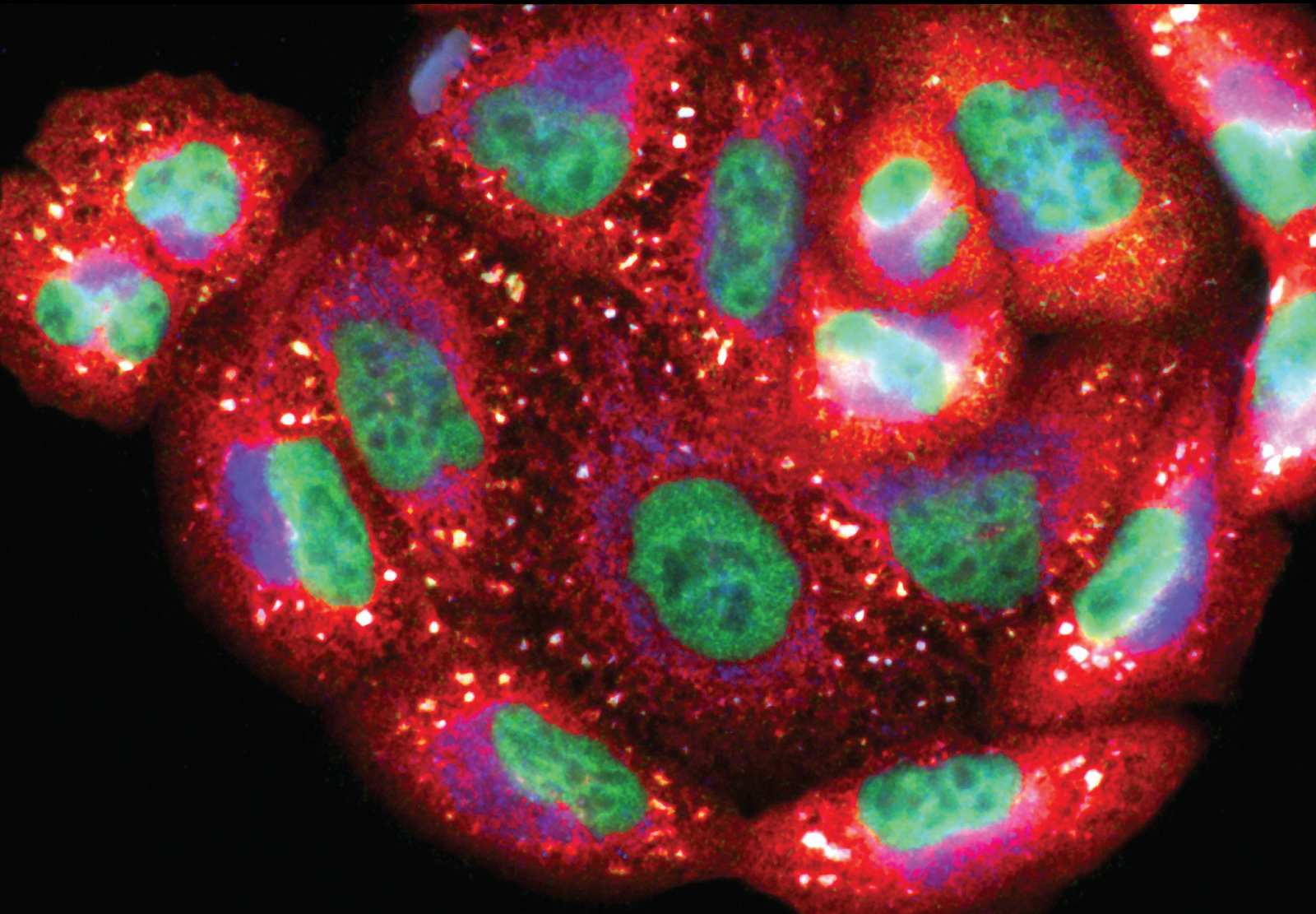# Strategies for Modulating Oxidative Stress Under Diverse Physiological and Pathological Conditions 2021

Lead Guest Editor: Karolina Szewczyk-Golec
Guest Editors: Jolanta Czuczejko, Przemko Tylzanowski, Joanna Lecka, and Manjit Singh Rana

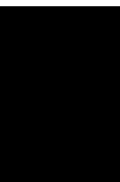# Strategies for Modulating Oxidative Stress Under Diverse Physiological and Pathological Conditions 2021

Strategies for Modulating Oxidative Stress Under Diverse Physiological and Pathological Conditions 2021

Lead Guest Editor: Karolina Szewczyk-Golec
Guest Editors: Jolanta Czuczejko, Przemko Tylzanowski, Joanna Lecka, and Manjit Singh Rana

Tim Hofer, Norway
John D. Horowitz, Australia
Silvana Hrelia, Italy
Dragan Hrncic, Serbia
Zebo Huang, China
Zhao Huang, China
Tarique Hussain, Pakistan
Stephan Immenschuh, Germany
Norsharina Ismail, Malaysia
Franco J. L, Brazil
Sedat Kacar, USA
Andleeb Khan, Saudi Arabia
Kum Kum Khanna, Australia
Neelam Khaper, Canada
Ramoji Kosuru, USA
Demetrios Kouretas, Greece
Andrey V. Kozlov, Austria
Chan-Yen Kuo, Taiwan
Gaocai Li, China
Guoping Li, USA
Jin-Long Li, China
Qiangqiang Li, China
Xin-Feng Li, China
Jialiang Liang, China
Adam Lightfoot, United Kingdom
Christopher Horst Lillig, Germany
Paloma B. Liton, USA
Ana Lloret, Spain
Lorenzo Loffredo, Italy
Camilo López-Alarcón, Chile
Daniel Lopez-Malo, Spain
Massimo Lucarini, Italy
Hai-Chun Ma, China
Nageswara Madamanchi, USA
Kenneth Maiese, USA
Marco Malaguti, Italy
Steven McAnulty, USA
Antonio Desmond McCarthy, Argentina
Sonia Medina-Escudero, Spain
Pedro Mena, Italy
Víctor M. Mendoza-Núñez, Mexico
Lidija Milkovic, Croatia
Alexandra Miller, USA
Sara Missaglia, Italy

Premysl Mladenka, Czech Republic
Sandra Moreno, Italy
Trevor A. Mori, Australia
Fabiana Morroni, Italy
Ange Mouithys-Mickalad, Belgium
Iordanis Mourouzis, Greece
Ryoji Nagai, Japan
Amit Kumar Nayak, India
Abderrahim Nemmar, United Arab
Emirates
Xing Niu, China
Cristina Nocella, Italy
Susana Novella, Spain
Hassan Obied, Australia
Pál Pacher, USA
Pasquale Pagliaro, Italy
Dilipkumar Pal, India
Valentina Pallottini, Italy
Swapnil Pandey, USA
Mayur Parmar, USA
Vassilis Paschalis, Greece
Keshav Raj Paudel, Australia
Ilaria Peluso, Italy
Tiziana Persichini, Italy
Shazib Pervaiz, Singapore
Abdul Rehman Phull, Republic of Korea
Vincent Pialoux, France
Alessandro Poggi, Italy
Zsolt Radak, Hungary
Dario C. Ramirez, Argentina
Erika Ramos-Tovar, Mexico
Sid D. Ray, USA
Muneeb Rehman, Saudi Arabia
Hamid Reza Rezvani, France
Alessandra Ricelli, Italy
Francisco J. Romero, Spain
Joan Roselló-Catafau, Spain
Subhadeep Roy, India
Josep V. Rubert, The Netherlands
Sumbal Saba, Brazil
Kunihiro Sakuma, Japan
Gabriele Saretzki, United Kingdom
Luciano Saso, Italy
Nadja Schroder, Brazil

Contents

Contents

Hindawi

Research Article

Protective Effect of Electroacupuncture on the Barrier Function of Intestinal Injury in Endotoxemia through HO-1/PINK1 Pathway-Mediated Mitochondrial Dynamics Regulation

Yuan Zhang [iD],[1] **Zhenzhen Meng,**[1] **Lina Wu** [iD],[1] **Xiuyun Liu** [iD],[2,3] **Chenxu Guo,**[1] **Jianbo Yu** [iD],[1] **Dong Ming,**[2,3] **Shuan Dong,**[1] **Yingya Cao,**[1] **and Xianhong Jiang**[1]

[1]*Department of Anesthesiology and Critical Care Medicine, Tianjin Nankai Hospital, Tianjin Medical University, Tianjin 300100, China*

[2]*Department of Biomedical Engineering, College of Precision Instruments and Optoelectronics Engineering, Tianjin University, Tianjin 300072, China*

[3]*Academy of Medical Engineering and Translational Medicine, Tianjin University, Tianjin 300072, China*

Correspondence should be addressed to Jianbo Yu; 30717008@nankai.edu.cn

Background and Aims. Endotoxemia (ET) is a common critical illness in patients receiving intensive care and is associated with high mortality and prolonged hospital stay. The intestinal epithelial cell dysfunction is regarded as the "engine" of deteriorated ET. Although electroacupuncture (EA) can mitigate endotoxin-induced intestinal epithelial cell dysfunction in ET, the mechanism through which EA improves endotoxin-induced intestinal injury for preventing ET deterioration needs further investigation. *Methods.* An in vivo ET model was developed by injecting lipopolysaccharide (LPS) in wild-type and PINK1-knockout mice. An in vitro model was also established by incubating epithelial cells in the serum samples obtained from both groups of mice. Hemin and zinc protoporphyrin IX (ZnPP) were applied to activate or inhibit heme oxygenase 1 (HO-1) production. EA treatment was performed for 30 min consecutively for 5 days before LPS injection, and on the day of the experiment, EA was performed throughout the process. Samples were harvested at 6 h after LPS induction for analyzing tissue injury, oxidative stress, ATP production, activity of diamine oxidase (DAO), and changes in the levels of HO-1, PTEN-induced putative kinase 1 (PINK1), mitochondrial fusion and fission marker gene, caspase-1, and interleukin 1 beta (IL-1β). *Results.* In the wild-type models (both in vivo and vitro), EA alleviated LPS-induced intestinal injury and mitochondrial dysfunction, as indicated by decreased reactive oxygen species (ROS) production and oxygen consumption rate (OCR) and reduced levels of mitochondrial fission proteins. EA treatment also boosted histopathological morphology, ATP levels, DAO activity, and levels of mitochondrial fusion proteins in vivo and vitro. The effect of EA was enhanced by hemin but suppressed by Znpp. However, EA + AP, Znpp, or hemin had no effects on the LPS-induced, PINK1-knocked out mouse models. *Conclusion.* EA may improve the HO-1/PINK1 pathway-mediated mitochondrial dynamic balance to protect the intestinal barrier in patients with ET.

1. Introduction

Endotoxemia (ET) is common in clinically ill patients receiving intensive care and can easily induce multiple organ dysfunction syndromes (MODS) and threaten patients' life. Intestinal epithelial cell dysfunction is considered the main cause of systemic inflammation, such as MODS after ET.

Early and effective interventions to prevent gut barrier dysfunction have been proved to be beneficial for patients with ET [1].

The mitochondria are highly dynamic organelles that undergo delicate fusion and fission cycles to maintain their functions and shape when cells experience metabolic or environmental stress [2]. In mammals, mitochondrial fusion
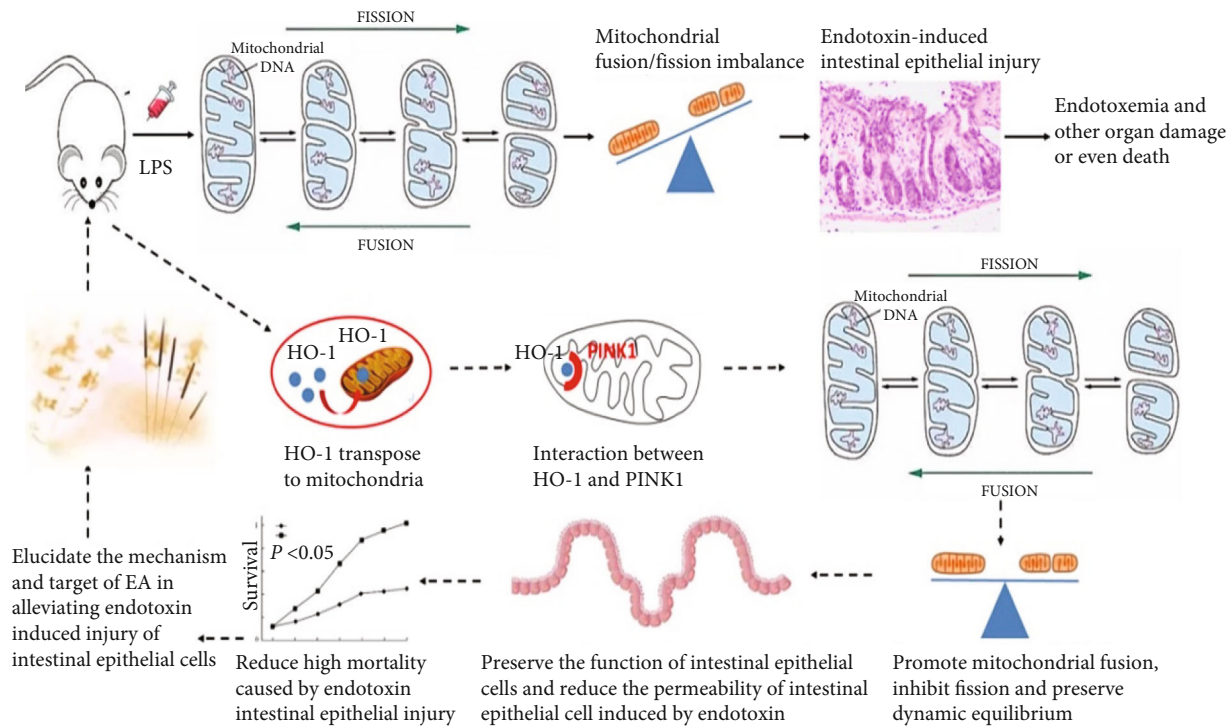
Figure 1: Outline of the experimental design.

is regulated by mitofusin 1 and 2 (Mfn1/2), situated in the outer membranes of the mitochondria, and optic atrophy 1 (OpA-1), situated in the inner membranes of the mitochondria. Mitochondrial fission is promoted by dynamin-related protein 1 (Drp1) in the cytoplasm and mitochondrial division protein 1 (Fis1) located in the outer membrane of the mitochondria [2, 3]. Dysregulation of these processes results in an abnormally fused or fragmented mitochondrial network that is unable to meet cellular energy demands.

Dysregulated mitochondrial dynamics has been found to be related to disease development and progression. Intestinal disease causing intestinal dysfunction has been reported to be related to disrupted mitochondrial dynamics [4]. Our previous studies have demonstrated that the mitochondria with a proper dynamic balance of fusion/fission could resist endotoxin-induced acute lung injury [5–7]. Previous studies have also proved that the progression of organ failure during sepsis is partially due to mitochondrial dysfunction initiated by oxidative stress, along with a decreased mitochondrial respiratory control ratio [8, 9]. However, whether modulating the mitochondrial fusion/fission balance can alleviate the gut barrier dysfunction in ET is currently unknown. Exploring a potential antioxidant to preserve mitochondrial dynamics may be a vital determinant for protecting the mitochondria from oxidative damage in animal models of sepsis-induced organ failure.

Heme oxygenase-1 (HO-1) can regulate mitochondrial dynamic equilibrium and impede oxidative cellular injury by catalyzing the breakdown of heme to free iron, carbon monoxide, and biliverdin in mammalian cells [10–12]. PTEN-induced putative kinase 1 (PINK1), the only kinase located mainly in the mitochondrial intima, has been found

to have a certain protective effect on the mitochondria during cellular stress, which is important in the HO-1 pathway. However, the basic mechanism remains to be investigated [13–15].

In recent years, electroacupuncture (EA) on proper acupoints (AP) has gained popularity as a nonpharmaceutical treatment for intestinal injury [16–18]. Our previous studies have demonstrated the protective effect of EA on ET-induced lung injury, wherein we found an increase in HO-1 expression and mitochondrial fusion activities [19–21]. However, whether EA is effective in protecting intestinal epithelial cells in patients with ET by regulating the mitochondrial fusion/division homeostasis is currently unknown. Therefore, in the present study, we hypothesized that EA may protect the intestinal epithelial cells in patients with ET by regulating the mitochondrial fusion/fission dynamics and protect the intestinal barrier by activating the HO-1/PINK1 pathway. Both wild-type and PINK1-knockout mice and cells were used in the study, and an ET model was established both in vivo and vitro. We attempted to validate our hypothesis to explore the basic mechanism of EA treatment for ET (Figure 1).

2. Materials and Methods

2.1. Ethics Approval.
All animal procedures were approved by the Animal Ethics and Welfare Committee of Nankai University (No.81803899) and performed according to the Guidelines for the Care and Use Experimental Animals.

2.2. Establishment of an In Vitro LPS-Induced Cell Intestinal Barrier Model.
Human colon adenocarcinoma cells (Caco-2

cells) were cultured in the DMEM complete medium (containing 20% fetal bovine serum) at 37°C in a 5% CO_2 incubator and passaged by trypsin digestion every 3–5 days. The cells were counted using a blood cell counting plate, which were seeded on the top of a Transwell chamber at a density of 2×10^5 cells/ml. Then, $400\,\mu l$ of cells and $600\,\mu l$ of DMEM complete medium were added to each well. After inoculation, the medium was changed every day. The growth status of cells was observed by determining trans-epithelial electrical resistance (TEER). After 21 days of culture, the cells were dense and well-connected per our observation under a light microscope, and TEER was significantly increased and stabilized at 450–$500\,\Omega$/cm, which indicated that an in vitro Caco-2 cell intestinal barrier model was established successfully. The intestinal barrier model cells were further exposed to LPS ($100\,\mu g$/mL, dissolved in 1 mL of 0.9% normal saline) for 24 h to establish an LPS-induced cell intestinal barrier model in vitro.

A certain amount of blood was taken from the heart of the mice treated with EA on AP via a 5 mL vacuum blood sampling needle. The blood was cooled for 1 h and centrifuged (2,500 rpm) for 25 min. The sediment was discarded, and the serum was retained. The serum was inactivated in a water bath at 56°C for 30 min and then sterilized using $0.22\,\mu M$ semipermeable membranes. The prepared serum was added to the Caco-2 cell intestinal barrier model at a ratio of 10%. After 12 h of incubation, the Caco-2 cell intestinal barrier model with EA on AP intervention was established [22]. The Caco-2 cells were subcultured for three passages. Tests were performed at each passage. Each test was repeated three times. Mycoplasma detection was performed through PCR analysis to ensure that the cells were not infected by mycoplasma [23].

2.3. Establishment of the Mouse Intestinal Injury Model of ET.
Eight-week-old, male C57BL/6 mice (weighing 18 to 22 g) were provided by the Laboratory Animal Center of Nankai University, Tianjin, China. The mice were caged individually at 30%–70% humidity (18 to 25°C) and acclimatized to a 12 h light-dark cycle, with access to food and water ad libitum. The animals were anesthetized and operated, as described previously [24]. To induce intestinal injury, 10 mg/kg LPS (dissolved in 1 mL of 0.9% normal saline) was injected intraperitoneally, and the control group was injected with an equal volume of normal saline. Further experimental details were described in our previous study [23]. The mice were sacrificed 6 h after the LPS injection, and the specimens were isolated for further analysis (the animals who died within 6 h were excluded). The mice were acclimated for three days prior to the experiments.

2.4. Different Groups of Cells and Mice with/without Treatment.
The cells were divided into 5 groups, namely control, LPS (LPS-induced cells), LPS + EA + AP group (LPS cells treated with EA on AP targets), LPS + EA + AP + ZnPP group (LPS cells treated with EA on AP targets and incubated with ZnPP), and LPS + EA + AP + hemin group (LPS cells treated with EA on AP targets and incubated with hemin). For EA intervention, the cells were cultured with the serum obtained from the LPS mice treated with EA. The cells were digested after 6 h. Then, the cell pel-

lets were resuspended in 1 mL phosphate buffer saline for complete homogenization. The supernatants of the cell homogenate were extracted by centrifugation at 4°C and 15,000 rpm for 10 min. The samples were frozen in liquid nitrogen and stored at -80°C until further assays.

The mice were divided into 5 groups, with 10 mice in each group: Control group (wild mice injected with normal saline), LPS group (mice injected with LPS), LPS + EA + AP group (LPS mice treated with EA on AP targets), LPS + EA + AP + ZnPP group (LPS mice treated with EA on AP targets and injected with ZnPP), and LPS + EA + AP + hemin group (LPS mice treated with EA on AP targets and injected with hemin). For the LPS + AP + EA group, the bilateral acupoints of Zusanli at 5 mm depth and Hegu at 1 mm depth were selected as the AP locations (for more details, please refer to supplementary materials and methods). During the treatment period, the needle handles were connected to a Han's nerve AP stimulator with a disperse-dense wave of 2 Hz/15 Hz frequency and 1 mA intensity applied. A daily 30 min EA treatment was performed for 5 days before administering the LPS injection. On the day of the experiment, EA was performed 30 min before the LPS injection. The needles were retained in the APs until the end of the experiment. On the other hand, the LPS + EA group received EA treatment on locations beyond the selected targets. An experienced acupuncturist identified the AP and non-AP targets. In the groups treated with drugs, ZnPP or hemin was injected via the tail vein; hemin was injected at the dose of 100 mg/kg dissolved in 1 mL of NaOH, and Znpp was injected at a dose of $10\,\mu$mol/kg dissolved in 1 mL of $NaHCO_3$.

All the mice were euthanized 6 h after LPS injection, and a 10 cm long small intestine was dissected from the terminal ileum. The small intestine was carved along with the antimesenteric attachment, and a mucosal homogenate was obtained. The mucosal homogenate (1 mL) was centrifuged at 15,000 rpm and 4°C for 5 min, and the cell pellets were resuspended in 1 mL phosphate buffer saline for complete homogenization. Then, the supernatant of the cell homogenate was extracted by centrifugation at 4°C and 15,000 rpm for 10 min. The samples were frozen in liquid nitrogen and stored at -80°C until further analysis.

2.5. Determining Mitochondrial Function.
The level of reactive oxygen species (ROS) in the intestinal mucosal epithelial cells was determined spectrofluorometrically using the DCFH-DA as a fluorescent dye. Briefly, the intestine mucosal cell suspension was treated with $10\,\mu$mol/L DCFH-DA at 37°C for 30 min in the dark. DCF fluorescence was monitored with Ex/Emof 480 nm/530 nm by using the Chameleon microplate reader (Hidex, Turku, Finland). The fluorescence intensity of the sample was determined as the differences relative to the initial fluorescence. The oxygen consumption rate (OCR) of the intestinal mucosal epithelial cells was detected using the Cayman oxygen consumption rate detection kit and analyzed by flow cytometer (Beckman Coulter, CA, USA). The data were analyzed using FlowJo software (Tree Star, OR, USA). The ATP level was determined using an ATP assay kit, and the absorbance of every well was

(a)

(b)
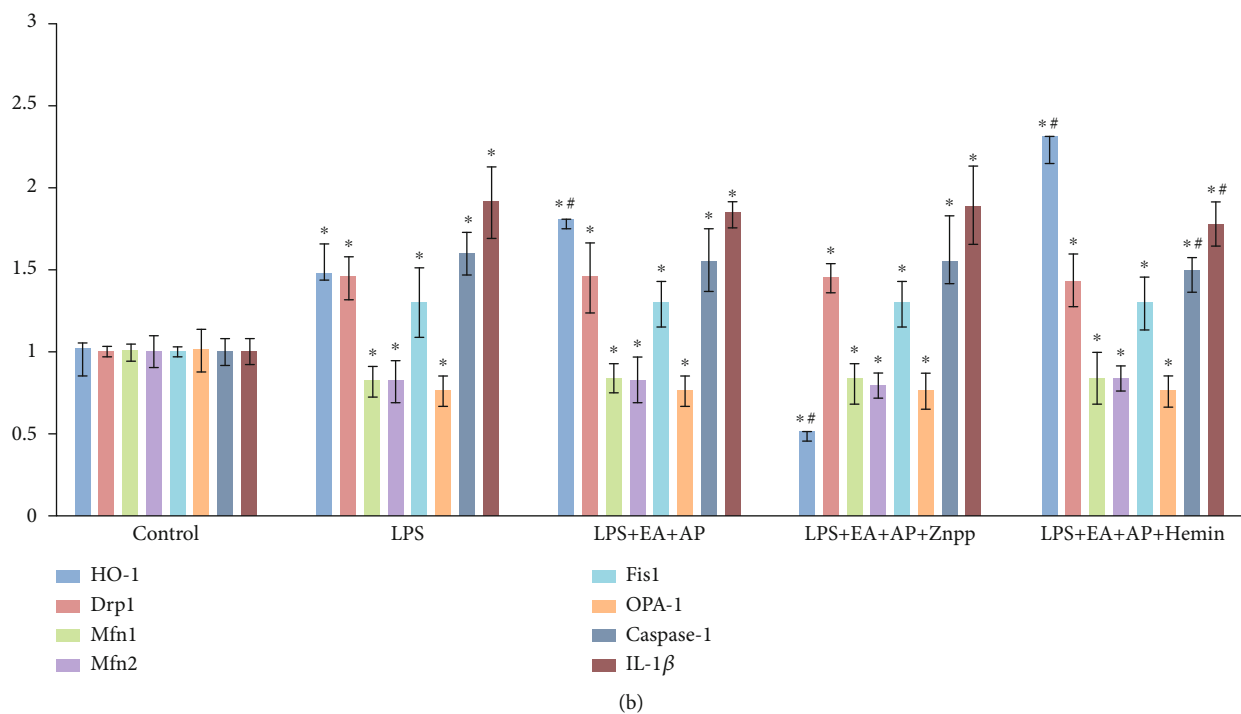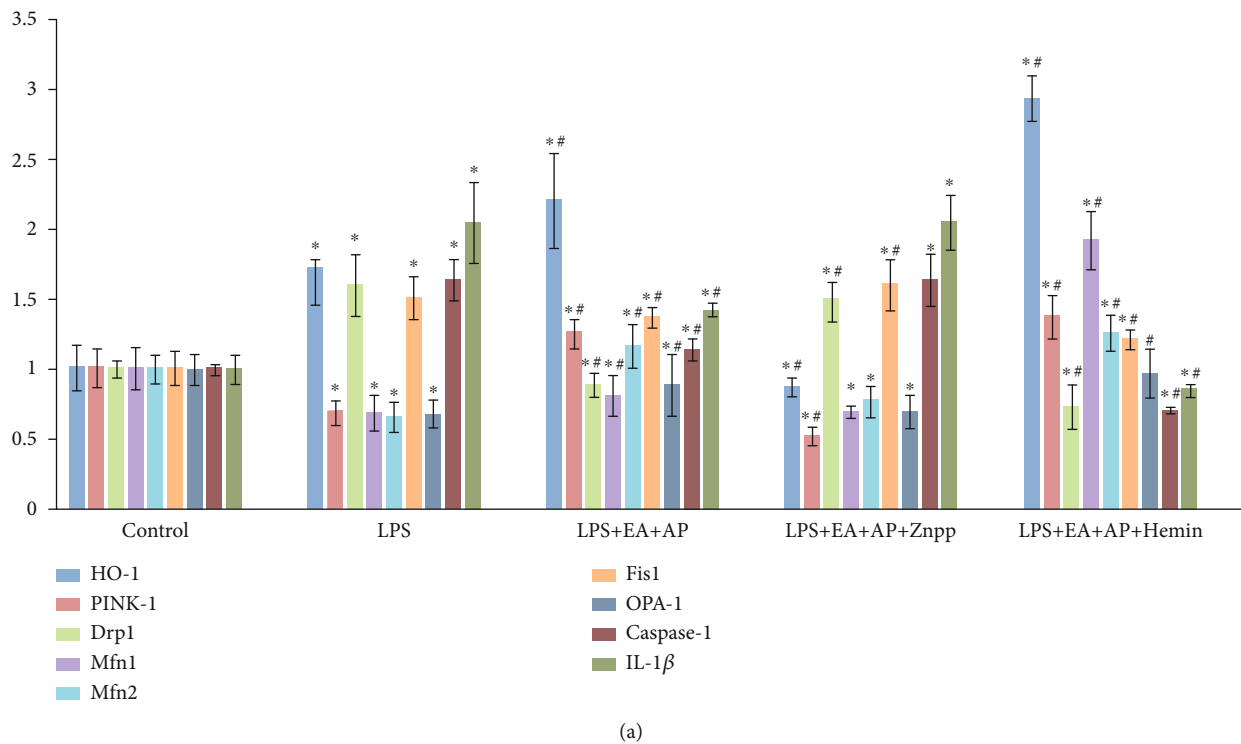
FIGURE 2: Continued.

(c)

(d)
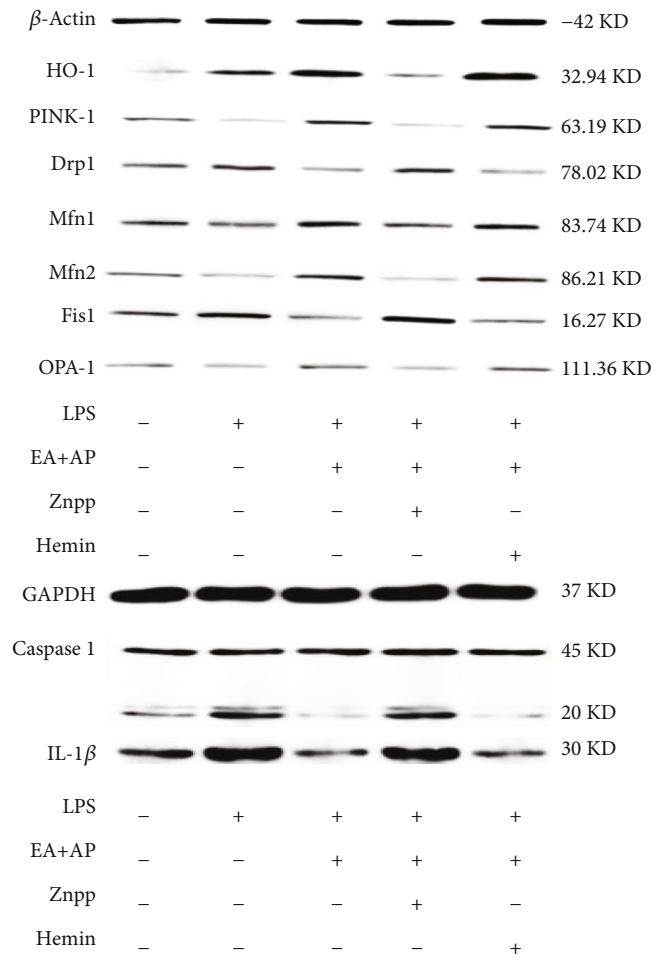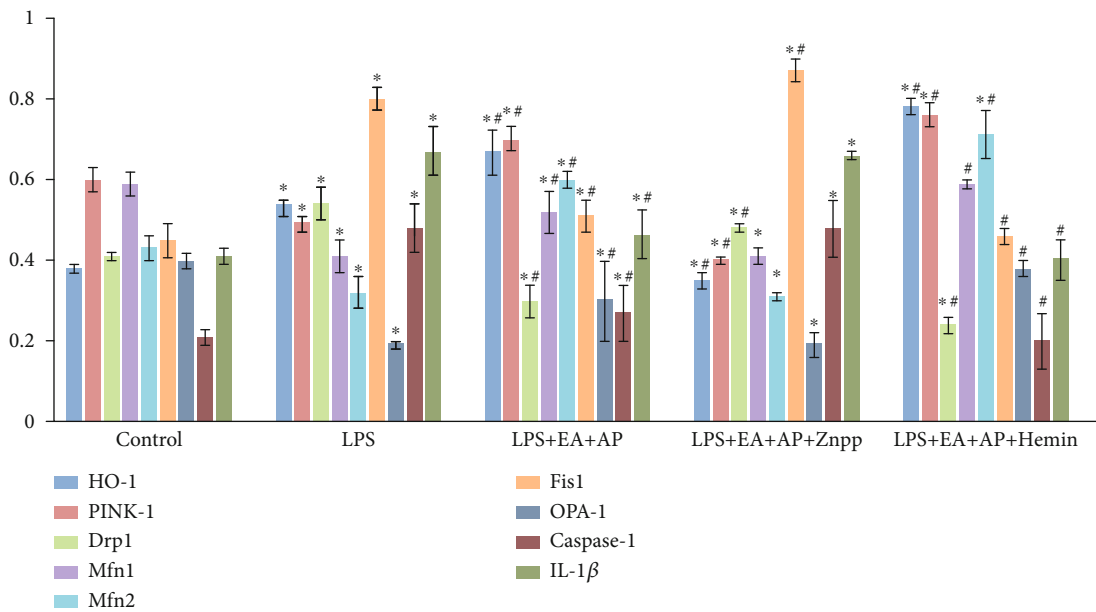
Figure 2: Continued.
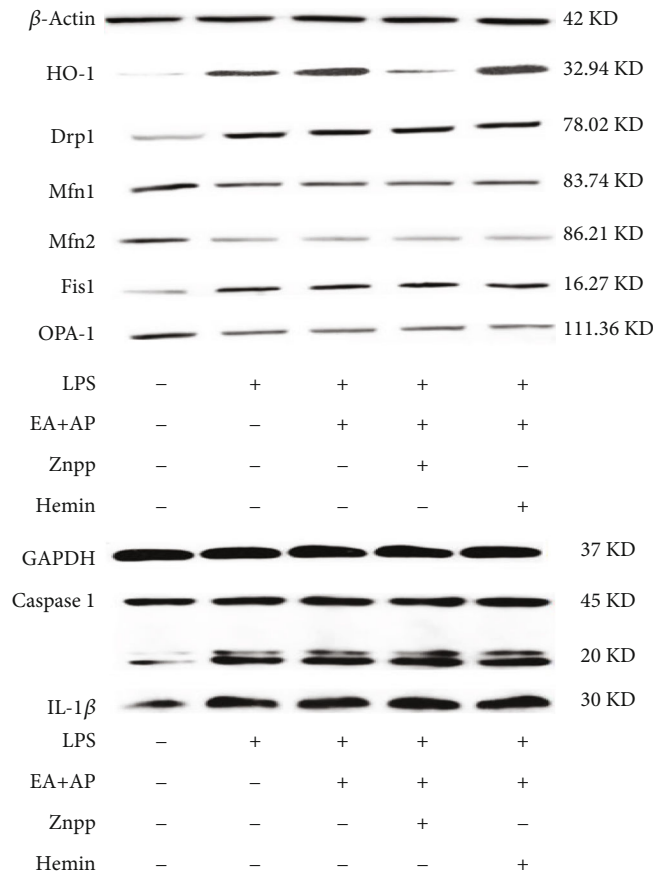
(e)
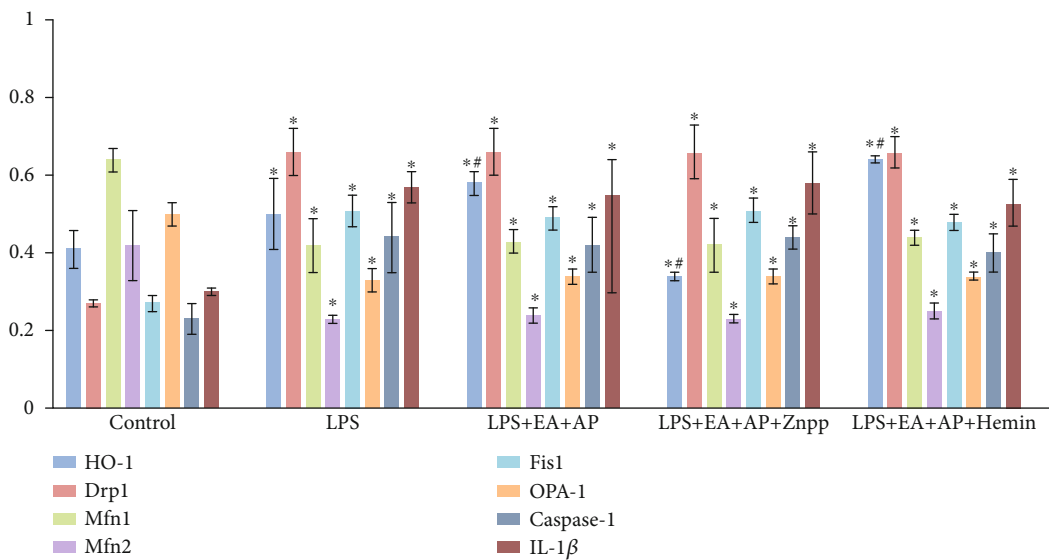
(f)

FIGURE 2: The levels of mRNAs (a, b) and proteins (c, d, e, and f) known as mitochondrial fusion/fission markers and pyroptosis factors in the wild-type mice (a, c, and d) and PINK1-knockout mice (b, e, and f). HO-1: heme oxygenase-1, PINK1: PTEN-induced putative kinase 1, Drp1: the dynamin-related protein 1, Mfn1/2: the mitofusin 1 and 2, Fis1: mitochondrial division protein 1, OpA-1: the optic atrophy 1, IL-1β: interleukin-1β, LPS: lipopolysaccharide, EA + AP: electroacupuncture (EA) performed on acupoint (AP), hemin: a substrate and inducer of HO-1, and ZnPP: zinc protoporphyrin IX, an inhibitor of HO-1, +/-. The mice were or were not treated with corresponding factors. β-Actin served as an internal standard to ensure similar gel loading of the starting material in each sample. The mRNA and protein levels are compared using the paired sample t-test. $*$: significant difference compared with the control mice ($P < 0.05$). $\#$: significant difference compared with the LPS-exposed mice ($P < 0.05$).

(a)

(b)

FIGURE 3: Continued.

β-Actin						42 KD
HO-1						32.94 KD
PINK-1						63.19 KD
Drp1						78.02 KD
Mfn1						83.74 KD
Mfn2						86.21 KD
Fis1						16.27 KD
OPA-1						111.36 KD
LPS	−	+	+	+	+	
EA+AP	−	−	+	+	+	
Znpp	−	−	−	+	−	
Hemin	−	−	−	−	+	

GAPDH						37 KD
Caspase 1						45 KD
						20 KD
IL-1β						30 KD
LPS	−	+	+	+	+	
EA+AP	−	−	+	+	+	
Znpp	−	−	−	+	−	
Hemin	−	−	−	−	+	
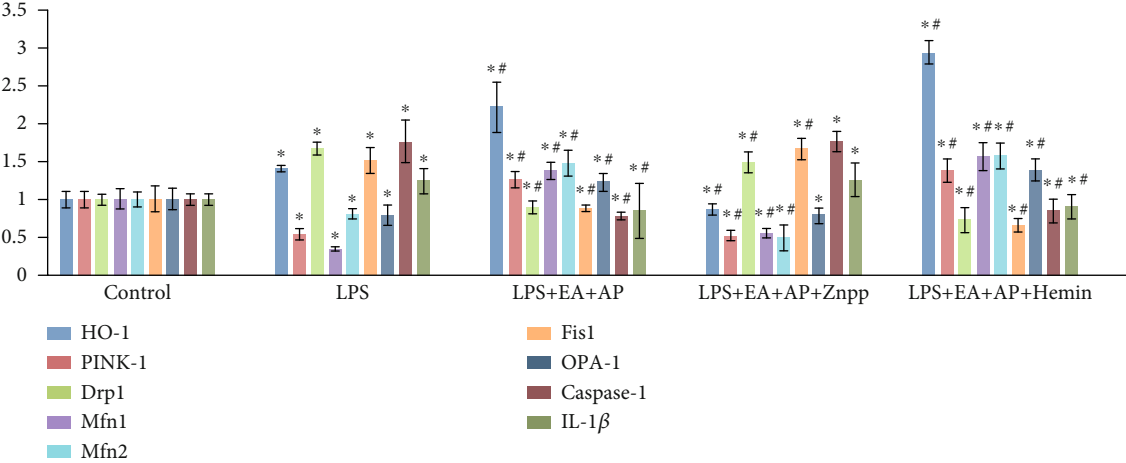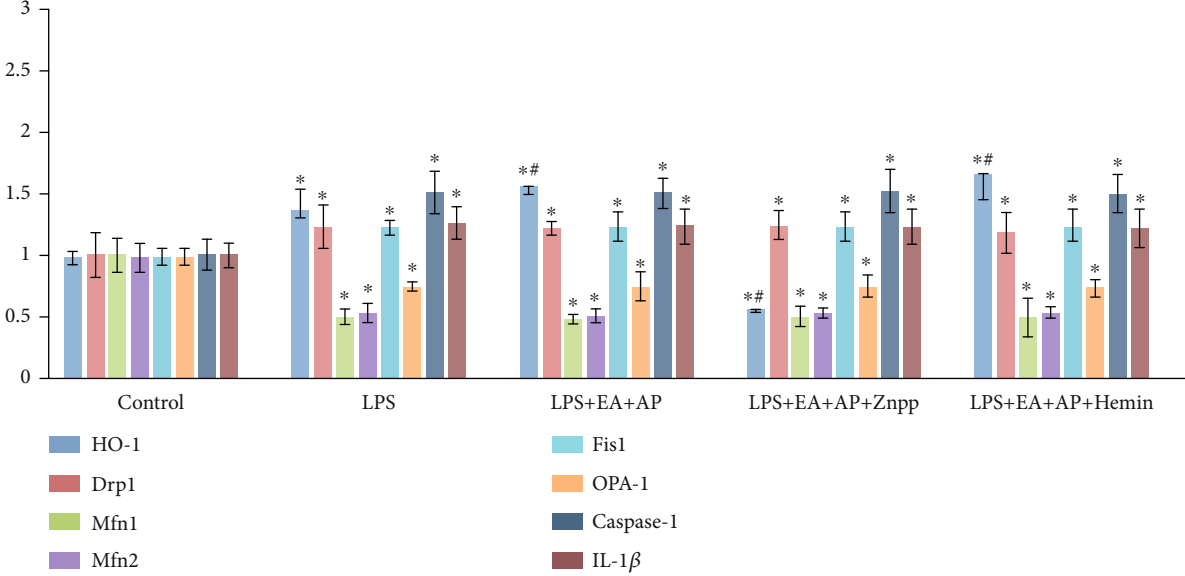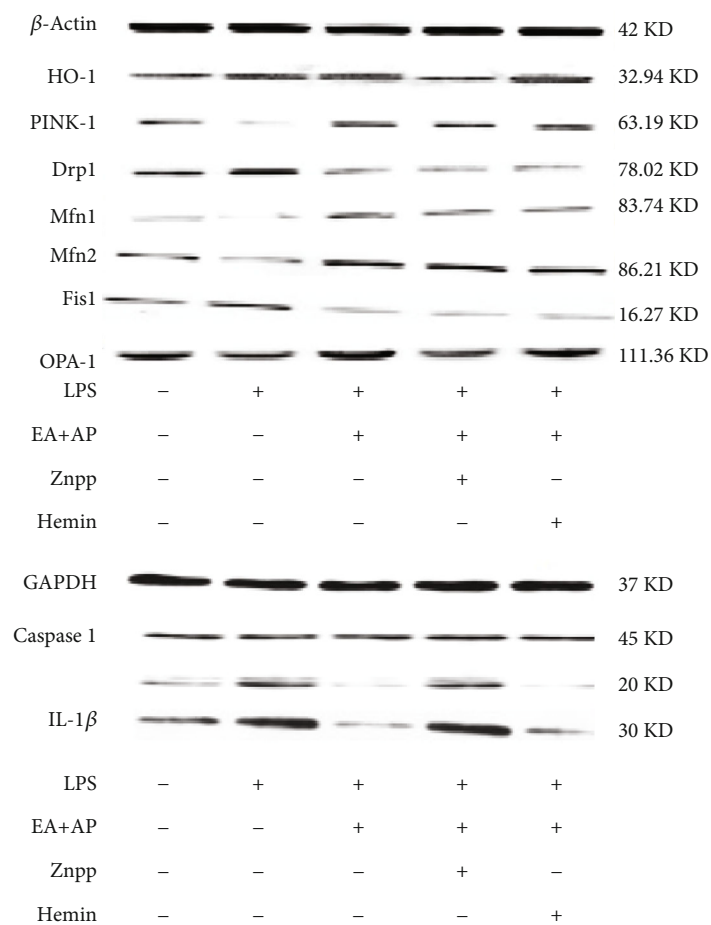
(c)

Figure 3: Continued.

(d)

Figure 3: Continued.

β-Actin					42 KD
HO-1					32.94 KD
Drp1					78.02 KD
Mfn1					83.74 KD
Mfn2					86.21 KD
Fis1					16.27 KD
OPA-1					111.36 KD
LPS	−	+	+	+	+
EA+AP	−	−	+	+	+
Znpp	−	−	−	+	−
Hemin	−	−	−	−	+
GAPDH					37 KD
Caspase 1					45 KD
					20 KD
IL-1β					30 KD
LPS	−	+	+	+	+
EA+AP	−	−	+	+	+
Znpp	−	−	−	+	−
Hemin	−	−	−	−	+

(e)

Figure 3: Continued.

(f)
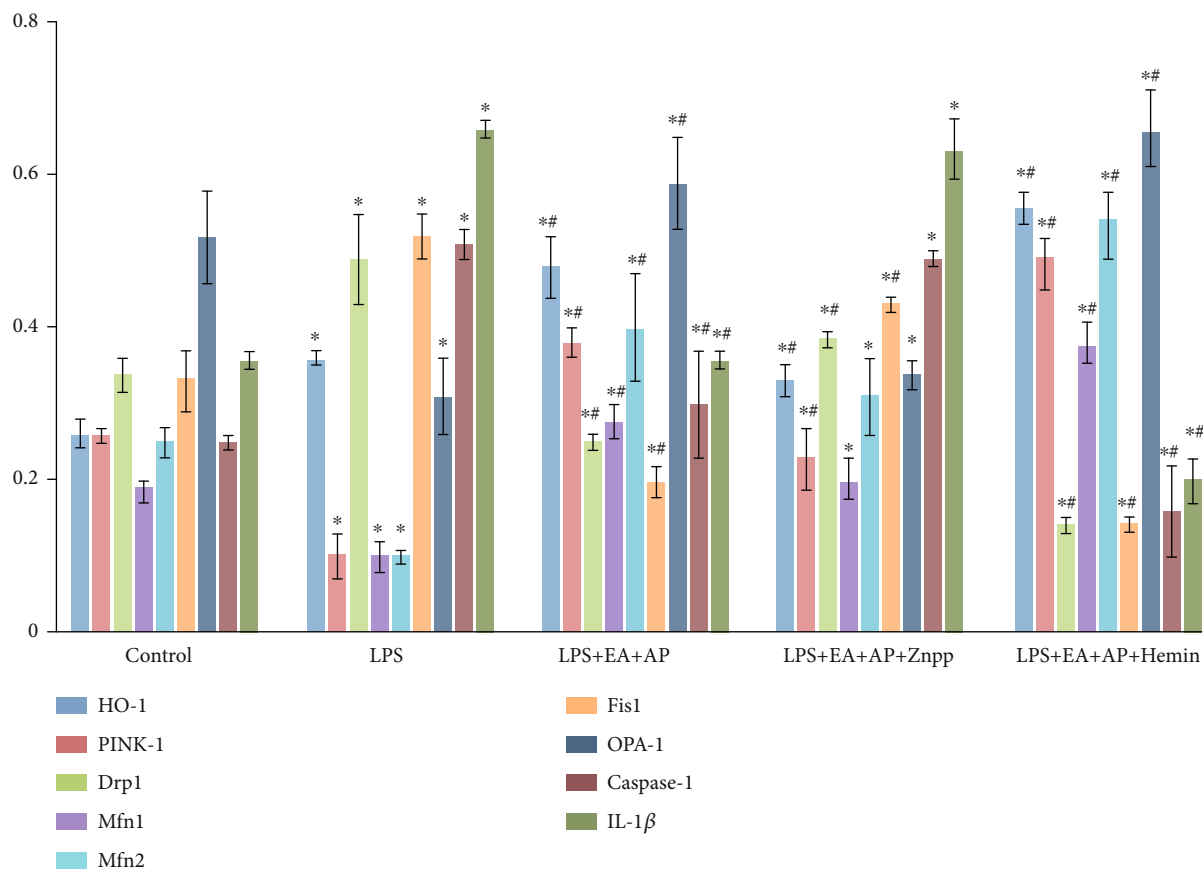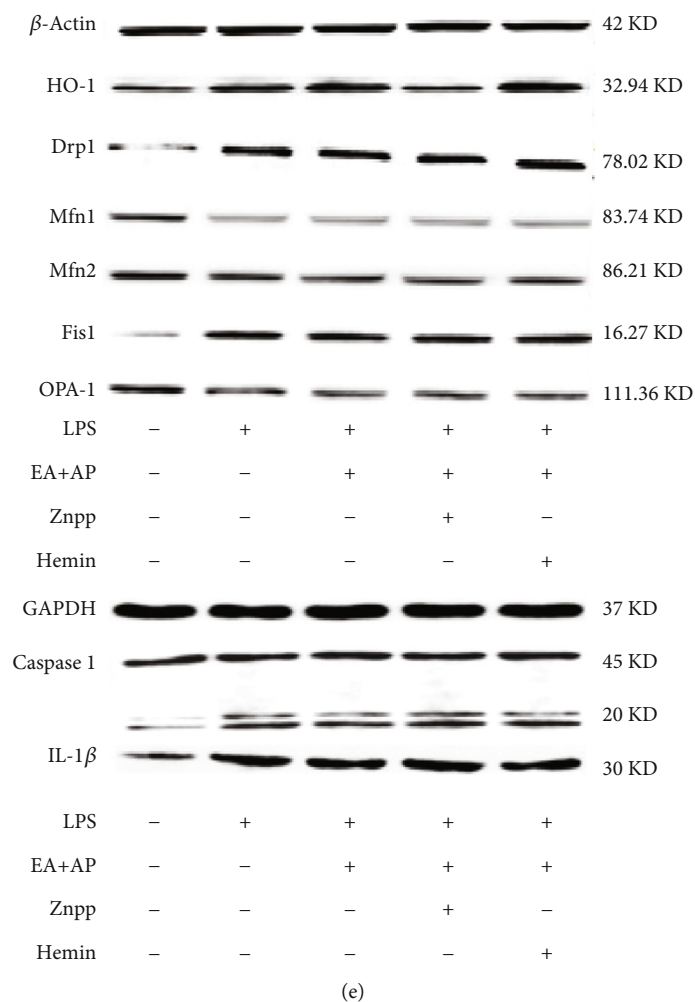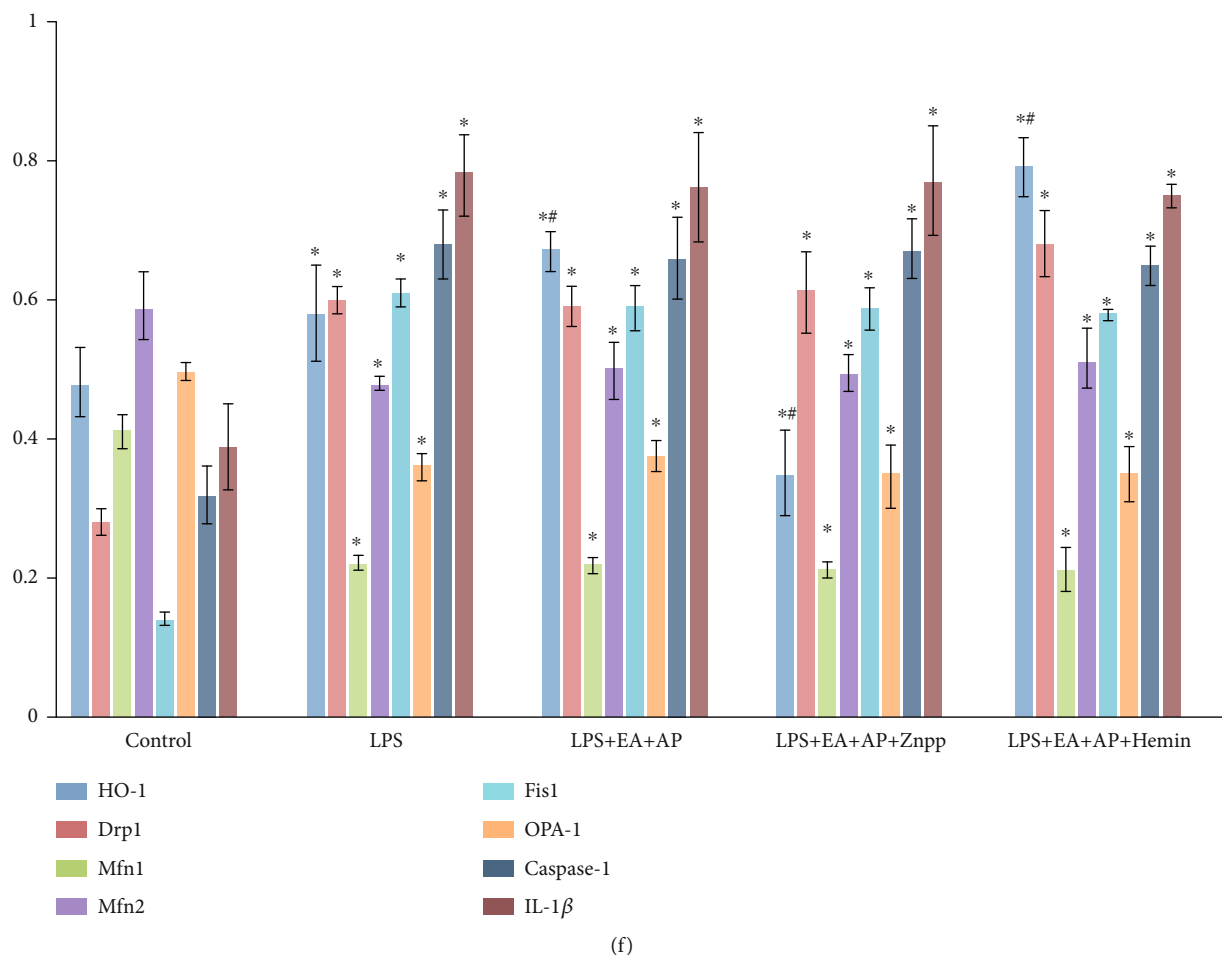
FIGURE 3: The levels of mRNAs (a, b) and proteins (c, d, e, and f) known as mitochondrial fusion/fission markers and pyroptosis factors in the wild-type Caco-2 cells (a, c, and d) and PINK1-knockout Caco-2 cells (b, e, and f). HO-1: heme oxygenase-1, PINK1: PTEN-induced putative kinase 1, Drp1: the dynamin-related protein 1, Mfn1/2: the mitofusin 1 and 2, Fis1: mitochondrial division protein 1, OpA-1: the optic atrophy 1, IL-1β: interleukin-1β, LPS: lipopolysaccharide, EA + AP: electroacupuncture (EA) performed on acupoint (AP), hemin: a substrate and inducer of HO-1, and ZnPP: zinc protoporphyrin IX, an inhibitor of HO-1, +/-. The cells were or were not treated with corresponding factors. β-Actin served as an internal standard to ensure similar gel loading of the starting material in each sample. The mRNA and protein levels were compared using the paired sample t-test. *: significant difference compared with the control cells ($P < 0.05$). #: significant difference compared with the LPS-exposed cells ($P < 0.05$).

monitored at the optical density (OD) of 570 nm by using a microplate reader (Bio-Tek Instruments, VT, USA) [25].

2.6. Assessment of the Extent of Intestinal Epithelial Cell Injury.
The extent of intestinal epithelial cell injury was assessed by determining the diamine oxidase (DAO) levels. The activity of DAO was determined by ELISA. The activity of DAO in animal plasma and cell culture supernatant samples was determined using the double antibody sandwich method. The specific methods used are as follows: first, the microplates were coated using the purified DAO antibody to make a solid-phase antibody. Second, standard DAO and animal plasma and cell culture supernatants were added to the coated microplates. Third, HRP-labeled DAO antibody was added to the microplates to form antibody antigen enzyme-labeled antibody complexes. After thorough washing, the substrate 3,3′,5,5′ -tetramethylbenzidine (TMB) of HR was

added for color development. The color of TMB turned blue because of the catalysis of the HRP enzyme and turned yellow under the action of the acid. The color density was positively correlated with the activity of DAO. The absorbance (OD value) was measured at a wavelength of 450 nm by using a microplate reader. The activity of DAO was calculated by determining the standard curve.

2.7. Real-Time Quantitative Reverse Transcription PCR.
Total RNA was isolated from cultured Caco-2 cells or mouse intestine mucosa by using a high-purity RNA kit (Roche, Switzerland). Total RNA was quantified using a spectrophotometer at 260 nm. Then, 2 μg of total RNA was reverse transcribed to produce first-strand cDNA by using the SYBR Green Master Mix on the ABI Prism 7000 sequence detector system (Applied Biosystems, Foster City, USA). The PCR conditions were as follows: predegeneration at 95°C for

(a)

(b)

(c)

(d)

(e)

(f)

Figure 4: Continued.

(g)

(h)
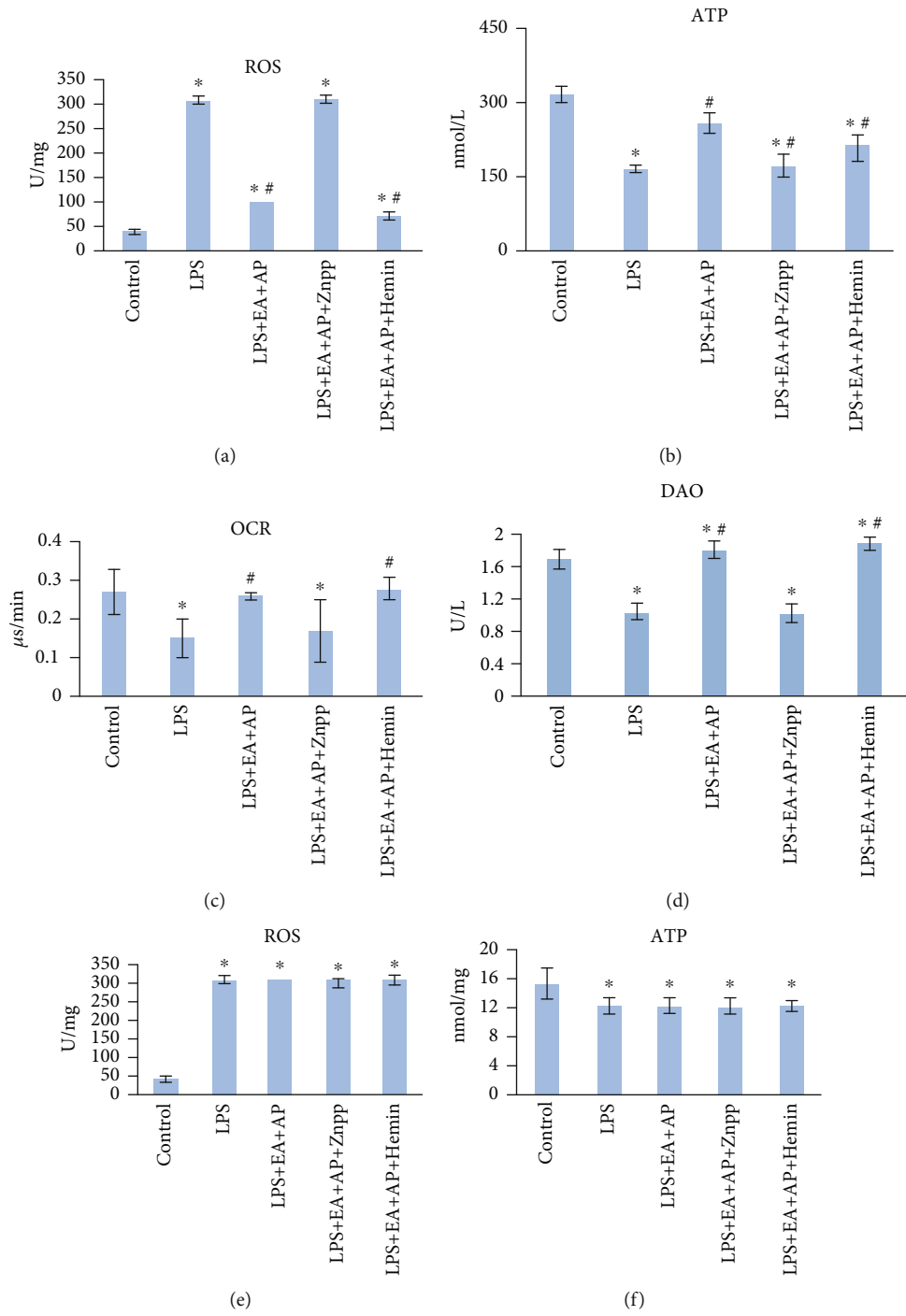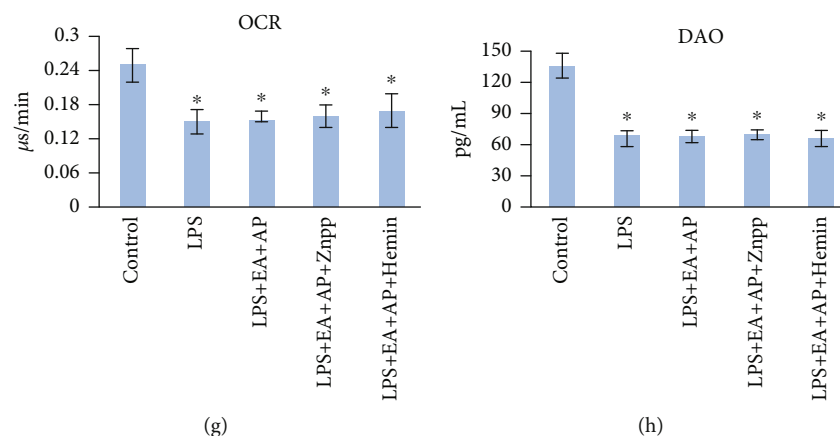
FIGURE 4: Effect of EA on ROS production, ATP content, OCR, and DAO levels in the LPS-exposed wild-type (a, b, c, and d) and PINK1-knockout mice (e, f, g, and h). LPS: lipopolysaccharide, EA + AP: electroacupuncture (EA) on acupoint (AP), hemin: a substrate and inducer of HO-1, ZnPP: zinc protoporphyrin IX, an inhibitor of HO-1, OCR: oxygen consumption rate, ROS: reactive oxygen species, DAO: diamine oxidase, and ATP: adenosine triphosphate. The mRNA and protein levels were compared using the paired sample t-test. *: significant difference compared with the control mice ($P < 0.05$). #: significant difference compared with the LPS-exposed mice ($P < 0.05$).

10 min, followed by 40 thermal cycles of denaturation for 30 s at 95°C; annealing for 5 s at 95°C; and extension for 30 s at 60°C. Specific primers used for marker genes of the status of the mitochondrial dynamic equilibrium are described in Supplementary Methods. The housekeeping gene β-actin served as an internal control to normalize all PCR products. Target gene expression was quantified using the comparative cycle threshold (C_T) methods [26, 27].

2.8. Western Blot Analysis. At the indicated time after pretreatment with various factors, the cultured Caco-2 cells or mouse intestine mucosa were homogenized in the ice-cold lysis buffer for 30 min. The protein extracts were centrifuged at 4°C and 15,000 rpm for 15 min, and the supernatants were quantified using the bicinchoninic acid protein assay kit (Thermo Fisher Scientific, MA, USA). Equal amounts of protein (50 μg per lane) were separated by 12% SDS-PAGE and then transferred to PVDF membranes (Bio-Rad, Hercules, CA, USA) by using the Bio-Rad transblot apparatus. The blots were washed with 1X Tris-buffered saline (TBS; 200 mmol/L Tris and 1.5 mol/L NaCl) three times and then blocked using 5% skim milk for 40 min at room temperature. The proteins were incubated overnight at 4°C with primary antibodies against HO-1 (1 : 500), PINK-1 (1 : 500), Drp1 (1 : 500), Mfn1 (1 : 400), Mfn2 (1 : 300), Fis1 (1 : 500), OPA1 (1 : 500), caspase-1 (1 : 500), IL-1β (1 : 500), and β-actin (1 : 500). The blots were washed with TBS-0.05% Tween 20 three times and incubated for 2 h at 37°C with HRP-conjugated secondary antibody (1 : 300). The protein signal was visualized using the Immobilon Western Chemiluminescent HRP Substrate detection reagent (Millipore, MA, USA) and imaged using Image Lab software (Bio-Rad, VA, USA). Finally, the proteins were quantified through densitometry using the Molecular Analyst Image-analysis Software (Bio-Rad Laboratories, CA, USA). The protein concentration of the marker genes was normalized to β-actin concentration by using the OD ratio.

2.9. Histopathological Examination of Cells and Observation of Mitochondrial Ultrastructure. After sacrificing the mice, 2 jejunum tissues were extracted from each mouse, of which one was used for histopathological examination and the other for observing the change in the mitochondrial ultrastructure. For the tissue histopathological examination, the jejunum tissues were cut into 5 mm sections, sliced into thin slices, fixed in 10% formalin, embedded in paraffin, and stained with hematoxylin and eosin (H&E) dye. We then evaluated the extent of injury to the intestine mucosa tissue according to inflammatory cell infiltration. To observe changes in the mitochondrial ultrastructure, the mucosal layer of the injured jejunum was fixed in 2.5% glutaraldehyde overnight at 4°C and then fixed in 1% aqueous osmium for 1 h, dehydrated with acetone, and embedded in resin based on routine protocols. The ultra-thin sections (<100 nm) were prepared using a microtome and mounted on copper grids. The mitochondrial ultrastructure was observed under a transmission electron microscope.

3. Results

3.1. The Mechanism of EA + AP Treatment in LPS-Induced Intestinal Injury In Vivo and In Vitro. The LPS-treated wild-type mice or cells and PINK1-knockout mice or cells were used to understand the mechanism of EA + AP treatment in LPS-induced intestinal injury both in vivo and in vitro (Figures 2 and 3). Figures 2(a), 2(c), and 2(d) and Figures 3(a), 3(c), and 3(d) show that LPS injection downregulated HO-1, PINK1, Mfn1, Mfn2, and OPA-1 mRNA expressions, decreasing respective protein levels ($P < 0.05$), and upregulated Drp1, Fis1, caspase-1, and IL-1β mRNA expressions, increasing respective protein levels, in the wild-type mice or cells ($P < 0.05$). When the wild-type mice and cells were subjected to EA + AP treatment, the mRNA and protein levels induced by LPS were alleviated (Figures 2 and 3; $P < 0.05$). Znpp (the HO-1 inhibitor) and hemin (a substrate and potent

(a)

(b)

(c)

(d)

(e)

(f)

FIGURE 5: Continued.

(g)

(h)
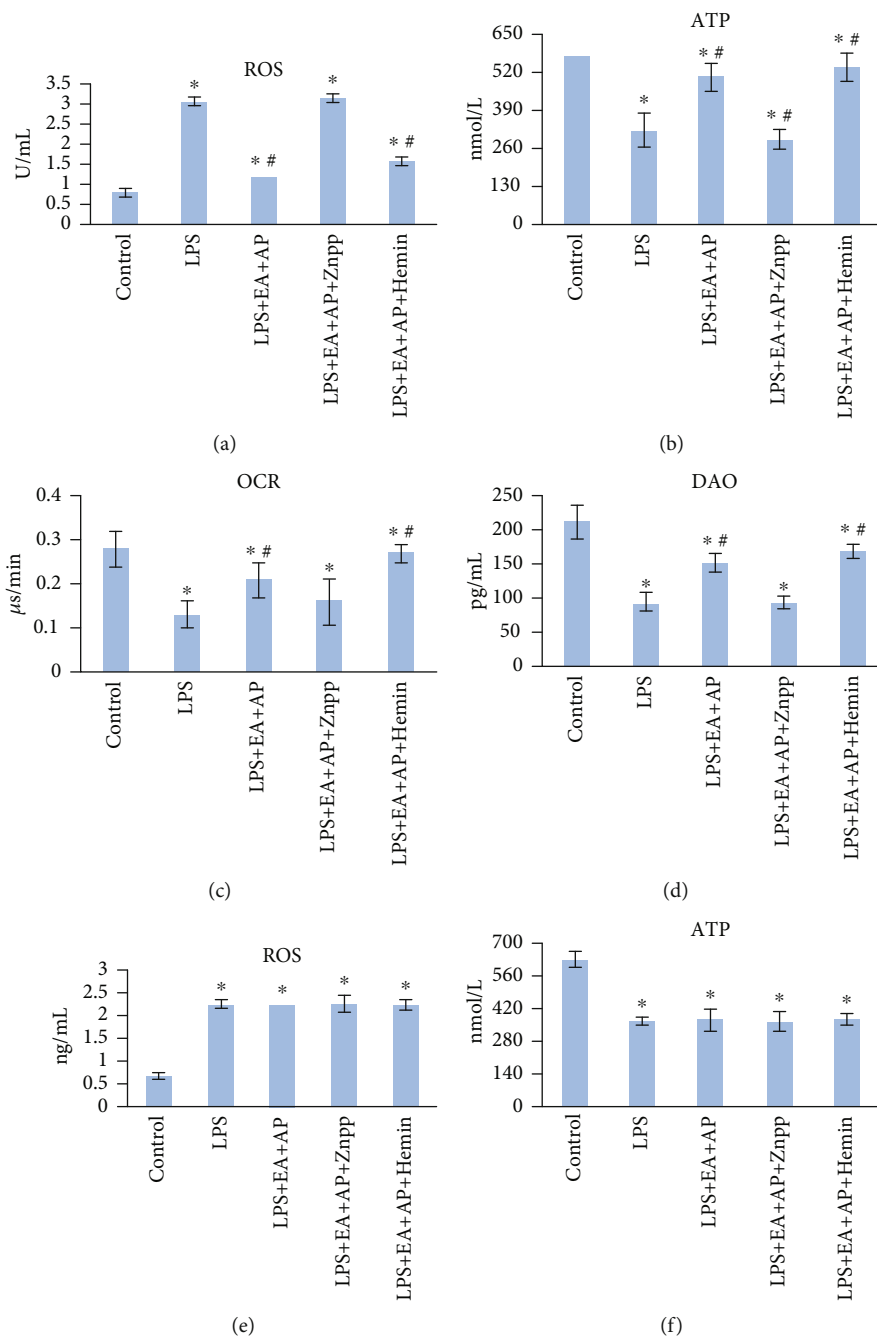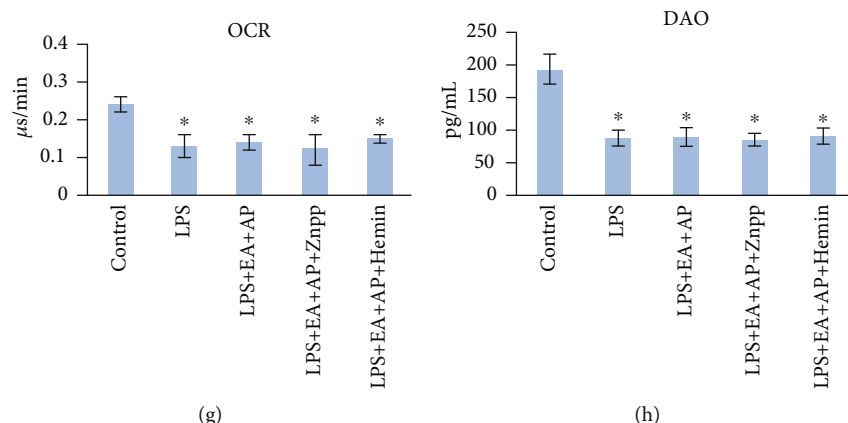
FIGURE 5: Effect of EA on ROS production, ATP content, OCR, and DAO levels in the LPS-exposed wild-type (a, b, c, and d) and PINK1-knockout mice (e, f, g, and h). LPS: lipopolysaccharide, EA + AP: electroacupuncture (EA) on acupoint (AP), hemin: a substrate and inducer of HO-1, ZnPP: zinc protoporphyrin IX, an inhibitor of HO-1, OCR: oxygen consumption rate, ROS: reactive oxygen species, DAO: diamine oxidase, and ATP: adenosine triphosphate. The mRNA and protein levels were compared using the paired sample t-test. *: significant difference compared with the control cells ($P < 0.05$). $^{\#}$: significant difference compared with the LPS-exposed cells ($P < 0.05$).

inducer of HO-1) were used alone to treat the wild-type mice and cells. The effect of EA + AP was reversed by the HO-1 inhibitor Znpp in the wild-type mice and cells; however, the HO-1 substrate and potent inducer hemin reversed the inhibitory effect of Znpp (Figures 2 and 3; $P < 0.05$).

However, the EA + AP, Znpp, and hemin treatments did not affect Drp1, Mfn1, Mfn2, Fis1, OPA-1, caspase-1, and IL-1β mRNA expressions and respective protein levels in the LPS-induced and PINK1-knockout mice and cells. (Figures 2(b), 2(e), and 2(f) and Figures 3(b), 3(e), and 3(f)).

3.2. EA Exerted a Protective Effect by Regulating the HO-1/ PINK1 Pathway in LPS-Induced Mitochondrial Dysfunction and Intestinal Epithelial Cell Injury In Vivo and In Vitro.

The four indices of mitochondrial function and intestinal epithelial cell injury degree, namely OCR, ROS, ATP, and DAO, were compared between the wild-type and PINK1-knockout mice and cells. As shown in Figures 4 and 5, LPS increased the ROS contents in the mitochondria (Figures 4(a), 4(e), 5(a), 5(e)), whereas it decreased the ATP (Figures 4(b), 4(f), 5(b), 5(f)), OCR (Figures 4(c), 4(g), 5(c), 5(g)), and DAO (Figures 4(d), 4(h), 5(d), 5(h)) levels ($P < 0.05$) in both the wild-type and PINK1-knockout mice and cells. The EA effect on the wild-type cells was reversed by Znpp, whereas hemin reinforced the effect of EA + AP in the wild-type mice and cells. EA + AP, Znpp, and hemin did not affect the LPS-induced and PINK1-knockout mice and cells.

3.3. EA Changed the Histopathological Morphology of LPS-Induced Intestinal Epithelium Tissues in the Wild-Type Mice.

As shown in Figure 6, the LPS group showed a decreased number of normal cells in the jejunal epithelial tissue than the control group. The tissues in the LPS group showed cellular vacuolization, swelling, desquamation, and interstitial edema. In the LPS + EA + AP group, the degree of the jejunal epithelial tissue injury was attenuated to a certain extent, which was shown by the increased normal cell density and reduced cellular vacuolization, swelling, desquamation, and interstitial edema. Additional treatment with

hemin augmented the effects of EA + AP. However, additional treatment with ZnPP weakened the protective effects of EA + AP (the LPS + EA + AP + ZnPP group), and hemin reinforced the effect of EA + AP against the LPS-induced jejunal epithelial tissue injury.

3.4. EA Changed the Mitochondrial Ultrastructure in the Wild-Type Mice.

As shown in Figure 7, LPS-induced mitochondrial edema and crest fracture (the LPS group) were attenuated by EA + AP treatment (the LPS + EA + AP group) and further attenuated by hemin (the LPS + EA + AP + hemin group). However, Znpp partially inhibited the protective effects of EA + AP (the LPS + EA + AP + Znpp group).

4. Discussion

This study showed that EA exerted a protective effect on ET-induced intestinal injury by regulating the HO-1/PINK1 pathway-mediated mitochondrial dynamics both in vitro and in vivo. The study showed that EA + AP can regulate the mitochondrial fusion/fission balance and preserve the mitochondrial function by increasing ATP production, DAO activity, and OCR; upregulating mitochondrial fusion marker gene expression; increasing respective protein levels; decreasing the ROS content and OCR; and downregulating mitochondrial fission marker gene expressions and the respective protein levels. The study also showed that the HO-1 inhibitor mitigates the positive effect of EA + AP on LPS-induced intestinal injury and that the positive effect of EA + AP can be enhanced by the HO-1 inducer hemin. To further investigate the role of HO-1, we used PINK1-knockout models and found that the protective effect of EA + AP against endotoxin-induced intestinal injury disappeared. The function of the intestinal epithelial barrier mainly depends on the balance between apoptosis and proliferation of intestinal epithelial cells [28]. Usually, the dynamic renewal of intestinal epithelial cells plays an important role in maintaining the normal structure and function of the intestinal epithelium. The destruction of the inherent
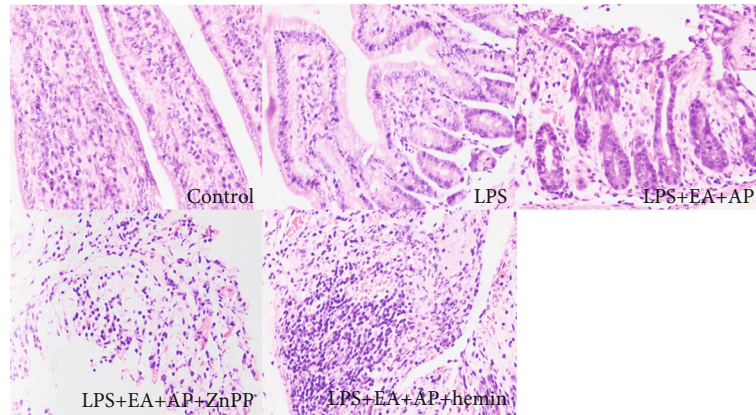
FIGURE 6: Microphotographs of histopathologic changes in the small intestine epithelial tissue stained with H&E. Representative images of H&E-stained small intestinal epithelial slices from the control group (mice were injected with normal saline instead of LPS), LPS group (the mouse intestinal injury model of ET), LPS + EA + AP group (the mouse intestinal injury model of ET treated by EA on AP), LPS + EA + AP + ZnPP group (the LPS +EA + AP group was injected with ZnPP), and LPS + EA + AP + hemin group (the LPS +EA + AP group was injected with hemin). H&E: hematoxylin and eosindye, LPS: lipopolysaccharide, EA: electroacupuncture, AP: acupoint, ET: endotoxemia, and Znpp: zinc protoporphyrin IX.
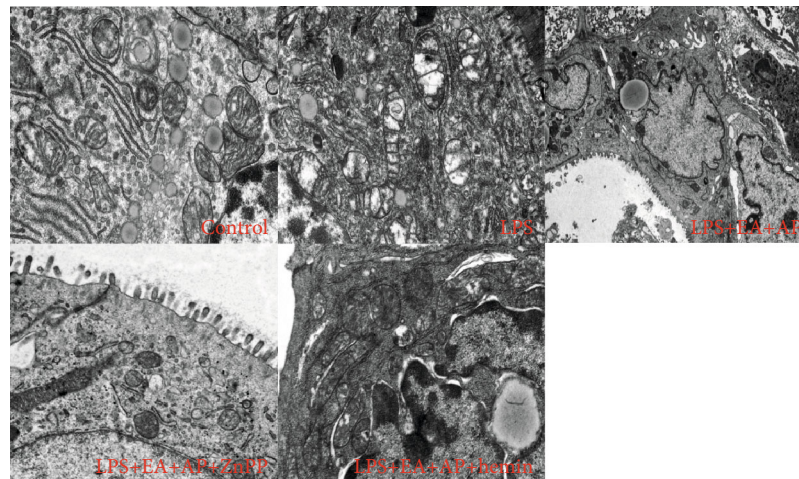
FIGURE 7: The change in the ultrastructure of the mitochondria in the small intestine epithelial cells. Electron microscopy images of the mitochondria in small intestine epithelial tissues from the control group (the mice were injected with normal saline instead of LPS), LPS group (the mouse intestinal injury model of ET), LPS + EA + AP group (the mouse intestinal injury model of ET treated by EA on AP), LPS + EA + AP + ZnPP group (the LPS + EA + AP group was injected with ZnPP), and LPS + EA + AP + hemin group (the LPS+ EA + AP group was injected with hemin). LPS: lipopolysaccharide, EA: electroacupuncture, AP: acupoint, ET: endotoxemia, and Znpp: zinc protoporphyrin IX.

dynamic balance of intestinal epithelial cells can cause intestinal injury. ET induces inflammatory factors in the gastrointestinal microenvironment, which can facilitate apoptosis by activating the proapoptotic signal in intestinal epithelial cells via the cell membrane death receptor [29]. Excessive apoptosis of intestinal epithelial cells may disrupt the intestinal epithelial barrier function and accelerate the migration of intestinal bacteria from the intestine to the systemic blood circulation along the mesenteric lymphatic vessels, thus inducing ET deterioration and MODS development [30].

Pyroptosis is a form of programmed cell death characterized by the cysteinyl aspartate-specific proteases-1 (caspase-

1) and the release of a large number of proinflammatory cytokines such as IL-1β [31–33]. Pyroptosis plays a role in the occurrence and development of infectious diseases including ET. The mitochondrion is the central link in the regulatory mechanism of apoptosis, in which tube network fragmentation occurs in the early stage of apoptosis [34]. Studies have proposed the concept of "microcirculation and mitochondrial distress syndrome", pointing out the fundamental role of mitochondrial dysfunction in ET pathogenesis [35].

The stability of mitochondrial dynamics (the dynamic process of mitochondrial fusion and division) is important to ensure the normal spatial structure and morphology of

the mitochondria [36]. In cells, mitochondria form a dynamic network structure by connecting with each other, which may represent an efficient energy-transport system or calcium channels between different regions of a cell. The dynamic balance of fusion/division maintains the stability of the morphological functions of mitochondria. Studies have shown that the imbalance of mitochondrial dynamics is involved in the occurrence and development of various acute/chronic major diseases. However, the underlying mechanism of mitochondrial dynamic destruction is unknown [37, 38]. Using the LPS-induced ET model, we showed that the mitochondrial fusion/division movement can be adjusted by regulating mitochondrial movement-related proteins, thus treating ET-induced intestine injury via restoring the mitochondrial dynamic balance [5, 7, 24].

ET increases free oxygen and nitrogen radicals and produces peroxynitrite. The persistently high levels of ROS and reactive nitrogen substances are harmful to the mitochondria, as they inhibit the mitochondrial respiratory chain function, thus reducing mitochondrial DNA replication and accelerating free radical generation. Hence, in this study, a vicious cycle of "free radical generation-mitochondrial structure destruction-free radical generation" was initiated. In the early stage of stress, fusion compensates for defects in mitochondria to maintain the energy needs. When mitochondrial damage exceeds a certain threshold, a mitochondrial division is much faster than fusion, resulting in the accumulation of many fragmented mitochondria in cells, which cannot be removed, causing irreversible damage to cells including intestinal epithelial cells [39, 40]. Therefore, the regulation of mitochondrial fusion/division and the maintenance of its dynamic stability are the prerequisite for the protection of the intestinal epithelial barrier function in ET.

Recent studies have shown that PINK1 plays an important role in regulating mitochondrial dynamics and mediating the autophagic clearance of damaged mitochondria [41, 42]. In this study, the positive effect of EA + AP was not observed on the ET-induced intestinal injury in the PINK1-knockout cells and mice. A possible reason is that HO-1 regulates mitochondrial homeostasis via PINK1 located in the mitochondrial intima.

5. Conclusions

EA + AP protects the intestine against endotoxin-induced injury by inducing HO-1 translocation to the mitochondrial intima, which may further regulate the mitochondrial fusion/division balance and protect the intestinal barrier function by activating PINK1. This study provides atheoretical basis for the novel therapy using EA on specific acupoints to treat ET-induced intestinal injury.

Abbreviations

ET: Endotoxemia
MODS: Multiple organ dysfunction syndrome
HO-1: Heme oxygenase-1
ELISA: Enzyme-linked immunosorbent assay;
PTEN: Phosphatase and tensin homolog
PINK1: PTEN induced putative kinase 1
LPS: Lipopolysaccharide
EA: Electroacupuncture
AP: Acupoint
Fis1: One of the key mitochondrial fission protein members
Znpp: Zinc protoporphyrin IX
OCR: Oxygen consumption rate
ROS: Reactive oxygen species
DAO: Diamine oxidase
Mfn 1/2: Mitofusin 1/2
OPA1: Optic atrophy 1
Drp1: Dynamin-related protein 1.

Data Availability

Data is available on reasonable request though email (Dr. JB Yu, 30717008@nankai.edu.cn).

Conflicts of Interest

The authors declare that they have no conflict of interest.

Authors' Contributions

Yuan Zhang and Jian-bo Yu contributed to the conception and planning of the research. Zhen-zhen Meng and Li-na Wu performed the experiments and assessed the data. Yuan Zhang wrote the first paper, and Xiu-yun Liu commented on previous versions of the manuscript. Chen-xu Guo, Dong Ming, and Shu-an Dong assisted to perform the experiments. Ying-ya Cao and Xian-hong Jiang assisted to analyze the data. All authors have read and agreed on the final contents of the manuscript. Yuan Zhang, Zhenzhen Meng, and Lina Wu contributed equally to the paper.

Acknowledgments

Supplementary Materials

Supplementary Table 1: primers of marker genes for qRT-PCR. Supplementary Figure 1: PINK1 gene knockout strategy. Supplementary Table 2: primers used for validating the efficiency of the designed cas9/sgRNA. Supplementary Table 3: the designed sgRNA sequences. Supplementary Figure 2: conversion products of EGE-WL-008-sgRNA4 and EGE-WL-008-sgRNA9. (Supplementary Materials)

References

[1] A.-C. Luissint, C. A. Parkos, and A. Nusrat, "Inflammation and the intestinal barrier: leukocyte-epithelial cell interactions, cell junction remodeling, and mucosal repair," Gastroenterology, vol. 151, no. 4, pp. 616–632, 2016.

[2] R. J. Youle and A. M. van der Bliek, "Mitochondrial fission, fusion, and stress," Science (New York, N.Y.), vol. 337, no. 6098, pp. 1062–1065, 2012.

[3] J. Bereiter-Hahn and M. Jendrach, "Mitochondrial dynamics," *International Review of Cell and Molecular Biology*, vol. 284, pp. 1–65, 2010.

[4] A. Bhattacharyya, R. Chattopadhyay, S. Mitra, and S. E. Crowe, "Oxidative stress: an essential factor in the pathogenesis of gastrointestinal mucosal diseases," *Physiological Reviews*, vol. 94, no. 2, pp. 329–354, 2014.

[5] J. B. Yu, J. Shi, D. Wang et al., "Heme oxygenase-1/carbon monoxide-regulated mitochondrial dynamic equilibrium contributes to the attenuation of endotoxin-induced acute lung injury in rats and in lipopolysaccharide-activated macrophages," *Anesthesiology*, vol. 125, no. 6, pp. 1190–1201, 2016.

[6] J. B. Yu, Y. Wang, Z. Li et al., "Effect of heme oxygenase-1 on mitofusin-1 protein in LPS-induced ALI/ARDS in rats," *Scientific Reports*, vol. 6, no. 1, p. 36530, 2016.

[7] J. Shi, J. B. Yu, W. Liu et al., "Carbon monoxide alleviates lipopolysaccharide-induced oxidative stress injury through suppressing the expression of Fis1 in NR8383 cells," *Experimental Cell Research*, vol. 349, no. 1, pp. 162–167, 2016.

[8] D. A. Lowes, N. R. Webster, M. P. Murphy, and H. F. Galley, "Antioxidants that protect mitochondria reduce interleukin-6 and oxidative stress, improve mitochondrial function, and reduce biochemical markers of organ dysfunction in a rat model of acute sepsis," *British Journal of Anaesthesia*, vol. 110, no. 3, pp. 472–480, 2013.

[9] M. D. Brand and D. G. Nicholls, "Assessing mitochondrial dysfunction in cells," *The Biochemical Journal*, vol. 435, no. 2, pp. 297–312, 2011.

[10] S. Bindu, C. Pal, S. Dey et al., "Translocation of heme oxygenase-1 to mitochondria is a novel cytoprotective mechanism against non-steroidal anti-inflammatory drug-induced mitochondrial oxidative stress, apoptosis, and gastric mucosal injury," *The Journal of Biological Chemistry*, vol. 286, no. 45, pp. 39387–39402, 2011.

[11] H. Zhou, F. Lu, C. Latham, D. S. Zander, and G. A. Visner, "Heme oxygenase-1 expression in human lungs with cystic fibrosis and cytoprotective effects against Pseudomonas aeruginosa in vitro," *American Journal of Respiratory and Critical Care Medicine*, vol. 170, no. 6, pp. 633–640, 2004.

[12] A. Agarwal and S. Bolisetty, "Adaptive responses to tissue injury: role of heme oxygenase-1," *Transactions of the American Clinical and Climatological Association*, vol. 124, pp. 111–122, 2013.

[13] D. A. Sliter, J. Martinez, L. Hao et al., "Parkin and PINK1 mitigate STING-induced inflammation," *Nature*, vol. 561, no. 7722, pp. 258–262, 2018.

[14] M. Bueno, Y. C. Lai, Y. Romero et al., "PINK1 deficiency impairs mitochondrial homeostasis and promotes lung fibrosis," *The Journal of Clinical Investigation*, vol. 125, no. 2, pp. 521–538, 2015.

[15] W. L. Chien, T. R. Lee, S. Y. Hung et al., "Increase of oxidative stress by a novel PINK1 mutation, P209A," *Free Radical Biology & Medicine*, vol. 58, pp. 160–169, 2013.

[16] Z. Liu, S. Yan, J. Wu et al., "Acupuncture for chronic severe functional constipation: a randomized trial," *Annals of Internal Medicine*, vol. 165, no. 11, pp. 761–769, 2016.

[17] S. S. M. Ng, W. W. Leung, T. W. C. Mak et al., "Electroacupuncture reduces duration of postoperative Ileus after laparoscopic surgery for colorectal cancer," *Gastroenterology*, vol. 144, no. 2, pp. 307–313.e1, 2013.

[18] Y. Zhang and J. Yu, "Effects of acupuncture of acupoints selected on postsurgical gastrointestinal dysfunction in patients undergoing nongastrointestinal abdominal surgery," *Chinese Journal of Anesthesiology*, vol. 36, no. 3, pp. 267–271, 2016.

[19] J. B. Yu, J. Shi, Y. Zhang et al., "Electroacupuncture ameliorates acute renal injury in lipopolysaccharide-stimulated rabbits via induction of HO-1 through the PI3K/Akt/Nrf2 pathways," *PLoS One*, vol. 10, no. 11, p. e0141622, 2015.

[20] J. B. Yu, S. A. Dong, X. Q. Luo et al., "Role of HO-1 in protective effect of electro-acupuncture against endotoxin shock-induced acute lung injury in rabbits," *Experimental Biology and Medicine (Maywood, N.J.)*, vol. 238, no. 6, pp. 705–712, 2013.

[21] Y. Zhang and J. B. Yu, "Effects of electroacupuncture on mitochondrial fusion-fission during endotoxin-induced acute lung injury in rabbits," *Chinese Journal of Anesthesiology*, vol. 38, no. 5, pp. 631–634, 2018.

[22] J. He and J. C. Yu, "Research progress on the effects of acupuncture-moxibustion serum," *Zhongguo Zhen Jiu = Chinese Acupuncture & Moxibustion*, vol. 34, no. 10, pp. 1042–1046, 2014.

[23] A. Hopert, C. C. Uphoff, M. Wirth, H. Hauser, and H. G. Drexler, "Mycoplasma detection by PCR analysis," *In Vitro Cellular & Developmental Biology. Animal*, vol. 29, no. 10, pp. 819–821, 1993.

[24] J. B. Yu, F. Zhou, S.-L. Yao, Z. H. Tang, M. Wang, and H. R. Chen, "Effect of heme oxygenase-1 on the kidney during septic shock in rats," *Translational Research: The Journal of Laboratory and Clinical Medicine*, vol. 153, no. 6, pp. 283–287, 2009.

[25] J. Han, J. H. Li, G. Bai et al., "Acanthopanax senticosuspolysaccharides-induced intestinal tight junction injury alleviationviainhibition of NF-κB/MLCK pathway in a mouse endotoxemia model," *World Journal of Gastroenterology*, vol. 23, no. 12, pp. 2175–2184, 2017.

[26] R. R. Bartz, H. B. Suliman, P. Fu et al., "Staphylococcus aureus sepsis and mitochondrial accrual of the 8-oxoguanine DNA glycosylase DNA repair enzyme in mice," *American Journal of Respiratory and Critical Care Medicine*, vol. 183, no. 2, pp. 226–233, 2011.

[27] T. D. Schmittgen and K. J. Livak, "Analyzing real-time PCR data by the comparative C_T method," *Nature Protocols*, vol. 3, no. 6, pp. 1101–1108, 2008.

[28] L. Khailova, D. N. Frank, J. A. Dominguez, and P. E. Wischmeyer, "Probiotic administration reduces mortality and improves intestinal epithelial homeostasis in experimental sepsis," *Anesthesiology*, vol. 119, no. 1, pp. 166–177, 2013.

[29] C. Han, Z. Ding, H. Shi, W. Qian, X. Hou, and R. Lin, "The role of probiotics in lipopolysaccharide-induced autophagy in intestinal epithelial cells," *Cellular Physiology and Biochemistry: International Journal of Experimental Cellular Physiology, Biochemistry, and Pharmacology*, vol. 38, no. 6, pp. 2464–2478, 2016.

[30] R. J. Haines, C. Y. Wang, C. G. Y. Yang, R. A. Eitnier, F. Wang, and M. H. Wu, "Targeting palmitoyl acyltransferase ZDHHC21 improves gut epithelial barrier dysfunction resulting from burn-induced systemic inflammation," *American Journal of Physiology. Gastrointestinal and Liver Physiology*, vol. 313, no. 6, pp. G549–G557, 2017.

[31] M. Lamkanfi, T.-D. Kanneganti, L. Franchi, and G. Núñez, "Caspase-1 inflammasomes in infection and inflammation," *Journal of Leukocyte Biology*, vol. 82, no. 2, pp. 220–225, 2007.

[32] J. Shi, Y. Zhao, Y. Wang et al., "Inflammatory caspases are innate immune receptors for intracellular LPS," *Nature*, vol. 514, no. 7521, pp. 187–192, 2014.

[33] S. Zhu, S. Ding, P. Wang et al., "Nlrp9b inflammasome restricts rotavirus infection in intestinal epithelial cells," *Nature*, vol. 546, no. 7660, pp. 667–670, 2017.

[34] A. Tanaka and R. J. Youle, "A chemical inhibitor of DRP1 uncouples mitochondrial fission and apoptosis," *Molecular Cell*, vol. 29, no. 4, pp. 409-410, 2008.

[35] C. Ince, "The microcirculation is the motor of sepsis," *Critical Care*, vol. 9, Suppl 4, pp. S13–S19, 2005.

[36] B. Westermann, "Mitochondrial fusion and fission in cell life and death," *Nature Reviews. Molecular Cell Biology*, vol. 11, no. 12, pp. 872–884, 2010.

[37] M. Zhan, C. Brooks, F. Liu, L. Sun, and Z. Dong, "Mitochondrial dynamics: regulatory mechanisms and emerging role in renal pathophysiology," *Kidney International*, vol. 83, no. 4, pp. 568–581, 2013.

[38] R. A. Stetler, R. K. Leak, Y. Gao, and J. Chen, "The dynamics of the mitochondrial organelle as a potential therapeutic target," *Journal of Cerebral Blood Flow and Metabolism: Official Journal of the International Society of Cerebral Blood Flow and Metabolism*, vol. 33, no. 1, pp. 22–32, 2013.

[39] T. Dey, P. Dutta, P. Manna et al., "Anti-proliferative activities of Vasicinone on lung carcinoma cells mediated via activation of both mitochondria-dependent and independent pathways," *Biomolecules & Therapeutics*, vol. 26, no. 4, pp. 409–416, 2018.

[40] A. S. Gonzalez, M. E. Elguero, P. Finocchietto et al., "Abnormal mitochondrial fusion-fission balance contributes to the progression of experimental sepsis," *Free Radical Research*, vol. 48, no. 7, pp. 769–783, 2014.

[41] A. L. Luz, T. R. Godebo, L. L. Smith, T. C. Leuthner, L. L. Maurer, and J. N. Meyer, "Deficiencies in mitochondrial dynamics sensitize Caenorhabditis elegans to arsenite and other mitochondrial toxicants by reducing mitochondrial adaptability," *Toxicology*, vol. 387, pp. 81–94, 2017.

[42] Y. J. Tang, Y. N. Niu, and H. Wang, "Advance on the molecular mechanism of Pink1/Parkin-mediated mitophagy," *Chinese Journal of Cell Biology*, vol. 39, no. 7, pp. 939–946, 2017.

Research Article

Inhibition of Xanthine Oxidase Protects against Sepsis-Induced Acute Kidney Injury by Ameliorating Renal Hypoxia

Ting-ting Wang [ID]**, Yi-wei Du, Wen Wang, Xiang-nan Li, and Hong-bao Liu** [ID]

Department of Nephrology, Tangdu Hospital, Air Force Military Medical University (Fourth Military Medical University),
Xi'an 710038, China

Correspondence should be addressed to Hong-bao Liu; xjsnlhb@fmmu.edu.cn

Xanthine oxidase (XO) utilizes molecular oxygen as a substrate to convert purine substrates into uric acid, superoxide, and hydrogen peroxide, which is one of the main enzyme pathways to produce reactive oxygen species (ROS) during septic inflammation and oxidative stress. However, it is not clear whether XO inhibition can improve sepsis-induced renal hypoxia in sepsis-induced acute kidney injury (SI-AKI) mice. In this study, pretreatment with febuxostat, an XO-specific inhibitor, or kidney knockdown of XO by shRNA in vivo significantly improved the prognosis of SI-AKI, not only by reducing the levels of blood urea nitrogen, serum creatinine, tumor necrosis factor-α, interleukin-6, and interleukin-1β in peripheral blood but also by improving histological damage and apoptosis, reducing the production of ROS, and infiltrating neutrophils and macrophages in the kidney. More importantly, we found that pharmacological and genetic inhibition of XO significantly improved renal hypoxia in SI-AKI mice by a hypoxia probe via fluorescence staining. This effect was further confirmed by the decrease in hypoxia-inducible factor-1α expression in the kidneys of mice with pharmacological and genetic inhibition of XO. In vitro, the change in XO activity induced by lipopolysaccharide was related to the change in hypoxia in HK-2 cells. Febuxostat and XO siRNA significantly relieved the hypoxia of HK-2 cells cultured in 2% oxygen and reversed the decrease in cell viability induced by lipopolysaccharide. Our results provide novel insights into the nephroprotection of XO inhibition in SI-AKI, improving cell hypoxia by inhibiting XO activity and reducing apoptosis, inflammation, and oxidative stress.

1. Introduction

Sepsis is the leading cause of acute renal injury (AKI) and is associated with increased morbidity and mortality in intensive care units [1, 2]. Palliative interventions such as fluid resuscitation, antibiotics, vasopressin, and renal replacement therapy are recommended to treat sepsis-induced AKI (SI-AKI) patients and wait passively for the kidney function to recover [3–5]. The experimental AKI induced by lipopolysaccharide (LPS), a key component of the outer membrane of gram-negative bacteria, is commonly used in vivo model closely recapitulating SI-AKI in humans, which hosts a complex inflammatory milieu comprising neutrophils, macrophages, epithelial cells, reactive oxygen species (ROS), proinflammatory mediators, and enzymes [6, 7]. An in-depth understanding of the SI-AKI pathophysiology is of great benefit to formulating effective mechanism-mediated treatment strategies.

Xanthine oxidase (XO) is one of the main enzyme pathways that produce ROS during oxidative stress and inflammation. It utilizes molecular oxygen to catalyze the oxidation of purine substrates (such as hypoxanthine and xanthine) to uric acid and generates superoxide ($O_2^{\bullet-}$) and hydrogen peroxide (H_2O_2) [8, 9]. XO has been suggested to participate in the pathogenesis of acute organ injury, including SI-AKI. Its activity and expression can be upregulated by various inflammatory stimuli, such as LPS, cytokines, and hypoxia [10–16]. Febuxostat, a selective and potent inhibitor of XO, can alleviate AKI, which may be related to antioxidant stress, anti-inflammation, and antiendoplasmic reticulum

stress and reducing uric acid production [17–19]. The protective role of febuxostat in animal models of SI-AKI has only recently been reported. Ramos and his colleagues [20] found that febuxostat, rather than allopurinol, improved renal function in experimental SI-AKI animals induced by LPS. The mechanism may be associated with antioxidant, anti-inflammatory, and antiapoptotic effects. Similarly, Ibrahim et al. [21] confirmed the protective effect of febuxostat on liver and kidney injuries in sepsis after cecal ligation through its antioxidant, anti-inflammatory, and antiapoptotic properties and the weakening of the c-Jun N-terminal kinase signaling pathway.

In addition to the inflammatory cascade and oxidative stress, renal ischemia/hypoxia is emerging as a common pathophysiological feature of SI-AKI, an essential driver in the transition and/or propensity for the progression from AKI to chronic kidney disease (CKD) [22, 23]. Based on the characteristic that XO utilizes molecular oxygen to catalyze purine substrates, we hypothesize that downregulation of XO can alleviate local hypoxia in renal tissue of the SI-AKI model, which has not been reported thus far. Therefore, this study is aimed at exploring the effects and potential mechanisms of XO inhibition on LPS-induced renal hypoxia in SI-AKI mice.

2. Materials and Methods

2.1. Chemicals and Reagents. LPS (Escherichia coli serotype O55:B5, L2880) was obtained from Sigma-Aldrich (USA). F4/80 (cat no. 29414-1-AP) and myeloperoxidase (MPO, cat no. 22225-1-AP) antibodies were from Proteintech (Wuhan, China), and hypoxia-inducible factor-1α (HIF-1α) antibody (cat no. BF8002) was from Affinity Biologicals (Jiangsu, China). XO (cat no. sc-398548) antibody was from Santa Cruz (USA). The XO activity assay kit (cat no. KTB1070), goat anti-mouse IgG H&L (DyLight 649) (cat no. A23610), goat anti-mouse IgG H&L (DyLight 488) (cat no. A23210), and goat anti-mouse IgG HRP (cat no. A21010) were purchased from Abbkine (Wuhan, China). Pimonidazole HCl and anti-pimonidazole mouse antibody was purchased from Hypoxyprobe (USA). ELISA kits for tumor necrosis factor-α (TNF-α, cat no. BMS607-3), interleukin-6 (IL-6, cat no. KMC0061), and IL-1β (cat no. KMC0061) were from Thermo Fisher Scientific (USA). The fluorescein (FITC) TUNEL Cell Apoptosis Detection Kit was from Servicebio (cat no. G1501, Wuhan, China). Dihydroethidium (DHE) for probing superoxide radicals was purchased from Beyotime (cat no. S0063, Shanghai, China).

2.2. Animals and Experimental Protocol. All animal experiments were conducted in strict accordance with the Guidelines for Care and Use of Laboratory Animals and were permitted by the Animal Welfare and Ethics Institution of the Fourth Military Medical University. Male C57BL/6 mice aged 6-8 weeks, weighing 20-25 g, were raised in the SPF laboratory of the Animal Experiment Center of the Air Force Military Medical University (Fourth Military Medical University). They were randomly divided into three groups: control (received water by gavage) group ($n = 10$), LPS

(10 mg/kg dissolved in sterile deionized water) only group ($n = 10$), and LPS+febuxostat (Feb, 10 mg/kg/day dissolved in saline) ($n = 10$). The mice were given febuxostat by gavage every 24 h for 7 days, followed by intraperitoneal injection of LPS. For XO knockdown in vivo, we constructed an AAV vector carrying XO shRNA (pAAV-shXO) with a target sequence of $5'$ AAGTGTAGCAATCGCGTCC $3'$ (Shanghai Genechem Co., Ltd). Mice were divided into two groups: LPS+pAAV-shNC (LPS+Ctrl-shR) and LPS+pAAV-shXO (LPS+XO-shR) ($n = 10$). AAV injection was conducted according to the previous research [24]. Briefly, mice were anesthetized with 50 mg/kg sodium pentobarbital, the abdominal hair of the mice was removed with a shaver, and the mice were fixed in a supine position on the operating table with tape. Make a longitudinal incision about 2.0 cm long along the midline of the abdomen below the costal margin. Then, renal vein was isolated and clamped, and 50 μl of 1× PBS containing $1E + 11$ V.G. of AAV was slowly injected using a 30 G needle. The clamp was removed after 15 min postinjection, and the incision sutured. Three weeks later, LPS was administered to induce SI-AKI in mice. Animals were ethically sacrificed by administrating pentobarbital sodium (Sigm-Aldrich, USA) at 24 h after LPS injection, and whole blood and kidneys were collected for further analysis.

2.3. Blood Physiochemical Assays. The whole blood collected from the eyeballs was centrifuged at 4°C and 4000 rpm for 10 min to acquire the serum sample. The levels of serum creatinine (Scr, cat no. C011-2-1) and blood urea nitrogen (BUN, cat no. C013-2-1) were measured according to the manufacturer's instructions using the creatinine and urea nitrogen assay kit (Nanjing Jiancheng, China).

2.4. Renal Histopathology. Kidney tissues were carefully separated, washed with ice-cold stroke-physiological saline solution, and stored in 4% paraformaldehyde. Hematoxylin and eosin (H&E) staining of paraffin-embedded kidney tissue slices was performed, and a double-blind method was utilized to assess the damage to renal tubular epithelial cells. H&E-stained sections were scored by calculating the percentage of tubules in corticomedullary junction that displayed cell necrosis, loss of brush border, cast formation, and tubular dilation as follows: 0, none; 1, <10%; 2, 11-25%; 3, 26-45%; 4, 46-75%; and 5, >76%. At least 10 randomly selected areas per mouse were assessed. The scores of ten fields per kidney section were averaged and used as the score of individual mouse kidneys.

2.5. Determination of XO Activity and Expression in Serum and Kidneys. After renal tissue homogenization, kidney XO activity was detected according to the manual instructions, and the XO activity in the serum was detected at the same time. XO expression in renal tissue was further detected by immunofluorescence. Briefly, kidney tissues were sliced into 5 μm sections, stained with XO antibody (1 : 100) for 18 h at 4°C, washed with phosphate buffered saline with Tween 20 (PBST), incubated with goat anti-mouse IgG (DyLight 488) (1 : 3000), and stained for 1 h at room temperature in the

dark. After washing with PBST, DAPI solution was added to stain the nucleus, and photos were taken with a laser confocal microscope (Leica SP8).

2.6. Determination of Hypoxia in Kidneys.

Hypoxyprobe, the component of which is pimonidazole hydrochloride, has been an effective approach to assessing hypoxia in cells [25]. Pimonidazole hydrochloride could be reduced, activated, and combined with thiol groups from peptides or proteins which could be detected with goat anti-mouse hypoxyprobe antibody. Twenty-four hours after the SI-AKI model was established, and the mice were injected intraperitoneally with 60 mg/kg hypoxyprobe and anesthetized with 50 mg/kg sodium pentobarbital 2 h later. The kidney tissues were collected and stored at -80°C. Kidney tissues were sliced into 5 μm sections, stained with goat anti-mouse hypoxyprobe antibody (1 : 200) for 18 h at 4°C. Kidney slices were washed with PBST; then, goat anti-mouse IgG (DyLight 649) (1 : 3000) was added and stained for 1 h at room temperature in the dark. After washing with PBST, DAPI solution was added to stain the nucleus, and photos were taken with a laser confocal microscope (Leica SP8).

2.7. Western Blot Analysis.

Equal amounts of protein from HK-2 cells or kidney tissue lysates were loaded and separated using 10% sodium dodecyl sulfate (SDS) polyacrylamide gels and transferred to polyvinylidene fluoride membranes (cat no. IPVH00010, Millipore, USA). The membranes were incubated with 5% nonfat milk for 1 h at room temperature and probed with HIF-1α or XO primary antibody for 18 h at 4°C, followed by a peroxidase-conjugated secondary antibody. Antibody-antigen complexes were detected using an ECL system (cat no. P0018AS, Beyotime, Shanghai, China). The intensity of each band was measured using ImageJ. The results were normalized to the intensity of beta-actin for standardization.

2.8. ROS Detection in Kidneys.

Dihydroethidium (DHE) was used to detect the ROS levels in the renal tissues, as previously reported [26]. The renal tissues were immersed in saccharose (30% w/v), embedded at the optimal cutting temperature (OCT), sliced into 5 μm sections, and stored at -20°C until fluorescence detection. Tissue sections were incubated with 10 μM DHE for 60 min at 37°C in a humidified chamber in the dark, incubated with DAPI solution at room temperature for 5 min, and kept in the dark. In the presence of superoxide anions, DHE is oxidized to ethidium, producing bright red fluorescence. After washing with PBS, sections were visualized and imaged via a laser confocal microscope (Leica SP8).

2.9. Macrophages and Neutrophils Infiltrated the Kidney Tissues.

Tissues were fixed with 4% paraformaldehyde and subsequently processed for immunofluorescence staining. MPO and F4/80 staining was performed after antigen retrieval (1% SDS for 3 min). MPO$^+$ and F4/80$^+$ cells were quantified by counting the number of stained cells per field. We collected 10-15 images of a kidney from each animal at 400x magnification with a laser confocal microscope (Leica SP8).

2.10. Cytokine Analysis.

The concentrations of the cytokines TNF-α, IL-6, and IL-1β in serum were measured with mouse TNF-α, IL-6, and IL-1β ELISA kits according to the instructions.

2.11. Kidney Terminal Deoxynucleotidyl Transferase dUTP Nick-End Labeling (TUNEL) Assay.

Kidney tissue TUNEL analysis was conducted in accordance with our previous research [27]. Briefly, kidney tissues were fixed with 4% paraformaldehyde (PFA) for 24 h at room temperature, followed by dehydration and paraffin embedding. Tissues were cut into 5 μm sections for immunofluorescence staining. The sections were incubated with TdT enzyme solution for 90 min at 37°C. Then, FITC-12-dUTP was added and incubated for 30 min at 37°C. The reaction was terminated by incubation in stop/wash buffer for 30 min at 37°C. The number of TUNEL-positive cell nuclei and the total numbers of cell nuclei stained with DAPI were counted in 10 random areas, and the percentages of the numbers of TUNEL-positive nuclei to the numbers of total cell nuclei were then calculated.

2.12. Cells and Experimental Protocol.

Cell culture experiments were performed using HK-2 cells, a human kidney proximal tubular cell line, which was purchased from the American Type Culture Collection. HK-2 cells at a concentration of 5×10^3/well in 96-well plates were cultured with or without LPS (10 μg/ml) in a trigas incubator (Thermo Fisher Scientific, USA) under 21% O_2 or 2% O_2 for 6 h in the presence or absence of febuxostat (100 μM). Then, we added 10 μL CCK-8 (Dojindo, Japan) to each well and measured the optical density (OD) values at 450 nm after 1 h of incubation. For hypoxia condition evaluation, HK-2 cells were thus divided into three groups: control, LPS (10 μg/ml), and LPS (10 μg/ml) plus febuxostat (100 μM). After administration of LPS and febuxostat, cells were incubated for 6 h. For XO knockdown analysis, HK-2 cells were transfected with siRNA of XO (XO-siR) or negative control (Ctrl-siR) using Lipofectamine® 2000 (Invitrogen) according to the manufacturer's protocol. The target sequence of si-XO was 5′-GGCATTGAGATGAAGTTCA-3′. The oligonucleotide dose used was 100 nM. All transfections were transient. Thirty-six hours later, the cells were treated with LPS (10 μg/ml) with or without 2% oxygen. Then, 150 μM pimonidazole HCl was added to the cells 1 h before being harvested for hypoxia evaluation, after fixation with 4% paraformaldehyde (PFA) for 20 min at room temperature. Anti-pimonidazole mouse antibody was incubated with the cells at 4°C for 18 h. Afterward, goat anti-mouse DyLight 488 antibody was added and incubated for 1 h at room temperature in the dark. Finally, confocal imaging was conducted with a Leica SP8 confocal microscope. For XO activity analysis, HK-2 cells at a concentration of 5×10^4/well in 6-well plates were cultured with or without LPS (10 μg/ml) in a trigas incubator under 21% O_2 or 2% O_2 for 6 h in the presence or absence of febuxostat (100 μM) or siXO transfection. After that, the cells were harvested for the XO activity assay conducted according to the assay kit instructions.

(a)

(b)

(c)

(d)

(e)

(f)

Figure 1: Continued.

(g)
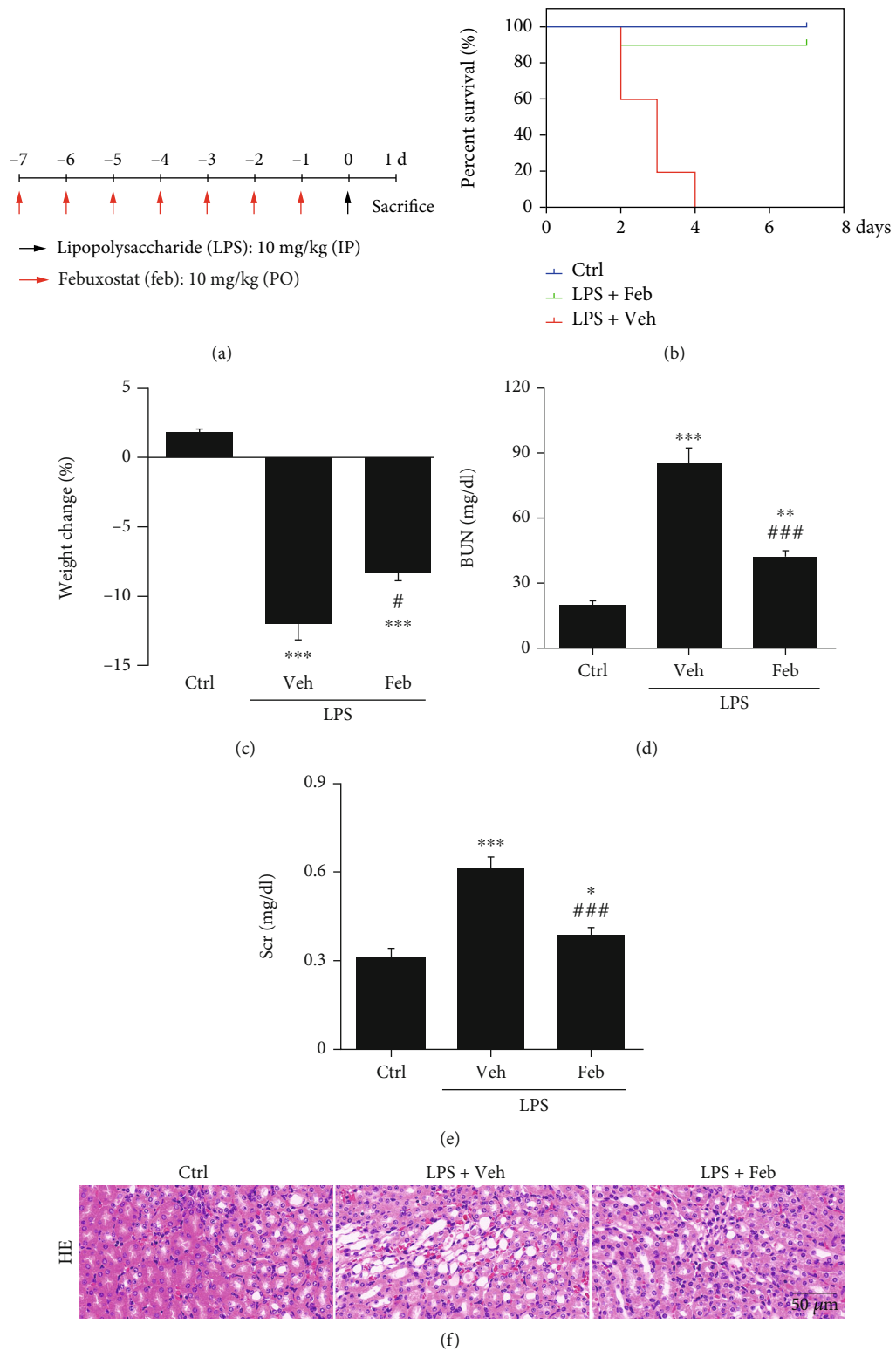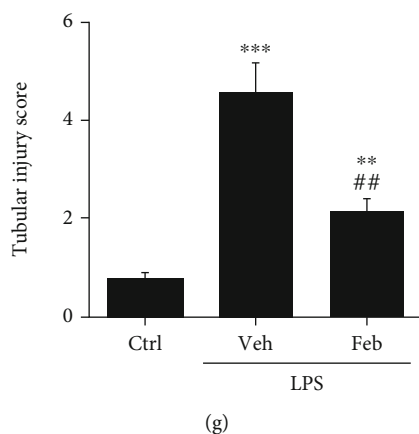
FIGURE 1: Therapeutical effects of febuxostat on attenuating renal injury in SI-AKI mice. (a) Mice pretreated with febuxostat (10 mg/kg/day, po.) for 7 days were administered intraperitoneal injections of LPS (10 mg/kg) and then were executed 24 h after LPS injection. (b) The death of mice in 7 days after intraperitoneal injection of LPS (10 mg/kg). (c–e) Body weight changes and BUN and Scr levels were measured at 24 h after the injection of LPS. (f, g) Histopathology analysis of the kidneys in SI-AKI mice was performed by hematoxylin-eosin (HE) staining (600x magnification), and the kidney tubular injury score was graded in a double-blinded manner. Scale bar = 50 μm. $^*P < 0.05$, $^{**}P < 0.01$, and $^{***}P < 0.001$ vs. Ctrl; $^{\#}P < 0.05$, $^{\#\#}P < 0.01$, and $^{\#\#\#}P < 0.001$ vs. LPS+Veh ($n = 10$). Ctrl: control; Veh: vehicle; LPS: lipopolysaccharide; Feb: febuxostat; BUN: blood urea nitrogen; Scr: serum creatinine.

2.13. Statistical Analysis. Data are presented as the mean ± standard deviation (SD). Differences between different data means were compared by using Student's *t*-test and one-way analysis of variance (ANOVA) followed by Dunnett's multiple comparison tests using GraphPad Prism 7. $P < 0.05$ indicates that the difference is statistically significant.

3. Results

3.1. Effects of Febuxostat on Attenuating Renal Injury in SI-AKI Mice. The schedule of LPS (10 mg/kg, ip.) and febuxostat (Feb, 10 mg/kg/day, po.) administration was outlined (Figure 1(a)). We first administered febuxostat daily one week before establishing the LPS-challenged SI-AKI model. We recorded the survival of SI-AKI mice with or without febuxostat pretreatment within one week (Figure 1(b)). Control mice exhibited 100% survival. Forty-eight hours after LPS administration, 40% of septic mice died, and after another 48 h, the remaining septic mice died. In contrast, febuxostat pretreatment dramatically increased the survival rate by 90% compared to the LPS group (Figure 1(b)). Therefore, the SI-AKI mice were killed 24 h after LPS injection for the subsequent experiments.

Febuxostat pretreatment showed remarkable resistance to weight loss in SI-AKI mice (Figure 1(c)). Induction of sepsis by LPS caused a significant increase in blood urea nitrogen (BUN, Figure 1(d)) and serum creatinine (Scr, Figure 1(e)) compared to the control group. Pretreatment with febuxostat exerted a significant decrease in BUN and Scr levels compared to the LPS group (Figures 1(d) and 1(e)). The specific histopathological features of SI-AKI showed that many renal tubular epithelial cells were vacuolated, the brush border was lost and flattened, and protein cast was also observed (Figure 1(f)). After febuxostat pretreatment, renal tubular epithelial cell injury was significantly improved (Figure 1(g)).

3.2. Febuxostat Relieves Serum and Renal Tissue XO Activity, and XO Knockdown Attenuates Kidney Injury in SI-AKI Mice. Although febuxostat has shown an inhibitory effect on XO activity in other kidney injury models, this effect has not been reported in SI-AKI animal models. Consistent with the changes in renal function and histology, SI-AKI mice displayed higher XO activity in the serum and kidneys than control mice, and the increase in XO activity induced by LPS was reversed by febuxostat pretreatment (Figures 2(a) and 2(b)). Immunofluorescence assays further confirmed that the increased expression of XO in the kidney induced by LPS was inhibited by febuxostat pretreatment (Figures 2(c) and 2(d)). To further confirm the role of XO in SI-AKI, we constructed an AAV vector with XO shRNA (pAAV-shXO), and administration of pAAV-shXO significantly inhibited XO expression in the kidney (Figures 2(e)–2(i)). Serum and kidney XO activity were also decreased by XO knockdown (Figures 2(j) and 2(k)). Moreover, renal function, as indicated by BUN and Scr levels, was protected from the marked increase induced by XO knockdown in SI-AKI mice (Figures 2(l) and 2(m)). HE staining of kidney tissues from each group showed that XO knockdown dampened kidney tubular injury in SI-AKI mice (Figures 2(n) and 2(o)).

3.3. The Inhibition of XO Improves Hypoxia and ROS Production in the Kidneys of SI-AKI Mice. XO is an enzyme that utilizes molecular oxygen to produce ROS. Still it is unclear whether the inhibition of XO can improve renal hypoxia in SI-AKI mice by reducing the utilization of molecular oxygen. The hypoxia distribution in renal tubular cells can be detected by fluorescence labeling of the hypoxia probe pimonidazole, which can conjugate with intracellular thios under hypoxia and then be detected with a pimonidazole secondary antibody. The fluorescence intensity of the hypoxia signal in the kidney tissue of the SI-AKI group was the strongest, while that of the febuxostat pretreatment

(a)

(b)

(c)

(d)

(e)

(f)

(g)

Figure 2: Continued.

(h)

(i)

(j)

(k)

(l)

(m)

Figure 2: Continued.

(n)

(o)
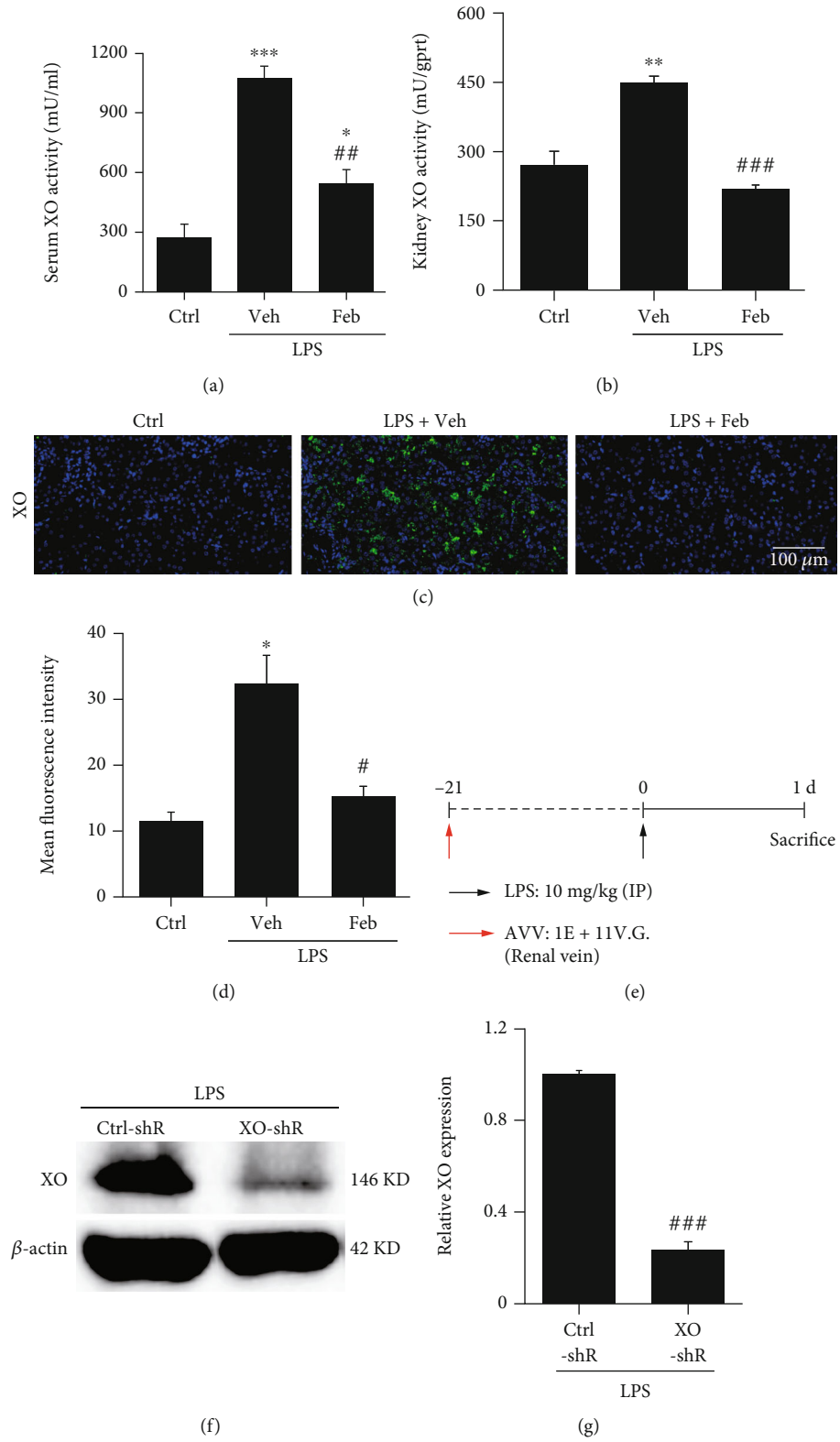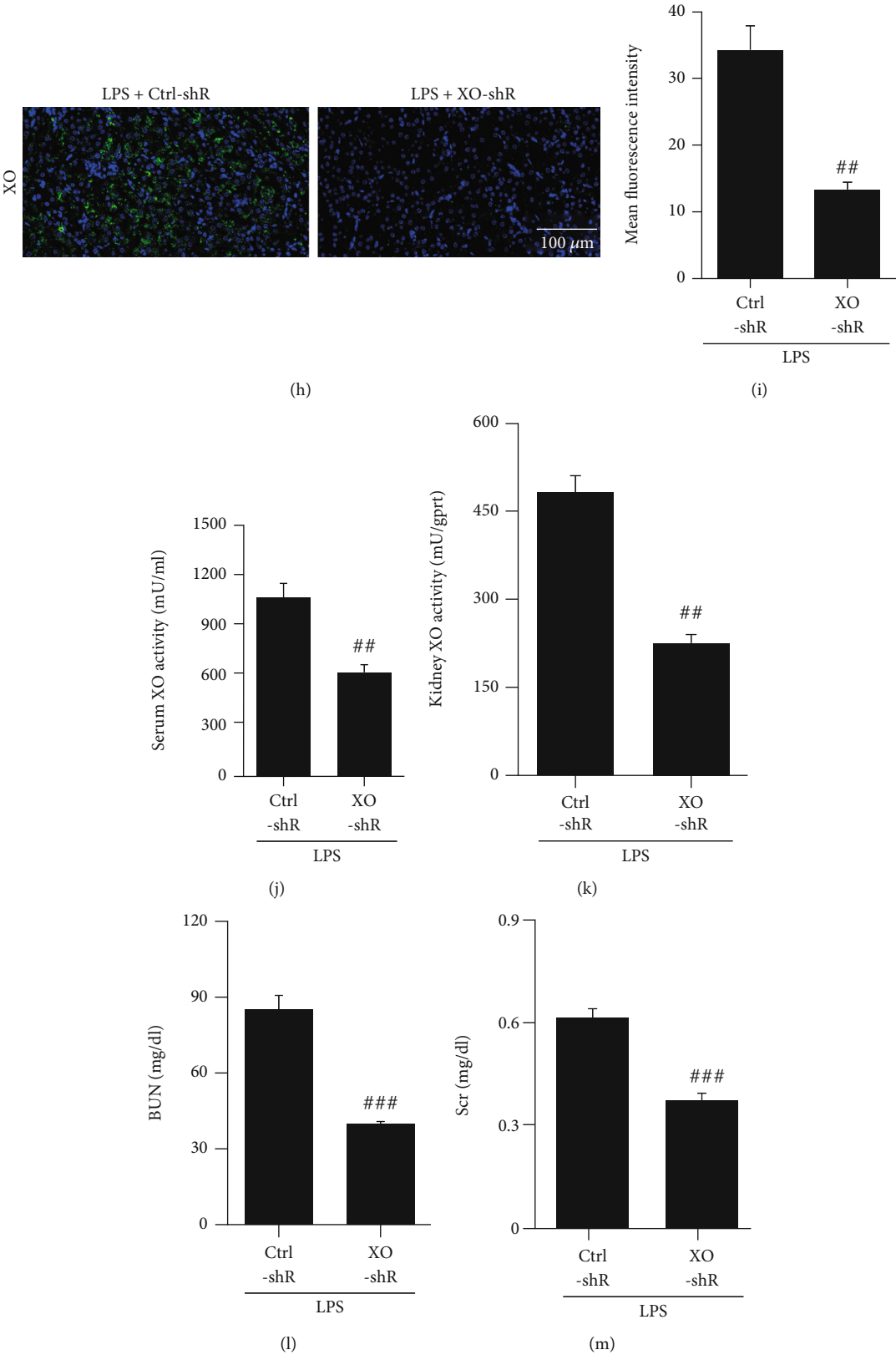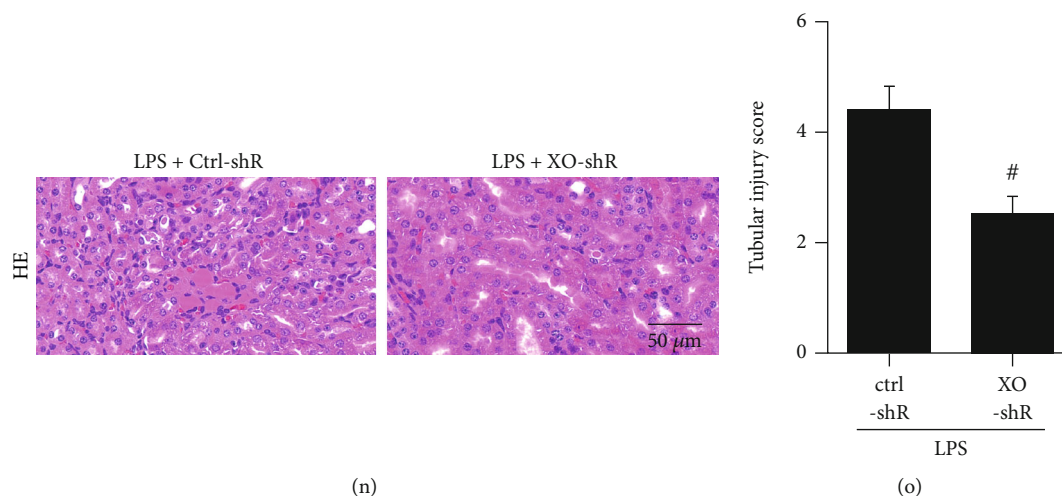
FIGURE 2: Febuxostat relieves serum and renal tissue XO activity, and XO knockdown attenuates kidney injury in SI-AKI mice. (a, b) The XO activity in serum and renal tissue homogenates was measured 24 h after LPS injection. XO could oxidize xanthine and produce $O_2^{\bullet-}$, which could react with WST-8, and the color of the reaction products could be detected with a micro reader at 450 nm. (c, d) Changes in XO expression in the kidneys of SI-AKI mice were detected by immunofluorescence assay (400x magnification). (e) Timeline of AAV injection displayed. (f–i) Knockdown of XO expression was confirmed using western blot and immunofluorescence assays. (j, k) Serum and renal XO activity were evaluated. (l, m) BUN and Scr were analyzed after downregulation of XO and challenge with LPS (10 mg/kg). (n, o) Representative images of kidney tissue are presented, and the injury score was graded in a double-blinded manner. $^*P < 0.05$, $^{**}P < 0.01$, and $^{***}P < 0.001$ vs. Ctrl; $^{\#}P < 0.05$, $^{\#\#}P < 0.01$, and $^{\#\#\#}P < 0.001$ vs. LPS+Veh or LPS+Ctrl-shR ($n = 10$). Ctrl: control; Veh: vehicle; LPS: lipopolysaccharide; Feb: febuxostat; XO: xanthine oxidase; BUN: blood urea nitrogen; Scr: serum creatinine.

group was significantly decreased (Figures 3(a) and 3(b)). We also detected the expression of HIF-1α in the kidneys of SI-AKI mice. The results showed that the expression of HIF-1α in the kidneys of SI-AKI mice was significantly higher than that in control mice. At the same time, febuxostat pretreatment decreased the expression of HIF-1α in the kidneys of SI-AKI mice (Figures 3(c) and 3(d)). In addition, DHE fluorescence staining showed that febuxostat pretreatment significantly decreased the level of ROS in the kidneys of LPS-induced SI-AKI mice (Figures 3(e) and 3(f)). We further investigated the impact of XO on hypoxia and ROS in SI-AKI mice by knocking down XO in the kidney using pAAV-shXO. Downregulation of XO improved severe hypoxic conditions (Figures 3(g) and 3(h)) in SI-AKI mice and inhibited HIF-1α expression in the kidney (Figures 3(i) and 3(j)). The ROS level was also decreased by XO knockdown (Figures 3(k) and 3(l)).

3.4. Hypoxia Increased LPS-Induced XO Activity in HK-2 Cells, but the Inhibition of XO Conversely Improved Hypoxia. Since we observed the protective effect of febuxostat against renal hypoxia in SI-AKI mice in vivo, we further evaluated the relationship between XO activity and cellular hypoxia and the role of febuxostat. For this purpose, HK-2 cells were treated with LPS (10 μg/ml)±febuxostat (100 μM) and cultured under normoxic (21% O_2, 5% CO_2, and 74% N_2) or hypoxic (2% O_2, 5% CO_2, and 93% N_2) conditions for 6 h in vitro. The results from the cell counting kit-8 (CCK-8) assay showed that hypoxia for 6 h did not change the viability of HK-2 cells, which was decreased by LPS, especially under the condition of hypoxic culture (Figure 4(a)). The above results indicated that febuxostat reversed the

increase in LPS-induced cytotoxicity under normoxia and hypoxia. Consistent with the results of CCK-8, LPS induced a slight increase in XO activity in HK-2 cells under normoxia and a significant increase in hypoxia, suggesting that hypoxia has a positive effect on the increase in XO activity induced by LPS (Figure 4(b)). Febuxostat inhibited the increase in XO activity induced by LPS under both normoxic and hypoxic conditions (Figure 4(b)). Importantly, the green fluorescence of the hypoxia probe showed that no obvious hypoxia occurred in HK-2 cells cultured in 21% oxygen with or without LPS±febuxostat treatment (Figures 4(c) and 4(d)). After culturing with 2% O_2 for 6 h, HK-2 cells showed weak green fluorescence but LPS significantly enhanced the green fluorescence brightness, while febuxostat significantly reduced LPS-induced hypoxia (Figures 4(c) and 4(d)). To further confirm the function of XO in hypoxia- and LPS-induced cell injury, we knocked down XO in vitro using siRNA (Figures 4(e) and 4(f)). Loss of XO also alleviated hypoxia- and LPS-induced cell injury (Figure 4(g)) and XO activity (Figure 4(h)) and further relieved hypoxia in HK-2 cells (Figures 4(i) and 4(j)).

3.5. The Inhibition of XO Reduced Inflammation and Apoptosis in SI-AKI Mice. Hypoxia and oxidative stress induce mitochondrial damage, which further leads to the release of inflammatory cytokines and subsequent cell death [10]. Therefore, we further focused on the effects of XO inhibition on inflammation and apoptosis in SI-AKI mice. The ELISA results showed that febuxostat pretreatment significantly reduced the levels of serum inflammatory factors such as TNF-α (Figure 5(a)), IL-1β (Figure 5(b)), and IL-6 (Figure 5(c)) in SI-AKI mice triggered by LPS.

(a)

(b)

(c)

(d)

(e)

(f)

(g)

(h)

Figure 3: Continued.

(i)

(j)

(k)

(l)
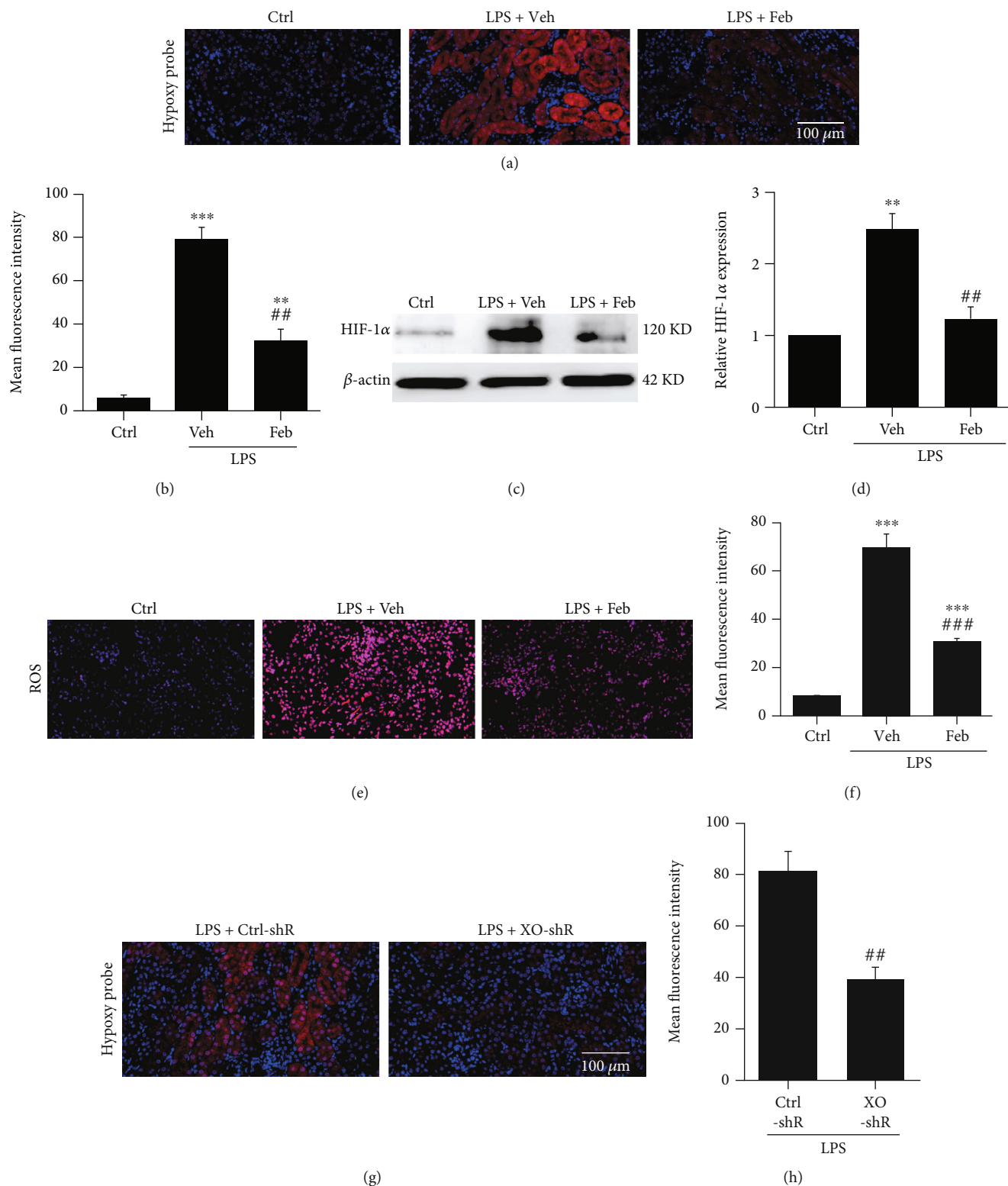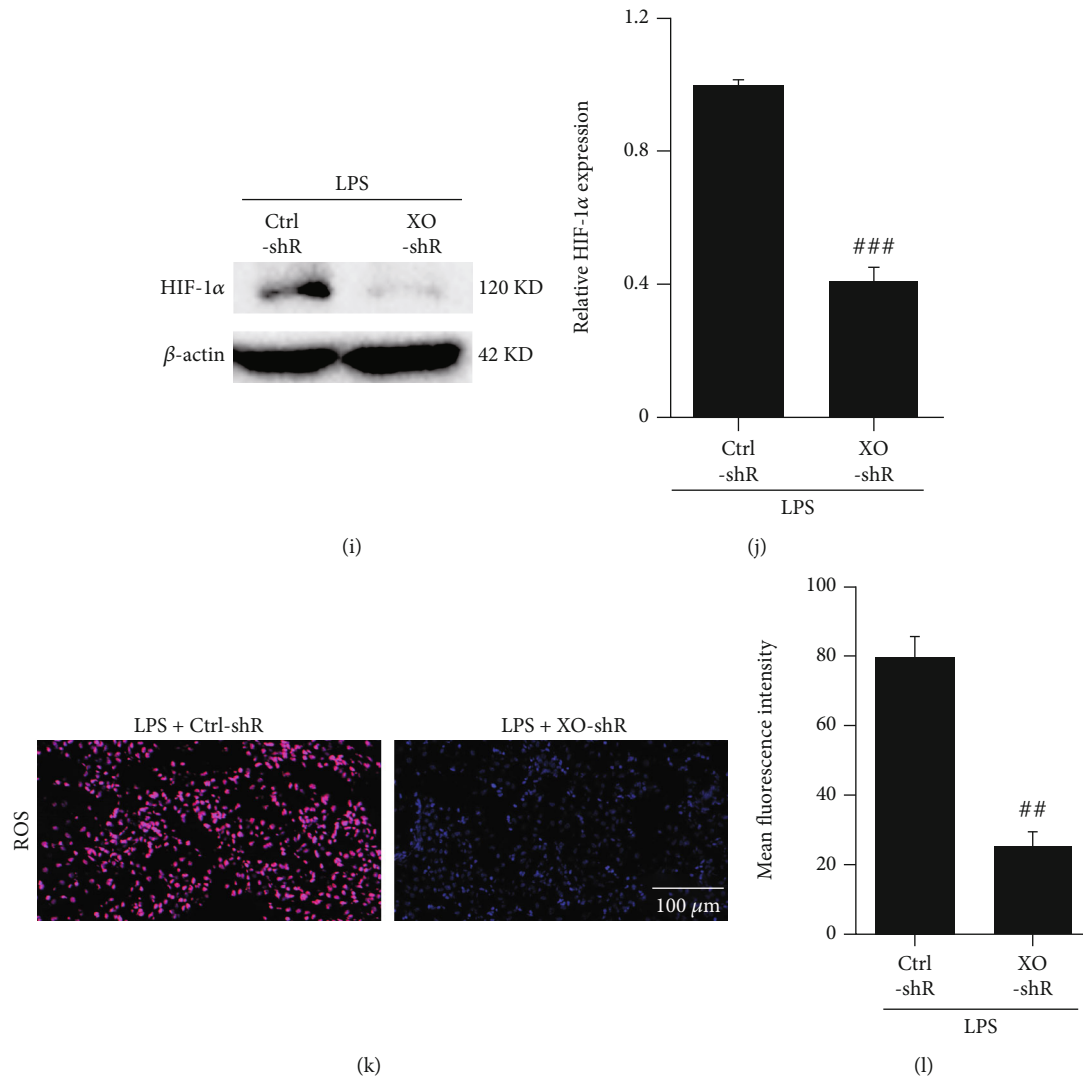
FIGURE 3: The inhibition of XO improves hypoxia and ROS production in the kidneys of SI-AKI mice. (a, b) Intracellular hypoxia in the kidneys of SI-AKI mice was detected by an immunofluorescence assay using a hypoxia probe (400x magnification). (c, d) Detection of HIF-1α protein expression in mouse renal homogenates by western blot. (e, f) The ROS level of kidney tissues was captured by CLSM at 24 h after LPS injection (dihydroethidium fluorescent staining, 400x magnification). (g, h) Intracellular hypoxia in the kidneys of SI-AKI mice after the knockdown of XO was captured by CLSM (400x magnification). (i, j) HIF-1α protein expression in SI-AKI mouse renal homogenates after downregulation of XO by western blot. (k, l) ROS levels in SI-AKI mouse renal tissue after the knockdown of XO were assessed using CLSM. Scale bar = 100 μm. $*P < 0.05$, $**P < 0.01$, and $***P < 0.001$ vs. control; $^{\#}P < 0.05$, $^{\#\#}P < 0.01$, and $^{\#\#\#}P < 0.001$ vs. LPS+Veh or LPS+Ctrl-shR ($n = 10$). Ctrl: control; Veh: vehicle; LPS: lipopolysaccharide; Feb: febuxostat; HIF: hypoxia-inducible factor; ROS: reactive oxygen species.

Immunofluorescence detection of neutrophils and macrophages in renal tissue labeled with MPO (Figures 5(d) and 5(g)) and F4/80 (Figures 5(e) and 5(h)), respectively, showed that the infiltration of neutrophils and macrophages at the outer stripe of the outer medulla of the kidneys in SI-AKI mice increased significantly. Febuxostat pretreatment remarkably reduced neutrophil and macrophage infiltration. TUNEL assay in the kidneys indicated that febuxostat pretreatment significantly decreased the number of apoptotic cells induced by LPS (Figures 5(f) and 5(i)). We further investigated the impact of XO on inflammation and cell apoptosis in SI-AKI mice by knocking down XO in the kidney using pAAV-shXO. Downreg-

ulation of XO reduced the levels of serum TNF-α (Figure 5(j)), IL-1β (Figure 5(k)), and IL-6 (Figure 5(l)) in SI-AKI mice. Furthermore, neutrophil (Figures 5(m) and 5(p)) and macrophage (Figures 5(n) and 5(q)) infiltration was also reduced by XO knockdown. Cell apoptosis in the kidney was prevented by XO downregulation, as suggested by TUNEL staining (Figures 5(o) and 5(r)).

4. Discussion

Lipopolysaccharide (LPS), which is a component of the outer membrane of gram-negative bacteria, has been the most widely studied pathogen-associated molecular pattern

(a)

(b)

(c)

(d)

(e)

Figure 4: Continued.

(f)

(g)

(h)

(i)

(j)
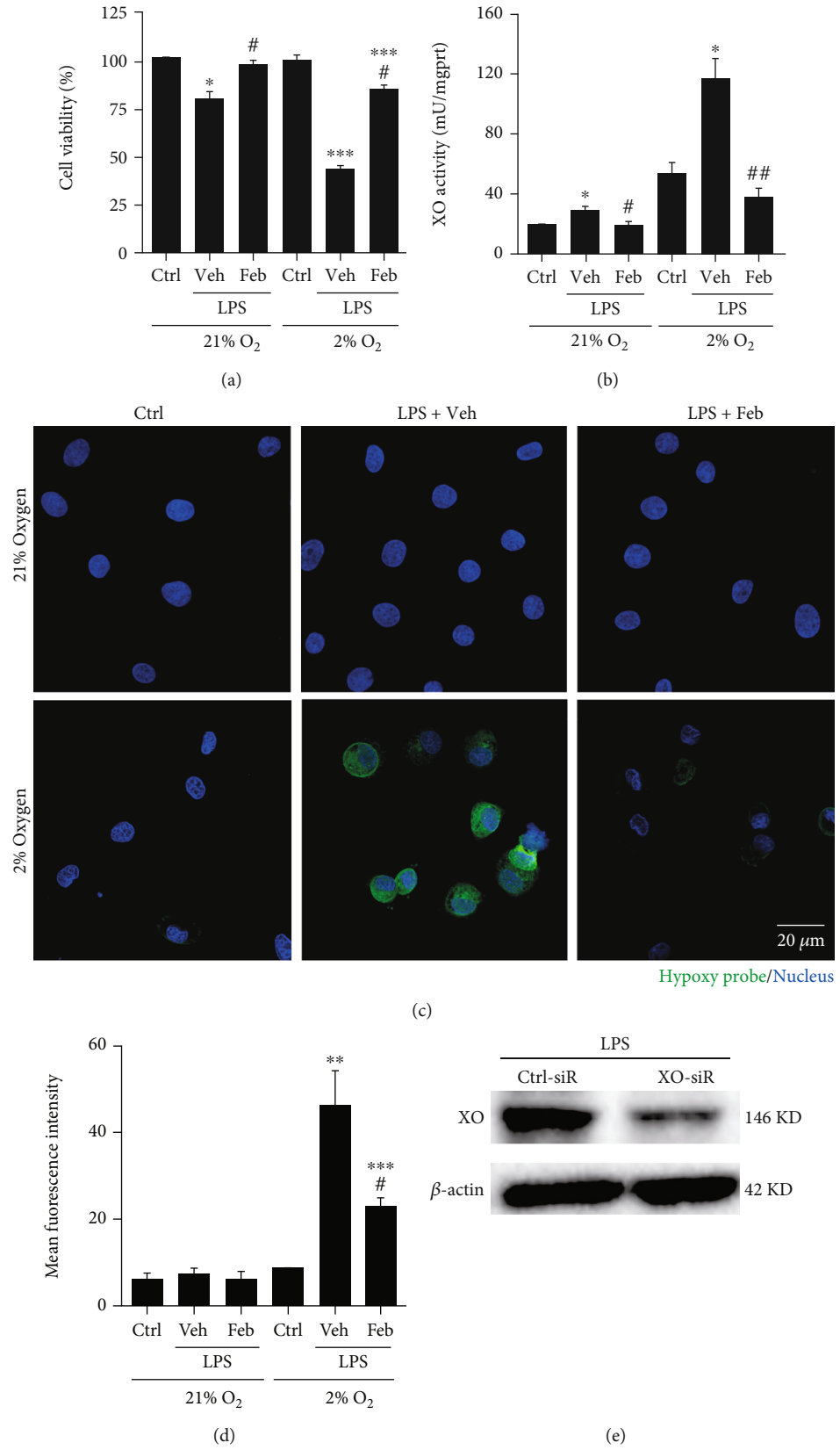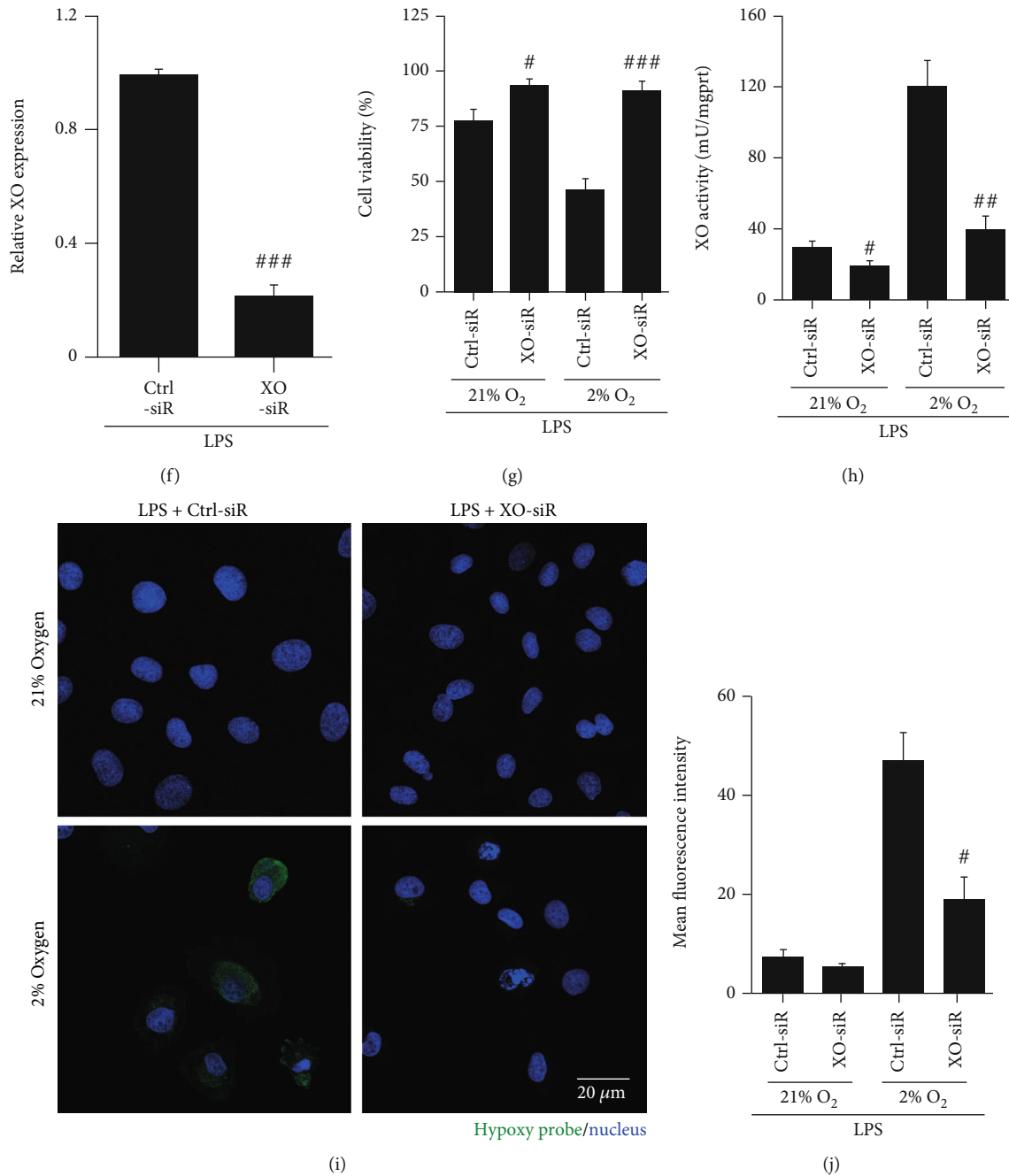
FIGURE 4: Hypoxia increased LPS-induced XO activity in HK-2 cells, but the inhibition of XO also improved hypoxia. (a) CCK8 showing the viability of HK-2 cells treated with LPS (10 μg/ml)±febuxostat (100 μM) under normoxic (21% O_2) and hypoxic (2% O_2) conditions for 6 h. (b) The XO activity of HK-2 cells treated with LPS±febuxostat under normoxic and hypoxic conditions for 6 h. (c, d) The intracellular hypoxia of HK-2 cells treated with LPS±febuxostat under normoxic and hypoxic conditions for 6 h was detected by an immunofluorescence assay using a hypoxia probe (800x magnification). (e, f) Knockdown of XO in HK-2 cells was confirmed using western blotting. (g) After the knockdown of XO with siRNA transfection, HK-2 cells were stimulated with LPS with 21% or 2% oxygen. Six hours later, the cells were harvested, and cell viability was assessed with the CCK8 method. (h) XO activity was assayed with the same method as in (b). (i, j) The intracellular hypoxia of HK-2 cells treated with LPS under normoxic and hypoxic conditions for 6 h was detected by an immunofluorescence assay using a hypoxia probe (800x magnification). Scale bar = 20 μm. $^{*}P < 0.05$, $^{**}P < 0.01$, and $^{***}P < 0.001$ vs. control; $^{\#}P < 0.05$, $^{\#\#}P < 0.01$, and $^{\#\#\#}P < 0.001$ vs. LPS+Veh or LPS+Ctr-siR ($n = 10$). Ctrl: control; Veh: vehicle; LPS: lipopolysaccharide; Feb: febuxostat; XO: xanthine oxidase.

(PAMP) in sepsis [28, 29]. LPS activates the Toll-like receptor to activate XO, which utilizes oxygen as a substrate to decompose hypoxanthine and xanthine into uric acid, producing superoxide and hydrogen peroxide during the reaction, and is mainly expressed during cellular stress or immune activation [30–32]. Hypoxemia caused by hemodynamic changes
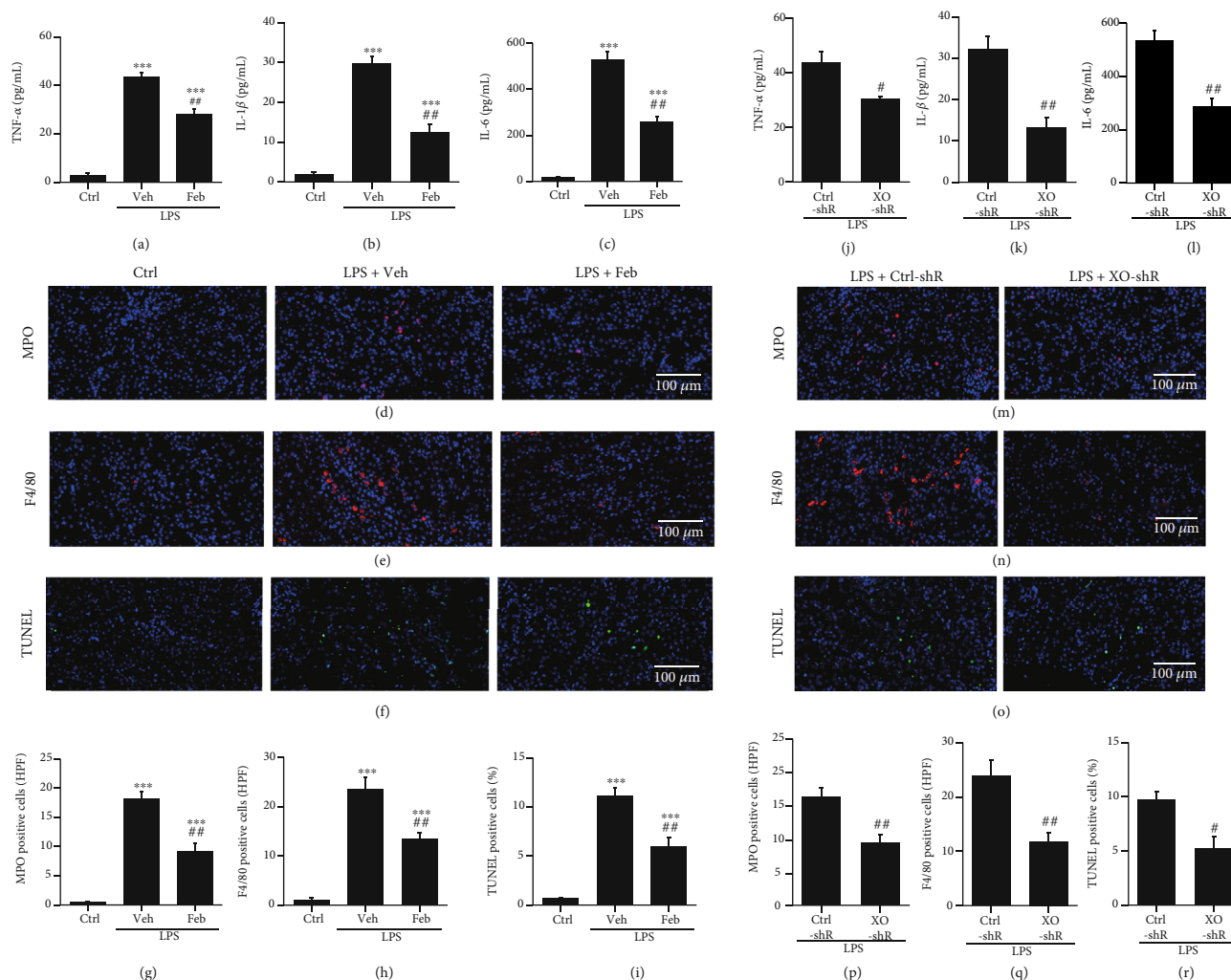
FIGURE 5: The inhibition of XO reduced inflammation and apoptosis in SI-AKI mice. (a–c) The levels of TNF-α, IL-1β, and IL-6 in renal homogenates of SI-AKI mice were detected by ELISA. (d, g) Immunofluorescence detection of neutrophils in the kidneys of SI-AKI mice by anti-MPO antibody (400x magnification). (e, h) Immunofluorescence detection of macrophages in the kidneys of SI-AKI mice by anti-F4/80 antibody (400x magnification). (f, i) Representative TUNEL-stained sections of the kidney in SI-AKI mice (400x magnification). Semiquantitative analysis of TUNEL-positive cells in each group is also displayed. (j–l) After the downregulation of XO, mice were treated with LPS (10 mg/kg), and the levels of TNF-α, IL-1β, and IL-6 in renal homogenates of SI-AKI mice were detected by ELISA. (m and p, n and q) After knockdown of XO with pAAV-shRNA, immunofluorescence detection of neutrophils and macrophages in the kidneys of SI-AKI mice by anti-MPO and anti-F4/80 antibodies (400x magnification). (o, r) Kidney cell apoptosis was analyzed with TUNEL staining in SI-AKI mice after XO knockdown. Scale bar = 100 μm. $^{*}P < 0.05$, $^{**}P < 0.01$, and $^{***}P < 0.001$ vs. control; $^{\#}P < 0.05$, $^{\#\#}P < 0.01$, and $^{\#\#\#}P < 0.001$ vs. LPS+Veh or LPS+Ctr-shR ($n = 10$). Ctrl: control; Veh; vehicle; LPS: lipopolysaccharide; Feb: febuxostat; TNF: tumor necrosis factor; IL: interleukin; MPO: myeloperoxidase; TUNEL: terminal deoxynucleotidyl transferase dUTP nick-end labeling.

in sepsis can also activate XO, which is widespread in ischemia–reperfusion models [8, 17, 20, 21, 33]. Several experimental and clinical studies have proven that XO activity has proinflammatory and prooxidative effects and can mediate vascular and endothelial dysfunction. The inhibition of XO by allopurinol or Feb has a protective effect [14, 15, 17–21, 33, 34]. In this study, we found that febuxostat, an XO-specific inhibitor, and knockdown of XO expression with pAAV-shXO showed antioxidant stress and anti-inflammatory effects and weakened the local hypoxia of renal tubular epithelial cells by inhibiting XO activity, thus alleviat-ing SI-AKI. The results of inhibition of XO in HK-2 cells with febuxostat and XO-siRNA in vitro showed that the downregulation of XO remarkably reduced the hypoxia condition in HK-2 cells induced by LPS and 2% oxygen. Taken together, our results indicated important roles of XO in oxidative stress- and hypoxia-induced injury in SI-AKI.

Currently, XO inhibitors approved by the US Food and Drug Administration (FDA) include three drugs, allopurinol, febuxostat, and topiroxostat, which all show antioxidant, anti-inflammatory, and renoprotective effects in addition to reducing uric acid [33]. Moreover, allopurinol and febuxostat

have been confirmed to play an important role in myocardial mechanoenergetic uncoupling. Febuxostat is superior to allopurinol in reducing systolic blood pressure, pulse-wave velocity, and left ventricular mass index in hyperuricemic patients undergoing cardiac surgery [35]. Moreover, febuxostat was more effective and faster than allopurinol in achieving the serum uric acid target in patients with gout [36]. Similarly, febuxostat has an advantage over topiroxostat in cardiorenal protection in hyperuricemic patients with cardiovascular disease [37, 38]. Recently, there have been only two reports on the treatment of SI-AKI with febuxostat showing that febuxostat improves the prognosis of SI-AKI animals through antioxidant stress and anti-inflammation [20, 21]. In this study, we also confirmed that pretreatment with febuxostat or kidney knockdown of XO by shRNA in vivo significantly improved the prognosis of SI-AKI mice by reducing the levels of BUN, Scr, TNF-α, IL-6, and IL-1β in peripheral blood and by improving histological damage, reducing kidney tubular cell apoptosis and ROS production, and inhibiting infiltration of neutrophils and macrophages in the kidneys. This suggests that the inhibition of XO has a nephroprotective effect on SI-AKI through anti-inflammation, antioxidant stress, and antiapoptosis.

Sepsis is often accompanied by organ dysfunction, poor tissue perfusion, or hypotension, which is bound to ischemia/hypoxia of damaged organs [2–6]. Renal dysfunction in sepsis is usually secondary to septic shock and sometimes to hypovolemia [39, 40]. AKI, including endotoxemia, can reduce tissue oxygen delivery and increase renal tissue oxygen consumption, resulting in renal medullary hypoxia, which can be the main driver of a cascade of events leading to renal tubular dysfunction, vascular injury, and cell injury [41]. This study found that LPS induced significant hypoxia in renal tubular epithelial cells through hypoxia probe fluorescence detection. However, pretreatment with febuxostat or kidney knockdown of XO by shRNA in vivo significantly improved renal hypoxia in SI-AKI mice, suggesting that the inhibition of XO elicits a favorable effect on alleviating renal medullary hypoxia in SI-AKI mice. We further evaluated the effect of pharmacologic (febuxostat) and genetic (XO siRNA) inhibition on XO activity and the viability of HK-2 cells under LPS and hypoxia in vitro. Our results showed that LPS caused a slight increase in XO activity under normoxia and a significant increase under hypoxia, accompanied by consistent changes in the degree of hypoxia, suggesting that the effect of LPS on XO activity is closely related to cell hypoxia. Importantly, for HK-2 cells treated with LPS, pharmacologic and genetic inhibition of XO improved cell hypoxia at 2% oxygen concentration and reversed the decrease in cell viability induced by LPS, suggesting the positive effect of inhibition of XO in improving cell hypoxia.

Hypoxia-inducible factor (HIF) is a cellular oxygen sensor that is a heterodimeric protein composed of an α subunit and a β subunit [42]. Under normoxia, the α subunit is unstable, degraded by the ubiquitin–proteasome system and does not function [42]. Under hypoxia, stabilization of the α subunit results in the formation of a dimer with the β subunit, which translocates to the nucleus, initiating mRNA synthesis for multiple genes [42, 43]. For example, it can upregulate erythropoietin and endothelial nitric oxide synthase (eNOS) and ameliorate tissue hypoxia [22]. However, HIF can be a double-edged sword because early onset of renal medullary hypoxia in sepsis prolongs the phases of tissue hypoxia, leading to the destabilization of HIF that aggravates oxidative and nitrosative injuries, culminating in AKI [44]. In addition, excessive production of HIF in response to prolonged hypoxia in severe sepsis can lead to excessive production of vasoconstrictive and ROS-induced proteins, such as inducible nitric oxide synthase (iNOS), thereby promoting fibrogenesis [22]. Although our study did not further explore the advantages and disadvantages of high expression of HIF-1α in the kidneys of SI-AKI mice, the decrease in HIF-1α expression in the kidneys of mice with pharmacological and genetic inhibition of XO did not rule out the improvement of cellular hypoxia increased the degradation of HIF-1α, which further enriched the effect of XO inhibition in improving renal medulla hypoxia.

5. Conclusions

In summary, we proposed for the first time that the nephroprotective effect of inhibiting XO in SI-AKI models occurred at least partly through inhibiting XO activity to reduce renal hypoxia, thereby decreasing oxidative stress, inflammation, and apoptosis and ultimately attenuating the pathological process of SI-AKI. Although the specific regulatory pathway of XO inhibition to improve cellular hypoxia has still not been comprehensively illuminated, the current work might provide novel insight into the choice of drugs for the prevention and treatment of SI-AKI.

Abbreviations

AKI: Acute kidney injury
SI-AKI: Sepsis-induced AKI
LPS: Lipopolysaccharide
Feb: Febuxostat
ROS: Reactive oxygen species
XO: Xanthine oxidase
CKD: Chronic kidney disease
BUN: Blood urea nitrogen
Scr: Serum creatinine
HIF: Hypoxia-inducible factor
DHE: Dihydroethidium
CLSM: Confocal laser-scanning microscope
MPO: Myeloperoxidase
TNF: Tumor necrosis factor
IL: Interleukin
TUNEL: Terminal deoxynucleotidyl transferase dUTP nick-end labeling.

Data Availability

All data related to this paper may also be requested from the corresponding authors (email: xjsnlhb@fmmu.edu.cn).

Conflicts of Interest

The authors declare that there are no conflicts of interest regarding the publication of this paper.

Authors' Contributions

Ting-ting Wang, Yi-wei Du, Wen Wang, and Xiang-nan Li contributed equally to this work.

Acknowledgments

References

[1] J. A. Kellum, P. Romagnani, G. Ashuntantang, C. Ronco, A. Zarbock, and H. J. Anders, "Acute kidney injury," *Nat. Rev. Dis. Prim.*, vol. 7, no. 1, 2021.

[2] C. L. Manrique-Caballero, G. Del Rio-Pertuz, and H. Gomez, "Sepsis-associated acute kidney injury," *Critical Care Clinics*, vol. 37, no. 2, pp. 279–301, 2021.

[3] T. Hellman, P. Uusalo, and M. J. Järvisalo, "Renal replacement techniques in septic shock," *International Journal of Molecular Sciences*, vol. 22, no. 19, p. 10238, 2021.

[4] K. Kalantari and M. H. Rosner, "Recent advances in the pharmacological management of sepsis-associated acute kidney injury," *Expert Review of Clinical Pharmacology*, vol. 14, no. 11, pp. 1401–1411, 2021.

[5] J. L. Koyner, "Sepsis and kidney injury," *Contributions to Nephrology*, vol. 199, pp. 56–70, 2021.

[6] A. Stasi, A. Intini, C. Divella et al., "Emerging role of lipopolysaccharide binding protein in sepsis-induced acute kidney injury," *Nephrology, Dialysis, Transplantation*, vol. 32, no. 1, pp. 24–31, 2016.

[7] K. Doi, A. Leelahavanichkul, P. S. T. Yuen, and R. A. Star, "Animal models of sepsis and sepsis-induced kidney injury," *The Journal of Clinical Investigation*, vol. 119, no. 10, pp. 2868–2878, 2009.

[8] H. M. Schmidt, E. E. Kelley, and A. C. Straub, "The impact of xanthine oxidase (XO) on hemolytic diseases," *Redox Biology*, vol. 21, p. 101072, 2019.

[9] S. S. Al-Shehri, J. A. Duley, and N. Bansal, "Xanthine oxidase-lactoperoxidase system and innate immunity: biochemical actions and physiological roles," *Redox Biology*, vol. 34, p. 101524, 2020.

[10] M. G. Battelli, L. Polito, M. Bortolotti, and A. Bolognesi, "Xanthine oxidoreductase-derived reactive species: physiological and pathological effects," *Oxidative Medicine and Cellular Longevity*, vol. 2016, 8 pages, 2016.

[11] N. Cantu-Medellin and E. E. Kelley, "Xanthine oxidoreductase-catalyzed reactive species generation: a process in critical need of reevaluation," *Redox Biology*, vol. 1, no. 1, pp. 353–358, 2013.

[12] H. Fu, J. Zhang, and M. Huang, "Topiroxostat ameliorates oxidative stress and inflammation in sepsis-induced lung injury," *Zeitschrift fur Naturforsch. - Sect. C Journal of Biosciences*, vol. 75, no. 11–12, pp. 425–431, 2020.

[13] M. Damarla, L. F. Johnston, G. Liu et al., "XOR inhibition with febuxostat accelerates pulmonary endothelial barrier recovery and improves survival in lipopolysaccharide-induced murine sepsis," *Physiological Reports*, vol. 5, no. 15, pp. 1–10, 2017.

[14] P. H. F. Gois, D. Canale, R. A. Volpini et al., "Allopurinol attenuates rhabdomyolysis-associated acute kidney injury: renal and muscular protection," *Free Radical Biology & Medicine*, vol. 101, pp. 176–189, 2016.

[15] T. Erol, A. Tekin, M. T. Katırcıbaşı et al., "Efficacy of allopurinol pretreatment for prevention of contrast-induced nephropathy: a randomized controlled trial," *International Journal of Cardiology*, vol. 167, no. 4, pp. 1396–1399, 2013.

[16] N. Yabuuchi, H. Hou, N. Gunda, Y. Narita, H. Jono, and H. Saito, "Suppressed hepatic production of indoxyl sulfate attenuates cisplatin-induced acute kidney injury in sulfotransferase 1a1-deficient mice," *International Journal of Molecular Sciences*, vol. 22, no. 4, p. 1764, 2021.

[17] K. Fujii, A. Kubo, K. Miyashita et al., "Xanthine oxidase inhibitor ameliorates postischemic renal injury in mice by promoting resynthesis of adenine nucleotides," *JCI Insight*, vol. 4, no. 22, 2019.

[18] K. J. Yang, J. H. Kim, Y. K. Chang, C. W. Park, S. Y. Kim, and Y. A. Hong, "Inhibition of xanthine oxidoreductase protects against contrast-induced renal tubular injury by activating adenosine monophosphate-activated protein kinase," *Free Radical Biology & Medicine*, vol. 145, pp. 209–220, 2019.

[19] A. N. A. Fahmi, G. S. G. Shehatou, A. M. Shebl, and H. A. Salem, "Febuxostat exerts dose-dependent renoprotection in rats with cisplatin-induced acute renal injury," *Naunyn-Schmiedeberg's Archives of Pharmacology*, vol. 389, no. 8, pp. 819–830, 2016.

[20] M. F. de Paula Ramos, C. V. Razvickas, F. T. Borges, and N. Schor, "Xanthine oxidase inhibitors and sepsis," *International Journal of Immunopathology and Pharmacology*, vol. 32, p. 205873841877221, 2018.

[21] Y. F. Ibrahim, R. R. Fadl, S. A. E. Ibrahim, M. F. Gayyed, A. M. A. Bayoumi, and M. M. M. Refaie, "Protective effect of febuxostat in sepsis-induced liver and kidney injuries after cecal ligation and puncture with the impact of xanthine oxidase, interleukin 1β, and c-Jun N-terminal kinases," *Human & Experimental Toxicology*, vol. 39, no. 7, pp. 906–919, 2020.

[22] C. P. Ow, A. Trask-Marino, A. H. Betrie, R. G. Evans, C. N. May, and Y. R. Lankadeva, "Targeting oxidative stress in septic acute kidney injury: From theory to practice," *Journal of Clinical Medicine*, vol. 10, no. 17, p. 3798, 2021.

[23] H. Scholz, F. J. Boivin, K. M. Schmidt-Ott et al., "Kidney physiology and susceptibility to acute kidney injury: implications for renoprotection," *Nature Reviews. Nephrology*, vol. 17, no. 5, pp. 335–349, 2021.

[24] C. J. Rocca, S. N. Ur, F. Harrison, and S. Cherqui, "RAAV9 combined with renal vein injection is optimal for kidney-targeted gene delivery: conclusion of a comparative study," *Gene Therapy*, vol. 21, no. 6, pp. 618–628, 2014.

[25] M. H. Ho, C. H. Yen, T. H. Hsieh et al., "CCL5 via GPX1 activation protects hippocampal memory function after mild traumatic brain injury," *Redox Biology*, vol. 46, article 102067, 2021.

[26] L. Zhou, P. Yu, T. T. Wang et al., "Polydatin attenuates cisplatin-induced acute kidney injury by inhibiting ferroptosis,"

Oxidative Medicine and Cellular Longevity, vol. 2022, 14 pages, 2022.

[27] H. B. Liu, Q. H. Meng, C. Huang, J. B. Wang, and X. W. Liu, "Nephroprotective effects of polydatin against ischemia/reperfusion injury: a role for the PI3K/Akt signal pathway," *Oxidative Medicine and Cellular Longevity*, vol. 2015, 13 pages, 2015.

[28] G. Gorecki, D. Cochior, C. Moldovan, and E. Rusu, "Molecular mechanisms in septic shock (review)," *Experimental and Therapeutic Medicine*, vol. 22, no. 4, pp. 1–5, 2021.

[29] C. Lelubre and J. L. Vincent, "Mechanisms and treatment of organ failure in sepsis," *Nature Reviews. Nephrology*, vol. 14, no. 7, pp. 417–427, 2018.

[30] V. Kumar, "Toll-like receptors in sepsis-associated cytokine storm and their endogenous negative regulators as future immunomodulatory targets," *International Immunopharmacology*, vol. 89, p. 107087, 2020.

[31] A. Ives, J. Nomura, F. Martinon et al., "Xanthine oxidoreductase regulates macrophage IL1β secretion upon NLRP3 inflammasome activation," *Nature Communications*, vol. 6, no. 1, pp. 1–11, 2015.

[32] Z. Doğanyiğit, A. Okan, E. Kaymak, D. Pandır, and S. Silici, "Investigation of protective effects of apilarnil against lipopolysaccharide induced liver injury in rats via TLR 4/ HMGB-1/ NF-κB pathway," *Biomed. Pharmacother.*, vol. 125, p. 109967, 2020.

[33] K. Vickneson and J. George, "Xanthine oxidoreductase inhibitors," *Handbook of Experimental Pharmacology*, vol. 264, pp. 205–228, 2021.

[34] S. Wei, T. Isagawa, M. Eguchi et al., "Febuxostat, a xanthine oxidase inhibitor, decreased macrophage matrix metalloproteinase expression in hypoxia," *Biomedicine*, vol. 8, no. 11, p. 470, 2020.

[35] A. Sezai, M. Soma, K. I. Nakata et al., "Comparison of febuxostat and allopurinol for hyperuricemia in cardiac surgery patients with chronic kidney disease (NU-FLASH trial for CKD)," *Journal of Cardiology*, vol. 66, no. 4, pp. 298–303, 2015.

[36] G. Desideri, M. Rajzer, M. Gerritsen et al., "Effects of intensive urate lowering therapy with febuxostat in comparison with allopurinol on pulse wave velocity in patients with gout and increased cardiovascular risk: the FORWARD study," *Eur Heart J Cardiovasc Pharmacother*, vol. 8, no. 3, pp. 236–242, 2022.

[37] A. Sezai, S. Unosawa, M. Taoka, S. Osaka, H. Sekino, and M. Tanaka, "Changeover trial of febuxostat and topiroxostat for hyperuricemia with cardiovascular disease: sub-analysis for chronic kidney disease (trofeo ckd trial)," *Annals of Thoracic and Cardiovascular Surgery*, vol. 26, no. 4, pp. 202–208, 2020.

[38] A. Sezai, K. Obata, K. Abe, S. Kanno, and H. Sekino, "Crossover trial of febuxostat and topiroxostat for hyperuricemia with cardiovascular disease (TROFEO trial)," *Circulation Journal*, vol. 81, no. 11, pp. 1707–1712, 2017.

[39] E. H. Post, J. A. Kellum, R. Bellomo, and J. L. Vincent, "Renal perfusion in sepsis: from macro- to microcirculation," *Kidney International*, vol. 91, no. 1, pp. 45–60, 2017.

[40] C. Ronco, R. Bellomo, and J. A. Kellum, "Acute kidney injury," *Lancet*, vol. 394, no. 10212, pp. 1949–1964, 2019.

[41] S. Peerapornratana, C. L. Manrique-Caballero, H. Gómez, and J. A. Kellum, "Acute kidney injury from sepsis: current concepts, epidemiology, pathophysiology, prevention and treatment," *Kidney International*, vol. 96, no. 5, pp. 1083–1099, 2019.

[42] P. Koivunen and T. Kietzmann, "Hypoxia-inducible factor prolyl 4-hydroxylases and metabolism," *Trends in Molecular Medicine*, vol. 24, no. 12, pp. 1021–1035, 2018.

[43] D. Bar-Or, M. M. Carrick, C. W. Mains, L. T. Rael, D. Slone, and E. N. Brody, "Sepsis, oxidative stress, and hypoxia: are there clues to better treatment?," *Redox Report*, vol. 20, no. 5, pp. 193–197, 2015.

[44] K. U. Eckardt, C. Rosenberger, J. S. Jürgensen, and M. S. Wiesener, "Role of hypoxia in the pathogenesis of renal disease," *Blood Purification*, vol. 21, no. 3, pp. 253–257, 2003.

Research Article

Inhibition of PLK3 Attenuates Tubular Epithelial Cell Apoptosis after Renal Ischemia–Reperfusion Injury by Blocking the ATM/P53-Mediated DNA Damage Response

Weiming Deng [1,2] **Xiangling Wei** [1] **Zhenwei Xie,**[1] **Rui Zhang,**[1] **Zhanwen Dong,**[1] **Jinhua Zhang,**[1] **You Luo** [1] **Qingdi Cheng,**[1] **Ruojiao Wang,**[1] **Heng Li** [1] **and Ning Na** [1]

[1]*Department of Kidney Transplantation, The Third Affiliated Hospital of Sun Yat-sen University, Guangzhou, Guangdong 510630, China*
[2]*The First Affiliated Hospital, Department of Urology, Hengyang Medical School, University of South China, Hengyang, Hunan 421001, China*

Correspondence should be addressed to Heng Li; liheng23@mail.sysu.edu.cn and Ning Na; naning@mail.sysu.edu.cn

Objective. Renal ischemia–reperfusion (I/R) injury is a major cause of acute kidney injury (AKI) in transplanted kidneys. This study was aimed at exploring the role of PLK3 (polo-like kinase 3) in renal I/R injury, focusing on its relationship with oxidative stress-induced DNA damage and renal tubular epithelial cell (TEC) apoptosis. *Methods*. TRAP-seq data from the development dataset GSE52004 and the validation dataset GSE121191 were analyzed using GEO2R. PLK3 overexpression plasmids and targeted silencing siRNAs were used in a model of hypoxia/reoxygenation (H/R) injury, and rAAV-9-PLK3-KD were administered to C57BL/6J mice exposed to I/R injury. The ATM-specific inhibitor KU-60019 was used to block the DNA damage response (DDR). Western blotting was performed to measure DDR- and apoptosis-associated protein expression. Cell viability was measured by CCK-8 reagent, and apoptosis was examined by flow cytometry and TUNEL assay. Furthermore, the fluorescent probes H_2DCFH-DA and DHE were used to measure ROS production in vitro. The MDA level and SOD activity were measured to assess oxidative stress in vivo. KIM-1 staining and Scr and BUN were used to evaluate kidney injury. *Results*. The mRNA and protein levels of PLK3 were markedly increased in the H/R injury and I/R injury models. GO terms showed that PLK3 was mainly involved in oxidative stress and DNA damage after renal I/R injury. Overexpression of PLK3 decreased cell viability and increased apoptosis. In contrast, targeted silencing of PLK3 expression decreased the Bax/Bcl-2 ratio by decreasing P53 phosphorylation, thereby reducing TEC apoptosis. Furthermore, KU-60019 reduced PLK3 activation and DDR-induced apoptosis, while overexpression of PLK3 reversed the mitigating effect of KU-60019 on TEC apoptosis. Similarly, rAAV-9-PLK3 KD mice exhibited a lower rate of TEC apoptosis and milder renal damage after I/R injury. *Conclusion*. We demonstrate for the first time that PLK3 is involved in oxidative stress-induced DNA damage and TEC apoptosis in renal I/R injury. Inhibition of PLK3 attenuates TEC apoptosis after I/R injury by blocking the ATM/P53-mediated DDR. Therefore, PLK3 may serve as a potential therapeutic target for ischemic AKI.

1. Introduction

Acute kidney injury (AKI) is a common complication that is associated with high morbidity and mortality, and medications that are effective in treating AKI are lacking [1]. Ischemia–reperfusion (I/R) injury is an inevitable process associated with renal transplantation and the main cause of AKI after transplantation. When the kidney is exposed to hypoxia and ischemic injury, the proximal tubules are the most vulnerable part of the structure [2, 3].

The oxidative stress caused by the excessive production of reactive oxygen species (ROS) during reperfusion is generally considered to be the major cause of tubular epithelial cell (TEC) injury [4]. ROS attack DNA and cause DNA double-strand breaks (DSBs), which are one of the most critical DNA lesions with respect to TEC survival and death during oxidative stress [5, 6]. DSBs activate the protein kinase ataxia telangiectasia mutation (ATM), which initiates DNA damage response (DDR) signals to downstream target genes, affecting cell cycle arrest, DNA repair, and apoptosis [7]. P53 is an intracellular transcription factor that regulates the expression of genes involved in growth arrest or apoptosis in response to various stress conditions, including DNA damage and hypoxia [8]. After DNA damage, P53 protein stability is affected by post-translational modification, including extensive phosphorylation. When DNA damage is severe and cannot be repaired, ATM stabilizes and activates P53 through phosphorylation at Ser15 and Ser20 to initiate the apoptosis cascade [9]. DNA damage occurs more frequently in proximal tubules than in distal tubules, and this trend may be related to subtle differences in sensitivity to damage and proliferation between these cell types [10]. Increasing evidence suggests that DNA damage and the related DDR play key roles in cisplatin-induced nephrotoxic AKI [11–13], but the current evidence on ischemic AKI remains poorly understood.

PLK3 is an evolutionarily conserved Ser/Thr protein kinase in the mammalian polo-like kinase (Plk) family that plays a vital role in the cell cycle and mitosis [14]. Unlike other PLKs, PLK3 acts as a tumor suppressor by blocking cell proliferation and inducing apoptosis [15–17]. PLK3 is often rapidly activated in response to various environmental stresses [18–20]. As an essential part of hypoxia regulation, PLK3 can directly phosphorylate HIF-1α and reduce its stability under hypoxic conditions [21]. Hypoxia/reoxygenation- (H/R-) induced PLK3 activation results in the direct phosphorylation of c-Jun, thereby promoting human corneal epithelial cell apoptosis [22]. When oxidative stress causes DNA damage, PLK3 can be phosphorylated in an ATM-dependent manner [23]. Therefore, the main function of PLK3 may be regulation of the stress response but not the cell cycle in mammals [24]. I/R injury-induced TEC apoptosis is a major factor in ischemic AKI in renal transplant patients. However, whether PLK3 is involved in the oxidative stress-induced DNA damage that leads to TEC apoptosis is still unclear.

In the current study, we provided compelling evidence that PLK3 promoted TEC apoptosis during ischemic AKI using a renal I/R injury model in vivo and a TEC H/R injury model in vitro. ROS generated by I/R injury caused DSBs, which activated PLK3 in an ATM-dependent manner, and then, PLK3 activated P53 to drive the DDR and apoptosis. Importantly, inhibiting PLK3 reduced apoptosis of TECs and attenuated renal injury in both the cellular and animal experiments. In conclusion, this study is the first to demonstrate that PLK3 plays a pivotal role in ischemic AKI and that inhibiting PLK3 may be a novel strategy for the prevention and treatment of renal I/R injury.

2. Materials and Methods

2.1. Bioinformatics Analysis. The gene expression profile GSE52004 was downloaded from the Gene Expression Omnibus (GEO) database (http://www.ncbi.nlm.nih.gov/geo/). The researchers developed a mouse line in which the translation profiles of specific cell types can be identified by utilizing cell-type specific CRE-driver lines and translating ribosomal affinity purification (TRAP) techniques. For this database, the researchers screened the cell-specific translational expression profiles of nephron (Six2), interstitial cell group (Foxd1), vascular endothelial cell (Cdh5), and macrophage/monocyte group (Lyz2) after renal I/R injury [25]. The TRAP-seq validation dataset was derived from GSE121191 [26]. Single-cell RNA-seq data from normal human kidney tissue were obtained from GSE131685 and analyzed with the Human Protein Atlas (https://www.proteinatlas.org/). We used the GEO2R online tool (http://www.ncbi.nlm.nih.gov/geo/geo2r/) to identify the differentially expressed genes (DEGs) and displayed these genes in the forms of a heatmap and column. The heatmap was generated by the imageGP (http://www.ehbio.com/ImageGP/index.php/Home/Index/index.html). To elucidate the function of PLK3 in renal I/R injury, the "clusterProfiler" R package was used to perform Gene Ontology (GO) functional enrichment analyses [27].

2.2. Cell Culture and the Induction of H/R In Vitro. The human proximal tubular cell line HK-2 was obtained from the American Type Culture Collection (Manassas, VA, USA) and validated by a short tandem repeat (STR) assay (IGE Biotech, Guangzhou, China). The cells were maintained in DMEM/F12 medium (Gibco, CA, USA) supplemented with 10% fetal bovine serum (Gibco, CA, USA), 100 IU/ml penicillin, and 100 μg/ml streptomycin (Gibco, CA, USA) in a 37°C humidified incubator with an atmosphere of 95% air and 5% CO_2. Before each experiment, HK-2 cells were seeded in six-well plates at a density of $1 - 5 \times 10^5$ cells per well and cultured in complete DMEM/F12 medium until they reached approximately 70-80% confluence. To induce hypoxic injury, the medium was replaced with serum- and glucose-free DMEM/F12 medium (Procell, Wuhan, China), and the cells were exposed to hypoxic conditions (1% O_2, 94% N_2, and 5% CO_2) in a humidified N_2-flushed hypoxic chamber (Eppendorf, GALAXY-48R) for different times. After exposure to hypoxia, the cells were cultured in complete DMEM/F12 medium for different times under normoxic conditions (5% CO_2 and 95% air) to allow reoxygenation. Control cells were maintained in complete medium in a normoxic cell incubator.

2.3. Animal Models of Renal I/R Injury. All the animal protocols were strictly conducted in accordance with institutional animal care policies and were approved by the Biomedical Ethics Committee of Sun Yat-sen University (Guangzhou, China). Male C57BL/6 mice (age 8-10 weeks and weight 22–25 g) were purchased from Guangdong Medical Experimental Animal Center. The mice were housed under pathogen-free conditions with a relative humidity of 50% and temperature of 25 ± 2°C and were

maintained under conditions of 12 h of light and 12 h of darkness. To establish the model of renal I/R injury, the mice were anesthetized with pentobarbital sodium (60 mg/kg, i.p.) and placed on a heating pad to maintain a core body temperature of 37°C. A median abdominal incision was made, and the bilateral renal pedicles were blocked with a nontraumatic vascular clamp (FT222T, B. BRAUN, Germany) for 30 min. Then, the clamp was released, and reperfusion was visually confirmed. The sham operation group only underwent renal pedicle exposure without clamping.

2.4. Recombinant Adeno-Associated Virus Serotype-9- (rAAV9-) Mediated PLK3 Knockdown (KD) in Mice. rAAV-9 was developed by and obtained from GeneChem (Shanghai, China). All the mice were randomly divided into 4 groups ($n = 6$ per group): the sham group, saline+IRI group, rAAV9+IRI group, and rAAV9-PLK3-KD+IRI group. Before the operation, a 34 G microinjection needle was used to slowly inject 50 μl of rAAV9-PLK3-KD plasmid at a concentration of 1×10^{11} vg/ml into the kidneys through the renal vein [28]. The animals were sacrificed 24 h after reperfusion, and blood and kidney tissue samples were collected for further analysis. The shRNA sequences were listed as follows: PLK3 shRNA sense (5′-3′): CTTTCTGGCCT CAAGTACT and control shRNA sense (5′-3′): CGCTGA GTACTTCGAAATGTC.

2.5. Analysis of Renal Function. Blood samples were collected from the submandibular vein, and then, the supernatant was collected after centrifugation. Creatinine and urea commercial kits (Nanjing Jiancheng Co., China) were used to calculate the levels of blood urea nitrogen (BUN) and creatinine according to the manufacturer's instructions.

2.6. Quantitative Real-Time PCR. Total RNA was extracted from HK-2 cells and mouse renal tissues with TRIzol reagent (Thermo Fisher Scientific, USA). The RNA yield was measured by NanoDrop 2000 (Thermo Scientific, USA). Subsequently, the HiScript III RT SuperMix+gDNA Wiper Kit (Vazyme, Nanjing, China) was used to reverse transcribe the RNA into cDNA. qRT–PCR analysis was performed using the ABI7500 system (Agilent Technologies, USA) with SYBR Green qPCR Master Mix (Vazyme, Nanjing, China). In all the PCR experiments, the expression levels of GAPDH (Homo sapiens) and β-actin (Mus musculus) were used as the internal references. Fold change in expression was quantified using the $2^{-\Delta\Delta Ct}$ method. The primers for the specific target genes (Supplementary table 1) were synthesized by IGE Biotech (Guangzhou, China).

2.7. Flow Cytometry. Cell apoptosis was examined by an Annexin-V-FITC/propidium iodide (PI) apoptosis detection kit (KeyGEN Biotech, Nanjing, China) after transfection and H/R treatment for the indicated times. HK-2 cells were collected and washed twice with phosphate-buffered saline (PBS). Then, the cells were stained with 5 μl of Annexin V-fluorescein isothiocyanate (FITC) and 5 μl of PI for 30 min in the dark at room temperature. A H_2DCFH-DA fluorescent probe was used to measure the production of ROS with

FITC parameter settings. Finally, the stained cells were scanned by an LSRFortessa™ flow cytometer (BD Biosciences, San Diego, CA, USA). The raw data were analyzed by FlowJo software (Tree Star Inc., Ashland, OR).

2.8. Cell Viability Assay. A Cell Counting Kit-8 (CCK-8) assay kit was used to assess cell viability. Transfected HK-2 cells were seeded in 96-well plates at a density of 5×10^3 cells/well and subjected to H/R injury. The plates were incubated for 3 h at 37°C in the dark after 10 μl of CCK-8 solution was added to each well. At the end of the experiments, a microplate reader was used to measure the absorbance at 450 nm. Cell viability was calculated as the percentage $= [(A - C)/(B - C)] \times 100\%$ (A: OD value of treatment group, B: OD value of control group, and C: OD value of blank group).

2.9. Measurement of Oxidative Stress Index Levels. The level of malondialdehyde (MDA) and the activity of superoxide dismutase (SOD) in mouse kidney tissues were measured using commercial kits (Jiancheng, Nanjing, China). Intracellular ROS accumulation was examined with a DHE probe (Beyotime, Nanjing, China) according to the manufacturer's instructions. After transfection and H/R treatment, HK-2 cells were incubated with 5 μmol/l DHE at 37°C for 30 min. Then, the cells were washed three times with serum-free cell culture medium, and red fluorescence was observed under a fluorescence microscope (Nikon, Tokyo, Japan). In addition, we examined the expression levels of PLK3 in a H_2O_2-induced oxidative stress model by stimulating HK-2 cells with different concentrations of H_2O_2 (50 μM, 100 μM, and 200 μM) for 6 h.

2.10. Immunofluorescence Analysis. To perform the immunofluorescence assay, samples were fixed with 4% paraformaldehyde for 30 min at room temperature. After being washed with PBST, the samples were permeabilized with 0.3% Triton X-100 for 10 min and then blocked with 5% goat serum for 30 min. Subsequently, the samples were incubated with primary antibodies overnight at 4°C. The primary antibodies used in the present study were specific for the following proteins: PLK3 (DF4471, 1 : 250, Afftiny) and rH2AX (YP0218, 1 : 250, Immunoway). Then, the samples were washed 3 times with PBST and incubated with fluorescent secondary antibodies at room temperature for 1 h. DAPI was used to label the nucleus, and the cells were mounted with antifading mounting medium (Applygen, Beijing, China). Images were captured with a fluorescence microscope (Nikon, Tokyo, Japan).

2.11. TUNEL Assay. Apoptotic cells were analyzed by a TUNEL BrightGreen apoptosis detection kit (Vazyme, Nanjing, China) and a One Step TUNEL Apoptosis Assay Kit (Beyotime, Nanjing, China) according to the manufacturer's instructions. Samples were incubated with buffer containing FITC-12-dUTP and recombinant TdT enzyme for 1 h at 37°C. The number of apoptotic cells in randomly selected visual fields was counted and analyzed in a blinded manner under a fluorescence microscope.

2.12. *Western Blotting*. Mouse kidneys and HK-2 cells were lysed with cold lysis buffer (0.25 M NaCl, 50 mM Tris-HCl pH 7.4, 0.5% NP 40, 1 mM EDTA, 1 mM Na_3VO_4, 1 mM NaF, 1% cocktail, and 1 mM PMSF). BCA reagent was used to determine the total protein concentration. The separated proteins were then electrophoretically transferred to a polyvinylidene fluoride membrane. After blocking with 5% fat-free milk in PBST for 2 h at room temperature, the samples were incubated with primary antibodies overnight at 4°C. After being washed three times, the membranes were incubated with horseradish peroxidase-conjugated secondary antibodies at room temperature for 60 min. Finally, an ECL substrate (sc2048, Santa Cruz) was used to visualize the immunoreactive bands. The main antibodies used for Western blot analysis included PLK3 (4896S, 1 : 1000, Cell Signaling), PLK3 (DF4471, 1 : 1000, Afftiny), ATM (ab199726, 1 : 1000, Abcam), p-ATM (ab81292, 1 : 1000, Abcam), P53 (ab179477, 1 : 1000, Abcam), P53 (YT3528, 1 : 1000, Immunoway), p-P53 (9287S, 1 : 1000, Cell Signaling), rH2AX (YP0218,1 : 1000, Immunoway), Bcl-2 (BF9103, 1 : 1000, Affinity), and Bax (GB12-690, 1 : 1000, Servicebio); the relative expression of the targeted protein was normalized to that of β-actin (AC026, 1 : 5000, ABclonal).

2.13. *Histopathological Evaluation and Immunohistochemistry*. After establishing the I/R injury mouse model, 4% paraformaldehyde was infused into the hearts of the mice until the kidneys were completely exsanguinated. The kidneys were harvested, fixed with 4% paraformaldehyde at room temperature, embedded in paraffin, and stained with hematoxylin and eosin. Pathological sections were evaluated under a microscope by a nephropathologist in a blinded manner. Renal tubule damage, including renal tubule dilation, tubular epithelial damage, and cast formation, was scored by determining the percentage of necrotic tubules, and renal tubule damage was graded from 0 to 4 [29].

A commercial kit (ZSGB-BIO, Beijing) was used to perform immunohistochemical staining. Briefly, the sections were incubated with anti-KIM-1 (1 : 500) overnight at 4°C and then incubated with a secondary antibody (1 : 100) for 1 h at room temperature. For quantification, the ratio of optical density was calculated with ImageJ software (version 1.52) to assess the staining intensity.

2.14. *Small Molecule Inhibitors, siRNAs, Plasmids, and Transfection*. The specific ATM inhibitor KU-60019 was purchased from MCE Co., Ltd. (Shanghai, China). PLK3-siRNA was designed and synthesized by IGE Co., Ltd. (Guangzhou, China). The siRNA sequences are shown in Supplementary Table 1. The PLK3 overexpression plasmid was constructed with a pcDNA3.1 vector with a 3× Flag tag. Before transfection, HK-2 cells were seeded in 6-well plates and incubated at 37°C in 5% CO_2 until they reached 60%-70% confluence. The siRNAs and plasmids were transfected by using Lipofectamine 2000 transfection reagent in Opti-MEM. The siRNA-NC and pcDNA3.1 vector served as the negative controls. After 6 h, the Opti-MEM was replaced with DMEM/F-12 medium supplemented with 10% FBS, and the cells were further cultured. Then, qRT–PCR

and Western blot were used to evaluate gene knockdown and overexpression efficiency.

2.15. *Statistical Analysis*. R software version 4.0.4 was used for bioinformatics analysis. All statistical analyses were performed using GraphPad Prism 8.0 (GraphPad, La Jolla, CA, U.S.A.). Data are presented as the mean ± SD. Two-tailed unpaired t-test was used for comparisons between two groups, and one-way analysis of variance (ANOVA) was used for multigroup comparisons. A value of $P < 0.05$ was considered statistically significant.

3. Results

3.1. *Identification of DEGs in Wild-Type (WT) Mice and Screened PLK3 in Four Distinct Cellular Subgroups*. A total of 821 (379 upregulated and 442 downregulated) DEGs were identified between the WT mice in the I/R injury (24 h) and sham groups from GSE52004 by GEO2R ($|logFC| > 1.5$, adj.$P < 0.05$) (Figure 1(a)). Interestingly, we found that PLK3 and the two most common markers of renal injury (Kim1 and Ngal) were among the top five upregulated DEGs (Figure 1(b)). PLK3 has not been previously described in studies of renal I/R injury, so we continued to compare the PLK3 translation profiles of four distinct cellular subgroups. PLK3 was highly expressed in all the cell groups, especially in interstitial cells (Foxd1) and TECs (Six2) (Figure 1(c)). The TRAP-seq validation dataset GSE121191 (adj.$P < 0.05$) also confirmed the significantly increased expression of PLK3 in renal TECs after 48 h of I/R injury (Figure 1(d)). Notably, the single-cell RNA-seq data from normal kidneys in the Human Protein Atlas indicated that the expression level of PLK3 in normal TECs was lower than that in immune cells (Figure 1(e)). GO enrichment analysis was used to verify the potential function of PLK3 in I/R injury. The TRAP-WT results suggested that PLK3 was significantly enriched in GO terms of biological processes, including oxidative stress, cell cycle, and DNA damage (Figure 1(f)). On the other hand, the TRAP-Nephron results suggested that PLK3 was mainly involved in the hypoxic response, oxygen level regulation, oxidative stress, and DNA damage response (Figure 1(g)). These biological processes are extremely important in ischemic AKI, suggesting that PLK3 may play an important role in renal I/R injury.

3.2. *PLK3 Was Upregulated in Response to H/R Injury in TECs and I/R Injury in the Renal Cortex*. We first examined the mRNA expression levels of PLK3 in HK-2 cells exposed to different hypoxic conditions and different reoxygenation times in the H/R model. The results showed that PLK3 mRNA expression was significantly higher in the H/R group than in the normoxia group, and its expression gradually increased with increasing hypoxia duration (Figure 2(a)). Similarly, PLK3 protein expression was also increased after H/R stimulation, and the highest protein level was observed after 24 h of hypoxia and 6 h of reoxygenation (Figure 2(b)). Since oxidative stress occurs mainly during the reoxygenation stage, we examined the changes in PLK3 expression in

(a)

(b)

(c)

(d)
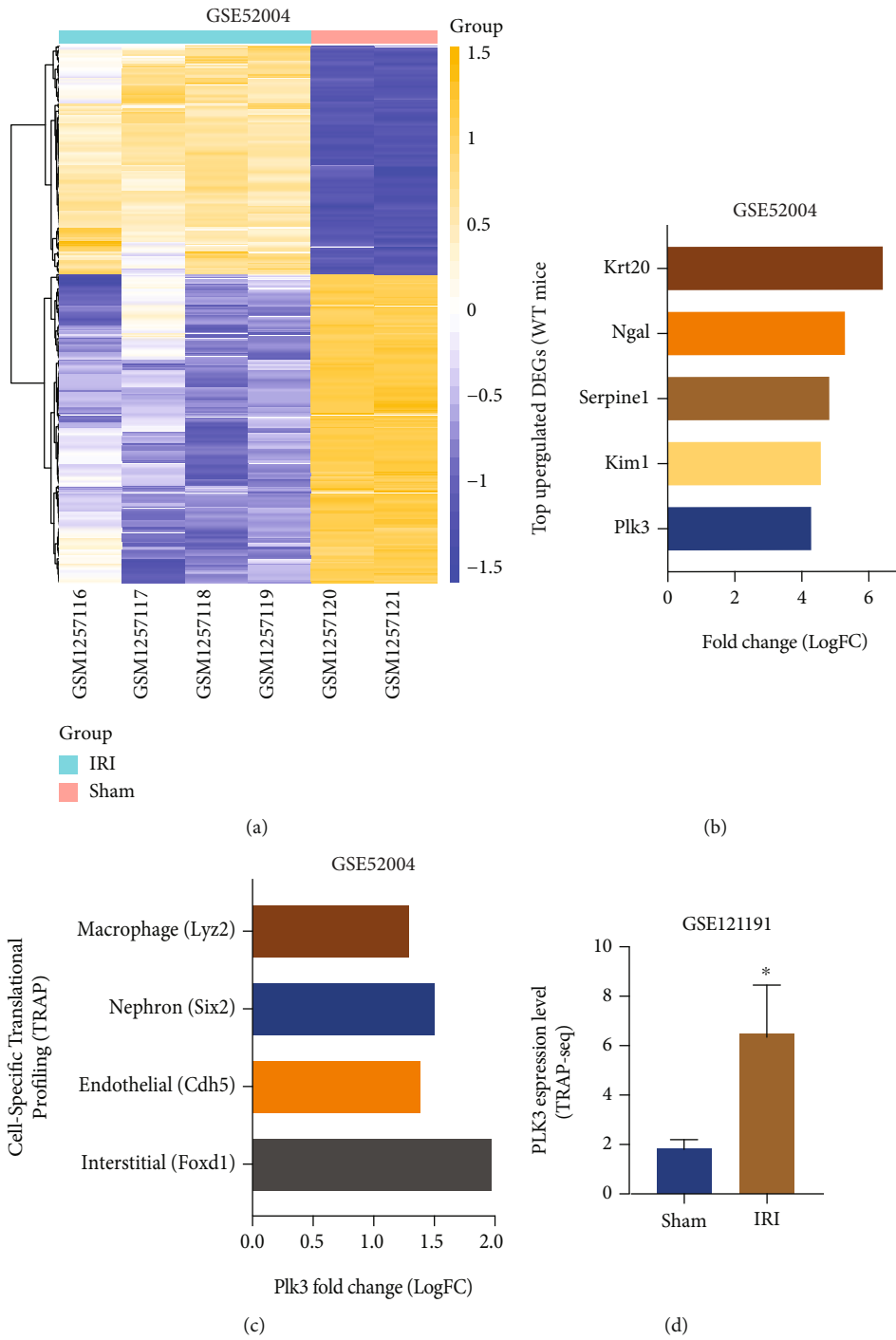
Figure 1: Continued.

(e)

(f)

Figure 1: Continued.

(g)
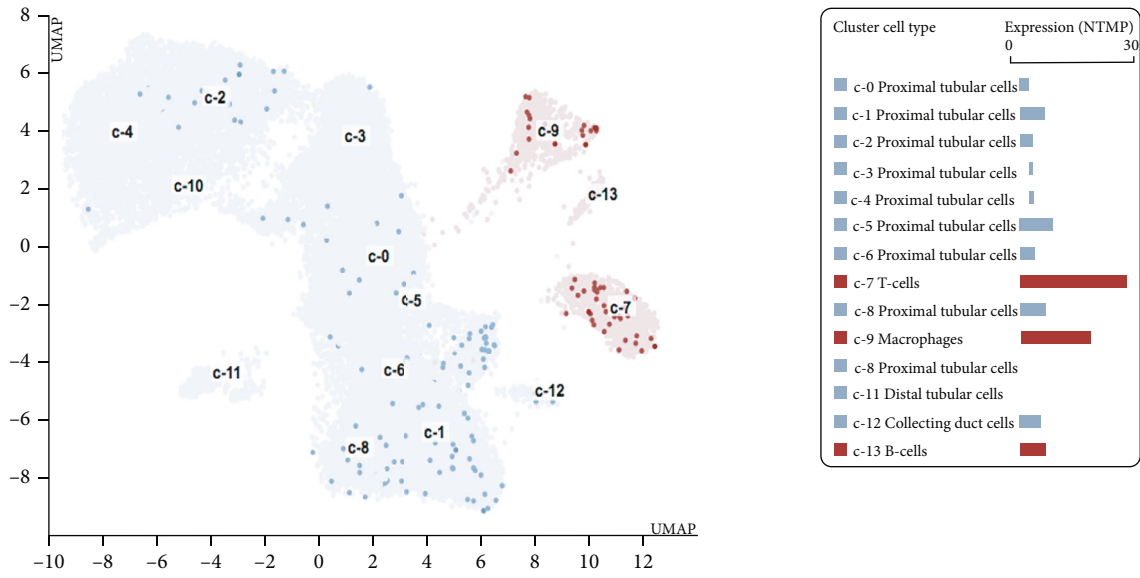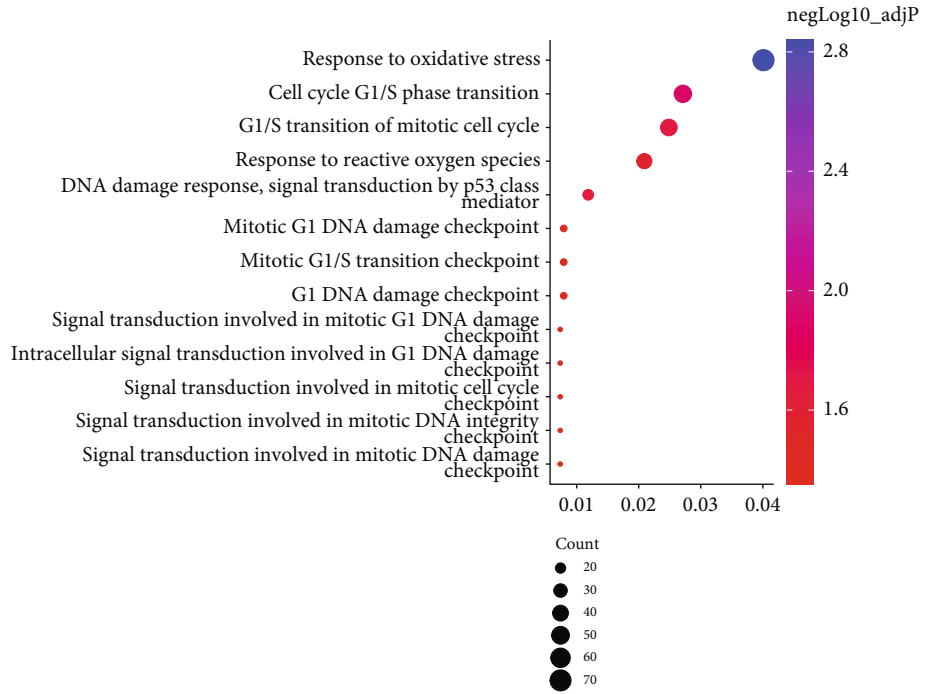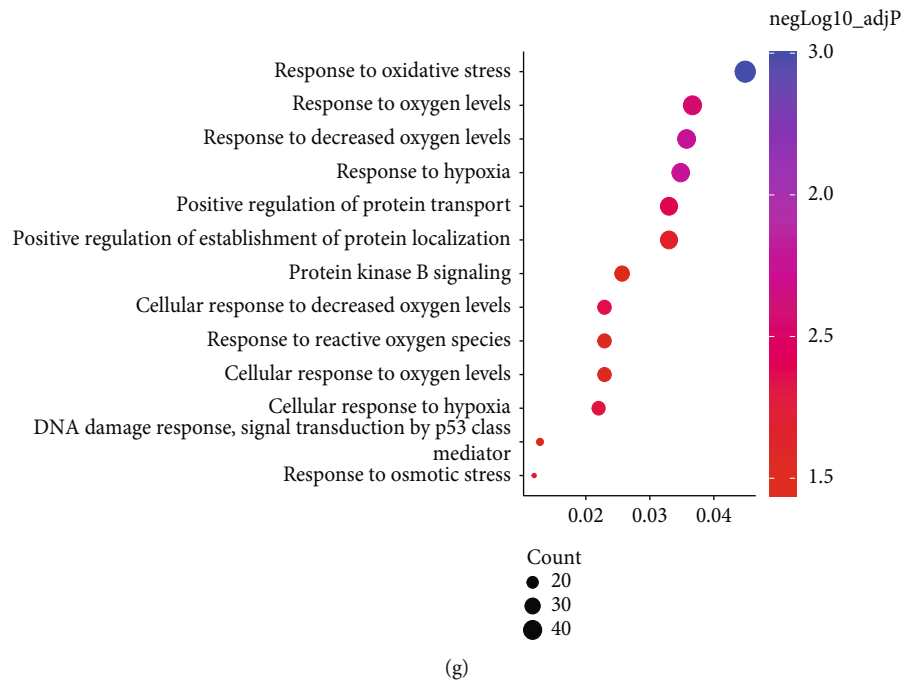
FIGURE 1: Bioinformatics analysis of PLK3 expression in renal TECs. (a) The heatmap shows the expression levels of the upregulated and downregulated DEGs (GSE52004). (b) Top 5 upregulated DEGs in TRAP-seq analysis of WT mice. (c) The expression level of PLK3 in four different cell subgroups 24 h after renal I/R injury. (d) The expression level of PLK3 in the TRAP-seq validation dataset (GSE121191) after renal I/R injury. (e) The expression level of PLK3 in single-cell RNA-seq data of normal kidney TECs derived from the Human Protein Atlas (GSE131685). (f) Bubble plots showing the enriched GO terms for PLK3-related biological processes in IRI vs. sham (TRAP-WT) DEGs. (g) Bubble plots showing the enriched GO terms for PLK3-related biological processes in IRI vs. sham (TRAP-Nephron) DEGs. The data are presented as the mean ± SD. $n = 3$. $^{*}P < 0.05$.

response to different reoxygenation times after 24 h of hypoxia, and the results demonstrated that PLK3 expression was higher at 6 h than at 3 h, and there was no additional increase after 6 h (Figure 2(c)). Therefore, 24 h of hypoxia and 6 h of reoxygenation were chosen as the time points for subsequent in vitro experiments.

In parallel, we examined the expression of PLK3 in the renal cortex by establishing a mouse model of I/R injury. Consistently, the mRNA and protein levels of PLK3 increased with increasing reperfusion time (Figures 2(d)–2(f)). Moreover, the kidney injury pathology score and enzymatic analyses results (creatinine and BUN levels) suggested that the kidney was most severely damaged at 24 h after the restoration of perfusion (Figures 2(g) and 2(h) and Supplementary Fig. 1A). In addition, the immunofluorescence results revealed a significant increase in PLK3-positive staining in renal tubules with increasing reperfusion time (Figure 2(e)). These results indicated that PLK3 was involved in the progression of renal I/R injury.

3.3. PLK3 Inhibition Enhanced Cell Viability and Reduced TEC Apoptosis in H/R Injury. We successfully constructed PLK3 overexpression plasmids and targeted siRNA sequences (Figures 3(a) and 3(b) and Figures 4(a) and 4(b)). First, a CCK-8 assay was used to measure cell viability. Compared with normoxic conditions, H/R injury significantly reduced the number of viable cells, while PLK3 overexpression further reduced cell viability (Figure 3(c)). However, silencing PLK3 expression enhanced cell viability

under H/R conditions (Figure 4(c)). To investigate the effect of PLK3 on H/R-induced apoptosis of TECs, the incidence of apoptosis was assessed by flow cytometry and TUNEL assays. Flow cytometry revealed that PLK3 overexpression increased TEC apoptosis (Figure 3(d)). Notably, PLK3-targeted siRNA reduced the percentage of apoptotic cells observed after H/R injury (Figure 4(d)). TUNEL assays showed that the PLK3 plasmid increased the number of TUNEL-positive cells compared to the number of TUNEL-positive cells in the group exposed to H/R alone (Figure 3(e)), while inhibiting PLK3 expression decreased the number of apoptotic TECs (Figure 4(e)).

3.4. I/R Injury- and H/R Injury-Induced Exacerbation of Oxidative Stress and DNA Damage in TECs. We investigated the degree of oxidative stress in the I/R injury and H/R injury models. Compared with those in the sham-operated group, the MDA levels were increased and SOD activity was decreased in the renal cortex in the I/R injury group (Figures 5(a) and 5(b)). The results also showed that oxidative stress damage worsened with prolonged reperfusion time. Additionally, $H_2DCFH-DA$ and DHE staining in the H/R model further confirmed this result (Figures 5(c) and 5(d)). These findings suggested that I/R or H/R exacerbated oxidative stress in TECs. In mammalian cells, rH2AX is a marker of DSBs in response to DNA damage [30]. Immunofluorescence analysis suggested a marked increase in γH2AX-positive TECs after H/R injury compared with that

(a)

(b)

(c)

(d)

Figure 2: Continued.

(e)

(f)

(g)

(h)
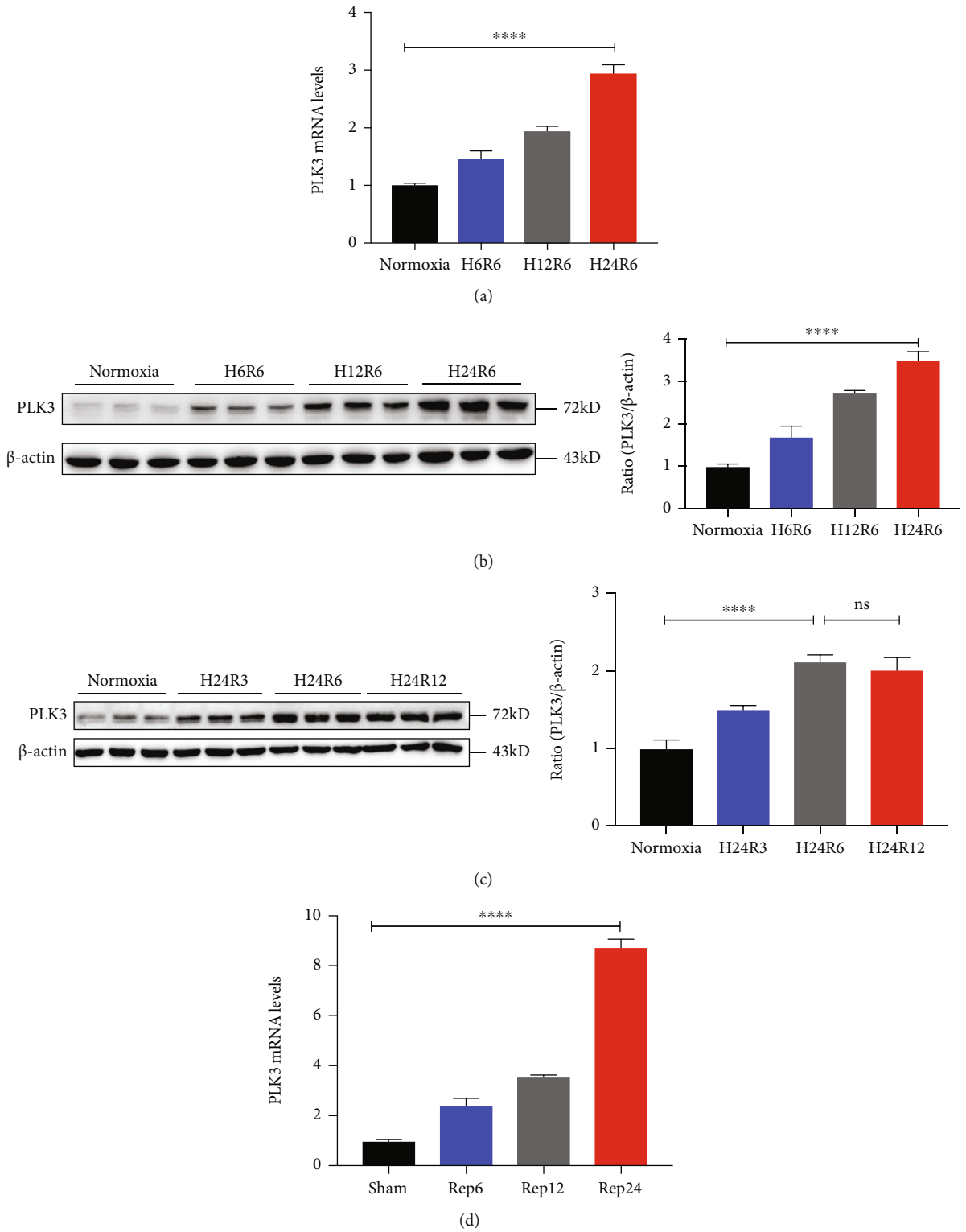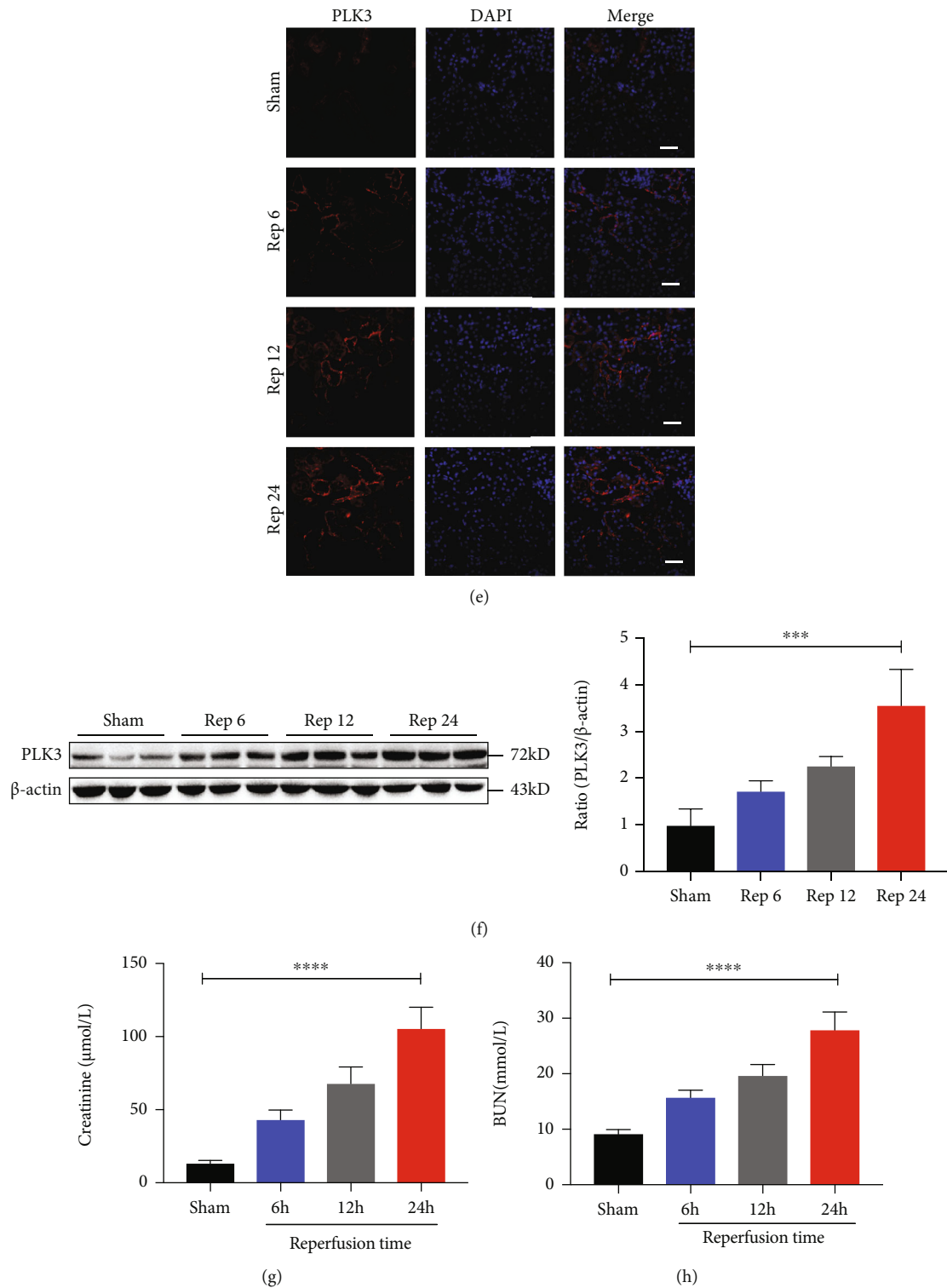
FIGURE 2: PLK3 expression was upregulated in TECs exposed to H/R injury and kidneys exposed to I/R injury. (a) PLK3 mRNA levels in HK-2 cells were measured by real-time RT–PCR after hypoxia and reoxygenation for different time periods. (b) PLK3 protein levels were measured by Western blot after different hypoxia time periods and the same reoxygenation time period. (c) PLK3 protein levels after the same hypoxia time period and different reoxygenation time periods. (d) PLK3 mRNA levels in the kidneys of C57BL/6J mice exposed to I/R were examined after 30 min of ischemia and different reperfusion times (6 h, 12 h, and 24 h). (e) PLK3 protein levels after different reperfusion times were observed by immunofluorescence (bar = 50 μM; magnification, 400x). (f) PLK3 protein levels were measured after different reperfusion times. (g-h) Creatinine and BUN levels after different reperfusion times. The data are presented as the mean ± SD. $n \geq 3$. $^*P < 0.05$, $^{**}P < 0.01$, $^{***}P < 0.001$, and $^{****}P < 0.0001$. BUN: blood urea nitrogen; H24R3: hypoxia for 24 h and reperfusion for 3 h; Rep24: ischemia for 30 min and reperfusion for 24 h.

(a)

(b)

(c)

(d)

Figure 3: Continued.

(e)
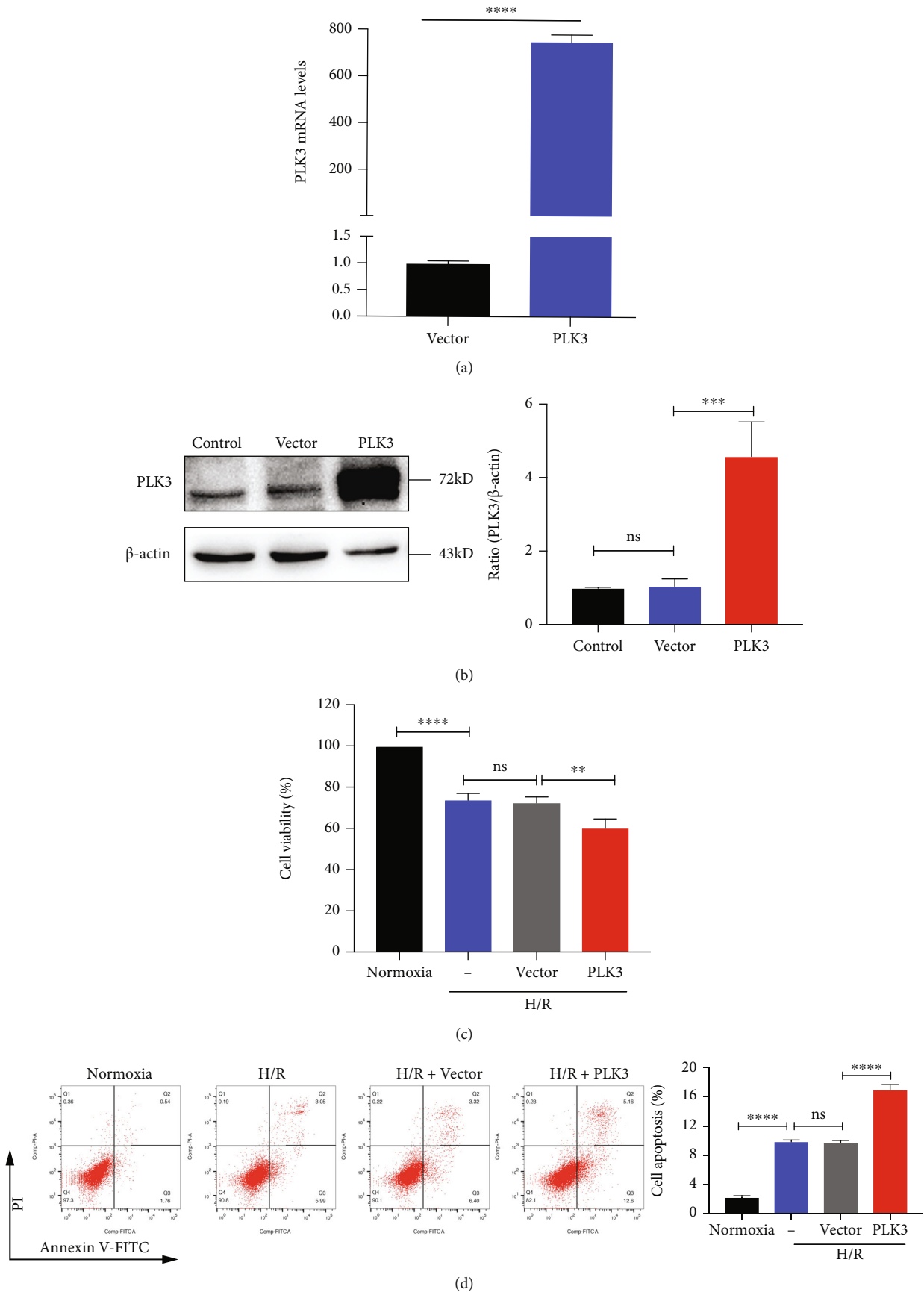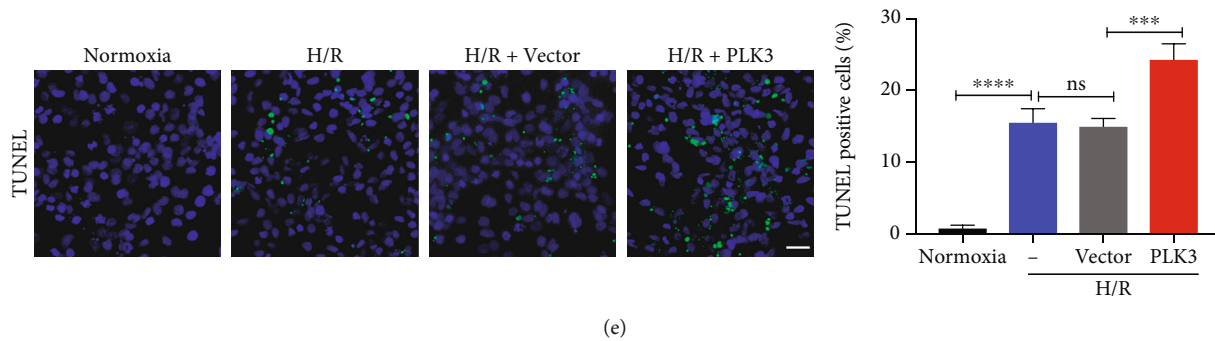
FIGURE 3: PLK3 overexpression promotes the TEC apoptosis caused by H/R injury. (a and b) Quantitative analysis and representative Western blot images of PLK3 mRNA and protein expression after transfection with the pcDNA3.1-flag-PLK3 plasmid. (c) CCK-8 reagent was used to evaluate the viability of HK-2 cells transfected with plasmids after H/R injury. (d) Representative graphs of the flow cytometry results showing apoptotic populations and quantitative analysis of apoptosis rates. (e) TUNEL staining to measure DNA fragmentation during apoptosis (bar = 50 μM; magnification, 400x). The data are presented as the mean ± SD. $n = 3$. $^{*}P < 0.05$, $^{**}P < 0.01$, $^{***}P < 0.001$, and $^{****}P < 0.0001$.

after exposure to normoxia (Figure 5(e)), and the Western blot results also confirmed significant upregulation of γH2AX protein levels. As shown in Figure 5(f), the ATM phosphorylation and P53 phosphorylation levels were dramatically elevated by H/R injury, further suggesting that the DDR could be induced after H/R injury. In addition, in the H_2O_2-induced oxidative stress model, we stimulated HK-2 cells with different concentrations of H_2O_2, and the results showed that the expression of PLK3 was significantly increased (Figures 5(g) and 5(h)). In summary, these findings suggest that H/R injury can induce oxidative stress-mediated DNA damage, which may be an essential factor for TEC apoptosis.

3.5. Inhibiting PLK3 Attenuated TEC Apoptosis by Regulating P53-Mediated Apoptosis Pathways in Response to H/R Injury. P53 can be activated to initiate apoptotic signaling after DNA damage. To investigate whether elevated PLK3 expression due to the DDR correlates with the phosphorylation and activation of P53, we examined the P53 phosphorylation levels in H/R-exposed TECs in which PLK3 expression was silenced. The results showed that low levels of PLK3 expression were accompanied by reduced P53 phosphorylation. Interestingly, knockdown of PLK3 expression did not alter the hypoxia-induced increase in total P53 levels. This result suggests that PLK3 acts as a protein kinase and is involved in the phosphorylation of P53 associated with the DDR. P53 activation may lead to apoptosis, and this effect is governed by a series of apoptotic genes, including Bcl-2 and Bax. Compared to cells cultured under normoxic conditions, cells exposed to H/R exhibited elevated expression of the proapoptotic gene Bax and decreased expression of the antiapoptotic gene Bcl-2. However, the expression of Bax in PLK3-KD TECs was significantly lower than that in si-NC-transfected cells, but Bcl-2 expression was elevated and the Bax/Bcl-2 ratio was reversed (Figure 6(a)). These results suggested that inhibiting PLK3 expression could attenuate downstream proapoptotic factors, leading to TEC apoptosis by reducing the phosphorylation of P53 during the DDR.

3.6. ATM Mediated the Induction of PLK3 in H/R Injury in TECs. ATM is one of the first sensors that is activated during the DDR. To determine whether ATM affects PLK3 expression, we used the specific ATM inhibitor KU-60019 and explored its inhibitory effect on PLK3 in HK-2 cells subjected to H/R for different times (Supplementary Fig. 2A). Western blot analysis showed that inhibiting p-ATM activation decreased the PLK3-induced P53 phosphorylation, thereby blocking the proapoptotic response downstream of P53 (Figure 6(b)). These results suggest that ATM, which is upstream of the DDR, can induce TEC apoptosis through the PLK3/P53 pathway in the presence of severe DNA damage.

3.7. The Alleviating Effects of ATM Inhibition on TEC Apoptosis Were Reversed by PLK3 Overexpression. We added KU-60019 to inhibit the DDR in HK-2 cells subjected to H/R injury and then transfected the cells with PLK3 overexpression plasmid. Western blot revealed no significant changes in the ATM phosphorylation levels, but the p-P53 levels were significantly increased, and the Bax/Bcl-2 ratio was elevated (Figure 7(a)). These results suggested that activation of PLK3, a downstream effector molecule of ATM, alone can also increase the phosphorylation of P53 to promote TEC apoptosis. In addition, we used flow cytometry and TUNEL assays to examine TEC apoptosis in vitro to verify these results (Figures 7(b) and 7(c)).

3.8. Knockdown of PLK3 Alleviated Renal Dysfunction and Tubular Damage in I/R-Induced AKI. PLK3 expression was disrupted in C57BL/6J mice by renal vein injection of the rAAV9-PLK3-KD plasmid (Figure 8(a)). Real-time PCR and Western blot showed that the PLK3 mRNA and protein levels were significantly downregulated after 28 days (Supplementary Fig. 2B-C). Body weight measurements suggested that the injection of the rAAV-9 virus had no significant effect on body weight (Supplementary Fig. 2D). In mice suffering from I/R injury, the serum creatinine and BUN levels were significantly increased, while PLK3-KD decreased the serum creatinine and BUN levels after I/R injury (Figures 8(b) and 8(c)). Renal tubular damage is

(a)

(b)

(c)

(d)

(e)
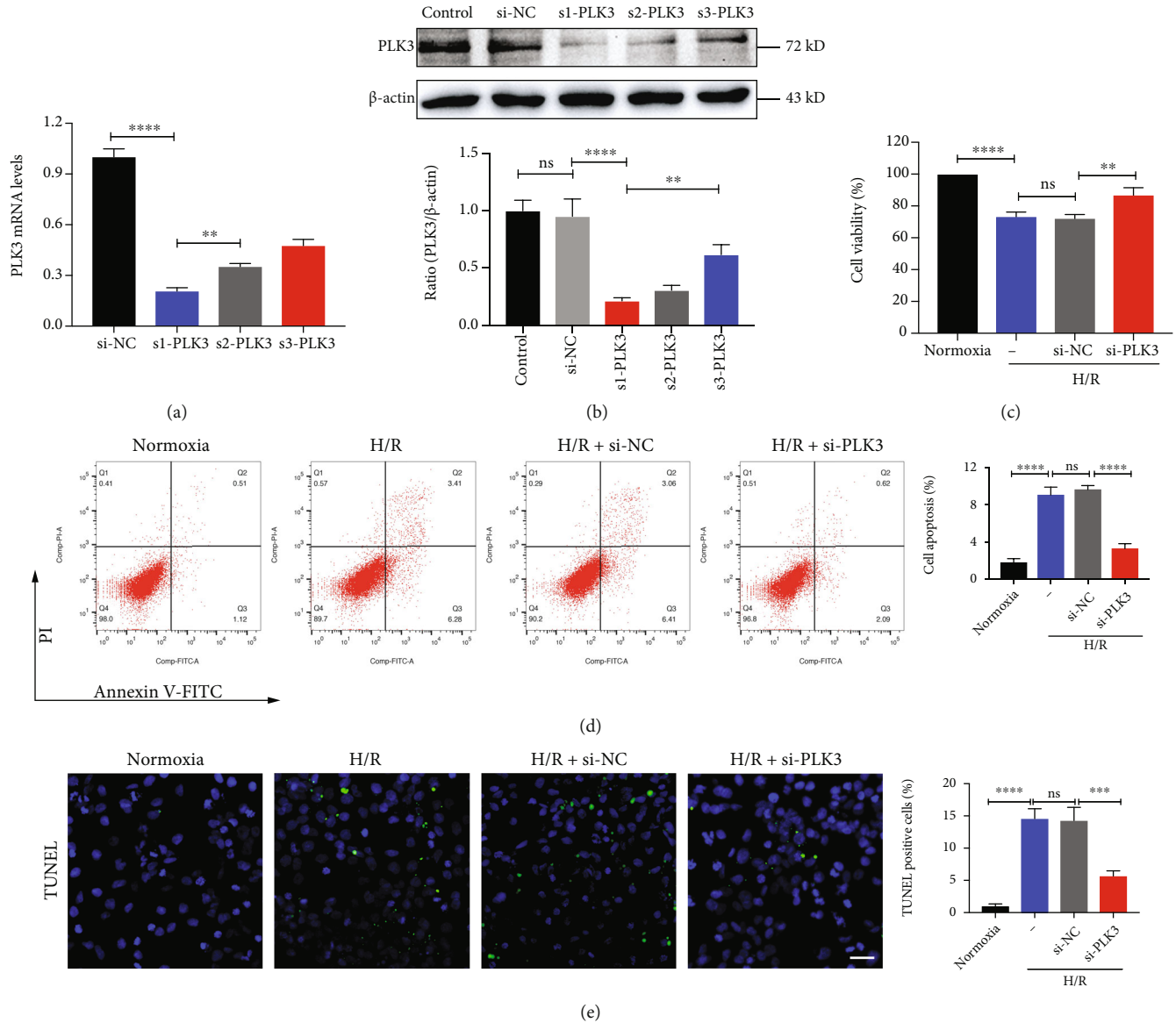
FIGURE 4: Targeted silencing of PLK3 expression reduces H/R-induced apoptosis in TECs. (a) qRT–PCR analysis of PLK3 mRNA expression after transfection with 100 nM PLK3-siRNA or scrambled oligonucleotide (si-NC). (b) Immunoblotting analysis of PLK3 silencing efficiency. (c) The viability of HK-2 cells was measured by CCK-8 assays. (d) Flow cytometry was performed to examine HK-2 cell apoptosis. (e) Representative images showing TUNEL-positive HK-2 cells after PLK3 silencing (bar = 50 μM; magnification, 400x). The data are presented as the mean ± SD. $n = 3$. $^{*}P < 0.05$, $^{**}P < 0.01$, $^{***}P < 0.001$, and $^{****}P < 0.0001$.

characterized by tubular dilatation, swelling, necrosis, and/or tubular congestion. Renal injury was evident in mice subjected to I/R injury, and PLK3-KD treatment alleviated this injury (Figure 8(d)). Immunohistochemical analysis of the expression of KIM-1, a marker of renal tubular injury, further confirmed that PLK3-KD attenuated I/R-induced AKI (Figure 8(d)). These results suggest that activating PLK3 in mice with I/R-induced AKI may be a key factor in susceptibility to AKI and that inhibiting PLK3 has a protective effect against ischemic AKI.

3.9. Inhibiting PLK3 Could Reduce TEC Apoptosis in I/R-Induced AKI. Immunofluorescence was performed to measure the expression of PLK3 in the renal cortical region,

and the results suggested that PLK3-positive staining was diminished in PLK3-KD mice compared with rAAV9 mice. The TUNEL assay was used to examine genomic DNA fragmentation during apoptosis, and the results revealed significantly decreased positive staining in the renal cortex of PLK3-KD mice, indicating that blocking PLK3 expression reduced apoptosis and DNA fragmentation in TECs (Figure 9(a)). Moreover, we extracted the renal cortex, which contains a large number of nephrons, from mice with I/R-induced AKI for Western blot. The results indicated that I/R injury enhanced P53 phosphorylation and Bax expression and decreased Bcl-2 expression compared with the control, whereas PLK3-deficient mice showed significantly reduced P53 phosphorylation and Bax expression and enhanced

(a)

(b)

(c)

(d)

(e)

Figure 5: Continued.

(f)

(g)

(h)
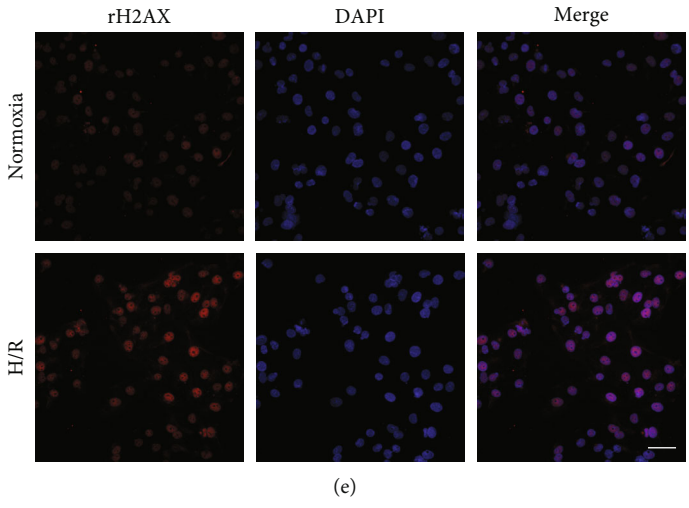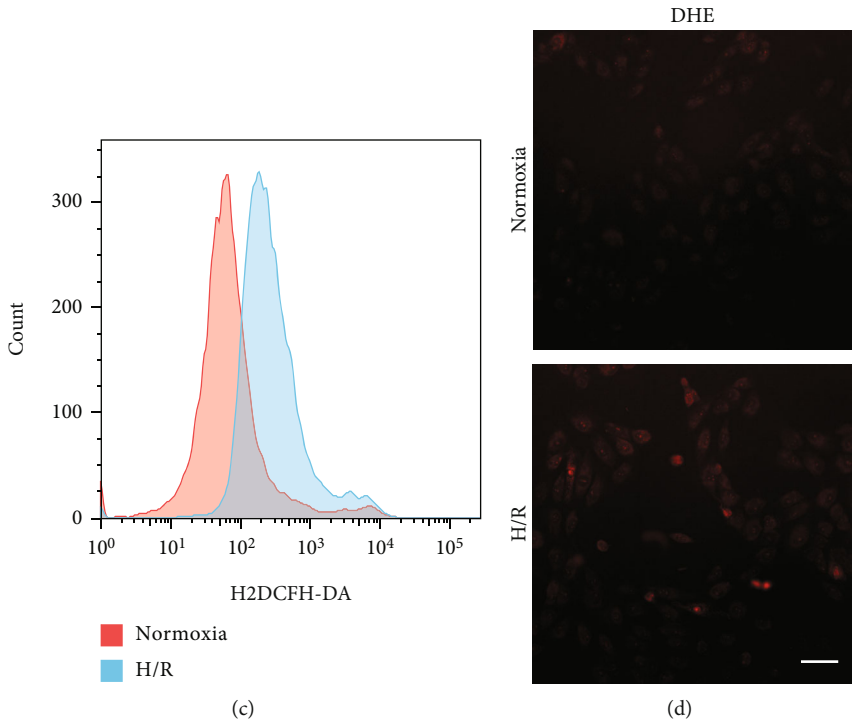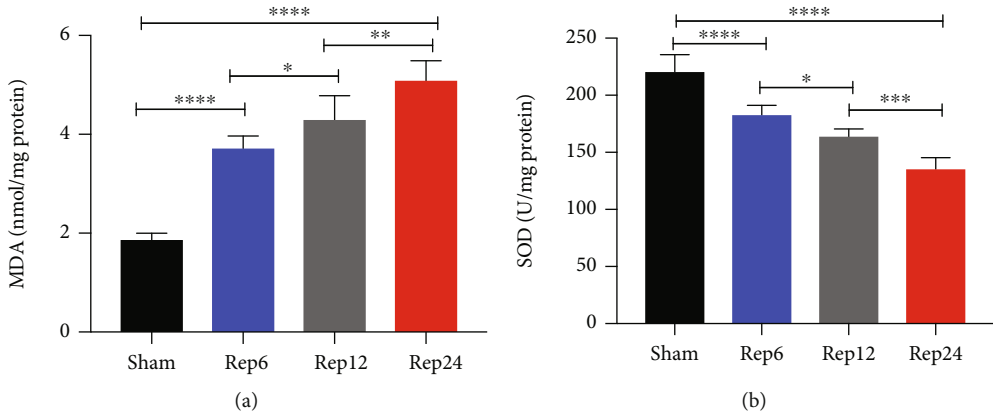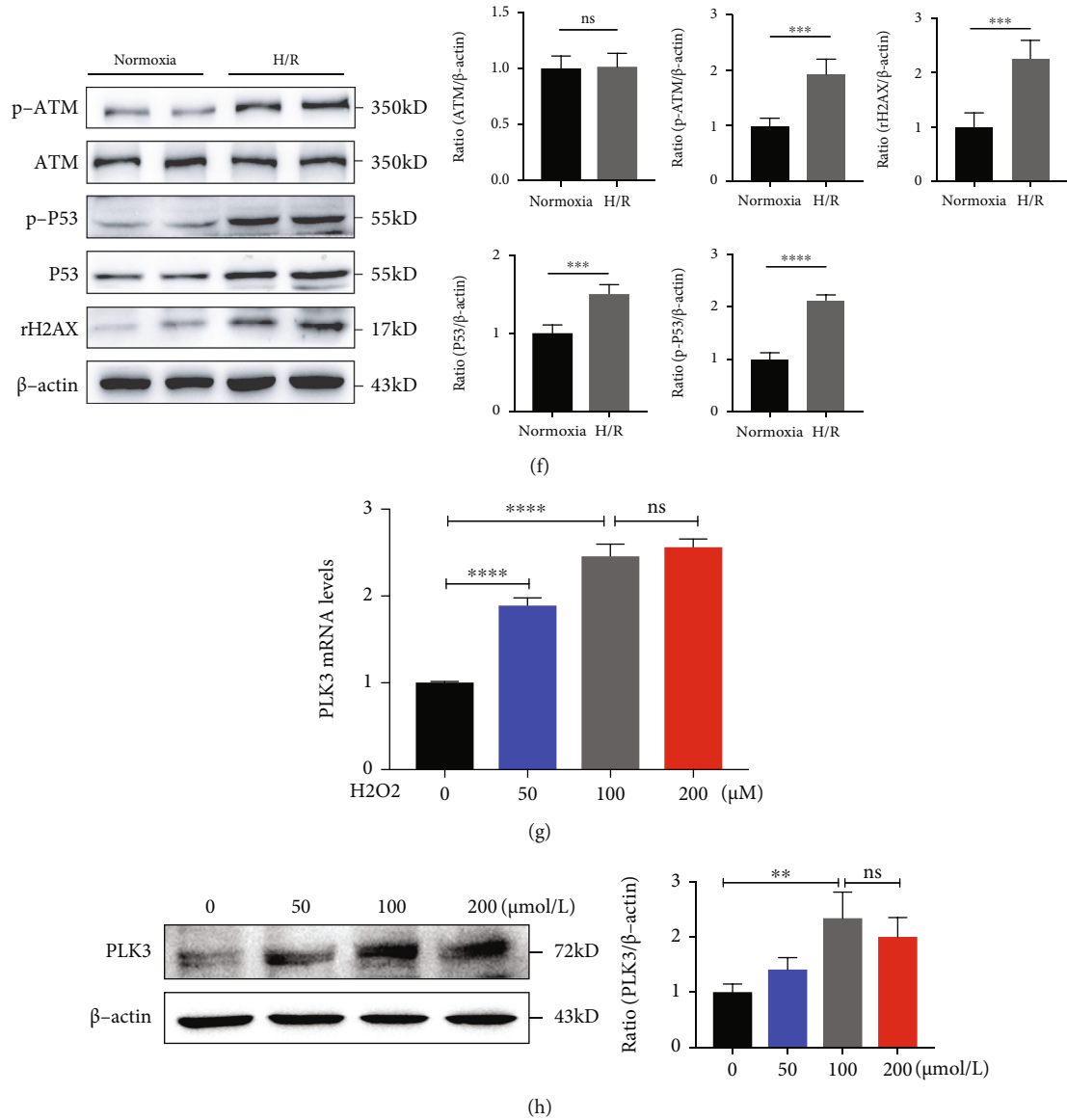
FIGURE 5: Oxidative stress and the DDR were induced during H/R injury in TECs and I/R injury in mouse kidneys. HK-2 cells were subjected to normoxia or hypoxia for 24 h/reoxygenation for 6 h. C57BL/6J male mice were subjected to sham operation or 30 min of bilateral renal ischemia, followed by 24 h of reperfusion. (a and b) MDA levels and SOD activity in renal cortex homogenates were analyzed. (c and d) Flow cytometric analysis of H_2DCFH-DA staining and cytofluorometric analysis of DHE staining were performed to measure the levels of cellular ROS production after H/R treatment (bar = 50 μM; magnification, 400x). (e) Representative images of immunofluorescence staining of γH2AX in TECs (bar = 50 μM; magnification, 400x). (f) The expression of DNA damage-related proteins was measured by Western blot after H/R injury. (g) PLK3 mRNA levels in the H_2O_2-induced oxidative stress model. (h) PLK3 protein levels after H_2O_2 stimulation. The data are presented as the mean ± SD. $n = 3$. $^*P < 0.05$, $^{**}P < 0.01$, $^{***}P < 0.001$, and $^{****}P < 0.0001$. DHE: dihydroethidium; MDA: malondialdehyde; SOD: superoxide dismutase.

Bcl-2 expression after I/R injury (Figure 9(b)). These results suggest that inhibiting PLK3 can reduce DNA damage and thus protect against TEC apoptosis during ischemic AKI.

4. Discussion

In a complex tissue such as the kidney, the high degree of cellular heterogeneity complicates the analysis of gene expression profiles derived from whole tissues. Comprehensive transcriptional profiles and gene expression profiles of specific cell types in complex tissues are essential for understanding the roles of genes in different cells [31]. The advantage of TRAP versus other gene expression profiling methodologies is that it allows in situ analysis of the mRNA profile of any genetically defined cell type, and the results match protein expression results more closely than the results of total RNA gene expression profiling [32]. Renal tubules are portion of the kidney that is most vulnerable to I/R injury, and renal tubules contribute most strongly to renal failure. To better characterize the molecular and
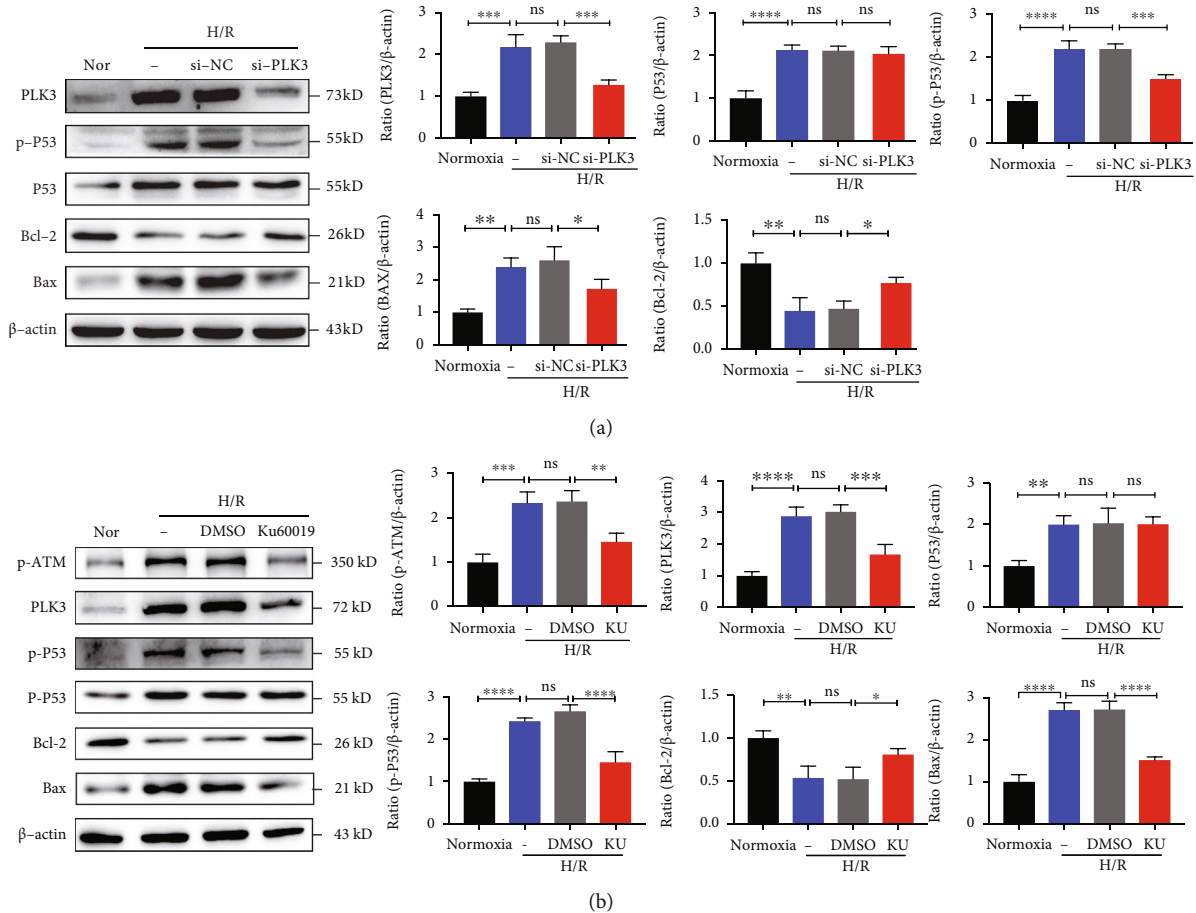
FIGURE 6: Inhibiting PLK3 attenuates TEC apoptosis via the ATM/P53 signaling pathway. (a) In the H/R injury model, the PLK3 protein levels and apoptosis-related protein levels were measured after targeted KD of PLK3 expression. (b) p-ATM protein levels, PLK3 protein levels, and apoptosis-related protein levels were measured by Western blot after the application of the specific ATM inhibitor KU-60019. The data are presented as the mean ± SD. $n = 3$. $^{*}P < 0.05$, $^{**}P < 0.01$, $^{***}P < 0.001$, and $^{****}P < 0.0001$. Nor: normoxia; Ku: KU-60019.

cellular events related to AKI, we used the TRAP-seq results in the GEO database to examine PLK3 expression in the translation profile of nephrons (tubules) exposed to IRI for 24 h.

GO analysis showed that PLK3 was mainly involved in oxidative stress and DNA damage after renal I/R injury. DNA damage has been reported to be involved in I/R injury in a variety of vital organs, including the testicular, brain, liver, and heart [33–36]. During renal I/R injury, DNA fragmentation in the renal tubules after DNA damage occurs as early as 12 h after reperfusion and increases within 24 h [37]. In vitro, significant DNA damage occurs in rat proximal renal TECs after 5 min of hypoxia and 30 min of reoxygenation, and DSBs are exacerbated in a time-dependent manner [38]. AKI caused by sepsis, ischemia, or nephrotoxic drugs can lead to rapidly progressive renal dysfunction. Genomic DNA damage plays a critical role in the phenotypic changes in TECs and the subsequent loss of renal function. In nephrotoxic and ischemic AKI, TRIP13 deletion leads to increased DNA damage and activation of apoptotic signaling, resulting in TEC injury [39]. Endogenous salbutamol-β treatment exacerbates sepsis-related and nephrotoxic AKI by activating the ROS/DNA damage/P53 apoptotic

pathway [11]. CCN2 exacerbates ischemic AKI by increasing the expression of γH2AX and p-P53 through oxidative DNA damage [40]. The degree of DNA damage is inversely correlated with the estimated glomerular filtration rate (eGFR) [41]. Therefore, activation of the DDR signaling pathway may represent a common mechanism that leads to AKI. Studies have confirmed that HMSCs and high-dose vitamin B12 protect renal function after I/R injury by reducing renal superoxide levels and lipid peroxidation, thereby attenuating the DDR and TEC apoptosis [42, 43]. After renal I/R injury, application of BA (boric acid) decreased the degree of DNA damage by preventing partially oxidative stress [44]. Our current study also confirmed that inhibition of PLK3, a phosphokinase directly involved in the DNA damage cascade response, protects TECs from renal I/R injury.

PLK3 has never been examined in the context of renal I/R injury. In the present study, we found significant upregulation of PLK3 expression in renal TECs in response to H/R injury and renal I/R injury. We observed renal injury and PLK3 expression changes in the I/R model with bilateral renal ischemia for 30 min and reperfusion for different times (6 h, 12 h, and 24 h). With the prolongation of reperfusion time, the expression of PLK3 showed the same trend as the

(a)

(b)

(c)
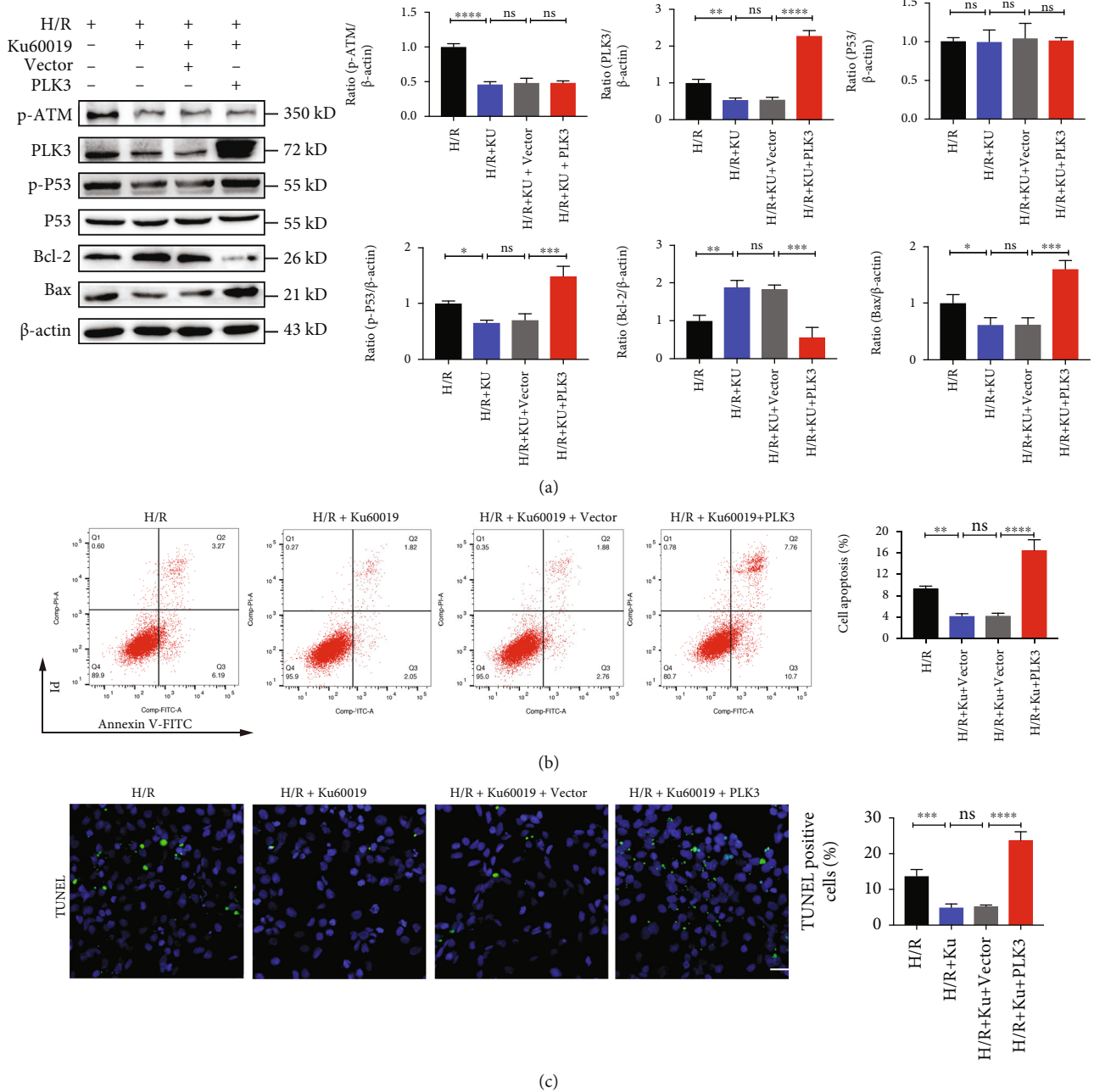
FIGURE 7: PLK3 overexpression reverses the effect of ATM inhibition in alleviating TEC apoptosis. (a) p-ATM protein levels, PLK3 protein levels, and apoptosis-related protein levels were measured by Western blot after the application of KU-60019 and PLK3 plasmid. (b) Flow cytometry was performed to examine the apoptosis of HK-2 cells after the administration of KU-60019 and PLK3 plasmids. (c) TUNEL assays showed the number of apoptotic HK-2 cells. The data are presented as the mean ± SD. $n = 3$. $^{*}P < 0.05$, $^{**}P < 0.01$, $^{***}P < 0.001$, and $^{****}P < 0.0001$.

indicators of renal function (creatinine and BUN), suggesting that the expression of PLK3 was related to the severity of renal injury. When cells are subjected to I/R injury, large amounts of ROS are produced, which disrupt the balance between oxidative and antioxidant systems and ultimately lead to oxidative stress [45]. ROS induced by I/R injury in vivo or H/R injury in vitro can lead to a series of severe damaging effects, such as lipid peroxidation, mitochondrial damage, and increased susceptibility to renal tubular injury

[46]. Similarly, DNA damage due to H/R injury in vitro is mainly caused by oxidative stress associated with the reoxygenation-induced production of ROS [47]. To confirm the occurrence of oxidative stress and DNA damage in our in vitro model, we used a ROS fluorescent probe to measure ROS production and immunofluorescence analysis to observe rH$_2$AX staining. The results showed significant oxidative stress and DSBs. To further confirm that PLK3 can be activated by oxidative stress, we measured PLK3 expression

(a)

(b)

(c)

(d)
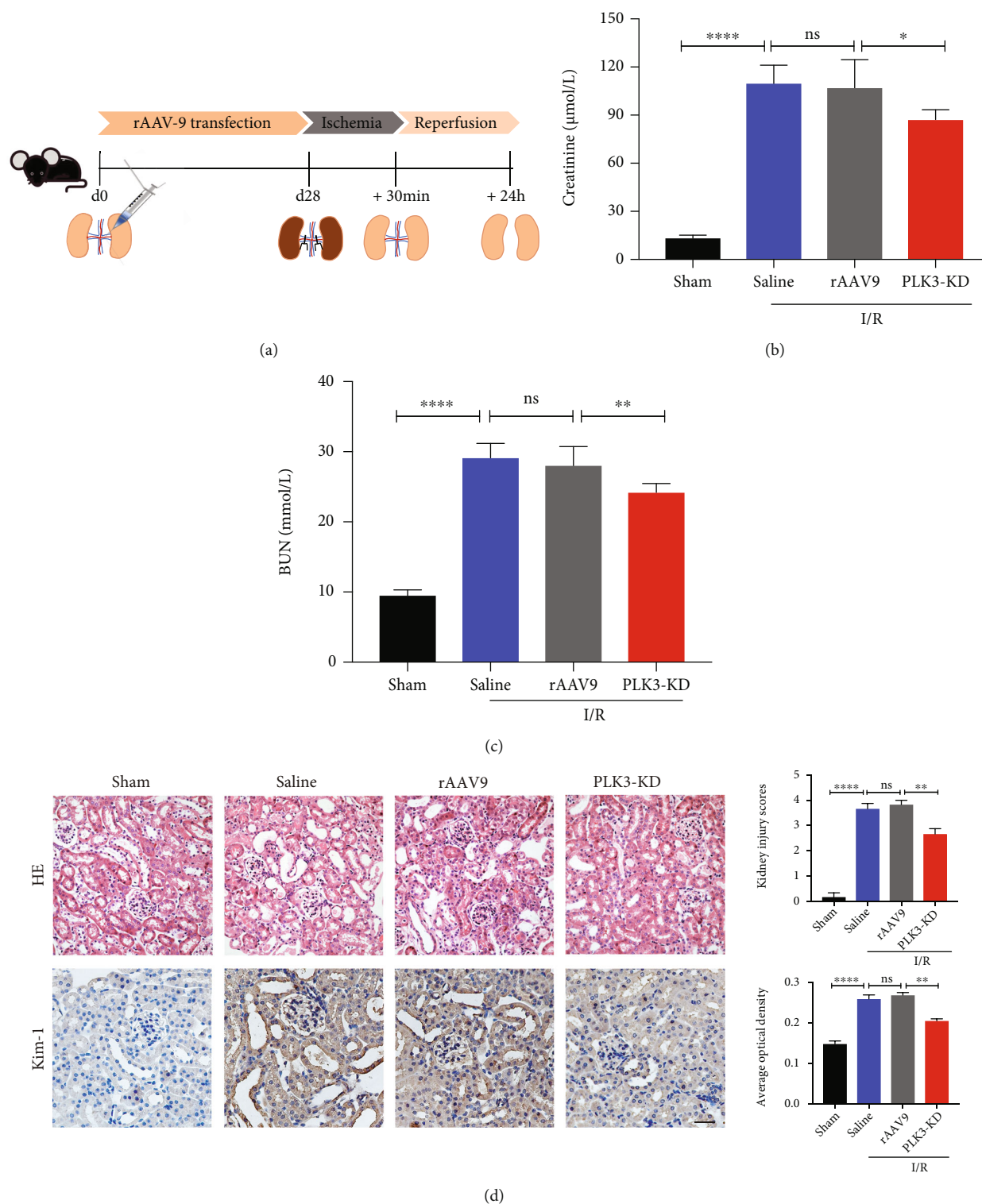
FIGURE 8: rAAV-9-mediated PLK3 KD attenuates I/R-induced AKI in mice. (a) Schematic diagram illustrating the animal experimental design. (b and c) Serum creatinine and BUN assays. (d) Sections of kidney tissue were stained with H&E, and tubular damage was quantified; KIM1 expression was examined by immunohistochemistry (bar = 50 μM; magnification, 400x). The data are presented as the mean ± SD. $n \geq 3$. $^{*}P < 0.05$, $^{**}P < 0.01$, and $^{****}P < 0.0001$.

and observed significantly elevated PLK3 expression in H$_2$O$_2$-stimulated HK-2 cells.

ATM plays dual roles in DNA damage due to I/R. It plays a protective role during ischemic preconditioning but

promotes cell death in lethal ischemic injury [48]. As one of the key transducers of the DDR, ATM undergoes rapid autophosphorylation at serine 1981 after DNA damage; then, ATM is recruited to the site of DNA damage to initiate

(a)

(b)
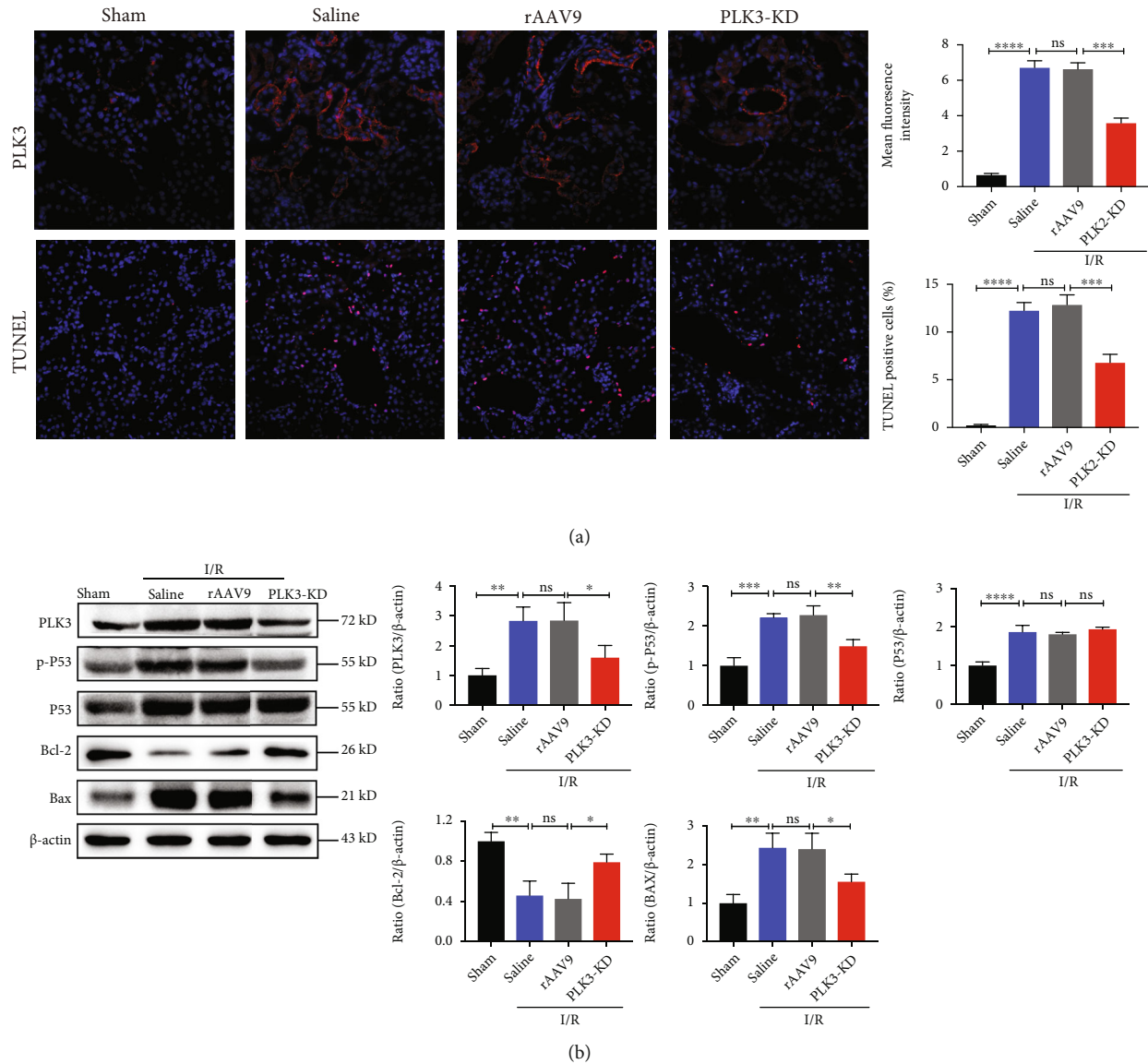
FIGURE 9: rAAV-9-mediated PLK3 KD alleviates I/R-induced TEC apoptosis in mice. (a) PLK3 expression was examined by immunofluorescence analysis; TUNEL analysis of apoptosis was performed (bar = 50 μM; magnification, 400x). (b) Western blot analysis of PLK3 and apoptosis-related protein expression levels. The data are presented as the mean ± SD. $n \geq 3$. $^*P < 0.05$, $^{**}P < 0.01$, $^{***}P < 0.001$, and $^{****}P < 0.0001$.

repair, but in the context of severe DNA damage, it initiates apoptosis [49]. In this study, we confirmed that ATM was rapidly phosphorylated at serine 1981, which led to the activation of the downstream kinase PLK3 during H/R injury. We confirmed that PLK3 overexpression exacerbated TEC apoptosis after H/R injury, while targeted silencing of PLK3 expression reduced apoptosis. Specific ATM inhibitors attenuated apoptosis in the presence of multiple DNA damage-inducing factors [50, 51]. Compared with KU-55933, KU-60019 is an improved ATM kinase-specific inhibitor that has a more potent inhibitory effect [52]. KU-60019 reduced the protein levels of p-ATM and PLK3 and reduced the phosphorylation of P53, thereby regulating the downstream Bax/Bcl-2 ratio and attenuating apoptosis. In the rescue assay, PLK3 overexpression reversed the cytoprotective effect of KU-60019 on the DDR. Furthermore, we

found that cell viability decreased after H/R injury, which may be related to the significant decrease in the nucleotide levels after hypoxia and the decrease in replication caused by DNA damage [53]. Our results suggest that silencing PLK3 expression during DDR injury can improve the viability of TECs.

Oxidative DNA damage, which can be induced by the ROS that are generated after renal I/R injury, directly induces TEC apoptosis [11, 54]. The TUNEL assay can detect DNA double-stranded and single-stranded breaks, which are markers of apoptosis after DNA damage [55]. Consistently, we found that H/R-induced apoptosis was accompanied by oxidative stress and the DDR. Accumulating evidence suggests that DNA damage and apoptosis are important steps in the pathogenesis of a variety of renal diseases [56, 57]. Consistent with previous studies [58], we also
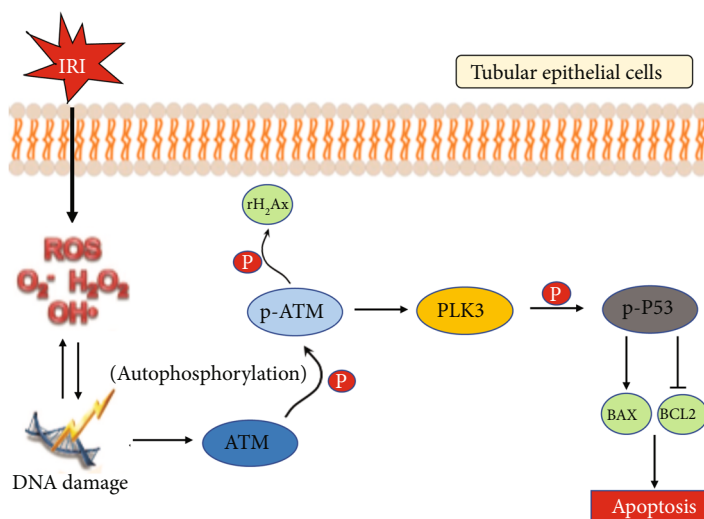
FIGURE 10: A schematic representation of the proposed mechanisms by which PLK3 regulates TEC apoptosis after DNA damage in response to oxidative stress. Renal I/R injury causes severe oxidative stress, and ROS attack double-stranded DNA, resulting in DSBs, which activate the ATM/PLK3/P53 signaling pathway in response to DNA damage, triggering the P53-dependent downstream apoptotic cascade, and thereby promoting TEC apoptosis.

found that P53 protein expression in renal tubules was very low under baseline physiological conditions and increased significantly after ischemic injury. P53 is the master player in DDR-induced apoptosis, and the phosphorylation of P53, rather than the total expression of this protein, is the key to the induction of apoptosis [59]. DNA damage signaling induces P53 phosphorylation and stabilization and enhances its robust transcriptional activity to initiate the apoptosis cascade [60]. In the intrinsic mitochondrial apoptotic pathway, the activation of Bax by P53 transcription leads to permeabilization of the outer mitochondrial membrane and the release of apoptotic factors, which further activate caspases to induce apoptosis. Conversely, Bcl-2 antagonizes Bax to prevent mitochondrial permeabilization and inhibit apoptosis. In our study, we confirmed that H/R injury and I/R injury significantly increased the level of P53 phosphorylation. After P53 transcriptional activity is enhanced, expression of the downstream proapoptotic factor Bax is also significantly increased, and expression of the survival protein Bcl-2 is reduced; thus, the intrinsic apoptosis cascade is initiated in TECs. However, targeted silencing of PLK3 expression in vitro or knockdown of PLK3 expression with rAAV-9 plasmids in vivo could block P53-mediated apoptosis by reducing the phosphorylation of P53 to alleviate ischemic AKI and protect renal function. These results suggest that PLK3 functions as a protein kinase in the DDR and regulates DNA damage-induced apoptosis by phosphorylating its substrate P53 (Figure 10). This study provides insight into the causal relationship among oxidative stress, oxidative DNA damage, and TEC apoptosis in renal I/R injury.

5. Conclusions

In summary, this study is the first to show that PLK3 is activated during renal I/R injury and associated with oxidative stress and DNA damage. Oxidative stress caused by excessive ROS production can lead to DSBs, which can activate ATM, as well as downstream signaling responses to DNA damage. PLK3 activation by phosphorylated ATM increases the phosphorylation of P53, which enhances the P53-mediated proapoptotic cascade to promote TEC apoptosis. Overall, inhibiting PLK3 attenuates renal I/R injury-induced apoptosis by blocking the ATM/P53-mediated DDR, suggesting that PLK3 could be the target of effective therapeutic strategies to treat I/R injury during kidney transplantation.

Data Availability

Data are available at NCBI GEO: GSE52004 and GSE121191.

Conflicts of Interest

All authors declare that they have no competing interests.

Authors' Contributions

Weiming Deng, Xiangling Wei, and Zhenwei Xie contributed equally to this work.

Acknowledgments

Supplementary Materials

Table 1: the primer sequence of PLK3 siRNA. Table 2: the primer sequence of qPCR. Supplementary data to this article can be found online. Figure 1: (A) renal tissues for H&E staining and quantification of tubular damage (bar = 50 μM;

magnification, 400x). (B and C) TUNEL assays showed the number of apoptotic after I/R injury (bar = 50 μM; magnification, 400x). The data are presented as the mean ± SD. $n \geq 3$. *$P < 0.05$, **$P < 0.01$, and ****$P < 0.0001$. PC: positive control; NC: negative control. Supplementary data to this article can be found online. Figure 2: (A) p-ATM protein levels, PLK3 protein levels were measured by Western blotting after the application of KU-60019. (B and C) PLK3 expression after I/R injury at day 21 and day 28 of rAAV9-PLK3-KD plasmid injection. (D) PLK3 mRNA expression after rAAV9-PLK3-KD plasmids injection was detected of by qPCR. (E) Body weight measurement of mice injected with rAAV9 vector and rAAV9-PLK3-KD plasmids. The data are presented as the mean ± SD. $n \geq 3$. *$P < 0.05$, ***$P < 0.001$, and ****$P < 0.0001$. 21d: 21 days; 28d: 28 days. Supplementary data to this article can be found online. *(Supplementary Materials)*

References

[1] A. Zuk and J. V. Bonventre, "Acute kidney injury," *Annual Review of Medicine*, vol. 67, no. 1, pp. 293–307, 2016.

[2] A. A. Sharfuddin and B. A. Molitoris, "Pathophysiology of ischemic acute kidney injury," *Nature Reviews. Nephrology*, vol. 7, no. 4, pp. 189–200, 2011.

[3] C. Barin-Le Guellec, "Ischemia/reperfusion-associated tubular cells injury in renal transplantation: can metabolomics inform about mechanisms and help identify new therapeutic targets?," *Pharmacological Research*, vol. 129, pp. 34–43, 2018.

[4] M. G. Snoeijs, A. van Bijnen, E. Swennen et al., "Tubular epithelial injury and inflammation after ischemia and reperfusion in human kidney transplantation," *Annals of Surgery*, vol. 253, no. 3, pp. 598–604, 2011.

[5] N. Ueda and S. V. Shah, "Endonuclease-induced DNA damage and cell death in oxidant injury to renal tubular epithelial cells," *The Journal of Clinical Investigation*, vol. 90, no. 6, pp. 2593–2597, 1992.

[6] O. A. Sedelnikova, D. R. Pilch, C. Redon, and W. M. Bonner, "Histone H2AX in DNA damage and repair," *Cancer Biology & Therapy*, vol. 2, no. 3, pp. 233–235, 2003.

[7] Y. Shiloh, "ATM and related protein kinases: safeguarding genome integrity," *Nature Reviews. Cancer*, vol. 3, no. 3, pp. 155–168, 2003.

[8] K. H. Vousden and X. Lu, "Live or let die: the cell's response to p53," *Nature Reviews. Cancer*, vol. 2, no. 8, pp. 594–604, 2002.

[9] N. H. Chehab, A. Malikzay, E. S. Stavridi, and T. D. Halazonetis, "Phosphorylation of Ser-20 mediates stabilization of human p53 in response to DNA damage," *Proceedings of the National Academy of Sciences of the United States of America*, vol. 96, no. 24, pp. 13777–13782, 1999.

[10] J. L. M. Digby, T. Vanichapol, A. Przepiorski, A. J. Davidson, and V. Sander, "Evaluation of cisplatin-induced injury in human kidney organoids," *American Journal of Physiology. Renal Physiology*, vol. 318, no. 4, pp. F971–F978, 2020.

[11] Q. B. Lu, Q. Du, H. P. Wang, Z. H. Tang, Y. B. Wang, and H. J. Sun, "Salusin-β mediates tubular cell apoptosis in acute kidney injury: involvement of the PKC/ROS signaling pathway," *Redox Biology*, vol. 30, p. 101411, 2020.

[12] H. Huang, C. Xu, Y. Wang et al., "Lethal (3) malignant brain tumor-like 2 (L3MBTL2) protein protects against kidney injury by inhibiting the DNA damage-p53-apoptosis pathway in renal tubular cells," *Kidney International*, vol. 93, no. 4, pp. 855–870, 2018.

[13] S. Zhu, N. Pabla, C. Tang, L. He, and Z. Dong, "DNA damage response in cisplatin-induced nephrotoxicity," *Archives of Toxicology*, vol. 89, no. 12, pp. 2197–2205, 2015.

[14] S. Zitouni, C. Nabais, S. C. Jana, A. Guerrero, and M. Bettencourt-Dias, "Polo-like kinases: structural variations lead to multiple functions," *Nature Reviews. Molecular Cell Biology*, vol. 15, no. 7, pp. 433–452, 2014.

[15] C. W. Conn, R. F. Hennigan, W. Dai, Y. Sanchez, and P. J. Stambrook, "Incomplete cytokinesis and induction of apoptosis by overexpression of the mammalian polo-like kinase, Plk3," *Cancer Research*, vol. 60, no. 24, pp. 6826–6831, 2000.

[16] C. Thangavel, E. Boopathi, S. Ciment et al., "The retinoblastoma tumor suppressor modulates DNA repair and radioresponsiveness," *Clinical Cancer Research*, vol. 20, no. 21, pp. 5468–5482, 2014.

[17] Y. Yang, J. Bai, R. Shen et al., "Polo-like kinase 3 functions as a tumor suppressor and is a negative regulator of hypoxia-inducible factor-1 alpha under hypoxic conditions," *Cancer Research*, vol. 68, no. 11, pp. 4077–4085, 2008.

[18] P. J. Donohue, G. F. Alberts, Y. Guo, and J. A. Winkles, "Identification by targeted differential display of an immediate early gene encoding a putative serine/threonine kinase," *The Journal of Biological Chemistry*, vol. 270, no. 17, pp. 10351–10357, 1995.

[19] L. Wang, W. Dai, and L. Lu, "Osmotic stress-induced phosphorylation of H2AX by polo-like kinase 3 affects cell cycle progression in human corneal epithelial cells," *The Journal of Biological Chemistry*, vol. 289, no. 43, pp. 29827–29835, 2014.

[20] E. Kis, T. Szatmari, M. Keszei et al., "Microarray analysis of radiation response genes in primary human fibroblasts," *International Journal of Radiation Oncology • Biology • Physics*, vol. 66, no. 5, pp. 1506–1514, 2006.

[21] D. Xu, Y. Yao, L. Lu, M. Costa, and W. Dai, "Plk3 functions as an essential component of the hypoxia regulatory pathway by direct phosphorylation of HIF-1alpha," *The Journal of Biological Chemistry*, vol. 285, no. 50, pp. 38944–38950, 2010.

[22] L. Wang, J. Gao, W. Dai, and L. Lu, "Activation of Polo-like kinase 3 by hypoxic stresses," *The Journal of Biological Chemistry*, vol. 283, no. 38, pp. 25928–25935, 2008.

[23] S. Xie, Q. Wang, H. Wu et al., "Reactive oxygen species-induced phosphorylation of p53 on serine 20 is mediated in part by polo-like kinase-3," *The Journal of Biological Chemistry*, vol. 276, no. 39, pp. 36194–36199, 2001.

[24] D. Xu, W. Dai, and C. Li, "Polo-like kinase 3, hypoxic responses, and tumorigenesis," *Cell Cycle*, vol. 16, no. 21, pp. 2032–2036, 2017.

[25] J. Liu, A. M. Krautzberger, S. H. Sui et al., "Cell-specific translational profiling in acute kidney injury," *The Journal of Clinical Investigation*, vol. 124, no. 3, pp. 1242–1254, 2014.

[26] M. Chang-Panesso, F. F. Kadyrov, M. Lalli et al., "FOXM1 drives proximal tubule proliferation during repair from acute ischemic kidney injury," *The Journal of Clinical Investigation*, vol. 129, no. 12, pp. 5501–5517, 2019.

[27] G. Yu, L. G. Wang, Y. Han, and Q. Y. He, "clusterProfiler: an R package for comparing biological themes among gene clusters," *OMICS*, vol. 16, no. 5, pp. 284–287, 2012.

[28] C. J. Rocca, S. N. Ur, F. Harrison, and S. Cherqui, "rAAV9 combined with renal vein injection is optimal for kidney-

targeted gene delivery: conclusion of a comparative study," *Gene Therapy*, vol. 21, no. 6, pp. 618–628, 2014.

[29] P. Jablonski, B. O. Howden, D. A. Rae, C. S. Birrell, V. C. Marshall, and J. Tange, "An experimental model for assessment of renal recovery from warm ischemia," *Transplantation*, vol. 35, no. 3, pp. 198–204, 1983.

[30] E. P. Rogakou, C. Boon, C. Redon, and W. M. Bonner, "Megabase chromatin domains involved in DNA double-strand breaks in vivo," *The Journal of Cell Biology*, vol. 146, no. 5, pp. 905–916, 1999.

[31] P. Moran, Y. Guo, R. Yuan et al., "Translating ribosome affinity purification (TRAP) for RNA isolation from endothelial cells in vivo," *Journal of Visualized Experiments*, vol. 147, no. 147, 2019.

[32] M. Heiman, R. Kulicke, R. J. Fenster, P. Greengard, and N. Heintz, "Cell type–specific mRNA purification by translating ribosome affinity purification (TRAP)," *Nature Protocols*, vol. 9, no. 6, pp. 1282–1291, 2014.

[33] F. Khashab, F. Al-Saleh, N. Al-Kandari, F. Fadel, and M. Al-Maghrebi, "JAK inhibition prevents DNA damage and apoptosis in testicular ischemia-reperfusion injury via modulation of the ATM/ATR/Chk pathway," *International Journal of Molecular Sciences*, vol. 22, no. 24, p. 13390, 2021.

[34] M. S. Sun, H. Jin, X. Sun et al., "Free radical damage in ischemia-reperfusion injury: an obstacle in acute ischemic stroke after revascularization therapy," *Oxidative Medicine and Cellular Longevity*, vol. 2018, Article ID 3804979, 17 pages, 2018.

[35] W. Zhang, S. Bi, P. Li et al., "In situ observation of mtDNA damage during hepatic ischemia-reperfusion," *Analytical Chemistry*, vol. 93, no. 14, pp. 5782–5788, 2021.

[36] L. Hu, Z. Wang, C. Carmone, J. Keijer, and D. Zhang, "Role of oxidative DNA damage and repair in atrial fibrillation and ischemic heart disease," *International Journal of Molecular Sciences*, vol. 22, no. 8, p. 3838, 2021.

[37] M. Schumer, M. C. Colombel, I. S. Sawczuk et al., "Morphologic, biochemical, and molecular evidence of apoptosis during the reperfusion phase after brief periods of renal ischemia," *The American Journal of Pathology*, vol. 140, no. 4, pp. 831–838, 1992.

[38] N. Ueda, P. D. Walker, S. M. Hsu, and S. V. Shah, "Activation of a 15-kDa endonuclease in hypoxia/reoxygenation injury without morphologic features of apoptosis," *Proceedings of the National Academy of Sciences of the United States of America*, vol. 92, no. 16, pp. 7202–7206, 1995.

[39] T. Hama, P. K. B. Nagesh, P. Chowdhury et al., "DNA damage is overcome by TRIP13 overexpression during cisplatin nephrotoxicity," *JCI Insight*, vol. 6, no. 22, 2021.

[40] F. A. Valentijn, S. N. Knoppert, G. Pissas et al., "CCN2 aggravates the immediate oxidative stress–DNA damage response following renal ischemia–reperfusion injury," *Antioxidants*, vol. 10, no. 12, p. 2020, 2021.

[41] B. A. Molitoris, "DNA damage response protects against progressive kidney disease," *The Journal of Clinical Investigation*, vol. 129, no. 11, pp. 4574-4575, 2019.

[42] F. Li, E. M. Bahnson, J. Wilder et al., "Oral high dose vitamin B12 decreases renal superoxide and post-ischemia/reperfusion injury in mice," *Redox Biology*, vol. 32, p. 101504, 2020.

[43] W.-C. Tseng, P.-Y. Lee, M.-T. Tsai et al., "Hypoxic mesenchymal stem cells ameliorate acute kidney ischemia-reperfusion injury via enhancing renal tubular autophagy," *Stem Cell Research & Therapy*, vol. 12, no. 1, 2021.

[44] F. Kar, C. Hacioglu, H. Senturk, D. B. Donmez, and G. Kanbak, "The role of oxidative stress, renal inflammation, and apoptosis in post ischemic reperfusion injury of kidney tissue: the protective effect of dose-dependent boric acid administration," *Biological Trace Element Research*, vol. 195, no. 1, pp. 150–158, 2020.

[45] C. T. Chien, P. H. Lee, C. F. Chen, M. C. Ma, M. K. Lai, and S. M. Hsu, "De novo demonstration and co-localization of free-radical production and apoptosis formation in rat kidney subjected to ischemia/reperfusion," *Journal of the American Society of Nephrology*, vol. 12, no. 5, pp. 973–982, 2001.

[46] C. Chen, W. Yao, S. Wu et al., "Crosstalk between connexin32 and mitochondrial apoptotic signaling pathway plays a pivotal role in renal ischemia reperfusion-induced acute kidney injury," *Antioxidants & Redox Signaling*, vol. 30, no. 12, pp. 1521–1538, 2019.

[47] E. M. Hammond, M. J. Dorie, and A. J. Giaccia, "ATR/ATM targets are phosphorylated by ATR in response to hypoxia and ATM in response to reoxygenation," *The Journal of Biological Chemistry*, vol. 278, no. 14, pp. 12207–12213, 2003.

[48] G. H. Xie, H. J. Dai, F. Liu et al., "A dual role of ATM in ischemic preconditioning and ischemic injury," *Cellular and Molecular Neurobiology*, vol. 40, no. 5, pp. 785–799, 2020.

[49] Z. Bencokova, M. R. Kaufmann, I. M. Pires, P. S. Lecane, A. J. Giaccia, and E. M. Hammond, "ATM activation and signaling under hypoxic conditions," *Molecular and Cellular Biology*, vol. 29, no. 2, pp. 526–537, 2009.

[50] H. Schweikl, C. Petzel, C. Bolay, K. A. Hiller, W. Buchalla, and S. Krifka, "2-Hydroxyethyl methacrylate-induced apoptosis through the ATM- and p53-dependent intrinsic mitochondrial pathway," *Biomaterials*, vol. 35, no. 9, pp. 2890–2904, 2014.

[51] X. H. Lu, V. B. Mattis, N. Wang et al., "Targeting ATM ameliorates mutant Huntingtin toxicity in cell and animal models of Huntington's disease," *Science Translational Medicine*, vol. 6, no. 268, article 268ra178, 2014.

[52] S. E. Golding, E. Rosenberg, N. Valerie et al., "Improved ATM kinase inhibitor KU-60019 radiosensitizes glioma cells, compromises insulin, AKT and ERK prosurvival signaling, and inhibits migration and invasion," *Molecular Cancer Therapeutics*, vol. 8, no. 10, pp. 2894–2902, 2009.

[53] I. M. Pires, Z. Bencokova, M. Milani et al., "Effects of acute versus chronic hypoxia on DNA damage responses and genomic instability," *Cancer Research*, vol. 70, no. 3, pp. 925–935, 2010.

[54] Y. T. Chen, C. C. Yang, Y. Y. Zhen et al., "Cyclosporine-assisted adipose-derived mesenchymal stem cell therapy to mitigate acute kidney ischemia-reperfusion injury," *Stem Cell Research & Therapy*, vol. 4, no. 3, p. 62, 2013.

[55] H. Chen, L. Wang, W. Wang et al., "ELABELA and an ELABELA fragment protect against AKI," *Journal of the American Society of Nephrology*, vol. 28, no. 9, pp. 2694–2707, 2017.

[56] M. Yan, C. Tang, Z. Ma, S. Huang, and Z. Dong, "DNA damage response in nephrotoxic and ischemic kidney injury," *Toxicology and Applied Pharmacology*, vol. 313, pp. 104–108, 2016.

[57] S. Kishi, C. R. Brooks, K. Taguchi et al., "Proximal tubule ATR regulates DNA repair to prevent maladaptive renal injury responses," *The Journal of Clinical Investigation*, vol. 129, no. 11, pp. 4797–4816, 2019.

[58] K. J. Kelly, Z. Plotkin, S. L. Vulgamott, and P. C. Dagher, "P53 mediates the apoptotic response to GTP depletion after renal ischemia-reperfusion: protective role of a p53 inhibitor," *Journal of the American Society of Nephrology*, vol. 14, no. 1, pp. 128–138, 2003.

[59] T. Shono, P. J. Tofilon, T. S. Schaefer, D. Parikh, T. J. Liu, and F. F. Lang, "Apoptosis induced by adenovirus-mediated p53 gene transfer in human glioma correlates with site-specific phosphorylation," *Cancer Research*, vol. 62, no. 4, pp. 1069–1076, 2002.

[60] T. M. Johnson, E. M. Hammond, A. Giaccia, and L. D. Attardi, "The p53QS transactivation-deficient mutant shows stress-specific apoptotic activity and induces embryonic lethality," *Nature Genetics*, vol. 37, no. 2, pp. 145–152, 2005.

Research Article

Bidirectional Effect of Repeated Exposure to Extremely Low-Frequency Electromagnetic Field (50 Hz) of 1 and 7 mT on Oxidative/Antioxidative Status in Rat's Brain: The Prediction for the Vulnerability to Diseases

Angelika Klimek [iD],[1] **Anna Nowakowska** [iD],[1] **Hanna Kletkiewicz** [iD],[1] **Joanna Wyszkowska** [iD],[1] **Justyna Maliszewska** [iD],[1] **Milena Jankowska** [iD],[1] **Lukasz Peplowski** [iD],[2] **and Justyna Rogalska** [iD][1]

[1]*Department of Animal Physiology and Neurobiology, Faculty of Biological and Veterinary Sciences, Nicolaus Copernicus University in Torun, 87-100, Poland*
[2]*Department of Biophysics, Institute of Physics, Faculty of Physics, Astronomy and Informatics Nicolaus Copernicus University in Torun, 87-100, Poland*

Correspondence should be addressed to Angelika Klimek; klimek@doktorant.umk.pl

Studies reported evidence for opposite effects of extremely low-frequency electromagnetic field (EMF): harmful, including the oxidative stress induction, and beneficial, such as the activation of antioxidant defense. People's exposure to EMF is often repeated or prolonged, and it is important to consider the cumulative effect of such kind of exposure on the organism. If changes evoked by repeated exposure to EMF are permanent, responsiveness to other stress factors can be modified. The aims of our study were (1) to evaluate changes in the levels of oxidative stress and antioxidant defense markers in the prefrontal cortex of adult rats after repeated exposure to 1 and 7 mT EMF and (2) to assess whether repeated EMF exposure can modify oxidative/antioxidative status in response to other stress factors. Rats were exposed to EMF 1 h/day for 7 days, one, twice, or three times. After each exposure, 8-isoprostanes, protein carbonyl groups, and the total antioxidant capacity were assessed. Part of the animals, after EMF treatment, was exposed to another stress factor—open field. Results showed that repeated exposure changed the oxidative/antioxidative status depending on the intensity of the EMF and the number of exposures. 1 mT EMF created weak changes in the oxidative status in the brain; however, 7 mT EMF moved the balance to a clearly higher level. The changes in the oxidative status after 1 mT EMF were enough to reduce, and after 7 mT EMF to intensify oxidative processes in response to the next stress. We concluded that the organism might adapt to "weak" EMF, while "strong" EMF exceeds the adaptive capacity of the organism and sensitizes it to subsequent stress, and thus may modulate vulnerability to diseases. Our results also provide new insights into the possible therapeutic properties of the magnetic field, as 1 mT EMF appears to have a potentially protective impact on the brain.

1. Introduction

The influence of the extremely low-frequency electromagnetic field (EMF) on living organisms is still being widely investigated. EMF includes frequencies in the range of 3-300 Hz, which also correspond to physiological brain oscillations [1]. The most common frequencies values in our environment are 50 Hz and 60 Hz [2, 3]. Nowadays, people are increasingly exposed to this type of electromagnetic field due to the increasing number of electrical devices in our urbanized environment. EMF exposure has been proved to be an important risk factor in the development of diseases

affecting the nervous system, such as anxiety or depression [4]. The brain is an organ extremely sensitive to oxidative stress because of the high amount of unsaturated lipids, energetics dependent on mitochondria, neurotransmitters' metabolism generating hydrogen peroxide (H_2O_2), the ability of neurotransmitters to autooxidation, and engagement of reactive oxygen species in Ca^{2+} signaling [5]. Oxidative stress underlies many neurodegenerative and neuropsychiatric disorders [6].

The results of studies concerning the effect of EMF (50/60 Hz) on oxidative stress and antioxidant defense are often contradictory or insufficient. It means that the answer to the question whether EMF has a beneficial or detrimental impact on the organism is not obvious. Some authors reported evidence for the harmful effects of EMF, including oxidative stress induction [7–9]. The increased level of one of the most common markers of lipid peroxidation, malondialdehyde (MDA), was noticed in a several studies on humans and animal models exposed to EMF [7, 8]. In addition, oxidative damages are often accompanied by a decrease in antioxidant defense [8–10]. On the other hand, the increase of reports on the benefits associated with exposure to EMF such as activation of antioxidant systems is observed [11–13]. These protective effects of EMF are also used in medicine, e.g., for the treatment of brain damages [13]. It is also important that EMF exposure experienced by people is often repeated or prolonged, but most research evaluates the effect of the single period of EMF exposure.

EMF is recognized as a mild stress factor [2, 14], which as other stress factors can result in different activations of stress response systems; it means that exposure to EMF can establish a new "set-point" for stress systems activity. However, the course of this phenomenon (the direction and dynamics) depends on the intensity of the electromagnetic field. As a consequence, the EMF-induced changes in stress hormones can boost "cellular hormesis" by activation of signaling pathways including oxidative/antioxidative processes in different ways [15].

Here, we propose the hypothesis that the impact of an extremely low-frequency electromagnetic field on oxidant/antioxidant balance is not definitely negative, and the direction and dynamics of EMF-induced changes depend on the value of magnetic flux density as well as on the number of exposures. During repeated exposure to some stress factor, the organism responds to each individual stressor; however, consequently, the cumulative effect of all exposures is observed. As a result, temporary or permanent regulatory changes can be evoked [16]. The first exposure to stress generates the stress-induced initial disruption in homeostasis. As the response, the processes to reestablish the balance are triggered and they require gene expression and protein synthesis that progresses over time; thus, the temporal feature of the response to repetitive stress is essential [17]. We assumed that the first exposure to EMF changes the oxidative/antioxidative status; thus, each next EMF exposure would overlap its level established under the previous EMF exposure.

Therefore, the first aim of the study was to evaluate the changes in the levels of oxidative stress as well as the antioxidant defense markers in the prefrontal cortex of adult rats

after repeated exposure to EMF of two different values of magnetic flux density (1 and 7 mT). The prefrontal cortex seems to be more sensitive to oxidative stress than other brain structures and concerning its role in the development of nervous system-related diseases; it appears to be relevant for research of the impact of EMF on oxidative/antioxidative status [18]. We have chosen to evaluate the effects of EMF of 1 and 7 mT. According to European Union Directive 2013/35/EU, the threshold value for magnetic flux density of the minor transient changes in the brain is set to a value of 1 mT EMF for 50 Hz. On the other hand, the exposure of workers to 50 Hz magnetic fields must be limited to the value 6 mT [19]. It has been shown that exposure to EMF of intensity higher than 6 mT causes measurable biological effects, e.g., increased lipid peroxidation [20, 21], DNA damage [22], and neuronal networks synchrony firing generation [23].

Then, we assumed that if the changes evoked by repeated exposure to EMF are permanent, the responsiveness to the other kinds of stress can be modified. It means that EMF can change the vulnerability of the organism to subsequent stress factors and thus to diseases, mainly related to the nervous system, in a two-way manner: compensatory or detrimental ones. Intriguingly, many nervous system-related disorders may be accounted for by a 'two-hit model' in which environmental stressors change the central nervous system function in the permanent way leading to changes in vulnerability to a "second hit," in turn leading to the onset of disease [24]. Thus, the second aim of the research was to assess whether the consequence of repeated EMF exposure can be the modification of the oxidative/antioxidative status in response to subsequent, other stress factors.

2. Materials and Methods

2.1. Animals. A total of 175 male adults (3-month-old) Wistar rats weighing 300-350 g were used throughout the experimentation. The number of animals in the research was planned in accordance with 3R principles (replacement, reduction, and refinement; EU Directive 2010/63/EU) [25]. Rats were housed in plastic cages in a temperature/humidity/light-controlled laboratory conditions ($22 \pm 2°C$, humidity $55 \pm 10\%$, 12 : 12 h light : dark cycle with lights on at 7:00 a.m.). Rodent laboratory feed and drinking water were provided ad libitum. All experimental procedures were approved by the Local Committee for Ethics in Animal Research in Bydgoszcz, Poland (decision number: 3/2018).

2.2. In Vivo Electromagnetic Field Exposure System. Animals were exposed to 50 Hz sinusoidal electromagnetic field of 1 mT and 7 mT (root mean square (RMS)) flux density, generated in a coil of 0.1 m in radius, designed by EiE (Elektronika i Elektromedycyna Sp. J., Otwock, Poland). This exposure system has been described in detail previously [3, 26]. The EMF was regulated during exposure by input current to the coil, and the magnetic flux density was measured before each experiment with a Gauss meter (Model GM2, AlphaLab, Inc., USA). The nonhomogeneity of the EMF within the area containing the animal's cage was < 15% (Figure 1). The temperature during all
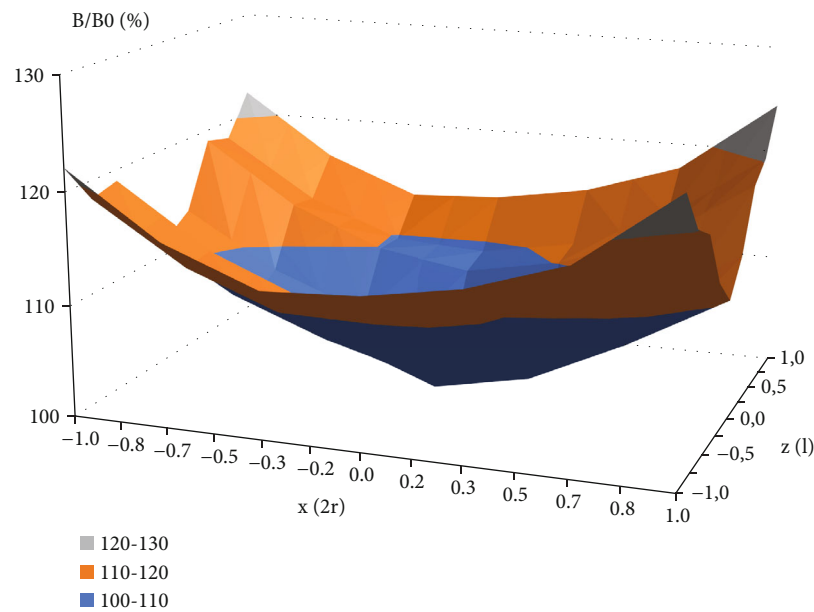
FIGURE 1: The plot of the mean value of magnetic flux density within the area of the animal's cage in the coil. Abbreviations: B: magnetic flux density vector, $B/B0$: normalized magnetic flux density relative to the value in the geometrical centre of the coil; z/l: normalized distance from the coil centre along z-axis; $x/2r$: normalized distance from the solenoid centre along x-axis; l: coil length; r: coil radius

experiments was monitored using thermocouples mounted in the animal cages, and it was set to $26 \pm 1°C$.

2.3. Experimental Design.

One week after habituation to the laboratory environment, the rats in individual plastic cages ($12 \, cm \times 20 \, cm \times 14 \, cm$, with a perforated plexiglass cover and wood shavings bedding) were put into the centre of the EMF coil. Exposure to "low" (1 mT) and "high" (7 mT) EMF was performed for three periods described as $E1$, $E2$, and $E3$. Each period included 7-day exposure, 1 h/1day. Rats subjected to the same experimental procedure except electromagnetic field exposure were used as the control.

The experimental design included two sets of experiments (Figure 2). During the first set of experiments, a part of rats ($n = 88$) after each period of EMF or control exposure ($E1$, $E2$, and $E3$) was decapitated to estimate the effect of EMF on oxidant/antioxidant status (8-isoprostanes (8-epi PGF2α), protein carbonyl (CP) groups, and level of total antioxidant capacity (TAC)—described in this research as "basal" (B) level) (Figure 2(a)). The remaining rats from each group ($n = 87$) were used during the second set of experiments (Figure 2(b)). The experiments as previously included one to three periods of EMF or control exposure ($E1$, $E2$, or $E3$), and after each of them the part of animals was exposed to another kind of stress factor—open field (OF) (size of the box: $100 \, cm \times 100 \, cm$, duration of the test: 5 min). It is a stress-induced procedure (exposure to a novel, open, light environment), which was proved to evoke the activation of brain stress systems. Then, the animals were decapitated for assessment of stress-induced changes in oxidant/antioxidant parameters as a consequence of previous exposure to EMF. To avoid the influence of the circadian

rhythm on the results, decapitation was performed between 10:00 and 12:00 am.

The rats were divided into six groups: (1) EMF/B/1mT: animals exposed to EMF (50 Hz, 1 mT), in which the basal (B) level of markers was assessed; (2) EMF/OF/1mT: animals exposed to EMF (50 Hz, 1 mT) and exposed to open field test (OF); (3) EMF/B/7mT: animals exposed to EMF (50 Hz, 7 mT) in which the basal (B) level of markers was assessed; (4) EMF/OF/7mT: animals exposed to EMF (50 Hz, 7 mT) and exposed to open field test (OF); (5) C/B: control animals subjected to the same experimental procedure as the experimental groups 1 and 3, except EMF exposure; (6) C/OF: control animals subjected to the same experimental procedure as the experimental groups 2 and 4, except EMF exposure.

2.4. Sample Collection.

After decapitation, the part of the brain (prefrontal cortex) was quickly dissected. Each fragment of tissue was weighed and immediately frozen in liquid nitrogen and stored at $-80°C$ until further biochemical analysis. For determination of oxidant/antioxidant status, brain samples were homogenized on ice in phosphate buffer pH 7.4. After centrifugation for 10 minutes at 12000 x g, the supernatants were collected in Eppendorf tubes and stored until they were used for the assessment of the level of protein carbonyl (CP) groups and 8-isoprostanes (8-epi PGF2α) as a result of proteins and phospholipid peroxidation, respectively, as well as the total nonenzymatic antioxidant capacity (TAC).

2.5. Determination of the Markers of Oxidant/Antioxidant Status Level.

Protein carbonyl (CP) groups and 8-isoprostanes (8-epi PGF2α) as well as total nonenzymatic antioxidant capacity (TAC) concentrations were determined with commercial

	1 week	2 weeks	3 weeks	4 weeks	5 weeks	6 weeks	7 weeks	8 weeks	9 weeks
Control 1 mT/7 mT	Exposure 1 (E1)				Exposure 2 (E2)				Exposure 3 (E3)

Oxidant status assessment　　　Oxidant status assessment　　　Oxidant status assessment

(a)

	1 week	2 weeks	3 weeks	4 weeks	5 weeks	6 weeks	7 weeks	8 weeks	9 weeks
Control 1 mT/7 mT	Exposure 1 (E1)				Exposure 2 (E2)				Exposure 3 (E3)

Open-field test and Oxidant status assessment　　Open-field test and Oxidant status assessment　　Open-field test and Oxidant status assessment

(b)

Figure 2: Experimental design. (a) First set of experiments: assessment of basal level of oxidative stress markers and antioxidants. (b) Second set of experiments: assessment of open field-induced level of oxidative stress markers and antioxidants.

kits according to the manufacturers' instructions. Each sample was assayed in triplicate. Colorimetric changes in the assay were detected using a multimode microplate reader Epoch 2 (BioTek Instruments, Inc., Winooski, UT, USA).

2.5.1. Determination of Protein Peroxidation. The level of end product of protein peroxidation-protein carbonyl (CP) groups was assayed using a Protein Carbonyl Content Assay Kit (Sigma-Aldrich, No MAK094, USA) based on their reaction with 2,4-dinitrophenylohydrazine (DNPH). Finally, dinitrophenyl (DNP) hydrazone adducts were formed and then were detected spectrophotometrically at 375 nm. The level of DNP was proportional to the concentrations of CP. The amount of carbonyl in the sample well was calculated per 1 mg of protein. Results were expressed as nanomoles per mg of protein.

2.5.2. Determination of Phospholipid Peroxidation. The level of end product of phospholipid peroxidation–8-isoprostanes (8-epi PGF2α) was assayed using 8-isoprostane ELISA Kit (Cayman Chemical, No 516351, USA). 8-Isoprostane has been proposed as a marker of oxidative stress and antioxidant deficiency. Isoprostanes are prostaglandin (PG) isomers that are generated from polyunsaturated fatty acids, mainly from arachidonic acid by a nonenzymatic process that involves peroxidation of membrane phospholipids by free radicals and reactive oxygen species. The absorbance of samples was measured at 406 nm. The concentration of 8-epi PGF2α was expressed as picograms per milliliter of sample.

2.5.3. Determination of Total Antioxidant Capacity. TAC was determined using a Total Antioxidant Capacity Assay Kit (Sigma-Aldrich, No MAK187, USA) in which concentrations of both small molecules and protein antioxidants were

determined. Determination of TAC is based on reduction Cu^{2+} to Cu^+ by both small molecules and proteins but using the Protein Mask prevents Cu^{2+} reduction by proteins. Finally, the amount of reduced Cu^+ ion enabling the analysis of small molecule antioxidants. The reduced Cu^+ ions chelate with a colorimetric probe. The absorbance (peak at 570 nm) is proportional to the TAC level in Trolox equivalents (a water-soluble vitamin E analogue used as an antioxidant standard). Results were calculated as nanomoles per milliliter of sample.

2.6. Data Analysis. To analyze the effect of repeated exposure to EMF on the markers of oxidative stress and total antioxidant capacity, we applied a general linear model (GLM) allowing to determine the effect of a combination of two fixed categorical factors: EMF intensity and number of exposures (1 mT, 7 mT vs. *E*1, *E*2, and *E*3). The levels of the open field-induced oxidative stress and antioxidant markers were compared to their basal levels for each group, respectively: C/B vs. C/OF, EMF/B/1mT vs. EMF/OF/1mT, and EMF/B/7mT vs. EMF/OF/7mT using GLM with open field/basal level and number of exposures as fixed categorical factors. If necessary the data were log-transformed after checking for normality (Shapiro-Wilk test) and homoscedasticity (Levene test). Differences between compared data were considered significant when $P < 0.05$. The analyses were carried out using SPSS 25.0 package (IBM Inc.).

3. Results

3.1. The Basal Level of Oxidative Stress Markers

3.1.1. Protein Carbonyl (CP) Groups. The intensity of EMF, as well as the number of exposures, had an influence on

TABLE 1: Results of statistical analysis of the oxidative markers concentrations in the prefrontal cortex.

	Dependent variable	Effect	df	F	P
a	CP basal level	Intensity of the electromagnetic field (mT)	2	22.133	*<0.001*
		Number of exposures (E1-E3)	2	16.681	*<0.001*
		(mT) × (E1-E3)	4	9.851	*<0.001*
		Error	68		
b	8-epi PGF2α basal level	Intensity of the electromagnetic field (mT)	2	15.231	*<0.001*
		Number of exposures (E1-E3)	2	0.191	0.827
		(mT) × (E1-E3)	4	2.343	0.063
		Error	73		
c	Open field-induced CP level	Intensity of the electromagnetic field (mT)	2	190.737	*<0.001*
		Number of exposures (E1-E3)	2	19.793	*<0.001*
		(mT) × (E1-E3)	4	12.051	*<0.001*
		Error	71		
d	Open field-induced 8-epi PGF2α level	Intensity of the electromagnetic field (mT)	2	13.921	*<0.001*
		Number of exposures (E1-E3)	2	0.657	0.522
		(mT) × (E1-E3)	4	7.753	*<0.001*
		Error	66		

F: GLM; statistically significant P value: indicated in italic; CP: protein carbonyl groups.

the basal level of CP groups in the prefrontal cortex. The CP groups' level increased with increasing EMF intensity, and the subsequent exposures enhanced the effect. There was also a significant interaction between these two factors (Table 1(a), Figure 3(a)). After first ($E1$) and second exposures ($E2$) to EMF of 1 mT the level of CP groups in the rat's brain did not differ from the control level; however, CP level after $E2$ was significantly higher than that after $E1$ ($P < 0.01$). After the third exposure ($E3$), CP level increased significantly compared to the control group ($P < 0.001$) and was also significantly higher than that noticed after $E1$ ($P < 0.001$) and $E2$ ($P < 0.01$). In animals exposed to EMF of 7 mT after $E1$, we observed a slight elevation in the level of the CP groups in comparison to control values, after $E2$ as well as after $E3$; however, the increase in CP level was significant ($P < 0.001$). Moreover, the statistically significant increase in the CP level after $E2$ was observed in comparison to that observed after $E1$ ($P < 0.01$), whereas after $E3$, the CP level was not significantly different from the value determined after $E2$. In animals exposed to EMF of 7 mT, the level of CP was enhanced in comparison to the value in the EMF/B/1mT group after $E1$ and $E2$ ($P < 0.001$) and the difference disappeared after $E3$.

3.1.2. 8-Isoprostanes (8-epi PGF2α). The level of 8-epi PGF2α after exposure to EMF was dependent only on the strength of the electromagnetic field (Table 1(b), Figure 3(b)). The exposure to EMF of 1 mT did not significantly affect the level of 8-epi PGF2α regardless of the number of exposures. Also, the analysis showed no clear differences between values of this parameter observed after $E1$ to $E3$. However, the tendency to decrease in the level of 8-epi PGF2α with each subsequent exposure was observed (Figure 3(b)). Otherwise, in the EMF/B/7mT group, the tendency to increase in the level of 8-epi

PGF2α with each next exposure was noticed (Figure 3(b)). After $E3$, the level of 8-epi PGF2α was clearly higher in the group exposed to EMF of 7 mT compared to the control group as well as to that in the EMF/B/1mT group ($P < 0.001$).

3.2. The Open Field-Induced Level of Oxidative Stress Markers

3.2.1. Protein Carbonyl (CP) Groups. The direction of changes in CP level in animals exposed to EMF of 1 mT and 7 mT after exposure to subsequent stress factor—open field test (EMF/OF/1mT and EMF/OF/7mT groups) coincided with their basal level observed only after exposure to electromagnetic field (EMF/B/1mT and EMF/B/7mT groups). Both intensity of the EMF and the number of exposures had an effect on the open field-induced level of CP groups. The interaction of both factors was also significant (Table 1(c), Figure 4(a)). There were no significant differences between the EMF/OF/1mT and C/OF groups after $E1$ and $E2$, but after $E3$ the level of CP in the group exposed to EMF of 1 mT was even lower in comparison to the value in the respective control group (C/OF) ($P < 0.001$). After a single exposure to EMF of 1 mT, the CP level was higher than that noticed after $E2$ and $E3$ ($P < 0.001$), while no significant difference was noticed between values after $E2$ and $E3$. The lowest value of CP groups in the EMF/OF/1mT group was observed after $E3$. The level of CP in the EMF/OF/7mT group was significantly increased compared to control animals after each exposure ($P < 0.001$) and was the highest after $E3$. The value observed after $E2$ was lower compared to both $E1$ and $E3$ ($P < 0.001$). Regardless of the number of exposures, the level of CP was always higher in the EMF/OF/7mT group in comparison to the values observed in the EMF/OF/1mT group ($P < 0.001$).

(a)

(b)
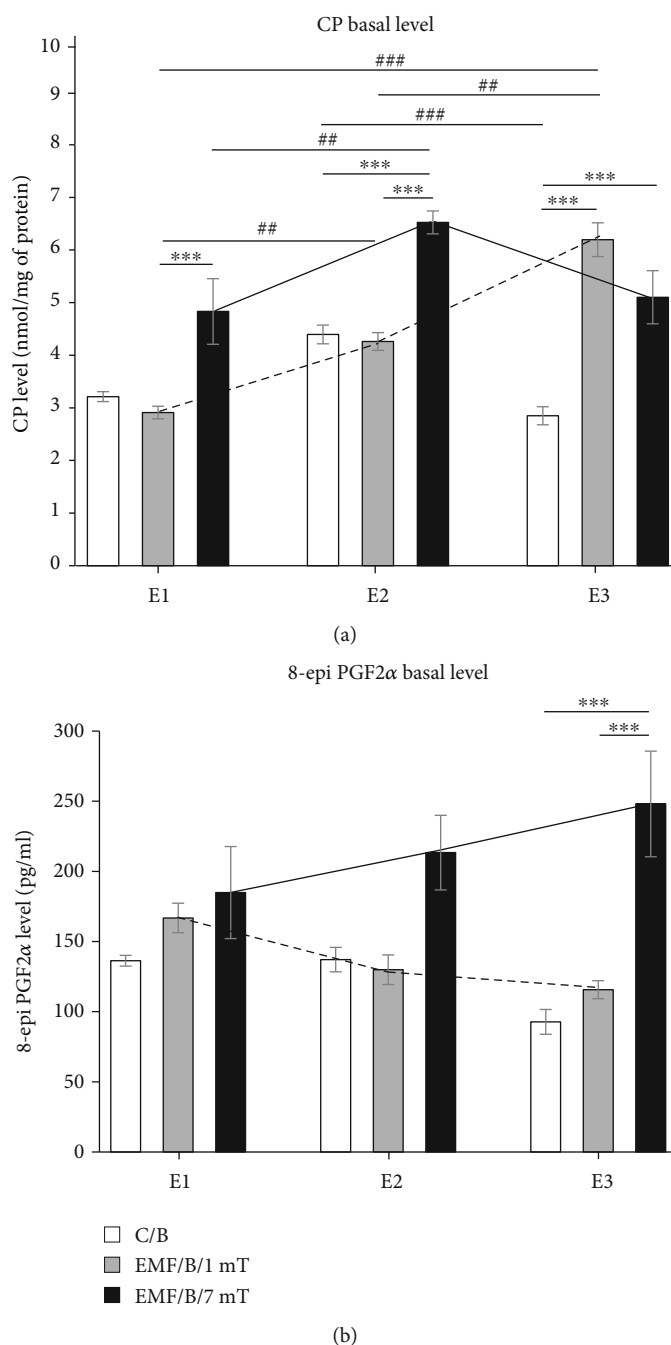
FIGURE 3: The basal level of oxidative stress markers: (a) CP groups and (b) 8-epi PGF2α in the prefrontal cortex of rat's brain. Animals were exposed once to three times (E1-E3) to EMF of 1 or 7 mT or control conditions. Values are presented as mean ± SEM. The lines show the direction of changes in the level of stress markers in 1 mT (dotted line) and 7 mT (solid line) groups after each subsequent exposure. Statistically significant differences between animals from the same group are denoted $^{\#\#}P < 0.01$ and $^{\#\#\#}P < 0.001$; and these between experimental groups are denoted $^{***}P < 0.001$.

3.2.2. 8-Isoprostanes (8-epi PGF2α). The direction of OF-induced changes in the 8-epi PGF2α level was similar to that in the basal level of this marker. A significant impact of EMF intensity and the combination of two factors (EMF intensity x number of exposures) was noticed (Table 1(d); Figure 4(b)). There was no significant difference in 8-epi PGF2α level between the control group (C/OF) and animals exposed to

EMF of 1 mT after E1; however, the level of this parameter after E2 was decreased compared to the control value ($P < 0.05$), and after E3, it returned to the control value. The decrease in 8-epi PGF2α level was also observed after E2 relative to E1 ($P < 0.05$). In the EMF/OF/7mT group, the clear increase of 8-epi PGF2α level compared to the control value was noticed only after E3 ($P < 0.001$); however, the tendency to increase
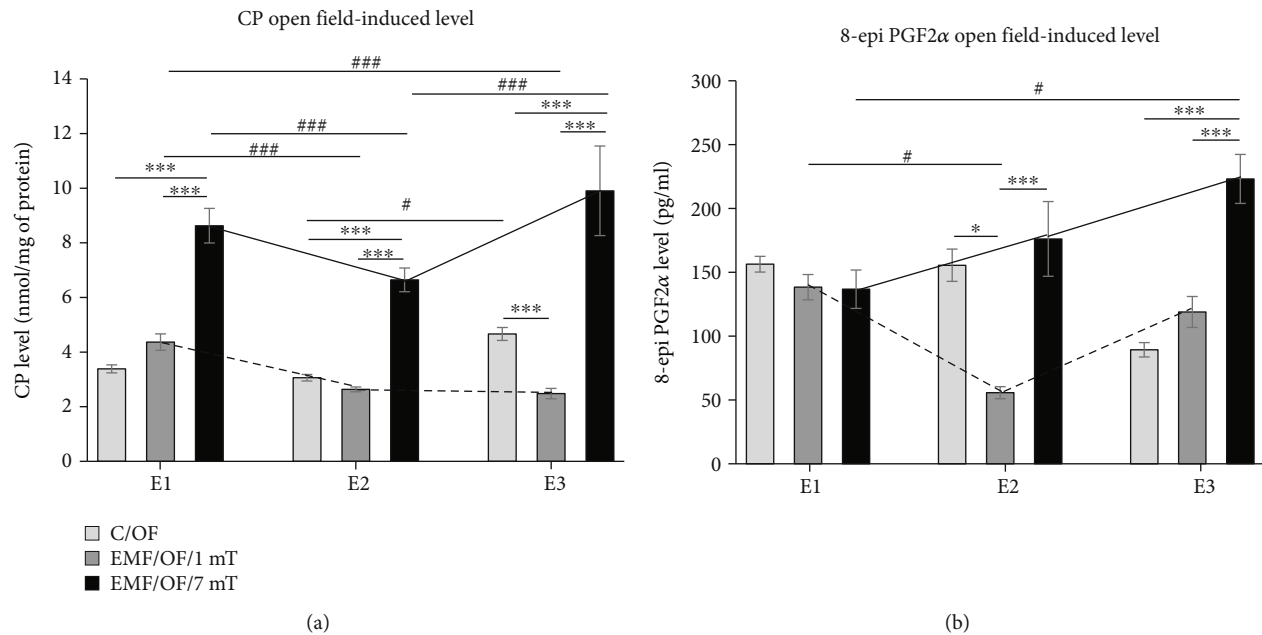
Figure 4: The open field-induced level of oxidative stress markers: (a) CP groups and (b) 8-epi PGF2α in the prefrontal cortex of rat's brain. Animals were exposed once to three times (E1-E3) to EMF of 1 or 7 mT or control conditions. Values are presented as mean ± SEM. The lines show the direction of changes in the level of stress markers in 1 mT (dotted line) and 7 mT (solid line) groups after each subsequent exposure. Statistically significant differences between animals from the same group are denoted $^{\#}P < 0.05$ and $^{\#\#\#}P < 0.001$, and these between experimental groups are denoted $^{*}P < 0.05$ and $^{***}P < 0.001$.

in the level of 8-epi PGF2α was noticed with each subsequent exposure. The level of 8-epi PGF2α after E3 was also significantly higher compared to its value after E1 ($P < 0.05$). After second and third exposures to EMF of 7 mT, the significant increase of 8-epi PGF2α level relative to 1 mT was noticed ($P < 0.001$).

3.3. Comparison between Basal Level and Open Field Test-Induced Level of Oxidative Stress Markers.
Table 2 presents the results of analysis comparing the basal levels of oxidative stress markers to their levels after the open field test for each group, respectively: C/B vs .C/OF, EMF/B/1mT vs. EMF/OF/1mT, and EMF/B/7mT vs. EMF/OF/7mT). The analysis showed that both the open field test and the number of exposures do not affect the CP level in the control group, only interaction of both factors had a significant influence on CP level in this group (Table 2(a)). In the group exposed to EMF of 1 mT, the CP level has been changed after open field, and the interaction between the open field test and the number of exposures also profoundly affected the CP level (Table 2(b)). In the group exposed to EMF of 7 mT, we have found the significant influence of the open field test on the increase in CP levels, and the number of exposures has no effect; however, the interaction between these factors was significant (Table 2(c)). The changes of 8-epi PGF2α level in the control group were dependent only on the number of exposures (Table 2(d)). The clearest effect of both factors as well as the interaction between them was noticed in rats exposed to EMF of 1 mT (Table 2(e)). In rats exposed to EMF of 7 mT, the 8-epi PGF2α level was not affected by any factor (Table 2(f)).

Valuable results were received when we evaluated the percentage changes in the level of stress markers in comparison to their level in the control C/B group separately after each exposure (set at 100%: reference value) (Figure 5).

CP level in the prefrontal cortex (Figure 5(a)) in group C/OF increased clearly after E3 (by 64%) in comparison to the C/B group. In the EMF/B/1 mT group, the level of CP was higher by 117% than that in the control group (C/B) after E3. Otherwise, after exposure to open field, the level of CP in rats previously exposed to EMF of 1 mT in comparison to the level in the EMF/B/1mT group was increased only after E1 (by 45%) and then was decreased even in comparison to both control groups (C/B and C/OF). In EMF/B/7mT, the level of CP after each subsequent exposure was higher in comparison to the value in the control group (C/B) (by 50 51 and 79%, respectively) and the open field test remarkably increased the level of the parameter after E1 (by 118%) and E3 (by 168%), except after E2 when the value of CP was similar to its basal level.

A similar direction of changes as in the case of CP groups level was observed in 8-epi PGF2α level in the control group as well as in groups exposed to EMF of 1 and 7 mT (Figure 5(b)). In the case of 8-epi PGF2α in animals exposed to EMF of 7 mT, the higher basal level of this marker should be noticed after each exposure in comparison to the control level (C/B) with its incredibly high level after E3 (267% of reference value). After OF test, the level of 8-epi PGF2α decreased slightly relative to its basal level in this group.

3.4. The Basal Level of Total Antioxidant Capacity (TAC).
The intensity of EMF, as well as EMF intensity × number

TABLE 2: Results of statistical analysis of effects of open field stress on oxidative stress markers level in relation to its basal level in each experimental group.

	Dependent variable/group	Effect	df	F	P
a	CP Control group	Open field effect	1	1.964	0.168
		Number of exposures ($E1$-$E3$)	2	2.253	0.118
		Number of exposures × open field effect	2	32.078	*<0.001*
		Error	42		
b	CP EMF/1mT	Open field effect	1	52.023	*<0.001*
		Number of exposures ($E1$-$E3$)	2	3.077	0.055
		Number of exposures × open field effect	2	66.370	*<0.001*
		Error	49		
c	CP EMF/7mT	Open field effect	1	47.966	*<0.001*
		Number of exposures ($E1$-$E3$)	2	1.876	0.164
		Number of exposures × open field effect	2	12.193	*<0.001*
		Error	48		
d	8-epi PGF2α Control group	Open field effect	1	2.995	0.091
		Number of exposures ($E1$-$E3$)	2	33.444	*<0.001*
		Number of exposures × open field effect	2	1.422	0.252
		Error	44		
e	8-epi PGF2α EMF/1mT	Open field effect	1	14.228	*<0.001*
		Number of exposures ($E1$-$E3$)	2	15.181	*<0.001*
		Number of exposures × open field effect	2	6.000	*0.005*
		Error	47		
f	8-epi PGF2α EMF/7mT	Open field effect	1	2.005	0.163
		Number of exposures ($E1$-$E3$)	2	2.649	0.081
		Number of exposures × open field effect	2	0.064	0.938
		Error	48		

F: GLM; statistically significant P value: indicated in italic; CP: protein carbonyl groups.

of exposures interaction, had a significant influence on TAC level (Table 3(a), Figure 6(a)). The level of TAC in animals exposed to EMF of both intensities was not significantly different from that noticed in the C/B group. In the group exposed to EMF of 1 mT, only after $E3$ the tendency to decrease in the TAC level in comparison to the control value was observed. The only detectable decrease of TAC level in the EMF/B/1mT group was observed after $E3$ relative to that after $E2$ ($P < 0.05$). The TAC level in animals exposed to EMF of 7 mT was lower than that in the EMF/B/1mT group after $E2$ ($P < 0.05$). However, the tendency to decrease in the value of TAC level in animals exposed to EMF of 7 mT was observed after each subsequent exposure relative to its level in the C/B group.

3.5. The Open Field-Induced Level of Total Antioxidant Capacity (TAC). The direction of changes in the open field test-induced level of TAC in all groups was similar as in the case of its basal level. The strength of the electromagnetic field, as well as the number of exposures, significantly influenced the changes of open field-induced TAC level. The interaction between both factors was also notable (Table 3(b), Figure 6(b)). After a single exposure to EMF of 1 mT, the TAC level was higher compared to the value in the respective control group (C/OF) ($P < 0.05$). After $E2$,

the value of TAC was comparable to the control level, and only after $E3$, it dropped significantly compared to the value in the control group ($P < 0.05$). In addition, in the EMF/OF/1mT group, the TAC level after $E1$ and $E2$ was clearly higher compared to that observed after $E3$ ($P < 0.001$). After first exposure to EMF of 7 mT, the level of TAC was significantly decreased compared to that in control animals exposed to OF (C/OF) ($P < 0.01$) as well as to its value in the EMF/OF/1mT group ($P < 0.001$). Moreover, in the EMF/OF/7mT group, the level of TAC was significantly decreased after $E1$ and $E3$ compared to that noticed after $E2$ ($P < 0.01$).

3.6. Comparison between Basal Level and Open Field Test-Induced Level of TAC. Any of the factors did not affect the TAC level in the control group (Table 4(a)). In the group exposed to EMF of 1 mT, the significant influence of the open field test and the number of exposures as well as their interaction on TAC level was found (Table 4(b)). In the 7 mT group, the number of exposures had a significant impact on TAC level. Moreover, the interaction between the open field test and the number of exposures was also significant (Table 4(c)).

The percentage changes in TAC level (Figure 7) in the control group after the open field test was clear. The value of antioxidant's level marker was increased in comparison
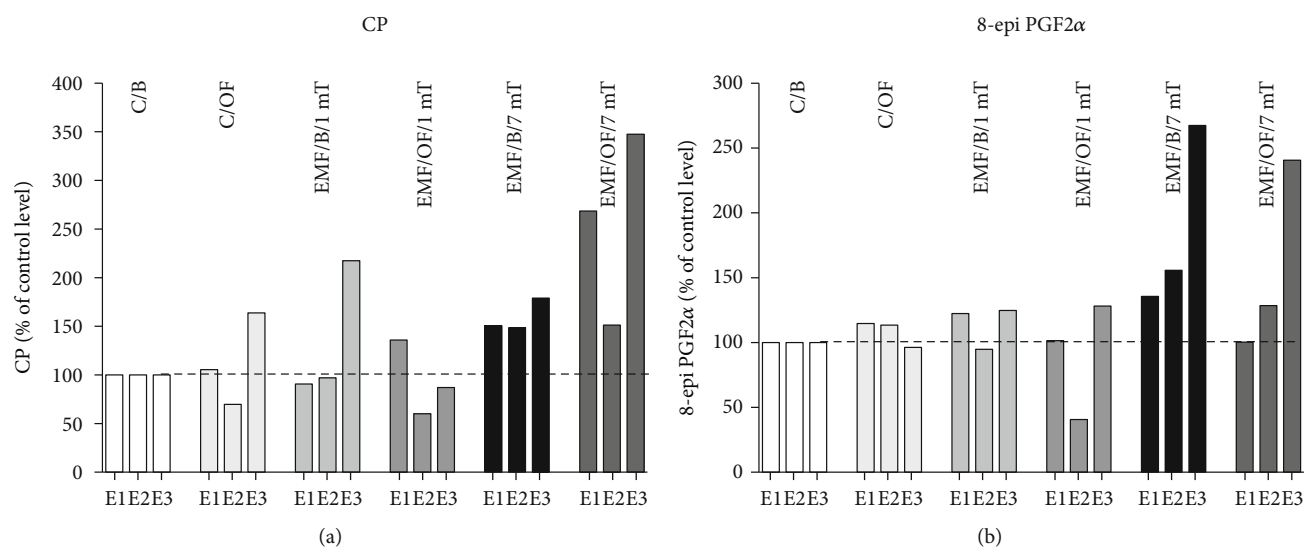
FIGURE 5: Percentage changes in the basal level as well as open field-induced level of oxidative stress markers: (a) CP groups and (b) 8-epi PGF2α in each experimental group in relation to their level in the control C/B group set at 100% after each subsequent exposure (E1-E3).

TABLE 3: Results of statistical analysis of the TAC level in the prefrontal cortex.

	Dependent variable	Effect	df	F	P
a	TAC basal level	Intensity of the electromagnetic field (mT)	2	5.088	*0.008*
		Number of exposures (E1-E3)	2	2.209	0.117
		(mT) × (E1-E3)	4	3.163	*0.018*
		Error	79		
b	Open field-induced TAC level	Intensity of the electromagnetic field (mT)	2	11.803	*<0.001*
		Number of exposures (E1-E3)	2	27.075	*<0.001*
		(mT) x (E1-E3)	4	11.086	*<0.001*
		Error	78		

F: GLM; statistically significant *P* value: indicated in italic; TAC: total antioxidant capacity.

to its basal level after E1 by 17%. In the EMF/OF/1mT group, the TAC amount was higher than that in the EMF/B/1mT group after E1 (by 45%) and E2 (by 15%), while after E3, the TAC level was close to its basal level. In rats from the EMF/B/7mT group after all exposures, the basal level of TAC was lower than that in the C/B group (by 13, 20, 3%, respectively). In the EMF/OF/7mT group, the noticed value of TAC after E1 was similar to the basal control value; after E2, the level of TAC was increased (by 24%); and then, after E3, the OF-induced level of TAC was decreased by 15% in comparison to values in EMF/B/7mT.

4. Discussion

Our experiments have shown that repeated exposure to the extremely low-frequency electromagnetic field (EMF) profoundly changes the oxidative/antioxidative status in the prefrontal cortex of rats in the EMF intensity- and number of exposure-dependent manner. The level of oxidative stress markers and antioxidants in rats exposed to EMF of 1 mT was not very different from the control value. In rats exposed

to EMF of 1 mT, a significantly increased protein carbonyl groups level was noticed only after third exposure compared to the control group. In the case of 8-isoprostanes, the exposure to EMF of 1 mT did not significantly affect their level; however, the tendency to decrease with each following exposure was noticed. Moreover, in the 1 mT EMF-exposed group, the profound change in the basal TAC level was not found. The level of TAC was a little, not significantly increased after the first and second exposures.

Generally, most research confirmed the antioxidative effects of EMF of ≤ 1 mT. Patruno et al. [12] observed elevated catalase (CAT) activity in cell culture (myelogenous leukemia cells: K562) after exposure to 50 Hz 1 mT EMF concomitantly with a decrease in the activity of inducible nitric oxide synthase (iNOS). In an animal model of Huntington's disease EMF (60 Hz and 0.7 mT), exposure reduced levels of oxidative stress biomarkers [27]. In C2C12 muscle cells, no change in reactive oxygen species (ROS) production was observed after exposure to EMF of 1 mT [11]. The research indicating that even low levels (≤ 1 mT) of a single EMF exposure can cause an increase in

FIGURE 7: Percentage changes in the basal level as well as open field-induced level of TAC in each experimental group in relation to their level in control C/B group set at 100% after each subsequent exposure (E1-E3).

Our results showed that EMF of 1 mT creates weak changes in oxidative status in the rat's brain. Many studies showed that stress induces the disruption in homeostasis [15, 32], and as a consequence, an overcompensation response is triggered to reestablish homeostasis, and such effect was seen in response to EMF of 1 mT after two first exposures. The compensatory mechanisms driven during first exposure to EMF seem to be able to maintain the oxidative equilibrium even after the second exposure, only after the third exposure the cumulative effect of all exposures as an increase in oxidative stress simultaneously with a discrete decrease of antioxidants was visible.

In animals exposed to EMF of 7 mT, the characteristic of changes in oxidative stress and antioxidative defence markers was quite different. The clear increase of CP groups was visible earlier than in the group exposed to EMF of 1 mT— already after the second exposure and remained high after the third exposure. Moreover, the tendency to increase in the level of 8-epi PGF2α with each subsequent exposure was noticed, and eventually, after E3, the 8-epi PGF2α level was significantly higher (more than 2.5 times) than that in the control group. In animals exposed to EMF of 7 mT, the tendency to decrease in the TAC level was observed after each subsequent exposure relative to its level in the control group. The present results indicate that the changes in TAC level were accompanied by a parallel increase in oxidative stress markers. The other research also showed that exposure to EMF (40-50 Hz) of intensities close to this used in our research (≥ 6 mT) alters oxidative stress and antioxidant defense parameters. In the serum of ICR mice, the level of MDA was significantly higher after exposure to EMF of 6, 8, and 10 mT, and simultaneously, the level of antioxidant enzyme superoxide dismutase (SOD) activity was decreased [8]. Similarly, in mouse brains subjected to EMF (8 mT), the levels of MDA, ROS, nitrogen oxide (NO), and nitric oxide synthase (NOS) were increased, whereas activities of antioxidants enzymes: SOD, CAT, and glutathione

peroxidase (GPx), were decreased [33]. The disturbance of oxidative status was also found in testes of rats (diabetic model) exposed to EMF (8.2 mT) in the form of elevated MDA and NO levels and diminished glutathione (GSH) level was found [34]. The measurements of oxidative stress markers in the rat's heart and plasma after exposure to EMF of 7 mT showed a significant increase in thiobarbituric acid reactive substances (TBARS) and H_2O_2 concentration and the diminished antioxidant defense decreased TAC, GSH, and total free thiol groups level [20]. In vitro studies confirmed that after exposure to electromagnetic field (8 mT), a decrease in the viability and morphological changes of the rat hippocampal neurons were observed with an increase in the level of MDA and ROS and a decrease in the activity of SOD [22]. Otherwise, opposite results have also been received, e.g., poststroke patients after EMF therapy (7 mT) showed improved enzymatic antioxidant activity [13]. As in the case of studies on the effects of EMF of lower intensities ≤ 1 mT, the abovementioned results are the consequence of continuous exposure for 14-28 days (day by day, 15 min-4 h/day) or as in the case of in vitro studies— one 90-min lasting treatment. The present results indicate that in such challenging stress situations as repeated exposure to EMF of 7 mT, the balance is disturbed in the direction of a higher level of oxidative stress. It also suggests that not all homotypic stressors cause response habituation. Responses to more "severe" stressors are maintained over time, perhaps due to the higher costs required to adapt to the particular situational demand [16]. Thus, the cumulative effect of repeated exposure to EMF of high intensity resulted in increased oxidative stress.

In our research, we identified the directions and dynamics of some mechanisms that may be brought into play in EMF-provoked changes. Although moderate stimulation by EMF (1 mT) even repeated might be not demanding for the organism, if strong (7 mT), it can lead to deleterious effects due to the increase in oxidative stress. The integrative

processes between all "players" determining oxidative/anti-oxidative balance appear to determine the final effect of EMF [2, 15]. As a result, even subtle changes in the brain can change the function of the neuronal circuits. An undisturbed oxidative/antioxidative balance is essential for the normal function of the organism. Unbalanced concentrations of oxidative processes products decrease the chance of overcompensation and increase brain vulnerability to other potentially dangerous events.

We have found that the exposure of rats to EMF of 1 mT influenced the oxidative/antioxidative status evolved in response to subsequent (heterogenous in relation to EMF) stress factor—open field test. EMF of 1 mT diminished the response to another stressor as the small elevation of open field-induced CP concentration was visible only after the first exposure to EMF, each next period of EMF-treatment decreased the level of the marker. In the case of 8-isoprostanes, their level was diminished after two first exposures, and after E3 received a similar value as in the respective group not-exposed to OF. In 1 mT EMF-treated rats, the augmented antioxidant defense in response to a new stress factor was visible after first exposure; then, the adaptation as the decrease in TAC level was observed. The changes in the TAC level can partly explain the reduction in oxidative stress in this group. Our results allowed us to conclude that the subtle changes in the level of oxidative status in animals repeatedly exposed to EMF of 1 mT were enough to change the profile of oxidative processes after exposure to another kind of stress factor— open field test. It suggests that it can be a kind of habituation, when one stressor diminishes the response to the second one [16].

The EMF of 7 mT disturbs the oxidative/antioxidative balance as the changes in oxidative stress markers as well as antioxidant capacity level were still clear after each subsequent exposure to the open field. The pattern and size of the changes in 8-epi PGF2α level after subsequent exposures to open field in rats previously exposed to EMF of 7 mT were close to the changes in basal level. The open field-induced CP level in rats exposed to EMF of 7 mT has been increasing with each subsequent exposure and was definitely higher than that in respective control as well as in the 1 mT EMF-exposed group. The response to first contact with a new stressor was also the significant decrease in TAC level, which then increased to the value not different from that in the respective control group. Thus, we suggest that the exposure to one stressor (EMF) sensitizes the organism to a second stressor (open field), resulting in a faster onset of oxidative stress and its higher level in 7 mT exposed animals in comparison to the values in 1 mT EMF-treated rats. Djordjevic et al. [35] have also found that in rats exposed to open field after EMF exposure (50 Hz, 10 mT, 24 h for 7 days) the levels of superoxide anion and nitrites in the hypothalamus were increased compared to the control group; however, the observed changes are the synergic effect of both factors, as the oxidative status of rats after EMF exposure was not evaluated in this research. Our results suggest that a high level of magnetic flux density (7 mT) of EMF is able to disturb the brain oxidative/antioxidative status, and to shift its set-point in the direction of increase of oxidative processes and as a consequence can augment the oxidative processes in response to the next stress events.

5. Conclusions

Summarizing, as we hypothesized, the level of EMF appears to be essential for direction and dynamics of the stress response: changes in oxidative/antioxidative parameters after exposure to 1 mT EMF were observed at a lower level than these after exposure to 7 mT EMF; moreover, the character of changes was also different. Our data confirmed that the exposure to EMF of 1 mT can establish a new "set-point" for cellular oxidative processes and may initiate cellular adaptation by activation of intrinsic signaling pathways directed into the decrease of oxidative stress, although the cumulative effect of repeated exposure cannot be definitely excluded. Otherwise, in the case of a stronger electromagnetic field (7 mT), the adaptive processes are not sufficient to counteract its detrimental effects. Consequently, EMF can change the vulnerability of the organism to subsequent stress factors and thus to diseases, mainly related to the nervous system. Our research for the first time showed the different "mode of action" of EMF in relation to oxidative/antioxidative status in the brain dependently on its magnetic flux density value. In addition, what is even more important, we proved that the effects of EMF can be permanent and influence the response of the organism to other stress events and in this way modulate the vulnerability to the diseases. We are convinced that the results of our research extended the knowledge on mechanisms of EMF's impact on human health. Further, the elucidation of the EMF-induced changes in the oxidative/antioxidative status is necessary to a reliable assessment of the influence of EMF on the brain. The obtained results can also provide a new view on possible therapeutic properties of the magnetic field as well as a new direction in the risk assessment of EMF exposure. As the 1 mT seems to have a potentially protective impact on the brain, the studies are worth continuing.

Data Availability

The data used to support the findings of this study are included within the article.

Conflicts of Interest

The authors declare that there is no conflict of interest regarding the publication of this paper.

Authors' Contributions

Acknowledgments

References

[1] G. Thut, C. Miniussi, and J. Gross, "The functional importance of rhythmic activity in the brain," *Current Biology*, vol. 22, no. 16, pp. R658–R663, 2012.

[2] Y. Touitou and B. Selmaoui, "The effects of extremely low-frequency magnetic fields on melatonin and cortisol, two marker rhythms of the circadian system," *Dialogues in Clinical Neuroscience*, vol. 14, no. 4, pp. 381–399, 2012.

[3] P. Bieńkowski and J. Wyszkowska, "Technical aspects of exposure to magnetic fields of extremely low frequencies (ELF) in biomedical research," *Medycyna Pracy*, vol. 66, no. 2, pp. 185–197, 2015.

[4] C. N. Black, M. Bot, P. G. Scheffer, P. Cuijpers, and B. W. Penninx, "Is depression associated with increased oxidative stress? A systematic review and meta-analysis," *Psychoneuroendocrinology*, vol. 51, pp. 164–175, 2015.

[5] J. N. Cobley, M. L. Fiorello, and D. M. Bailey, "13 reasons why the brain is susceptible to oxidative stress," *Redox Biology*, vol. 15, pp. 490–503, 2018.

[6] S. Salim, "Oxidative stress and the central nervous system," *The Journal of Pharmacology and Experimental Therapeutics*, vol. 360, no. 1, pp. 201–205, 2017.

[7] M. El-Helaly and E. Abu-Hashem, "Oxidative stress, melatonin level, and sleep insufficiency among electronic equipment repairers," *Indian journal of occupational and environmental medicine*, vol. 14, no. 3, pp. 66–70, 2010.

[8] X. Luo, M. Chen, Y. Duan et al., "Chemoprotective action of lotus seedpod procyanidins on oxidative stress in mice induced by extremely low-frequency electromagnetic field exposure," *Biomedicine & Pharmacotherapy*, vol. 82, pp. 640–648, 2016.

[9] Y. Sun, Z. Shi, Y. Wang et al., "Coupling of oxidative stress responses to tricarboxylic acid cycle and prostaglandin E2 alterations in *Caenorhabditis* elegans under extremely low-frequency electromagnetic field," *International Journal of Radiation Biology*, vol. 94, no. 12, pp. 1159–1166, 2018.

[10] J. Frahm, M. O. Mattsson, and M. Simkó, "Exposure to ELF magnetic fields modulate redox related protein expression in mouse macrophages," *Toxicology Letters*, vol. 192, no. 3, pp. 330–336, 2010.

[11] C. Morabito, F. Rovetta, M. Bizzarri, G. Mazzoleni, G. Fanò, and M. A. Mariggiò, "Modulation of redox status and calcium handling by extremely low frequency electromagnetic fields in C2C12 muscle cells: a real-time, single-cell approach," *Free Radical Biology & Medicine*, vol. 48, no. 4, pp. 579–589, 2010.

[12] A. Patruno, S. Tabrez, M. Pesce, S. Shakil, M. A. Kamal, and M. Reale, "Effects of extremely low frequency electromagnetic field (ELF-EMF) on catalase, cytochrome P450 and nitric oxide synthase in erythro-leukemic cells," *Life Sciences*, vol. 121, pp. 117–123, 2015.

[13] N. Cichoń, M. Bijak, E. Miller, and J. Saluk, "Extremely low frequency electromagnetic field (ELF-EMF) reduces oxidative stress and improves functional and psychological status in ischemic stroke patients," *Bioelectromagnetics*, vol. 38, no. 5, pp. 386–396, 2017.

[14] R. Szemerszky, D. Zelena, I. Barna, and G. Bárdos, "Stress-related endocrinological and psychopathological effects of short- and long-term 50 Hz electromagnetic field exposure in rats," *Brain Research Bulletin*, vol. 81, no. 1, pp. 92–99, 2010.

[15] A. Klimek and J. Rogalska, "Extremely low-frequency magnetic field as a stress factor-really detrimental?-insight into literature from the last decade," *Brain sciences*, vol. 11, no. 2, p. 174, 2021.

[16] J. P. Herman, J. M. McKlveen, S. Ghosal et al., "Regulation of the hypothalamic-pituitary-adrenocortical stress response," *Comprehensive Physiology*, vol. 6, no. 2, pp. 603–621, 2016.

[17] E. J. Calabrese, "Overcompensation stimulation: a mechanism for hormetic effects," *Critical Reviews in Toxicology*, vol. 31, no. 4-5, pp. 425–470, 2001.

[18] J. W. Gawryluk, J. F. Wang, A. C. Andreazza, L. Shao, and L. T. Young, "Decreased levels of glutathione, the major brain antioxidant, in post-mortem prefrontal cortex from patients with psychiatric disorders," *The International Journal of Neuropsychopharmacology*, vol. 14, no. 1, pp. 123–130, 2011.

[19] *Directive 2013/35/EU of the European Parliament and of the Council of 26 June 2013 on the minimum health and safety requirements regarding the exposure of workers to the risks arising from physical agents (electromagnetic fields)*, 2013.

[20] A. Goraca, E. Ciejka, and A. Piechota, "Effects of extremely low frequency magnetic field on the parameters of oxidative stress in heart," *Journal of Physiology and Pharmacology*, vol. 61, no. 3, pp. 333–338, 2010.

[21] E. Ciejka, P. Kleniewska, B. Skibska, and A. Goraca, "Effects of extremely low frequency magnetic field on oxidative balance in brain of rats," *Journal of Physiology and Pharmacology*, vol. 62, no. 6, pp. 657–661, 2011.

[22] C. Yin, X. Luo, Y. Duan et al., "Neuroprotective effects of lotus seedpod procyanidins on extremely low frequency electromagnetic field-induced neurotoxicity in primary cultured hippocampal neurons," *Biomedicine & Pharmacotherapy*, vol. 82, pp. 628–639, 2016.

[23] A. C. Calvo and M. J. Azanza, "Synaptic neurone activity under applied 50 Hz alternating magnetic fields," *Comparative Biochemistry and Physiology. Part C, Pharmacology, Toxicology & Endocrinology*, vol. 124, no. 1, pp. 99–107, 1999.

[24] T. M. Maynard, L. Sikich, J. A. Lieberman, and A. S. LaMantia, "Neural development, cell-cell signaling, and the "two-hit" hypothesis of schizophrenia," *Schizophrenia Bulletin*, vol. 27, no. 3, pp. 457–476, 2001.

[25] *Directive 2010/63/EU of the European Parliament and of the Council of 22 September 2010 on the protection of animals used for scientific purposes*, 2010.

[26] T. Trawiński, M. Szczygieł, J. Wyszkowska, and K. Kluszczyński, "Analysis of magnetic field distribution and

mechanical vibration of magnetic field exciter under different voltage supply," *Information Technologies in Biomedicine*, vol. 69, pp. 613–622, 2010.

[27] I. Tasset, F. J. Medina, I. Jimena et al., "Neuroprotective effects of extremely low-frequency electromagnetic fields on a Huntington's disease rat model: effects on neurotrophic factors and neuronal density," *Neuroscience*, vol. 209, pp. 54–63, 2012.

[28] C. Merla, M. Liberti, C. Consales et al., "Evidences of plasma membrane-mediated ROS generation upon ELF exposure in neuroblastoma cells supported by a computational multiscale approach," *Biochimica et Biophysica Acta - Biomembranes*, vol. 1861, no. 8, pp. 1446–1457, 2019.

[29] A. M. Eleuteri, M. Amici, L. Bonfili et al., "50 Hz Extremely Low Frequency Electromagnetic Fields Enhance Protein Carbonyl Groups Content in Cancer Cells: Effects on Proteasomal Systems," *Journal of Biomedicine & Biotechnology*, vol. 2009, Article ID 834239, 10 pages, 2009.

[30] M. Z. Akdag, S. Dasdag, E. Ulukaya, A. K. Uzunlar, M. A. Kurt, and A. Taşkin, "Effects of extremely low-frequency magnetic field on caspase activities and oxidative stress values in rat brain," *Biological Trace Element Research*, vol. 138, no. 1-3, pp. 238–249, 2010.

[31] M. Z. Akdag, S. Dasdag, D. U. Cakir, B. Yokus, G. Kizil, and M. Kizil, "Do 100- and 500-μT ELF magnetic fields alter beta-amyloid protein, protein carbonyl and malondialdehyde in rat brains?," *Electromagnetic Biology and Medicine*, vol. 32, no. 3, pp. 363–372, 2013.

[32] A. Zimmermann, M. A. Bauer, G. Kroemer, F. Madeo, and D. Carmona-Gutierrez, "When less is more: hormesis against stress and disease," *Microbial Cell*, vol. 1, no. 5, pp. 150–153, 2014.

[33] Y. Duan, Z. Wang, H. Zhang et al., "The preventive effect of lotus seedpod procyanidins on cognitive impairment and oxidative damage induced by extremely low frequency electromagnetic field exposure," *Food & Function*, vol. 4, no. 8, pp. 1252–1262, 2013.

[34] D. Kuzay, C. Ozer, B. Sirav, A. G. Canseven, and N. Seyhan, "Oxidative effects of extremely low frequency magnetic field and radio frequency radiation on testes tissues of diabetic and healthy rats," *Bratislavské Lekárske Listy*, vol. 118, no. 5, pp. 278–282, 2017.

[35] N. Z. Djordjevic, M. G. Paunović, and A. S. Peulić, "Anxiety-like behavioural effects of extremely low-frequency electromagnetic field in rats," *Environmental Science and Pollution Research International*, vol. 24, no. 27, pp. 21693–21699, 2017.

Research Article

Mitochondrial DNA Efflux Maintained in Gingival Fibroblasts of Patients with Periodontitis through ROS/mPTP Pathway

Jia Liu [ID],[1,2] **Yanfeng Wang,**[1,2] **Qiao Shi,**[1,2] **Xiaoxuan Wang,**[1,2] **Peihui Zou,**[1,2] **Ming Zheng** [ID],[3] **and Qingxian Luan** [ID][1,2]

[1]*Department of Periodontology, Peking University School and Hospital of Stomatology, Beijing, China*
[2]*National Center of Stomatology & National Clinical Research Center for Oral Diseases & National Engineering Research Center of Oral Biomaterials and Digital Medical Devices, China*
[3]*Department of Physiology and Pathophysiology, Peking University Health Science Center, Beijing, China*

Correspondence should be addressed to Ming Zheng; zhengm@bjmu.edu.cn and Qingxian Luan; kqluanqx@bjmu.edu.cn

Mitochondria have their own mitochondrial DNA (mtDNA). Aberrant mtDNA is associated with inflammatory diseases. mtDNA is believed to induce inflammation via the abnormal mtDNA release. Periodontitis is an infectious, oral inflammatory disease. Human gingival fibroblasts (HGFs) from patients with chronic periodontitis (CP) have shown to generate higher reactive oxygen species (ROS) that cause oxidative stress and have decreased mtDNA copy number. Firstly, cell-free mtDNA was identified in plasma from CP mice through qRT-PCR. Next, we investigated whether mtDNA efflux was maintained in primary cultures of HGFs from CP patients and the possible underlying mechanisms using adenovirus-mediated transduction live cell imaging and qRT-PCR analysis. Here, we reported that mtDNA was increased in plasma from the CP mice. Additionally, we confirmed that CP HGFs had significant mtDNA efflux from mitochondria compared with healthy HGFs. Furthermore, lipopolysaccharide (LPS) from *Porphyromonas gingivalis* can also cause mtDNA release in healthy HGFs. Mechanistically, LPS upregulated ROS levels and mitochondrial permeability transition pore (mPTP) opening by inhibition of pyruvate dehydrogenase kinase (PDK)2 expression, resulting in mtDNA release. Importantly, mtDNA efflux was even persistent in HGFs after LPS was removed and cells were passaged to the next three generations, indicating that mtDNA abnormalities were retained in HGFs in vitro, similar to the primary hosts. Taken together, our results elucidate that mtDNA efflux was maintained in HGFs from periodontitis patients through abnormal ROS/mPTP activity. Therefore, our work indicates that persistent mtDNA efflux may be a possible diagnostic and therapeutic target for patients with periodontitis.

1. Introduction

Periodontal inflammation is known to affect 20%-50% of the global population, and it often interacts with other inflammatory diseases such as heart disease and diabetes [1–3]. Periodontitis is associated with lipopolysaccharide (LPS) from the cell walls of gram-negative bacteria-mediated inflammatory responses and represents the most common cause of teeth loss [1, 4, 5]. Increasing evidences suggest that mitochondrial dysfunction appears to result in periodontitis during LPS stimulus [6–8]. As such, abnormal mitochondria are considered to be one of the major contributors to the periodontitis development. Several mitochondrial compo-

nents, including mitochondrial DNA (mtDNA), have also been implicated in inflammatory responses [9].

mtDNA exists in mitochondrial matrix and is in intimate contact with the electron transport chain, one of the principal sources of reactive oxygen species (ROS). Therefore, mtDNA is particularly susceptible to oxidation, which can cause mutations and damages, leading to the pathogenesis of inflammation [10]. ROS production and ROS produced in mitochondria (mtROS) are indeed significantly enhanced in human gingival fibroblasts (HGFs) after LPS stimulation or from periodontitis hosts [11]. These results indicate that oxidative stress is induced during periodontitis [12]. According to current studies linking oxidative stress to

decreased mtDNA copy number [13, 14], it is becoming clear that mtDNA disruption may be associated with chronic inflammation [15]. Consistent with this assumption, previous research has also demonstrated that mtDNA deletion is present in the gingival tissues of patients with periodontitis [16]. Moreover, a decrease in mtDNA in periodontitis rats suggested that aberrant mtDNA might contribute to aggravated periodontitis [7]. Considering our recent observation that HGFs and gingival tissues of patients with periodontitis in vitro had decreased mtDNA levels and decreased mitochondrial matrix protein expression, especially in pyruvate dehydrogenase kinase 2 (PDK2) when compared with those from healthy subjects [8], suggesting that mtDNA and mitochondria disruption in peripheral HGFs might replicate the mitochondrial dysfunction observed in vivo during periodontitis development. Therefore, we hypothesized that abnormal mtDNA might be maintained in HGFs in vitro connecting the disease in vivo with a certain mechanism. Answering these problems will improve our understanding of the periodontitis etiology, and it might lead to new treatment options.

Superresolution imaging demonstrated that mtDNA constitutes one copy of mtDNA and a number of different proteins, presenting densely compacted nucleoids [17]. Mitochondrial transcription factor A (TFAM) is the most notable mtDNA nucleoid protein that can be assumed to specifically recognize mtDNA [15]. mtDNA can escape from mitochondria and release into the cytoplasm under various pathological situations [18, 19]. Multiple major factors have been attributed to driving mtDNA release from damaged mitochondria, including the opening of mitochondrial permeability transition pore (mPTP), mitochondrial stress, and calcium overload [20–22]. Nonetheless, the biological mechanisms provide limited information on this process during periodontitis conditions. Our recent study demonstrated that mitochondria in HGFs from periodontitis patients appeared to retain many of the damaged features, as observed in donors [8]. In addition, previous studies have suggested that the primary host has profound influence on the cells in vitro, such as higher oxidative stress in HGFs of periodontitis patients than that of healthy individuals [8, 23]. However, differences of mtDNA release in HGFs from chronic periodontitis (CP) patients and healthy HGFs have not been tested and if this abnormal intracellular mtDNA activity would last need to be further elucidated. Thus, therapies targeting mtDNA may become a potential approach to patients suffered from severe recurrent periodontitis.

The mPTP spans the mitochondrial inner membrane, and its formation is associated with various cellular stresses [24, 25]. Interestingly, the opening of mPTP has been detected in the metabolic stress observed in inflammatory diseases [26]. More recently, using an in vitro and in vivo approach, studies have shown that genetic removal of one of the mPTP component proteins ameliorated mtDNA release into the cytoplasm during the neuroinflammatory response [20]. Pharmacological inhibition of mPTP by cyclosporin A (CsA) has also been shown to be effective in preventing mtDNA leakage into the cytoplasm [20]. Despite

these results in previous studies, the notion that the opening of mPTP may directly drive mtDNA efflux remains controversial and is still unclear in periodontitis. It has been reported that ROS contributes directly to mPTP opening during ischemia-reperfusion [27]. As a result of cellular ROS and mtROS outburst, mPTP opening can be activated. Nevertheless, its association with mPTP involved in mtDNA efflux in periodontitis is scarcely understood.

In this study, we discovered the differences in the mtDNA efflux process, ROS levels, and mPTP opening between primary HGFs, isolated from patients with CP and age-matched periodontally healthy patients. This elevated mtDNA efflux together with high ROS levels, and mPTP opening in CP HGFs could be more enhanced in response to LPS. Furthermore, this identified mtDNA efflux as an important modifier could be maintained in HGFs even withdrawing the LPS stimulation after passages. Consequently, we explored if the ROS/mPTP pathway involving in the mtDNA efflux along with the progression of periodontitis. This may be a promising target for early diagnosing periodontitis and provides preclinical evidence for therapeutic strategy to people with periodontal inflammation tolerating common anti-microorganism therapy.

2. Materials and Methods

2.1. Ethics Approval. The study was approved by the Review Board and Ethics Committee of Peking University Health Science Center (PKUS-SIRB-2013017) and conducted in agreement with the Declaration of Helsinki II. Written informed consent was obtained from all subjects before inclusion in the study. All animal work was approved by the Review Board and Ethics Committee of Peking University Health Science Center (LA2018076).

2.2. Animals and Experimental Groups. Specific-pathogen-free male C57BL/6 wild-type mice (6-wk-old) (Figure 1(a)) were purchased from Experimental Animal Laboratory, Peking University Health Science Center, in compliance with established polices. All mice were randomly divided into the normal control groups or CP groups of four mice each. The control group was left untreated, and the CP group had their maxillary second molar tooth ligated with a 5-0 silk ligature (Roboz Surgical Instrument Co, MD, USA) (Figure 1(a)). The ligatures remained in place in CP groups throughout the experimental period. All mice were sacrificed at three weeks postligation (Figure 1(a)). Microcomputed tomography (CT) was used for assuring the CP model was established successfully.

2.3. Microcomputed Tomography. In brief, after sacrificing the mice, the maxillary teeth were carefully dissected and soft tissues were removed. The sample was fixed with 4% paraformaldehyde for 24 h, and scanned using the μCT50 (Scanco Medical) with a resolution of 1024×1024, pixel size of $15 \times 15 \mu$m, and layer spacing of 15μm. The region of interest was assessed by 3D reconstructed. Bone loss was evaluated by 3D micro-CT.

(a)

(b)

(c)

(d)
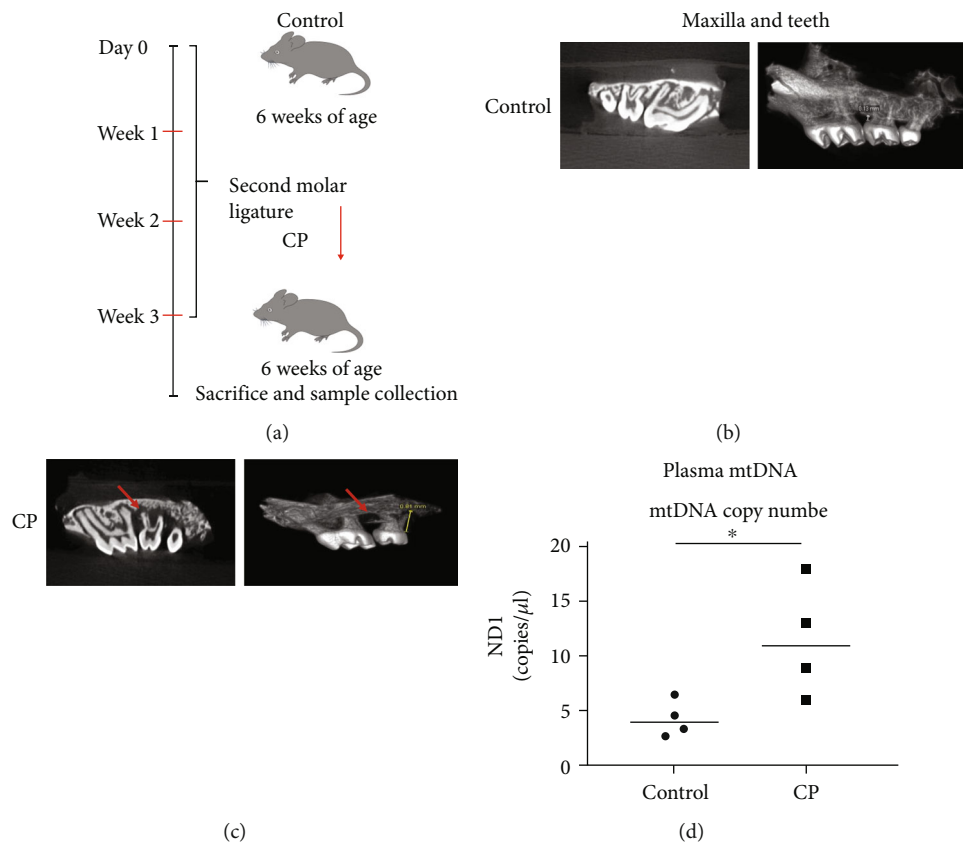
FIGURE 1: Cell-free- (cf-) mtDNA in plasma from chronic periodontitis mice and control healthy mice. (a) 5-0 silk suture was sutured for three weeks passing around the maxillary second molar in 6-week-old mice for establishing experimental chronic periodontitis (CP) mouse model. Control normal mice had no treatment. (b–c) Micro-CT showed obviously increased bone loss in CP mice after ligation for three weeks when compared to the control group. One representative image for 2-dimensional and 3-Dmode is shown. The red arrow represents bone loss areas. The yellow line indicates the distance between cement-enamel junction (CEJ) and alveolar bone crest (AEJ). (d) ND1 levels in plasma between CP and control mice ($n = 4$). $^*p < 0.05$.

2.4. Human Subjects.

HGFs were obtained from six CP patients and six age-matched healthy donors. These participants were recruited from the Department of Periodontology, Peking University School and Hospital of Stomatology. The exclusion criteria included smoking and systemic health issues including hypertension, diabetes, and immune-related diseases within the past six months. CP was defined according to the American Academy of Periodontology and European Federation of Periodontology criteria based on staging and grading [28]. CP patients included in this study were grade B and stage III. Gingival tissues from CP were acquired through flap surgery, with PD ≥ 6 mm. Tissues in the healthy group were harvested during crown lengthening surgery, with PD < 4 mm. Table 1 lists the detailed characteristics of the participants.

2.5. Primary Culture of HGFs.

HGFs were prepared from the gingival tissues of six CP patients and six healthy controls during periodontal surgery. Cells were grown in Dulbecco's modified Eagle's medium supplemented with 10% fetal bovine serum (Gibco, Thermo Fisher Scientific, USA) and 1% penicillin-streptomycin. The cells were incubated at 37°C with 5% CO_2. The medium was changed after a week. In approximately two weeks, the cells reached subconfluency

TABLE 1: Clinical characteristics at surgery site of patients included in this study.

Abbreviation	Number of patients	Range of age	Percent women	BI PD (mm)	CAL (mm)
Con	6	27-40	50	1-2	0-0.5
CP	6	33-45	66.7	6-10	4-7

and the pieces of gingival tissue were removed from the culture flask. Cells from the third to the eighth passage were used in the subsequent study.

2.6. Cell Treatment and Stimulation.

HGFs from healthy and CP patients were stimulated with or without 5 μg/mL LPS from Porphyromonas gingivalis (P.g) (ATCC33277, Standard, InvivoGen, San Diego, CA, USA) for 24 h. To investigate whether inflammatory features of donors were retained in HGFs, HGFs from healthy donors were treated with 5 μg/mL of LPS for 24 h, followed by discarding the medium then passaging to the next three generations for analysis. The cells were assessed by indicated assays and compared with cells from healthy donors that were directly stimulated with the same amount of LPS for the same time.

TABLE 2: List of primers for real-time PCR studies.

Gene	Primer	Sequence
ND 1	Forward primer	5′-CACACTAGCAGAGACCAACCGAAC-3′
	Reverse primer	5′-CGGCTATGAAGAATAGGGCGAAGG-3′
18S rRNA	Forward primer	5′-GACTCAACACGGGAAACCTCACC-3′
	Reverse primer	5′-ACCAGACAAATCGCTCCACCAAC-3′

2.7. Cellular ROS and Mitochondrial ROS (mtROS) Detection.

$2′,7′$-Dichlorodihydrofluorescein diacetate (H2DCF-DA) (Sigma-Aldrich, St. Louis, MO) and MitoSOX Red (Invitrogen, Carlsbad, CA) were used to detect total ROS and mtROS, respectively, as previously described [11]. HGFs were loaded with H2DCF-DA ($10\,\mu$M) or MitoSOX Red ($5\,\mu$M) for 30 min and then observed using a microscope [11]. To inhibit ROS levels, HGFs were preincubated with 3 mM N-acetylcysteine (NAC) (Sigma Aldrich, St. Louis, MO) for 2 h. The mtROS scavenger $50\,\mu$M Mito-TEMPO (Santa Cruz Biotech, Dallas, TX) were pretreated for 2 h.

2.8. Western Blotting.

Proteins were extracted from HGFs using ice-cold radioimmunoprecipitation (RIPA) lysis buffer (Solarbio). After being quantified by BCA (Thermo Fisher Scientific), the protein samples were mixed with loading buffer (Solarbio), separated by electrophoresis on SDS-PAGE. The proteins in the gel were transferred on a polyvinylidene fluoride (PVDF) membrane (Beyotime). The membranes were blocked with 5% skimmed milk (Solarbio) and incubated overnight at 4°C with primary antibody. The membranes were washed with Tris-buffered saline and incubated with secondary antibody for 90 min at room temperature. The PVDF membranes were subjected to chemiluminescence detection using an ECL Western Blotting Detection Kit (Solarbio).

2.9. DNA Isolation and mtDNA Quantification by Quantitative Real-Time Polymerase Chain Reaction (qRT-PCR).

Genomic DNA from HGFs was extracted using the Universal Genomic DNA Kit (ZOMAN, Beijing, China), following the manufacturer's instructions. The mtDNA levels in HGFswere assessed using primers against mitochondrial genes (ND1), while nuclear 18S rRNA served as a loading control. Detailed ND1 and 18S rRNA sequences are presented in Table 2. Cytosolic mtDNA extraction was performed according to the methods established by West et al. [29]. The plasma from the mice was centrifuged at $1000\,g$ for 5 min, and then the supernatant was centrifuged a second time at $5000\,g$ for 10 min. The top 80% of the volume can be used for cell-free- (cf-) mtDNA quantification. DNA from cell supernatants, cf-mtDNA in plasma, and cytosol DNA ($200\,\mu$L) were isolated using the QIAamp DNA Mini Kit (Qiagen, Germany). ND1 levels in the samples were analyzed according to a standard curve based on ND1 plasmid (Sangon, Shanghai, China) levels.

2.10. Adenovirus Transduction for Mitochondria and mtDNA Detection.

HGFs were transduced with adenovirus encoding the mitochondrial outer-membrane protein Tomm 20 bearing a mCherry fluorescence protein. mtDNA was detected by coexpression of TFAM, tagged with the green fluorescent protein (GFP) variant mNeonGreen. HGFs were seeded on 10 mm round confocal glass coverslips at a density of 50% and were infected with specified amounts of the Tomm 20-mCherry and TFAM-mNeonGreen adenoviruses. Forty-eight hours after transduction, the medium was changed, and the cells were processed for further analysis.

2.11. Live Cell Imaging Microscopy.

Live cells were captured using a fluorescence microscope (TCS-STED; Leica, Wetzlar, Germany) with a $63\times$ oil immersion objective. For all experiments, HGFs were grown in 10 mm round glass bottom confocal wells (Cedarlane, Southern Ontario, Canada). Laser excitation was achieved at 488 nm for mNeonGreen and 561 nm for mCherry. LPS treatment was performed after sample mounting in the medium chamber, if needed. HGFs expressing Tomm 20-mCherry and TFAM-mNeonGreen were imaged serially at every 10 s for 10-15 min. Image processing and analysis were performed using ImageJ (NIH, http://rsb.info.nih.gov/ij/) and Huygens Professional software (Scientific Volume Imaging, Amsterdam, Holland).

2.12. Detection of mPTP Opening.

HGFs were incubated with 50 mM cobalt chloride for 15 min, before treatment with $1\,\mu$M Calcein Green AM (Solarbio, Beijing, China) for 30 min. Free Calcein quenching by cobalt chloride preserved mitochondrial integrity, which could be used to indicate mPTP opening. Calcein fluorescence was detected by confocal microscopy (Leica) using a 488 nm excitation wavelength. Quantification of the Calcein fluorescence intensity was conducted by analyzing 20 cells for every indicated condition using ImageJ software. To prevent mPTP opening, HGFs were preincubated with $0.5\,\mu$M cyclosporine A (CsA; Sigma) for 2 h, following the manufacturer's recommendations.

2.13. Flow Cytometric Analysis.

Cells were briefly washed with $1\times$ phosphate-buffered saline (PBS), resuspended in $1\times$ binding buffer, and centrifuged at $300\times g$ for 10 min. The pellets were resuspended with $1\times$ binding buffer at a density of 1×10^6 cells/mL. Cells were replated in a flow cytometric tube at a density of 1×10^5 cells/mL and processed for Annexin V-FITC staining (Solarbio, Beijing, China)for 10 min at 20-25°C. Subsequently, the cells were

(a)

(b)

(c)

(d)

(e)

(f)

FIGURE 2: Continued.

(g)

(h)

(i)
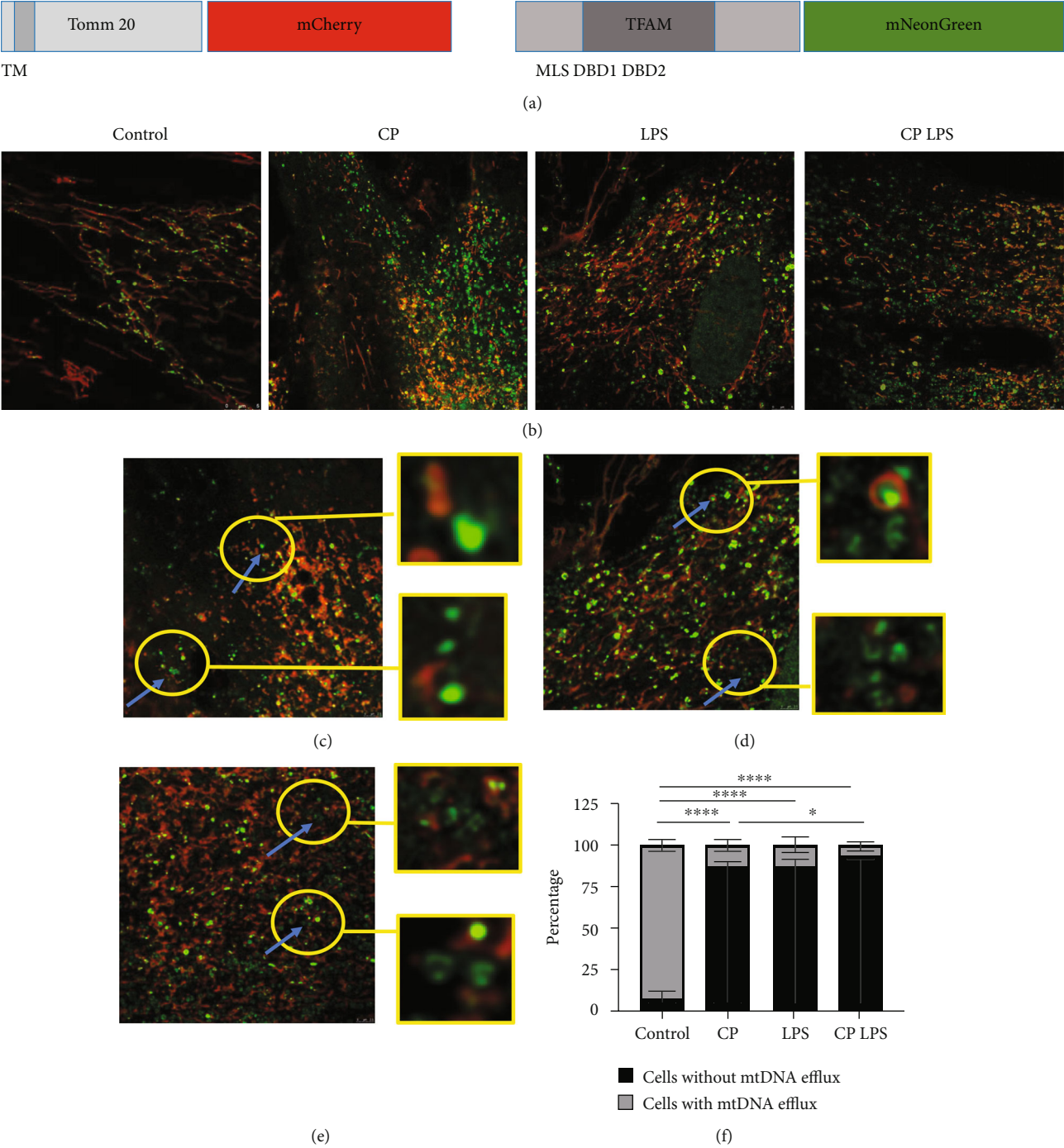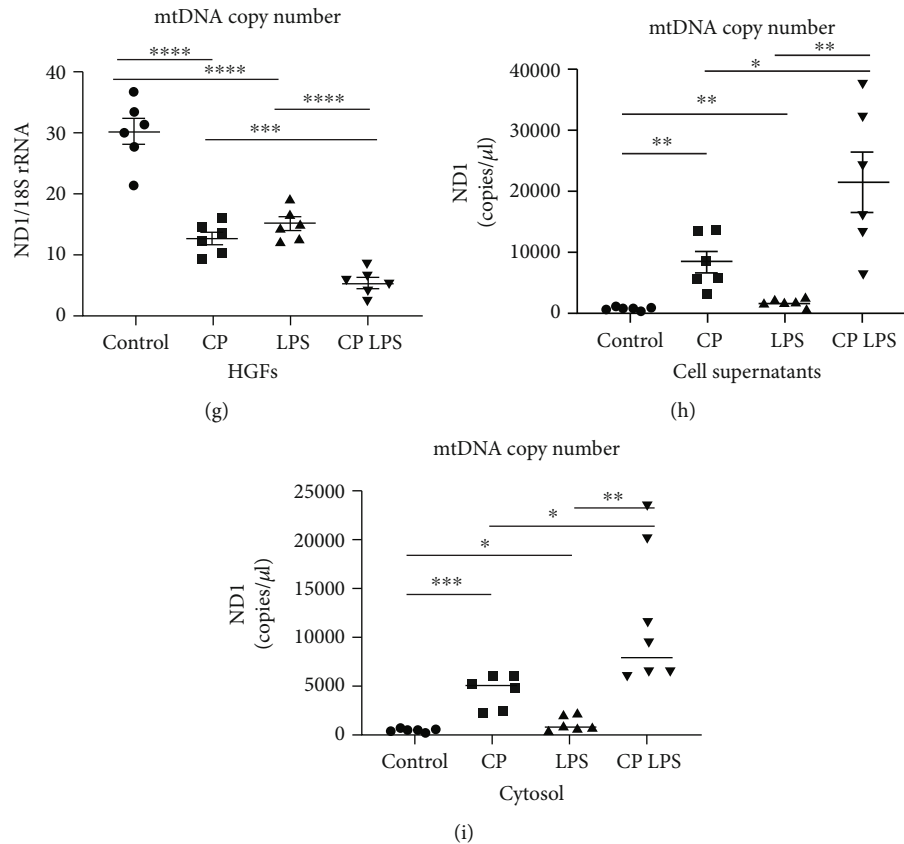
Figure 2: mtDNA released from mitochondria in human gingival fibroblasts from patients with chronic periodontitis. (a) Using fluorescent fusion proteins to visualize mitochondria (Tomm 20-mCherry) and mtDNA (TFAM-mNeonGreen). TM: transmembrane domain; MLS: mitochondrial localization sequence; DBD1 and DBD2: DNA binding domain-1 and DNA binding domain-2. (b) Typical illustration of the human gingival fibroblasts (HGFs) for mitochondria and mtDNA among control, CP, and with or without LPS stimulation (5 μg/mL, 24 h) groups (scale bars: 5 μm). (c) Still image of mtDNA efflux in HGFs from CP patients (scale bar: 2.5 μm, see Movie 1). (d) Still image of mtDNA efflux in HGFs with LPS stimulation (scale bar: 2.5 μm, see Movie 2). (e) Still image showing mtDNA efflux in HGFs from CP patients with LPS stimulation (scale bar: 2.5 μm, see Movie 3). (f) Percentage of HGFs with, without mtDNA efflux. Data are the mean ± SE of 20 fields in each group. (g–i) mtDNA in HGFs, cell supernatants, and cell cytosol. Data are obtained by six independent experiments. $^*p < 0.05$, $^{**}p < 0.01$, $^{***}p < 0.001$, and $^{****}p < 0.0001$.

stained with propidium iodide (PI) for 5 min at 20-25°C and analyzed for apoptosis by flow cytometry.

2.14. Statistical Analysis. Data are expressed as the mean ± standard error (SE). All p values were determined by two-way Student's t-test or one-way analysis of variance (ANOVA) with a post hoc Student Knewman-Keuls test for multiple comparisons. Significant differences were accepted at $p < 0.05$. Statistical analysis was performed using GraphPad Prism software (version 9.00; GraphPad Software).

3. Results

3.1. mtDNA Release from Mitochondria during Periodontitis Development. Micro-CT results revealed that alveolar bone around the ligated molar was significantly reduced in CP mice compared to control mice, suggesting experimental periodontitis in the CP group established (Figures 1(b) and 1(c)). Intriguingly, mtDNA in plasma from CP mice were enriched compared to age-matched wild-type control mice

(Figure 1(d)). These results indicated that mtDNA release might be involved in periodontitis development. However, mtDNA efflux in HGFs during periodontitis is still unclear. Next, we transduced primary HGFs with adenovirus encoding Tomm 20-mCherry and TFAM-mNeonGreen to show mitochondria and mtDNA, respectively (Figure 2(a)). mtDNA were detected robust release into the cytoplasm in CP HGFs (Figure 2(b)). This process was also found by real-time microscopy (Figure 2(c), Movie 1). In contrast, no mtDNA efflux was detected in healthy HGFs (Movie S1). LPS caused remarkable mtDNA release in healthy HGFs and led to more significant mtDNA release in periodontitis-affected samples (Figures 2(b)–2(d), and 2(e), Movie 2 and 3).Next, we calculated a significant increase in the percentage of HGFs with mtDNA efflux in CP HGFs as compared with that in control HGFs (Figure 2(f)). LPS treatment caused marked increase in the percentage of HGFs with mtDNA efflux compared with those without LPS treatment in healthy and CP states (Figure 2(f)). Moreover, qRT-PCR confirmed that mtDNA release into cytosol and out of cells during periodontitis (Figures 2(g)–2(i)). These results
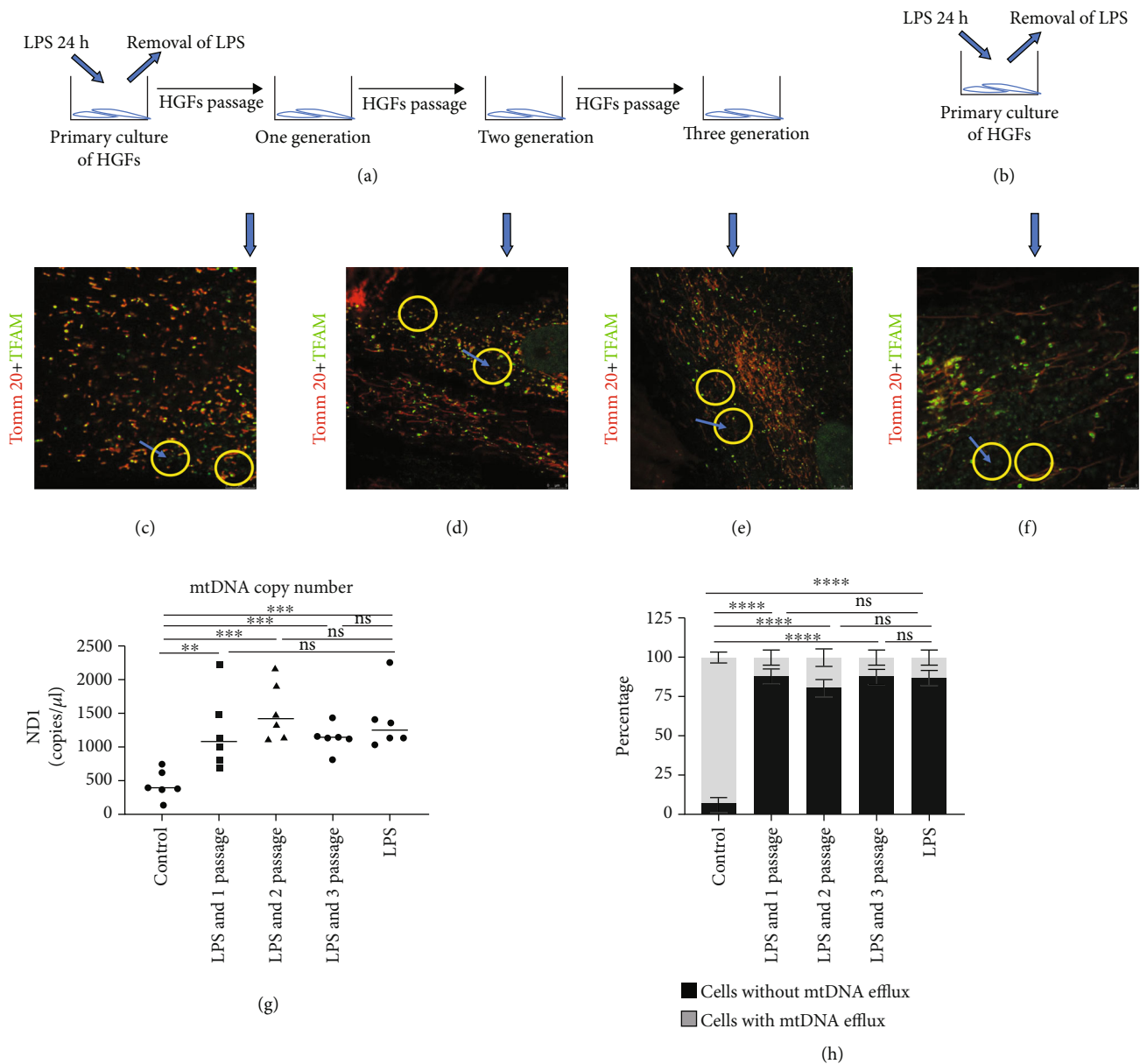
Figure 3: mtDNA efflux maintained inhuman gingival fibroblasts during periodontitis. (a) Human gingival fibroblasts (HGFs) were treated with lipopolysaccharide (LPS) (5 μg/mL, 24 h), which was later removed from the culture medium. These LPS-treated HGFs were cultured to next three generations for analysis. (b) HGFs were cultured with LPS direct stimulation (5 μg/mL, 24 h), which will be directly analyzed for mtDNA activity. (c–e) Images of HGFs in the A group for analysis after passaging three generations, respectively. (f) Images of HGFs in the B group. Scale bars: 5 μm. (g) mtDNA levels in cytosol among the five groups of HGFs. $n = 6$. (h) Percentage of HGFs with, without mtDNA efflux. Data in (h) are the mean ± standard error (SE) of 20 fields per group. ns = no significant difference. $^{**} p < 0.01$, $^{***}p < 0.001$, and $^{****}p < 0.0001$.

indicated that mtDNA release might be involved in periodontitis development.

3.2. mtDNA Efflux Maintained in HGFs during Periodontitis.

LPS is a principal factor that determines the periodontal inflammation; we decided to clarify if LPS causes mtDNA efflux maintained in HGFs. In these experiments, healthy HGFs were exposed to LPS stimulation for 24 h. Next, LPS was removed and HGFs were cultured into the next three generations for analysis (Figure 3(a)). In contrast, healthy HGFs were directly treated with LPS for 24 h (Figure 3(b)).

The results showed that LPS reinforced the mtDNA efflux effect even in the next three generational HGFs (Figures 3 (c)–3(e)). No significant differences were observed compared to the LPS directly treated HGFs (Figure 3(f)). Next, we examined the mtDNA levels in the cytosol using qRT-PCR analyzing these groups. LPS directly stimulated HGFs, and LPS treatment following passages of HGFs were both enriched in cytosolic mtDNA (Figure 3(g)). In addition, the percentages of HGFs with mtDNA efflux between LPS direct treatment and LPS treatment followed by HGFs passages were similar (Figure 3(h)). These results suggest that LPS treatment can

(a)

(b)

(c)

(d)

Figure 4: Continued.

(e)
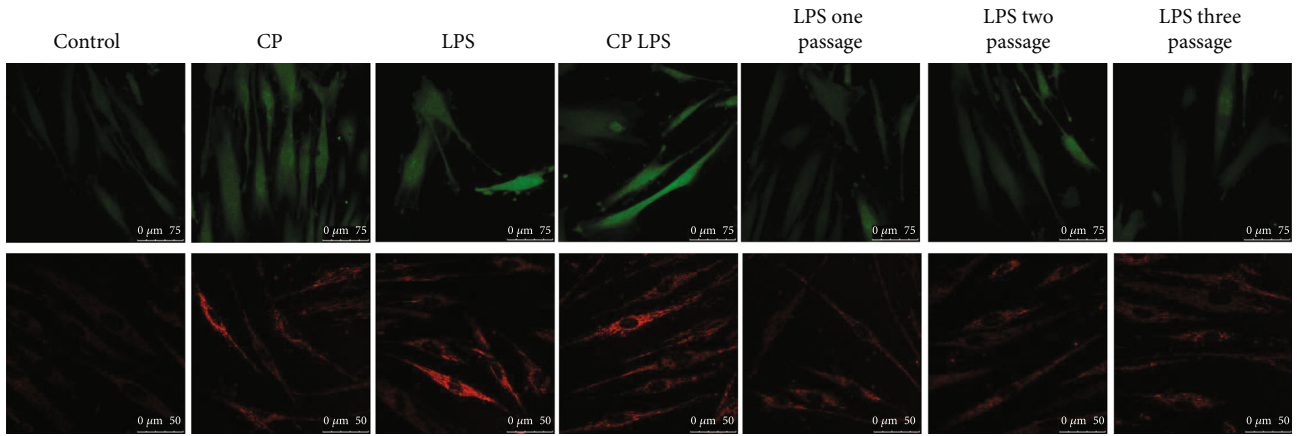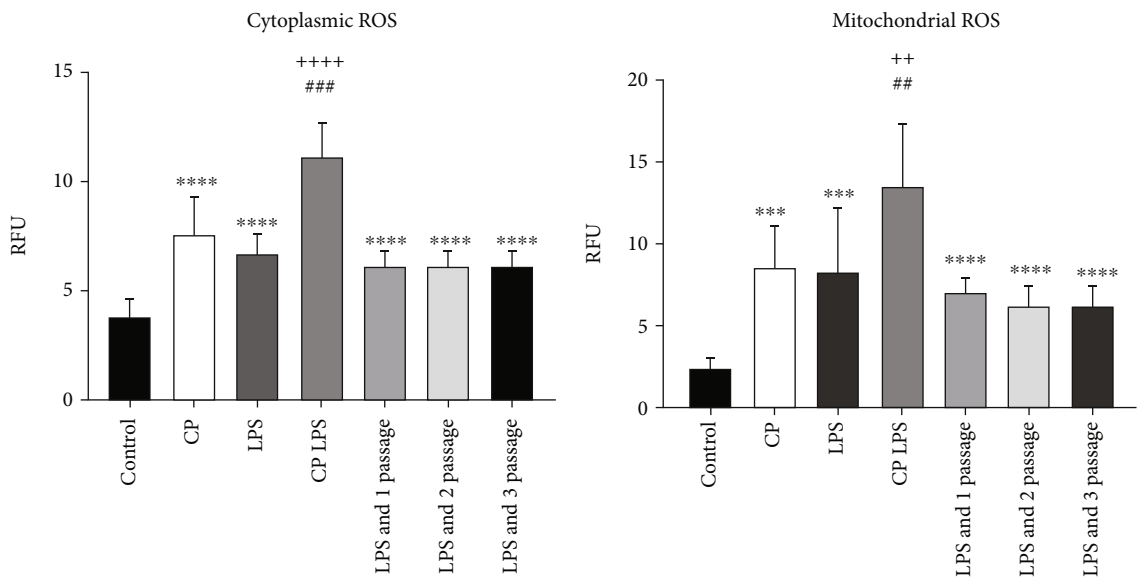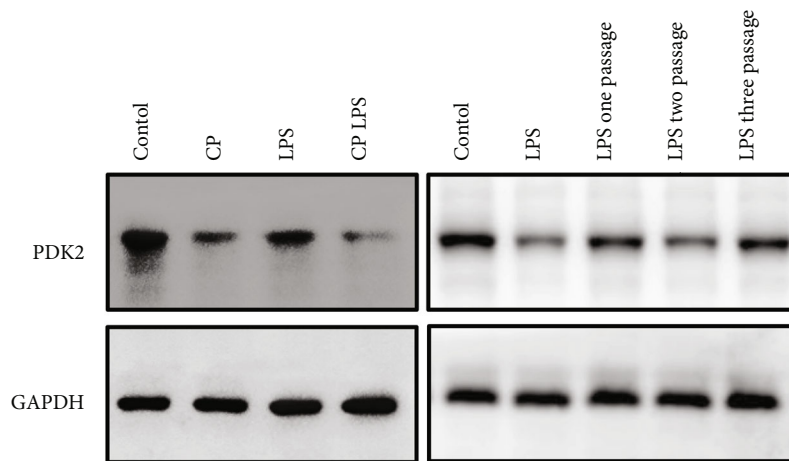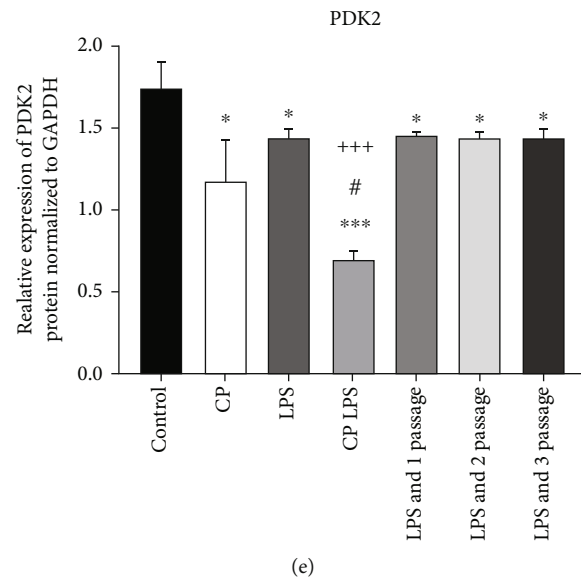
Figure 4: Reactive oxygen species (ROS) and mitochondrial ROS is overproduction in human gingival fibroblasts from chronic periodontitis patients. (a) Human gingival fibroblasts (HGFs) were incubated with $2',7'$-dichlorodihydrofluorescein diacetate (H2DCF-DA) ($10\,\mu$M, 30 minutes) to indicate the ROS levels (green) in HGFs (scale bars: $75\,\mu$m). HGFs were incubated with MitoSOX Red ($5\,\mu$M, 30 minutes) to visualize mitochondrial ROS (mtROS) levels (red) (scale bars: $50\,\mu$m). (b, c) The arbitrary fluorescence intensity of ROS and mtROS in (a) were calculated by ImageJ based on per 10 cells in each group from (a). Data represent the mean ± standard error (SE) from 10 cells from each group. (d) Western blot to evaluate the protein expression of pyruvate dehydrogenase kinase 2 (PDK2). Glyceraldehyde-3-phosphate dehydrogenase (GAPDH) as the loading control. (e) Quantification of each band intensity with respect to loading control in D. $n = 3$ (LPS: $5\,\mu$g/mL). Statistically significant p value is indicated as follows: $^*p < 0.05$, $^{***}p < 0.001$, and $^{****}p < 0.0001$ as compared with the control group; $^\#p < 0.05$, $^{\#\#}p < 0.01$, and $^{\#\#\#}p < 0.001$ as compared with the CP group; $^{++}p < 0.01$, $^{+++}p < 0.001$, and $^{++++}p < 0.0001$ as compared with the LPS group.

enhance this mtDNA efflux phenomenon, and the facilitative mtDNA release effects can be maintained in HGFs even in the next-generations HGFs, which is consistent with those mtDNA release of CP HGFs and CP mice.

3.3. ROS and mtROS Is Overproduction in HGFs from CP Patients.

To investigate in further details how mtDNA efflux effect remained during periodontitis at cellular level, we firstly analyzed the ROS and mtROS levels in HGFs from different hosts. Control healthy HGFs had the lowest ROS and mtROS levels (Figure 4(a)). HGFs from CP had significantly greater levels of ROS and mtROS (Figure 4(a)). We found that the ROS and mtROS were more activated in the presence of LPS compared to those in the absence of LPS groups (Figure 4(a)). In addition, LPS can affect ROS and mtROS even in the next three generations HGFs (Figure 4 (a)). Furthermore, the levels of these fluorescent signals reflecting ROS and mtROS levels in Figure 4(a) were calculated by ImageJ (Figures 4(b) and 4(c)). Western blot analysis showed PDK2 exhibited decreased expression in CP HGFs (Figures 4(d) and 4(e)). Meanwhile, the expression levels of PDK2 were also reduced after LPS stimulation and showed low levels even in the next three-generation HGFs (Figures 4(d) and 4(e)). In summary, CP HGFs are primed for ROS activation, and LPS can persistently upregulate the ROS levels in HGFs by suppressing the PDK2 expression. Its regulation may contribute to this mtDNA efflux process.

3.4. mPTP Opening in HGFs from CP Patients via ROS Activation.

mPTP opening in HGFs was indicative using Calcein AM fluorescence (Figure 5(a)). Control HGFs showed strong green fluorescence (Figure 5(a)), suggesting that mPTP remained in a closed state under normal condition [30]. However, the fluorescence was hardly detected in CP HGFs (Figure 5(a)). LPS further resulted in a much more decrease in fluorescence in the control and CP groups (Figure 5(a)). Decreased level of fluorescence signal was also detected in the LPS treated following passaging three generational HGFs (Figure 5(b)). A significant increase in fluorescence was observed in HGFs in the presence of CsA when compared with that in the absence of CsA (Figures 5(a)–5 (d)). It was shown that inhibition of ROS and mtROS activation contributes to suppression of mPTP opening (Figures 5 (a)–5(d)). Collectively, these data show that CP HGFs display mPTP opening and that mPTP opening in the LPS-treated HGFs was maintained within the HGFs even in the later three generations. Additionally, this observed mPTP opening is dependent on ROS activation.

3.5. mtDNA Release in CP HGFs via ROS and mPTP Opening.

We performed real-time fluorescent microscopy for control, CP, LPS treatment, and CP LPSHGFs in the presence of CsA (Figure 6(a)). It was observed that mtDNA displayed mild or no efflux in the four CsA-treated groups of HGFs (Figure 6(a)). These data demonstrated that mPTP was critical for the mtDNA release under these conditions.

(a)

(b)

Figure 5: Continued.

(c)
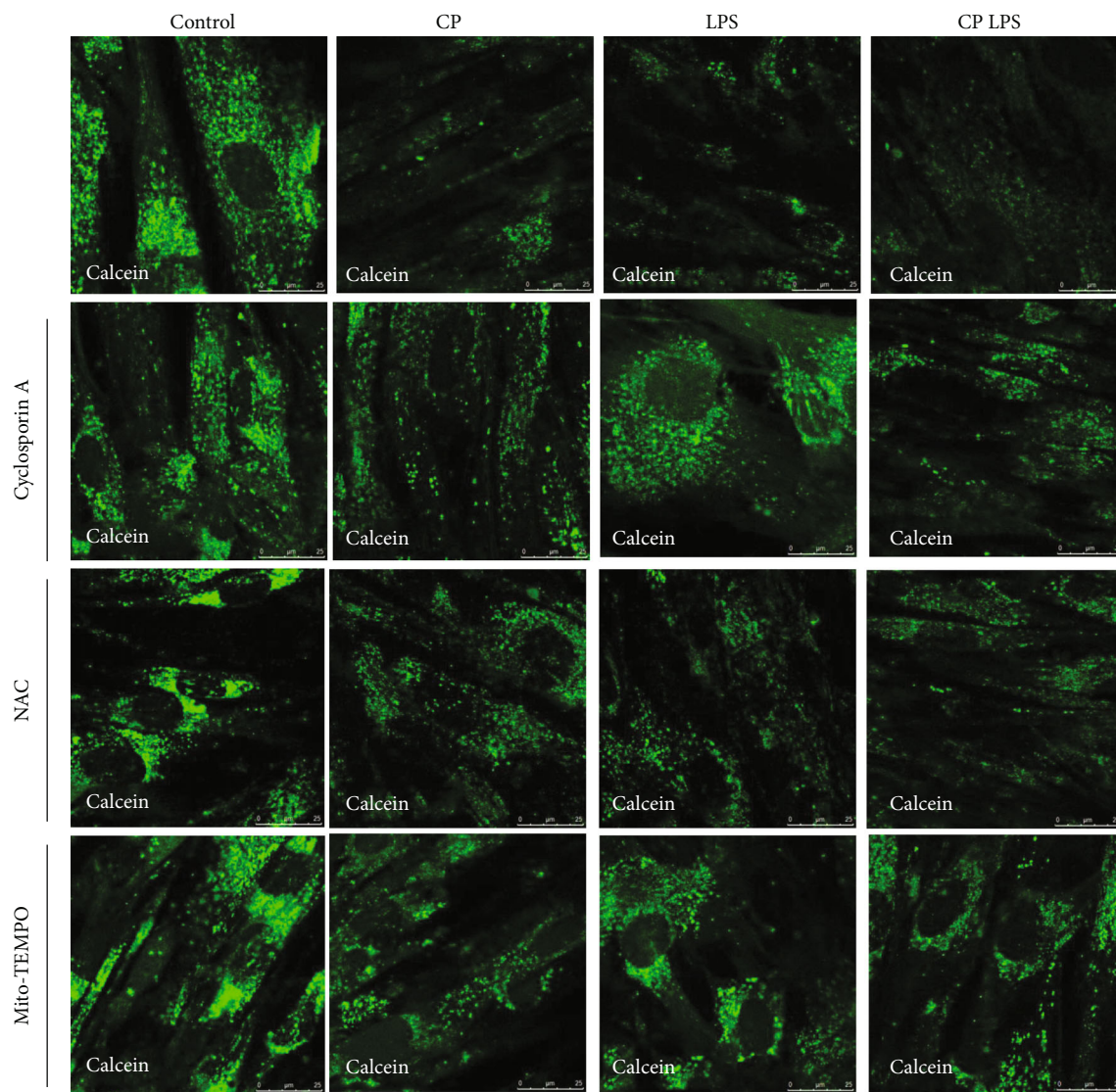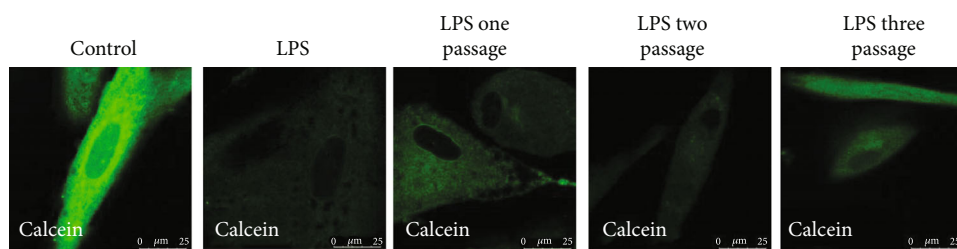
(d)
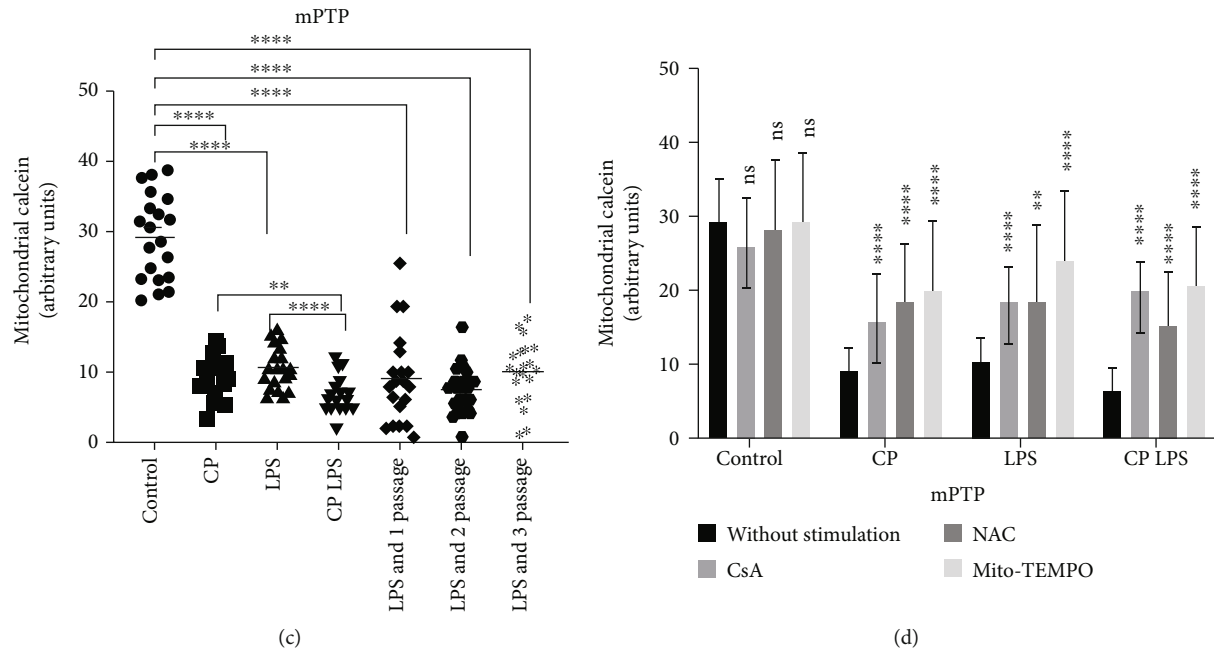
Figure 5: Human gingival fibroblasts (HGFs) from chronic periodontitis presented active mitochondrial permeability transition pore opening via reactive oxygen species. (a) Human gingival fibroblasts (HGFs) were loaded with cobalt chloride (50 mM, 15 minutes) and Calcein AM (green) to determine the opening of the mitochondrial permeability transition pore (mPTP) in HGFs in the presence or absence of lipopolysaccharide (LPS) treatment (5 μg/mL, 24 h). The opening of mPTP in HGFs was measured after cyclosporin A (CsA) (0.5 μM, 2 h) or N-acetylcysteine (NAC) (3 mM, 2 h)or Mito-TEMPO (50 μM, 2 h) treatment (scale bars: 25 μm). (b) Images for mPTP opening in the control, LPS-treated, and LPS-treated group after passaging three generations (scale bars: 25 μm). (c) Quantification of the observed Calcein green signal in HGFs from (a, b). Mean ± SE are indicated ($n = 20$ cells). The CP group was observed a lower signal; LPS was also observeda lower signal compared with control HGFs. LPS can aggravate this lower signal in the control and CP groups, and this phenomenon can be retained in HGFs after LPS was removed and passaged to next three generations as compared with the control group. (d) The intensity of the indicated Calcein green signal was detected per 20 cells from the control, CP, LPS, and CP LPS groups with CsA, NAC, and Mito-TEMPO treatment compared to HGFs without any treatment, respectively. CsA, NAC, and Mito-TEMPO all downregulated the signal in the LPS, CP, and CP LPS groups, while they fail to induce this phenomenon in control HGFs. p values were determined by 1-way analysis of variance followed by post hoc tests. $^{**}p < 0.01$ and$^{****}p < 0.0001$; ns: not significant.

We performed qRT-PCR to detect the cytosolic mtDNA levels by the inhibitors of mPTP, ROS, and mtROS. CsA, NAC, and Mito-TEMPO all decreased the cytosolic mtDNA levels in the CP, LPS, and CP LPS groups when compared with the three groups without any treatment, whereas the control group showed similar cytosolic mtDNA levels in the presence and absence of CsA and NAC (Figure 6(b)). We also showed that Mito-TEMPO slightly decreased cytosolic mtDNA concentration in healthy HGFs (Figure 6(b)). When we examined the difference in apoptosis of HGFs among the four groups, we found that HGFs from CP, LPS, and CP LPS showed no significant apoptosis when compared with the HGFs of control healthy donors (Fig. S1). Cumulatively, these results provide further evidence that ROS-mPTP opening causes mtDNA release in CP and LPS-treated HGFs.

4. Discussion

Mitochondrial dysfunction is an important component of periodontitis pathogenesis [31], as defects in mitochondrial structure and function have been shown in periodontitis in our previous work [8]. mtDNA is crucial for mitochondrial

function. It is known that mtDNA has structural similarities with microbial DNA [32]. Hence, mtDNA could result in an inflammatory response when released into the cytoplasm or extracellular milieu in susceptible patients. These mtDNA characteristics confirmed the significant role of mtDNA in the pathogenesis of inflammation-related diseases in humans. In this study, we examined mtDNA efflux activity and extent using confocal microscopy and qRT-PCR analysis between primary HGFs from periodontitis patients and healthy donors. We demonstrated for the first time that mtDNA released from the mitochondria in HGFs from CP patients. LPS stimuli was found to trigger this mtDNA efflux activity and keep these properties within the HGFs for some periods.

Studies have previously identified that mtDNA is found outside the mitochondria and sometimes even outside the cells in certain circumstances [33, 34]. mtDNA release was first reported that LPS pointed to extrude mtDNA into the cytoplasm [35]. Another key evidence for mtDNA extruding into the extracellular space is that LPS induces neutrophil extracellular traps (NETs) formation, largely consisting of mtDNA [36, 37]. This mtDNA release may result in substantial tissue damage, leading to chronic inflammation.

(a)

(b)
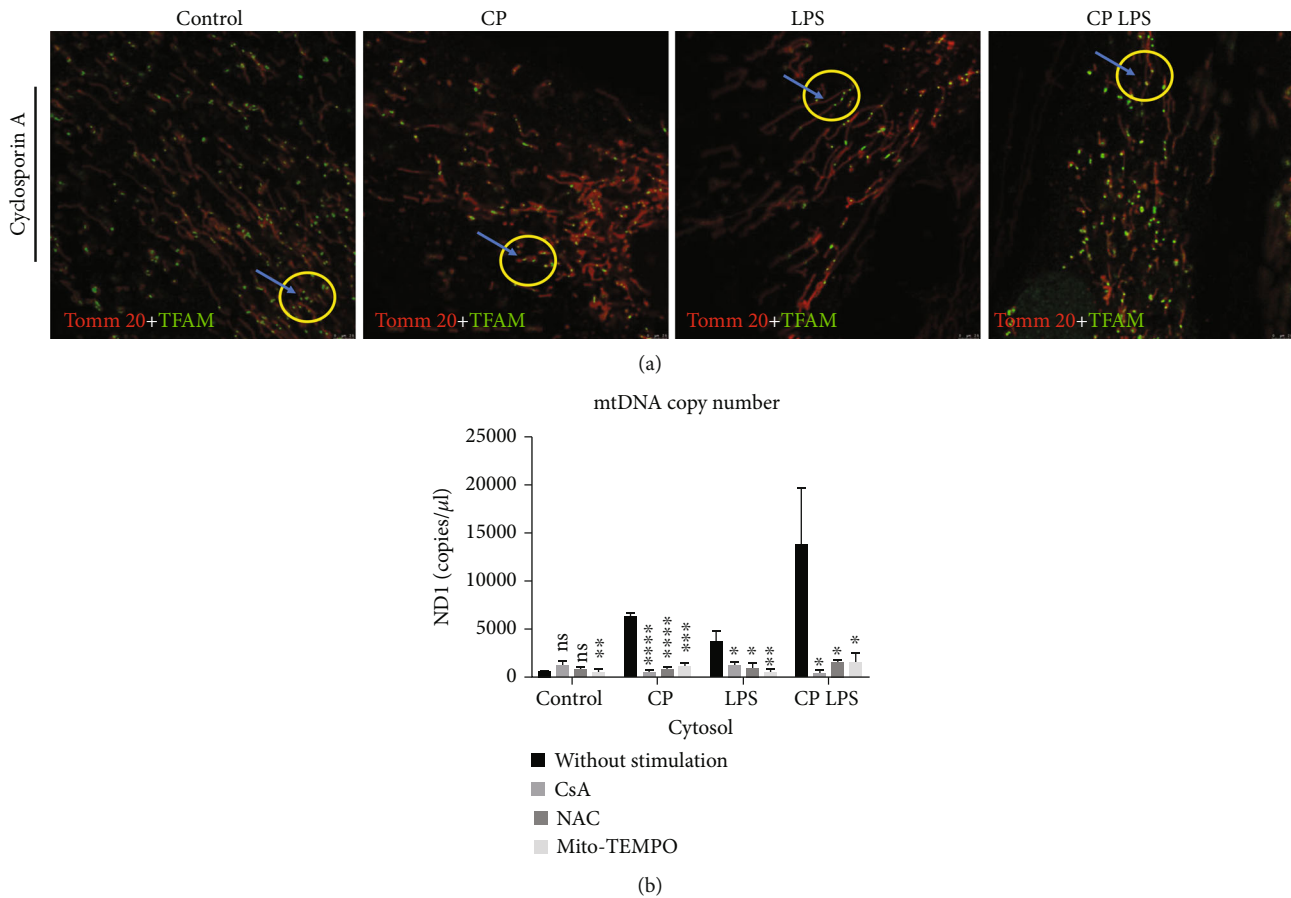
FIGURE 6: mtDNA release from mitochondria in human gingival fibroblasts of chronic periodontitis patients via reactive oxygen species-mitochondrial permeability transition pore pathways. (a) Human gingival fibroblasts (HGFs) from the control, chronic periodontitis (CP), and lipopolysaccharide (LPS) stimulation infection ($5\,\mu$g/mL, 24 h), and CP LPS groups were pretreated with $0.5\,\mu$M cyclosporin A (CsA) for 2 h and subjected to analysis for mtDNA release. HGFs expressing Tomm 20-mCherry (red) and TFAM-mNeonGreen (green) revealed mtDNA nucleoid presented along with mitochondria. Yellow circles and blue arrows mark areas where mtDNA (green) clearly stops efflux from mitochondria (red). Scale bars: $2.5\,\mu$m. See Movies 4, 5, 6, and 7). (b) Bar graphs illustrate the average mtDNA levels in cytosol among four groups of HGFs with or without CsA, N-acetylcysteine (NAC) (3 mM, 2 h), and Mito-TEMPO ($50\,\mu$M, 2 h) treatment. All quantified data represent the mean $\pm$ SE. p values were determined by 1-way analysis of variance followed by post hoc tests. Graphs represent at least 3 independent experiments. $^{*}p < 0.05$, $^{**}\,p < 0.01$, $^{***}p < 0.001$, and$^{****}p < 0.0001$; ns: not significant.

Periodontitis is a kind of chronic inflammatory disease driving the destruction of soft and hard periodontal tissues such as gingiva recession and alveolar bone loss [5], suggesting a role for mtDNA efflux in the periodontitis. Consistent with the reported mtDNA efflux in other studies, we identified a significant increased mtDNA levels in the plasma from CP mice, implying an association with periodontitis and this mtDNA efflux. One study demonstrated that the mtDNA outside of mitochondria was found to be crucial for inflammation via inducing bone-destructing immunity [38]. Owing to the mtDNA accumulation in the plasma of CP mice, little is known about the mtDNA function and activity in HGFs during periodontitis. In the context of periodontitis, in vitro studies of periodontitis patients have confirmed alterations in mitochondrial structure, function, and hyperoxidative stress in HGFs and gingival tissues compared to normal individuals [8, 12], which indicates that there may be a correlation between periodontitis progression and mitochondrial dysfunction in HGFs from different hosts. Interestingly, we confirmed that aberrant mtDNA release into cytosol and supernatants of HGFs from CP patients. It is evident that LPS stimulation could also induce this phenomenon in healthy HGFs. The observed high mtDNA levels in the cytosol and supernatants of CP HGFs were more significant in the presence of LPS than in HGFs without LPS, indicating that mtDNA release was maintained in inflamed cells. It is possible that LPS, a major trigger of periodontitis, enables mtDNA to release from mitochondria in periodontitis mouse model and periodontitis patients, but the retained mtDNA efflux in HGFs from CP patients was inadequate to understand.

Our data showed that LPS increased ROS levels and mPTP opening, and it also led to this variation in next three generational HGFs. This comparison of mtDNA efflux activity between the next three generations HGFs after LPS stimuli and direct LPS treatment was similar, in line with the above findings. In addition, we demonstrated that LPS upregulated ROS generation through PDK2 inhibition even in the next three generations HGFs. It was reported that

PDK2 activation has beneficial effects on ROS suppression [39]. Thus, we reasoned that LPS might mediate irreversible high ROS generation by downregulation of PDK2 expression [6, 40], leading to sustained increased mtDNA release activity even in the next-generation HGFs without LPS stimulation. As widely reported in the literature, LPS activated Toll-like receptor (TLR) was abundantly expressed in the inflammatory cells, leading to the ROS production as well as the lower PDK2 expression [8, 41]. Some reported that ROS triggered mtDNA damages and release into cytosol in cancer [42]. Another study showed that mitochondrial ROS induced inflammation dependent on disrupting mtDNA maintenance [15]. In agreement, other study detected that LPS induced accumulation of free mtDNA outside of mitochondria contributing to inflammation via TLR9 activation [43]. We provided herein the proof of mtDNA efflux arising from LPS mediating ROS activation by blocking PDK2 in HGFs. The exact reason for this phenomenon is unclear. It is crucial to note that studies have observed the transfer of entire mitochondria between cells [44]. However, whether the entire mitochondria or mtDNA is transferred is controversial [45]. Therefore, mtDNA is thought to be a signal molecule that spreads inflammatory signals across a population of cells. This suggests that inflammation could spread between cells via the detection of mtDNA [9]. Based on these results, we propose that LPS modulates mtDNA efflux remained in HGFs closely linked to sustained ROS overproduction.

Some studies have concluded mtDNA release in the context of cell apoptosis [46], while other studies have indicated that mPTP opening leads to increased mtDNA release [46]. Given that cell apoptosis was similar among our divided groups, the role of mPTP opening in mtDNA release in HGFs was focused. Based on the inhibitory effect of CsA on mPTP opening, CsA successfully restored mtDNA efflux from mitochondria and reduced mtDNA levels in cytosol within inflamed HGFs. These results highlight that mPTP opening potentially modulates mtDNA release in HGFs with periodontitis. One of the possible physiological mechanisms mediating increased mPTP opening could be linked to ROS increase in inflammatory HGFs. Exceeding levels of ROS can trigger mPTP opening via mitochondrial ATP-sensitive potassium channels, and voltage-dependent anion channel-1 oligomerization, suggesting that ROS works as an important molecular leading to downstream mPTP opening and eventually disruption of cellular functions [47, 48]. Of note, earlier, Bullon's work together with our recent work demonstrated that HGFs and gingival tissues from CP patients were observed impaired mitochondria and higher oxidative stress [8, 12, 49]. As a result of cellular ROS and mtROS outburst, mPTP opening can be activated. According to our data, we confirmed positive relationship between ROS overproduction and mPTP opening in inflammatory HGFs. In addition, ROS and mPTP both played a critical role in mtDNA release during periodontitis. Our results highlight that ROS could be one possible explanation for mPTP opening, contributing to mtDNA release in HGFs during periodontitis.

5. Conclusion

In summary, mtDNA efflux maintained in primary HGFs could reflect mitochondrial dysfunction detected in peri-

odontitis. This work provides initial preclinical evidence for a new candidate biomarker for mtDNA efflux in HGFs predicting periodontitis. In addition to this focused investigation of mtDNA efflux in HGFs during inflammation, our results also indicate that ROS/mPTP pathway could be the principal mediator of mtDNA efflux in inflamed HGFs. Further investigation is needed to determine how mtDNA release causes periodontitis, which may reveal new therapeutic strategies for the treatment of patients with periodontitis.

Data Availability

The datasets generated and analyzed during the current study are available from the corresponding authors on reasonable request.

Conflicts of Interest

The authors declare no conflict of interest.

Authors' Contributions

J. Liu, M. Zheng, and Q. Luan designed the study. J. Liu performed the experiments. J. Liu, X. Wang, P. Zou, Y. Wang, and Q. Shi analyzed the data. J. Liu wrote the manuscript. All authors contributed to editing the manuscript and approved the final manuscript.

Acknowledgments

Supplementary Materials

Supplementary 1. Fig. S1: measurement of cell apoptosis by Annexin V binding and propidium iodide (PI) uptake. Human gingival fibroblasts (HGFs) were from control donors (A) or chronic periodontitis (CP) patients (B). Control cells were treated with lipopolysaccharide (LPS) (5 μg/mL, 24 h) (C), and CP cells were treated with LPS (5 μg/mL, 24 h) (D). These four groups of HGFs were harvested for cell apoptosis analysis by flow cytometry 24 h after LPS treatment or without LPS treatment.

Supplementary 2. Movie. S1: mtDNA does not release from mitochondria in human gingival fibroblasts from healthy control donors in real time movie. Human gingival fibroblasts (HGFs) from control hosts were transduced with vector encoding the mitochondrial outer-membrane protein Tomm 20 bearing a mCherry fluorescence to illustrate mitochondria (red). Meanwhile, HGFs were also transduced with mitochondrial transcription factor A (TFAM) tagged with the green fluorescent protein (GFP) variant mNeonGreen to detect mtDNA (green) (scale bar: 7.5 μm).

References

[1] J. M. Albandar, C. Susin, and F. J. Hughes, "Manifestations of systemic diseases and conditions that affect the periodontal attachment apparatus: case definitions and diagnostic considerations," *Journal of Periodontology*, vol. 89, pp. S183–S203, 2018.

[2] F. Lakschevitz, G. Aboodi, H. Tenenbaum, and M. Glogauer, "Diabetes and periodontal diseases: interplay and links," *Current Diabetes Reviews*, vol. 7, no. 6, pp. 433–439, 2011.

[3] Y. Chang, H. G. Woo, J. Park, J. S. Lee, and T. J. Song, "Improved oral hygiene care is associated with decreased risk of occurrence for atrial fibrillation and heart failure: a nationwide population-based cohort study," *Eur J PrevCardiol.*, vol. 27, no. 17, pp. 1835–1845, 2020.

[4] Y. Li, Z. Lu, L. Zhang, K. L. Kirkwood, M. F. Lopes-Virella, and Y. Huang, "Acid sphingomyelinase deficiency exacerbates LPS-induced experimental periodontitis," *Oral Diseases*, vol. 26, no. 3, pp. 637–646, 2020.

[5] C. A. Ramseier, A. Anerud, M. Dulac et al., "Natural history of periodontitis: disease progression and tooth loss over 40 years," *Journal of Clinical Periodontology*, vol. 44, no. 12, pp. 1182–1191, 2017.

[6] J. Liu, J. Zeng, X. Wang, M. Zheng, and Q. Luan, "P53 mediates lipopolysaccharide-induced inflammation in human gingival fibroblasts," *Journal of Periodontology*, vol. 89, no. 9, pp. 1142–1151, 2018.

[7] X. Sun, Y. Mao, P. Dai et al., "Mitochondrial dysfunction is involved in the aggravation of periodontitis by diabetes," *Journal of Clinical Periodontology*, vol. 44, no. 5, pp. 463–471, 2017.

[8] J. Liu, X. Wang, F. Xue, M. Zheng, and Q. Luan, "Abnormal mitochondrial structure and function are retained in gingival tissues and human gingival fibroblasts from patients with chronic periodontitis," *Journal of Periodontal Research*, vol. 57, no. 1, pp. 94–103, 2022.

[9] J. Bai, C. Cervantes, J. Liu et al., "DsbA-L prevents obesity-induced inflammation and insulin resistance by suppressing the mtDNA release-activated cGAS-cGAMP-STING pathway," *Proceedings of the National Academy of Sciences*, vol. 114, no. 46, pp. 12196–12201, 2017.

[10] K. W. Chung, P. Dhillon, S. Huang et al., "Mitochondrial damage and activation of the STING pathway lead to renal inflammation and fibrosis," *Cell Metabolism*, vol. 30, no. 4, pp. 784–799.e5, 2019.

[11] C. Zhu, Y. Zhao, X. Wu et al., "The therapeutic role of baicalein in combating experimental periodontitis with diabetes via Nrf2 antioxidant signaling pathway," *Journal of Periodontal Research*, vol. 55, no. 3, pp. 381–391, 2020.

[12] J. Liu, X. Wang, M. Zheng, and Q. Luan, "Oxidative stress in human gingival fibroblasts from periodontitis versus healthy counterparts," *Oral Diseases*, 2021.

[13] H. C. Lee and Y. H. Wei, "Mitochondrial biogenesis and mitochondrial DNA maintenance of mammalian cells under oxidative stress," *The International Journal of Biochemistry & Cell Biology*, vol. 37, no. 4, pp. 822–834, 2005.

[14] Y. Quan, Y. Xin, G. Tian, J. Zhou, and X. Liu, "Mitochondrial ROS-modulated mtDNA: a potential target for cardiac aging," *Oxidative Medicine and Cellular Longevity*, vol. 2020, Article ID 9423593, 11 pages, 2020.

[15] M. Zhao, Y. Wang, L. Li et al., "Mitochondrial ROS promote mitochondrial dysfunction and inflammation in ischemic acute kidney injury by disrupting TFAM-mediated mtDNA maintenance," *Theranostics.*, vol. 11, no. 4, pp. 1845–1863, 2021.

[16] C. F. Canakçi, A. Tatar, V. Canakçi, Y. Cicek, S. Oztas, and R. Orbak, "New evidence of premature oxidative DNA damage: mitochondrial DNA deletion in gingival tissue of patients with periodontitis," *Journal of Periodontology*, vol. 77, no. 11, pp. 1894–1900, 2006.

[17] C. Kukat, C. A. Wurm, H. Spåhr, M. Falkenberg, N. G. Larsson, and S. Jakobs, "Super-resolution microscopy reveals that mammalian mitochondrial nucleoids have a uniform size and frequently contain a single copy of mtDNA," *Proceedings of the National Academy of Sciences*, vol. 108, pp. 13534–13539, 2011.

[18] X. Zhang, X. Wu, Q. Hu et al., "Mitochondrial DNA in liver inflammation and oxidative stress," *Life Sciences*, vol. 236, article 116464, 2019.

[19] L. Yuan, Y. Mao, W. Luo et al., "Palmitic acid dysregulates the Hippo-YAP pathway and inhibits angiogenesis by inducing mitochondrial damage and activating the cytosolic DNA sensor cGAS-STING-IRF3 signaling mechanism," *The Journal of Biological Chemistry*, vol. 292, no. 36, pp. 15002–15015, 2017.

[20] C. H. Yu, S. Davidson, C. R. Harapas et al., "TDP-43 triggers mitochondrial DNA release via mPTP to activate cGAS/STING in ALS," *Cell*, vol. 183, no. 3, pp. 636–649.e18, 2020.

[21] J. Kim, R. Gupta, L. P. Blanco et al., "VDAC oligomers form mitochondrial pores to release mtDNA fragments and promote lupus-like disease," *Science*, vol. 366, no. 6472, pp. 1531–1536, 2019.

[22] X. Zhang, Y. Wang, M. Chen, and M. Zeng, "Hexavalent chromium-induced apoptosis in Hep3B cells is accompanied by calcium overload, mitochondrial damage, and AIF translocation," *Ecotoxicology and Environmental Safety*, vol. 208, article 111391, 2021.

[23] F. Puhm, T. Afonyushkin, U. Resch et al., "Mitochondria are a subset of extracellular vesicles released by activated monocytes and induce type I IFN and TNF responses in endothelial cells," *Circulation Research*, vol. 125, no. 1, pp. 43–52, 2019.

[24] W. X. Sun, H. Y. Zheng, and J. Lan, "Edaravone protects osteoblastic cells from dexamethasone through inhibiting oxidative stress and mPTP opening," *Molecular and Cellular Biochemistry*, vol. 409, no. 1-2, pp. 51–58, 2015.

[25] Y. Yang, Y. Tian, X. Guo, S. Li, W. Wang, and J. Shi, "Ischemia injury induces mPTP opening by reducing Sirt3," *Neuroscience*, vol. 468, pp. 68–74, 2021.

[26] A. Krishnamoorthy, M. Sevanan, S. Mani, M. Balu, S. Balaji, and P. Ramajayan, "Chrysin restores MPTP induced neuroinflammation, oxidative stress and neurotrophic factors in an acute Parkinson's disease mouse model," *Neuroscience Letters*, vol. 709, article 134382, 2019.

[27] L. K. Seidlmayer, V. V. Junettner, S. Kettlewell, E. V. Pavlov, L. A. Blatter, and E. N. Dedkova, "Distinct mPTP activation mechanisms in ischaemia-reperfusion: contributions of Ca²⁺, ROS, pH, and inorganic polyphosphate," *Cardiovascular Research*, vol. 106, no. 2, pp. 237–248, 2015.

[28] M. S. Tonetti, H. Greenwell, and K. S. Kornman, "Staging and grading of periodontitis: framework and proposal of a new classification and case definition," *Journal of Periodontology*, vol. 89, pp. S159–S172, 2018.

[29] A. P. West, W. Khoury-Hanold, M. Staron et al., "Mitochondrial DNA stress primes the antiviral innate immune response," *Nature*, vol. 520, no. 7548, pp. 553–557, 2015.

[30] W. N. Pei, H. J. Hu, F. Liu, B. Xiao, Y. B. Zuo, and W. Cui, "C-reactive protein aggravates myocardial ischemia/reperfusion

injury through activation of extracellular-signal-regulated kinase 1/2," *Journal Of Geriatric Cardiology*, vol. 15, pp. 492–503, 2018.

[31] P. Bullon, H. N. Newman, and M. Battino, "Obesity, diabetes mellitus, atherosclerosis and chronic periodontitis: a shared pathology via oxidative stress and mitochondrial dysfunction?," *Periodontology 2000*, vol. 2014, no. 64, pp. 139–153, 2014.

[32] Z. Wu, S. Oeck, A. P. West et al., "Mitochondrial DNA stress signalling protects the nuclear genome," *Nature Metabolism*, vol. 1, no. 12, pp. 1209–1218, 2019.

[33] Z. Al Amir Dache, A. Otandault, R. Tanos et al., "Blood contains circulating cell-free respiratory competent mitochondria," *The FASEB Journal*, vol. 34, no. 3, pp. 3616–3630, 2020.

[34] P. Pérez-Treviño, M. Velásquez, and N. García, "Mechanisms of mitochondrial DNA escape and its relationship with different metabolic diseases," *Biochimica et Biophysica Acta (BBA)-Molecular Basis of Disease*, vol. 1866, no. 6, article 165761, 2020.

[35] K. Nakahira, J. A. Haspel, V. A. Rathinam et al., "Autophagy proteins regulate innate immune responses by inhibiting the release of mitochondrial DNA mediated by the NALP3 inflammasome," *Nature Immunology*, vol. 12, no. 3, pp. 222–230, 2011.

[36] C. Mikacenic, R. Moore, V. Dmyterko et al., "Neutrophil extracellular traps (NETs) are increased in the alveolar spaces of patients with ventilator-associated pneumonia," *Critical Care*, vol. 22, no. 1, p. 358, 2018.

[37] J. Cedervall, A. Hamidi, and A. K. Olsson, "Platelets, NETs and cancer," *Thrombosis Research*, vol. 164, pp. S148–S152, 2018.

[38] A. Zheleznyak, M. Mixdorf, L. Marsala et al., "Orthogonal targeting of osteoclasts and myeloma cells for radionuclide stimulated dynamic therapy induces multidimensional cell death pathways," *Theranostics.*, vol. 11, no. 16, pp. 7735–7754, 2021.

[39] X. Zhao, S. Li, Y. Mo et al., "DCA protects against oxidation injury attributed to cerebral ischemia- reperfusion by regulating glycolysis through PDK2-PDH-Nrf2 axis," *Oxidative Medicine and Cellular Longevity*, vol. 2021, Article ID 5173035, 12 pages, 2021.

[40] Y. Gao, J. Li, J. Li et al., "Tetrahydroxy stilbene glycoside alleviated inflammatory damage by mitophagy via AMPK related PINK1/Parkin signaling pathway," *Biochemical Pharmacology*, vol. 177, article 113997, 2020.

[41] H. Wu, Y. Wang, Y. Zhang et al., "Breaking the vicious loop between inflammation, oxidative stress and coagulation, a novel anti-thrombus insight of nattokinase by inhibiting LPS- induced inflammation and oxidative stress," *Redox Biology*, vol. 32, article 101500, 2020.

[42] A. N. Cheng, L. C. Cheng, C. L. Kuo et al., "Mitochondrial Lon-induced mtDNA leakage contributes to PD-L1-mediated immunoescape via STING-IFN signaling and extracellular vesicles," *Journal for Immunotherapy of Cancer*, vol. 8, no. 2, article e001372, 2020.

[43] W. Kaewduangduen, P. Visitchanakun, W. Saisorn et al., "Blood bacteria-free DNA in septic mice enhances LPS-induced inflammation in mice through macrophage response," *International Journal of Molecular Sciences*, vol. 23, no. 3, p. 1907, 2022.

[44] J. L. Spees, S. D. Olson, M. J. Whitney, and D. J. Prockop, "Mitochondrial transfer between cells can rescue aerobic respiration," *Proc Natl Acad Sci USA.*, vol. 103, no. 5, pp. 1283–1288, 2006.

[45] K. McArthur, L. W. Whitehead, J. M. Heddleston et al., "BAK/BAX macropores facilitate mitochondrial herniation and mtDNA efflux during apoptosis," *Science*, vol. 359, no. 6378, p. 6047, 2018.

[46] V. Izzo, J. M. Bravo-San Pedro, V. Sica, G. Kroemer, and L. Galluzzi, "Mitochondrial permeability transition: new findings and persisting uncertainties," *Trends in Cell Biology*, vol. 26, no. 9, pp. 655–667, 2016.

[47] J. Teixeira, F. Basit, H. G. Swarts et al., "Extracellular acidification induces ROS- and mPTP-mediated death in HEK293 cells," *Redox Biology*, vol. 15, pp. 394–404, 2018.

[48] A. Daiber, "Redox signaling (cross-talk) from and to mitochondria involves mitochondrial pores and reactive oxygen species," *Biochimica et Biophysica Acta (BBA)-Bioenergetics*, vol. 1797, pp. 897–906, 2010.

[49] P. Bullon, A. Pugnaloni, I. Gallardo, G. Machuca, A. Hevia, and M. Battino, "Ultrastructure of the gingiva in cardiac patients treated with or without calcium channel blockers," *Journal of Clinical Periodontology*, vol. 30, no. 8, pp. 682–690, 2003.

Research Article

Chrysin Attenuates Fructose-Induced Nonalcoholic Fatty Liver in Rats via Antioxidant and Anti-Inflammatory Effects: The Role of Angiotensin-Converting Enzyme 2/Angiotensin (1-7)/Mas Receptor Axis

Hala Attia [1,2] **Norah Albekairi** [1] **Layal Albdeirat** [3] **Arwa Soliman** [3] **Reem Rajab** [3] **Hend Alotaibi** [1] **Rehab Ali** [1] **and Amira Badr** [1,4]

[1]*Department of Pharmacology and Toxicology, College of Pharmacy, King Saud University, Riyadh 11495, Saudi Arabia*
[2]*Department of Biochemistry, College of Pharmacy, Mansoura University, Mansoura 35516, Egypt*
[3]*College of Pharmacy, King Saud University, Riyadh 11495, Saudi Arabia*
[4]*Department of Pharmacology and Toxicology, College of Pharmacy, Ain Shams University, Heliopolis, Cairo, Egypt*

Correspondence should be addressed to Hala Attia; hsalem@ksu.edu.sa

Aim. Nonalcoholic fatty liver disease (NAFLD) is the hepatic manifestation of metabolic syndrome, and if untreated, it may propagate into end-stage liver disease. The classical arm of the renin-angiotensin system (RAS) has a fundamental role in triggering oxidative stress and inflammation, which play potential roles in the pathogenesis of NAFLD. However, the nonclassical alternative axis of RAS, angiotensin- (Ang-) converting enzyme 2 (ACE2)/Ang (1-7)/Mas receptor, opposes the actions of the classical arm, mitigates the metabolic dysfunction, and improves hepatic lipid metabolism rendering it a promising protective target against NAFLD. The current study is aimed at investigating the impact of chrysin, a well-known antioxidant flavonoid, on this defensive RAS axis in NAFLD. *Methods.* Rats were randomly distributed and treated daily for eight weeks as follows: the normal control, chrysin control (50 mg/kg, p.o), NAFLD group (received 20% fructose in drinking water), and treated groups (25 and 50 mg/kg chrysin given orally and concomitantly with fructose). Diminazene aceturate (DIZE) (15 mg/kg, s.c.) was used as a reference ACE2 activator. *Key Findings.* High fructose induced significant weight gain, hepatocyte degeneration with fat accumulation, and inflammatory cell infiltration (as examined by H&E staining). This was accompanied by a substantial increase in liver enzymes, glucose, circulating and hepatic triglycerides, lipid peroxides, inflammatory cytokines, and Ang II (the main component of classical RAS). At the same time, protein levels of ACE2, Ang (1-7), and Mas receptors were markedly reduced. Chrysin (25 and 50 mg/kg) significantly ameliorated these abnormalities, with a prominent effect of the dose of 50 mg/kg over DIZE and the lower dose in improving ACE2, Ang (1-7), and Mas. *Significance.* Chrysin is a promising efficient protective remedy against NAFLD; mechanisms include the activation of ACE2/Ang (1-7)/Mas axis.

1. Introduction

Nonalcoholic fatty liver disease (NAFLD) is considered the hepatic component of metabolic syndrome [1]. The hallmark of NAFLD is the accumulation of triglycerides (TG) by more than 5-10% of liver weight, which occurs without associated secondary causes such as excessive alcohol consumption, viral or autoimmune hepatitis, or congenital hepatic disorders [2]. NAFLD is one of the main contributors to morbidity and mortality worldwide because of the rapid progression into end-stage liver disease and liver malignancy [3]. The estimated global prevalence of NAFLD

is 25%, increasing to 55.5% in patients with type II diabetes mellitus (T2DM) and 60–80% in people with obesity [4, 5].

Multiple aetiologies of NAFLD have been suggested, including oxidative stress, induction of mitochondrial dysfunction, disturbance of endoplasmic reticulum, and insulin resistance (IR) [6]. In adipose tissue, IR impairs the antilipolytic action of insulin, with a resultant increase of free fatty acids (FFA) release with high circulating FFA available for subsequent hepatic uptake. In response to systemic IR, hyperinsulinemia develops, which stimulates hepatic *de novo* lipogenesis accompanied with the impairment of FFA β-oxidation, culminating in the accumulation of TG in the liver and the progression to fatty liver [3, 7].

The renin-angiotensin system (RAS) has a fundamental role in triggering oxidative stress and inflammation as well as regulating insulin sensitivity that is closely related to NAFLD [8], and thus, RAS was documented as one of the contributors to the development and the progression of NAFLD [9, 10]. The RAS includes a classical axis, angiotensin-converting enzyme (ACE)/angiotensin (Ang) II/type 1 angiotensin receptor (AT1R), and an alternative axis: (ACE2)/Ang 1-7/Mas receptor axis [11]. The classical RAS axis starts with the cleavage of angiotensinogen, produced in the liver, to Ang I by renin, produced by the kidney. This is followed by the ACE-catalysed conversion of Ang I to Ang II, which can bind to the AT1R [12], leading to Ang II-mediated prooxidation, inflammation, and vascular effects. This axis can contribute to the pathogenesis of NAFLD via the stimulation of IR, *de novo* lipogenesis, mitochondrial dysfunction, reactive oxygen species (ROS) generation, and production of proinflammatory cytokine [10, 12, 13].

Meanwhile, an alternative axis, ACE2/Ang (1-7)/Mas receptor, appears to function against the ACE/Ang II/AT1 axis in the liver [14–17]. Ang II is degraded by the ACE2 enzyme into Ang (1-7), which antagonizes the deleterious effects of Ang II mainly via Mas receptors [16, 18, 19]. Researchers have found that activating the ACE2/Ang1-7/ Mas axis mitigates the metabolic dysfunction and prevents NAFLD [17, 18] mainly via improving hepatic IR and FFA oxidation along with inhibiting liver lipogenesis and inflammation [20–22]. Cao et al. [20] reported that, in mice, Ang (1–7)/ACE2 alleviated steatosis, oxidative stress, and inflammation induced by FFA, but deletion of ACE2 exacerbated their development. Moreover, the overexpression of ACE2 in db/db mice improved fatty liver, suggesting its potential role in preventing and treating hepatic lipid metabolism [20]. Yang et al. [18] determined that ACE2 knockouts could exacerbate high fructose-induced fat deposition in the liver, promoting inflammatory mediators such as nuclear factor kappa B (NF-κB). Based on these findings, targeting the ACE2/Ang (1-7)/Mas axis could represent a pharmacological approach for protecting against NAFLD.

Several drugs are being tested for their ability to protect against or prevent NAFLD including those targeting the hepatic TG accumulation, oxidative stress, inflammation, or liver fibrosis [23], while little attention is gained toward the protective arm of RAS.

Flavonoids, which are found in plants in high concentrations, have been gaining attention in the past decade, particularly in relation to NAFLD [24]. Chrysin (5,7-dihydroxyflavone) is a well-known flavonoid found in blue passion flower (*Passiflora caerulea*), Indian trumpet flower (*Oroxylum indicum*), honey, and propolis [25]. In addition to anti-inflammatory and antioxidant properties, it inhibits atherogenesis and hyperlipidemia [25–27]. It has many pharmacological activities such as neuroprotective, antidiabetic, anticancer, nephroprotective, cardioprotective, antiarthritic, and antiasthmatic [25]. Chrysin has shown hepatoprotective effects against several hepatotoxins like ethanol [28], carbon tetrachloride [29], ammonia [30], and paracetamol [31]. Recently, chrysin has been found to reduce plasma Ang II level and to regulate the classical arm of RAS in L-NAME hypertensive rats [32]. Notably, it has been reported to ameliorate NAFLD via its antioxidant effect [33]. However, its impact on the RAS, particularly the protective arm, in NAFLD has not been studied yet. Therefore, the present work is aimed at investigating the role of chrysin in ameliorating NAFLD via the activation of the ACE2/Ang 1-7/Mas axis. The impact of chrysin on this axis was compared with diminazene aceturate (DIZE), a well-known ACE2 activator commonly used in many animal models [34–36].

Fructose (fruit sugar) is a monosaccharide present in many plants such as sugar cane, sugar beets, and corn. It is mainly added as a sweetener in the form of high-fructose corn syrup to a variety of processed foods and beverages, such as desserts, pastries, and soft drinks [37]. It is now generally thought that increased fructose consumption is one of the major causes of chronic metabolic diseases, including obesity, diabetes, and NAFLD [38, 39]. When added to highly consumed beverages, fructose can cause steatosis in only seven days [40]. Being a highly lipogenic monosaccharide, high fructose consumption leads to IR and finally fatty liver [38]. In this regard, fructose overload in chow or drinking water is a commonly used model of NAFLD in rats [41] and was used in the current study to investigate the impact of chrysin on the ACE2/Ang (1-7)/Mas axis in NAFLD.

2. Materials and Methods

2.1. Chemicals and Kits. Chrysin, DIZE, and fructose were purchased from Sigma-Aldrich (St. Louis, MO, USA). A variety of colorimetric kits were obtained from BioDiagnostic Company (Egypt) for the assay of lipid peroxides, reduced glutathione (GSH), liver enzymes, and serum levels of glucose and TG. The colorimetric kit used to quantify hepatic TG (# MAK266) was obtained from Sigma-Aldrich (St. Louis, MO, USA). ELISA kits for the assay of inflammatory markers including tumor necrosis factor-α (TNF-α), interleukin-6 (IL-6), and NF-κB were provided from MyBioSource (San Diego, CA, USA). Rabbit monoclonal anti-ACE2 antibody (ab108252) was purchased from Abcam (Cambridge, MA, USA). Rabbit polyclonal anti-Mas receptor (sc135063) antibody was purchased from Santa Cruz Biotechnology. Rabbit polyclonal ant-Ang II (MBS286234) and anti-Ang 1-7 (MBS2112534) antibodies were obtained from MyBioSource (San Diego, CA, USA). Monoclonal rabbit anti-beta-actin (β-actin) and secondary goat anti-rabbit horseradish peroxidase- (HRP-) conjugated antibody (# 7074) were purchased from Cell Signaling Technology (Beverly, MA, USA).

2.2. Animals. Forty-eight Wistar rats weighed between 150 and 200 g were provided from Prince Naïf Bin Abdulaziz Health Research Center, King Saud University, Riyadh, Saudi Arabia. The animal protocol was designed to minimize pain or discomfort to the animals. The rats were placed in individual cages as four rats per cage at a temperature of $22°C \pm 2°C$ and relative humidity of $50\% \pm 5\%$ with a 12 h light/dark cycle. In addition to standard rodent chow, the rats were allowed free access to water. Before experiments began, the animals were allowed to acclimate for 1 week to the animal house conditions. The local Ethics Committee at King Saud University approved the experimental procedures (Ethics reference No: SE-19-108).

2.3. Study Design. The rats were weighed, randomly divided into six groups (eight rats/each), and treated daily for eight weeks as follows: Group 1: normal control received carboxymethylcellulose (CMC, 0.5% in normal saline) by oral gavage. Group 2: drug control received 50 mg/kg chrysin (dissolved in 0.5% CMC solution) by oral gavage. Group 3 was the model group given 20% fructose in drinking water [42–46] + equivalent volume of 0.5% CMC (the vehicle of chrysin) orally. Groups 4 and 5 were treated, respectively, with 25 and 50 mg/kg chrysin dissolved in 5% CMC, concomitant with 20% fructose. Group 6: rats received DIZE (15 mg/kg, s.c., dissolved in normal saline) + equivalent volume of 0.5% CMC concomitant with 20% fructose. DIZE was used as a reference ACE2 activator.

2.4. Preparation of Serum and Liver Homogenate. At the end of the experiment, fasted rats were reweighed and the body gain was calculated. Rats were then anesthetized with carbon dioxide, and the serum was separated from the blood after it had been collected, allowed to clot, and centrifuged for 20 minutes at 3500 rpm.

Liver tissues were removed, rinsed with normal saline, and weighed for the calculation of liver index as follows: liver index = liver weight/body weight × 100. The liver was then divided into three parts: the first part was homogenized in phosphate-buffered saline (PBS) and used for assessing hepatic TG, oxidative stress, and inflammatory markers. Another part of the liver was stored in liquid nitrogen for western blot analysis of ACE2, Ang (1-7), Mas R, and Ang II. To detect the structural changes and fat deposition, a third part was fixed in 4% formalin for histological examination using hematoxylin and eosin staining (H&E).

2.5. Histological Examination. A small part of liver tissue was fixed in 4% phosphate-buffered formalin at 4°C for 24 hours. After fixation, samples were dehydrated using ascending grades of alcohol, embedded in paraffin, and processed using rotary microtome to prepare 5 μm thick paraffin sections. For staining, sections were deparaffinized by the incubation in a 60°C-heated oven for 1 hour, followed by the immersion in xylene for 10 minutes, and then rehydrated using descending concentrations of ethanol followed by the immersion in xylene for 10 minutes and then rehydrated using descending concentrations of ethanol. Finally, the sections were stained with H&E for examination of any structural abnormalities

and inflammatory cell infiltration. The examination of the slides was performed under a light microscope, and digital images were captured using Olympus CKX 41 microscope (Olympus Optical Co., Ltd., Tokyo).

2.6. Assessment of Fasting Glucose, TG, and Liver Function Tests. Using the commercial kits, serum was used to assess glucose, TG, and liver enzymes including alanine aminotransferase (ALT) and aspartate aminotransferase (AST) according to the manufacturers' instructions.

2.7. Assay of Hepatic TG. Hepatic TAG was quantified using a colorimetric quantification kit according to the manufacturer's instructions. First, 100 mg of liver tissue was homogenized in 1 ml of 5% Nonidet P 40 (NP-40, # 74385) in distilled H_2O. The homogenate was heated at 80–100°C in a water bath for 2–5 minutes or until the Nonidet P 40 became cloudy. The homogenate was allowed to cool to room temperature. The heating process was repeated one more time to solubilize all TG. The homogenate was then centrifuged for 2 min to remove any insoluble substances, and the supernatant was diluted 10-fold with water before the assay. Briefly, 50 μl of the Master Reaction Mix was added to 50 μl of each sample and standard, mixed well, and incubated for 40 minutes at room temperature. The absorbance of the colored product was measured at 570 nm.

2.8. Assay of Lipid Peroxidation and GSH. Hepatic levels of malondialdehyde (MDA, a final product of the peroxidation process of cell membrane lipids) and GSH (a critical nonenzymatic antioxidant) were determined using colorimetric kits according to manufacturers' instructions. For determination of MDA, 200 μl of sample homogenate or standard was mixed with 1 ml of thiobarbituric acid (TBA) reagent. The mixture was incubated at a temperature of 95°C for 30 min, and the absorbance of the pink-colored TBA reactive product was measured at 535 nm against the reagent blank. For GSH, 0.5 ml of hepatic homogenate was mixed with 0.5 ml of trichloroacetic acid to precipitate protein, then the mixture was centrifuged, and 0.5 ml of the supernatant was mixed with 100 μl of 5,5$'$-dithiobis (2-nitrobenzoic acid) reagent and the absorbance of the yellow-colored product was measured at 405 nm against reagent blank.

2.9. Assay of Inflammatory Markers. According to the manufacturers' instructions, the hepatic levels of the proinflammatory cytokines, TNF-α and IL-6, and their regulatory transcription factor, NF-κB, were assayed using the ELISA technique.

2.10. Western Blot Analysis of Ang II, ACE2, Ang (1-7), and Mas Receptor. Ang II, ACE2, Ang (1-7), and Mas receptor protein levels were determined by Western blotting. A total of about 100 mg of liver tissue was homogenized in a phosphatase inhibitor cocktail and protease inhibitor-containing radioimmunoprecipitation assay (RIPA) buffer at ice-cold temperature. The homogenate was centrifuged, and the lysate protein concentrations were determined using a Direct Detect® infrared spectrometer (Millipore). Using polyacrylamide gel electrophoresis with sodium dodecyl

sulphate as the stationary phase, the extracted proteins were separated and electrophoretically transferred to polyvinylidene difluoride membranes. After being blocked with 5% bovine serum albumin in Tris-buffered saline (TBS) at room temperature for 1 h, the blots were incubated overnight at 4°C with the primary antibodies including anti-Ang II (1 : 200), anti-ACE2 (1 : 500), anti-Ang (1-7) (1 : 1000), and anti-Mas receptor (1 : 1000). After washing with TBS, the membranes were incubated with goat anti-rabbit HRP-conjugated secondary antibodies (1 : 1000), for 2 hours at room temperature. Bio-Rad Universal Hood II Gel Doc System was used to visualize the immunoreactive bands developed using chemiluminescent detection reagents. We quantified the intensities of the different protein bands using ImageJ software and normalized them to the loading control (β-actin).

2.11. Statistical Analysis.
Data were expressed as the mean ± SEM. Statistical comparisons were performed using one-way analysis of variance (ANOVA) followed by the Tukey-Kramer test as post hoc multiple tests. GraphPad Prism Software Inc. (San Diego, CA, USA) was used for the statistical analysis. Results were considered significant at a P value less than 0.05.

3. Results

3.1. Effect of Chrysin on Liver Architecture in High-Fructose-Induced NAFLD in Rats (Figure 1).
Liver sections from both standard control (a, b) and chrysin control (c, d) showed normal liver architecture including intact hepatic lobules with normal hepatocytes, portal areas, and central veins. However, liver sections from rats received 20% fructose alone showed loss of hepatic architecture as revealed by degeneration and ballooning of hepatocytes, pyknotic nuclei, and dilated blood sinusoids in addition to extensive fat droplet deposition (steatosis) and inflammatory cell infiltration (e, f, and g). Concomitant treatment with chrysin at dose 25 (h, i) and 50 mg/kg (j, k) showed marked improvement of hepatic architecture with remarkable attenuation of the cell degeneration, fat disposition, and inflammatory infiltration.

3.2. Effect of Chrysin on the Activities of Liver Enzymes (ALT, AST) in High-Fructose-Induced NAFLD in Rats (Figure 2).
In the present study, fructose feeding resulted in a significant increase in the serum levels of ALT (75.46 ± 1.84 vs. 64.45 ± 1.43 U/l, $P < 0.01$) and AST (87.46 ± 2.52 vs. 71.84 ± 2.55 U/l, $P < 0.01$) when compared to the normal control group. The fructose-induced elevation of ALT was significantly ameliorated by the treatment with 25 mg/kg (69.44 ± 1.88 vs. 75.46 ± 1.84, $P < 0.05$) and 50 mg/kg (65.65 ± 2.24 vs. 75.46 ± 1.84, $P < 0.01$) of chrysin compared to the activities in the fructose feeding group. Similarly, the high activities of AST were alleviated by the concomitant treatment with 25 and 50 mg/kg chrysin (77.9 ± 1.92 and 77.09 ± 1.9, respectively, vs. 87.46 ± 2.52, $P < 0.05$). No significant differences in liver enzyme activities were observed between the normal control and chrysin control. Also, no significant difference was observed between rats treated with 25 and 50 mg/kg chrysin.

3.3. Effect of Chrysin on the Weight Gain and Liver Index in High-Fructose-Induced NAFLD in Rats (Figure 3).
Rats fed with high fructose showed a highly significant weight gain compared to the normal control (86.14 ± 6.57 vs. 44 ± 6.76, $P < 0.001$). This weight gain was significantly ameliorated by the simultaneous ingestion of 25 mg/kg chrysin (59.86 ± 6.24 vs. 86.14 ± 6.57, $P < 0.05$) and to a greater extent with the dose of 50 mg/kg (48 ± 4.18 vs. 86.14 ± 6.57, $P < 0.001$) compared to the gain experienced with the fructose alone.

Concerning liver index (as a measure of fat accumulation), rats received fructose showed a significant elevation in liver index compared to the normal control (3.1 ± 0.19 vs. 2.64 ± 0.03, $P < 0.001$). However, this increase was significantly attenuated by the supplementation with 25 and 50 mg/kg of chrysin (2.73 ± 0.066 and 2.78 ± 0.07, respectively, vs. 3.1 ± 0.19, $P < 0.001$). However, no significant difference was observed between rats treated with 25 and 50 mg/kg chrysin in terms of weight gain and liver index.

3.4. Effect of Chrysin on the Serum and Hepatic Levels of Triglycerides (TG) in High-Fructose-Induced NAFLD in Rats (Figure 4).
As revealed by Figure 4, rats received 20% fructose showed a highly significant increase in both sera (98.2 ± 2.7 vs. 61.34 ± 5.2 mg/dl, $P < 0.001$) and hepatic levels of TG (169.4 ± 5.9 vs. 67.6 ± 2.8, $P < 0.001$) compared to the normal control. Chrysin at both doses markedly improved TG levels both in serum (71.65 ± 4.5 and 62.8 ± 5.7 vs. 98.2 ± 2.7, $P < 0.001$) and liver tissue (105.6 ± 5.7 and 92.8 ± 3.5 vs. 169.4 ± 5.9, $P < 0.001$).

3.5. Effect of Chrysin on Serum Levels of Fasting Glucose in High-Fructose-Induced NAFLD in Rats (Figure 5).
Rats fed with 20% fructose alone revealed a marked increase in the serum fasting glucose (193.4 ± 14.99 vs. 90.08 ± 8.7 mg/dl, $P < 0.001$) compared to the normal control. Concomitant treatment with 25 and 50 mg/kg chrysin significantly alleviated the hyperglycemia induced by fructose (142.8 ± 11.3 vs. 193.4 ± 14.99, $P < 0.05$ and 125.3 ± 8.86 vs. 193.4 ± 14.99, $P < 0.001$, respectively) with a prominent effect with the dose 50 mg/kg. However, no significant difference was observed between rats treated with 25 and 50 mg/kg chrysin.

3.6. Effect of Chrysin on the Extent of Lipid Peroxidation and the Levels of GSH in High-Fructose-Induced NAFLD in Rats (Figure 6).
In the present study, there was a marked elevation in the hepatic levels of MDA in rats ingested with 20% fructose compared to the normal control (72.81 ± 2.54 vs. 45.32 ± 1.74 nmol/g tissue, $P < 0.001$). This elevation of MDA was associated with a significant reduction of GSH (9.6 ± 0.64 vs. 13.09 ± 0.34 mg/g tissue, $P < 0.001$), which reflects the oxidant/antioxidant imbalance in the liver. MDA elevation was alleviated by the concomitant treatment with 25 and 50 mg/kg of chrysin (57.42 ± 2.6 and 55.46 ± 2.35, respectively, vs. 72.81 ± 2.54, $P < 0.001$). In addition, the GSH depletion was attenuated by administration of 25 mg/kg (12.18 ± 0.35 vs. 9.6 ± 0.64, $P < 0.01$) and 50 mg/kg chrysin (13.06 ± 0.24 vs. 9.6 ± 0.64, $P < 0.001$).
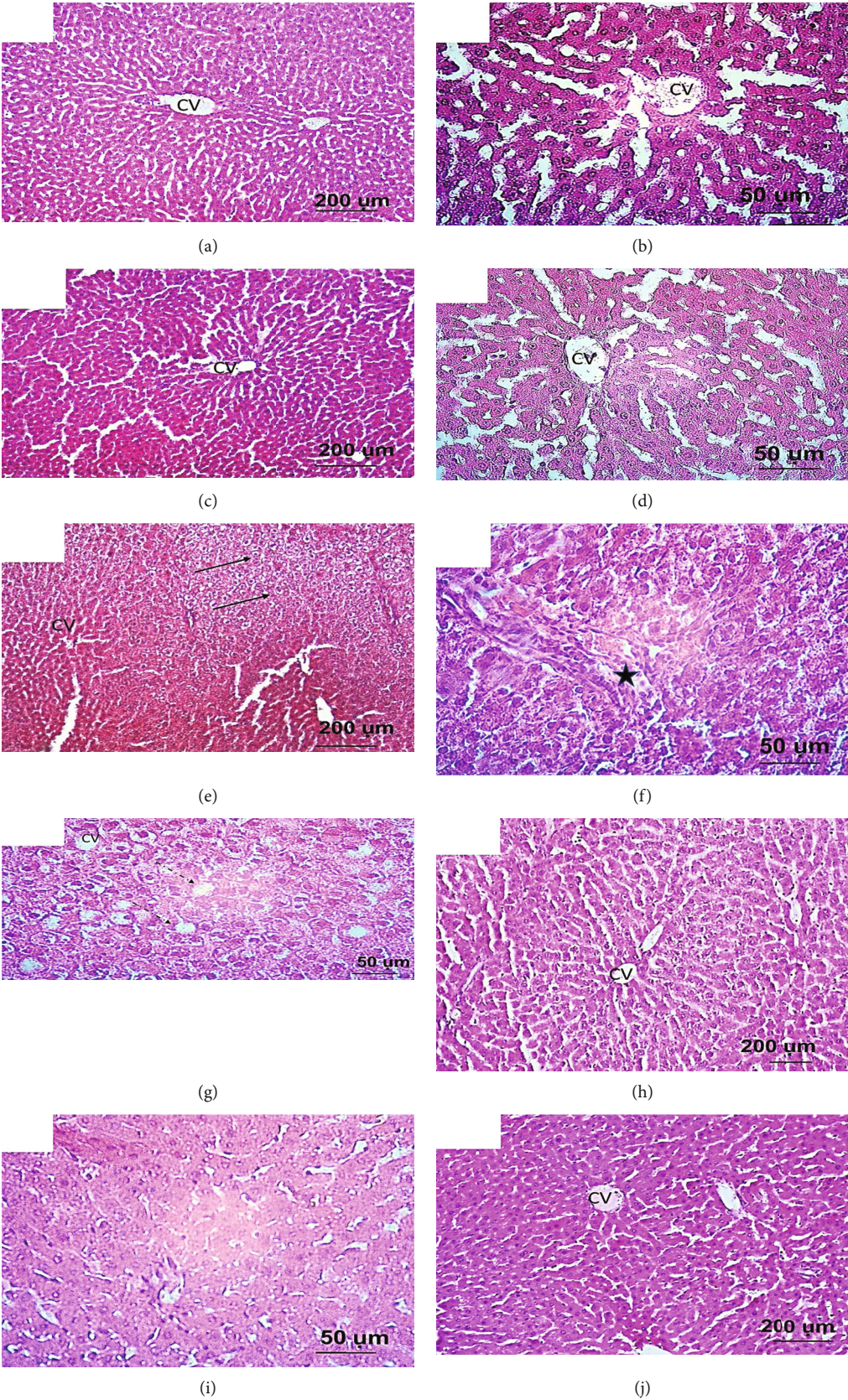
Figure 1: Continued.
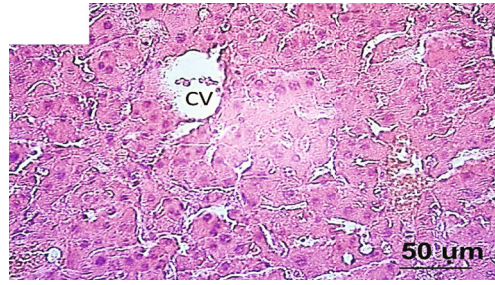
(k)

FIGURE 1: Light photographs of liver sections stained with H&E. (a, b) Liver sections from the normal rat group showing normal hepatic architecture which comprised of intact hepatic lobules with normal hepatocytes, portal area, and central veins (CV). (c, d) Liver sections from rat received only chrysin (50 mg/kg) showing apparently healthy hepatic lobules with normal hepatocytes appearance. (e, f, g) Liver sections from rats received 20% fructose showing loss of intact liver architecture which characterized by extensive fat droplet disposition (steatosis, dashed arrows), ballooning of hepatocytes and pyknotic nuclei (arrows), and inflammatory cell infiltration (star). Additionally, the blood sinusoids are dilating. (h, i) Liver sections from rat received 20% fructose and concomitantly treated with chrysin (25 mg/kg). (j, k) Liver sections from rat received 20% fructose and concomitantly treated with chrysin (50 mg/kg), showing marked improvement in the hepatic appearance with lesser or completely lacking of fatty disposition and inflammatory cells.
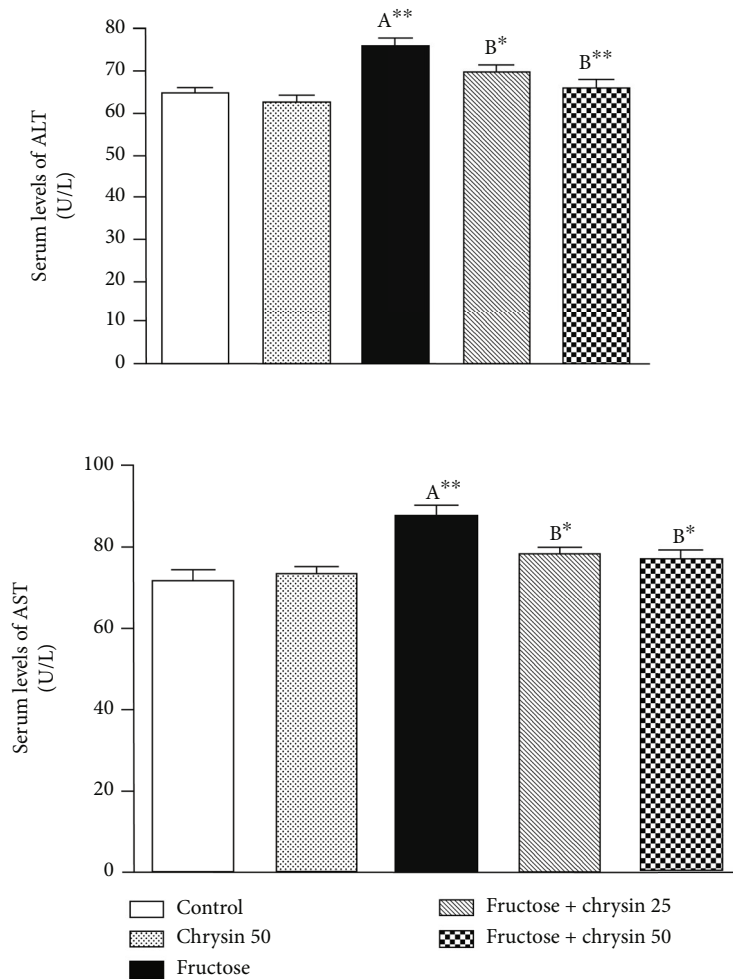
FIGURE 2: The effect of 25 and 50 mg/kg chrysin on alanine aminotransferase (ALT) and aspartate aminotransferase (AST) in high-fructose-induced NAFLD. Values are expressed as the mean ± SEM. (A) Significantly different from the normal control group. (B) Significantly different from fructose-induced NAFLD. $^{**}P < 0.01$ and $^{*}P < 0.05$.
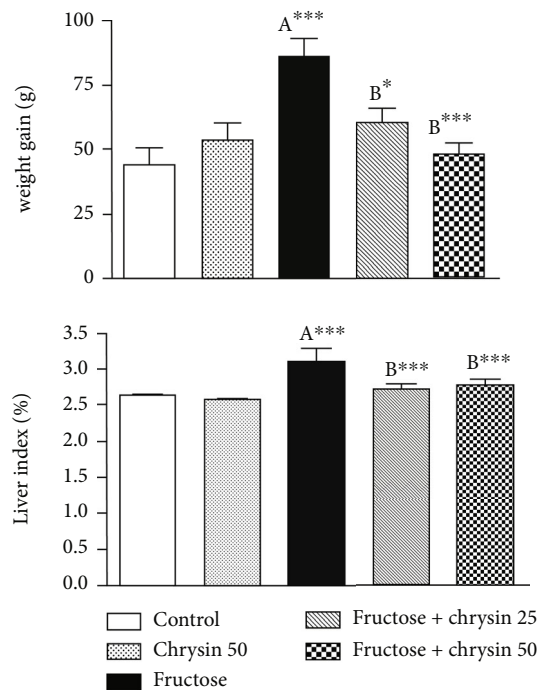
FIGURE 3: The effect of 25 and 50 mg/kg chrysin on body weight gain and liver index in high-fructose-induced NAFLD. Values are expressed as the mean ± SEM. (A) Significantly different from the normal control group. (B) Significantly different from fructose-induced NAFLD. $^{***}P < 0.001$ and $^{*}P < 0.05$.

3.7. Effect of Chrysin on the Hepatic Levels of Inflammatory Markers in High-Fructose-Induced NAFLD in Rats (Figure 7).

As shown in Figure 7, there are dramatic increases in the hepatic levels of inflammatory markers including TNF-α (84.2 ± 5.2 vs. 15.8 ± 0.6 pg/mg protein, $P < 0.001$), IL-6 (123.9 ± 4.6 vs. 48.1 ± 2.02 pg/mg protein, $P < 0.001$) and NF-κB (72.3 ± 3.2 vs. 45.3 ± 1.7 pg/mg tissue, $P < 0.001$) in rats received 20% fructose compared to the normal control. This inflammatory response was markedly ameliorated by chrysin at 25 and 50 mg/kg ($P < 0.001$). The dose 50 mg/kg revealed significant improvement in TNF-α (31.1 ± 4.6 vs. 43.8 ± 1.7, $P < 0.05$), IL-6 (56.2 ± 3.6 vs. 72.4 ± 3.9, $P < 0.05$) and NF-κB (48 ± 1.4 vs. 55 ± 2.1, $P < 0.05$) compared to the levels elicited by the dose 25 mg/kg.

3.8. Effect of Chrysin on the Protein Levels of Ang II in High-Fructose-Induced NAFLD in Rats (Figure 8).

In the present study, a high intake of fructose led to an approximately 6-fold increase in protein levels of Ang II ($P < 0.001$), reflecting stimulation of the classical axis of RAS as an essential mechanism of the NAFLD induced by fructose. Cotreatment with both 25 and 50 mg/kg of chrysin significantly mitigated the elevation of Ang II (3.16 ± 0.3 and 2.1 ± 0.11-fold, respectively, vs. 5.75 ± 0.31-fold, $P < 0.001$) with the prominent effect of the dose 50 mg/kg compared to the dose 25 mg/kg ($P < 0.01$). It is noted that the dose 50 mg/kg elicited significant mitigated the expression of Ang II compared to DIZE (2.1 ± 0.11 vs. 3.18 ± 0.22, $P < 0.01$).
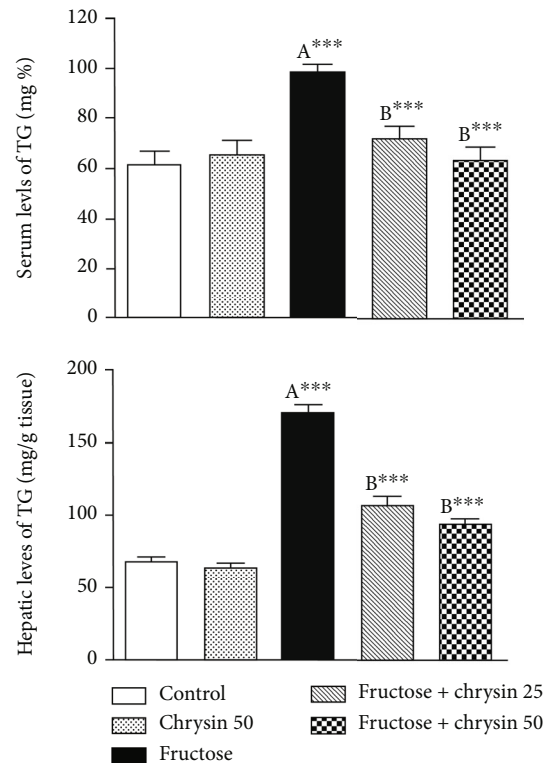
FIGURE 4: The effect of 25 and 50 mg/kg chrysin on serum and hepatic levels of triglycerides (TG) in high-fructose-induced NAFLD. Values are expressed as the mean ± SEM. (A) Significantly different from the normal control group. (B) Significantly different from fructose-induced NAFLD. $^{***}P < 0.001$.

3.9. Effect of Chrysin on the Protein Levels of ACE2, Ang (1-7), and Mas Receptors in High-Fructose-Induced NAFLD in Rats (Figure 9).

Our results revealed that high fructose caused dramatic depletion of protein levels of ACE 2, Ang (1-7), and Mas receptor by approximately 70% ($P < 0.001$) compared to the normal control supporting that the impairment of this RAS axis is implicated in fructose-induced NAFLD. The protein levels of ACE 2, Ang (1-7), and Mas receptors were significantly improved by the treatment with DIZE, chrysin 25 ($P < 0.01$), and to a greater extent with chrysin 50 mg/kg ($P < 0.001$). Chrysin (50 mg/kg) has a notable superior effect over DIZE and chrysin (25 mg/kg) in improving the levels of ACE-2 ($P < 0.05$), Ang (1-7) ($P < 0.001$), and Mas receptor ($P < 0.05$).

4. Discussion

The main finding of the present study is that chrysin at doses 25 and 50 mg/kg alleviates the protein expression of Ang II in the liver while enhancing ACE2, Ang (1–7), and Mas receptor protein expression in the fructose model of NAFLD. The effect of the lower dose is comparable to the impact of DIZE, while the higher dose elicits a superior impact than the DIZE and the lower dose. Therefore, chrysin may contribute to reducing the progression of NAFLD via modulating the hepatic RAS.
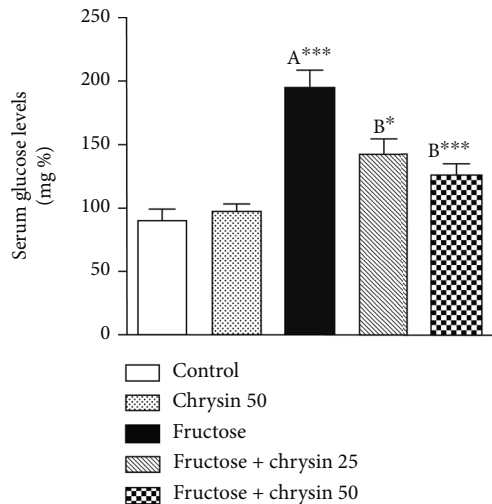
FIGURE 5: The effect of 25 and 50 mg/kg chrysin on serum levels of fasting blood glucose in high-fructose-induced NAFLD. Values are expressed as the mean ± SEM. (A) Significantly different from the normal control group. (B) Significantly different from fructose-induced NAFLD. $***P < 0.001$ and $*P < 0.05$.
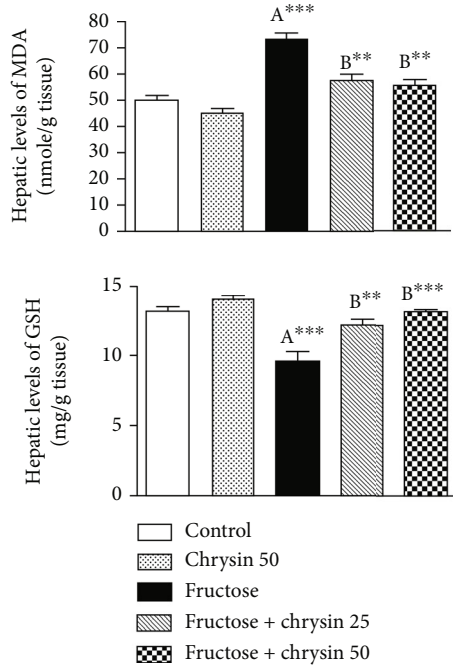
FIGURE 6: The effect of 25 and 50 mg/kg chrysin on hepatic levels of malondialdehyde (MDA) and reduced glutathione (GSH) in high-fructose-induced NAFLD. Values are expressed as the mean ± SEM. (A) Significantly different from the normal control group. (B) Significantly different from fructose-induced NAFLD. $***P < 0.001$ and $**P < 0.01$.

FIGURE 7: The effect of 25 and 50 mg/kg chrysin on hepatic levels of inflammatory markers, including tumor necrosis factor-α (TNF-α), interleukin-6 (IL-6), and nuclear factor kappa B (NF-κB) in high-fructose-induced NAFLD. Values are expressed as the mean ± SEM. (A) Significantly different from the normal control group. (B) Significantly different from fructose-induced NAFLD. (C) Significantly different from fructose+chrysin 25. $***P < 0.001$, $**P < 0.01$, and $*P < 0.05$.

documented by elevated hepatic TG content and fat droplets observed after H&E staining.

In the presence of liver damage, the cytosolic enzymes of hepatocytes, ALT and AST, are released into the bloodstream [49]. This study found that fructose feeding significantly raised the levels of ALT and AST in serum, suggesting the increased permeability of the cell membrane that triggers the leakage of these intracellular transaminases into circulation. This result is consistent with previous works [33, 38, 39] and may be explained in terms of high-fructose-induced formation of ROS, which attack phospholipids in membranes, causing cell membrane rupture [33, 38]. Chrysin at either dose (25 or 50 mg/kg) significantly inhibited the serum elevation of liver enzymes, reflecting the membrane stability induced by chrysin. This result coincided with a remarkable attenuation of the cell degeneration in H&E staining. The effect of chrysin to on liver function

The high-fructose model of NAFLD in experimental animals has been widely used as a reliable and reproducible one [41]. In this regard and consistent with previous works [46–48], fructose in the present study was associated with liver injury associated with increased fat accumulation, as
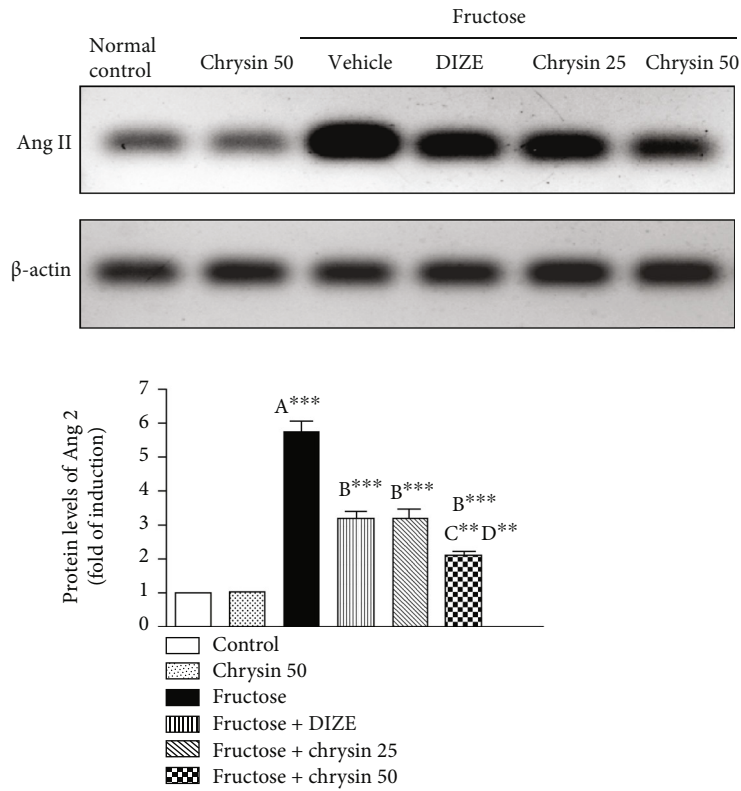
FIGURE 8: Representative immunoblots and quantitative analysis of the protein levels of Ang II in liver tissues of the controls, NAFLD, DIZE, and chrysin-treated groups. $^{**}P < 0.01$ and $^{***}P < 0.001$. (A) Significantly different from the normal control group. (B) Significantly different from fructose-induced NAFLD. (C) Significantly different from fructose+chrysin 25. (D) Significantly different from fructose+DIZE.
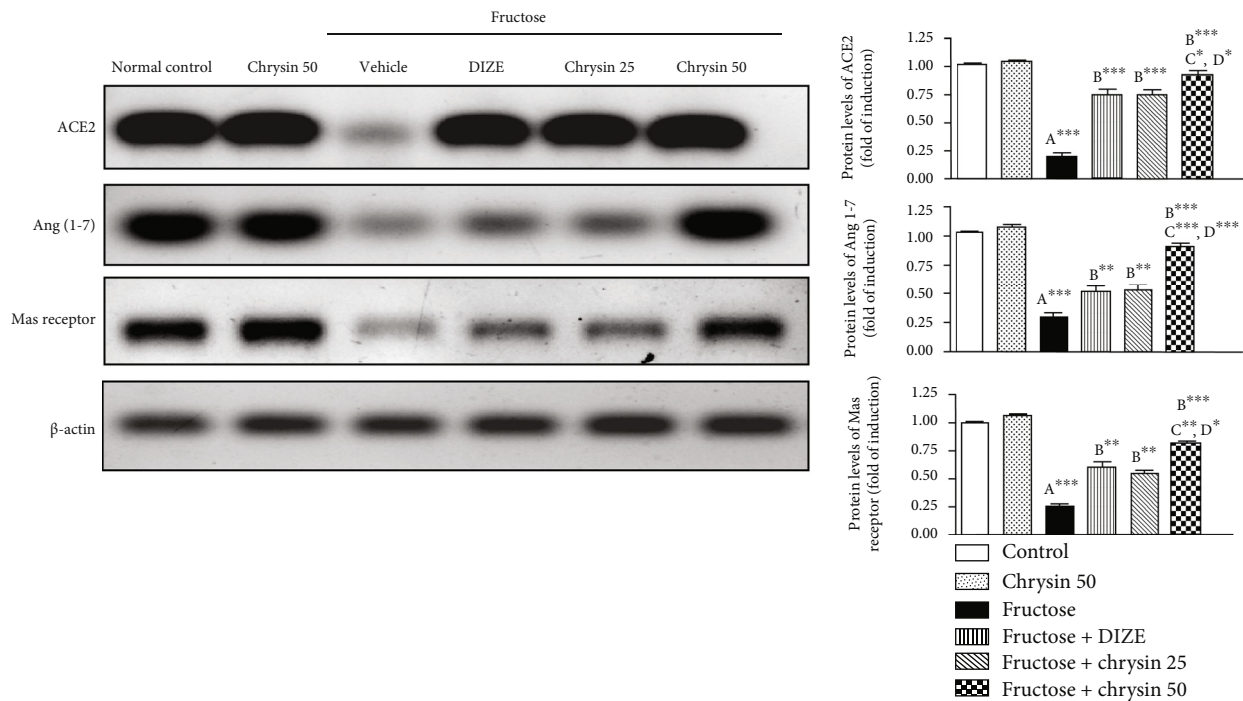
FIGURE 9: Representative immunoblots and quantitative analysis of the protein levels of ACE2, Ang 1-7, and Mas receptor in liver tissues of the controls, NAFLD, DIZE, and chrysin-treated groups. $^{*}P < 0.05$, $^{**}P < 0.01$, and $^{***}P < 0.001$. (A) Significantly different from the normal control group. (B) Significantly different from fructose-induced NAFLD. (C) Significantly different from fructose+chrysin 25. (D) Significantly different from fructose+DIZE.

marker enzymes is previously reported [33, 50–54] and could be explained in terms of its antioxidant characteristics [25].

In the liver, TG is derived from dietary sources or *de novo* lipogenesis. The consumption of high-fructose diets is documented to be lipogenic [38, 47]. This is attributed to its rapid uptake and utilization through the liver. Inside the liver, fructose is rapidly metabolized by fructokinase to fructose-1-phophate that plays a role as a carbon atom donor for the synthesis of TG [48]; thus, fructose can be considered as an efficient inducer of *de novo* lipogenesis and increased secretion and hepatic storage of TG [48]. In addition, dietary fructose increases *de novo* lipogenesis by upregulating the lipogenic enzymes that accelerate TG synthesis in the hepatocytes [40, 55]. Fat accumulates in the liver as a result of this enhanced lipogenesis is associated with increased liver weight and body weight [33, 56] which could explain the significant weight gain and liver index observed in our study in the rats fed with high fructose. The results of these experiments are consistent with our observations where the serum and hepatic TG levels increased significantly with fructose consumption simultaneously with fat deposition and fat infiltration, as observed by H&E staining. The weight gain, high liver index, and elevated TG levels (both in the serum and liver tissue) observed in the current study were markedly reduced by chrysin supplementation. These data are in agreement with those of Pai et al. [33] and Pushpavalli et al. [57] and support the findings concerning the antihyperlipidemic effects of chrysin [26, 27, 58–60], which is exerted probably via elevating the activity of lipoprotein lipase (LPL) which hydrolyses the extra TG [27] and downregulating the action of the lipogenic enzymes, e.g., fatty acid synthase [59].

Fructose also induced hyperglycemia. This is because the liver converts a significant amount of fructose into glucose [55]. Moreover, the high levels of TG in the bloodstream, caused by fructose, cause IR, thereby adds to increasing blood sugar levels [48]. These findings are in harmony with our results and the work of Tappy [55] and Pai et al. [33]. Both doses of chrysin significantly alleviated this hyperglycemia, indicating the ability of chrysin to reduce IR and improve glucose metabolism in fructose-induced NAFLD; this result is consistent with recent work by Pai et al. [33] and Satyanarayana et al. [61].

In the pathogenesis of high-fructose-induced NAFLD, oxidative stress plays a crucial role [46, 47]. An indication of oxidative stress in this study is the augmented hepatic levels of MDA which is associated with depleted levels of GSH, an essential cellular antioxidant that acts against redox imbalance restoring insulin sensitivity in obesity-associated metabolic syndrome [62]. These findings reflect the oxidant/antioxidant imbalance in the liver, which results in oxidative stress. Here, we reported that chrysin (25 and 50 mg/kg) significantly ameliorated this imbalance, suggesting increased scavenging ability of free radicals and the hepatoprotective effect via antioxidant properties. The chrysin's antioxidant activity has been reported in several animal models via different mechanisms [50–53, 60, 63–65].

Due to the generation of ROS triggered by high fructose in addition to fat accumulation, hepatic proinflammatory cytokines will be continuously generated from the Kupffer cells [3, 66]. There is evidence that NAFLD is associated with elevated TNF-α and IL-6 levels, cytokines that play a crucial role in systemic and local inflammation [67]. In this context, our results also showed significantly higher levels of TNF-α and IL-6 after fructose feeding than when fed with a standard control diet. It is also reported that oxidative stress will trigger inflammatory pathways involving NF-κB [3]. It has been demonstrated that NF-κB contributes to the development of NAFLD and steatohepatitis by regulating the expression of several genes involved in the inflammatory process [68–70]. The highly expressed levels of NF-κB in the current study could explain the inflammatory response evoked in our model of NAFLD. The fructose-induced inflammatory response was markedly ameliorated by chrysin, particularly with the dose of 50 mg/kg. Similarly, several studies demonstrated the hepatoprotective activity of chrysin by reducing the production of inflammatory cytokines [33, 50, 52, 63, 64]. This effect could be attributed to the suppression of NF-κB. In many other studies, NF-κB was a common pathway by which chrysin has been shown to exert its beneficial effects [52, 64, 65, 71].

In the next step, we investigated whether the protective role of chrysin against NAFLD has mediated via the modulation of RAS, either the harmful classical axis (represented by Ang II) or the alternative protective arm comprising ACE2/Ang 1-7/Mas receptor. The effects of chrysin were compared with those elicited by DIZE, a well-known ACE2 activator.

Prior studies demonstrated that the hepatic local classical RAS axis is upregulated during NAFLD [18, 72, 73]. RAS's classical arm is dominated by Ang II which contributes to NAFLD pathogenesis through multiple mechanisms, including the induction of IR, *de novo* lipogenesis, mitochondrial dysfunction, ROS generation, and proinflammatory cytokine production [10, 12]. Ang II-infused rats, for example, displayed increased IL-6 expression in the liver, as well as increased monocyte recruitment and overall inflammation [74]. In addition, elevated Ang II is associated with increased FFAs, resulting in FFA flux to the liver and promoting the increase of TG [75]. Frantz et al. [17], in a study of rats with high fructose intake, found that ACE activity and Ang II protein expression increased which is consistent with our own finding, indicating that the classical RAS axis may play a role in the pathogenesis of high-fructose-induced NAFLD. This augmentation of Ang II may contribute to oxidative stress, inflammation, hyperglycemia, and hypertriglyceridemia induced by fructose. Cotreatment with both doses of chrysin, particularly 50 mg/kg, significantly mitigated the elevation of Ang II, suggesting an association between the hepatoprotective effect mediated by chrysin and the normalization of the classic axis of RAS. The prior study revealed that chrysin administration led to a reduction in plasma Ang-II levels in comparison to rats untreated. Free radical scavenging activity and increased plasma NO activity might explain this effect, which regulates the RAS system and reduces plasma Ang-II levels [32].

An important role of ACE2 in the RAS involves its role in degrading Ang II in order to produce cytoprotective effects. ACE2 shows its protective effects by reducing Ang II and producing Ang (1–7) [76, 77], which, by binding to Mas receptors, antagonizes the detrimental effects of Ang II [16, 18, 19]. Studies have shown that Ang (1–7) can improve glucose tolerance, insulin sensitivity, glucose uptake, and TG and cholesterol levels, accompanied with reduced abdominal fat mass [15]. Accordingly, there has been evidence that the activation of the ACE2/Ang1-7/Mas receptor axis protects against NAFLD through multiple mechanisms including inhibition of hepatic lipogenesis, enhancement of FFA oxidation, and inhibition of inflammation [20–22]. Cao et al. [20] showed that the deletion of ACE2 enhanced hepatic steatosis, oxidative stress, and inflammation in ACE2 knockout mice, and that both proteins, ACE2 and Ang (1–7), ameliorated inflammation, oxidative stress, and hepatic steatosis in FFA-induced HepG2 cells. Further, they demonstrated that overexpression of ACE2 reduced hyperglycemia and fatty liver in db/db mice. They proposed that Ang (1-7)/ACE2/Mas pathway effect is mediated through regulation of lipid-metabolizing genes [20]. According to Yang et al. [18], mice with a high-fructose diet gained significantly more body weight and liver weight than the controls, and that the lack of ACE2 further contributed to this effect. This suggests that enhancing hepatic ACE2/Ang (1-7)/MAS may provide a therapeutic strategy for counteracting the detrimental effects of high fructose in liver tissue.

In the current study, we reported that high fructose led to a dramatic decrease in the protein levels of ACE2, Ang (1-7), and Mas receptor in hepatic tissue, supporting that the impairment of this RAS axis is involved in high-fructose-induced NAFLD. Similarly, in a rat model of fructose-fed NAFLD [17], a dysregulation of the hepatic RAS coupled with an upregulation of ACE/ACE2, AngII/Ang (1-7), and Mas/AT1R ultimately led to liver steatosis. Simultaneous treatment with DIZE, chrysin 25, and chrysin 50 showed a marked improvement of the protein levels of ACE 2/Ang 1-7/Mas receptor with a prominent effect of the dose 50 mg/kg over DIZE or the lower dose of chrysin. This finding indicates that the beneficial effects, such as hypoglycemic, hypolipidemic, and anti-inflammatory effects exerted by chrysin in this model of NAFLD, could be mediated via enhancing the expression of ACE2/Ang (1-7)/Ras receptor axis of RAS in the liver. Using chrysin to modulate this RAS axis suppresses the inflammation induced by fructose ingestion, so we concluded that the ACE2/Ang (1-7)/MAS is downregulated during NAFLD and that it is essential for chrysin in preventing liver damage. Chrysin upregulates the ACE2/Ang (1-7)/Mas axis and antagonizes fatty liver. These findings provide a novel insight into the mechanism of chrysin in NAFLD therapy.

5. Conclusion

Daily supplementation with chrysin at either 25 or 50 mg/kg body weight can be used to protect NAFLD efficiently. Depleting the augmented levels of Ang II and upregulating the components of the protective axis of RAS, including ACE2, Ang (1-7), and Mas, represent a potential protective mechanism, particularly with the dose of 50 mg/kg.

Abbreviations

ACE: Angiotensin-converting enzyme
ALT: Alanine aminotransferase
Ang II: Angiotensin II
AST: Aspartate aminotransferase
AT1R: Type 1 angiotensin receptor
CMC: Carboxymethylcellulose
DIZE: Diminazene aceturate
FFAs: Free fatty acids
GSH: Reduced glutathione
H&E: Hematoxylin and eosin staining
HRP: Horseradish peroxidase
IL-6: Interleukin-6
IR: Insulin resistance
MDA: Malondialdehyde
NAFLD: Nonalcoholic fatty liver disease
NF-κB: Nuclear factor kappa B
PBS: Phosphate-buffered saline
RAS: Renin-angiotensin system
ROS: Reactive oxygen species
TBS: Tris-buffered saline
TG: Triglycerides
TNF-α: Tumor necrosis factor-α.

Data Availability

The biochemical and molecular data used to support the findings of this study are included within the article.

Conflicts of Interest

The authors declare that there are no conflicts of interest.

Acknowledgments

References

[1] A. M. Diehl and C. Day, "Cause, pathogenesis, and treatment of nonalcoholic steatohepatitis," *The New England Journal of Medicine*, vol. 377, no. 21, pp. 2063–2072, 2017.

[2] N. Chalasani, Z. Younossi, J. E. Lavine et al., "The diagnosis and management of nonalcoholic fatty liver disease: practice guidance from the American Association for the Study of Liver Diseases," *Hepatology*, vol. 67, no. 1, pp. 328–357, 2018.

[3] R. M. Carr, A. Oranu, and V. Khungar, "Nonalcoholic fatty liver disease: pathophysiology and management," *Gastroenterology Clinics of North America*, vol. 45, no. 4, pp. 639–652, 2016.

[4] L. Caballeria and P. Torán, "The fatty liver epidemic: an analysis from the primary care," *Atencion Primaria*, vol. 51, no. 9, pp. 525-526, 2019.

[5] Z. Younossi, F. Tacke, M. Arrese et al., "Global perspectives on nonalcoholic fatty liver disease and nonalcoholic steatohepatitis," *Hepatology*, vol. 69, no. 6, pp. 2672–2682, 2019.

[6] E. Buzzetti, M. Pinzani, and E. A. Tsochatzis, "The multiple-hit pathogenesis of non-alcoholic fatty liver disease (NAFLD)," *Metabolism*, vol. 65, no. 8, pp. 1038–1048, 2016.

[7] Q. Liu, S. Bengmark, and S. Qu, "The role of hepatic fat accumulation in pathogenesis of non-alcoholic fatty liver disease (NAFLD)," *Lipids in Health and Disease*, vol. 9, no. 1, p. 42, 2010.

[8] Y. Marcus, G. Shefer, K. Sasson et al., "Angiotensin 1-7 as means to prevent the metabolic syndrome: lessons from the fructose-fed rat model," *Diabetes*, vol. 62, no. 4, pp. 1121–1130, 2013.

[9] Y. Z. Xu, X. Zhang, L. Wang et al., "An increased circulating angiotensin II concentration is associated with hypoadiponectinemia and postprandial hyperglycemia in men with nonalcoholic fatty liver disease," *Internal Medicine*, vol. 52, no. 8, pp. 855–861, 2013.

[10] Y. Wei, S. E. Clark, E. M. Morris et al., "Angiotensin II-induced non-alcoholic fatty liver disease is mediated by oxidative stress in transgenic TG(mRen2)27(Ren2) rats," *Journal of Hepatology*, vol. 49, no. 3, pp. 417–428, 2008.

[11] K. M. Mirabito Colafella, D. M. Bovée, and A. H. J. Danser, "The renin-angiotensin-aldosterone system and its therapeutic targets," *Experimental Eye Research*, vol. 186, article 107680, 2019.

[12] P. Paschos and K. Tziomalos, "Nonalcoholic fatty liver disease and the renin-angiotensin system: implications for treatment," *World Journal of Hepatology*, vol. 4, no. 12, pp. 327–331, 2012.

[13] Y. Wu, K. L. Ma, Y. Zhang et al., "Lipid disorder and intrahepatic renin–angiotensin system activation synergistically contribute to non-alcoholic fatty liver disease," *Liver International*, vol. 36, no. 10, pp. 1525–1534, 2016.

[14] C. H. Osterreicher, K. Taura, S. De Minicis et al., "Angiotensin-converting-enzyme 2 inhibits liver fibrosis in mice," *Hepatology*, vol. 50, no. 3, pp. 929–938, 2009.

[15] S. H. Santos, J. F. Braga, E. G. Mario et al., "Improved lipid and glucose metabolism in transgenic rats with increased circulating angiotensin-(1-7)," *Arteriosclerosis, Thrombosis, and Vascular Biology*, vol. 30, no. 5, pp. 953–961, 2010.

[16] X. Cao, F. Y. Yang, Z. Xin, R. R. Xie, and J. K. Yang, "The ACE2/Ang-(1-7)/Mas axis can inhibit hepatic insulin resistance," *Molecular and Cellular Endocrinology*, vol. 393, no. 1-2, pp. 30–38, 2014.

[17] E. D. C. Frantz, R. F. Medeiros, I. G. Giori et al., "Exercise training modulates the hepatic renin-angiotensin system in fructose-fed rats," *Experimental Physiology*, vol. 102, no. 9, pp. 1208–1220, 2017.

[18] M. Yang, X. Ma, X. Xuan, H. Deng, Q. Chen, and L. Yuan, "Liraglutide attenuates non-alcoholic fatty liver disease in mice by regulating the local renin-angiotensin system," *Frontiers in Pharmacology*, vol. 11, p. 432, 2020.

[19] J. F. Giani, M. A. Mayer, M. C. Muñoz et al., "Chronic infusion of angiotensin-(1-7) improves insulin resistance and hypertension induced by a high-fructose diet in rats," *American Journal of Physiology. Endocrinology and Metabolism*, vol. 296, no. 2, pp. E262–E271, 2009.

[20] X. Cao, F. Yang, T. Shi et al., "Angiotensin-converting enzyme 2/angiotensin-(1-7)/Mas axis activates Akt signaling to ameliorate hepatic steatosis," *Scientific Reports*, vol. 6, no. 1, article 21592, 2016.

[21] J. D. Feltenberger, J. M. Andrade, A. Paraíso et al., "Oral formulation of angiotensin-(1-7) improves lipid metabolism and prevents high-fat diet-induced hepatic steatosis and inflammation in mice," *Hypertension*, vol. 62, no. 2, pp. 324–330, 2013.

[22] M. C. Muñoz, J. F. Giani, V. Burghi et al., "The Mas receptor mediates modulation of insulin signaling by angiotensin-(1-7)," *Regulatory Peptides*, vol. 177, no. 1-3, pp. 1–11, 2012.

[23] Y. Rotman and A. J. Sanyal, "Current and upcoming pharmacotherapy for non-alcoholic fatty liver disease," *Gut*, vol. 66, no. 1, pp. 180–190, 2017.

[24] M. Mazidi, N. Katsiki, and M. Banach, "A higher flavonoid intake is associated with less likelihood of nonalcoholic fatty liver disease: results from a multiethnic study," *The Journal of Nutritional Biochemistry*, vol. 65, pp. 66–71, 2019.

[25] R. Mani and V. Natesan, "Chrysin: sources, beneficial pharmacological activities, and molecular mechanism of action," *Phytochemistry*, vol. 145, pp. 187–196, 2018.

[26] J. J. Ramírez-Espinosa, J. Saldaña-Ríos, S. García-Jiménez et al., "Chrysin induces antidiabetic, antidyslipidemic and anti-inflammatory effects in athymic nude diabetic mice," *Molecules*, vol. 23, no. 1, p. 67, 2018.

[27] R. Anandhi, P. A. Thomas, and P. Geraldine, "Evaluation of the anti-atherogenic potential of chrysin in Wistar rats," *Molecular and Cellular Biochemistry*, vol. 385, no. 1-2, pp. 103–113, 2014.

[28] M. Tahir and S. Sultana, "Chrysin modulates ethanol metabolism in Wistar rats: a promising role against organ toxicities," *Alcohol and Alcoholism*, vol. 46, no. 4, pp. 383–392, 2011.

[29] K. V. Anand, R. Anandhi, M. Pakkiyaraj, and P. Geraldine, "Protective effect of chrysin on carbon tetrachloride (CCl4)-induced tissue injury in male Wistar rats," *Toxicology and Industrial Health*, vol. 27, no. 10, pp. 923–933, 2011.

[30] M. Renuka, N. Vijayakumar, and A. Ramakrishnan, "Chrysin, a flavonoid attenuates histological changes of hyperammonemic rats: a dose dependent study," *Biomedicine & Pharmacotherapy*, vol. 82, no. 345–354, pp. 345–354, 2016.

[31] E. Eldutar, F. M. Kandemir, S. Kucukler, and C. Caglayan, "Restorative effects of chrysin pretreatment on oxidant–antioxidant status, inflammatory cytokine production, and apoptotic and autophagic markers in acute paracetamol-induced hepatotoxicity in rats: an experimental and biochemical study," *Journal of Biochemical and Molecular Toxicology*, vol. 31, no. 11, article e21960, 2017.

[32] R. Veerappan and T. Malarvili, "Chrysin pretreatment improves angiotensin system, cGMP concentration in L-NAME induced hypertensive rats," *Indian Journal of Clinical Biochemistry*, vol. 34, no. 3, pp. 288–295, 2019.

[33] S. A. Pai, R. P. Munshi, F. H. Panchal, I. S. Gaur, and A. R. Juvekar, "Chrysin ameliorates nonalcoholic fatty liver disease in rats," *Naunyn-Schmiedeberg's Archives of Pharmacology*, vol. 392, no. 12, pp. 1617–1628, 2019.

[34] Y. Qi, J. Zhang, C. T. Cole-Jeffrey et al., "Diminazene aceturate enhances angiotensin-converting enzyme 2 activity and attenuates ischemia-induced cardiac pathophysiology," *Hypertension*, vol. 62, no. 4, pp. 746–752, 2013.

[35] E. Velkoska, S. K. Patel, K. Griggs, and L. M. Burrell, "Diminazene aceturate improves cardiac fibrosis and diastolic dysfunction in rats with kidney disease," *PLoS One*, vol. 11, no. 8, p. e0161760, 2016, eCollection.

[36] C. Castardeli, C. L. Sartório, E. B. Pimentel, L. Forechi, and J. G. Mill, "The ACE 2 activator diminazene aceturate (DIZE) improves left ventricular diastolic dysfunction following myocardial infarction in rats," *Biomedicine & Pharmacotherapy*, vol. 107, pp. 212–218, 2018.

[37] P. M. Sulis, K. Motta, A. M. Barbosa et al., "Impact of fish oil supplementation and interruption of fructose ingestion on glucose and lipid homeostasis of rats drinking different concentrations of fructose," *BioMed Research International*, vol. 2017, Article ID 4378328, 16 pages, 2017.

[38] B. H. Mai and L. J. Yan, "The negative and detrimental effects of high fructose on the liver, with special reference to metabolic disorders," *Diabetes, Metabolic Syndrome and Obesity: Targets and Therapy*, vol. 12, no. 12, pp. 821–826, 2019.

[39] I. Alqarni, Y. A. Bassiouni, A. M. Badr, and R. A. Ali, "Telmisartan and/or chlorogenic acid attenuates fructose-induced non-alcoholic fatty liver disease in rats: implications of crosstalk between angiotensin, the sphingosine kinase/sphingoine-1-phosphate pathway, and TLR4 receptors," *Biochemical Pharmacology*, vol. 164, pp. 252–262, 2019.

[40] N. Chalasani and G. Szabo, "Pathogenesis of NAFLD and NASH," in *Alcoholic and Non-Alcoholic Fatty Liver Disease*, pp. 71–102, Springer, Cham, Switzerland, 1st ed edition, 2016.

[41] T. Kawasaki, K. Igarashi, T. Koeda et al., "Rats fed fructose-enriched diets have characteristics of nonalcoholic hepatic steatosis," *The Journal of Nutrition*, vol. 139, no. 11, pp. 2067–2071, 2009.

[42] T. Mengesha, N. Gnanasekaran, and T. Mehare, "Hepatoprotective effect of silymarin on fructose induced nonalcoholic fatty liver disease in male albino Wistar rats," *BMC Complementary Medicine and Therapies*, vol. 21, no. 1, p. 104, 2021.

[43] N. Mamikutty, Z. C. Thent, and S. F. Haji, "Fructose-drinking water induced nonalcoholic fatty liver disease and ultrastructural alteration of hepatocyte mitochondria in male Wistar rat," *BioMed Research International*, vol. 2015, Article ID 895961, 7 pages, 2015.

[44] Y. C. Li, J. Y. Qiao, B. Y. Wang, M. Bai, J. D. Shen, and Y. X. Cheng, "Paeoniflorin ameliorates fructose-induced insulin resistance and hepatic steatosis by activating LKB1/AMPK and AKT pathways," *Nutrients*, vol. 10, no. 8, article 1024, 2018.

[45] T. T. Nyakudya, E. Mukwevho, P. Nkomozepi, and K. H. Erlwanger, "Neonatal intake of oleanolic acid attenuates the subsequent development of high fructose diet-induced nonalcoholic fatty liver disease in rats," *Journal of Developmental Origins of Health and Disease*, vol. 9, no. 5, pp. 500–510, 2018.

[46] F. Armutcu, M. Kanter, A. Gurel, and M. Unalacak, "Excessive dietary fructose is responsible for lipid peroxidation and steatosis in the rat liver tissues," *Turkiye Klinikleri Journal of Medical Sciences*, vol. 27, pp. 164–169, 2007.

[47] E. A. Abd El-Haleim, A. K. Bahgat, and S. Saleh, "Resveratrol and fenofibrate ameliorate fructose-induced nonalcoholic steatohepatitis by modulation of genes expression," *World Journal of Gastroenterology*, vol. 22, no. 10, pp. 2931–2948, 2016.

[48] H. Basciano, L. Federico, and K. Adeli, "Fructose, insulin resistance, and metabolic dyslipidemia," *Nutrition & Metabolism (London)*, vol. 2, no. 1, article 5, 2005.

[49] A. J. G. Hanley, K. Williams, A. Festa, L. E. Wagenknecht, J. R. D'Agostino, and S. M. Haffner, "Liver markers and development of the metabolic syndrome: the insulin resistance atherosclerosis study," *Diabetes*, vol. 54, no. 11, pp. 3140–3147, 2005.

[50] B. G. Baykalir, A. S. Arslan, S. I. Mutlu et al., "The protective effect of chrysin against carbon tetrachloride-induced kidney and liver tissue damage in rats," *International Journal for Vitamin and Nutrition Research*, vol. 91, no. 5-6, pp. 427–438, 2021.

[51] F. Koc, M. Y. Tekeli, M. Kanbur, M. Ö. Karayigit, and B. C. Liman, "The effects of chrysin on lipopolysaccharide-induced sepsis in rats," *Journal of Food Biochemistry*, vol. 44, no. 9, article e13359, 2020.

[52] Y. He, Z. Xia, D. Yu et al., "Hepatoprotective effects and structure-activity relationship of five flavonoids against lipopolysaccharide/d-galactosamine induced acute liver failure in mice," *International Immunopharmacology*, vol. 68, pp. 171–178, 2019.

[53] A. Mohammadi, S. Kazemi, M. Hosseini et al., "Chrysin effect in prevention of acetaminophen-induced hepatotoxicity in rat," *Chemical Research in Toxicology*, vol. 32, no. 11, pp. 2329–2337, 2019.

[54] S. Rashid, N. Ali, S. Nafees et al., "Alleviation of doxorubicin-induced nephrotoxicity and hepatotoxicity by chrysin in Wistar rats," *Toxicology Mechanisms and Methods*, vol. 23, no. 5, pp. 337–345, 2013.

[55] L. Tappy, "Fructose-containing caloric sweeteners as a cause of obesity and metabolic disorders," *The Journal of Experimental Biology*, vol. 221, Suppl_1, 2018.

[56] K. L. Stanhope, J. M. Schwarz, N. L. Keim et al., "Consuming fructose-sweetened, not glucose-sweetened, beverages increases visceral adiposity and lipids and decreases insulin sensitivity in overweight/obese humans," *The Journal of Clinical Investigation*, vol. 119, no. 5, pp. 1322–1334, 2009.

[57] G. Pushpavalli, C. Veeramani, and K. V. Pugalendi, "Influence of chrysin on hepatic marker enzymes and lipid profile against D-galactosamine-induced hepatotoxicity rats," *Food and Chemical Toxicology*, vol. 48, no. 6, pp. 1654–1659, 2010.

[58] M. Amir Siddiqui, A. J. Badruddeen, S. Uddin et al., "Chrysin modulates protein kinase IKKε/TBK1, insulin sensitivity and hepatic fatty infiltration in diet-induced obese mice," *Drug Development Research*, vol. 83, pp. 194–207, 2022.

[59] C. M. John and S. Arockiasamy, "Enhanced inhibition of adipogenesis by chrysin via modification in redox balance, lipogenesis, and transcription factors in 3T3-L1 adipocytes in comparison with hesperidin," *Journal of the American College of Nutrition*, vol. 30, pp. 1–13, 2021.

[60] S. Yuvaraj, T. Ramprasath, B. Saravanan, V. Vasudevan, S. Sasikumar, and G. S. Selvam, "Chrysin attenuates high-fat-diet-induced myocardial oxidative stress via upregulating eNOS and Nrf2 target genes in rats," *Molecular and Cellular Biochemistry*, vol. 476, no. 7, pp. 2719–2727, 2021.

[61] K. Satyanarayana, K. Sravanthi, I. A. Shaker, R. Ponnulakshmi, and J. Selvaraj, "Role of chrysin on expression of insulin signaling molecules," *Journal of Ayurveda and Integrative Medicine*, vol. 6, no. 4, pp. 248–258, 2015.

[62] K. L. Hoehn, A. B. Salmon, C. Hohnen-Behrens et al., "Insulin resistance is a cellular antioxidant defense mechanism," *Proceedings of the National Academy of Sciences of the United States of America*, vol. 106, no. 42, pp. 17787–17792, 2009.

[63] M. Samini, T. Farkhondeh, M. Azimi-Nezhad, and S. Samarghandian, "Chrysin's impact on oxidative and inflammation damages in the liver of aged male rats," *Endocrine, Metabolic & Immune Disorders Drug Targets*, vol. 21, no. 4, pp. 743–748, 2021.

[64] Y. Temel, S. Kucukler, S. Yıldırım, C. Caglayan, and F. M. Kandemir, "Protective effect of chrysin on cyclophosphamide-induced hepatotoxicity and nephrotoxicity via the inhibition of oxidative stress, inflammation, and apoptosis," *Naunyn-Schmiedeberg's Archives of Pharmacology*, vol. 393, no. 3, pp. 325–337, 2020.

[65] S. A. El-Marasy, S. A. El Awdan, and R. M. Abd-Elsalam, "Protective role of chrysin on thioacetamide-induced hepatic encephalopathy in rats," *Chemico-Biological Interactions*, vol. 299, pp. 111–119, 2019.

[66] S. M. Alwahsh, M. Xu, F. C. Schultze et al., "Combination of alcohol and fructose exacerbates metabolic imbalance in terms of hepatic damage, dyslipidemia, and insulin resistance in rats," *PLoS One*, vol. 9, no. 8, article e104220, 2014.

[67] E. Matthew Morris, J. A. Fletcher, J. P. Thyfault, and R. S. Rector, "The role of angiotensin II in nonalcoholic steatohepatitis," *Molecular and Cellular Endocrinology*, vol. 378, no. 1-2, pp. 29–40, 2013.

[68] Y. Guo, J. X. Li, T. Y. Mao, W. H. Zhao, L. J. Liu, and Y. L. Wang, "Targeting Sirt1 in a rat model of high-fat diet-induced non-alcoholic fatty liver disease: comparison of Gegen Qinlian decoction and resveratrol," *Experimental and Therapeutic Medicine*, vol. 14, no. 5, pp. 4279–4287, 2017.

[69] R. P. Cunningham, M. P. Moore, A. N. Moore et al., "Curcumin supplementation mitigates NASH development and progression in female Wistar rats," *Physiological Reports*, vol. 6, no. 14, article e13789, 2018.

[70] M. Malaguarnera, M. Di Rosa, F. Nicoletti, and L. Malaguarnera, "Molecular mechanisms involved in NAFLD progression," *Journal of Molecular Medicine*, vol. 87, no. 7, pp. 679–695, 2009.

[71] A. Ciceu, C. Balta, H. Herman et al., "Complexation with random methyl-β-cyclodextrin and (2-hidroxypropyl)-β-cyclodextrin enhances in vivo anti-fibrotic and anti-inflammatory effects of chrysin via the inhibition of NF-κB and TGF-β1/Smad signaling pathways and modulation of hepatic pro/anti-fibrotic miRNA," *International Journal of Molecular Sciences*, vol. 22, no. 4, p. 1869, 2021.

[72] G. Sansoe, M. Aragno, and F. Wong, "Pathways of hepatic and renal damage through non-classical activation of the renin-angiotensin system in chronic liver disease," *Liver International*, vol. 40, no. 1, pp. 18–31, 2020.

[73] K. M. Kim, J. H. Roh, S. Lee, and J. H. Yoon, "Clinical implications of renin-angiotensin system inhibitors for development and progression of non-alcoholic fatty liver disease," *Scientific Reports*, vol. 11, no. 1, p. 2884, 2021.

[74] M. Moreno, L. N. Ramalho, P. Sancho-Bru et al., "Atorvastatin attenuates angiotensin II-induced inflammatory actions in the liver," *American Journal of Physiology. Gastrointestinal and Liver Physiology*, vol. 296, no. 2, pp. G147–G156, 2009.

[75] A. D. de Kloet, E. G. Krause, and S. C. Woods, "The renin angiotensin system and the metabolic syndrome," *Physiology & Behavior*, vol. 100, no. 5, pp. 525–534, 2010.

[76] S. M. Bindom, C. P. Hans, H. Xia, A. H. Boulares, and E. Lazartigues, "Angiotensin I-converting enzyme type 2 (ACE2) gene therapy improves glycemic control in diabetic mice," *Diabetes*, vol. 59, no. 10, pp. 2540–2548, 2010.

[77] E. D. Frantz, C. Crespo-Mascarenhas, A. R. Barreto-Vianna, M. B. Aguila, and C. A. Mandarim-de-Lacerda, "Renin-angiotensin system blockers protect pancreatic islets against diet-induced obesity and insulin resistance in mice," *PLoS One*, vol. 8, no. 7, article e67192, 2013.

Research Article

Nrf2-Mediated Ferroptosis Inhibition Exerts a Protective Effect on Acute-on-Chronic Liver Failure

Jing Wu [1], **Ran Xue** [2], **Muchen Wu** [1], **Xuehong Yin** [1], **Bangxiang Xie** [3], **and Qinghua Meng** [1]

[1]*Department of Liver Disease, Beijing You-An Hospital, Capital Medical University, Beijing 100069, China*
[2]*Key Laboratory of Carcinogenesis and Translational Research (Ministry of Education), Department of Gastrointestinal Oncology, Peking University Cancer Hospital & Institute, Beijing 100036, China*
[3]*Beijing Youan Hospital, Beijing Institute of Hepatology, Capital Medical University, Beijing 100069, China*

Correspondence should be addressed to Bangxiang Xie; yhxych7201@ccmu.edu.cn
and Qinghua Meng; meng_qh0805@ccmu.edu.cn

Although massive hepatocyte cell death and oxidative stress constitute major events of acute-on-chronic liver failure (ACLF), the relationship of ferroptosis with ACLF has yet to be explored. Nuclear factor erythroid 2-related factor 2 (Nrf2) is a key regulator of ferroptosis. However, if Nrf2 modulates ACLF through ferroptosis remains unknown. Here, the liver tissues of ACLF patients were collected and murine models of ACLF using carbon tetrachloride, D-galactosamine, and lipopolysaccharide as well as an H_2O_2-induced hepatocyte injury model were established. Upon ACLF, livers exhibited key features of ferroptosis, including lipid peroxidation (increase in malondialdehyde whereas a decrease in glutathione and nicotinamide adenine dinucleotide phosphate), and increased mRNA expression of prostaglandin-endoperoxide synthase-2 (PTGS2). Ferroptosis inducer RSL-3 treatment aggravated liver damage, while ferroptosis inhibitor Ferrostatin-1 administration alleviated ACLF severity, manifesting with improved liver histopathological lesions and reduced serum ALT and AST. Compared with normal liver tissue, Nrf2 was upregulated in ACLF patients and murine models. Pharmacological activation of Nrf2 (Bardoxolone Methyl) attenuated liver damage, prevented lipid peroxidation, upregulated PTGS2 mRNA expression, and improved ferroptosis-specific mitochondrial morphology in vivo. In contrast, Nrf2 inhibitor ML385 exacerbated lipid peroxidation and liver injury. Collectively, Nrf2 plays a protective role in ACLF progression through repressing ferroptosis, which provides promising therapeutic cues for ACLF.

1. Introduction

Acute-on-chronic liver failure (ACLF) is a distinct clinical entity when chronic liver disease undergoes acute insults. ACLF is complicated with organ failures, characterized by rapid deteriorated course and high short-term mortality [1]. Globally, it is estimated that 24% to 40% of patients with cirrhosis admitted to hospitals were diagnosed with ACLF [2]. Deciphering ACLF pathogenesis and developing therapeutic strategies have become unmet needs and critical priority. Nevertheless, molecular mechanisms of progressive

liver failure have hitherto not been fully understood, and ACLF remains one of the most challenging problems in clinic. Therefore, intense research efforts to delay disease progression are urgently required.

Hepatic cell death is a crucial molecular event of ACLF. Although apoptosis [3], autophagy [4], and necrosis [5] have been proposed in ACLF, whether other types of cell death are pathophysiological mechanisms underlying ACLF has not been explored. Ferroptosis is a novel mode of iron-dependent cell death manifesting with overwhelming lipid peroxidation and loss of cellular redox homeostasis [6].

Ferroptosis is morphologically, genetically, and biochemically distinct from other types of cell death [7, 8]. Accumulating evidence suggests that ferroptosis plays an unneglectable role in regulating disease development and progression, including neoplastic [9], neurological [10], and heart diseases [11]. Given that the liver is highly predisposed to oxidative damage and iron accumulation has been involved in multiple liver diseases [12], ferroptosis is a potential contributor to various liver diseases. Dysregulated iron homeostasis has been reported in patients with ACLF [13]. Specifically, increased circulating levels of total iron and ferritin were observed in ACLF patients relative to normal controls. Since aberrant iron metabolism is a potential predictor of multiorgan failure and mortality in patients with ACLF [13, 14], we hypothesized that ferroptosis contributed to ACLF pathogenesis. To the best of our knowledge, there has been no clear demonstration of association between ferroptosis and ACLF.

The nuclear factor erythroid 2-related factor 2 (Nrf2) is a vital nuclear transcription factor, which controls a battery of cellular defensive genes to maintain redox homeostasis and cell survival [15]. Recently, Nrf2 has been identified as a regulator of ferroptosis. For example, in neoplastic diseases, Nrf2-mediated ferroptosis suppressed tumor growth and sensitized cancer cells to antitumor drugs [16, 17]. In acute or chronic tissue/cell damage, Nrf2 stabilization could restrain ferroptosis and subsequently relieve injury [18]. Specifically, activation of Keap1/Nrf2-ARE signaling pathway in response to dehydroabietic acid could eliminate reactive oxygen species (ROS) accumulation and suppress ferroptosis, which consequently, improved nonalcoholic fatty liver disease [19]. However, little is known whether ferroptosis is a mechanism through which Nrf2 confers a protective effect on ACLF.

The purpose of this study was to investigate if ferroptosis participates in ACLF pathogenesis and to unveil underlying molecular mechanisms. Major features of clinical ACLF were recapitulated through establishing murine models with carbon tetrachloride (CCl4), D-galactosamine (D-gal), and lipopolysaccharide (LPS). A hepatocyte injury model was established by treating L02 cells with H_2O_2 in vitro. Successful establishment of ACLF model was confirmed by features of ACLF in terms of laboratory parameters and liver histopathology. Then, mice were treated with either ferroptosis inducer or inhibitor to assess effects of ferroptosis on liver injury. Finally, we explored if Nrf2 could protect from liver injury through ferroptosis by using either inducer or inhibitor of Nrf2.

2. Materials and Methods

This study was conducted following the Declaration of Helsinki. All animal experiments were performed according to the guidelines of Animal Experiments and Experimental Animal Welfare Committee at Capital Medical University. This study was approved by the Ethical Committee of Beijing You-An Hospital, Capital Medical University (No. AEEI-2020-195).

2.1. Mice and Experimental Design. Male BALB/c mice between 6 and 8 weeks of age were purchased from the Bei-

jing Weitong Lihua Experimental Animal Ltd. Co. (license: SCXK11-00-0008). Mice were housed in a standard environmental condition with sterile water and diet, the 23°C laboratory room temperature, 12 h of light and 12 h of darkness, and 50% indoor humidity were acclimated for two weeks before experimentation. ACLF models were constructed as follows: mice were injected intraperitoneally (i.p.) with 0.2 ml CCl4 in olive oil (CCl4/olive oil volume = 1 : 5, twice a week) for 8 weeks, and subsequently with a high frequency (three times a week) for 4 weeks. Twenty-four hours later, mice were challenged i.p. with LPS (10 μg/kg) and D-gal (500 mg/kg).

Mice were randomly divided into six groups. Group 1 ($n = 3$), normal control: mice received 0.2 ml of saline (0.9%, v/v) in water (twice a week for 8 weeks and 3 times a week for 4 weeks). Group 2, ACLF ($n = 6$): ACLF models were constructed as described above. Group 3 ($n = 6$), ACLF + ferroptosis activation: mice were administrated i.p. with ferroptosis inducer RSL-3 (10 mg/kg, Abmole, USA) three times a week for 4 weeks. Group 4 ($n = 6$), ACLF + ML385: mice were injected i.p. with Nrf2 inhibitor ML385 (30 mg/kg, Abmole, USA) four times per week for 4 weeks. Group 5 ($n = 6$), ACLF + Baroxolone Methyl (BM): mice were administrated with BM (10 mg/kg, dissolved in olive oil, Abmole, USA) by gavage once every other day for 4 weeks. Group 6 ($n = 6$), ACLF + Ferrostatin-1 (Fer-1): mice were treated with i.p. injection of Fer-1(10 mg/kg, Abmole, USA) three times a week for 4 weeks. The experimental regimen was described in Figure 1.

2.2. Patients. Between January 2019 and June 2021, five transplant recipients who fulfilled diagnostic criteria of Asian Pacific Association for the Study of the Liver (APASL) [20] for ACLF were included in this study. Normal liver tissues were obtained from liver transplant donors, serving as the healthy control. Exclusion criteria included multiple organ failure, fulminant hepatic failure, complicated liver cancer, long-term immunosuppressive therapy, and age less than 18 years. Informed consent was obtained from each participant before enrollment. This study was approved by the Ethical Committee of Beijing You-An Hospital, Capital Medical University (No. LL-2018-119-K).

2.3. Western Blot. The cells and liver tissues were lysed in lysis buffer and centrifuged at 4°C and 12000 rpm for 30 min. Nuclear proteins were extracted with the Nuclear Protein Extraction Kit (Solarbio, China). After assessment of concentrations, proteins were denatured using 5× sodium dodecyl sulfate (SDS) loading buffer at 100°C for 5 min. Protein mixtures were separated on 8-12% SDS-polyacrylamide gel electrophoresis and transferred to polyvinylidene difluoride membrane. After blocked with 5% defat milk at room temperature for 1 h, the membrane was incubated with the primary antibody against Nrf2 (Cell Signaling Technology, MA, USA), HO-1(Abcam, Cambridge, UK), and NQO1(Abcam, Cambridge, UK) overnight at 4°C. The next day, after washed for three times with Tris Buffered Saline with Tween 20 (TBST), the membrane was incubated with goat antirabbit horseradish peroxidase-conjugated secondary antibodies
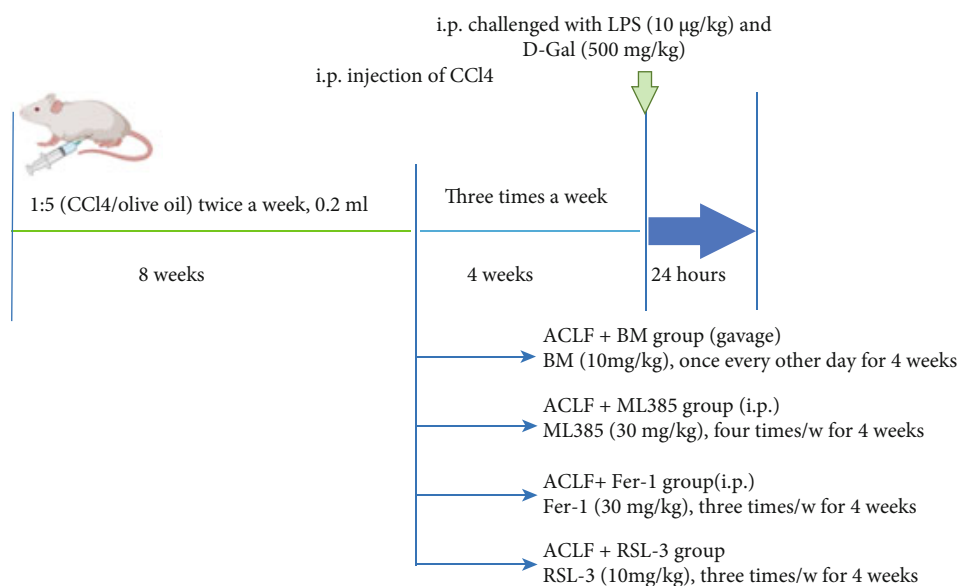
FIGURE 1: The experimental regimen applied in this study.

TABLE 1: Primers used in this study.

	Gene	Forward	Reverse
	PTGS2	5′-TGAGCATCTACGGTTTGCTG-3′	5′-TGCTTGTCTGGAACAACTGC-3′
Human	GAPDH	5′-TGTCATGGCAGAAGTACCTG-3′	5′-GTTAACTGGGGAGCCTGCTC-3′
	HO-1	5′-CCAGGCAGAGAATGCTGAGTTC-3′	5′-AAGACTGGGCTCTCCTTGTTGC-3′
	NQO-1	5′-CCTGCCATTCTGAAAGGCTGGT-3′	5′-GTGGTGATGGAAAGCACTGCCT-3′
Mouse	PTGS2	5′-CTGCGCCTTTTCAAGGATGG-3′	5′-GGGGATACACCTCTCCACCA-3′
	GAPDH	5′-CAAAGCAAAGATGCTCCACA-3′	5′-ATCGCATGAACCTTGTTTCC-3′

(Cell Signaling Technology, MA, USA) for 1 h at room temperature and washed for three times with TBST. Subsequently, the bands were visualized using an enhanced chemiluminescence detection kit (Thermo Fisher Scientific, USA) according to the manufacturer's instructions.

2.4. Liver Histopathology and Immunohistochemical Assays. As previously described [21], the liver tissues collected from different groups were fixed with formaldehyde and embedded in paraffin. Haematoxylin–eosin and Masson's trichrome staining were conducted to evaluate liver histological features and tissue fibrosis. Formalin-fixed paraffin-embedded liver tissues were stained with antibodies against Nrf2 (Sigma-Aldrich, St. Louis, MO, USA). The morphology was assessed under an electron microscope (Nikon Eclipse 80i, Tokyo, Japan). Representative pictures of liver sections from all groups were displayed.

2.5. Enzyme-Linked Immunosorbent Assay (ELISA). ELISA kits (RayBiotech, Norcross, GA) were applied to detect hepatic protein levels of IL-6 and tumor necrosis factor (TNF)-α according to the manufacturer's protocol.

2.6. Serum Biochemistry. Serum alanine aminotransferase (ALT) and aspartate aminotransferase (AST) were detected by an automated chemical analyzer (Olympus Company, Tokyo, Japan).

2.7. Hepatic Content of Malondialdehyde (MDA) and Glutathione (GSH). According to the manufacturer's recommendations, MDA and GSH levels were measured using corresponding detection kits (Beyotime, Beijing, China). Absorbance values of samples were measured at 532 nm and 412 nm, respectively.

2.8. Iron Assay. Hepatic iron concentration was determined by Iron Assay Kit (No. ab83366, Abcam) according to the manufacturer's instruction.

2.9. Cell Culture. Human cell line L02 was cultured in Dulbecco's Modified Eagle's Medium (DMEM) (Gibco, Gaithersburg, MD, USA) containing 10% fetal bovine serum (FBS) (Gibco, Gaithersburg, MD, USA) and grown at 37°C and 5% CO_2 humidified atmosphere. Cells were treated with H_2O_2 (300 μM) (Invitrogen, Carlsbad, CA, USA) for 30 h for

(a)

(b)

(c)

(d)
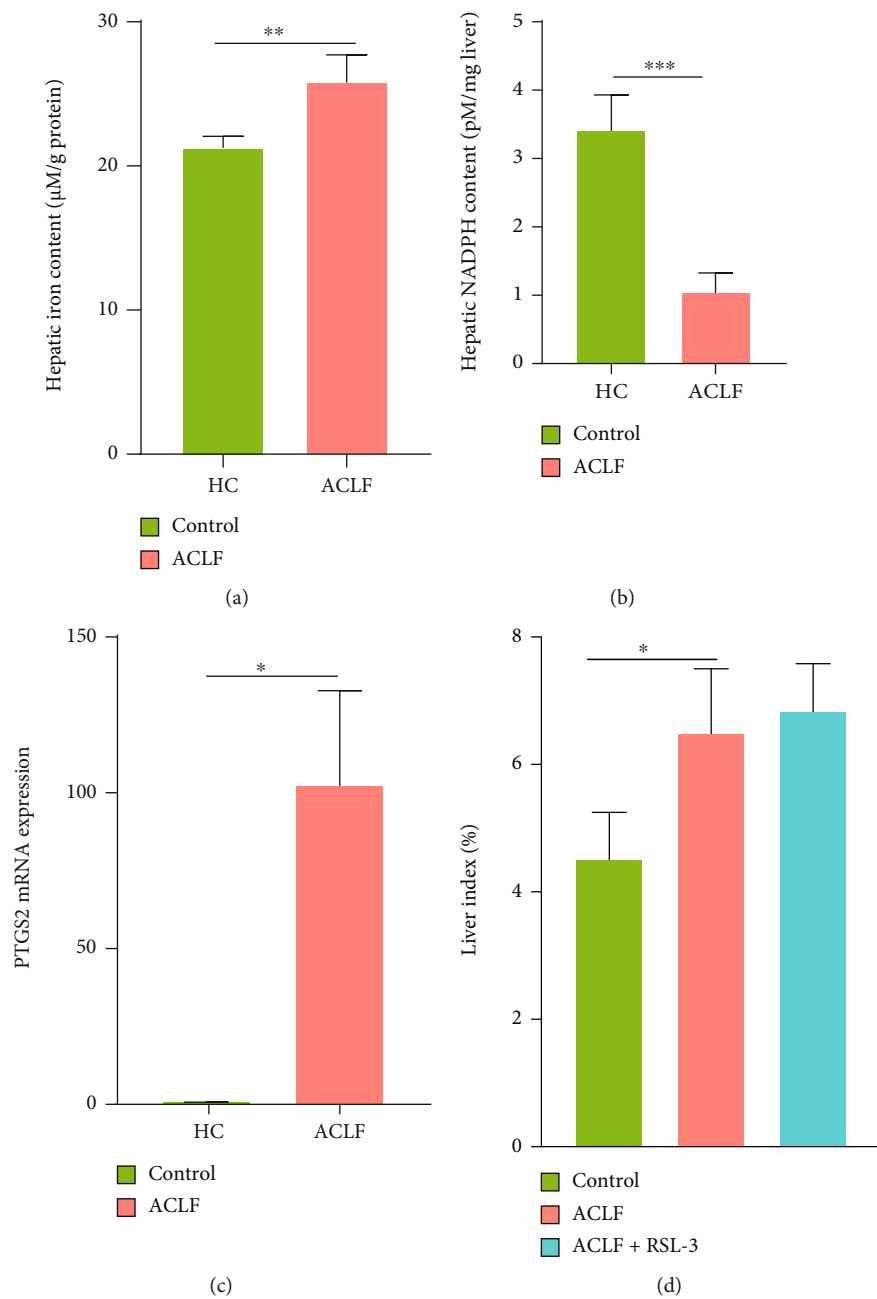
Figure 2: Continued.

(e)

(f)

(g)

FIGURE 2: Continued.

(h)

(i)

(j)

(k)
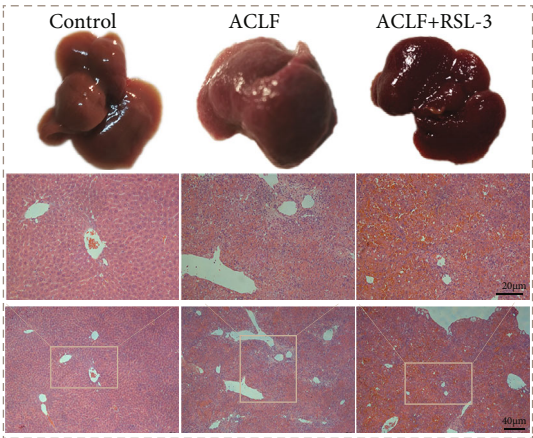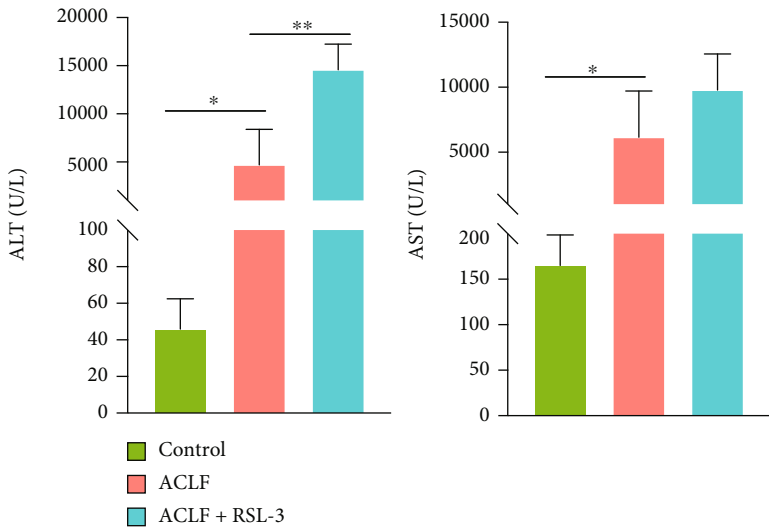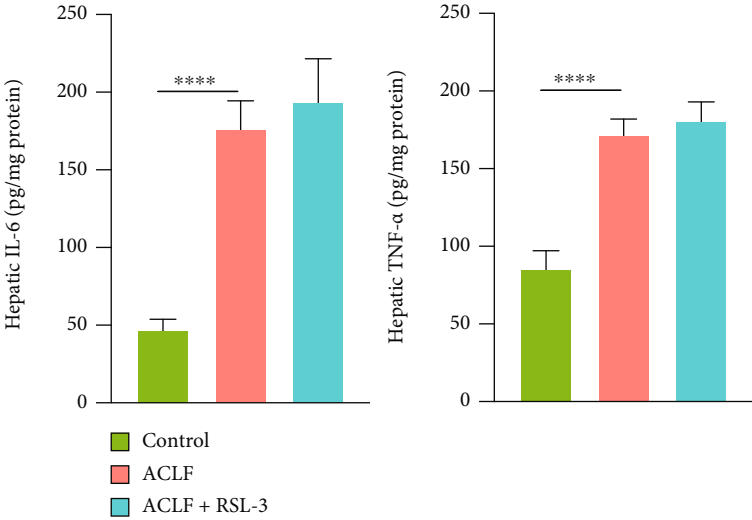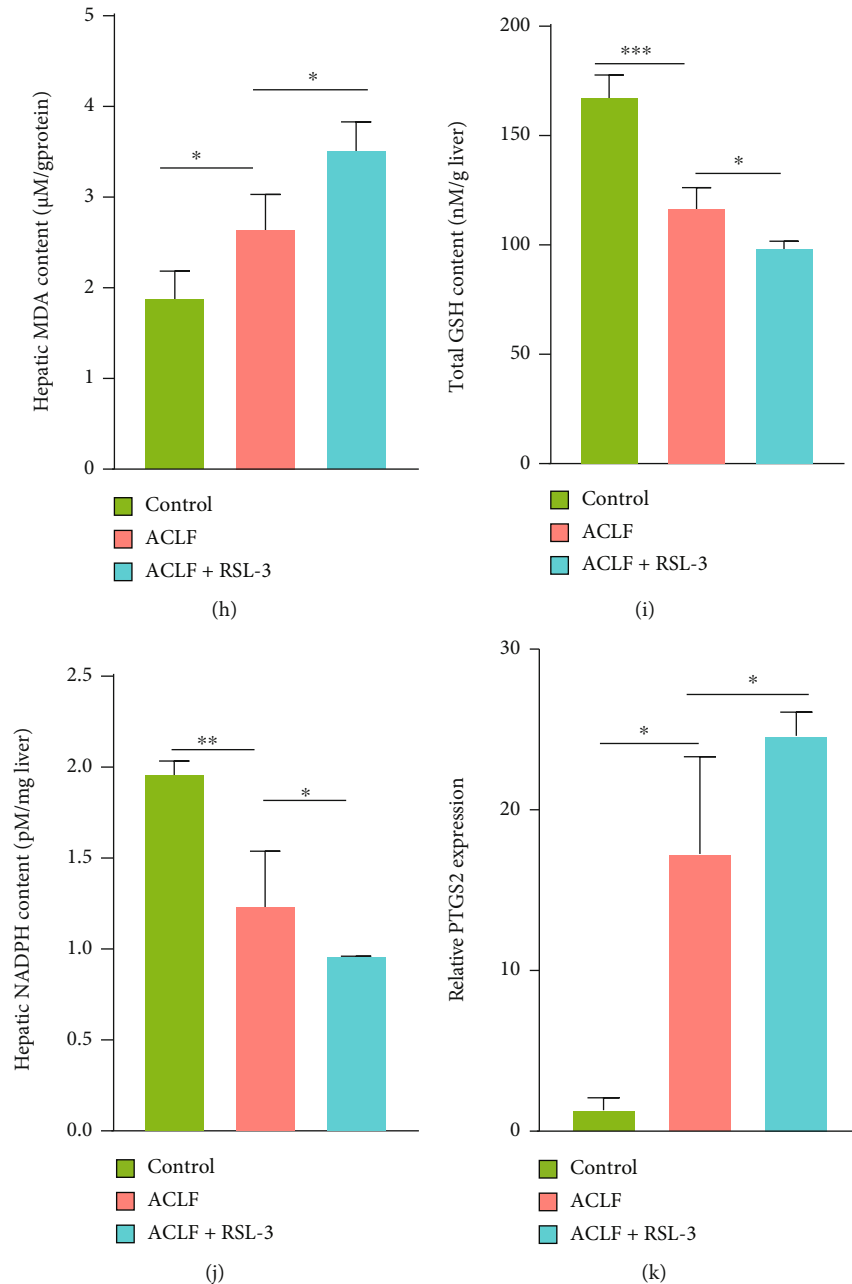
FIGURE 2: Ferroptosis aggravated liver injury in ACLF mice models. (a) Hepatic iron content both in healthy controls and ACLF patients was measured (HC $n = 3$, ACLF $n = 5$). (b) Hepatic NADPH content was decreased in ACLF patients relative to healthy controls (HC $n = 3$, ACLF $n = 5$). (c) PTGS2 mRNA expression was increased in patients with ACLF compared with healthy controls (HC $n = 3$, ACLF $n = 5$). (d) The livers of the ACLF+RSL-3-treated mice were slightly heavier than those of ACLF mice although without statistical significance. (e) Representative images of morphologic and histopathological features of the control, ACLF, and ACLF+RSL-3-treated mice. Original magnification ×100 (Bar = 40 μm) and ×200 (Bar = 20 μm). (f and g) Serum ALT and AST levels and hepatic inflammatory cytokines (IL-6, TNF-α) were assessed. (h–j) Lipid peroxidation was analyzed through comparing hepatic GSH, NADPH, and MDA in the three groups. (k) The expression of PTGS2 mRNA was measured by qRT-PCR. Data are expressed as mean ± SD $^*p < 0.05$, $^{**}p < 0.01$, $^{***}p < 0.001$, $^{****}p < 0.0001$. $n = 3$ (control, ACLF+RSL-3), $n = 6$ (ACLF). ALT = alanine aminotransferase; AST = aspartate aminotransferase; ACLF = acute-on-chronic liver failure; GSH = glutathione; IL-6 = interleukin-6; MDA = malondialdehyde; NADPH = nicotinamide adenine dinucleotide phosphate; PTGS2 = prostaglandin-endoperoxide synthase-2; qRT-PCR = quantitative real-time polymerase chain reaction; TNF-α = tumor necrosis factor alpha.

hepatocyte injury model. Moreover, cells were treated with or without inducer or inhibitor of ferroptosis or Nrf2 for mechanistic exploration.

2.10. Cell Viability Assay. Cell Counting Kit-8 (CCK-8, Abmole, USA) was used to assess proliferation of cells with different treatments. Briefly, 3×10^3 L02 cells were seeded

(a)

(b)

(c)

(d)

Figure 3: Continued.

(e)

(f)
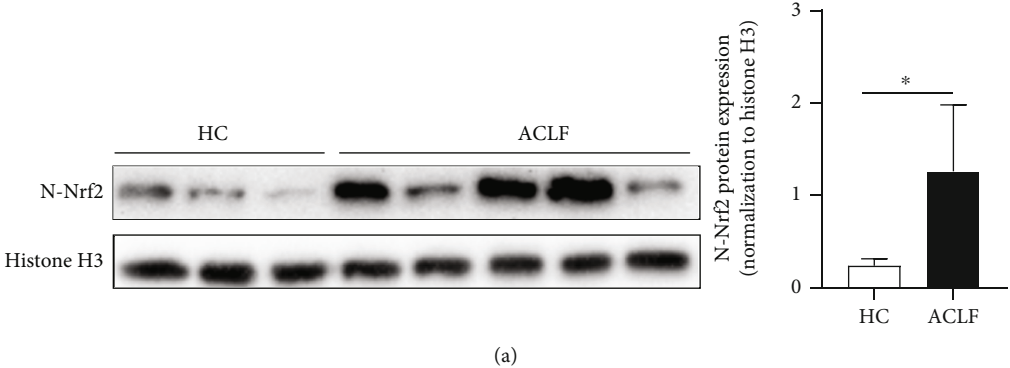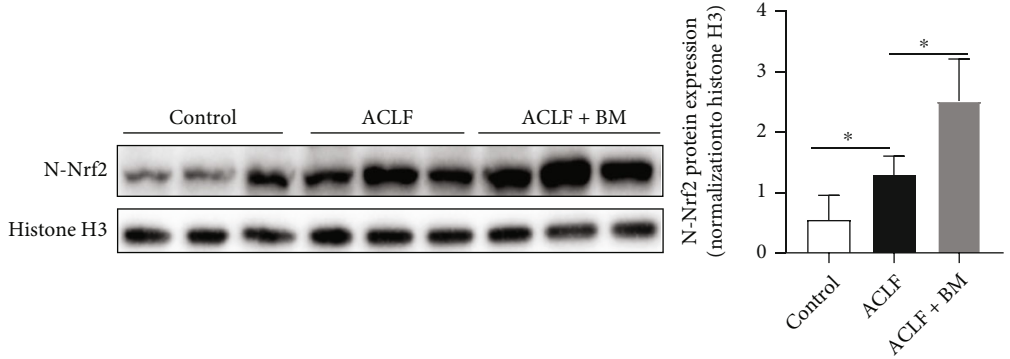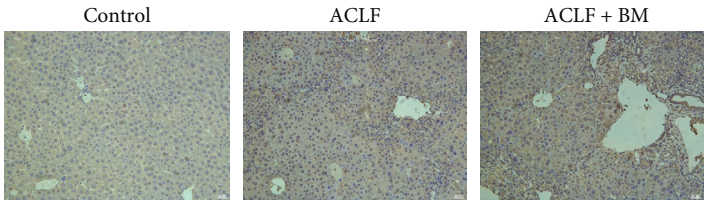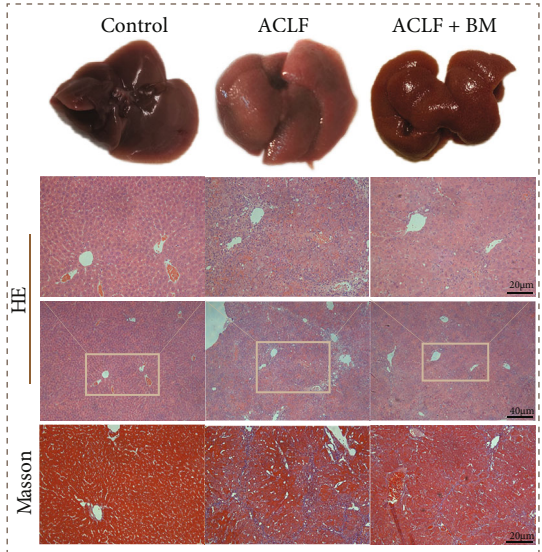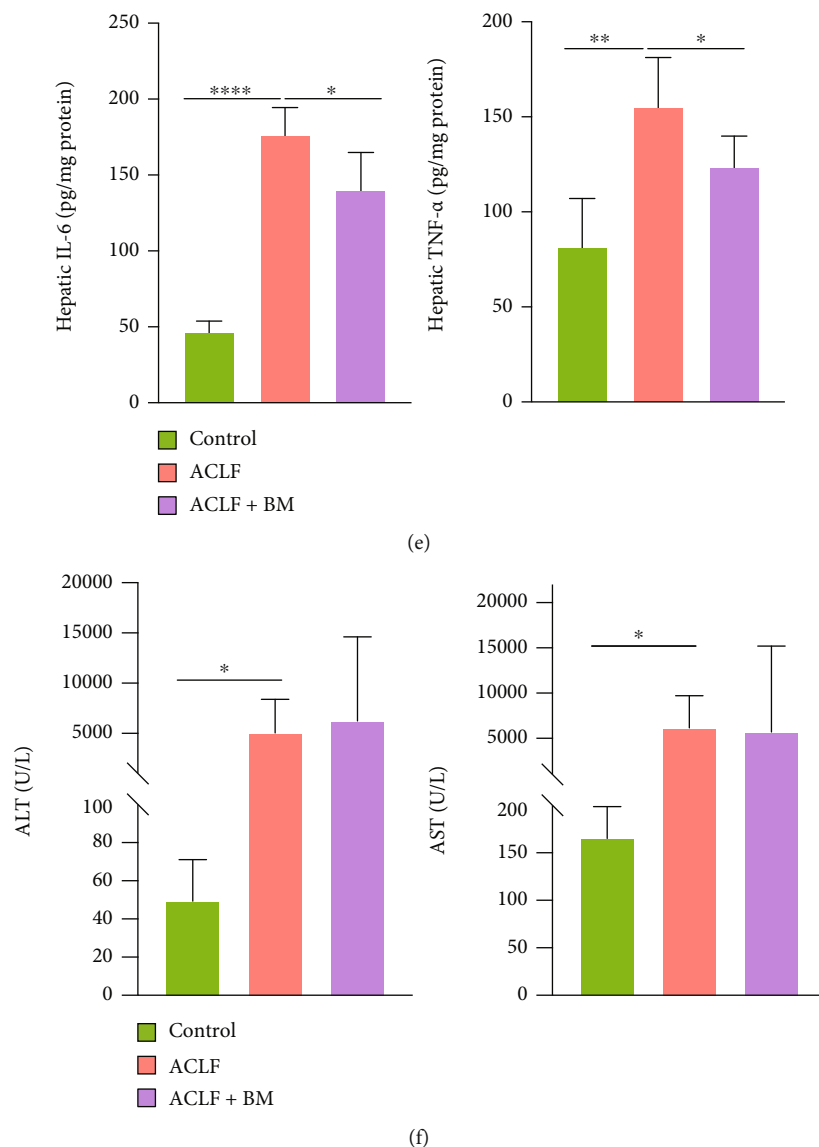
FIGURE 3: Activation of Nrf2 ameliorated liver injury in vivo. (a and b) The protein expression of Nrf2 in the liver tissues was confirmed by western blot (HC $n = 3$, ACLF $n = 5$). (c) The results of immunohistochemical staining indicated that Nrf2 translocated into the nucleus and activated in the pathologic context of ACLF, and BM treatment further augmented its activation. Original magnification ×200 (Bar = 20 μm). (d) Improvement of morphologic and histopathological features in the BM treatment group implied the protective effect of Nrf2 on ACLF. Original magnification ×100 (Bar = 40 μm) and ×200 (Bar = 20 μm). (e) Hepatic protein levels of IL-6 and TNF-α were measured. (f) BM treatment did not significantly decrease serum levels of ALT and AST. $^*p < 0.05$, $^{**}p < 0.01$, $^{****}p < 0.0001$. $n = 3$ (control), $n = 6$ (ACLF), $n = 5$ (ACLF+BM). ALT = alanine aminotransferase; AST = aspartate aminotransferase; ACLF = acute-on-chronic liver failure; BM = bardoxolone methyl; IL-6 = interleukin-6; Nrf2 = nuclear factor erythroid 2-related factor 2; TNF-α = tumor necrosis factor alpha.

in 96-well plates and incubated for 24 h. Afterwards, cells were pretreated with BM (0.2 μM), Fer-1(0.25 μM), and ML385 (10 μM) for 12 h, respectively, and H$_2$O$_2$ (300 μM) for 30 h. For the positive control group, cells were treated with Erastin (E, 10 μM, an inducer of ferroptosis) for 30 h. Later, 10 μL CCK-8 working solution was added to corresponding culture medium and incubated for 2 h at 37°C. Finally, absorbance was evaluated at 450 nm using a microplate reader.

2.11. Lipid Peroxidation Assay. Indicated cells were stained with 5 μM BODIPY® 581/591 C11 dye for 30 min at 37°C

in the dark. After the incubation, cells were washed twice with phosphate buffer saline (PBS) and resuspended in 400 μL PBS. Flow cytometry analysis was conducted using a BD FACSCalibur system.

2.12. Transmission Electron Microscopy (TEM). Liver tissues were fixed with glutaraldehyde (2.5%) and washed for three times with phosphate-buffered solution. After embedded in 1% agarose, samples were dehydrated in 30%, 50%, 70%, 80%, and 95% ethanol for 20 min, in Acetone for 15 min, and then embedded in Acetone. Resin blocks were cut to 60-80 nm-thin fragments on ultramicrotome. The tissue

(a)

(b)

(c)

(d)

FIGURE 4: Continued.

(e)
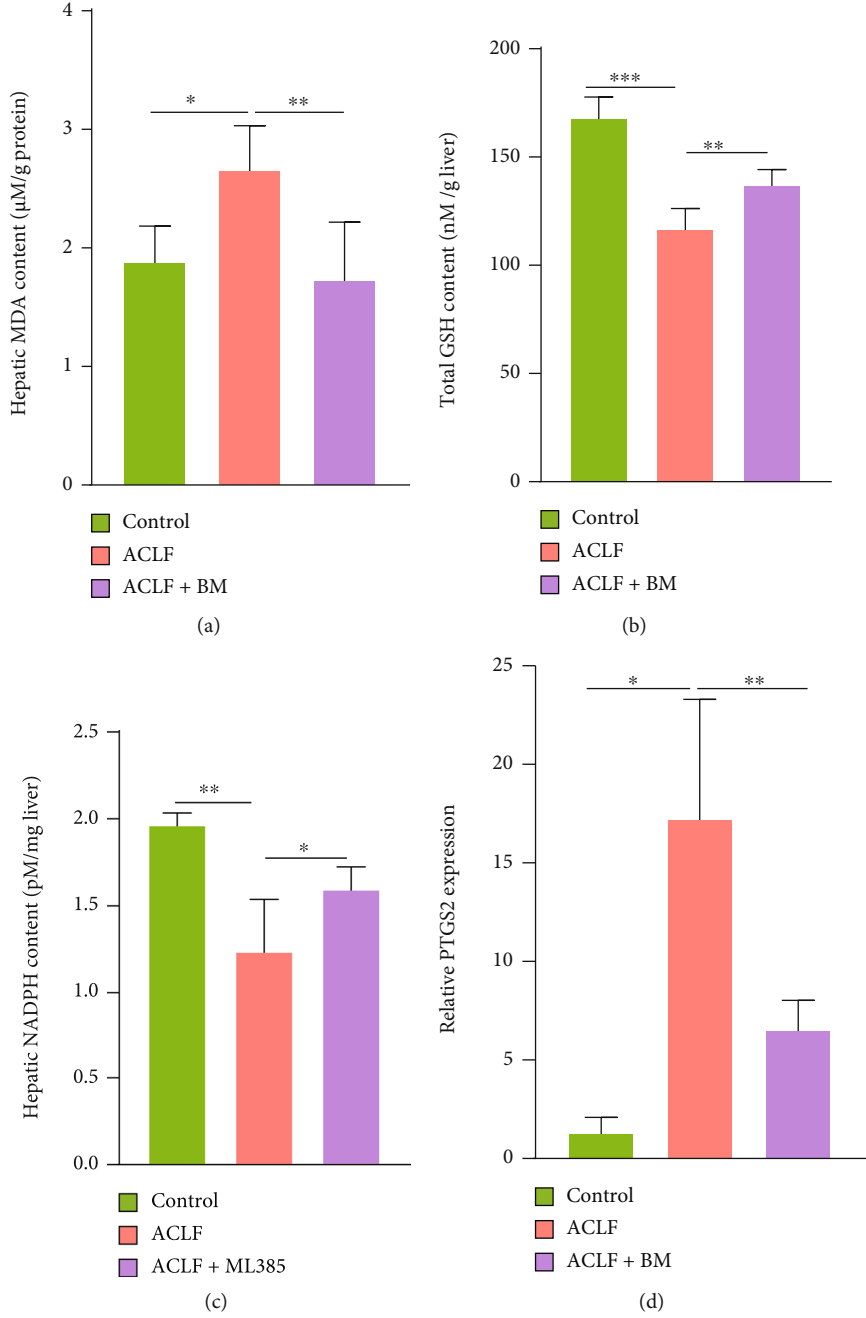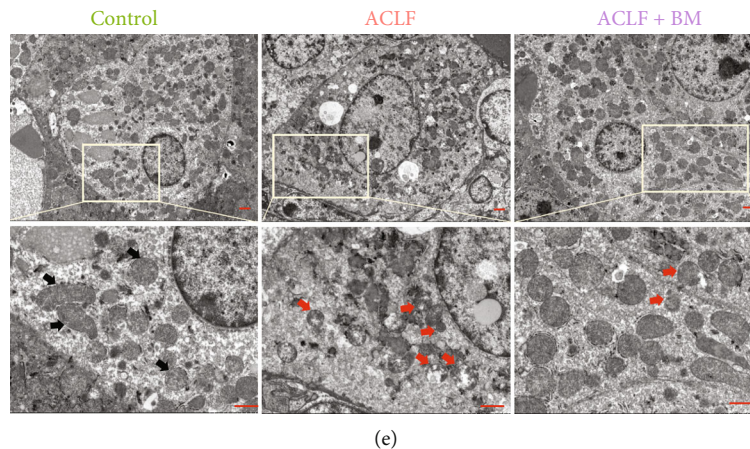
Figure 4: Activation of Nrf2 mitigated lipid peroxidation. (a) Hepatic MDA content was measured in all three groups. (b) Total GSH concentration was detected. (c) Hepatic NADPH content was measured. (d) The relative mRNA expression of ferroptosis-related gene PTGS2 in the liver tissues. (e) Increased mitochondrial outer membrane rupture and diminished mitochondrial ridges were seen in the ACLF group under electron microscopy, while BM treatment improved these morphological changes. Bar = 10 μm. Black arrows indicate normal mitochondria; red arrows indicate shrunken and ruptured mitochondria. $^*p < 0.05$, $^{**}p < 0.01$, $^{***}p < 0.001$. $n = 3$ (control), $n = 6$ (ACLF), $n = 5$ (ACLF+BM). ACLF = acute-on-chronic liver failure; BM = bardoxolone methyl; GSH = glutathione; MDA = malondialdehyde; NADPH = nicotinamide adenine dinucleotide phosphate; Nrf2 = nuclear factor erythroid 2-related factor 2; PTGS2 = prostaglandin-endoperoxide synthase-2.

was fished out onto cuprum grids. After staining, images were taken under TEM (JEM-1200; Jeol Ltd.) at 80 kV with representative pictures being depicted.

2.13. Quantitative Real-Time Polymerase Chain Reaction (qRT-PCR). TRIzol reagent (Invitrogen, Carlsbad, CA, USA) was used for total RNA isolation according to the manufacturer's instructions. Isolated RNA was reverse transcribed into cDNA using the PrimeScript RT reagent kit (TaKaRa Biotechnology, Beijing, China). Finally, real-time PCR was performed using the TB Green Premix Ex Taq™ (Tli RNaseH Plus) kit (TaKaRa Biotechnology, Beijing, China) on an ABI ViiA 7 Real-Time PCR System (ABI, USA) according to the manufacturer's protocol. The relative gene expression was normalized to glyceraldehyde-3-phosphate dehydrogenase (GAPDH). The thermal cycling conditions were as follows: 95°C for 30 s; 40 cycles of 95°C for 5 s and 60°C for 30 s; and dissociation at 95°C for 15 s, 60°C for 60 s, and 95°C for 15 s. Primers used in this study were listed in Table 1.

2.14. Statistical Analysis. The GraphPad Prism 8.0 software was used to conduct statistical analysis. Data were expressed as means ± standard deviation (SD). Unpaired Student's t-test and Mann–Whitney U test were used to evaluate the differences between groups. A p value < 0.05 was considered statistically significant.

3. Results

3.1. Induction of Ferroptosis Aggravated Liver Injury in ACLF Murine Models. Human hepatic iron concentration was evaluated in the healthy controls and ACLF patients. Compared with the healthy controls, hepatic iron content was significantly increased in ACLF (Figure 2(a)), consistent

with previous studies [13]. Decreased hepatic nicotinamide adenine dinucleotide phosphate (NADPH) content, an established signature of ferroptosis [22, 23], was observed in ACLF relative to the healthy controls (Figure 2(b)). In addition, the mRNA expression of prostaglandin-endoperoxide synthase-2 (PTGS2), another typical feature of ferroptosis [22], was elevated in ACLF (Figure 2(c)). We speculated that ferroptosis was implicated in ACLF pathogenesis.

To verify this hypothesis, a mouse model was established to recapitulate major characteristics of clinical ACLF using CCl4, LPS, and D-gal (Figure 1). Induction of ferroptosis, through treatment with RSL-3, an inducer of ferroptosis [24], reinforced liver damage. As shown in Figures 2(d) and 2(e), in the control group, the livers were smooth and rosy with intact hepatic structure; while in the ACLF group, the livers were smaller and harder, with blunt edges and small nodules. Disordered hepatic lobule structure, substantial hepatic cell death, and advanced fibrosis with nodule formation, as major characteristics of ACLF [1], were observed in the successfully established ACLF group. Of note, these histopathological lesions were more evident in the livers of RSL-3-treated mice. Consistent with an increase in histopathological severity, serum biochemical indicators (ALT and AST) were elevated in response to RSL-3 treatment (Figure 2(f)). Regarding inflammatory cytokines, however, no significantly increased hepatic IL-6 and TNF-α were observed in response to RSL-3 treatment compared with the ACLF group (Figure 2(g)). In parallel with aggravated liver damage, several indicators of lipid peroxidation, (a) MDA (Figure 2(h)), an end product of lipid peroxidation, was higher in the ACLF group and the highest in the RSL-3 treatment group; (b) GSH and NADPH showed an opposite trend (Figures 2(i) and 2(j)). Similarly, the mRNA expression of PTGS2 was elevated along with increased

(a)

(b)

Figure 5: Continued.

(c)

(d)

(e)

FIGURE 5: Continued.

(f)

(g)
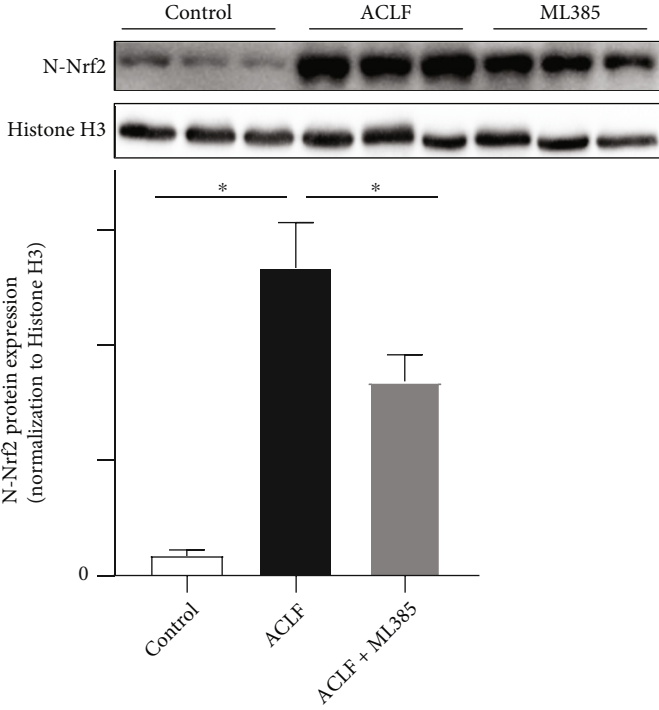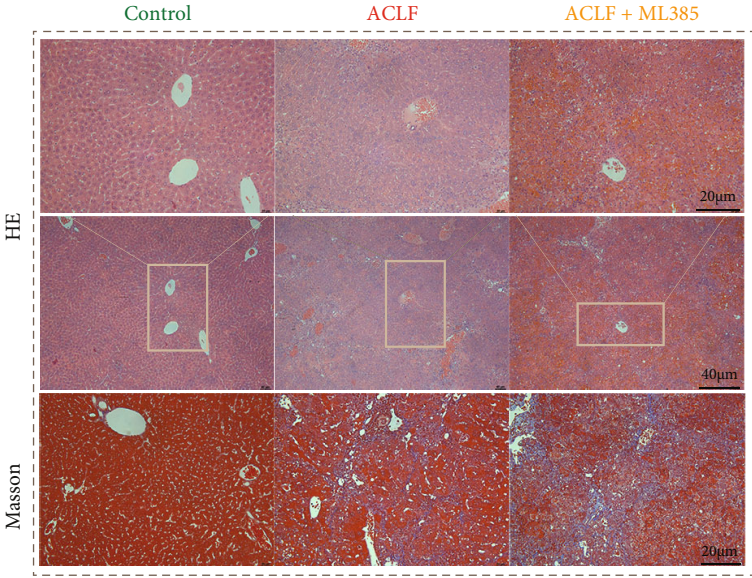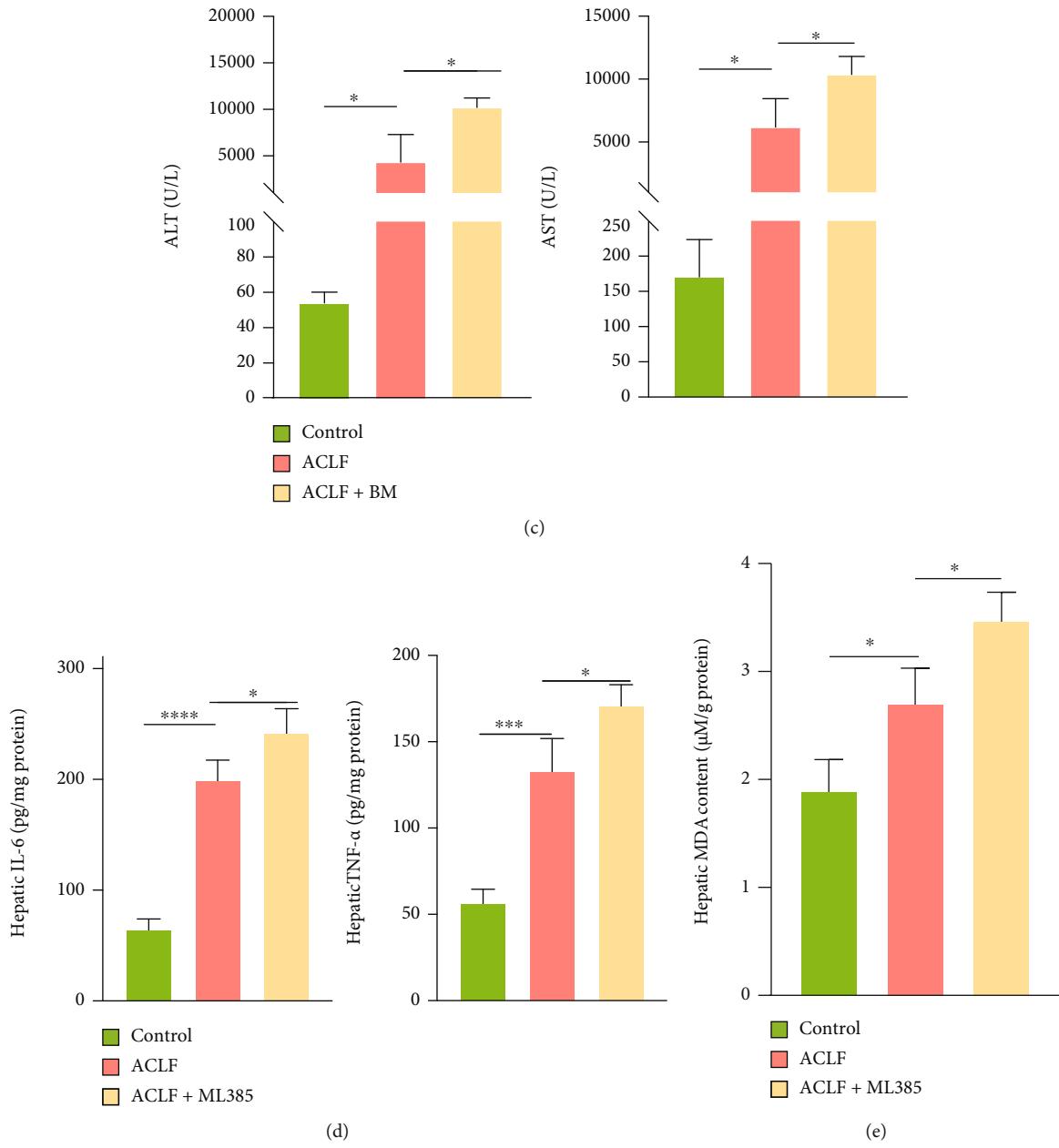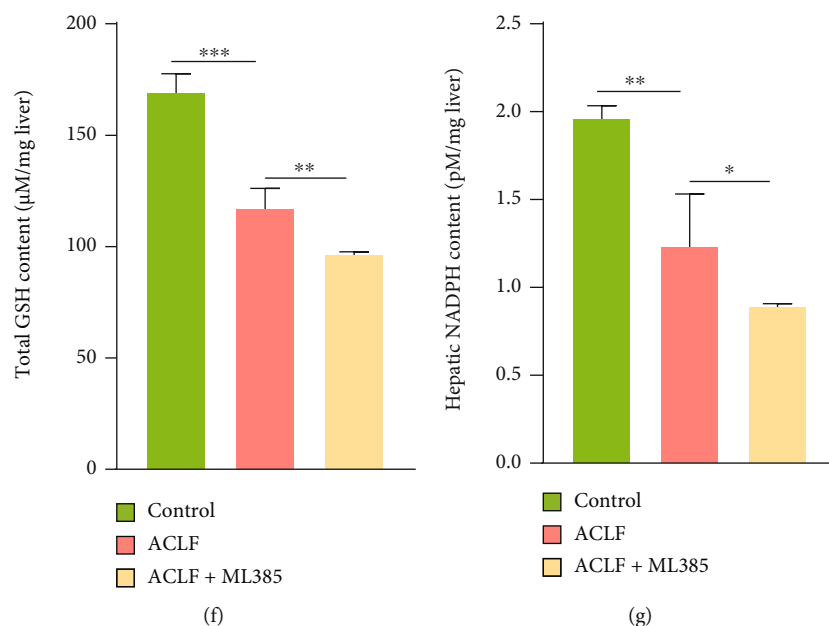
FIGURE 5: Nrf2 inhibition promoted the onset of lipid peroxidation and aggravated liver injury in mice. (a) Results of western blot confirmed the successful inhibition of Nrf2 using ML385 in vivo ($n = 3$). (b) The mice treated with ML385 demonstrated a more severe liver injury (hepatocytes necrosis, destruction of the lobular structure, infiltration of inflammatory cells, obvious vascular congestion, and hemorrhage) compared with the ACLF mice. Original magnification ×100 (Bar = 40 μm) and ×200 (Bar = 20 μm). (c) Significantly increased serum ALT and AST suggested the aggravated liver damage of mice treated with ML385. (d) ML385 treatment also increased the protein levels of inflammatory cytokines (IL-6, TNF-α). (e–g) The mice treated with ML385 showed increased lipid peroxidation as evidenced by decreased hepatic GSH and NADPH content and increased hepatic MDA levels. $^{*}p < 0.05$, $^{**}p < 0.01$, $^{****}p < 0.0001$. $n = 3$ (control), $n = 6$ (ACLF), $n = 3$ (ACLF+ML385). ALT = alanine aminotransferase. AST = aspartate aminotransferase; ACLF = acute-on-chronic liver failure; GSH = glutathione; IL-6 = interleukin-6; MDA = malondialdehyde; Nrf2 = nuclear factor erythroid 2-related factor 2; NADPH = nicotinamide adenine dinucleotide phosphate; TNF-α = tumor necrosis factor alpha.

severity of liver injury in the ACLF and RSL-3 groups (Figure 2(k)). Collectively, ferroptosis might act as a deleterious factor, which aggravated liver damage and promoted disease progression in ACLF.

3.2. Activation of Nrf2 Inhibited Ferroptosis and Ameliorated Liver Injury In Vivo. Nrf2-mediated defensive network might protect against various pathologic injuries and engage in regulating ferroptosis [25]. When being activated, Nrf2 was translocated to nuclear and initiated downstream anoxidative genes [26, 27]. Our preliminary results showed that nuclear protein expressions of Nrf2 were significantly increased in the liver tissues of ACLF patients compared with normal ones (Figure 3(a)). In addition, at mRNA levels, NAD(P) H quinone dehydrogenase, quinone 1 (NQO1), a pivotal target gene of Nrf2, was upregulated in ACLF liver tissues compared with normal ones (Supplemental Figure 1). Therefore, we speculated that Nrf2 might have a protective role in ferroptosis-provoked liver damage. BM is a common agent to activate Nrf2 [28, 29]. Nrf2 was activated in vivo in the BM group, as revealed by increased nuclear protein expression of Nrf2 relative to the ACLF group (Figure 3(b)). As expected, immunohistochemical staining of Nrf2 demonstrated the same results as western blots (Figure 3(c)). Specifically, in the control group, a small proportion of Nrf2 positive cells were diffusely distributed in the cytoplasm. In contrast, in the ACLF group, a large proportion of Nrf2

positive cells in the nuclei were identified. In the BM group, Nrf2 expressed in nuclei was largely augmented. Alongside Nrf2 activation was attenuated severity of ACLF, which was confirmed by gross morphological and histopathological features of the livers (Figure 3(d)). Specifically, Nrf2-activated livers demonstrated mitigated inflammation and hepatocytes death along with improved hepatic lobule structure disorder. In addition, this pattern was confirmed by decreased hepatic inflammatory indicators, such as IL-6 and TNF-α (Figure 3(e)). Contrary to our expectation, BM treatment failed to reduce the serum levels of ALT and AST (Figure 3(f)).

Furthermore, the potential role of Nrf2 in ferroptosis during ACLF was examined. As shown in Figures 4(a)–4(c), BM increased hepatic content of GSH and NADPH whereas decreased content of MDA. In addition, PTGS2 was downregulated in response to BM treatment (Figure 4(d)). Apart from lipid peroxidation, mitochondrial morphology was examined. Compared to the control group, the liver tissues from the ACLF group displayed smaller mitochondria morphology with diminished mitochondria crista, as well as rupture of outer mitochondrial membrane, all of which were specific morphological features of ferroptosis [7], whereas BM treatment improved this morphological phenotype (Figure 4(e)). Accordingly, Nrf2 activation inhibited ferroptosis, which might hold a substantial potential in attenuating liver damage in ACLF.

(a)

(b)

Figure 6: Continued.

(c)

(d)

(e)

(f)

(g)

FIGURE 6: Continued.

(h)
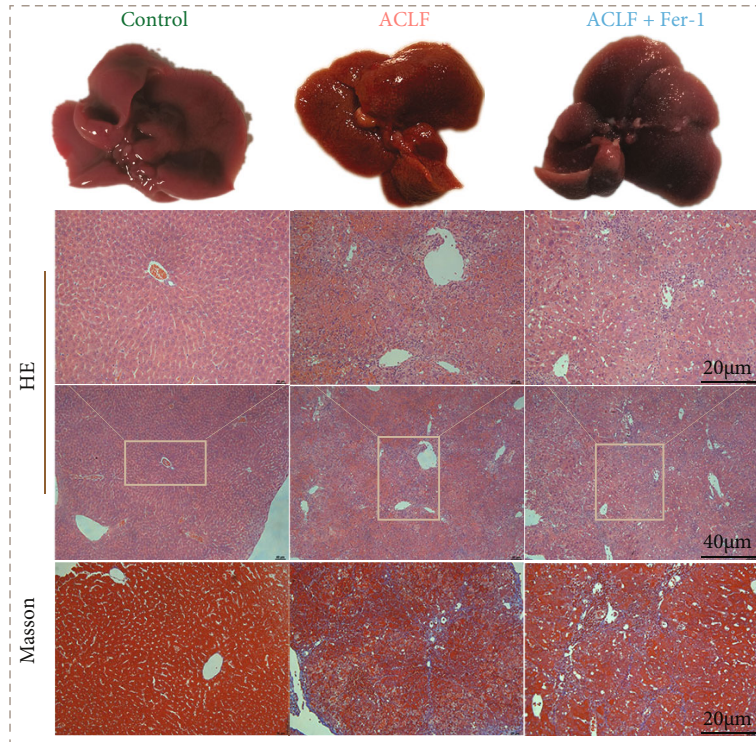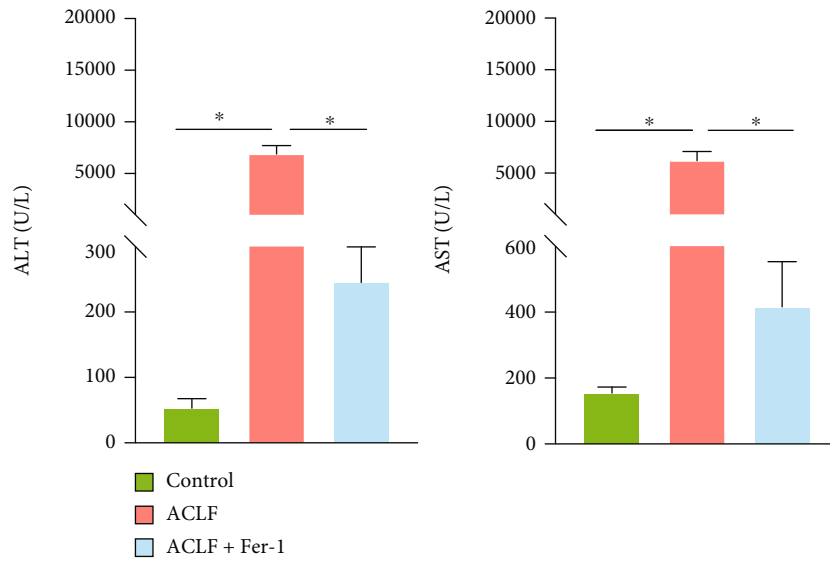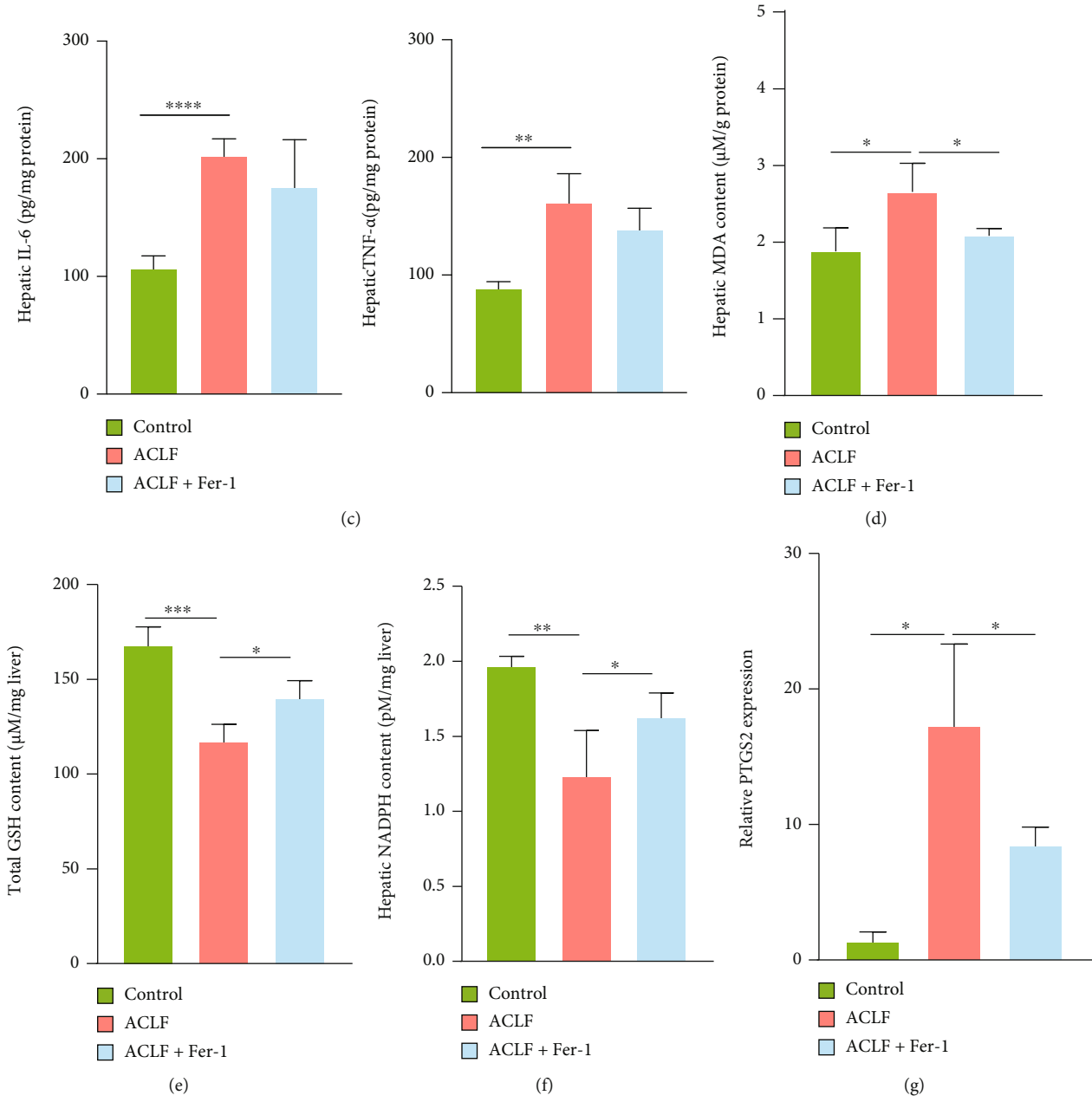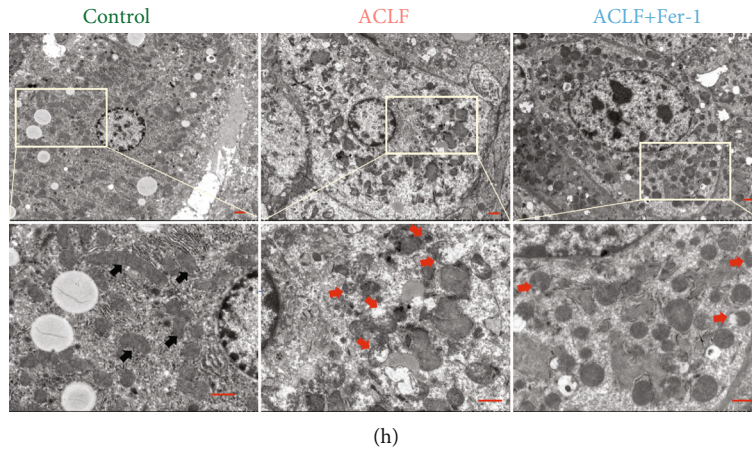
FIGURE 6: Repression of ferroptosis attenuates the severity of ACLF in vivo. (a) Representative images of morphological and histopathologic traits. Original magnification ×100 (Bar = 40 μm) and ×200 (Bar = 20 μm). (b) Fer-1 treatment significantly reduced the serum levels of ALT and AST. (c) Inhibition of ferroptosis failed to decrease the hepatic IL-6 and TNF-α concentrations. (d–f) Increased hepatic GSH and NADPH and decreased hepatic MDA were observed in mice treated with Fer-1. (g) The mRNA expression of ferroptosis-related gene PTGS2 was decreased in mice treated with Fer-1. (h) Fer-1 treatment improved ferroptosis-specific mitochondrial morphology. Bar = 10 μm. Black arrows indicate normal mitochondria; red arrows indicate shrunken and ruptured mitochondria. $^*p < 0.05$, $^{**}p < 0.01$, $^{***}p < 0.001$, $^{****}p < 0.0001$. $n = 3$(control), $n = 6$ (ACLF), $n = 5$ (ACLF+Fer-1). ALT = alanine aminotransferase; AST = aspartate aminotransferase; ACLF = acute-on-chronic liver failure; Fer-1 = ferrostatin-1; GSH = glutathione; IL-6 = interleukin-6; MDA = malondialdehyde; NADPH = nicotinamide adenine dinucleotide phosphate; PTGS2 = prostaglandin-endoperoxide synthase-2; TNF-α = tumor necrosis factor alpha.

3.3. Nrf2 Inhibition Promoted the Onset of Lipid Peroxidation and Corresponded to a More Severe Liver Injury.

To verify that Nrf2 was required in improving lipid peroxidation and liver damage, ML385, an inhibitor of Nrf2 [30], was used to inactivate Nrf2. As demonstrated by western blot, nuclear content of Nrf2 was decreased, confirming inactivation of Nrf2 (Figure 5(a)). Consistent with decrease in Nrf2, more severe histopathologic lesions, such as hepatocytes necrosis, destruction of the lobular structure, infiltration of inflammatory cells, obvious vascular congestion, and hemorrhage and tissue fibrosis were observed in the ML385 group compared to the ACLF group (Figure 5(b)). Convergently, liver damage assessed by serum biochemical parameters including ALT and AST was exacerbated in the ML385-treated mice (Figure 5(c)). As Nrf2 inhibited inflammatory response, inflammatory factors including IL-6 and TNF-α were augmented in the Nrf2-inhibited livers (Figure 5(d)). As for oxidative stress, the liver tissue from ML385-treated mice demonstrated the highest content of MDA, whereas GSH and NADPH were markedly decreased compared with the ACLF group and controls (Figure 5(e)–5(g)). Taken together, targeting Nrf2 might hold a potential therapeutic value in treating ACLF.

3.4. Inhibiting Ferroptosis Attenuated the Severity of ACLF In Vivo.

To confirm functions of ferroptosis in ACLF, ACLF mice were treated with ferroptosis-specific inhibitor Fer-1. Interestingly, Fer-1 ameliorated ACLF severity, manifesting with improved liver morphology and histopathologic lesions (e.g., reduced granules and improved lobule structure) (Figure 6(a)). Consistently, liver injury was revealed by critical indicators. Specifically, liver function indices (ALT and AST) in the Fer-1 treatment group were lower than that in the ACLF group, indicating a protective effect of Fer-1 on liver function (Figure 6(b)). Moreover, protein levels of hepatic inflammatory cytokines (IL-6 and TNF-α) were decreased in Fer-1-treated mice relative to the ACLF group (Figure 6(c)). Consistent with improved liver function, reduced lipid peroxidation was identified, evidenced by increased hepatic GSH and NADPH whereas decreased hepatic MDA in Fer-1-treated mice (Figures 6(d)–6(f)). Similarly, PTGS2 mRNA expression was reduced after Fer-1 treatment, indicating an improved lipid oxidative stress status (Figure 6(g)). In addition, TEM demonstrated improved ferroptosis-specific mitochondrial morphology after Fer-1 treatment (Figure 6(h)).

3.5. H_2O_2 Exposure Induced Ferroptosis in L02 Cells.

To further explore engagement of ferroptosis in ACLF, a hepatocyte injury model was established via treating L02 cells with H_2O_2 for 30 h. Cells were divided into 4 groups as follows: control, ACLF, ACLF + Fer-1, and control + Erastin (E) (serving as the positive control). CCK-8 assay indicated that H_2O_2 inhibited cell viability, as exhibited in the control+E group, whereas Fer-1 reversed growth inhibition, as evidenced by improved viability in the ACLF+Fer-1 group (Figure 7(a)). L02 cells grew slowly and became skinnier, accompanied by decreased attachment following H_2O_2 and Erastin treatment. These cells eventually exhibited a "ballooning" phenotype because of plasma membrane destabilization, cytoskeletal rearrangements, and disruption of proteostasis [31]. By contrast, Fer-1 improved morphology (Figure 7(b)). H_2O_2 increased lipid ROS in a comparable pattern to Erastin treatment, which was counteracted by Fer-1 (Figure 7(c)). In parallel, compared with the control group, increased MDA whereas decreased GSH were

(a)

(b)

(c)

(d)

Figure 7: Continued.

(e)

(f)

(g)
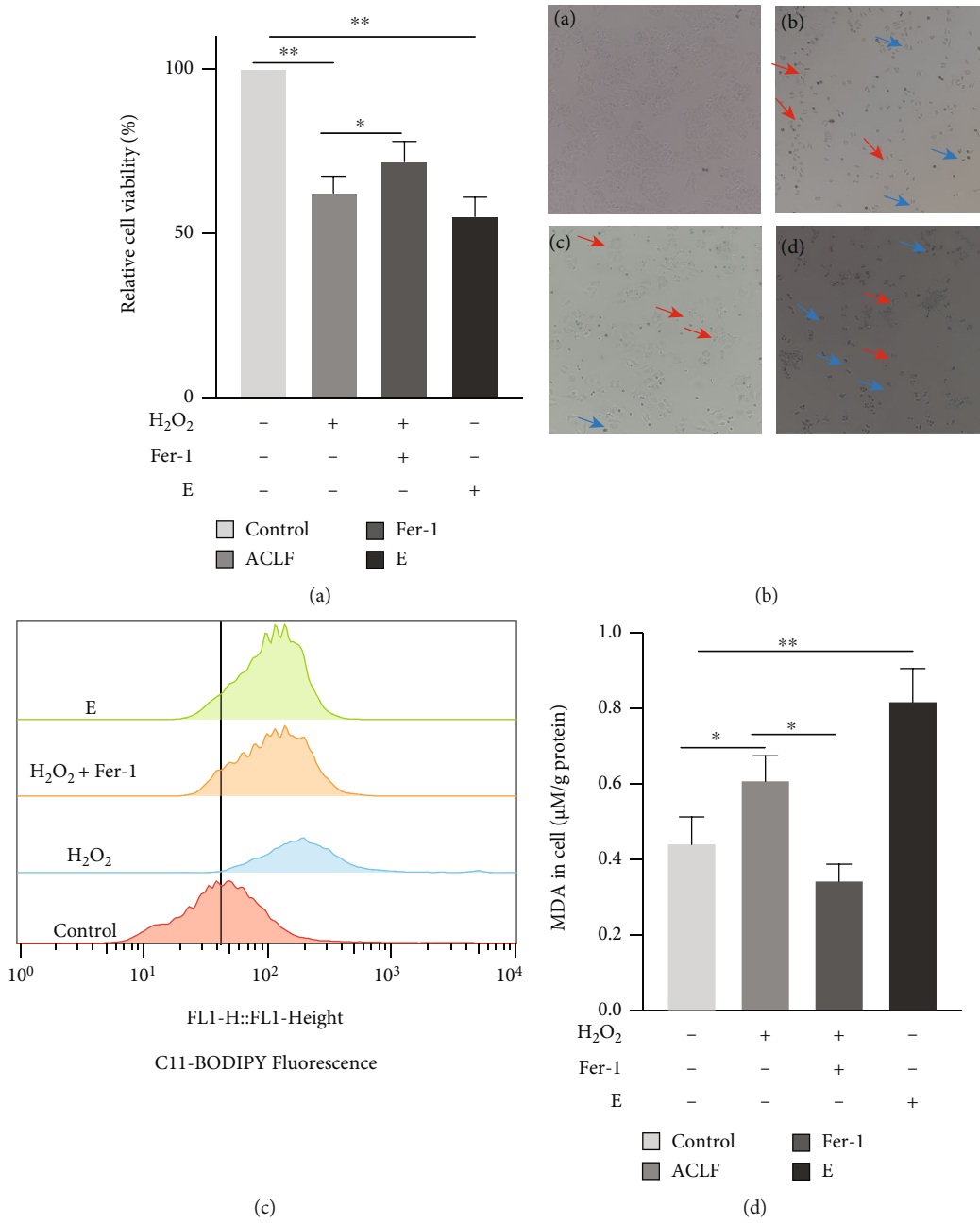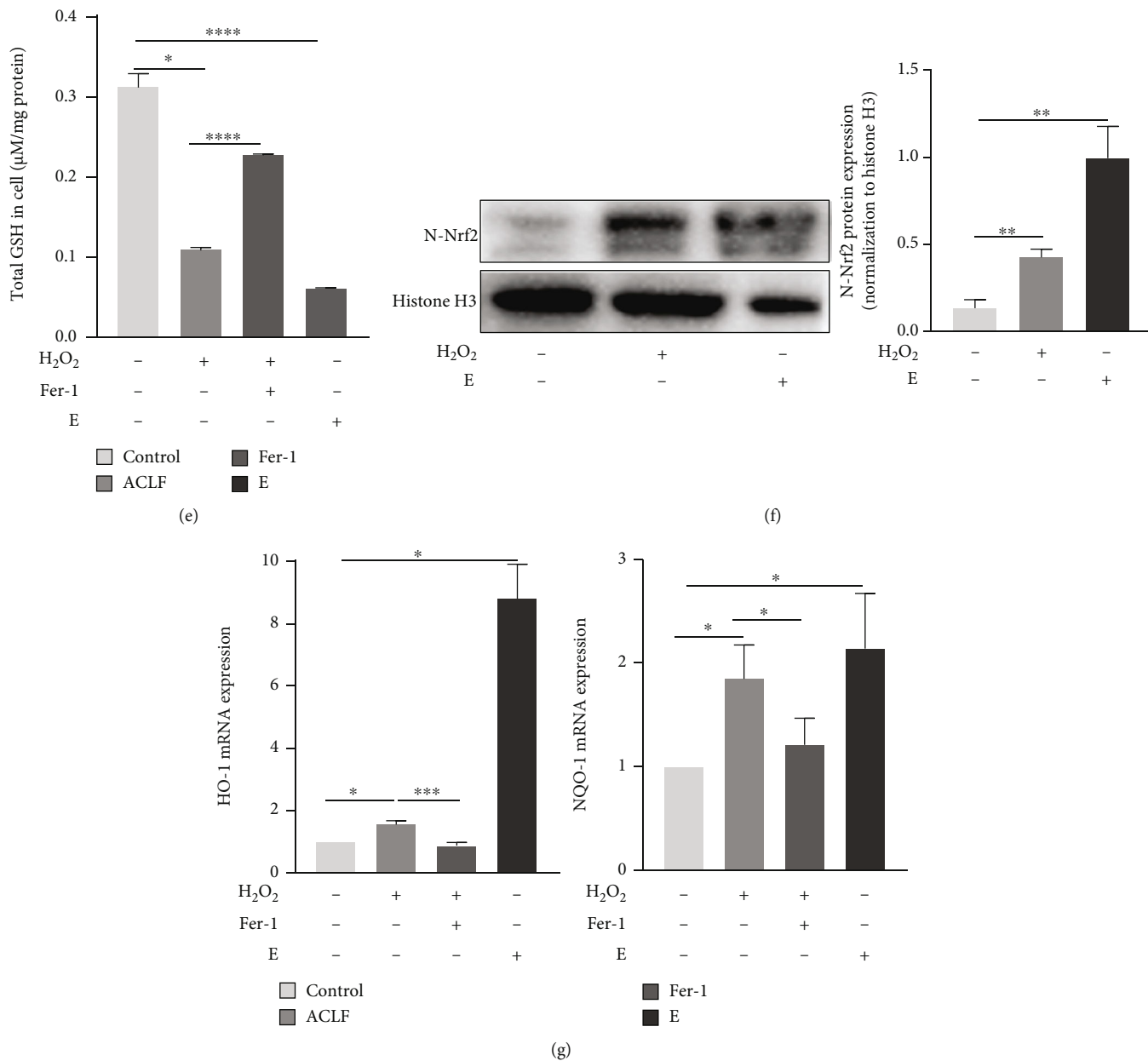
FIGURE 7: H_2O_2 exposure induced ferroptosis in L02 cells. (a) Relative cell viability was confirmed by the CCK-8 assay ($n = 6$). (b) L02 cells underwent ferroptosis-specific morphologic phenotype (cells shrunk at first and eventually exhibiting a balloon-type) after being treated with H_2O_2 or Erastin. The blue and red arrows indicate shrunken and balloon phenotypes, respectively ((a) normal L02 cells. (b) L02 cells treated with H_2O_2. (c) L02 cells co-treated with Fer-1 and H_2O_2. (d) L02 cells exposed to Erastin). Original magnification ×200. (c) Cells were stained with 5 μM BODIPY® 581/591 C11 to detect the content of cellular lipid peroxide through flow cytometry ($n = 3$). (d and e) Cellular content MDA and total GSH were measured, respectively ($n = 3$). (f) Protein expression of Nrf2 was elevated after cells were treated with H_2O_2 or Erastin compared with normal L02 cells ($n = 3$). (g) The mRNA expression of HO-1 and NQO1 was elevated in response to H_2O_2 and Erastin treatment ($n = 3$). $^*p < 0.05$, $^{**}p < 0.01$, $^{***}p < 0.001$. CCK-8 = Cell Counting Kit-8; Fer-1 = ferrostatin-1; GSH = glutathione; HO-1 = heme oxygenase-1; MDA = malondialdehyde; NQO1 = NAD(P) H quinone dehydrogenase, quinone 1.

observed in the H_2O_2 and Erastin treatment groups, which was rescued by Fer-1 (Figures 7(d) and 7(e)). Simultaneously, nuclear protein expression of Nrf2 was upregulated after H_2O_2 and Erastin treatment (Figure 7(f)). In addition, at protein (Supplementary Figure 2) and mRNA levels (Figure 7(g)), Nrf2 target genes heme oxygenase-1 (HO-1) and NQO1 were upregulated in response to H_2O_2 and

Erastin treatment. Collectively, H_2O_2 treatment contributed to ferroptosis in L02 cells.

3.6. Nrf2 Protected against H_2O_2-Induced Hepatotoxicity via Inhibiting Ferroptosis In Vitro. To explore effects of Nrf2 on H_2O_2-induced cell injury, BM (0.2 μM) and ML385 (10 μM) were applied to activate or inhibit Nrf2. As shown in

(a)

(b)

(c)

FIGURE 8: Continued.

FL1-H::FL1-Height

C11-BODIPY fluorescence

(d)

(e)

(f)
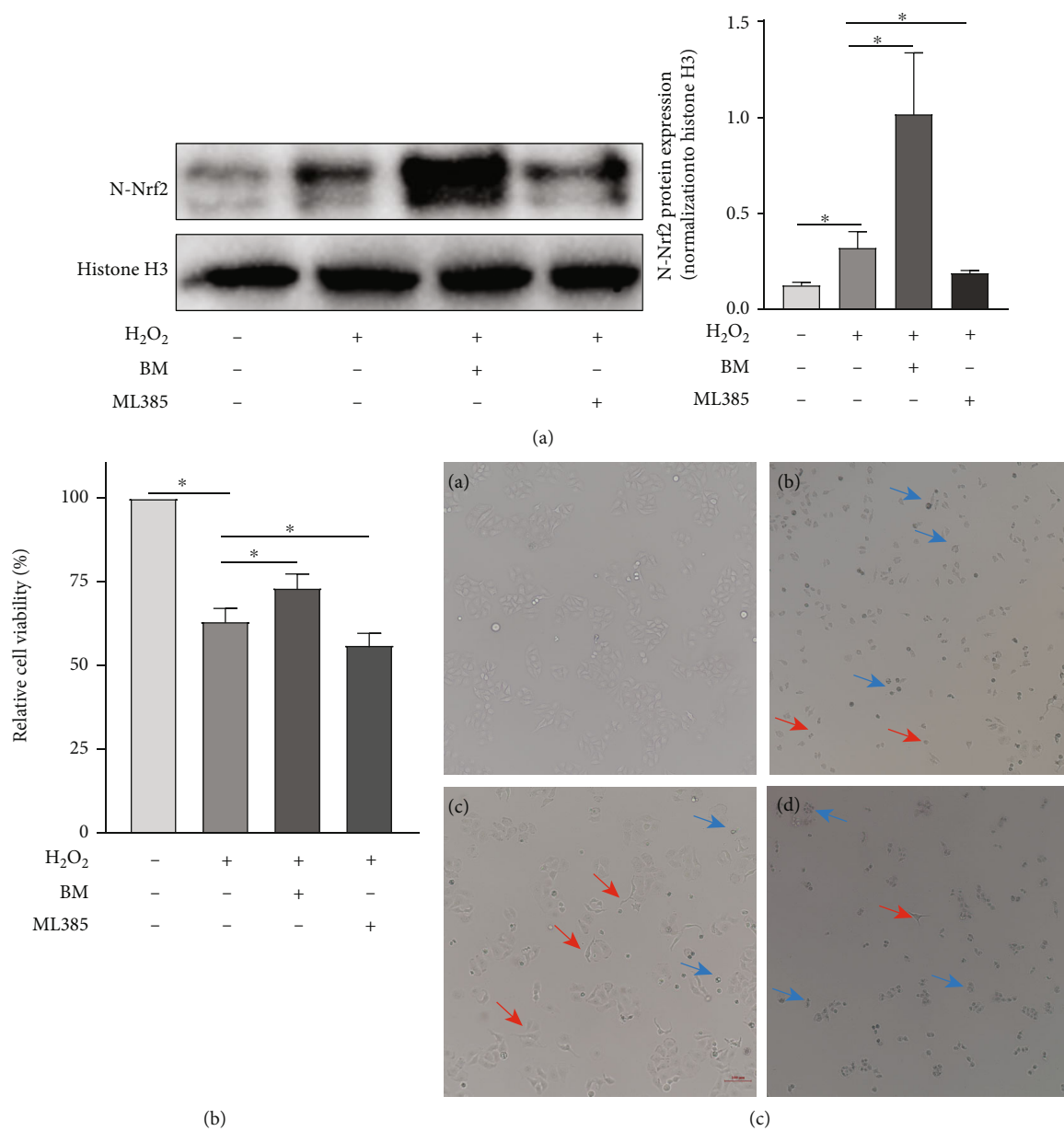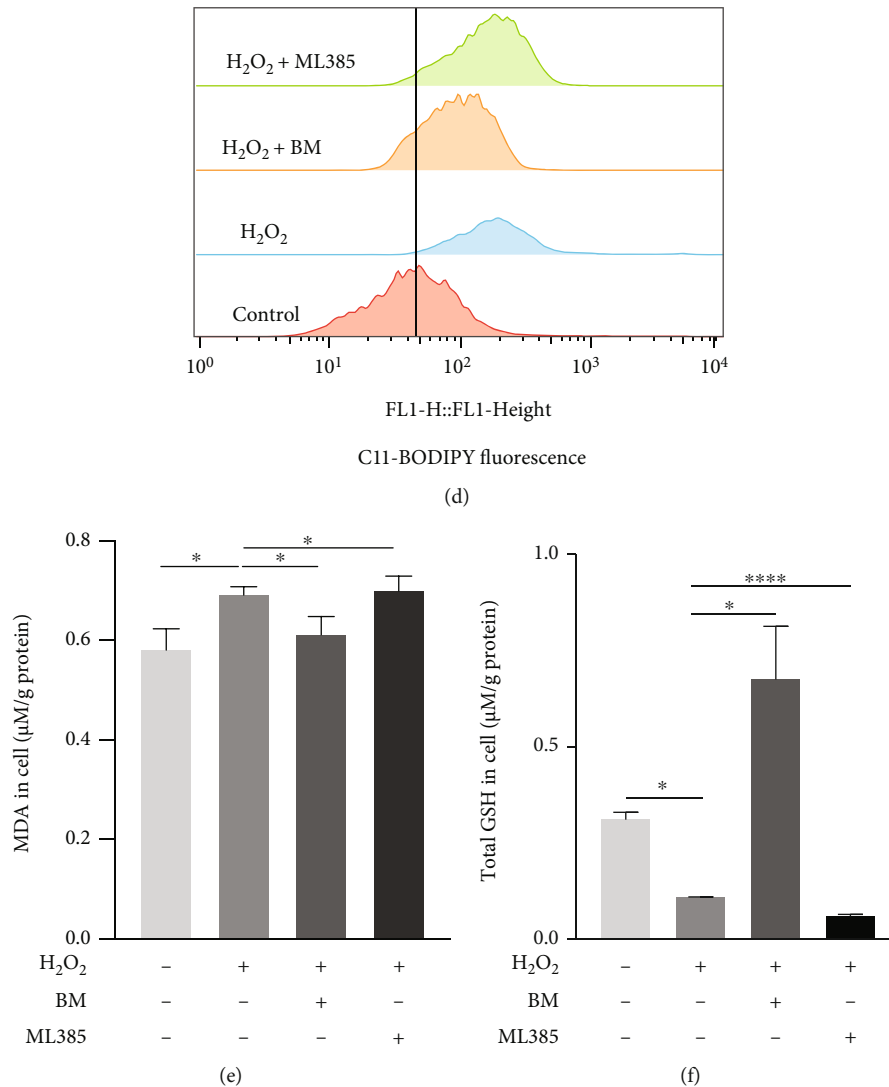
FIGURE 8: Nrf2 protected against H_2O_2-induced hepatocytes injury via inhibiting ferroptosis. (a) The results of western blot suggested the successful activation or inhibition of Nrf2 in vitro ($n = 3$). (b) BM treatment significantly increased the cell viability of L02 cells with H_2O_2 exposure, while ML385 significantly decreased L02 cell viability treated with H_2O_2 ($n = 4$). (c) BM treatment reduced the number of cells showing ferroptosis-specific morphologic phenotype. The blue and red arrows indicate shrunken and balloon phenotype, respectively. Original magnification ×200. (d) Flow cytometry was used to detect the content of cellular lipid peroxide after treating cells with 5 μM BODIPY® 581/591 C11 ($n = 3$). (e and f) Cellular GSH and MDA content were measured. $^*p < 0.05$, $^{****}p < 0.0001$. BM = Bardoxolone Methyl; GSH = glutathione; MDA = malondialdehyde; Nrf2 = nuclear factor erythroid 2-related factor.

Figure 8(a), nuclear expression of Nrf2 was increased upon BM treatment whereas decreased upon ML385 treatment, suggesting that Nrf2 was activated or inactivated, respectively. The mRNA (Supplemental Figure 1) and protein expression (Supplemental Figure 2) of HO-1 and NQO1 changed accordingly in response to activation or inhibition of Nrf2, respectively. BM treatment improved cell viability and morphologic features, while ML385 treatment had opposite effects (Figures 8(b) and 8(c)). These results indicated that Nrf2 might exert a protective effect on H_2O_2-induced cell damage. Effects of Nrf2 on H_2O_2-induced ferroptosis were investigated in L02 cells. BM treatment decreased lipid peroxidation during ACLF, as evidenced by reduced level of lipid ROS in the BM treatment group relative to the ACLF group (Figure 8(d)).

In contrast, ML385 treatment augmented the accumulation of lipid ROS. Likewise, ML385 treatment aggravated the increase in MDA whereas decrease in GSH in L02 cells (Figures 8(e) and 8(f)). Taken together, Nrf2 could protect L02 cells from H_2O_2-induced ferroptosis.

4. Discussion

In this study, ferroptosis has been identified to participate in pathogenesis of ACLF, while inhibition of ferroptosis through activating Nrf2-mediated pathway is a potential strategy to prevent ACLF progression. Characterized by a heterogeneous and intertwined pathophysiological process and high short-term mortality, ACLF constitutes a significant threat to public health worldwide without clinically

effective treatments [32]. Unveiling ACLF pathogenesis and seeking effective therapeutic targets would be a focus of clinical and basic research. Here, through establishing ACLF models by treating mice with CCl4, LPS, and D-Gal along with a hepatocyte injury model, for the first time we demonstrate participation of ferroptosis in ACLF pathogenesis as evidenced by the following: (1) ACLF livers exhibit key features of ferroptosis including lipid peroxidation [6, 23] (increase in MDA content whereas decrease in GSH and NADPH in ACLF models), upregulation of PTGS2, and presence of ferroptosis-specific mitochondrial morphology; (2) activation of ferroptosis exacerbates lipid peroxidation and leads to more severe liver damage, while inhibiting ferroptosis with ferroptosis inhibitor Fer-1 [8] largely abrogates injury and restores liver damage.

Ferroptosis is an iron-dependent nonapoptotic form of cell death resulting from excessive iron accumulation and lipid peroxidation. Massive iron accumulation, increased lipid peroxidation, and deficiency in cellular antioxidation are recognized as main pathological pillars during ferroptotic cascade [33]. Recently, accumulating evidence has indicated involvement of ferroptosis in liver diseases. Ferroptosis may contribute to liver injury and promote disease progression in acute or chronic liver diseases, such as ischemia/reperfusion-related injury and nonalcoholic fatty liver disease [8, 24]. Despite evidence that iron overload and increased oxidative stress have been revealed in ACLF patients, especially those with multiorgan failure [13, 14, 34, 35], no studies have investigated association between ferroptosis and ACLF, representing a gap in knowledge. For the first time, our current study has demonstrated that ferroptosis is responsible for aggravated liver damage in ACLF. Thus, inhibiting ferroptosis alleviates the severity of ACLF, providing novel therapeutic cues based on ferroptosis.

Nrf2 is a stress-inducible transcription factor that elicits defense to protect cells from oxidative injury through regulation of a host of defensive and detoxification genes [36] involved in iron metabolism, glutathione synthesis, and metabolism of reactive intermediates [37, 38]. Notably, most of its target genes are critical for ferroptosis. In addition, antiferroptosis mediators including glutathione peroxidase 4 (Gpx4) [39], Ferroptosis Suppressor Protein 1 (FSP1) [40], and system Xc⁻ [41] are all target genes of Nrf2. Thus, Nrf2-mediated antioxidant defense is integral in mitigating lipid peroxidation and ferroptosis prevention. For pathologic conditions where ferroptosis functions as a detrimental factor in disease development, activation of Nrf2 may play a beneficial role in attenuating damage through removing overwhelmed lipid peroxidation and unrelenting cell death [19]. For example, ferroptosis was activated after seawater drowning, and repression of ferroptosis relieved lung damage [30]. Further mechanical studies using inhibitor/inducer of Nrf2 suggested that activation of Nrf2 improved the severity of acute lung injury via decreasing lipid peroxidation [30].

In the present study, nuclear expression of Nrf2 was upregulated in ACLF model and hepatocyte injury model, implying that Nrf2 may activate adaptively to combat increased lipid peroxidation. The end products of lipid peroxidation themselves, including MDA and 4-hydroxynonenal (4-HNE), are potent initiators of lipid peroxidation [42]. As such, pharmacologically activated Nrf2 might have a synergistic effect with originally activated Nrf2 to control rapidly increased lipid peroxidation. To test this hypothesis, inhibitor/inducer of Nrf2 (ML385 and BM) was applied. As expected, BM treatment induced Nrf2 expression, improved cell viability, reduced MDA and lipid ROS, and restored depleted GSH in L02 cells after H_2O_2 exposure. As depicted in liver histopathology, BM treatment reduced histological lesions in ACLF mice. Mounting evidence has revealed the important role of Nrf2 in ameliorating inflammatory responses [43–46]. Consistently proinflammatory cytokines TNF-α and IL-6 were decreased in BM-treated mice compared with ACLF mice, suggesting a reduced inflammatory response. In addition, increased GSH and NADPH whereas decreased MDA and PTGS2 mRNA expression suggested that BM mitigated ferroptosis in vivo. Inhibitory effects of Nrf2 on ferroptosis were verified by using Nrf2 inhibitor ML385. As expected, ML385 exerted opposite effects to BM. Overall, Nrf2 could attenuate liver damage via inhibiting ferroptosis and inflammatory response in ACLF. Although inhibiting ferroptosis may have an anti-inflammatory effect [47], our current study observed no significant decrease in TNF-α and IL-6 in mice treated with ferroptosis inhibitor compared with ACLF mice. More research is needed to determine potential roles of ferroptosis in inflammatory response in ACLF. Previous studies indicated that BM might increase serum aminotransferase levels through inducing expression of aminotransferases as an on-target effect [48], which may partly explain why ALT and AST levels were not decreased after BM treatment in mice (Figure 3(f)).

Despite novel findings, some limitations of this study should be kept in mind. Bardoxolone Methyl is a potent noncytotoxic activator of Nfr2 and has been tested in clinical trials for chronic kidney and malignant diseases [49, 50]. However, because of multifunctional property such as an inhibitor nuclear factor-κB [51], precise net effects of Nrf2 on ferroptosis in ACLF should be examined via genetic manipulation of Nrf2. In addition, upstream regulators of Nrf2 in ACLF need investigation.

5. Conclusions

In summary, our present study provides the first evidence that ferroptosis is a major RCD in ACLF. Inhibiting ferroptosis by Nrf2 could alleviate liver damage and prevent hepatocyte death. This study implies that targeting Nrf2-mediated ferroptosis may be a promising therapeutic approach in treating ACLF. Bardoxolone Methyl may be a potential new treatment option for ACLF patients.

Data Availability

The data that support the findings of this study are available from the corresponding author upon reasonable request.

Conflicts of Interest

The authors declare that they have no competing interests.

Authors' Contributions

J.W. and M.W. performed the experiments. J.W. and R.X. analyzed the data. J. W. wrote the first draft of the manuscript. B.X., J.W., M. W, X.Y., and R.X. participated in the critical discussion. Q.M. contributed to the research design and finalized the manuscript.

Acknowledgments

Supplementary Materials

Supplementary 1. Figure 1: the mRNA expression of Nrf2 target genes. A. The mRNA expression of NQO1 was upregulated in ACLF patients relative to healthy controls. (HC $n = 3$, ACLF $n = 5$). B. The mRNA expression of HO-1 was increased after H_2O_2 exposure, and BM treatment augmented its expression, while ML385 inhibited its expression ($n = 3$).

Supplementary 2. Figure 2: the protein expression of Nrf2 target genes. A. The protein expressions of NQO1 and HO-1 were increased in response to H_2O_2 and Erastin treatment, while Fer-1 treatment reversed the effect of H_2O_2 ($n = 3$). B. The protein expressions of HO-1 and NQO1 were increased after H_2O_2 exposure, and BM treatment augmented its expression, while ML385 inhibited its expression ($n = 3$). ACLF, acute-on-chronic liver failure; BM, Bardoxolone Methyl; E, Erastin; Fer-1, ferrostatin-1; HO-1, heme oxygenase-1; NQO1, NAD(P) H quinone dehydrogenase, quinone 1.

References

[1] S. K. Sarin and A. Choudhury, "Acute-on-chronic liver failure: terminology, mechanisms and management," *Nature Reviews Gastroenterology & Hepatology*, vol. 13, no. 3, pp. 131–149, 2016.

[2] K. Sargenti, H. Prytz, E. Nilsson, and E. Kalaitzakis, "Predictors of mortality among patients with compensated and decompensated liver cirrhosis: the role of bacterial infections and infection-related acute-on-chronic liver failure," *Scandinavian Journal of Gastroenterology*, vol. 50, no. 7, pp. 875–883, 2015.

[3] D. Adebayo, V. Morabito, F. Andreola et al., "Mechanism of cell death in acute-on-chronic liver failure: a clinico-pathologic-biomarker study," *Liver International*, vol. 35, no. 12, pp. 2564–2574, 2015.

[4] R. Xue, J. Yang, L. Jia et al., "Mitofusin2, as a protective target in the liver, controls the balance of apoptosis and autophagy in

acute-on-chronic liver failure," *Frontiers in Pharmacology*, vol. 10, p. 601, 2019.

[5] Y. Zou, T. Chen, M. Han et al., "Increased killing of liver NK cells by Fas/Fas ligand and NKG2D/NKG2D ligand contributes to hepatocyte necrosis in virus-induced liver failure," *The Journal of Immunology*, vol. 184, no. 1, pp. 466–475, 2010.

[6] S. J. Dixon and B. R. Stockwell, "The hallmarks of ferroptosis," *Annual Review of Cancer Biology*, vol. 3, no. 1, pp. 35–54, 2019.

[7] S. J. Dixon, K. M. Lemberg, M. R. Lamprecht et al., "Ferroptosis: an iron-dependent form of nonapoptotic cell death," *Cell*, vol. 149, no. 5, pp. 1060–1072, 2012.

[8] J. Wu, Y. Wang, R. Jiang et al., "Ferroptosis in liver disease: new insights into disease mechanisms," *Cell Death Discovery*, vol. 7, no. 1, pp. 1–9, 2021.

[9] B. R. Stockwell, X. Jiang, and W. Gu, "Emerging mechanisms and disease relevance of ferroptosis," *Trends in Cell Biology*, vol. 30, no. 6, pp. 478–490, 2020.

[10] J. R. Wu, Q. Z. Tuo, and P. Lei, "Ferroptosis, a recent defined form of critical cell death in neurological disorders," *Journal of Molecular Neuroscience*, vol. 66, no. 2, pp. 197–206, 2018.

[11] X. Fang, H. Wang, D. Han et al., "Ferroptosis as a target for protection against cardiomyopathy," *Proceedings of the National Academy of Sciences*, vol. 116, no. 7, pp. 2672–2680, 2019.

[12] J. Wu and Q.-H. Meng, "Current understanding of the metabolism of micronutrients in chronic alcoholic liver disease," *World Journal of Gastroenterology*, vol. 26, no. 31, pp. 4567–4578, 2020.

[13] J. S. Maras, R. Maiwall, H. Harsha et al., "Dysregulated iron homeostasis is strongly associated with multiorgan failure and early mortality in acute-on-chronic liver failure," *Hepatology*, vol. 61, no. 4, pp. 1306–1320, 2015.

[14] T. Bruns, R. Nuraldeen, M. Mai et al., "Low serum transferrin correlates with acute-on-chronic organ failure and indicates short-term mortality in decompensated cirrhosis," *Liver International*, vol. 37, no. 2, pp. 232–241, 2017.

[15] K. Taguchi and M. Yamamoto, "The KEAP1–NRF2 system as a molecular target of cancer treatment," *Cancers*, vol. 13, no. 1, article 46, 2021.

[16] Q. Wang, C. Bin, Q. Xue et al., "GSTZ1 sensitizes hepatocellular carcinoma cells to sorafenib-induced ferroptosis via inhibition of NRF2/GPX4 axis," *Cell Death & Disease*, vol. 12, no. 5, pp. 1–16, 2021.

[17] X. Sun, Z. Ou, R. Chen et al., "Activation of the p62-Keap1-NRF2 pathway protects against ferroptosis in hepatocellular carcinoma cells," *Hepatology*, vol. 63, no. 1, pp. 173–184, 2016.

[18] C. Wang, T. Liu, Y. Tong et al., "Ulinastatin protects against acetaminophen-induced liver injury by alleviating ferroptosis via the SIRT1/NRF2/HO-1 pathway," *American Journal of Translational Research*, vol. 13, no. 6, pp. 6031–6042, 2021.

[19] G. Gao, Z. Xie, E. W. Li et al., "Dehydroabietic acid improves nonalcoholic fatty liver disease through activating the Keap1/Nrf2-ARE signaling pathway to reduce ferroptosis," *Journal of Natural Medicines*, vol. 75, no. 3, pp. 540–552, 2021.

[20] S. K. Sarin, A. Choudhury, M. K. Sharma et al., "Acute-on-chronic liver failure: consensus recommendations of the Asian Pacific association for the study of the liver (APASL): an update," *Hepatology International*, vol. 13, no. 4, pp. 353–390, 2019.

[21] M. Wang, C.-Y. Liu, T. Wang et al., "(+)-Clausenamide protects against drug-induced liver injury by inhibiting

hepatocyte ferroptosis," *Cell Death & Disease*, vol. 11, no. 9, pp. 1–15, 2020.

[22] H. Wang, P. An, E. Xie et al., "Characterization of ferroptosis in murine models of hemochromatosis," *Hepatology*, vol. 66, no. 2, pp. 449–465, 2017.

[23] K. Shimada, M. Hayano, N. C. Pagano, and B. R. Stockwell, "Cell-line selectivity improves the predictive power of pharmacogenomic analyses and helps identify NADPH as biomarker for ferroptosis sensitivity," *Cell Chemical Biology*, vol. 23, no. 2, pp. 225–235, 2016.

[24] J. Qi, J.-W. Kim, Z. Zhou, C. W. Lim, and B. Kim, "Ferroptosis affects the progression of nonalcoholic steatohepatitis via the modulation of lipid peroxidation-mediated cell death in mice," *The American Journal of Pathology*, vol. 190, no. 1, pp. 68–81, 2020.

[25] T. W. Kensler, N. Wakabayashi, and S. Biswal, "Cell survival responses to environmental stresses via the Keap1-Nrf2-ARE pathway," *Annual Review of Pharmacology and Toxicology*, vol. 47, no. 1, pp. 89–116, 2007.

[26] Y. Lv, H. Jiang, S. Li et al., "Sulforaphane prevents chromium-induced lung injury in rats via activation of the Akt/GSK-3β/Fyn pathway," *Environmental Pollution*, vol. 259, article 113812, 2020.

[27] D. Yang, Q. Yang, N. Fu et al., "Hexavalent chromium induced heart dysfunction via Sesn2-mediated impairment of mitochondrial function and energy supply," *Chemosphere*, vol. 264, no. 2, article 128547, 2021.

[28] A. K. Kalvala, R. Kumar, B. Sherkhane, C. Gundu, V. K. Arruri, and A. Kumar, "Bardoxolone methyl ameliorates hyperglycemia induced mitochondrial dysfunction by activating the keap1-Nrf2-ARE pathway in experimental diabetic neuropathy," *Molecular Neurobiology*, vol. 57, no. 8, pp. 3616–3631, 2020.

[29] R. Wu, H. Zhang, M. Zhao et al., "_Nrf2_ in keratinocytes protects against skin fibrosis via regulating epidermal lesion and inflammatory response," *Biochemical Pharmacology*, vol. 174, article 113846, 2020.

[30] Y. B. Qiu, B. B. Wan, G. Liu et al., "Nrf2 protects against seawater drowning-induced acute lung injury via inhibiting ferroptosis," *Respiratory Research*, vol. 21, no. 1, pp. 1–16, 2020.

[31] M. Dodson, R. Castro-Portuguez, and D. D. Zhang, "NRF2 plays a critical role in mitigating lipid peroxidation and ferroptosis," *Redox Biology*, vol. 23, article 101107, 2019.

[32] R. Hernaez, E. Solà, R. Moreau, and P. Ginès, "Acute-on-chronic liver failure: an update," *Gut*, vol. 66, no. 3, pp. 541–553, 2017.

[33] W. S. Yang and B. R. Stockwell, "Ferroptosis: death by lipid peroxidation," *Trends in Cell Biology*, vol. 26, no. 3, pp. 165–176, 2016.

[34] G. R. Assis-Mendonça, M. Cunha-Silva, M. F. Fernandes et al., "Massive iron overload and acute-on-chronic liver failure in a patient with Diamond–Blackfan anaemia: a case report," *BMC Gastroenterology*, vol. 20, no. 1, pp. 1–7, 2020.

[35] H. Liu, T. Han, J. Tian et al., "Monitoring oxidative stress in acute-on-chronic liver failure by advanced oxidation protein products," *Hepatology Research*, vol. 42, no. 2, pp. 171–180, 2012.

[36] G. M. DeNicola, F. A. Karreth, T. J. Humpton et al., "Oncogene-induced Nrf2 transcription promotes ROS detoxification and tumorigenesis," *Nature*, vol. 475, no. 7354, pp. 106–109, 2011.

[37] J. D. Hayes and A. T. Dinkova-Kostova, "The Nrf2 regulatory network provides an interface between redox and intermediary metabolism," *Trends in Biochemical Sciences*, vol. 39, no. 4, pp. 199–218, 2014.

[38] J. Y. Chan and M. Kwong, "Impaired expression of glutathione synthetic enzyme genes in mice with targeted deletion of the Nrf2 basic-leucine zipper protein," *Biochimica et Biophysica Acta (BBA)-Gene Structure and Expression*, vol. 1517, no. 1, pp. 19–26, 2000.

[39] Q. Liu and K. Wang, "The induction of ferroptosis by impairing STAT3/Nrf2/GPx4 signaling enhances the sensitivity of osteosarcoma cells to cisplatin," *Cell Biology International*, vol. 43, no. 11, pp. 1245–1256, 2019.

[40] B. N. Chorley, M. R. Campbell, X. Wang et al., "Identification of novel NRF2-regulated genes by ChIP-Seq: influence on retinoid X receptor alpha," *Nucleic Acids Research*, vol. 40, no. 15, pp. 7416–7429, 2012.

[41] L. Feng, K. Zhao, L. Sun et al., "SLC7A11 regulated by NRF2 modulates esophageal squamous cell carcinoma radiosensitivity by inhibiting ferroptosis," *Journal of Translational Medicine*, vol. 19, no. 1, pp. 1–16, 2021.

[42] H. Yin, L. Xu, and N. A. Porter, "Free radical lipid peroxidation: mechanisms and analysis," *Chemical Reviews*, vol. 111, no. 10, pp. 5944–5972, 2011.

[43] H. Lu, X. Sun, M. Jia et al., "Rosiglitazone suppresses renal crystal deposition by ameliorating tubular injury resulted from oxidative stress and inflammatory response via promoting the Nrf2/HO-1 pathway and shifting macrophage polarization," *Oxidative Medicine and Cellular Longevity*, vol. 2021, 19 pages, 2021.

[44] X. Wang, Z. Lv, B. Han et al., "The aggravation of allergic airway inflammation with dibutyl phthalate involved in Nrf2-mediated activation of the mast cells," *Science of The Total Environment*, vol. 789, article 148029, 2021.

[45] Q. Yang, B. Han, S. Li et al., "The link between deacetylation and hepatotoxicity induced by exposure to hexavalent chromium," *Journal of Advanced Research*, vol. 35, pp. 129–140, 2022.

[46] N. Deng, H. Jiang, P. Wu et al., "Inhibition of the Nrf2/p38MAPK pathway involved in deltamethrin-induced apoptosis and fibrosis in quail kidney," *Food and Chemical Toxicology*, vol. 155, article 112382, 2021.

[47] Y. Sun, P. Chen, B. Zhai et al., "The emerging role of ferroptosis in inflammation," *Biomedicine & Pharmacotherapy*, vol. 127, article 110108, 2020.

[48] R. J. Church and P. B. Watkins, "The challenge of interpreting alanine aminotransferase elevations in clinical trials of new drug candidates," *Clinical and Translational Science*, vol. 14, no. 2, pp. 434–436, 2021.

[49] D. S. Hong, R. Kurzrock, J. G. Supko et al., "A phase I first-in-human trial of bardoxolone methyl in patients with advanced solid tumors and lymphomas," *Clinical Cancer Research*, vol. 18, no. 12, pp. 3396–3406, 2012.

[50] D. De Zeeuw, T. Akizawa, P. Audhya et al., "Bardoxolone methyl in type 2 diabetes and stage 4 chronic kidney disease," *New England Journal of Medicine*, vol. 369, no. 26, pp. 2492–2503, 2013.

[51] Y. Y. Wang, Y. X. Yang, H. Zhe, Z. X. He, and S. F. Zhou, "Bardoxolone methyl (CDDO-Me) as a therapeutic agent: an update on its pharmacokinetic and pharmacodynamic properties," *Drug Design, Development and Therapy*, vol. 8, pp. 2075–2088, 2014.

Research Article

General Rehabilitation Program after Knee or Hip Replacement Significantly Influences Erythrocytes Oxidative Stress Markers and Serum ST2 Levels

Maciej Idzik [ID],[1] **Jakub Poloczek** [ID],[2,3] **Bronisława Skrzep-Poloczek** [ID],[4] **Elżbieta Chełmecka** [ID],[5] **Jerzy Jochem** [ID],[4] **and Dominika Stygar** [ID][4]

[1]*Independent Public Health Care, Opole Cancer Centre prof. Tadeusz Koszarowski, Katowicka 45-061 Street, 46-020 Opole, Poland*
[2]*Department of Rehabilitation, 3rd Specialist Hospital in Rybnik, Energetyków 46 Street, 44-200 Rybnik, Poland*
[3]*Department of Internal Medicine, Diabetology, And Nephrology, Faculty of Medical Sciences in Zabrze, Medical University of Silesia, Katowice, Poland*
[4]*Department of Physiology, Faculty of Medical Sciences in Zabrze, Medical University of Silesia, Jordana Street 19, 41-808 Katowice, Poland*
[5]*Department of Statistics, Department of Instrumental Analysis, Faculty of Pharmaceutical Sciences in Sosnowiec, Medical University of Silesia, Ostrogórska 31 Street, 41-200 Katowice, Poland*

Correspondence should be addressed to Dominika Stygar; dstygar@gmail.com

The survival of erythrocytes in the circulating blood depends on their membranes' structural and functional integrity. One of the mechanisms that may underlie the process of joint degeneration is the imbalance of prooxidants and antioxidants, promoting cellular oxidative stress. The study is aimed at observing the effects of the 21-day general rehabilitation program on the erythrocytes redox status and serum ST2 marker in patients after knee or hip replacement in the course of osteoarthritis. Erythrocytes and serum samples were collected from 36 patients. We analyzed the selected markers of the antioxidant system in the erythrocytes: catalase (CAT), glutathione reductase (glutathione disulfide reductase (GR, GSR)), total superoxide dismutase activity (SOD), glutathione peroxidase (GPx), glutathione transferase (GST) activity, and cholesterol and lipofuscin (LPS) concentration. In serum, we analyzed the concentration of the suppression of tumorigenicity 2 (ST2) marker. After the 21-day general rehabilitation program, the total SOD and GPx activity, measured in the hemolysates, significantly increased ($p < 0.001$) while LPS, cholesterol, and ST2 levels in serum significantly decreased ($p < 0.001$). General rehabilitation reduces oxidative stress in patients after knee or hip replacement in the course of osteoarthritis. Individually designed, regular physical activity is the essential element of the postoperative protocol, which improves the redox balance helping patients recover after the s4urgery effectively.

1. Introduction

Osteoarthritis (OA) is the most common form of arthritis, one of the most common joint disorders in the world [1]. Osteoarthritis of the knee and hip is a common condition in the elderly [1]. Since no effective treatment options for osteoarthritis or osteoarthritis modifying therapies exist, joint replacement remains the only treatment [2]. However, OA pathogenesis and the accompanying pain are two com-

monly researched therapeutic targets that, if approached correctly, should help prevent disease progression and relieve the patients from pain [2].

Regardless of its type, postoperative rehabilitation significantly reduces pain, increases the range of motion and muscle strength, and limits the use of pain medications [3, 4]. However, strenuous exercise increases oxygen uptake and energy requirements, which intensifies the mitochondrial energy metabolism and promotes the formation of free

radicals and oxidative stress [5]. Cellular oxidative stress resulting from the imbalance of prooxidants and antioxidants is thought to be one of the mechanisms that may underlie the process of joint degeneration [6].

Erythrocytes are one of the many cell types in which a redox imbalance can occur. Fatty acids in the membranes, elevated oxygen levels, and the presence of hemoglobin inside make erythrocytes a natural target for free radicals [7]. The oxidative processes in the erythrocytes entail membrane injury, modifications of the membrane's structural and functional elements, and changes in the membrane architecture. All these processes cause an increase in erythrocytes' mean osmotic fragility and inhibition of Mg^{2+} and Ca^{2+} ATPase activity [7]. The survival of erythrocytes in the circulating blood plasma depends on the structural and functional integrity of their membranes, which determines the mechanical behavior of cells. Erythrocytes express several physiological defenses against intracellular oxidative stress, including cellular antioxidant enzymes: superoxide dismutase (SOD), catalase (CAT), glutathione reductase (GR), glutathione peroxidase (GPx), and glutathione S-transferase (GST) [7, 8]. Reactive oxygen species (ROS), such as superoxide radicals, hydrogen peroxide, and especially hydroxyl radical, are toxic for cells. They modify amino acid residues and oxidize sulfhydryl groups in proteins, break peptide bonds, remove metals in metalloproteins, depolymerize nucleic acids, cause point mutations, and also oxidize polysaccharides and polyunsaturated fatty acids. Protection against toxic and mutagenic ROS is provided by enzymes of antioxidative defense, with SOD and CAT being the most important of them [9].

The intensity of oxidative stress can be assessed using various general and specific indicators [10]. Lipofuscin (LPS) as a product of unsaturated fatty acid oxidation is considered one of them. Lipofuscin formation is directly related to an increased concentration of other oxidative stress markers. Reactive oxygen species are too short-lived to be detected directly. However, they react with lipids and produce lipid peroxidation products that may serve as indirect biomarkers of *in vivo* oxidative stress status and related diseases. Malondialdehyde (MDA) is one of the principal and most studied low-molecular-weight end products of lipid peroxidation. The high cytotoxicity of MDA results from its ability to bind proteins or nucleic acids [11]. Malondialdehyde (MDA) cross-links erythrocytes' phospholipids and proteins which impairs a variety of membrane-related functions and leads to their diminished survival and death [12].

Dysregulation of ST2/IL-33 signaling and suppression of tumorigenicity 2 (ST2) marker production is observed in various inflammatory diseases such as cardiac disease [13–16], inflammatory bowel disease (IBD) [17–20], graft-versus-host disease (GVHD) [21–28], and type-2 diabetes [29–32]. ST2 was first discovered to function as a mediator of type 2 inflammatory responses [33]. Targeting ST2 demonstrated protective effects in the respiratory [34], skin [35], and kidney [36] diseases and autoimmune neurological pathologies [37].

Pain and disability are the two most frequent OA complications, which lead to a significant reduction in a patient's

physical activity. The decreased physical capacity and sedentary lifestyle negatively influence the heart muscle condition, leading to comorbid heart diseases [38]. The American Heart Association and American College of Cardiology indicated ST2 as an important factor of heart failure: it predicts hospitalization and death in patients and, together with natriuretic peptides, shows a prognostic value [39]. Our previous study reported that a 21-day general rehabilitation significantly improved patients' physical efficiency and exercise capacity after hip or knee replacement [40]. Rheumatic diseases are chronic inflammatory disorders in which the immune system attacks itself and the body's organs [41]. A growing number of studies have demonstrated a critical role of the IL-33/ST2 axis in rheumatic diseases, including systemic lupus erythematosus (SLE), rheumatoid arthritis (RA), primary Sjögren's syndrome (pSS), systemic sclerosis (SSc), psoriatic arthritis (PsA), gout, and ankylosing spondylitis (AS), indicating a promising potential for IL-33/ST2-targeting therapy in rheumatic disease [41]. Although the alterations in the blood induced by physical training influence changes in other tissues, the effects of physical training-induced oxidative stress on blood have not been extensively investigated. However, changes in erythrocytes' properties can lead to impaired oxygen transport and result in cell and tissue hypoxia [42]. Our previous work presented significant changes in the plasma parameters related to the 21-day postoperative general rehabilitation [40]. Since, selected in this work, oxidative stress markers and also ST2 are important and sensitive indicators of inflammatory, prooxidative, and cardiac status, we aimed to observe the effects of 21-day general rehabilitation program on the erythrocytes' redox status and changes in ST2 serum levels in patients after knee or hip surgical replacement in the course of osteoarthritis.

2. Materials and Methods

2.1. Ethical Statement and Permissions. The study was approved by the Ethics Committee of the Medical University of Silesia in Katowice (KNW/002/KB1/106/17 issued on 03/10/2017) and followed the Declaration of Helsinki guidelines. Every participant of the study was informed about the study protocol, its benefits, and possible risks. All participants returned the written informed consent before the study started.

2.2. Study Group. Patients were recruited in the outpatients' clinic and the Department of Rehabilitation, 3rd Specialist Hospital in Rybnik, 2017-2018. The study included patients that in the prior 6 months underwent hip or knee arthroplasty due to advanced degenerative disease. The study excluded any patients with other inflammatory or immune disease, cancer, ischemic heart disease, heart, kidney, or liver failure.

Upon the arrival to the outpatients' clinic, each patient was initially examined and interviewed. The initial examination consisted of the resting electrocardiogram (ECG) and blood pressure measurement. The body mass and height measurements were also recorded. The interview is aimed

at identifying patients with inflammatory disorders, infections, renal or hepatic insufficiencies, active coronary artery disease, diabetes, heart failure, hormonal replacement therapy, or supplementation with antioxidants. All patients with the above-mentioned health deficiencies occurring 3 months before the study were excluded from the study.

Eventually, the study included 41 patients after total hip ($n = 29$; 71%) or knee ($n = 12$; 29%) replacement. Twenty-two of them were men, and 19 were women (54% and 46%, respectively), aged 61.0 ± 8.1 years on average. The day the study started, they were 89.6 ± 9.7 days after the replacement surgery. Five patients were excluded from the oxidative stress markers analyses due to health conditions diagnosed during the study course.

2.3. General Rehabilitation Program. A 21-day general rehabilitation program started ca. 90 days after knee or hip endoprosthesis implantation. The program constituted physiotherapy, daily living activities training, and education on nutrition. The daily sessions were conducted for 45 min, from 8:00 to 8:45 a.m. The individual rehabilitation program consisted of aerobic walking (30-45 min), strength training (20-30 min), rotor/bicycle training (30-45 min), and a cool-down phase (15 min). The patients were asked to continue the activities at home to sustain the effects at the beneficial level [43]. The responsible physiotherapist individually adjusted the type of exercises (strength and balance exercises) and training modalities (number and sets of repetitions, duration of resting time) for each patient and then monitored their progress.

Before starting and after completing the 21-day general rehabilitation program, each patient underwent the 6-minute walk test (6MWT) [44] to track changes in the patient's functional exercise capacity and assess the effectiveness of the rehabilitation program [45, 46]. The results of the 6-minute walk test (6MWT) after a 21-day general rehabilitation in the studied patients were presented in Skrzep-Poloczek et al. [40].

2.4. Blood Collection. Blood samples (5 mL) were collected from the ulnar vein the day before the first and the day after the last rehabilitation session (in the morning, at 8:00 a.m, before breakfast). The blood was collected to the standard blood tubes with EDTA (1.6 mg/mL EDTA-K3) and into tubes with a clot activator (S-Monovette, SARSTEDT, AG & Co. KG, Numbrecht, Germany).

The samples for serum analysis were centrifuged at 1500 g for 10 min at 4°C, transferred into 1 mL cryotubes, and stored at −80°C for later analyses. The pellet was washed with PBS buffer (0.01 M, 0.14 M NaCl, and pH 7.4) three times, and the separated erythrocytes were cooled to 4°C and then also stored at −80°C for later analysis. Before the analysis, erythrocytes were thawed, diluted with distilled water, and then again cooled to 4°C.

2.5. Oxidative stress markers, cholesterol, and ST2 analysis. To assess the status of the antioxidant system in the erythrocytes, we determined the activity of catalase (CAT), glutathione reductase (glutathione disulfide reductase (GR, GSR)),

total superoxide dismutase activity (SOD), glutathione peroxidase (GPx), and glutathione transferase (GST). Additionally, we analyzed lipofuscin (LPS), cholesterol concentration in the erythrocytes, and suppression of tumorigenicity 2 (ST2) marker concentration in blood serum, to assess the intensity of the patients' oxidative stress during the rehabilitation program.

2.5.1. Catalase (CAT) Activity (EC 1.11.1.6). CAT activity was determined using the Aebi method [47]. In short, the hemolysate homogenate was mixed with the TRIS/HCl buffer (50 mM, pH 7.4). The reaction was initiated with freshly prepared H_2O_2. The hydrogen peroxide decomposition rate was measured spectrophotometrically at 240 nm. CAT activity was expressed as units per 1 g of hemoglobin (IU/g Hb).

2.5.2. Glutathione Reductase (GR) Activity (EC 1.8.1.7). GR activity was determined using the kinetic method [48]. The changes in absorbance, resulting from the changes in NADPH concentration after reaction with oxidized glutathione, were measured at 340 nm. GR activity was expressed as μmol of NADPH utilized in 1 min per 1 g of hemoglobin (IU/g Hb).

2.5.3. Superoxide Dismutase (SOD) Activity (EC 1.15.1.1). Total SOD activity was determined using the Oyanagui method [49]. In short, xanthine oxidase catalyzes the production of superoxide anion that with hydroxylamine produces nitroso ion. The nitroso ion reacts with n-(1-naphthyl)ethylenediamine and sulfanilic acid, and the concentration of the product of this reaction can be measured spectrophotometrically at 550 nm. The total SOD activity was presented as nitrite units (NU) per mg of hemoglobin, where one NU represents 50% blockage of nitrite ions formation [49].

2.5.4. Glutathione Peroxidase (GPx) Activity (EC 1.11.1.9). Glutathione peroxidase (GPx) was measured using Paglia and Valentine's kinetic method [50], recording the decrease of absorbance at 340 nm. The GPx activity was expressed in U/g Hb, where one unit of enzyme activity (U) represents the amount of enzyme causing oxidation of 1 μmol NADPH in 1 min at 25°C.

2.5.5. Glutathione S-Transferase (GST) Activity (EC 2.5.1.18). GST activity was determined using the Habig and Jakoby kinetic method [51]. In short, the reaction mixture with reduced glutathione was added to hemolysate samples, and after initial stabilization, 1-chloro-2,3-dinitrobenzene was added. The changes in absorbance were measured at 340 nm for at least 3 min. The GST activity was expressed as μmol of thioether formed within 1 min per 1 g of hemoglobin (IU/g Hb).

2.5.6. Lipofuscin (LPS) Concentration. LPS concentration was determined as described by Tsuchida et al. [52]. The serum was mixed with ethanol-ether (3 : 1; v/v), shaken, and centrifuged. The fluorescence intensity was measured at 345 nm (for absorbance) and 430 nm (for emission) in a

dissolved solid. LPS concentration was expressed in relative lipid extract fluorescence (RF), where 100 RF corresponds to the fluorescence of $0.1 \, \mu g/mL$ of quinidine sulfate in 0.1 N sulfuric acid. The inter- and intra-assay coefficients of variations (CV) were 2.8% and 9.7%, respectively.

2.5.7. Total Cholesterol Concentration. Total cholesterol was measured in erythrocytes membrane lipid extracts using a commercial enzymatic assay (Waco Chemicals GmbH, Neuss, Germany) based on Allain et al.'s methodology [53]. The assay detection limit was 1.8 mg/dL. The intra- and interassay precision were <1.1% for both indicators. The results are expressed as milligram of total membrane cholesterol per deciliter.

2.5.8. Suppression of Tumorigenicity 2 (ST2) Marker Concentration. Suppression of tumorigenicity 2 (ST2) marker concentration was determined using the Quantikine Human ST2/IL-1 R4 Immunoassay kit (R&D Systems, Minneapolis, MN, United States). The assay was calibrated according to the manufacturer's recommendations. The values were normalized to a standard curve. ST2 concentration was determined using the Cobas analyzer (Cobas 6000e501, Roche Diagnostics, Mannheim, Germany). The test sensitivity was 13.5 pg/mL, and the assay range was 31.3-2000 pg/mL.

2.5.9. Protein Concentration. Hemoglobin concentration in hemolysates was determined using the modified Drabkin method [54].

2.6. Statistical Analysis. Statistical analysis was performed using STATISTICA 12.5 PL (StatSoft, Cracow, Poland). The mean value ± SD (for a normal distribution) and median with lower–upper quartile range (for data with skewed or nonnormal distribution) were chosen to express the interval data. The Shapiro–Wilk test and the quantile-quantile plot evaluated the distribution of variables. The homogeneity of variances was checked with Levene's test. The Mann–Whitney U-test, the nonparametric Kruskal–Wallis test, or the two-way parametric ANOVA with *post hoc* contrast analysis was used for data comparison. The data with skewed distribution were log-transformed before analysis. A $p < 0.05$ was considered statistically significant, and all the tests were two-tailed.

3. Results

The study included 41 patients after hip or knee replacement surgery. The mean age of the patients was 59.0 ± 7.0 years (range: 40-72 years). Women constituted 46.3% of the study group. There were no statistically significant differences in the age of the patients depending on their sex ($p = 0.859$). The location of lesions depending on the age of the patients was also analyzed, and no significant differences were found in both groups ($p = 0.978$) (Table 1).

3.1. General Health Indicators. Our previous work presented the biochemical and morphological characteristics of the blood of patients before and after the 21-day general rehabil-

TABLE 1: Relationship between gender, age, and type of joints affected by osteoarthritis in patients included in a 21-day general rehabilitation program after knee or hip surgical replacement. The results are presented as mean ± SD or median.

		Age (years)	t	p
Gender	Women	59.3 ± 5.4	0.179	0.859
	Men	58.9 ± 8.3		
Operated joint	Knee	59.0 ± 4.5	0.028	0.978
	Hip	59.1 ± 7.9		

itation program [40]. Here, we assessed whether the biochemical parameters analyzed in the patients' serum changed compared to the laboratory norm [55].

3.2. C-Reactive Protein (CRP). Before starting the 21-day rehabilitation program, all patients showed no signs of infection, and their health status was confirmed by CRP parameter < 5 mg/L. However, after completing the 21-day rehabilitation program, this parameter showed even lower values, as it decreased significantly in 80% of patients (Table 2).

The applicable standards of erythrocyte sedimentation rate (ESR) for women and men take into account their age. Reference values for women < 60 years are 3-15 mm/h, for women ≥ 60 years are 3-20 mm/h, for men < 60 years are 1-10 mm/h, and for men ≥ 60 years are 1-15 mm/h. Analysis of the results showed that before the 21-day rehabilitation program, the ESR values were above the norm in six patients (1 woman and 5 men). After the 21-day rehabilitation program, the ERS values fit within the norm for female patients, while in 3 men, the ESR values were above the norm (Table 2).

3.3. Glucose. Glucose concentration in the range of 3.9-5.5 mmol/L is considered normal. Before the therapy, 13 patients had elevated glucose levels, and after the therapy, elevated glucose levels were noted for only 6 patients. Values below the norm, both before and after the 21-day rehabilitation program, were observed only in 1 patient.

3.4. Creatinine. The reference values for creatinine in healthy individuals are 60-120 μmol/L for men and 50-110 μmol/L for women. The creatinine levels fit within the norm in all patients, both before and after the 21-day rehabilitation program.

3.5. Platelets. The platelet count of 150-400 K/μL is considered normal. The platelet count was below the norm before the therapy for one patient, and it slightly increased after the 21-day rehabilitation program. The platelet count was within the normal range of healthy individuals in the remaining patients both before and after the 21-day rehabilitation program.

3.6. Hematocrit. All women had hematocrit within the normal range (35–45%) before and after the 21-day rehabilitation program. However, the hematocrit of 7 male patients

TABLE 2: Change in the general health indicators in the blood of patients after knee or hip replacement subjected to the 21-day general rehabilitation program. The results are presented as a number (%) of cases.

Parameter	Amelioration (N (%))	No change (N (%))	Deterioration (N (%))
CRP (mg/L)	33 (80%)	2 (5%)	6 (15%)
ESR (mm/h)	27 (66%)	1 (2%)	13 (32%)
Glucose (mmol/L)	13 (32%)	26 (63%)	2 (5%)

Abbreviations: CRP: C-reactive protein, ESR: erythrocyte sedimentation rate.

before the rehabilitation was below the lower limit of its norm (the normal range for male patients is 40–50%). After the rehabilitation, only 5 male patients presented hematocrit values below the norm.

3.7. Red Blood Cells (RBC).

The norm of red blood cells count is 3,500,000-5,200,000/μL (3.5–5.2 M/μL) for women and 4,200,000-5,400,000/μL (4.2–5.4 M/μL for men. Before the 21-day rehabilitation program, 5 men had low RBC count, while after the rehabilitation, the RBC count was low in three male patients. As for female patients, 3 women had a high RBC count before the rehabilitation, while after the 21-days rehabilitation program, the RBC count was normal in all female patients.

3.8. Hemoglobin (HGB).

The normal hemoglobin range for women is 12-16 g/dL and 14-18 g/dL for men. Low HGB levels were noted in 11 male patients before and 9 male patients after the 21-day rehabilitation program. The HGB levels in female patients fit within the normal limits before and after the 21-day rehabilitation program.

3.9. White Blood Cells (WBC).

The reference norm value of white blood cells count is 4,000-10,000 leukocytes/mm³. The elevated leukocyte count was observed only in one patient before the rehabilitation started, and all study participants presented normal WBC count after the rehabilitation concluded.

3.10. Total Cholesterol.

The norm for cholesterol level for healthy individuals is <190 mg/dL. Only 4 patients presented normal cholesterol levels before the rehabilitation started, and only 5 after it concluded. Although most patients presented elevated cholesterol levels, it is worth noting that in 78% of patients (32 individuals), the cholesterol level decreased after the 21-day rehabilitation program.

3.11. High-Density Lipoprotein (HDL).

The norm for high-density lipoprotein is 40-80 mg/dL for women, and 35-70 mg/dL for men. Thirteen female patients had low HDL levels before the rehabilitation started, and nine women after it. Only one male patient presented a low HDL level before the rehabilitation. In the whole study group, the decreased HDL level was observed in 11 patients (male and female together).

3.12. Triglycerides (TG).

Triglyceride reference values are as follows: correct result < 150 mg/dL. Before the 21-day rehabilitation program, 18 patients (44%) had normal TG levels, and after the rehabilitation concluded, the normal TG levels were observed in 26 patients (63%).

3.13. Low-Density Lipoprotein (LDL).

The normal level of low-density lipoprotein (LDL) is <115 mg/dL. The correct LDL concentration was noted only in 3 patients (7%) before the rehabilitation started and 5 patients (12%) after the rehabilitation concluded. A decrease in LDL concentration in the course of the 21-day rehabilitation program was found in 11 patients (27%).

3.14. Oxidative Stress Markers, Cholesterol, and ST2.

A 21-day rehabilitation program significantly influenced the levels of selected oxidative stress markers: SOD and GPx assessed in erythrocytes hemolysates, as well as LPS, cholesterol, and ST2 assessed in serum obtained from patients after knee or hip replacement. CAT, GR, and GST activities were the same as before the 21-day rehabilitation program (Table 3).

After a 21-day rehabilitation program, the total SOD activity increased on average by 63.5 ± 23.7 NU/mg Hb (95% CI: 55.4-71.6) and GPx activity increased by 11.2 ± 8.2 NU/g Hb (95% CI: 8.5-14.0). On the contrary, LPS concentration in the serum decreased by 86.6 RF (95% CI: 24.9-84.4, cholesterol levels decreased by 16.4 ± 19.3 mg/dL (95% CI: 9.9-23.0), and the ST2 level decreased by 0.2 ± 0.1 ng/mL (95% CI: 0.1-0.2).

4. Discussion

Our previous work presented biochemical and morphological characteristics of the blood of patients before and after the 21-day general rehabilitation program [40]. We reported that the individually designed general rehabilitation positively affected the patients' blood glucose and lipids concentrations. Glucose, total cholesterol, LDL, and TG were significantly lower, and HDL levels were significantly higher when compared to their initial levels. Also, we observed that C-reactive protein, platelets, and hematocrit were lower after the rehabilitation proving that general rehabilitation helped reduce inflammation and prevent clot formation [40].

Hypoxia leads to decreased antioxidant defense in muscles and other organs. The decreased activity of superoxide dismutase (SOD) and lower glutathione levels have been observed under hypoxic conditions [42]. Oxygen generates reactive oxygen species (ROS) production necessary for cell signaling processes. Nevertheless, ROS also exerts detrimental effects on organs function including the heart's function [42]. In this study, we assessed the impact of postoperative rehabilitation on oxidative stress markers, cholesterol, and ST2 measured in erythrocytes of patients after hip or knee replacement surgery in the course of osteoarthritis. We analyzed catalase (CAT), glutathione reductase (glutathione disulfide reductase (GR, GSR)), total superoxide dismutase (SOD), glutathione peroxidase (GPx), and glutathione transferase (GST) activities, lipofuscin (LPS), and cholesterol concentration in the erythrocytes, as well as ST2 concentration

TABLE 3: Oxidative stress markers levels in hemolysates and lipofuscin (LPS), cholesterol, and suppression of tumorigenicity 2 (ST2) levels in serum of patients ($n = 36$) after knee or hip replacement before and after a 21-day general rehabilitation program. The results are presented as mean ± SD or median and lower–upper quartile.

Oxidative stress markers	Before rehabilitation	After rehabilitation	Δ = after – before	t	p
CAT activity (IU/g Hb)	700.5 (649.2-748.4)	678.8 (650.0-750.8)	—	—	0.643
GR activity (IU/g Hb)	9.3 ± 1.7	9.2 ± 2.1	—	0.34	0.734
SOD activity (NU/mg Hb)	232.0 ± 19.2	295.5 ± 31.3	63.5	15.88	<0.001
GPx activity (IU/g Hb)	60.0 ± 9.0	71.2 ± 10.9	8.2	8.23	<0.001
GST activity (IU/g Hb)	0.41 ± 0.09	0.42 ± 0.11	—	0.95	0.349
LPS (RF)	314.9 ± 102.7	260.2 ± 48.9	-86.6	3.74	<0.001
Cholesterol (mg/dL)	234.0 ± 35.0	217.6 ± 31.5	-16.4	5.10	<0.001
ST2 (ng/mL)	0.69 ± 0.11	0.51 ± 0.13	-0.18	8.99	< 0.001

Abbreviations: CAT: catalase, GPx: glutathione peroxidase, GR: glutathione reductase, GST: glutathione S-transferase, Hb: hemoglobin, LPS: lipofuscin, RF: relative lipid extract fluorescence, SOD: total superoxide dismutase, ST2: suppression of tumorigenicity 2 marker.

in serum. To the best of our knowledge, this is the first study designed to compare the oxidative stress markers, cholesterol, and ST2 marker, measured in erythrocytes or serum, before and after the general rehabilitation cycle. Our results show a significant increase in SOD and GPx activity in erythrocytes and a significant decrease in ST2 marker concentration in the serum. Simultaneously, we observed a reduction in LPS and total cholesterol concentration in patients' erythrocytes. A previous study on patients with hip or knee replacement enrolled into the general rehabilitation program [40] showed that physical rehabilitation improves serum oxidative stress parameters and positively affects patients' general health. The patients showed improved glucose and lipid profiles and inflammation and blood clotting parameters [40]. They also presented greater physical efficiency and exercise capacity, as determined by the 6-minute walk test (6MWT). After the rehabilitation process, the patients walked a longer distance in 6MWT, but their body mass remained the same [40]. Osteoarthritis affects patients' antioxidative and oxidative metabolism by significantly impairing antioxidant defense [56]. Antioxidants ensure the proper functioning of the organism by neutralizing reactive oxygen species. In mature erythrocytes, SOD, CAT, and GPx participate in this process [57]. They control ROS production and limit or repair damage caused by them [58]. The interventional antioxidants, also known as free radical scavengers, creating the antioxidant barrier [59] include SOD, CAT, and GPx. They remove ROS from the cellular and intercellular spaces and extracellular fluids, such as plasma, lymphatic fluid, cerebrospinal fluid, and articular synovial fluid [60]. The family of SOD enzymes comprises three isoforms with different structural characteristics of the prosthetic group (containing Mn or Cu and Zn), compartmentalization, and functional significance. In mature erythrocytes, the Cu/Zn isoform (SOD1) catalyzes the superoxide anion dismutation. The superoxide anion is formed mostly by Hb autoxidation. The produced hydrogen peroxide is degraded to oxygen and water by CAT and GPx. In nonpathological conditions, GPx degrades most of the H_2O_2 by oxidizing GSH into GSSG [57]. Here, we confirm

that total SOD and GPx activity in erythrocytes increased after regular, individually adjusted physical activity during 21-day general rehabilitation after hip or knee replacement. Our previous study showed that total SOD activity measured in patients' serum also increased after 21 days of general rehabilitation. The effects of 21-day general rehabilitation, adjusted to the patient's abilities, designed and controlled by a physiotherapist, were compatible with results obtained by other research groups and resulted from the oxidative stress after physical training [40]. Oxidative stress is an essential factor that modulates the progression of complications triggered by physical activity implemented as a therapy. Teixeira et al. [61] demonstrated that the erythrocyte SOD activity was higher in kayakers and canoeists. Evelson et al. [62] determined that resting SOD activity in well-trained rugby players was higher than men with a sedentary lifestyle. Melikoglu et al. [63] also reported that SOD and GPx activities were higher in basketball players than in men with a sedentary lifestyle. Other researchers showed that GPx activity is associated with the maximal oxygen uptake attained by specific training, and its increased activity reflects adaptation to the exercise-induced oxidative stress [64]. Here, we observed the same tendency in total SOD and GPx activity in erythrocytes of patients who underwent knee or hip replacement and were enrolled in a 21-day controlled and individualized therapeutic physical activity. Moderate physical activity, appropriately matched with the fitness level of post hip or knee surgery patients, leads to significantly increased exercise capacity and induces multiple physiological changes in the body including changes in blood biochemistry and metabolism [40]. Physical activity increases blood oxygenation, tissue perfusion, and oxygen metabolism leading to mild oxidative stress [42]. Mild oxidative stress induced by physical activity may evoke adaptive changes, such as increased expression of antioxidant enzymes causing a general improvement in the function of tissue antioxidative systems [42].

Reactive oxygen species oxidize proteins, enzymes, lipids, and other macromolecules. Lipofuscin is produced from secondary products of membrane lipids peroxidation

reacting with amino groups of phospholipids, proteins, etc. Lipofuscin is considered a less specific marker of lipid peroxidation than malondialdehyde [65]. It is stored in lysosomes, decreasing their phagocytic activity and ability to degrade the nonefficient and damaged mitochondria, a phenomenon accompanying the aging process [66–68]. Lipofuscin is a fluorescent complex mixture composed of highly oxidized cross-linked macromolecules (proteins, lipids, and sugars) with multiple metabolic origins [69]. The nature and structure of LPS complexes vary among tissues and show temporal heterogeneity in oxidized proteins (30–70%), lipids (20–50%), metals cations (2%), and sugar residues content. Due to its polymeric and highly cross-linked nature, LPS cannot be degraded or cleared by exocytosis. It accumulates within the lysosomes and cell cytoplasm of long-lived postmitotic and senescent animal cells [69]. To the best of our knowledge, there are barely any studies linking lipofuscin concentration with osteoarthritis and joint replacement in humans. Moreover, this subject was never analyzed in the context of lipofuscin serum level and its changes after physical rehabilitation. This study documents a significant reduction in LPS levels in hemolysates of the patients after a 21-day systemic physical activity. In our previous study, serum lipofuscin concentration significantly decreased after the 21-day general rehabilitation program. We also report that lipofuscin in erythrocytes decreases after the 21-day general rehabilitation program. We assume that high lipofuscin concentration is associated with high oxidative stress resulting from precedent joint damage and recent surgery. The rehabilitation program positively affected, meaning reduced, the oxidative stress in the patients and contributed to the subsequent reduction of lipofuscin concentration, as expected from literature analysis [40, 70].

Oxidation changes membrane permeability resulting in hemolysis which may reflect endovascular destruction of the erythrocytes. The extravascular mechanisms may include cell deformation and changes in antigenicity [71]. Lipid peroxidation causes polymerization of membrane components and decreases cells' deformability [72]. Lipid oxidation products, such as oxidized cholesterol and oxidized unsaturated fatty acyl groups of phospholipids, may affect membrane bilayer structure and function. Phospholipids uptaken from plasma repair the oxidized lipids of the erythrocytes membrane since they cannot be synthesized *de novo*. Overall, lipid peroxidation decreases membrane fluidity [73]. The surface receptor molecules that allow cells to respond to hormones and cytokines and are involved in the maintenance of correct ion balance within the cells can be inactivated during lipid peroxidation [74]. Redox imbalance and oxidative stress-induced membrane shedding increase the cholesterol/phospholipids ratio in the erythrocyte membrane, decreasing membrane fluidity [75] and consequently elevating osmotic resistance [76–78]. Higher cholesterol level in the erythrocyte membrane affects its mechanical properties [79, 80]. During erythrocyte physiological aging, senescent erythrocytes show an increased cholesterol/phospholipids ratio and subsequent increased membrane osmotic resistance [77]. Increased cholesterol/phospholipids ratio is observed in various pathological conditions such as diabetes

[75], chronic alcoholism [81], and multiple sclerosis [82]. The significant elevations in HDL-C and LDL-C serum levels were noted after a 21-day physical rehabilitation [40]. The observed changes may be related to modulation of the erythrocytes' membrane fluidity that enhances its functionality. The cholesterol content in the erythrocyte membrane reflects the blood cholesterol levels of high- and low-density lipoproteins [83]. The increase in the cholesterol content, until a critical level, stabilizes the erythrocyte membrane and keeps its fluidity critical for its functions. Beyond this critical level, the increased cholesterol content decreases the membrane's fluidity and impairs its functions [83]. HDL plays a major role throughout the body by removing excess cholesterol from membranes, so they gain greater stability, but altogether, it ensures the critical flow necessary to perform the membrane functions. In our previous paper, we observed the increased HDL serum levels. We concluded that it indicated that the mechanisms removing the excess of cholesterol are more efficient in the membranes of extrahepatic tissues and cells, and they ensure the membrane critical fluidity and promote the so-called reverse transport of cholesterol to the liver [40, 83]. Our study showed a reduction of cholesterol levels accompanied by reduced LPS levels. We consider that the changes result from the protective mechanism stimulated by controlled physical activity of the patients related to the 21-day general rehabilitation program.

The suppressor of tumorigenicity 2 (ST2) is expressed on many different cells, mostly of hematopoietic origin, where IL-33 induces the production of cytokines and chemokines, cell activation, or chemotaxis [84–88]. Like other members of the IL-1 receptor family, ST2 also exists in a soluble form (sST2), generated by alternative mRNA splicing. This soluble form acts as a decoy receptor and inhibits IL-33 signaling [89]. Elevated sST2 concentrations have been reported in the serum of patients suffering from various disorders, including systemic lupus erythematosus, atopic dermatitis, asthma, trauma, septic shock, and myocardial infarction. Several studies suggested that IL-33 and ST2 are involved in the inflammatory process that leads to arthritis. It is known that IL-33 and ST2 are expressed in the synovium of patients with rheumatoid arthritis [90–92]. To date, only a few studies analyzed the relationship between serum ST2 levels and osteoarthritis severity and development. Sacitharan et al. [93] studied tissues from OA patients and reported an upregulation of IL-33 in the synovial fluid and both IL-33 and its receptor ST2 in chondrocytes. The *in vitro* experiments on human chondrocytes cells showed that exogenous IL-33 stimulated human chondrocytes to produce cartilage-degrading proteases. Also, in the experimental mice model, exogenous IL-33 augmented the disease in animals with experimentally induced OA by destabilization of the medial meniscus (DMM) [93]. Interleukin- (IL-) 33 is a type of cytokine, which is a ligand for ST2, and belongs to the IL-1 receptor (IL-1R) family [94]. Li et al. [94] investigated the possible pathophysiological role of IL-33/sST2 in ankylosing spondylitis (AS). The authors reported that the serum levels of IL-33/sST2 were remarkably higher in the patients with AS than the healthy groups. Elevated levels of IL-33/sST2

were detected in the patients with peripheral arthritis, sST2 was higher in the patients with hip involvement, and IL-33/sST2 may regulate the immunological or inflammatory process of AS [94]. He et al. [95] showed that IL-33 and ST2 are elevated in human and murine OA. Moreover, neutralizing IL-33 and ST2 reduced cartilage degradation and pain *in vivo* and was associated with a marked decrease in the production of cartilage-degrading proteases alongside an increased expression of chondrogenic markers [95]. Pharmacological usage of monoclonal antibodies to block either IL-33 or ST2 helped diminish the pain and joint damage in mice with DMM-induced OA. It suggests that IL-33 can potentially be a future therapeutic target for OA [95]. In the presented study, we assessed the ST2 parameter in order to determine whether the tested biomarkers could help with identifying patients who benefited the most from the general 21-day rehabilitation process. So far, no scientific reports have studied ST2 in the context of physical rehabilitation of patients with OA. Our study shows a significant reduction in ST2 concentration in the serum of patients after knee or hip replacement in the course of osteoarthritis subjected to the 21-day general rehabilitation program. We may conclude that ST2 is one of the many inflammation-related parameters that are altered in patients with OA who underwent hip or knee replacement and the general rehabilitation program. The general rehabilitation program reduces the inflammatory processes measured by the ST2 parameter.

5. Conclusions

General rehabilitation is an effective, natural, and therapeutic procedure reducing the levels of oxidative stress markers such as LPS, as well as cholesterol and ST2 in patients, who underwent knee and hip replacement in the course of osteoarthritis. Individually designed, regular physical activity is an essential element of the postoperative protocol, which improves the redox balance and helps patients recover after the surgery effectively.

Data Availability

Data are available on request due to privacy/ethical restrictions.

Conflicts of Interest

The authors declare that there is no conflict of interest regarding the publication of this paper.

Authors' Contributions

M.I., B.S-P., and D.S. are responsible for the conceptualization; B.S-P., J.P., D.S., and. M.I. for the methodology; D.S., B.S-P., E.CH., and M.I. for the formal analysis; M.I., J.P., B.S-P., D.S., and J.J. for the investigation; D.S. and E.CH for the data curation; D.S. and M.I. for the writing—original draft preparation; D.S., M.I., J.P., and J.J. for the writing—review and editing; D.S. for the visualization; B.S.-P., D.S., and

M.I. for the supervision; B.S-P. and D.S. for the project administration; and M.I. for the funding acquisition. All authors have read and agreed to the published version of the manuscript.

References

[1] F. Domínguez-Navarro, C. Igual-Camacho, A. Silvestre-Muñoz, S. Roig-Casasús, and J. M. Blasco, "Effects of balance and proprioceptive training on total hip and knee replacement rehabilitation: a systematic review and meta-analysis," *Gait & Posture*, vol. 62, pp. 68–74, 2018.

[2] S. Glyn-Jones, A. J. Palmer, R. Agricola et al., "Osteoarthritis," *Lancet*, vol. 386, pp. 376–387, 2015.

[3] M. Łyp, R. Kaczor, A. Cabak et al., "A water rehabilitation program in patients with hip osteoarthritis before and after total hip replacement," *Medical Science Monitor*, vol. 22, pp. 2635–2642, 2016.

[4] M. S. Ha, D. Y. Kim, and Y. H. Baek, "Effects of hatha yoga exercise on plasma malondialdehyde concentration and superoxide dismutase activity in female patients with shoulder pain," *Journal of Physical Therapy Science*, vol. 27, no. 7, pp. 2109–2112, 2015.

[5] S. Vyas, H. Sharma, and R. K. Vyas, "Role of malondialdehyde in the serum of rheumatoid arthritis and osteoarthritis," *Journal of Postgraduate Medical Institute*, vol. 30, no. 1, pp. 58–61, 2016.

[6] R. S. Bhattacharya and V. Gupta, "Efficacy of vitamin E in knee osteoarthritis management of north Indian geriatric population," *Therapeutic Advances in Musculoskeletal Disease*, vol. 4, no. 1, pp. 11–19, 2012.

[7] H. Ben Saad, I. Nasri, A. Elwej et al., "A mineral and antioxidant-rich extract from the red marine algae Alsidium corallinum exhibits cytoprotective effects against potassium bromate-induced erythrocyte oxidative damages in mice," *Biological Trace Element Research*, vol. 160, no. 1, pp. 85–96, 2014.

[8] M. Cay and M. Naziroglu, "Effects of intraperitoneally-administered vitamin E and selenium on the blood biochemical and haematological parameters in rats," *Cell Biochemistry and Function*, vol. 17, no. 2, pp. 143–148, 1999.

[9] M. Zámocký, B. Gasselhuber, P. G. Furtmüller, and C. Obinger, "Molecular evolution of hydrogen peroxide degrading enzymes," *Archives of Biochemistry and Biophysics*, vol. 525, no. 2, pp. 131–144, 2012.

[10] M. N. Paliwal, A. N. Sontakke, and P. Paliwal, "Study of serum malondialdehyde and reduced glutathione level in patients with osteoarthritis," *Journal of Evolution of Medical and Dental Sciences*, vol. 2, no. 30, pp. 5682–5687, 2013.

[11] H. Esterbauer, "Estimation of peroxidative damage. A critical review," *Pathologie Biologie*, vol. 44, no. 1, pp. 25–28, 1996.

[12] A. Ścibior, A. Adamczyk, D. Gołębiowska, and J. Kurus, "Evaluation of lipid peroxidation and the level of some elements in rat erythrocytes during separate and combined vanadium and magnesium administration," *Chemico-Biological Interactions*, vol. 293, pp. 1–10, 2018.

[13] C. Caselli, "Inflammation in cardiac disease: focus on Interleukin-33/ST2 pathway," *Inflammation and Cell Signaling*, vol. 1, no. 2, article e149, 2014.

[14] M. M. Ciccone, F. Cortese, M. Gesualdo et al., "A novel cardiac bio-marker: ST2: a review," *Molecules*, vol. 18, no. 12, pp. 15314–15328, 2013.

[15] M. Shimpo, D. A. Morrow, E. O. Weinberg et al., "Serum levels of the interleukin-1 receptor family member ST2 predict mortality and clinical outcome in acute myocardial infarction," *Circulation*, vol. 109, no. 18, pp. 2186–2190, 2004.

[16] E. O. Weinberg, M. Shimpo, S. Hurwitz, S. Tominaga, J. L. Rouleau, and R. T. Lee, "Identification of serum soluble ST2 receptor as a novel heart failure biomarker," *Circulation*, vol. 107, no. 5, pp. 721–726, 2003.

[17] C. J. Beltrán, L. E. Núñez, D. Díaz-Jiménez et al., "Characterization of the novel ST2/IL-33 system in patients with inflammatory bowel disease," *Inflammatory Bowel Disease*, vol. 16, no. 7, pp. 1097–1107, 2010.

[18] L. Pastorelli, R. R. Garg, S. B. Hoang et al., "Epithelial-derived IL-33 and its receptor ST2 are dysregulated in ulcerative colitis and in experimental Th1/Th2 driven enteritis," *Proceedings of the National Academy of Sciences of the United States of America*, vol. 107, no. 17, pp. 8017–8022, 2010.

[19] D. Díaz-Jiménez, L. E. Núñez, C. J. Beltrán et al., "Soluble ST2: a new and promising activity marker in ulcerative colitis," *World Journal of Gastroenterology*, vol. 17, no. 17, pp. 2181–2190, 2011.

[20] D. Díaz-Jiménez, M. De la Fuente, K. Dubois-Camacho et al., "Soluble ST2 is a sensitive clinical marker of ulcerative colitis evolution," *BMC Gastroenterology*, vol. 16, no. 1, p. 103, 2016.

[21] M. T. Vander Lugt, T. M. Braun, S. Hanash et al., "ST2 as a marker for risk of therapy-resistant graft-versus-host disease and death," *New England Journal Medicine*, vol. 369, no. 6, pp. 529–539, 2013.

[22] D. M. Ponce, P. Hilden, C. Mumaw et al., "High day 28 ST2 levels predict for acute graft-versus-host disease and transplant-related mortality after cord blood transplantation," *Blood*, vol. 125, no. 1, pp. 199–205, 2015.

[23] G. B. McDonald, L. Tabellini, B. E. Storer, R. L. Lawler, P. J. Martin, and J. A. Hansen, "Plasma biomarkers of acute GVHD and nonrelapse mortality: predictive value of measurements before GVHD onset and treatment," *Blood*, vol. 126, no. 1, pp. 113–120, 2015.

[24] J. E. Levine, T. M. Braun, A. C. Harris et al., "A prognostic score for acute graft-versus-host disease based on biomarkers: a multicentre study," *The Lancet Haematology*, vol. 2, no. 1, pp. e21–e29, 2015.

[25] J. Yu, B. E. Storer, K. Kushekhar et al., "Biomarker panel for chronic graft-versus-host disease," *Journal of Clinical Oncology*, vol. 34, no. 22, pp. 2583–2590, 2016.

[26] M. Abu Zaid, J. Wu, C. Wu et al., "Plasma biomarkers of risk for death in a multicenter phase 3 trial with uniform transplant characteristics post-allogeneic HCT," *Blood*, vol. 129, no. 2, pp. 162–170, 2017.

[27] M. J. Hartwell, U. Özbek, E. Holler et al., "An early-biomarker algorithm predicts lethal graft-versus-host disease and survival," *JCI Insight*, vol. 2, no. 3, article e89798, 2017.

[28] C. G. Kanakry, G. Bakoyannis, S. M. Perkins et al., "Plasma-derived proteomic biomarkers in human leukocyte antigen-haploidentical or human leukocyte antigen-matched bone marrow transplantation using post-transplantation cyclophosphamide," *Haematologica*, vol. 102, no. 5, pp. 932–940, 2017.

[29] C. Pei, M. Barbour, K. J. Fairlie-Clarke, D. Allan, R. Mu, and H. R. Jiang, "Emerging role of interleukin-33 in autoimmune diseases," *Immunology*, vol. 141, no. 1, pp. 9–17, 2014.

[30] R. A. Johnpulle, S. Paczesny, D. K. Jung et al., "Metabolic complications precede alloreactivity and are characterized by changes in suppression of tumorigenicity 2 signaling," *Biology of Blood and Marrow Transplantation*, vol. 23, no. 3, pp. 529–532, 2017.

[31] M. Miller, D. Purves, A. McConnachie et al., "Soluble ST2 associates with diabetes but not established cardiovascular risk factors: a new inflammatory pathway of relevance to diabetes?," *PLoS One*, vol. 7, no. 10, article e47830, 2012.

[32] Y. H. Lin, R. C. Zhang, L. B. Hou et al., "Distribution and clinical association of plasma soluble ST2 during the development of type 2 diabetes," *Practice*, vol. 118, pp. 140–145, 2016.

[33] C. Meisel, K. Bonhagen, M. Löhning et al., "Regulation and function of T1/ST2 expression on CD4+ T cells: induction of type 2 cytokine production by T1/ST2 cross-linking," *Journal of Immunology*, vol. 166, no. 5, pp. 3143–3150, 2001.

[34] X. Liu, M. Li, Y. Wu, Y. Zhou, L. Zeng, and T. Huang, "Anti-IL-33 antibody treatment inhibits airway inflammation in a murine model of allergic asthma," *Biochemical and Biophysical Research Communications*, vol. 386, no. 1, pp. 181–185, 2009.

[35] C. Li, I. Maillet, C. Mackowiak et al., "Experimental atopic dermatitis depends on IL-33R signaling via MyD88 in dendritic cells," *Cell Death and Disease*, vol. 8, no. 4, article e2735, 2017.

[36] G. H. Park, H. K. Shinn, J. H. Kang, W. J. Na, Y. H. Kim, and C. S. Park, "Anti-interleukin-33 reduces ovalbumin-induced nephrotoxicity and expression of kidney injury molecule-1," *International Neurourology Journal*, vol. 20, no. 2, pp. 114–121, 2016.

[37] M. Li, Y. Li, X. Liu, X. Gao, and Y. Wang, "IL-33 blockade suppresses the development of experimental autoimmune encephalomyelitis in C57BL/6 mice," *Journal of Neuroimmunology*, vol. 247, no. 1-2, pp. 25–31, 2012.

[38] C. de Gregorio, "Physical training and cardiac rehabilitation in heart failure patients," in *Heart Failure: From Research to Clinical Practice. Advances in Experimental Medicine and Biology*, vol. 1067, Springer, Cham, 2018.

[39] C. W. Yancy, M. Jessup, B. Bozkurt et al., "ACCF/AHA guideline for the management of heart failure: a report of the American College of Cardiology Foundation/American Heart Association Task Force on practice guidelines," *Journal of American College of Cardiology*, vol. 62, pp. e147–e239, 2013.

[40] B. Skrzep-Poloczek, J. Poloczek, E. Chełmecka et al., "General, 21-day postoperative rehabilitation program has beneficial effect on oxidative stress markers in patients after total hip or knee replacement," *Oxidative Medicine and Cellular Longevity Volume*, vol. 2020, 9 pages, 2020.

[41] X. Liu, Y. Xiao, Y. Pan, H. Li, S. G. Zheng, and W. Su, "The role of the IL-33/ST2 axis in autoimmune disorders: friend or foe?," *Cytokine and Growth Factor Reviews*, vol. 50, pp. 60–74, 2019.

[42] K. Gwozdzinski, A. Pieniazek, J. Bernasinska-Slomczewska, J. Brzeszczynska, R. Irzmanski, and A. Jegier, "Alterations in the properties of red blood cells in men with coronary artery diseases after comprehensive cardiac rehabilitation," *Cardiology Research and Practice*, vol. 2020, Article ID 6478785, 9 pages, 2020.

[43] Y. Li, Y. Su, S. Chen et al., "The effects of resistance exercise in patients with knee osteoarthritis: a systematic review and

meta-analysis," *Clinical Rehabilitation*, vol. 30, no. 10, pp. 947–959, 2016.

[44] ATS Committee on Proficiency Standards for Clinical Pulmonary Function Laboratories, "ATS Statement: Guidelines for the Six-Minute Walk Test," *American Journal of Respiratory and Critical Care Medicine*, vol. 166, no. 1, pp. 111–117, 2002.

[45] C. Fiorina, E. Vizzardi, R. Lorusso et al., "The 6-min walking test early after cardiac surgery. Reference values and the effects of rehabilitation programme," *European Journal of Cardio-Thoracic Surgery*, vol. 32, no. 5, pp. 724–729, 2007.

[46] R. W. Bohannon and R. Crouch, "Minimal clinically important difference for change in 6-minute walk test distance of adults with pathology: a systematic review," *Journal of Evaluation in Clinical Practice*, vol. 23, no. 2, pp. 377–381, 2017.

[47] H. Aebi, "Catalase in vitro," *Methods in Enzymology*, vol. 105, pp. 121–126, 1984.

[48] I. Carlberg and B. Mannervik, "Glutathione reductase," *Methods in Enzymology*, vol. 113, pp. 484–490, 1985.

[49] Y. Oyanagui, "Reevaluation of assay methods and establishment of kit for superoxide dismutase activity," *Analytical Biochemistry*, vol. 142, no. 2, pp. 290–296, 1984.

[50] D. E. Paglia and W. N. Valentine, "Studies on the quantitative and qualitative characterization of erythrocyte glutathione peroxidase," *The Journal of Laboratory and Clinical Medicine*, vol. 70, no. 1, pp. 158–169, 1967.

[51] W. H. Habig and W. B. Jakoby, "Assays for differentiation of glutathione S-transferases," *Methods in Enzymology*, vol. 77, pp. 398–405, 1981.

[52] M. Tsuchida, T. Miura, K. Mizutani, and K. Aibara, "Fluorescent substances in mouse and human sera as a parameter of in vivo lipid peroxidation," *Biochimica et Biophysica Acta*, vol. 834, no. 2, pp. 196–204, 1985.

[53] C. C. Allain, L. S. Poon, C. S. G. Chan, W. Richmond, and P. C. Fu, "Enzymatic determination of total serum cholesterol," *Clinical Chemistry*, vol. 20, no. 4, pp. 470–475, 1974.

[54] P. Balasubramaniam and P. Malathi, "Comparative study of hemoglobin estimated by Drabkin's and Sahli's methods," *Journal of Postgraduate Medicine*, vol. 38, no. 1, pp. 8-9, 1992.

[55] M. Pietruczuk and A. Bartoszko-Tyczkowska, "Laboratory Diagnostics," in *Klinikleitfaden Labordiagnostik (Clinical Guide)*, Elsevier Urban & Partner, Wrocław, Poland, 2013.

[56] M. Paździor, M. Kiełczykowska, J. Kurzepa, D. Luchowska-Kocot, J. Kocot, and I. Musik, "The oxidative stress in knee osteoarthritis patients. An attempt of evaluation of possible compensatory effects occurring in the disease development," *Medicina*, vol. 55, no. 5, p. 150, 2019.

[57] V. Kuhn, L. Diederich, T. S. Keller IV et al., "Red blood cell function and dysfunction: redox regulation, nitric oxide metabolism, anemia," *Antioxidants & Redox Signaling*, vol. 26, no. 13, pp. 718–742, 2017.

[58] M. Valko, D. Leibfritz, J. Moncol, M. T. D. Cronin, M. Mazur, and J. Telser, "Free radicals and antioxidants in normal physiological functions and human disease," *International Journal of Biochemistry and Cellular Biology*, vol. 39, no. 1, pp. 44–84, 2007.

[59] D. M. Olszewska-Słonina, D. Matewski, G. Drewa et al., "Oxidative equilibrium in the prophylaxis of degenerative joint changes: an analysis of pre- and postoperative activity of antioxidant enzymes in patients with hip and knee osteoarthritis," *Medical Science Monitor*, vol. 16, no. 5, pp. 238–245, 2010.

[60] M. Skrzycki and H. Czeczot, "Extracellular superoxide dismutase (EC-SOD) – structure, properties and functions," *Postepy Higieny i Medycyny Doświadczalnej*, vol. 58, pp. 301–311, 2004.

[61] V. Teixeira, H. Valente, S. Casal, F. Marquez, and P. Moreira, "Antioxidant status, oxidative stress, and damage in elite trained kayakers and canoeists and sedentary controls," *International Journal of Sport Nutrition and Exercise Metabolism*, vol. 19, no. 5, pp. 443–456, 2009.

[62] P. Evelson, G. Gambino, M. Travacio et al., "Higher antioxidant defences in plasma and low density lipoproteins from rugby players," *European Journal of Clinical Investigation*, vol. 32, no. 11, pp. 818–825, 2002.

[63] M. A. Melikoglu, M. Kaldirimci, D. Katkat, I. Sen, I. Kaplan, and K. Senel, "The effect of regular long term training on antioxidant enzymatic activities," *The Journal of Sports Medicine and Physical Fitness*, vol. 48, no. 3, pp. 388–390, 2008.

[64] S. Goto and Z. Radak, "Hormetic effects of reactive oxygen species by exercise: a view from animal studies for successful aging in human," *Dose-Response*, vol. 8, no. 1, 2010.

[65] J. Koska, D. Syrova, P. Blazicek et al., "Malondialdehyde, lipofuscin and activity of antioxidant enzymes during physical exercise in patients with essential hypertension," *Journal of Hypertension*, vol. 17, no. 4, pp. 529–535, 1999.

[66] P. Luo, F. Gao, D. Niu et al., "The role of autophagy in chondrocyte metabolism and osteoarthritis: a comprehensive research review," *BioMed Research International*, vol. 2019, Article ID 5171602, 7 pages, 2019.

[67] Y. Kakimoto, C. Okada, N. Kawabe et al., "Myocardial lipofuscin accumulation in ageing and sudden cardiac death," *Scientific Reports*, vol. 9, no. 1, p. 3304, 2019.

[68] J. Aiken, E. Bua, Z. Cao et al., "Mitochondrial DNA deletion mutations and sarcopenia," *Annals of the New York Academy of Sciences*, vol. 959, no. 1, pp. 412–423, 2002.

[69] A. Moreno-García, A. Kun, O. Calero, M. Medina, and M. Calero, "An overview of the role of lipofuscin in age-related neurodegeneration," *Frontiers in Neuroscience*, vol. 12, p. 464, 2018.

[70] A. Terman and U. T. Brunk, "Oxidative stress, accumulation of biological "garbage", and aging," *Antioxidants & Redox Signaling*, vol. 8, no. 1-2, pp. 197–204, 2006.

[71] D. Chiu, B. Lubin, and S. Shonet, "Erythrocyte membrane lipid reorganization during sickling process," *British Journal of Haematology*, vol. 41, pp. 223–234, 1979.

[72] C. W. M. Haest, G. Plasa, D. Kamp, and B. Deuticke, "Spectrin as a stabilizer of the phospholipid asymmetry in the human erythrocyte membrane," *Biochimica et Biophysica Acta*, vol. 509, no. 1, pp. 21–32, 1978.

[73] C. Richter, "Biophysical consequences of lipid-peroxidation in membranes," *Chemistry and Physics of Lipids*, vol. 44, pp. 175–189, 1987.

[74] C. K. Daniels and D. B. Goldstein, "Movement of free cholesterol from lipoprotein on lipid vesicles into erythrocytes. Acceleration by ethanol in vitro," *Molecular Pharmacology*, vol. 21, pp. 694–700, 1982.

[75] H. G. Allen, J. C. Allen, L. C. Boyd, B. P. Alston-Mills, and G. P. Fenner, "Determination of membrane lipid differences in insulin resistant diabetes mellitus type 2 in whites and blacks," *Nutrition*, vol. 22, no. 11-12, pp. 1096–1102, 2006.

[76] L. T. McGrath, A. F. Douglas, E. McClean et al., "Oxidative stress and erythrocyte membrane fluidity in patients

undergoing regular dialysis," *Clinica Chimica Acta*, vol. 235, no. 2, pp. 179–188, 1995.

[77] P. Caprari, A. Scuteri, A. M. Salvati et al., "Aging and red blood cell membrane: a study of centenarians," *Experimental Gerontology*, vol. 34, no. 1, pp. 47–57, 1999.

[78] J. Brzeszczynska, M. Luciak, and K. Gwozdzinski, "Alterations of erythrocyte structure and cellular susceptibility in patients with chronic renal failure: effect of haemodialysis and oxidative stress," *Free Radical Research*, vol. 42, no. 1, pp. 40–48, 2008.

[79] H. A. Wilson-Ashworth, Q. Bahm, J. Erickson et al., "Differential detection of phospho- lipid fluidity, order, and spacing by fluorescence spectroscopy of bis-pyrene, prodan, nystatin, and merocyanine 540," *Biophysics Journal*, vol. 91, pp. 4091–4101, 2006.

[80] L. J. Gonzalez, E. Gibbons, R. W. Bailey et al., "The influence of membrane physical properties on microvesicle release in human erythrocytes," *PMC Biophysics*, vol. 2, no. 1, p. 7, 2009.

[81] P. Maturu, D. R. Vaddi, P. Pannuru, and V. Nallanchakravarthula, "Alterations in erythrocyte membrane fluidity and Na /K - ATPase activity in chronic alcoholics," *Molecular and Cellular Biochemistry*, vol. 339, no. 1-2, pp. 35–42, 2010.

[82] G. M. Hon, M. S. Hassan, S. J. van Rensburg et al., "Red blood cell membrane fluidity in the etiology of multiple sclerosis," *Journal of Membrane Biology*, vol. 232, no. 1-3, pp. 25–34, 2009.

[83] L. F. Paraiso, A. F. M. Gonçalves-e-Oliveira, L. M. Cunha et al., "Effects of acute and chronic exercise on the osmotic stability of erythrocyte membrane of competitive swimmers," *PLoS One*, vol. 12, no. 2, article e0171318, 2017.

[84] D. Moulin, O. Donzé, D. Talabot-Ayer, F. Mézin, G. Palmer, and C. Gabay, "Interleukin (IL)-33 induces the release of pro-inflammatory mediators by mast cells," *Cytokine*, vol. 40, no. 3, pp. 216–225, 2007.

[85] M. Komai-Koma, D. Xu, Y. Li, A. . N. . J. McKenzie, I. . B. McInnes, and F. . Y. Liew, "IL-33 is a chemoattractant for human Th2 cells," *European Journal of Immunology*, vol. 37, no. 10, pp. 2779–2786, 2007.

[86] M. D. Smithgall, M. R. Comeau, B. R. Park Yoon, D. Kaufman, R. Armitage, and D. E. Smith, "IL-33 amplifies both Th1- and Th2-type responses through its activity on human basophils, allergen-reactive Th2 cells, iNKT and NK cells," *International Immunology*, vol. 20, pp. 1019–1030, 2008.

[87] T. Pecaric-Petkovic, S. A. Didichenko, S. Kaempfer, N. Spiegl, and C. A. Dahinden, "Human basophils and eosinophils are the direct target leukocytes of the novel IL-1 family member IL-33," *Blood*, vol. 113, no. 7, pp. 1526–1534, 2009.

[88] E. Bourgeois, L. P. Van, M. Samson et al., "The pro-Th2 cytokine IL-33 directly interacts with invariant NKT and NK cells to induce IFN-gamma production," *European Journal of Immunology*, vol. 39, pp. 1046–1055, 2009.

[89] H. Hayakawa, M. Hayakawa, A. Kume, and S. I. Tominaga, "Soluble ST2 blocks IL-33 signaling in allergic airway inflammation," *Journal of Biological Chemistry*, vol. 282, pp. 26369–26380, 2007.

[90] V. Carriere, L. Roussel, N. Ortega et al., "IL-33,the IL-1-like cytokine ligand forST2 receptor, is a chromatin-associated nuclear factor in vivo," *Proceedings of the National Academy of Sciences of the United States of America*, vol. 104, pp. 282–287, 2007.

[91] G. Palmer, D. Talabot-Ayer, C. Lamacchia et al., "Inhibition of interleukin-33 signaling attenuates the severity of experimental arthritis," *Arthritis and Rheumatology*, vol. 60, no. 3, pp. 738–749, 2009.

[92] D. Xu, H. R. Jiang, P. Kewin et al., "IL-33 exacerbates antigen-induced arthritis by activating mast cells," *Proceedings of the National Academy of Sciences of the United States of America*, vol. 105, no. 31, pp. 10913–10918, 2008.

[93] P. K. Sacitharan, S. J. Snelling, and J. R. Edwards, "Aging mechanisms in arthritic disease," *Discovery Medicine*, vol. 14, pp. 345–352, 2012.

[94] X. Li, T. Lin, C. Qi et al., "Elevated serum level of IL-33 and sST2 in patients with ankylosing spondylitis," *Journal of Investigative Medicine*, vol. 61, no. 5, pp. 848–851, 2013.

[95] Z. He, Y. Song, Y. Yi et al., "Blockade of IL-33 signalling attenuates osteoarthritis," *Clinical and Translational Immunology*, vol. 9, no. 10, article e1185, 2020.

Research Article

High Temperature-Induced Oxidative Stress Affects Systemic Zinc Homeostasis in Broilers by Regulating Zinc Transporters and Metallothionein in the Liver and Jejunum

Chuanpi Xiao [ID],[1,2] **Linglian Kong,**[1] **Xue Pan,**[1] **Qidong Zhu,**[1] **Zhigang Song** [ID],[1] **and Nadia Everaert**[2]

[1]*Department of Animal Science, Shandong Agricultural University, Taian, Shandong 271018, China*
[2]*Precision Livestock and Nutrition Unit, Gembloux Agro-Bio Tech, University of Liège, Gembloux 5030, Belgium*

Correspondence should be addressed to Zhigang Song; zhigangs@sdau.edu.cn

To investigate the change in zinc homeostasis of broilers under heat stress, 512 broiler chickens were raised to the age of 28 days. The broilers were then assigned to heat stress and normal temperature (36.0°C vs. 26.0°C) groups for 7 days. The results showed that oxidative stress induced by high temperature had a negative effect on the growth performance of broilers. Heat stress altered zinc homeostasis and led to a redistribution of zinc in broilers, which was reflected in increased zinc concentrations in the jejunum, liver, and tibia. Upregulation of the expression of the zinc exporter *ZnT1* and importers *ZIP8* and *ZIP14* in the jejunum indicated that more zinc was absorbed and transported from the jejunum into the blood, while the liver increased its capacity to hold zinc through upregulation of metallothionein (*MT*) expression, which was achieved by reducing *ZnT1* expression and upregulating the expression of the importer *ZIP3*. The pathway was mediated by zinc transporters, but the capacity of *MT* to chelate and release zinc ions also played a crucial role. The mechanism of alterations in zinc homeostasis under heat stress was revealed by the changes in zinc transporters and *MT* levels in the intestine and liver. Heat stress also altered cecal microbial diversity and reduced the relative abundances of *Bilophila* and *Dialister*. In conclusion, broilers altered systemic zinc homeostasis through the regulation of zinc transporters and *MT* in the liver and jejunum to resist oxidative stress induced by high temperature.

1. Introduction

With global warming and the aggravation of the greenhouse effect, heat stress has become a challenge that cannot be ignored in animal husbandry. In poultry production, broilers have shown great growth potential with the improvement of modern breeding technology [1]. However, the increased growth rate will accelerate metabolism and likely lead to heat stress; the lack of sweat glands in broilers is not conducive to heat dissipation. Heat stress could cause physiological system disorders in broilers, including immune system damage, respiratory alkalosis, and hormone secretion disorders [2]. These phenomena could lead to oxidative stress by affecting mitochondrial function and changing reactive oxygen species (ROS) levels, thereby causing

oxidative damage to proteins and lipids and changes in the levels of oxidative stress markers, such as malondialdehyde (MDA), glutathione peroxidase (GPX), and superoxide dismutase (SOD) [3, 4]. When heat stress occurs, the heat shock protein (HSP) family begins to act as a stress indicator and cell protector [5]. A large number of studies have shown that the *HSP70* protein is related to the immune function of birds, such as controlling the transcription of various genes in response to immune stimulation by regulating the activity of nuclear factor kappa light chain enhancer of B cells (*NF-κB*) [6].

Zinc, an essential trace element, participates in a variety of enzyme reactions and affects various biological processes, such as digestion, absorption, and metabolism of nutrients in animals [7]. Therefore, the metabolism and

homeostasis of zinc is a complex physiological process. An increasing amount of evidence indicates that many protein families, such as metallothionein (MT) and zinc-regulated transporters (Zrts), iron-regulated transporter- (Irt-) like proteins, and zinc transporters, play major roles in zinc metabolism and homeostasis [8]. MT is a family of low-molecular metal-binding proteins that are rich in cysteine and usually bind zinc in cells to serve as a zinc reservoir [9]. MT is not only a zinc reservoir but also a potential diagnostic biological marker of intracellular zinc content. MT also participates in a variety of physiological processes, including oxidative stress and immune function [10]. Zrt- and Irt-like proteins (ZIPs) belong to the SLC39A family and transport zinc into the cytoplasm from extracellular or cellular organelles; zinc transporters (ZnTs) belong to the SLC30A family and transport zinc from the cytoplasm to the outside of the cell, functioning in zinc mobilization across biological membranes. Thus far, 10 ZnT transporters and 14 ZIP transporters have been discovered [11]. In an inflammatory or oxidative stress state, the level of hepatic MT can rise rapidly, while the expression of the zinc finger protein A20 is altered; moreover, NF-κB is negatively regulated to inhibit the production of inflammatory cytokines [12].

Adding zinc to feed has positive effects on animal growth and immunity. According to the National Research Council (NRC, 1994), the requirement of zinc for broilers is 40.0 ppm; approximately 100 ppm zinc from different sources is typically added to feed to optimize animal performance [13, 14]. The underlying mechanisms could be attributed to altered intestinal histomorphology and reduced inflammation and oxidative stress [15, 16] resulting in improved growth of broilers. Increasing lines of evidence indicate that zinc is redistributed in animals under conditions of oxidative stress and immune challenge [17, 18]. However, changes in zinc homeostasis in broilers under heat stress conditions and the regulatory mechanism have not been reported.

In this study, we investigated the changes in systemic zinc homeostasis and the regulatory mechanism in broilers under oxidative stress and inflammation caused by heat stress. The role of zinc transporters and metallothioneins in the regulation of zinc metabolism under heat stress conditions was innovatively revealed.

2. Materials and Methods

All experimental procedures were approved by the Ethics Committee of Shandong Agricultural University and performed in accordance with the Guidelines for Experimental Animals of the Ministry of Science and Technology (Beijing, People's Republic of China). All feeding and euthanasia procedures were performed with full consideration of animal welfare.

2.1. Experimental Design and Management. A total of 512 28-day-old male broiler chicks (Arbor Acre) with similar weights were randomly divided into two treatment groups, each of which included 16 replicates (cages) and 16 birds

per cage. The two treatments were as follows: half of the birds were assigned to temperature treatment at $36.0 \pm 1°C$ (heat stress group, HT) for 7 days; birds in the other treatment group were raised at a normal temperature of $26.0 \pm 1°C$ (CON). All birds were given free access to pellet feed and water during the rearing period. The basal diet composition and nutrition levels of the basal diet are listed in Table 1. During the first 3 days, the average relative humidity was maintained at approximately 70.0% and was maintained between 55.0% and 65.0% thereafter. In the first week of life, the birds were given 23 h of light and 1 h of darkness; this schedule was gradually changed to 20 h of light and 4 h of darkness by the end of the 35-day test. All broilers were vaccinated by means of drinking water. Newcastle disease (ND) and infectious bronchitis (IB) vaccines were administered on day 6 and infectious bursal disease (IBD) vaccine on day 12. The use of antibiotics was strictly prohibited to ensure the effectiveness of the test.

2.2. Growth Performance. At 35 days of age, feed consumption was recorded to calculate the average daily feed intake (ADFI) for each replicate. The birds were weighed to calculate the average daily gain (ADG). The feed conversion ratio (FCR) was defined as ADFI : ADG. Mortality data were recorded and included in the FCR calculation.

2.3. Sample Collection. One bird was randomly selected from each cage at 35 days of age after the measurement of growth performance. Blood samples were collected intravenously with a sterile syringe from the wing, placed in a glass tube without anticoagulant, and centrifuged at 3000 rpm at 4°C for 10 min after being left to stand for 30 min. Serum was obtained and stored at -20°C for biochemical analysis. The birds were euthanized by cervical dislocation after obtaining blood samples. Approximately 2 cm segments were excised from the midjejunum (from the entry point of the bile duct to Meckel's diverticulum), flushed repeatedly with a cold saline solution, and immediately immersed in a 4% paraformaldehyde solution for histological examination. Tissue samples of approximately 1 g to 2 g were collected from the jejunum and liver, rapidly frozen in liquid nitrogen, and stored at -80°C for further analysis. Tibia from both sides were dissected carefully and stored at -20°C until analysis. All birds selected were fasted for eight hours before the procedure.

2.4. Analysis of Oxidative Stress and Cytokines in Serum. The total SOD (T-SOD) activity and MDA, aspartate aminotransferase (AST), and alanine aminotransferase (ALT) levels were measured in the serum by using diagnostic kits purchased from Nanjing Jiancheng Biotechnology Institute (Nanjing, China). All determination procedures were performed strictly according to the manufacturer's instructions. The intra-assay coefficient of variation (CV) was less than 5%, and the interassay CV was less than 8%.

Endotoxin, interleukin 1β (IL-1β), interleukin 4 (IL-4), interleukin 6 (IL-6), interleukin 10 (IL-10), and tumor necrosis factor-α (TNF-α) in serum were detected using ELISA kits (MLBIO Co., Shanghai, China) according to the

TABLE 1: Composition and nutritional levels of the basal diet.

Item	1-21 days	22-35 days
Ingredient (%)		
Corn	49.98	54.9
Soybean meal (46%)	35.75	30.5
Corn protein flour (60%)	3.80	3.10
Salt	0.280	0.280
Limestone	1.75	1.62
Dicalcium phosphate	1.55	1.40
Soybean oil	5.10	6.50
Vitamin premix	0.050	0.050
Mineral premix	0.200	0.200
Choline chloride (50%)	0.100	0.100
Methionine (99%)	0.350	0.350
Lysine (70%)	0.800	0.750
Threonine (98.5%)	0.290	0.250
Phytase (20000 U)	0.020	0.020
Total	100	100
Nutritional level		
Metabolizable energy	3100 (kcal/kg)	3200 (kcal/kg)
Crude protein	23.5	21.0
Lysine	1.39	1.20
Methionine+cystine	1.02	0.920
Calcium	1.00	0.900
Total phosphorus	0.990	0.900
Available phosphorus	0.500	0.450

Provided per kilogram of compound diet: vitamin A: 12000 IU; vitamin D3: 5000 IU; vitamin E: 80 mg; vitamin K: 3.2 mg; vitamin B1: 3.2 mg; vitamin B2: 8.6 mg; nicotinic acid: 65 mg; pantothenic acid: 20 mg; vitamin B6: 4.3 mg; biotin: 0.22 mg; folic acid: 2.2 mg; vitamin B12: 0.017 mg; I: 1.50 mg; Fe: 80 mg; Mn: 120 mg; Se: 0.3 mg; Cu: 16 mg; and Zn: 110 mg. The nutrition level was calculated.

manufacturer's instructions. The inter- and intra-assay CVs were less than 10%.

2.5. Zinc and Metallothionein Concentrations. The serum concentration of zinc was measured by an inductively coupled plasma optical emission spectroscopy instrument (ICAP 7000, Thermo, USA). Each serum sample (75 μL) was placed in a centrifuge tube with 600 μL of HNO_3 (5%) and 75 μL of hydrogen peroxide (30%). The centrifuge tubes were placed in a water bath at 60°C for 2 h, and 750 μL of HNO_3 (5%) was added. The mixed solution was centrifuged for 15 min (8000 r/min), and the supernatant was stored at 4°C until measurement. The concentrations of zinc in the tibia, liver, jejunum, and cecal contents were evaluated via flame atomic absorption spectrometry (SpectrAA50/55, Warman Corporation, Palo Alto, CA, USA). The tibiae were boiled in deionized water for 10 min, soaked in ether for 96 h, degreased, and dried at 105°C to constant weight. The liver and jejunum tissues were freeze dried for 24 h and weighed. The samples from the tibia, liver, and jejunum were ashed in a muffle oven (550-600°C for 24 h). Ash content

was measured and expressed as dry degreased weight. The ash of the sample was dissolved with 0.6 mol/L hydrochloric acid and filtered. The solution was stored at 4°C before determination.

The concentrations of MT in the liver and jejunum were measured using ELISA kits (MLBIO Co., Shanghai, China) according to the manufacturer's instructions. The inter- and intra-assay CVs were less than 10%.

2.6. Total RNA Extraction and Real-Time PCR. Total RNA in the jejunum was extracted with TRIzol reagent (Invitrogen, San Diego, USA). The concentration and purity of each RNA sample were detected using a NanoDrop spectrophotometer (ND-2000, Thermo Scientific, Wilmington, USA). RNA integrity was detected by 1% agarose gel electrophoresis. Reverse transcription of 1 μg of total RNA was performed using a PrimeScript® RT reagent kit (RR047A, TaKaRa, Japan). RT-PCR analysis was performed to determine gene expression by using TB Green Premix Ex Taq (RR820A, Takara, Japan) in an ABI 7500 Real-Time PCR System (Thermo Scientific, Wilmington, USA). The reaction program included the following: predenaturation at 95°C for 10 s, followed by 40 cycles of denaturation at 95°C for 5 s and annealing and extension at 60°C for 40 s. Each reaction was repeated in triplicate wells, and the primer sequences are shown in Table 2. The amplification efficiencies of the primers were calculated using a standard curve. The specificities of the amplified products were verified by the melting curve. The geometric mean of the expression of β-actin and glyceraldehyde-3-phosphate dehydrogenase (GAPDH) was used to normalize the expression of the target genes. Relative gene expression levels of each target gene were analyzed using the $2^{-\Delta\Delta ct}$ method.

2.7. Western Blot Analysis. Frozen liver and jejunum samples were crushed into powder in liquid nitrogen, and protein extraction was performed using a total protein extraction kit (CW Biotech, Beijing, China) as specified by the manufacturer's instructions. After the protein concentration of the sample was determined using the BCA protein analysis kit (Beyotime Institute of Biotechnology, Beijing, China), a 40 μg protein sample was loaded into a 10% sodium dodecyl sulfate-polyacrylamide gel for electrophoresis (New Cell & Molecular Biotech Co., Suzhou, China). The protein was separated in electrophoresis buffer at a constant voltage of 150 mV and then transferred to a polyvinylidene difluoride (PVDF) membrane (Invitrogen, Carlsbad, CA, USA) with transfer buffer (Beyotime Institute of Biotechnology, Beijing, China) at a constant current of 400 mA. After membrane transfer, the PVDF membrane was immersed in blocking buffer for 0.5 h and then incubated overnight with primary antibodies at 4°C. Primary antibodies against ZnT1 (1:500) and GAPDH (1:2000) were purchased from Bioss Technology Inc. After three washes with TBST buffer, a secondary horseradish peroxidase-conjugated antibody (Beyotime Institute of Biotechnology, Beijing, China) was incubated at room temperature for 1 h. Finally, the protein blot strips were visualized in a gel imager using ECL kits (Beyotime Institute of Biotechnology, Beijing, China), and signals were

TABLE 2: Nucleotide sequences of real-time PCR primers.

Gene	Accession number	Primer sequence, $5' \rightarrow 3'$	Product size (bp)
ZnT1	NM_001389457.1	F: CTTCGCTTAGCATTTCTT	75
		R: TCTCCGATTTAGTCCTTCT	
DMT1	NM_001128102.2	F: AGCCGTTCACCACTTATTTCG	129
		R: GGTCCAAATAGGCGATGCTC	
ZIP3	NM_144564.4	F: GGGCACTTTCTTGTTCATCACC	105
		R: GCAGCATAACCCAGCACCAG	
ZIP8	XM_040671236.1	F: TGTAAATGTCTCGGTGGG	159
		R: CAAGATGGCTATGGAGGT	
ZIP14	XM_040689606.1	F: GTTCTGCCCCGCTGTCCT	96
		R: GGTCTGCCCTCCTCCGTCT	
MT	NM_205275.1	F:GCAACAACTGTGCCAAGGGC	138
		R: TTTCGTGGTCCCTGTCACCC	
MTF-1	XM_015297695.3	F: CCTGGTTCAACTCCTATGC	278
		R: TCAAACGGCTTCTCCTTA	
NF-λB	NM_205129	F:GTGTGAAGAAACGGGAACTG	203
		R: GGCACGGTTGTCATAGATGG	
A20	XM_003640919.2	F:GACATCGTGCTAACAGCTTGGA	141
		R: AGAAAAGAGGTATCAGGCACAAC	
S100A9	NM_001305151.1	F: TTGAGAAGCAGCTTGCCAACTAC	187
		R: TGCTGTTGCTGGTGGTCCTC	
HSP70	NM_001006685.1	F: TCTCATCAAGCGTAACACCAC	104
		R: TCTCACCTTCATACACCTGGAC	
β-Actin	NM_205518.1	F: ATGTGGATCAGCAAGCAGGAGTA	127
		R: TTTATGCGCATTTATGGGTTTTGT	
GADPH	NM_204305	F: ACATGGCATCCAAGGAGTGAG	266
		R: GGGGAGACAGAAGGGAACAGA	

MT: metallothionein; ZIP: zinc-regulated transporter, iron-regulated transporter-like protein; ZnT: zinc transporter; DMT1: divalent metal transporter 1; MTF-1: metal transcription factor-1; NF-κB: nuclear factor kappa-B; HSP70: heat shock protein 70; GAPDH: glyceraldehyde-3-phosphate dehydrogenase.
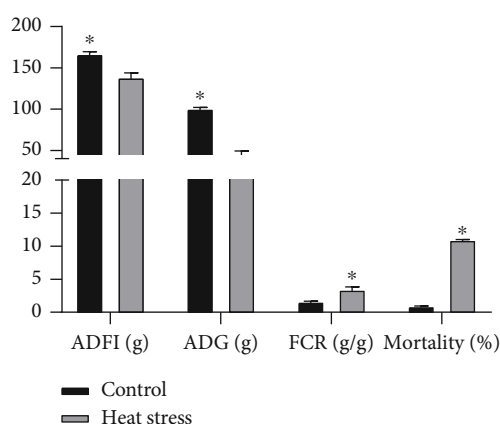
FIGURE 1: Effects of heat stress on growth performance. ADG: average daily gain; ADFI: average daily feed intake; FCR: feed conversion ratio.

quantified using the measurement software in the imager. GAPDH protein was used as an internal control for all the immunoblotting bands to obtain the corresponding expression of the target proteins.

TABLE 3: Effects of heat stress on serum parameters and cytokine levels.

Temperature	Control	Heat stress	P value
MDA (nmol/mL)	3.11 ± 0.127	3.09 ± 0.274	0.9491
T-SOD (U/mL)	100 ± 7.48^b	120 ± 5.27^a	0.0472
Endotoxin (EU/mL)	0.317 ± 0.0338^b	0.469 ± 0.0484^a	0.0153
IL-1β (ng/L)	28.0 ± 3.50	29.4 ± 2.68	0.7442
IL-4 (ng/L)	129 ± 7.08^b	219 ± 25.1^a	0.0012
IL-6 (ng/L)	63.8 ± 8.64^b	118 ± 11.0^a	0.0011
IL-10 (ng/L)	100 ± 9.84^b	182 ± 18.1^a	0.0001
TNF-α (ng/L)	171 ± 12.1	158 ± 11.3	0.4471

MDA: malondialdehyde; T-SOD: total superoxide dismutase; IL-4: interleukin 4; IL-6: interleukin 6; IL-10: interleukin 10; IL-1β: interleukin 1β; TNF-α: tumor necrosis factor-α. Values are expressed as the mean ± SD ($n = 8$). Different superscripts (a, b) in the same line indicate significant differences ($P < 0.05$).

2.8. 16S rRNA Gene Amplicon Sequencing. Samples of cecal contents were collected on ice after slaughter and immediately stored in a -80°C freezer for subsequent analysis. Microbial DNA extraction from cecum contents was

(a)

(b)
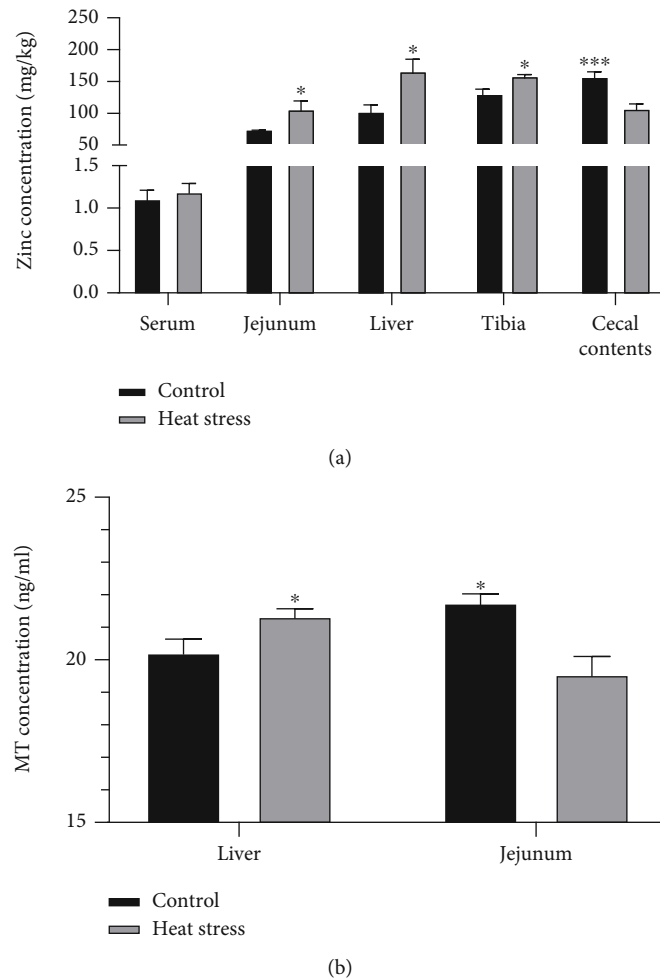
Figure 2: Zinc and metallothionein concentrations in different tissues of broilers were affected by heat stress. (a) Zinc concentrations in the serum, jejunum, liver, tibia, and cecal contents of broilers; (b) *MT* concentrations in the liver and jejunum of broilers. *MT*: metallothionein.

performed according to the instructions of the E.Z.N.A.® soil kit (Omega Bio-Tek, Norcross, GA, USA). The DNA concentration and purity were measured using a NanoDrop 2000 spectrophotometer, and the quality of DNA extraction was determined using 1% agarose gel electrophoresis. PCR amplification of the V3-V4 variable region of the bacterial 16S rRNA gene was performed using the 338F and 806R primers. The PCR conditions consisted of an initial denaturing program for 3 min at 95°C, 27 cycles (95°C for 30 s, 55°C annealing for 30 s, and 72°C for 30 s), and a final extension step at 72°C for 10 min (PCR instrument: GeneAmp9700 produced by ABI). PCRs were performed in a 20 μL mixture: 4 μL of 5X FastPfu buffer, 2 μL of 2.5 mM dNTPs, 0.8 μL of primer (5 μM), 0.4 μL of FastPfu polymerase, and 10 ng of DNA template. PCR products were recovered using a 2% agarose gel, purified using an AxyPrep DNA Gel Extraction Kit (Axygen Biosciences, Union City, CA, USA) and quantified using QuantiFluor™-ST (Promega, USA).

Purified amplicons were pooled in equimolar amounts and paired-end sequenced (2 × 300) on an Illumina MiSeq platform (Illumina, San Diego, USA) according to standard protocols. Quantitative Insights Into Microbial Ecology 2 (QIIME2) software was used for quality screening of the

raw sequences and quality filtering and pruning, denoising, merging, and chimera removal of the demultiplexed sequence of each sample were carried out to obtain the amplicon sequence variation feature table. According to the 338F/806R primers, the database obtained in the previous step was pruned to the V3-V4 region to obtain the species classification table. After all contaminating mitochondrial and chloroplast sequences were removed, appropriate methods, including ANCOM, ANOVA, Kruskal-Wallis test, and LEfSe, were used to identify bacteria with differential abundances between samples and groups. QIIME2 core diversity was used to calculate the horizontal alpha diversity index of feature sequences, including observed operational taxonomic units (OTUs), Chao1 abundance estimator, Shannon diversity index, and Faith's phylogenetic diversity index. The beta diversity index included Bray-Curtis, unweighted UniFrac, and weighted UniFrac indices, which were used to evaluate the structural changes in microbial communities between samples and are presented in principal coordinate analysis (PCoA) and nonmetric dimensional scaling (NMDS) diagrams. Partial least squares discriminant analysis in R software was used as a monitoring model to reveal the relationship between the

(a)

(b)

(c)
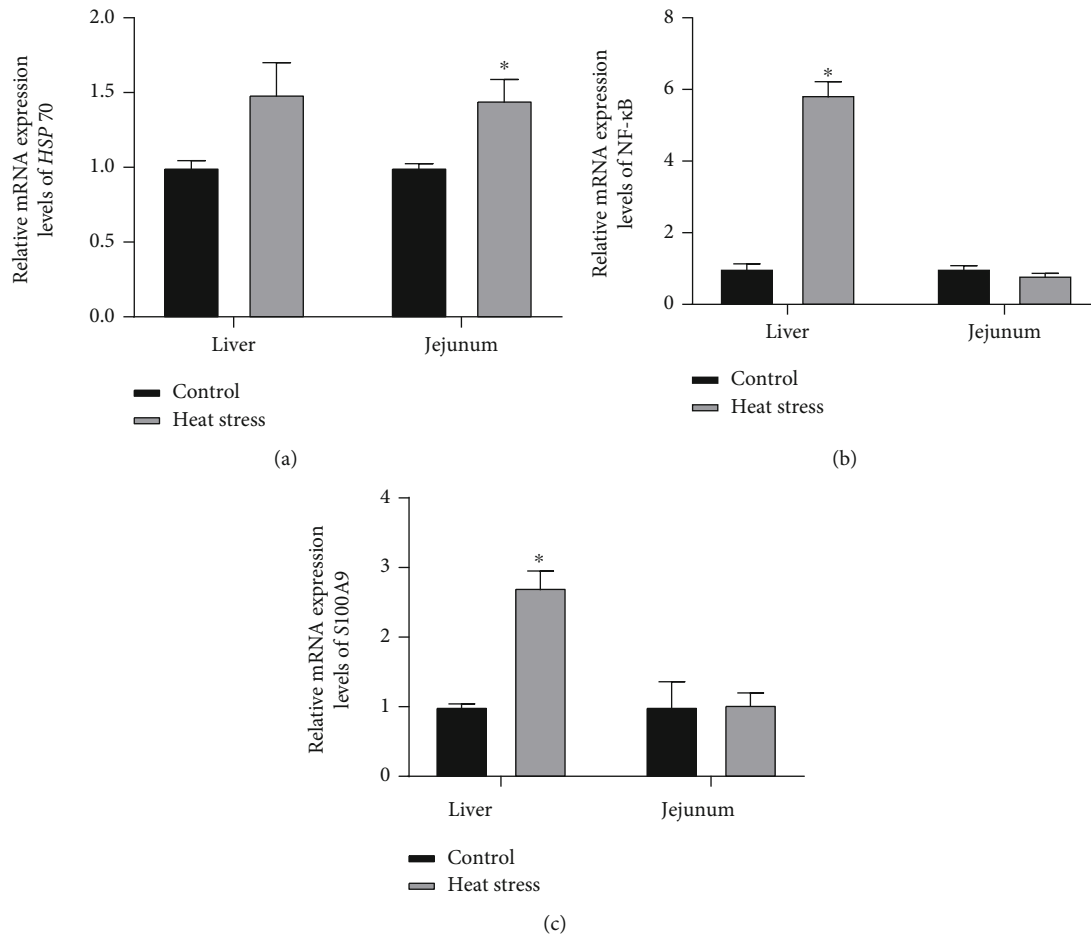
Figure 3: Influence of heat stress on the gene expression of *HSP70* (a), *NF-κB* (b), and *S100A9* (c) in the liver and jejunum. *HSP70*: heat shock protein 70; *NF-κB*: nuclear factor kappa light chain enhancer of B cells.

microbial community and sample category. The R package "Vegan" redundancy analysis method was used to reveal potential associations between microbial communities and related environmental factors. Spearman rank correlation coefficients were calculated using cooccurrence analysis to show associations between species based on the relative abundances of major microbial species in the samples. The parameters used in the analysis were set as the defaults.

2.9. *Statistical Analysis.* Data are presented as the mean ± SD . All data were analyzed through normal distribution determination. Growth performance was analyzed on a replicate (per cage) basis while other indicators were analyzed on an individual basis. Differences in the treatments were analyzed with a *t*-test in SPSS 22.0 (SPSS. Inc., Chicago, USA). Significance was set as $P < 0.05$.

3. Results

3.1. *Growth Performance.* Heat stress had a significant effect on growth performance. As shown in Figure 1, heat stress significantly reduced the ADFI and ADG ($P < 0.05$) and increased the FCR and mortality of 35-day-old broilers ($P < 0.05$).

3.2. *Analysis of Oxidative Stress and Cytokines in Serum.* The heat stress group had higher ($P < 0.05$) T-SOD and endotoxin levels in serum (Table 3). No significant difference was found in serum MDA levels ($P > 0.05$) between the heat stress and normal temperature groups. The levels of serum IL-4, IL-6, and IL-10 increased ($P < 0.05$) under heat stress. No significant effect was observed in serum IL-1β and TNF-α levels ($P > 0.05$) between the heat stress and normal temperature groups.

3.3. *Zinc Concentration in Tissues and Cecal Contents.* As shown in Figure 2(a), the concentration of zinc increased ($P < 0.05$) in the jejunum, liver, and tibia in response to heat stress, while the opposite result was observed in the cecal contents. However, heat stress had no significant effects ($P > 0.05$) on the serum concentration of zinc. The results indicated that zinc was redistributed under heat stress.

3.4. *MT Concentration in Tissues.* Figure 2(b) summarizes the *MT* concentration in the liver and jejunum. Heat stress increased ($P < 0.05$) the *MT* concentration in the liver. Moreover, the *MT* concentration in the jejunum was decreased under heat stress conditions ($P < 0.05$).
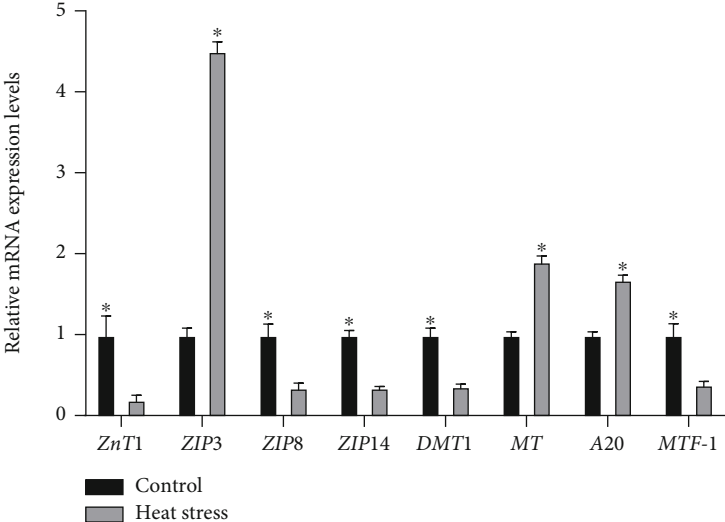
(a)
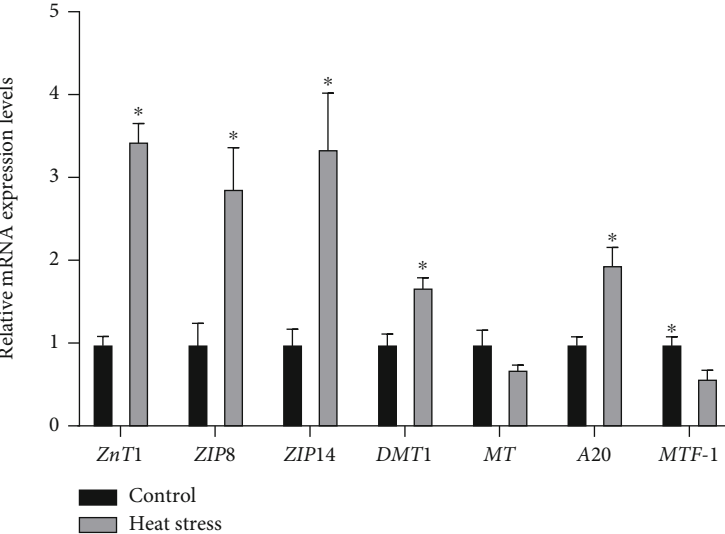
(b)

Figure 4: Continued.
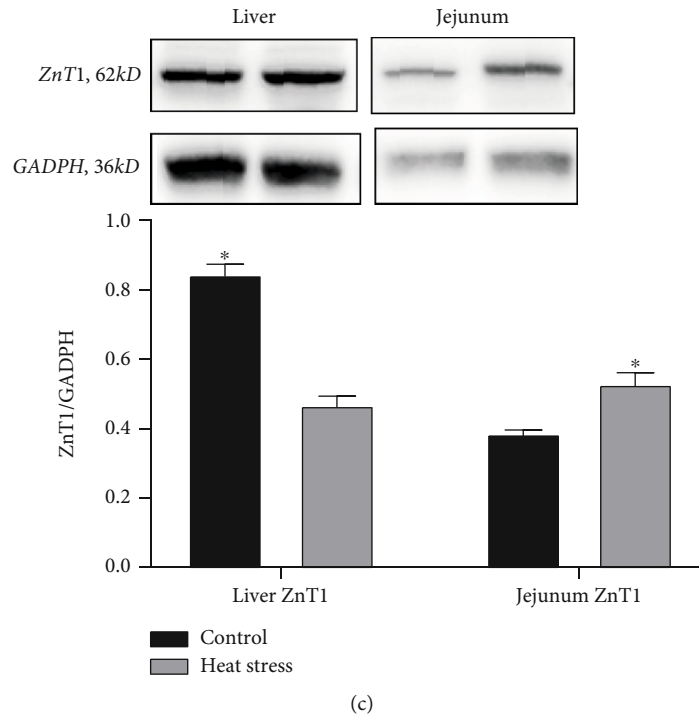
FIGURE 4: Influence of heat stress on gene and protein expression in the liver and jejunum. (a) Zinc transporter- and zinc transporter regulation-related genes in the liver; (b) zinc transporter- and zinc transporter regulation-related genes in the jejunum; (c) protein expression of *ZnT1* in the liver and jejunum. *MT*: metallothionein; ZIP: zinc-regulated transporter, iron-regulated transporter-like protein; ZnT: zinc transporter; *DMT1*: divalent metal transporter 1; *MTF-1*: metal transcription factor-1.

3.5. mRNA Expression of Jejunal and Hepatic Genes. Figure 3(a) shows the mRNA expression of *HSP70* in the jejunum and liver after heat stress. We also determined the mRNA expression levels of the immune and inflammatory genes calprotectin *NF-κB* and *S100A9* (Figures 3(b) and 3(c)). In general, the expression of the *HSP70* gene in the jejunum was upregulated after heat stress ($P < 0.05$). Moreover, the expression levels of *S100A9* and *NF-κB* in the liver were upregulated ($P < 0.05$).

Figure 4 shows that heat stress altered zinc metabolism in the liver and jejunum, which plays a crucial role in regulating systemic zinc homeostasis. The expression of the zinc transporters *ZnT1*, *ZIP8*, and *ZIP14* was downregulated ($P < 0.05$), and that of the divalent metal transporter 1 (*DMT1*) showed the same trend ($P < 0.05$) in the liver. The mRNA expression of the zinc importer *ZIP3* was significantly upregulated ($P < 0.05$) in the livers of heat-stressed broilers (Figure 4(a)). Moreover, heat stress increased the gene expression levels ($P < 0.05$) of zinc transporters (*ZnT1*, *ZIP8*, and *ZIP14*) and *DMT1* in the jejunum (Figure 4(b)). Heat stress resulted in higher gene expression levels of *MT* and the zinc finger protein *A20* ($P < 0.05$) in the liver, and *A20* expression showed the same trend in the jejunum. The expression of metal-binding transcription factor-1 (*MTF-1*) was downregulated ($P < 0.05$) in both organs.

3.6. Protein Expression of Jejunal and Hepatic Genes. As shown in Figure 4(c), heat stress elevated the protein expression of *ZnT1* in the liver but decreased the protein expres-

sion of *ZnT1* in the jejunum ($P < 0.05$). This result confirmed the same trend as the gene expression results.

3.7. Composition and Community Diversity of the Cecal Microbiota. In 35-day-old broilers, 174 OTUs were identical in the cecal contents of both the heat stress group and normal temperature group, while 198 and 151 OTUs were unique to the normal temperature group and heat stress group, respectively (Figure 5(a)). *β*-Diversity analysis using unweighted UniFrac distance did not show specific clustering between the two treatments (Figure 5(b)). As shown in Figure 5(c), heat stress significantly decreased the Chao1, PD, Shannon, and Simpson indices of *α* diversity ($P < 0.05$).

Phylum level-based analyses showed that over 95% of the cecal microbiota in both treatment groups was dominated by three major phyla: *Bacteroidetes*, *Firmicutes*, and *Proteobacteria* (Figure 6). There was no significant effect of heat stress on the relative abundance of the cecum microbial community at the phylum level. Taxonomic analysis of the relative abundances of the 20 predominant genera in each group was used to confirm specific changes in the microbial community (Figure 7(a)). The results showed that heat stress reduced the relative abundances of *Bilophila* and *Dialister* at the genus level (Figure 7(b)).

4. Discussion

Heat stress causes a variety of physiological changes, such as oxidative stress and immune function suppression, leading to increased mortality and decreased feed efficiency, body

(a)

(b)

(c)
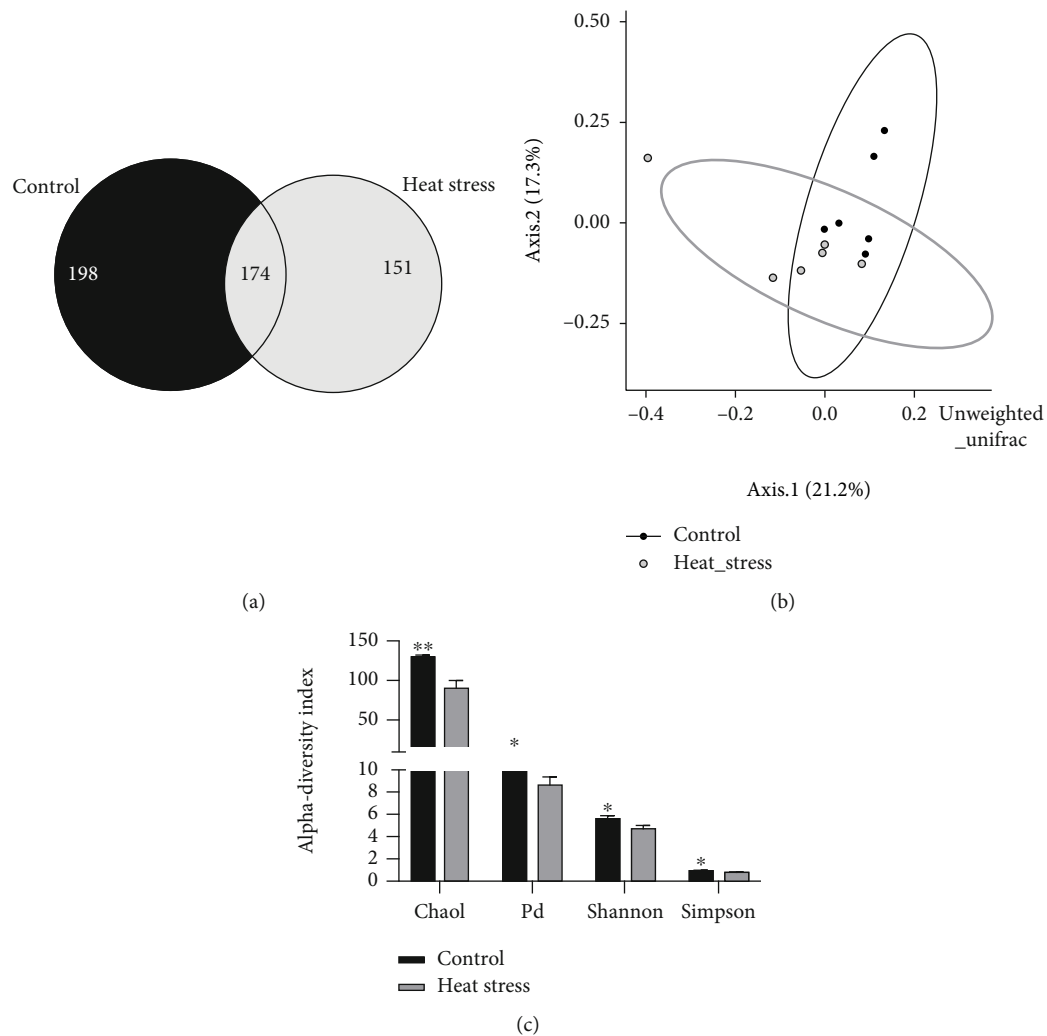
FIGURE 5: Heat stress altered the community diversity of the cecal microbiota. (a) Venn diagram based on the OTU level. (b) PCoA plots of β diversity based on OTUs. (c) α-Diversity based on the Chao1, PD, Shannon, and Simpson indices.

weight, and feed intake [19, 20]. In the present study, heat stress decreased broiler performance, as manifested by the decrease in ADFI and ADG. High temperatures increased mortality in broilers from 1% to 11%, while feed conversion rates more than doubled. The effect of heat stress has been reported to be responsible for the decrease in feed intake as well as layer weight, feed utilization, and egg production and quality [21]. Birds need to breathe to release heat at high ambient temperatures. A previous study indicated that eating is restricted during heat stress because birds cannot simultaneously breathe and eat. Therefore, birds spend more time panting than eating when exposed to high temperatures [22]. Another reason is that hyperthermic birds aim to reduce metabolic heat by eating less to decrease heat generation [23].

High temperatures can cause oxidative stress. The levels of MDA and T-SOD can effectively assess the antioxidant balance of animals [24]. The activity of antioxidant enzymes in the liver and serum significantly increase with increasing environmental temperature [25]. In the present study, heat stress increased the T-SOD content in broiler serum as a

protective response to oxidative stress [26]. Exposure to acute heat stress (35.0°C, 3 h) resulted in increased liver lipid peroxidation in broilers. However, heat stress did not affect the serum MDA level of broilers, which may be related to the duration of exposure to heat stress. Under heat stress conditions, the blood flow distribution changes from the visceral capillaries to the peripheral capillaries, resulting in a rapid drop in body temperature [27]. However, reduced visceral blood flow may lead to hypoxia in gastrointestinal tissues [28], oxidative stress damage, and increased permeability to pathogens and related endotoxins [29]. Heat stress increases the serum endotoxin (ET) content, suggesting increased intestinal permeability.

HSP is a protein chaperone in cells that senses oxidative damage and plays a role in cell protection under various stresses [30]. Consistent with the present study, previous work has reported that the expression of *HSP70* increased in the presence of oxidative stress [31]. The *NF-κB* pathway is a ubiquitous participator in the expression of proinflammatory cytokines, such as IL-1β, IL-6, IL-8, and TNF-α, after an inflammatory challenge with lipopolysaccharide (LPS)

[32]. Heat stress can activate the expression of *NF-κB* in the liver and jejunum of birds, leading to the secretion of a series of proinflammatory cytokines [33, 34]. Calprotectin is also a biomarker of inflammation and belongs to the S100 protein family, whose expression is elevated in the gut and liver following inflammatory infection [35]. In the present study, the expression levels of *NF-κB* and *S100A9* were upregulated in the liver, similar to those of *HSP70* in the jejunum. Hence, oxidative stress caused by heat stress can change the expression of immune regulatory genes and inflammatory marker genes and eventually lead to an increase in the serum levels of anti-inflammatory cytokines (IL-4, IL-6, and IL-10).

As a classical type 2 nutrient, zinc should be ingested frequently, and its homeostasis must be regulated accurately [36]. After heat stress, zinc in the liver was redistributed, and *MT* gene expression in the liver was upregulated, indicating that the liver increased zinc storage in response to oxidative stress, as demonstrated by the increase in zinc content in the liver, tibia, and jejunum. In the carrier-mediated process of zinc absorption [37], zinc can be absorbed into intestinal epithelial cells through the enterocyte apical membrane by *DMT1* and ZIP family transporters [38] and then stored for binding with metallothionein. The zinc exporter *ZnT1* is located at the basolateral membrane and contributes to the transport of zinc from the intestine into the portal vein circulation. The liver plays an important role in zinc homeostasis due to its rich content and fast exchange in the metabolism of zinc [39]. Zinc uptake by the liver is necessary for the plasma through the regulation of transporter proteins. The importer *ZIP3* is involved in the transport of zinc from serum to the liver, where zinc is stored in cells after binding to metallothionein and transported out of the liver by the exporter *ZnT1* [40].

Our results suggested that zinc was redistributed in the jejunum and liver after heat stress. The expression levels of zinc importers (*DMT1*, *ZIP8*, and *ZIP14*) and the exporter *ZnT1* increased in the jejunum, indicating that more zinc was absorbed from the intestinal tract as evidenced by a decrease in the concentration of zinc in the intestinal contents. More interestingly, the expression of *ZIP3* increased and that of *ZnT1* decreased, which meant that the liver needed more zinc reserves, as reflected by the higher contents of liver *MT* and zinc. Heat stress altered zinc homeostasis in chickens, as reflected in the increased zinc contents in tissues and bone. The adjustment of zinc transporter levels in different organs played an incredible role in increasing the ability of zinc to be absorbed in the intestine, while the liver, as a major organ of metabolism, had an increased ability to store zinc. Oxidative stress and immune challenge process is accompanied by a decrease in serum zinc concentration and an increase in liver zinc concentration providing antioxidant defense system [41]. Similar to the results after seven days of Salmonella infection in broilers [42], we did not find a decrease trend in serum zinc concentrations after heat stress, which should be attributed to the adaptation of broilers to temperature and adequate zinc content in the feed.

Accumulating evidence shows that oxidative stress can alter the expression of zinc transporters [43]. *ZIP14* directly
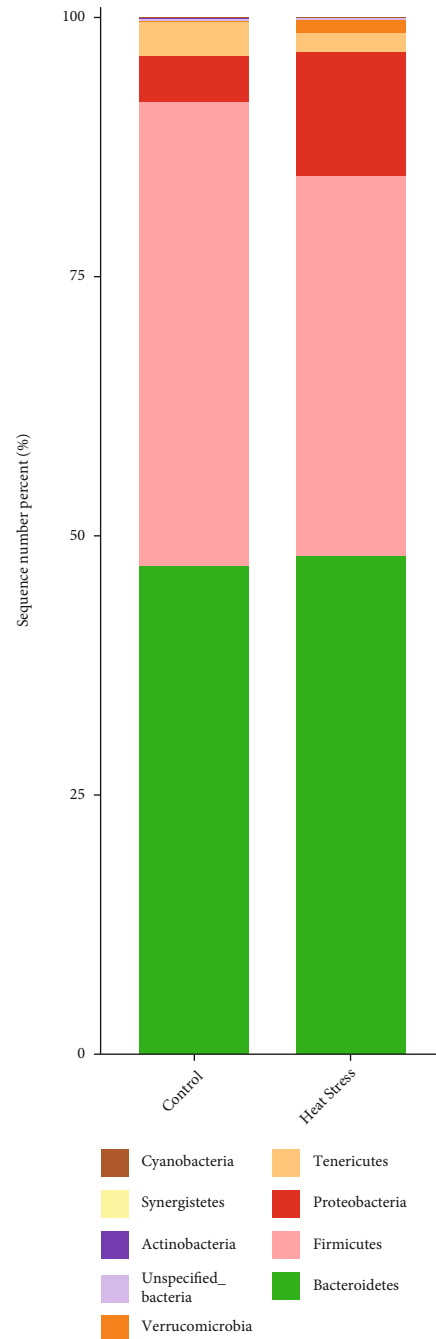
FIGURE 6: Average relative abundances of predominant bacteria at the phylum level in cecal contents.

or indirectly promotes intestinal zinc absorption and regulates zinc metabolism in response to inflammatory stimuli in the liver [44]. Oxidative stress induced by chronic alcohol exposure can downregulate the expression of the zinc transporter *ZIP14* in mouse hepatocytes [45]. In aged cardiomyocytes, the *ZIP8* level has been found to decrease with increasing ROS levels [46]. *ZIP8* and *ZIP14* are configured differently from the other members of the ZIP family because a histidine is replaced by glutamic acid [47], which may be the key to their immunity and antioxidant roles. As the only zinc-sensitive transcription factor, *MTF-1* is
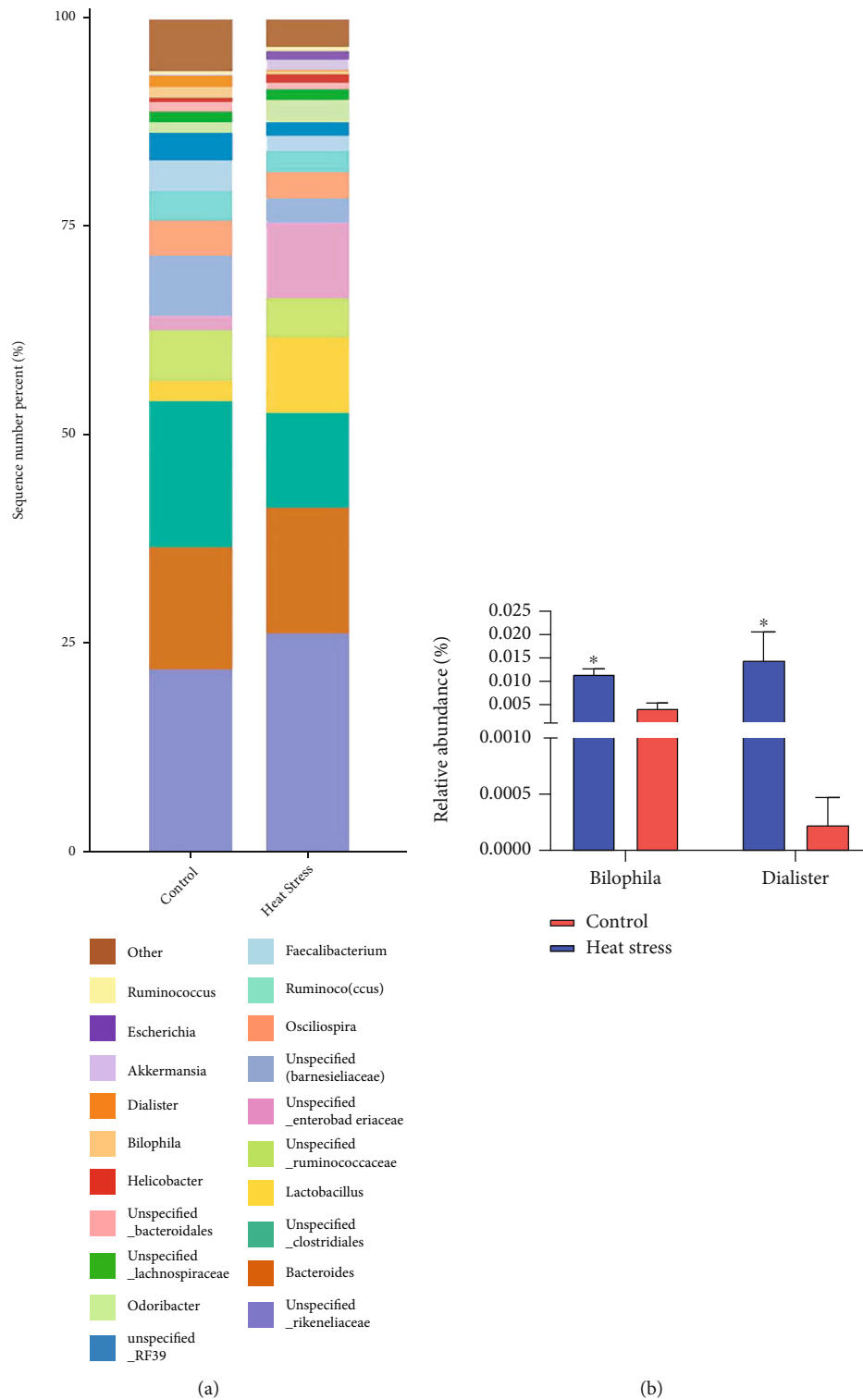
FIGURE 7: Alteration of the cecal microbiota at the genus level. (a) Average relative abundances of predominant bacteria (top 20) at the genus level in cecal contents. (b) Relative abundances of *Bilophila* and *Dialister*.

involved in zinc concentration sensing and *MT* regulation [48]. *MT* not only regulates the concentration of free zinc in cells but also affects the production of ROS in cells to resist stress by regulating the expression of *NF-κB* [49]. Zinc concentration affects the expression of the zinc finger protein *A20*, which in turn changes the ability of *NF-κB* to assemble with DNA and reduces the inflammatory response caused by oxidative stress [50]. Heat stress decreased the expression of *MTF-1* and increased the expression of *A20* in the liver and jejunum, indicating that the increase in the tissue zinc concentration downregulated the expression of the sensing gene *MTF-1*, while the zinc finger protein *A20*

activated the anti-inflammatory effect of *NF-κB*. These modifications support the physiological significance of greater accumulation of zinc in tissues for the promotion of zinc-mediated antioxidant actions.

The cecal microbiota resists inflammatory bowel disease and metabolic disorders and helps maintain normal barrier function and antioxidant capacity [51, 52]. Our results confirm that heat stress alters the microbial composition of the broiler cecum and that lower levels of intestinal microbes may be associated with the negative effects of heat stress on intestinal health and microbial community stability. We did not find significant correlations between heat stress and the cecum microbiota at the phylum level, similar to previous findings in yellow-feathered broilers [53]. At the genus level, heat stress treatment reduced the relative abundances of *Bilophila* and *Dialister*. *Bilophila* is involved in the anaerobic metabolic pathway that converts the substrate taurine, which is abundant in the gut microbiota, into the toxic metabolite hydrogen sulfide. A reduction in the relative abundance of *Bilophila* predicts a weakening of intestinal immune stimulation and the inflammatory response after heat stress treatment [54]. In the gut microbiota of pigs fed higher levels of lysine-chelated zinc diets, *Dialister* had a high relative abundance, promoting the decarboxylation of succinate to propionate [55]. Propionic acid is a short-chain fatty acid (SCFA), and zinc can result in the enrichment of beneficial SCFAs by increasing the abundance of corresponding bacteria in the gut, thereby influencing the composition of the microbiota to promote zinc absorption by the host [56]. In our study, heat stress enhanced intestinal absorption of zinc via transporter proteins, leading to a low-zinc environment in the gut and resulting in a decrease in the relative abundance of *Dialister*. Therefore, the reduction in cecum microbial abundance in broiler chickens due to heat stress is associated with an attenuated inflammatory response and a low-zinc environment in the intestine.

5. Conclusions

Heat stress could cause oxidative stress and immune challenge in broilers, which can be reflected in the decrease in production performance. Our results confirmed the remodeling of zinc homeostasis in broilers under heat stress and identified the role of zinc transporters and metallothionein in the liver and jejunum during this process. The effects of heat stress on the gut microbiota seem to be involved in the redistribution of zinc, which will be further explored in future studies.

Abbreviations

ROS: Reactive oxygen species
MDA: Malondialdehyde
GPX: Glutathione peroxidase
T-SOD: Total superoxide dismutase
HSP: Heat shock protein
NF-κB: Nuclear factor kappa light chain enhancer of B cells
MT: Metallothionein

ZIP: Zinc-regulated transporter:
ZnT: Zinc transporter, iron-regulated transporter-like protein
ADFI: Average daily feed intake
ADG: Average daily gain
FCR: Feed conversion ratio
AST: Aspartate aminotransferase
ALT: Alanine aminotransferase
CV: Coefficient of variation
IL-1β: Interleukin 1β
IL-4:   Interleukin 4
IL-6:   Interleukin 6
IL-10:   Interleukin 10
TNF-α: Tumor necrosis factor-α
GADPH: Glyceraldehyde-3-phosphate dehydrogenase
DMT1:   Divalent metal transporter 1
MTF-1:   Metal transcription factor-1
PVDF: Polyvinylidene difluoride
OTUs: Operational taxonomic units.

Data Availability

The 16S rRNA sequence data used to support the findings of this study have been deposited in the GenBank repository (PRJNA770158).

Conflicts of Interest

The authors declare no conflicts of interest.

Acknowledgments

References

[1] C. W. Tallentire, I. Leinonen, and I. Kyriazakis, "Breeding for efficiency in the broiler chicken: a review," *Agronomy for Sustainable Development*, vol. 36, no. 4, p. 66, 2016.

[2] L. Liu, M. Ren, K. Ren, Y. Jin, and M. Yan, "Heat stress impacts on broiler performance: a systematic review and meta- analysis," *Poultry Science*, vol. 99, no. 11, pp. 6205–6211, 2020.

[3] N. K. Emami, U. Jung, B. Voy, and S. Dridi, "Radical response: effects of heat stress-induced oxidative stress on lipid metabolism in the avian liver," *Antioxidants*, vol. 10, no. 1, p. 35, 2021.

[4] S. J. Hosseini-Vashan, A. Golian, and A. Yaghobfar, "Growth, immune, antioxidant, and bone responses of heat stress-exposed broilers fed diets supplemented with tomato pomace," *International Journal of Biometeorology*, vol. 60, no. 8, pp. 1183–1192, 2016.

[5] J. Uerlings, Z. G. Song, X. Y. Hu et al., "Heat exposure affects jejunal tight junction remodeling independently of adenosine monophosphate-activated protein kinase in 9-day-old broiler chicks," *Poultry Science*, vol. 97, no. 10, pp. 3681–3690, 2018.

[6] K. Kumada, N. Fuse, T. Tamura, C. Okamori, and S. Kurata, "HSP70/DNAJA3 chaperone/cochaperone regulates NF-κB activity in immune responses," *Biochemical and Biophysical Research Communications*, vol. 513, no. 4, pp. 947–951, 2019.

[7] G. Wu, *Principles of Animal Nutrition*, CRC Press, 2017.

[8] T. Kambe, Y. Yamaguchi-Iwai, R. Sasaki, and M. Nagao, "Overview of mammalian zinc transporters," *Cellular and Molecular Life Sciences: CMLS*, vol. 61, no. 1, pp. 49–68, 2004.

[9] A. K. Baltaci, K. Yuce, and R. Mogulkoc, "Zinc metabolism and metallothioneins," *Biological Trace Element Research*, vol. 183, no. 1, pp. 22–31, 2018.

[10] E. Mocchegiani, L. Costarelli, R. Giacconi, F. Piacenza, A. Basso, and M. Malavolta, "Zinc, metallothioneins and immunosenescence: effect of zinc supply as nutrigenomic approach," *Biogerontology*, vol. 12, no. 5, pp. 455–465, 2011.

[11] T. Kambe, T. Tsuji, A. Hashimoto, and N. Itsumura, "The physiological, biochemical, and molecular roles of zinc transporters in zinc homeostasis and metabolism," *Physiological Reviews*, vol. 95, no. 3, pp. 749–784, 2015.

[12] A. S. Prasad, B. Bao, F. W. Beck, and F. H. Sarkar, "Zinc-suppressed inflammatory cytokines by induction of A20-mediated inhibition of nuclear factor-κB," *Nutrition*, vol. 27, no. 7-8, pp. 816–823, 2011.

[13] A. Gheisari, A. Sanei, A. Samie, M. Gheisari, and M. Toghyani, "Effect of diets supplemented with different levels of manganese, zinc, and copper from their organic or inorganic sources on egg production and quality characteristics in laying hens," *Biological Trace Element Research*, vol. 142, no. 3, pp. 557–571, 2011.

[14] Y. Attia, A. Abd Al-Hamid, H. Zeweil et al., "Effect of dietary amounts of inorganic and organic zinc on productive and physiological traits of white Pekin ducks," *Animal*, vol. 7, no. 6, pp. 895–900, 2013.

[15] C. Bortoluzzi, B. S. Vieira, and T. J. Applegate, "Influence of dietary zinc, copper, and manganese on the intestinal health of broilers under Eimeria challenge," *Frontiers in Veterinary Science*, vol. 7, p. 13, 2020.

[16] V. Kloubert, I. Wessels, J. Wolf et al., "Zinc deficiency leads to reduced interleukin-2 production by active gene silencing due to enhanced CREMα expression in T cells," *Clinical Nutrition*, vol. 40, no. 5, pp. 3263–3278, 2020.

[17] K. Sahin, N. Sahin, O. Kucuk, A. Hayirli, and A. S. Prasad, "Role of dietary zinc in heat-stressed poultry: a review," *Poultry Science*, vol. 88, no. 10, pp. 2176–2183, 2009.

[18] Z. Zhou, L. Wang, Z. Song, J. T. Saari, C. J. McClain, and Y. J. Kang, "Zinc supplementation prevents alcoholic liver injury in mice through attenuation of oxidative stress," *The American Journal of Pathology*, vol. 166, no. 6, pp. 1681–1690, 2005.

[19] S. Wasti, N. Sah, and B. Mishra, "Impact of Heat Stress on Poultry Health and Performances, and Potential Mitigation Strategies," *Animals*, vol. 10, no. 8, p. 1266, 2020.

[20] Y. A. Attia and S. S. Hassan, "Broiler tolerance to heat stress at various dietary protein/energy levels," *European Poultry Science*, vol. 81, no. 10.1399, 2017.

[21] W. Deng, X. Dong, J. M. Tong, and Q. Zhang, "The probiotic _Bacillus licheniformis_ ameliorates heat stress-induced impairment of egg production, gut morphology, and intestinal mucosal immunity in laying hens[1]," *Poultry Science*, vol. 91, no. 3, pp. 575–582, 2012.

[22] L. A. Mack, J. N. Felver-Gant, R. L. Dennis, and H. W. Cheng, "Genetic variations alter production and behavioral responses following heat stress in 2 strains of laying hens," *Poultry Science*, vol. 92, no. 2, pp. 285–294, 2013.

[23] I. Belhadj Slimen, T. Najar, A. Ghram, and M. Abdrrabba, "Heat stress effects on livestock: molecular, cellular and meta-

bolic aspects, a review," *Journal of Animal Physiology and Animal Nutrition*, vol. 100, no. 3, pp. 401–412, 2016.

[24] Y. A. Attia, M. A. Al-Harthi, and H. M. Abo El-Maaty, "The effects of different oil sources on performance, digestive enzymes, carcass traits, biochemical, immunological, antioxidant, and morphometric responses of broiler chicks," *Frontiers in Veterinary Science*, vol. 7, p. 181, 2020.

[25] G. Y. Tan, L. Yang, Y. Q. Fu, J. H. Feng, and M. H. Zhang, "Effects of different acute high ambient temperatures on function of hepatic mitochondrial respiration, antioxidative enzymes, and oxidative injury in broiler chickens," *Poultry Science*, vol. 89, no. 1, pp. 115–122, 2010.

[26] M. J. Thomas, "The role of free radicals and antioxidants," *Nutrition*, vol. 16, no. 7-8, pp. 716–718, 2000.

[27] M. Shakeri, E. Oskoueian, H. H. Le, and M. Shakeri, "Strategies to combat heat stress in broiler chickens: unveiling the roles of selenium, vitamin E and vitamin C," *Veterinary Sciences*, vol. 7, no. 2, p. 71, 2020.

[28] D. M. Hall, G. R. Buettner, L. W. Oberley, L. Xu, R. D. Matthes, and C. V. Gisolfi, "Mechanisms of circulatory and intestinal barrier dysfunction during whole body hyperthermia," *American Journal of Physiology. Heart and Circulatory Physiology*, vol. 280, no. 2, pp. H509–H521, 2001.

[29] M. Shakeri, J. J. Cottrell, S. Wilkinson et al., "Dietary betaine improves intestinal barrier function and ameliorates the impact of heat stress in multiple vital organs as measured by Evans blue dye in broiler chickens," *Animals*, vol. 10, no. 1, p. 38, 2020.

[30] X. Cong, Q. Zhang, H. Li et al., "Puerarin ameliorates heat stress-induced oxidative damage and apoptosis in bovine Sertoli cells by suppressing ROS production and upregulating Hsp72 expression," *Theriogenology*, vol. 88, pp. 215–227, 2017.

[31] S. Tang, B. Yin, J. Xu, and E. Bao, "Rosemary reduces heat stress by inducing CRYAB and HSP70 expression in broiler chickens," *Oxidative Medicine and Cellular Longevity*, vol. 2018, Article ID 7014126, 2018.

[32] B. R. B. Pires, R. Silva, and G. M. Ferreira, "NF-kappaB: two sides of the same coin," *Genes*, vol. 9, no. 1, p. 24, 2018.

[33] C. Orhan, F. Akdemir, N. Sahin et al., "Chromium histidinate protects against heat stress by modulating the expression of hepatic nuclear transcription factors in quail," *British Poultry Science*, vol. 53, no. 6, pp. 828–835, 2012.

[34] K. Sahin, C. Orhan, F. Akdemir, M. Tuzcu, C. Iben, and N. Sahin, "Resveratrol protects quail hepatocytes against heat stress: modulation of the Nrf 2 transcription factor and heat shock proteins," *Journal of Animal Physiology and Animal Nutrition*, vol. 96, no. 1, pp. 66–74, 2012.

[35] M. Abildtrup, G. H. Kingsley, and D. L. Scott, "Calprotectin as a biomarker for rheumatoid arthritis: a systematic review," *The Journal of Rheumatology*, vol. 42, no. 5, pp. 760–770, 2015.

[36] M. T. Baer and J. C. King, "Tissue zinc levels and zinc excretion during experimental zinc depletion in young men," *The American Journal of Clinical Nutrition*, vol. 39, no. 4, pp. 556–570, 1984.

[37] J. Condomina, T. Zornoza-Sabina, L. Granero, and A. Polache, "Kinetics of zinc transport in vitro in rat small intestine and colon: interaction with copper," *European Journal of Pharmaceutical Sciences: Official Journal of the European Federation for Pharmaceutical Sciences*, vol. 16, no. 4-5, pp. 289–295, 2002.

[38] S. Hojyo and T. Fukada, "Zinc transporters and signaling in physiology and pathogenesis," *Archives of Biochemistry and Biophysics*, vol. 611, pp. 43–50, 2016.

[39] N. E. Krebs and K. M. Hambidge, "Zinc metabolism and homeostasis: the application of tracer techniques to human zinc physiology," *Zinc Biochemistry, Physiology, and Homeostasis*, vol. 14, no. 3/4, pp. 397–412, 2001.

[40] R. E. Dempski, "The cation selectivity of the ZIP transporters," *Current Topics in Membranes*, vol. 69, pp. 221–245, 2012.

[41] J. P. Liuzzi, L. A. Lichten, S. Rivera et al., "Interleukin-6 regulates the zinc transporter Zip 14 in liver and contributes to the hypozincemia of the acute-phase response," *Proceedings of the National Academy of Sciences of the United States of America*, vol. 102, no. 19, pp. 6843–6848, 2005.

[42] A. Wu, S. Bai, X. Ding et al., "The systemic zinc homeostasis was modulated in broilers challenged by salmonella," *Biological Trace Element Research*, vol. 196, no. 1, pp. 243–251, 2020.

[43] D. D. Marreiro, K. J. Cruz, J. B. Morais, J. B. Beserra, J. S. Severo, and A. R. de Oliveira, "Zinc and Oxidative Stress: Current Mechanisms," *Antioxidants*, vol. 6, no. 2, p. 24, 2017.

[44] T. B. Aydemir, S. M. Chang, G. J. Guthrie et al., "Zinc transporter ZIP14 functions in hepatic zinc, iron and glucose homeostasis during the innate immune response (endotoxemia)," *PLoS One*, vol. 7, no. 10, article e48679, 2012.

[45] Q. Sun, Q. Li, W. Zhong et al., "Dysregulation of hepatic zinc transporters in a mouse model of alcoholic liver disease," *American Journal of Physiology. Gastrointestinal and Liver Physiology*, vol. 307, no. 3, pp. G313–G322, 2014.

[46] Y. Olgar, E. Tuncay, and B. Turan, "Mitochondria-targeting antioxidant provides cardioprotection through regulation of cytosolic and mitochondrial Zn2+ levels with re-distribution of Zn2+-Transporters in aged Rat Cardiomyocytes," *International Journal of Molecular Sciences*, vol. 20, no. 15, p. 3783, 2019.

[47] H. Fujishiro, Y. Yano, Y. Takada, M. Tanihara, and S. Himeno, "Roles of ZIP8, ZIP14, and DMT1 in transport of cadmium and manganese in mouse kidney proximal tubule cells," *Metallomics*, vol. 4, no. 7, pp. 700–708, 2012.

[48] G. W. Stuart, P. F. Searle, and R. D. Palmiter, "Identification of multiple metal regulatory elements in mouse metallothionein-I promoter by assaying synthetic sequences," *Nature*, vol. 317, no. 6040, pp. 828–831, 1985.

[49] A. Wu, P. Tymoszuk, D. Haschka et al., "Salmonella utilizes zinc to subvert antimicrobial host defense of macrophages via modulation of NF-κB signaling," *Infection and Immunity*, vol. 85, no. 12, p. 12, 2017.

[50] C. I. Morgan, J. R. Ledford, P. Zhou, and K. Page, "Zinc supplementation alters airway inflammation and airway hyperresponsiveness to a common allergen," *Journal of Inflammation*, vol. 8, no. 1, p. 36, 2011.

[51] F. Sommer, J. M. Anderson, R. Bharti, J. Raes, and P. Rosenstiel, "The resilience of the intestinal microbiota influences health and disease," *Nature Reviews Microbiology*, vol. 15, no. 10, pp. 630–638, 2017.

[52] A. M. Shehata, V. K. Paswan, Y. A. Attia et al., "Managing gut microbiota through in ovo nutrition influences early-life programming in broiler chickens," *Animals*, vol. 11, no. 12, p. 3491, 2021.

[53] Y. Huang, H. Lv, Y. Song, C. Sun, Z. Zhang, and S. Chen, "Community composition of cecal microbiota in commercial yellow broilers with high and low feed efficiencies," *Poultry Science*, vol. 100, no. 4, article 100996, 2021.

[54] S. C. Peck, K. Denger, A. Burrichter, S. M. Irwin, E. P. Balskus, and D. Schleheck, "A glycyl radical enzyme enables hydrogen sulfide production by the human intestinal bacterium *Bilophila wadsworthia*," *Proceedings of the National Academy of Sciences of the United States of America*, vol. 116, no. 8, pp. 3171–3176, 2019.

[55] R. Pieper, T. H. Dadi, L. Pieper et al., "Concentration and chemical form of dietary zinc shape the porcine colon microbiome, its functional capacity and antibiotic resistance gene repertoire," *The ISME Journal*, vol. 14, no. 11, pp. 2783–2793, 2020.

[56] S. Reed, M. Knez, A. Uzan et al., "Alterations in the gut (Gallus gallus) microbiota following the consumption of zinc biofortified wheat (Triticum aestivum)-based diet," *Journal of Agricultural and Food Chemistry*, vol. 66, no. 25, pp. 6291–6299, 2018.

Research Article

Effect of Li-ESWT on Testicular Tissue and Function in Androgen-Deficient Rat Model

Wen Jie Tian,[1,2,3,4] Seung Hwan Jeon,[5] Hyuk Jin Cho,[2] U-Syn Ha,[2] Sung-Hoo Hong,[2] Ji Youl Lee,[2] Jun Jie Piao,[2,3] Zhong Cheng Xin,[4,6] Ye Gang Chen,[4,6] Hong Yu Feng,[4,6] Sae Woong Kim,[2,3,4] Woong Jin Bae ⓘ,[2,3,4] and Mahadevan Raj Rajasekaran ⓘ[7]

[1]*Department of Urology, Second Hospital of Jilin University, China*
[2]*Department of Urology, College of Medicine, The Catholic University of Korea, Seoul, Republic of Korea*
[3]*Catholic Integrative Medicine Research Institute, The Catholic University of Korea, Seoul, Republic of Korea*
[4]*China-Korea Joint Research Center for Male Reproductive and Sexual Medicine, Tianjin Institute of Urology, Tianjin, China*
[5]*Department of Clinical Laboratory Science, Suwon Science College, Hwaseong, Republic of Korea*
[6]*Department of Male Reproductive and Sexual Medicine and Department of Urology, The Second Hospital of Tianjin Medical University, Tianjin, China*
[7]*Department of Urology, San Diego School of Medicine, University of California, CA, USA*

Correspondence should be addressed to Woong Jin Bae; bwoong@catholic.ac.kr
and Mahadevan Raj Rajasekaran; mrajasekaran@health.ucsd.edu

Low-intensity extracorporeal shockwave therapy (Li-ESWT), as a microenergy therapy, has the effects of inhibiting oxidative stress, antiapoptosis, and tissue repair, which is increasingly applied to a variety of diseases. Our research aims to explore the protective effects of Li-ESWT in the aging rat model and its possible molecular mechanism through in vivo and in vitro experiments. In vitro, TM3 Leydig cells incubated with H_2O_2 were treated with Li-ESWT at 4 energy levels (0.01, 0.05, 0.1, and 0.2 mJ/mm^2). In vivo, we employed an androgen-deficient rat model to simulate male aging and treated it with Li-ESWT at three different energy levels (0.01, 0.05, and 0.2 mJ/mm^2). Li-ESWT increased the expression of vascular endothelial growth factor (VEGF) in TM3 cells, improved antioxidant capacity, and reduced apoptosis, with the effect being most significant at 0.05 mJ/mm^2 energy level. In androgen-deficient rat model, LI-ESWT can improve sperm count, motility, and serum testosterone level, enhancing tissue antioxidant capacity and antiapoptotic ability, and the effect is most significant at 0.05 mJ/mm^2 energy level. Therefore, Li-ESWT at an appropriate energy level can improve sperm count, motility, and serum testosterone levels in androgen-deficient rat models, reduce oxidative stress in the testis, and increase antioxidant capacity and antiapoptotic abilities. The mechanism of this condition might be related to the increased VEGF expression in Leydig cells by Li-ESWT.

1. Introduction

Aging is a complex phenomenon attributed to developmental, genetic defects, environmental, disease, and hereditary factors, which accumulate adverse changes that increase disease risk [1]. Androgen-deficient is a common manifestation of aging in men, affecting up to 25% of older men, more than 10% of whom present as clinical symptoms of hypogonad-

ism [2]. Johnson et al. [3] reported that the volume of testis increases in adolescence, peaks at the age of 30, and significantly declines after the age of 60. Testicular volume in elderly men is positively correlated with serum testosterone [4]. In previous studies, a comparative analysis [5] investigated the variation of testicular structure and function of 30 men age between 22-48 and 50-76 years, indicating that the average total number of Leydig cells in the oldest group

decreased by 44% and thus affected the production of testosterone. However, some research results suggest the opposite conclusion [6, 7]. Although age-related regulation of the Leydig cell population remains controversial, some evidence in the literature shows that change in the maintenance of the redox balance within the Leydig cells affects their function. Previous research revealed that the superoxide content in aging Leydig cells is remarkably higher than in young Leydig cells [8]. Furthermore, the evidence of elevated levels of reactive oxygen species has been reported to be detected in 30-80% of infertile men's semen, showing that oxidative stress plays a critical role in male infertility. Oxidative stress can negatively affect fertility through a variety of pathways, interference with spermatozoa capacitation, and peroxidative damage to sperm membranes, proteins, and DNA, which are deleterious to the sperm's potential and decrease the chances of the fertilized egg developing into a healthy early embryo [9].

In urology, low-intensity extracorporeal shockwave therapy (Li-ESWT) is mainly used for Peyronie disease, chronic pelvic pain, and erectile dysfunction [10–12]. However, the effect of Li-ESWT on testicles and sperm is not well understood, so there are concerns about using Li-ESWT to treat male diseases. Studies have shown [13] that Li-ESWT has the effect of inhibiting oxidative stress and antiapoptosis. In our previous study, we found that Li-ESWT showed a dramatic promotion effect on the expression of vascular endothelial growth factor (VEGF) in the cavernous body [14, 15], and VEGF can stimulate the release of testosterone in Leydig cells [16]. Therefore, we hypothesized that Li-ESWT might positively affect testicles in older men.

The purpose of the present study was to investigate the restorative effects of Li-ESWT in the androgen-deficient rat model and to investigate the mechanism of Li-ESWT in TM3 Leydig cells in vitro.

2. Materials and Methods

2.1. In Vitro Immunofluorescence and Western Blot Testing Using TM3 Mouse Leydig Cells. TM3 cells, an immature mouse Leydig cell line (Korean Cell Line Bank, Seoul, Korea), were cultured in Dulbecco's modified Eagle's medium (DMEM)/F-12 medium (GIBCO, Life Technologies Co., USA) supplemented with 10% heat-inactivated fetal bovine serum (FBS; GIBCO) in a humidified atmosphere with 5% CO_2/95% air at 37°C.

Cells (1×10^6 cells) were plated on 6-well plates (Corning) in 10% FBS/DMEM/F-12 and subsequently incubated for 24 h. Oxidative cell stress was induced by treatment with $40 \mu M$ H_2O_2 for 2 hours. Cells in each treatment group were given different energy levels of Li-ESWT (CENOWAVE; HNT MEDICAL Co., Ltd., Seoul, Korea) with 300 shocks each time, once a day, for a total of 7 times a week. TM3 cells were immobilized with 4% PFA for 15 min, then treated with cold methanol for 15 min, and permeated with 0.2% Triton X-100 in PBS at 4°C for 15 min. After washing with PBS, TM3 cells were incubated in a blocking solution (PBS containing 10% goat serum). TM3 cells were then combined with an anti-VEGF (1 : 500 dilution; Santa Cruz Biotechnol-

ogy, USA) and β-actin (1 : 500 dilution; Santa Cruz Biotechnology, USA), staying overnight at 4°C. On the second day, TM3 cells were mixed with goat anti-rabbit IgG H&L (FITC) (1 : 100; Abcam, UK); after washing with PBS at room temperature for 2 h, the nuclei were identified by DAPI for 15 min and then rinsed with PBS and sealed.

Cells (1×10^6 cells) were plated on 6-well plates (Corning) in 10% FBS/DMEM/F-12 and subsequently incubated for 24 h. Oxidative cell stress was induced by treatment with $40 \mu M$ H_2O_2 for 2 hours. Cells in each treatment group were given different energy levels L with 300 shocks each time, once a day, for a total of 7 times a week. After processing, we gathered all cellular proteins by placing cells in a lysis buffer consisting of 0.1% sodium dodecyl sulfate in phosphate-buffered saline, followed by brief sonication. Protein concentration was identified by a bicinchoninic acid protein assay (Pierce Chemical Co., USA). Thirty micrograms of total cellular protein was separated by 12% SDS-polyacrylamide gel electrophoresis and then transferred to nitrocellulose membranes. Blots were probed with an antibody specific for the following proteins: β-actin (1: 1000 dilution; Santa Cruz Biotechnology, USA), HO-1 (1: 1000 dilution; Cell Signaling Technology, USA), Nrf2 (1: 500 dilution; Santa Cruz Biotechnology, USA), SOD (1 : 1000, dilution; Abcam, UK), NF-κB (1 : 2000, dilution; Abcam, UK), and COX-2(1 : 1000 dilution; Cell Signaling Technology, USA). The binding antibody of each blot was evaluated by enhancing chemiluminescence (Western blot detection kit; Amersham Pharmacia Biotech, USA), which was assessed with horseradish peroxidase-conjugated secondary antibody.

2.2. Animal Groups and Treatment Protocol. This study was investigated in strict accordance with the recommendations in the Guide for the Care and Use of Laboratory Animals of the National Institutes of Health. The protocol was approved by the Institutional Animal Care and Use Committee in School of Medicine, The Catholic University of Korea (CUMC-2019-0072-03).

Male Sprague-Dawley (SD) rats 270-300 g (8 weeks of age) were randomly divided into four groups (6 rats in each group), which were submitted to (1) receive an intramuscular injection of normal saline (control); (2) receive a subcutaneous injection of an LHRH agonist (leuprolide acetate, Leuplin®; Takeda Pharmaceutical Co., Osaka, Japan) for four weeks to induce androgen-deficient (Leuplin); (3) after induction of androgen-deficient, 0.01 mJ/mm² Li-ESWT was used for four weeks, once a week, 300 shocks each time (ESWT_0.01); (4) after induction of androgen-deficient, 0.05 mJ/mm² Li-ESWT was used for 4 weeks with the same frequency (ESWT_0.05); and (5) after induction of androgen-deficient, 0.2 mJ/mm² Li-ESWT was used for 4 weeks with the same frequency (ESWT_0.2). After 4 weeks, the animals in all groups were sacrificed, and the testes, epididymides, and blood samples were obtained.

2.3. Evaluation of Sperm Count and Motility in Caudal Epididymis. The right epididymis tissue was collected and minced and placed in normal saline containing 0.5% bovine

serum albumin at 37°C and filtered. The sperm suspension was placed on preheated glass slides at 37°C. The sperm count was measured by Neubauer hemocytometer under 400x light microscope. The sperm count represented the number of sperm in 1 ml medium. Freshly collected left epididymis tissue was used for sperm motility analysis. Motile sperm percentage is more than 300 sperm randomly selected under the microscope, counting the motile sperm rate [17]. Each sample was counted three times.

2.4. Measurement of Germinal Cell Layer Thickness.
Testicles were collected, washed with precooled PBS, and immediately impended in 4% paraformaldehyde for over 24 hours. The testicular tissue was corrected and placed into an automatic tissue processor for gradient ethanol dehydration. The sample was embedded in paraffin and cut into $4 \mu m$ sections. Testicular specimens were dewaxed with xylene and ethanol, stained with hematoxylin and eosin, dehydrated, and fixed. Morphological changes of the testis were observed under a microscope, and the thickness of germinal cell layer was measured at 10 representative sites in the seminiferous tubules at random to complete image collection and analysis [18].

2.5. Serum Testosterone Levels.
Before the rats were sacrificed, venous blood of inferior vena cava was taken, and serum testosterone level was measured by testosterone ELISA kit (Competitive ELISA, Immobilized antigen, RTC001R, BioVendor, Czech Republic). Place $10 \mu l$ of sample (each specimen has three wells) with new disposable tips into appropriate wells dispensed in $100 \mu l$ of incubation buffer into each well. Added was $50 \mu l$ enzyme conjugate into each well which was incubated for 60 min at room temperature. This was discarded and well rinsed 4 times with diluted washing solution ($300 \mu l$ per well). Then, $200 \mu l$ of substrate solution was added to each well and incubated standing for 30 min. The reaction was stopped by adding $50 \mu l$ of stop solution to each well and the absorbance determined for each well at 450 nm. Repeat the test 3 times.

2.6. Measurement of Oxidative Stress.
We used 8-hydroxy-2-deoxyguanosine (8-OHdG) level as a biomarker to detect DNA damage in testicular tissue and detected antioxidant levels in vivo by measuring superoxide dismutase (SOD) in testicular tissue. Total DNA was extracted from the testis using the DNeasy Blood & Tissue Kit (Qiagen, Valencia, CA, USA) and DNA oxidation Kit (Highly Sensitive 8-OHdG Check ELISA; Japan Institute for the Control of Aging, Fukuroi, Japan). After adding $3,3',5,5'$-tetramethyl-benzidine for color development, the absorbance was measured at 450 nm. The tissue sample concentrations were measured using standard curves and DNA concentrations were corrected. The SOD activity (CuZnSOD and Mn SOD) in tissues was measured by SOD Assay Kit-WST (DG-SOD400, 400 tests, Dojindo), and the reduction rate of nitroblue tetrazolium mediated by superoxide was monitored by spectrophotometer at 450 nm.

2.7. TUNEL Staining.
Apoptotic cells were detected in situ by indirect TUNEL assay using anti-digoxin antibody bound to fluorescein reporter molecule. Testicular tissue sections were blocked with 0.1% Triton X-100 for 5 minutes and then washed with PBS. Terminal deoxyribonucleotidyl transferase-mediated dUTP-digoxigenin nick-end labeling (TUNEL, ApopTag In Situ Apoptosis Detection Kits, Millipore, MA, USA) detection solution was dropped on each section and then incubated at 37°C in the dark which lasted for an hour. After rinsing with PBS, DAPI nuclei were stained for 5 minutes. After rinsing with PBS, sections were fixed with 50% glycerol. For the control group, the TUNEL solution was replaced by PBS. The sections were observed under a fluorescence microscope.

2.8. Animal Testicular Tissue Western Blot Analysis.
We collected testicular histone proteins from each group, placed the crushed testicular tissue in a phosphate-buffered saline solution consisting of 0.1% sodium dodecyl sulfate, and then performed a brief ultrasound. The protein concentration was determined by the diphenylphenol acid protein assay (Pierce Chemical Co., USA). Thirty micrograms of total testicular tissue protein was separated by 12% SDS-polyacrylamide gel electrophoresis and transferred to nitrocellulose membranes. Specific antibodies were used to detect the following proteins: β-actin (1 : 1000 dilution; Santa Cruz Biotechnology, USA), HO-1 (1 : 1000 dilution; Cell Signaling Technology, USA), Nrf2 (1 : 500 diluted; Santa Cruz Biotechnology, USA), SOD (1 : 1000, dilution; Abcam, UK), BCL-xL (1 : 1000 dilution; Cell Signaling Technology, USA), Bax (1 : 1000 dilution; Cell Signaling Technology, USA), and Cleaved Caspase-3 (Caspase-3) (1 : 1000 dilution; Cell Signaling Technology, USA). The binding antibody of each blot was evaluated by enhancing chemiluminescence (Western blot detection kit; Amersham Pharmacia Biotech, USA), which was assessed with horseradish peroxidase-conjugated secondary antibody.

2.9. Statistical Analysis.
Statistical analyses were carried out using SPSS 16.0 (SPSS Inc., Chicago, USA). The data was expressed as mean ± standard deviation. ANOVA test was used for data conforming to normal distribution, and the Scheffe test was used for comparison between groups. $P < 0.05$ was considered significant.

3. Results

3.1. Protective Effect of Li-ESWT on TM3 Leydig Cells in Vitro.
Western blot analysis was conducted to determine whether Li-ESWT could prevent oxidative stress damage of TM3 Leydig cells induced by H_2O_2. As shown in Figure 1(a), compared with normal TM3 Leydig cells, the expression of Nrf2/HO-1 and SOD decreased significantly after incubation with H_2O_2 ($P < 0.01$). The expression level increased after Li-ESWT treatment, and the increase was most significant at $0.05 \, mJ/mm^2$ energy level ($P < 0.01$), which is also confirmed by quantitative analysis in Figure 1(b).

At the same time, as shown in Figure 1(c), NF-κB/COX-2 expression was significantly increased after H_2O_2

(a)

(b)

(c)

(d)
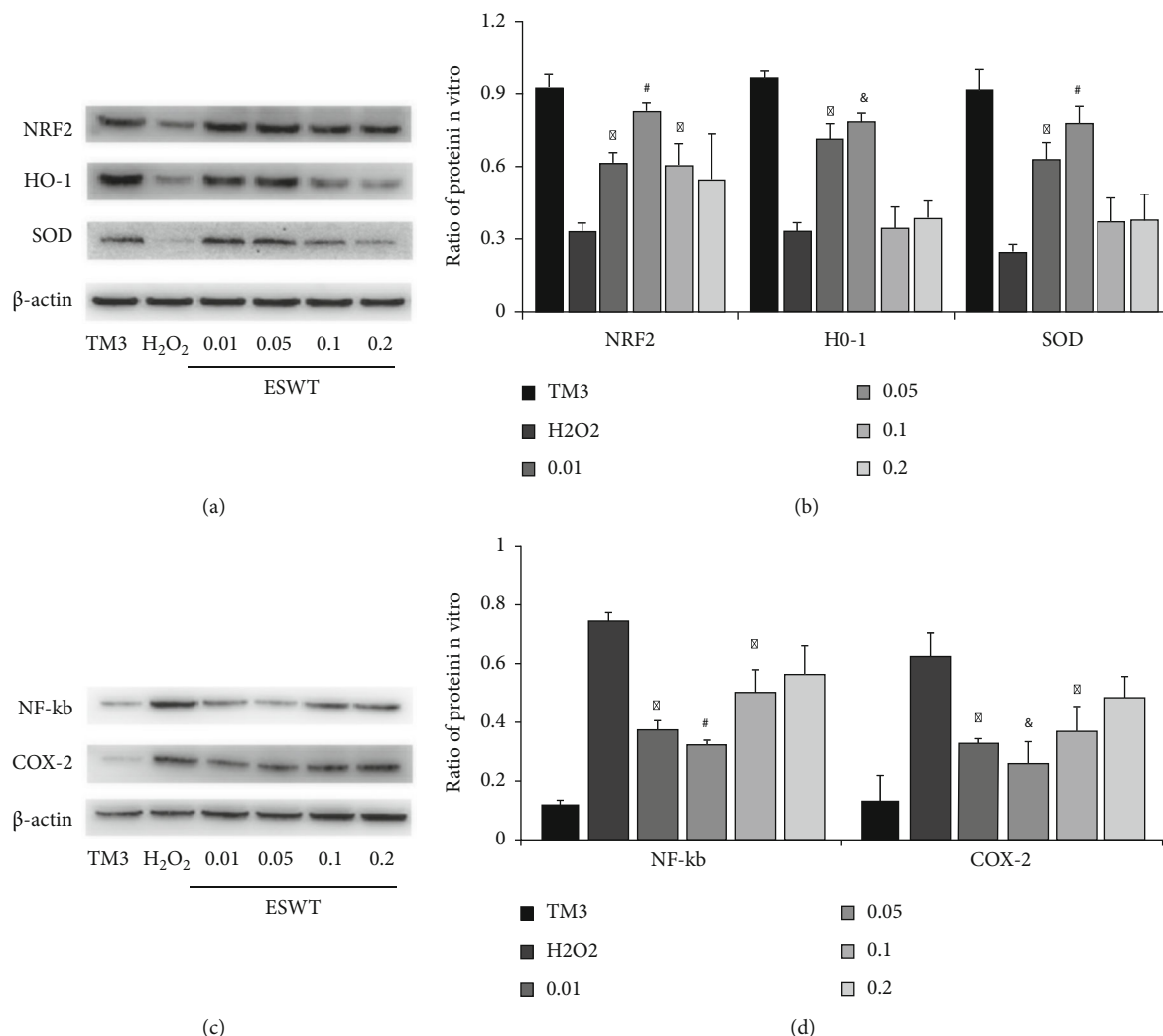
FIGURE 1: Effect of Li-ESWT on protein expression in H_2O_2-treated TM3 Leydig cells in vitro. (a) The expression levels of Nrf2, HO-1, and SOD in cells of each group were detected by Western blot. (b) The expression of Nrf2, HO-1, and SOD in each group was quantitatively analyzed. (c) The expression levels of NF-κB and COX-2 in each group were detected by Western blot. (d) The expression levels of NF-κB and COX-2 in each group were quantitatively analyzed. $^*P < 0.01$ compared with H_2O_2 group. $^\#P < 0.01$ compared with ESWT_0.01, ESWT_0.1, and ESWT_0.2 group. $^\&P < 0.01$ compared with ESWT_0.2. Normal control was normal TM3 Leydig cell group. H_2O_2 was the TM3 Leydig cell group treated with H_2O_2. ESWT_0.01 was the group of TM3 Leydig cells treated with H_2O_2 followed by 0.01 mJ/ mm^2 Li-ESWT treatment. ESWT_0.05, ESWT_0.1, and ESWT_0.2 were treated by the same method with different energy levels.

incubation compared with normal TM3 Leydig cells ($P < 0.01$). This indicated increased apoptosis. The expression decreased after Li-ESWT treatment, and the decrease was most significant at 0.05 mJ/mm^2 level ($P < 0.01$), which was also confirmed by the quantitative analysis in Figure 1(d). These results indicated that Li-ESWT could effectively prevent oxidative stress injury and reduce apoptosis of TM3 Leydig cells induced by H_2O_2, and the effect was most obvious at the energy level of 0.05 mJ/mm^2.

3.2. Effect of Li-ESWT on VEGF Expression in TM3 Leydig Cells in Vitro. The effect of Li-ESWT on VEGF expression in TM3 Leydig cells was analyzed by immunofluorescence staining. As shown in Figure 2(a), compared with normal TM3 Leydig cells, the VEGF expression was significantly

reduced after incubation with H_2O_2 ($P < 0.01$). The expression level increased after Li-ESWT treatment, and the increase was most significant at 0.05 mJ/mm^2 energy level ($P < 0.01$). The quantitative analysis in Figure 2(b) also confirmed this, with an approximately 4-fold increase in the expression. This suggests that Li-ESWT can effectively increase the expression of VEGF in TM3 Leydig cells damaged by oxidative stress.

3.3. In Vivo, Li-ESWT Preserves Testicular Function and Improves Serum Testosterone Levels. There was no significant difference in body weight among the groups. Table 1 lists the average weight of the testis for each group. After 8 weeks, the androgen-deficient group had significantly less testicular weight than the normal control group ($P < 0.01$).
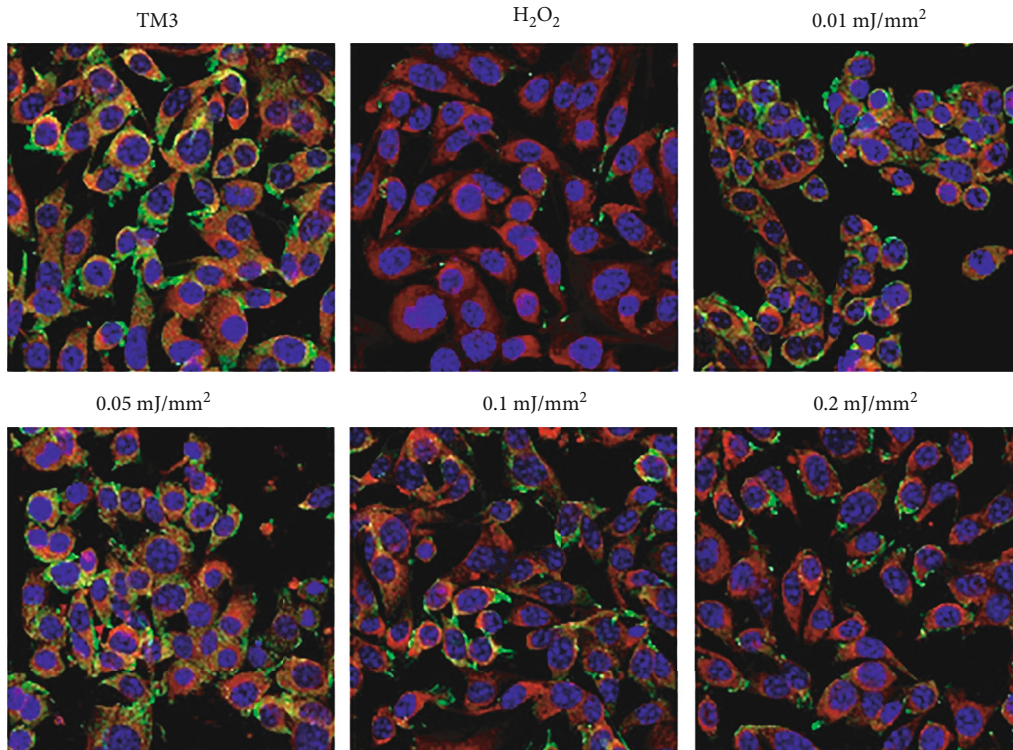
(a)
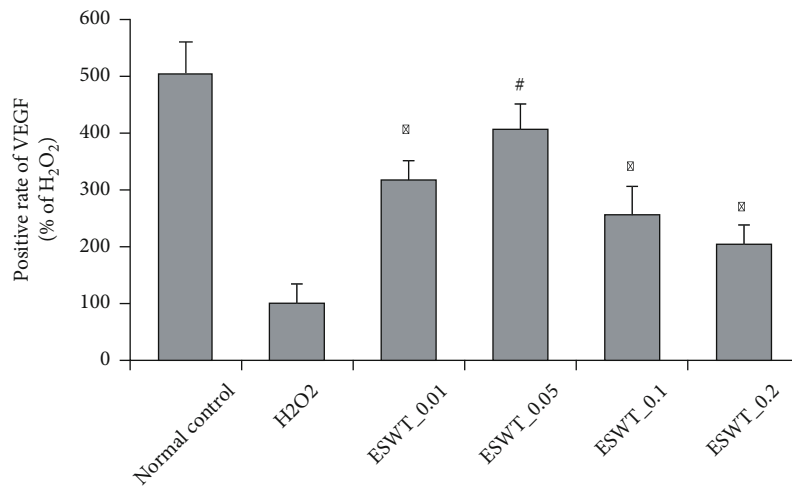
(b)

Figure 2: Effect of Li-ESWT on VEGF expression in H_2O_2-treated TM3 Leydig cells in vitro. (a) Representative images of VEGF expression in each group. Blue is DAPI, red is β-actin, and green is VEGF. (b) Positive rate of VEGF in each group. Each bar chart shows the mean (standard deviation). *$P < 0.01$ compared with H_2O_2 group. #$P < 0.01$ compared with ESWT_0.01, ESWT_0.1, and ESWT_0.2 group. Normal control was normal TM3 Leydig cell group. H_2O_2 was the TM3 Leydig cell group treated with H_2O_2. ESWT_0.01 was the group of TM3 Leydig cells treated with H_2O_2 followed by 0.01 mJ/mm^2 Li-ESWT treatment. ESWT_0.05, ESWT_0.1, and ESWT_0.2 were treated by the same method with different energy levels.

After Li-ESWT treatment, the testis weight was increased and the energy level was significantly increased at 0.05 mJ/mm^2 ($P < 0.01$).

The testicular structure was normal, with mature vas deferens and complete spermatogenic sequence. But as shown in Figure 3, the density of spermatogenic cells decreased significantly in the androgen-deficient group compared with the normal control group ($P < 0.01$), and tissue degradation and even incomplete spermatogenic sequence could be seen in some vas deferens. Li-ESWT treatment improved with a significant increase in energy levels at 0.05 mJ/mm^2 ($P < 0.01$) (Table 1).

Serum testosterone levels were significantly lower in the androgen-deficient group than in the normal control group ($P < 0.01$), and it was improved after Li-ESWT treatment, but the degree of improvement in each group was not

TABLE 1: Comparison of testicular health parameters. Data show mean ± standard deviation. Analysis of variance test. $^{*}P < 0.01$ compared with the control group. $^{\#}P < 0.01$ compared with Leuplin group.

	Testicular weight (g)	Sperm count ($\times10^6$/g cauda)	% of motile spermatozoa	Diameter of seminiferous tubules (μm)	Serum testosterone (ng/ml)
Control	1.96 ± 0.09	233.3 ± 37.05	59.86 ± 11.31	301.58 ± 10.26	3.07 ± 0.33
Leuplin	$1.14 \pm 0.24^{*}$	$109.67 \pm 31.34^{*}$	$21.88 \pm 13.33^{*}$	$120.32 \pm 12.55^{*}$	$1.28 \pm 0.52^{*}$
ESWT 0.01	1.25 ± 0.2	110 ± 16.09	25.45 ± 7.1	134.74 ± 8.33	1.30 ± 0.24
ESWT 0.05	$1.50 \pm 0.28^{\#}$	$161.1 \pm 27.62^{\#}$	$39.13 \pm 5.49^{\#}$	$178.36 \pm 9.95^{\#}$	1.67 ± 0.30
ESWT 0.2	1.46 ± 0.26	150.34 ± 30.86	33.03 ± 5.35	148.21 ± 12.21	1.58 ± 0.37
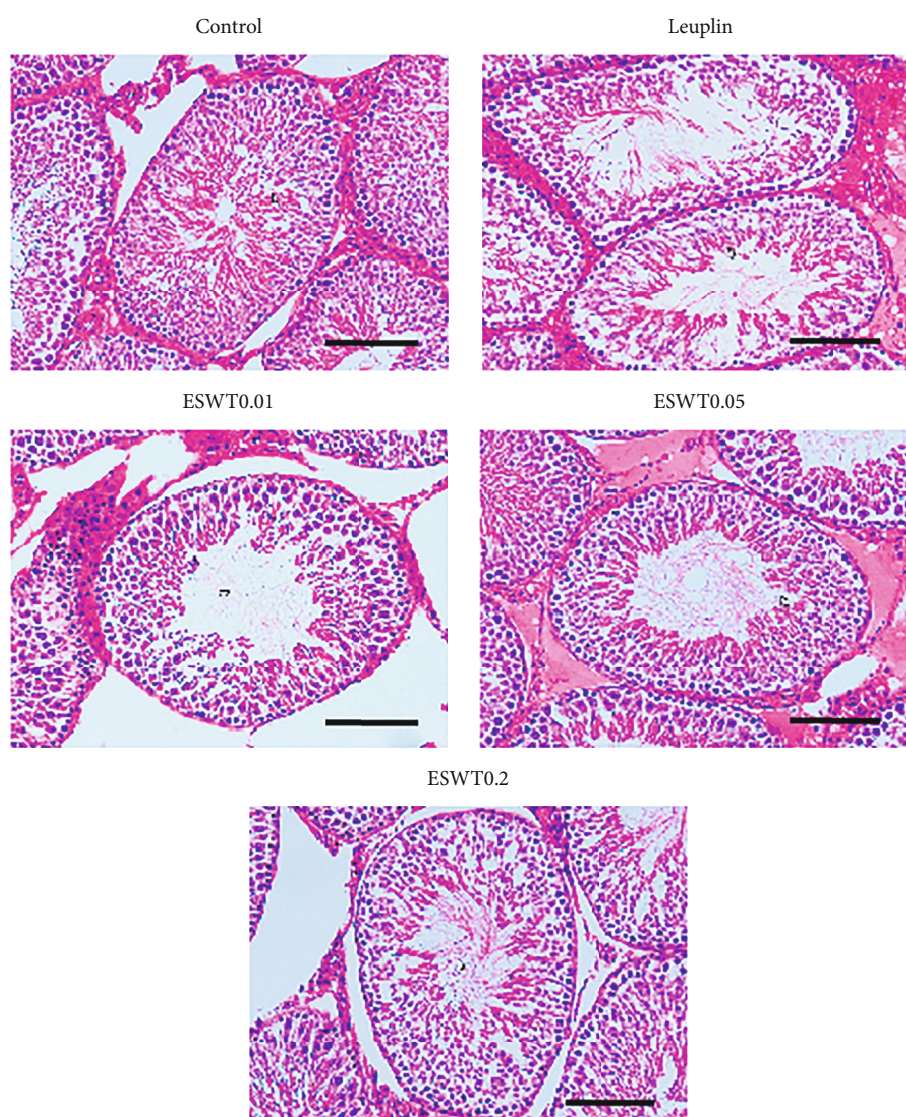
FIGURE 3: Pathological appearance of testicular tissue (hematoxylin and eosin staining). Compared with the normal control group, the germinal cell layer was narrower in the androgen deprivation group. The scale in the figure represents 100μm.

statistically significant compared with the androgen-deficient group (Table 1).

3.4. In Vivo, Li-ESWT Reduced Oxidative Stress and Apoptosis. ELISA showed that the mean expression of 8-OHdG (Figure 4(a)) in the androgen-deficient group was significantly higher than that in the normal group, while the mean expression of SOD (Figure 4(b)) was significantly lower. Li-ESWT treatment reversed and was most obvious at 0.05 mJ/mm^2 energy level ($P < 0.01$).
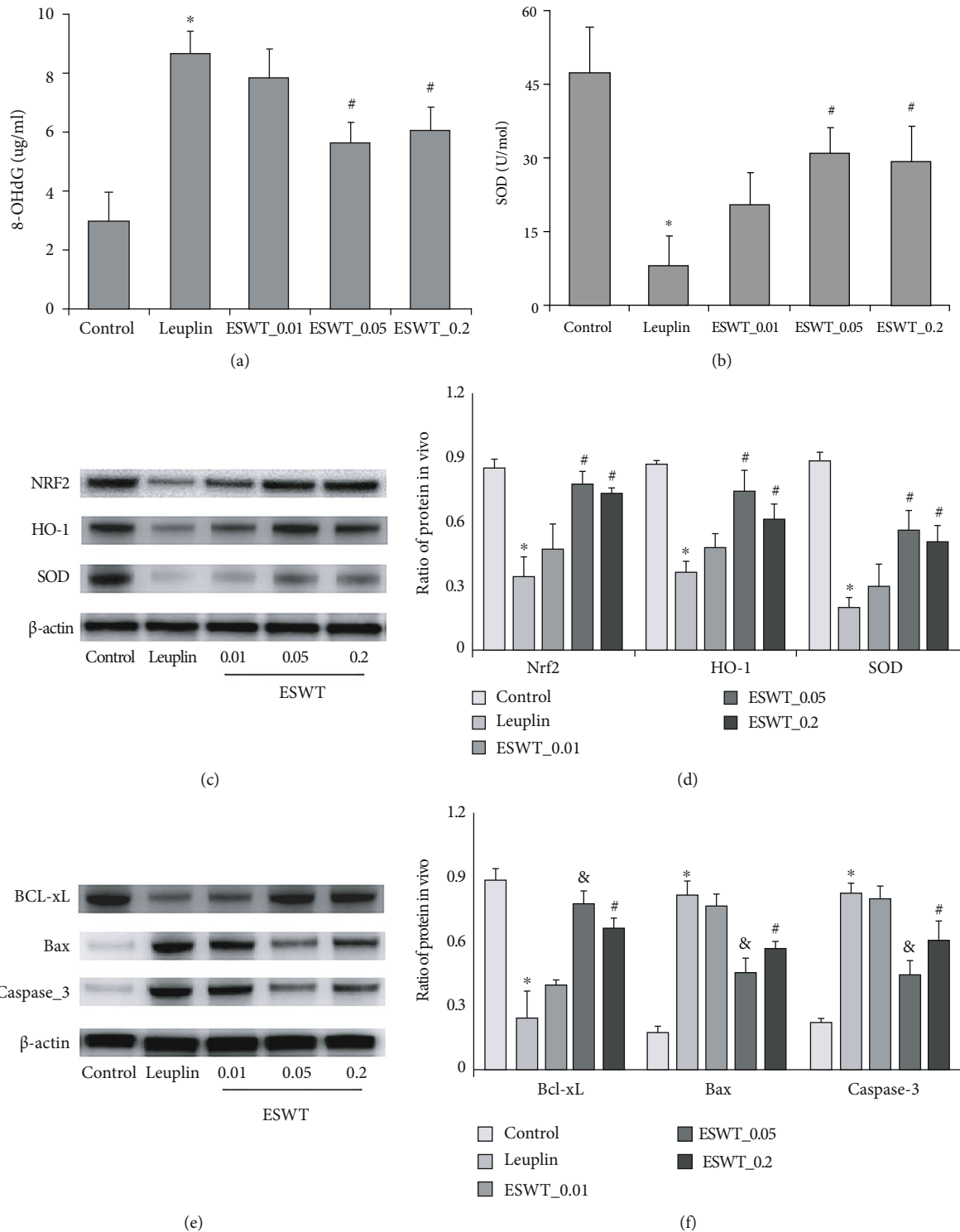
FIGURE 4: Comparison of 8-OHdG (a) and SOD (b) expression levels by ELISA. (c) The expression levels of Nrf2, HO-1, and SOD in each group were detected by Western blot. (d) The expressions of Nrf2, HO-1, and SOD in each group were quantitatively analyzed. (e) The expression levels of Bcl-xL, Bax, and Caspase-3 in each group were detected by Western blot. (f) The expressions of Bcl-xL, Bax, and Caspase-3 in each group were quantitatively analyzed. $^{*}P < 0.01$ compared with the control group. $^{#}P < 0.01$ compared with Leuplin group. $^{&}P < 0.01$ compared with ESWT_0.01 and ESWT_0.2 groups.

(a)

(b)
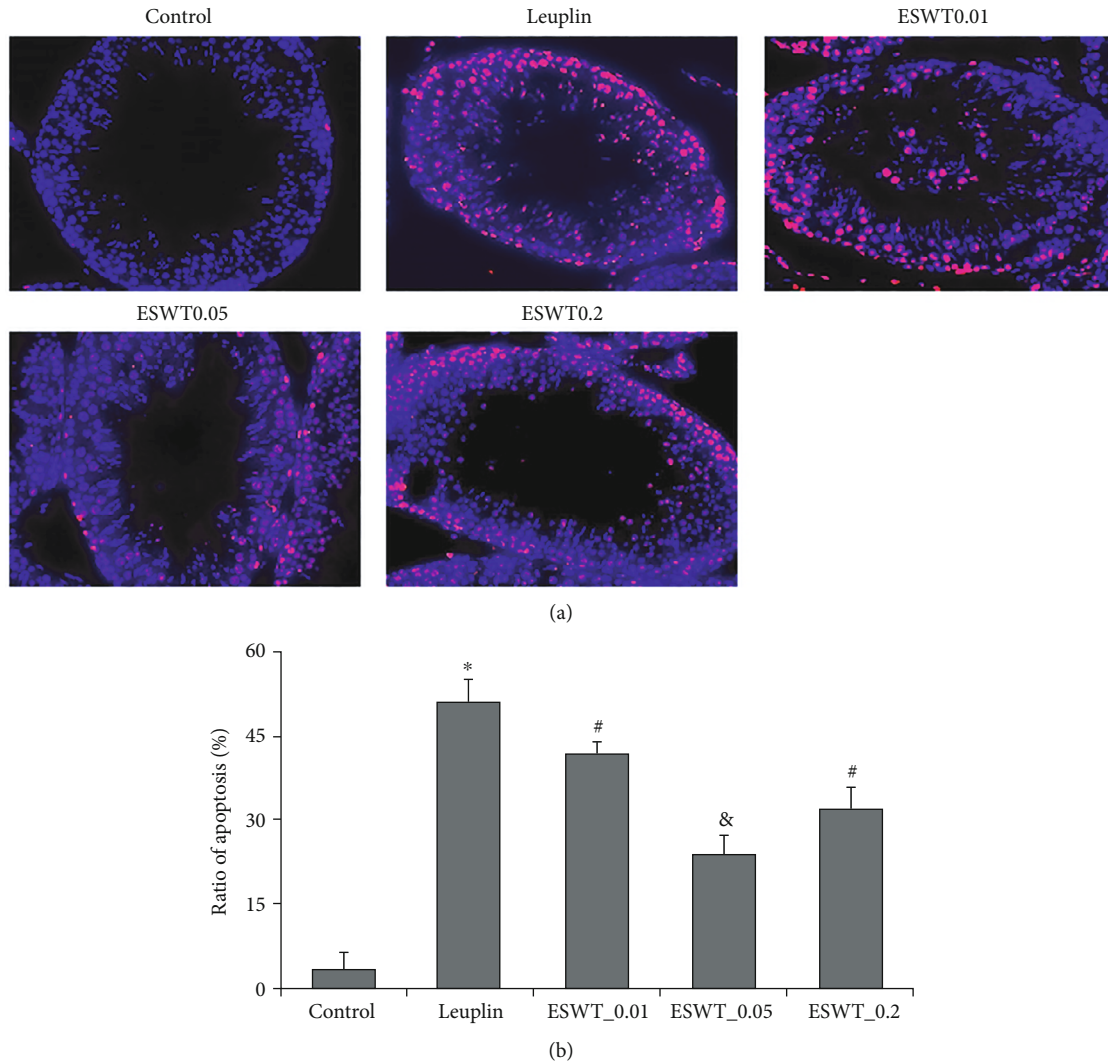
FIGURE 5: TUNEL assay to detect the effect of Li-ESWT on apoptosis of testicular tissue. (a) The representative image of each group: blue is DAPI and red is TUNEL positive. (b) The positive rate of TUNEL detection in each group. $^{*}P < 0.01$ compared with the control group. $^{\#}P < 0.01$ compared with Leuplin group. $^{\&}P < 0.01$ compared with ESWT_0.01 and ESWT_0.2 groups.

As shown in Figure 4(c), the expression of Nrf2/HO-1 and SOD in the androgen-deficient group was significantly decreased compared with the normal group ($P < 0.01$). Li-ESWT treatment reversed and was most obvious at 0.05 mJ/mm^2 energy level ($P < 0.01$) (Figure 4(f)).

At the same time, as shown in Figure 4(e), the expression of Caspase-3 and Bax was significantly increased in the androgen-deficient group compared with the normal group, while the expression of Bcl-xL was significantly decreased, which was reversed after Li-ESWT treatment, and was most obvious at 0.05 mJ/mm^2 energy level ($P < 0.01$) (Figure 4(f)).

Dark red apoptotic cells were observed in the testis during TUNEL assay (Figure 5(a)). The androgen-deficient group was significantly increased compared with the normal control group and decreased after Li-ESWT treatment, with a significant decrease in energy levels at 0.05 mJ/mm^2 ($P < 0.01$), which is also confirmed by the quantitative analysis in Figure 5(b).

4. Discussion

In vitro cell experiments in this study, we set Li-ESWT at 4 energy levels (0.01, 0.05, 0.1, and 0.2 mJ/mm^2). The results suggested that Li-ESWT could increase the expression of VEGF in TM3 cells, improve antioxidant capacity, and reduce apoptosis, and the effect was most significant at the energy level of 0.05 mJ/mm^2. In androgen-deficient rat model, we set the Li-ESWT at 3 energy levels (0.01, 0.05, and 0.2 mJ/mm^2). The results suggested that Li-ESWT could improve the sperm count, motility, serum testosterone level, tissue antioxidant capacity, and antiapoptotic ability. The effect was most significant at 0.05 mJ/mm^2 energy level.

The transcription factor Nrf2 is a redox-sensitive transcription factor. It regulates the expression of HO-1 and confers cytoprotection against oxidative stress [19, 20]. Activation of Nrf2/HO-1 pathway can lead to increased SOD level in mouse kidneys [21, 22]. Previous research has

shown that Nrf2 expression and related genes exhibit an age-dependent decrease in aged rats [23, 24]. This was consistent with our results. In androgen-deficient rat model, Nrf2/HO-1 expression and SOD level in rat testicular tissue were decreased, and the oxidative damage marker 8-OHdG was significantly increased, which was improved after Li-ESWT treatment. In our previous study [25], it was found that the expression level of Nrf2/HO-1 in TM3 stromal cells significantly decreased after oxidative stress. In the present research, the expression of Nrf2/HO-1 in TM3 cells was decreased after H_2O_2 treatment, while the expression level was increased after Li-ESWT treatment, which was consistent with the results of previous studies.

Apoptosis plays multiple roles in the normal growth and development of individual organisms and critical roles in maintaining normal, balanced homeostasis; however, excessive spontaneous apoptosis by generating increased intracellular reactive oxygen species production may cause organ dysfunction. Abbate et al. [26] have suggested that the expression of COX-2 in nonmyocytes in acute myocardial infarction was correlated with the induction of inflammation and severity of apoptosis. COX-2 expression is regulated by various transfactors, such as NF-κB, which can bind to corresponding promoter regions to regulate transcription [27, 28]. COX-2 overexpression is associated with activation of NF-κB signaling pathway [29]. In our cell experiments, NF-κB and COX-2 were significantly increased after H_2O_2 treatment and decreased after Li-ESWT treatment. At the same time, the expression of TUNEL index, Caspase-3, and Bax was significantly increased, while the expression of Bcl-xL was significantly decreased in the androgen-deficient animal model. However, these changes can be reversed with Li-ESWT treatment, and the Bax/Bcl-xL ratio was reduced. Therefore, we believe that Li-ESWT can reduce tissue oxidative stress and apoptosis, improve antioxidant capacity and stromal cell activity, and at the same time increase serum testosterone level, further promoting sperm production.

Li-ESWT is an acoustic wave that produces mechanical forces to produce shear stress on the cell membrane, cytoskeleton, and extracellular matrix, thereby exerting biological effects [30, 31]. It has been reported that Li-ESWT can stimulate the upregulation of tissue repair markers such as VEGF [32–34] and reduce oxidative stress [35]. In our in vitro cell experiments, it was found that VEGF expression in TM3 cells decreased after H_2O_2 treatment and significantly increased after Li-ESWT treatment. Studies have shown that VEGF subtypes, as a gene regulator, are necessary for the maintenance of spermatogonia, sperm production, and male fertility [16]. Therefore, according to the results of this experiment, we believe that Li-ESWT may play an active role in testis by increasing the expression of VEGF in stromal cells. At the same time, we need to further study the mechanism.

Some studies have shown that Li-ESWT has a negative effect on testicles, contrary to our results [36–38], which may be related to the use of different energy levels. In our study, the optimal energy level obtained by cell and animal experiments was 0.05 mJ/mm². In animal experiments, the results of 0.01 mJ/mm² energy level were compared with the Leuplin group. Although the average value was changed, there was no statistical difference. Meanwhile, some results of 0.2 mJ/mm² energy level were not statistically different from 0.05 mJ/mm² energy level, but the average value was changed. This suggests that Li-ESWT energy level directly impacts its effect, and high energy level may reduce Li-ESWT effect. However, when Li-ESWT treated penis and other parts or even applied ESWT gravel energy to testis, the energy received by the testis was necessarily different from the energy given in our experiment, so the impact was unknown.

In this experiment, we intended to target aging male hypoandrogens with partial androgen deficiency rather than complete castration, so low-dose leuprorelin injection helped to establish this model. And we may study further experiments using older rat models. Although the average serum testosterone level increased after Li-ESWT treatment, there was no statistical difference. Meanwhile, we did not set sufficient energy level gradient in animal experiments. Although the results showed that the energy level of 0.05 mJ/mm² was the best and different from other energy levels, this may not mean that this is the true optimal level, so we may need further research.

5. Conclusion

Both our experiments have confirmed that Li-ESWT with appropriate energy levels can improve sperm count, motility, and serum testosterone levels in androgen-deficient rat models. It can reduce oxidative stress in the testis and increase antioxidant capacity and antiapoptotic capacity, and the effect is most obvious at 0.05 mJ/mm² energy level. We believe the mechanism underlying these findings may be related to the increase of VEGF expression in Leydig cells by Li-ESWT. Li-ESWT may serve as a new noninvasive and effective treatment to improve testicular function and sperm quality in middle-aged and elderly men. Meanwhile, we can also expect Li-ESWT to play a positive role in the oxidative stress lesions of the testis or other organs caused by obesity, metabolic diseases, or other injuries.

Data Availability

The data used to support the finding of this study are available from the corresponding author upon request.

Conflicts of Interest

The authors declare that they have no conflicts of interest.

Acknowledgments

References

[1] D. Harman, "Aging: phenomena and theories," *Annals of the New York Academy of Sciences*, vol. 854, no. 1, pp. 1–7, 1998.

[2] R. Golan, J. M. Scovell, and R. Ramasamy, "Age-related testosterone decline is due to waning of both testicular and hypothalamic-pituitary function," *The Aging Male*, vol. 18, no. 3, pp. 201–204, 2015.

[3] L. Johnson, C. S. Petty, and W. B. Neaves, "Age-related variation in seminiferous tubules in men. A stereologic evaluation," *Journal of Andrology*, vol. 7, no. 5, pp. 316–322, 1986.

[4] A. M. Mahmoud, S. Goemaere, Y. El-Garem, I. Van Pottelbergh, F. H. Comhaire, and J. M. Kaufman, "Testicular volume in relation to hormonal indices of gonadal function in community-dwelling elderly men," *The Journal of Clinical Endocrinology & Metabolism*, vol. 88, no. 1, pp. 179–184, 2003.

[5] W. B. Neaves, L. Johnson, J. C. Porter, C. R. Parker Jr., and C. S. Petty, "Leydig cell numbers, daily sperm production, and serum gonadotropin levels in aging men," *The Journal of Clinical Endocrinology & Metabolism*, vol. 59, no. 4, pp. 756–763, 1984.

[6] L. H. Honoré, "Ageing changes in the human testis: a light-microscopic study," *Gerontology*, vol. 24, no. 1, pp. 58–65, 1978.

[7] I. Ichihara, H. Kawamura, and L. J. Pelliniemi, "Ultrastructure and morphometry of testicular Leydig cells and the interstitial components correlated with testosterone in aging rats," *Cell and Tissue Research*, vol. 271, no. 2, pp. 241–255, 1993.

[8] H. Chen, D. Cangello, S. Benson et al., "Age-related increase in mitochondrial superoxide generation in the testosterone-producing cells of Brown Norway rat testes: relationship to reduced steroidogenic function?," *Experimental Gerontology*, vol. 36, no. 8, pp. 1361–1373, 2001.

[9] A. Agarwal, N. Parekh, M. K. Panner Selvam et al., "Male oxidative stress infertility (MOSI): proposed terminology and clinical practice guidelines for management of idiopathic male infertility," *The World Journal of Men's Health*, vol. 37, no. 3, pp. 296–312, 2019.

[10] D. Hatzichristou, "Low-intensity extracorporeal shock waves therapy (LI-ESWT) for the treatment of erectile dysfunction: where do we stand?," *European Urology*, vol. 71, no. 2, pp. 234–236, 2017.

[11] E. Chung and R. Cartmill, "Evaluation of clinical efficacy, safety and patient satisfaction rate after low-intensity extracorporeal shockwave therapy for the treatment of male erectile dysfunction: an Australian first open-label single-arm prospective clinical trial," *BJU International*, vol. 115, Suppl 5, pp. 46–49, 2015.

[12] H. Lei, H. Xin, R. Guan et al., "Low-intensity Pulsed Ultrasound Improves Erectile Function in Streptozotocin- induced Type I Diabetic Rats," *Urology*, vol. 86, no. 6, pp. 1241.e11–1241.e18, 2015.

[13] C. C. Hsiao, W. H. Huang, K. H. Cheng, and C. T. Lee, "Low-energy extracorporeal shock wave therapy ameliorates kidney function in diabetic nephropathy," *Oxidative Medicine and Cellular Longevity*, vol. 2019, Article ID 8259645, 2019.

[14] S. H. Jeon, K. R. Shrestha, R. Y. Kim et al., "Combination therapy using human adipose-derived stem cells on the cavernous nerve and low-energy shockwaves on the corpus cavernosum in a rat model of post-prostatectomy erectile dysfunction," *Urology*, vol. 88, pp. 226.e1–226.e9, 2016.

[15] H. C. Jeong, S. H. Jeon, Z. G. Qun et al., "Effects of next-generation low-energy extracorporeal shockwave therapy on erectile dysfunction in an animal model of diabetes," *The World Journal of Men's Health*, vol. 35, no. 3, pp. 186–195, 2017.

[16] N. Lu, K. M. Sargent, D. T. Clopton et al., "Loss of vascular endothelial growth factor A (VEGFA) isoforms in the testes of male mice causes subfertility, reduces sperm numbers, and alters expression of genes that regulate undifferentiated spermatogonia," *Endocrinology*, vol. 154, no. 12, pp. 4790–4802, 2013.

[17] K. W. Ko, J. Y. Chae, S. W. Kim et al., "The effect of the partial obstruction site of the renal vein on testis and kidney in rats: is the traditional animal model suitable for varicocele research?," *Korean Journal of Urology*, vol. 51, no. 8, pp. 565–571, 2010.

[18] W. J. Bae, U. S. Ha, J. B. Choi et al., "Protective effect of decursin extracted from Angelica gigas in male infertility via Nrf2/HO-1 signaling pathway," *Oxidative Medicine and Cellular Longevity*, vol. 2016, Article ID 5901098, 2016.

[19] A. Loboda, M. Damulewicz, E. Pyza, A. Jozkowicz, and J. Dulak, "Role of Nrf2/HO-1 system in development, oxidative stress response and diseases: an evolutionarily conserved mechanism," *Cellular and Molecular Life Sciences*, vol. 73, no. 17, pp. 3221–3247, 2016.

[20] P. Balasubramanian and V. D. Longo, "Linking Klotho, Nrf2, MAP kinases and aging," *Aging*, vol. 2, no. 10, pp. 632-633, 2010.

[21] C. Dai, S. Tang, S. Deng et al., "Lycopene attenuates colistin-induced nephrotoxicity in mice via activation of the Nrf2/HO-1 pathway," *Antimicrobial Agents and Chemotherapy*, vol. 59, no. 1, pp. 579–585, 2015.

[22] E. N. Kim, J. H. Lim, M. Y. Kim et al., "Resveratrol, an Nrf2 activator, ameliorates aging-related progressive renal injury," *Aging*, vol. 10, no. 1, pp. 83–99, 2018.

[23] P. H. Shih and G. C. Yen, "Differential expressions of antioxidant status in aging rats: the role of transcriptional factor Nrf2 and MAPK signaling pathway," *Biogerontology*, vol. 8, no. 2, pp. 71–80, 2007.

[24] H. Zhang, K. J. A. Davies, and H. J. Forman, "Oxidative stress response and Nrf2 signaling in aging," *Free Radical Biology and Medicine*, vol. 88, no. Part B, pp. 314–336, 2015.

[25] W. J. Bae, G. Q. Zhu, S. W. Choi et al., "Antioxidant and anti-fibrotic effect of a herbal formulation in vitro and in the experimental andropause via Nrf2/HO-1 signaling pathway," *Oxidative Medicine and Cellular Longevity*, vol. 2017, Article ID 6024839, 2017.

[26] A. Abbate, D. Santini, G. G. L. Biondi-Zoccai et al., "Cyclo-oxygenase-2 (COX-2) expression at the site of recent myocardial infarction: friend or foe?," *Heart*, vol. 90, no. 4, pp. 440–443, 2004.

[27] A. G. Asting, H. Carén, M. Andersson, C. Lönnroth, K. Lagerstedt, and K. Lundholm, "COX-2 gene expression in colon cancer tissue related to regulating factors and promoter methylation status," *BMC Cancer*, vol. 11, no. 1, p. 238, 2011.

[28] M. H. Chung, D. H. Kim, H. K. Na et al., "Genistein inhibits phorbol ester-induced NF-κB transcriptional activity and COX-2 expression by blocking the phosphorylation of p65/RelA in human mammary epithelial cells," *Mutation Research, Fundamental and Molecular Mechanisms of Mutagenesis*, vol. 768, pp. 74–83, 2014.

[29] H. N. Kim, D. H. Kim, E. H. Kim et al., "Sulforaphane inhibits phorbol ester-stimulated IKK-NF-κB signaling and COX-2 expression in human mammary epithelial cells by targeting NF-κB activating kinase and ERK," *Cancer Letters*, vol. 351, no. 1, pp. 41–49, 2014.

[30] M. C. d'Agostino, K. Craig, E. Tibalt, and S. Respizzi, "Shock wave as biological therapeutic tool: from mechanical stimulation to recovery and healing, through mechanotransduction," *International Journal of Surgery*, vol. 24, no. Part B, pp. 147–153, 2015.

[31] L. Gerdesmeyer, M. Maier, M. Haake, and C. Schmitz, "Physical-technical principles of extracorporeal shockwave therapy (ESWT)," *Orthopade*, vol. 31, no. 7, pp. 610–617, 2002.

[32] A. Aicher, C. Heeschen, K. Sasaki, C. Urbich, A. M. Zeiher, and S. Dimmeler, "Low-energy shock wave for enhancing recruitment of endothelial progenitor Cells," *Circulation*, vol. 114, no. 25, pp. 2823–2830, 2006.

[33] Y. J. Chen, T. Wurtz, C. J. Wang et al., "Recruitment of mesenchymal stem cells and expression of TGF-beta 1 and VEGF in the early stage of shock wave-promoted bone regeneration of segmental defect in rats," *Journal of Orthopaedic Research*, vol. 22, no. 3, pp. 526–534, 2004.

[34] M. Yoshida, T. Nakamichi, T. Mori, K. Ito, H. Shimokawa, and S. Ito, "Low-energy extracorporeal shock wave ameliorates ischemic acute kidney injury in rats," *Clinical and Experimental Nephrology*, vol. 23, no. 5, pp. 597–605, 2019.

[35] Y. T. Chen, C. C. Yang, C. K. Sun et al., "Extracorporeal shock wave therapy ameliorates cyclophosphamide-induced rat acute interstitial cystitis though inhibiting inflammation and oxidative stress-in vitro and in vivo experiment studies," *American Journal of Translational Research*, vol. 6, no. 6, pp. 631–648, 2014.

[36] Z.-J. Zang, Q. Liu, J. Hu et al., "The impact of low-intensity extracorporeal shock wave therapy on testicular function in adult rats," *Andrology*, vol. 6, no. 6, pp. 936–942, 2018.

[37] Y. L. Deng, D. Z. Luo, and H. G. Chen, "Effects of high-energy shock waves on testes of Wistar rats," *Journal of Endourology*, vol. 7, no. 5, pp. 383–386, 1993.

[38] P. Philippou, D. J. Ralph, and A. G. Timoney, "The impact of shock wave lithotripsy on male fertility: a critical analysis of existing evidence," *Urology*, vol. 79, no. 3, pp. 492–500, 2012.

Hindawi

Research Article

The Effect of Enalapril, Losartan, or Not Antihypertensive on the Oxidative Status in Renal Transplant Recipients

Jorge Andrade-Sierra ⓘ,[1] Mónica Lizbeth Morales-Guillén ⓘ,[1] Andrés García-Sánchez ⓘ,[2] Elodia Nataly Díaz-de la Cruz ⓘ,[2] José Ignacio Cerrillos-Gutiérrez ⓘ,[1] Enrique Rojas-Campos ⓘ,[1] and Alejandra Guillermina Miranda-Díaz ⓘ[2]

[1]Nephrology and Transplantation Division, UMAE, National Medical Center of the West, Mexican Institute of Social Security, Guadalajara, Jalisco, Mexico
[2]Department of Physiology, University Center for Health Sciences, University of Guadalajara, Mexico

Correspondence should be addressed to Alejandra Guillermina Miranda-Díaz; kindalex1@outlook.com

The clinical and biochemical improvement observed in kidney transplant (RT) recipients is remarkable. The correct functioning of the allograft depends on various factors such as the donor's age, the alloimmune response, the ischemia-reperfusion injury, arterial hypertension, and the interstitial fibrosis of the allograft, among others. Antihypertensive drugs are necessary for arterial hypertension patients to avoid or reduce the probability of affecting graft function in RT recipients. Oxidative stress (OS) is another complex pathophysiological process with the ability to alter posttransplant kidney function. The study's objective was to determine the effect of the administration of Enalapril, Losartan, or not antihypertensive medication on the oxidative state in RT recipients at the beginning of the study and one year of follow-up. All patients included in the study found significant overexpression of the oxidative damage marker to DNA and the antioxidant enzymes superoxide dismutase (SOD) and glutathione peroxidase (GPx). In contrast, it was found that the determination of the total antioxidant capacity decreased significantly in the final determination at one year of follow-up in all the patients who ingested Enalapril and Losartan. We found dysregulation of the oxidative state characterized mainly by oxidative damage to DNA and a significant increase in antioxidant enzymes, which could suggest a compensatory effect against the imbalance of the oxidative state.

1. Introduction

Chronic allograft dysfunction (CAD) is a progressive and irreversible entity and is a cause of long-term kidney transplant failure [1–3]. The mechanisms of damage that contribute to CAD involve immunological [4] and nonimmunological [3] aspects, which conditions the formation of interstitial fibrosis and tubular atrophy (IFTA) [5]. On the other hand, the oxidative stress (OS) characterized by the imbalance between the generation of oxidative compounds and the antioxidant defense mechanisms could be resulted in allograft damage, especially when immunosuppression in renal transplantation is based on the use of calcineurin inhibitors (CNI) inducing endothelial dysfunction, hypertension, and increased renal

nephrotoxicity, characterized by renal vasoconstriction, interstitial fibrosis, and arterial hypertrophy [6–9]. The generation of oxidative compounds is physiologically essential as part of the defense mechanism against the invasion of microorganisms, malignant cells, tissue repair, and healing. When the deregulated activation of OS occurs, it can cause vascular damage favoring the progression of atherosclerosis due to oxidative damage directly to cellular components, leading to impaired cell function, aging, and activation of apoptosis [10]. Lipoperoxidation products (LPO) damage lipoproteins present in the cell membrane, leading to the formation of toxic reactive aldehydes and promoting more significant lipid peroxidation, ultimately affecting many lipid molecules [10]. On the other hand, the 8-hydroxy-2$'$-deoxyguanosine (8-

OHdG) is a sensitive and specific marker of oxidative damage to DNA [11].

Various therapeutic interventions are used to minimize kidney graft damage associated with CNI including the use of angiotensin-converting enzyme (ACE) inhibitors and angiotensin receptor blockers (ARBs) [12–14]. ACE inhibitors or ARBs are drugs with potent antihypertensive and renoprotective effects that are underutilized because it can cause elevated potassium and deleterious effect on renal hemodynamics with elevated serum creatinine (sCr) levels at some RT recipients, in addition to contradictory results in patients and graft survival in RT [15–17]. Nevertheless, the angiotensin II induces OS *in vitro* and *in vivo* and selectively blocks AT1 recipients ameliorated nonhemodynamic effects (reduction of OS) in renal nephrotoxicity due to CNI [18, 19]. Likewise the used of ACE inhibitors may potentiate protective mechanisms against long-term complications of CNI treatments (reducing effects on OS, fibrogenesis, and chronic rejection) [6].

The study's objective was to determine the effect of the administration of Enalapril, Losartan, or not antihypertensive on the oxidative state in RT recipients at the beginning of the study and one year of follow-up.

2. Patients and Methods

An open, randomized clinical trial was conducted with a control group. It was carried out in the Transplant Division of the High Specialty Medical Unit of the Hospital de Especialidades, Centro Médico Nacional de Occidente of the Mexican Institute of Social Security in Guadalajara, Jalisco, Mexico. The sample size was based on the formula to evaluate mean differences for clinical trials [20]. Three study groups were formed; thirteen patients with RT did not require any antihypertensive. Thirteen RT patients received Enalapril as an antihypertensive regimen. Thirteen RT patients received Losartan as an antihypertensive regimen in the posttransplant period. Recipients of a RT, from a living related donor (DVR) or living unrelated donor (DVNoR), agreed to participate and signed the letter of consent under information.

Patients who received an RT from a deceased donor, from a donor >55 years, with renal comorbidities at the time of the study (urolithiasis, infections, and diabetes), with blood dyscrasias, second transplantation, treatment with nonsteroidal anti-inflammatory drugs, statins, spironolactone, and pentoxifylline and patients with neurodegenerative processes or who withdrew the letter of consent under information were excluded.

Baseline determinations were made the day before RT and at one year of posttransplant follow-up. Type of donor and cold and hot ischemia time were recorded.

2.1. Immunosuppression Induction and Maintenance Scheme. TAC carried out the induction of immunosuppression at doses of 0.12 mg/kg/day divided into two doses, mycophenolate mofetil 2 g/day, and methylprednisolone 500 mg (day 0), polyclonal antibodies (thymoglobulin 1-1.5 mg/kg/day or humanized monoclonal antibodies inter-

leukin 2Rα basiliximab 20 mg at day 0 and 4 posttransplant). The immunization maintenance scheme was carried out by administering TAC at 0.1-0.2 mg/kg (the dose was modified according to serum levels). The target levels of TAC on days 1-30 posttransplantation were 9-15 ng/mL and from day 31 to 365 posttransplantation 8-10 ng/mL. The dose of mycophenolate mofetil was administered 1 g twice a day. Prednisone was administered at 1 mg/kg/day from the start of RT and was reduced to 0.1 mg/kg/day in the second month after transplantation [21].

2.2. Clinical and Biochemical Measurements. Patients were classified according to body mass index (BMI) 18.5-24.9 kg/m² (normal weight), 25 to 29.9 kg/m² (overweight), and ≥30 kg/m² (obesity) [22], and the blood pressure was determined [23]. The biochemical data of plasma glucose and blood TAC levels were determined, maintaining levels of 9-15 ng/mL from 1-30 days and 8-10 ng/mL from 31-365 days after transplantation. The sCr levels were expressed in mg/dL and sCr clearance in 24?h urine was determined using the formula sCr debugging: sCr = sCr urinary (mg/dL) × 24 h urinary volume (mL) × sCr (mg/dL) × 1440 × body surface (m²).

The clearance of sCr was calculated with the formula: MDRD = GFR (mL/min × 1.73 m²) = 186 × CrS − 1.154 × (age) − 0.203 × (0.742 in case of being a woman)[24].

2.3. Oxidants

2.3.1. Products of Lipoperoxidation (LPO). The serum LPO was measured using an FR12 assay kit (Oxford Biomedical Research Inc®., Oxford, MI, USA). Plasma samples treated with N-methyl-2-phenylindole were centrifuged at 12,791 rpm for 10 min, and the supernatant was obtained. The supernatant was added to a microplate, and the absorbance was measured at 586 nm. The duplicate standard intra-assay CV was 6.4%.

2.3.2. Nitric Oxide (NO). Before the assay, plasma samples were deproteinized by adding zinc sulfate (6 mg of zinc sulfate was added to 400 μL of the sample) and vortexed for one min, and the samples were centrifuged at 10,000 × g for 10 min at 4°C. For measuring NO, the kit NB98, Oxford Biochemical, Oxford, MI, USA, was used. The colorimetric signal was read at 540 nm. The duplicate standard intra-assay CV was 7.9%.

2.4. Antioxidants

2.4.1. Superoxide Dismutase. The kit (SOD No. 706002, Cayman Chemical Company®, USA) was used. The serum samples were diluted at 1:2 in sample buffer before the colorimetric assay. Color development was read at a wavelength of 440 nm. The dilution factor was used to calculate the results. The duplicate standard intra-assay CV was 5.4%.

2.4.2. Glutathione Peroxidase (GPx). The assay kit GPx 703,102 was used (Cayman Chemical Company®, USA). Plasma samples (20 μL) were added to a microplate of 96 wells with 70 μL of buffer, 50 μL of glutathione and

glutathione reductase mixture, and $50\,\mu$L of NADPH. The activity was obtained by measuring the absorbance decrease at 340 nm every min for 20 min. The activity is expressed as nmol/min/mL. The duplicate of positive control intra-assay CV was 1.5%.

2.4.3. Total Antioxidant Capacity. The total antioxidant capacity (TAC) quantification was done following the Total Antioxidant Power Kit (No. TA02.090130, Oxford Biomedical Research®). The serum samples and standards were diluted at 1 : 40, and $200\,\mu$L was placed in each well of a microplate. The concentration was expressed as mM equivalents of Trolox (an analog of vitamin E). The duplicate standard intra-assay CV was 5.7%.

2.5. Statistical Analysis. The results are presented in measures of central tendency and dispersion. The qualitative variables were determined in frequencies and percentages; the chi-square test was used when required. The results are expressed as mean ± standard deviation. The normality of data was determined, and the Shapiro-Wilk test was performed. For intragroup differences, the Wilcoxon rank test was used. The Kruskal-Wallis test was used for intergroup differences. The different letter denotes statistically significant difference using the Dunn-Bonferroni paired test. All $p \leq 0.05$ values were considered statistically significant.

2.6. Ethical Considerations. The study adhered to the ethical principles for medical research in human beings stipulated in the Declaration of Helsinki 64th General Assembly, Fortaleza, Brazil, October 2013 and in the Belmont Report. The Standards of Good Clinical Practice and the International Conference on Harmonization were followed. The study was category III (risk more significant than the minimum). The following provision of the General Health Law in Mexico on health research, Title Two, of the Ethical Aspects of research in human beings, Chapter I, Article 17 Letter of Consent Under Information, was required with the signature of witnesses. The study was approved by the Local Ethics and Research Committee with registration 2018-1001-214, before Cofepris 17CI11 020 146 and before Bioethics with number 11 CEI 003 20188080. The clinical trial registration number is NCT05232370.

3. Results

The recipients of the three RT groups were young patients ($p < 0.01$). Kidney donors were <50 years. The male gender predominated in the three study groups. Age showed a difference in the group that did not require antihypertensive medication 29 ± 3.83 years vs. those treated with Enalapril 24.38 ± 1.61 years ($p \leq 0.01$). The stature of the patients treated with Enalapril was greater than that of the other groups ($p \leq 0.01$). The number of transfusions and the time of hot and cold ischemia were similar in the three study groups (Table 1).

3.1. Clinical Data. The patients who did not require antihypertensive medication and those who ingested Losartan gained weight in the one-year follow-up measurement. The BMI increased significantly in the final determination in those who ingested Losartan ($p < 0.01$). Patients with RT who did not require antihypertensive medication kept their blood pressure normal throughout the study. Thirteen patients who had elevated baseline systolic and diastolic blood pressure (134.62 ± 7.54 mmHg and 87.31 ± 4.34 mmHg) ($p < 0.01$) were administered with Enalapril. After one year of follow-up of the patients who ingested Enalapril, their blood pressure was significantly modified (systolic 127.8 ± 4 mmHg and diastolic 78.92 ± 1.5 mmHg, $p < 0.01$). The thirteen patients with baseline systolic blood pressure values of 140 ± 4.83 mmHg and diastolic 89.92 ± 5.48 mmHg ($p < 0.01$) were administered with Losartan. In the determination at one year of follow-up, the systolic blood pressure was modified to 131.31 ± 7 mmHg and diastolic to 80.77 ± 5.3 mmHg ($p < 0.01$). Glucose decreased its concentration in the group without antihypertensive medication in the final determination with 137.38 ± 80.42 mg/dL baseline vs. 90.46 ± 17.46 mg/dL final ($p = 0.03$). The sCr levels were similar in the three groups in the baseline determination. At the end of the study, an apparent decrease in sCr levels was shown in the three study groups. The patients who did not require antihypertensive medication obtained sCr levels in the baseline determination, 12.84 ± 3.77 mg/dL vs. 1.18 ± 0.15 mg/dL at one year of follow-up ($p < 0.01$). Those who ingested Enalapril had baseline sCr levels of 12.16 ± 4.63 mg/dL and final levels of 1.17 ± 0.21 mg/dL ($p < 0.01$). The baseline sCr levels in those who ingested Losartan were 13.38 ± 1.79 mg/dL and at one year of follow-up 2.6 ± 3.27 mg/dL ($p < 0.01$). Area concentration in the three groups was different ($p = 0.02$), the group without antihypertensive was 122.92 ± 37.74 mg/dL at baseline levels vs. 31.39 ± 6.68 mg/dL in the final determination ($p < 0.01$). In those who ingested Enalapril, the baseline urea determination was 155.59 ± 28.3 mg/dL vs. 30.82 ± 5.05 mg/dL at the end of follow-up ($p < 0.01$). For the group treated with Losartan, the baseline urea levels were 127.40 ± 32.11 mg/dL vs. 70.04 ± 72.94 mg/dL at the end of follow-up ($p < 0.04$). TAC levels were homogeneous in the three study groups between the baseline results and one year of follow-up (Table 2).

3.2. Oxidative Stress Markers

3.2.1. LPO and Nitric Oxide Metabolites (NO). Table 3 shows the results of the LPO levels with the significant increase in LPO between the basal levels 5.6 ± 2.61 mM, and the final levels 8.65 ± 1.09 mM ($p \leq 0.01$) in patients who did not require antihypertensive medication can be seen. The LPO levels in the patients taking Enalapril and Losartan were similar between baseline and final results. NO metabolites did not show significant differences between the baseline and final results in the three study groups.

3.2.2. Marker of Oxidative Damage to DNA. The baseline levels of the oxidative damage marker to DNA in patients who did not require antihypertensive drugs were 68.88 ± 11 ng/mL with a significant increase at one year of follow-up, 74.47 ± 0.39 ng/mL ($p < 0.01$). At one year of follow-

TABLE 1: Inherent data to renal transplantation.

	Not antihypertensive	Enalapril	Losartan	p
Age (years)	29 ± 3.83^a	24.38 ± 1.61	28.46 ± 3.53	$<0.01^*$
Donor age (years)	37 ± 10.5	35.62 ± 7.32	39.54 ± 12.32	0.617
Transfusions	1.69 ± 0.48	1.62 ± 0.51	1.38 ± 0.51	0.273
Cold ischemia	56.46 ± 25.62	57.46 ± 17.08	70.01 ± 23.32	0.239
Warm ischemia	144.38 ± 101.41	122.62 ± 23.79	102.85 ± 19.21	0.237
Height (m)	1.68 ± 0.07	1.78 ± 0.08	1.72 ± 0.08^b	$<0.01^*$

The results are expressed as mean ± standard deviation. [a]vs. Enalapril. [b]vs. Losartan. *ANOVA of a factor.

up, the levels of those who ingested Enalapril increased significantly to 74.29 ± 0.63 ng/mL ($p = 0.02$) vs. baseline levels 52.94 ± 21.45 ng/mL. The same behavior was observed in the patients who ingested Losartan; in the baseline determination, 62.71 ± 19.6 ng/mL was obtained with a significant increase at one year of follow-up of 73.78 ± 1.88 ng/mL ($p < 0.01$). Significant intragroup differences were obtained (Table 3).

3.2.3. Antioxidants. A significant increase in the enzyme superoxide dismutase (SOD) activity was observed in the three study groups. In patients who did not require antihypertensive medication, baseline levels were 0.3 ± 0.2 U/L and at the end of follow-up 1.17 ± 0.63 U/L ($p < 0.01$). The activity of the SOD enzyme in the basal Enalapril group was 0.39 ± 0.17 U/L vs. at one year of follow-up 1.31 ± 0.67 U/L ($p < 0.01$). The activity of the SOD enzyme at the end of the follow-up of those who ingested Losartan was 1.19 ± 0.46 vs. the basal activity of the enzyme 0.25 ± 0.21 U/L ($p < 0.01$) (Table 3).

The GPx enzyme only showed a significant increase in its activity for the group that did not require antihypertensive treatment with 343.76 ± 214.82 nmol/min/mL (baseline) vs. 518.15 ± 163 nmol/min/mL (final) ($p = 0.03$). GPx activity in those who ingested Enalapril and Losartan was similar.

The determination of the total antioxidant capacity (CAT) showed a significant decrease in its baseline concentration of 59.78 ± 1.89 μM in patients who did not require antihypertensive treatment vs. the final determination 17.52 ± 3.4 μM ($p < 0.01$). Patients who ingested Enalapril also decreased CAT levels between baseline 65.45 ± 18.99 μM vs. the levels obtained at the end of the follow-up 14.2 ± 3.2 μM ($p < 0.01$). A similar situation was observed in the patients who ingested Losartan where the baseline levels were 61.10 ± 24.07 μM, and a significant decrease was observed at the end of the study 20.7 ± 5.3 μM ($p < 0.01$) (Table 3).

4. Discussion

Significant overexpression of the oxidative DNA damage marker in the determination at one year of follow-up in the RT recipients who did not require antihypertensive medication is striking; the same phenomenon occurred in those who ingested Enalapril and Losartan. Changes in the epige-

nome and DNA methylation also could be implicated in each of the processes mentioned above to affect the kidney or other organ systems [25]. The increased expression of the oxidative damage marker to DNA can partially explain inflammation and cellular senescence, which could accelerate premature vascular aging at RT recipients [26–28]. Nuclear erythroid factor 2 (NRF2) signaling related to nuclear erythroid factor 2 (NRF2) and vitamin K play a crucial role in counteracting OS, DNA damage, senescence, and inflammation, thus activating NRF2 and supplementation with vitamin K which could offer an attractive therapeutic target in patients undergoing RT [29].

The antioxidant activity of the SOD enzyme was found to be significantly increased in the final determination in the three groups of patients, those treated with Enalapril and Losartan and those that did not require antihypertensive medication, possibly trying to compensate for the oxidative imbalance that occurs in the posttransplant period. Two antioxidants antagonize free radicals, including the antioxidant enzymes SOD, GPx, and catalase, and non-enzymatic antioxidants such as vitamin E, C, β-carotene, and coenzyme Q. The enzyme SOD is considered the first line of antioxidants capable of antagonizing the imbalance of the redox state. Following the present study, a significant increase in the activity of the SOD enzyme has recently been reported in patients undergoing hemodialysis [30]. The activity of the antioxidant enzyme GPx was found to be significantly increased in patients who did not require antihypertensive medication, possibly trying to compensate for the significant increase in LPO found in the determination at one year of follow-up. Some investigations mention the importance of mitochondrial deterioration and cell death due to apoptosis as a mechanism of nephrotoxicity manifested by an increase in LPO [31]. It was recently reported that circulating malondialdehyde concentration is independently associated with the long-term risk of cardiovascular mortality in RT recipients with relatively lower renal function [32].

In addition to traditional cardiovascular risk factors, the attention of RT recipients has focused on other complex pathophysiological processes related to posttransplant renal function, including the effect of OS. It is widely known that OS is increased in CKD and is further aggravated by renal replacement therapies. OS is associated with the appearance of atherosclerosis, left ventricular hypertrophy, and cardiorenal syndrome [26]. Various mechanisms have been proposed to explain the association between OS and atherosclerosis;

TABLE 2: Biochemical and anthropometric data.

	Not antihypertensive n-13			Enalapril n-13			Losartan n-13			
	Baseline	One year	WCX	Baseline	1 year	WCX	Baseline	One year	WCX	K-W
Weight (kg)	67.08 ± 11.51[b]	68.31 ± 10.94[b]	0.05*	73.73 ± 12.93	74.46 ± 10.97	0.2	71.46 ± 13.11	74.08 ± 11.34	0.03*	0.03**
BMI (km/m^2)	23.77 ± 3.56	23.97 ± 3.51	0.2	23.11 ± 3.37	23.32 ± 3.19	0.9	24.42 ± 3.63	25.27 ± 3.08	<0.01*	0.05**
SBP (mmHg)	119.23 ± 3.88[a,b]	122.54 ± 2.54[a,b]	<0.01*	134.62 ± 7.54	127.8 ± 4	<0.01*	140 ± 4.83	131.31 ± 7	<0.01*	<0.01**
DBP (mmHg)	78.62 ± 2.5[a,b]	76.62 ± 3[b]	0.03*	87.31 ± 4.34	78.92 ± 1.5	<0.01*	89.92 ± 5.48	80.77 ± 5.3	<0.01*	<0.01**
Glucose (mg/dL)	137.38 ± 80.42	90.46 ± 17.46	0.03*	104.85 ± 31.48	87.08 ± 18.5	0.2	107.31 ± 35.03	103.23 ± 38.65	0.5	NS
Creatinine (mg/dL)	12.84 ± 3.77	1.18 ± 0.15	<0.01*	12.16 ± 4.63	1.17 ± 0.21	<0.01*	13.38 ± 1.79	2.6 ± 3.27	<0.01*	NS
Urea (mg/dL)	122.92 ± 37.74[a]	31.39 ± 6.68	<0.01*	155.59 ± 28.30	30.82 ± 5.05	<0.01*	127.40 ± 32.11	70.04 ± 72.94	0.04*	0.02**
Potassium mmol/L	4.14 ± 0.63	4.10 ± 0.50	NS	4.33 ± 0.75	4.01 ± 0.50	NS	4.69 ± 0.68	4.47 ± 0.64	NS	NS
Leukocytes (%)	11.95 ± 4.87	8.76 ± 1.73	0.1	11.2 ± 8.78	9.03 ± 1.89	0.3	10.62 ± 2.89	8.86 ± 2.47	0.05*	0.2
Lymphocytes (%)	11.08 ± 11.82[a]	22.16 ± 7.53	0.04*	21.43 ± 10.73[b]	20.06 ± 8.4	0.5	8.87 ± 4.45	15.93 ± 7.18	<0.01*	<0.01**
Hemoglobin (mg/dL)	11.14 ± 1.45	12.36 ± 0.69	<0.01*	10.23 ± 1.88	12.58 ± 34.38	<0.01*	10.58 ± 1.57	12.17 ± 1.61	0.02*	NS
Hematocrit (%)	35.28 ± 4.64	38.52 ± 3.01	0.6	34.75 ± 9.98	37.94 ± 3.68	0.1	31.88 ± 3.2	37.05 ± 5.59	<0.01*	NS
Platelets (μL)	230.62 ± 48.25[a,b]	283.46 ± 51.5	<0.01*	282.46 ± 25.46	322.69 ± 59.3	0.1	295.46 ± 41.56	331.77 ± 71.13	0.02*	<0.01**
TAC levels	10.24 ± 7.33	14.78 ± 8.06	NS	8.88 ± 5.03	11.32 ± 1.47	NS	10.29 ± 4.3	11.92 ± 4.4	NS	NS

The results are expressed as mean ± standard deviation. [a]vs. Enalapril. [b]vs. Losartan. *Wilcoxon rank test. **Kruskal-Wallis test. [a,b]The different letter denotes statistically significant difference using the Dunn-Bonferroni paired test. BMI: body mass index; SBP: systolic blood pressure; DBP: diastolic blood pressure; NS: nonsignificant.

TABLE 3: Oxidative stress markers.

	Not antihypertensive n-13			Enalapril n-13			Losartan n-13	
	Baseline	One year	WCX	Baseline	One year	WCX	Baseline	One year
Oxidants								
LPO (mM)	5.6 ± 2.61	8.65 ± 1.09	<0.01*	5.08 ± 3.11	9.5 ± 2.68	0.1	8.73 ± 8.6	7.45 ± 3.81
NO (μg/mL)	374.56 ± 42.97	350.8 ± 111.32	0.8	382.8 ± 42.06	343.51 ± 138.46	0.3	352.2 ± 47.46	401.51 ± 72.06
Oxidative damage to DNA								
8-OHdG (ng/mL)	68.88 ± 11[a]	74.47 ± 0.39	<0.01*	52.94 ± 21.45	74.29 ± 0.63	0.02*	62.71 ± 19.6	73.78 ± 1.88
Antioxidants								
SOD (U/L)	0.3 ± 0.2	1.17 ± 0.63	<0.01*	0.39 ± 0.17	1.31 ± 0.67	<0.01*	0.25 ± 0.21	1.19 ± 0.46
GPx (nmol/min/mL)	343.76 ± 214.82	518.15 ± 163	0.03*	288.70 ± 212.12	493.1 ± 264.06	0.9	448.61 ± 146.96	442.3 ± 242.67
TAC (μM)	59.78 ± 1.89	17.52 ± 3.4	<0.01*	65.45 ± 18.99	14.2 ± 3.2[b]	<0.01*	61.10 ± 24.07	20.7 ± 5.3

The results are expressed as mean ± standard deviation. [a]vs. Enalapril. [b]vs. Losartan. **Kruskal-Wallis test. *Wilcoxon rank test. [a,b]The different letter denotes statistical significant difference using the Dunn-Bonferroni paired test. LPO: lipoperoxides; NO: nitric oxide; 8-OHdG: 8-hydroxy2′-deoxyguanosine; SOD: superoxide dismutase; GPx: glutathione peroxidase. TAC: total antioxidant capacity.

among them are the following: (a) OS promotes enzymatic modification of circulating lipids and lipoproteins, (b) reactive oxygen species (ROS) are capable of directly conditioning dysfunction of endothelial [33], (c) immune system promotes a chronic proinflammatory state, and (d) OS promotes osteoblastic differentiation of vascular cells [34].

Indeed, the quality of life is low in patients with CKD; however, RT can improve the quality of life similar to healthy individuals [35]. The clinical and biochemical improvement observed in the RT recipients included in the present study is notable. However, some medications can delay kidney function in RT recipients, including adjusting immunosuppressive therapy, treating high blood pressure with ACEI drugs, ARA II type 1 drugs, calcium channel blocking drugs, and lipid control [36]. ACE inhibitors and type 1 ARBs may slow the progression of kidney disease by offering antiproteinuric effects [37, 38]. In 2013, the possible antioxidant protective effect related to the uptake of the Enalapril superoxide radical was reported by protecting the vascular endothelium against ROS in a dose-dependent manner in isolated abdominal aortas from rabbits and spontaneously hypertensive rats [39, 40].

Losartan is a potent, orally active, and selective nonpeptide blocker of the angiotensin II receptor type 1. Losartan reduces blood pressure, proteinuria, serum uric acid level, and posttransplant erythrocytosis. Losartan has positive effects on renal excretory function in adult CKD patients and RT recipients [41, 42]. Losartan increases proximal tubular caveolin 1. The intrarenal angiotensin II is probably involved in the downregulation of caveolin one during hypertension and kidney injury [43]. The HSP70i chaperone protein translocated to the plasma membrane, and its colocalization with caveolin one could be involved in the mechanism responsible for the cytoprotective effect of Losartan in the proximal tubules by decreasing OS through the downregulation of the NADPH oxidase Nox4 subunit [44]. However, these antihypertensives can have serious adverse events including hyperkalemia and metabolic acidosis [45]. In the present study, potassium levels did not change significantly in the final determination.

Various factors have been associated with increased cardiovascular risk in RT recipients during the postoperative period, such as the development of diabetes mellitus, arterial hypertension, dyslipidemia, and obesity [46]. Approximately 50% of patients gain weight after RT as a factor regardless of nutritional status before transplantation [47]. Increased body weight and its negative metabolic consequences may be associated with negative results after RT [48]. Per the preceding, in the present study, we found that patients who did not require antihypertensive medication and those who ingested Losartan significantly increased their weight at one year of follow-up, which could condition metabolic alterations with adverse effects evolution of RT.

The determination of sCr and urea and the estimation of GFR through different equations are considered biomarkers of kidney graft function used routinely in clinical transplantation. The sensitivity and specificity of these biomarkers are low, but they are inexpensive and readily accessible [49, 50]. In the present study, the levels of sCr and urea decreased significantly in the final determination as expected.

Another benefit of RT is the improvement in hemoglobin levels found in the three study groups in the determination at one year of follow-up under the previously reported. The authors found improvement in hemoglobin and hematocrit in patients with RT treated with TAC [51].

We consider that it is essential to monitor the expression of the oxidative damage marker to DNA, oxidants, and the activity of antioxidant enzymes as well as the function of the transplanted organ in addition to traditional kidney function tests to detect early alterations that can be corrected early to avoid the loss of the transplanted organ.

In conclusion, all the patients included in the study, regardless of the management with or without antihypertensive, presented overexpression of the marker of oxidative DNA damage, a significant increase in the activity of the SOD enzyme, and a significant decrease in the total antioxidant capacity as a systemic buffer of the redox state, which could suggest oxidative state imbalance. The increase in the activity of the SOD enzyme in all patients, including the increase in the GPx enzyme in patients who did not require antihypertensive medication, could suggest a compensatory effect in light of the significant increase in LPO in this group of patients. The present study results suggest that the determination of other markers in addition to those traditionally requested is required: sCr, urea, potassium, and glomerular filtration rate.

The limitations of the study are based on the small number of patients included and the short length of follow-up.

The study's strengths are based on the fact that it is a prospective cohort study before and after in patients with de novo RT with follow-up at one year. Soon, another study will be carried out with a longer follow-up time and a larger sample size.

Data Availability

Clinical data is restricted to protect the confidentiality of the participants and against misuse of the information. The data may be shared by the Mexican Social Security Institute (IMSS) through the approval of the Institution's Ethics Committee. Data used to support the findings of this study will be made available by the corresponding author provided the criteria for access to confidential data.

Conflicts of Interest

There is no conflict of interest to report.

References

[1] B. J. Nankivell and D. R. J. Kuypers, "Diagnosis and prevention of chronic kidney allograft loss," *Lancet*, vol. 378, no. 9800, pp. 1428–1437, 2011.

[2] T. Fujiwara, S. Teruta, S. Tsudaka, K. Ota, and H. Matsuda, "Clinical courses of graft failure caused by chronic allograft dysfunction in kidney transplantation," *Transplantation Proceedings*, vol. 49, no. 1, pp. 49–52, 2017.

[3] E. Günay, T. Çelebi, S. Şen et al., "Investigation of the factors affecting allograft kidney functions: results of 10 years," *Transplantation Proceedings*, vol. 51, no. 4, pp. 1082–1085, 2019.

[4] J. Sellarés, D. G. de Freitas, M. Mengel et al., "Understanding the causes of kidney transplant failure: the dominant role of antibody-mediated rejection and nonadherence," *American Journal of Transplantation*, vol. 12, no. 2, pp. 388–399, 2012.

[5] M. Arias, D. Serón, F. Moreso, O. Bestard, and M. Praga, "Chronic renal allograft damage: existing challenges," *Transplantation*, vol. 91, no. 9S, pp. S4–S25, 2011.

[6] L. A. Calò, P. A. Davis, B. Giacon et al., "Oxidative stress in kidney transplant patients with calcineurin inhibitor-induced hypertension: effect of ramipril," *Journal of Cardiovascular Pharmacology*, vol. 40, no. 4, pp. 625–631, 2002.

[7] L. M. Ruiz-Muñoz, F. Vidal-Vanaclocha, and I. Lampreabe, "Enalaprilat inhibits hydrogen peroxide production by murine mesangial cells exposed to high glucose concentrations," *Nephrology, Dialysis, Transplantation*, vol. 12, no. 3, pp. 456–464, 1997.

[8] A. C. Akbasli, K. Keven, B. Erbay, and S. Nebioglu, "Changes in oxidative stress in renal graft patients receiving calcineurin inhibitors: cyclosporine versus tacrolimus," *Experimental and Clinical Transplantation*, vol. 10, no. 5, pp. 439–445, 2012.

[9] P. S. Satyanarayana and K. Chopra, "Oxidative stress-mediated renal dysfunction by cyclosporine A in rats: attenuation by trimetazidine," *Renal Failure*, vol. 24, no. 3, pp. 259–274, 2002.

[10] G. Pizzino, N. Irrera, M. Cucinotta et al., "Oxidative stress: harms and benefits for human health," *Oxidative Medicine and Cellular Longevity*, vol. 2017, Article ID 8416763, 13 pages, 2017.

[11] A. R. Proteggente, T. G. England, A. Rehman, C. A. Rice-Evans, and B. Halliwell, "Gender differences in steady-state levels of oxidative damage to DNA in healthy individuals," *Free Radical Research*, vol. 36, no. 2, pp. 157–162, 2002.

[12] H. J. Lim, H. H. Lee, A. J. Kim et al., "Renin-angiotensin-aldosterone system blockade in critically ill patients is associated with increased risk for acute kidney injury," *The Tohoku Journal of Experimental Medicine*, vol. 238, no. 1, pp. 17–23, 2016.

[13] B. Sayin, B. Canver, B. Gurlek Demirci, T. Colak, B. H. Ozdemir, and M. Haberal, "Renin-angiotensin system blockage and avoiding high doses of calcineurin inhibitors prevent interstitial fibrosis and tubular atrophy in kidney transplant recipients," *Experimental and Clinical Transplantation*, vol. 15, no. 1, pp. 32–36, 2017.

[14] S. M. Cockfield, S. Wilson, P. M. Campbell et al., "Comparison of the effects of standard vs low-dose prolonged-release tacrolimus with or without ACEi/ARB on the histology and function of renal allografts," *American Journal of Transplantation*, vol. 19, no. 6, pp. 1730–1744, 2019.

[15] A. Zakrzewska, L. Tylicki, and A. Debska-Slizien, "Cardiovascular and renal outcomes of renin-angiotensin system blockade in renal transplant recipients," *Transplantation Proceedings*, vol. 50, no. 6, pp. 1834–1837, 2018.

[16] S. Hiremath, D. A. Fergusson, N. Fergusson, A. Bennett, and G. A. Knoll, "Renin-angiotensin system blockade and long-term clinical outcomes in kidney transplant recipients: a meta-analysis of randomized controlled trials," *American Journal of Kidney Diseases*, vol. 69, no. 1, pp. 78–86, 2017.

[17] C. G. Sreeadhara, R. Narayanaswamy, U. Lingaraju, V. Leelavathi, and S. M. Shivaprasad, "Early initiation of angiotensin-converting enzyme inhibitors in postrenal transplant period: a study from a state-run tertiary care center," *Saudi Journal of Kidney Diseases and Transplantation*, vol. 29, no. 3, pp. 637–642, 2018.

[18] V. Chander, D. Singh, N. Tirkey, H. Chander, and K. Chopra, "Amelioration of cyclosporine nephrotoxicity by irbesartan, a selective AT1 receptor antagonist," *Renal Failure*, vol. 26, no. 5, pp. 467–477, 2004.

[19] S. S. Padi and K. Chopra, "Selective angiotensin II type 1 receptor blockade ameliorates cyclosporine nephrotoxicity," *Pharmacological Research*, vol. 45, no. 5, pp. 413–420, 2002.

[20] T. Cvetković, R. Veličković-Radovanović, A. Stefanović et al., "Oxidative and nitrosative stress in stable renal transplant recipients with respect to the immunosuppression protocol - differences or similarities," *Journal of Medical Biochemistry*, vol. 34, no. 3, pp. 295–303, 2015.

[21] P. F. Katsakiori, E. P. Papapetrou, G. C. Sakellaropoulos, D. S. Goumenos, G. C. Nikiforidis, and C. S. Flordellis, "Factors affecting the long-term response to tacrolimus in renal transplant patients: pharmacokinetic and pharmacogenetic approach," *International Journal of Medical Sciences*, vol. 7, no. 2, pp. 94–100, 2010.

[22] World Health Organization, "Obesity and overweight," 2016, https://www.who.int/news-room/fact-sheets/detail/obesity-and-overweight.

[23] J. Lopes, M. Fonseca, A. Torres-Costoso et al., "Low- and moderate-intensity aerobic exercise acutely reduce blood pressure in adults with high-normal/grade I hypertension," *Journal of Clinical Hypertension*, vol. 22, no. 9, pp. 1732–1736, 2020.

[24] I. López-Pelayo, M. A. Mazuecos Blanca, M. V. García Palacios, F. Galán Sánchez, F. López Rodríguez, and M. A. Bailén García, "How to manage kidney transplant recipients: deciding between glomerular filtration rate-estimating equations, creatinine clearance and albumin-creatinine ratio, or albumin excretion," *Experimental and Clinical Transplantation*, vol. 17, no. 4, pp. 450–456, 2019.

[25] L. Heylen, B. Thienpont, M. Naesens, D. Lambrechts, and B. Sprangers, "The emerging role of DNA methylation in kidney transplantation: a perspective," *American Journal of Transplantation*, vol. 16, no. 4, pp. 1070–1078, 2016.

[26] L. Dai, L. J. Schurgers, P. G. Shiels, and P. Stenvinkel, "Early vascular ageing in chronic kidney disease: impact of inflammation, vitamin K, senescence and genomic damage," *Nephrology, Dialysis, Transplantation*, vol. 35, no. 2, pp. ii31–ii37, 2020.

[27] A. Posadzy-Małaczyńska, M. Kosch, M. Hausberg et al., "Large artery wall properties in dialyse and renal transplant patients with normal blood pressure," *Wiadomości Lekarskie*, vol. 57, no. 11-12, pp. 611–616, 2004.

[28] A. García-Sánchez, J. I. Gámez-Nava, E. N. Díaz-de la Cruz et al., "The effect of visceral abdominal fat volume on oxidative stress and proinflammatory cytokines in subjects with normal Weight, Overweight and Obesity," *Diabetes, Metabolic Syndrome and Obesity: Targets and Therapy*, vol. 13, pp. 1077–1087, 2020.

[29] M. Guerrero-Hue, S. Rayego-Mateos, C. Vázquez-Carballo et al., "Protective role of Nrf2 in renal disease," *Antioxidants*, vol. 10, no. 1, p. 39, 2021.

[30] T. Soleymanian, A. Ranjbar, M. Alipour, M. R. Ganji, and I. Najafi, "Impact of kidney transplantation on biomarkers of oxidative stress and inflammation," *Iranian Journal of Kidney Diseases*, vol. 9, no. 5, pp. 400–405, 2015.

[31] R. Heidari, S. Behnamrad, Z. Khodami, M. M. Ommati, N. Azarpira, and A. Vazin, "The nephroprotective properties of taurine in colistin-treated mice is mediated through the regulation of mitochondrial function and mitigation of oxidative

stress," *Biomedicine & Pharmacotherapy*, vol. 109, pp. 103–111, 2019.

[32] M. Yepes-Calderón, C. G. Sotomayor, R. O. B. Gans et al., "Post-transplantation plasma malondialdehyde is associated with cardiovascular mortality in renal transplant recipients: a prospective cohort study," *Nephrology, Dialysis, Transplantation*, vol. 35, no. 3, pp. 512–519, 2020.

[33] V. Cachofeiro, M. Goicochea, S. G. de Vinuesa, P. Oubiña, V. Lahera, and J. Luño, "Oxidative stress and inflammation, a link between chronic kidney disease and cardiovascular disease: new strategies to prevent cardiovascular risk in chronic kidney disease," *Kidney International. Supplement*, vol. 74, pp. S4–S9, 2008.

[34] N. Mody, F. Parhami, T. A. Sarafian, and L. L. Demer, "Oxidative stress modulates osteoblastic differentiation of vascular and bone cells," *Free Radical Biology & Medicine*, vol. 31, no. 4, pp. 509–519, 2001.

[35] M. M. Iqbal, N. Rahman, M. Alam et al., "Quality of life is improved in renal transplant recipients versus that shown in patients with chronic kidney disease with or without dialysis," *Experimental and Clinical Transplantation*, vol. 18, no. 1, pp. 64–67, 2020.

[36] D. Serón, F. Moreso, and J. M. Grinyó, "Prevention and management of late renal allograft dysfunction," *Journal of Nephrology*, vol. 14, no. 2, pp. 71–79, 2001.

[37] N. J. Webb, C. Lam, T. Loeys et al., "Randomized, double-blind, controlled study of losartan in children with proteinuria," *Clinical Journal of the American Society of Nephrology*, vol. 5, no. 3, pp. 417–424, 2010.

[38] N. J. Webb, S. Shahinfar, T. G. Wells et al., "Losartan and enalapril are comparable in reducing proteinuria in children," *Kidney International*, vol. 82, no. 7, pp. 819–826, 2012.

[39] J. H. Kim, H. Kim, Y. H. Kim, W. S. Chung, J. K. Suh, and S. J. Kim, "Antioxidant effect of captopril and enalapril on reactive oxygen species-induced endothelial dysfunction in the rabbit abdominal aorta," *The Korean Journal of Thoracic and Cardiovascular Surgery*, vol. 46, no. 1, pp. 14–21, 2013.

[40] G. Chandran, K. N. Sirajudeen, N. S. Yusoff, M. Swamy, and M. S. Samarendra, "Effect of the antihypertensive drug enalapril on oxidative stress markers and antioxidant enzymes in kidney of spontaneously hypertensive rat," *Oxidative Medicine and Cellular Longevity*, vol. 2014, Article ID 608512, 10 pages, 2014.

[41] R. Holgado, F. Anaya, and D. Del Castillo, "Angiotensin II type 1 (AT1) receptor antagonists in the treatment of hypertension after renal transplantation," *Nephrology, Dialysis, Transplantation*, vol. 16, no. 1, pp. 117–120, 2001.

[42] A. L. Kamper and A. H. Nielsen, "Uricosuric effect of losartan in patients with renal transplants," *Transplantation*, vol. 72, no. 4, pp. 671–674, 2001.

[43] V. Bocanegra, W. Manucha, M. R. Peña, V. Cacciamani, and P. G. Vallés, "Caveolin-1 and Hsp70 interaction in microdissected proximal tubules from spontaneously hypertensive rats as an effect of losartan," *Journal of Hypertension*, vol. 28, no. 1, pp. 143–155, 2010.

[44] P. G. Vallés, V. Bocanegra, V. V. Costantino, A. F. Gil Lorenzo, M. E. Benardon, and V. Cacciamani, "The renal antioxidative effect of losartan involves heat shock protein 70 in proximal tubule cells," *Cell Stress & Chaperones*, vol. 25, no. 5, pp. 753–766, 2020.

[45] H. Sakallı, E. Baskın, U. S. Bayrakcı, G. Moray, and M. Haberal, "Acidosis and hyperkalemia caused by losartan and enalapril in pediatric kidney transplant recipients," *Experimental and Clinical Transplantation*, vol. 12, no. 4, pp. 310–313, 2014.

[46] S. Palepu and G. V. Prasad, "New-onset diabetes mellitus after kidney transplantation: current status and future directions," *World Journal of Diabetes*, vol. 6, no. 3, pp. 445–455, 2015.

[47] W. Chan, J. A. Bosch, D. Jones, P. G. McTernan, A. C. Phillips, and R. Borrows, "Obesity in kidney transplantation," *Journal of Renal Nutrition*, vol. 24, no. 1, pp. 1–12, 2014.

[48] E. F. Pedrollo, C. Corrêa, B. B. Nicoletto et al., "Effects of metabolic syndrome on kidney transplantation outcomes: a systematic review and meta-analysis," *Transplant International*, vol. 29, no. 10, pp. 1059–1066, 2016.

[49] A. Abbasian Ardakani, A. R. Sattar, J. Abolghasemi, and A. Mohammadi, "Correlation between kidney function and sonographic texture features after allograft transplantation with corresponding to serum creatinine: a lng term follow-up study," *Journal of Biomedical Physics & Engineering*, vol. 10, no. 6, pp. 713–726, 2020.

[50] Š. Borštnar, Ž. Večerić-Haler, E. Boštjančič et al., "Uromodulin and microRNAs in kidney transplantation-association with kidney graft function," *International Journal of Molecular Sciences*, vol. 21, no. 16, p. 5592, 2020.

[51] J. Sułowicz, D. Cieniawski, E. Ignacak, A. Bętkowska-Prokop, M. Kuźniewski, and W. Sułowicz, "Comparison of kidney transplant function, lipid metabolism disorders, and glucose and hemoglobin concentration in transplant patients treated with proliferation signal inhibitor (everolimus) or calcineurin inhibitor (tacrolimus)," *Transplantation Proceedings*, vol. 52, no. 8, pp. 2347–2351, 2020.

Research Article

Cyclic Polypeptide D7 Protects Bone Marrow Mesenchymal Cells and Promotes Chondrogenesis during Osteonecrosis of the Femoral Head via Growth Differentiation Factor 15-Mediated Redox Signaling

Jiazheng Chen [1], **Zichen Cui** [2,3] **Yi Wang,** [1] **Linmao Lyu** [4] **Changgong Feng,** [2,3] **Dianjie Feng,** [1] **Yifan Cheng,** [1] **Ziqing Li** [2,3] **and Shui Sun** [1,2,3]

[1]*Department of Joint Surgery, Shandong Provincial Hospital, Cheeloo College of Medicine, Shandong University, Jinan, Shandong 250012, China*

[2]*Department of Joint Surgery, Shandong Provincial Hospital Affiliated to Shandong First Medical University, Jinan, Shandong 250021, China*

[3]*Orthopaedic Research Laboratory, Medical Science and Technology Innovation Center, Shandong First Medical University & Shandong Academy of Medical Sciences, Jinan, Shandong 250117, China*

[4]*Department of Emergency Medicine, Qilu Hospital of Shandong University, Jinan, China*

Correspondence should be addressed to Ziqing Li; liziqing@sdfmu.edu.cn and Shui Sun; sunshui@sdfmu.edu.cn

Osteonecrosis of the femoral head (ONFH) is a debilitating disease that is closely associated with the clinical application of high-dose glucocorticoids. Elevated oxidative stress contributes to the pathophysiological changes observed in ONFH. The lack of effective treatments besides surgical intervention highlights the importance of finding novel therapeutics. Our previous studies demonstrated that D7, a cyclic polypeptide, enhances the adhesion, expansion, and proliferation of bone marrow mesenchymal stem cells (BMSCs). Therefore, in this study, we investigated the therapeutic effects of D7 against ONFH in BMSCs and evaluated the underlying mechanisms. First, we screened for ONFH risk factors. Then, we applied D7 treatment to steroid-induced ONFH (SONFH) in an in vitro model produced by dexamethasone (DEX) to further elucidate the underlying mechanisms. We found negative correlations among oxidative stress marker expression, growth differentiation factor 15 (GDF15) levels, and ONFH. Furthermore, we demonstrated that DEX inhibited the proliferation and induced apoptosis of BMSCs by suppressing GDF15/AKT/mammalian target of rapamycin (mTOR) signaling. D7 alleviated DEX-induced BMSCs injury and restored the chondrogenic function of BMSCs by activating GDF15/AKT/mTOR signaling. In addition, DEX-induced excessive reactive oxygen species (ROS) generation was an upstream trigger of GDF15-mediated signaling, and D7 ameliorated this DEX-induced redox imbalance by restoring the expression of antioxidants, including superoxide dismutase (SOD) 1, SOD2, and catalase, via regulation of GDF15 expression. In conclusion, our findings revealed the potential therapeutic effects of D7 in SONFH and showed that this protective function may be mediated via inhibition of DEX-induced ROS and activation of GDF15/AKT/mTOR signaling, thereby providing insights into the potential applications of D7 in SONFH treatment.

1. Introduction

Osteonecrosis of the femoral head (ONFH) is a progressive disease that causes collapse of the joint cartilage and the femoral head, leading to substantial hip pain and loss of joint function [1, 2]. Clinical application of glucocorticoids (GCs) is the leading cause of ONFH, also called steroid-induced ONFH (SONFH). The pathophysiological changes

associated with SONFH include disruption of bone marrow-derived mesenchymal stem cells (BMSCs) self-renewal; acceleration of an imbalance among osteogenic, chondrogenic, and adipogenic differentiation [3]; circulatory impairment [4]; modified artery constriction [5]; and intramedullary pressure changes [6]. To date, numerous surgical procedures have been applied for ONFH treatment, including total hip arthroplasty (THA) and joint-preserving surgeries, such as core decompression (CD), osteotomy, and free vascularized fibular grafting. Additionally, CD combined with cell transplantation prevents early-stage ONFH from femoral head collapse and delays the need for THA [7]. Although these treatments can substantially improve the quality of life of patients, postoperative complications, such as infection, deep vein thromboembolism, peroneal nerve palsy, proximal femoral fracture, ankle functional impairment, dislocation, periprosthetic fracture, and prosthesis loosening, cannot be neglected [8–10]. Therefore, it is essential to identify novel therapeutic targets in early-stage ONFH to prevent further pathophysiological changes and to delay surgical interventions.

Reactive oxygen species (ROS) contribute to the pathogenesis of SONFH [11]. Under normal physiological conditions, ROS are produced by cell metabolism. A balanced level of ROS plays a significant role in cell homeostasis and signal transduction [12]. However, under stress conditions, the balance between the formation and degradation of ROS is disrupted, resulting in oxidant accumulation [13] and further inducing endoplasmic reticulum stress, DNA damage, mitochondrial dysfunction, and BCL-2/BAX apoptosis pathway activation [14]. Application of high doses of GCs induces severe oxidative stress by boosting the accumulation of intracellular ROS [15], thereby leading to apoptosis of BMSCs and further deterioration of the osteogenic and chondrogenic differentiation of BMSCs [16–18]. Oxidative stress also causes vascular endothelial dysfunction, resulting in blood vessel injury, which is another cause of SONFH pathogenesis [12]. Therefore, ROS activators have been used for establishing ONFH models in basic research [11], and reducing oxidative stress may constitute a therapeutic strategy for SONFH treatment.

Growth differentiation factor 15 (GDF15), also known as macrophage inhibitory cytokine-1, plays an important role in ROS generation and serves as a marker of oxidative stress in many diseases [19–21]. GDF15 is a member of the cell stress-responsive transforming growth factor β superfamily [22] and has been reported to suppress ROS generation via activation of the SMAD1 signaling pathway [23]. However, the specific role of GDF15 in bone metabolism is unclear. Westhrin et al. reported that GDF15 promotes osteoclast differentiation and inhibits osteoblast differentiation in multiple myeloma [24], whereas Symmank et al. demonstrated that mechanical stimulation can induce periodontal ligament cells to secrete more GDF15 and promote osteoblast differentiation [25]. Moreover, for several other types of cells, the AKT/mammalian target of rapamycin (mTOR) pathway acts downstream of GDF, and GDF15 could promote the survival and proliferation of cells via the activation of AKT/mTOR signaling pathway [26–28]. At the same time, the AKT/mTOR signaling pathway is closely associated with ROS, as its activation protects cells from ROS accumulation and restores the balance of ROS [29, 30]. Nonetheless, the mechanisms through which GDF15/AKT/mTOR signaling mediates the pathophysiological changes in association with SONFH and whether this signaling pathway can restore the redox balance in BMSCs under GC conditions are largely unknown.

In our previous study, we had screened cyclic polypeptide D7 from the cyclic peptide phage display library (Ph.D.-C7C) by phage display technology [31]. Phage display is a robust, high-throughput screening strategy in which a library of peptide or protein variants is expressed on the outside of a phage virion, and the genetic material encoding each variant is present on the inside of the virion [32]. Based on the different binding affinities of the cyclic peptide and the target cell, we screened D7 through three or four biopanning procedures, following previously described protocols [33, 34]. In addition, we demonstrated that D7 could enhance the adhesion, expansion, and proliferation of BMSCs on β-tricalcium phosphate scaffolds [31], in contrast to the pathophysiological changes related to SONFH.

Hence, in this study, we aimed to investigate the therapeutic effects of D7 on BMSCs proliferation and differentiation under SONFH conditions and elucidate the underlying mechanisms.

2. Methods and Materials

2.1. Reagents and Antibodies. Reagents for cell transfection were obtained from RIBOBIO (cat. no. C10511-05; Guangzhou, China). siRNA-GDF15 was synthesized by GEKYGENE (Shanghai, China). Reagents for cell differentiation and detection included ascorbic acid (cat. no. A8960-5G; Sigma-Aldrich, USA), dexamethasone (DEX; MCE, USA), paraformaldehyde (PFA), transforming growth factor (TGF)-β_1 (cat. no. P01137; Peprotech, China), insulin, transferrin, and sodium selenite (ITS; cat. no. I3146; Sigma-Aldrich), and N-Acetyl-L-cysteine (NAC; cat. no. A9165; Sigma-Aldrich). Primary antibodies for Western blotting (WB) and immunofluorescence (IF) staining used in this study were from the following sources: anti-AKT (cat. no. 10176-2-AP), anti-phospho-AKT (cat. no. 66444-4-Ig), anti-glyceraldehyde 3-phosphate dehydrogenase (cat. no. 60004-1-Ig), anti-BCL-XL (cat. no. 10783-1-AP), BCL-2 (cat. no. 26593-1-AP), anti-BAX (cat. no. 50599-2-Ig), anti-poly (ADP-ribose) polymerase (PARP; cat. no. 66520-1-Ig), anti-aggrecan (cat. no. 13880-1-AP), anti-matrix metalloproteinase (MMP) 13 (cat. no. 18165-1-AP), anti-CD29 (cat. no. 12594-1-AP), anti-collagen type 2 (COL2; cat. no. 28459-1-AP), and anti-mTOR (cat. no. 66888-1-Ig) from Proteintech (China); anti-phospho-mTOR (cat. no. 5536S) from Cell Signaling Technology (Danvers, MA, USA); anti-GDF15 (cat. no. 27455-4-AP) from Santa Cruz Biotechnology (Dallas, TX, USA); and anti-SOX9 from Abcam (USA). Secondary antibodies for WB, including anti-mouse (cat. no. SA00001-1) and anti-rabbit (cat. no. SA00001-2) antibodies, were from Proteintech. Secondary antibodies for IF, including anti-mouse (cat. no. SA00003-

1) and anti-rabbit (cat. no. SA00003-2) antibodies, were from Proteintech.

2.2. Synthesis of Peptides.
The synthesis of peptides was performed as previously described [35]. The cyclic peptide (amino acid sequence CDNVAQSVC) contained seven amino acids; each amino acid terminus was conjugated with a pair of cysteine residues that formed an intramolecular disulfide linkage. All peptides were synthesized by solid-phase peptide synthesis using fluorenylmethyloxycarbonyl chemistry (Scilight-Peptide, Inc., Beijing, China).

2.3. Cell Culture.
Sprague–Dawley rat BMSCs were purchased from Cyagen Biosciences, Inc. (cat. no. RASMX-01001; Guangzhou, China). BMSCs were grown at 37°C with a 5% CO_2 atmosphere in complete medium (α-minimum essential medium (α-MEM) containing 10% fetal bovine serum (FBS) and 1% penicillin/streptomycin). The cells were passaged when they reached 70–80% confluence, and only passages 3–6 were used for experiments.

2.4. Western Blotting.
WB was performed as previously described, with slight modifications [36]. Cells were lysed using ice-cold RIPA buffer containing 1% phenylmethylsulfonyl fluoride and 1% phosphatase inhibitor. Human tissue samples were added to RIPA lysis buffer at a ratio of 10 mg per 100 μL. A tissue grinder was used to break the tissue. Protein concentrations were measured using BCA assays according to the manufacturer's instructions. Equal amounts of protein (20 μg) were separated by sodium dodecyl sulfate polyacrylamide gel electrophoresis on 10% or 12% gels and transferred to polyvinylidene difluoride membranes. After blocking in TBST containing 5% fat-free milk, the membranes were incubated overnight at 4°C with primary antibodies. All primary antibodies were used at a dilution of 1:1000, except for anti-cleaved-caspase 3, which was used at a dilution of 1:500. The secondary antibody (diluted 1:5000) was incubated with membranes for 1 h at room temperature. Finally, the protein signals were visualized using Immobilon Western Chemiluminescent HRP Substrate (cat. no. WBKLS0500; Merck Millipore, Germany).

2.5. Reverse Transcription Quantitative Polymerase Chain Reaction (RT-qPCR).
RT-qPCR was performed as previously described [13]. We extracted total RNA using TRIzol reagent (TaKaRa Bio, China). One microgram RNA was used to synthesize cDNA using a PrimeScriptRT reagent Kit with gDNA Eraser (TaKaRa Bio). The sequences of the specific primers are shown in Table 1. PCR amplification was performed using a Roche LightCycler 480II (Roche, Basel, Switzerland). We analyzed the relative levels of gene expression using the $2^{-\triangle\triangle CT}$ method, with β-actin as an endogenous control.

2.6. Cell Viability Assay.
Cell viability was evaluated using Cell Counting Kit-8 (CCK-8) assays (cat. no. HY-K0301; MCE, USA). Briefly, 5000 cells were seeded into each well of a 96-well plate and cultured in α-MEM containing 10% FBS. After treatment with DEX and other reagents for 72 h, the cells were washed thrice with phosphate-buffered saline (PBS). Then, 10 μL CCK-8 solution in 100 μL α-MEM was added to each well. After incubation for 2 h at 37°C in the dark, the absorbance was measured using a microplate reader at a wavelength of 450 nm.

2.7. Lactate Dehydrogenase (LDH) Release Assay.
LDH release assays were performed as previously described [36]. Briefly, LDH was released from necrotic or apoptotic cells into the culture medium. BMSCs were seeded into 24-well plates and cultured in serum-free α-MEM with DEX and treated for 48 h. LDH activity was measured using a commercially available assay kit (Roche). The optical density was measured using a spectrophotometer at a wavelength of 490 nm.

2.8. EdU Incorporation Assay.
Cell proliferation was evaluated by monitoring DNA synthesis using EdU incorporation assays. Briefly, 5000 cells/well were seeded into 96-well plates and incubated in α-MEM containing 10% FBS with specific treatments for 24 h. Next, EdU was diluted to 10 μM and added to each well for 2 h. The EdU working solution provided in the kit (cat. no. C6015; Suzhou Yuheng Biotechnology, China) was mixed according to the manufacturer's instructions. Subsequently, the cells were fixed with 4% PFA for 20 min, permeabilized with 0.5% Triton X-100 in PBS for 5 min, blocked with 3% bovine serum albumin (BSA) for 1 h, and mixed with 100 μL reagent according to the manufacturer's protocol.

2.9. Intracellular ROS Measurement.
The level of intracellular ROS was evaluated using a reactive oxygen species assay kit (cat. no. S0033; Beyotime Biotechnology, Shanghai, China). Cells were seeded in six-well plates at a density of 30% and then transfected with siRNA for 24 h. DCFH-DA was then diluted in serum-free culture medium at a ratio of 1:1000 to a final concentration of 10 μM. The cell culture medium was removed, and 1 mL diluted DCFH-DA was added to each well. After 30 min, DEX and D7 treatments were applied, and cells were again transfected with siRNA. Fluorescence intensity was observed by fluorescence microscopy after 30 min.

2.10. In Vitro Chondrogenic Induction of BMSCs.
Chondrogenic differentiation of BMSCs was performed following a previously described method, with slight modifications [37]. BMSCs were plated into 12-well plates at a density of 2×10^5 cells/well and incubated with α-MEM containing 10% FBS at 37°C and 5% CO_2 for 24 h. After reaching 80% confluence, the cells were cultured in α-MEM containing 10% FBS, 1% penicillin-streptomycin, 1% ITS (Sigma-Aldrich), 100 nM DEX (MCE), 10 ng TGF-β1 (PeproTech), and 10 mg/mL ascorbic acid. Chondrogenic differentiation of BMSCs was induced for 21 days, during which time the medium was replaced every other day. The cells were then stained with Alcian blue.

2.11. Alcian Blue Staining.
After incubation in chondrogenic inductive medium for 21 days, the cells were fixed in 4% PFA for 15 min. Thereafter, the cells were exposed to Alcian

TABLE 1: Primer sequences for quantitative real-time PCR.

Gene	Forward primer	Reverse primer
ACTB	GGAGATTACTGCCCTGGCTCCTA	GACTCATCGTACTCCTGCTTGCTG
SOD1	GGCAAAGGTGGAAATGAAGAAA	CAGTTTAGCAGGACAGCAGATGAG
SOD2	CATACTTGGTGTGAGCTGCTCTTGA	TTTGATGGCCTTATGATGACAGTGA
GPX1	AGGAGAATGGCAAGAATGAAGAGA	GGAAGGTAAAGAGCGGGTGAG
GR	TGCCCTGGGTTGGAGATCATA	TGGTCATACATGCAGGGTAGAGACA
CAT	GAACATTGCCAACCACCTGAAAG	GTAGTCAGGGTGGACGTCAGTGAA

ACTB: β-Actin; *SOD1*: superoxide dismutase 1; *SOD2*: superoxide dismutase 2; *GPX1*: glutathione peroxidase; *GR*: glutathione reductase; *CAT*: catalase.

(a)

(b)

(c)

(d)

(e)
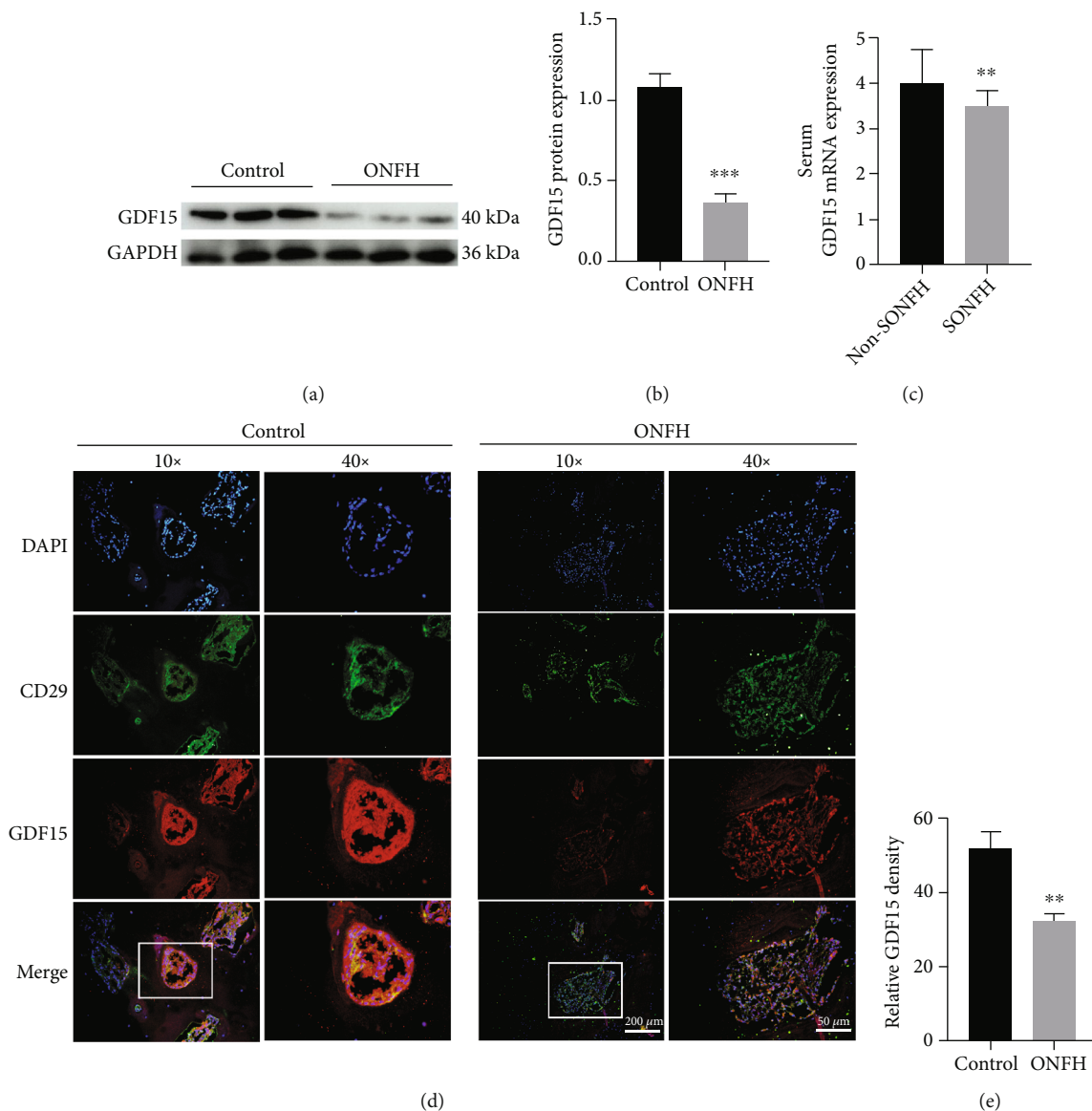
FIGURE 1: GDF15 expression is suppressed in ONFH samples. (a) Western blotting analysis of GDF15 expression in the ONFH and control groups ($n = 3$). (b) Quantitative analysis of the data from (a). $^{***}p < 0.01$ versus the control group. (c) GDF15 expression in the GSE123568 dataset. (d) GDF15 expression in BMSCs from SONFH and healthy (control) femoral head tissues, as analyzed by immunofluorescence staining using anti-CD29 and GDF15 antibodies. (e) Quantitative analysis of the data from (d). $^{**}p < 0.01$ versus the control group. Quantitative data are presented as means ± SD. $^{**}p < 0.01$ versus the non-SONFH group.
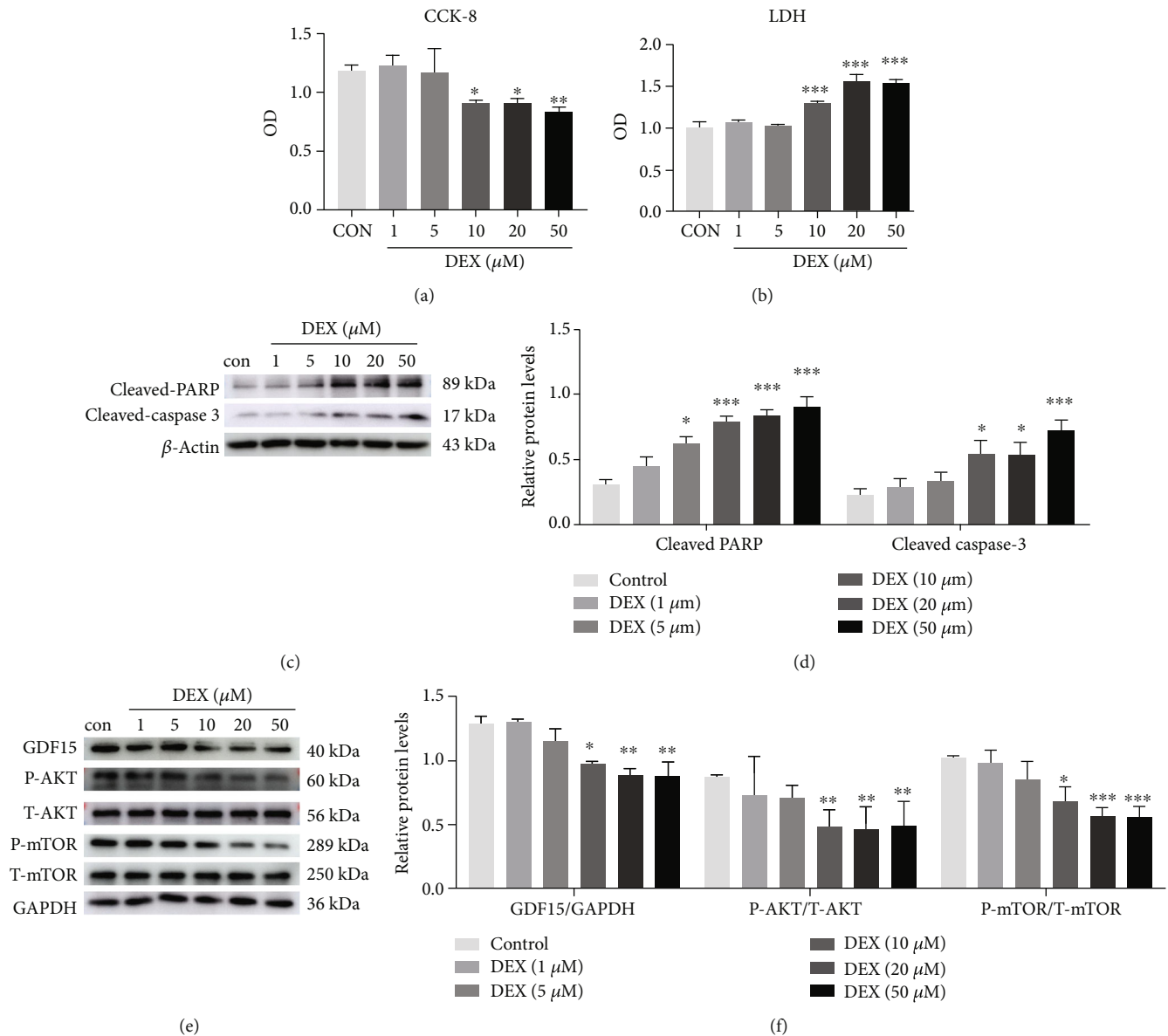
FIGURE 2: DEX inhibits BMSCs proliferation and induces BMSCs apoptosis via suppression of GDF15 expression and downregulation of AKT/mTOR signaling. (a) BMSCs viability following DEX stimulation, as evaluated by CCK-8 assays ($n = 3$). $^{*}p < 0.05$, $^{**}p < 0.01$ versus the control. Cells were incubated with complete medium for 2 days. (b) BMSCs apoptosis induced by DEX stimulation was measured by LDH release assays ($n = 3$). $^{***}p < 0.001$ versus the control. Cells were treated with DEX in serum-free medium for 48 h. (c) Western blotting (WB) analysis of the effects of DEX (0–$50 \mu M$) on the expression of apoptosis-related proteins (cleaved-PARP and cleaved-caspase 3) in BMSCs. Cells were treated with DEX in serum-free medium for 48 h before protein extraction. (d) Quantitative analysis of the data from (c) ($n = 3$). $^{*}p < 0.05$, $^{***}p < 0.001$ versus the control. (e) WB analysis of the effects of DEX (0–$50 \mu M$) on GDF15 expression and AKT/mTOR phosphorylation in BMSCs. Cells were treated with DEX in complete medium for 48 h before protein extraction. (f) Quantitative analysis of the data from (e) ($n = 3$). $^{*}p < 0.05$, $^{**}p < 0.01$, $^{***}p < 0.001$ versus the control. Quantitative data are presented as means ± SD.

acidizing fluid (Solarbio, Beijing, China) for 3 min and Alcian staining solution for 30 min.

2.12. Immunofluorescence Staining. IF staining of cells was performed as previously described [38], and BMSCs were seeded on cover slips at an appropriate density (30–40% confluence). Twenty-four hours later, the cells were incu-

bated with different treatments for 24 h. Cells were fixed with 4% PFA for 30 min and permeabilized with 0.5% Triton X-100 in PBS for 10 min. The cells were then blocked with 1% BSA for 1 h at room temperature. After incubation with primary antibody (anti-GDF15 diluted at 1 : 100) overnight at 4°C, the cells were incubated with the specific secondary antibody for 1 h and 4′,6-diamidino-2-phenylindole (DAPI;

(a)

(b)

(c)

(d)
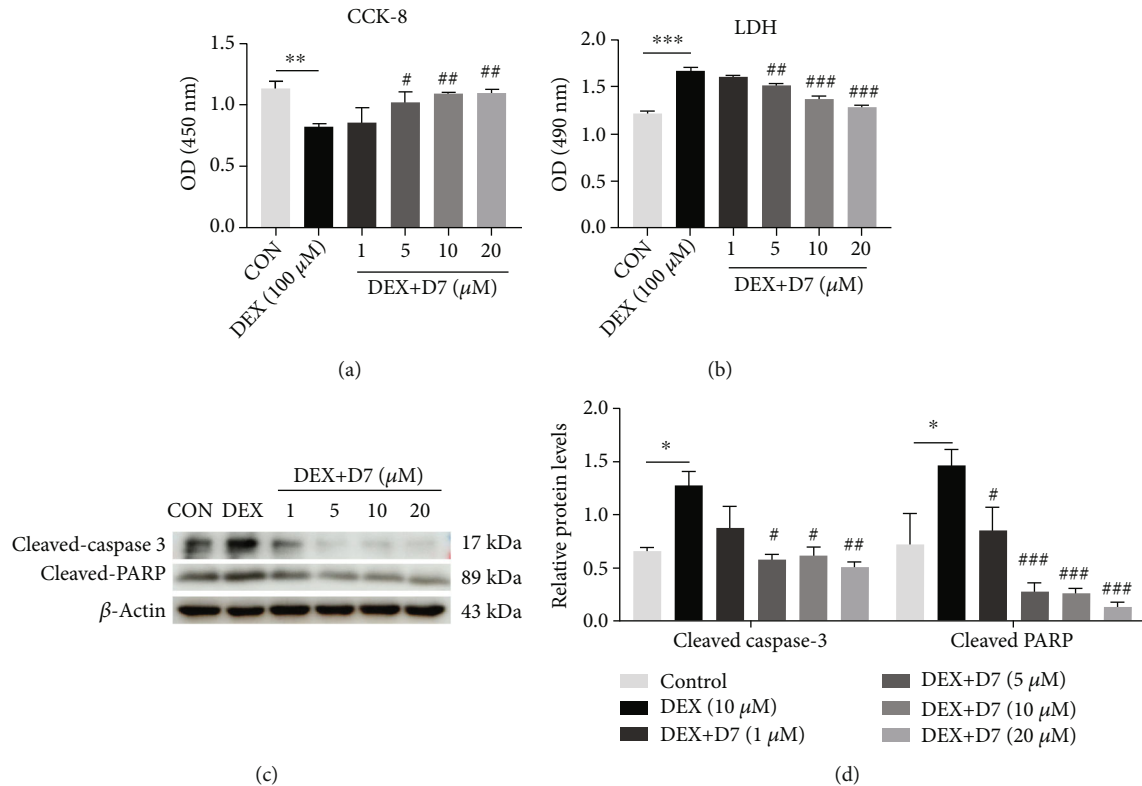
FIGURE 3: D7 alleviates DEX-induced BMSCs damage in a concentration-dependent manner. (a) The viability of BMSCs following DEX and D7 stimulation was examined by CCK-8 assays ($n = 3$). $^{**}p < 0.01$ versus the control; $^{#}p < 0.05$, $^{##}p < 0.01$ versus DEX (10 μM). Cells were incubated with complete medium for 2 days. (b) BMSCs apoptosis following DEX and D7 stimulation was examined by LDH release assays ($n = 3$). $^{***}p < 0.001$ versus the control; $^{##}p < 0.01$, $^{###}p < 0.001$ versus DEX (10 μM). Cells were treated with DEX and D7 in serum-free medium for 48 h before protein extraction. (c) WB analysis of the effects of D7 on cleaved-PARP and cleaved-caspase 3 levels in BMSCs ($n = 3$). $^{***}p < 0.001$ versus the control; $^{###}p < 0.001$ versus DEX (10 μM). Cells were treated with DEX and D7 in serum-free medium for 48 h before protein extraction. (d) Quantitative analysis of the data from (c) ($n = 3$). $^{*}p < 0.05$ versus the control group; $^{#}p < 0.05$, $^{##}p < 0.01$, $^{###}p < 0.001$ versus DEX (10 μM). Quantitative data are presented as means ± SD.

cat. no. C0065; Solarbio) for 5 min, sealed, and visualized using a Nikon fluorescence microscope (Axio Observer 3; Carl Zeiss AG, Germany).

After tissue isolation, human tissues were fixed in PFA for 48 h. Subsequently, tissues were decalcified in 10% ethylenediaminetetraacetic acid (EDTA)/PBS for 1 month. Decalcification was considered complete when a needle could easily penetrate the bone tissue. After embedding in paraffin, tissues were cut into 7 μM-thick tissue sections for IF staining. After deparaffinization, the sample slices were used for IF staining. Briefly, the slices were placed in antigen repair solution, using a microwave oven at 100 W for 3 min to boil, followed by 50 W for 7 min. Heating was then stopped, and the samples were allowed to cool normally for 20–30 min. The slices were then permeabilized with 0.5% Triton-100X for 5 min and blocked with horse serum for 1 h at room temperature. After incubation with primary antibody (anti-CD29 diluted at 1 : 200; anti-GDF15 diluted at 1 : 100) overnight at 4°C, the slices were incubated with the specific secondary antibody for 1 h and DAPI (cat. no. C0065; Solarbio) for 5 min. Finally, the slices were incubated with Autofluo Quencher (cat. no. C1212; APPLYGEN, Beijing,

China) for 10 min and covered with mounting medium, antifading (cat. no. S2100; Solarbio). The slices were sealed and visualized using a fluorescence microscope (Axio Observer 3; Carl Zeiss AG). All procedures involving human tissues were performed following protocols approved by the Shandong Provincial Hospital (Shandong, China; NSFC: No. 2019-187).

2.13. Terminal Deoxynucleotidyl Transferase dUTP Nick-End Labeling (TUNEL) Assay. Apoptotic cells were identified using a TUNEL staining kit (cat. no. KGA7072; KeyGEN BioTECH, China), as previously described [39]. Cells were seeded onto 24-well cover glasses and cultured in serum-free α-MEM with specific reagents for 48 h. The cells were then subjected to TUNEL staining according to the manufacturer's instructions, sealed, and visualized under a fluorescence microscope. Green staining indicated TUNEL-positive cells, and the percentage of positive cells was calculated in three random fields.

2.14. Flow Cytometry. The level of intracellular ROS was evaluated using a reactive oxygen species assay kit (cat. no.

(a)

(b)

(c)

(d)

(e)

(f)
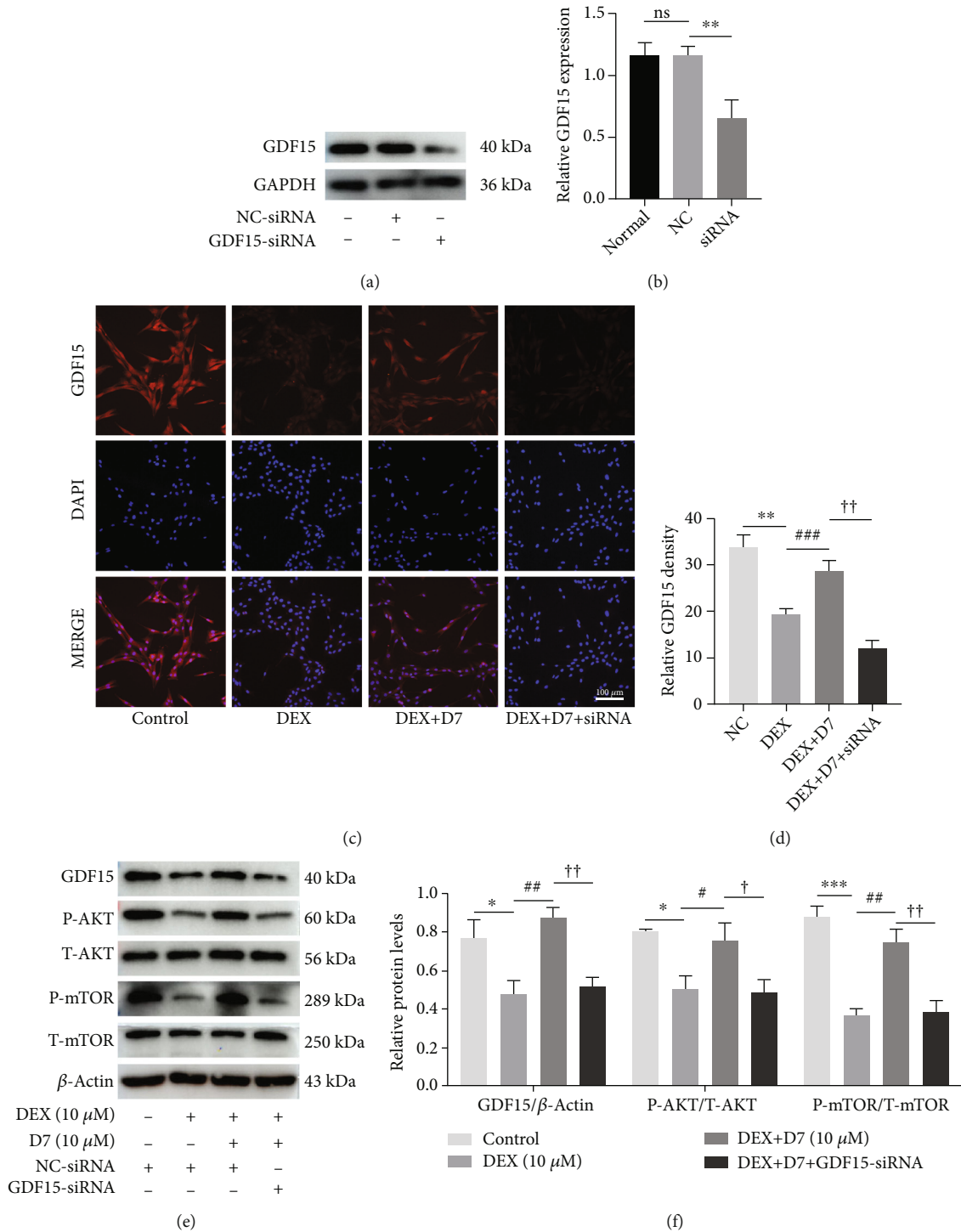
Figure 4: D7 restores DEX-dependent inhibition of AKT/mTOR signaling via upregulation of GDF15 expression in BMSCs. (a) Western blotting (WB) analysis of the efficiency of siRNA-GDF15 transfection. Cells were transfected with siRNA and incubated with complete medium for 48 h. (b) Quantitative analysis of data from (a) ($n = 3$). $^{**}p < 0.01$ versus the normal and negative control groups. (c) Immunofluorescence analysis of GDF15 expression in BMSCs under different experimental conditions. Cells were transfected with siRNA and treated with different reagents for 24 h. (d) Quantitative analysis of data from (c) ($n = 3$). $^{**}p < 0.01$ versus the NC group; $^{###}p < 0.001$ versus the DEX group; $^{††}p < 0.01$ versus the DEX + D7 group. (e) WB analysis of GDF15 expression and AKT/mTOR phosphorylation in BMSCs under different experimental conditions. (f) Quantitative analysis of data from (e) ($n = 3$). $^{*}p < 0.05$, $^{***}p < 0.001$ versus the control group; $^{#}p < 0.05$, $^{##}p < 0.01$ versus the DEX group; $^{†}p < 0.05$, $^{††}p < 0.01$ versus the DEX + D7 group. Quantitative data are presented as means ± SD.
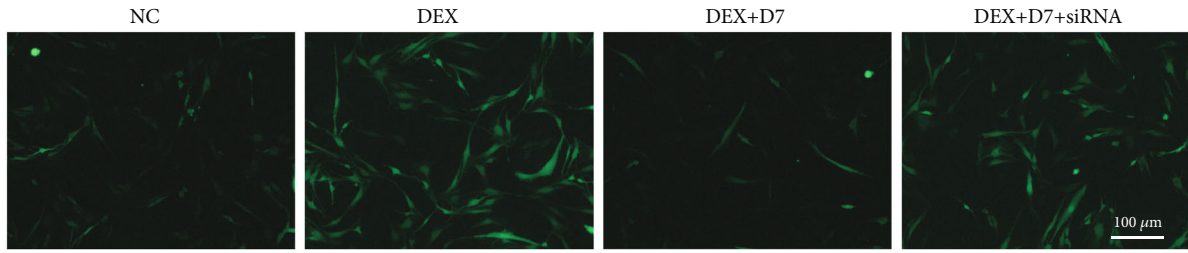
(a)
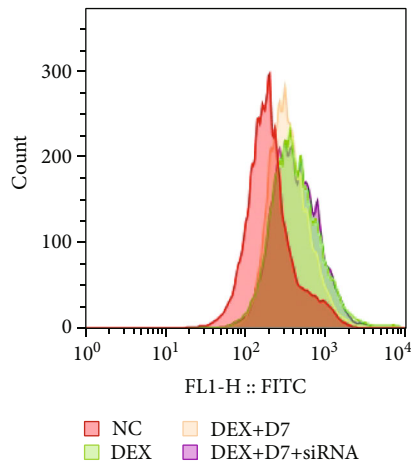
(b)
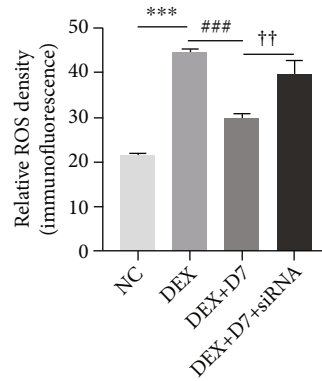
(c)
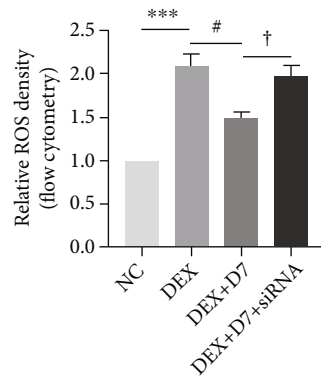
(d)
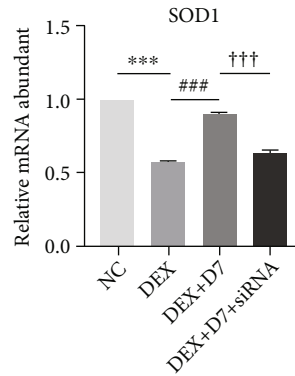
(e)
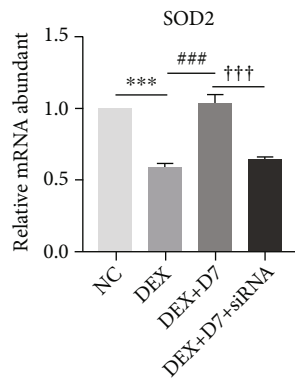
(f)
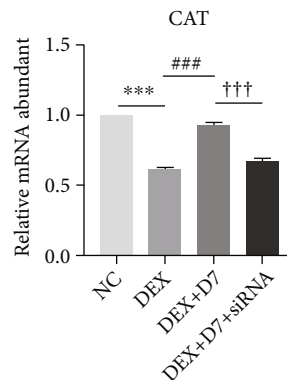
(g)

Figure 5: Continued.

(h)

(i)
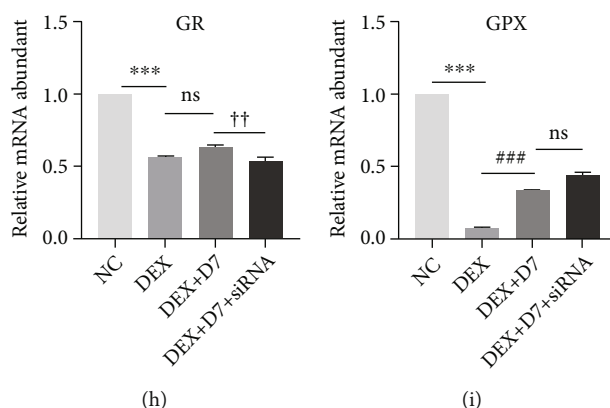
FIGURE 5: D7 reduces DEX-induced oxidative stress via regulation of GDF15 expression. (a) DCFH-DA assays were used to evaluate intracellular ROS levels in BMSCs under different experimental conditions. Cells were loaded with DCFH-DA for 30 min and treated with different reagents for 30 min. (b) The density of DCFH-DA was detected by flow cytometry. Cells were loaded with DCFH-DA for 30 min and treated with different reagents for 30 min. (c) Quantitative analysis of data from (a) ($n = 3$). ***$p < 0.001$ versus the NC group; ###$p < 0.001$ versus the DEX group; †††$p < 0.001$ versus the DEX + D7 group. (d) Quantitative analysis of data from (b) ($n = 3$). *** $p < 0.001$ versus the NC group; #$p < 0.05$ versus the DEX group; †$p < 0.05$ versus the DEX + D7 group. (e–i) mRNA levels of *SOD1*, *SOD2*, *CAT*, *GR*, and *GPX* under different experimental conditions, normalized to *ACTB* expression ($n = 3$). Cells were treated with different reagents for 24 h. Quantitative data are presented as means ± SD.

S0033; Beyotime Biotechnology, Shanghai, China). Cells were seeded in 6-well plates to reach 30% confluency and then transfected with siRNA for 24 h. DEX (10 μM) and D7 (10 μM) treatments were added into indicated culture medium. After 30 min, cells were digested with trypsin for 5 min. After stopping digestion with culture medium containing 10% FBS, cells were collected into 15 mL centrifuge tube, and centrifuged at 1500 rpm for 5 min. The cells were then resuspended with cold PBS and centrifuged again (1500 rpm for 5 min). Next, 1 mL diluted DCFH-DA solution (10 μM) was added to each tube. Cells were cultured at 37°C in a 5% CO$_2$ atmosphere for 30 min and shook every 5 min. Cells were then washed with PBS and centrifuged thrice. Thereafter, cells were resuspended in 400 μL PBS and transferred to the flow cytometry test tube. The flow cytometry was used at the excitation wavelength of 488 nm and the emission wavelength of 525 nm to detect the fluorescence value.

2.15. Data Source. The dataset of GSE123568 included 40 samples, 10 of which were normal patient serum samples and 30 were SONFH serum samples. The data were deposited by Zhang et al. and downloaded from the GEO database (https://www.ncbi.nlm.nih.gov/geo/query/acc.cgi?acc=GSE123568) [40]. The datasets were obtained based on the GPL15207 platform, and the probe identification number was 11716663_a_at ([PrimeView] Affymetrix Human Gene Expression Array).

2.16. Statistical Analysis. All data are presented as means ± standard deviations (SDs; $n > 3$). *T*-tests were used for comparisons between two groups, and one-way analysis of variance was used for comparisons between more than two sets of data. Statistical significance was set at $p < 0.05$. All statistical analyses were performed with GraphPad Prism 8.0 software (GraphPad Software).

3. Results

3.1. GDF15 Expression is Suppressed in ONFH Samples. To explore GDF15 expression levels during ONFH, we evaluated GDF15 expression in patients without ONFH (controls) and patients with ONFH. Using WB, we found that GDF15 protein levels were significantly downregulated in ONFH samples (Figure 1(a)). This result was further verified by data mining from the GEO dataset deposited by Zhang et al. (GSE123568; Figure 1(c)). The dataset included 40 serum samples, of which 10 were obtained from controls and 30 were obtained from patients with SONFH. As shown in Figure 1(c), GDF15 expression was markedly downregulated in the SONFH group. Additionally, we found that GDF15 expression in the BMSCs population was dramatically decreased under ONFH conditions (Figure 1(d)). Taken together, these results indicated that there was a negative correlation between GDF15 expression and ONFH and that BMSCs were one of the main cell populations affected in the bone microenvironment.

3.2. DEX Inhibits BMSCs Proliferation and Induces BMSCs Apoptosis via Suppression of GDF15 Expression and Downregulation of AKT/mTOR Signaling. To elucidate the functional roles of GDF15 and its downstream signaling in BMSCs during SONFH, DEX was used for a series of functional assays in vitro. Using CCK-8 assays, we found that BMSCs proliferation was inhibited by DEX stimulation when the concentration exceeded 10 μM (Figure 2(a)). By contrast, BMSCs apoptosis was significantly enhanced by DEX stimulation, as measured by evaluation of LDH activity and cleaved-PARP and cleaved-caspase 3 levels (Figures 2(b)–2(d)). We further investigated whether GDF15 was involved in these DEX-dependent changes and evaluated the signaling pathways involved in this mechanism. As expected, WB results demonstrated relationships

(a)

(b)

(c)

(d)

(e)

(f)

Figure 6: Continued.

(g)

(h)
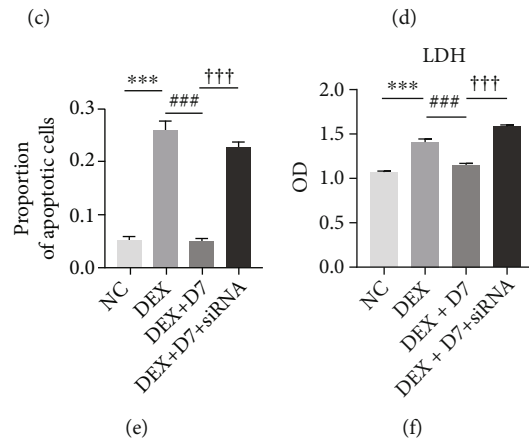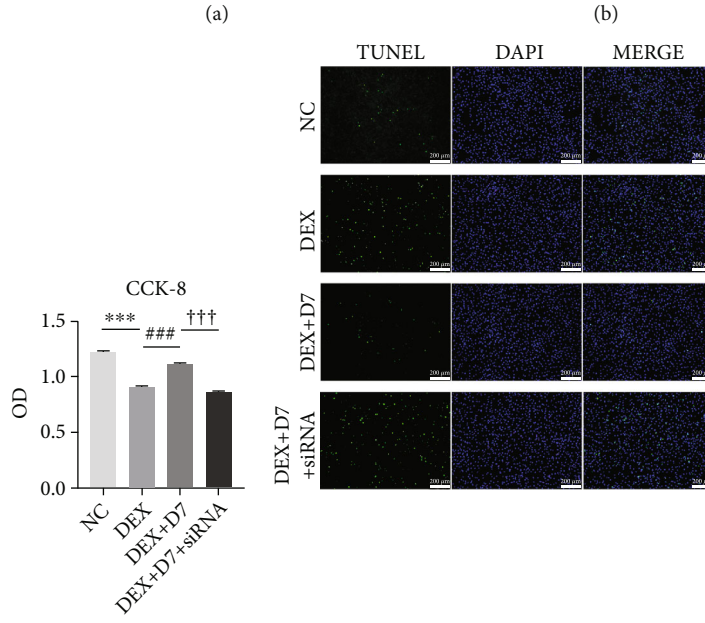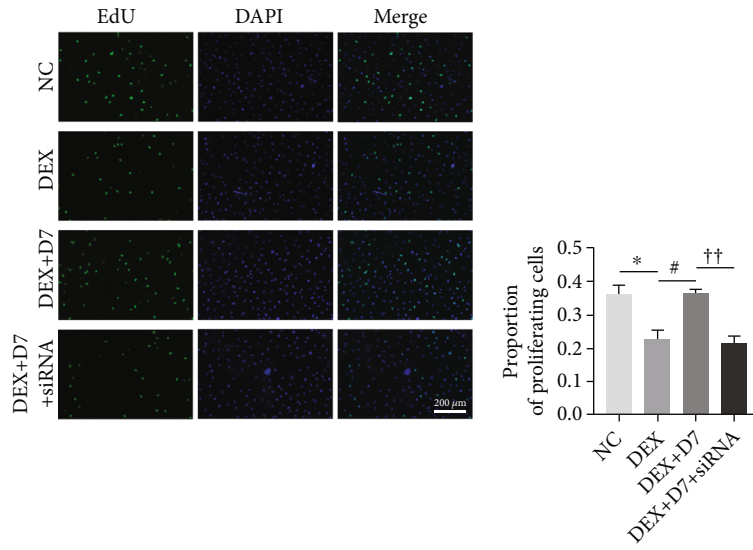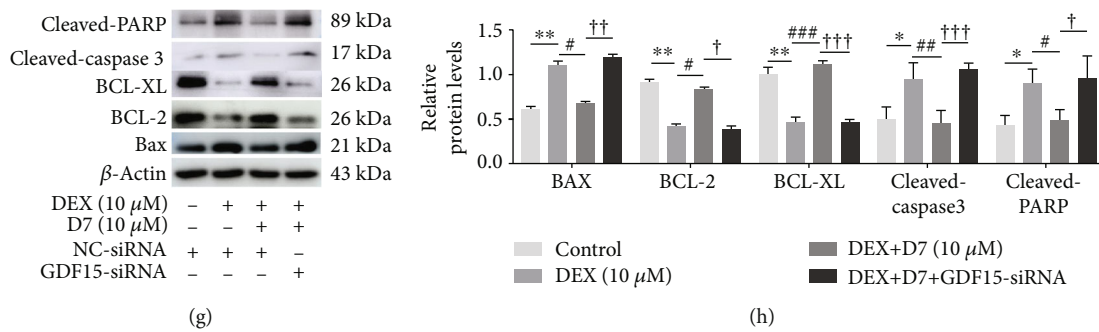
Figure 6: D7 restores BMSCs viability and reduces BMSCs apoptosis via GDF15 expression. (a) EdU assays were performed to evaluate the proportion of proliferating BMSCs under different experimental conditions. Cells were treated with different reagents for 24 h and were then incubated with EdU solution for 2 h. (b) Quantitative analysis of data from (a) ($n = 3$). $^*p < 0.05$ versus the NC group; $^\#p < 0.05$ versus the DEX group; $^{††}p < 0.01$ versus the DEX + D7 group. (c) Viability of BMSCs under different conditions was examined by CCK-8 assays ($n = 3$). $^{***}p < 0.001$ versus the NC group; $^{\#\#\#}p < 0.001$ versus the DEX group; $^{†††}p < 0.001$ versus the DEX + D7 group. (d) TUNEL assays were performed to measure the proportion of apoptotic BMSCs under different conditions. Cells were incubated in serum-free medium for 48 h before detection. (e) Quantitative analysis of data from (d) ($n = 3$). $^{***}p < 0.001$ versus the NC group; $^{\#\#\#}p < 0.001$ versus the DEX group; $^{†††}p < 0.001$ versus the DEX + D7 group. (f) Apoptosis of BMSCs under different condition was measured by LDH assays ($n = 3$). Cells were incubated in serum-free medium for 48 h before detection. $^{***}p < 0.001$ versus the NC group; $^{\#\#\#}p < 0.001$ versus the DEX group; $^{†††}p < 0.001$ versus the DEX + D7 group. (g) Western blotting analysis of the expression of some apoptosis-related proteins in BMSCs under different experimental conditions. Cells were incubated in serum-free medium for 48 h before lysis. (h) Quantitative analysis of data from (g) ($n = 3$). $^*p < 0.05$, $^{**}p < 0.01$ versus the NC group; $^\#p < 0.05$, $^{\#\#}p < 0.01$, $^{\#\#\#}p < 0.001$ versus the DEX group; $^†p < 0.05$, $^{††}p < 0.01$, $^{†††}p < 0.001$ versus the DEX + D7 group. Quantitative data are presented as means ± SD.

between GDF15 suppression and DEX stimulation (Figures 2(e) and 2(f)), wherein AKT/mTOR signaling was believed to be a downstream pathway. These results suggested a pivotal role of GDF15/AKT/mTOR signaling in DEX-induced damage to BMSCs self-renewal.

3.3. D7 Alleviates DEX-Induced BMSCs Damage in a Concentration-Dependent Manner.
Our previous study demonstrated that the specific affinity cyclic peptide D7 could enhance the adhesion, expansion, and proliferation of BMSCs on β-tricalcium phosphate scaffolds [31]; therefore, we tested the potential therapeutic effects of D7 on DEX-induced BMSCs damage. To our surprise, D7 exhibited a powerful rescue effect against DEX-induced BMSCs damage, as demonstrated by concentration-dependent amelioration of BMSCs proliferation in CCK-8 assays (Figure 3(a)) and reduced expression of apoptosis markers, including LDH activity, cleaved-PARP levels, and cleaved-caspase 3 levels (Figures 3(b)–3(d)).

3.4. D7 Restores DEX-Dependent Inhibition of AKT/mTOR Signaling via Upregulation of GDF15 Expression in BMSCs.
Considering the pivotal role of GDF15/AKT/mTOR signaling in DEX-induced BMSCs damage, we next investigated whether this signaling pathway was also involved in the therapeutic effects of D7. siRNA-GDF15 was introduced for further studies, and the efficiency of the siRNA effect was evaluated by WB (Figures 4(a) and 4(b)). Consistent with our previous results, IF staining demonstrated that GDF15 expression was suppressed in the presence of DEX stimulation, whereas D7 restored GDF15 activation (Figures 4(c) and 4(d)). In addition, transfection with GDF15-siRNA strongly blocked D7-dependent restoration of GDF15 expression, indicating a regulatory role for GDF15 in mediating the therapeutic effects of D7 against DEX-induced

BMSCs damage (Figures 4(c) and 4(d)). This mechanism was further supported by the WB results, wherein the DEX-dependent inhibition of AKT/mTOR activity was restored by D7 via GDF15 upregulation and then partially blocked after GDF15-siRNA transfection (Figures 4(e) and 4(f)). These findings indicated the downstream roles of the AKT/mTOR signaling pathway in the therapeutic effects of D7 against DEX-induced BMSCs damage.

3.5. D7 Reduces DEX-Induced Oxidative Stress via Regulation of GDF15 Expression.
GDF15 serves as a marker of oxidative stress and inflammation in many diseases and pathophysiological assessments [19–21]. Therefore, we next tested whether GDF15 had similar effects on the therapeutic action of D7 against DEX-induced BMSCs damage and whether ROS functioned upstream of GDF15 during this process because DEX enhances ROS levels and induces cell death in chondrocytes [41, 42]. Using the DCFH-DA probe, we found that intracellular ROS levels increased dramatically in DEX-stimulated BMSCs and decreased rapidly after D7 addition (Figures 5(a) and 5(c)). These results were further verified by DCFH-DA flow cytometry analysis (Figures 5(b) and 5(d)). However, when GDF15 expression was inhibited by siRNA, D7 partially reduced DEX-induced ROS production in BMSCs (Figures 5(a) and 5(c)). Then, we used N-acetyl-l-cysteine (NAC) to suppress DEX-induced oxidative stress to verify that ROS functioned upstream of GDF15/AKT/mTOR signaling. As expected, the activation of GDF15/AKT/mTOR signaling suppressed by DEX was restored by NAC treatment (Supplement Figure 1a and 1b).

We then evaluated the responses of antioxidant proteins to determine whether the defense system of oxidative stress contributed to the GDF15-mediated therapeutic effects of D7. qPCR showed that DEX reduced the expression of all

(a)

(b)

(c)
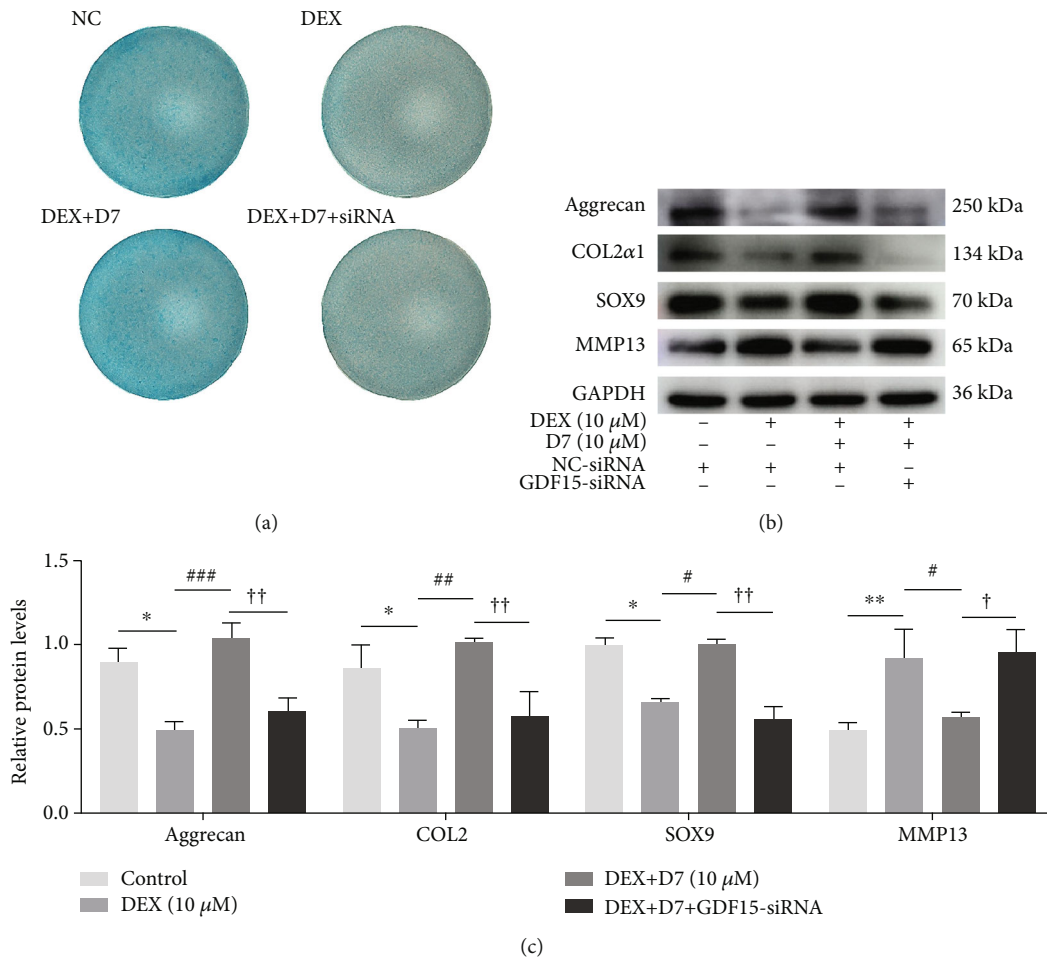
FIGURE 7: D7 promotes chondrogenesis following DEX stimulation via GDF15 expression. (a) Representative images of Alcian blue staining. Chondrogenic differentiation was induced in BMSCs for 21 days. (b) WB analysis of the expression of some chondrogenesis-related proteins, including Aggrecan, SOX9, COL2, and MMP13. Chondrogenesis was induced for 14 days. (c) Quantitative analysis of data from (b) ($n = 3$). $^*p < 0.05$, $^{**}p < 0.01$ versus the NC group; $^#p < 0.05$, $^{##}p < 0.03$, $^{###}p < 0.001$ versus DEX (10μM); $^\dagger p < 0.05$, $^{\dagger\dagger}p < 0.01$ versus the DEX + D7 group. Quantitative data are presented as means ± SD.

five antioxidant genes. However, D7 only restored the expression of superoxide dismutase (*SOD*) 1, *SOD2*, and catalase (*CAT*) via a mechanism involving GDF15 (Figures 5(e)–5(g)). Glutathione reductase (*GR*) and glutathione peroxidase (*GPX*) were either not responsive to D7 treatment or were not regulated by GDF15 (Figures 5(h) and 5(i)). Taken together, these results suggested that D7 reduced DEX-induced ROS activity and restored the redox balance via regulation of GDF15 expression.

3.6. D7 Restores BMSCs Viability and Reduces BMSCs Apoptosis via GDF15 Expression.

We next determined whether GDF15-mediated signaling affected the therapeutic action of D7 against DEX-induced BMSCs damage. As expected, the proliferation of BMSCs damaged by DEX treatment was restored after D7 addition in the presence of GDF15, as demonstrated by EdU and CCK-8 assays (Figures 6(a)–6(c)) Moreover, apoptosis indices, as evaluated by TUNEL assays and LDH release tests, were all reduced (Figures 6(d)–6(f)). These results were further validated at

the protein level; the expression levels of apoptosis-related proteins, including cleaved-PARP and cleaved-caspase 3, were decreased, whereas those of antiapoptotic proteins, including BCL-2 and BCL-XL, were increased (Figures 6(g) and 6(h)), supporting the involvement of GDF15-mediated signaling in the therapeutic effects of D7.

3.7. D7 Promotes Chondrogenesis following DEX Stimulation via GDF15 Expression.

Because of the therapeutic effects of D7 on DEX-induced BMSCs damage, we next evaluated whether the chondrogenic differentiation of BMSCs under DEX conditions could benefit from D7 addition. As expected, D7 promoted the chondrogenic differentiation of DEX-treated BMSCs, and the effect of D7 was partially blocked by GDF15-siRNA transfection (Figure 7(a)). These results were further verified by WB analysis of protein expression. Notably, D7 increased the expression levels of Aggrecan (ACAN), COL2, and SOX9 and reduced the expression of MMP13. However, GDF15-siRNA transfection significantly blocked the D7-enhanced expression of
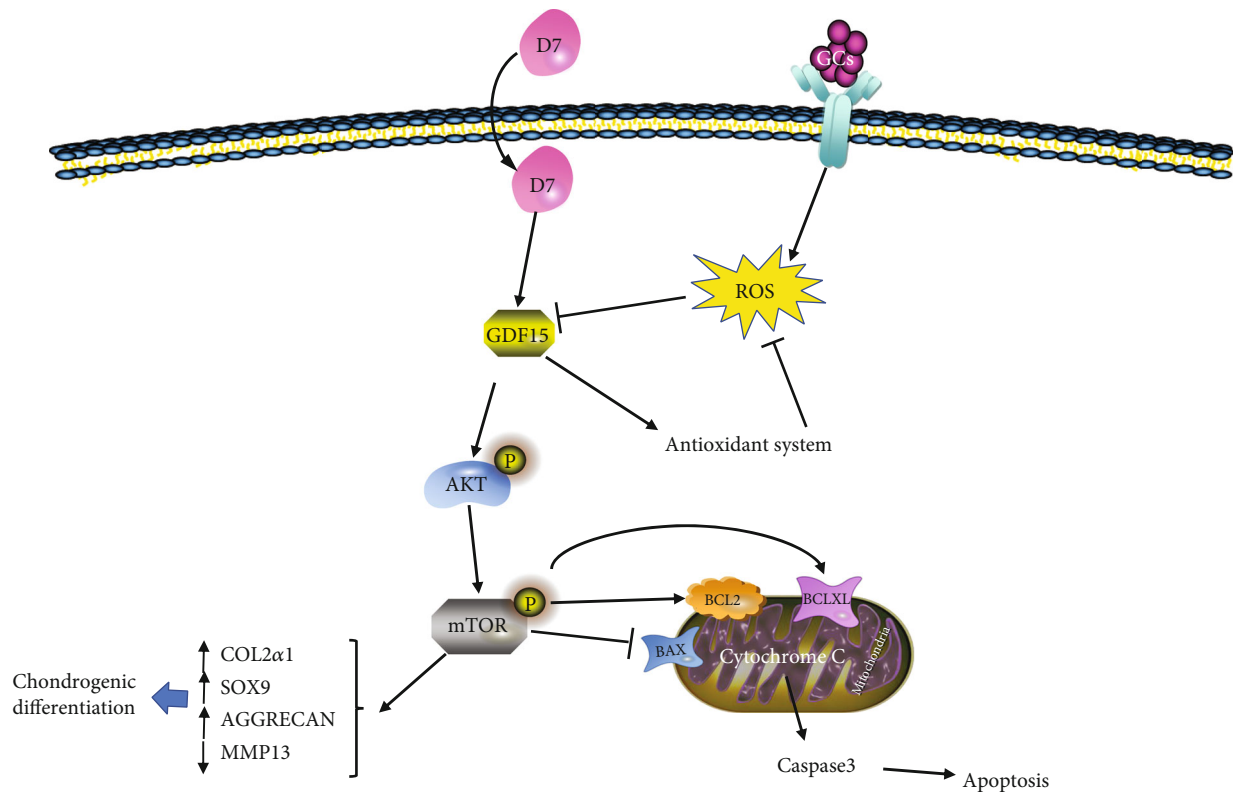
FIGURE 8: Schematic diagram showing the underlying mechanism through which D7 prevents SONFH. Glucocorticoids lead to the accumulation of ROS in BMSCs, thereby inhibiting GDF15/AKT/mTOR signaling and further causing damage to BMSCs. D7 restores the expression of GDF15, activates the oxidative stress defense system, and restores the balance of oxidative stress. GDF15 further activates the AKT/mTOR signaling pathway to protect BMSCs from SONFH.

chondrogenesis-related proteins, indicating a regulatory role of GDF15 during D7-induced chondrogenic differentiation in the presence of DEX (Figures 7(b) and 7(c)).

4. Discussion

In our previous study, we had demonstrated that the cyclic polypeptide D7 has a specific affinity to BMSCs [35]. To the best of our knowledge, our study is the first to demonstrate that D7 protected BMSCs against DEX-induced SONFH in vitro. In the current study, we found that D7 promoted the viability of BMSCs in the presence of DEX and reduced DEX-induced cell apoptosis. Activation of the GDF15/AKT/mTOR signaling pathway contributed to the protective roles of D7 in the DEX-induced SONFH model. Furthermore, activation of GDF15/AKT/mTOR signaling contributed to the suppressive effects of D7 on oxidative stress, mediated by restoration of SOD1, SOD2, and CAT expression. Additionally, D7 promoted BMSCs chondrogenesis through GDF15/AKT/mTOR signaling during SONFH (Figure 8). These results established the potential therapeutic effects of D7 in SONFH for the first time.

GCs are a common cause of ONFH as well as many other bone diseases [43, 44]. By inducing the accumulation of ROS, DEX promotes osteoblast apoptosis, inhibits the osteoblastic differentiation of BMSCs, and activates osteoclasts [16–18]. In this study, we also found that DEX could

cause severe damage to BMSCs, including inhibition of cell proliferation and acceleration of cell apoptosis, via the regulation of BCL-2 family and caspase3 expression, and the suppression on GDF15/AKT/mTOR signaling. The chondrogenesis of BMSCs was therefore significantly inhibited by DEX treatment. Moreover, we found that DEX activated intracellular ROS by inhibiting the expression of the antioxidant proteins SOD1, SOD2, GR, GPX1, and CAT.

In our previous study, we screened a BMSCs-specific affinity peptide, D7, using phage display technology [35]. Similar peptides, such as RGD, have been used in the treatment of ONFH and have shown some therapeutic effects [45, 46]. Compared with RGD, D7 has specific affinity for BMSCs and the ability to recruit BMSCs more effectively. In this study, we showed that D7 treatment could alleviate the BMSCs injury caused by DEX. Furthermore, D7 was found to restore the chondrogenic function of BMSCs. In addition, D7 reestablished the balance of oxidative stress by regulating the expression of SOD1, SOD2, and CAT and exerted protective effects by activating GDF15/AKT/ mTOR signaling.

Deregulation of the expression and function of cytokines belonging to the TGF-β family always contribute to the apoptosis and oxidative. Apoptosis is one of the important forms of cell death, and it plays an important role in the pathogenesis and progression of femoral head necrosis [47]. The BCL-2 family can regulate cell apoptosis. BAX,

BCL-2, and BCL-XL are important regulators belonging to the BCL-2 family that control apoptosis. BAX can inhibit the activity of BCL-XL, while BCL-2 can inhibit BAX expression. Caspase family also plays an important role in the process of apoptosis. BCL-2 can inhibit the conversion of cytochrome C into caspase3, thereby inhibiting apoptosis. In this study, we showed that GDF15 expression was suppressed in femoral head tissue from patients with ONFH. Consistent with this, we also found that GDF15 expression was lower in the serum of patients with SONFH than in healthy controls. Importantly, DEX decreased GDF15 expression and inhibited the AKT/mTOR signaling pathway. D7 could upregulate the expression of BCL-2 and BCL-XL by activating GDF15/AKT/mTOR signaling and suppressed the expression of BAX, which further inhibited the formation of caspase3 and further alleviated cell apoptosis. For oxidative stress, GC can mediate the accumulation of oxygen free radicals by inhibiting the expression of antioxidant proteins. In this study, we also found GC inhibited the expression of SOD1, SOD2, GR, GPX1, and CAT to activate oxidative stress. According to other reports, GDF15/AKT/mTOR signaling is closely related to oxidative stress, wherein the activation of this signaling could suppress ROS accumulation [19–21, 23, 29, 48, 49]. In our study, D7 treatment was observed to inhibit the GC-induced oxidative stress by restoring the expression levels of SOD1, SOD2, CAT, and GPX. The silencing of GDF15 significantly reverses the antioxidant effect of D7 by downregulating the expression of SOD1, SOD2, and CAT. In general, GDF15/AKT/mTOR signal inhibited GC-induced oxidative stress by upregulating the expression of SOD1, SOD2, and CAT. Furthermore, as a member of the TGF-β superfamily, GDF15 is closely related to the differentiation of BMSCs [25] and contributes to the pathological progression of SONFH. In our study, D7 treatment could restore the chondrogenic differentiation function of BMSCs, whereas siRNA-GDF15 transfection inhibited the D7-induced chondrogenic differentiation of BMSCs.

Overall, our findings clarified the interactions among D7, GDF15, oxidative stress, and SONFH. However, further in vivo experiments are needed to clarify the therapeutic effects of D7-containing scaffolds in animal models of SONFH.

In conclusion, we demonstrated the protective effects of D7 against DEX-induced SONFH in vitro and found that these protective effects may be mediated by inhibition of DEX-induced ROS and activation of GDF15/AKT/mTOR signaling. Our research provides insights into the potential applications of D7 in the treatment of SONFH.

Data Availability

The data will be made available after being requested from the corresponding author.

Conflicts of Interest

The authors declare that they have no competing interests.

Authors' Contributions

Jiazheng Chen designed experiments, conceived the experiments, and wrote the manuscript. Zichen Cui, Yi Wang, Linmao Lyu, Changgong Feng, Dianjie Feng, and Yifan Cheng contributed to cell research data; Shui Sun and Ziqing Li participated in the analysis and polished the manuscript. All authors approved the final version.

Acknowledgments

Supplementary Materials

Supplemental Figure 1: NAC restores DEX-dependent inhibition of GDF15/AKT/mTOR signaling. (a) WB analysis of GDF15 expression and AKT/mTOR phosphorylation in BMSCs under DEX and NAC treatment. (b) Quantitative analysis of data from (a). $^*p < 0.05$ versus the NC group; $^\#p < 0.05$ versus the DEX group. (Supplementary Materials)

References

[1] C. Powell, C. Chang, S. M. Naguwa, G. Cheema, and M. E. Gershwin, "Steroid induced osteonecrosis: an analysis of steroid dosing risk," Autoimmunity reviews, vol. 9, no. 11, pp. 721–743, 2010.

[2] Y. Qi, Y. Zhu, Y. Cao et al., "Association between MMP-3 polymorphisms among Chinese patients with osteonecrosis of the femoral head," Oncotarget, vol. 8, no. 65, pp. 108859–108866, 2017.

[3] X. Li, L. Jin, Q. Cui, G. J. Wang, and G. Balian, "Steroid effects on osteogenesis through mesenchymal cell gene expression," Osteoporosis International, vol. 16, no. 1, pp. 101–108, 2005.

[4] J. R. Urbaniak, A. V. Seaber, and L. E. Chen, "Assessment of ischemia and reperfusion injury," Clinical orthopaedics and related research, vol. 334, no. 334, pp. 30–36, 1997.

[5] W. Drescher, D. Varoga, T. R. Liebs et al., "Femoral artery constriction by norepinephrine is enhanced by methylprednisolone in a rat model," JBJS, vol. 88, pp. 162–166, 2006.

[6] C. H. Yeh, J. K. Chang, Y. H. Wang, M. L. Ho, and G. J. Wang, "Ethanol may suppress Wnt/beta-catenin signaling on human bone marrow stroma cells: a preliminary study," Clinical orthopaedics and related research, vol. 466, no. 5, pp. 1047–1053, 2008.

[7] L. Mao, P. Jiang, X. Lei et al., "Efficacy and safety of stem cell therapy for the early-stage osteonecrosis of femoral head: a systematic review and meta-analysis of randomized controlled trials," Stem cell research & therapy, vol. 11, no. 1, p. 445, 2020.

[8] P. Sadoghi, M. Liebensteiner, M. Agreiter, A. Leithner, N. Böhler, and G. Labek, "Revision surgery after total joint arthroplasty: a complication-based analysis using worldwide arthroplasty registers," vol. 28, no. 8, pp. 1329–1332, 2013.

[9] W. C. Eward, C. A. Rineer, J. R. Urbaniak, M. J. Richard, and D. S. Ruch, "The vascularized fibular graft in precollapse osteonecrosis: is long-term hip preservation possible?," Clinical

Orthopaedics and Related Research, vol. 470, no. 10, pp. 2819–2826, 2012.

[10] Y. S. Gao, S. B. Chen, D. X. Jin, J. G. Sheng, X. G. Cheng, and C. Q. Zhang, "Modified surgical techniques of free vascularized fibular grafting for treatment of the osteonecrosis of femoral head: results from a series of 407 cases," *Microsurgery*, vol. 33, no. 8, pp. 646–651, 2013.

[11] T. Ichiseki, Y. Ueda, S. Katsuda, K. Kitamura, A. Kaneuji, and T. Matsumoto, "Oxidative stress by glutathione depletion induces osteonecrosis in rats," *Rheumatology*, vol. 45, no. 3, pp. 287–290, 2006.

[12] Y. Kubo, W. Drescher, A. Fragoulis et al., "Adverse effects of oxidative stress on bone and vasculature in corticosteroid-associated osteonecrosis: potential role of nuclear factor erythroid 2-related factor 2 in cytoprotection," *Antioxidants & redox signaling*, vol. 35, no. 5, pp. 357–376, 2021.

[13] G. Luo, Z. Li, Y. Wang et al., "Resveratrol protects against titanium particle-induced aseptic loosening through reduction of oxidative stress and inactivation of NF-κB," *Inflammation*, vol. 39, no. 2, pp. 775–785, 2016.

[14] P. H. Willems, R. Rossignol, C. E. Dieteren, M. P. Murphy, and W. J. Koopman, "Redox homeostasis and mitochondrial dynamics," *Cell metabolism*, vol. 22, no. 2, pp. 207–218, 2015.

[15] M. I. LJ and R. M. Sapolsky, "Sapolsky, Glucocorticoids increase the accumulation of reactive oxygen species and enhance adriamycin-induced toxicity in neuronal culture," *Experimental neurology*, vol. 141, no. 2, pp. 201–206, 1996.

[16] N. K. Lee, Y. G. Choi, J. Y. Baik et al., "A crucial role for reactive oxygen species in RANKL-induced osteoclast differentiation (short title: role for ROS in osteoclastogenesis)," *Blood*, vol. 106, no. 3, pp. 852–859, 2005.

[17] X. C. Bai, D. Lu, J. Bai et al., "Oxidative stress inhibits osteoblastic differentiation of bone cells by ERK and NF-kappaB," *Biochemical and biophysical research communications*, vol. 314, no. 1, pp. 197–207, 2004.

[18] S. Deng, G. Dai, S. Chen et al., "Dexamethasone induces osteoblast apoptosis through ROS-PI3K/AKT/GSK3β signaling pathway," *Biomedicine & Pharmacotherapy*, vol. 110, pp. 602–608, 2019.

[19] L. Wallentin, Z. Hijazi, U. Andersson et al., "Growth differentiation factor 15, a marker of oxidative stress and inflammation, for risk assessment in patients with atrial fibrillation: insights from the Apixaban for Reduction in Stroke and Other Thromboembolic Events in Atrial Fibrillation (ARISTOTLE) trial," *Circulation*, vol. 130, no. 21, pp. 1847–1858, 2014.

[20] D. Sánchez-Infantes, M. Nus, M. Navas-Madroñal et al., "Oxidative stress and inflammatory markers in abdominal aortic aneurysm," *Antioxidants*, vol. 10, no. 4, 2021.

[21] K. K. Tiwari, B. Moorthy, and K. Lingappan, "Role of GDF15 (growth and differentiation factor 15) in pulmonary oxygen toxicity," *Toxicology in Vitro*, vol. 29, no. 7, pp. 1369–1376, 2015.

[22] S. N. Breit, D. A. Brown, and V. W. Tsai, "The GDF15-GFRAL pathway in health and metabolic disease: friend or foe?," *Annual Review of Physiology*, vol. 83, pp. 127–151, 2021.

[23] Y. L. Li, J. T. Chang, L. Y. Lee et al., "GDF15 contributes to radioresistance and cancer stemness of head and neck cancer by regulating cellular reactive oxygen species via a SMAD-associated signaling pathway," *Oncotarget*, vol. 8, no. 1, pp. 1508–1528, 2017.

[24] M. Westhrin, S. H. Moen, T. Holien et al., "Growth differentiation factor 15 (GDF15) promotes osteoclast differentiation and inhibits osteoblast differentiation and high serum GDF15 levels are associated with multiple myeloma bone disease," *Haematologica*, vol. 100, no. 12, pp. e511–e514, 2015.

[25] J. Symmank, S. Zimmermann, J. Goldschmitt et al., "Mechanically-induced GDF15 secretion by periodontal ligament fibroblasts regulates osteogenic transcription," *Scientific Reports*, vol. 9, no. 1, article 11516, 2019.

[26] J. Y. Huang, Y. Y. Wang, S. Lo et al., "Visfatin mediates malignant behaviors through adipose-derived stem cells intermediary in breast cancer," *Cancers*, vol. 12, no. 1, 2019.

[27] J. Corre, E. Labat, N. Espagnolle et al., "Bioactivity and prognostic significance of growth differentiation factor GDF15 secreted by bone marrow mesenchymal stem cells in multiple myeloma," *Cancer research*, vol. 72, no. 6, pp. 1395–1406, 2012.

[28] H. Liu, J. Liu, L. Si, C. Guo, W. Liu, and Y. Liu, "GDF-15 promotes mitochondrial function and proliferation in neuronal HT22 cells," *Journal of Cellular Biochemistry*, vol. 120, no. 6, pp. 10530–10547, 2019.

[29] X. Zhang, C. Hu, C. Y. Kong et al., "FNDC5 alleviates oxidative stress and cardiomyocyte apoptosis in doxorubicin-induced cardiotoxicity via activating AKT," *Cell Death & Differentiation*, vol. 27, no. 2, pp. 540–555, 2020.

[30] Z. D. Zhang, Y. J. Yang, X. W. Liu et al., "The protective effect of aspirin eugenol ester on oxidative stress to PC12 cells stimulated with H(2)O(2) through regulating PI3K/Akt signal pathway," *Oxidative Medicine and Cellular Longevity*, vol. 2021, Article ID 5527475, 14 pages, 2021.

[31] T. Sun, Z. Man, C. Peng, G. Wang, and S. Sun, "A specific affinity cyclic peptide enhances the adhesion, expansion and proliferation of rat bone mesenchymal stem cells on β-tricalcium phosphate scaffolds," *Molecular medicine reports*, vol. 20, no. 2, pp. 1157–1166, 2019.

[32] G. J. Smith, "Filamentous fusion phage: novel expression vectors that display cloned antigens on the virion surface," *Science*, vol. 228, no. 4705, pp. 1315–1317, 1985.

[33] H. Ramaraju, S. Miller, and D. H. Kohn, "Dual-functioning peptides discovered by phage display increase the magnitude and specificity of BMSC attachment to mineralized biomaterials," *Biomaterials*, vol. 134, pp. 1–12, 2017.

[34] Y. Pi, X. Zhang, J. Shi et al., "Targeted delivery of non-viral vectors to cartilage in vivo using a chondrocyte-homing peptide identified by phage display," *Biomaterials*, vol. 32, no. 26, pp. 6324–6332, 2011.

[35] G. Wang, Z. Man, N. Zhang et al., "Biopanning of mouse bone marrow mesenchymal stem cell affinity for cyclic peptides," *Molecular medicine reports*, vol. 19, no. 1, pp. 407–413, 2019.

[36] L. Lyu, J. Chen, W. Wang et al., "Scoparone alleviates Ang II-induced pathological myocardial hypertrophy in mice by inhibiting oxidative stress," *Journal of cellular and molecular medicine*, vol. 25, no. 6, pp. 3136–3148, 2021.

[37] K. Tie, M. Wu, Y. Deng et al., "Histone hypo-acetylation of Sox9 mediates nicotine-induced weak cartilage repair by suppressing BMSC chondrogenic differentiation," *Stem cell research & therapy*, vol. 9, no. 1, p. 98, 2018.

[38] A. Y. Ng, Z. Li, M. M. Jones et al., "Regulator of G protein signaling 12 enhances osteoclastogenesis by suppressing Nrf2-dependent antioxidant proteins to promote the generation of reactive oxygen species," *Elife*, vol. 8, 2019.

[39] J. He, H. Xiao, B. Li et al., "The programmed site-specific delivery of the angiostatin sunitinib and chemotherapeutic paclitaxel for highly efficient tumor treatment," *Journal of Materials Chemistry B*, vol. 7, no. 32, pp. 4953–4962, 2019.

[40] T. Li, Y. Zhang, R. Wang et al., "Discovery and validation an eight-biomarker serum gene signature for the diagnosis of steroid-induced osteonecrosis of the femoral head," *Bone*, vol. 122, pp. 199–208, 2019.

[41] C. Shen, G. Q. Cai, J. P. Peng, and X. D. Chen, "Autophagy protects chondrocytes from glucocorticoids-induced apoptosis via ROS/Akt/FOXO3 signaling," *Osteoarthritis and Cartilage*, vol. 23, no. 12, pp. 2279–2287, 2015.

[42] Y. Huang, G. Q. Cai, J. P. Peng, and C. Shen, "Glucocorticoids induce apoptosis and matrix metalloproteinase-13 expression in chondrocytes through the NOX4/ROS/p38 MAPK pathway," *The Journal of steroid biochemistry and molecular biology*, vol. 181, pp. 52–62, 2018.

[43] M. Zaidi, L. Sun, L. J. Robinson et al., "ACTH protects against glucocorticoid-induced osteonecrosis of bone," *Proceedings of the National Academy of Sciences*, vol. 107, no. 19, pp. 8782–8787, 2010.

[44] M. Maruyama, A. Nabeshima, C. C. Pan et al., "The effects of a functionally-graded scaffold and bone marrow-derived mononuclear cells on steroid-induced femoral head osteonecrosis," *Biomaterials*, vol. 187, pp. 39–46, 2018.

[45] Z. Man, D. Sha, S. Sun et al., "In vitro bioactivity study of RGD-coated titanium alloy prothesis for revision total hip arthroplasty," *BioMed Research International*, vol. 2016, Article ID 8627978, 7 pages, 2016.

[46] Q. Mao, H. Jin, F. Liao, L. Xiao, D. Chen, and P. Tong, "The efficacy of targeted intraarterial delivery of concentrated autologous bone marrow containing mononuclear cells in the treatment of osteonecrosis of the femoral head: a five year follow-up study," *Bone*, vol. 57, no. 2, pp. 509–516, 2013.

[47] S. C. Tao, T. Yuan, B. Y. Rui, Z. Z. Zhu, S. C. Guo, and C. Q. Zhang, "Exosomes derived from human platelet-rich plasma prevent apoptosis induced by glucocorticoid-associated endoplasmic reticulum stress in rat osteonecrosis of the femoral head via the Akt/Bad/Bcl-2 signal pathway," *Theranostics*, vol. 7, no. 3, pp. 733–750, 2017.

[48] Z. Zhao, P. Zhang, W. Li et al., "Pegylated recombinant human arginase 1 induces autophagy and apoptosis via the ROS-activated AKT/mTOR pathway in bladder cancer cells," *Oxidative Medicine and Cellular Longevity*, vol. 2021, Article ID 5510663, 13 pages, 2021.

[49] Z. D. Zhang, Y. J. Yang, X. W. Liu et al., "The protective effect of aspirin eugenol ester on oxidative stress to PC12 cells stimulated with H_2O_2 through regulating PI3K/Akt signal pathway," *Oxidative Medicine and Cellular Longevity*, vol. 2021, Article ID 5527475, 2021.

Research Article

Effect of Normobaric Hypoxia on Alterations in Redox Homeostasis, Nitrosative Stress, Inflammation, and Lysosomal Function following Acute Physical Exercise

Mateusz Maciejczyk [iD],[1] **Anna Zalewska** [iD],[2] **Małgorzata Gryciuk,**[3] **Katarzyna Hodun,**[4] **Miłosz Czuba,**[5] **Kamila Płoszczyca,**[6] **Małgorzata Charmas,**[7] **Jerzy Sadowski,**[7] **and Marcin Baranowski**[4]

[1]*Department of Hygiene, Epidemiology and Ergonomics, Medical University of Bialystok, 2C Adama Mickiewicza Street, 15-022 Bialystok, Poland*
[2]*Department of Restorative Dentistry and Experimental Dentistry Laboratory, Medical University of Bialystok, 24A Marii Sklodowskiej-Curie Street, 15-276 Bialystok, Poland*
[3]*Students Scientific Club "Biochemistry of Civilization Diseases" at the Department of Hygiene, Epidemiology and Ergonomics, Medical University of Bialystok, 2c Mickiewicza Street, 15-233 Bialystok, Poland*
[4]*Department of Physiology, Medical University of Bialystok, 2C Adama Mickiewicza Street, 15-022 Bialystok, Poland*
[5]*Faculty of Rehabilitation, Józef Piłsudski University of Physical Education in Warsaw, Marymoncka 34, 00-968 Warsaw, Poland*
[6]*Department of Kinesiology, Institute of Sport-National Research Institute, Trylogii 2, 01-982 Warsaw, Poland*
[7]*Department of Biochemistry and Physiology, Faculty of Physical Education and Sport in Biała Podlaska, Józef Piłsudski University of Physical Education in Warsaw, Akademicka 2, 21-500 Biała Podlaska, Poland*

Correspondence should be addressed to Mateusz Maciejczyk; mat.maciejczyk@gmail.com

Hypoxia is a recognized inducer of oxidative stress during prolonged physical activity. Nevertheless, previous studies have not systematically examined the effects of normoxia and hypoxia during acute physical exercise. The study is aimed at evaluating the relationship between enzymatic and nonenzymatic antioxidant barrier, total antioxidant/oxidant status, oxidative and nitrosative damage, inflammation, and lysosomal function in different acute exercise protocols under normoxia and hypoxia. Fifteen competitive athletes were recruited for the study. They were subjected to two types of acute cycling exercise with different intensities and durations: graded exercise until exhaustion (GE) and simulated 30 km individual time trial (TT). Both exercise protocols were performed under normoxic and hypoxic (FiO$_2$ = 16.5%) conditions. The number of subjects was determined based on our previous experiment, assuming the test power = 0.8 and α = 0.05. We demonstrated enhanced enzymatic antioxidant systems during hypoxic exercise (GE: ↑ catalase (CAT), ↑ superoxide dismutase; TT: ↑ CAT) with a concomitant decrease in plasma reduced glutathione. In athletes exercising in hypoxia, redox status was shifted in favor of oxidation reactions (GE: ↑ total oxidant status, ↓ redox ratio), leading to increased oxidation/nitration of proteins (GE: ↑ advanced oxidation protein products (AOPP), ↑ ischemia-modified albumin, ↑ 3-nitrotyrosine, ↑ S-nitrosothiols; TT: ↑ AOPP) and lipids (GE: ↑ malondialdehyde). Concentrations of nitric oxide and its metabolites (peroxynitrite) were significantly higher in the plasma of hypoxic exercisers with an associated increase in inflammatory mediators (GE: ↑ myeloperoxidase, ↑ tumor necrosis factor-alpha) and lysosomal exoglycosidase activity (GE: ↑ N-acetyl-β-hexosaminidase, ↑ β-glucuronidase). Our study indicates that even a single intensive exercise session disrupts the antioxidant barrier and leads to increased oxidative and nitrosative damage at the systemic level. High-intensity exercise until exhaustion (GE) alters redox homeostasis more than the less intense exercise (TT, near the anaerobic threshold) of longer duration (20.2 ± 1.9 min vs. 61.1 ± 5.4 min—normoxia; 18.0 ± 1.9 min vs. 63.7 ± 3.0 min—hypoxia), while hypoxia significantly exacerbates oxidative stress, inflammation, and lysosomal dysfunction in athletic subjects.

1. Introduction

An inevitable consequence of functioning under aerobic conditions is the production of reactive oxygen (ROS) and nitrogen species (RNS). ROS and RNS are typical by-products of oxygen metabolism and important messengers in cellular signal processing. Under physiological conditions, ROS and RNS are involved in energy metabolism, erythropoiesis, muscle contraction, and other biochemical processes [1–3]. The signaling activity of free radicals is based on the modulation of several transcription factors, e.g., NF-κB (nuclear factor kappa-light-chain-enhancer of activated B cells) and HIF-1 (hypoxia-inducible factor-1), which results in S-nitrosylation of proteins and induction of second-order transmitter formation, as well as changes in cellular redox status [4–6]. However, ROS and RNS overproduction and/or insufficient antioxidant defense can cause redox imbalance, leading to cellular damage by oxidation and nitration. Such a state is defined as oxidative and nitrosative stress, which plays an essential role in many contemporary diseases, including metabolic [7, 8], neurodegenerative [9, 10], autoimmune [11, 12], and neoplastic disorders [13, 14]. Interestingly, factors inducing oxidative and nitrosative stress involve physical exercise [2, 15–17]. It was shown that overproduction of ROS/RNS occurs both during and after training [2, 15, 16]. A direct source of free radicals is the activity of mitochondrial enzymes and membrane oxidases (e.g., NADPH oxidase (NOX)), disturbances of ion homeostasis (especially iron and calcium ions), or changes in lysosomal function. The rate of ROS formation depends on the intensity and duration of exercise, the degree of training of the subjects, their age, sex, and diet [2, 15, 16, 18, 19]. It was shown that regular long-term aerobic exercise, especially at high intensity, is responsible for a significant increase in oxidative stress through intensified oxygen consumption [19–21]. Lipid peroxidation of muscle cells results in decreased fluidity and higher permeability of cellular membranes and enhanced oxidation of proteins and their tissue aggregation, as well as ROS-mediated DNA injury, causing an inflammatory response, delayed muscle soreness, and the release of intramuscular enzymes into the blood [15, 22, 23]. Nevertheless, little is known on redox homeostasis, nitrosative stress, and inflammatory response after acute physical intervention.

Nowadays, altitude/hypoxic training is becoming increasingly popular in sports [24–27]. Exposure to hypoxia leads to stimulation of HIF-1, which, apart from regulation of erythropoiesis and angiogenesis, is also a regulator of activity of glycolytic enzymes, mainly phosphofructokinase (PFK-1) [28, 29]. Therefore, improvements in aerobic and anaerobic capacity may occur. However, hypoxia and subsequent reoxygenation are also responsible for ROS/RNS overproduction, during prolonged exposure to altitude, as well as during intermittent hypoxic training [29–31]. This is caused by disruption of the mitochondrial respiratory chain, disturbances in arachidonic acid metabolism, or migration/activation of immune cells during regular physical activity [24, 25, 30, 31]. Nevertheless, there is a lack of studies evaluating the relationship between antioxidant systems, oxidative and nitrosative cell damage, inflammation, and lysosomal function under normoxic and hypoxic conditions. We speculate that even acute physical exercise can induce oxidative stress and inflammation, and hypoxia can exacerbate these disorders. As interest in high-altitude sports grows, it is essential to understand the differences in redox homeostasis between various protocols of acute physical intervention. Previous studies have examined only a few aspects of redox homeostasis [30, 32, 33] and ultimately have not systematically studied the effects of normoxia and hypoxia during acute exercise. Therefore, the present study is aimed at evaluating the relationship between (1) enzymatic and nonenzymatic antioxidant barrier, (2) total antioxidant/oxidant status, (3) oxidative and (4) nitrosative cell damage, (5) biomarkers of inflammation, and (6) lysosomal function in different protocols (different intensity and duration) performed under normoxic and hypoxic conditions.

2. Materials and Methods

2.1. Participants. The investigation conformed with the principles outlined in the Declaration of Helsinki and was approved by the Bioethics Committee of the Medical University of Bialystok (approval no. R-I-002/325/2019). All subjects gave their informed consent before their inclusion in the study.

Fifteen well-trained male competitive athletes (12 cyclists and 3 triathlonists) aged 25.4 ± 8.4 years, with BMI of $21.6 \pm 1.8 \, kg/m^2$, body fat content of $9.2 \pm 2.1\%$, and VO_2max of $61.4 \pm 3.1 \, mL/kg/min$ were recruited for the study. Their average training experience was 6.3 ± 2.0 years. Only candidates with a valid medical certificate confirming the absence of contraindications to the practice of competitive sport activity were accepted.

2.2. Experimental Design. The subjects were tested on two occasions, separated by 14 days, in normoxic and hypoxic ($FiO_2 = 16.5\%$, equivalent to 2,000 m asl) conditions applied in random order. The tests were performed in a laboratory room equipped with a normobaric hypoxia system (AirZone 25, Air Sport, Poland) allowing to freely manipulate the oxygen concentration in the room air. Temperature (19°C), humidity (50%), and CO_2 concentration (700–800 ppm) were controlled and held constant. The study participants were blinded to exercise conditions. The athletes were instructed to maintain their regular diet and supplementation throughout the experiment and avoid caffeine intake for 24 h preceding each test. All participants arrived at the camp one day before the start of each test series and consumed the same meals throughout their stay (40 kcal/kg/d, 50% carbohydrates, 20% proteins, and 30% fats).

On the first day of each stay, two hours after a light breakfast, the subjects performed graded cycling exercise beginning with a workload of 120 W, which was subsequently increased by 40 W every 3 minutes until volitional exhaustion. The total duration of exposure to hypoxia during this test was ~35 min. On the second day, following 24 h of rest and two hours after a light breakfast, the athletes performed a simulated 30 km individual time trial (TT) in a

mountainous terrain. The TT was preceded by a 15 min warm-up, carried out according to the individual preferences of the athletes, under the same oxygen concentration as during the main exercise. The total duration of exposure to hypoxia during this test was ~90 min. Both tests were performed on subjects' personal bicycles connected to an electromagnetic bicycle trainer (Cyclus 2, RBM Elektronik-Automation GmbH, Leipzig, Germany). During each test series, the athletes were allowed to consume water ad libitum. The oxygen saturation of arterial blood (SpO_2) and heart rate (HR) was measured using the WristOx2 pulse oximeter (Nonin Medical Inc., Plymouth, USA).

2.3. Blood Collection.

Blood samples were taken from the antecubital vein into 4 mL EDTA tubes at three-time points: before the exercise, immediately after its completion, and following 30 min of rest. They were kept on ice until centrifugation at $375 \times g$ for 10 min at 4°C. Platelet-rich plasma was transferred to a fresh plastic tube, and the leukocyte-rich buffy coat was thoroughly removed. Separated erythrocytes were suspended in ice-cold PBS and centrifuged at $800 \times g$ for 10 min, and the upper layer and the remaining buffy coat were discarded. Red blood cells were then resuspended in PBS and flash-frozen in liquid nitrogen. Platelet-rich plasma was centrifuged at $2000 \times g$ for 10 min to sediment platelets. The supernatant was then transferred to a fresh plastic tube and recentrifuged at $5000 \times g$ for 10 minutes to obtain platelet-free plasma. All samples were stored at -80°C until analysis.

2.4. Biochemical Assays.

All reagents were of analytical grade and purchased (unless otherwise stated) from Sigma-Aldrich (Nümbrecht, Germany, or Saint Louis, MO, USA). Redox determinations were performed in duplicate assays: assessment of antioxidant enzymes in erythrocyte samples and assessment of nonenzymatic antioxidants, oxidative and nitrosative stress products, inflammatory mediators, and lysosomal enzymes in the plasma samples. The absorbance and fluorescence were determined using an Infinite M200 PRO multimode microplate reader (Tecan Group Ltd., Männedorf, Switzerland). The results were then standardized to 1 mg of total protein content, as reported in several other publications [34–40]. The total protein level was evaluated with the bicinchoninic acid (BCA) method, using a commercial kit (Thermo Scientific PIERCE BCA Protein Assay (Rockford, IL, USA)), with bovine serum albumin (BSA) as a standard. Redox determinations were performed no more than two months after the samples were frozen.

2.5. Enzymatic Antioxidant Barrier.

Catalase (CAT, E.C. 1.11.1.6) activity was measured with the method developed by Aebi [41], by evaluation of hydrogen peroxide decomposition, measured spectrophotometrically at the wavelength of 240 nm. One unit of CAT was defined as the amount of the enzyme which is needed to decompose one nmol of hydrogen peroxide within 1 minute. The results are presented as nmol H_2O_2/min/mg protein.

The activity of glutathione peroxidase (GPx, E.C. 1.11.1.9) was determined using Paglia and Valentine's method [42] based on the conversion of NADPH (reduced nicotinamide adenine dinucleotide) to $NADP^+$ (nicotinamide adenine dinucleotide cation). The measurements were performed spectrophotometrically at 340 nm. One unit of GPx was represented as the amount of the enzyme necessary to catalyze the oxidation of 1 μmol of NADPH within 1 minute [43]. The results are presented as mU/mg protein.

Glutathione reductase (GR, E.C. 1.8.1.7) activity was evaluated spectrophotometrically with the Mize and Langdon [44] method at the wavelength of 340 nm. It was assumed that one unit of GR catalyzing oxidation of 1 μmol of NADPH within 1 minute. The results are presented as mU/mg protein.

The activity of superoxide dismutase (SOD, E.C. 1.15.1.1) was determined with the spectrophotometric method, according to Misra and Fredovich [45]. The absorbance changes accompanying adrenaline oxidation to adrenochrome were measured at the wavelength of 480 nm. One SOD unit corresponds to the amount of enzyme reducing adrenaline oxidation by 50%. The results are presented as mU/mg protein.

2.6. Nonenzymatic Antioxidant Barrier.

The uric acid (UA) concentration was measured spectrophotometrically at the wavelength of 490 nm using the commercial kit (QuantiChromTMUric Acid Assay Kit DIUA-250; BioAssay Systems, Hayward, CA, USA) according to the manufacturer's instructions. The results are presented as μmol/mg protein.

The concentration of reduced (GSH) and oxidized (GSSG) glutathione was evaluated colorimetrically. The determination was based on the enzymatic reaction between NADPH, DTNB (5,5′-Dithiobis-(2-nitrobenzoic acid), and GR. In order to determine GSSG concentration, the samples were incubated with 2-vinylpiridine to inhibit glutathione oxidation after neutralization with 1 M chlorhydrol triethanolamine to pH 6-7. The concentration of GSH was calculated as a difference in the levels of total glutathione and GSSG. The measurements were taken at the 412 nm wavelength [46, 47]. The results are presented as μmol/mg protein.

Oxidation/reduction potential (redox ratio) was calculated based on the formula = $[GSH]^2/[GSSG]$ [48].

2.7. Antioxidant Status.

Total antioxidant capacity (TAC) was determined by the Erel's method [49]. 2,2-Azinobis (3-ethylbenzene-thiazoline-6-sulfonate) (ABTS) was mixed with potassium persulfate and incubated at room temperature for 12 hours to obtain $ABTS^+$. In the next step, 1 mL of $ABTS^+$ was added to 10 μL of samples, and the absorbance was read 735 nm wavelength. Results of decolorization were linear with increasing Trolox concentrations. The results are presented as μmol/mg protein.

Total oxidant status (TOS) was evaluated colorimetrically by Erel's method [50], using the oxidation reaction of Fe^{2+} to Fe^{3+} ions. Fe^{3+} ions were then detected using xylenol orange. The results are presented as nmol H_2O_2 equivalent/mg protein.

The oxidative stress index (OSI) was calculated using the formula: OSI = [TOS, μmol H_2O_2 equivalent/L[/[TAC, mmol Trolox/L] × 10 [51, 52].

2.8. Oxidative Stress. The concentration of thiobarbituric acid reactive substances (TBARS) was measured colorimetrically using thiobarbituric acid (TBA) method. 1,1,3,3-Tetraethoxypropane was used as the standard, and determination was performed at 535 nm [53, 54]. The results are presented as μmol/mg protein.

The spectrophotometric detection evaluated the concentration of advanced oxidation protein products (AOPP). Potassium iodide and acetic acid were added to the wells, and the absorbance was read immediately at 340 nm [55, 56]. The results are presented as μmol/mg protein.

Ischemia modified albumin (IMA) concentration was determined colorimetrically at 470 nm. The determination was based on the measurement of the exogenous cobalt (Co^{2+}) binding facility of human plasma albumin [57, 58]. The results are presented as μmol/mg protein.

2.9. Nitrosative Stress. Nitrate/nitrite (NOx) concentration was determined spectrofluorimetrically. Stable decomposition products of nitric oxide (NO) from the Griess reaction were evaluated by measuring absorbance at 543 nm wavelength [59]. The results are presented as μmol/mg protein.

The peroxynitrite level was determined spectrophotometrically by measurement of the absorbance of nitrophenol at the wavelength of 320 nm. The nitrophenol production resulted from the decomposition of peroxynitrite followed by nitration of glycyltyrosine and 4-hydroxyphenyloacetic acid (4-HPA) [60, 61]. The results are presented as μmol/mg protein.

3-Nitrotyrosine (3-NT) level was measured using the ELISA method. According to the manufacturer's instructions, a commercial kit (Nitrotyrosine ELISA; Immundiagnostik AG, Bensheim, Germany) was used. The results are presented as μmol/mg protein.

S-Nitrosothiol concentration was measured spectrophotometrically based on the reaction of the Cu^{2+} ions with the Griess reagent [62]. The solution was shaken and incubated for 20 minutes, after which the absorbance was measured at 490 nm [63]. The results are presented as nmol/mg protein.

2.10. Inflammation and Lysosomal Function. Myeloperoxidase (MPO, EC 1.11.2.2) activity was analyzed spectrophotometrically using sulfanilamide hexadecyl trimethylammonium, ortho-dianisidinedihydrochloride, and hydrogen peroxide [37, 64]. The absorbance was measured at 450 nm. The results are presented as mU/mg protein.

The tumor necrosis factor-alpha (TNF-α) level was determined by the ELISA method using a commercially available kit (EIAab Science Inc. Wuhan; Wuhan, China) according to the manufacturer's instructions. The results are presented as pg/mL.

The activity of N-acetyl-β-hexosaminidase (HEX, EC 3.2.1.52) and β-glucuronidase (GLU, EC 3.2.1.31) was estimated colorimetrically at 405 nm using 4-nitrophenyl-N-acetyl-β-glucosaminide (HEX) and 4-nitrophenyl-β-D-glucuronide (GLU) as a substrate reaction [65, 66]. The results are presented as pKat/mg protein.

2.11. Statistical Analysis. Statistical analysis was performed using GraphPad Prism 8.4.3 for macOS (GraphPad Software, Inc. La Jolla, USA). The normality of the distribution was assessed using the Shapiro–Wilk test, while homogeneity of variance used the Levene test. For comparison of quantitative variables, the two-way analysis of variance (ANOVA) followed by the original FDR method of Benjamini and Hochberg was used. Multiplicity adjusted p value was also calculated. The relationship between the assessed biomarkers was evaluated using the Pearson correlation coefficient. The statistical significance level was set at $p < 0.05$.

The number of subjects was determined based on our previous experiment, assuming the test power $= 0.8$ and $\alpha = 0.05$ (online *ClinCalc* sample size calculator). Erythrocyte GSH-Px, plasma GSH, TAC, TBARS, AOPP, and peroxynitrite were used for calculations, and the minimum number of subjects should be 13 (in one group).

3. Results

3.1. Exercise Performance. The duration of the GE under normoxic conditions was 20.2 ± 1.9 min, and the maximal work rate amounted to 5.1 ± 0.3 W/kg of body weight. The SpO_2 was 98.0 ± 0.8 and $91.9 \pm 3.0\%$ at rest and at the end of the exercise, respectively. The heart rate at the point of exhaustion was 193 ± 8 bpm. In hypoxia, the average duration of the exercise was 18.0 ± 1.9 min, whereas the maximal work rate was 4.6 ± 0.4 W/kg. The SpO_2 was 93.3 ± 3.4 and $84.3 \pm 5.4\%$ at rest and at the point of exhaustion, respectively. The heart rate at the end of the exercise was 190 ± 9 bpm.

The duration of the TT in normoxia was 61.1 ± 5.4 min, and the average work rate was 3.6 ± 0.3 W/kg of body weight. The SpO_2 amounted to 97.8 ± 2.0 and $93.6 \pm 2.3\%$ at rest and at the end of the exercise, respectively. The average heart rate was 176 ± 9, 177 ± 8, and 179 ± 10 bpm after 10, 20, and 30 km of the TT, respectively. Under hypoxic conditions, the TT lasted 63.7 ± 3.0 min, whereas the average work rate was 3.3 ± 0.2 W/kg. The SpO_2 was 93.3 ± 3.8 and $86.5 \pm 2.7\%$ at rest and at the end of the TT, respectively. The mean heart rate was 174 ± 11, 176 ± 13, and 180 ± 12 bpm after 10, 20, and 30 km of the TT, respectively.

3.2. Enzymatic Antioxidant Barrier. In normoxia, after the (GE) activity of glutathione reductase (GR) increased by 9% ($p = 0.0464$), while after 30 minutes of resting, the activity of catalase (CAT) rose 25.4% ($p = 0.0003$), and the activity of glutathione peroxidise (GPx) decreased by 13% ($p = 0.0081$), all comparing to the preexercise activity. In hypoxia, the postexercise activity of CAT and superoxide dismutase (SOD) was consecutively 28% ($p = 0.0002$) and 59.8% ($p < 0.0001$) greater than preexercise. After resting, the activity of CAT was 41.6% higher ($p < 0.0001$) than before the GE, and SOD activity was 33.9% lower ($p < 0.0001$) comparing to the evaluation performed immediately after exercise. When comparing the enzymatic activity in groups exercising hypoxia to those exercising normoxia, the CAT activity was 24% higher ($p = 0.0088$) before the GE. In postexercise measurement, the activity of CAT

was 6% higher ($p < 0.0001$), the activity of GPx was 12.1% lower ($p = 0.0175$), and the activity of SOD was 71.7% greater ($p < 0.0001$). Moreover, the activity of CAT after resting was 41.6% higher ($p < 0.0001$) in hypoxia (Figure 1, GE).

After 30 km TT in normoxia, the activity of CAT and SOD after the exercise rose 18.8% ($p = 0.0386$) and 17.1% ($p = 0.046$) consecutively, and after resting for 30 minutes, the activity of GPx and SOD increased by 15.2% ($p < 0.0001$) and 22.3% ($p = 0.01$), respectively, all comparing to the activity before exercising. If compared to the post-exercise value, after resting, the activity of GPx decreased by 24.4% ($p = 0.0009$). After the exercise in hypoxia, there was a significant increase in the activity of CAT (17.2%; $p = 0.0242$) and SOD (47.9%; $p < 0.0001$). Furthermore, the activity of SOD after resting was 24.4% lower ($p = 0.0009$) than after the exercise. Before TT, the activity of CAT in hypoxia was 18.9% ($p < 0.0001$) greater than in normoxia and 17.4% ($p = 0.0233$) greater after the exercise, while the postexercise SOD activity was 10.5% ($p = 0.003$) lower in hypoxia than in normoxia. Evaluation taken 30 minutes after the end of TT revealed that in hypoxia, the activity of GPx and SOD was significantly lower than in normoxia—18.7% ($p < 0.0001$) and 19.9% ($p = 0.0051$), respectively (Figure 1, TT).

3.3. Nonenzymatic Antioxidant Barrier. There were no significant changes in concentration of uric acid (UA), reduced (GSH), and oxidized (GSSG) glutathione or value of redox ratio in normoxia after GE compared to those values before exercise. However, after 30 minutes rest, the concentration of UA increased by 18.7% ($p = 0.0058$), while concentration of GSH and redox ratio lessened by 11.9% ($p = 0.0031$) and 24.8% ($p = 0.0017$) consecutively, comparing to preexercise values. Redox ratio decreased also in comparison to postexercise value (18%, $p = 0.0343$). In hypoxia, comparing to the measurements taken before exercise, immediately after GE, concentration of UA increased by 23.6% ($p = 0.0006$), and concentration of GSH and redox ratio decreased by 18% ($p = 0.0002$) and 31.1% ($p = 0.0053$) consecutively after the exercise. After 30 minutes of resting, redox ratio was 33.5% lower ($p = 0.0028$). Moreover, concentration of GSH and redox ratio was significantly lower in hypoxia than in normoxia both before (GSH 15%, $p = 0.0002$; redox ratio 29.3%, $p < 0.0001$) and after (GSH 30%, $p < 0.0001$; redox ratio 51.3%, $p < 0.0001$) GE, as well as after 30 minutes rest (GSH 19.7%, $p < 0.0001$; redox ratio 37.4%, $p = 0.0004$) (Figure 2, GE).

In normoxia, the concentration of GSH and redox ratio declined significantly after 30 km time trial—19% ($p < 0.0001$) and 31.6% ($p < 0.0001$), respectively. Thirty minutes after finishing the TT, UA concentration raised by 18.8% ($p = 0.0143$), and concentration of GSH (13%, $p = 0.0048$) and redox ratio (25.8%, $p = 0.0009$) decreased significantly compared to the values observed before conducting the time trial, while the GSSG concentration increased by 7.79% ($p = 0.0366$) comparing to the measurement taken immediately after the exercise. In hypoxia, 30 km time trial affected significantly the content of UA (increased by 22.3%, $p = 0.0018$), GSH (decreased by 35%, $p < 0.0001$), and redox ratio (decreased by 55%, $p < 0.0001$). After resting, there was a significant decrease in

GSH concentration (27.5%, $p < 0.0001$) and redox ratio (48.8%, $p < 0.0001$) in comparison to those before TT, while GSSG content was 7.8% higher ($p = 0.038$) than right after the exercise. Moreover, postexercise content of UA was 27% greater ($p = 0.0003$) in hypoxia than in normoxia, while the concentration of GSH and redox ratio was significantly lower in hypoxia—24.2% ($p < 0.0001$) and 39.7% ($p = 0.0005$), respectively. After 30 minutes of resting, GSH content and redox ratio were 20.9% ($p = 0.0001$) and 36.8% ($p < 0.0001$) lower in hypoxia than in normoxia (Figure 2, TT).

3.4. Antioxidant Status. Total oxidant status (TOS) was raised by graded exercise until exhaustion in normoxia by 31.9% ($p = 0.0485$), while total antioxidant capacity (TAC) and oxidative stress index (OSI) were not affected. Moreover, after 30 minutes of resting, TOS increased by 51.9% ($p = 0.0016$), and OSI increased by 55.8% ($p = 0.0023$) comparing to the preexercise. In hypoxia, both TAC and TOS were elevated after exercising—by 20.8% ($p = 0.0025$) and 29.7% ($p = 0.0228$), respectively. There were also significant rises of all described measurements after 30 minutes of rest in relation to the values observed before the exercise (TAC—13.6%, $p = 0.044$; TOS—56.5%, $p < 0.0001$; OSI—37.1%, $p = 0.0276$). TOS was also 20.6% higher ($p = 0.0399$) after resting than immediately after GE. Furthermore, postexercise TAC was 26.2% greater ($p = 0.0003$) in hypoxia than in normoxia, whereas both TAC and TOS values after resting were higher in hypoxia as well (26.4%, $p = 0.0442$; 28%, $p = 0.009$, respectively) (Figure 3, GE).

In normoxia, total antioxidant capacity was increased by 30 km time trial by 34.8% ($p = 0.0023$) while oxidative stress index was elevated by 39.7% ($p = 0.0021$). After resting, TAC was raised by 16.9% ($p = 0.0006$) compared to preexercise values and by 19.9% ($p = 0.0001$) compared to postexercise measurement. OSI was 28.4% ($p = 0.0021$) lower after resting than immediately after TT. Hypoxia did not affect postexercise markers' values, but resting for 30 minutes led to 12.6% growth ($p = 0.0104$) comparing to the preexercise analysis. There were no significant differences between preexercise values comparing normoxia and hypoxia, although postexercise TAC was 10.3% higher ($p = 0.0392$) in hypoxia than in normoxia (Figure 3, TT).

3.5. Oxidative Stress. Graded exercise until exhaustion in normoxia did not influence oxidative stress marker concentration assessed directly after exercise. However, there were significant changes in TBARS (24% increase compared to preexercise value, $p = 0.0017$) and ischemia modified protein (IMA) (15.9% increase compared to postexercise value, $p = 0.0121$) contents when measured after 30 minutes of rest. In hypoxia, TBARS concentration was elevated by 25.8% ($p = 0.0002$), and advanced oxidation protein product (AOPP) content was increased by 18.8% ($p < 0.0001$) immediately after exercise. After the rest, the significant increase of the concentration of all evaluated substances was observed—TBARS by 42.2% ($p < 0.0001$), AOPP by 43.8% ($p < 0.0001$), and IMA by 27.6% ($p < 0.0001$) comparing to the values before GE and TBARS by 13% (0.0141), AOPP by 21% ($p < 0.0001$), and IMA by 17.2% ($p = 0.0003$) comparing to the values after GE.
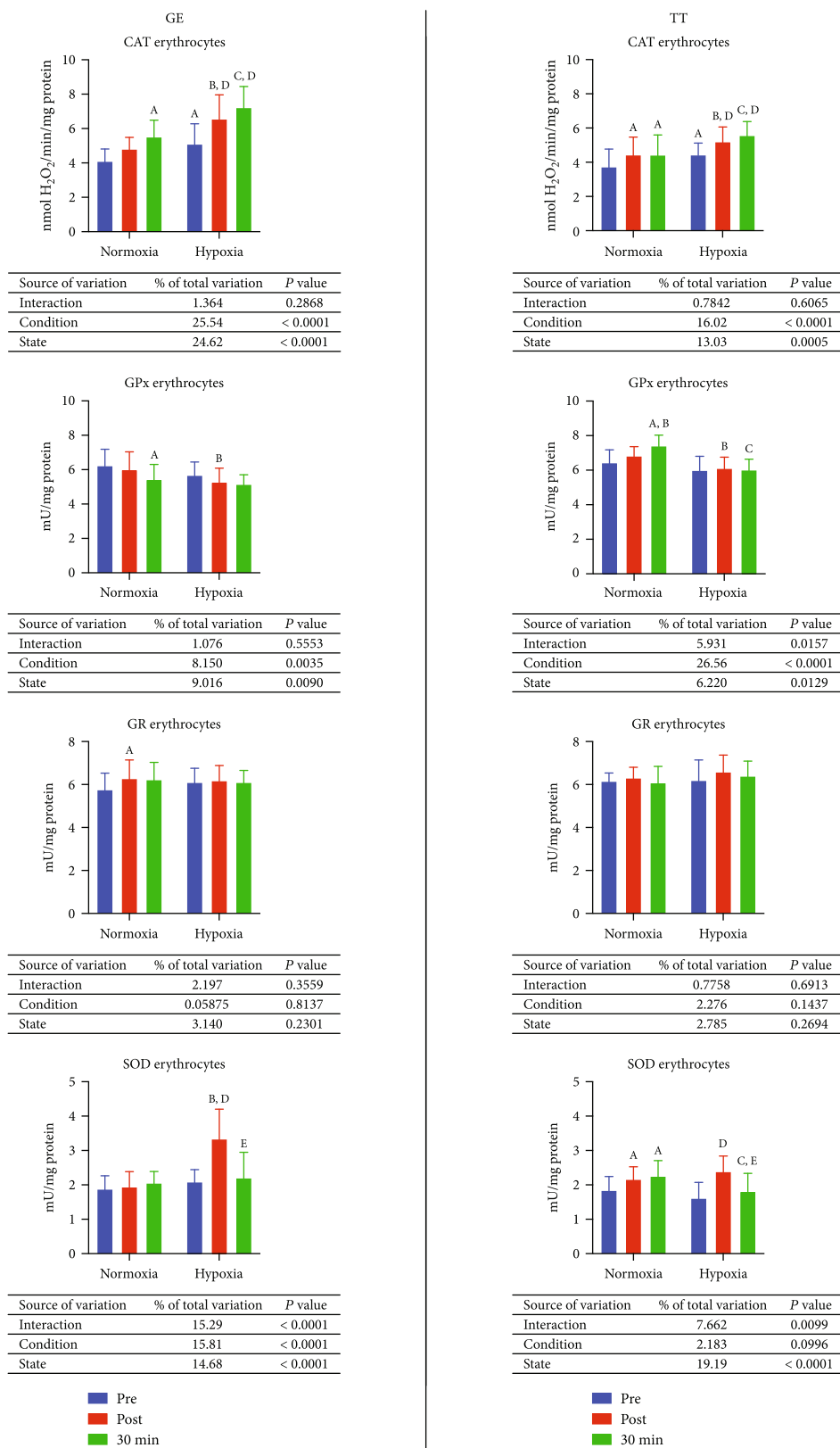
FIGURE 1: Effect of graded exercise until exhaustion (GE) and 30 km time trial (TT) on the enzymatic antioxidant barrier in normoxia and hypoxia. CAT: catalase; GPx: glutathione peroxidase; GR: glutathione reductase; SOD: superoxide dismutase. a, $p < 0.05$ vs. the value before exercise in normoxia; b, $p < 0.05$ vs. the value after the exercise in normoxia; c, $p < 0.05$ vs. the value after the exercise and 30 min of rest in normoxia; d, $p < 0.05$ vs. the value after the exercise in hypoxia; e, $p < 0.05$ vs. the value after the exercise in hypoxia; f, $p < 0.05$ vs. the value after the exercise 30 min of rest in hypoxia.
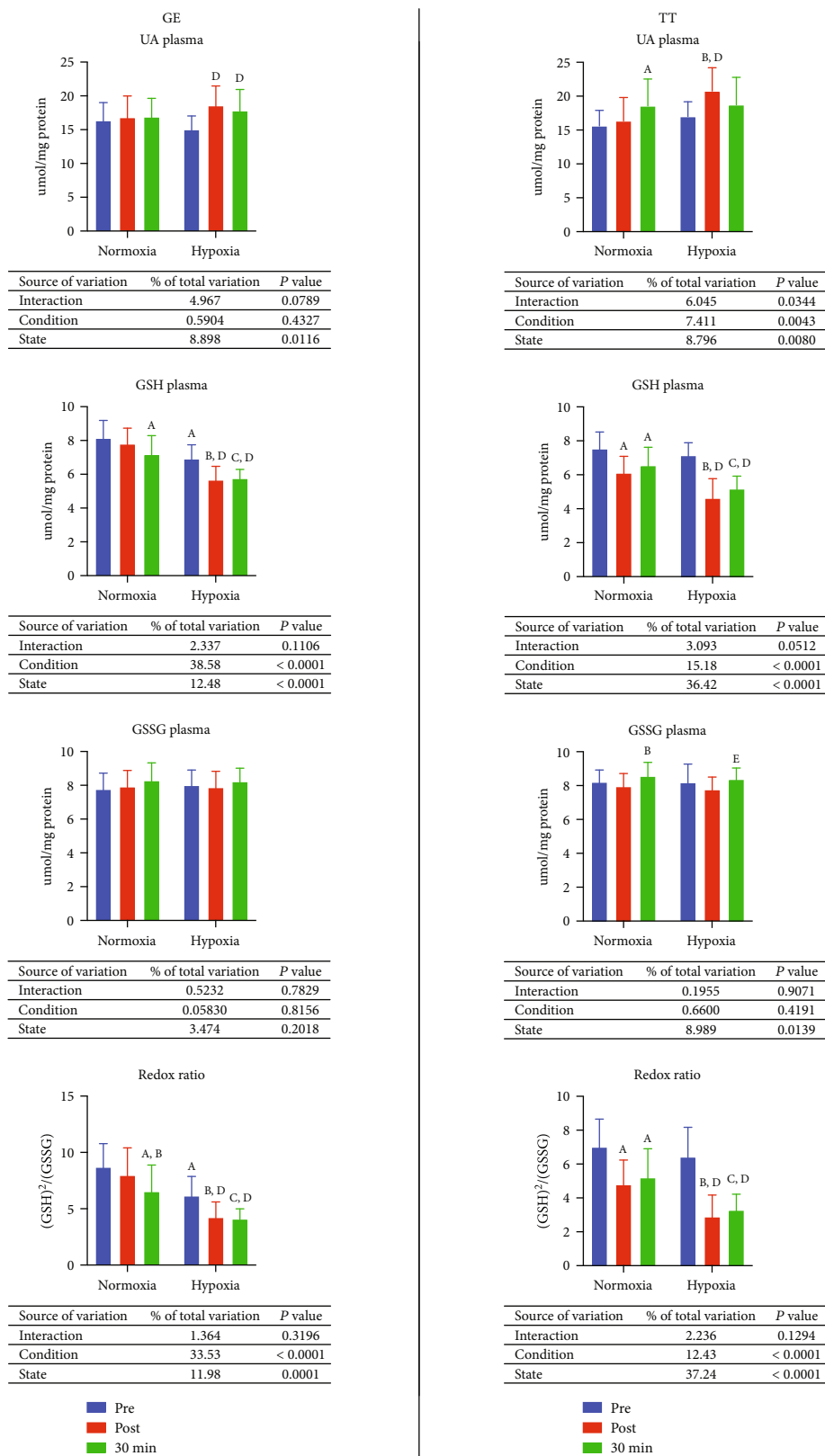
FIGURE 2: Effect of graded exercise until exhaustion (GE) and 30 km time trial (TT) on the nonenzymatic antioxidant barrier in normoxia and hypoxia. GSH: reduced glutathione; GSSG: oxidized glutathione; UA: uric acid. a, $p < 0.05$ vs. the value before exercise in normoxia; b, $p < 0.05$ vs. the value after the exercise in normoxia; c, $p < 0.05$ vs. the value after the exercise and 30 min of rest in normoxia; d, $p < 0.05$ vs. the value after the exercise in hypoxia; e, $p < 0.05$ vs. the value after the exercise in hypoxia; f, $p < 0.05$ vs. the value after the exercise 30 min of rest in hypoxia.
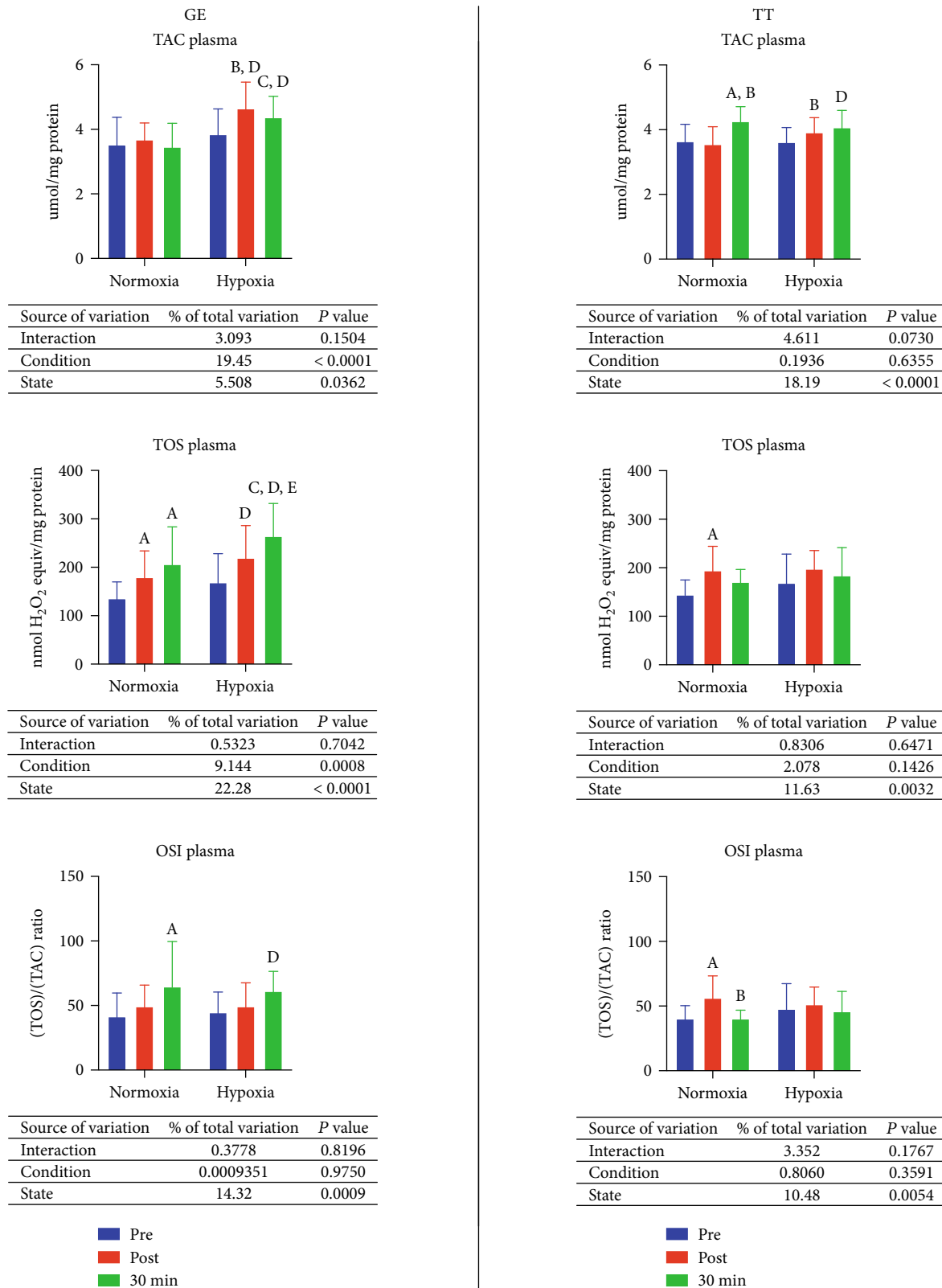
FIGURE 3: Effect of graded exercise until exhaustion (GE) and 30 km time trial (TT) on antioxidant status in normoxia and hypoxia. OSI: oxidative stress index; TAC: total antioxidant capacity; TOS: total oxidant status. a, $p < 0.05$ vs. the value before exercise in normoxia; b, $p < 0.05$ vs. the value after the exercise in normoxia; c, $p < 0.05$ vs. the value after the exercise and 30 min of rest in normoxia; d, $p < 0.05$ vs. the value after the exercise in hypoxia; e, $p < 0.05$ vs. the value after the exercise in hypoxia; f, $p < 0.05$ vs. the value after the exercise 30 min of rest in hypoxia.

There were also no differences between preexercise concentrations in normoxia and hypoxia, while contents of all described substances were significantly higher in hypoxia than in normoxia after the GE—TBARS 29.4% ($p < 0.0001$), AOPP 16.5% ($p = 0.0032$), and IMA 20.1% ($p = 0.0016$)—and after 30 minutes of resting—TBARS 29.7% ($p < 0.0001$), AOPP 21% ($p < 0.0001$), and IMA 21.5% ($p = 0.0001$) (Figure 4, GE).

After 30 km time trial in normoxia, the concentration of TBARS was increased by 21.5% ($p = 0.0034$), and the content of AOPP was 12.9% ($p = 0.0401$) higher. After 30 minutes of rest, the TBARS concentration was elevated by 16.1% ($p = 0.0267$). In hypoxia, all postexercise oxidative stress markers' concentrations were elevated—TBARS by 42.7% ($p < 0.0001$), AOPP by 49% ($p < 0.0001$), and IMA by 19.4% ($p = 0.0101$). Directly after the exercise, but after 30 minutes, the content of TBARS decreased by 11.5% ($p = 0.0328$). There were no differences between preexercise values in hypoxia and normoxia. The concentration of AOPP after TT in hypoxia was 24.2% greater ($p < 0.0001$) than in normoxia. After the rest, the contents of AOPP and IMA were also higher in hypoxia—39% ($p < 0.0001$) and 15.7% ($p = 0.0407$) consecutively (Figure 4, TT).

3.6. Nitrosative Stress.

Besides 29.8% increase ($p = 0.0014$) in peroxynitrite level after 30 minutes of resting in relation to the pre-GE value and 18.8% decrease ($p = 0.0291$) in S-nitrosothiol concentration after the rest compared to the measurement conducted directly after exercise, there was no other influence of GE in normoxia on nitrosative stress markers. In hypoxia, the 3-nitrotyrosine (3-NT) level was elevated by 15.9% ($p = 0.0223$) after the exercise. After resting, levels of peroxynitrite and 3-NT and concentration of S-nitrosothiols increased by 15.6% ($p = 0.0397$), 41.1% ($p < 0.0001$), and 31.2% ($p = 0.0034$), respectively, in comparison to the preexercise evaluation. Moreover, 3-NT level and S-nitrosothiol content were greater after 30 minutes of resting than immediately after exercise (21.8%, $p = 0.0004$; 29%, $p = 0.0055$ consecutively). Comparing the group exercising in hypoxia to the group exercising in normoxia—in hypoxia, before exercise, the content of NO_x was 20.2% higher ($p = 0.0144$), and the level of peroxynitrite was 21.1% greater ($p = 0.0219$). In comparison, after exercise, the NO_x concentration and peroxynitrite level were 20.3% ($p = 0.007$) and 16.4% ($p = 0.0393$) higher, and S-nitrosothiol concentration was 17.3% lower ($p = 0.044$). Furthermore, 30 minutes after finishing the exercise, NO_x concentration, 3-NT level, and S-nitrosothiol content were also significantly higher in hypoxia—18.5% ($p = 0.0133$), 25.4% ($p < 0.0001$), and 31.4% ($p = 0.0055$), respectively (Figure 5, GE).

After a 30 km TT in normoxia, the only significant change was 16.4% ($p = 0.0083$) increase in peroxynitrite level. In hypoxia, the level of peroxynitrite rose 13.5% ($p = 0.0252$) after the exercise, while the level of 3-NT increased by 13.1% ($p = 0.0193$) after 30 minutes of rest, both comparing to the preexercise levels. Moreover, before the exercise, the concentration of 3-NT was 12.7% higher ($p = 0.0228$) in hypoxia than normoxia. No other significant changes were observed (Figure 5, TT).

3.7. Inflammation and Lysosomal Function.

After graded exercise until exhaustion in normoxia, there were no significant changes in the activity of myeloperoxidase (MPO), level of tumor necrosis factor-alpha (TNF-α), or the activity of N-acetyl-β-hexosaminidase (HEX) and β-glucuronidase (GLU). After 30 minutes of resting, level of TNF-α and the activity of GLU increased by 36.6% ($p = 0.0279$) and 33.3% ($p = 0.0322$) comparing to preexercise, and the level of TNF-α rose 35% ($p = 0.033$) comparing to postexercise value as well. In hypoxia, the activity of all examined enzymes, as well as the level of TNF-α, increased after resting comparing to the measurement taken before exercise (MPO—52.4%, $p = 0.0002$; TNF-α—71%, $p < 0.0001$; HEX—47.7%, $p < 0.0001$; GLU—105.4%, $p < 0.0001$). The level of TNF-α and activity of HEX and GLU were significantly higher after rest also comparing to the assessment performed directly after exercise—43.9% ($p = 0.0014$), 47.7% ($p < 0.0001$), and 84.7% ($p < 0.0001$), respectively. No significant differences between inflammation and lysosomal function markers between values in normoxia and hypoxia were observed in measurements performed before and after GE. However, after 30 minutes, activity of all investigated enzymes and level of TNF-α were higher in hypoxia than in normoxia—MPO 34.4% ($p = 0.005$), TNF-α 28.3% ($p = 0.0161$), HEX 46% ($p < 0.0001$), and GLU 34.9% ($p = 0.0031$) (Figure 6, GE).

After 30 km TT in normoxia, the activity of GLU increased by 29.8% ($p = 0.038$) considering pre-TT values. In hypoxia, the level of TNF-α raised by 38.3% ($p = 0.0109$) subsequently to the exercise, while after 30 minutes, the activity of GLU raised by 6.4% ($p = 0.0012$) comparing to the activity before exercise and by 9% ($p < 0.0001$) comparing to the activity directly after exercise, and the activity of HEX increased by 17.2% ($p = 0.043$) in relation to postexercise measurement. Comparing exercising in hypoxia to exercising in normoxia, the preexercise GLU activity in hypoxia was 31.7% ($p = 0.0279$) higher, while the postexercise activity of MPO was 33.6% ($p = 0.454$) greater too. After resting, the activity of GLU was also 7.2% higher ($p = 0.0002$) in hypoxia (Figure 6, TT).

3.8. Correlations.

The results of correlation analysis are shown in Figure 7. Of particular note is the negative correlation between GSH and TOS levels ($r = -0.465$; $p = 0.001$) and the positive correlation between peroxynitrite and TOS ($r = 0.458$; $p = 0.001$) in the GE group in normoxic conditions. In the GE group in hypoxia, AOPP levels correlated positively with 3-NT content ($r = 0.571$; $p < 0.0001$) and GLU activity ($r = 0.62$; $p < 0.0001$), whereas IMA levels correlated with 3-NT ($r = 0.55$; $p < 0.0001$) and GLU ($r = 0.487$; $p < 0.0001$). Interestingly, UA concentration was also correlated negatively with WRmax ($r = -0.326$; $p = 0.029$). In the TT group in normoxia, GSH concentration ($r = -0.496$; $p < 0.0001$) and redox ratio ($r = -0.496$; $p = 0.001$) correlated negatively with CAT activity, whereas in hypoxia, UA concentration correlated positively with SOD activity ($r = 0.487$; $p = 0.013$), and GSH correlated negatively with TBARS ($r = -0.486$; $p < 0.0001$) and AOPP level ($r = -0.605$; $p = 0.0001$). Similarly, redox ratio correlated negatively with
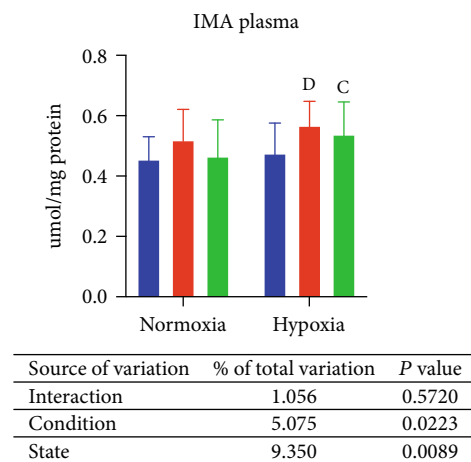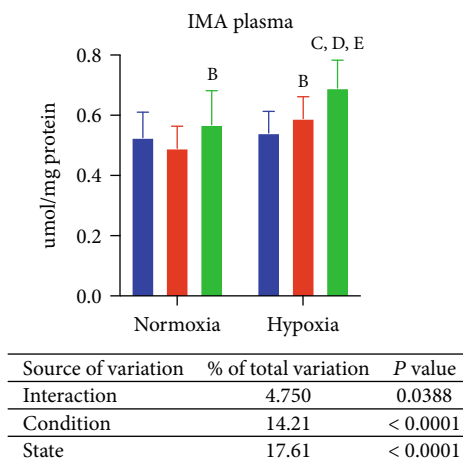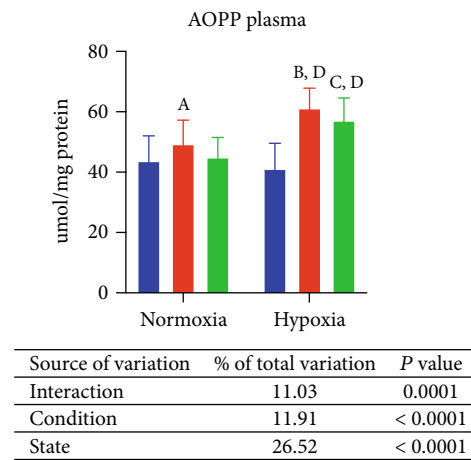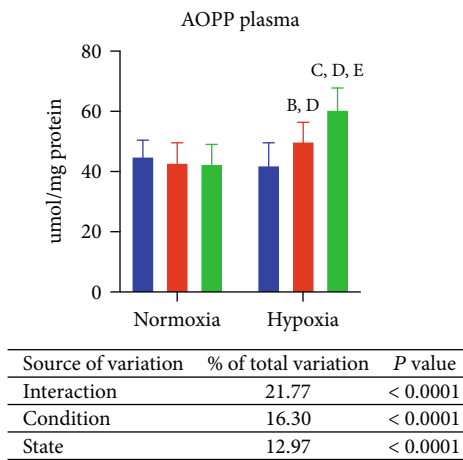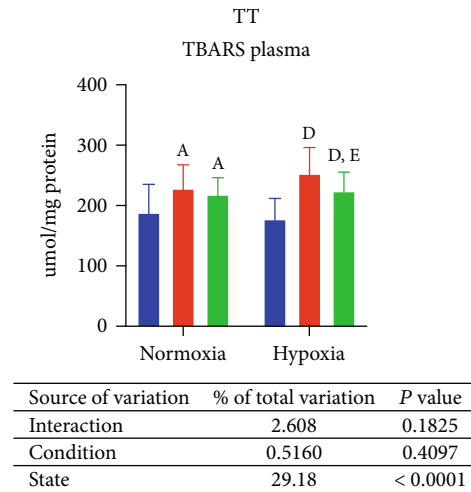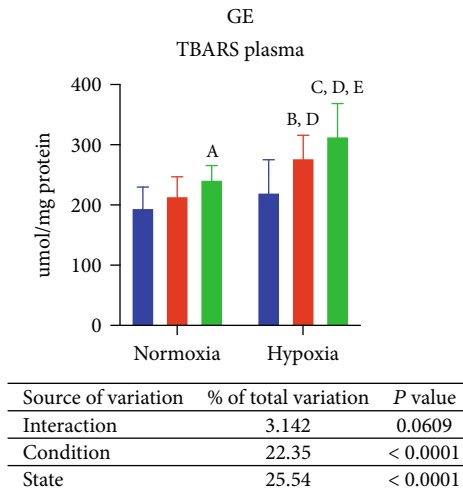
FIGURE 4: Effect on graded exercise until exhaustion (GE) and 30 km time trial (TT) on oxidative stress in normoxia and hypoxia. AOPP: advanced oxidation protein products; IMA: ischemia modified albumin; TBARS: thiobarbituric acid reactive substances. a, $p < 0.05$ vs. the value before exercise in normoxia; b, $p < 0.05$ vs. the value after the exercise in normoxia; c, $p < 0.05$ vs. the value after the exercise and 30 min of rest in normoxia; d, $p < 0.05$ vs. the value after the exercise in hypoxia; e, $p < 0.05$ vs. the value after the exercise in hypoxia; f, $p < 0.05$ vs. the value after the exercise 30 min of rest in hypoxia.
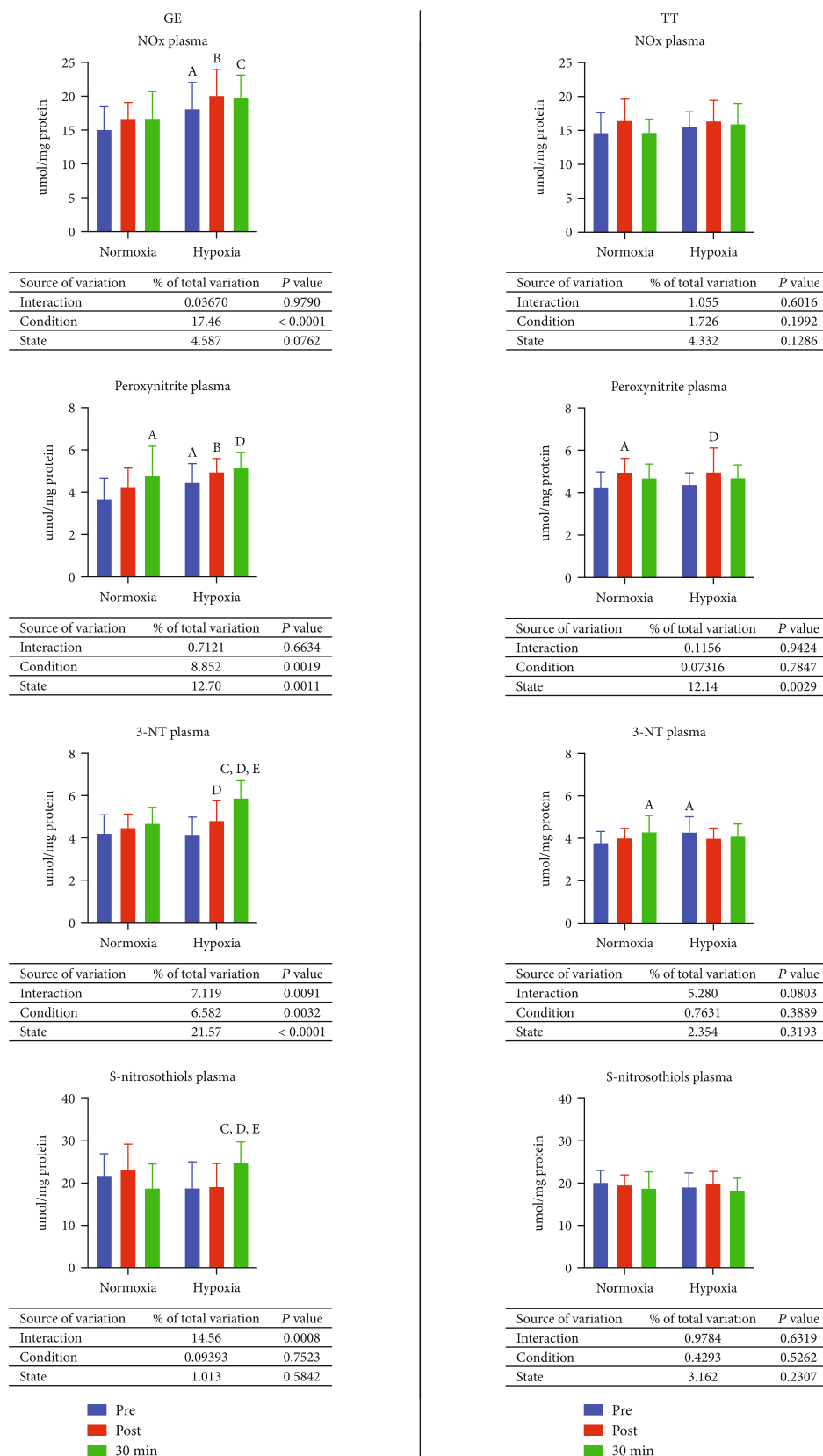
FIGURE 5: Effect on graded exercise until exhaustion (GE) and 30 km time trial (TT) on nitrosative stress in normoxia and hypoxia. 3-NT: 3-nitrotyrosine; NO_x: nitrate/nitrite. a, $p < 0.05$ vs. the value before exercise in normoxia; b, $p < 0.05$ vs. the value after the exercise in normoxia; c, $p < 0.05$ vs. the value after the exercise and 30 min of rest in normoxia; d, $p < 0.05$ vs. the value after the exercise in hypoxia; e, $p < 0.05$ vs. the value after the exercise in hypoxia; f, $p < 0.05$ vs. the value after the exercise 30 min of rest in hypoxia.

GE

MPO

Source of variation	% of total variation	P value
Interaction	5.751	0.0487
Condition	3.305	0.0612
State	8.167	0.0145

TNF-a

Source of variation	% of total variation	P value
Interaction	2.068	0.2841
Condition	4.256	0.0243
State	20.73	< 0.0001

HEX

Source of variation	% of total variation	P value
Interaction	12.00	0.0009
Condition	0.05343	0.7961
State	16.33	< 0.0001

GLU

Source of variation	% of total variation	P value
Interaction	6.992	0.0097
Condition	0.5052	0.4032
State	28.03	< 0.0001

TT

MPO

Source of variation	% of total variation	P value
Interaction	3.523	0.1835
Condition	2.298	0.1368
State	2.437	0.3073

TNF-a

Source of variation	% of total variation	P value
Interaction	4.473	0.1130
Condition	0.03636	0.8493
State	5.389	0.0732

HEX

Source of variation	% of total variation	P value
Interaction	0.1088	0.9431
Condition	8.398	0.0034
State	7.982	0.0164

GLU

Source of variation	% of total variation	P value
Interaction	11.18	0.0014
Condition	5.960	0.0072
State	11.93	0.0009

■ Pre
■ Post
■ 30 min

FIGURE 6: Effect on graded exercise until exhaustion (GE) and 30 km time trial (TT) on inflammation and lysosomal function in normoxia and hypoxia. GLU: β-glucuronidase; HEX: N-acetyl-β-hexosaminidase; MPO: myeloperoxidase; TNF-α: tumor necrosis factor-alpha. a, $p < 0.05$ vs. the value before exercise in normoxia; b, $p < 0.05$ vs. the value after the exercise in normoxia; c, $p < 0.05$ vs. the value after the exercise and 30 min of rest in normoxia; d, $p < 0.05$ vs. the value after the exercise in hypoxia; e, $p < 0.05$ vs. the value after the exercise in hypoxia; f, $p < 0.05$ vs. the value after the exercise 30 min of rest in hypoxia.
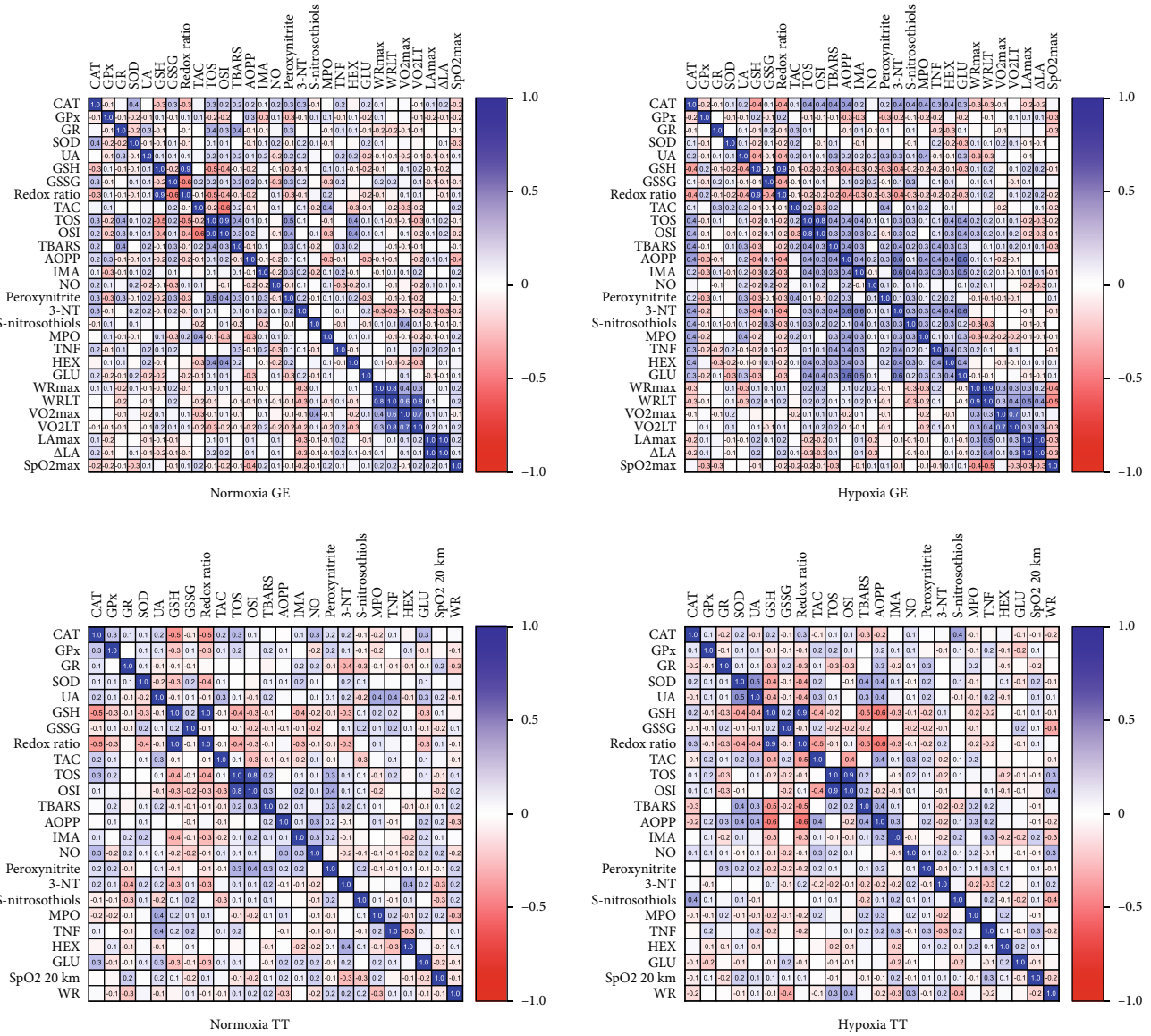
Figure 7: Correlation heat maps between redox and exercise parameters.

TAC ($r = -0.451$; $p = 0.001$), TBARS ($r = -0.468$; $p = 0.001$), and AOPP ($r = -0.615$; $p < 0.0001$) concentrations (Figure 7).

4. Discussion

Our study is the first to evaluate the effect of different acute exercise protocols performed under normoxia and hypoxia on antioxidant status, oxidative and nitrosative damage, inflammation, and lysosomal function. We have shown that both graded exercise until exhaustion (GE) and 30 km time trial (TT) impair the efficiency of antioxidant systems and induce oxidative and nitrosative stress, with hypoxia causing more significant disruption in redox homeostasis and inflammation.

In recent years, there has been a marked increase in interest in mountain sports [67]. Apart from its undoubted advantages, this type of activity is not without health risks. Limited oxygen diffusion through the pulmonary capillaries

contributes to tissue hypoxia and the overproduction of free radicals [32, 67]. ROS sources under these conditions include primarily reduced partial pressure of oxygen in the air (hypobaric hypoxia), intense physical activity, and autooxidation of catecholamines. Although various adaptive mechanisms can partially compensate for tissue hypoxia (e.g., hyperventilation, tachycardia, increased cardiac output, and enhanced hemoglobin and erythrocytes content), the most effective blood response does not appear until several days later [32].

The present study generally demonstrated the strengthening of enzymatic antioxidant systems during hypoxic exercise (GE: ↑ CAT, ↑ SOD; TT: ↑ CAT vs. normoxia). Changes in the enzymatic antioxidant barrier may reflect various functional/pathophysiological states. The initial increase in enzyme activity is usually adaptation to higher production of ROS and RNS, whereas the subsequent decrease results from depletion of the antioxidant reserves.

Of particular note are the erythrocyte enzymes (GPx and CAT) that degrade hydrogen peroxide. GPx plays a key role in H_2O_2 degradation at physiological concentrations by reducing hydrogen peroxide with the simultaneous conversion of GSH to its oxidized form (GSSG). However, under H_2O_2 overproduction, CAT exhibits greater enzymatic activity as evidenced by the Michaelis–Menten constant (Km) for GPx (1×10^{-6} M) and CAT (2.4×10^{-4} M) [68, 69]. Although we did not directly assess the rate of free radical formation, the increase in CAT and decrease in GPx activity (versus normoxia) indicate a higher intensity of oxidative processes during hypoxic exercise. Enhanced plasma TOS in hypoxia also supports this hypothesis. It is well known that TOS determines the total amount of oxidants in a biological system [50]. Considering that free radicals can mutually enhance their production, TOS provides more information than evaluation of individual ROS/RNS separately. However, what could constitute an additional source of free radicals in hypoxic exercise? During tissue hypoxia (as during tissue ischemia), xanthine dehydrogenase is converted to XO, donating an electron to molecular oxygen. The reaction catalyzed by XO produces superoxide anions and hydrogen peroxide [2, 30, 31, 70], explaining the increase in SOD and CAT activity under hypoxic exercise. However, overactivation of nitric oxide synthases (NOS), especially inducible NOS (iNOS), also occurs in these conditions [71, 72]. Excess nitric oxide (NO) concentrations inhibit cytochrome oxidase activity, which in turn intensifies $O_2^{-\bullet}$ production [73, 74]. If the full O_2 supply is restored, there is an increased formation of ROS referred to as the "oxygen paradox" [75, 76]. Therefore, enhanced CAT activity observed in our study is not surprising (increase at each time interval versus normoxic exercise). Interestingly, the activity of antioxidant enzymes (CAT, SOD) and total oxidative capacity (TOS, OSI) were also relatively higher in high-intensity exercise until exhaustion (GE). If O_2 supply to the cells is insufficient, energy is produced in the low-efficiency process of anaerobic glycolysis, leading to an increase in H^+ ions and lactate concentrations. The consequence is the loss of ability to maintain ionic homeostasis, particularly an increase in the extracellular concentration of K^+ and the accumulation of Na^+ and Ca^{2+}, which is responsible for ROS overproduction [77, 78].

The signaling effects of hydrogen peroxide are associated with proteins recording changes in cellular redox status. The molecules responsible for transmitting the H_2O_2 signal to the nucleus are low molecular weight thiols, of which reduced glutathione is an essential intracellular source [79, 80]. Therefore, it is not surprising that GSH concentrations were significantly lower in athletes exercising in hypoxia compared to normoxia. Since GSSG concentrations and GR activity were unchanged, the decrease in GSH concentration may be due to the oxidation of enzymes responsible for glutathione synthesis or the formation of S-conjugates with glutathione and proteins. In addition to its antioxidant role, GSH participates in DNA replication and apoptosis and regulates the thiol groups of proteins in their reduced state [81, 82]. Therefore, maintenance of adequate GSH levels is crucial for proper cellular function. In our study, despite

strengthening the antioxidant barrier under hypoxia, there was a redox imbalance in favor of oxidative reactions (GE: ↑ TOS, ↓ redox ratio). This results in enhanced oxidation of plasma proteins (GE: ↑ AOPP, ↑ IMA; TT: ↑ AOPP) and lipids (GE: ↑ TBARS), which indicates the occurrence of systemic oxidative stress. This may be confirmed by the negative correlation between GSH concentration and TBARS and AOPP and between redox ratio and TAC, TBARS, and AOPP. Of particular note is the increase in IMA levels during hypoxic exercise. IMA is the earliest biomarker of tissue ischemia, whereas decreased oxygen saturation, ischemic reperfusion, acidosis, sodium/calcium pump dysfunction, and higher oxidative stress are factors causing conformational changes of albumin [57]. The increase in total antioxidant capacity may also be controversial (GE: ↑ TAC both after exercise and hypoxia vs. normoxia). Nevertheless, 70-80% of plasma TAC represents nonenzymatic uric acid (UA), with a robust prooxidant effect in high concentrations [83, 84]. UA can generate free radicals by reacting with peroxynitrite or forming alkylated proteins, lipids, and carbohydrates [85]. Higher UA concentrations were observed in previous studies after one-time and regular high-intensity physical training [2, 20, 86–88]. UA is the end product of purine catabolism formed in a XO-catalyzed reaction from xanthine. Under hypoxic/ischemic conditions, hypoxanthine formed from ATP decomposition is accumulated in the cell and then metabolized to xanthine with the generation of ROS/RNS upon reperfusion [89, 90].

The H_2O_2 production may also be affected by nitric oxide metabolism [91, 92]. In our study, higher NO_x bioavailability with a concomitant increase in CAT activity could be explained by intensified peroxynitrite ($ONOO^-$) formation influenced by an acute hypoxic intervention. Indeed, the superoxide radicals formed in the XO-catalyzed pathway react with NO to generate the highly reactive $ONOO^-$ [92]. Peroxynitrite is a powerful oxidizing and nitrating agent that initiates lipid peroxidation and oxidation of thiols/aromatic amino acids with an efficiency of at least 1000-fold higher than hydrogen peroxide [93, 94]. Tyrosine residues are particularly sensitive to $ONOO^-$ damage; hence, the increase in 3-NT concentrations (both after exercise and in hypoxic conditions) is not surprising. Interestingly, peroxynitrite formation occurs typically under increased systemic inflammation [93, 94]. This may be supported by the results of our study (GE: ↑ NO, ↑ $ONOO^-$, ↑ MPO, ↑ TNF-α). Of particular note is higher MPO activity after hypoxic exercise. Indeed, MPO is released by neutrophils and monocytes during inflammatory cell activation [95]. It is involved in hypochlorous acid production, which exacerbates oxidative stress and initiates acute inflammation [95, 96]. It is well known that higher secretion of cytokines, chemokines, and growth factors is a physiological response to decreased arterial blood O_2 saturation and microdamage of muscle fibers. Activated neutrophils and macrophages can remove fragments of damaged muscle tissue induced by NO and H_2O_2 signaling [97, 98]. Simultaneously, IL-1, IL-2, IL-6, and TNF-α may stimulate white blood cells to produce significant amounts of NO through prolonged iNOS activation [99, 100]. In these conditions, XO and

NOX are also induced, which, by positive feedback, enhances nitrosative cell injury (GE: ↑ NO_x, ↑ $ONOO^-$, ↑ 3-NT). A consequence of enhanced inflammatory response and oxidative/nitrosative stress can be damage to the lysosomal membrane and the release of lysosomal enzymes into the circulation (GE: ↑ HEX, ↑ GLU). Interestingly, lysosomal dysfunction, mitochondrial energy metabolism, and impaired ion homeostasis are essential sources of ROS during physical exercise [101–103]. However, NO signaling activity may also depend on protein S-nitrosylation, as evidenced by increased S-nitrosothiols under hypoxic conditions. It is well known that NO-mediated protein S-nitrosylation plays a vital role in the adaptation to endurance exercise/hypoxia by increasing the PGC-1α (peroxisome proliferator-activated receptor gamma coactivator 1-alpha) expression [104, 105]. Nevertheless, enhanced S-nitrosylation can also end in the formation of protein disulfide and a nitroxyl residue, which irreversibly alters the biological properties of proteins.

Physical exercise is indicated in both health and disease. Although our study does not explain it, individuals with diseases with oxidative stress etiology (e.g., metabolic, neurodegenerative, and immune diseases) should be cautious during acute hypoxic training. This may exacerbate disturbances in redox homeostasis and inflammation. Antioxidant supplementation during acute hypoxic exercise also remains an open question.

Unfortunately, our work has numerous limitations. These include the relatively small number of participants and the evaluation of only selected biomarkers of oxidative stress, inflammation, and lysosomal function. Our study also does not explain the molecular mechanisms responsible for the observed redox disturbances. Research on nonprofessional athletes is also essential.

To summarize, our study shows that even a single session of physical exercise disrupts the enzymatic and nonenzymatic antioxidant barrier leading to enhanced oxidative and nitrosative damage at a systemic level. High-intensity exercise of short duration alters redox homeostasis more than prolonged aerobic exercise, while hypoxia significantly exacerbates oxidative stress, inflammation, and lysosomal dysfunction in athletic subjects. Although we have reported the most commonly assessed circulating redox biomarkers, further studies are needed to elucidate the molecular basis of the observed relationships. Studies on larger groups of athletes are also advisable.

Data Availability

The datasets generated for this study are available on request to the corresponding author.

Ethical Approval

The investigation conformed with the principles outlined in the Declaration of Helsinki and was approved by the Bioethics Committee of the Medical University of Bialystok (approval no. R-I-002/325/2019).

Conflicts of Interest

There is no conflict of interests.

Acknowledgments

References

[1] H. Sies and D. P. Jones, "Reactive oxygen species (ROS) as pleiotropic physiological signalling agents," *Nature Reviews. Molecular Cell Biology*, vol. 21, pp. 363–383, 2020.

[2] F. He, J. Li, Z. Liu, C.-C. Chuang, W. Yang, and L. Zuo, "Redox mechanism of reactive oxygen species in exercise," *Frontiers in Physiology*, vol. 7, p. 486, 2016.

[3] V. I. Lushchak, "Free radicals, reactive oxygen species, oxidative stress and its classification," *Chemico-Biological Interactions*, vol. 224, pp. 164–175, 2014.

[4] P. D. Ray, B. W. Huang, and Y. Tsuji, "Reactive oxygen species (ROS) homeostasis and redox regulation in cellular signaling," *Cellular Signalling*, vol. 24, no. 5, pp. 981–990, 2012.

[5] M. J. Morgan and Z. G. Liu, "Crosstalk of reactive oxygen species and NF-κB signaling," *Cell Research*, vol. 21, no. 1, pp. 103–115, 2011.

[6] P. Poprac, K. Jomova, M. Simunkova, V. Kollar, C. J. Rhodes, and M. Valko, "Targeting free radicals in oxidative stress-related human diseases," *Trends in Pharmacological Sciences*, vol. 38, no. 7, pp. 592–607, 2017.

[7] B. Choromańska, P. Myśliwiec, J. Dadan, A. Maleckas, A. Zalewska, and M. Maciejczyk, "Effects of age and gender on the redox homeostasis of morbidly obese people," *Free Radical Biology & Medicine*, vol. 175, pp. 108–120, 2021.

[8] J. Styskal, H. Van Remmen, A. Richardson, and A. B. Salmon, "Oxidative stress and diabetes: what can we learn about insulin resistance from antioxidant mutant mouse models?," *Free Radical Biology & Medicine*, vol. 52, no. 1, pp. 46–58, 2012.

[9] M. Maciejczyk, A. Zalewska, and K. Gerreth, "Salivary redox biomarkers in selected neurodegenerative diseases," *Journal of Clinical Medicine*, vol. 9, no. 2, p. 497, 2020.

[10] B. Halliwell, "Oxidative stress and neurodegeneration: where are we now?," *Journal of Neurochemistry*, vol. 97, no. 6, pp. 1634–1658, 2006.

[11] L. J. S. Da Fonseca, V. Nunes-Souza, M. O. F. Goulart, and L. A. Rabelo, "Oxidative stress in rheumatoid arthritis: what the future might hold regarding novel biomarkers and add-on therapies," *Oxidative Medicine and Cellular Longevity*, vol. 2019, Article ID 7536805, 16 pages, 2019.

[12] K. Morawska, M. Maciejczyk, Ł. Popławski, A. Popławska-Kita, A. Krętowski, and A. Zalewska, "Enhanced salivary and general oxidative stress in Hashimoto's thyroiditis women in euthyreosis," *Journal of Clinical Medicine*, vol. 9, no. 7, p. 2102, 2020.

[13] J. Zińczuk, K. Zaręba, J. Kamińska et al., "Association of tumour microenvironment with protein glycooxidation, DNA damage, and nitrosative stress in colorectal cancer,"

Cancer Management and Research, vol. 13, pp. 6329–6348, 2021.

[14] M. Valko, C. J. Rhodes, J. Moncol, M. Izakovic, and M. Mazur, "Free radicals, metals and antioxidants in oxidative stress-induced cancer," *Chemico-Biological Interactions*, vol. 160, no. 1, pp. 1–40, 2006.

[15] M. Finkler, D. Lichtenberg, and I. Pinchuk, "The relationship between oxidative stress and exercise," *Journal of Basic and Clinical Physiology and Pharmacology*, vol. 25, no. 1, pp. 1–11, 2014.

[16] S. K. Powers, R. Deminice, M. Ozdemir, T. Yoshihara, M. P. Bomkamp, and H. Hyatt, "Exercise-induced oxidative stress: friend or foe?," *Journal of Sport and Health Science*, vol. 9, pp. 415–425, 2020.

[17] C. Simioni, G. Zauli, A. M. Martelli et al., "Oxidative stress: role of physical exercise and antioxidant nutraceuticals in adulthood and aging," *Oncotarget*, vol. 9, pp. 17181–17198, 2018.

[18] M. Valko, D. Leibfritz, J. Moncol, M. T. D. Cronin, M. Mazur, and J. Telser, "Free radicals and antioxidants in normal physiological functions and human disease," *The International Journal of Biochemistry & Cell Biology*, vol. 39, pp. 44–84, 2007.

[19] R. J. Bloomer and K. H. Fisher-Wellman, "Blood oxidative stress biomarkers: influence of sex, exercise training status, and dietary intake," *Gender Medicine*, vol. 5, no. 3, pp. 218–228, 2008.

[20] T. Kawamura and I. Muraoka, "Exercise-induced oxidative stress and the effects of antioxidant intake from a physiological viewpoint," *Antioxidants*, vol. 7, p. 119, 2018.

[21] A. Vezzoli, L. Pugliese, M. Marzorati, F. R. Serpiello, A. La Torre, and S. Porcelli, "Time-course changes of oxidative stress response to high-intensity discontinuous training versus moderate-intensity continuous training in masters runners," *PLoS One*, vol. 9, article e87506, 2014.

[22] A. Z. Jamurtas, "Exercise-induced muscle damage and oxidative stress," *Antioxidants*, vol. 7, p. 50, 2018.

[23] J. Kruk, H. Y. Aboul-Enein, A. Kładna, and J. E. Bowser, "Oxidative stress in biological systems and its relation with pathophysiological functions: the effect of physical activity on cellular redox homeostasis," *Free Radical Research*, vol. 53, pp. 497–521, 2019.

[24] J. A. Sinex and R. F. Chapman, "Hypoxic training methods for improving endurance exercise performance," *Journal of Sport and Health Science*, vol. 4, pp. 325–332, 2015.

[25] B. Feriche, A. García-Ramos, A. J. Morales-Artacho, and P. Padial, "Resistance training using different hypoxic training strategies: a basis for hypertrophy and muscle power development," *Sports Medicine - Open*, vol. 3, p. 12, 2017.

[26] M. Czuba, O. Fidos-Czuba, K. Płoszczyca, A. Zając, and J. Langfort, "Comparison of the effect of intermittent hypoxic training vs. the live high, train low strategy on aerobic capacity and sports performance in cyclists in normoxia," *Biology of Sport*, vol. 35, pp. 39–48, 2018.

[27] M. Czuba, G. Bril, K. Płoszczyca et al., "Intermittent hypoxic training at lactate threshold intensity improves aiming performance in well-trained biathletes with little change of cardiovascular variables," *BioMed Research International*, vol. 2019, 1287517 pages, 2019.

[28] G. L. Semenza, "HIF-1 and mechanisms of hypoxia sensing," *Current Opinion in Cell Biology*, vol. 13, pp. 167–171, 2001.

[29] A. Wiśniewska, K. Płoszczyca, and M. Czuba, "Changes in erythropoietin and vascular endothelial growth factor following the use of different altitude training concepts," *The Journal of Sports Medicine and Physical Fitness*, vol. 60, 2020.

[30] J. Nagasawa, T. Kizaki, and H. Ohno, "Exercise and oxidative stress in hypoxia," *Journal in Physical Fitness, Sports Medicine*, vol. 2, pp. 481–486, 2013.

[31] C. Ballmann, G. McGinnis, B. Peters et al., "Exercise-induced oxidative stress and hypoxic exercise recovery," *European Journal of Applied Physiology*, vol. 114, pp. 725–733, 2014.

[32] G. Viscor, J. R. Torrella, L. Corral et al., "Physiological and biological responses to short-term intermittent hypobaric hypoxia exposure: from sports and mountain medicine to new biomedical applications," *Frontiers in Physiology*, vol. 9, p. 814, 2018.

[33] A. Raberin, E. Nader, J. Lopez Ayerbe et al., "Pro-oxidant/antioxidant balance during a prolonged exposure to moderate altitude in athletes exhibiting exercise-induced hypoxemia at sea-level," *Lifestyles*, vol. 11, p. 228, 2021.

[34] L. J. S. da Fonseca, V. Nunes-Souza, S. Guedes Gda, G. Schettino-Silva, M. A. Mota-Gomes, and L. A. Rabelo, "Oxidative status imbalance in patients with metabolic syndrome: role of the myeloperoxidase/hydrogen peroxide axis," *Oxidative Medicine and Cellular Longevity*, vol. 2014, Article ID 898501, 14 pages, 2014.

[35] J. Carracedo, R. Ramírez-Carracedo, I. de Toda et al., "Protein carbamylation: a marker reflecting increased age-related cell oxidation," *International Journal of Molecular Sciences*, vol. 19, 2018.

[36] S. Sabuncuoğlu, B. Kuşkonmaz, D. Uckun Çetinkaya, and H. Özgüneş, "Evaluation of oxidative and antioxidative parameters in pediatric hematopoietic SCT patients," *Bone Marrow Transplantation*, vol. 47, pp. 651–656, 2012.

[37] B. Choromańska, P. Myśliwiec, M. Łuba et al., "The impact of hypertension and metabolic syndrome on nitrosative stress and glutathione metabolism in patients with morbid obesity," *Oxidative Medicine and Cellular Longevity*, vol. 2020, Article ID 1057570, 10 pages, 2020.

[38] A. Hohl, J. da Silva Gullo, C. C. P. Silva et al., "Plasma levels of oxidative stress biomarkers and hospital mortality in severe head injury: a multivariate analysis," *Journal of Critical Care*, vol. 27, pp. 523.e11–523.e19, 2012.

[39] G. Colombo, F. Reggiani, D. Cucchiari et al., "Plasma protein carbonylation in haemodialysed patients: focus on diabetes and gender," *Oxidative Medicine and Cellular Longevity*, vol. 2018, Article ID 4149681, 12 pages, 2018.

[40] J. A. Detterich, H. Liu, S. Suriany et al., "Erythrocyte and plasma oxidative stress appears to be compensated in patients with sickle cell disease during a period of relative health, despite the presence of known oxidative agents," *Free Radical Biology & Medicine*, vol. 141, pp. 408–415, 2019.

[41] H. Aebi, "[13] Catalase in vitro," *Methods in Enzymology*, vol. 105, pp. 121–126, 1984.

[42] D. E. Paglia and W. N. Valentine, "Studies on the quantitative and qualitative characterization of erythrocyte glutathione peroxidase," *The Journal of Laboratory and Clinical Medicine*, vol. 70, pp. 158–169, 1967.

[43] P. Żukowski, M. Maciejczyk, J. Matczuk et al., "Effect of N-acetylcysteine on antioxidant defense, oxidative modification, and salivary gland function in a rat model of insulin resistance," *Oxidative Medicine and Cellular Longevity*, vol. 2018, Article ID 6581970, 11 pages, 2018.

[44] C. E. Mize and R. G. Langdon, "Hepatic glutathione reductase: I. Purification and general kinetic properties," *The Journal of Biological Chemistry*, vol. 237, pp. 1589–1595, 1962.

[45] H. P. Misra and I. Fridovich, "The role of superoxide anion in the autoxidation of epinephrine and a simple assay for superoxide dismutase," vol. 105, pp. 121–126, 1972.

[46] M. S. Moron, J. W. Depierre, and B. Mannervik, "Levels of glutathione, glutathione reductase and glutathione S-transferase activities in rat lung and liver," *Biochimica et Biophysica Acta, General Subjects*, vol. 582, pp. 67–78, 1979.

[47] E. Żebrowska, A. Chabowski, A. Zalewska, and M. Maciejczyk, "High-sugar diet disrupts hypothalamic but not cerebral cortex redox homeostasis," *Nutrients*, vol. 12, 2020.

[48] B. Choromańska, P. Myśliwiec, T. Kozłowski et al., "Antioxidant barrier and oxidative damage to proteins, lipids, and DNA/RNA in adrenal tumor patients," *Oxidative Medicine and Cellular Longevity*, vol. 2021, Article ID 5543531, 19 pages, 2021.

[49] O. Erel, "A novel automated direct measurement method for total antioxidant capacity using a new generation, more stable ABTS radical cation," *Clinical Biochemistry*, vol. 37, pp. 277–285, 2004.

[50] O. Erel, "A new automated colorimetric method for measuring total oxidant status," *Clinical Biochemistry*, vol. 38, pp. 1103–1111, 2005.

[51] J. Toczewska, M. Maciejczyk, T. Konopka, and A. Zalewska, "Total oxidant and antioxidant capacity of gingival crevicular fluid and saliva in patients with periodontitis: review and clinical study," *Antioxidants.*, vol. 9, 2020.

[52] S. Zengin, B. Al, P. Yarbil et al., "An assessment of oxidant/antioxidant status in patients with snake envenomation," *Emergency Medizinhistorisches Journal*, vol. 31, pp. 48–52, 2014.

[53] J. A. Buege and S. D. Aust, "[30] Microsomal lipid peroxidation," *Methods in Enzymology*, vol. 52, pp. 302–310, 1978.

[54] N. Bakan, S. Taysi, Ö. Yilmaz et al., "Glutathione peroxidase, glutathione reductase, Cu–Zn superoxide dismutase activities, glutathione, nitric oxide, and malondialdehyde concentrations in serum of patients with chronic lymphocytic leukemia," *Clinica Chimica Acta*, vol. 338, pp. 143–149, 2003.

[55] J. Škrha, M. Prázný, J. Hilgertová, J. Kvasnička, M. Kalousová, and T. Zima, "Oxidative stress and endothelium influenced by metformin in type 2 diabetes mellitus," *European Journal of Clinical Pharmacology*, vol. 63, pp. 1107–1114, 2007.

[56] K. Drygalski, E. Fereniec, A. Zalewska, A. Krętowski, M. Żendzian-Piotrowska, and M. Maciejczyk, "Phloroglucinol prevents albumin glycation as well as diminishes ROS production, glycooxidative damage, nitrosative stress and inflammation in hepatocytes treated with high glucose," *Biomedicine & Pharmacotherapy*, vol. 142, p. 111958, 2021.

[57] D. Bar-Or, E. Lau, and J. V. Winkler, "A novel assay for cobalt-albumin binding and its potential as a marker for myocardial ischemia - a preliminary report," *The Journal of Emergency Medicine*, vol. 19, no. 4, pp. 311–315, 2000.

[58] B. Choromańska, P. Myśliwiec, M. Łuba et al., "Bariatric surgery normalizes protein glycoxidation and nitrosative stress in morbidly obese patients," *Antioxidants.*, vol. 9, pp. 1–19, 2020.

[59] M. B. Grisham, G. G. Johnson, and J. R. Lancaster, "Quantitation of nitrate and nitrite in extracellular fluids," *Methods in Enzymology*, vol. 268, pp. 237–246, 1996.

[60] A. Skutnik-Radziszewska, M. Maciejczyk, I. Flisiak et al., "Enhanced inflammation and nitrosative stress in the saliva and plasma of patients with plaque psoriasis," *Journal of Clinical Medicine*, vol. 9, no. 3, p. 745, 2020.

[61] J. S. Beckman, H. Ischiropoulos, L. Zhu et al., "Kinetics of superoxide dismutase- and iron-catalyzed nitration of phenolics by peroxynitrite," *Archives of Biochemistry and Biophysics*, vol. 298, pp. 438–445, 1992.

[62] E. Bechtold and S. B. King, "Chemical methods for the direct detection and labeling of S-nitrosothiols," *Antioxidants & Redox Signaling*, vol. 17, pp. 981–991, 2012.

[63] B. Choromańska, P. Myśliwiec, T. Kozłowski et al., "Cross-talk between nitrosative stress, inflammation and hypoxia-inducible factor in patients with adrenal masses," *Journal of Inflammation Research*, vol. 14, pp. 6317–6330, 2021.

[64] M. F. Garça, M. Aslan, B. Tuna, A. Kozan, and H. Cankaya, "Serum myeloperoxidase activity, total antioxidant capacity and nitric oxide levels in patients with chronic otitis media," *The Journal of Membrane Biology*, vol. 246, no. 7, pp. 519–524, 2013.

[65] M. Maciejczyk, A. Kossakowska, J. Szulimowska et al., "Lysosomal exoglycosidase profile and secretory function in the salivary glands of rats with streptozotocin-induced diabetes," *Journal Diabetes Research*, vol. 2017, article 9580398, 13 pages, 2017.

[66] J. Marciniak, A. Zalewska, J. Popko, and K. Zwierz, "Optimization of an enzymatic method for the determination of lysosomal N-acetyl-β-D-hexosaminidase and β-glucuronidase in synovial fluid," *Clinical Chemistry and Laboratory Medicine*, vol. 44, pp. 933–937, 2006.

[67] M. Burtscher, M. Niedermeier, and H. Gatterer, "Editorial on the special issue on "Mountain Sports Activities: Injuries and Prevention"," *International Journal of Environmental Research and Public Health*, vol. 18, p. 1405, 2021.

[68] J. Zińczuk, M. Maciejczyk, K. Zaręba et al., "Pro-Oxidant Enzymes, Redox Balance and Oxidative Damage to Proteins, Lipids and DNA in Colorectal Cancer Tissue. Is Oxidative Stress Dependent on Tumour Budding and Inflammatory Infiltration?," *Cancers*, vol. 12, 2020.

[69] B. J. Day, "Catalase and glutathione peroxidase mimics," *Biochemical Pharmacology*, vol. 77, no. 3, pp. 285–296, 2009.

[70] L. Matta, T. S. Fonseca, C. C. Faria et al., "The effect of acute aerobic exercise on redox homeostasis and mitochondrial function of rat white adipose tissue," *Oxidative Medicine and Cellular Longevity*, vol. 2021, Article ID 4593496, 15 pages, 2021.

[71] E. Y. Dyakova, L. V. Kapilevich, V. G. Shylko, S. V. Popov, and Y. Anfinogenova, "Physical exercise associated with NO production: signaling pathways and significance in health and disease," *Frontiers in Cell and Development Biology*, vol. 3, 2015.

[72] A. V. Nosarev, L. V. Smagliy, Y. Anfinogenova, S. V. Popov, and L. V. Kapilevich, "Exercise and NO production: relevance and implications in the cardiopulmonary system," *Frontiers in Cell and Development Biology*, vol. 2, 2015.

[73] D. Z. Levett, B. O. Fernandez, H. L. Riley et al., "The role of nitrogen oxides in human adaptation to hypoxia," *Scientific Reports*, vol. 1, p. 109, 2011.

[74] R. A. Dweik, "Nitric oxide, hypoxia, and superoxide: the good, the bad, and the ugly!," *Thorax*, vol. 60, pp. 265–267, 2005.

[75] A. Hadanny and S. Efrati, "The hyperoxic-hypoxic paradox," *Biomolecules*, vol. 10, p. 958, 2020.

[76] S. Dane, S. Taysi, M. Gul, F. Akcay, and A. Gunal, "Acute exercise induced oxidative stress is prevented in erythrocytes of male long distance athletes," *Biology of Sport*, vol. 25, 2008.

[77] J. T. Reeves, E. E. Wolfel, H. J. Green et al., "Oxygen transport during exercise at altitude and the lactate paradox: lessons from Operation Everest II and Pikes Peak," *Exercise and Sport Sciences Reviews*, vol. 20, pp. 275–296, 1992.

[78] P. Moghetti, E. Bacchi, C. Brangani, S. Donà, and C. Negri, "Metabolic effects of exercise," *Sports Endocrinology*, vol. 47, pp. 44–57, 2016.

[79] H. S. Marinho, C. Real, L. Cyrne, H. Soares, and F. Antunes, "Hydrogen peroxide sensing, signaling and regulation of transcription factors," *Redox Biology*, vol. 2, pp. 535–562, 2014.

[80] C. C. Winterbourn, "Hydrogen peroxide reactivity and specificity in thiol-based cell signalling," *Biochemical Society Transactions*, vol. 48, pp. 745–754, 2020.

[81] K. Aquilano, S. Baldelli, and M. R. Ciriolo, "Glutathione: New roles in redox signaling for an old antioxidant," *Frontiers in Pharmacology*, vol. 5, 2014.

[82] M. Jozefczak, T. Remans, J. Vangronsveld, and A. Cuypers, "Glutathione is a key player in metal-induced oxidative stress defenses," *International Journal of Molecular Sciences*, vol. 13, pp. 3145–3175, 2012.

[83] I. Peluso and A. Raguzzini, "Salivary and urinary total antioxidant capacity as biomarkers of oxidative stress in humans," *Pathology Research International*, vol. 2016, 14 pages, 2016.

[84] A. Janaszewska and G. Bartosz, "Assay of total antioxidant capacity: comparison of four methods as applied to human blood plasma," *Scandinavian Journal of Clinical and Laboratory Investigation*, vol. 62, pp. 231–236, 2002.

[85] C. Gersch, S. P. Palii, W. Imaram et al., "Reactions of peroxynitrite with uric acid: formation of reactive intermediates, alkylated products and triuret, and in vivo production of triuret under conditions of oxidative stress," *Nucleosides, Nucleotides & Nucleic Acids*, vol. 28, pp. 118–149, 2009.

[86] S. Mohamed, N. Lamya, and M. Hamda, "Effect of maximal versus supra-maximal exhausting race on lipid peroxidation, antioxidant activity and muscle-damage biomarkers in long-distance and middle-distance runners, Asian," *The Journal of Sports Medicine*, vol. 7, pp. e27902–e27902, 2016.

[87] C. Thomas, P. Sirvent, S. Perrey, E. Raynaud, and J. Mercier, "Relationships between maximal muscle oxidative capacity and blood lactate removal after supramaximal exercise and fatigue indexes in humans," *Journal of Applied Physiology*, vol. 97, pp. 2132–2138, 2004.

[88] M. Wiecek, M. Maciejczyk, J. Szymura, and Z. Szygula, "Sex differences in oxidative stress after eccentric and concentric exercise," *Redox Report*, vol. 22, pp. 478–485, 2017.

[89] G. Glantzounis, E. Tsimoyiannis, A. Kappas, and D. Galaris, "Uric acid and oxidative stress," *Current Pharmaceutical Design*, vol. 11, no. 32, pp. 4145–4151, 2005.

[90] P. Higgins, J. Dawson, and M. Walters, "The potential for xanthine oxidase inhibition in the prevention and treatment of cardiovascular and cerebrovascular disease," *Cardiovascular Psychiatry and Neurology*, vol. 2009, Article ID 282059, 9 pages, 2009.

[91] S. Thomas, S. Kotamraju, J. Zielonka, D. R. Harder, and B. Kalyanaraman, "Hydrogen peroxide induces nitric oxide and proteosome activity in endothelial cells: a bell-shaped signaling response," *Free Radical Biology & Medicine*, vol. 42, pp. 1049–1061, 2007.

[92] W. Xie, J. L. Parker, and C. L. Heaps, "Effect of exercise training on nitric oxide and superoxide/H_2O_2 signaling pathways in collateral-dependent porcine coronary arterioles," *Journal of Applied Physiology*, vol. 112, pp. 1546–1555, 2012.

[93] R. Radi, "Nitric oxide, oxidants, and protein tyrosine nitration," *Proceedings of the National Academy of Sciences of the United States of America*, vol. 101, no. 12, pp. 4003–4008, 2004.

[94] R. Radi, J. S. Beckman, K. M. Bush, and B. A. Freeman, "Peroxynitrite-induced membrane lipid peroxidation: the cytotoxic potential of superoxide and nitric oxide," *Archives of Biochemistry and Biophysics*, vol. 288, no. 2, pp. 481–487, 1991.

[95] D. Odobasic, A. R. Kitching, and S. R. Holdsworth, "Neutrophil-mediated regulation of innate and adaptive immunity: the role of myeloperoxidase," *Journal of Immunology Research*, vol. 2016, Article ID 2349817, 11 pages, 2016.

[96] J. P. Eiserich, S. Baldus, M. L. Brennan et al., "Myeloperoxidase, a leukocyte-derived vascular NO oxidase," *Science (80-.)*, vol. 296, no. 5577, pp. 2391–2394, 2002.

[97] T. A. Butterfield, T. M. Best, and M. A. Merrick, "The dual roles of neutrophils and macrophages in inflammation: a critical balance between tissue damage and repair," *Journal of Athletic Training*, vol. 41, no. 4, pp. 457–465, 2006.

[98] F. Pizza, J. Peterson, J. Baas, and T. Koh, "Interplay between neutrophils and skeletal muscle after exercise. What's going on?," *Physiology News*, vol. 61, no. Winter 2005, pp. 32-33, 2006.

[99] E. Supruniuk, M. Maciejczyk, A. Zalewska, J. Górski, and A. Chabowski, "Blood profile of cytokines, chemokines, growth factors, and redox biomarkers in response to different protocols of treadmill running in rats," *International Journal of Molecular Sciences*, vol. 21, 2020.

[100] É. Cerqueira, D. A. Marinho, H. P. Neiva, and O. Lourenço, "Inflammatory effects of high and moderate intensity exercise—a systematic review," *Frontiers in Physiology*, vol. 10, 2020.

[101] Z. Zhang, P. Yue, T. Lu, Y. Wang, Y. Wei, and X. Wei, "Role of lysosomes in physiological activities, diseases, and therapy," *Journal of Hematology & Oncology*, vol. 14, p. 79, 2021.

[102] A. Salminen, K. Hongisto, and V. Vihko, "Lysosomal changes related to exercise injuries and training-induced protection in mouse skeletal muscle," *Acta Physiologica Scandinavica*, vol. 120, pp. 15–19, 1984.

[103] H. Nohl and L. Gille, "Lysosomal ROS formation," *Redox Report*, vol. 10, pp. 199–205, 2005.

[104] J. Bouviere, R. S. Fortunato, C. Dupuy, J. P. Werneck-de-Castro, D. P. Carvalho, and R. A. Louzada, "Exercise-stimulated ROS sensitive signaling pathways in skeletal muscle," *Antioxidants.*, vol. 10, p. 537, 2021.

[105] T. Geng, P. Li, M. Okutsu et al., "PGC-1alpha plays a functional role in exercise-induced mitochondrial biogenesis and angiogenesis but not fiber-type transformation in mouse skeletal muscle," *American Journal of Physiology. Cell Physiology*, vol. 298, pp. C572–C579, 2010.

Review Article

Ferroptosis: A New Regulatory Mechanism in Osteoporosis

Pan Liu [ID],[1,2] **Wenzhao Wang** [ID],[3] **Zheng Li**,[4] **Yao Li**,[1,2] **Xiaoping Yu** [ID],[5,6] **Ji Tu** [ID],[7]
and Zhengdong Zhang [ID][1,2,8]

[1]*School of Clinical Medicine, Chengdu Medical College, Chengdu 610500, China*
[2]*The First Affiliated Hospital of Chengdu Medical College, Chengdu 610500, China*
[3]*Department of Orthopedics, West China Hospital of Sichuan University, Chengdu 610041, China*
[4]*People's Hospital of Jiulongpo District, Chongqing 400050, China*
[5]*School of Public Health, Chengdu Medical College, Chengdu 610500, China*
[6]*Basic Medical College of Chengdu University, Chengdu 610500, China*
[7]*Spine Labs, St. George & Sutherland Clinical School, University of New South Wales, Sydney, Australia*
[8]*Department of Orthopedics, The First Affiliated Hospital of Chengdu Medical College, Chengdu 610500, China*

Correspondence should be addressed to Xiaoping Yu; cyggwsyxp@sina.com, Ji Tu; ji.tu@student.unsw.edu.au,
and Zhengdong Zhang; doctorzzd@vip.qq.com

Osteoporosis can be caused by a multitude of factors and is defined by a decrease in bone density and mass caused by the destruction of bone microstructure, resulting in increased bone brittleness. Thus, it is a systemic bone disease in which patients are prone to fracture. The role of ferroptosis in the pathogenesis of osteoporosis has become a topic of growing interest. In this review, we discuss the cell morphology, basic mechanisms of ferroptosis, the relationship between ferroptosis and osteoclasts and osteoblasts, as well as the relationship between ferroptosis and diabetic osteoporosis, steroid-induced osteoporosis, and postmenopausal osteoporosis. Emerging biomedical research has provided new insights into the roles of ferroptosis and osteoporosis, such as in cellular function, signaling pathways, drug inhibition, and gene silencing. The pathophysiology and mechanism of ferroptosis and osteoporosis need to be further studied and elucidated to broaden our understanding of iron metabolism and immune regulation. Studies using animal models of osteoporosis in vivo and cell models in vitro will help clarify the relationship between ferroptosis and osteoporosis and provide research ideas for the elucidation of new mechanisms and development of new technologies and new drugs for the treatment of osteoporosis in the future.

1. Introduction

Cell death includes apoptosis, pyroptosis, necrosis, autophagy, ferroptosis, and other death mechanisms. Before the concept of ferroptosis was revealed, one study showed that the regulation of iron metabolism and the maintenance of iron homeostasis have indispensable biological roles in the human pathophysiological process. In 2003, Dolma et al. [1] found that the small molecule erastin can induce RAS mutations in tumor cells, leading to cell death in a manner different from traditional apoptosis. In 2008, using high-throughput small-molecule screening technology, it was found that Ras selective lethal small molecules could kill human foreskin fibroblasts (BJeLR) in a nonapoptotic manner [2]; however, neither apoptosis inhibitors nor necrostatin inhibitors (Necrostatin-1) [3] could reverse cell death induced by erastin and RSLs. In contrast, the antioxidant vitamin E and the iron-chelating agent deferoxamine mesylate (DFO) can inhibit cell death [4], indicating that ferroptosis is an iron-dependent cell death process. In 2012, Dixon et al. named this process erastin-induced cell death with distinct morphological, genetic, and biochemical characteristics [5].

Iron, an essential trace element for humans and a necessary substance for life, plays a vital role in many biochemical processes, including oxygen transport, enzymatic reactions,

and immune reactions. With accumulating research, various physiological and pathological processes, such as tumor, Parkinson's disease, atherosclerosis, viral infection, osteoporosis, immune response, and ischemia-reperfusion injury, have been found to be related to ferroptosis [6–8], and ferroptosis is expected to become a new research direction for disease treatment.

Interestingly, a growing number of studies have reported a relationship between ferroptosis and osteoporosis. Here, we summarize the basic pathological features of ferroptosis and the relationship between ferroptosis and osteoclasts and osteoblasts. We also summarize the relationship between ferroptosis and osteoporosis and show how ferroptosis regulates diabetic osteoporosis (DOP), glucocorticoid-induced osteoporosis (GIOP), and postmenopausal osteoporosis (PMOP).

2. Morphological Characteristics of Ferroptosis

Ferroptosis was delineated as a type of regulated cell death (RCD) by the Nomenclature Committee on Cell Death in 2018. It is initiated by oxidative perturbations in the intracellular microenvironment, which are constitutively controlled by glutathione peroxidase 4 (GPX4) and can be inhibited by iron-chelating agents and lipophilic antioxidants [9]. Ferroptosis is distinguished from apoptosis [10], necrosis [11], autophagy [12], and pyroptosis [13] by a varying set of morphological characteristics, inducing factors, and regulatory pathways.

Cancer cells undergoing ferroptosis are generally round, small, and scattered [1]. In human prepuce fibroblast BJeLR cells treated with erastin, several effects were observed: mitochondria atrophied and decreased in number, membrane density increased, the normal structure of mitochondrial cristae was destroyed, nuclear size was normal but lacked chromatin aggregation, and cell membranes were blistered without rupturing [5, 14–16]. These morphological features can help to distinguish ferroptosis from other modes of cell death, such as apoptosis, necrosis, pyroptosis, and autophagy.

3. Mechanisms and Regulation of Ferroptosis

3.1. Iron Metabolism and Ferroptosis. Iron is involved in the synthesis of various important proteases and is an essential element in the life activities of the body [17, 18]. Iron overload caused by abnormal iron metabolism is one of the main characteristics of ferroptosis. Binding of ferric acid to transferrin is the main mechanism for circulation of iron in the bloodstream. Circulating iron enters cells by binding to transferrin receptor 1 (TFR1) on the cell membrane, where the six-transmembrane epithelial antigen of prostate 3 (STEAP3) reduces ferric iron to ferrous iron. Finally, divalent metal transporter 1 (DMT1) releases divalent iron into the labile iron pool (LIP) in the cytoplasm. LIP enables the active uptake of free iron in the cytoplasm, as well as recovery of iron in ferritin and mitochondria, and large quantities of LIP are present in lysosomes [19]. Lysosomes are therefore considered the main organelles responsible for cellular

ferroptosis [20]. Excess bivalent iron is transported extracellularly by ferroportin 1 (FPN1) and stored in ferritin heavy chain 1 and ferritin light chain 1 (FTL1) [21, 22].

Under physiological conditions, ferritin provides a strong buffer that regulates physiological responses to iron deficiency and excess, maintaining homeostasis [23]. Under pathological conditions, iron overload can induce ferroptosis by producing ROS through Fenton and Haber–Weiss reactions [24, 25]. Studies have shown that DFO, an iron chelator, can inhibit ferroptosis caused by intracellular iron overload [26, 27]. In addition, a high iron diet can lead to serious heart damage, and the ferroptosis inhibitor ferrostatin-1 mitigates the damage caused by ferroptosis [28]. Under physiological conditions, mitochondrial ferritin (FtMt) regulates the free iron content in the mitochondria and maintains normal mitochondrial iron metabolism. FtMt overexpression can reverse erastin-induced ferroptosis both in vivo and in vitro [29, 30]. In neurological diseases, mitochondrial transferrin mitoferrin 1/2 (Mfrn1/2) on the inner mitochondrial membrane is found to be destroyed, resulting in abnormal iron metabolism in the mitochondria [31].

Iron metabolism has been implicated in the occurrence and development of ferroptosis. However, the role of systemic iron regulation in the cellular role of iron deposits and ferritinophagy remains elusive. Whether systemic iron levels fully determine the effect of ferroptosis on the disease remains to be clarified.

3.2. Ferroptosis Mediated by P53. P53 is an important tumor suppressor gene with important roles in cell cycle inhibition, apoptosis, tumorigenesis, and aging [32–34]. mRNA and protein expression levels of SLC7A11 were significantly decreased after the upregulation of p53 gene expression, which confirmed that SLC7A11 is a new target of the p53 gene [35, 36]. p53-silenced H1299 cells were treated with ROS, and there was no change in cell activity. In contrast, cells with activated p53 that were treated with ROS had a 90% death rate. After adding the ferroptosis inhibitor, ferrostatin-1, the cell death rate decreased by approximately 40%, indicating that p53 can induce ferroptosis [37]. Recent studies have shown that P53 can inhibit the uptake of cystine by system xc$^-$ by downregulating the expression of the SLC7A11 subunit, resulting in a decrease in cystine-dependent glutathione peroxidase activity and cell antioxidant capacity and an increase in lipid ROS, leading to cellular ferroptosis [38].

3.3. Voltage-Dependent Anion Channels with Ferroptosis. Mitochondria, the main regulators of oxidative phosphorylation, play an important role in oxidative stress and are major producers of ROS [39, 40]. Iron can reach the mitochondrial matrix by passing through the outer mitochondrial membrane and inner mitochondrial membrane, subsequently regulating the physiological functions of important organelles in the mitochondria [41]. Mitochondria also play an important role in the regulation of ferroptosis [42]. Under erastin induction, the voltage-dependent anion channel protein 2/3 (VDAC2/3) on the outer mitochondrial membrane is opened, leading to iron

accumulation in the mitochondria. However, the detailed mechanism underlying the role of erastin and VDAC2/3 is still being explored [43].

3.4. Ferroptosis Induced by Inhibition of GPX4 and Cysteine-Glutamate Transporter Receptors (System xc⁻). GPX4, an important specific marker of ferroptosis [44], can reduce lipid peroxides to lipid alcohols and hydrogen peroxide to water during ferroptosis [45]. Both GPX4 knockout and the use of the small molecule inhibitor RSL3 antagonism against GPX4 could effectively induce ferroptosis [46–49]. L-glutathione (GSH) is composed of glycine, glutamate, and cysteine and is an important antioxidant in the oxidative stress response, widely present in cells in the form of reduced GSH and oxidized glutathione (GSSG) [50]. The degradation of lipid peroxides by GPX4 requires GSH for the provision of electrons to complete the process [20]. GSH synthesis requires intracellular uptake of cysteine, which is mediated by the sodium-dependent system xc⁻ (also named the cystine/glutamate antiporter), a disulfide-linked heterodimer composed of a heavy chain (4F2hc, gene name SLC3A2), and a light chain (xCT, gene name SLC7A11). The sodium-dependent system xc⁻ transports extracellular cystine into the cell and further converts it to cysteine, which is then used in GSH biosynthesis [5, 51–55]. Studies have shown that selective inhibition of system xc⁻ leads to a decrease in intracellular GSH, which aggravates ROS accumulation and eventually leads to ferroptosis [56, 57]. Although a regulatory mechanism between GXP4 and ferroptosis is known to exist, the roles of GXP4 in different RCD and the mechanism of information transduction pathways remain unclear.

3.5. Ferroptosis Mediated by Lipid Peroxidation. Lipid peroxidation is another key factor in ferroptosis. Recent studies [58] have shown that lipid peroxides can destroy the stability of the lipid bilayer, causing disintegration of the cell membrane. Lipidomics analyses have indicated that both AA and adrenic acid containing phosphatidyl ethanolamine are lipid products of ferroptosis, which can undergo spontaneous peroxidation in the presence of hydroxyl radicals (produced by the Fenton reaction between redox-active iron divalent and hydrogen peroxide) [46, 59, 60]. Polyunsaturated fatty acids (PUFAs) are prone to lipid peroxidation, owing to the presence of highly active hydrogen atoms in methylene bridges. Hydroxyl radicals can directly interact with PUFAs in membrane phospholipids through chain reactions to form lipid peroxides, which attack the cytomembrane and trigger morphological changes in ferroptosis [61, 62]. Derivatives resulting from the decomposition of lipid peroxides, including 4-hydroxynonenal (4-HNE) and malondialdehyde (MDA), can react with nucleic acids and proteins, leading to further cell destruction [63, 64]. These derivatives can also be used as important molecular markers for the detection of ferroptosis and lipid peroxidation. In addition, divalent iron can be used as a cofactor of lipoxygenase (LOX) to catalyze lipid peroxidation of PUFAs [65]. Recent studies have shown [62]

that both lysophosphatidylcholine acyltransferase 3 (LPCAT3) and ACSL4 are involved in lipid peroxidation of membrane PUFAs, and they serve as important molecular markers of ferroptosis.

In the upper panel, we can see that ferroptosis involves multiple signaling pathways and their regulators (Figure 1). Understanding these signaling molecules and their transduction pathways is of great significance in the pathophysiology of ferroptosis.

3.6. Ferroptosis with Osteoclasts and Osteoblasts. Over the last two decades, the relationship between iron and osteoporosis has attracted increasing attention. Studies have reported that disorders of iron metabolism, including iron deficiency and iron overload, can lead to osteoporosis [66–70]. The homeostasis and integrity of bone tissue are maintained by maintaining a balance between osteoclastic and osteogenic activities, and the remodeling process of bone tissue is a continuous cycle. Osteoclasts mainly play the role of bone resorption, whereas osteoblasts mainly play the role of bone reconstruction, such as the formation, mineralization, and secretion of osteocytes. They mutually restrict and balance the metabolism of bone tissues [71, 72]. Song et al. found that FA complementation group D2 (FANCD2) suppresses erastin-induced ferroptosis in bone mesenchymal stem cells (BMSCs), and FANCD2 reduces iron accumulation and lipid peroxidation in ferroptosis [73]. This is due to the multidirectional differentiation potential of BMSCs. These results suggest that ferroptosis may also occur during the targeted differentiation of BMSCs under certain circumstances.

3.7. Ferroptosis May Occur in Osteoclasts. Osteoclasts are large multinucleated cells formed by the fusion of mononuclear macrophage lineage or BMSCs by the inductive form of receptor activator of nuclear factor-kappa B ligand (RANKL) and perform the function of bone resorption. Iron ions can promote osteoclast differentiation and bone resorption by producing ROS [74]. The iron chelator DFO inhibits osteoclast formation in vitro [75]. Liu et al. found the iron-starvation response and ferritinophagy under normoxia in the process of osteoclast differentiation confirmed the involvement of ferroptosis; following RANKL stimulation, MDA and prostaglandin endoperoxide synthase 2 (PTGS2) gene expression in bone marrow-derived macrophages (BMDMs) were increased, GSH and iron levels in the culture medium supernatant decreased, and iron accumulation in mitochondria was observed [76].

3.8. Ferroptosis May Occur in Osteoblasts. Osteoblasts play an important role in bone regeneration and play a leading role in the synthesis, secretion, and mineralization of the bone matrix [77]. Previous studies have shown that the inhibitory effect of iron on the osteogenic differentiation of MSCs is proposed, and iron overload in mice is associated with increased ferritin and decreased RUNX family transcription factor 2 (RUNX2) levels in compact bone osteoprogenitor cells [69]. A high dose of dexamethasone
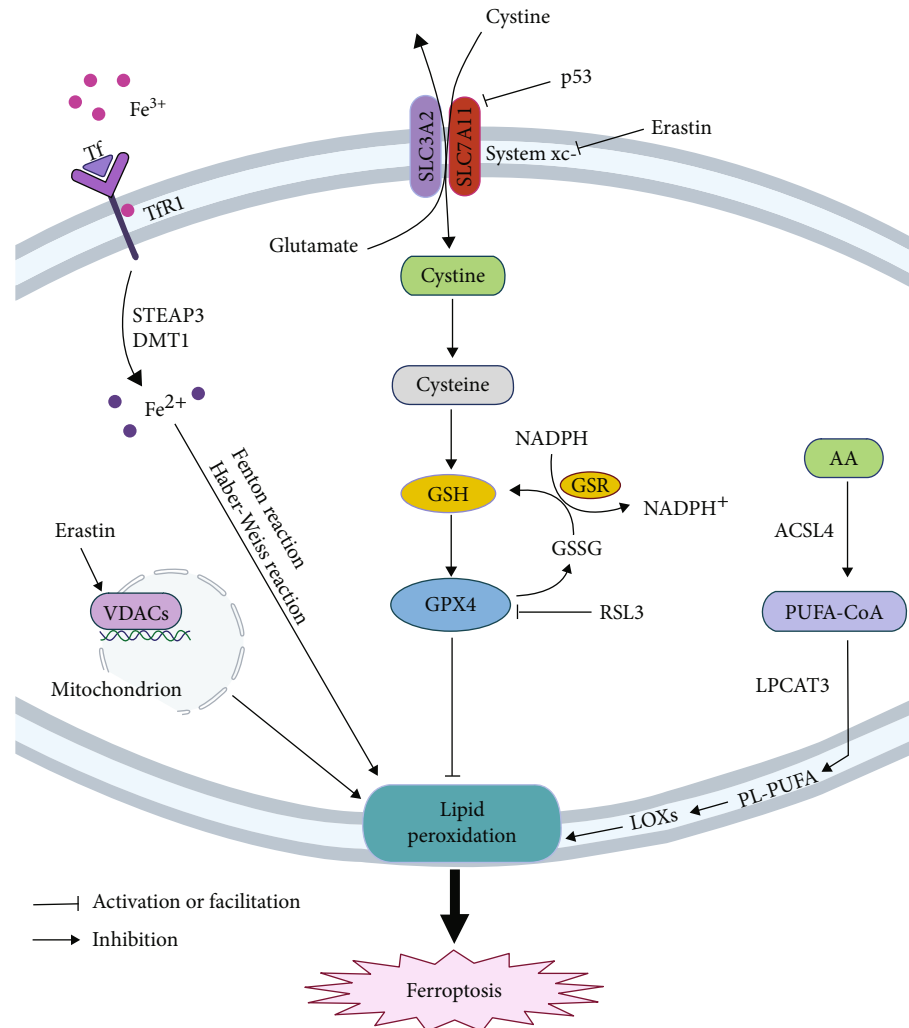
FIGURE 1: The mechanism of ferroptosis. Circulating iron enters cells by binding to TFR1 on the cell membrane, where the STEAP3 reduces ferric iron to ferrous iron. DMT1 releases the divalent iron into a labile iron pool in the cytoplasm, and iron overload can induce ferroptosis by producing ROS through the Fenton and Haber–Weiss reactions. The sodium-dependent system xc⁻ transports extracellular cystine into the cell and further converts it to cysteine. The selective inhibitor of system xc⁻ leads to a decrease in intracellular GSH, which aggravates ROS accumulation and eventually leads to ferroptosis; P53 can inhibit the uptake of cystine by system xc⁻ via downregulating the expression of the SLC7A11 subunit, resulting in a decrease in cystine-dependent glutathione peroxidase activity and cell antioxidant capacity and an increase in lipid ROS, leading to ferroptosis of cells; RSL3 can induce ferroptosis by antagonizing GPX4; Hydroxyl radicals can directly interact with PUFAs in membrane phospholipids through chain reactions to form lipid peroxides, inducing ferroptosis.

(10 μM dexamethasone) may activate osteoblasts to induce ferroptosis by downregulating GPX4 and system xc⁻ [78]. Subsequent studies found that GPX4 was significantly reduced, ROS levels were increased in MC3T3 cells induced by high glucose, and mitochondria were generally smaller and less tubular, with a darker-stained membrane with distinctly disrupted inner membrane folding. In addition, the ability of MC3T3 to differentiate into osteoblasts and the formation of mineralized nodules was decreased in a high glucose environment, and similar phenomena were observed in osteoblasts in mice [79, 80].

Based on the results of the above studies, we hypothesized that ferroptosis of osteoclasts would reduce the occurrence of bone resorption, while ferroptosis of osteoblasts would lead to reduced bone formation.

4. Potential Relationship between Ferroptosis and Osteoporosis

Osteoporosis is a metabolic bone disease, involving an imbalance between the bone resorptive functions of osteoclasts and bone forming functions of osteoblasts. This imbalance leads to loss of bone mass and strength, resulting in the increased risk of fragility fractures and a progressive decrease in healing ability following fractures [81–83]. Global rates of hip fractures, vertebral fractures, and wrist fractures caused by osteoporosis have increased, emerging as a major global public health problem [84] with approximately 8.9 million people worldwide experiencing osteoporotic fractures each year [85]. It is estimated that by 2050, hip fractures in elderly men will increase by 310%, and hip

fractures in elderly women will increase by 240% [86]. Preventing and effectively treating the occurrence and development of osteoporosis are therefore an urgent priority in global health.

4.1. Ferroptosis and DOP. Approximately 1 in 11 adults worldwide have diabetes, and 90% have type 2 diabetes [87]. Diabetes mellitus is often associated with osteoporosis [88] that this is often associated to multiple factors. It has been suggested that the factors contributing to reduced bone formation include oxidative stress caused by high blood sugar and accumulation of advanced glycation end products (AGEs) in collagen [88, 89]. Other studies suggest that low concentrations of insulin and insulin-like growth factor 1 (IGF-1) may affect osteogenic activity and lead to osteoporosis [90]. Antidiabetic drugs, such as thiazolidinedione, have been shown to negatively affect bone metabolism and fracture risk [91, 92]. However, the detailed pathological mechanism is not fully understood and is still being explored. In addition, patients with diabetes often have complications such as vision loss and neuropathy, which can increase the risk of falls and fractures. An in-depth study of the pathological mechanism of DOP would help to improve the prediction of DOP risk, as well as enable timely and reasonable prevention and treatment of brittle fractures caused by osteoporosis.

Iron metabolism is often disturbed in patients with diabetes [93–95]. Iron is also a strong oxidant that can promote the production of many reactive oxygen free radicals. Indicators of iron metabolism (transferrin, ferritin, hepcidin, transferrin receptor, etc.) can directly or indirectly affect the occurrence and development of type 2 diabetes [94]. Ferroptosis results in the production of abundant ROS through the Fenton reaction, which causes the accumulation of lipid peroxides and cell damage [96]. Wang et al. [80] detected the expression of FtMt and the occurrence of ferroptosis in the bone tissue of a (T2DOP) rat model of type 2 diabetes. They found that overexpression of FtMt reduced oxidative stress induced by excess iron under high glucose conditions to inhibit the occurrence of ferroptosis in osteoblasts, while the silencing of FtMt induced mitochondrial autophagy of T2DOP through the ROS/PINK1/Parkin signaling pathway. This suggests that FtMt may be a potential target for the treatment of T2DOP. Meanwhile, it was found that ferroptosis of osteoblasts increased following mitochondrial activation by carbonyl cyanide-M-chlorophenyl-hydrazine (CCCP, a mitochondrial agonist). Additionally, several other effects were observed: decreased expression of GPX4, osteocalcin (OCN), alkaline phosphatase (ALP), and osteoprotegerin (OPG), decreased mineralized nodules, increased ROS levels, and increased lipid peroxide. In contrast, treatment of the CCCP group with ferroptosis inhibitors was able to rescue ferroptosis. Ma et al. [79] found that high glucose induced ferroptosis in the bone tissue of a T2DOP rat model by increasing the consumption of ROS/lipid peroxidation/GSH. More importantly, melatonin (N-acetyl-5-methoxy-tryptamine) significantly reduced the level of ferroptosis by activating the Nrf2/HO-1 signaling pathway in vivo and in vitro and improved the osteogenic ability of MC3T3-E1
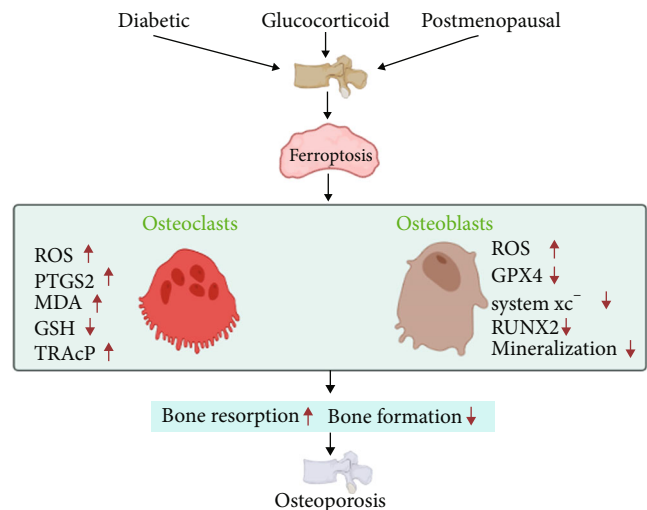
FIGURE 2: Diabetic, glucocorticoid, and postmenopausal induce ferroptosis in osteoclasts and osteoblasts. The subsequent loss of bone mass contributes to osteoporosis. RUNX2: Runt-related transcription factor 2; TRAcP: tartrate resistance acid phosphatase.

cells. Based on these studies, we speculated that the occurrence of T2DOP was correlated with iron homeostasis imbalance and ferroptosis in osteoblasts. Nonetheless, the detailed mechanisms require further investigation.

4.2. Ferroptosis and GIOP. Ferroptosis is a recently discovered form of cell death characterized by lipid peroxidation caused by the downregulation of GPX4 and system xc⁻. It is involved in GIOP. Yang et al. [97] found that high-dose and long-term use of steroid hormones can alter antioxidant capacity, reduce the activity and function of osteoblasts, and lead to osteoporosis and osteonecrosis. Endothelial cell-secreted exosomes (EC-Exos) are important mediators of cell-to-cell communication and are involved in many physiological and pathological processes. By inhibiting ferritin-phagocytosis-dependent ferroptosis, EC-Exos reversed the inhibitory effect of glucocorticoid-induced osteoblasts on osteogenesis. Lu et al. [78] established a GIOP model with a high dose of dexamethasone and found that high-dose dexamethasone ($10\,\mu$M) can induce ferroptosis of osteoblasts, possibly by downregulating GPX4 and system xc⁻. KEGG-based gene set enrichment analysis was performed to demonstrate the activation of the ferroptosis pathway. Extracellular vesicles extracted from bone marrow-derived endothelial progenitor cells inhibited activation of the ferroptosis pathway by restoring GPX4 and system xc⁻. The changes in the expression of ferroptosis markers, such as SLC3A2, SLC7A11, and GPX4, were further confirmed using RNA-seq. EPC-EVS reversed dexamethasone-induced changes in cysteine and oxidative damage markers, such as MDA, GSH, and glutathione disulfide (GSSG), and improved skeletal parameters in mice. EPC-EVS reversed dexamethasone-induced changes in cysteine and oxidative damage markers, such as MDA, GSH, and GSSG, and improved skeletal parameters in mice. They suggested that EPC-EVS prevents glucocorticoid-induced osteoporosis in

TABLE 1: Interventions and reagents targeting ferroptosis for osteoporosis.

Intervention methods or reagents	Mechanism	Effects on cells	Reference
2ME2 (2-methoxyestradiol)	Targeting HIF-1α and ferritin	Inducing the ferroptosis of osteoclasts	[76]
EPC-EVs	Restoring GPX4 and system xc$^-$ levels	Inhibiting ferroptotic pathway of osteoblasts	[78]
Melatonin	Activating the Nrf2/ho-1 signaling	Reducing ferroptosis in MC3T3-E1	[79]
Silencing FtMt	Inducing mitophagy via ROS/PINK1/Parkin pathway	Inhibiting ferroptosis of osteoblasts	[80]
CCCP (mitophagy agonist)	Activating mitochondria	Promoting ferroptosis of osteoblasts	[80]
EC-exos	Inhibiting ferritin-phagocytosis-dependent ferroptosis	Reversing the inhibitory effect of glucocorticoid on osteoblasts	[97]

mice by inhibiting the ferroptotic pathway of osteoblasts. However, further research is needed to elucidate the ferroptosis mechanisms associated with GIOP.

4.3. Ferroptosis and PMOP. PMOP is caused by estrogen deficiency in postmenopausal women. Estrogen deficiency is associated with insufficient differentiation of osteoblasts and increased activity of osteoclasts, ultimately leading to decreased bone mass and increased bone fragility [98]. A significant association between low serum iron levels and PMOP has been reported [66, 99]. Abraham et al. [100] found that dietary iron (or related factors) may have a protective effect against bone loss in the postmenopausal spine. Ni et al. [76] found a correlation between ferroptosis and RANKL-induced osteoclast differentiation and iron-starvation response, and ferritinophagy promoted the ferroptosis of osteoclasts induced by RANKL. In vivo, the HIF-1α-specific inhibitor 2-methoxyestradiol (2ME2) was found to prevent bone loss in OVX mice. The authors, therefore, proposed that the induction of ferroptosis of osteoclasts by targeting HIF-1α and ferritin could be an alternative treatment for osteoporosis.

Together, these findings show that patients with osteoporosis often experience iron metabolism disorders, oxidative stress, and lipid peroxidation, leading to ferroptosis (Figure 2). This suggests that the regulation of ferroptosis of osteoclasts or osteoblasts may provide a potential therapeutic strategy for osteoporosis (Table 1).

5. Conclusion

Owing to consistent research efforts, osteoporosis has developed from a highly disabling disease to a disease that can be managed. Existing drugs and biologics marketed to treat osteoporosis have some clinical efficacy, but are associated with side effects including cancer, osteonecrosis of the jaw, and adverse effects on liver and kidney function. Improved antiosteoporosis treatment is therefore a significant priority for medical researchers and clinicians.

In this review, we have summarized the cell morphology, cell characteristics, and pathogenesis of ferroptosis, as well as the relationship between ferroptosis and osteoporosis. Ferroptosis is an iron-dependent nonapoptotic form of RCD, which is closely related to the pathophysiological processes of various human diseases. It is accompanied by disorders of iron metabolism and energy metabolism, upregulation of inflammation and oxidative stress, and functional impairment of important organelles in cells.

Elucidating the molecular mechanisms of ferroptosis and osteoporosis can provide substantial insights into the field of bone metabolism and immunity, enabling the discovery of new therapeutics with fewer side effect for the prevention and treatment of osteoporosis. At present, these encouraging research results have generated great interest in further exploring the mechanisms underlying iron-dependent cell death and osteoporosis. The interaction and crosstalk among osteoclasts, osteoblasts, and osteocytes should be considered in the treatment of osteoporosis. Research on ferroptosis is still at a relatively early stage, and the specific mechanism, nodal molecules, and related signaling pathways of ferroptosis remain unclear. Further study is required to explore these newly discovered mechanisms, their associated signaling pathways and molecular targets, to develop effective treatment methods. The use of osteoporosis models in castrated mice, diabetic mice, and aging mice will help to determine the relationship between osteoporosis and ferroptosis and guide research for further understanding and effectively treating osteoporosis.

Conflicts of Interest

The authors declare that the research was conducted in the absence of any commercial or financial relationships that could be construed as a potential conflict of interest.

Authors' Contributions

PL, XY, JT, and ZZ generated the ideas, reviewed the publications, and wrote the manuscript. WW, ZL, and YL participated in the discussions.

Acknowledgments

References

[1] S. Dolma, S. L. Lessnick, W. C. Hahn, and B. R. Stockwell, "Identification of genotype-selective antitumor agents using synthetic lethal chemical screening in engineered human tumor cells," *Cancer Cell*, vol. 3, no. 3, pp. 285–296, 2003.

[2] W. S. Yang and B. R. Stockwell, "Synthetic lethal screening identifies compounds activating iron-dependent, nonapoptotic cell death in oncogenic-RAS-harboring cancer cells," *Chemistry & Biology*, vol. 15, no. 3, pp. 234–245, 2008.

[3] N. Werthmoller, B. Frey, R. Wunderlich, R. Fietkau, and U. S. Gaipl, "Modulation of radiochemoimmunotherapy-induced B16 melanoma cell death by the pan-caspase inhibitor zVAD-fmk induces anti-tumor immunity in a HMGB1-, nucleotide- and T-cell-dependent manner," *Cell Death & Disease*, vol. 6, no. 5, article e1761, 2015.

[4] Y. Li, X. Zeng, D. Lu, M. Yin, M. Shan, and Y. Gao, "Erastin induces ferroptosis via ferroportin-mediated iron accumulation in endometriosis," *Human Reproduction*, vol. 36, no. 4, pp. 951–964, 2021.

[5] S. J. Dixon, K. M. Lemberg, M. R. Lamprecht et al., "Ferroptosis: an iron-dependent form of nonapoptotic cell death," *Cell*, vol. 149, no. 5, pp. 1060–1072, 2012.

[6] C. Mao, X. Liu, Y. Zhang et al., "DHODH-mediated ferroptosis defence is a targetable vulnerability in cancer," *Nature*, vol. 593, no. 7860, pp. 586–590, 2021.

[7] S. Wen, T. Aki, K. Unuma, and K. Uemura, "Chemically induced models of Parkinson's disease: history and perspectives for the involvement of ferroptosis," *Frontiers in Cellular Neuroscience*, vol. 14, article 581191, 2020.

[8] Y. Le, Z. Zhang, C. Wang, and D. Lu, "Ferroptotic cell death: new regulatory mechanisms for metabolic diseases," *Endocrine, Metabolic & Immune Disorders Drug Targets*, vol. 21, no. 5, pp. 785–800, 2021.

[9] L. Galluzzi, I. Vitale, S. A. Aaronson et al., "Molecular mechanisms of cell death: recommendations of the nomenclature committee on cell death 2018," *Cell Death and Differentiation*, vol. 25, no. 3, pp. 486–541, 2018.

[10] R. Mirzayans and D. Murray, "Do TUNEL and other apoptosis assays detect cell death in preclinical studies?," *International Journal of Molecular Sciences*, vol. 21, no. 23, p. 9090, 2020.

[11] J. Wu, J. Ye, W. Kong, S. Zhang, and Y. Zheng, "Programmed cell death pathways in hearing loss: a review of apoptosis, autophagy and programmed necrosis," *Cell Proliferation*, vol. 53, no. 11, article e12915, 2020.

[12] L. Galluzzi, E. H. Baehrecke, A. Ballabio et al., "Molecular definitions of autophagy and related processes," *The EMBO Journal*, vol. 36, no. 13, pp. 1811–1836, 2017.

[13] P. Liu, Z. Zhang, and Y. Li, "Relevance of the pyroptosis-related inflammasome pathway in the pathogenesis of diabetic kidney disease," *Frontiers in Immunology*, vol. 12, article 603416, 2021.

[14] H. Yu, P. Guo, X. Xie, Y. Wang, and G. Chen, "Ferroptosis, a new form of cell death, and its relationships with tumourous diseases," *Journal of Cellular and Molecular Medicine*, vol. 21, no. 4, pp. 648–657, 2017.

[15] Y. Xie, X. Song, X. Sun et al., "Identification of baicalein as a ferroptosis inhibitor by natural product library screening," *Biochemical and Biophysical Research Communications*, vol. 473, no. 4, pp. 775–780, 2016.

[16] C. Han, Y. Liu, R. Dai, N. Ismail, W. Su, and B. Li, "Ferroptosis and its potential role in human diseases," *Frontiers in Pharmacology*, vol. 11, p. 239, 2020.

[17] T. Nakamura, I. Naguro, and H. Ichijo, "Iron homeostasis and iron-regulated ROS in cell death, senescence and human diseases," *Biochimica et Biophysica Acta - General Subjects*, vol. 1863, no. 9, pp. 1398–1409, 2019.

[18] R. P. L. van Swelm, J. F. M. Wetzels, and D. W. Swinkels, "The multifaceted role of iron in renal health and disease," *Nature Reviews Nephrology*, vol. 16, no. 2, pp. 77–98, 2020.

[19] S. Torii, R. Shintoku, C. Kubota et al., "An essential role for functional lysosomes in ferroptosis of cancer cells," *The Biochemical Journal*, vol. 473, no. 6, pp. 769–777, 2016.

[20] B. R. Stockwell, J. P. Friedmann Angeli, H. Bayir et al., "Ferroptosis: a regulated cell death nexus linking metabolism, redox biology, and disease," *Cell*, vol. 171, no. 2, pp. 273–285, 2017.

[21] H. Drakesmith, E. Nemeth, and T. Ganz, "Ironing out ferroportin," *Cell Metabolism*, vol. 22, no. 5, pp. 777–787, 2015.

[22] R. P. Zhou, Y. Chen, X. Wei et al., "Novel insights into ferroptosis: implications for age-related diseases," *Theranostics*, vol. 10, no. 26, pp. 11976–11997, 2020.

[23] N. Abbaspour, R. Hurrell, and R. Kelishadi, "Review on iron and its importance for human health," *Journal of Research in Medical Sciences: The Official Journal of Isfahan University of Medical Sciences*, vol. 19, no. 2, pp. 164–174, 2014.

[24] H. Yu, C. Yang, L. Jian et al., "Sulfasalazine-induced ferroptosis in breast cancer cells is reduced by the inhibitory effect of estrogen receptor on the transferrin receptor," *Oncology Reports*, vol. 42, no. 2, pp. 826–838, 2019.

[25] N. Kajarabille and G. O. Latunde-Dada, "Programmed cell-death by ferroptosis: antioxidants as mitigators," *International Journal of Molecular Sciences*, vol. 20, no. 19, p. 4968, 2019.

[26] H. Wang, P. An, E. Xie et al., "Characterization of ferroptosis in murine models of hemochromatosis," *Hepatology*, vol. 66, no. 2, pp. 449–465, 2017.

[27] H. F. Deng, L. X. Yue, N. N. Wang et al., "Mitochondrial iron overload-mediated inhibition of Nrf2-HO-1/GPX4 assisted ALI-induced nephrotoxicity," *Frontiers in Pharmacology*, vol. 11, article 624529, 2020.

[28] X. Fang, Z. Cai, H. Wang et al., "Loss of cardiac ferritin H facilitates cardiomyopathy via Slc7a11-mediated ferroptosis," *Circulation Research*, vol. 127, no. 4, pp. 486–501, 2020.

[29] M. Gao, J. Yi, J. Zhu et al., "Role of mitochondria in ferroptosis," *Molecular Cell*, vol. 73, no. 2, pp. 354–363.e3, 2019.

[30] X. Chen, C. Yu, R. Kang, and D. Tang, "Iron metabolism in ferroptosis," *Frontiers in Cell and Development Biology*, vol. 8, article 590226, 2020.

[31] D. M. Ward and S. M. Cloonan, "Mitochondrial iron in human health and disease," *Annual Review of Physiology*, vol. 81, no. 1, pp. 453–482, 2019.

[32] A. L. C. Ong and T. S. Ramasamy, "Role of Sirtuin1-p53 regulatory axis in aging, cancer and cellular reprogramming," *Ageing Research Reviews*, vol. 43, pp. 64–80, 2018.

[33] J. A. McCubrey and Z. N. Demidenko, "Recent discoveries in the cycling, growing and aging of the p53 field," *Aging*, vol. 4, no. 12, pp. 887–893, 2012.

[34] E. Leveille and N. A. Johnson, "Genetic events inhibiting apoptosis in diffuse large B cell lymphoma," *Cancers*, vol. 13, no. 9, p. 2167, 2021.

[35] L. Jiang, N. Kon, T. Li et al., "Ferroptosis as a p53-mediated activity during tumour suppression," *Nature*, vol. 520, no. 7545, pp. 57–62, 2015.

[36] B. Chu, N. Kon, D. Chen et al., "ALOX12 is required for p53-mediated tumour suppression through a distinct ferroptosis pathway," *Nature Cell Biology*, vol. 21, no. 5, pp. 579–591, 2019.

[37] L. Jiang, J. H. Hickman, S. J. Wang, and W. Gu, "Dynamic roles of p53-mediated metabolic activities in ROS-induced stress responses," *Cell Cycle*, vol. 14, no. 18, pp. 2881–2885, 2015.

[38] G. Lei, Y. Zhang, T. Hong et al., "Ferroptosis as a mechanism to mediate p53 function in tumor radiosensitivity," *Oncogene*, vol. 40, no. 20, pp. 3533–3547, 2021.

[39] M. Chen-Goodspeed, A. N. Lukan, and C. W. Dessauer, "Modeling of $G\alpha_s$ and $G\alpha_i$ regulation of human type V and VI adenylyl cyclase∗," *The Journal of Biological Chemistry*, vol. 280, no. 3, pp. 1808–1816, 2005.

[40] D. J. Klionsky, A. K. Abdel-Aziz, S. Abdelfatah et al., "Guidelines for the use and interpretation of assays for monitoring autophagy (4th edition)," *Autophagy*, vol. 17, pp. 1–382, 2021.

[41] B. T. Paul, D. H. Manz, F. M. Torti, and S. V. Torti, "Mitochondria and iron: current questions," *Expert Review of Hematology*, vol. 10, no. 1, pp. 65–79, 2017.

[42] Y. Takashi, K. Tomita, Y. Kuwahara et al., "Mitochondrial dysfunction promotes aquaporin expression that controls hydrogen peroxide permeability and ferroptosis," *Free Radical Biology & Medicine*, vol. 161, pp. 60–70, 2020.

[43] Y. Yang, M. Luo, K. Zhang et al., "Nedd4 ubiquitylates VDAC2/3 to suppress erastin-induced ferroptosis in melanoma," *Nature Communications*, vol. 11, no. 1, p. 433, 2020.

[44] W. S. Yang, R. SriRamaratnam, M. E. Welsch et al., "Regulation of ferroptotic cancer cell death by GPX4," *Cell*, vol. 156, no. 1-2, pp. 317–331, 2014.

[45] R. P. Brandes, N. Weissmann, and K. Schroder, "Nox family NADPH oxidases: molecular mechanisms of activation," *Free Radical Biology & Medicine*, vol. 76, pp. 208–226, 2014.

[46] J. P. Friedmann Angeli, M. Schneider, B. Proneth et al., "Inactivation of the ferroptosis regulator Gpx4 triggers acute renal failure in mice," *Nature Cell Biology*, vol. 16, no. 12, pp. 1180–1191, 2014.

[47] X. Sui, R. Zhang, S. Liu et al., "RSL3 drives ferroptosis through GPX4 inactivation and ROS production in colorectal cancer," *Frontiers in Pharmacology*, vol. 9, p. 1371, 2018.

[48] J. Ye, X. Jiang, Z. Dong, S. Hu, and M. Xiao, "Low-concentration PTX and RSL3 inhibits tumor cell growth synergistically by inducing ferroptosis in mutant p53 hypopharyngeal squamous carcinoma," *Cancer Management and Research*, vol. -Volume 11, pp. 9783–9792, 2019.

[49] A. M. Vuckovic, V. Bosello Travain, L. Bordin et al., "Inactivation of the glutathione peroxidase GPx4 by the ferroptosis-inducing molecule RSL3 requires the adaptor protein 14-3-3ε," *FEBS Letters*, vol. 594, no. 4, pp. 611–624, 2020.

[50] H. J. Forman, H. Zhang, and A. Rinna, "Glutathione: overview of its protective roles, measurement, and biosynthesis," *Molecular Aspects of Medicine*, vol. 30, no. 1-2, pp. 1–12, 2009.

[51] J. Lewerenz, S. J. Hewett, Y. Huang et al., "The cystine/glutamate antiporter system x(c)(-) in health and disease: from molecular mechanisms to novel therapeutic opportunities," *Antioxidants & Redox Signaling*, vol. 18, no. 5, pp. 522–555, 2013.

[52] P. Koppula, L. Zhuang, and B. Gan, "Cystine transporter SLC7A11/xCT in cancer: ferroptosis, nutrient dependency, and cancer therapy," *Protein & Cell*, vol. 12, no. 8, pp. 599–620, 2021.

[53] J. K. M. Lim, A. Delaidelli, S. W. Minaker et al., "Cystine/glutamate antiporter xCT (SLC7A11) facilitates oncogenic RAS transformation by preserving intracellular redox balance," *Proceedings of the National Academy of Sciences of the United States of America*, vol. 116, no. 19, pp. 9433–9442, 2019.

[54] C. D. Poltorack and S. J. Dixon, "Understanding the role of cysteine in ferroptosis: progress & paradoxes," *The FEBS Journal*, vol. 10, 2021.

[55] H. Tu, L. J. Tang, X. J. Luo, K. L. Ai, and J. Peng, "Insights into the novel function of system xc- in regulated cell death," *European Review for Medical and Pharmacological Sciences*, vol. 25, no. 3, pp. 1650–1662, 2021.

[56] B. Proneth and M. Conrad, "Ferroptosis and necroinflammation, a yet poorly explored link," *Cell Death and Differentiation*, vol. 26, no. 1, pp. 14–24, 2019.

[57] S. Y. Zhou, G. Z. Cui, X. L. Yan et al., "Mechanism of ferroptosis and its relationships with other types of programmed cell death: insights for potential interventions after intracerebral hemorrhage," *Frontiers in Neuroscience*, vol. 14, article 589042, 2020.

[58] M. M. Gaschler and B. R. Stockwell, "Lipid peroxidation in cell death," *Biochemical and Biophysical Research Communications*, vol. 482, no. 3, pp. 419–425, 2017.

[59] J. Z. Haeggstrom and C. D. Funk, "Lipoxygenase and leukotriene pathways: biochemistry, biology, and roles in disease," *Chemical Reviews*, vol. 111, no. 10, pp. 5866–5898, 2011.

[60] R. Shah, M. S. Shchepinov, and D. A. Pratt, "Resolving the role of lipoxygenases in the initiation and execution of ferroptosis," *ACS Central Science*, vol. 4, no. 3, pp. 387–396, 2018.

[61] H. F. Yan, T. Zou, Q. Z. Tuo et al., "Ferroptosis: mechanisms and links with diseases," *Signal Transduction and Targeted Therapy*, vol. 6, no. 1, p. 49, 2021.

[62] S. Doll, B. Proneth, Y. Y. Tyurina et al., "ACSL4 dictates ferroptosis sensitivity by shaping cellular lipid composition," *Nature Chemical Biology*, vol. 13, no. 1, pp. 91–98, 2017.

[63] H. Feng and B. R. Stockwell, "Unsolved mysteries: how does lipid peroxidation cause ferroptosis?," *PLoS Biology*, vol. 16, no. 5, article e2006203, 2018.

[64] A. Ayala, M. F. Munoz, and S. Arguelles, "Lipid peroxidation: production, metabolism, and signaling mechanisms of malondialdehyde and 4-hydroxy-2-nonenal," *Oxidative Medicine and Cellular Longevity*, vol. 2014, Article ID 360438, 2014.

[65] W. S. Yang, K. J. Kim, M. M. Gaschler, M. Patel, M. S. Shchepinov, and B. R. Stockwell, "Peroxidation of polyunsaturated fatty acids by lipoxygenases drives ferroptosis," *Proceedings of the National Academy of Sciences of the United States of America*, vol. 113, no. 34, pp. E4966–E4975, 2016.

[66] P. D'Amelio, M. A. Cristofaro, C. Tamone et al., "Role of iron metabolism and oxidative damage in postmenopausal bone loss," *Bone*, vol. 43, no. 6, pp. 1010–1015, 2008.

[67] H. Okabe, T. Suzuki, E. Uehara, M. Ueda, T. Nagai, and K. Ozawa, "The bone marrow hematopoietic

microenvironment is impaired in iron-overloaded mice," *European Journal of Haematology*, vol. 93, no. 2, pp. 118–128, 2014.

[68] J. Che, J. Yang, B. Zhao et al., "The effect of abnormal iron metabolism on osteoporosis," *Biological Trace Element Research*, vol. 195, no. 2, pp. 353–365, 2020.

[69] E. Balogh, E. Tolnai, B. Nagy Jr. et al., "Iron overload inhibits osteogenic commitment and differentiation of mesenchymal stem cells via the induction of ferritin," *Biochimica et Biophysica Acta*, vol. 2016, pp. 1640–1649, 1862.

[70] Q. Cheng, X. Zhang, J. Jiang et al., "Postmenopausal iron overload exacerbated bone loss by promoting the degradation of type I collagen," *BioMed Research International*, vol. 2017, Article ID 1345193, 2017.

[71] H. Zhao, Y. Ito, J. Chappel, N. W. Andrews, S. L. Teitelbaum, and F. P. Ross, "Synaptotagmin VII regulates bone remodeling by modulating osteoclast and osteoblast secretion," *Developmental Cell*, vol. 14, no. 6, pp. 914–925, 2008.

[72] B. Kolodziejska, N. Stepien, and J. Kolmas, "The influence of strontium on bone tissue metabolism and its application in osteoporosis treatment," *International Journal of Molecular Sciences*, vol. 22, no. 12, p. 6564, 2021.

[73] X. Song, Y. Xie, R. Kang et al., "FANCD2 protects against bone marrow injury from ferroptosis," *Biochemical and Biophysical Research Communications*, vol. 480, no. 3, pp. 443–449, 2016.

[74] P. Jia, Y. J. Xu, Z. L. Zhang et al., "Ferric ion could facilitate osteoclast differentiation and bone resorption through the production of reactive oxygen species," *Journal of Orthopaedic Research*, vol. 30, no. 11, pp. 1843–1852, 2012.

[75] K. A. Ishii, T. Fumoto, K. Iwai et al., "Coordination of PGC-1β and iron uptake in mitochondrial biogenesis and osteoclast activation," *Nature Medicine*, vol. 15, no. 3, pp. 259–266, 2009.

[76] S. Ni, Y. Yuan, Z. Qian et al., "Hypoxia inhibits RANKL-induced ferritinophagy and protects osteoclasts from ferroptosis," *Free Radical Biology & Medicine*, vol. 169, pp. 271–282, 2021.

[77] R. Florencio-Silva, G. R. Sasso, E. Sasso-Cerri, M. J. Simoes, and P. S. Cerri, "Biology of bone tissue: structure, function, and factors that influence bone cells," *BioMed Research International*, vol. 2015, Article ID 421746, 2015.

[78] J. Lu, J. Yang, Y. Zheng, X. Chen, and S. Fang, "Extracellular vesicles from endothelial progenitor cells prevent steroid-induced osteoporosis by suppressing the ferroptotic pathway in mouse osteoblasts based on bioinformatics evidence," *Scientific Reports*, vol. 9, no. 1, p. 16130, 2019.

[79] H. Ma, X. Wang, W. Zhang et al., "Melatonin suppresses ferroptosis induced by high glucose via activation of the Nrf2/HO-1 signaling pathway in type 2 diabetic osteoporosis," *Oxidative Medicine and Cellular Longevity*, vol. 2020, Article ID 9067610, 2020.

[80] X. Wang, H. Ma, J. Sun et al., "Mitochondrial ferritin deficiency promotes osteoblastic ferroptosis via mitophagy in type 2 diabetic osteoporosis," *Biological Trace Element Research*, vol. 200, no. 1, pp. 298–307, 2022.

[81] J. E. Compston, M. R. McClung, and W. D. Leslie, "Osteoporosis," *Lancet*, vol. 393, no. 10169, pp. 364–376, 2019.

[82] Y. Yamamoto, T. Chiba, S. Dohmae, K. Higashi, and A. Nakazawa, "Osteoporosis medication after fracture in older adults: an administrative data analysis," *Osteoporosis International*, vol. 32, no. 6, pp. 1245-1246, 2021.

[83] M. de Wit, C. Cooper, P. Tugwell et al., "Practical guidance for engaging patients in health research, treatment guidelines and regulatory processes: results of an expert group meeting organized by the World Health Organization (WHO) and the European Society for Clinical and Economic Aspects of Osteoporosis, Osteoarthritis and Musculoskeletal Diseases (ESCEO)," *Aging Clinical and Experimental Research*, vol. 31, no. 7, pp. 905–915, 2019.

[84] T. Sozen, L. Ozisik, and N. Calik Basaran, "An overview and management of osteoporosis," *European Journal of Rheumatology*, vol. 4, no. 1, pp. 46–56, 2017.

[85] E. Hernlund, A. Svedbom, M. Ivergard et al., "Osteoporosis in the European Union: medical management, epidemiology and economic burden. A report prepared in collaboration with the International Osteoporosis Foundation (IOF) and the European Federation of Pharmaceutical Industry Associations (EFPIA)," *Archives of Osteoporosis*, vol. 8, no. 1-2, p. 136, 2013.

[86] M. A. Bass, A. Sharma, V. K. Nahar et al., "Bone mineral density among men and women aged 35 to 50 years," *The Journal of the American Osteopathic Association*, vol. 119, no. 6, pp. 357–363, 2019.

[87] Y. Zheng, S. H. Ley, and F. B. Hu, "Global aetiology and epidemiology of type 2 diabetes mellitus and its complications," *Nature Reviews Endocrinology*, vol. 14, no. 2, pp. 88–98, 2018.

[88] P. Anagnostis, S. A. Paschou, N. N. Gkekas et al., "Efficacy of anti-osteoporotic medications in patients with type 1 and 2 diabetes mellitus: a systematic review," *Endocrine*, vol. 60, no. 3, pp. 373–383, 2018.

[89] J. N. Farr, M. T. Drake, S. Amin, L. J. Melton 3rd, L. K. McCready, and S. Khosla, "In vivo assessment of bone quality in postmenopausal women with type 2 diabetes," *Journal of Bone and Mineral Research*, vol. 29, no. 4, pp. 787–795, 2014.

[90] S. Epstein and D. LeRoith, "Diabetes and fragility fractures – a burgeoning epidemic?," *Bone*, vol. 43, no. 1, pp. 3–6, 2008.

[91] N. Napoli, On behalf of the IOF Bone, Diabetes Working Group et al., "Mechanisms of diabetes mellitus-induced bone fragility," *Nature Reviews Endocrinology*, vol. 13, no. 4, pp. 208–219, 2017.

[92] C. Eller-Vainicher, E. Cairoli, G. Grassi et al., "Pathophysiology and management of type 2 diabetes mellitus bone fragility," *Journal Diabetes Research*, vol. 2020, article 7608964, 2020.

[93] S. N. Rajpathak, J. P. Crandall, J. Wylie-Rosett, G. C. Kabat, T. E. Rohan, and F. B. Hu, "The role of iron in type 2 diabetes in humans," *Biochimica et Biophysica Acta*, vol. 1790, no. 7, pp. 671–681, 2009.

[94] J. Liu, Q. Li, Y. Yang, and L. Ma, "Iron metabolism and type 2 diabetes mellitus: a meta-analysis and systematic review," *Journal of Diabetes Investigation*, vol. 11, no. 4, pp. 946–955, 2020.

[95] J. A. Simcox and D. A. McClain, "Iron and diabetes risk," *Cell Metabolism*, vol. 17, no. 3, pp. 329–341, 2013.

[96] G. C. Forcina and S. J. Dixon, "GPX4 at the crossroads of lipid homeostasis and ferroptosis," *Proteomics*, vol. 19, no. 18, article e1800311, 2019.

[97] R. Z. Yang, W. N. Xu, H. L. Zheng et al., "Exosomes derived from vascular endothelial cells antagonize glucocorticoid-induced osteoporosis by inhibiting ferritinophagy with resultant limited ferroptosis of osteoblasts," *Journal of Cellular Physiology*, vol. 236, no. 9, pp. 6691–6705, 2021.

[98] R. Eastell, "Treatment of postmenopausal osteoporosis," *The New England Journal of Medicine*, vol. 338, no. 11, pp. 736–746, 1998.

[99] E. Okyay, C. Ertugrul, B. Acar, A. R. Sisman, B. Onvural, and D. Ozaksoy, "Comparative evaluation of serum levels of main minerals and postmenopausal osteoporosis," *Maturitas*, vol. 76, no. 4, pp. 320–325, 2013.

[100] R. Abraham, J. Walton, L. Russell et al., "Dietary determinants of post-menopausal bone loss at the lumbar spine: a possible beneficial effect of iron," *Osteoporosis International*, vol. 17, no. 8, pp. 1165–1173, 2006.

Research Article

Oxidative Stress in Plasma from Patients with Marfan Syndrome Is Modulated by Deodorized Garlic Preliminary Findings

Israel Pérez-Torres [ID],[1] **María Elena Soto** [ID],[2] **Linaloe Manzano-Pech** [ID],[1]
Eulises Díaz-Diaz [ID],[3] **Elizabeth Soria-Castro** [ID],[1] **María Esther Rubio-Ruíz** [ID],[4]
and Verónica Guarner-Lans [ID][4]

[1]*Department of Cardiovascular Biomedicine, Instituto Nacional de Cardiología "Ignacio Chávez", Juan Badiano 1, Sección XVI,*
Tlalpan, México City 14080, Mexico
[2]*Department of Immunology, Instituto Nacional de Cardiología "Ignacio Chávez", Juan Badiano 1, Sección XVI, Tlalpan,*
México City 14080, Mexico
[3]*Department of Reproductive Biology, Instituto Nacional de Ciencias Médicas y Nutrición Salvador Zubirán, Vasco de Quiroga 15,*
Sección XVI, Tlalpan, México City 14000, Mexico
[4]*Department of Physiology, Instituto Nacional de Cardiología "Ignacio Chávez", Juan Badiano 1, Sección XVI, Tlalpan,*
México City 14080, Mexico

Correspondence should be addressed to Verónica Guarner-Lans; gualanv@yahoo.com

Marfan syndrome (MFS) is a genetic disorder of connective tissue that affects the fibrillin-1 protein (FBN-1). It is associated with the formation of aneurysms, damage to the endothelium and oxidative stress (OS). Allium sativum (garlic) has antioxidant properties; therefore, the goal of this study was to show the antioxidant effect of deodorized garlic (DG) on antioxidant enzymes and OS markers in the plasma of patients with MFS. The activity of antioxidant enzymes such as extracellular superoxide dismutase (EcSOD), peroxidases, glutathione peroxidase (GPx), gluthatione-S-tranferase (GST), and thioredoxin reductase (TrxR) was quantified, and nonenzymatic antioxidant system markers including lipid peroxidation (LPO), carbonylation, nitrates/nitrites, GSH, and vitamin C in plasma were determined in patients with MFS before and after treatment with DG. The results show that DG increased the activity of the EcSOD, peroxidases, GPx, GST, TrxR ($p \leq 0.05$) and decrease LPO, carbonylation, and nitrates/nitrites ($p \leq 0.01$). However, glutathione was increased ($p = 0.01$) in plasma from patients with MFS. This suggests that treatment with garlic could lower the OS threshold by increasing the activity of antioxidant enzymes and could help in the prevention and mitigation of adverse OS in patients with MFS.

1. Introduction

Marfan syndrome (MFS) is a disorder of genetic origin with an autosomal dominant character that affects the gene that encodes for the fibrillin-1 protein (FBN-1), therefore altering connective tissue. It is associated with deformity and dysfunction of elastic fibers, which results in structural and functional damage to the structure of the aorta causing micro dissection of the middle layer and degeneration [1]. Damage to the aortic tissue in MFS is accompanied by oxidative stress (OS), vascular dysfunction, and loss of the contractile function and the endothelium-dependent relaxation [1].

OS is caused by an imbalance between the production of reactive oxygen species (ROS) and the ability to rapidly detoxify their intermediate reagents or repair the damage caused by them through the employment of biological antioxidant systems [2]. Biological macromolecules such as lipids, carbohydrates, proteins, and nucleic acids are altered by instability in their structures caused by their reaction with

ROS [3]. Excess ROS and reactive nitrogen species are implicated in cardiovascular disease (CVD). ROS are produced by several pathways including mitochondria, xanthine oxidase, NADPH oxidase, and inducible nitric oxide synthase (iNOS) [4]. There is an inverse association between the risk of degenerative diseases where there is an increase in OS and the consumption of medicinal plants. Therefore, it is important to seek for strategies to improve the antioxidant capacity in these diseases including MFS. One of these strategies implies the use of garlic which has antioxidant properties. The intake of therapeutic medicinal plants that containing antioxidants can reduce oxidation at the endogenous level, thus diminishing the negative consequences derived from OS [3]. Recent work indicates that cursive sativum (garlic) has antioxidant properties and reduces the OS present in CVD [5]. Deodorized garlic (DG) extracts contain phytochemicals and lipid-soluble organ sulfur compounds, such as dial-lyl-thiosulfonate (allicin) and selenium that protect against OS [6]. DG in tablets has fewer harmful side effects than raw garlic [6]. Furthermore, DG has beneficial effects for treatment of ROS-mediated CVD [7].

DG stabilizes compounds with antioxidant properties such as allicin, S-allyl-cysteine (SAC), and S-allylmercaptocysteine (SAMC) [5]. These stable compounds exert antioxidant actions by eliminating ROS, increasing the activity of cellular antioxidant enzymes such as superoxide dismutase superoxide dismutase (SOD) isoforms, catalase and GPx, and GSH levels. In a review where garlic supplementation was analyzed and that included four meta-analyses, garlic reduced systolic and diastolic blood pressure. In another study using garlic supplementation, there was a reduction of total cholesterol [8]. Furthermore, DG had more consistent benefits than raw garlic, and rare adverse reactions were documented with established limited causality [9].

The participation of OS in the progression of aortic damage in MFS has been described [10]. LPO causes vasomotor dysfunction in the thoracic aorta associated with OS, which is related to a decrease in eNOS and an increase in the iNOS pathways, and a decrease in the activity of the superoxide dismutase (SOD) isoforms [11].

Due to the aforementioned information and to the lack of reports on the antioxidant properties of DG on OS in patients with MS, the goal of this study was to show the antioxidant effect of DG in the plasma of MFS patients.

2. Materials and Methods

2.1. Population in Study. This was a controlled, open, analytical, prospective, and longitudinal (before-after) study that included 13 patients of either sex, 6 men, and 7 women, that were admitted to the Ignacio Chávez National Cardiology Institute consecutively with aortic root dilation (>50 mm). The dilation was demonstrated by magnetic resonance angiography.

The cases included MFS patients, classified by the Ghent criteria in 1996 [12]. Once the patients completed the inclusion criteria, a cardiological investigation of the clinical condition of each patient was analyzed, including various clinical indications of their cardiac pathology.

Studies including clotting times, radiographs, electrocardiography, anesthetic evaluation, and current medical treatment were obtained, and care was taken that the cases were not under treatment with antioxidants, allopurinol, or inhibitors of the probable pathways involved in the production of ROS. Exclusion criteria taken into account were a doubtful diagnosis and/or the lack of agreement to sign the informed consent form for the research study.

Each patient was explained and asked for their approval to include their plasma in this project, doubts were clarified, and an informed consent was obtained to take a blood sample (baseline) and another subsequent blood sample two months after starting the DG treatment when the intervention was concluded.

2.2. Healthy Subjects. The control group consisted of 13 healthy men and/or women, who were previously evaluated by an expert cardiologist and rheumatologist to verify that they did not have MFS. Routine laboratory tests were

TABLE 1: Demographic characteristic Marfan syndrome patients.

	Total	Men ($n = 6$)	Women ($n = 7$)	p
Median (min-max)				
Age	26 (14-51)	26 (14-51)	30 (16-42)	
BMI	24 (12-30)	23 (12-25)	24 (18-30)	
(mg/dL)				
Glucose	90 ± 7	92 ± 9	88 ± 5	NS
CrS	0.67 ± 0.17	0.78 ± 0.20	0.58 ± 0.09	NS
CT	166 ± 40	154 ± 24	176 ± 50	NS
HDL	50 ± 13	47 ± 12	53 ± 15	NS
LDL	96 ± 28	93 ± 30	99 ± 29	NS
TG	119 ± 59	122 ± 85	117 ± 32	NS
Score				
Ghent criteria	8 (62)	4 (66.6)	4 (57)	NS
Ectopia lentis	4 (31)	1 (17)	3 (43)	NS
Aortic dilatation	9 (69)	5 (83)	4 (57)	NS
Systemic score	13 (100)	6 (100)	7 (100)	NS
HFA	9 (69)	5 (83)	4 (57)	NS

Abbreviations: BMI: body mass index; CT: cholesterol; CrS: creatinine serum; HDL: high-density lipoprotein; LDL: low-density lipoprotein: HFA: hereditary family antecedent; TG: triglycerides.

TABLE 2: Blood chemistry in healthy subjects.

Glucose (mg/dL)	85.84 ± 5.49
SCr (mg/dL)	0.77 ± 0.02
CT (mg/dL)	174.38 ± 5.56
HDL (mg/dL)	41.23 ± 1.81
LDL (mg/dL)	97.23 ± 4.46
TG (mg/dL)	109.23 ± 15.62

Abbreviations: SCr: serum creatinine; CT: cholesterol; HDL: high-density lipoprotein; LDL: low-density lipoprotein; TG: triglycerides.

Table 3: Redox biomarkers of the nonenzymatic system in the plasma.

Parameters (ml of plasma)	HS	MFS basal	MFS + DG
LPO (nmol MDA)	5.25 ± 0.56	$11.06 \pm 0.69^{**}$	$8.33 \pm 0.45^{*}$
Carbonylation (nmol carbonyls)	$0.08 \pm 3.57 \times 10^{-3}$	$0.11 \pm 3.30 \times 10^{-3**}$	$0.09 \pm 3.08 \times 10^{-3**}$
NO_3^-/NO_2^- (nM)	1.45 ± 0.12	$2.46 \pm 0.19^{**}$	1.63 ± 0.19†
GSH (nM)	$0.06 \pm 2.42 \times 10^{-3}$	$0.05 \pm 1.76 \times 10^{-3**}$	$0.06 \pm 4.17 \times 10^{-3*}$
Vitamin C (μM)	0.20 ± 0.01	$0.18 \pm 6.70 \times 10^{-3}$	$0.19 \pm 7.08 \times 10^{-3}$

**HS vs. MFS basal, $p \leq 0.001$, †MFS vs. MFS + garlic, $p \leq 0.001$, and *HS and MFS + garlic vs. MFS, $p = 0.01$. Abbreviations: DG: deodorized garlic; HS: healthy subjects; MFS: Marfan syndrome; LPO: lipid peroxidation; NO_3^-/NO_2^-: nitrate and nitrite ratio; GSH: gluthatione.
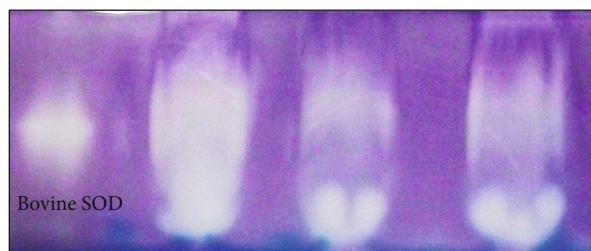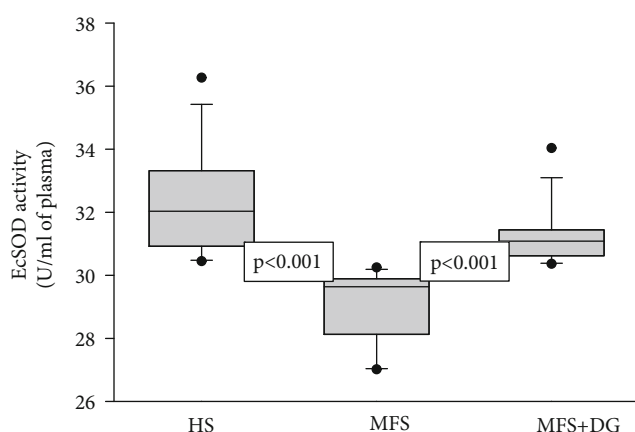
Figure 1: Deodorized garlic increases EcSOD activity in Marfan syndrome patients. HS: healthy subjects; MFS: Marfan syndrome; MFS + DG: Marfan syndrome plus deodorized garlic. (a) is a native gel representative of the EcSOD activity. Riboflavin and TEMED, in the presence of UV light and oxygen, produce superoxide radicals; NBT and SOD compete for them, where SOD is present; the gel remains transparent, whereas reduced NBT turns it purple-blue. The whole scanning shown represents the activity of the enzyme.

performed to determine triglycerides and cholesterol-HDL, cholesterol-LDL, glucose serum creatinine, and total cholesterol. In addition, echocardiography, computed tomography, or magnetic resonance imaging were performed to rule out aortic damage. Healthy subjects (HS) were not taking anti-inflammatory drugs, antioxidants, DG, or statins. Medications that could interfere with the outcome of the study, such as non steroidal antiinflammatory drugs NSAIDs, lipid-lowering drugs, and antioxidant supplements were discontinued.
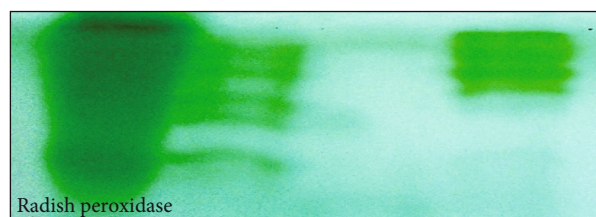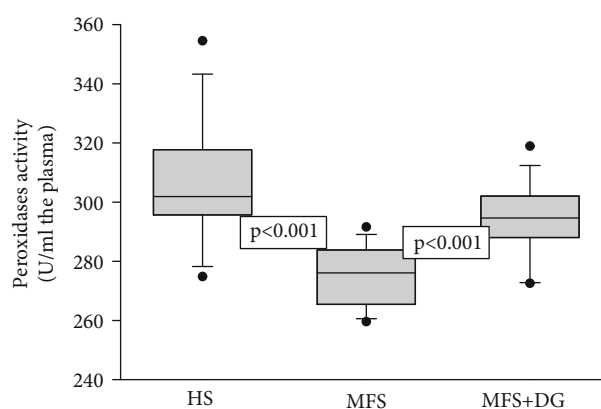
Figure 2: Effect of deodorozid garlic administration on peroxidase activity in healthy subjects and Marfan syndrome patients. A representative native gel is shown below the histogram, where peroxidases are present; the gel remains transparent. and the 3,3,5,5-tetramethylbenzidine is oxidized, showing a green coloration. Abbreviations: HS: healthy subjects; MFS: Marfan syndrome; MFS + DG: Marfan syndrome plus deodorized garlic.

2.3. Ethical Considerations. The research protocol was approved by the Research and Ethics Committee of our institution (institutional protocol number: PT-18-101). The study was carried out according to the international ethical standards and the General Health Law, as well as according to the Helsinki declaration, modified at the Congress of Tokyo, Japan, and with informed consent of patients and controls [13].

2.4. Treatment. Cursive sativum Chinese garlic tablets (Ajo-lín Forte® plus, Deodorized Garlic) of 500 mg were ingested orally with water, every 12 hours for 2 months in MFS patients. The nutrition facts of the tablets showed a total fat of 750 mg, 600 μg of sodium, 20 g carbohydrates, and 0 g protein.

(a)

(b)

(c)
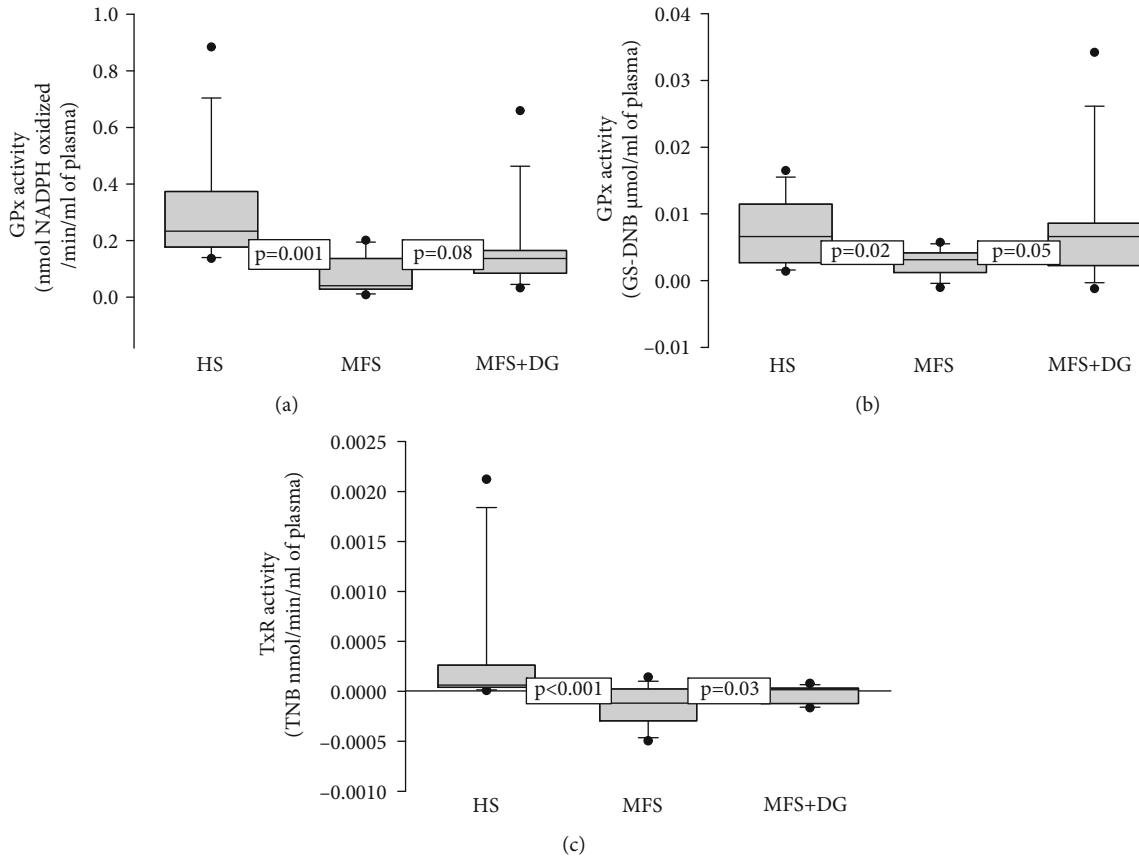
FIGURE 3: Average activities of GPx (a), GST (b), and TrxR (c) in HS ($n = 13$), MFS patients ($n = 13$), and MFS after DG treatment Abbreviations: HS: healthy subjects; MFS: Marfan syndrome; MFS + DG: Marfan syndrome plus deodorized garlic.

(a)

(b)
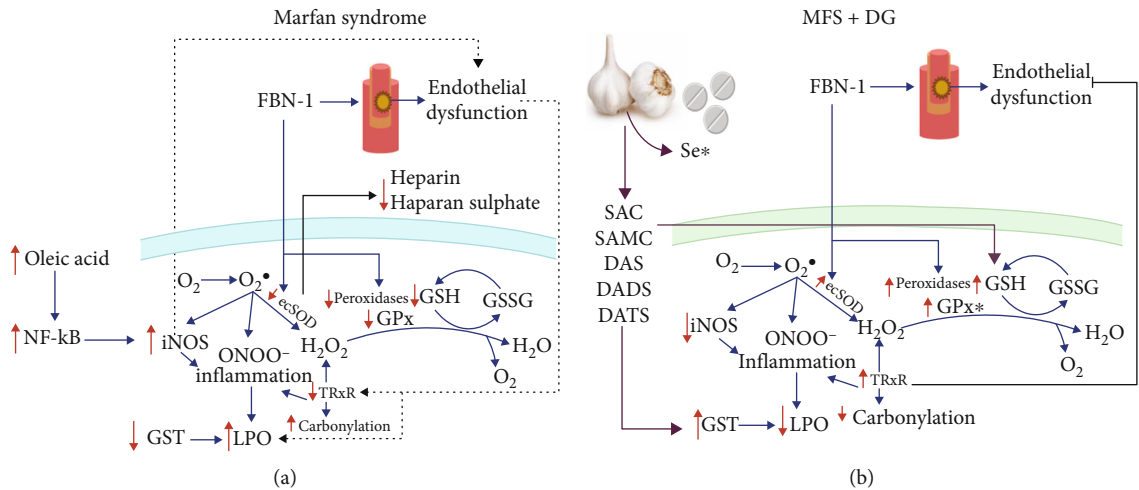
FIGURE 4: Contributions of deodorized garlic in the antioxidant systems in Marfan syndrome. *Enzymes stimulated by selenium. Abbreviations: DADS: diallyl disulfide; DAS: diallyl sulfide; DATS: diallyl trisulfide; DG: deodorized garlic; EcSOD: extracellular superoxide dismutase; FBN-1: fibrillin-1 gene; GPx: glutathione peroxidase; GSH: glutathione; GSSG: oxidized glutathione; GST: gluthatione-S-transferase; H_2O_2: hydrogen peroxide; iNOS: inducible nitric oxide synthase; LPO: lipoperoxidation; NF-κB: nuclear factor κ-light-chain-enhancer of activated B cells; O_2-: superoxide anion; ONOO−: peroxynitrite; SAC: S-allyl-cysteine; SAMC: S-allylmercaptocysteine; Se: selenium.

2.5. Blood Sample Collection. Five ml of blood per patient was collected and centrifuged for 20 min at 936 g at 4°C. The red blood cell pellet was discarded, and the plasma was collected in aliquots of 400 μl and stored at −30°C until used. Blood samples were obtained from each patient before the treatment and after the two months of treatment with the DG.

2.6. EcSOD and Peroxidase Activities. The extracellular activity of super oxide dismutase (EcSOD) was determined in plasma by nondenaturing gel electrophoresis and nitro blue tetrazolium (NBT) staining as described by Pérez-Torres et al. [14] 25 μl of plasma was applied directly, without boiling, to a nondenaturing 10% polyacrylamide gel. The electrophoresis was carried out at 120 volts for 4 hours. Subsequently, the gel was incubated in a 2.45 mM NBT solution for 20 min, then the liquid was discarded, and the gel was incubated in a 28 mM EDTA solution, containing 36 mM potassium phosphate (pH 7.8) and 0.028 mM riboflavin. After 10 min of incubation under dark conditions, the nitro blue tetrazolium stain for O_2^- was viewed by UV light exposure for another 10 min. Purified SOD from bovine erythrocytes with a specific activity of 112 U/mg of protein (Sigma-Aldrich, St. Louis, MO, USA) was used as a positive control.

For the activities of peroxidases, 35 μl of horseradish peroxidase was loaded to a final concentration of 178.5 μg as a standard, and 25 μl of plasma in the same conditions of the native gel was run as previously described. To observe the activity of the peroxidases, the gel was washed with distilled water three times, during 5 min, and it was then incubated with a mixture of 3 mg/ml 3,3,5,5-tetramethylbenzidine dissolved in a solution of ethanol: acetic acid: water (1 : 1 : 1) with H_2O_2 for 10 min in the dark [15]. In these conditions, where peroxidases are present, the gel remains transparent and 3, 3, 5, 5-tetramethylbenzidine is oxidized showing a green coloration. The gels for EcSOD and peroxidase activities were analyzed by densitometry with a Kodak Image® 3.5 system.

2.7. Glutathione Peroxidase and Glutathione-S-Transferase. Glutathione peroxidase and glutathione-S-transferase activities were determinate spectrophotometrically in plasma of each patient as previously described [15]. 100 μl of plasma was suspended in 1.6 ml of 50 mM phosphate buffer (pH 7.3), with added 0.2 mM reduced nicotinamide adenine nucleotide phosphate NADPH, 1 mM GSH, and 1 UI/ml glutathione reductase. The mixture was incubated for 1 min at 37°C, then 100 μl of 0.25 mM H_2O_2 was added to start the reaction, and the absorbance was monitored for 6 min at 340 nm. Activity is expressed in nmol of NADPH oxidized/min/ml plasma with an extinction coefficient of 6220 M^{-1} cm^{-1} at 340 nm for NADPH.

For glutathione-S-transferase (GST) activity, 700 μl of phosphate buffer (0.1 M, pH 6.5) supplemented with 100 μl GSH 0.1 mM and 100 μl 1-chloro-2,4-dinitrobenzene (CDNB) 0.1 mM was added to 100 μl of plasma. The sample was incubated and monitored for 10 min at 37°C at 340 nm [16]. Values of GST activity were expressed in U/min/ml

of plasma. The GST activity is expressed as units of GS-DNB μmol/min/ml of plasma with an extinction coefficient of 14150 M^{-1} cm^{-1}.

2.8. Thioredoxin Reductase. Thioredoxin reductase activity (TrxR) was assessed as described previously [17]. 100 μl of plasma suspended in 3 ml of 0.1 mM phosphate buffer (KH_2PO_4, pH 7.0) was added to 0.2 mM NADPH, 1 mM EDTA, and 0.1 mg/ml bovine serum albumin. The sample were read in the presence of 20 μl of the specific TrxR inhibitor (10 μM auranofin), and together with a duplicate of the sample without the inhibitor was determined indirectly by the amount of DTNB in the presence of NADPH to form 2 moles of TNB. The DTNB oxidation is monitored at 412 nm at 37°C for 6 min with an extinction coefficient of 13600 M^{-1} cm^{-1}.

2.9. Lipid Peroxidation. Fatty acids are converted to malondialdehyde which in the presence of thiobarbituric acid develop a pink color which was read at 532 nm. 50 μl CH_3-OH with 4% BHT plus phosphate buffer pH 7.4 was added to 100 μl of plasma. The mixture was shaken vigorously in vortex for 5 seconds and then incubated in water bath at 37°C for 30 min. 1.5 ml of 0.8 M thiobarbituric acid was then added, and the sample was incubated in a water bath at boiling temperature for 1 hour. After this time and to stop the reaction, the samples were placed on ice; 1 ml 5% KCl was added to each sample as well as 4 ml n-butanol; they were shaken in vortex for 30 sec and centrifuged at 4000 rpm at room temperature for 2 min. Then, the n-butanol phase was extracted, and the absorbance was measured. The calibration curve was obtained using tetraethoxypropane as standard [15].

2.10. Carbonylation. Protein carbonylation was detected spectrophotometrically as previously described [15]. 100 μl of plasma were added to 500 μl of HCl 2.5 N. Another sample with 500 μl of 2,4-dinitrophenylhydrazine and incubated in the dark at room temperature for one hour, shaking with a vortex every 15 min, was run in parallel. At the end of the incubation period, 500 μl of 20% trichloroacetic acid were added, and the sample was centrifuged at 15,000 × g for 5 min. The supernatant was discarded. Two washings were performed, first removing the precipitate with a sealed capillary tube by adding 1 ml ethanol/ethyl acetate. It was incubated for 10 min, and centrifuging at 15,000× g for 10 min. Finally, 1 ml of 6 M guanidine hydrochloride in 20 mM KH_2PO_4 pH 2.3 was added. The mixture was incubated again at 37°C for 30 min. Absorbance was read in a spectrophotometer at 370 nm, using water bidistilled as blank and a molar absorption coefficient of 22,000 M^{-1} cm^{-1}.

2.11. NO_3^-/NO_2^- Ratio. The NO_3^- was reduced to NO_2^- by the nitrate reductase enzyme reaction and detected by the technique of the Griess as previously described [15]. The NO_3^- was reduced to NO_2^- by the nitrate reductase enzyme reaction. 100 μl of plasma previously deproteinized with 0.5 N, NaOH and 10%, $ZnSO_4$ was mixed, and the supernatant was incubated for 30 min at 37°C in presence of nitrate reductase (5 units). At the end of the incubation period,

200 μl of sulfanilamide 1% and 200 μl of N-naphthyl-ethyldiamine 0.1% were added, and the total volume was adjusted to 1 ml. The absorbance was measured at 540 nm.

2.12. GSH Concentration. 100 μl of plasma previously deproteinized with 20% trichloroacetic acid (vol/vol) and centrifugated to 10,000 x g for 5 min was added to 800 μl of phosphate buffer 50 mM, pH 7.3, and plus 100 μl of 1 M. The GSH concentration was determined as described previously [15] using Ellman's reagent (5,5′-dithiobis-2-nitrobenzoic acid). The mixture was incubated at room temperature for 5 min, and absorbance was read at 412 nm.

2.13. Vitamin C. For measuring vitamin C levels, 20% trichloroacetic acid was added to 100 μl of plasma. After vigorous shaking, the samples were kept in an ice bath for 5 min and centrifuged at 5000 rpm for 5 min; 200 μl of Folin-Ciocalteu reagent 0.20 mM was added to the supernatant. The mixture was shaken vigorously in a vortex for 5 seconds and incubated for 10 min. The absorbance was measured at 760 nm. The calibration curve was obtained using ascorbic acid standard solution [15].

2.14. Statistical Analysis. The data are presented as the mean ± SE. Differences were considered as statistically significant when $p \leq 0.05$. Statistical significance between MFS patients was determined by the Mann–Whitney rank sum test followed by the normality test (Shapiro-Wilk). Statistical significance was determined by one-way ANOVA test, followed by Tukey's post hoc test using Sigma Plot 14 program (Systat Software Inc. 2107, San Jose, CA95131 EE.UU. North First Street, Suite 360).

3. Results

3.1. General Characteristics. A total of 13 patients with MFS and 13 healthy subjects (HS) were studied. Age in patients with MFS had a median of 26 years with a minimum of 14 and a maximum of 51. The body mass index in MFS patients had a median value of 24 with a minimum of 12 and a maximum of 30. Demographic characteristics of the MFS patients are shown in Table 1, and the blood chemistry of healthy subjects is shown in Table 2. The distribution and frequency of the Ghent criteria of each of the patients are shown in Table 3.

3.2. Extra Cellular Superoxide Dismutase and Peroxidase Activities. Our results show that EcSOD activity was significantly increased in HS and MFS + DG patients ($p < 0.001$), in comparison to MFS patients (Figure 1). The activity of peroxidases was significantly increased in HS and MFS + DG patients in comparison to MFS patients ($p < 0.001$) (Figure 2).

3.3. GPx, GST, and TxrR Activities. The results of the activity of GPx showed a significant decrease in the MFS patients compared to HS ($p = 0.001$). However, the treatment with DG in MFS patients only showed a tendency to an increase ($p = 0.08$) without reaching a significant value (Figure 3(a)). Our results show that the GST activity was sig-

nificantly decreased in the MFS patients when compared to HS and MFS + DG patients ($p = 0.02$ and $p = 0.05$, respectively, Figure 3(b)). The TrxR in MFS patients was significantly decreased when compared to that in the HS and MFS + DG subjects ($p < 0.001$ and $p = 0.03$, respectively, Figure 3(c)).

3.4. Non Enzymatic Antioxidant System Markers: Lipid Peroxidation and Carbonylation. The OS indicators in the plasma of the experimental groups are shown in Table 3. There was a significant increase in LPO ($p \leq 0.001$ and $p = 0.01$), carbonylation ($p \leq 0.001$), and NO_3^-/NO_2^- ratio levels in the MFS group in comparison to the HS and MFS + DG groups ($p \leq 0.001$ and $p = 0.01$, respectively). However, the GSH levels showed a decrease in MFS patients with a significant difference compared to the HS and MFS + DG groups, respectively ($p \leq 0.001$ and $p = 0.01$). Vitamin C levels showed no significant changes in the groups.

4. Discussion

The medicinal use of garlic in folk medicine is extremely old, and thousands of investigations have shown its beneficial effects on different pathologies such as hypertension, dyslipidemias, insulin resistance, and OS to mention a few. The beneficial effects of garlic are due to organ sulfuric compounds, such as allicin, E/Z-ajoene, SAC, S-allyl-cysteine sulfoxide (alliin), SAMC, diallyl sulfide (DAS), diallyl disulfide (DADS), diallyl trisulfide (DATS), gamma-glutamyl tripeptides, and sulfur dioxide(SO_2) among others [3].

On the other hand, in animal models and in humans with MFS, there is formation of aortic aneurysms and pseudoaneurysms which is accompanied by endothelial dysfunction, chronic inflammation, increase in the expression and activity of metalloproteinase, and a decrease of the antioxidant enzymes. These alterations are due to the genetic mutation of the FBN-1 gene [18].

The objective of this work was to show the antioxidant effect of DG in the plasma of MFS patient. As far as we know, there are no studies to date that show the beneficial effect of garlic in this syndrome. Figure 4 summarizes the results of this study on DG treatment in the plasma of the MFS patients.

4.1. Superoxide Dismutase. SOD isoforms participate as the first line of detoxification against the O_2^- anion reducing it to H_2O_2. This enzyme is expressed in blood vessels primarily on the surface of vascular smooth muscle cells and the subendothelial space. It contains a binding domain that links it to proteoglycans and heparan sulphates which are expressed on the cell surface. This enzyme may be secreted into the extracellular space and is found in plasma [19]. The results in this study suggest that the decrease of EcSOD activity could contribute to OS in MFS patients [20]. The mutation of FBN-1 is also associated with a decrease in heparin/heparan sulphate for which the EcSOD has a binding domain. Genetic factors such as polymorphisms in the heparin binding domain alter the expression or activity of this enzyme [21]. Regarding the alterations of the expression or activity

of this enzyme by medicinal plants that provide antioxidants in MFS patients, it was previously found that an infusion of *Hibiscus sabdariffa L.* increased its activity [11]. Our results show that the treatment with DG increases the EcSOD activity in MFS patients. The beneficial effect of garlic is due to the organ sulfuric compounds such SAC and SAMC responsible for the transcription of some antioxidant enzymes such as SOD isoforms through the NrF2 pathway [22]. In addition, this result suggests that the O_2^- anion concentration decreases but that H_2O_2 increases.

4.2. GPx Activity. To detoxify the H_2O_2, the cell antioxidant system is provided with other enzymes that employ it as a substrate. 12% of the EcSOD functions are related to the activity of some of the GPx isoforms [11]. GPx isoforms catalyze the oxidation reaction of glutathione (GSH) to glutathione disulfide using H_2O_2. It recycles some of the molecules attacked by H_2O_2 and peroxidized organic molecules [23]. However, the activity of GPx is reduced by prooxidative conditions such as an inflammatory state which may induce further the accumulation of ROS [24]. Our results show that the GPx activity in plasma of the MFS patients was decreased as had been previously reported [25], and that the DG treatment tended to increase it and thus contribute to the reduction of OS. Several studies have reported that organ sulfuric compounds from garlic can induce the expression of the GPx gene [26]. Another study showed that garlic administration activated the phosphorylation of the Nuclear factor erythroid 2-related factor 2 which was associated to an increased in the transcription of the GPx genes [27]. The DG treatment can also provide selenium, an essential micronutrient for the catalytic center of the several antioxidant enzymes such as GPx and TrxR, thus favoring an increase in their activity. In patients with the Loeys-Dietz syndrome, a severe variant of the MFS, there is a decrease in GPx, GST, TrxR, selenium, and Nrf2 expression [28]. However, in MFS patients, the involvement of selenium requires further study.

4.3. Activity of Peroxidases. Other antioxidant enzymes that contribute to reduce H_2O_2 to water are peroxidases. These enzymes play an important role in innate immunity and in other physiologically important processes like apoptosis and cell signaling [29]. Our results show that the activity of peroxidases decreases in MFS patients. This may be due to the FBN-1 mutation since the fibrillins constitute the backbone of microfibrils in the extracellular matrix of elastic and nonelastic tissues [30]. Furthermore, the low activity of these enzymes can contribute to background oxidation which is favored, in part, by the increase in the H_2O_2 in MFS patients. Treatment with DG increased the activity of these enzymes, which reduce OS. In HepG2 cells, incubation DAS increases both mRNA and expression of heme oxygenase-1 (HO-1), which is a type deperoxidase [31].

4.4. TrxR Activity. TrxR possesses a selenocysteine in its catalytic site [32]. Moderate OS can induce a compensatory increase in the TrxR activity and reduce the oxidative modification of proteins present in several pathologies [33].

However, TrxR is decreased in chronic pathologies with severe OS and metabolic disturbances [34]. In endothelial dysfunction, TxrR decreases, and this is associated with a prothrombotic and proinflammatory state [35]. The thioredoxin system in mammals consists of two antioxidant components, the thioredoxin (Trx) and TrxR. The TrxR enzyme catalyzes the reduction of disulfide in the active site of Trx in the presence of NADPH. It improves the mal function of the proteins, cellular receptors, and/or enzymes [36]. The results of this study suggest that the decrease in TrxR activity in MFS patients could be associated to the background OS. These changes are associated to the lack of disulphide bonds formed among microfibrils where the thioredoxin system is essential to reduce these bridges [37]. However, the DG treatment favored an increase in the activity of this enzyme, which could contribute to decrease the OS and increase the reduction between the disulphide bonds in the microfibrils. The beneficial effect of garlic is associated to organ sulfur compound such the DATS, which modulate the expression and activity of the Trx/TrxR system [37, 38]. These sulfur conjugates may favor an increase in the H_2S production in the presence of reduced Trx. [38]. H_2S is a lipophilic molecule that controls important processes in the cell including the regulation of the Keap1-Nrf2 pathway [3].

4.5. GST Activity. Another enzyme that showed a decrease in its activity in MFS patients was GST. This is a phase II drug-metabolizing enzyme which detoxifies a wide variety of electrophilic xenobiotics by catalyzing their conjugation to GSH. It also reduces many organic hydroperoxides into alcohols [39]. The decrease in the activity of this enzyme could favor the accumulation of the LPO products including 4-hydroxy-2-transnonenal [40]. However, treatment with DG favored an increase in the activity of this enzyme. Different compounds of garlic are linked to the increase in the activity of this enzyme including DADS and DATS which significantly increased the GST activities in liver damage [41]. Another study demonstrated that organ sulfur compounds increased the activity and mRNA of GST, and this effect was associated to DAS, DADS, and DATS [42]. Furthermore, the reduction of the activities of GST and GPx can also be caused by GSH depletion, since both enzymes depend on it [43].

4.6. Redox Biomarkers of the Nonenzymatic System. GSH is the most abundant endogenous intracellular antioxidant present within cells. This tripeptide inactivates the O_2^- anion and the hydroxyl radical. Irreversible cell damage happens when the cell is unable to maintain its intracellular concentration of GSH [44]. Our results show that the GSH concentration was significantly diminished in the MFS patients. However, the treatment with DG increased the GSH concentration favoring the reduction of OS through the provision of a larger amount of this antioxidant molecule that also acts as a substrate for GPx and GST [45]. GSH can be obtained through the diet by consuming foods like garlic, which contains thioallyl compounds such as the DAS DADS and DATS. These compounds maintain the intracellular GSH level modulating its increase and preventing its

depletion probably through the enzymes that participate in the GSH synthesis [46].

4.7. NO_3^-/NO_2^- Ratio, Lipoperoxidation, and Carbonylation. The endothelial dysfunction in MFS patients may inactivate eNOS and increase the iNOS expression/activity leading to an enhanced production of NO which contributes to inflammation [41]. In previous studies in MFS patients, oleic acid was increased, and it may elevate NF-KB which participates in the overproduction of iNOS [47]. Our results show an increase in the NO_3^-/NO_2^- ratio in MFS patients. NO metabolites may participate in the chronic inflammation present in this syndrome. Moreover, the loss of the redox homeostasis together with the induction of the iNOS expression/activity and with the subsequent exacerbation of NO through NF-κB activation could lead to the formation of peroxynitrites ($ONOO^-$). $ONOO^-$ affects protein functions by modifying essential reactive thiol groups and/or tyrosine residues, thereby leading to the formation of oxidized thiol groups or the formation of 3-nitrotyrosine in proteins. These alterations in proteins can induce S-nitrosylation [48]. S-nitrosylation may also regulate the expression of proinflammatory genes. Furthermore, S-nitrosylation impairs both endothelium-dependent and -independent relaxation, and these effects are accompanied by irreversible inactivation of the antioxidant enzymes [49]. However, the treatment with DG favors the inhibition of iNOS [50]. A recent study demonstrated that SAC administration in rats significantly decreased the expression of NF-κB, tumor necrosis factor, and iNOS, exerting a protective effect against toxicity [45]. $ONOO^-$ is also an important intermediary in both LPO and carbonylation [51]. We analyzed the LPO and carbonylation levels in our experimental groups. LPO is a marker of damage to cell membranes, and carbonylation is a marker of protein damage by ROS. The DG treatment was able to reduce both indices through its sulfur components by modulating the antioxidant enzymes.

5. Conclusions and Perspectives

Our results demonstrated that MFS is associated with the presence of OS, and that the treatment with DG may be effective in diminishing this parameter by increasing the antioxidant defense in the plasma of patients with MFS.

The application of alternative therapies such garlic which have antioxidants properties could help in the prevention and mitigation of adverse OS in the MFS patients and thereby have a beneficial impact on patient survival. These relevant findings suggest the need of conducting multicentric studies or systematic studies providing therapies with antioxidants that may improve the redox state of these patients and that may be appropriate to the clinical context of each particular subject.

Data Availability

The datasets generated and analyzed during the current study are available from the corresponding author on reasonable request.

Conflicts of Interest

The authors declare no conflict of interest.

Authors' Contributions

I.P.-T. designed the study, made some the laboratory determination, and wrote the manuscript and the statistical study. M.E.S. recruited patients, followed the treatment in patients, and made some the laboratory determination. L.M.-P. designed and made the graphical abstract and Figure 4. E.D.D. performed the blood biochemistry. E.S.-C. and M.E.R.-R. took blood samples from both MFS patients and healthy subjects. V.G.-L. revised and structured the manuscript. All authors have read and agreed to the published version of the manuscript. Israel Pérez-Torres and María Elena Soto share first authorship of the paper.

References

[1] Q. Du, D. Zhang, Y. Zhuang, Q. Xia, T. Wen, and H. Jia, "The molecular genetics of Marfan syndrome," *International Journal of Medical Sciences*, vol. 18, pp. 2752–2766, 2021.

[2] S. S. Portelli, B. D. Hambly, R. W. Jeremy, and E. N. Robertson, "Oxidative stress in genetically triggered thoracic aortic aneurysm: role in pathogenesis and therapeutic opportunities," *Redox Report*, vol. 26, pp. 45–52, 2021.

[3] I. Pérez-Torres, V. Castrejón-Téllez, M. E. Soto, M. E. Rubio-Ruiz, L. Manzano-Pech, and V. Guarner-Lans, "Oxidative stress, plant natural antioxidants, and obesity," *International Journal of Molecular Sciences*, vol. 22, p. 1786, 2021.

[4] T. Donia and A. Khamis, "Management of oxidative stress and inflammation in cardiovascular diseases: mechanisms and challenges," *Environmental Science and Pollution Research International*, vol. 28, pp. 34121–34153, 2021.

[5] R. Mirondo and S. Barringer, "Deodorization of garlic breath by foods, and the role of polyphenol oxidase and phenolic compounds," *Journal of Food Science*, vol. 81, pp. C2425–C2430, 2016.

[6] A. Harauma and T. Moriguchi, "Aged garlic extract improves blood pressure in spontaneously hypertensive rats more safely than raw garlic," *The Journal of Nutrition*, vol. 136, pp. 769S–773S, 2006.

[7] R. Munch and S. A. Barringer, "Deodorization of garlic breath volatiles by food and food components," *Journal of Food Science*, vol. 79, pp. C526–C533, 2014.

[8] J. S. Kwak, J. Y. Kim, J. E. Paek et al., "Garlic powder intake and cardiovascular risk factors: a meta-analysis of randomized controlled clinical trials," *Nutrition Research and Practice*, vol. 8, pp. 644–654, 2014.

[9] R. Varshney and M. J. Budoff, "Garlic and heart disease," *The Journal of Nutrition*, vol. 146, pp. 416S–421S, 2016.

[10] M. M. van Andel, M. Groenink, A. H. Zwinderman, B. J. M. Mulder, and V. de Waard, "The potential beneficial effects of resveratrol on cardiovascular complications in Marfan syndrome patients-insights from rodent-based animal studies," *International Journal of Molecular Sciences*, vol. 20, p. 1122, 2019.

[11] M. E. Soto, A. Zuñiga-Muñoz, V. Guarner Lans, E. J. Duran-Hernández, and I. Pérez-Torres, "Infusion of hibiscus sabdariffa L. modulates oxidative stress in patients with Marfan syndrome," *Mediators of Inflammation*, vol. 2016, Article ID 8625203, 12 pages, 2016.

[12] L. Faivre, G. Collod-Beroud, L. Adès et al., "The new Ghent criteria for Marfan syndrome: what do they change?," *Clinical Genetics*, vol. 81, pp. 433–442, 2012.

[13] "World Medical Association. Declaration of Helsinki. Ethical principles for medical research involving human subjects," *Journal of the American Medical Association*, vol. 310, pp. 2191–2194, 2013.

[14] I. Pérez-Torres, P. Roque, M. El Hafidi, E. Diaz-Diaz, and G. Baños, "Association of renal damage and oxidative stress in a rat model of metabolic syndrome. Influence of gender," *Free Radical Research*, vol. 43, pp. 761–771, 2009.

[15] F. L. Rodríguez-Fierros, V. Guarner-Lans, M. E. Soto et al., "Modulation of renal function in a metabolic syndrome rat model by antioxidants in Hibiscus sabdariffa L," *Molecules*, vol. 26, p. 2074, 2021.

[16] L. Flohé and W. A. Günzler, "Assays of glutathione peroxidase," *Methods in Enzymology*, vol. 105, pp. 114–121, 1984.

[17] A. Holmgren and M. Björnstedt, "Thioredoxin and thioredoxin reductase," *Methods in Enzymology*, vol. 252, pp. 199–208, 1995.

[18] P. N. Robinson, E. Arteaga-Solis, C. Baldock et al., "The molecular genetics of Marfan syndrome and related disorders," *Journal of Medical Genetics*, vol. 43, pp. 769–787, 2006.

[19] L. G. M. Pech, S. Caballero-Chacón, V. Guarner-Lans, E. Díaz-Díaz, A. M. Gómez, and I. Pérez-Torres, "Effect of oophorosalpingo-hysterectomy on serum antioxidant enzymes in female dogs," *Scientific Reports*, vol. 9, p. 9674, 2019.

[20] Z. Yan and H. R. Spaulding, "Extracellular superoxide dismutase, a molecular transducer of health benefits of exercise," *Redox Biology*, vol. 32, p. 101508, 2020.

[21] K. Karlsson and S. L. Marklund, "Heparin-induced release of extracellular superoxide dismutase to human blood plasma," *The Biochemical Journal*, vol. 242, pp. 55–59, 1987.

[22] J. Yang, X. Song, Y. Feng et al., "Natural ingredients-derived antioxidants attenuate H(2)O(2)-induced oxidative stress and have chondroprotective effects on human osteoarthritic chondrocytes via Keap1/Nrf2 pathway," *Free Radical Biology & Medicine*, vol. 152, pp. 854–864, 2020.

[23] J. C. Whitin, S. Bhamre, D. M. Tham, and H. J. Cohen, "Extracellular glutathione peroxidase is secreted basolaterally by human renal proximal tubule cells," *American Journal of Physiology. Renal Physiology*, vol. 283, pp. F20–F28, 2002.

[24] Y. S. Lee, A. Y. Kim, J. W. Choi et al., "Dysregulation of adipose glutathione peroxidase 3 in obesity contributes to local and systemic oxidative stress," *Molecular Endocrinology*, vol. 22, pp. 2176–2189, 2008.

[25] A. M. Zúñiga-Muñoz, I. Pérez-Torres, V. Guarner-Lans et al., "Glutathione system participation in thoracic aneurysms from patients with Marfan syndrome," *VASA*, vol. 46, pp. 177–186, 2017.

[26] M. I. El-Barbary, "Detoxification and antioxidant effects of garlic and curcumin in Oreochromis niloticus injected with aflatoxin B1 with reference to gene expression of glutathione peroxidase (GPx) by RT-PCR," *Fish Physiology and Biochemistry*, vol. 42, pp. 617–629, 2016.

[27] U. Franco-Enzástiga, R. A. Santana-Martínez, C. A. Silva-Islas, D. Barrera-Oviedo, M. E. Chánez-Cárdenas, and P. D. Maldonado, "Chronic administration of S-allylcysteine activates Nrf2 factor and enhances the activity of antioxidant enzymes in the striatum, frontal cortex and hippocampus," *Neurochemical Research*, vol. 42, pp. 3041–3051, 2017.

[28] M. E. Soto, L. G. Manzano-Pech, V. Guarner-Lans et al., "Oxidant/antioxidant profile in the thoracic aneurysm of patients with the Loeys-Dietz syndrome," *Oxidative Medicine and Cellular Longevity*, vol. 2020, Article ID 5392454, 17 pages, 2020.

[29] I. I. Vlasova, "Peroxidase activity of human hemoproteins: keeping the fire under control," *Molecules*, vol. 23, p. 2561, 2018.

[30] K. A. Zeyer and D. P. Reinhardt, "Fibrillin-containing microfibrils are key signal relay stations for cell function," *The Journal of Cell Communication and Signaling*, vol. 9, pp. 309–325, 2015.

[31] P. Gong, B. Hu, and A. I. Cederbaum, "Diallyl sulfide induces heme oxygenase-1 through MAPK pathway," *Archives of Biochemistry and Biophysics*, vol. 432, pp. 252–260, 2004.

[32] J. Lu and A. Holmgren, "The thioredoxin antioxidant system," *Free Radical Biology & Medicine*, vol. 66, pp. 75–87, 2014.

[33] E. S. J. Arnér, "Effects of mammalian thioredoxin reductase inhibitors," *Handbook of Experimental Pharmacology*, vol. 264, pp. 289–309, 2021.

[34] A. A. Tinkov, G. Bjørklund, A. V. Skalny et al., "The role of the thioredoxin/thioredoxin reductase system in the metabolic syndrome: towards a possible prognostic marker?," *Cellular and Molecular Life Sciences*, vol. 75, pp. 1567–1586, 2018.

[35] J. Kirsch, H. Schneider, J. I. Pagel et al., "Endothelial dysfunction, and a prothrombotic, proinflammatory phenotype is caused by loss of mitochondrial thioredoxin reductase in endothelium," *Arteriosclerosis, Thrombosis, and Vascular Biology*, vol. 36, pp. 1891–1899, 2016.

[36] E. Chupakhin and M. Krasavin, "Thioredoxin reductase inhibitors: updated patent review (2017-present)," *Expert Opinion on Therapeutic Patents*, vol. 31, pp. 745–758, 2021.

[37] S. Schrenk, C. Cenzi, T. Bertalot, M. T. Conconi, and R. Di Liddo, "Structural and functional failure of fibrillin-1 in human diseases (review)," *International Journal of Molecular Medicine*, vol. 41, pp. 1213–1223, 2018.

[38] Y. Liu, Y. Zhao, Z. Wei et al., "Targeting thioredoxin system with an organosulfur compound, diallyl trisulfide (DATS), attenuates progression and metastasis of triple-negative breast cancer (TNBC)," *Cellular Physiology and Biochemistry*, vol. 50, pp. 1945–1963, 2018.

[39] W. Chih-Chung, S. Lee-Yan, C. Haw-Wen, K. Wei-Wen, T. Shun-Jen, and L. Chong-Kuei, "Differential effects of garlic oil and its three major organosulfur components on the hepatic detoxification system in rats," *Journal of Agricultural and Food Chemistry*, vol. 50, pp. 378–383, 2002.

[40] A. Rahal, A. Kumar, V. Singh et al., "Oxidative stress, prooxidants, and antioxidants: the interplay," *BioMed Research International*, vol. 2014, Article ID 761264, 19 pages, 2014.

[41] T. Fukao, T. Hosono, S. Misawa, T. Seki, and T. Ariga, "The effects of allyl sulfides on the induction of phase II detoxification enzymes and liver injury by carbon tetrachloride," *Food and Chemical Toxicology*, vol. 42, pp. 743–749, 2004.

[42] C. C. Wu, L. Y. Sheen, H. W. Chen, S. J. Tsai, and C. K. Lii, "Effects of organosulfur compounds from garlic oil on the antioxidation system in rat liver and red blood cells," *Food and Chemical Toxicology,*, vol. 39, no. 6, pp. 563–569, 2002.

[43] J. Rybka, D. Kupczyk, K. Kędziora-Kornatowska et al., "Glutathione-related antioxidant defense system in elderly patients treated for hypertension," *Cardiovascular Toxicology*, vol. 11, pp. 1–9, 2011.

[44] R. V. Sekhar, S. G. Patel, A. P. Guthikonda et al., "Deficient synthesis of glutathione underlies oxidative stress in aging and can be corrected by dietary cysteine and glycine supplementation," *The American Journal of Clinical Nutrition*, vol. 94, pp. 847–853, 2011.

[45] J. Borlinghaus, F. Albrecht, M. C. Gruhlke, I. D. Nwachukwu, and A. J. Slusarenko, "Allicin: chemistry and biological properties," *Molecules*, vol. 19, no. 8, pp. 12591–12618, 2014.

[46] C. Rodrigues and S. S. Percival, "Immunomodulatory effects of glutathione, garlic derivatives, and hydrogen sulfide," *Nutrients*, vol. 11, p. 295, 2019.

[47] M. E. Soto, A. V. Iturriaga-Hernández, V. Guarner-Lans et al., "Participation of oleic acid in the formation of the aortic aneurysm in Marfan syndrome patients," *Prostaglandins & Other Lipid Mediators*, vol. 123, pp. 46–55, 2016.

[48] J. Dairou, B. Pluvinage, J. Noiran et al., "Nitration of a critical tyrosine residue in the allosteric inhibitor site of muscle glycogen phosphorylase impairs its catalytic activity," *Journal of Molecular Biology*, vol. 372, pp. 1009–1021, 2007.

[49] H. Choi, K. J. Allahdadi, R. C. Tostes, and R. C. Webb, "Augmented S-nitrosylation contributes to impaired relaxation in angiotensin II hypertensive mouse aorta: role of thioredoxin reductase," *Journal of Hypertension*, vol. 29, pp. 2359–2368, 2011.

[50] K. M. Kim, S. B. Chun, M. S. Koo et al., "Differential regulation of NO availability from macrophages and endothelial cells by the garlic component S-allyl cysteine," *Free Radical Biology & Medicine*, vol. 30, pp. 747–756, 2001.

[51] S. G. Turowski, K. E. Jank, and H. L. Fung, "Inactivation of hepatic enzymes by inhalant nitrite–in vivo and in vitro studies," *The AAPS Journal*, vol. 9, no. 3, pp. E298–E305, 2007.

Review Article

Cold Physical Plasma in Cancer Therapy: Mechanisms, Signaling, and Immunity

Fatemeh Faramarzi [ID],[1,2] Parisa Zafari [ID],[2,3] Mina Alimohammadi,[3]
Mohammadreza Moonesi [ID],[2,4] Alireza Rafiei [ID],[2,3] and Sander Bekeschus [ID][2,5]

[1]*Student Research Committee, School of Medicine, Mazandaran University of Medical Science, Iran*
[2]*Department of Immunology, School of Medicine, Mazandaran University of Medical Science, Sari, Iran*
[3]*Department of Immunology, School of Medicine, Shahid Beheshti University of Medical Science, Tehran, Iran*
[4]*Department of Hematology, School of Medicine, Tabriz University of Medical Sciences, Tabriz, Iran*
[5]*ZIK plasmatis, Leibniz Institute for Plasma Science and Technology (INP), Greifswald, Germany*

Correspondence should be addressed to Alireza Rafiei; rafiei1710@gmail.com
and Sander Bekeschus; sander.bekeschus@inp-greifswald.de

Despite recent advances in therapy, cancer still is a devastating and life-threatening disease, motivating novel research lines in oncology. Cold physical plasma, a partially ionized gas, is a new modality in cancer research. Physical plasma produces various physicochemical factors, primarily reactive oxygen and nitrogen species (ROS/RNS), causing cancer cell death when supplied at supraphysiological concentrations. This review outlines the biomedical consequences of plasma treatment in experimental cancer therapy, including cell death modalities. It also summarizes current knowledge on intracellular signaling pathways triggered by plasma treatment to induce cancer cell death. Besides the inactivation of tumor cells, an equally important aspect is the inflammatory context in which cell death occurs to suppress or promote the responses of immune cells. This is mainly governed by the release of damage-associated molecular patterns (DAMPs) to provoke immunogenic cancer cell death (ICD) that, in turn, activates cells of the innate immune system to promote adaptive antitumor immunity. The pivotal role of the immune system in cancer treatment, in general, is highlighted by many clinical trials and success stories on using checkpoint immunotherapy. Hence, the potential of plasma treatment to induce ICD in tumor cells to promote immunity targeting cancer lesions systemically is also discussed.

1. Introduction

Cold physical plasma is a partially ionized gas operated at or around body temperature [1], and the term "plasma" in this work relates to this gas plasma and not to the protein-rich liquid of blood plasma. Physical plasmas are multicomponent systems as several plasma properties are described, including electrons and ions, electric fields, mild thermal and UV radiation, and reactive oxygen and nitrogen species. The latter will be abbreviated as ROS hereafter as most RNS also contain oxygen. It was recently outlined that ROS are major biomedical effectors of physical plasma treatment in biology and medicine [2].

Physical plasma is produced by different types of plasma devices such as the plasma jet [3–8], dielectric barrier discharge (DBD) [9–13], floating-electrode dielectric barrier discharge (FE-DBD) [14, 15], atmospheric pressure glow discharge torch (APGD-t) [16, 17], plasma brush [18], microhollow cathode discharge air plasma jet [19], microwave plasma torch [20], and nanosecond plasma gun [21]. Plasma jets and DBDs are particularly suitable for biomedical applications as these devices have already entered clinical practice [22]. The first report of using plasma in oncology was published in 2007 by showing the inactivation of melanoma cells *in vitro* following plasma treatment [14]. After that, more studies provided evidence of the anticancer

capacity of plasma in several cancer types such as the brain [23–25], skin [26–29], breast [30–34], colorectal [35–37], lung [38–40], cervical [41–43], leukemia [44–48], pancreatic [49–54], liver [55–57], and head and neck [58–60]. Because of altered metabolism and mitochondrial dysfunction, cancer cells are often found to produce more intracellular ROS than nonmalignant cells [61–63]. In some studies, enhanced intracellular ROS in cancer cells makes them more susceptible to cell death induced by extracellular ROS [64, 65]. Among the extracellular ROS generated via plasma are superoxide anion, hydrogen peroxide, peroxynitrite, nitrite, nitrate, hydroxyl radicals, atomic oxygen, ozone, and singlet delta oxygen [66]. One hypothesis is that aquaporin transporters [67, 68] and lower levels of cholesterol in the membrane of cancer cells compared to a nonmalignant cell [69] increase the permeation of ROS through the cancer cell membrane, presumably via lipid peroxidation [70, 71]. As a result, more plasma-produced ROS are being transported to cancer cells, ultimately augmenting cell death. Cell death is a consequence of intracellular signaling regulated by pathways such as signal transducer and activator of transcription 3 (STAT3), MAP-kinase (MAPK) [72], and phosphatidylinositol 3-kinases (PI3K) via AKT (protein kinase B) [73]. Thus, plasma treatment can selectively target cancer cells because of their unique properties [67, 69].

Moreover, several pharmacological and physics approaches have been combined with plasma treatment to additively or synergistically augment toxicity in cancer cells. This includes radiotherapy [74–76], pulsed electric fields [77, 78], hyperthermia [79], photodynamic therapy [80], established anticancer drugs [81–85], and novel anticancer compounds [86, 87] including nanoparticles and emulsions [88–103]. This current will not focus on these aspects due to the broad nature of the combination approaches. Instead, plasma treatment has been described to directly or indirectly affect the immune system's cells, which may be harnessed in antitumor therapy [104], and current concepts are described that address this framework. Altogether, this review is aimed at unfolding the mechanisms, pathways, and immune-related activities involved in plasma cancer therapy.

2. Plasma Devices in Cancer Treatment

Analyzing plasma devices from different perspectives, including assessing their safety aspects, the capacity of ROS production, and cellular response to oxidative eustress and distress, are critical steps in examining how plasma works in cancer treatment. For a detailed overview of plasma physics, the reader is referred to reviews on this topic [105–107], while this section intends to give a brief overview to the biomedical audience. There are three major types of plasma sources including (1) DBD plasmas, also called "direct" plasma sources, that use the human body as an electrode; (2) plasma needles/plasma jets, also called "indirect" plasma sources, producing a discharge between two electrodes (Figure 1); and (3) hybrid plasma source, the combination of both (1) and (2) plasma sources [108]. The use of these plasma-producing systems depends on the study's purpose,

and plasma jets seem more common than DBD plasmas based on several reports [109]. DBD plasmas' advantage is that they do not require a particular gas flow as needed in plasma jets, in which usually a noble gas is excited using high-frequency electrodes. In most cases with DBDs, the DBD electrode needs to be close to the target, and its diameter varies from several millimeters to centimeters [110]. Unlike DBDs, plasma jets use three common gases, including helium (He), argon (Ar), and nitrogen (N_2), that determine the efficiency and pattern of ROS production [111]. Other critical parameters in operating plasma jets are, for instance, gas flow rate, applied voltage, and the distance from the nozzle to the target. For example, increasing the distance from the target to a jet nozzle decreases the concentration and variety of most reactive species reaching that target, while some, like ozone, are often found to be increased [112]. Also, changes in the feed gas flux are accompanied by changes in the reactive species composition, especially when the flow switches from laminar to turbulent [113, 114]. Another critical factor is exposure time. It is well known from microbiology studies that the growth inhibition zones of bacteria grown on agar increase with a rise in plasma treatment time [115]. Likewise, the plasma treatment time dictates the extent of biological responses, e.g., apoptosis [110, 116]. Also, exposure time can modulate the secretion of cell-signaling molecules, such as growth factors and cytokines [117]. The plasma devices' operating conditions affect the type and amount of reactive species products, especially in cancer cells [6, 118, 119]. Therefore, regulating these conditions improves plasma efficiency in inhibiting cancer cells (Table 1).

One device that has been successfully employed in cancer treatment in patients [120, 121] is the atmospheric pressure argon plasma jet kINPen MED (Figure 2). Generally, medical plasmas are multicomponent systems, while it has been established that the biological activity of plasma treatment is mainly mediated via ROS/RNS and subsequent redox signaling [2, 122]. The ROS/RNS generation process is briefly described. For plasma jets, a gas is fed into the device. Usually, noble gases such as argon, helium, and neon are used to be ionized easily. These ionized gases are subsequently expelled into the ambient air. Reaction with oxygen and nitrogen takes place, generating reactive oxygen and nitrogen species. Within the plasma plume, hundreds of chemical reactions occur [123, 124], leading to the simultaneous generation of a large variety of reactive species [125]. These species have varying concentrations along the axis of the plasma jet and are characterized by individual travel distance and deterioration kinetics in the ambient air [126–128]. This aspect complicates the identification of exact species types and concentrations being delivered to the biological target. As a general measure of species quantification, liquids can be exposed to plasma to identify some species such as nitric oxide, singlet oxygen, hydrogen peroxide, hydroxyl radical, nitrite, nitrate, peroxynitrite, and ozone, based on established redox chemistry assays [66, 129–133]. Notably, there is no tool available to simultaneously investigate all types of species being generated in the plasma gas phase or treated liquids. This also holds true
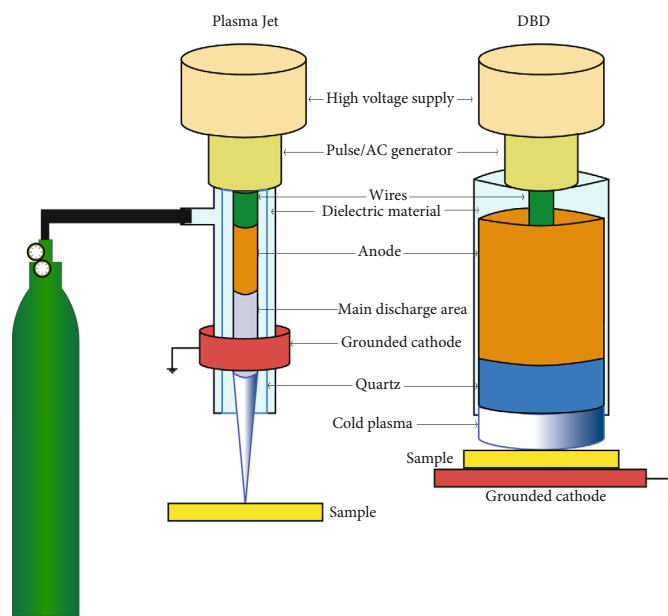
FIGURE 1: Schematic of the principles of plasma jets and dielectric barrier discharges (DBD). In plasma jets, the gas flow is required for the generation of cold physical plasma, while the plasma provided by DBD is created in ambient air. Plasma jets are grounded, while many DBD systems use the treatment target as a grounded cathode to produce cold physical plasma. Many types of gases can be used. Usually, noble gases such as argon, helium, and neon are employed, but air ionization is also feasible with specific parameter setups.

for plasma-treated tissues, as tools for assessing such species directly in such context are currently not available [134].

3. Cell Death Signaling in Cancer Cells

Several cell death modalities are known, including necrosis, apoptosis, necroptosis, autophagy, and pyroptosis [135]. These pathways can be a therapeutic target for the control and destruction of cancer cells. Deregulation of cell death signaling is a distinctive feature of cancer cells, and many cancer therapies target the apoptosis signaling machinery, including cell death receptors and mitochondrial signaling pathways [136, 137]. Direct plasma treatment or plasma-treated liquid (PTL) increases the intracellular ROS affecting different factors in cell death signaling in tumor cells [138]. Accordingly, targeting proteins or kinases involved in cell death signaling can efficiently induce apoptosis and death in the cancer cell. In the following, it will be outlined which pathways are involved in plasma-mediated cell death (Figure 3).

3.1. Apoptosis. It has been found that the ROS produced by plasma can induce cell death in cancer cells by activation of four MAPK pathways, including ERK1/2, c-Jun N-terminal kinase (JNK), p38 MAPK, and ERK5. The JNK and p38 pathways have a crucial role in the induction of apoptosis and the stress of the cells [139]. The activation of these pathways involves proapoptosis Bcl-2 proteins such as BAX and BAK that initiate intrinsic or mitochondrial cell death signaling. Also, p38 MAPK and JNK can upregulate p53 activity that controls cancer growth and triggers cell death in cancer cells [140].

p53 is a tumor suppressor protein involved in stress responses and intrinsic and extrinsic apoptosis pathways [141]. The phosphorylation of p53 triggers the intrinsic apoptosis pathway by activating the BH3 domain of proapoptotic proteins such as Puma, Noxa, Bad, Bax, Bak, and apoptosis-execution factors such as Apaf1 [136]. Also, p53 can initiate extrinsic apoptotic pathway signaling through cell death receptors such as Fas. Following activation of one of the two (or both) pathways, downstream caspases are activated, and apoptosis occurs. High levels of p53 protein in plasma-treated leukemia cells confirm p53-induced apoptosis [46, 136]. Moreover, increased Bax, Bcl-2, and caspase 8 expression in cancer cells after plasma treatment showed the effect of plasma on intrinsic and extrinsic pathways [46].

The ERK pathway is another MAPK pathway that coordinately regulates some essential biological functions of the cells, such as proliferation, differentiation, cycle regulation, apoptosis, and tissue formation. Also, this pathway can be related to tumor proliferation and invasion/metastasis [139]. Accordingly, the regulation of this pathway can be essential in inhibiting tumor cell growth. Plasma therapy has been shown to dramatically increase ERK1/2 phosphorylation and activate caspases in cancer cells, leading to their death [142].

Elevated intracellular ROS activates tumor suppressor proteins and kinases, suppressing the oncogenic PI3K/AKT pathway. Thus, inhibition of the PI3K/AKT pathway initiates cancer cell death [140]. PI3K/AKT signaling mediates a wide range of cellular functions, including transcription, translation, proliferation, growth, and survival. This pathway maintains the balance between cell proliferation and apoptosis in cancer cells and is associated with metastasis

TABLE 1: Plasma devices and their characteristics and outcomes in tumor cells.

Plasma device	Gas/modality	ROS/RNS investigated	Species/cell or tissue type	Biological consequence			Ref.
				Proliferation	Apoptosis	Migration	
Plasma jet	He/direct	O	Human (G361 melanoma)	→	n.i.	→	[4]
Plasma jet	He, O_2/direct	O and OH	Human (HCT-116, SW480 colorectal carcinoma)	→	↑	→	[35]
Plasma jet	Ar/indirect	OH, singlet oxygen radicals, NO_2	Human (NOS2, NOS3 epithelial ovarian carcinoma)	→	↑	n.i.	[236]
Plasma jet	He, O_2/direct	O and OH	Human (BHP10-3 and TPC1 thyroid papillary carcinoma cell lines)	=	=	→	[73]
Plasma jet	Ar/indirect	H_2O_2	Human (SK-Mel-147 melanoma cell line)	=	=	-	[237]
Plasma jet	He/indirect	OH	Human (RPMI8226 and LP-1 MM cell line)	→	↑	→	[238]
Plasma jet	Ar/indirect	H_2O_2	Human (HEC-1 and GCIY endometrial and gastric cancer)	→	n.i.	n.i.	[239]
Plasma jet	Air/indirect	H_2O_2	Human (ES2, SKOV3, and WI-38 cell lines)	=	↑	→	[240]
Plasma jet	Air/direct and indirect	OH	Human (U87 MG brain cancer cells)	→	↑	n.i.	[241]
DBD plasma	Air/direct	-	Human melanoma cell line (ATCC A2058)	n.i.	↑	n.i.	[14]
DBD plasma	Air/direct	O_3, NO, HO_2, H_2O_2, OH, O	Human (MCF10A breast cancer)	=	↑	n.i.	[12]
DBD plasma	Air/direct and indirect	O_2^-, H_2O_2	Human (U87MG glioblastoma) and Human (HCT-116 colorectal carcinoma)	→	↑	n.i.	[15]
DBD plasma	Air/direct	-	Human (T98G brain cancer cell line)	→	↑	n.i.	[11]
DBD Plasma	Air/direct	-	Human (T98G malignant)	→	n.i.	n.i.	[13]
DBD plasma	Air/direct	H_2O_2 and NOx	Human (H460 lung cancer cell lines)	n.i.	↑	→	[10]
DBD plasma	Air/direct	H_2O_2, O_3, OH	Human (A549 lung adenocarcinoma epithelial cells)	→	↑	→	[110]
DBD plasma	Air/indirect (plasma-treated macrophages)	N_2	Human (U251MG and U87MG cells) cocultured with plasma-treated macrophages	→	↑	→	[178]

DBD: dielectric barrier discharge; HPMCs: human primary mesothelial cells; HEC-1: human endometrial carcinoma; PTL: plasma-treated liquid; ROS: reactive oxygen species; Ar: argon; He: helium; O_2: oxygen; N_2: nitrogen; NOx: nitric oxides; NO: nitric oxide; H_2O_2: hydrogen peroxide; HO_2: hyperoxide; O_3: ozone; O_2^-: superoxide; O: atomic oxygen; OH: hydroxyl radicals; NO_2: nitric dioxide; n.i.: not investigated.
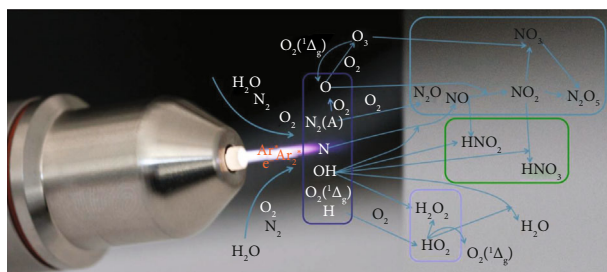
Figure 2: The atmospheric pressure argon plasma jet kINPen. The kINPen is a certified medical product in Europe and is regularly employed in dermatology. First initial trials in human cancer patients have been employed. Reproduced from [125].

in some tumors [143]. Also, PI3K/AKT activation has been shown to play a critical role in inhibiting p53. Indeed, plasma therapy downregulates the PI3K/AKT pathway and induces p53-mediated apoptosis and cancer cell death [97]. Nitric oxide (NO), a product of NOX activity in some tumor and innate immune cells, has pro- and anticancer effects. Depending on its intracellular level, low NO levels can promote tumor cell growth, while high NO levels usually cause the tumor cell to die [144]. Physical plasma treatment enhances intracellular NO levels in cancer cells, leading to MAPK p38 activation [144]. This plasma-derived NO was shown to significantly increase the presence of active caspases 3 and 8, confirming the role of plasma in activating caspase cascade and inducing cell death [144].

Moreover, activating protein-1 (AP-1) as a dimeric transcription factor, Fra-1, and c-Jun (highly expressed in invasive cancers) enhance cancer cells' migration and proliferation. Their phosphorylation is often regulated by MAP kinases such as JNK and p38 [145]. Plasma treatment can modulate the expression of AP-1 related transcription factors in cancer cells such as leukemia. It has been reported that JUND, a subfamily of Jun, can trigger phagocyte activation and cytokine secretion such as IL-8 in plasma-treated THP-1 cells [146].

Another pathway involved in cancer cell death is signal transducer and activator of transcription 3 (STAT3) signaling. STAT3 has a role in proliferation, survival, migration, invasion, and angiogenesis [147]. Therefore, targeting this pathway can be efficient in cancer cell inhibition. Plasma-treated osteosarcoma showed an initiation in the apoptotic pathway by reducing phosphorylation in the AMPK or STAT3 pathways, which had an inhibitory effect on cancer cells' growth [148]. Further experiments are needed to explain the effect of plasma on the STAT3 pathway in this area.

3.2. Autophagy. Autophagy is a process that occurs in all cells to eliminate dysfunctional or damaged cell organelles. The autophagic process plays a double-edged sword role in cancer progression [149]. Regulation of autophagy is mediated by tumor suppressor proteins such as LC3 and Beclin-1, leading to cancer cells' death. Various environmental stressors such as starvation, hypoxia, and growth factor deprivation can convert LC3 to LC3-II by conjugating a lipid

molecule called phosphatidylethanolamine (PE) to incorporate into the autophagosome membrane. Also, Beclin-1 is involved in the very early stage of autophagosome formation [149, 150]. Plasma-produced ROS increased autophagosome formation through activate ERK1/2 and induce LC3. This is presumably due to ROS stimulating the JNK pathway to phosphorylate Bcl-2 and releasing Beclin-1 associated with LC3 involved in autophagic cell death [151, 152]. Using PTL decreases the phosphorylated mTOR and AKT protein levels, which is critical for cancer cell viability. Besides, PTL increases LC3B expression in endometrial cancer cells. So PTL can inhibit cell viability while inducing autophagic cell death in endometrial cancer cells [153]. Moreover, PTL treatment increases the level of LC3A/B, p-ERK kinase, which is involved in Beclin-1-related autophagy. Indeed PTL induces apoptosis of pancreatic cancer cells through the ROS-dependent autophagy pathway [154]. As a result, JNK phosphorylates the c-Jun protein, which leads to the production of AP-1, which in turn promotes the expression of many genes such as Bax and FasL [151].

3.3. Pyroptosis. Pyroptosis is another type of programmed cell death mediated by the gasdermin family which includes GSDMA, GSDMB, GSDMC, and DFNA5/GSDME [155]. Pyroptosis has some characteristics of apoptosis as well as necrosis. Pyroptotic cells undergo nuclear condensation and chromatin DNA fragmentation, similar to apoptotic cells. In parallel, cell membrane pore formation, cell swelling, cell membrane rupture, and the release of proinflammatory mediators, including IL-1β, IL-18, ATP, and HMGB14 during pyroptosis, occur, sharing similar features to necrosis. Therefore, pyroptosis is an inflammatory form of cell death and has a bilateral role in tumor cell progression. Plasma treatment was shown to induce pyroptosis in cancer cells via ROS, promoting the phosphorylation of JNK and increasing cytoplasmic cytochrome C levels [156]. These pathways induced caspase 9 and caspase 3 activation by cleaving GSDME, which induces pyroptosis in cancer cells [157].

3.4. Ferroptosis. Ferroptosis is an iron-dependent and reactive oxygen species- (ROS-) reliant cell death distinct from apoptosis, classic necrosis, autophagy, and other forms of cell death at morphologic, biochemical, and genetic levels [158–160]. Ferroptosis is mainly based on cytological changes, including decreased mitochondrial cristae, a ruptured outer mitochondrial membrane, and a condensed mitochondrial membrane. Excessive membrane lipid peroxidation and the occurrence of oxidative stress cause cell abnormalities in ferroptosis [160]. This form of cell death can be induced by small molecules such as erastin and Ras-selective lethal small molecules (RSL). Also, iron and ROS accumulation, activation of the MAPK pathway, and release of arachidonic acid mediators trigger this type of cell death. However, xCT (SLC7A11) and glutathione peroxidase 4 (GPX4) are critical regulators of ferroptosis [159]. In addition, p53 might act as a rheostat, preventing ferroptosis under basal or low ROS stress while promoting ferroptosis in high oxidative stress conditions [161]. p53 represses the
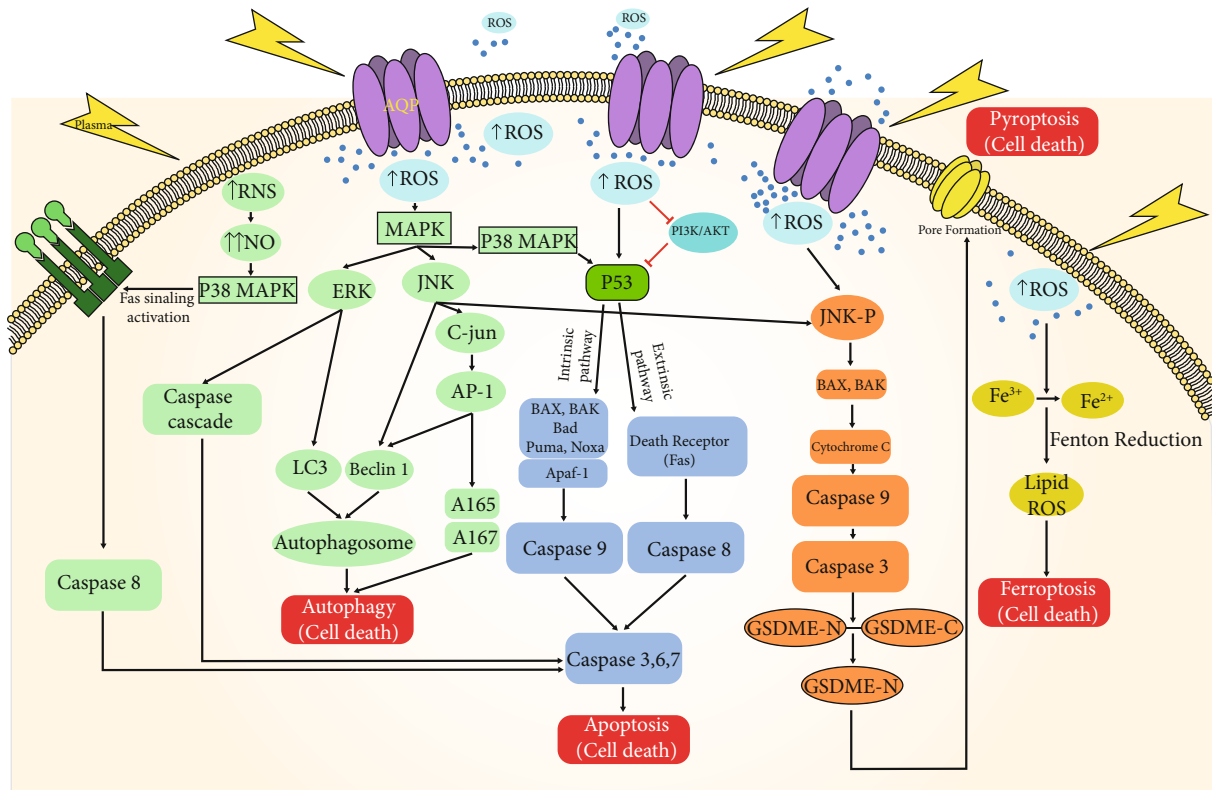
FIGURE 3: Model of three cell death signaling pathways in plasma-treated cancer cells. Plasma exposure increases aquaporin transporters in cancer cell membranes that allow the transport of H_2O_2 into the cells. Additionally, plasma treatment oxidizes cellular membranes, leading to cell death signaling. The excessive intracellular ROS contribute to the initiation of the cell death signaling (e.g., apoptosis, autophagy, pyroptosis, and ferroptosis) in cancer cells, partially through the activation of the MAPK pathway.

expression of SLC7A11, a vital component of the cystine/glutamate antiporter. Hence, p53 can inhibit cystine uptake and sensitizes cells to ferroptosis [162]. Moreover, another study implicated that plasma treatment increases cell death in the samples with lower xCT expression than samples with higher xCT expression [163].

Excess irons are the basis for ferroptosis. Interestingly, redox-active iron pools (i.e., Fe_2^+) via Fenton reaction can directly catalyze lipid peroxides, which cause ferroptosis [162]. Accordingly, it was hypothesized that plasma exposure could induce destruction of the shell of ferritin and simultaneous reduction from Fe(III) to Fe(II), resulting in Fenton reaction to cause oxidative cell death [164]. Also, plasma exposure may kill oral squamous carcinoma cells through ferroptosis, dependent on ample catalytic Fe(II) [165]. Further studies are required to demonstrate the effect of plasma therapy in cancer cell ferroptosis.

4. Immune Cell Activation Followed by Plasma Treatment

Plasma treatment can affect the activation of immune cells and their ability to provide effective antitumor immunity [166]. As currently known, antitumor immune responses consist of innate and adaptive immunity that interacts and acts on cancer cells by various means [104]. The innate immune system can both foster and limit cancer progres-

sion through direct interaction with tumor cells and the activation of other cells in the tumor microenvironment (TME) [167, 168].

4.1. Immunogenic Cancer Cell Death (ICD). Induction of cell death is an expected valuable outcome in plasma-treated cancer cells. It may also cause tumor cells to externalize or secrete many types of damage-associated molecular patterns (DAMPs), including ATP, high mobility group protein B1 (HMGB1), calreticulin (CRT), and heat shock protein 90 (HSP90), leading to the recruitment of immune cells [169]. CRT and ATP are critical for innate immune cell activation to uptake dead tumor cells to occur in the inflammatory context. This mediates an antitumor immune response by promoting DC maturation and antigen presentation, resulting in T-cell responses against tumor cells [170].

It has been demonstrated that nonthermal plasma treatment induces ICD by the generation of ROS [171] and other charged species [166] and increases the immunogenicity of tumor cells. Plasma upregulates immunogenic cell surface molecules such as MHC-I [172] and surface-exposed calreticulin (ecto-CRT). The latter acts as an *Eat Me* signal facilitating the recognition, engulfment, and processing of tumor cells by APCs. High levels of extracellular ATP following plasma therapy [173] act as a *Find Me* signal for the recruitment and activation of APCs in tumor microenvironments (Figure 4). Increased expression of CD45, a
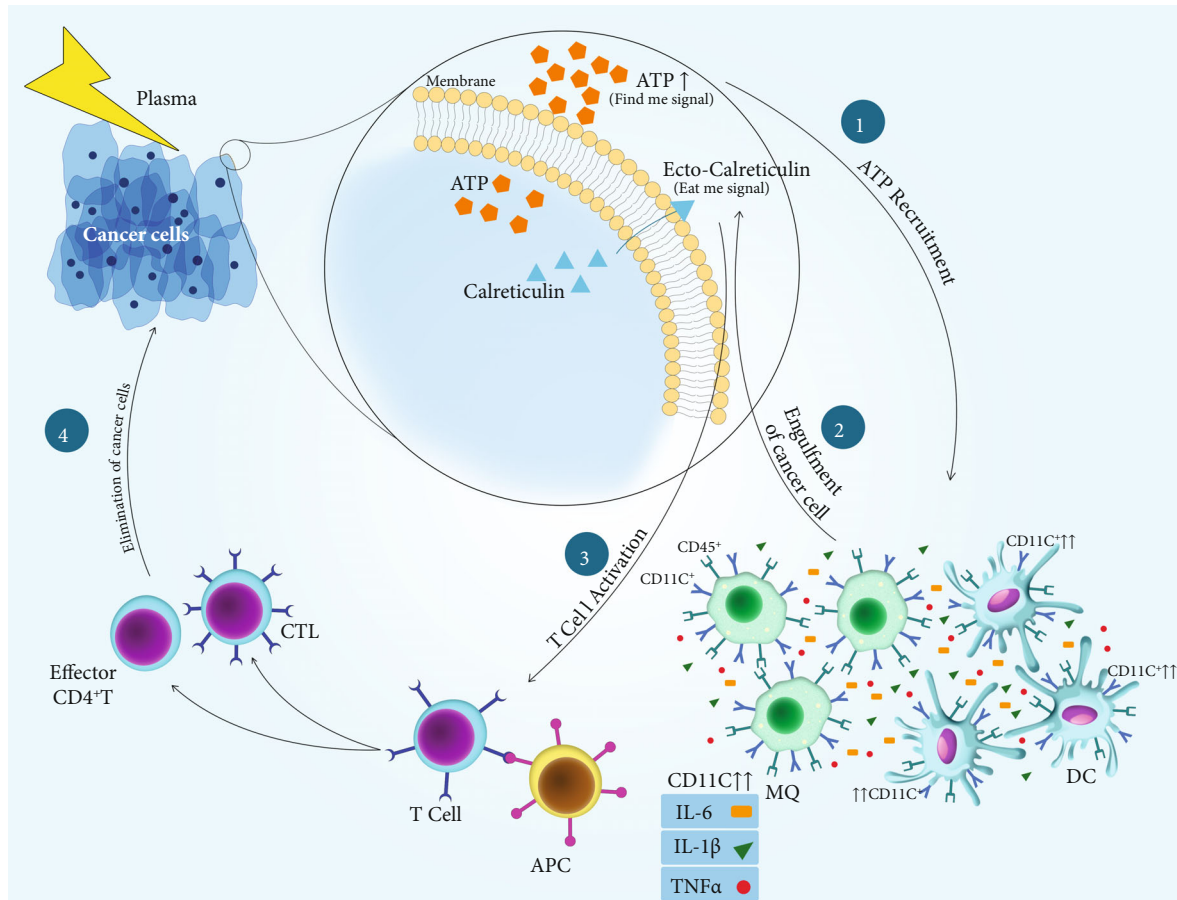
FIGURE 4: Model of plasma-induced immunogenic cell death in cancer cells. Plasma exposure leads to an increase in DAMP signaling (e.g., ATP and calreticulin), which (1) provides inflammatory stimuli for (2) promoting the processing of cancer cells by APCs. Consequently, (3) activated APCs promote the development and activation of (4) effector T-cells, capable of precisely and systemically eradicating cancer cells distant from the site of plasma treatment.

leukocyte marker, and CD11c, an APC marker, in the tumor microenvironment of BALB/c mice exposed to the plasma suggested additional leukocytes' recruitment, including APCs, presumably via DAMP signaling [174, 175].

4.2. Macrophages. Macrophages are critical immune cells in the TME and play a pivotal role in immune homeostasis. In response to a wide variety of environmental conditions, macrophages can differentiate and polarize into different phenotypes of M1 and M2. Tumor cells release and express molecules that hijack macrophages, supporting tumor growth [176]. In some cancer types, such as in the pancreas and brain, up to 50% of the cells are macrophages, continually supporting angiogenesis and phagocytose, silently and without inflammation, dead tumor cells. These are called tumor-associated (M2) macrophages. M2 macrophages express CD163 (scavenger receptor) and CD206 (mannose receptor) as anti-inflammatory markers and arginase. In addition, they release IL-10, TGF-β, and PGE2 and have a higher expression of PD-L1 that can repress antitumor T-cell responses. In turn, however, macrophages can also be licensed to kill tumor cells in the presence of proper proinflammatory stimuli, called proinflammatory (M1) macro-

phages [167]. M1 macrophages, as classically activated macrophages, express CD68, CD80, and CD86 costimulatory molecules and can control tumor progression by releasing TNF-α, IL-1β, IL-12, and iNOS. In the appropriate setting, some cytokines such as INF-γ can convert M2 macrophages to the M1 phenotype in the TME [177, 178]. Another study, however, found an M2 skewing of monocyte-derived macrophages with plasma treatment [179]. While plasma-treated monocytes generated ROS and were susceptible to plasma-induced cell death, as shown before [180], plasma-treated macrophages were not [178].

Using human monocytes, plasma treatment was shown to exacerbate M1 macrophages' cytotoxic activity against tumor cells. This was accompanied by an increased expression of CD86 (M1 marker) and low levels of CD163 and CD206 (M2 markers) on the THP-1-derived macrophages [178]. A similar increase of toxicity was made in A549 lung cancer cells during coculture with THP-1-derived macrophage *in vitro* [181]. Another study reported that the rate of cell death in a plasma-treated nasopharyngeal carcinoma cell line (CNE-1) cocultured with native (M0) macrophages (macrophages) was higher than the presence of macrophages, possibly due to the increase in extracellular ATP

[182]. In such coculture systems of cell-line-derived macrophages and tumor cells, elevated levels of TNF-α were also linked to the increased cytotoxicity observed [183]. TNF-α inhibits the tumor progression by activating CD8$^+$ T-cells and induces inflammatory cytokines such as IL-1, IL-6, IL-8, and cytotoxic factors like NO and ROS produced by macrophages and NK cells [184, 185]. Strikingly, recent evidence suggests that plasma treatment supports monocytes' differentiation process into macrophage-like cells. In contrast to the other studies, this was found in cell lines and using primary monocytes isolated from the human blood [186]. Moreover, plasma treatment of cancer cells and culturing monocytes in these DAMP-containing cancer cell supernatants promoted monocyte activation [123] and their cytotoxicity upon coculture with tumor cells [187].

4.3. *Cross-Talk between Dendritic Cells and T-Cells.* Activation of T-cells and the generation of long-lived memory cells in the tumor microenvironment (TME) are the critical target of cancer therapies. CD8$^+$ T-cells are the key player in the adaptive immune system for the direct killing of cancer cells via the release of cytotoxins, such as perforin and granzyme B. Effector CD4$^+$ T-cells in response to an antigenic tumor can secrete cytokines such as IFN-γ, TNF-α, and IL-2 that limit tumor progression and help the activation of CD8$^+$ CTL in a later stage [188]. Activation of adaptive T-cell responses depends on antigen recognition, so antigen-presenting cells (APC) such as DCs play a critical role in stimulating an adaptive immune response, especially cytotoxic CD8$^+$ T-cells and CD4$^+$ T-cells. DCs are innate immune cells known as professional APC and play a crucial role in linking innate and adaptive immune responses. DCs phagocytose, process, and present the tumor antigens to naïve antigen-specific CD4$^+$ or CD8$^+$ T-cells via major histocompatibility complexes (MHC) II and I, respectively. There are two major subsets of DC: classical/conventional DC (cDC) and plasmacytoid DC (pDC). pDC produces type I interferons, which are essential in the stimulation of anti-tumor immune response. They can also generate regulatory T-cells (T$_{reg}$) in the tumor microenvironment, which favors tumor progression. Depending on their subtype, cDCs present tumor antigens to prime both CD8$^+$ and CD4$^+$ T-cells [189].

It was previously speculated that plasma-derived ROS treatment of tumor cells initiates the cancer-immunity cycle by promoting ICD, DC maturation, and priming of antitumor T-cells in the draining lymph node [190, 191]. A recent *in vivo* report supports this claim by providing evidence for ICD and subsequent DC activation together with checkpoint therapy-augmented plasma and abscopal effects in a melanoma model [192]. Using the same cell type but a different type of plasma source, ICD and the subsequent protection from tumor growth in a preventive vaccination model were shown, and mechanistically, the effects were deduced to the action of short-lived ROS [193]. *In vitro*, plasma-treated PBS activity on tumor cells may be involved in DC maturation. Also, higher levels of TNF-α and IFN-γ and decreased levels of immunosuppressive cytokines such as TGF-β produced by DC cocultured with tumor cells exposed

to plasma-treated PBS an immune-enhancing effect of this approach [194]. Moreover, other in vitro studies suggested a distinct cytokine profile and modest but evident DC activation in the presence of directly plasma-killed tumor cells [74, 173]. It was recently reported for a translational research-relevant plasma jet accredited as a medical device in Europe that plasma treatment not only induced ICD in melanoma cells that were successfully used as a preventive vaccine in mice but also was accompanied by an increased influx of CD4$^+$ and CD8$^+$ T-cells in the TME along with their increased activation and memory phenotype [195]. Moreover, increased efficacy of plasma treatment was demonstrated when combined with a toll-like-receptor (TLR) agonist activating DCs and superior efficacy of one plasma-derived ROS cocktail rich in atomic oxygen over other ROS cocktails. These findings corroborated previous reports on increased T-cell infiltrates in plasma-treated syngeneic melanomas *in vivo* [196, 197]. In addition, it was recently shown in vitro and in vivo that the immunogenicity plasma-treated protein can confer immunoprotection in mice against melanoma growth [198], giving rise to entire novel concepts in plasma oncotherapy [199].

5. Clinical Trials and Case Series on Plasma Therapy in Medicine including Cancer

In vivo and *in vitro* studies in plasma medicine have shown promising results, encouraging clinicians to evaluate plasma therapy in clinical settings across several types of diseases (Table 2). Since there is only a few reports on plasma anti-cancer studies, other clinical applications are described as well in the following. For each plasma device, such studies must demonstrate safe plasma treatment in the first clinical step.

5.1. *Case Series.* Several case series and reports have reported on the use of different plasma devices in humans to treat disease. In Greifswald, Germany, clinicians investigated the clinical application of cold physical plasma treatment in 21 patients with advanced head and neck cancer in a palliative setting. This study was aimed at evaluating tumor surface changes and the ratio of apoptotic cancer cells, respectively, in group I and group II. Among the 12 patients in group I, there was no enhanced or stimulated tumor growth under two weeks after cold physical plasma treatment. The result of 9 patients in group II showed more frequent apoptotic cells in tissue areas treated by plasma than in untreated areas [120, 121, 200].

Moreover, German clinicians used a plasma device to treat six patients suffering from wound healing disturbances after maxillofacial surgical procedures. The size and localization of the defect were different among all cases, so plasma therapy was initiated at various postsurgery times, ranging from 2 to 42 weeks. The primary outcome showed complete healing, defined as wound closure and the absence of any signs of infection. Besides, the secondary outcomes showed complete remission after 48 weeks of plasma treatment. In that study, several therapeutic properties of plasma, including antibacterial effect, stimulation of tissue

TABLE 2: Clinical case series and trials on plasma therapy in medicine.

Study type	Year	# of pat.	Condition	Plasma source/certification	Outcome with plasma treatment	Allocation	Ref.
Case series	2015	11	Infected wounds	kINPen MED (certified)	Complete healing of the wounds	N/A	[242]
Case series	2016	21	Advanced head and neck cancer	kINPen MED (certified)	No enhanced tumor growth and more apoptotic cell kill	N/A	[121]
Case report	2016	1	Percutaneous driveline infection	kINPen MED (certified)	Completed regression of local infection	N/A	[243]
Case series	2016	4	Nonhealing wounds	kINPen MED (certified)	Completed wound repair	N/A	[202]
Case series	2017	6	Nonhealing wounds	PlasmaDerm (certified)	Completed remission	N/A	[201]
Case series	2017	5	Actinic keratosis	FE-DBD (not certified)	17 lesions: 9 showed full regression, 3 significantly improved, 5 showed no change	N/A	[203]
Case series	2018	2	Warts	FE-DBD (not certified)	Patient 1: wart cleared; patient 2: wart improved but not cleared	N/A	[205]
Case series	2018	4	Therapy-resistant corneal infections	kINPen MED (certified)	Significantly elimination of pathogens	N/A	[244]
Case series	2018	7	Actinic keratosis	SteriPlas (certified)	Overall decline of actinic keratosis characteristics	N/A	[204]
Case series	2020	5	Warts	FE-DBD (not certified)	4 warts cleared, 1 did not change	N/A	[206]
Clinical trial	2011-2012	14	Chronic venous leg ulcers	PlasmaDerm (certified)	Significantly improved ulcer size-reduction	Random	[245]
Clinical trial	2016-2020	100	Actinic keratosis, acne, verruca plana	Plasma to treat skin lesions and acne	Successful cure in most of them	Nonrandom	[210]
Clinical trial	2017-2020	55	Facial wrinkles, rhytides	J-Plasma He-jet (FDA approved)	Significant improvement, no serious adverse events	N/A	[246]
Clinical trial	2017-2020	170	Cervical intraepithelial neoplasia	Plasma treatment	Pathological remission and HPV reduction	Nonrandom	[208]
Clinical trial	2017-2018	25	Intact skin, experimental contaminant added to patient skin	Plasma	Safety, efficacy, and efficiency of plasma for burn wound treatment	Nonrandom	[247]
Clinical trial	2017-2019	5	Onychomycosis of toenail	Plasma treatment	Mycological cure, evident nail growth	N/A	[248]
Clinical trial	2019	100	Wound healing	Cold argon Plasma	Ongoing, no results have been yet reported	Random	[249]
Clinical trial	2020	40	Androgenetic alopecia	Plasma-treated aqueous-alcohol solution	Ongoing, no results have been yet reported	N/A	[211]

repair, regeneration, neovascularization, and skin microcirculation, were considered. Based on the results, plasma is a promising approach to treat chronic healing disorders of wounds resulting from CMF surgery [201]. Another study by the same authors evaluated the effect of plasma therapy on wound healing disorder following the radial forearm free flap (RFFF) procedure. The endpoint of this therapy showed the successful remission of wounds. It was concluded that plasma treatment possibly is a new therapeutic modality to avoid repeated surgery [202].

Actinic keratosis (AK) was another skin disease that has been investigated to be treated using plasma. In one study, 17 lesions were plasma-treated and followed up for one month without interval evaluation. Three lesions improved significantly, and the condition of five lesions did not worsen. Interestingly, none of the patients experienced side effects, such as pain and inflammation during treatment [203]. All patients showed a decline in AK characteristics such as erythema, scaling, crusts, and thickness, and in some cases, the total lesion number was decreased [204].

The efficacy of plasma therapy has also been investigated in the treatment of wart lesions. The results of one study revealed that all lesions of the first patient faded after 2 to 3 plasma exposure cycles. In a second patient, however, the lesions were improved but did not disappear completely [205]. The same authors demonstrated that plasma exposure could also be an effective modality for wart treatment in pediatric patients [206]. The plasma device used in this study is currently not approved by the FDA. Nevertheless, plasma treatment was suggested to induce apoptosis in malignant cells *ex vivo* [207], so it seems likely that this also holds for premalignant cells. However, clinical data are insufficient to confirm the plasma mechanism in improving the wart [206].

Overall, plasma therapy is a novel promising therapeutic tool in managing tumor cells and the recovery of infection, postoperative wound healing, actinic keratosis, and wart disorders.

5.2. Clinical Trials. The first registered clinical trial on plasma cancer treatment was initiated in Tübingen, Germany, in 2017 to manage cervical intraepithelial neoplasia. Approximately 170 patients were planned to participate in the study. Final results, however, were not reported yet apart from the observation that pathological remission and HPV reduction were secondary outcomes [208]. In 2019, a U.S. company used plasma to treat 20 patients with breast and lung cancer after standard treatments, including chemotherapy, radiation, and surgery. Preliminary results suggested a preferential targeting of tumor cells, but further confirmation is awaited. This technology was the first to be approved in an FDA phase I clinical trial in August 2019 [209]. Moreover, the Skin Center Dermatology Group investigated the effect of plasma to treat 100 subjects with skin disorders. This study enrolled 100 participants suffering from actinic keratosis, acne, or verruca plana. The results of the plasma treatment were successful in most cases and showed no side effects. However, this study has not yet been completed and final results are awaited

[210]. A recent clinical study examined the effect of plasma in the treatment of hair loss. This study started on June 8, 2020, and is currently recruiting. However, no results have yet been reported [211].

6. Side Effects of Plasma Treatment

Any medical treatment has to meet both efficacy and safety requirements. While many studies had investigated the efficacy of plasma treatment in many types of diseases, studies on their safe applications are less frequent. The main agents of biomedical plasma effects, ROS, are also produced during physiological processes in the body. Hence, ROS are not toxic or dangerous *per se*, but their exacerbated concentration or application frequency might be. To understand this from a practical point of view, it needs to be mentioned that H_2O_2 at molar concentrations (e.g., 3% equals 1M) is used for wound disinfection and dentistry. For comparison, to reach the concentration of 1M H_2O_2 in 1 ml of a saline solution, this would translate to a plasma treatment time of 30.000 min (or 500 h) for an accredited argon plasma jet [212]. For *in vitro*, *in vivo* (mice), and patient treatment with this jet, typical treatment times are between 5 s and 3 min [213, 214]. This calculation emphasizes that the ROS doses generated with plasma treatment range from inducing ROS-related (cell death) signaling rather than overloading the cells with necrotic doses of ROS and would account for most medically suited plasma devices currently in use.

Nevertheless, several safety studies have been performed, especially for the well-characterized kINPen MED [215]. This plasma jet does not generate mutagenic events, as shown using the OECD-accredited HRPT test and the cytokinesis-block micronucleus assay [216, 217]. Notably, the phosphorylation of the histone 2A-X seems a secondary event due to plasma-induced cell death rather than direct DNA damage [218]. *In vivo*, no formation of micronuclei was observed [219]. In a wound-healing model in mice, the animals were plasma-treated for seven days using the kINPen, and one year later, the animals were investigated using MR-imaging, CT-scanning, histopathology, and tumor marker analysis in the blood and tissues [220]. No tumor formation or any other detrimental long-term effect was observed. Concerning mucosal tissue in mice, plasma exposure caused mild inflammation, and the epithelial layers healed without showing signs of hyperplasia or dysplasia [221]. Side effects in patients were recently summarized [215] and currently extended to the first 5-year follow-up in plasma-treated wounds [222]. In patients suffering from advanced squamous cell carcinoma of the head and neck, some side effects such as bad taste, fatigue, and bleeding were seen in some cases after plasma treatment. However, all of the side effects were mild to moderate and not life-threatening [223].

For plasma devices other than the kINPen MED, safety has been implied as well, albeit less systemically. For instance, this accounts for the PlasmaDerm and SteriPlas devices [224–227], and the efficacy and safety of plasma wound treatment have been reviewed in a meta-analysis recently [228]. Moreover, the number of clinical trials

indicates a preevaluation (e.g., CE mark in Europe) of the safety across many other plasma sources as a prerequisite to clinical use. In Europe, several medical plasma device types have been employed over the last seven years in over 100 clinical centers and thousands of applications already without any note of severe side effects. It is important to note that there are many plasma devices for cosmetic application on several international markets, but their safety has been addressed to a minimal extent only in most cases. Besides, several plasma devices or device modifications that are not in clinical use yet but are aimed for such application have undergone in vitro or in vivo risk assessments already [229–234]. A DIN spec has been published in Germany that suggests several assays that should be performed for a standard characterization of medical plasma devices [235]. A DIN spec is a legal norm in Germany that describes detailed methods and assays to characterize a product, process, or device based on industry consensus. Current efforts are aimed at generating a respective ISO-norm for the safety of plasma devices that would harmonize risk assessments to ensure the safety and efficacy of plasma treatment of human diseases.

7. Conclusion

This review summarizes the recent advances in understanding plasma therapy in medicine, emphasizing cancer treatment. Studies of plasma therapy in the clinical setting have only begun, but promising results were reported so far. Cold physical plasma alters many features of tumor cells, ultimately leading to their demise. Plasma also promotes inflammatory signaling pathways that can augment antitumor responses by innate and adaptive immune cells. Further studies are required to demonstrate the effect of plasma on memory cells' generation against tumor cells. Because plasma releases tumor-associated antigens and facilitates antigen processing, using a combination of plasma and immunotherapy regimens, such as immune checkpoint inhibitors, possibly enhances antitumor immune responses.

Conflicts of Interest

The authors declare that no conflict of interest exists with the publication of this article.

Authors' Contributions

All authors prepared the draft and finalized the manuscript. Alireza Rafiei and Sander Bekeschus contributed equally to this work as last authors.

References

[1] K. D. Weltmann, E. Kindel, T. von Woedtke, M. Hähnel, M. Stieber, and R. Brandenburg, "Atmospheric-pressure plasma sources: prospective tools for plasma medicine," *Pure and Applied Chemistry*, vol. 82, no. 6, pp. 1223–1237, 2010.

[2] A. Privat-Maldonado, A. Schmidt, A. Lin et al., "Ros from physical plasmas: redox chemistry for biomedical therapy," *Oxidative Medicine and Cellular Longevity*, vol. 2019, Article ID 9062098, 29 pages, 2019.

[3] A. Shashurin, M. Keidar, S. Bronnikov, R. A. Jurjus, and M. A. Stepp, "Living tissue under treatment of cold plasma atmospheric jet," *Applied Physics Letters*, vol. 93, no. 18, p. 181501, 2008.

[4] H. J. Lee, C. H. Shon, Y. S. Kim, S. Kim, G. C. Kim, and M. G. Kong, "Degradation of adhesion molecules of g361 melanoma cells by a non-thermal atmospheric pressure microplasma," *New Journal of Physics*, vol. 11, no. 11, article 115026, 2009.

[5] J. Y. Kim, Y. Wei, J. Li et al., "Single-cell-level microplasma cancer therapy," *Small*, vol. 7, no. 16, pp. 2291–2295, 2011.

[6] H. J. Ahn, K. I. Kim, G. Kim, E. Moon, S. S. Yang, and J. S. Lee, "Atmospheric-pressure plasma jet induces apoptosis involving mitochondria via generation of free radicals," *PLoS One*, vol. 6, no. 11, article e28154, 2011.

[7] S. Mashayekh, H. Rajaee, M. Akhlaghi, B. Shokri, and Z. M. Hassan, "Atmospheric-pressure plasma jet characterization and applications on melanoma cancer treatment (b/16-f10)," *Physics of Plasmas*, vol. 22, no. 9, article 093508, 2015.

[8] K. Kim, J. D. Choi, Y. C. Hong et al., "Atmospheric-pressure plasma-jet from micronozzle array and its biological effects on living cells for cancer therapy," *Applied Physics Letters*, vol. 98, no. 7, article 073701, 2011.

[9] M. Kuchenbecker, N. Bibinov, A. Kaemlimg, D. Wandke, P. Awakowicz, and W. Viöl, "Characterization of dbd plasma source for biomedical applications," *Journal of Physics D: Applied Physics*, vol. 42, no. 4, article 045212, 2009.

[10] K. Panngom, K. Y. Baik, M. K. Nam, J. H. Han, H. Rhim, and E. H. Choi, "Preferential killing of human lung cancer cell lines with mitochondrial dysfunction by nonthermal dielectric barrier discharge plasma," *Cell Death & Disease*, vol. 4, no. 5, article e642, 2013.

[11] N. K. Kaushik, H. Uhm, and E. H. Choi, "Micronucleus formation induced by dielectric barrier discharge plasma exposure in brain cancer cells," *Applied Physics Letters*, vol. 100, 2012.

[12] S. Kalghatgi, C. M. Kelly, E. Cerchar et al., "Effects of nonthermal plasma on mammalian cells," *PLoS One*, vol. 6, article e16270, 2011.

[13] N. K. Kaushik, P. Attri, N. Kaushik, and E. H. Choi, "A preliminary study of the effect of dbd plasma and osmolytes on t98g brain cancer and hek non-malignant cells," *Molecules*, vol. 18, pp. 4917–4928, 2013.

[14] G. Fridman, A. Shereshevsky, M. M. Jost et al., "Floating electrode dielectric barrier discharge plasma in air promoting apoptotic behavior in melanoma skin cancer cell lines," *Plasma Chemistry and Plasma Processing*, vol. 27, pp. 163–176, 2007.

[15] M. Vandamme, E. Robert, S. Lerondel et al., "Ros implication in a new antitumor strategy based on non-thermal plasma," *International Journal of Cancer*, vol. 130, pp. 2185–2194, 2012.

[16] M. Leduc, S. Coulombe, and R. L. Leask, "Atmospheric pressure plasma jet deposition of patterned polymer films for cell culture applications," *IEEE Transactions on Plasma Science*, vol. 37, pp. 927–933, 2009.

[17] S. Coulombe, V. Léveillé, S. Yonson, and R. L. Leask, "Miniature atmospheric pressure glow discharge torch (APGD-t) for local biomedical applications," *Pure and Applied Chemistry*, vol. 78, pp. 1147–1156, 2006.

[18] Y. Duan, C. Huang, and Q. S. Yu, "Cold plasma brush generated at atmospheric pressure," *The Review of Scientific Instruments*, vol. 78, article 015104, 2007.

[19] J. F. Kolb, A. A. H. Mohamed, R. O. Price et al., "Cold atmospheric pressure air plasma jet for medical applications," *Applied Physics Letters*, vol. 92, article 241501, 2008.

[20] N. Y. Babaeva, G. V. Naidis, D. V. Tereshonok et al., "Production of active species in an argon microwave plasma torch," *Journal of Physics D: Applied Physics*, vol. 51, 2018.

[21] L. Brulle, M. Vandamme, D. Ries et al., "Effects of a non thermal plasma treatment alone or in combination with gemcitabine in a MIA PaCa2-luc orthotopic pancreatic carcinoma model," *PLoS One*, vol. 7, 2012.

[22] H.-R. Metelmann, T. von Woedtke, and K.-D. Weltmann, *Comprehensive Clinical Plasma Medicine*, 2018.

[23] N. D. Almeida, A. L. Klein, E. A. Hogan et al., "Cold atmospheric plasma as an adjunct to immunotherapy for glioblastoma multiforme," *World Neurosurgery*, vol. 130, pp. 369–376, 2019.

[24] Z. Chen, H. Simonyan, X. Cheng et al., "A novel micro cold atmospheric plasma device for glioblastoma both in vitro and in vivo," *Cancers (Basel)*, vol. 9, 2017.

[25] M. Adhikari, B. Adhikari, A. Adhikari et al., "Cold atmospheric plasma as a novel therapeutic tool for the treatment of brain cancer," *Current Pharmaceutical Design*, vol. 26, pp. 2195–2206, 2020.

[26] G. Pasqual-Melo, R. K. Gandhirajan, I. Stoffels, and S. Bekeschus, "Targeting malignant melanoma with physical plasmas," *Clinical Plasma Medicine*, vol. 10, pp. 1–8, 2018.

[27] C. Schneider, L. Gebhardt, S. Arndt et al., "Acidification is an essential process of cold atmospheric plasma and promotes the anti-cancer effect on malignant melanoma cells," *Cancers (Basel)*, vol. 11, 2019.

[28] D. K. Yadav, M. Adhikari, S. Kumar et al., "Cold atmospheric plasma generated reactive species aided inhibitory effects on human melanoma cells: an in vitro and in silico study," *Scientific Reports*, vol. 10, p. 3396, 2020.

[29] A. Rafiei, F. Sohbatzadeh, S. Hadavi, S. Bekeschus, M. Alimohammadi, and R. Valadan, "Inhibition of murine melanoma tumor growth in vitro and in vivo using an argon-based plasma jet," *Clinical Plasma Medicine*, vol. 19-20, 2020.

[30] L. Xiang, X. Xu, S. Zhang, D. Cai, and X. Dai, "Cold atmospheric plasma conveys selectivity on triple negative breast cancer cells both in vitro and in vivo," *Free Radical Biology & Medicine*, vol. 124, pp. 205–213, 2018.

[31] S. Park, H. Kim, H. W. Ji et al., "Cold atmospheric plasma restores paclitaxel sensitivity to paclitaxel-resistant breast cancer cells by reversing expression of resistance-related genes," *Cancers (Basel)*, vol. 11, p. 2011, 2019.

[32] S. Bekeschus, M. Lippert, K. Diepold, G. Chiosis, T. Seufferlein, and N. Azoitei, "Physical plasma-triggered ros induces tumor cell death upon cleavage of hsp90 chaperone," *Scientific Reports*, vol. 9, p. 4112, 2019.

[33] M. Wang, B. Holmes, X. Cheng, W. Zhu, M. Keidar, and L. G. Zhang, "Cold atmospheric plasma for selectively ablating

[34] Z. Yazdani, P. Mehrabanjoubani, P. Biparva, and A. Rafiei, "Cytotoxicity effect of cold atmospheric plasma on melanoma (B16-F10), breast (MCF-7) and lung (A549) cancer cell lines compared with normal cells," *Journal of Mazandaran University of Medical Sciences*, vol. 30, pp. 38–48, 2020.

[35] C. H. Kim, J. H. Bahn, S. H. Lee et al., "Induction of cell growth arrest by atmospheric non-thermal plasma in colorectal cancer cells," *Journal of Biotechnology*, vol. 150, pp. 530–538, 2010.

[36] C. H. Kim, S. Kwon, J. H. Bahn et al., "Effects of atmospheric nonthermal plasma on invasion of colorectal cancer cells," *Applied Physics Letters*, vol. 96, article 243701, 2010.

[37] S. Bekeschus, E. Freund, K. Wende, R. K. Gandhirajan, and A. Schmidt, "Hmox1 upregulation is a mutual marker in human tumor cells exposed to physical plasma-derived oxidants," *Antioxidants (Basel)*, vol. 7, 2018.

[38] H. M. Joh, J. Y. Choi, S. J. Kim, T. H. Chung, and T. H. Kang, "Effect of additive oxygen gas on cellular response of lung cancer cells induced by atmospheric pressure helium plasma jet," *Scientific Reports*, vol. 4, p. 6638, 2014.

[39] Y. J. Cheng, C. K. Lin, C. Y. Chen et al., "Plasma-activated medium as adjuvant therapy for lung cancer with malignant pleural effusion," *Scientific Reports*, vol. 10, p. 18154, 2020.

[40] E. A. Golubitskaya, O. S. Troitskaya, E. V. Yelak et al., "Cold physical plasma decreases the viability of lung adenocarcinoma cells," *Acta Naturae*, vol. 11, pp. 16–19, 2019.

[41] L. Feil, A. Koch, R. Utz et al., "Cancer-selective treatment of cancerous and non-cancerous human cervical cell models by a non-thermally operated electrosurgical argon plasma device," *Cancers (Basel)*, vol. 12, 2020.

[42] M. A. Jezeh, T. Tayebi, M. R. Khani, H. Niknejad, and B. Shokri, "Direct cold atmospheric plasma and plasma-activated medium effects on breast and cervix cancer cells," *Plasma Processes and Polymers*, vol. 17, no. 11, 2020.

[43] B. S. Kwon, E. H. Choi, B. Chang, J. H. Choi, K. S. Kim, and H. K. Park, "Selective cytotoxic effect of non-thermal micro-dbd plasma," *Physical Biology*, vol. 13, article 056001, 2016.

[44] E. Turrini, R. Laurita, E. Simoncelli et al., "Plasma-activated medium as an innovative anticancer strategy: insight into its cellular and molecular impact on in vitro leukemia cells," *Plasma Processes and Polymers*, vol. 17, no. 10, p. 2000007, 2020.

[45] S. Bekeschus, K. Wende, M. M. Hefny et al., "Oxygen atoms are critical in rendering thp-1 leukaemia cells susceptible to cold physical plasma-induced apoptosis," *Scientific Reports*, vol. 7, p. 2791, 2017.

[46] E. Turrini, R. Laurita, A. Stancampiano et al., "Cold atmospheric plasma induces apoptosis and oxidative stress pathway regulation in t-lymphoblastoid leukemia cells," *Oxidative Medicine and Cellular Longevity*, vol. 2017, Article ID 4271065, 13 pages, 2017.

[47] S. Bekeschus, A. Schmidt, L. Bethge et al., "Redox stimulation of human THP-1 monocytes in response to cold physical plasma," *Oxidative Medicine and Cellular Longevity*, vol. 2016, Article ID 5910695, 11 pages, 2016.

[48] M. Thiyagarajan, H. Anderson, and X. F. Gonzales, "Induction of apoptosis in human myeloid leukemia cells by remote

exposure of resistive barrier cold plasma," *Biotechnology and Bioengineering*, vol. 111, pp. 565–574, 2014.

[49] A. Azzariti, R. M. Iacobazzi, R. Di Fonte et al., "Plasma-activated medium triggers cell death and the presentation of immune activating danger signals in melanoma and pancreatic cancer cells," *Scientific Reports*, vol. 9, p. 4099, 2019.

[50] K. R. Liedtke, S. Diedrich, O. Pati et al., "Cold physical plasma selectively elicits apoptosis in murine pancreatic cancer cells in vitro and in ovo," *Anticancer Research*, vol. 38, pp. 5655–5663, 2018.

[51] Z. Chen, L. Lin, E. Gjika, X. Cheng, J. Canady, and M. Keidar, "Selective treatment of pancreatic cancer cells by plasma-activated saline solutions," *IEEE Transactions on Radiation and Plasma Medical Sciences*, vol. 2, pp. 116–120, 2018.

[52] S. Bekeschus, E. Freund, C. Spadola et al., "Risk assessment of kINPen plasma treatment of four human pancreatic cancer cell lines with respect to metastasis," *Cancers (Basel)*, vol. 11, p. 1237, 2019.

[53] Y. Sato, S. Yamada, S. Takeda et al., "Effect of plasma-activated lactated Ringer's solution on pancreatic cancer cells in vitro and in vivo," *Annals of Surgical Oncology*, vol. 25, pp. 299–307, 2018.

[54] R. Verloy, A. Privat-Maldonado, E. Smits, and A. Bogaerts, "Cold atmospheric plasma treatment for pancreatic cancer-the importance of pancreatic stellate cells," *Cancers (Basel)*, vol. 12, 2020.

[55] B. Smolkova, M. Lunova, A. Lynnyk et al., "Non-thermal plasma, as a new physicochemical source, to induce redox imbalance and subsequent cell death in liver cancer cell lines," *Cellular Physiology and Biochemistry*, vol. 52, pp. 119–140, 2019.

[56] X. H. Zhang, M. J. Li, R. L. Zhou, K. C. Feng, and S. Z. Yang, "Ablation of liver cancer cells in vitro by a plasma needle," *Applied Physics Letters*, vol. 93, 2008.

[57] J. Duan, X. Lu, and G. He, "The selective effect of plasma activated medium in an in vitro co-culture of liver cancer and normal cells," *Journal of Applied Physics*, vol. 121, article 013302, 2017.

[58] J. Berner, C. Seebauer, S. K. Sagwal et al., "Medical gas plasma treatment in head and neck cancer-challenges and opportunities," *Applied Sciences*, vol. 10, 2020.

[59] C. Welz, S. Emmert, M. Canis et al., "Cold atmospheric plasma: a promising complementary therapy for squamous head and neck cancer," *PLoS One*, vol. 10, article e0141827, 2015.

[60] R. Guerrero-Preston, T. Ogawa, M. Uemura et al., "Cold atmospheric plasma treatment selectively targets head and neck squamous cell carcinoma cells," *International Journal of Molecular Medicine*, vol. 34, pp. 941–946, 2014.

[61] S. Galadari, A. Rahman, S. Pallichankandy, and F. Thayyullathil, "Reactive oxygen species and cancer paradox: to promote or to suppress?," *Free Radical Biology & Medicine*, vol. 104, pp. 144–164, 2017.

[62] J. N. Moloney and T. G. Cotter, "Ros signalling in the biology of cancer," *Seminars in Cell & Developmental Biology*, vol. 80, pp. 50–64, 2018.

[63] A. Glasauer and N. S. Chandel, "Targeting antioxidants for cancer therapy," *Biochemical Pharmacology*, vol. 92, pp. 90–101, 2014.

[64] H. Kong and N. S. Chandel, "Regulation of redox balance in cancer and T cells," *The Journal of Biological Chemistry*, vol. 293, pp. 7499–7507, 2018.

[65] D. Trachootham, J. Alexandre, and P. Huang, "Targeting cancer cells by ros-mediated mechanisms: a radical therapeutic approach?," *Nature Reviews Drug Discovery*, vol. 8, pp. 579–591, 2009.

[66] K. Wende, T. von Woedtke, K. D. Weltmann, and S. Bekeschus, "Chemistry and biochemistry of cold physical plasma derived reactive species in liquids," *Biological Chemistry*, vol. 400, pp. 19–38, 2018.

[67] D. Yan, A. Talbot, N. Nourmohammadi, J. H. Sherman, X. Cheng, and M. Keidar, "Toward understanding the selective anticancer capacity of cold atmospheric plasma–a model based on aquaporins (review)," *Biointerphases*, vol. 10, article 040801, 2015.

[68] M. Yusupov, D. Y. Yan, R. M. Cordeiro, and A. Bogaerts, "Atomic scale simulation of H_2O_2 permeation through aquaporin: toward the understanding of plasma cancer treatment," *Journal of Physics D: Applied Physics*, vol. 51, 2018.

[69] J. Van der Paal, C. Verheyen, E. C. Neyts, and A. Bogaerts, "Hampering effect of cholesterol on the permeation of reactive oxygen species through phospholipids bilayer: possible explanation for plasma cancer selectivity," *Scientific Reports*, vol. 7, p. 39526, 2017.

[70] J. Van der Paal, E. C. Neyts, C. C. W. Verlackt, and A. Bogaerts, "Effect of lipid peroxidation on membrane permeability of cancer and normal cells subjected to oxidative stress," *Chemical Science*, vol. 7, pp. 489–498, 2016.

[71] C. M. Wolff, J. F. Kolb, K. D. Weltmann, T. von Woedtke, and S. Bekeschus, "Combination treatment with cold physical plasma and pulsed electric fields augments ros production and cytotoxicity in lymphoma," *Cancers (Basel)*, vol. 12, p. 845, 2020.

[72] L. Bundscherer, S. Nagel, S. Hasse et al., "Non-thermal plasma treatment induces mapk signaling in human monocytes," *Open Chemistry*, vol. 13, pp. 606–613, 2015.

[73] J. W. Chang, S. U. Kang, Y. S. Shin et al., "Non-thermal atmospheric pressure plasma inhibits thyroid papillary cancer cell invasion via cytoskeletal modulation, altered MMP-2/-9/uPA activity," *PLoS One*, vol. 9, article e92198, 2014.

[74] G. Pasqual-Melo, S. K. Sagwal, E. Freund et al., "Combination of gas plasma and radiotherapy has immunostimulatory potential and additive toxicity in murine melanoma cells in vitro," *International Journal of Molecular Sciences*, vol. 21, p. 1379, 2020.

[75] L. Lin, L. Wang, Y. Liu, C. Xu, Y. Tu, and J. Zhou, "Nonthermal plasma inhibits tumor growth and proliferation and enhances the sensitivity to radiation in vitro and in vivo," *Oncology Reports*, vol. 40, pp. 3405–3415, 2018.

[76] J. Lafontaine, J. S. Boisvert, A. Glory, S. Coulombe, and P. Wong, "Synergy between non-thermal plasma with radiation therapy and olaparib in a panel of breast cancer cell lines," *Cancers (Basel)*, vol. 12, 2020.

[77] C. M. Wolff, A. Steuer, I. Stoffels et al., "Combination of cold plasma and pulsed electric fields – a rationale for cancer patients in palliative care," *Clinical Plasma Medicine*, vol. 16, 2019.

[78] E. Griseti, J. Kolosnjaj-Tabi, L. Gibot et al., "Pulsed electric field treatment enhances the cytotoxicity of plasma-

activated liquids in a three-dimensional human colorectal cancer cell model," *Scientific Reports*, vol. 9, p. 7583, 2019.

[79] R. Moniruzzaman, M. U. Rehman, Q. L. Zhao et al., "Cold atmospheric helium plasma causes synergistic enhancement in cell death with hyperthermia and an additive enhancement with radiation," *Scientific Reports*, vol. 7, p. 11659, 2017.

[80] M. Wang, B. M. Geilich, M. Keidar, and T. J. Webster, "Killing malignant melanoma cells with protoporphyrin ix-loaded polymersome-mediated photodynamic therapy and cold atmospheric plasma," *International Journal of Nanomedicine*, vol. 12, pp. 4117–4127, 2017.

[81] C. Y. Chen, Y. C. Cheng, and Y. J. Cheng, "Synergistic effects of plasma-activated medium and chemotherapeutic drugs in cancer treatment," *Journal of Physics D: Applied Physics*, vol. 51, 2018.

[82] G. Daeschlein, A. Hillmann, D. Gumbel et al., "Enhanced anticancer efficacy by drug chemotherapy and cold atmospheric plasma against melanoma and glioblastoma cell lines in vitro," *IEEE Transactions on Radiation and Plasma Medical Sciences*, vol. 2, pp. 153–159, 2018.

[83] K. R. Liedtke, E. Freund, M. Hermes et al., "Gas plasma-conditioned Ringer's lactate enhances the cytotoxic activity of cisplatin and gemcitabine in pancreatic cancer in vitro and in ovo," *Cancers (Basel)*, vol. 12, p. 123, 2020.

[84] G. E. Conway, A. Casey, V. Milosavljevic et al., "Non-thermal atmospheric plasma induces ROS-independent cell death in U373MG glioma cells and augments the cytotoxicity of temozolomide," *British Journal of Cancer*, vol. 114, pp. 435–443, 2016.

[85] E. Gjika, S. Pal-Ghosh, M. E. Kirschner et al., "Combination therapy of cold atmospheric plasma (cap) with temozolomide in the treatment of U87MG glioblastoma cells," *Scientific Reports*, vol. 10, p. 16495, 2020.

[86] S. Mitra, P. Bhartiya, N. Kaushik et al., "Plasma-treated flammulina velutipes-derived extract showed anticancer potential in human breast cancer cells," *Applied Sciences*, vol. 10, p. 8395, 2020.

[87] P. Shaw, N. Kumar, D. Hammerschmid, A. Privat-Maldonado, S. Dewilde, and A. Bogaerts, "Synergistic effects of melittin and plasma treatment: a promising approach for cancer therapy," *Cancers (Basel)*, vol. 11, 2019.

[88] A. Jalili, S. Irani, and R. Mirfakhraie, "Combination of cold atmospheric plasma and iron nanoparticles in breast cancer: gene expression and apoptosis study," *Oncotargets and Therapy*, vol. 9, pp. 5911–5917, 2016.

[89] M. Adhikari, B. Adhikari, B. Ghimire, S. Baboota, and E. H. Choi, "Cold atmospheric plasma and silymarin nanoemulsion activate autophagy in human melanoma cells," *International Journal of Molecular Sciences*, vol. 21, 2020.

[90] M. Adhikari, N. Kaushik, B. Ghimire et al., "Cold atmospheric plasma and silymarin nanoemulsion synergistically inhibits human melanoma tumorigenesis via targeting HGF/c-MET downstream pathway," *Cell Communication and Signaling: CCS*, vol. 17, p. 52, 2019.

[91] S. Aryal and G. Bisht, "New paradigm for a targeted cancer therapeutic approach: a short review on potential synergy of gold nanoparticles and cold atmospheric plasma," *Biomedicine*, vol. 5, 2017.

[92] X. Q. Cheng, W. Murphy, N. Recek et al., "Synergistic effect of gold nanoparticles and cold plasma on glioblastoma cancer

therapy," *Journal of Physics D: Applied Physics*, vol. 47, article 335402, 2014.

[93] X. Q. Cheng, K. Rajjoub, J. Sherman et al., "Cold plasma accelerates the uptake of gold nanoparticles into glioblastoma cells," *Plasma Processes and Polymers*, vol. 12, pp. 1364–1369, 2015.

[94] B. B. Choi, M. S. Kim, U. K. Kim, J. W. Hong, H. J. Lee, and G. C. Kim, "Targeting neu protein in melanoma cells with non-thermal atmospheric pressure plasma and gold nanoparticles," *Journal of Biomedical Nanotechnology*, vol. 11, pp. 900–905, 2015.

[95] Z. He, K. Liu, E. Manaloto et al., "Cold atmospheric plasma induces ATP-dependent endocytosis of nanoparticles and synergistic U373MG cancer cell death," *Scientific Reports*, vol. 8, p. 5298, 2018.

[96] S. Irani, Z. Shahmirani, S. M. Atyabi, and S. Mirpoor, "Induction of growth arrest in colorectal cancer cells by cold plasma and gold nanoparticles," *Archives of Medical Science*, vol. 11, pp. 1286–1295, 2015.

[97] N. K. Kaushik, N. Kaushik, K. C. Yoo et al., "Low doses of PEG-coated gold nanoparticles sensitize solid tumors to cold plasma by blocking the PI3K/AKT-driven signaling axis to suppress cellular transformation by inhibiting growth and EMT," *Biomaterials*, vol. 87, pp. 118–130, 2016.

[98] G. Kim, S. R. Park, G. C. Kim, and J. K. Lee, "Targeted cancer treatment using anti-egfr and -tfr antibody-conjugated gold nanoparticles stimulated by nonthermal air plasma," *Plasma Medicine*, vol. 1, pp. 45–54, 2011.

[99] G. C. Kim, G. J. Kim, S. R. Park et al., "Air plasma coupled with antibody-conjugated nanoparticles: a new weapon against cancer," *Journal of Physics D: Applied Physics*, vol. 42, article 032005, 2009.

[100] W. Li, H. Yu, D. Ding et al., "Cold atmospheric plasma and iron oxide-based magnetic nanoparticles for synergetic lung cancer therapy," *Free Radical Biology & Medicine*, vol. 130, pp. 71–81, 2019.

[101] R. Wahab, N. Kaushik, F. Khan et al., "Gold quantum dots impair the tumorigenic potential of glioma stem-like cells via beta-catenin downregulation in vitro," *International Journal of Nanomedicine*, vol. 14, pp. 1131–1148, 2019.

[102] H. Yu, H. Wang, S. Wang et al., "Paclitaxel-loaded core–shell magnetic nanoparticles and cold atmospheric plasma inhibit non-small cell lung cancer growth," *ACS Applied Materials & Interfaces*, vol. 10, pp. 43462–43471, 2018.

[103] W. Zhu, S. J. Lee, N. J. Castro, D. Yan, M. Keidar, and L. G. Zhang, "Synergistic effect of cold atmospheric plasma and drug loaded core-shell nanoparticles on inhibiting breast cancer cell growth," *Scientific Reports*, vol. 6, p. 21974, 2016.

[104] J. M. Pitt, A. Marabelle, A. Eggermont, J. C. Soria, G. Kroemer, and L. Zitvogel, "Targeting the tumor microenvironment: removing obstruction to anticancer immune responses and immunotherapy," *Annals of Oncology*, vol. 27, pp. 1482–1492, 2016.

[105] R. Brandenburg, "Dielectric barrier discharges: progress on plasma sources and on the understanding of regimes and single filaments," *Plasma Sources Science and Technology*, vol. 26, article 053001, 2017.

[106] J. Winter, R. Brandenburg, and K. D. Weltmann, "Atmospheric pressure plasma jets: an overview of devices and new directions," *Plasma Sources Science and Technology*, vol. 24, article 064001, 2015.

[107] X. Lu, G. V. Naidis, M. Laroussi, S. Reuter, D. B. Graves, and K. Ostrikov, "Reactive species in non-equilibrium atmospheric-pressure plasmas: generation, transport, and biological effects," *Physics Reports*, vol. 630, pp. 1–84, 2016.

[108] J. Gay-Mimbrera, M. C. Garcia, B. Isla-Tejera, A. Rodero-Serrano, A. V. Garcia-Nieto, and J. Ruano, "Clinical and biological principles of cold atmospheric plasma application in skin cancer," *Advances in Therapy*, vol. 33, pp. 894–909, 2016.

[109] D. Yan, J. H. Sherman, and M. Keidar, "Cold atmospheric plasma, a novel promising anti-cancer treatment modality," *Oncotarget*, vol. 8, pp. 15977–15995, 2017.

[110] S. B. Karki, E. Yildirim-Ayan, K. M. Eisenmann, and H. Ayan, "Miniature dielectric barrier discharge nonthermal plasma induces apoptosis in lung cancer cells and inhibits cell migration," *BioMed Research International*, vol. 2017, Article ID 8058307, 12 pages, 2017.

[111] H. M. Joh, S. J. Kim, T. H. Chung, and S. H. Leem, "Comparison of the characteristics of atmospheric pressure plasma jets using different working gases and applications to plasma-cancer cell interactions," *AIP Advances*, vol. 3, 2013.

[112] A. Schmidt-Bleker, R. Bansemer, S. Reuter, and K.-D. Weltmann, "How to produce an nox- instead of ox-based chemistry with a cold atmospheric plasma jet," *Plasma Processes and Polymers*, vol. 13, pp. 1120–1127, 2016.

[113] S. Iseni, A. Schmidt-Bleker, J. Winter, K. D. Weltmann, and S. Reuter, "Atmospheric pressure streamer follows the turbulent argon air boundary in a MHz argon plasma jet investigated by OH-tracer PLIF spectroscopy," *Journal of Physics D: Applied Physics*, vol. 47, article 152001, 2014.

[114] S. Iseni, S. Zhang, A. F. H. van Gessel et al., "Nitric oxide density distributions in the effluent of an RF argon APPJ: effect of gas flow rate and substrate," *New Journal of Physics*, vol. 16, article 123011, 2014.

[115] P. Bourke, D. Ziuzina, L. Han, P. J. Cullen, and B. F. Gilmore, "Microbiological interactions with cold plasma," *Journal of Applied Microbiology*, vol. 123, pp. 308–324, 2017.

[116] S. Bekeschus, A. Schmidt, F. Niessner, T. Gerling, K. D. Weltmann, and K. Wende, "Basic research in plasma medicine - a throughput approach from liquids to cells," *Journal of Visualized Experiments*, no. 129, article e56331, 2017.

[117] S. Arndt, M. Landthaler, J. L. Zimmermann et al., "Effects of cold atmospheric plasma (CAP) on ss-defensins, inflammatory cytokines, and apoptosis-related molecules in keratinocytes in vitro and in vivo," *PLoS One*, vol. 10, article e0120041, 2015.

[118] M. Akhlaghi, H. Rajaei, A. S. Mashayekh et al., "Determination of the optimum conditions for lung cancer cells treatment using cold atmospheric plasma," *Physics of Plasmas*, vol. 23, 2016.

[119] E. Gjika, S. Pal-Ghosh, A. Tang et al., "Adaptation of operational parameters of cold atmospheric plasma for in vitro treatment of cancer cells," *ACS Applied Materials & Interfaces*, vol. 10, pp. 9269–9279, 2018.

[120] H.-R. Metelmann, C. Seebauer, V. Miller et al., "Clinical experience with cold plasma in the treatment of locally advanced head and neck cancer," *Clinical Plasma Medicine*, vol. 9, pp. 6–13, 2018.

[121] M. Schuster, C. Seebauer, R. Rutkowski et al., "Visible tumor surface response to physical plasma and apoptotic cell kill in head and neck cancer," *Journal of Cranio-Maxillo-Facial Surgery*, vol. 44, pp. 1445–1452, 2016.

[122] A. Schmidt and S. Bekeschus, "Redox for repair: cold physical plasmas and Nrf2 signaling promoting wound healing," *Antioxidants (Basel)*, vol. 7, p. 146, 2018.

[123] A. Schmidt-Bleker, J. Winter, A. Bosel, S. Reuter, and K. D. Weltmann, "On the plasma chemistry of a cold atmospheric argon plasma jet with shielding gas device," *Plasma Sources Science and Technology*, vol. 25, article 015005, 2016.

[124] A. Schmidt-Bleker, J. Winter, S. Iseni, M. Dunnbier, K. D. Weltmann, and S. Reuter, "Reactive species output of a plasma jet with a shielding gas device-combination of ftir absorption spectroscopy and gas phase modelling," *Journal of Physics D: Applied Physics*, vol. 47, article 145201, 2014.

[125] S. Reuter, T. von Woedtke, and K. D. Weltmann, "The kINPen-a review on physics and chemistry of the atmospheric pressure plasma jet and its applications," *Journal of Physics D: Applied Physics*, vol. 51, 2018.

[126] M. Dünnbier, M. M. Becker, S. Iseni et al., "Stability and excitation dynamics of an argon micro-scaled atmospheric pressure plasma jet," *Plasma Sources Science and Technology*, vol. 24, 2015.

[127] M. Dunnbier, A. Schmidt-Bleker, J. Winter et al., "Ambient air particle transport into the effluent of a cold atmospheric-pressure argon plasma jet investigated by molecular beam mass spectrometry," *Journal of Physics D: Applied Physics*, vol. 46, article 435203, 2013.

[128] K. Wende, P. Williams, J. Dalluge et al., "Identification of the biologically active liquid chemistry induced by a nonthermal atmospheric pressure plasma jet," *Biointerphases*, vol. 10, article 029518, 2015.

[129] H. Jablonowski, J. Santos Sousa, K. D. Weltmann, K. Wende, and S. Reuter, "Quantification of the ozone and singlet delta oxygen produced in gas and liquid phases by a non-thermal atmospheric plasma with relevance for medical treatment," *Scientific Reports*, vol. 8, p. 12195, 2018.

[130] P. J. Bruggeman, M. J. Kushner, B. R. Locke et al., "Plasma-liquid interactions: a review and roadmap," *Plasma Sources Science and Technology*, vol. 25, no. 5, article 053002, 2016.

[131] H. Jablonowski, A. Schmidt-Bleker, K. D. Weltmann, T. von Woedtke, and K. Wende, "Non-touching plasma-liquid interaction - where is aqueous nitric oxide generated?," *Physical Chemistry Chemical Physics*, vol. 20, pp. 25387–25398, 2018.

[132] C. E. Anderson, N. R. Cha, A. D. Lindsay, D. S. Clark, and D. B. Graves, "The role of interfacial reactions in determining plasma-liquid chemistry," *Plasma Chemistry and Plasma Processing*, vol. 36, pp. 1393–1415, 2016.

[133] H. Jablonowski and T. von Woedtke, "Research on plasma medicine-relevant plasma–liquid interaction: what happened in the past five years?," *Clinical Plasma Medicine*, vol. 3, pp. 42–52, 2015.

[134] E. M. Hanschmann, J. R. Godoy, C. Berndt, C. Hudemann, and C. H. Lillig, "Thioredoxins, glutaredoxins, and peroxiredoxins–molecular mechanisms and health significance: from cofactors to antioxidants to redox signaling," *Antioxidants & Redox Signaling*, vol. 19, pp. 1539–1605, 2013.

[135] L. Galluzzi, I. Vitale, S. A. Aaronson et al., "Molecular mechanisms of cell death: recommendations of the nomenclature committee on cell death 2018," *Cell Death and Differentiation*, vol. 25, no. 3, pp. 486–541, 2018.

[136] G. Pistritto, D. Trisciuoglio, C. Ceci, A. Garufi, and G. D'Orazi, "Apoptosis as anticancer mechanism: function

and dysfunction of its modulators and targeted therapeutic strategies," *Aging (Albany NY)*, vol. 8, pp. 603–619, 2016.

[137] K. M. Debatin, "Apoptosis pathways in cancer and cancer therapy," *Cancer Immunology, Immunotherapy*, vol. 53, pp. 153–159, 2004.

[138] G. Bauer, D. Sersenova, D. B. Graves, and Z. Machala, "Cold atmospheric plasma and plasma-activated medium trigger rons-based tumor cell apoptosis," *Scientific Reports*, vol. 9, p. 14210, 2019.

[139] Y. J. Guo, W. W. Pan, S. B. Liu, Z. F. Shen, Y. Xu, and L. L. Hu, "ERK/MAPK signalling pathway and tumorigenesis," *Experimental and Therapeutic Medicine*, vol. 19, pp. 1997–2007, 2020.

[140] M. Ishaq, M. M. Evans, and K. K. Ostrikov, "Effect of atmospheric gas plasmas on cancer cell signaling," *International Journal of Cancer*, vol. 134, pp. 1517–1528, 2014.

[141] P. Bragado, A. Armesilla, A. Silva, and A. Porras, "Apoptosis by cisplatin requires p53 mediated p38alpha MAPK activation through ROS generation," *Apoptosis*, vol. 12, pp. 1733–1742, 2007.

[142] N. Kaushik, N. Uddin, G. B. Sim et al., "Responses of solid tumor cells in dmem to reactive oxygen species generated by non-thermal plasma and chemically induced ROS systems," *Scientific Reports*, vol. 5, p. 8587, 2015.

[143] M. Osaki, M. Oshimura, and H. Ito, "PI3K-Akt pathway: its functions and alterations in human cancer," *Apoptosis*, vol. 9, pp. 667–676, 2004.

[144] J. Xia, W. Zeng, Y. Xia et al., "Cold atmospheric plasma induces apoptosis of melanoma cells via sestrin2-mediated nitric oxide synthase signaling," *Journal of Biophotonics*, vol. 12, article e201800046, 2019.

[145] S. A. E. Ibrahim, A. Abudu, E. Johnson, N. Aftab, S. Conrad, and M. Fluck, "The role of AP-1 in self-sufficient proliferation and migration of cancer cells and its potential impact on an autocrine/paracrine loop," *Oncotarget*, vol. 9, pp. 34259–34278, 2018.

[146] A. Schmidt, K. Rodder, S. Hasse et al., "Redox-regulation of activator protein 1 family members in blood cancer cell lines exposed to cold physical plasma-treated medium," *Plasma Processes and Polymers*, vol. 13, pp. 1179–1188, 2016.

[147] J. F. Liu, W. W. Deng, L. Chen et al., "Inhibition of JAK2/STAT3 reduces tumor-induced angiogenesis and myeloid-derived suppressor cells in head and neck cancer," *Molecular Carcinogenesis*, vol. 57, pp. 429–439, 2018.

[148] J. Tornin, M. Mateu-Sanz, A. Rodriguez, C. Labay, R. Rodriguez, and C. Canal, "Pyruvate plays a main role in the antitumoral selectivity of cold atmospheric plasma in osteosarcoma," *Scientific Reports*, vol. 9, p. 10681, 2019.

[149] C. W. Yun and S. H. Lee, "The roles of autophagy in cancer," *International Journal of Molecular Sciences*, vol. 19, 2018.

[150] Z. Hamurcu, N. Delibasi, S. Gecene et al., "Targeting LC3 and beclin-1 autophagy genes suppresses proliferation, survival, migration and invasion by inhibition of cyclin-D1 and uPAR/integrin beta1/Src signaling in triple negative breast cancer cells," *Journal of Cancer Research and Clinical Oncology*, vol. 144, pp. 415–430, 2018.

[151] M. Alimohammadi, M. Golpur, F. Sohbatzadeh et al., "Cold atmospheric plasma is a potent tool to improve chemotherapy in melanoma in vitro and in vivo," *Biomolecules*, vol. 10, 2020.

[152] L. Shi, F. Ito, Y. Wang et al., "Non-thermal plasma induces a stress response in mesothelioma cells resulting in increased endocytosis, lysosome biogenesis and autophagy," *Free Radical Biology & Medicine*, vol. 108, pp. 904–917, 2017.

[153] N. Yoshikawa, W. Liu, K. Nakamura et al., "Plasma-activated medium promotes autophagic cell death along with alteration of the mTOR pathway," *Scientific Reports*, vol. 10, p. 1614, 2020.

[154] X. Zhen, H. N. Sun, R. Liu, H. S. Choi, and D. S. Lee, "Non-thermal plasma-activated medium induces apoptosis of Aspc1 cells through the ROS-dependent autophagy pathway," *In Vivo*, vol. 34, pp. 143–153, 2020.

[155] Y. Fang, S. Tian, Y. Pan et al., "Pyroptosis: a new frontier in cancer," *Biomedicine & Pharmacotherapy*, vol. 121, article 109595, 2020.

[156] X. Xia, X. Wang, Z. Cheng et al., "The role of pyroptosis in cancer: pro-cancer or pro-"host"?," *Cell Death & Disease*, vol. 10, p. 650, 2019.

[157] X. Yang, G. Chen, K. N. Yu et al., "Cold atmospheric plasma induces GSDME-dependent pyroptotic signaling pathway via ROS generation in tumor cells," *Cell Death & Disease*, vol. 11, p. 295, 2020.

[158] J. Y. Cao and S. J. Dixon, "Mechanisms of ferroptosis," *Cellular and Molecular Life Sciences*, vol. 73, pp. 2195–2209, 2016.

[159] Y. Xie, W. Hou, X. Song et al., "Ferroptosis: process and function," *Cell Death and Differentiation*, vol. 23, pp. 369–379, 2016.

[160] Y. Mou, J. Wang, J. Wu et al., "Ferroptosis, a new form of cell death: opportunities and challenges in cancer," *Journal of Hematology & Oncology*, vol. 12, p. 34, 2019.

[161] B. Hassannia, P. Vandenabeele, and T. Vanden Berghe, "Targeting ferroptosis to iron out cancer," *Cancer Cell*, vol. 35, pp. 830–849, 2019.

[162] L. Jiang, N. Kon, T. Li et al., "Ferroptosis as a p53-mediated activity during tumour suppression," *Nature*, vol. 520, pp. 57–62, 2015.

[163] S. Bekeschus, S. Eisenmann, S. K. Sagwal et al., "Xct (slc7a11) expression confers intrinsic resistance to physical plasma treatment in tumor cells," *Redox Biology*, vol. 30, article 101423, 2020.

[164] T. Furuta, L. Shi, and S. Toyokuni, "Non-thermal plasma as a simple ferroptosis inducer in cancer cells: a possible role of ferritin," *Pathology International*, vol. 68, pp. 442-443, 2018.

[165] K. Sato, L. Shi, F. Ito et al., "Non-thermal plasma specifically kills oral squamous cell carcinoma cells in a catalytic Fe(ii)-dependent manner," *Journal of Clinical Biochemistry and Nutrition*, vol. 65, pp. 8–15, 2019.

[166] A. Lin, B. Truong, S. Patel et al., "Nanosecond-pulsed DBD plasma-generated reactive oxygen species trigger immunogenic cell death in A549 lung carcinoma cells through intracellular oxidative stress," *International Journal of Molecular Sciences*, vol. 18, p. 966, 2017.

[167] Y. Liu and G. Zeng, "Cancer and innate immune system interactions: translational potentials for cancer immunotherapy," *Journal of Immunotherapy*, vol. 35, pp. 299–308, 2012.

[168] A. Marcus, B. G. Gowen, T. W. Thompson et al., "Recognition of tumors by the innate immune system and natural killer cells," *Advances in Immunology*, vol. 122, pp. 91–128, 2014.

[169] D. V. Krysko, A. D. Garg, A. Kaczmarek, O. Krysko, P. Agostinis, and P. Vandenabeele, "Immunogenic cell death

and damps in cancer therapy," *Nature Reviews. Cancer*, vol. 12, pp. 860–875, 2012.

[170] J. Zhou, G. Wang, Y. Chen, H. Wang, Y. Hua, and Z. Cai, "Immunogenic cell death in cancer therapy: present and emerging inducers," *Journal of Cellular and Molecular Medicine*, vol. 23, pp. 4854–4865, 2019.

[171] S. Bekeschus, A. Mueller, V. Miller, U. Gaipl, and K.-D. Weltmann, "Physical plasma elicits immunogenic cancer cell death and mitochondrial singlet oxygen," *IEEE Transactions on Radiation and Plasma Medical Sciences*, vol. 2, pp. 138–146, 2018.

[172] S. Bekeschus, K. Rödder, B. Fregin et al., "Toxicity and immunogenicity in murine melanoma following exposure to physical plasma-derived oxidants," *Oxidative Medicine and Cellular Longevity*, vol. 2017, Article ID 4396467, 12 pages, 2017.

[173] K. Rödder, J. Moritz, V. Miller et al., "Activation of murine immune cells upon co-culture with plasma-treated B16F10 melanoma cells," *Applied Sciences*, vol. 9, p. 660, 2019.

[174] A. G. Lin, B. Xiang, D. J. Merlino et al., "Non-thermal plasma induces immunogenic cell death in vivo in murine CT26 colorectal tumors," *Oncoimmunology*, vol. 7, article e1484978, 2018.

[175] K. R. Liedtke, E. Freund, C. Hackbarth, C.-D. Heidecke, L.-I. Partecke, and S. Bekeschus, "A myeloid and lymphoid infiltrate in murine pancreatic tumors exposed to plasma-treated medium," *Clinical Plasma Medicine*, vol. 11, pp. 10–17, 2018.

[176] J. Cook and T. Hagemann, "Tumour-associated macrophages and cancer," *Current Opinion in Pharmacology*, vol. 13, pp. 595–601, 2013.

[177] T. F. Gajewski, H. Schreiber, and Y. X. Fu, "Innate and adaptive immune cells in the tumor microenvironment," *Nature Immunology*, vol. 14, pp. 1014–1022, 2013.

[178] N. K. Kaushik, N. Kaushik, M. Adhikari et al., "Preventing the solid cancer progression via release of anticancer-cytokines in co-culture with cold plasma-stimulated macrophages," *Cancers (Basel)*, vol. 11, 2019.

[179] L. Crestale, R. Laurita, A. Liguori et al., "Cold atmospheric pressure plasma treatment modulates human monocytes/macrophages responsiveness," *Plasma*, vol. 1, pp. 261–276, 2018.

[180] S. Bekeschus, J. Kolata, A. Muller et al., "Differential viability of eight human blood mononuclear cell subpopulations after plasma treatment," *Plasma Medicine*, vol. 3, pp. 1–13, 2013.

[181] A. Lin, B. Truong, G. Fridman, A. A. Fridman, and V. Miller, "Immune cells enhance selectivity of nanosecond-pulsed dbd plasma against tumor cells," *Plasma Medicine*, vol. 7, 2017.

[182] A. Lin, B. Truong, A. Pappas et al., "Uniform nanosecond pulsed dielectric barrier discharge plasma enhances antitumor effects by induction of immunogenic cell death in tumors and stimulation of macrophages," *Plasma Processes and Polymers*, vol. 12, pp. 1392–1399, 2015.

[183] N. K. Kaushik, N. Kaushik, B. Min et al., "Cytotoxic macrophage-released tumour necrosis factor-alpha (TNF-alpha) as a killing mechanism for cancer cell death after cold plasma activation," *Journal of Physics D: Applied Physics*, vol. 49, article 084001, 2016.

[184] J. Jackute, M. Zemaitis, D. Pranys et al., "Distribution of M1 and M2 macrophages in tumor islets and stroma in relation to prognosis of non-small cell lung cancer," *BMC Immunology*, vol. 19, p. 3, 2018.

[185] B. W. Tse, K. F. Scott, and P. J. Russell, "Paradoxical roles of tumour necrosis factor-alpha in prostate cancer biology," *Prostate Cancer*, vol. 2012, Article ID 128965, 8 pages, 2012.

[186] E. Freund, J. Moritz, M. Stope, C. Seebauer, A. Schmidt, and S. Bekeschus, "Plasma-derived reactive species shape a differentiation profile in human monocytes," *Applied Sciences*, vol. 9, 2019.

[187] S. Bekeschus, V. Ressel, E. Freund, N. Gelbrich, A. Mustea, and M. B. Stope, "Gas plasma-treated prostate cancer cells augment myeloid cell activity and cytotoxicity," *Antioxidants (Basel)*, vol. 9, p. 323, 2020.

[188] S. Y. Gun, S. W. L. Lee, J. L. Sieow, and S. C. Wong, "Targeting immune cells for cancer therapy," *Redox Biology*, vol. 25, article 101174, 2019.

[189] C. Fu and A. Jiang, "Dendritic cells and cd8 t cell immunity in tumor microenvironment," *Frontiers in Immunology*, vol. 9, p. 3059, 2018.

[190] S. Bekeschus, R. Clemen, and H.-R. Metelmann, "Potentiating anti-tumor immunity with physical plasma," *Clinical Plasma Medicine*, vol. 12, pp. 17–22, 2018.

[191] M. Khalili, L. Daniels, A. Lin et al., "Non-thermal plasma-induced immunogenic cell death in cancer: a topical review," *Journal of Physics D: Applied Physics*, vol. 52, 2019.

[192] G. Chen, Z. Chen, D. Wen et al., "Transdermal cold atmospheric plasma-mediated immune checkpoint blockade therapy," *Proceedings of the National Academy of Sciences of the United States of America*, vol. 117, no. 7, pp. 3687–3692, 2020.

[193] A. Lin, Y. Gorbanev, J. De Backer et al., "Non-thermal plasma as a unique delivery system of short-lived reactive oxygen and nitrogen species for immunogenic cell death in melanoma cells," *Advanced Science*, vol. 6, p. 1802062, 2019.

[194] J. van Loenhout, T. Flieswasser, L. Freire Boullosa et al., "Cold atmospheric plasma-treated pbs eliminates immunosuppressive pancreatic stellate cells and induces immunogenic cell death of pancreatic cancer cells," *Cancers (Basel)*, vol. 11, no. 10, 2019.

[195] S. Bekeschus, R. Clemen, F. Niessner, S. K. Sagwal, E. Freund, and A. Schmidt, "Medical gas plasma jet technology targets murine melanoma in an immunogenic fashion," *Advanced Science*, vol. 7, p. 1903438, 2020.

[196] K. Mizuno, Y. Shirakawa, T. Sakamoto, H. Ishizaki, Y. Nishijima, and R. Ono, "Plasma-induced suppression of recurrent and reinoculated melanoma tumors in mice," *IEEE Transactions on Radiation and Plasma Medical Sciences*, vol. 2, pp. 353–359, 2018.

[197] K. Mizuno, K. Yonetamari, Y. Shirakawa, T. Akiyama, and R. Ono, "Anti-tumor immune response induced by nanosecond pulsed streamer discharge in mice," *Journal of Physics D: Applied Physics*, vol. 50, p. 12LT01, 2017.

[198] R. Clemen, E. Freund, D. Mrochen et al., "Gas plasma technology augments ovalbumin immunogenicity and OT-II T cell activation conferring tumor protection in mice," *Advanced Science*, vol. 8, p. 2003395, 2021.

[199] R. Clemen and S. Bekeschus, "ROS cocktails as an adjuvant for personalized antitumor vaccination?," *Vaccine*, vol. 9, 2021.

[200] H. R. Metelmann, C. Seebauer, R. Rutkowski, M. Schuster, S. Bekeschus, and P. Metelmann, "Treating cancer with cold physical plasma: on the way to evidence-based medicine," *Contributions to Plasma Physics*, vol. 58, pp. 415–419, 2018.

[201] S. Hartwig, S. Preissner, J. O. Voss et al., "The feasibility of cold atmospheric plasma in the treatment of complicated

wounds in cranio-maxillo-facial surgery," *Journal of Cranio-Maxillo-Facial Surgery*, vol. 45, pp. 1724–1730, 2017.

[202] S. Hartwig, C. Doll, J. O. Voss, M. Hertel, S. Preissner, and J. D. Raguse, "Treatment of wound healing disorders of radial forearm free flap donor sites using cold atmospheric plasma: a proof of concept," *Journal of Oral and Maxillofacial Surgery*, vol. 75, pp. 429–435, 2017.

[203] P. C. Friedman, V. Miller, G. Fridman, A. Lin, and A. Fridman, "Successful treatment of actinic keratoses using nonthermal atmospheric pressure plasma: a case series," *Journal of the American Academy of Dermatology*, vol. 76, pp. 349-350, 2017.

[204] M. Wirtz, I. Stoffels, J. Dissemond, D. Schadendorf, and A. Roesch, "Actinic keratoses treated with cold atmospheric plasma," *Journal of the European Academy of Dermatology and Venereology*, vol. 32, pp. e37–e39, 2018.

[205] P. C. Friedman, V. Miller, G. Fridman, and A. Fridman, "Use of cold atmospheric pressure plasma to treat warts: a potential therapeutic option," *Clinical and Experimental Dermatology*, vol. 44, pp. 459–461, 2019.

[206] P. C. Friedman, G. Fridman, and A. Fridman, "Using cold plasma to treat warts in children: a case series," *Pediatric Dermatology*, vol. 37, pp. 706–709, 2020.

[207] S. Bekeschus, J. Moritz, I. Helfrich et al., "Ex vivo exposure of human melanoma tissue to cold physical plasma elicits apoptosis and modulates inflammation," *Applied Sciences*, vol. 10, 2020.

[208] M. Linneweh, "Physical cold atmospheric plasma for the treatment of cervical intraepithelial neoplasia (capcin)," 2017, https://clinicaltrials.gov/ct2/show/NCT03218436.

[209] J. Canady, "Canady helios cold plasma scalpel treatment at the surgical margin and macroscopic tumor sites," 2019, https://clinicaltrials.gov/ct2/show/NCT04267575.

[210] P. C. Friedman, "Using a cold atmospheric plasma device to treat skin disorders," 2016, https://clinicaltrials.gov/ct2/show/NCT02759900.

[211] P. C. Friedman, "Cold plasma to treat hair loss," 2020, https://clinicaltrials.gov/ct2/show/NCT04379752.

[212] S. Bekeschus, J. Kolata, C. Winterbourn et al., "Hydrogen peroxide: a central player in physical plasma-induced oxidative stress in human blood cells," *Free Radical Research*, vol. 48, pp. 542–549, 2014.

[213] B. Stratmann, T. C. Costea, C. Nolte et al., "Effect of cold atmospheric plasma therapy vs standard therapy placebo on wound healing in patients with diabetic foot ulcers: a randomized clinical trial," *JAMA Network Open*, vol. 3, article e2010411, 2020.

[214] A. Schmidt, T. von Woedtke, B. Vollmar, S. Hasse, and S. Bekeschus, "Nrf2 signaling and inflammation are key events in physical plasma-spurred wound healing," *Theranostics*, vol. 9, pp. 1066–1084, 2019.

[215] S. Bekeschus, A. Schmidt, K.-D. Weltmann, and T. von Woedtke, "The plasma jet kINPen – a powerful tool for wound healing," *Clinical Plasma Medicine*, vol. 4, pp. 19–28, 2016.

[216] K. Wende, S. Bekeschus, A. Schmidt et al., "Risk assessment of a cold argon plasma jet in respect to its mutagenicity," *Mutation Research, Genetic Toxicology and Environmental Mutagenesis*, vol. 798-799, pp. 48–54, 2016.

[217] S. Bekeschus, A. Schmidt, A. Kramer et al., "High throughput image cytometry micronucleus assay to investigate the presence or absence of mutagenic effects of cold physical plasma," *Environmental and Molecular Mutagenesis*, vol. 59, pp. 268–277, 2018.

[218] S. Bekeschus, C. S. Schütz, F. Nießner et al., "Elevated H2AX phosphorylation observed with kINPen plasma treatment is not caused by ROS-mediated DNA damage but is the consequence of apoptosis," *Oxidative Medicine and Cellular Longevity*, vol. 2019, Article ID 8535163, 15 pages, 2019.

[219] S. Kluge, S. Bekeschus, C. Bender et al., "Investigating the mutagenicity of a cold argon-plasma jet in an HET-MM model," *PLoS One*, vol. 11, article e0160667, 2016.

[220] A. Schmidt, T. V. Woedtke, J. Stenzel et al., "One year follow-up risk assessment in SKH-1 mice and wounds treated with an argon plasma jet," *International Journal of Molecular Sciences*, vol. 18, 2017.

[221] L. Jablonowski, T. Kocher, A. Schindler et al., "Side effects by oral application of atmospheric pressure plasma on the mucosa in mice," *PLoS One*, vol. 14, article e0215099, 2019.

[222] R. Rutkowski, G. Daeschlein, T. von Woedtke, R. Smeets, M. Gosau, and H. R. Metelmann, "Long-term risk assessment for medical application of cold atmospheric pressure plasma," *Diagnostics (Basel)*, vol. 10, 2020.

[223] M. Schuster, R. Rutkowski, A. Hauschild et al., "Side effects in cold plasma treatment of advanced oral cancer—clinical data and biological interpretation," *Clinical Plasma Medicine*, vol. 10, pp. 9–15, 2018.

[224] H.-R. Metelmann, T. Von Woedtke, and K.-D. Weltmann, *Comprehensive Clinical Plasma Medicine: Cold Physical Plasma for Medical Application*, Springer, 2018.

[225] J. Heinlin, G. Isbary, W. Stolz et al., "A randomized two-sided placebo-controlled study on the efficacy and safety of atmospheric non-thermal argon plasma for pruritus," *Journal of the European Academy of Dermatology and Venereology*, vol. 27, pp. 324–331, 2013.

[226] G. Isbary, J. L. Zimmermann, T. Shimizu et al., "Non-thermal plasma—more than five years of clinical experience," *Clinical Plasma Medicine*, vol. 1, pp. 19–23, 2013.

[227] V. Boxhammer, Y. F. Li, J. Koritzer et al., "Investigation of the mutagenic potential of cold atmospheric plasma at bactericidal dosages," *Mutation Research*, vol. 753, pp. 23–28, 2013.

[228] O. Assadian, K. J. Ousey, G. Daeschlein et al., "Effects and safety of atmospheric low-temperature plasma on bacterial reduction in chronic wounds and wound size reduction: a systematic review and meta-analysis," *International Wound Journal*, vol. 16, pp. 103–111, 2019.

[229] E. Timmermann, R. Bansemer, T. Gerling et al., "Piezoelectric-driven plasma pen with multiple nozzles used as a medical device: risk estimation and antimicrobial efficacy," *Journal of Physics D: Applied Physics*, vol. 54, 2021.

[230] L. Miebach, E. Freund, S. Horn et al., "Tumor cytotoxicity and immunogenicity of a novel v-jet neon plasma source compared to the kINPen," *Scientific Reports*, vol. 11, p. 136, 2021.

[231] A. Lehmann, F. Pietag, and T. Arnold, "Human health risk evaluation of a microwave-driven atmospheric plasma jet as medical device," *Clinical Plasma Medicine*, vol. 7-8, pp. 16–23, 2017.

[232] S. Kos, T. Blagus, M. Cemazar, G. Filipic, G. Sersa, and U. Cvelbar, "Safety aspects of atmospheric pressure helium plasma jet operation on skin: in vivo study on mouse skin," *PLoS One*, vol. 12, article e0174966, 2017.

[233] F. Nejat, N.-S. Nabavi, M.-A. Nejat, H. Aghamollaei, and K. Jadidi, "Safety evaluation of the plasma on ocular surface tissue: an animal study and histopathological findings," *Clinical Plasma Medicine*, vol. 14, 2019.

[234] D. Xu, Q. Cui, Y. Xu et al., "Systemic study on the safety of immuno-deficient nude mice treated by atmospheric plasma-activated water," *Plasma Science and Technology*, vol. 20, 2018.

[235] M. S. Mann, R. Tiede, K. Gavenis et al., "Introduction to din-specification 91315 based on the characterization of the plasma jet kINPen® med," *Clinical Plasma Medicine*, vol. 4, pp. 35–45, 2016.

[236] F. Utsumi, H. Kajiyama, K. Nakamura et al., "Effect of indirect nonequilibrium atmospheric pressure plasma on antiproliferative activity against chronic chemo-resistant ovarian cancer cells in vitro and in vivo," *PLoS One*, vol. 8, article e81576, 2013.

[237] A. Schmidt, S. Bekeschus, T. von Woedtke, and S. Hasse, "Cell migration and adhesion of a human melanoma cell line is decreased by cold plasma treatment," *Clinical Plasma Medicine*, vol. 3, pp. 24–31, 2015.

[238] D. Xu, X. Luo, Y. Xu et al., "The effects of cold atmospheric plasma on cell adhesion, differentiation, migration, apoptosis and drug sensitivity of multiple myeloma," *Biochemical and Biophysical Research Communications*, vol. 473, pp. 1125–1132, 2016.

[239] J. I. Ikeda, H. Tanaka, K. Ishikawa, H. Sakakita, Y. Ikehara, and M. Hori, "Plasma-activated medium (PAM) kills human cancer-initiating cells," *Pathology International*, vol. 68, pp. 23–30, 2018.

[240] K. Nakamura, Y. Peng, F. Utsumi et al., "Novel intraperitoneal treatment with non-thermal plasma-activated medium inhibits metastatic potential of ovarian cancer cells," *Scientific Reports*, vol. 7, p. 6085, 2017.

[241] M. Akter, A. Jangra, S. A. Choi, E. H. Choi, and I. Han, "Non-thermal atmospheric pressure bio-compatible plasma stimulates apoptosis via p38/MAPK mechanism in U87 malignant glioblastoma," *Cancers (Basel)*, vol. 12, 2020.

[242] G. Daeschlein, M. Napp, S. Lutze et al., "Skin and wound decontamination of multidrug-resistant bacteria by cold atmospheric plasma coagulation," *Journal der Deutschen Dermatologischen Gesellschaft*, vol. 13, pp. 143–150, 2015.

[243] L. Hilker, T. von Woedtke, K. D. Weltmann, and H. G. Wollert, "Cold atmospheric plasma: a new tool for the treatment of superficial driveline infections," *European Journal of Cardio-Thoracic Surgery*, vol. 51, pp. 186-187, 2017.

[244] H. H. Reitberger, M. Czugala, C. Chow et al., "Argon cold plasma-a novel tool to treat therapy-resistant corneal infections," *American Journal of Ophthalmology*, vol. 190, pp. 150–163, 2018.

[245] F. Brehmer, H. A. Haenssle, G. Daeschlein et al., "Alleviation of chronic venous leg ulcers with a hand-held dielectric barrier discharge plasma generator (PlasmaDerm(®) VU-2010): results of a monocentric, two-armed, open, prospective, randomized and controlled trial (NCT01415622)," *Journal of the European Academy of Dermatology and Venereology*, vol. 29, pp. 148–155, 2015.

[246] J. D. Holcomb, M. Kelly, T. K. Hamilton, and J. B. DeLozier 3rd., "A prospective study evaluating the use of helium plasma for dermal resurfacing," *Lasers in Surgery and Medicine*, 2020.

[247] E. Middelkoop, "Cold plasma for wound treatment, safety study," 2017, https://clinicaltrials.gov/ct2/show/NCT03007264.

[248] J. N. Roe, "Early feasibility study to evaluate the efficacy and safety of the renewalnail™ plasma treatment system in patients with mild to moderate onychomycosis (fungal nail)," 2017, https://clinicaltrials.gov/ct2/show/NCT03072550.

[249] N. V. Tuktagulov, "Cold argon plasma (CAP) application in the wound treatment after open hemorrhoidectomy," 2019, https://clinicaltrials.gov/ct2/show/NCT03907306.

Research Article

Parameters of Oxidative Stress, Vitamin D, Osteopontin, and Melatonin in Patients with Lip, Oral Cavity, and Pharyngeal Cancer

Jarosław Nuszkiewicz [ID],[1] **Jolanta Czuczejko** [ID],[2,3] **Marta Maruszak** [ID],[3] **Marta Pawłowska** [ID],[1] **Alina Woźniak** [ID],[1] **Bogdan Małkowski** [ID],[4] and **Karolina Szewczyk-Golec** [ID][1]

[1]*Department of Medical Biology and Biochemistry, Faculty of Medicine, Ludwik Rydygier Collegium Medicum in Bydgoszcz, Nicolaus Copernicus University in Toruń, 24 Karłowicza St., 85-092 Bydgoszcz, Poland*

[2]*Department of Psychiatry, Faculty of Medicine, Ludwik Rydygier Collegium Medicum in Bydgoszcz, Nicolaus Copernicus University in Toruń, 9 M. Curie Skłodowskiej St., 85-094 Bydgoszcz, Poland*

[3]*Department of Nuclear Medicine, Oncology Centre Prof, Franciszek Łukaszczyk Memorial Hospital, Bydgoszcz, 2 Dr I. Romanowskiej St., 85-796 Bydgoszcz, Poland*

[4]*Department of Diagnostic Imaging, Faculty of Health Sciences, Ludwik Rydygier Collegium Medicum in Bydgoszcz, Nicolaus Copernicus University in Toruń, 2 Dr I. Romanowskiej St., 85-796 Bydgoszcz, Poland*

Correspondence should be addressed to Jarosław Nuszkiewicz; jnuszkiewicz@cm.umk.pl

Lip, oral cavity, and pharyngeal cancers (LOCP) constitute a group of rare neoplasms with unfavorable prognosis. So far, not much is known about the role of vitamin D and oxidative stress in the pathogenesis of LOCP in the European population. The aim of the study was to determine the concentrations of vitamin D, osteopontin, melatonin, and malondialdehyde (MDA) as markers of oxidative stress and/or inflammation, as well as the activities of antioxidant enzymes in the course of LOCP. The vitamin D, melatonin, and osteopontin concentrations in blood serum, the MDA levels in erythrocytes and blood plasma, and the activities of superoxide dismutase (SOD-1), catalase (CAT), and glutathione peroxidase (GPx) in erythrocytes were measured in blood samples taken from 25 LOCP patients of middle age (YCG), 20 LOCP elderly patients (OCG), and 25 healthy middle-aged volunteers. In both cancer groups, decreases in vitamin D and CAT, as well as increases in osteopontin and blood plasma MDA, were observed. An increase in GPx activity in YCG and a decrease in melatonin level in OCG were found. The results indicate the vitamin D deficiency and disturbed oxidant-antioxidant homeostasis in LOCP patients. Osteopontin seems to be associated with LOCP carcinogenesis and requires further research.

1. Introduction

Lip, oral cavity, and pharyngeal cancers (LOCP) belong to the most common head and neck cancers worldwide. Moreover, scientific analyses indicate that the incidence of this type of neoplasm will increase in the future. According to data, in 2012, 529,500 new cases of LOCP were detected worldwide, which corresponds to 3.6% of all cancers [1, 2]. Mortality in 2012 from this group of neoplasms was estimated at 292,300 cases, which corresponds to 3.6% of deaths

due to neoplastic diseases [1, 2]. Projections for 2035 show a 62% increase in the number of cases to around 856,000 cases annually [1]. Cancers of lip, oral cavity, and pharynx are considered together because they are characterized by similar risk factors. Neoplasms belonging to this group affect male much more often than female, and the age group 50-70 years is particularly vulnerable [3–5]. In addition, this type of cancer is especially common in south-central Asia [1]. The main risk factors for the development of LOCP cancer include smoking [6], alcohol consumption [7, 8],

infections caused by Epstein-Barr virus (EBV) [9], and *human papillomavirus* (HPV) [10]. Early diagnosis and treatment initiation significantly increases patient survival; unfortunately, most cases are detected in the advanced stage of the disease, which lowers the 5-year survival rate to about 40% [3].

Pathogenesis of lip, oral cavity, and pharyngeal cancers is still not clear and is believed to be multifactorial in origin. Few studies indicate the participation of extracellular matrix and fibroblast changes, immune system, and oxidative stress in the pathogenesis of oral submucous fibrosis, leading to cancer of the oral cavity [11]. Additionally, molecular pathogenesis of head and neck cancer is associated with deletion in region located at chromosome 9p21–22 containing p16 tumor suppressor gene [12]. An inherent element of carcinogenesis and neoplastic disease is the increased generation of reactive oxygen species (ROS) [13–18]. Moreover, cancer cells synthesize and secrete cytokines that modulate inflammation and significantly increases ROS generation [19]. The disturbance of homeostasis by ROS generated in exceeding of physiological capacity of adaptation leads to oxidative stress [20–22]. Although the disease has a specific localization, systemic symptoms of oxidative stress are observed in patients [23, 24]. ROS are a group of chemical molecules which are characterized by the presence of nonpair electrons and high chemical reactivity [25]. The most important ROS include superoxide anion (O_2^-), hydrogen peroxide (H_2O_2), hydroxyl radical (OH^-), and singlet oxygen ($^1O_2$) [20, 25]. Due to high chemical reactivity, ROS modify proteins, lipids, and genetic material [26, 27]. The effect of lipid peroxidation is damage to cell membranes, and the main markers of this process is malondialdehyde (MDA) and 4-hydroxynonenal [28]. Antioxidants play an important role in maintaining the redox balance [29]. Endogenous antioxidants include enzymes such as superoxide dismutases (SODs), catalase (CAT), and glutathione peroxidases (GPxs) [30]. The antioxidant defense is also constituted by small endo- and exogenous biomolecules such as vitamins A, C, and E, melatonin, and glutathione (GSH) [31, 32]. The role of vitamin D as an antioxidant remains ambiguous due to inconclusive research results [33].

Vitamin D is a biomolecule with pleiotropic properties. Calcitriol (1,25-dihydroxycholecalciferol) plays the most important role among the group of compounds called vitamin D [34]. Chemical compounds belonging to this group can be absorbed with food, most often in the form of cholecalciferol and ergocalciferol [35, 36]. Another source of vitamin D is the endogenous synthesis under the influence of ultraviolet radiation (UV) and hydroxylases found in the liver and kidney. The substrate for this process is 7-dehydrocholesterol [37]. Despite endogenous synthesis and the presence of vitamin D in food products, vitamin D deficiencies affect a significant part of the population worldwide [38–40]. Vitamin D is involved in the regulation of calcium-phosphate homeostasis, which is of particular importance for the functioning of the skeletal system [41]. Calcitriol, acting through the vitamin D receptor (VDR), reduces oxidative stress by increasing the level of SODs, GPxs, and GSH expression [33, 42]. Moreover, it was observed that vitamin

D reduced the secretion of proinflammatory cytokines, decreasing the level of oxidative stress [43]. The role of vitamin D and its derivatives in cancer is still under investigation. The results of the studies conducted so far are not unequivocal. Some researchers point to a significant role of vitamin D deficiency on cancer mortality, while no effect on morbidity [44–46]. On the contrary, some studies do not link cancer with vitamin D levels [47].

Research indicates a positive correlation between the concentration of vitamin D and osteopontin [48, 49]. Osteopontin is a glycoprotein secreted by osteoblasts and osteoclasts involved in shaping the correct bone structure [50]. The presence of this glycoprotein is not limited to the skeletal system. Osteopontin was found in many tissues and body fluids such as brain astrocytes, kidney, smooth muscle, saliva, and milk [50–52]. Tumor cells of lung, gastric, prostate, ovarian, and colorectal cancer were also found to secrete osteopontin [50]. In the course of neoplastic diseases, an increase in the concentration of osteopontin was observed along with an increase in the level of proinflammatory cytokines [53–55]. Osteopontin was found to be a modulator of the immune response [54]. The relationship between osteopontin and oxidative stress has not been analyzed frequently. The results of the research indicate that the concentration of osteopontin positively correlates with the markers of increased oxidative stress [56–59].

Melatonin (N-acetyl-5-methoxytryptamine) is a hormone synthesized and secreted by pinealocytes in the circadian rhythm [60, 61]. Gastrointestinal tract, lymphocytes, ovaries, skin, and retina are sources of extrapineal melatonin independent of the circadian rhythms [62]. The melatonin molecule contains an indole ring that neutralizes ROS directly [63, 64]. Moreover, research indicates that melatonin decreases the level of ROS by activating the silent information regulator 1 (SIRT1) pathway [65]. Melatonin may also indirectly affect the oxidant–antioxidant balance, stimulating the expression of genes encoding antioxidant enzymes, such as SODs and GPxs [66]. In addition to its direct and indirect action, melatonin inactivates ROS through its metabolites, namely, N1-acetyl-N2-formyl-5-methoxykynuramine (AFMK) and N1-acetyl-5-methoxykynuramine (AMK) [67]. The pleiotropic role of melatonin as endo- and paracrine hormone has been analyzed in carcinogenesis [68, 69]. Scientists indicated an oncostatic role of melatonin in breast, ovarian, prostate, oral, gastric, and colorectal tumors [70]. One of the mechanisms of the oncostatic action of melatonin seems to be based on the reduction of ROS levels [71, 72]. Moreover, melatonin was found to hinder angiogenesis and increase apoptosis of cancer cells [73]. However, little is known about the role of melatonin in LOCP cancer.

So far, only a few studies on the activity of antioxidant enzymes and lipid peroxidation markers in patients with LOCP have been conducted. The results described in the literature are not unequivocal. A decrease in SOD, CAT, and GPx activities with an increase in MDA concentration has been most frequently reported [74–76]. Still, according to some other research, no changes in the activity of antioxidant enzymes in the course of LOCP have been observed

[77]. The relationship between the activity of antioxidant enzymes and vitamin D and osteopontin and melatonin has not been studied. Examining the mechanisms related to vitamin D, osteopontin, melatonin, and oxidative stress in the course of LOCP seems to be important for a better understanding of the patophysiology of this type of cancer, as well as for finding new methods of treatment and prevention. Thus, the aim of this study was to determine the activities of selected antioxidant enzymes, as well as the concentrations of vitamin D, osteopontin, melatonin, and MDA in the course of lip, oral cavity, and pharyngeal cancer.

2. Materials and Methods

2.1. Participants. The study involved 45 patients diagnosed with *carcinoma* in situ of lip, oral cavity, or pharynx according to the International Classification of Diseases–11th Revision (ICD-11)–2E60.0 [78]. The patients were divided into two groups according to their age, namely, younger cancer group (YCG) and older cancer group (OCG). The classification of patients into age groups was based on the United Nations report, which stated that old age begins after the age of 65 [79]. The participants were treated at the Oncology Center, Prof. Franciszek Łukaszczyk Memorial Hospital, Bydgoszcz, Poland. The patients were referred for planning radiotherapy using positron emission tomography–computed tomography (PET/CT) after FDG ([18F]-fluorodeoxyglucose) administration. The patients with G1 squamous cell carcinoma, G2 squamous cell carcinoma, and nonkeratinizing G2 squamous cell carcinoma in histopathological analysis were included in the study. The patients with other grade and type of tumor were excluded from the study. The control group consisted of 25 healthy volunteers. The criteria of exclusion from the control group were associated conditions known to be caused by or to result in oxidative stress or involving disruption of the oxidant-antioxidant equilibrium (cancer, diabetes, cardiovascular, and infectious diseases). A survey was conducted among the people qualified for the study. The questions concerned tobacco addiction and vitamin D supplementation. The characteristics of the study and control groups are presented in Table 1. The study was approved by the Bioethics Committee of the Nicolaus Copernicus University in Toruń functioning at Collegium Medicum in Bydgoszcz, Poland (consent no. KB 221/2018).

2.2. Study Design. The patients were eligible for the study on the day of planning for radiotherapy. Blood samples were collected by qualified medical personnel in the morning (between 8:00 AM and 9:00 AM) after overnight fasting from median cubital vein just prior to the administration of the radiopharmaceutical. Every blood sample was collected into two polypropylene tubes. First tube (vol. 6 mL) contained a clotting activator to obtain blood serum, and another tube (vol. 10 mL) was covered with K_2EDTA to obtain blood plasma. The tubes were immediately transported under reduced temperature condition to the laboratory for centrifugation (6,000 g for 10 min at 4°C). After centrifugation, blood serum and plasma were separated

and stored at -80°C for further analysis. The blood morphotic elements remaining after centrifugation were washed three times with a phosphate-buffered saline (PBS) at a ratio of 1:3 and each time centrifuged (6,000 g for 10 min at 4°C) to remove leukocytes and thrombocytes. The red blood cells obtained in this method were mixed with the PBS solution to obtain erythrocytic suspension with a 50% hematocrite index.

2.3. Biochemical Analysis. The activity of selected antioxidant enzymes was determined in erythrocytic suspension with the use of spectrophotometric methods. Activity of Zn/Cu-superoxide dismutase (SOD-1; EC 1.15.1.1) was assayed according to the Misra and Fridovich method [80]. Analysis was based on the inhibition of adrenaline oxidation to adrenochrome in alkaline solution at 37°C, which induced a change in the absorbance at 480 nm. Activity of SOD-1 was expressed in IU/g Hb. CAT (EC 1.11.1.6) activity was determined with the use of the Beers and Sizer method [81] by measuring the decrease in the absorbance at 240 nm of a solution of hydrogen peroxide decomposed by the enzyme at 37°C. CAT activity was expressed in IU/g Hb. Activity of cytosolic glutathione peroxidase (GPx; EC 1.11.1.9) was assessed using the method of Paglia and Valentine [82]. The principle of the method for measuring GPx activity is based on the ability of the enzyme to reduce hydrogen peroxide with a simultaneous oxidation of GSH as a coenzyme at 37°C, measured at 340 nm. Activity of GPx was expressed in IU/g Hb. Erythrocytic and plasma MDA concentrations were determined with the method of Buege and Aust [83] in the modification of Esterbauer and Cheeseman [84]. The MDA concentration was expressed as the concentration of thiobarbituric acid-reactive substances (TBARS), measured at 532 nm at room temperature. The MDA concentration in erythrocytes was expressed in nmol/g Hb and in blood plasma in nmol/mL. Hemoglobin (Hb) concentration was evaluated using the Drabkin method [85]. Hemoglobin and selected hemoglobin derivatives under the influence of potassium ferricyanide are oxidized to methemoglobin. The absorbance is measured at 540 nm at room temperature.

Serum concentrations of melatonin, vitamin D, and osteopontin were determined with commercially available enzyme immune assay kits. The kits were used accordingly: an enzyme-linked immunosorbent assay kit for melatonin (Cloud-Clone Corp., Houston, TX, USA), a competitive enzyme-linked immunosorbent assay kit for 25(OH)-vitamin D (Immundiagnostik AG, Bensheim, Germany), and a sandwich enzyme-linked immunosorbent assay kit for human osteopontin (BioVendor, Brno, Czech Republic). The measurements were made according to manufacturer's instructions. The enzyme immune assay kits used in the study contain the reagents necessary for the study, standard concentration analytes, blank, and control samples. The principle of the assay is to bind the antigen by specific anti-human monoclonal antibodies that coat the wells of microplates found in the kits. The antigen concentration was determined from the calibration curve. The concentrations of melatonin, vitamin D, and osteopontin were expressed in pg/mL, ng/mL, and nmol/L, respectively.

TABLE 1: Anthropometric and clinical characteristic of patients with lip, oral cavity, or pharyngeal cancer and healthy volunteers (control group). Each value is mean ± S.E.M. YCG: younger cancer group; OCG: older cancer group, $^*p < 0.05$ vs. OCG.

Parameter	YCG	OCG	Control group
n (male/female)	25 (15/10)	20 (14/6)	25 (11/14)
Age [yrs]	58.24 ± 1.29*	69.7 ± 1.49	55.36 ± 1.17*
Body mass [kg]	72.53 ± 3.95	71.39 ± 3.52	71.02 ± 2.22
Height [cm]	168.92 ± 1.84	168.55 ± 1.52	169.88 ± 1.72
BMI [kg/m^2]	25.09 ± 0.99	25.00 ± 1.02	24.50 ± 0.47
Current smoker (y/n)	7/18	5/15	4/21
Vitamin D supplementation (y/n)	5/20	4/16	8/17

2.4. Statistical Analysis. Statistical analysis was performed using the Statistica 13.3 (TIBCO Software Inc.). The results were presented as means ± S.E.M. Statistical analysis included Student's *t*-test for independent samples, for the comparison of study group and control group, Shapiro-Wilk test to test hypothesis of normal distribution, Levene's test to asses homogeneity of variances. Pearson's correlation coefficient was used to quantify the relationship between the parameters measured. The level of significance was set at $p < 0.05$.

3. Results

Anthropometric and clinical characteristic of patients with lip, oral cavity, or pharyngeal cancer and healthy group were presented in Table 1. No significant differences were found between YCG and control group. There was a statistically significant difference in the age of the patients between the YCG, control group, and OCG.

The SOD-1 activity was similar in all groups and amounted to 738 ± 21 IU/g Hb in YCG, 735 ± 19 IU/g Hb in OCG, and 755 ± 18 IU/g Hb in control group. The statistically lower CAT activity was observed in YCG ($59.34 ± 2.68 10^4 ×$ IU/g Hb) and OCG ($58.11 ± 2.47 10^4 ×$ IU/g Hb) groups compared to the control group ($70.19 ± 1.87 10^4 ×$ IU/g Hb). The activity of GPx in YCG was 8.54 ± 0.75 IU/g Hb and was significantly higher compared to the control group (6.45 ± 0.58 IU/g Hb). In OCG, the mean GPx activity was 7.44 ± 0.76 IU/g Hb. The results concerning the activity of antioxidant enzymes are presented in Figure 1.

There were no statistically significant differences in the concentration of erythrocytic MDA in YCG (27.52 ± 4.23 nmol/g Hb), OCG (31.74 ± 6.21 nmol/g Hb), and control group (25.66 ± 1.98 nmol/g Hb). Significantly higher concentrations of MDA were observed in the plasma of YCG and OCG patients, amounting to 0.55 ± 0.02 and 0.56 ± 0.01 nmol/mL, respectively. In the control group, the plasma MDA level was 0.42 ± 0.02 nmol/mL. The melatonin level in OCG was 62.12 ± 4.70 pg/mL and was significantly lower than in the control group (84.33 ± 6.54 pg/mL). The concentration of melatonin in YCG was 72.83 ± 5.80 pg/mL, and no statistically significant differences were observed in relation to the other study groups. Figure 2 shows the concentration of MDA and melatonin in the graphs.

The concentration of 25(OH)-vitamin D in the serum of the healthy people was 82.57 ± 4.28 ng/mL. Considerably lower values were observed in YCG and OCG, amounting to 63.55 ± 7.36 ng/mL and 48.42 ± 7.09 ng/mL, respectively. The levels of osteopontin in the LOCP patient groups were significantly higher compared to the healthy group. The concentration of osteopontin in YCG and OCG was 16.04 ± 2.69 nmol/L and 14.98 ± 2.48 nmol/L, respectively, while in the control group, it was 9.78 ± 0.72 nmol/L. Figure 3 shows the graphs of 25(OH)-vitamin D and osteopontin concentration in the study groups.

The obtained data were also tested for the presence of correlations. In YCG, statistically significant negative correlations were observed between GPx and body mass ($r = -0.51$, $p = 0.009$), GPx and BMI ($r = -0.52$, $p = 0.007$), and CAT and vitamin D ($r = -0.42$, $p = 0.036$), whereas a significant positive correlation was found between plasma MDA and osteopontin ($r = 0.53$, $p = 0.007$) (see Figure 4). In the control group, a positive correlation between SOD-1 and erythrocytic MDA ($r = 0.44$, $p = 0.026$) and a negative correlation between body mass and erythrocytic MDA ($r = -0.39$, $p = 0.049$) were observed (Figure 5). No statistically significant correlations were found in OCG.

4. Discussion

As mentioned earlier, LOCP are relatively rare compared to other neoplastic diseases. Due to the small number of patients with such a diagnosis, there are few studies in which the mechanisms of antioxidant defense and the concentration of melatonin, osteopontin, and vitamin D were analyzed [74–77, 86–99]. Figure 6 presents putative mechanisms linking oxidative stress, antioxidant enzymes, vitamin D, osteopontin, and melatonin in LOCP carcinogenesis.

In the present study, specific modifications in the oxidant-antioxidant homeostasis, including a decrease in CAT and increases in GPx (in YCG) and blood plasma MDA, were found in the LOCP patients when compared to the healthy people. Moreover, GPx activity was found to negatively correlate with body mass and BMI in the YCG. Surprisingly, no statistically significant differences in SOD-1 activity were observed. This result is in contrast with the findings of other studies. In the study conducted by Gurudath et al. [86], a decrease in SOD-1 activity in patients with cancer of oral cavity was indicated. The study group

(a)

(b)

(c)
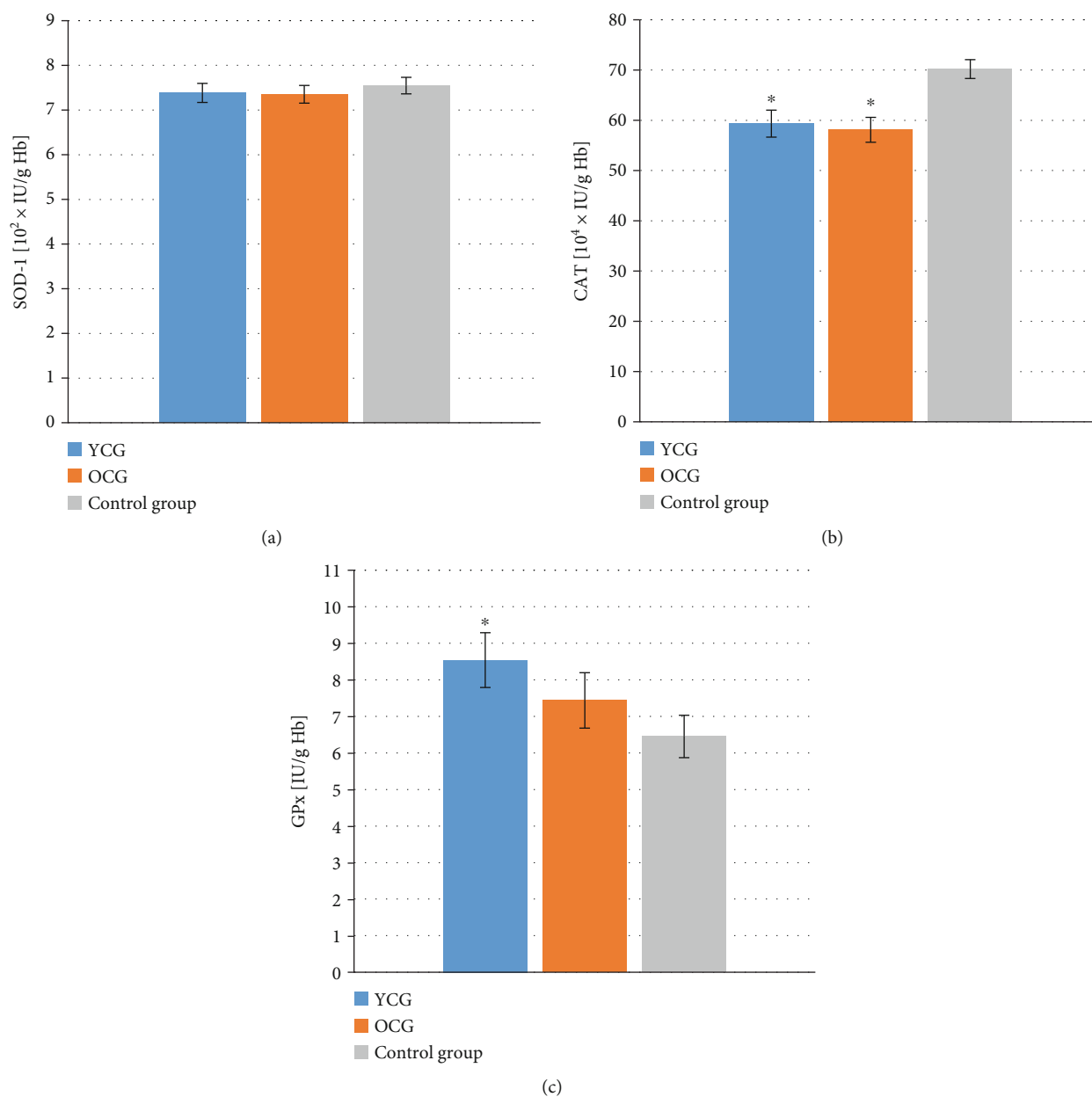
Figure 1: Activity of antioxidant enzymes in the erythrocytes of patients with lip, oral cavity, or pharyngeal cancer depending on age and in the healthy group. (a) Zn/Cu-superoxide dismutase (SOD-1) activity, (b) catalase (CAT) activity, (c) cytosolic glutathione peroxidase (GPx) activity. YCG: younger cancer group—mean age 58.24 ± 1.29 yrs; OCG: older cancer group—mean age 69.70 ± 1.49 yrs. Data are presented as the means ± S.E.M. $^*p < 0.05$ vs. control group.

consisted of 25 patients with oral cancer. Only smokers and tobacco chewers were included. Average age of the examined subjects was 53 yrs. The control group consisted of 25 healthy people; no information was provided on smoking or chewing tobacco in this group. Also, in the study of Subapriya et al. [87], the activity of SOD in group of 12 patients with oral precancerous lesions or oral cancer was tested. All subjects included in the study were between 35 and 60 yrs old and smoked or chewed tobacco. The cancer patients showed significantly lower SOD activity compared to the control group. Sabitha and Shyamaladevi [76] analyzed 12 blood samples obtained from patients with stage III oral can-

cer. The authors did not provide the age or information about the addictions of people participating in the study. Also, in that study, a significant decrease in SOD activity was observed in the course of cancer. Similarly, in the research by Manoharan et al. [75] decreased SOD activity was observed. A group of 46 men with oral cancer aged 40 to 60 years old was examined. The control group was free from smoking and chewing tobacco; no such information was provided in the context of the study group. Decreased activity of SOD in red blood cells was also reported by Patel et al. [77]. The age range for oral cancer patients was 22-75 years with a median of 45 years. A group of 126 patients, 113

(a)

(b)

(c)
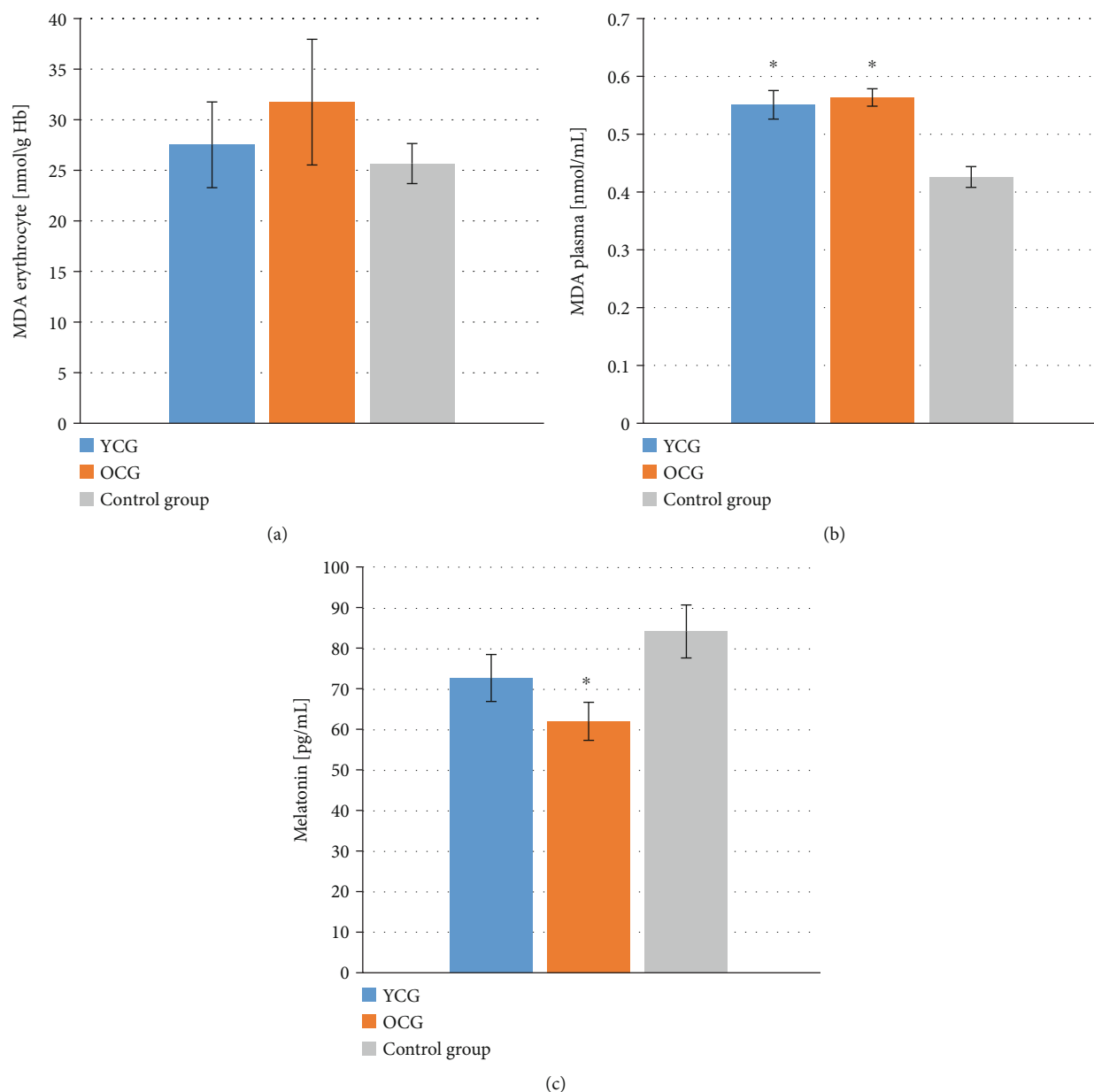
FIGURE 2: Concentration of malondialdehyde (MDA) and melatonin in patients with lip, oral cavity, or pharyngeal cancer depending on age and in the healthy group. (a) Erythrocytic MDA concentration, (b) plasma MDA concentration, (c) melatonin concentration. YCG: younger cancer group—mean age 58.24 ± 1.29 yrs; OCG: older cancer group—mean age 69.70 ± 1.49 yrs. Data are presented as the means $\pm$ S.E.M. $^*p < 0.05$, vs. control group.

of whom smoked or chewed tobacco, was tested. Different results were observed in the study of Huo et al. [74]. In their study, a group of 25 patients of both sexes aged 40 to 45 diagnosed with oral squamous cell carcinoma were investigated. Only smokers and tobacco chewers were included in the study. A healthy control group was free of tobacco chewing and smoking habits. The activity of SOD and CAT, as well as the level of erythrocytic MDA, was tested. SOD activity was higher in the group with neoplastic disease. In the case of observed in the present study lower CAT activity in the LOCP patients, similar results were reported by Huo et al. [74], Subapriya et al. [87], Sabitha and Shyamaladevi [76], and Manoharan et al. [75]. On the contrary, Patel

et al. [77] did not observe any statistically significant changes in catalase activity in oral cancer patients. In the present study, we noted significantly higher GPx activity in the middle-aged LOCP patients than in the control group. The different results were described by Gurudath et al. [86], Subapriya et al. [87], Sabitha and Shyamaladevi [76], and Manoharan et al. [75]. The authors of these studies observed that GPx activity decreased in the course of cancer. In our study, erythrocytic MDA showed no statistically significant variability between the studied groups, unlike MDA level in blood plasma, which was higher in the cancer patients. In the other studies, increases in the level of MDA in plasma or serum and red blood cells in patients with cancers of

(a)

(b)
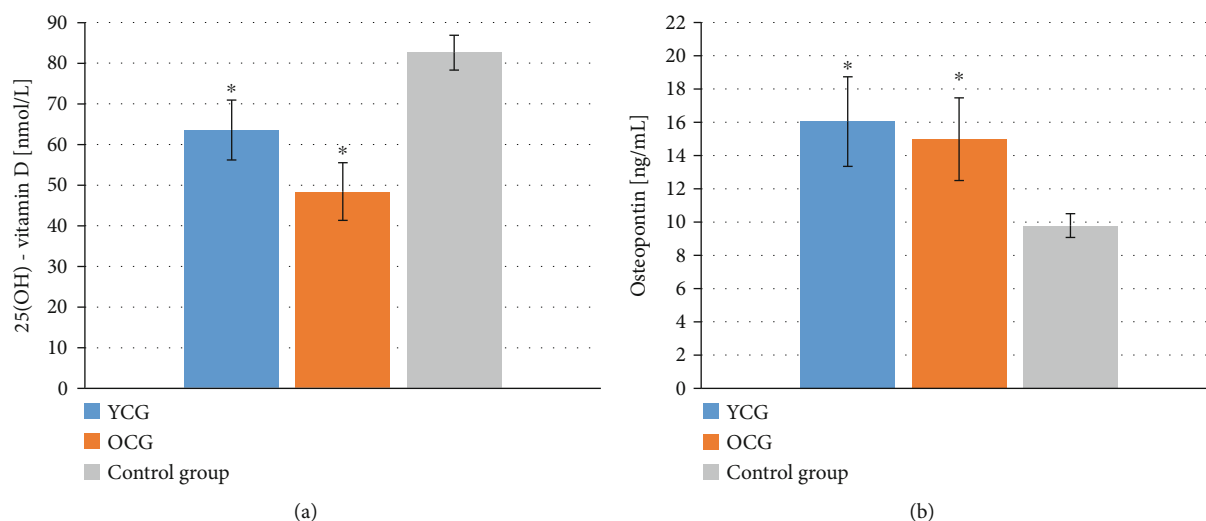
FIGURE 3: Concentration of 25(OH)-vitamin D and osteopontin in the blood serum of patients with lip, oral cavity, or pharyngeal cancer depending on age and in the healthy group. (a) 25(OH)-vitamin D concentration, (b) osteopontin concentration. YCG: younger cancer group—mean age 58.24 ± 1.29 yrs; OCG: older cancer group—mean age 69.70 ± 1.49 yrs. Data are presented as the means ± S.E.M. $^*p <$ 0.05 vs. control group.
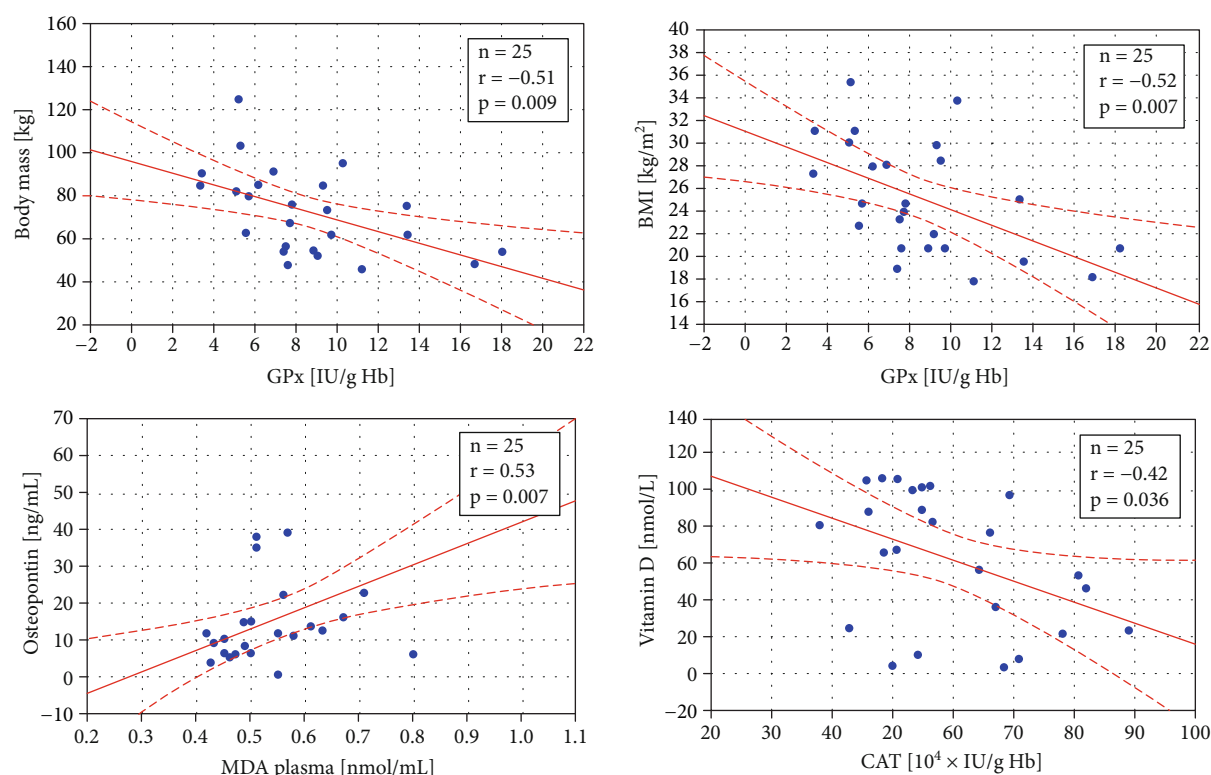
FIGURE 4: Statistically significant correlations in the younger cancer group (mean age 58.24 ± 1.29 yrs) between body mass and glutathione peroxidase (GPx) activity, body mass index (BMI) and GPx, osteopontin and plasma malondialdehyde (MDA) level, and vitamin D concentration and catalase (CAT) activity. The regression line is marked with a solid line, while the confidence intervals of 0.95 are marked with a dashed line.

the oral cavity and pharynx were unanimously indicated [74–76, 88–90].

Considering the differences between the studies, it is worth noting that the analyzed studies were conducted on small groups of patients of the Asian population (mainly India) [74–77, 86–90]. Additionally, in the study groups, a significant proportion of patients were smokers or chewing tobacco. The relationship between tobacco addiction and ROS generation, which leads to an increase in the level of oxidative stress, was confirmed in numerous studies [100,

n = 25
r = −0.39
p = 0.049

n = 25
r = 0.44
p = 0.026
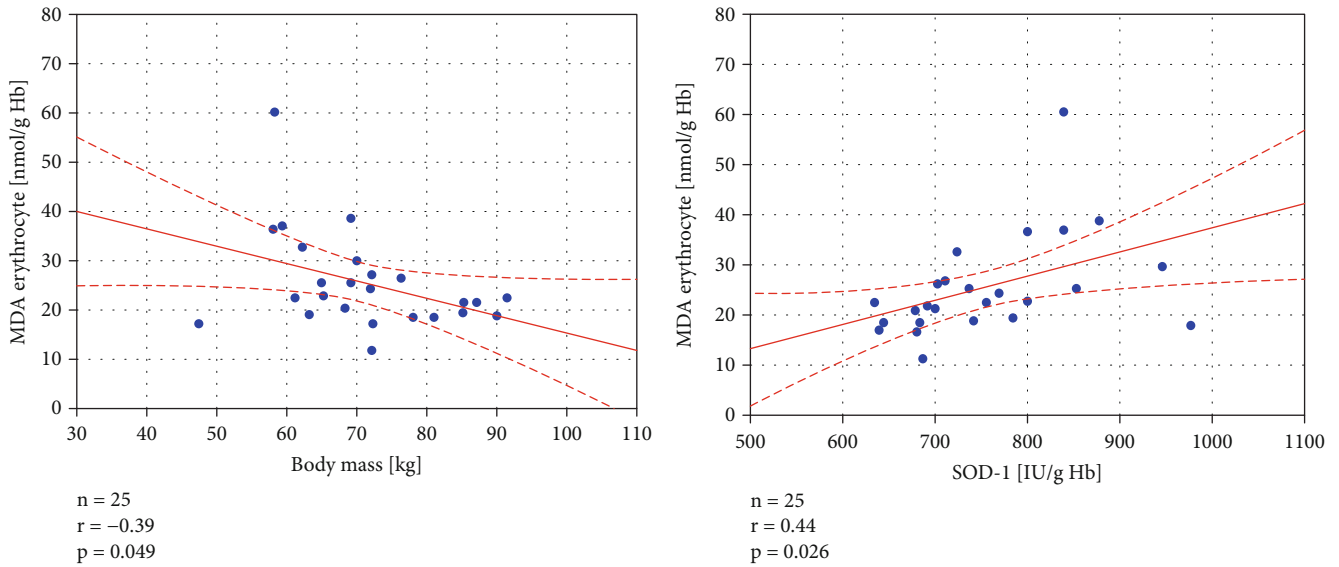
FIGURE 5: Statistically significant correlations in the healthy, control group between erythrocyte malondialdehyde (MDA) level and body mass, erythrocyte MDA concentration, and Zn/Cu-superoxide dismutase (SOD-1) activity. The regression line is marked with a solid line, while the confidence intervals of 0.95 are marked with a dashed line.
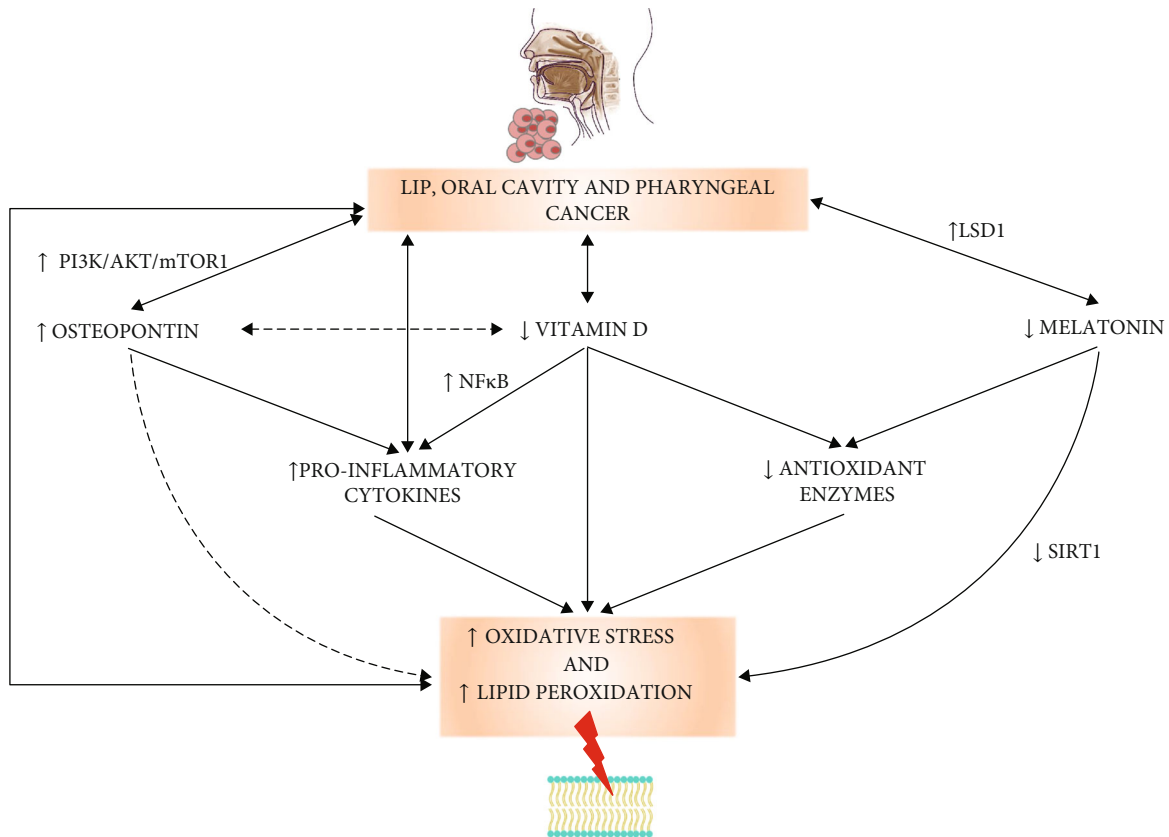
FIGURE 6: Putative mechanisms linking oxidative stress, antioxidant enzymes, vitamin D, osteopontin, and melatonin in lip, oral cavity, and pharyngeal cancer. Abbreviations used: LSD1: lysine-specific demethylase; NFκB: nuclear factor kappa-light-chain-enhancer of activated B cells; PI3K/AKT/mTOR1: phosphoinositide 3-kinase/protein kinase B/mechanistic target of rapamycin; SIRT1: silent information regulator 1.

101], so this factor could significantly influence the obtained results. The age of the patients is also known to have an impact on the oxidant-antioxidant balance of the organism [102, 103]. The discussed studies were carried out on patients from the age of 40, whereas in the present study, the patients were older [102, 103]. It is worth mentioning that the activity of SOD-1 is dependent on the zinc level in the diet, whereas GPx is an enzyme dependent on selenium. Deficiencies resulting from an unbalanced diet may reduce the activity of SOD-1 and/or GPx. The lower activity of GPx in OCG compared to YCG may be the evidence of selenium deficiency in the diet of the elderly patients with LOCP cancer. Hydrogen peroxide (H_2O_2) is a substrate for both CAT and GPxs [104, 105]. In the present study, lower CAT and higher GPx activities were observed in the cancer patients compared to the healthy control group. The lower activity of CAT might be compensated by the increase in GPx activity. Thus, the glutathione-related antioxidant defense seems to be predominant in the patients. In summary, the results of the present study point to the increased ROS generation and reduction of antioxidant defense mechanisms, which are characteristic of neoplastic diseases [18]. Increased levels of lipid peroxidation and MDA could be a consequence of the disturbance of oxidant-antioxidant homeostasis and might be involved in the carcinogenesis.

Research by Liu et al. [91] indicates the important role of melatonin as a ROS scavenger in oral cancer. The research was conducted on human umbilical vein endothelial cells (HUVECs) and six human oral cancer cell lines, including SCC25, SCC9, Tca8113, Cal27, FaDu, and human normal oral keratinocytes (hNOKs). The addition of melatonin (1 mM) to the culture medium significantly reduced the level of ROS in the Cal27 and FaDu cells. Concurrently, melatonin reduced the proliferation and induced the apoptosis of oral cancer cells. Observed inactivation of ROS-reliant Akt signaling significantly decreased the mobility of cancer cells. Inhibition of angiogenesis and reduction in tumor mass were also found. Yang et al. [92] analyzed oral squamous cell carcinoma (OSCC) tissue arrays. The reduction of lysine-specific demethylase (LSD1) expression under the influence of melatonin (0.1 g/mL) was described. Lower LSD-1 expression significantly reduced tumor cell proliferation. Human nasopharyngeal carcinoma (HONE-1), NPC-39, and NPC-BM cell line incubated in a solution containing melatonin (50 ng/mL) were investigated by Ho et al. [93]. Presence of melatonin inhibited TPA-induced cell motility by regulating the matrix metalloproteinase-9 (MMP-9) expression in nasopharyngeal neoplasm cells. Many scientists point to the protective role of melatonin in oral and nasopharyngeal cavity diseases mainly by reducing oxidative stress [106–109]. However, in the present study, a statistically significant lower melatonin concentration in patients with lip, oral cavity, or pharynx cancer compared to the healthy group was only observed in OCG. During the aging, the synthesis and secretion of melatonin are reduced [110]. It could indicate that melatonin deficiency is not particularly involved in the pathogenesis of LOCP [106–109].

Vitamin D deficiency was found to correlate with mortality in the course of neoplastic diseases [44–46]. Calcitriol modulates immune response of the tumor microenvironment through the inactivation of the NFκB (nuclear factor kappa-light-chain-enhancer of activated B cells) pathway [46]. The reference value for vitamin D in blood plasma is 75-125 nmol/L [111]. In our study, we observed that in the group of cancer patients, the vitamin D concentration was below the normal level. It is in accordance with the results of another research. Vitamin D deficiency was found to correlate with mortality in the course of neoplastic diseases [44–46]. The role of vitamin D in oral squamous cell carcinoma was investigated by Verma et al. [94]. Female C57BL/6 mice exposed to 4-nitroquinoline-1-oxide (4NQO) carcinogen were used. The animals were supplemented with vitamin D in the dose of 25-10,000 IU. The inhibition of tumor growth was observed. Beneficial effect in lowering oral mucositis in patients with head and neck cancer was also described by Bakr et al. [95]. The study involved 45 patients treated with radiotherapy divided into three groups. Two groups received topical oral vitamin D gel. Before the intervention, the levels of vitamin D in the blood serum of the patients were found to be deficient. The applied treatment not only reduced oral mucositis but also increased the level of vitamin D in the blood serum of patients. Also, Anand et al. [96] described vitamin D deficiency in oral cavity cancer patients. Moreover, the VDR overexpression in the course of oral cavity neoplasms was indicated in that study. Additionally, vitamin D appeared to play a special role in maintaining oral cavity health [112]. The surprising result of the present study is the negative correlation between CAT activity and vitamin D in the cancer group, suggesting that some regulatory mechanisms might be involved in the course of the disease. Undoubtedly, the role of vitamin D and its deficiency in LOCP cancer requires further research [112].

A significantly higher concentration of osteopontin was observed in our study in the LOCP patients. Also, Jeyasivanesan et al. [97] observed elevated osteopontin levels in patients with oral squamous cell carcinoma. Significant expression of osteopontin in salivary gland tumors was demonstrated in the study by Darling et al. [98]. Muramatsu et al. [99] analysed the effect of osteopontin levels on the invasiveness of oral cavity neoplasms. The study, performed on human oral squamous cell carcinoma cell lines, namely, HSC2, HSC3, HSC4, SAS, KB, and BSC-OF, revealed that high levels of osteopontin may increase the probability of metastasis. However, the mechanisms that link osteopontin and oral carcinomas have been not fully described yet. Presumably, osteopontin binds to integrin A4β1 and CD44 receptors, activating phosphoinositide 3-kinase/protein kinase B/mechanistic target of rapamycin (PI3K/AKT/mTOR1) pathway. In next step, mTOR1 regulates estrogen-related receptor alpha (ERRα), which binds to DNA and active transcription of osteopontin [113]. Overexpression of osteopontin was associated with increased angiogenesis, cancer cell proliferation, mobility, survival, invasion, and metastasis [113]. The positive correlation between osteopontin and lipid peroxidation, found in the present study, points to the association of the protein with deleterious oxidative processes in plasma membranes. Undoubtedly, these relations should be under further investigation.

The present study has some limitations. The small number of participants is a limiting factor. However, to the best of the authors' knowledge, no study has been conducted with the participation of patients with lip, oral cavity, and pharyngeal cancer of the European population, in which the mechanisms of antioxidant defense and the role of melatonin, vitamin D, and osteopontin were simultaneously analyzed.

5. Conclusions

The obtained results indicate a disruption of oxidant-antioxidant homeostasis in the lip, oral cavity, and pharyngeal cancer patients. Impaired antioxidant enzymatic defense and increased lipid peroxidation, correlated with high levels of osteopontin, were determined in this type of cancer. According to the results of the conducted study, melatonin seems not to be involved in the pathogenesis of the analyzed group of neoplasms. However, vitamin D deficiency in the LOCP patients was found. The role of elevated osteopontin in the pathogenesis of lip, oral cavity, and pharyngeal carcinoma requires further research. The simultaneous testing of vitamin D and osteopontin levels seems to be particularly noteworthy.

Data Availability

Data are available on request due to privacy/ethical restrictions.

Conflicts of Interest

The authors declare no conflict of interest.

Authors' Contributions

J.N., K.S.-G., and J.C. are responsible for the conceptualization; J.N., J.C., M.M., and. K.S.-G. for the methodology; J.N. and K.S.-G. for the formal analysis; J.N. K.S.-G., J.C., M.M., and M.P. for the investigation; J.N. for the data curation; J.N. for the writing—original draft preparation; J.N. and K.S.-G. for the writing—review and editing; J.N. for the visualization; A.W. and B.M. for the supervision; J.N. and K.S.-G. for the project administration; and A.W for the funding acquisition. All authors have read and agreed to the published version of the manuscript.

Acknowledgments

References

[1] K. D. Shield, J. Ferlay, A. Jemal et al., "The global incidence of lip, oral cavity, and pharyngeal cancers by subsite in 2012," *CA: a Cancer Journal for Clinicians*, vol. 67, no. 1, pp. 51–64, 2017.

[2] *World Health Organization International Agency for Research on Cancer Global Cancer Observatory* https://gco.iarc.fr/.

[3] D. Hashim, E. Genden, M. Posner, M. Hashibe, and P. Boffetta, "Head and neck cancer prevention: from primary prevention to impact of clinicians on reducing burden," *Annals of Oncology*, vol. 30, no. 5, pp. 744–756, 2019.

[4] K. Saika and T. Matsuda, "International comparison of lip, oral cavity and pharynx cancer incidence," *Japanese Journal of Clinical Oncology*, vol. 50, no. 4, pp. 479–480, 2020.

[5] B. Gupta, N. W. Johnson, and N. Kumar, "Global epidemiology of head and neck cancers: a continuing challenge," *Oncology*, vol. 91, no. 1, pp. 13–23, 2016.

[6] T. D. Ellington, S. J. Henley, V. Senkomago et al., "Trends in incidence of cancers of the oral cavity and pharynx — United States 2007–2016," *MMWR. Morbidity and Mortality Weekly Report*, vol. 69, no. 15, pp. 433–438, 2020.

[7] N. Schwartz, D. Nishri, S. Chin Cheong, N. Giesbrecht, and J. Klein-Geltink, "Is there an association between trends in alcohol consumption and cancer mortality? Findings from a multicountry analysis," *European Journal of Cancer Prevention*, vol. 28, no. 1, pp. 45–53, 2019.

[8] L. C. S. Thuler, R. F. de Menezes, and A. Bergmann, "Cancer cases attributable to alcohol consumption in Brazil," *Alcohol*, vol. 54, pp. 23–26, 2016.

[9] Y.-P. Chen, A. T. C. Chan, Q.-T. Le, P. Blanchard, Y. Sun, and J. Ma, "Nasopharyngeal carcinoma," *The Lancet*, vol. 394, no. 10192, pp. 64–80, 2019.

[10] B. C. Leonard, E. D. Lee, N. E. Bhola et al., "ATR inhibition sensitizes HPV− and HPV+ head and neck squamous cell carcinoma to cisplatin," *Oral Oncology*, vol. 95, pp. 35–42, 2019.

[11] V. Rai, S. Bose, S. Saha, and C. Chakraborty, "Evaluation of oxidative stress and the microenvironment in oral submucous fibrosis," *Heliyon*, vol. 5, no. 4, article e01502, 2019.

[12] H. Ram, J. Sarkar, H. Kumar, R. Konwar, M. L. B. Bhatt, and S. Mohammad, "Oral cancer: risk factors and molecular pathogenesis," *Journal of Maxillofacial and Oral Surgery*, vol. 10, no. 2, pp. 132–137, 2011.

[13] S. Reuter, S. C. Gupta, M. M. Chaturvedi, and B. B. Aggarwal, "Oxidative stress, inflammation, and cancer: how are they linked?," *Free Radical Biology & Medicine*, vol. 49, no. 11, pp. 1603–1616, 2010.

[14] J. G. Gill, E. Piskounova, and S. J. Morrison, "Cancer, oxidative stress, and metastasis," *Cold Spring Harbor Symposia on Quantitative Biology*, vol. 81, pp. 163–175, 2016.

[15] I. I. C. Chio and D. A. Tuveson, "ROS in cancer: the burning question," *Trends in Molecular Medicine*, vol. 23, no. 5, pp. 411–429, 2017.

[16] S. Chikara, L. D. Nagaprashantha, J. Singhal, D. Horne, S. Awasthi, and S. S. Singhal, "Oxidative stress and dietary phytochemicals: role in cancer chemoprevention and treatment," *Cancer Letters*, vol. 413, pp. 122–134, 2018.

[17] Y.-H. Lin, "MicroRNA networks modulate oxidative stress in cancer," *International Journal of Molecular Sciences*, vol. 20, no. 18, p. 4497, 2019.

[18] S. Sajadimajd and M. Khazaei, "Oxidative stress and cancer: the role of Nrf2," *Current Cancer Drug Targets*, vol. 18, no. 6, pp. 538–557, 2018.

[19] M. Murata, "Inflammation and cancer," *Environmental Health and Preventive Medicine*, vol. 23, no. 1, p. 50, 2018.

[20] A. V. Kudryavtseva, G. S. Krasnov, A. A. Dmitriev et al., "Mitochondrial dysfunction and oxidative stress in aging and cancer," *Oncotarget*, vol. 7, no. 29, pp. 44879–44905, 2016.

[21] B. L. Tan, M. E. Norhaizan, and W.-P.-P. Liew, "Nutrients and oxidative stress: friend or foe?," *Oxidative Medicine and Cellular Longevity*, vol. 2018, Article ID 9719584, 2018.

[22] S. K. Saha, S. B. Lee, J. Won et al., "Correlation between oxidative stress, nutrition, and cancer initiation," *International Journal of Molecular Sciences*, vol. 18, no. 7, p. 1544, 2017.

[23] P. Poprac, K. Jomova, M. Simunkova, V. Kollar, C. J. Rhodes, and M. Valko, "Targeting free radicals in oxidative stress-related human diseases," *Trends in Pharmacological Sciences*, vol. 38, no. 7, pp. 592–607, 2017.

[24] J. E. Klaunig, "Oxidative stress and cancer," *Current Pharmaceutical Design*, vol. 24, no. 40, pp. 4771–4778, 2019.

[25] V. Sosa, T. Moliné, R. Somoza, R. Paciucci, H. Kondoh, and M. E. LLeonart, "Oxidative stress and cancer: an overview," *Ageing Research Reviews*, vol. 12, no. 1, pp. 376–390, 2013.

[26] L.-D. Kajarabille, "Programmed cell-death by ferroptosis: antioxidants as mitigators," *International Journal of Molecular Sciences*, vol. 20, no. 19, p. 4968, 2019.

[27] R. K. Gupta, A. K. Patel, N. Shah et al., "Oxidative stress and antioxidants in disease and cancer: a review," *Asian Pacific Journal of Cancer Prevention*, vol. 15, no. 11, pp. 4405–4409, 2014.

[28] A. Ayala, M. F. Muñoz, and S. Argüelles, "Lipid peroxidation: production, metabolism, and signaling mechanisms of malondialdehyde and 4-hydroxy-2-nonenal," *Oxidative Medicine and Cellular Longevity*, vol. 2014, Article ID 360438, 2014.

[29] H. Sies, "Oxidative stress: a concept in redox biology and medicine," *Redox Biology*, vol. 4, pp. 180–183, 2015.

[30] X. G. Lei, J.-H. Zhu, W.-H. Cheng et al., "Paradoxical roles of antioxidant enzymes: basic mechanisms and health implications," *Physiological Reviews*, vol. 96, no. 1, pp. 307–364, 2016.

[31] G. Murdaca, A. Tonacci, S. Negrini et al., "Emerging role of vitamin D in autoimmune diseases: an update on evidence and therapeutic implications," *Autoimmunity Reviews*, vol. 18, no. 9, p. 102350, 2019.

[32] W. A. C. K. Koekkoek and A. R. H. van Zanten, "Antioxidant vitamins and trace elements in critical illness," *Nutrition in Clinical Practice*, vol. 31, no. 4, pp. 457–474, 2016.

[33] G. Hajiluian, M. Abbasalizad Farhangi, G. Nameni, P. Shahabi, and M. Megari-Abbasi, "Oxidative stress-induced cognitive impairment in obesity can be reversed by vitamin D administration in rats," *Nutritional Neuroscience*, vol. 21, no. 10, pp. 744–752, 2018.

[34] D.-H. Kim, C. A. Meza, H. Clarke, J.-S. Kim, and R. C. Hickner, "Vitamin D and endothelial function," *Nutrients*, vol. 12, no. 2, p. 575, 2020.

[35] L. R. Wilson, L. Tripkovic, K. H. Hart, and S. A. Lanham-New, "Vitamin D deficiency as a public health issue: using vitamin D2 or vitamin D3 in future fortification strategies," *The Proceedings of the Nutrition Society*, vol. 76, no. 3, pp. 392–399, 2017.

[36] G. Cardwell, J. Bornman, A. James, and L. Black, "A review of mushrooms as a potential source of dietary vitamin D," *Nutrients*, vol. 10, no. 10, p. 1498, 2018.

[37] A. Hanel and C. Carlberg, "Vitamin D and evolution: pharmacologic implications," *Biochemical Pharmacology*, vol. 173, p. 113595, 2020.

[38] S.-W. Chang and H.-C. Lee, "Vitamin D and health - the missing vitamin in humans," *Pediatrics and Neonatology*, vol. 60, no. 3, pp. 237–244, 2019.

[39] M. Sosa Henríquez and M. J. Gómez de Tejada Romero, "Cholecalciferol or calcifediol in the management of vitamin D deficiency," *Nutrients*, vol. 12, no. 6, p. 1617, 2020.

[40] Y. Zhang, F. Fang, J. Tang et al., "Association between vitamin D supplementation and mortality: systematic review and meta-analysis," *BMJ*, vol. 366, p. l4673, 2019.

[41] G. A. S. Casseb, M. P. Kaster, and A. L. S. Rodrigues, "Potential role of vitamin D for the management of depression and anxiety," *CNS Drugs*, vol. 33, no. 7, pp. 619–637, 2019.

[42] S. J. Wimalawansa, "Vitamin D deficiency: effects on oxidative stress, epigenetics, gene regulation, and aging," *Biology*, vol. 8, no. 2, pp. 15–30, 2019.

[43] M. Olszowiec-Chlebna, A. Koniarek-Maniecka, A. Brzozowska, A. Błauż, B. Rychlik, and I. Stelmach, "Vitamin D inhibits proinflammatory cytokines in the airways of cystic fibrosis patients infected by Pseudomonas aeruginosa- pilot study," *Italian Journal of Pediatrics*, vol. 45, no. 1, p. 41, 2019.

[44] N. Keum, D. H. Lee, D. C. Greenwood, J. E. Manson, and E. Giovannucci, "Vitamin D supplementation and total cancer incidence and mortality: a meta- analysis of randomized controlled trials," *Annals of Oncology*, vol. 30, no. 5, pp. 733–743, 2019.

[45] S. Minisola, F. Ferrone, V. Danese et al., "Controversies surrounding vitamin D: focus on supplementation and cancer," *International Journal of Environmental Research and Public Health*, vol. 16, no. 2, p. 189, 2019.

[46] M. A. Zmijewski, "Vitamin D and human health," *International Journal of Molecular Sciences*, vol. 20, no. 1, p. 145, 2019.

[47] B. Goulão, F. Stewart, J. A. Ford, G. MacLennan, and A. Avenell, "Cancer and vitamin D supplementation: a systematic review and meta-analysis," *The American Journal of Clinical Nutrition*, vol. 107, no. 4, pp. 652–663, 2018.

[48] B. Enkhjargal, J. Malaguit, W. M. Ho et al., "Vitamin D attenuates cerebral artery remodeling through VDR/AMPK/eNOS dimer phosphorylation pathway after subarachnoid hemorrhage in rats," *Journal of Cerebral Blood Flow and Metabolism*, vol. 39, no. 2, pp. 272–284, 2019.

[49] J. van de Peppel and J. P. T. M. van Leeuwen, "Vitamin D and gene networks in human osteoblasts," *Frontiers in Physiology*, vol. 5, pp. 1–10, 2014.

[50] M. A. Icer and M. Gezmen-Karadag, "The multiple functions and mechanisms of osteopontin," *Clinical Biochemistry*, vol. 59, pp. 17–24, 2018.

[51] L. Sayegh, G. E.-H. Fuleihan, and A. H. Nassar, "Vitamin D in endometriosis: a causative or confounding factor?," *Metabolism*, vol. 63, no. 1, pp. 32–41, 2014.

[52] B. Enkhjargal, D. W. McBride, A. Manaenko et al., "Intranasal administration of vitamin D attenuates blood–brain barrier disruption through endogenous upregulation of osteopontin and activation of CD44/P-gp glycosylation signaling after subarachnoid hemorrhage in rats," *Journal of*

Cerebral Blood Flow and Metabolism, vol. 37, no. 7, pp. 2555–2566, 2017.

[53] A.-S. Lamort, I. Giopanou, I. Psallidas, and G. T. Stathopoulos, "Osteopontin as a link between inflammation and cancer: the thorax in the spotlight," *Cell*, vol. 8, no. 8, p. 815, 2019.

[54] L. M. Castello, D. Raineri, L. Salmi et al., "Osteopontin at the crossroads of inflammation and tumor progression," *Mediators of Inflammation*, vol. 2017, Article ID 4049098, 22 pages, 2017.

[55] H. Miki, A. Okito, M. Akiyama, T. Ono, N. Tachikawa, and K. Nakahama, "Genetic and epigenetic regulation of osteopontin by cyclic adenosine 3' 5'-monophosphate in osteoblasts," *Gene*, vol. 763, p. 145059, 2020.

[56] P. Georgiadou, E. Iliodromitis, C. Varounis et al., "Relationship between plasma osteopontin and oxidative stress in patients with coronary artery disease," *Expert Opinion on Therapeutic Targets*, vol. 12, no. 8, pp. 917–920, 2008.

[57] M. Kocak, "The effect of antithyroid drugs on osteopontin and oxidative stress in graves' disease," *Acta Endocrinologica*, vol. 15, no. 2, pp. 221–224, 2019.

[58] J. Trostel, L. D. Truong, C. Roncal-Jimenez et al., "Different effects of global osteopontin and macrophage osteopontin in glomerular injury," *American Journal of Physiology-Renal Physiology*, vol. 315, no. 4, pp. F759–F768, 2018.

[59] T. Wolak, H. Kim, Y. Ren, J. Kim, N. D. Vaziri, and S. B. Nicholas, "Osteopontin modulates angiotensin II-induced inflammation, oxidative stress, and fibrosis of the kidney," *Kidney International*, vol. 76, no. 1, pp. 32–43, 2009.

[60] A. T. Slominski, R. Hardeland, M. A. Zmijewski, R. M. Slominski, R. J. Reiter, and R. Paus, "Melatonin: a cutaneous perspective on its production, metabolism, and functions," *The Journal of Investigative Dermatology*, vol. 138, no. 3, pp. 490–499, 2018.

[61] X. Meng, Y. Li, S. Li et al., "Dietary sources and bioactivities of melatonin," *Nutrients*, vol. 9, no. 4, p. 367, 2017.

[62] N. Ferlazzo, G. Andolina, A. Cannata et al., "Is melatonin the cornucopia of the 21st century?," *Antioxidants*, vol. 9, no. 11, p. 1088, 2020.

[63] S.-Y. Wang, X.-C. Shi, and P. Laborda, "Indole-based melatonin analogues: synthetic approaches and biological activity," *European Journal of Medicinal Chemistry*, vol. 185, p. 111847, 2020.

[64] R. Hardeland, "Melatonin and the electron transport chain," *Cellular and Molecular Life Sciences*, vol. 74, no. 21, pp. 3883–3896, 2017.

[65] G. Xu, J. Zhao, H. Liu, J. Wang, and W. Lu, "Melatonin inhibits apoptosis and oxidative stress of mouse Leydig cells via a SIRT1-dependent mechanism," *Molecules*, vol. 24, no. 17, p. 3084, 2019.

[66] R. He, M. Cui, H. Lin et al., "Melatonin resists oxidative stress-induced apoptosis in nucleus pulposus cells," *Life Sciences*, vol. 199, pp. 122–130, 2018.

[67] J. Jaworek, A. Leja-Szpak, K. Nawrot-Porąbka et al., "Effects of melatonin and its analogues on pancreatic inflammation, enzyme secretion, and tumorigenesis," *International Journal of Molecular Sciences*, vol. 18, no. 5, p. 1014, 2017.

[68] W. Talib, "Melatonin and cancer hallmarks," *Molecules*, vol. 23, no. 3, p. 518, 2018.

[69] R. Reiter, S. Rosales-Corral, D.-X. Tan et al., "Melatonin, a full service anti-cancer agent: inhibition of initiation, pro-

gression and metastasis," *International Journal of Molecular Sciences*, vol. 18, no. 4, p. 843, 2017.

[70] Y. Li, S. Li, Y. Zhou et al., "Melatonin for the prevention and treatment of cancer," *Oncotarget*, vol. 8, no. 24, pp. 39896–39921, 2017.

[71] S. Proietti, A. Cucina, M. Minini, and M. Bizzarri, "Melatonin, mitochondria, and the cancer cell," *Cellular and Molecular Life Sciences*, vol. 74, no. 21, pp. 4015–4025, 2017.

[72] F. Moradkhani, M. Moloudizargari, M. Fallah, N. Asghari, H. Heidari Khoei, and M. H. Asghari, "Immunoregulatory role of melatonin in cancer," *Journal of Cellular Physiology*, vol. 235, no. 2, pp. 745–757, 2020.

[73] S. Bhattacharya, K. K. Patel, D. Dehari, A. K. Agrawal, and S. Singh, "Melatonin and its ubiquitous anticancer effects," *Molecular and Cellular Biochemistry*, vol. 462, no. 1-2, pp. 133–155, 2019.

[74] W. Huo, Z.-M. Li, X.-Y. Pan, Y.-M. Bao, and L.-J. An, "Antioxidant enzyme levels in pathogenesis of oral squamous cell carcinoma (OSCC)," *Drug Research*, vol. 64, no. 11, pp. 629–632, 2014.

[75] S. Manoharan, K. Kolanjiappan, K. Suresh, and K. Panjamurthy, "Lipid peroxidation & antioxidants status in patients with oral squamous cell carcinoma," *The Indian Journal of Medical Research*, vol. 122, pp. 529–534, 2005.

[76] K. E. Sabitha and C. S. Shyamaladevi, "Oxidant and antioxidant activity changes in patients with oral cancer and treated with radiotherapy," *Oral Oncology*, vol. 35, no. 3, pp. 273–277, 1999.

[77] P. Patel, J. Patel, F. Shah, S. Shukla, and P. Shah, "Role of nitric oxide and antioxidant enzymes in the pathogenesis of oral cancer," *Journal of Cancer Research and Therapeutics*, vol. 5, no. 4, p. 247, 2009.

[78] *World Health Organization International classification of diseases for mortality and morbidity statistics (11th Revision)*https://icd.who.int/browse11/l-m/en.

[79] United Nations, *Population Division World Population Ageing*, Department of Economic and Social Affairs, 2015.

[80] H. P. Misra and I. Fridovich, "The role of superoxide anion in the autoxidation of epinephrine and a simple assay for superoxide dismutase," *The Journal of Biological Chemistry*, vol. 247, no. 10, pp. 3170–3175, 1972.

[81] R. F. Beers and I. W. Sizer, "A spectrophotometric method for measuring the breakdown of hydrogen peroxide by catalase," *The Journal of Biological Chemistry*, vol. 195, no. 1, pp. 133–140, 1952.

[82] D. E. Paglia and W. N. Valentine, "Studies on the quantitative and qualitative characterization of erythrocyte glutathione peroxidase," *The Journal of Laboratory and Clinical Medicine*, vol. 70, pp. 158–169, 1967.

[83] J. A. Buege and S. D. Aust, "Microsomal lipid peroxidation," in *In Methods in Enzymology Vol. 52*, pp. 302–310, Academic press, United States, 1978.

[84] H. Esterbauer and K. H. Cheeseman, "[42] Determination of aldehydic lipid peroxidation products: Malonaldehyde and 4-hydroxynonenal," in *Oxygen Radicals in Biological Systems Part B: Oxygen Radicals and Antioxidants vol. 186*, pp. 407–421, Elsevier, 1990.

[85] D. L. Drabkin, "Spectrophotometric studies: XIV. The crystallographic and optical properties of the hemoglobin of man in comparison with those of other species," *The Journal of Biological Chemistry*, vol. 164, no. 2, pp. 703–723, 1946.

[86] S. Gurudath, K. S. Ganapathy, A. Pai, S. Ballal, and M. L. Asha, "Estimation of superoxide dismutase and glutathione peroxidase in oral submucous fibrosis, oral leukoplakia and oral cancer - a comparative study," *Asian Pacific Journal of Cancer Prevention*, vol. 13, no. 9, pp. 4409–4412, 2012.

[87] R. Subapriya, R. Kumaraguruparan, S. Nagini, and A. Thangavelu, "Oxidant-antioxidant status in oral precancer and oral cancer patients," *Toxicology Mechanisms and Methods*, vol. 13, no. 1, pp. 77–81, 2003.

[88] V. Marakala, M. Malathi, and A. R. Shivashankara, "Lipid peroxidation and antioxidant vitamin status in oral cavity and oropharyngeal cancer patients," *Asian Pacific Journal of Cancer Prevention*, vol. 13, no. 11, pp. 5763–5765, 2012.

[89] U. U. Malik, I. A. Siddiqui, Z. Hashim, and S. Zarina, "Measurement of serum paraoxonase activity and MDA concentrations in patients suffering with oral squamous cell carcinoma," *Clinica Chimica Acta*, vol. 430, pp. 38–42, 2014.

[90] R. Chole, R. Patil, A. Basak, K. Palandurkar, and R. Bhowate, "Estimation of serum malondialdehyde in oral cancer AND precancer and its association with healthy individuals, gender, alcohol, and tobacco abuse," *Journal of Cancer Research and Therapeutics*, vol. 6, no. 4, p. 487, 2010.

[91] R. Liu, H. Wang, M. Deng et al., "Melatonin Inhibits Reactive Oxygen Species-Driven Proliferation, Epithelial- Mesenchymal Transition, and Vasculogenic Mimicry in Oral Cancer," *Oxidative Medicine and Cellular Longevity*, vol. 2018, Article ID 3510970, 2018.

[92] C.-Y. Yang, C.-K. Lin, C.-H. Tsao et al., "Melatonin exerts anti-oral cancer effect via suppressing LSD1 in patient-derived tumor xenograft models," *Oncotarget*, vol. 8, no. 20, pp. 33756–33769, 2017.

[93] H.-Y. Ho, C.-W. Lin, M.-H. Chien et al., "Melatonin suppresses TPA-induced metastasis by downregulating matrix metalloproteinase-9 expression through JNK/SP-1 signaling in nasopharyngeal carcinoma," *Journal of Pineal Research*, vol. 61, no. 4, pp. 479–492, 2016.

[94] A. Verma, V. K. Vincent-Chong, H. DeJong, P. A. Hershberger, and M. Seshadri, "Impact of dietary vitamin D on initiation and progression of oral cancer," *The Journal of Steroid Biochemistry and Molecular Biology*, vol. 199, p. 105603, 2020.

[95] I. S. Bakr, A. M. Zaki, R. M. El-Moslemany, and R. O. Elsaka, "Vitamin D oral gel for prevention of radiation-induced oral mucositis: a randomized clinical trial," *Oral Diseases*, vol. 27, no. 5, pp. 1197–1204, 2021.

[96] A. Anand, S. Singh, A. A. Sonkar et al., "Expression of vitamin D receptor and vitamin D status in patients with oral neoplasms and effect of vitamin D supplementation on quality of life in advanced cancer treatment," *Contemporary Oncology*, vol. 2, pp. 145–151, 2017.

[97] D. Jeyasivanesan, S. Mohamed, D. Pandiar, and S. Basheer, "Immunohistochemical analysis of osteopontin expression in oral squamous cell carcinoma," *Indian Journal of Dental Research*, vol. 30, no. 4, p. 539, 2019.

[98] M. R. Darling, M. Gauthier, L. Jackson-Boeters, T. D. Daley, A. F. Chambers, and A. B. Tuck, "Osteopontin expression in salivary gland tumours," *Oral Oncology*, vol. 42, no. 4, pp. 363–369, 2006.

[99] T. Muramatsu, K. Shima, K. Ohta et al., "Inhibition of osteopontin expression and function in oral cancer cell lines by antisense oligonucleotides," *Cancer Letters*, vol. 217, no. 1, pp. 87–95, 2005.

[100] M. Taylor, T. Carr, O. Oke et al., "E-cigarette aerosols induce lower oxidative stress in vitro when compared to tobacco smoke," *Toxicology Mechanisms and Methods*, vol. 26, no. 6, pp. 465–476, 2016.

[101] R. Carnevale, S. Sciarretta, F. Violi et al., "Acute impact of tobacco vs electronic cigarette smoking on oxidative stress and vascular function," *Chest*, vol. 150, no. 3, pp. 606–612, 2016.

[102] S. Abrahams, W. L. Haylett, G. Johnson, J. A. Carr, and S. Bardien, "Antioxidant effects of curcumin in models of neurodegeneration, aging, oxidative and nitrosative stress: a review," *Neuroscience*, vol. 406, pp. 1–21, 2019.

[103] J. Luo, K. Mills, S. le Cessie, R. Noordam, and D. van Heemst, "Ageing, age-related diseases and oxidative stress: what to do next?," *Ageing Research Reviews*, vol. 57, p. 100982, 2020.

[104] B. Speckmann, H. Steinbrenner, T. Grune, and L.-O. Klotz, "Peroxynitrite: from interception to signaling," *Archives of Biochemistry and Biophysics*, vol. 595, pp. 153–160, 2016.

[105] A. Sofo, A. Scopa, M. Nuzzaci, and A. Vitti, "Ascorbate peroxidase and catalase activities and their genetic regulation in plants subjected to drought and salinity stresses," *International Journal of Molecular Sciences*, vol. 16, no. 12, pp. 13561–13578, 2015.

[106] G. Gómez-Moreno, J. Guardia, M. Ferrera, A. Cutando, and R. Reiter, "Melatonin in diseases of the oral cavity," *Oral Diseases*, vol. 16, no. 3, pp. 242–247, 2010.

[107] R. J. Reiter, S. A. Rosales-Corral, X. Y. Liu, D. Acuna-Castroviejo, G. Escames, and D.-X. Tan, "Melatonin in the oral cavity: physiological and pathological implications," *Journal of Periodontal Research*, vol. 50, no. 1, pp. 9–17, 2015.

[108] A. Cutando, J. Aneiros-Fernández, J. Aneiros-Cachaza, and S. Arias-Santiago, "Melatonin and cancer: current knowledge and its application to oral cavity tumours," *Journal of Oral Pathology & Medicine*, vol. 40, no. 8, pp. 593–597, 2011.

[109] S. Najeeb, Z. Khurshid, S. Zohaib, and M. S. Zafar, "Therapeutic potential of melatonin in oral medicine and periodontology," *The Kaohsiung Journal of Medical Sciences*, vol. 32, no. 8, pp. 391–396, 2016.

[110] R. Hardeland, "Aging, melatonin, and the pro- and anti-inflammatory networks," *International Journal of Molecular Sciences*, vol. 20, no. 5, p. 1223, 2019.

[111] P. Pludowski, M. F. Holick, W. B. Grant et al., "Vitamin D supplementation guidelines," *The Journal of Steroid Biochemistry and Molecular Biology*, vol. 175, pp. 125–135, 2018.

[112] J. Botelho, V. Machado, L. Proença, A. S. Delgado, and J. J. Mendes, "Vitamin D deficiency and oral health: a comprehensive review," *Nutrients*, vol. 12, no. 5, p. 1471, 2020.

[113] E. S. Santos, J. C. Ramos, A. L. O. C. Roza, B. A. L. A. Mariz, and A. F. Paes Leme, "The role of osteopontin in oral cancer: a brief review with emphasis on clinical applications," *Oral Diseases*, pp. 1–10, 2020.

Research Article

The Possible Role of *Bifidobacterium longum* BB536 and *Lactobacillus rhamnosus* HN001 on Locomotor Activity and Oxidative Stress in a Rotenone-Induced Zebrafish Model of Parkinson's Disease

Ovidiu-Dumitru Ilie [iD],[1] **Emanuela Paduraru,**[2] **Madalina-Andreea Robea,**[1]
Ioana-Miruna Balmus,[3] **Roxana Jijie,**[3] **Mircea Nicoara,**[1] **Alin Ciobica** [iD],[1]
Ilinca-Bianca Nita,[4] **Romeo Dobrin** [iD],[5] **and Bogdan Doroftei**[4]

[1]*Department of Biology, Faculty of Biology, "Alexandru Ioan Cuza" University, Carol I Avenue, No 20A, 700505 Iasi, Romania*
[2]*Faculty of Geography and Geology, "Alexandru Ioan Cuza" University, Carol I Avenue, No 20A, 700505 Iasi, Romania*
[3]*Department of Exact and Natural Sciences, Institute of Interdisciplinary Research, "Alexandru Ioan Cuza" University, Carol I Avenue, No 11, 700506 Iasi, Romania*
[4]*Faculty of Medicine, University of Medicine and Pharmacy "Grigore T. Popa", University Street, No 16, 700115 Iasi, Romania*
[5]*Department of Psychiatry, Faculty of Medicine, University of Medicine and Pharmacy "Grigore T. Popa", University Street, No 16, 700115 Iasi, Romania*

Correspondence should be addressed to Romeo Dobrin; romeodobrin2002@gmail.com

Received 2 September 2021; Accepted 13 September 2021; Published 14 October 2021

Academic Editor: Jolanta Czuczejko

Background. As every organ within the body, the brain is also extremely susceptible to a plethora of noxious agents that change its chemistry. One component frequently found in current products against harmful species to crops is rotenone whose effect under prolonged exposure has been demonstrated to cause neurodegenerative disorders such as Parkinson's disease. The latest reports have indeed revealed that rotenone promotes Parkinson's in humans, but studies aiming to show congruent effects in zebrafish (*Danio rerio*) are lacking. *Material and Methods*. In this context, the aim of the present study was to demonstrate how chronic administration of rotenone for 3 weeks impairs the locomotor activity and sociability and induces oxidative stress in zebrafish. *Results*. There were no statistically significant differences following the analysis of their social interaction and locomotor tests ($p > 0.05$). However, several exceptions have been noted in the control, rotenone, and probiotics groups when we compared their locomotor activity during the pretreatment and treatment interval ($p < 0.05$). We further assessed the role of rotenone in disturbing the detoxifying system as represented by three enzymes known as superoxide dismutase (SOD), glutathione peroxidase (GPx), and malondialdehyde (MDA). Despite the fact that there were no statistically significant changes within SOD and GPx levels between the control group and rotenone, probiotics, and rotenone + probiotics ($p > 0.05$), relevant changes have been observed between the analyzed groups ($p < 0.05$ and $p < 0.005$, respectively). On the other hand, significant differences ($p < 0.05$) have been observed for MDA when we analyzed the data between the control group and the other three groups. *Conclusions*. Our results suggest that rotenone can be successfully used to trigger Parkinson's disease-related symptomatology in zebrafish.

1. Introduction

Parkinson's disease (PD) is the second most common neuro-degenerative disorder after Alzheimer's disease (AD) and is expected to advance by 2050. According to the latest published statistics, the incidence and prevalence fluctuate around 4.5-21, respectively, 18-328 cases at 100,000 individuals per year (~10 million worldwide). Although of onset is in the range of the fourth and seventh decades of life, the existing evidence refutes this hypothesis [1].

Mechanistically speaking, PD is characterized by a constant loss of dopaminergic and cholinergic neurons from the substantia nigra pars compacta (SNpc) and posterior motor nucleus of the vagus. Furthermore, it is characterized by the continuous storage and aggregation of the α-synuclein within the central nervous system (CNS) [2].

Despite best efforts, the etiology of PD remains obscure, recent studies revealing that PD actually possesses a multi-factorial substrate, reflected by major phenotypic changes. Specifically, the clinical signs exhibited by patients are grouped under the umbrella of the Parkinsonism spectrum and include essential tremor, stiffness, bradykinesia, and impaired postural balance [2].

Regarding its origin, PD has been shown to be caused by exposure to exogenous stressors (pesticides, heavy metals, or illicit substances) [3], either by abnormal gene expression, with or without family aggregation. By default, these determinants may gradually induce autosomal dominant PD or autosomal recessive juvenile PD [4]. However, people diagnosed and treated with antipsychotics are prone to significant side effects, a phenomenon known as drug-induced Parkinson's syndrome (PID) [5].

Cumulatively, it can be argued that PD is gradually triggered by various factors, but there are also situations in which the cause is idiopathic. Here was another long-time discussion due to the clinical heterogeneity and overlap between PD dementia, Lewy body dementia, and other types, which is why the nomenclature has been constantly reevaluated [6].

One common and usually underexplored feature of PD patients, yet crucial, is the role of anxiety [7] and depression [8] as promoters and/or pointers of PD. Analogous for healthy patients exposed to prolonged stress states as a risk group. The associated changes of the brain's chemistry have been extensively discussed from both perspectives [9, 10], and especially the petulant and abnormal oxidative stress (OS) that disrupts the physiological status of the redox potential [11]. The missing link of this puzzle could be the gut microbiota due to its ability to shape humans behavior and development, regardless of age, sex, and health status [12].

The most powerful vehicle used in clinical practice to diminish PD-related symptomatology and the associated comorbidities causative or not are probiotics [13]. These are live microorganisms known to have a helpful role in improving digestive function [14, 15]. Their implication in PD was often suggested in the last years [13, 16, 17]. Along this, there are not too many studies to sustain their importance in the PD diet but, until now, the evidence strongly supports probiotics [18]. It has been demonstrated in three

distinct randomized controlled trials that probiotics have the capacity to ameliorate all related-gastrointestinal deficiencies (constipation) in patients compared with the placebo. More precisely, the authors administered between 1 and 3 month strains of *Streptococcus*, *Enterococcus*, and especially *Bifidobacterium* and *Lactobacillus* and observed an improvement in life's quality, changes in fecal calprotectin, and less bowel deficiencies. However, the results following Unified Parkinson's Disease Rating Scale remained low despite the therapy [18–20].

Various animal models are being used in modeling PD disorder in order to observe the mechanisms or even possible find new therapeutic interventions in ameliorating and/or treating it. The successful usage of *Danio rerio* as a model for neurologic disorders is due to its main advantages such as physiological homology to human individuals, short time of replication, and low cost of breeding as compared to other experimental models, and it is also suitable for drug development studies [21]. Its implication in PD modeling was described and published in many reports over the years [22–27].

The pesticide rotenone was often used for inducing PD symptoms in rodents but also there are several studies which assessed rotenone's impact on zebrafish [28–31]. Rotenone was for a long time utilized in several commercialized insecticides, pesticides, or piscicides [24]. Beside behavioral aspects, rotenone is able to intervene in the OS balance by influencing enzymes level responsible with antioxidant role [32].

Having as support all these data, the aim of this study was to determine if probiotics brought a beneficial role in reducing the oxidative status and reestablishment potential of the motor impairment in a zebrafish PD model.

2. Material and Methods

2.1. Animal Husbandry. A total of sixty adults (6-8 months old) wild-type (WT) zebrafish (*Danio rerio*) were purchased from a local breeder. The fish were accommodated three weeks to laboratory conditions and kept in a 90 L recirculating dechlorinated water aquarium. Both aquariums (housing and experimental) respected the standard parameters as $26 \pm 2°C$ temperature, pH 7.5, with a 14 h light/10 h night cycle [33]. Water was changed daily in the experimental tanks. The adults were fed twice per day with TetraMin Flakes.

2.2. Ethical Approval. This experiment was performed by respecting the EU Commission Recommendation (2007), Directive 2010/63/EU of the European Parliament, and the Council of 22 September 2010 regarding protection, accommodation, and care of animals for scientific/experimental purposes [34, 35]. The current protocol was approved by the Ethical Committee of the Faculty of Biology, "Alexandru Ioan Cuza" University of Iasi with the registration number 11/25.05.2021.

2.3. Chemicals

2.3.1. Rotenone. Rotenone ($C_{23}H_{22}O_6$) was purchased from Toronto Research Chemicals, North York, Canada (Cat#

R700580), under a white powder that has been dissolved in distilled water until we reached a $2 \mu g L^{-1}$ concentration that was further administered daily for 21 days [30, 36].

2.3.2. Probiotics. Zircombi (ALFASIGMAS.p.A.) is a dedicated food supplement for people, having the appearance of a white powder that was purchased from a local pharmacy. It contains two strains—*Bifidobacterium longum* BB536-4 × 10^9 CFU (150 mg) and *Lactobacillus rhamnosus* HN001-1 × 10^9 CFU (25 mg) and Vit B$_6$-1.4 mg. We dissolved this mixture in ¼ water using a 100 ml rated balloon being administered half an hour before routine feeding in rearing water to ensure the ingestion as indicated by Valcarce et al. and obtaining as follows: $3 mg L^{-1}$ BB536, $0.5 mg L^{-1}$ HN001, and $0.02 mg L^{-1}$ vit. B$_6$ [37].

2.4. Design Protocol. After the accommodation period was over, they were subsequently divided into four equal groups ($n = 15$) and placed in small 10 L tanks for another two days in order to adapt to the new environment. Afterward, we assessed their swimming performance and sociability to determine whether or not are differences between pretreatment and treatment period. The groups were as follows: group 1 (control), group 2 (probiotics), group 3 (rotenone), and group 4 (rotenone + probiotics). The substances were daily renewed after water changing. The entire study lasted 21 days, and at the end of the experimental period, fishes were killed in water with ice at a temperature under 5°C [38].

2.5. Behavioral Assessment. The social interaction test was performed daily to evaluate the changes induced by rotenone and the possible behavior benefic role of probiotics. For this, we used a modified cross maze labyrinth closed by a slit and transformed into a T maze (10 h × 50 l × 50 w cm) filled with system water (5 cm) [39, 40]. The social stimulus was placed in the left arm of the T maze (Figure 1). The locomotor activity test was performed in the same maze. Once introduced, each fish was let to acclimate to the new conditions for half a minute. Movement was registered with a professional camera placed above the experimental chamber over a period of 240 seconds. Parameters were analyzed using EthoVision XT 11.5 software (Noldus Information Technology, Wageningen, The Netherlands). We focused on 3 specific parameters such as the total distance swam (cm), velocity (cm s^{-1}), and active status (s) for locomotor activity test and the time spent in the left arm (s) for social interaction test.

2.6. Oxidative Stress Measurement and Sample Preparation. Superoxide dismutase determination kit (SOD, 19160-1KT-F), Glutathione Peroxidase Cellular Activity Assay Kit (GPx, CGP1-1KT), and Protein Quantification Kit-Rapid (51254-KT) were purchased from Merck, Germany. All the analyses were performed according to the manufacturer's instructions. Malondialdehyde (MDA) levels were assessed by thiobarbituric acid-reactive assay following a preestablished work protocol [41].

At the end of chronic exposure period, each fish was individually well homogenized in a 10 volume of ice-cold saline (0.90% NaCl). Each sample was centrifuged at 5500 rpm for 10 min in accordance with the already estab-
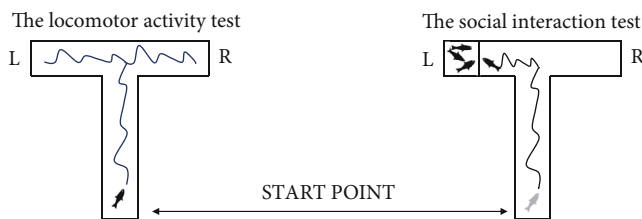
Figure 1: The experimental designs of zebrafish behavioral testing adapted to T-maze.

lished protocols by Jin et al. [42] and Ni et al. [43]. The supernatant obtained was aliquoted into 2 ml Eppendorf tubes for the subsequent determination of oxidative biomarkers levels. A spectrophotometer at distinct wavelengths (Specord 210 Plus producer Analytik Jena, Germany) was used to assess each enzyme activity.

2.7. Statistical Analysis. Through the Shapiro-Wilk test, we first analyzed the normality and distribution of the data, Microsoft Excel 2010 being used for editing, sorting, and coding of the raw data. The data was then exported into OriginPro v.9.3 (2016) software (OriginLab Corporation, Northampton, MA, USA). Thereafter, we used one-way ANOVA and Tukey HSD test to verify and certify whether or not there are significant different variances among investigated parameters from the start until endpoint [39, 44]. For the abovementioned behavioral parameters, data are presented as average ± SEM. For OS, we calculated the variance between the control and the experimental groups performing multiple comparisons; data expressed as average ± SEM. $p < 0.05$ was regarded as statistically significant.

3. Results

3.1. The Impact of Rotenone and Probiotics on Zebrafish Swimming Performance. According to our swimming performance, parameters as the total distance swam and the average velocity showed no pronounced effects of rotenone or probiotics administration after 21 days. Regarding the total distance swam, all the experimental groups recorded several changes between pretreatment and treatment period. The control group showed several picks of activity during experimental period compared to the pretreatment days as: D_10 (1240.03 ± 169.9 cm, $p = 0.01$ Tukey, ANOVA), D_13 (1209.58 ± 71.7 cm, $p = 0.02$ Tukey, ANOVA), and D_15 (1220.13 ± 104.2 cm, $p = 0.02$ Tukey, ANOVA) vs. 620.7 ± 127.8 cm. The second group exposed to rotenone did not present significant changes during the treatment excepting D_6 (1369.2 ± 255.8 cm, $p = 0.008$ Tukey, ANOVA) and D_14 (1642.9 ± 165.1 cm, $p = 0.002$ Tukey, ANOVA).

The third group treated with probiotics showed an increase of distance swam in the first days of the treatment with a highest value for the D_5 (1626.4 ± 138.2 cm, $p = 0.006$ Tukey, ANOVA). After 1 week of administration, the trend was composed from ups and downs as it can be seen in Figure 2. When rotenone and probiotics were administrated together, the activity of this parameter did not record important modifications ($p > 0.05$ ANOVA).
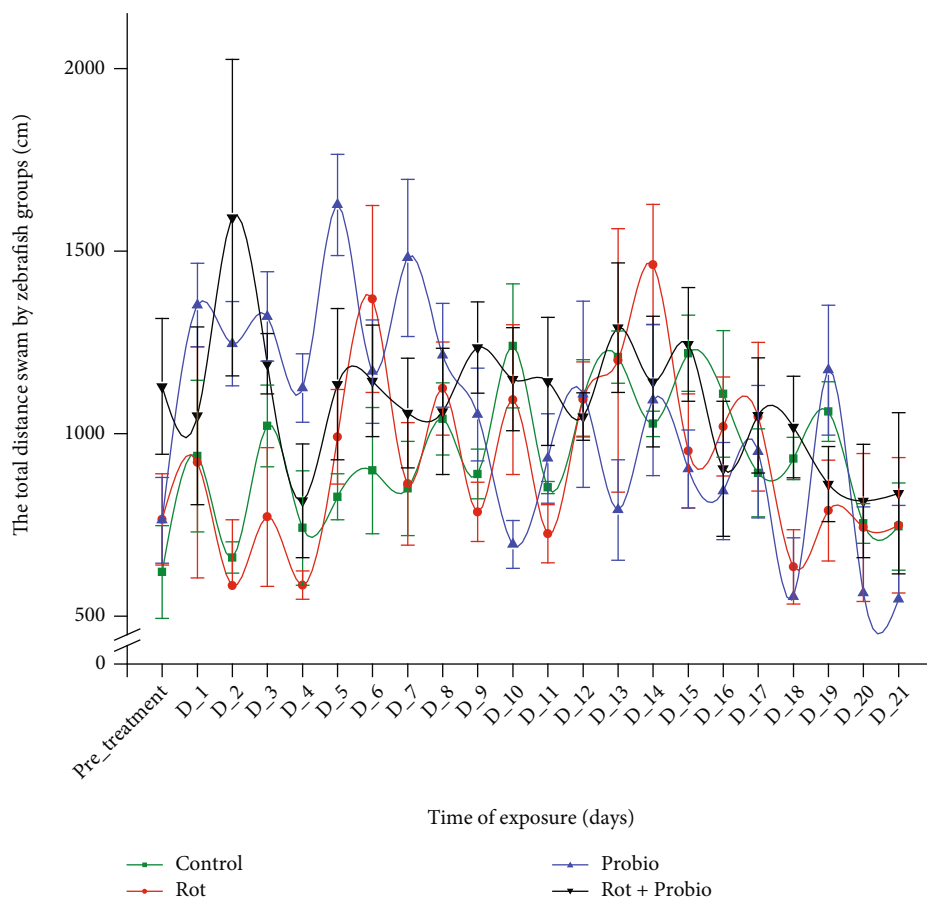
FIGURE 2: The total distance swam by experimental groups during locomotor activity test ($n = 15$). Green: control group, red: rotenone ($2\,\mu g\,L^{-1}$), blue: probiotics ($3\,mg\,L^{-1}$ BB536, $0.5\,mg\,L^{-1}$ HN001, and $0.02\,mg\,L^{-1}$ vit. B_6), black: rotenone ($2\,\mu g\,L^{-1}$) and probiotics ($3\,mg\,L^{-1}$ BB536, $0.5\,mg\,L^{-1}$ HN001, and $0.02\,mg\,L^{-1}$ vit. B_6). The groups mean was compared to pretreatment days mean, and the results were represented as average ± SEM.

No significant changes were observed for control, rotenone, and mixture group regarding the velocity parameter ($p > 0.05$ ANOVA). The trend was similar for the probiotic group excepting the short boost of hyperactivity in D_5 (6.77 ± 0.57 cm/s, $p = 0.005$ Tukey, ANOVA) compared to the pretreatment: 3.18 ± 0.42 cm/s (Figure 3).

We also determined the active status which measures the time spent by fish being active during the session. In the pretreatment days, fish from the control group showed a decrease in time moving, but its activity during the whole experimental period was following a constant trend. Fish exposed to rotenone recorded increases in time spent moving as D_6 (224.8 ± 10.8 s, $p = 0.03$ Tukey, ANOVA), D_8 (228.8 ± 5.22 s, $p = 0.02$ Tukey, ANOVA), D_12 (227.2 ± 3.52 s, $p = 0.02$ Tukey, ANOVA), D_14 (236.3 ± 1.50 s, $p = 0.007$ Tukey, ANOVA), D_16 (232.1 ± 3.78 s, $p = 0.01$ Tukey, ANOVA), and D_17 (223.5 ± 4.55 s, $p = 0.04$ Tukey, ANOVA) in comparison to 139.8 ± 12.7 s of pretreatment time. Regarding the activity for the third group treated with probiotics, its activity was similar with those observed for the abovementioned parameters and increases in the first part of the administration and then ups and downs. However, there was no statistically significant difference for the mixture group ($p > 0.05$ ANOVA) (Figure 4).

3.2. No Effect of Rotenone and Probiotic Administration on Zebrafish Sociability.
No significant changes were observed for the control and rotenone group ($p > 0.05$ ANOVA). The single administration of rotenone or probiotics did not have any effect on zebrafish sociability after 21 days of exposure as it can be seen in Figure 5. Moreover, a similar effect was also observed for the last group excepting D_19 when time spent next to the group increased considerably compared to pretreatment period (182.5 ± 16.5 s vs. 56.2 ± 19.8 s, $p = 0.01$ Tukey, ANOVA).

3.3. Oxidative Stress.
While analyzing the data regarding OS after 21 days of rotenone administration in zebrafish individuals, we noted several changes (Figure 6). For SOD, there was no statistically significant difference between the control group and the other three ($p > 0.05$) but rather when we compared the rotenone group with probiotics ($p = 0.014$) and probiotics + rotenone ($p = 0.011$). SOD level dropped in the rotenone-exposed group compared to the control group. Instead, the probiotics group showed an increase in SOD activity, result which was expected to obtain knowing the fact that probiotics can enhance SOD expression in living cells [45] and the differential response of each body depending on the organ investigated [46]. Meanwhile, the
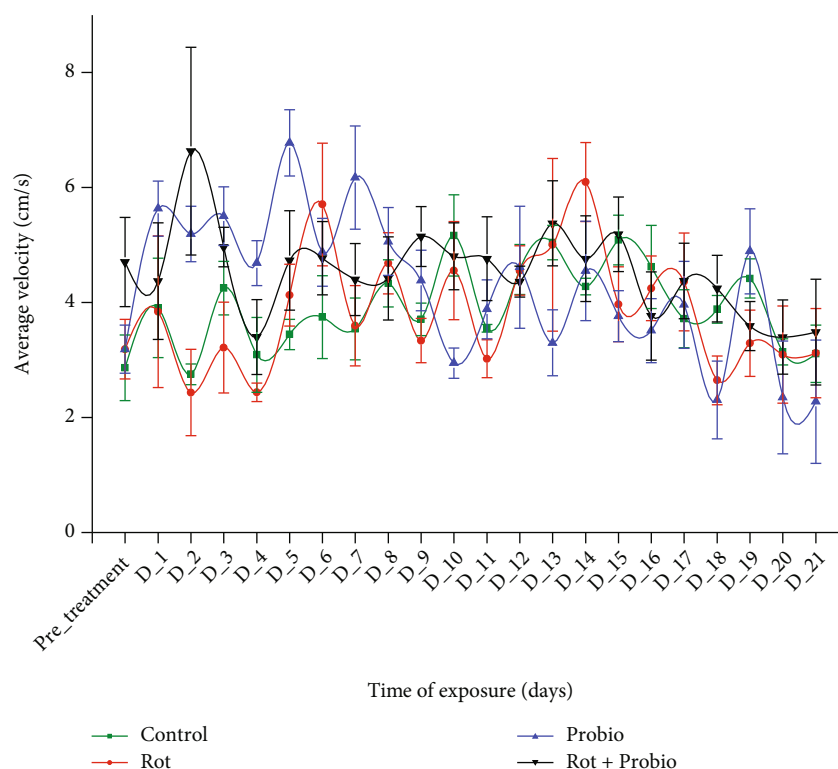
FIGURE 3: The average velocity of the experimental groups recorded during locomotor activity test ($n = 15$). Green: control group, red: rotenone ($2 \mu g \, L^{-1}$), blue: probiotics ($3 \, mg \, L^{-1}$ BB536, $0.5 \, mg \, L^{-1}$ HN001, and $0.02 \, mg \, L^{-1}$ vit. B$_6$), black: rotenone ($2 \mu g \, L^{-1}$) and probiotics ($3 \, mg \, L^{-1}$ BB536, $0.5 \, mg \, L^{-1}$ HN001, and $0.02 \, mg \, L^{-1}$ vit. B$_6$). The group mean was compared to pretreatment days mean, and the results were represented as average ± SEM.

last group exposed to rotenone and probiotics had also an increase in SOD level but still with no considerable change compared to control.

In the case of GPx, analogous results were obtained since there were no statistically significant differences between the control group and the rest of the groups investigated ($p > 0.05$). On the other hand, there was a significant change of GPx level when compared rotenone group with probiotics ($p = 0.001$) and rotenone + probiotics ($p = 0.004$) groups. It is already known that OS is often reported as a risk factor in PD development [47–49]. SOD and GPx are considered to be the first line defense against free radicals [50] and a diet supplementation with Lactobacillus fermentum enhance the antioxidant system as reported by Wang et al. [51]. A similar pattern has been also observed for GPx despite the fact that no significant difference, whereas the level of SOD is compensatory increased. Based on these considerations, there is certainty of the existence of OS. The possible explanation is that Bifidobacterium longum BB536 and Lactobacillus rhamnosus HN001 modulate anxiety state in Danio rerio but at the same time promote a hyperlocomotor activity [52], hence, these abnormal levels of OS biomarkers.

Furthermore, the main marker of lipidic peroxidation, MDA, presented significant high levels ($p < 0.05$) in the control group as compared with probiotics ($p = 0.033$) and in contrast with rotenone and probiotics ($p = 0.032$). Also, there were significant changes in terms of MDA levels between the rotenone group and probiotics ($p = 0.009$) and

rotenone + probiotics ($p = 0.01$) groups, respectively. Congruent with other studies, it appears that MDA is significantly increased after 30 days of $2 \, mg \, L^{-1}$ rotenone administration [46], Bifidobacterium longum BB536 being a reliable bacteria attributed to the reestablishment of the antioxidant system [53].

4. Discussion

A variety of reports have highlighted that fish, among other aquatic organisms, are deeply sensitive to pollutants and also to natural compounds used as pesticide. In our study, chronic administration of rotenone was performed in zebrafish adults, and its effect on behavior and OS was measured. We observed that administration of $2 \mu g \, L^{-1}$ rotenone had impacted the total distance travelled during test session presenting ups and downs compared to the pretreatment time. For example, Khotimah et al. [54] reported a decreased motility after 2 weeks of $5 \mu g/L$ rotenone administration. As already reported by Wang et al. [30] and our team, there were no significant differences in terms of locomotor impairment, thus, further highlighting the fact that PD triggering in Danio rerio is dependent on dosage and time of administration. These changes in locomotor activity can be a consequence of mitochondrial dysfunction which is responsible with ATP production or/and overproduction of free radicals. It was suggested that these abovementioned can lead to dopamine deficiency and apoptosis by the study
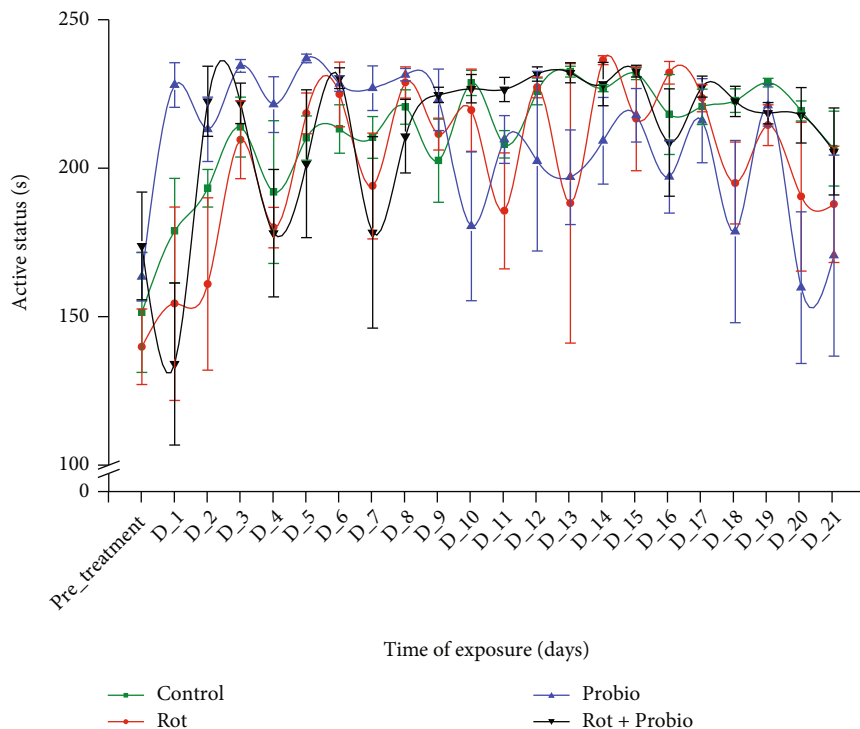
FIGURE 4: The active status of the experimental groups recorded during locomotor activity test ($n = 15$). Green: control group, red: rotenone ($2 \mu g \, L^{-1}$), blue: probiotics ($3 \, mg \, L^{-1}$ BB536, $0.5 \, mg \, L^{-1}$ HN001, and $0.02 \, mg \, L^{-1}$ vit. B_6), black: rotenone ($2 \mu g \, L^{-1}$) and probiotics ($3 \, mg \, L^{-1}$ BB536, $0.5 \, mg \, L^{-1}$ HN001, and $0.02 \, mg \, L^{-1}$ vit. B_6). The groups mean was compared to pretreatment days mean, and the results were represented as average ± SEM.
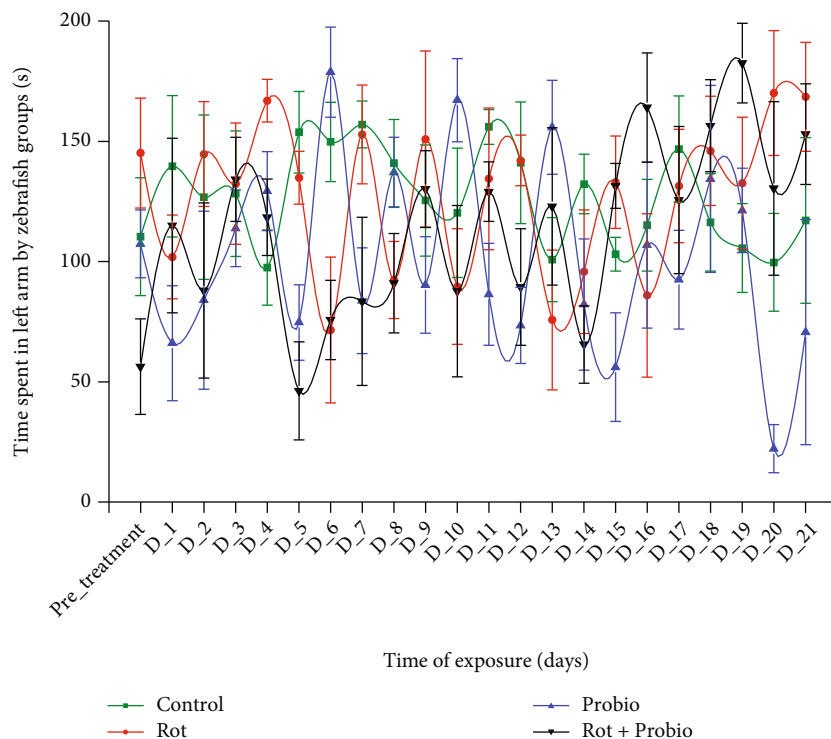
FIGURE 5: The time spent in the left arm by the experimental groups recorded during social interaction test ($n = 15$). Green: control group, red: rotenone ($2 \mu g \, L^{-1}$), blue: probiotics ($3 \, mg \, L^{-1}$ BB536, $0.5 \, mg \, L^{-1}$ HN001, and $0.02 \, mg \, L^{-1}$ vit. B_6), black: rotenone ($2 \mu g \, L^{-1}$) and probiotics ($3 \, mg \, L^{-1}$ BB536, $0.5 \, mg \, L^{-1}$ HN001, and $0.02 \, mg \, L^{-1}$ vit. B_6). The groups mean was compared to pretreatment days mean, and the results were represented as average ± SEM.
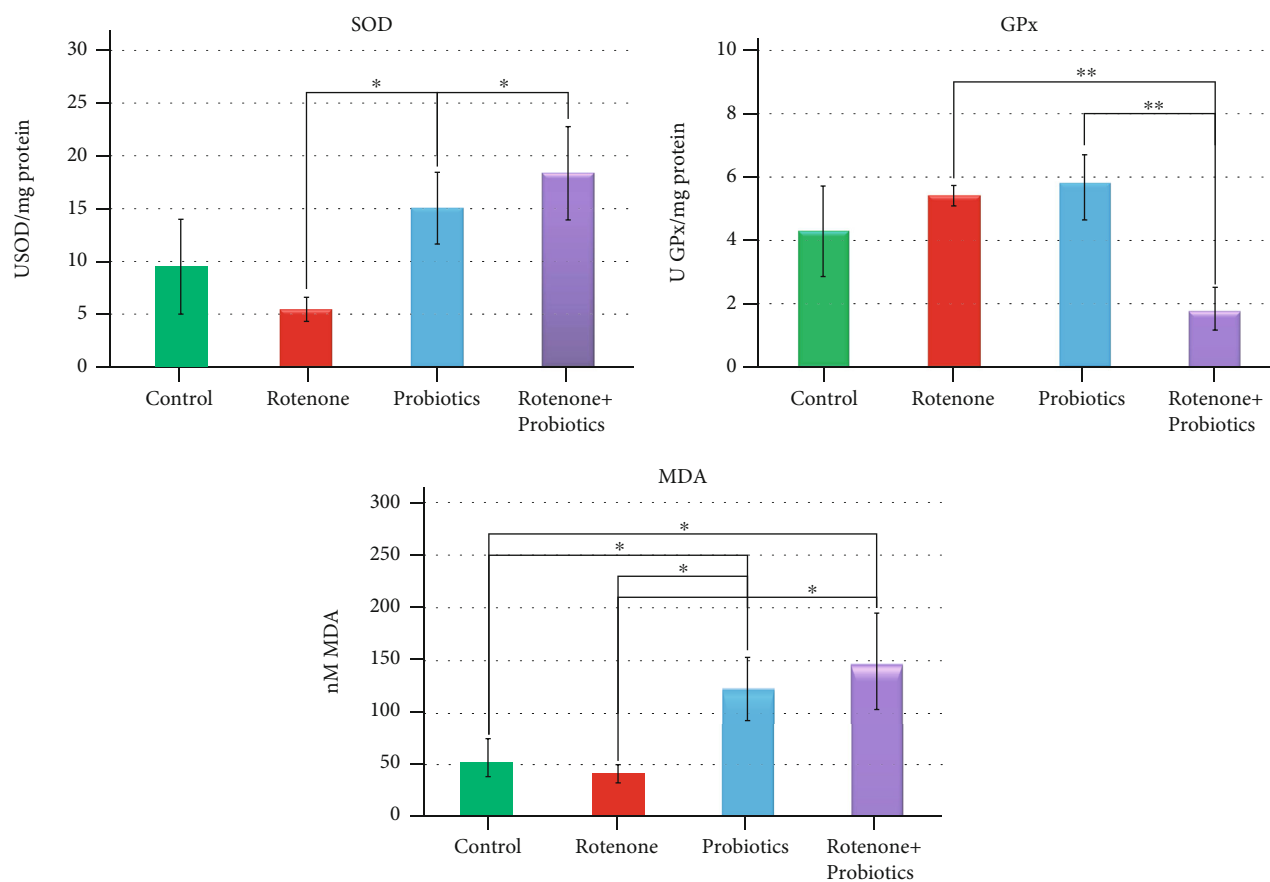
Figure 6: The activity of superoxide dismutase (SOD), glutathione peroxidase (GPx), and malondialdehyde (MDA) levels in zebrafish chronically exposed to rotenone and probiotics. Data were expressed as average ± SEM ($^*p < 0.05$; $^{**}p < 0.005$).

of Khotimah and his team in 2015 after chronic treatment of zebrafish with $5\,\mu g\,L^{-1}$ rotenone for 28 days [54]. One year later Khatri and Juvekar also evaluated the influence of $5\,\mu g\,L^{-1}$ rotenone on swimming behavior after 14 days of treatment [55].

When rotenone and probiotics were given together, this parameter did not show any significant changes. This could be an effect triggered by probiotic presence in the medium based on the third group results exposed only to probiotics where their activity was particularly increased in the first week of the treatment than the normal behavior recorded in the pretreatment.

It is interesting to observe that active status was different in the case of the second and forth group which received rotenone, respectively, rotenone and probiotics in the first day of treatment. Rotenone administration led to a hazardous zebrafish activity for all the period in comparison to the rotenone and probiotics group whose activity was adjusted after only 1 week of probiotic treatment.

To determine if rotenone has certain effects on zebrafish sociability the social interaction test was performed daily. According to our data, no significant impact on sociability was registered, fish manifesting contradictory behavior day after day. Even probiotic administration did not induce important advances in zebrafish social domain; it just sustains the normal activity. It was showed that the adminis-

tration of probiotics together with oxytocin could have a positive influence on social domain in an ASD mouse model [56].

OS is a common risk factor often reported in PD pathogenesis [48, 57]. Described as imbalance between antioxidants and oxidants, OS generates serious cellular damage which causes, mainly, neuronal degeneration [58]. In our study, we observed several changes in the antioxidant enzymes activity and an increased level of lipidic peroxidation. Treatment with $2\,\mu g\,L^{-1}$ rotenone for 21 days leads to a decrease in SOD level which was in agreement with Khan's study observations made on PD patients regarding OS markers [49]. On the other hand, SOD production was encouraged by probiotics. For example, diet supplementation with *Lactobacillus fermentum* could increase the level of SOD and GPx in pigs [51].

Exposing adult zebrafish to $2\,mg\,L^{-1}$ rotenone for 30 days showed significant activity of MDA and decreased SOD level both intestines and brain for glutathione-S-transferase (GST) and catalase (CAT) level [46]. Neurodegeneration and OS have also been recorded after experimental exposure of human liver HepG2 cells to a range between 12.5 and $250\,\mu M$ rotenone for 24 hours [59]. If rotenone favors OS, probiotic presence can stimulate the antioxidant system as it was demonstrated in our study by high levels of SOD and GPX.

Due to potentially antioxidant role, probiotics started to receive more attention, and since OS was linked to altered gut microbiota. The gut-brain axis is an important interaction which has been reported to be disrupted in PD individuals [60–62].

For example, Bhattaraiet al. and Dodiya and coauthors [63, 64] administered 10 mg/kg/day of rotenone for six and twelve weeks, respectively, and brought several solid arguments in this context. The administration for a period of 6 weeks led to a loss of tyrosine hydroxylase (TH) neurons in both conventionally raised mice and germ-free. In parallel, it resulted in a decrease in motor strength and coordination. The researchers concluded that chronic rotenone intake did not cause dysbiosis, rather a shift among bacterial load and increased in the first month and permeability in conventionally raised mice. On the other hand, it promoted elevated urinary cortisol, intestinal hyperpermeability, and a diminished abundance of lactic bacteria (*Lactobacillus*) in restraint stress mice by comparison with the control during the first month and a half. Moreover, rotenone alone without restraint stress disrupted the colonic expression of the tight junction protein ZO-1 and increased the protein level of α-syn in the colon, N-tyrosine as a marker of OS, and myenteric plexus enteric glial cell-glial fibrillary acidic protein expression by comparing with the control group. In the restraint stress rotenone-induced was observed analogous changes as in the rotenone alone group with several exceptions; intestinal hyperpermeability, an abnormal expression of Occludin and Claudin1, and increased ratio of fecal *Akkermania* and endotoxemia. Nevertheless, an intraperitoneal injection of 2.75 mg/kg rotenone, 5 days per week for 1 month promoted GI dysfunctionalities like diarrhea and delayed gastric emptying. The subsequent microbiota analyses revealed alterations along the small intestine and colon, whereas histological examination indicates a mucosal thickening and goblet cell hyperplasia in the colon [65].

Nonetheless, *Bifidobacterium longum* BB536 and *Lactobacillus rhamnosus* HN001 are two probiotic strains that have been previously administered also in patients suffering from irritable bowel syndrome (IBS). Specifically, there was a statistically significant decrease ($p < 0.0001$) within two parameters regarding "abdominal pain" and "bloating" and overall severity of disease between IBS patients and placebo. The beneficial effects were more detectable in IBS-diarrhea patients as indicated by the Bristol scale ($p < 0.00001$) in contrast with placebo ($p = 0.04$), while in IBS-constipation, there was only a slight improvement ($p = 0.06$) [66]. Similar findings were made by another team in which they enrolled lactose intolerance patients vs. placebo. This time, the physical symptoms panel as indicated by "bloating" ($p = 0.028$) and "constipation" ($p = 0.045$) were ameliorated in lactose intolerance patients as compared to placebo.

Another preliminary study revealed an increased load of both these species in pre- and postprandial individuals that persisted even after one month following the end of oral intake. At the phyla level, there was observed a significant decrease of *Firmicutes*, *Proteobacteria* as compared with the sample collected prior to the actual procedure. At the species level, the authors noted an increased abundance

of several microorganisms including *Blautia producta/wexlerae*, *Haemophilus ducrey*, *Akkermansia muciniphila*, *Roseburia faecis*, and *Ruminococcus gnavus* during follow-up, followed by a reduction of *Holdemania filiformis*, *Escherichia vulneris*, *Gemmiger formicilis*, and *Streptococcus sinensis* [67].

This mixture has been also successfully administered in rat models. According to the results of Alsheraji et al., [53] *Bifidobacterium longum* BB536 reduced total cholesterol, very-low, low and high-density lipoprotein cholesterol, and atherosclerotic index amounts, concomitantly with that of liver-lipid deposition and adipocyte size. In the same study, they demonstrated that the plasma MDA level significantly decreased after the administration of *Bifidobacterium longum* BB536.

Bifidobacterium longum BB536 and *Lactobacillus rhamnosus* HN001, in combination and/or individually, possess the ability to inhibit the activity of the major Gramnegative strains, even opportunistic pathogenic entities such as *Candida* [68, 69]. Different teams of researchers have also revealed in several other occasions that rotenone causes a dysfunction of the rat's and mice's gastrointestinal microbiota as well. Precisely, there was observed a decrease of *Bifidobacterium* genus, as well as in *Firmicutes* and *Bacteroides* phyla [70, 71].

5. Conclusions

It can be concluded based on our results that rotenone is a potent toxic agent that can be successfully used to trigger PD-related symptomatology in *Danio rerio*. Furthermore, it can offer a pathway to improve our knowledge regarding the etiology of PD, and these observations can be in the future further extrapolated to human individuals. Even though *Bifidobacterium longum* BB536 and *Lactobacillus rhamnosus* HN001 did not improve the locomotor activity, nor diminish oxidative status in zebrafish but rather induced a hyper-activity, our study offered a new perspective in contrast with the existing information.

Data Availability

The datasets used and analyzed during the current study are available from the corresponding author on reasonable request.

Conflicts of Interest

The authors declare no conflict of interest.

References

[1] E. R. Dorsey, A. Elbaz, E. Nichols et al., "Global, regional, and national burden of Parkinson's disease, 1990-2016: a systematic analysis for the global burden of disease study 2016," *Lancet Neurology*, vol. 17, no. 11, pp. 939–953, 2018.

[2] W. Poewe, K. Seppi, C. M. Tanner et al., "Parkinson disease," *Nature Reviews Disease Primers*, vol. 3, no. 1, 2017.

[3] N. Ball, W.-P. Teo, S. Chandra, and J. Chapman, "Parkinson's disease and the environment," *Frontiers in Neurology*, vol. 10, p. 218, 2019.

[4] P.-L. Zhang, Y. Chen, C.-H. Zhang, Y.-X. Wang, and P. Fernandez-Funez, "Genetics of Parkinson's disease and related disorders," *Journal of medical genetics*, vol. 55, no. 2, pp. 73–80, 2018.

[5] F. Brigo, R. Erro, A. Marangi, K. Bhatia, and M. Tinazzi, "Differentiating drug-induced parkinsonism from Parkinson's disease: an update on non-motor symptoms and investigations," *Parkinsonism & Related Disorders*, vol. 20, no. 8, pp. 808–814, 2014.

[6] C. Marras, A. Lang, B. P. van de Warrenburg et al., "Nomenclature of genetic movement disorders: recommendations of the international Parkinson and movement disorder society task force," *Movement Disorders*, vol. 31, no. 4, pp. 436–457, 2016.

[7] J. J. Chen and L. Marsh, "Anxiety in Parkinson's disease: identification and management," *Therapeutic Advances in Neurological Disorders*, vol. 7, no. 1, pp. 52–59, 2014.

[8] L. Marsh, "Depression and Parkinson's disease: current knowledge," *Current Neurology and Neuroscience Reports*, vol. 13, no. 12, p. 409, 2013.

[9] L. Mah, C. Szabuniewicz, and A. J. Fiocco, "Can anxiety damage the brain?," *Current Opinion in Psychiatry*, vol. 29, no. 1, pp. 56–63, 2016.

[10] S. C. Trifu, A. C. Trifu, E. Aluaș, M. A. Tătaru, and R. V. Costea, "Brain changes in depression," *Romanian Journal of Morphology and Embryology*, vol. 61, no. 2, pp. 361–370, 2020.

[11] V. Dias, E. Junn, and M. M. Mouradian, "The role of oxidative stress in Parkinson's disease," *Journal of Parkinson's Disease*, vol. 3, no. 4, pp. 461–491, 2013.

[12] S. M. Jandhyala, R. Talukdar, C. Subramanyam, H. Vuyyuru, M. Sasikala, and D. Nageshwar Reddy, "Role of the normal gut microbiota," *World Journal of Gastroenterology*, vol. 21, no. 29, pp. 8787–8803, 2015.

[13] A. H. Tan, J. W. Hor, C. W. Chong, and S.-Y. Lim, "Probiotics for Parkinson's disease: current evidence and future directions," *JGH Open*, vol. 5, no. 4, pp. 414–419, 2021.

[14] M. Kechagia, D. Basoulis, S. Konstantopoulou et al., "Health benefits of probiotics: a review," *International Scholarly Research Notices*, vol. 2013, Article ID 481651, 7 pages, 2013.

[15] R. George Kerry, J. K. Patra, S. Gouda, Y. Park, H.-S. Shin, and G. Das, "Benefaction of probiotics for human health: a review," *Journal of Food and Drug Analysis*, vol. 26, no. 3, pp. 927–939, 2018.

[16] L. Magistrelli, A. Amoruso, L. Mogna et al., "Probiotics may have beneficial effects in Parkinson's disease: in vitro evidence," *Frontiers in Immunology*, vol. 10, p. 969, 2019.

[17] P. Gazerani, "Probiotics for Parkinson's disease," *International Journal of Molecular Sciences*, vol. 20, no. 17, p. 4121, 2019.

[18] O. R. Tamtaji, M. Taghizadeh, R. Daneshvar Kakhaki et al., "Clinical and metabolic response to probiotic administration in people with Parkinson's disease: a randomized, double-blind, placebo-controlled trial," *Clinical Nutrition*, vol. 38, no. 3, pp. 1031–1035, 2019.

[19] M. Barichella, C. Pacchetti, C. Bolliri et al., "Probiotics and prebiotic fiber for constipation associated with Parkinson disease," *Neurology*, vol. 87, no. 12, pp. 1274–1280, 2016.

[20] A. H. Tan, S.-Y. Lim, K. K. Chong et al., "Probiotics for constipation in Parkinson disease," *Neurology*, vol. 96, pp. e772LP–e782LP, 2020.

[21] R. L. Vaz, T. F. Outeiro, and J. J. Ferreira, "Zebrafish as an animal model for drug discovery in Parkinson's disease and other movement disorders: a systematic review," *Frontiers in Neurology*, vol. 9, p. 347, 2018.

[22] Y. Vijayanathan, F. T. Lim, S. M. Lim et al., "6-OHDA-lesioned adult zebrafish as a useful Parkinson's disease model for dopaminergic neuroregeneration," *Neurotoxicity Research*, vol. 32, no. 3, pp. 496–508, 2017.

[23] M. E. Nunes, T. E. Muller, M. M. Braga et al., "Chronic treatment with paraquat induces brain injury, changes in antioxidant defenses system, and modulates behavioral functions in zebrafish," *Molecular Neurobiology*, vol. 54, no. 6, pp. 3925–3934, 2017.

[24] M.-A. Robea, I.-M. Balmus, A. Ciobica et al., "Parkinson's disease-induced zebrafish models: focussing on oxidative stress implications and sleep processes," *Oxidative Medicine and Cellular Longevity*, vol. 2020, Article ID 1370837, 15 pages, 2020.

[25] C.-W. Feng, Z.-H. Wen, S.-Y. Huang et al., "Effects of 6-hydroxydopamine exposure on motor activity and biochemical expression in zebrafish (Danio rerio) larvae," *Zebrafish*, vol. 11, no. 3, pp. 227–239, 2014.

[26] J. W. Bortolotto, G. P. Cognato, R. R. Christoff et al., "Long-term exposure to paraquat alters behavioral parameters and dopamine levels in adult zebrafish (Danio rerio)," *Zebrafish*, vol. 11, no. 2, pp. 142–153, 2014.

[27] C. Milanese, J. J. Sager, Q. Bai et al., "Hypokinesia and reduced dopamine levels in zebrafish lacking β\- and γ1-synucleins," *The Journal of Biological Chemistry*, vol. 287, no. 5, pp. 2971–2983, 2012.

[28] S. Martel, J. Y. Keow, and M. Ekker, "Rotenone neurotoxicity causes dopamine neuron loss in zebrafish," *University of Ottawa Journal of Medicine*, vol. 5, no. 2, pp. 16–21, 2015.

[29] K. M. Melo, R. Oliveira, C. K. Grisolia et al., "Short-term exposure to low doses of rotenone induces developmental, biochemical, behavioral, and histological changes in fish," *Environmental Science and Pollution Research*, vol. 22, no. 18, pp. 13926–13938, 2015.

[30] Y. Wang, W. Liu, J. Yang et al., "Parkinson's disease-like motor and non-motor symptoms in rotenone-treated zebrafish," *Neurotoxicology*, vol. 58, pp. 103–109, 2017.

[31] M. A. Robea, S. A. Strungaru, C. Lenzi, M. Nicoara, and A. Ciobica, "The importance of rotenone in generating neurological and psychiatric features in zebrafish-relevance for a Parkinson's disease model," *Academy of Romanian Scientists*, vol. 7, pp. 59–67, 2018.

[32] V. Bashkatova, M. Alam, A. Vanin, and W. J. Schmidt, "Chronic administration of rotenone increases levels of nitric oxide and lipid peroxidation products in rat brain," *Experimental Neurology*, vol. 186, no. 2, pp. 235–241, 2004.

[33] B. Reed and M. Jennings, "Guidance on the housing and care of zebrafish danio rerio," in *Guidance on the housing and care of zebrafish Danio rerio*, pp. 21–41, Royal Society for the Prevention of Cruelty to Animals (RSPCA), Horsham, UK, 2011.

[34] "Commission Recommendation Guidelines for the accommodation and care of animals used for experimental and other scientific purposes (notified under document number C(2007) 2525)," *Official Journal of the European Union*, vol. 50., 2007.

[35] "Directive 63 The protection of animals used for scientific purposes," *Official Journal of the European Union*, vol. 53, 2010.

[36] S. Bretaud, S. Lee, and S. Guo, "Sensitivity of zebrafish to environmental toxins implicated in Parkinson's disease," *Neurotoxicology and Teratology*, vol. 26, no. 6, pp. 857–864, 2004.

[37] D. G. Valcarce, M. F. Riesco, J. M. Martínez-Vázquez, and V. Robles, "Diet supplemented with antioxidant and anti-inflammatory probiotics improves sperm quality after only one spermatogenic cycle in zebrafish model," *Nutrients*, vol. 11, no. 4, 2019.

[38] A. M. Valentim, F. J. van Eeden, U. Strähle, and I. A. S. Olsson, "Euthanizing zebrafish legally in Europe: are the approved methods of euthanizing zebrafish appropriate to research reality and animal welfare?," *EMBO Reports*, vol. 17, no. 12, pp. 1688-1689, 2016.

[39] S.-A. Strungaru, G. Plavan, A. Ciobica et al., "Acute exposure to gold induces fast changes in social behavior and oxidative stress of zebrafish (*Danio rerio*)," *Journal of Trace Elements in Medicine and Biology*, vol. 50, pp. 249–256, 2018.

[40] M. A. Robea, R. Jijie, M. Nicoara et al., "Vitamin C attenuates oxidative stress and behavioral abnormalities triggered by fipronil and pyriproxyfen insecticide chronic exposure on zebrafish juvenile," *Antioxidants*, vol. 9, no. 10, p. 944, 2020.

[41] I.-M. Balmus, R. Lefter, A. Ciobica et al., "Preliminary biochemical description of brain oxidative stress status in irritable bowel syndrome contention-stress rat model," *Medicina*, vol. 55, no. 12, p. 776, 2019.

[42] Y. Jin, Z. Liu, F. Liu, Y. Ye, T. Peng, and Z. Fu, "Embryonic exposure to cadmium (II) and chromium (VI) induce behavioral alterations, oxidative stress and immunotoxicity in zebrafish (*Danio rerio*_)," *Neurotoxicology and Teratology*, vol. 48, pp. 9–17, 2015.

[43] H. Ni, L. Peng, X. Gao et al., "Effects of maduramicin on adult zebrafish (*Danio rerio*): acute toxicity, tissue damage and oxidative stress," *Ecotoxicology and Environmental Safety*, vol. 168, pp. 249–259, 2019.

[44] R. Jijie, G. Solcan, M. Nicoara, D. Micu, and S.-A. Strungaru, "Antagonistic effects in zebrafish (*Danio rerio*) behavior and oxidative stress induced by toxic metals and deltamethrin acute exposure," *Science of the Total Environment*, vol. 698, p. 134299, 2020.

[45] L. Kong, Z. Xiong, X. Song et al., "Enhanced antioxidant activity in Streptococcus thermophilus by high-level expression of superoxide dismutase," *Frontiers in Microbiology*, vol. 11, p. 2786, 2020.

[46] İ. Ünal, Ü. V. Üstündağ, P. S. Ateş et al., "Rotenone impairs oxidant/antioxidant balance both in brain and intestines in zebrafish," *The International Journal of Neuroscience*, vol. 129, no. 4, pp. 363–368, 2019.

[47] J. Blesa, I. Trigo-Damas, A. Quiroga-Varela, and V. R. Jackson-Lewis, "Oxidative stress and Parkinson's disease," *Frontiers in Neuroanatomy*, vol. 9, p. 91, 2015.

[48] L. Puspita, S. Y. Chung, and J.-W. Shim, "Oxidative stress and cellular pathologies in Parkinson's disease," *Molecular Brain*, vol. 10, no. 1, p. 53, 2017.

[49] Z. Khan and S. A. Ali, "Oxidative stress-related biomarkers in Parkinson's disease: a systematic review and meta-analysis," *Iran. J. Neurol.*, vol. 17, no. 3, pp. 137–144, 2018.

[50] O. M. Ighodaro and O. A. Akinloye, "First line defence antioxidants-superoxide dismutase (SOD), catalase (CAT) and glutathione peroxidase (GPX): their fundamental role in the entire antioxidant defence grid," *Alexandria Journal of Medicine*, vol. 54, no. 4, pp. 287–293, 2018.

[51] A. N. Wang, X. W. Yi, H. F. Yu, B. Dong, and S. Y. Qiao, "Free radical scavenging activity of Lactobacillus fermentum in vitro and its antioxidative effect on growing–finishing pigs," *Journal of Applied Microbiology*, vol. 107, no. 4, pp. 1140–1148, 2009.

[52] D. J. Davis, E. C. Bryda, C. H. Gillespie, and A. C. Ericsson, "Microbial modulation of behavior and stress responses in zebrafish larvae," *Behavioural Brain Research*, vol. 311, pp. 219–227, 2016.

[53] S. H. al-Sheraji, I. Amin, A. Azlan, M. Y. Manap, and F. A. Hassan, "Effects ofBifidobacterium longumBB536 on lipid profile and histopathological changes in hypercholesterolaemic rats," *Microbe*, vol. 6, no. 5, pp. 661–668, 2015.

[54] H. Khotimah, S. Sumitro, and M. Widodo, "Zebrafish Parkinson's model: rotenone decrease motility, dopamine, and increase α-synuclein aggregation and apoptosis of zebrafish brain," *International Journal of PharmTech Research*, vol. 8, pp. 614–621, 2015.

[55] D. Khatri and A. Juvekar, "Abrogation of locomotor impairment in a rotenone-induced Drosophila melanogaster and zebrafish model of Parkinson's disease by ellagic acid and curcumin," *International Journal of Nutrition, Pharmacology, Neurological Diseases*, vol. 6, no. 2, pp. 90–96, 2016.

[56] X.-J. Kong, J. Liu, J. Li et al., "Probiotics and oxytocin nasal spray as neuro-social-behavioral interventions for patients with autism spectrum disorders: a pilot randomized controlled trial protocol," *Pilot and Feasibility Studies*, vol. 6, no. 1, 2020.

[57] M. Hemmati-Dinarvand, S. Saedi, M. Valilo et al., "Oxidative stress and Parkinson's disease: conflict of oxidant-antioxidant systems," *Neuroscience Letters*, vol. 709, p. 134296, 2019.

[58] A. Masato, N. Plotegher, D. Boassa, and L. Bubacco, "Impaired dopamine metabolism in Parkinson's disease pathogenesis," *Molecular Neurodegeneration*, vol. 14, no. 1, p. 35, 2019.

[59] M. A. Siddiqui, J. Ahmad, N. N. Farshori et al., "Rotenone-induced oxidative stress and apoptosis in human liver HepG2 cells," *Molecular and Cellular Biochemistry*, vol. 384, no. 1-2, pp. 59–69, 2013.

[60] M. C. Houser and M. G. Tansey, "The gut-brain axis: is intestinal inflammation a silent driver of Parkinson's disease pathogenesis?," *NPJ Parkinson's disease*, vol. 3, no. 1, 2017.

[61] G. G. Ortiz, "Gut-brain axis: role of microbiota in Parkinson's disease and multiple sclerosis," in *Eat, Learn, Remember*, IntechOpen, Rijeka, 2019.

[62] S. F. Santos, H. L. de Oliveira, E. S. Yamada, B. C. Neves, and A. Pereira Jr., "The gut and Parkinson's disease-a bidirectional pathway," *Frontiers in Neurology*, vol. 10, p. 574, 2019.

[63] Y. Bhattarai, J. Si, M. Pu et al., "Role of gut microbiota in regulating gastrointestinal dysfunction and motor symptoms in a mouse model of Parkinson's disease," *Gut Microbes*, vol. 13, no. 1, p. 1866974, 2021.

[64] H. B. Dodiya, C. B. Forsyth, R. M. Voigt et al., "Chronic stress-induced gut dysfunction exacerbates Parkinson's disease phenotype and pathology in a rotenone-induced mouse model of Parkinson's disease," *Neurobiology of Disease*, vol. 135, p. 104352, 2020.

[65] M. E. Johnson, A. Stringer, and L. Bobrovskaya, "Rotenone induces gastrointestinal pathology and microbiota alterations in a rat model of Parkinson's disease," *Neurotoxicology*, vol. 65, pp. 174–185, 2018.

[66] L. Bonfrate, D. M. Di Palo, G. Celano et al., "Effects of Bifidobacterium longum BB536 and Lactobacillus rhamnosus

HN001 in IBS patients," *European Journal of Clinical Investigation*, vol. 50, no. 3, article e13201, 2020.

[67] M. Toscano, R. de Grandi, L. Stronati, E. de Vecchi, and L. Drago, "Effect ofLactobacillus rhamnosusHN001 andBifidobacterium longumBB536 on the healthy gut microbiota composition at phyla and species level: a preliminary study," *World Journal of Gastroenterology*, vol. 23, no. 15, pp. 2696–2704, 2017.

[68] R. Inturri, A. Stivala, P. M. Furneri, and G. Blandino, "Growth and adhesion to HT-29 cells inhibition of Gram-negatives by Bifidobacterium longum BB536 e Lactobacillus rhamnosus HN001 alone and in combination," *European Review for Medical and Pharmacological Sciences*, vol. 20, no. 23, pp. 4943–4949, 2016.

[69] R. Inturri, L. Trovato, G. L. Volti, S. Oliveri, and G. Blandino, "*In vitro* inhibitory activity of *Bifidobacterium longum* BB536 and *Lactobacillus rhamnosus* HN001 alone or in combination against bacterial and *Candida* reference strains and clinical isolates," *Heliyon*, vol. 5, no. 11, 2019.

[70] P. Perez-Pardo, H. B. Dodiya, P. A. Engen et al., "Gut bacterial composition in a mouse model of Parkinson's disease," *Beneficial Microbes*, vol. 9, no. 5, pp. 799–814, 2018.

[71] X. Yang, Y. Qian, S. Xu, Y. Song, and Q. Xiao, "Longitudinal analysis of fecal microbiome and pathologic processes in a rotenone induced mice model of Parkinson's disease," *Frontiers in Aging Neuroscience*, vol. 9, p. 441, 2018.

Research Article

Cannabidiol Decreases Metalloproteinase Activity and Normalizes Angiogenesis Factor Expression in UVB-Irradiated Keratinocytes from Psoriatic Patients

Agnieszka Gęgotek [ID],[1] Sinemyiz Atalay [ID],[1] Adam Wroński [ID],[2] Agnieszka Markowska [ID],[1] and Elżbieta Skrzydlewska [ID][1]

[1]*Department of Analytical Chemistry, Medical University of Bialystok, Poland*
[2]*Dermatological Specialized Center "DERMAL" NZOZ in Bialystok, Poland*

Correspondence should be addressed to Elżbieta Skrzydlewska; elzbieta.skrzydlewska@umb.edu.pl

The development of psoriasis is associated with the consequences of oxidative stress and inflammation leading to metabolic changes locally, in the skin cells, and systemically, in the blood. Therefore, the aim of this study was to analyze the effect of psoriasis vulgaris (PsV) and psoriatic arthritis (PsA) on the basal plasma/keratinocyte levels of matrix metalloproteinases (MMPs), tissue inhibitors of matrix metalloproteinases (TIMPs), and angiogenesis factors, as well as to evaluate the effect of CBD on these parameters in keratinocytes isolated from psoriatic/healthy individuals with and without in vitro irradiation by UVB. A quantitative chemiluminescent method of detection based on an ELISA protocol and zymography technique was used during analysis. It was shown that activity levels of MMP-9 and TIMP-2 in PsA plasma were higher than in PsV. Changes in the proteolytic activity were accompanied by an increase in markers of angiogenesis (angiopoietin-2, HGF, VEGF, TNFα, PDGF, FGF), where in the specific case of angiopoietin-2 and TNFα, the overexpression in PsV was significantly stronger than in PsA. CBD application to keratinocytes partially restored levels of MMP-1/2/3/7 and TIMP-1/2 (in an effect which was particularly enhanced by UVB irradiation), as well as levels of the examined angiogenic factors except TNFα (levels of which were increased in psoriatic keratinocytes and decreased in healthy keratinocytes). Presented results indicate that CBD may be suggested as an antiangiogenic factor that reduces the proinflammatory action of UVB in psoriatic keratinocytes and partially has a protective effect for healthy keratinocytes.

1. Introduction

Psoriasis vulgaris (PsV) is one of the most common immune-mediated inflammatory diseases, which affects approximately 4% of the adult population [1]. Its symptoms are mainly related to excessive exfoliation of the epidermis; however, the underlying cause of the disease is related to dysfunction of the entire human immune system [2]. As a result, not only do metabolic disturbances occur in skin cells, changing its condition and appearance, but damage also occurs to internal structures such as joints, as observed in psoriatic arthritis (PsA) [2]. To date, a number of factors in the pathogenesis of psoriasis (stress, environmental pollu-tion, xenobiotics, genetic factors) have been defined [3], and various metabolic pathways involved in the development of this disease have been described, including inflammatory and oxidative stress (and their metabolic consequences), leading to excessive stimulation of keratinocytes (KCs) for proliferation, as well as the formation of leukocyte infiltrates into the dermis and vascular angiogenesis [4, 5]. Considering the fact that psoriasis is an immune inflammatory disease associated with an increased level of proinflammatory factors, mainly at the site of damage (skin, joints), an important issue is to determine the role of the proteolytic/antiproteolytic balance resulting from the levels or activity of matrix metalloproteinases (MMPs) and their inhibitors (tissue

inhibitors of MMPs: TIMPs) in the pathogenesis of psoriasis, with the precise determination of the molecular mechanisms of this disease and therapy.

Extracellular MMPs belong to a large family of multidomain zinc endopeptidases. They are one of the most important proteolytic enzyme families which degrade components of the extracellular matrix, maintaining their physiological level, which is particularly meaningful in the case of skin cell migration and wound-healing. Moreover, MMPs are involved in many physiological processes, such as apoptosis or angiogenesis, especially in the human skin exposed to UV rays [6]. Oxidative stress markers and oxidatively modified lipids, levels of which are elevated in psoriasis and after UV irradiation, increase the expression of certain MMP genes and/or these enzymes' activities, both in blood and in psoriatic skin lesions [7, 8]. In the case of psoriasis, MMP activation is key to the incidence of structural changes in the epidermis via the modification of intracellular contacts and the composition of the extracellular matrix and to the promotion of angiogenesis in the skin, which favors the infiltration of immune cells [9]. Moreover, in addition to metabolic changes, these enzymes are additionally stimulated by UV radiation commonly used in the most psoriatic skin phototherapies [10]. This increased MMP activity has also been linked to other pathologies, including tumor cell spreading (metastasis), arthritis, periodontal disease, cardiovascular disease, and neurodegenerative diseases [11]. To prevent the negative effects of the MMP overexpression in the body, levels of endogenous inhibitors of these enzymes (TIMPs) are tightly physiologically regulated, as is the MMP:TIMP ratio. These balances may be dysregulated under pathological conditions [12].

Research is underway to identify compounds, including natural ones that would aid treatment. So far, the natural phytocannabinoid cannabidiol (CBD) has proved to be a promising candidate, especially for use in pharmacotherapy combined with UV phototherapy [13]. CBD is characterized by its antioxidant, as well as anti-inflammatory properties, consisting of support for endocannabinoids in their interaction with specific transmembrane receptors, such as cannabinoid receptors and TRPVs (transient receptor potential channels—vanilloid subtype) or PPARs (peroxisome proliferator-activated receptors) [14]. These features allow the determination of CBD as a cytoprotective compound, especially in relation to UV-irradiated skin cells [15]. Moreover, CBD has been found to reduce MMP secretion and activity, as well as upregulation of MMP inhibitors such as TIMP-1 in various types of cancer development [16, 17]. This inhibitory effect of CBD on MMPs was also observed in unchanged skin fibroblasts [18]. So far, CBD is used extensively in skincare products to avoid inflammation, dryness, and the generation of free radicals in irritated tissue [19]. However, its protective properties are constantly being considered in the design of new therapeutic applications [20].

Therefore, the aim of this study was as follows: firstly, to analyze how the development of PsV and PsA affect the expression of basic MMPs and their inhibitors, as well as growth/angiogenesis factors in plasma, and secondly, to deter-

mine the effect of CBD on these parameters in KCs isolated from psoriatic patients and irradiated in vitro with UVB, simulating the conditions experienced under phototherapy.

2. Materials and Methods

2.1. Material

2.1.1. Plasma Sample Collection. Plasma samples were obtained from the blood of 20 patients with psoriasis vulgaris (12 females and 8 men, mean age: 37) and from 20 people with diagnosed psoriatic arthritis (9 females and 11 men, mean age: 36). The control group was composed of 10 healthy females and 10 healthy men (in total: 20, mean age: 36). All psoriasis vulgaris patients were chosen on the basis of having a diagnosis of plaque psoriasis for at least 6 months prior, with at least 10% of the total body surface area affected. The severity of psoriasis was assessed using the Psoriasis Area and Severity Index (PASI) score (median 21; range 15–25). Patients with psoriatic arthritis were diagnosed on the basis of a questionnaire CASPAR (Classification Criteria for Psoriatic Arthritis). None of the respondents received topical, oral, or injectable medications during the 4 weeks before the study, and none had comorbidities, had been a smoker, or had abused alcohol. The presence of other both skin as well as systemic diseases excluded patients from the study. The study was conducted in accordance with the Declaration of Helsinki, and the protocol for the collection of all (blood or skin) samples was approved by the Local Bioethics Committee in Medical University of Bialystok (Poland), No. R-I-002/289/2017. Written informed consent was obtained from all participants.

Blood was collected into EDTA tubes and, to prevent oxidation in obtained samples, butylhydroxytoluene (BHT) was used. Plasma was then obtained by spinning for 25 min in $300 \times g$. Isolated material was stored at -80°C before further analysis.

2.1.2. Cell Line Derivation. KC cell lines were isolated from psoriatic skin biopsies of 5 randomly chosen patients with psoriasis vulgaris (2 men and 3 women; age range 25–48 years, mean 40). Biopsies were also taken from five healthy people (sex- and age-matched individuals forming a control group; age range 27–51 years, mean 41) who had moles, which were removed along with the adjacent skin. Skin biopsies were obtained from active psoriasis lesions from the elbow or knee area. The samples were collected using the classical surgical method. After skin decontamination, infiltration anesthesia with 1% lignocaine was applied, and then skin fragments of approximately 5-8 mm were collected. Samples immediately after biopsy were destined for histopathological examination (hematoxylin-eosin staining, data showed previously [21]). The remaining material was incubated overnight at 4°C in dispase (1 mg/mL) to separate epidermis from dermis. Following incubation, the epidermis, mainly composed of KCs, was digested using trypsin/EDTA in a 20 min incubation at 37°C. Separated KCs were washed in PBS and resuspended in growing medium: Keratinocyte Serum-Free Medium (Gibco, Grand Island,

NY) supplemented with fetal bovine serum (10%), penicillin (50 U/ml), and streptomycin (50 μg/ml). Cells were then cultured under standard conditions in a humidified atmosphere of 5% CO_2 at 37°C. Cell culture purity and uniformity were controlled based on the KC morphology observation.

2.1.3. Cell Treatment and Medium Collection. When KCs formed all derived lines reached 70% confluence, cells were exposed to UVB (312 nm) radiation in cold PBS (4°C) to avoid heat stress and oxidation of the medium components. Used wavelength corresponds to the wavelength of the UVB radiation (Narrow Band) used in the phototherapy of psoriasis [22]. KCs were irradiated on ice at a distance of 15 cm from an assembly of 6 UV lamps (Bio-Link Crosslinker BLX 312; Vilber Lourmat, Germany) at 6 W each, corresponding to a flux of 4.08 mW/cm². Total UVB dose was 60 mJ/cm², which resulted in the death of approximately 30% of KCs. After irradiation, KCs were incubated for 24 hours under standard conditions in medium without supplementation with growth factors. To analyze the effect of CBD on these cells, a suspension of CBD in ethanol was added to a final concentration of 4 μM (the final concentration of ethanol was 0.3%). Following incubation (24 h), the medium from was harvested and frozen at -80°C before further analysis.

2.2. Methods

2.2.1. Metalloproteinase Activity. Activity of metalloproteinases MMP-2 and MMP-9 was measured using gelatin zymography [23]. Samples were electrophoretically separated on an 8% gel containing gelatin (2 mg/ml). MMP activity was induced by incubation of the gel for 20 hours in 37°C in Tris-HCl buffer (50 mM, pH 7.8) with $CaCl_2$ (5 mM) and Triton X-100 (0.1%). Following incubation, the gel was stained in Coomassie Blue. Next, densitometric analysis of light fringes on a dark background was carried out using a Versa Doc System and Quantity One software (Bio-Rad Laboratories Inc., CA, USA).

2.2.2. Protein Expression. Levels of metalloproteinases MMP-1, MMP-2, MMP-3, MMP-7, and MMP-9 and their inhibitors, TIMP-1 and TIMP-2, as well as growing factors/angiogenesis HGF, VEGF, PDFG, FGF, IL-8, angiopoietin-2, and TNFα, were measured using commercially available kits (Q-Plex™ Human MMP (6-Plex) no. 340949HU and Q-Plex™ Human Angiogenesis (9-Plex) no. 150249HU, Quansys Biosciences, UT, USA) [24]. These assays use a quantitative chemiluminescent method of detection based on an ELISA protocol. These assays used two different antibodies specific for their respective targets. Samples, as well as calibrators, were pipetted into wells of a 96-well plate arrayed with analyte specific anti-bodies that captured chosen protein within 1 hour. Specific proteins were immobilized to their locations in the array. After washing away any unbound protein, a mixture that contains biotinylated analyte specific antibodies was added and incubated for 1 hour. The biotinylated antibodies completed the sandwich for each specific arrayed analyte. After washing away unbound biotinylated antibody, streptavidin-horseradish peroxidase (SHRP) was added for

20 min. Following an additional wash, the signal reading was performed by Q-ViewTM Imager LS with Q-View Sotware (Quansys Biosciences, Logan, UT, USA) according to the manufacturer protocols and method improvements available online at https://www.quansysbio.com/support/tech-tips/. Protein levels were read according to the respective calibration curves in the range: 49.38–12,000 pg/ml (MMP-1), 329.22–80,000 pg/ml (MMP-2), 18.52–4500 pg/ml (MMP-3), 7.41–1800 pg/ml (MMP-7), 181.07–44,000 pg/ml (MMP-9), 13.7–10,000 pg/ml (Ang-2), 6.9–5000 pg/ml (FGF), 19.2–14,000 pg/ml (HGF), 5.5–4000 pg/ml (PDGF), 13.7–10,000 pg/ml (TIMP-1), 27.4–20,000 pg/ml (TIMP-2), 5.5–4000 pg/ml (TNFα), 2.7–2000 pg/ml (VEGF), and 2.7–2000 pg/ml (IL-8). The image of the obtained curves, as well as the distribution of measurement spots, is presented in Figure 1.

All results were normalized against total protein concentration, as measured by the Bradford assay [25].

2.3. Statistical Analysis. Data were analyzed using standard statistical analyses, including multivariate analysis (one-way ANOVA). The Shapiro-Wilk and the Leven tests were used to check the normality of the data distribution and the homogeneity of variance. Results are expressed as the mean ± standard deviation (SD).

3. Results

The metabolic changes resulting from the development of psoriasis are inextricably linked to the increased plasma levels/activity of MMPs in patients diagnosed with both PsV and PsA. Our results confirm this finding, especially in the case of MMP-1 and MMP-7, where an increase of 25–60% was observed in the plasma of PsV and PsA patients compared to the level of these MMPs in the control group (Figure 2). Moreover, the plasma level of MMP-3 in psoriasis patients (both PsV and PsA) was more than twice as high as in the control group. Also, the levels of MMP-2 and MMP-9 were increased in psoriatic plasma, with significant differences observed in different forms of the disease: MMP-2 levels were higher than in plasma from healthy subjects by about 60% in PsV and by 25% in PsA, while MMP-3 levels increased by 53% in PsV and by 125% in PsA (Figure 2). The differences in the levels of these enzymes also coincided with changes in their activities. MMP-2 from PsV patient plasma digested gelatin more strongly than this same enzyme from PsA patient plasma. An inverse relationship was observed for the bands etched by MMP-9 (Figure 3). The findings of increased MMPs level/activity in psoriasis plasma were accompanied with enhanced expression of tissue inhibitors of MMPs (TIMPs) (Figure 2). TIMP-1 level was increased in plasma of both PsV and PsA patients by 40% and 25%, respectively, while the TIMP-2 level was significantly increased (by 24%) only in plasma of PsV patients comparing to healthy subjects.

Parallel to the disturbances in MMP activity in the plasma of psoriatic patients, significant changes were observed in the expression of the angiogenesis markers and growth factors in the plasma of both PsV and PsA patients
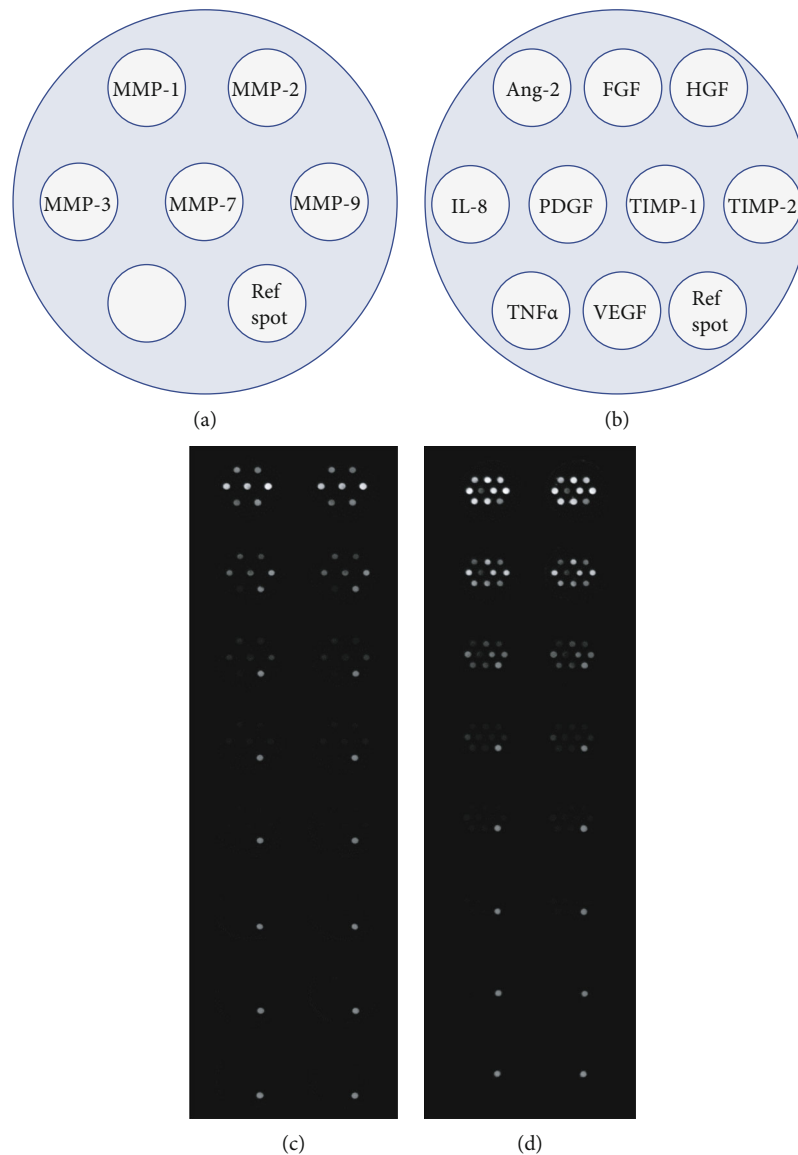
FIGURE 1: The spot distribution in the Q-Plex™ Human MMP (a) and Q-Plex™ Human Angiogenesis (b) and the images of the obtained curves for targeted proteins (c, d).

(Figure 4). A higher increase in these transcripts was observed for angiopoietin-2 and TNFα in plasma of PsV patients, which was 50% more than in the control. The same parameters were also increased in plasma of PsA patients and were around 15% higher comparing to healthy subjects. Further, the expression of IL-8, HGF, and PDGF was enhanced in psoriatic patient plasma by at least 35%. Across VEGF and FGF levels, no significant changes were observed compared to controls except for the FGF expression in PsA patient plasma, which was decreased by approximately 7%.

Observed changes in the plasma of psoriatic patients were also reflected in the levels studied in isolated skin cells cultured in vitro. In the medium collected from psoriatic KCs, levels of MMPs (MMP-1/2/3) were significantly higher than in medium from parallel cultured KCs isolated from healthy individuals (increases of 4.4 times, 2.4 times, and 1.5 times, respectively) (Figure 4). Further, UVB radiation

significantly enhanced MMP levels in medium of cultured psoriatic or control cells. However, this increase was greater in control cells than in psoriatic cells, e.g., the MMP-1 level in control cells following UVB exhibited a 5.7-fold increase, while in psoriatic KCs, this increase was only 1.4-fold. For all assessed MMPs (MMP-1/2/3/7), CBD caused significant reduction of their level in UVB-treated KCs. However, MMP-3 and MMP-7 levels were decreased by CBD more in UVB irradiated psoriatic KCs than in UV-irradiated healthy cells, while the MMP-1 and MMP-2 expression was reduced by CBD significantly more in UV-irradiated healthy cells as compared with the reaction of psoriatic KCs (Figure 4). Moreover, the TIMP expression in the medium of KCs was enhanced in psoriatic cells by compared to healthy cells by 32% for TIMP-1 and by 187% for TIMP-2. However, treatment of healthy cells with UVB radiation or CBD caused only moderate changes in the TIMP expression,
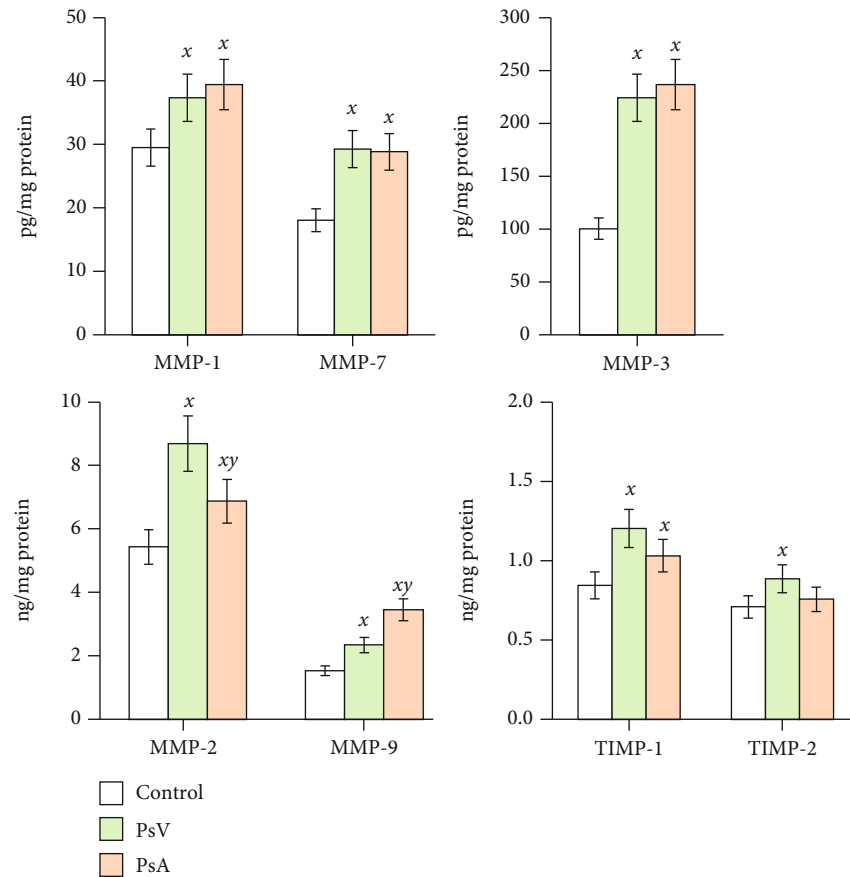
FIGURE 2: The level of metalloproteinases (MMP-1, MMP-2, MMP-3, MMP-7, and MMP-9) and metalloproteinase inhibitors (TIMP-1/2) in plasma of patients with psoriasis vulgaris (PsV, $n = 20$) and psoriatic arthritis (PsA, $n = 20$) compared to plasma of healthy subjects (control group, $n = 20$). Mean values ± SD are presented; [x] statistically significant differences vs. control group, $p < 0.05$; [y] statistically significant differences vs. PsA group, $p < 0.05$.

while psoriatic KCs responded in a more significant manner. It was observed that UVB radiation caused an increase of 60% for TIPM-1 and 90% for TIMP-2 in psoriatic cells, while CBD significantly reduced the UVB-induced expression of these molecules by approximately 65–70% (Figure 5).

Psoriatic changes in skin KCs were also related to the level of released into the medium growing factors and angiogenesis markers (Figure 6). Psoriasis development was associated with an increase in the level of angiopoietin-2 and HGF by 25%, of PDGF by 80%, of TNFα and VEGF twice, and of FGF three times as compared to healthy cells. Moreover, psoriatic KCs were also more sensitive to the experimental treatments, e.g., the expression of HGF in healthy cells was unwavering due to UVB radiation and CBD supplementation, while in psoriatic KCs, UVB induced double increase, which was prevented by CBD treatment. A similar character of changes following cell treatment was observed in the case of angiopoietin-2, PDGF, and VEGF, wherein UVB radiation resulted in a maximum of 30% increase in the expression in control cells and a 2-to-3-fold increase in psoriatic cells. Further, CBD treatment of these cells following UVB irradiation caused a decrease in these protein levels by approximately 15% in healthy KCs and 50–80% in psoriatic cells. The strongest effect of UVB and CBD

action was visible in the changes of the FGF expression, where UVB caused a 3- and 5-fold increase in healthy and psoriatic cells, respectively, and CBD prevented these changes by 65% and 85%, respectively. CBD did not decrease only the level of proinflammatory factor TNFα, which is also strongly increased in psoriatic cells with and without UVB radiation, as well as following CBD treatment. On the other hand, CBD reduced the level of TNFα to the control level in KCs obtained from healthy people and treated with UVB (Figure 6).

4. Discussion

The healthy appearance of the human skin has always been seen as an indicator of a healthy body condition. Therefore, hyperexfoliation of the epidermis caused by chronic inflammation in patients with psoriasis vulgaris (PsV) is not only a dermocosmetic problem but may indicate serious pathological changes in the body, even leading to the development of other diseases, such as metabolic syndrome or Leśniowski's disease (Crohn's disease), or may cause psychological/psychiatric disorders [26]. A comorbid disease classically associated with PsV is psoriatic arthritis (PsA). It is not known what factors lead to the development of PsA in some cases

(a)

(b)

(c)
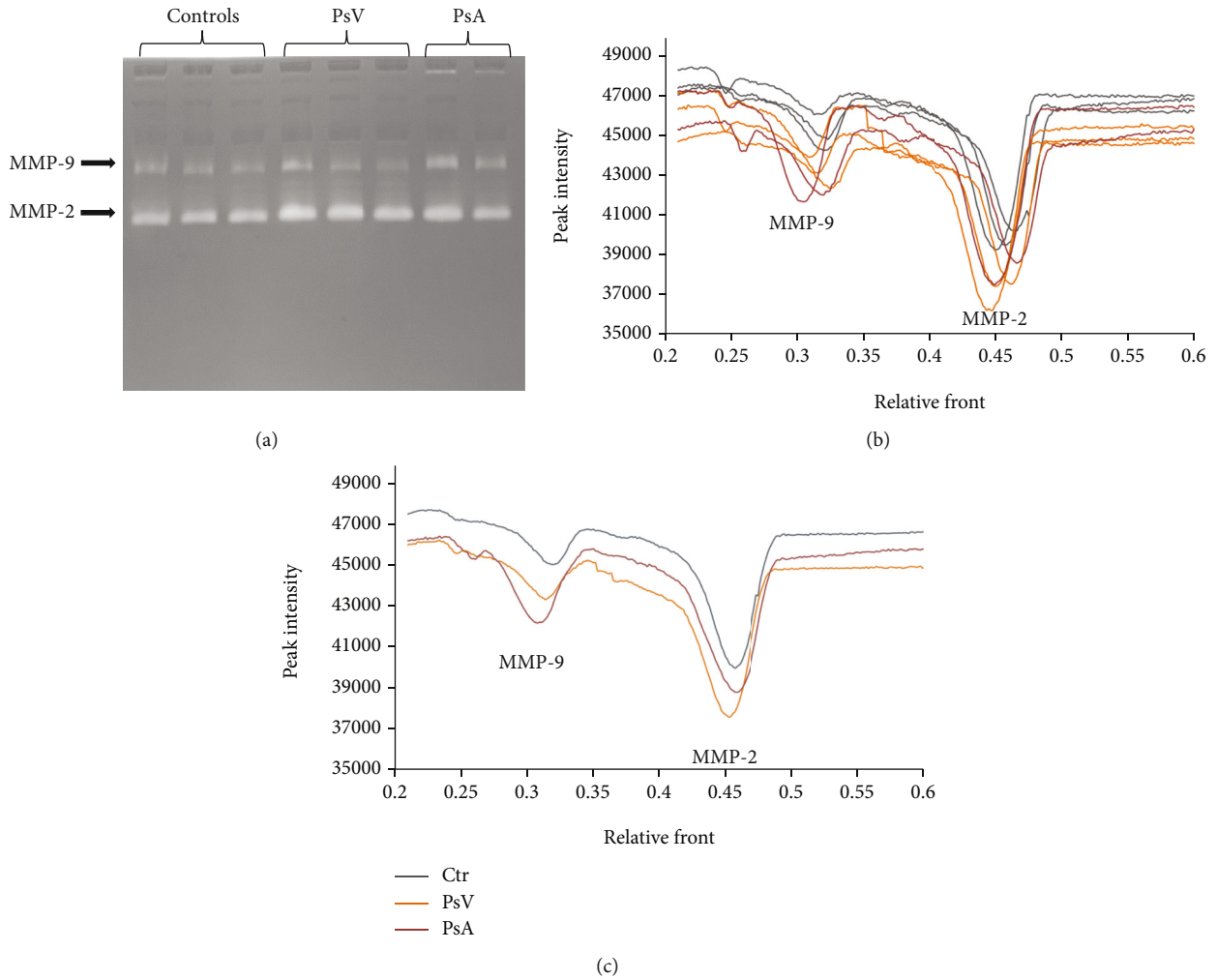
Figure 3: The activity of metalloproteinases (MMP-2 and MMP-9) in plasma of patients with psoriasis vulgaris and psoriatic arthritis compared to plasma of healthy subjects (control group). Presented results are (a) image of gelatin zymography, (b) the intensity of the signals for individual lines, and (c) the average of data from each group.
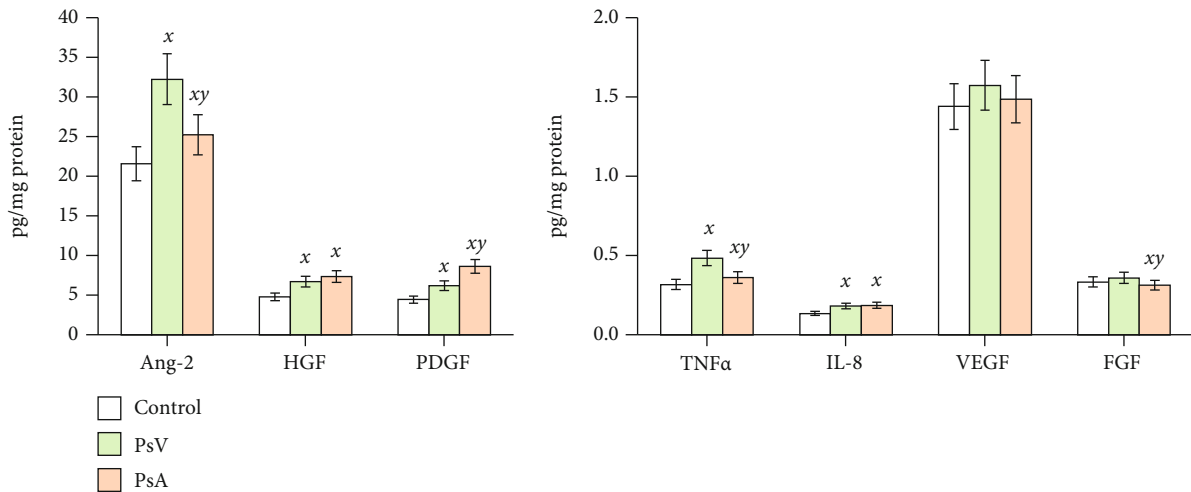
Figure 4: The level of the growth factors and markers of angiogenesis (angiopoietin-2, HGF, PDGF, TNFα, IL-8, VEGF, FGF) in plasma of patients with psoriasis vulgaris (PsV, $n = 20$) and psoriatic arthritis (PsA, $n = 20$) compared to plasma of healthy subjects (control group, $n = 20$). Mean values $\pm$ SD are presented. [x] statistically significant differences vs. control group, $p < 0.05$; [y] statistically significant differences vs. PsA group, $p < 0.05$.
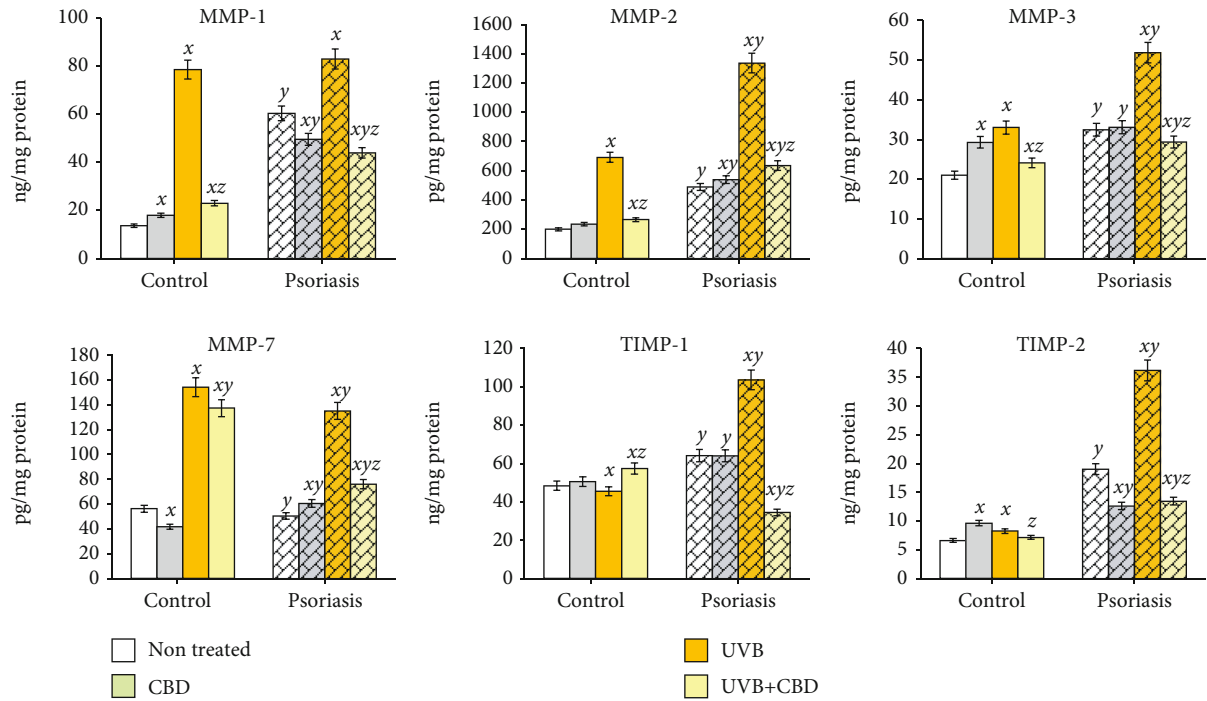
Figure 5: The level of metalloproteinases (MMP-1, MMP-2, MMP-3, and MMP-7) and metalloproteinase inhibitors (TIMP-1/2) in medium of keratinocytes isolated from psoriatic patents ($n = 5$) or healthy subjects ($n = 5$) and cultured following UVB irradiation ($60\,mJ/cm^2$) for 24 h with or without cannabidiol (CBD, $4\,\mu M$). Mean values $\pm$ SD are presented; [x] statistically significant differences vs. non treated group (control or psoriatic, respectively), $p < 0.05$; [y] statistically significant differences between psoriatic and respective-treated control group, $p < 0.05$; [z] statistically significant differences between UVB + CBD and only UVB-treated group, $p < 0.05$.
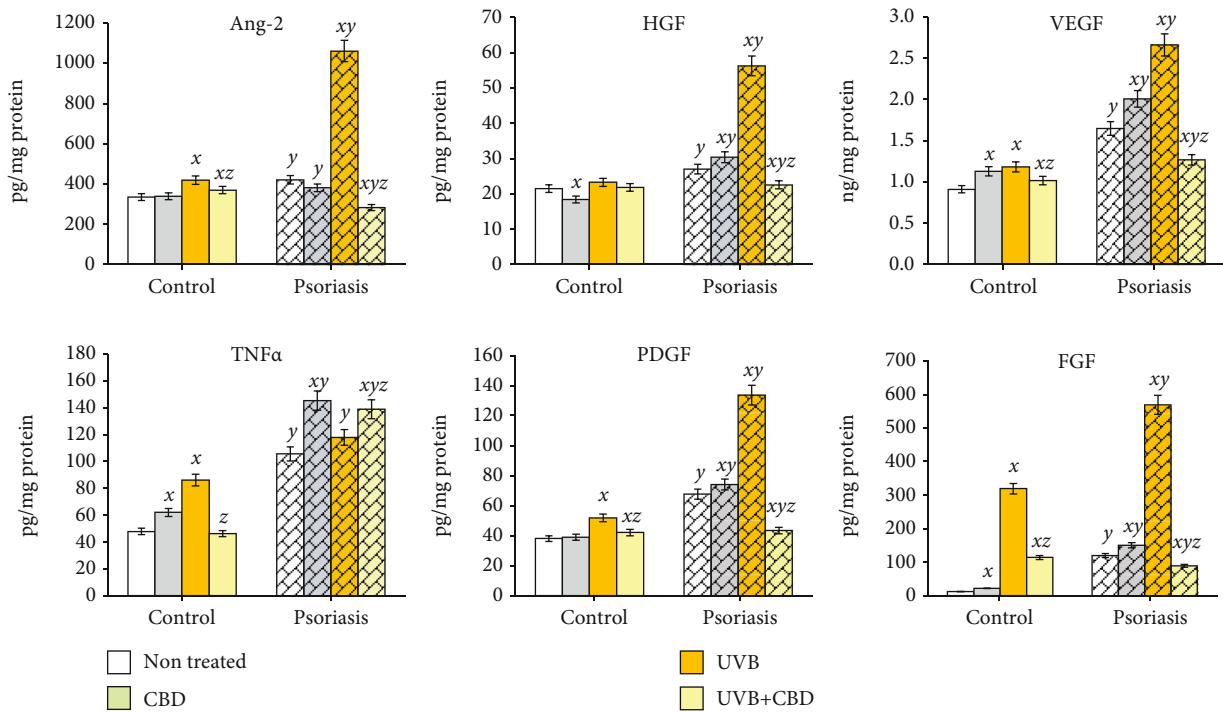
Figure 6: The level of growing factors and markers of angiogenesis (angiopoietin-2, TNFα, HGF, VEGF, PDGF, FGF) in medium of keratinocytes isolated from psoriatic patents ($n = 5$) or healthy subjects ($n = 5$) and cultured following UVB irradiation ($60\,mJ/cm^2$) for 24 h with or without cannabidiol (CBD, $4\,\mu M$). Mean values $\pm$ SD are presented. [x] statistically significant differences vs. non-treated group (control or psoriatic, respectively), $p < 0.05$; [y] statistically significant differences between psoriatic and respective-treated control group, $p < 0.05$; [z] statistically significant differences between UVB + CBD and only UVB-treated group, $p < 0.05$.

of PsV [2], but many reports indicate that changes in the metabolic profile and activity of plasma proteins/blood cells differ significantly in both diseases [27, 28], which indicates the need for careful analysis to determine the most effective treatments in each case.

All significant changes occurred in cellular metabolism are usually reflected in the body fluids protein profile. This also is visible in the case of psoriasis, where changes in skin cell metabolism are reflected in plasma composition [29]. So far, the reorganization of the psoriatic epidermis connected with protease and peptidase stimulation has been observed also as the increased level of these proteins in patients' plasma [30]. Among these, MMPs can also be mentioned [9]. The major functions of MMPs are remodeling and degradation of extra-cellular matrix and cell membranes during various biological processes, such as cell migration and KC proliferation, as well as angiogenesis. There are five subfamilies of MMPs: collagenases, gelatinases, stromelysins, matrilysins, and membrane-type MMP; however, all are involved in the degradation of collagens, proteoglycans, and various glycoproteins. Their stimulation or repression might be regulated at the level of biosynthesis, while their activity can be directly modified by growth factors, cytokines, or tissue inhibitors of MMPs (TIMPs) [12].

It has been known for many years that psoriasis is associated with increased activity of various types of MMPs [9]; however, presented in this study are results which for the first time clearly indicate that in the case of plasma MMPs with collagenase or stromelysin activity, there are no differences between PsV and PsA patients, while gelatinases such as MMP-2 and MMP-9 significantly differentiate these two types of psoriasis. The plasma level as well as the activity of the MMP-9 in PsA is higher than in PsV, which makes the symptoms of this disease closer to that of rheumatoid arthritis (RA) [31]. However, in RA, MMP-2 is present only in latent form [32], while in PsA as in PsV, both level and activity are significantly increased. Moreover, these results are accompanied with increased level of MMP inhibitors TIMP-1 and -2. TIMPs act by binding to MMPs prevent their catalytic activity which, in the case of psoriasis, could limit inflammatory response and the scope of epidermal changes. Therefore, in the body's protective response, an increase in TIMP levels has been found in psoriatic patients' plasma [8]. The increased expression of TIMP-2 in PsV patient plasma also differentiates them from patients with PsA, where this was not observed. The inhibitory effect of TIMP-2-specific inhibition on MMP-2 (previous findings show a strong balance between MMP-2 and TIMP-2 in the case of cancer cells [33]) can explain the observed lack of TIMP-2 overexpression in PsA patient plasma.

These findings, showing an increase in MMP activity in psoriatic patient plasma, are also accompanied by increased markers of angiogenesis. New blood vessel formation in PsV patients favors Th1 and Th17 lymphocyte migration, as well as distribution of KC proliferation stimulators including growth factors, which additionally accelerates the pathogenesis of psoriasis [34]. However, one previous study suggests that abnormalities of vessel architecture and circulating levels of angiogenic growth factors have been observed in

both psoriasis and atherosclerosis [35]. In the present study, most of the analyzed markers of angiogenesis in psoriatic patient plasma are similarly upregulated in both PsV and PsA; however, in the case of angiopoietin-2 and TNFα, the overexpression in PsV is significantly stronger than in PsA. Angiopoietin-2 (which is responsible for activation of the Tie-2 receptor) destabilizes blood vessel maturation, preparing them for new sprout formation and stronger psoriatic lesson invasion [36]. Additionally, it has been found that angiopoietin-2 is upregulated by VEGF and FGF [37], which were found to be elevated in PsV patients. Moreover, similar data for the TNFα expression differentiating PsV and PsA have been observed previously in psoriatic granulocytes [5], suggesting weaker proinflammatory signaling in PsA than in PsV, connected with stimulation or silencing by the protective mechanisms of the joints. Therefore, the inflammatory processes might be stronger in patients with PsV than in PsA. As a result, the mild variant of PsV is 10 times more frequently efficiently treated than severe form of psoriasis including PsA [38].

When analyzing the pathogenesis of psoriasis vulgaris, it is difficult to state unequivocally whether bothersome skin changes are the result of changes in the level of plasma signaling molecules, including proinflammatory cytokines, factors stimulating KC proliferation, as well as angiogenesis, or whether changes in the level of these factors in the plasma result directly from changes in epidermal cell metabolism [3]. This problem results from the complexity of the pathogenesis of psoriasis, the development of which consists of both environmental and genetic factors [4]. Regardless of this, skin cells are in constant communication with the immune cells present in the plasma and the signaling factors produced by them. Therefore, changes in plasma are reflected by changes in psoriatic KC metabolism and vice versa [21]. The increase in MMPs and growing factor level in plasma observed in this study from psoriatic patients may be the result of KC hyperproliferation, as well as a stimulus for the further development of the disease. Similar MMP level increase in psoriatic skin cells has been previously observed and has been associated with the induction of their expansion by IL-17 released from activated T lymphocytes [7].

All changes described in plasma markers indicating disturbances in organism homeostasis may have a detrimental effect on normal psoriatic patient functioning; therefore, this study proposes CBD as a potential compound that will decrease negative symptoms of psoriasis observed in skin KCs, especially after their UVB irradiation, received during phototherapy. CBD, because of its lipophilic nature, is wildly used in skincare products to avoid dryness of the skin [19]. Moreover, its antioxidant and anti-inflammatory properties provide protection of both healthy or psoriatic skin cells against oxidative stress caused by UV radiation [13–15, 39]. The effect of CBD on the level of MMPs in UVB irradiated KCs has not been studied so far; however, the results of studies from cancer cells indicate an inhibitory effect of CBD on MMPs, which is important in preventing the development of cancer [16, 17]. The results of this study show that CBD significantly decreases only MMP-7 level in healthy

cells; however, it shows strong inhibitory effect for MMP-1/2/3/7 in UV-irradiated KCs, especially in the case of psoriatic cells. Other studies also show that CBD has the strongest inhibitory effect on MMPs in skin cells exposed to proinflammatory factors, e.g., TNFα [40], which is additionally increased in psoriatic KCs after UVB irradiation. Similar effects of CBD under inflammatory conditions connected with rheumatoid arthritis development are observed in synovial fibroblasts, where CBD decreases MMP-3 level by activating transient receptor potential ankyrin (TRPA1), and increasing intracellular calcium levels [41].

On the other hand, CBD as well as UVB irradiation in various ways affects the level of MMP inhibitors (TIMPs) in both control and psoriatic KCs. While in healthy cells, UVB irradiation and CBD treatment (separately or together) only slightly influence the levels of TIPM-1/2; in psoriatic cells, a strong increase is observed in TIMP level following UVB irradiation. Psoriatic skin cells are continuously stimulated to proliferation; therefore, their metabolism is still maintained at a high level, and thus the observed reaction is significant compared to healthy cells. Moreover, this may be a result of the protective role of TIMPs against UVB-induced degradation of collagen and elastic fibers [42]. Therefore, a CBD-induced decrease in TIMP levels following UVB radiation could potentially be of great importance in phototherapy of psoriasis. To date, many findings show that CBD increases TIMP levels primarily in cancer cells, which, via MMP inhibition, prevents cancer cell migration [17, 43, 44]. In the case of psoriatic skin cells, the effect is the opposite, similarly to umbilical vein endothelial cells [45]. This may be connected with other TIMP actions in KCs, including growth and apoptosis induction, as well as angiogenesis regulation [46], which require special regulation during the hyperproliferation of epidermal cells in psoriatic patients.

As mentioned, angiogenesis plays an important role in psoriasis development, and compared to healthy cells, psoriatic KCs are much more responsive to UVB radiation by overproducing growth factors and angiogenesis markers. However, in most cases, CBD significantly decreases these proteins' expression, which can prevent UVB-induced angiogenesis. Moreover, the natural stimulation of cell proliferation after UVB radiation is observed as the increased expression of HGF, VEGF, PDGF, or FGF only in psoriatic cells and is inhibited by CBD. Similar CBD effects have been observed in the case of VEGF or FGF in human prostate or colon cancer with enhanced cell proliferation [40, 47], similar to that seen in psoriasis. This suggests that CBD may support UVB phototherapy of psoriasis by limiting proliferative signaling in irradiated cells.

The results of this study indicate that CBD regulates the proteolytic/antiproteolytic balance in relation to the extracellular matrix, both in healthy and psoriatic cells. However, in the case of the proinflammatory factor TNFα, CBD significantly differentiates the direction of changes taking place in healthy and psoriatic KCs exposed to UVB radiation. It has long been known that TNFα, as a signaling molecule, not only induces a proinflammatory response of cells but is also a factor actively promoting the development of psori-

asis [48]. Moreover, the TNFα expression is stimulated in skin KCs also in response to UVB radiation [49]. However, the antioxidant and anti-inflammatory properties of CBD contribute to the prevention of TNFα generation in control cells, what demonstrates the protective effect of this phytocannabinoid [50]. Simultaneously, CBD induces the proinflammatory action of UVB in relation to psoriatic cells by enhancing the TNFα level. However TNFα has been shown to inhibit the following: the secretion by plasmacytoid dendritic cells (pDC) of interferon gamma (IFNγ—an immunoregulatory cytokine that induces the release of inflammatory cytokines), the proliferation of KCs, and the maintenance of psoriasis [51]. Therefore, taking this into account, it can be suggested that CBD enhances the effects of narrowband UVB phototherapy.

5. Conclusion

In this study, it was shown that increased plasma levels of MMP-9 and TIMP-2, as well as angiogenic growth factors (mainly Ang-2), differentiate PsV from PsA. At the same time, these increased plasma levels are accompanied by a significant increase in the transcription factor TNFα. This indicates a significant exacerbation of metabolic/pathological changes in PsV patients. Therefore, the application of CBD with antioxidant and anti-inflammatory properties to UVB irradiated KCs has shown very significant effects. CBD has been found to prevent the disruption of the proteolytic/antiproteolytic balance established by extracellular matrix proteases and their inhibitors in both control and psoriatic KCs, especially in those exposed to UVB radiation. Moreover, on the basis of the obtained results, CBD can be indicated as an antiangiogenic factor, significantly reducing the level of all assessed angiogenic growth factors. At the same time, the anti-inflammatory effect of CBD is manifested by a decrease in the level of TNFα in KCs of the healthy skin, but an increase in the level of this transcription factor in psoriatic KCs, especially those exposed to UVB rays. Thus, CBD may prove to be the drug with beneficial effects on both healthy and psoriatic KCs, which may have important clinical implications.

Data Availability

The data used to support the findings of this study are included within the article.

Conflicts of Interest

The authors declare that there is no conflict of interest regarding the publication of this article.

Acknowledgments

References

[1] I. M. Michalek, B. Loring, and S. M. John, "A systematic review of worldwide epidemiology of psoriasis," *J Eur Acad Dermatol Venereol*, vol. 31, no. 2, pp. 205–212, 2017.

[2] Q. Li, V. Chandran, L. Tsoi et al., "Quantifying differences in heritability among psoriatic arthritis (PsA), cutaneous psoriasis (PsC) and psoriasis vulgaris (PsV)," *Sci. Rep*, vol. 10, no. 1, p. 4925, 2020.

[3] E. Ogawa, Y. Sato, A. Minagawa, and R. Okuyama, "Pathogenesis of psoriasis and development of treatment," *J. Dermatol*, vol. 45, no. 3, pp. 264–272, 2018.

[4] A. Rendon and K. Schäkel, "Psoriasis pathogenesis and treatment," *Int. J. Mol. Sci*, vol. 20, no. 6, p. 1475, 2019.

[5] E. Ambrożewicz, P. Wójcik, A. Wroński et al., "Pathophysiological alterations of redox signaling and endocannabinoid system in granulocytes and plasma of psoriatic patients," *Cells*, vol. 7, p. 159, 2018.

[6] P. Brenneisen, H. Sies, and K. Scharffetter-Kochanek, "Ultraviolet-B irradiation and matrix Metalloproteinases," *Annals of the New York Academy of Sciences*, vol. 973, no. 1, pp. 31–43, 2002.

[7] N. L. Starodubtseva, V. V. Sobolev, A. G. Soboleva, A. A. Nikolaev, and S. A. Bruskin, "Genes expression of metalloproteinases (MMP-1, MMP-2, MMP-9, and MMP-12) associated with psoriasis," *Russian Journal of Genetics*, vol. 47, no. 9, pp. 1117–1123, 2011.

[8] I. Flisiak, P. Zaniewski, and B. Chodynicka, "Plasma TGF-β1, TIMP-1, MMP-1 and IL-18 as a combined biomarker of psoriasis activity," *Biomarkers*, vol. 13, no. 5, pp. 549–556, 2008.

[9] A. Mezentsev, A. Nikolaev, and S. Bruskin, "Matrix metalloproteinases and their role in psoriasis," *Gene*, vol. 540, no. 1, pp. 1–10, 2014.

[10] F. Almutawa, N. Alnomair, Y. Wang, I. Hamzavi, and H. W. Lim, "Systematic review of UV-based therapy for psoriasis," *American Journal of Clinical Dermatology*, vol. 14, no. 2, pp. 87–109, 2013.

[11] S. Amar, L. Smith, and G. B. Fields, "Matrix metalloproteinase collagenolysis in health and disease," *Biochim. Biophys. Acta - Mol. Cell Res.*, vol. 1864, no. 11, pp. 1940–1951, 2017.

[12] J. Salimi Sartakhti, M. H. Manshaei, and M. Sadeghi, "MMP-TIMP interactions in cancer invasion: An evolutionary game-theoretical framework," *Journal of Theoretical Biology*, vol. 412, pp. 17–26, 2017.

[13] I. Jarocka-Karpowicz, M. Biernacki, A. Wroński, A. Gęgotek, and E. Skrzydlewska, "Cannabidiol effects on phospholipid metabolism in keratinocytes from patients with psoriasis vulgaris," *Biomolecules*, vol. 10, p. 367, 2020.

[14] S. Atalay, I. Jarocka-Karpowicz, and E. Skrzydlewska, "Antioxidative and anti-inflammatory properties of Cannabidiol," *Antioxidants.*, vol. 9, p. 21, 2019.

[15] A. Gęgotek, S. Atalay, P. Domingues, and E. Skrzydlewska, "The differences in the proteome profile of cannabidiol-treated skin fibroblasts following UVA or UVB irradiation in 2D and 3D cell cultures," *Cell*, vol. 8, p. 995, 2019.

[16] M. Solinas, P. Massi, V. Cinquina et al., "Cannabidiol, a non-psychoactive cannabinoid compound, inhibits proliferation and invasion in U87-MG and T98G glioma cells through a multitarget effect," *PLoS One*, vol. 8, article e76918, 2013.

[17] R. Ramer, J. Merkord, H. Rohde, and B. Hinz, "Cannabidiol inhibits cancer cell invasion via upregulation of tissue inhibitor of matrix metalloproteinases-1," *Biochemical Pharmacology*, vol. 79, pp. 955–966, 2010.

[18] S. Y. Rawal, M. K. Dabbous, and D. A. Tipton, "Effect of cannabidiol on human gingival fibroblast extracellular matrix metabolism: MMP production and activity, and production of fibronectin and transforming growth factor β," *Journal of Periodontal Research*, vol. 47, pp. 320–329, 2012.

[19] N. Jhawar, E. Schoenberg, J. V. Wang, and N. Saedi, "The growing trend of cannabidiol in skincare products," *Clinics in Dermatology*, vol. 37, pp. 279–281, 2019.

[20] C. M. White, "A review of human studies assessing cannabidiol's (CBD) therapeutic actions and potential," *Journal of Clinical Pharmacology*, vol. 59, pp. 923–934, 2019.

[21] A. Gęgotek, P. Domingues, A. Wroński, E. Ambrożewicz, and E. Skrzydlewska, "The proteomic profile of keratinocytes and lymphocytes in psoriatic patients," *Proteomics - Clin. Appl.*, vol. 13, pp. 1–11, 2019.

[22] I. B. Walters, L. H. Burack, T. R. Coven, P. Gilleaudeau, and J. G. Krueger, "Suberythemogenic narrow-band UVB is markedly more effective than conventional UVB in treatment of psoriasis vulgaris," *Journal of the American Academy of Dermatology*, vol. 40, pp. 893–900, 1999.

[23] B. Gogly, N. Groult, W. Hornebeck, G. Godeau, and B. Pellat, "Collagen zymography as a sensitive and specific technique for the determination of subpicogram levels of interstitial collagenase," *Analytical Biochemistry*, vol. 255, pp. 211–216, 1998.

[24] A. Nelson, R. Parr, A. Tyler, and C. Lyman, "The results of a continuing collaboration between PATH and Quansys Biosciences Q-Plex™ Human Micronutrient (7-Plex) Version 2.0, 2020," http://www.quansysbio.com (accessed December 3, 2020).

[25] M. Bradford, "A rapid and sensitive method for the quantitation of microgram quantities of protein utilizing the principle of protein-dye binding," *Analytical Biochemistry*, vol. 72, pp. 248–254, 1976.

[26] M. D. Oliveira, B. D. Rocha, and G. V. Duarte, "Psoriasis: classical and emerging comorbidities," *An. Bras. Dermatol*, vol. 90, no. 1, pp. 9–20, 2015.

[27] P. Wójcik, A. Gęgotek, A. Wroński, A. Jastrzab, A. Zebrowska, and E. Skrzydlewska, "Effect of redox imbalance on protein modifications in lymphocytes of psoriatic patients," *Journal of Biochemistry*, vol. 167, pp. 323–331, 2020.

[28] P. Wójcik, M. Biernacki, A. Wroński et al., "Altered lipid metabolism in blood mononuclear cells of psoriatic patients indicates differential changes in psoriasis vulgaris and psoriatic arthritis," *International Journal of Molecular Sciences*, vol. 20, p. 4249, 2019.

[29] R. Rashmi, K. S. J. Rao, and K. H. Basavaraj, "A comprehensive review of biomarkers in psoriasis," *Clinical and Experimental Dermatology*, vol. 34, pp. 658–663, 2009.

[30] A. Gęgotek, P. Domingues, A. Wroński, P. Wójcik, and E. Skrzydlewska, "Proteomic plasma profile of psoriatic patients," *Journal of Pharmaceutical and Biomedical Analysis*, vol. 155, pp. 185–193, 2018.

[31] B. L. Gruber, D. Sorbi, D. L. French et al., "Markedly elevated serum MMP-9 (gelatinase B) levels in rheumatoid arthritis: a potentially useful laboratory marker," *Clinical Immunology and Immunopathology*, vol. 78, pp. 161–171, 1996.

[32] G. Giannelli, R. Erriquez, F. Iannone et al., "MMP-2, MMP-9, TIMP-1 and TIMP-2 levels in patients with rheumatoid

arthritis and psoriatic arthritis," *Clinical and experimental rheumatology*, vol. 22, no. 3, pp. 335–338, 2004.

[33] D. C. Jinga, A. Blidaru, I. Condrea et al., "MMP-9 and MMP-2 gelatinases and TIMP-1 and TIMP-2 inhibitors in breast cancer: correlations with prognostic factors," *Journal of Cellular and Molecular Medicine*, vol. 10, pp. 499–510, 2006.

[34] R. Heidenreich, M. Röcken, and K. Ghoreschi, "Angiogenesis drives psoriasis pathogenesis," *International Journal of Experimental Pathology*, vol. 90, pp. 232–248, 2009.

[35] A. W. Armstrong, S. V. Voyles, E. J. Armstrong, E. N. Fuller, and J. C. Rutledge, "Angiogenesis and oxidative stress: common mechanisms linking psoriasis with atherosclerosis," *Journal of Dermatological Science*, vol. 63, pp. 1–9, 2011.

[36] T. Markham, R. Mullan, L. Golden-Mason et al., "Resolution of endothelial activation and down-regulation of Tie2 receptor in psoriatic skin after infliximab therapy," *Journal of the American Academy of Dermatology*, vol. 54, pp. 1003–1012, 2006.

[37] S. J. Mandriota and M. S. Pepper, "Regulation of angiopoietin-2 mRNA levels in bovine microvascular endothelial cells by cytokines and hypoxia," *Circulation Research*, vol. 83, pp. 852–859, 1998.

[38] O. Ahlehoff, G. H. Gislason, M. Charlot et al., "Psoriasis is associated with clinically significant cardiovascular risk: a Danish nationwide cohort study," *Journal of Internal Medicine*, vol. 270, pp. 147–157, 2011.

[39] S. Atalay, I. Dobrzyńska, A. Gęgotek, and E. Skrzydlewska, "Cannabidiol protects keratinocyte cell membranes following exposure to UVB and hydrogen peroxide," *Redox Biology*, vol. 36, p. 101613, 2020.

[40] M. Honarmand, F. Namazi, A. Mohammadi, and S. Nazifi, "Can cannabidiol inhibit angiogenesis in colon cancer?," *Comp. Clin. Path.*, vol. 28, pp. 165–172, 2019.

[41] T. Lowin, R. Tingting, J. Zurmahr, T. Classen, M. Schneider, and G. Pongratz, "Cannabidiol (CBD): a killer for inflammatory rheumatoid arthritis synovial fibroblasts," *Cell Death & Disease*, vol. 11, pp. 1–11, 2020.

[42] U. Yokose, A. Hachiya, P. Sriwiriyanont et al., "The endogenous protease inhibitor TIMP-1 mediates protection and recovery from cutaneous Photodamage," *The Journal of Investigative Dermatology*, vol. 132, pp. 2800–2809, 2012.

[43] S. Jeong, M. J. Jo, H. K. Yun et al., "Cannabidiol promotes apoptosis via regulation of XIAP/Smac in gastric cancer," *Cell Death & Disease*, vol. 10, pp. 1–13, 2019.

[44] R. Ramer, K. Bublitz, N. Freimuth et al., "Cannabidiol inhibits lung cancer cell invasion and metastasis *via* intercellular adhesion molecule-1," *The FASEB Journal*, vol. 26, pp. 1535–1548, 2012.

[45] M. Solinas, P. Massi, A. Cantelmo et al., "Cannabidiol inhibits angiogenesis by multiple mechanisms," *British Journal of Pharmacology*, vol. 167, pp. 1218–1231, 2012.

[46] E. Lambert, E. Dassé, B. Haye, and E. Petitfrère, "TIMPs as multifacial proteins," *Critical Reviews in Oncology/Hematology*, vol. 49, pp. 187–198, 2004.

[47] M. Sharma, J. B. Hudson, H. Adomat, E. Guns, and M. E. Cox, "<i>In Vitro</i> Anticancer activity of plant-derived cannabidiol on prostate cancer cell lines," *Pharmacology & Pharmacy*, vol. 5, no. 8, pp. 806–820, 2014.

[48] C. N. Young, J. I. Koepke, L. J. Terlecky, M. S. Borkin, S. L. Boyd, and S. R. Terlecky, "Reactive oxygen species in tumor necrosis factor-α-activated primary human keratinocytes: implications for psoriasis and inflammatory skin disease," *The Journal of Investigative Dermatology*, vol. 128, pp. 2606–2614, 2008.

[49] M. M. Bashir, M. R. Sharma, and V. P. Werth, "UVB and pro-inflammatory cytokines synergistically activate TNF-α production in keratinocytes through enhanced gene transcription," *The Journal of Investigative Dermatology*, vol. 129, pp. 994–1001, 2009.

[50] S. Burstein, "Cannabidiol (CBD) and its analogs: a review of their effects on inflammation," *Bioorganic Med. Chem.*, vol. 23, pp. 1377–1385, 2015.

[51] J. Wang, N. Kaplan, S. Wang et al., "Autophagy plays a positive role in induction of epidermal proliferation," *The FASEB Journal*, vol. 34, pp. 10657–10667, 2020.

Research Article

Hydrogen Sulfide Attenuates Angiotensin II-Induced Cardiac Fibroblast Proliferation and Transverse Aortic Constriction-Induced Myocardial Fibrosis through Oxidative Stress Inhibition via Sirtuin 3

Lulu Liu [1,2] **Weiwei Gong,** [1] **Shuping Zhang,** [1] **Jieru Shen,** [1] **Yuqin Wang,** [1]
Yun Chen, [1] **and Guoliang Meng** [1]

[1]*Department of Pharmacology, School of Pharmacy, Nantong University, Nantong, 226001 Jiangsu, China*
[2]*Department of Pharmacy, Affiliated Maternity & Child Health Care Hospital of Nantong University, Nantong 226001, China*

Correspondence should be addressed to Guoliang Meng; mengguoliang@ntu.edu.cn

Academic Editor: Joanna Lecka

Sirtuin 3 (SIRT3) is critical in mitochondrial function and oxidative stress. Our present study investigates whether hydrogen sulfide (H_2S) attenuated myocardial fibrosis and explores the possible role of SIRT3 on the protective effects. Neonatal rat cardiac fibroblasts were pretreated with NaHS followed by angiotensin II (Ang II) stimulation. SIRT3 was knocked down with siRNA technology. SIRT3 promoter activity and expression, as well as mitochondrial function, were measured. Male wild-type (WT) and SIRT3 knockout (KO) mice were intraperitoneally injected with NaHS followed by transverse aortic constriction (TAC). Myocardium sections were stained with Sirius red. Hydroxyproline content, collagen I and collagen III, α-smooth muscle actin (α-SMA), and dynamin-related protein 1 (DRP1) expression were measured both *in vitro* and *in vivo*. We found that NaHS enhanced SIRT3 promoter activity and increased SIRT3 mRNA expression. NaHS inhibited cell proliferation and hydroxyproline secretion, decreased collagen I, collagen III, α-SMA, and DRP1 expression, alleviated oxidative stress, and improved mitochondrial respiration function and membrane potential in Ang II-stimulated cardiac fibroblasts, which were unavailable after SIRT3 was silenced. *In vivo*, NaHS reduced hydroxyproline content, ameliorated perivascular and interstitial collagen deposition, and inhibited collagen I, collagen III, and DRP1 expression in the myocardium of WT mice but not SIRT3 KO mice with TAC. Altogether, NaHS attenuated myocardial fibrosis through oxidative stress inhibition via a SIRT3-dependent manner.

1. Introduction

Myocardial fibrosis is a cardiac interstitial remodeling characterized by excessive cardiac fibroblast proliferation, collagen deposition, and abnormal distribution [1, 2]. It is closely related to hypertension, chronic heart failure, hypertrophic cardiomyopathy, dilated cardiomyopathy, viral myocarditis, and many other cardiovascular diseases, which is a potential risk factor of sudden cardiac death [3–7]. However, there is no ideal strategy for the treatment of myocardial fibrosis.

Hydrogen sulfide (H_2S) is considered to be the third gasotransmitter after nitric oxide (NO) and carbon monoxide (CO) [8, 9]. Endogenous H_2S is catalyzed by cystathionine-β-synthase (CBS), cystathionine-γ-lyase (CSE), 3-mercaptopyruvate sulfurtransferase (3-MST), and so on [10, 11]. The enzymes are tissue-specific distributed in different systems. CBS is a key enzyme to produce H_2S in the nervous system, while CSE is mainly in the cardiovascular system [12, 13]. Previous studies verified that H_2S had protective effects against atherosclerosis, myocardial hypertrophy, myocardial ischemia-reperfusion injury, endothelial

cell damage, spermatogenic failure, and testicular dysfunction [13–21]. Moreover, we also found that H$_2$S donor GYY4137 alleviated myocardial fibrosis in spontaneously hypertensive rats [22]. However, the detailed mechanism by which H$_2$S attenuated cardiac fibroblast proliferation *in vitro* and myocardial fibrosis *in vivo* remains unclear.

Silent information regulator 2 (SIR2), a highly conserved NAD-dependent family histone deacetylase, serves as a cell sensor for energy utilization and metabolism regulation [23, 24]. SIR2 is widely found in mammals and consists of seven members including sirtuin 1 (SIRT1) to sirtuin 7 (SIRT7). The SIR2 family plays a role in metabolism, cancer, and other physiological and pathological processes [25, 26]. Sirtuin 3 (SIRT3) is a member of histone deacetylase III to mediate redox signaling [27]. Previous research has demonstrated that H$_2$S was capable of increasing SIRT3 to improve mitochondrial function and attenuate oxidative stress. We found that H$_2$S improved endothelium-dependent relaxation of aortic and mesenteric arteries in paraquat-administrated wild-type (WT) mice but not SIRT3 knockout (KO) mice [18]. H$_2$S reduced superoxide anion production in angiotensin II- (Ang II-) stimulated cardiomyocytes, but this effect is significantly weakened after SIRT3 was knocked down. H$_2$S protected against myocardial hypertrophy in WT mice but not SIRT3 KO mice [16]. However, it is not known whether H$_2$S protects against cardiac fibroblast proliferation and myocardial fibrosis via SIRT3 activation.

Therefore, our present study investigates whether H$_2$S attenuated cardiac fibroblast proliferation *in vitro* and myocardial fibrosis *in vivo* and explores the possible role of SIRT3 on the protective effects.

2. Materials and Methods

2.1. Cardiac Fibroblast Culture and Treatment. After anesthesia by isoflurane, neonatal Sprague Dawley rats aged 1 to 3 days old were killed by decapitation. Then, the left ventricular myocardium was cut into small pieces followed by digestion with trypsin in a constant temperature water bath of 37°C for 5-8 minutes. After about 10 times, all supernatants except the first time were mixed. Next, Dulbecco's modified Eagle's medium (DMEM, Wisent Inc., Montreal, QC, Canada) containing 10% fetal bovine serum (FBS, Wisent Inc., Montreal, QC, Canada) was timely added to stop excessive digestion. After centrifugation, fresh DMEM containing 10% FBS was used to resuspend the cell precipitate. After differential adhesion for 4 h, the cardiomyocytes in the medium were abandoned while confluent cardiac fibroblasts adhered to the walls. Cardiac fibroblasts of the 2nd or 3rd passage were used in our further experiments. Cells were then administrated with NaHS (50 μM, Sigma-Aldrich, St. Louis, MO), a common H$_2$S donor, for 4 h followed by Ang II (100 nM, Sigma-Aldrich, St. Louis, MO) stimulation for an additional 24 h.

2.2. Cell Proliferation and Hydroxyproline Content Measurement. Cell proliferation was represented as cardiac fibroblast number enhancement, which was determined by Cell Counting Kit-8 (CCK-8, Beyotime, Shanghai, China)

as the previous study [4]. The content of hydroxyproline in the cell culture medium and in the myocardium was detected according to our previous research [4, 22].

2.3. Luciferase Reporter Assay. Neonatal rat cardiac fibroblasts were transfected with the SIRT3 promoter luciferase fusion plasmid using the Lipofectamine 3000 reagent (Invitrogen, Carlsbad, CA, USA), and the pRL-TK reporter plasmid served as a control reporter. After changing by the fresh medium with 10% FBS 24 h later, cells were incubated with NaHS (50 μM) for 4 h and subsequently stimulated by Ang II (100 nM) for 24 h. Next, the cell lysis buffer was added to harvest the cells. The luciferase activity was detected with a dual-luciferase reporter assay system (Promega, Madison, WI, USA). Activity of the SIRT3 promoter was assessed by the relative luciferase activities compared with pRL-TK, which was normalized to control in triplicate.

2.4. SIRT3 RNA Interference. After starvation for 24 h, the mixture of the SIRT3 siRNA or nonspecific control siRNA (NC siRNA) and the Lipofectamine 3000 reagent was added into cardiac fibroblasts. SIRT3 siRNA (5′-CCAUCUUU-GAACUAGGCUUTT-3′ and 5′-AAGCCUAGUUCAAA-GAUGGTT-3′) or NC siRNA with random sequences was commercially synthesized (GenePharma, Shanghai, China). The expression of SIRT3 mRNA and protein was measured by real-time PCR and western blot, respectively, to evaluate the efficiency of SIRT3 siRNA transfection after 48 h. Some other cells were stimulated with NaHS (50 μM) for 4 h followed by Ang II (100 nM) stimulation for 24 h after siRNA was transfected into the cardiac fibroblasts.

2.5. Immunofluorescence. After treatment, cardiac fibroblasts were fixed by polyformaldehyde for 10 min followed by incubation with phosphate-buffered solution (PBS) containing 0.3% Triton X-100 at room temperature for 20 min. The anti-α-smooth muscle actin (α-SMA, 1 : 50; Bioss, Beijing, China) or anti-dynamin-related protein 1 (DRP1, 1 : 50; Cell Signaling Technology, Danvers, MA, USA) antibody was added into cells at 4°C overnight followed by Cy3- or Alexa Fluor 488-conjugated IgG (1 : 500; Beyotime, Shanghai, China) incubation at room temperature for 2 h the next day. Nuclei were stained by DAPI (4′,6-diamidino-2-phenylindole) (Beyotime, Shanghai, China). Then, cardiac fibroblasts were visualized and photographed with a fluorescence microscope (Nikon, Tokyo, Japan).

2.6. Measurement of Superoxide Formation. After treatment as the above description, the cardiac fibroblasts were incubated with dihydroethidium (DHE, 2 μM, in the Krebs-HEPES buffer) at 37°C without light for 30 min. The level of superoxide in cells, presented as DHE fluorescence intensity, was detected with a laser confocal microscope (Leica, Wetzlar, Germany).

2.7. Assessment of Mitochondrial Respiration Function. The mitochondrial respiration oxygen consumption rate (OCR) was measured as the previous description by a Seahorse Extracellular Flux Analyzer (XF-96, Seahorse Bioscience,

Santa Clara, CA, USA) [16]. After being plated in XF-96-well plates, the cardiac fibroblasts were subjected to siRNA transfection and treatment as described above. Then, the medium was changed into unbuffered DMEM containing glucose (10 mM), pyruvate (10 mM), and GlutaMAX (2 mM, Invitrogen, Carlsbad, CA, USA). Basal respiration was first obtained. After ATP synthesis was inhibited by oligomycin (Oligo, 2 μg/mL), ATP generation during respiration was measured. Then, respiratory reserve capacity and maximal respiration were detected after uncoupler carbonyl cyanide 4-(trifluoromethoxy)phenylhydrazone (FCCP, 2 μM) was added into the cells. Finally, rotenone and antimycin A (rot & AA, 4 μM) were applied to completely block oxygen consumption.

2.8. Assessment of Mitochondrial Membrane Potential ($\Delta\psi m$). After treatment, the cardiac fibroblasts were incubated in JC-1 staining solution (Beyotime, Shanghai, China) at 37°C without light for 20 min. The level of mitochondrial membrane potential ($\Delta\psi m$) was presented as the ratio of red fluorescence by aggregates of JC-1 to green fluorescence by monomers of JC-1, which were detected with a laser confocal microscope.

2.9. Animal Treatment. Male 8-week-old 129S1/SvImJ WT mice and SIRT3 KO mice were fed in the Experimental Animal Center of Nantong University according to the US National Institutes of Health Guidelines for Care and Use of Laboratory Animals (approval no. NTUERLAUA-20160224).

WT mice and SIRT3 KO mice were intraperitoneally administrated by NaHS (50 μmol·kg^{-1}·day^{-1}) once daily, and normal saline (NS) was given as a control. After 2 weeks, mice were intraperitoneally injected with a mixture of ketamine (100 mg·kg^{-1}) and xylazine (5 mg·kg^{-1}) to induce anesthesia which was confirmed by loss of reflex to toe pinching. Then, thoracotomy was performed to expose the aortic arch, and transverse aortic constriction (TAC) was carried out by tying a 6-0 nylon suture ligature against a 26-gauge needle. The needle was withdrawn immediately to form an incomplete constriction. The mice with the same operating procedures without constriction served as sham controls. After surgery, all mice went on being treated by NaHS or NS for another 2 weeks [28]. During the experiments, systolic blood pressure (SBP) was monitored by a noninvasive blood pressure analysis system (Visitech Systems, Apex, NC, USA) with the tail-cuff method every week.

2.10. Determination of H$_2$S Concentration in the Plasma and H$_2$S Production in the Myocardium. The H$_2$S level was determined using a H$_2$S-specific microelectrode connected to a free radical analyzer (World Precision Instruments, Sarasota, FL, USA) in light of the previous description [16]. A standard curve was obtained by the current value in different concentrations (0, 0.5, 1, 2, 4, and 8 μM) of Na$_2$S stock solution. H$_2$S in the myocardium was determined in tissue homogenates. The homogenates were incubated in the assay mixture (500 μL) containing 460 μL tissue homogenates, 20 μL L-cysteine (10 mmol/L), and 20 μL pyridoxal 5$'$-phosphate (2 mmol/L) at 37°C in tightly sealed vials for 30 min. Then, the plasma or homogenate was dropped into the reaction solution, and there was a significant change in the current value. The H$_2$S level in the plasma or the myocardium can be calculated according to the standard curve.

2.11. Sirius Red Staining. After washing 3 times, myocardial paraffin sections about 5 μm thick were stained with saturated picric acid-Sirius red without light for 30 min. Then, the nuclei were lightly stained with Mayer's hematoxylin staining solution. Finally, the collagen deposition in the myocardium was observed and photographed with a microscope. The ratio of the perivascular collagen area (PVCA) to the luminal area (LA) was calculated to assess the degree of perivascular fibrosis in the myocardium. The collagen volume fraction (CVF), as the ratio of the interstitial collagen area to the myocardial area, was statistically analyzed to evaluate the degree of interstitial fibrosis.

2.12. Quantitative Real-Time PCR. Expressions of mRNA were carried out by real-time PCR following the MIQE guidelines. Extracted RNA from cardiac fibroblasts or the myocardium with the TRIzol reagent (Takara, Kyoto, Japan) was subjected to reverse transcription according to the introduction of the PrimeScript™ RT Master Mix Kit (Takara, Kyoto, Japan). Amplification of cDNA was carried out three times in the PCR System (ABI 7500, ABI, Carlsbad, CA, USA) by SYBR (Takara, Kyoto, Japan) with 18S as the housekeeping gene. All sequences of the sense primers and antisense primers are listed below (Table 1).

2.13. Western Blots. Protein samples extracted from cardiac fibroblasts or the left ventricular myocardium were separated by 10% or 6% sodium dodecyl sulfate- (SDS-) polyacrylamide gel electrophoresis (PAGE). Then, the proteins in the gel were transferred onto membranes of polyvinylidene fluoride (PVDF) (Millipore, Billerica, MA, USA). After the membranes were blocked with 5% nonfat milk at room temperature for 2 h, the membranes with proteins were incubated overnight with an appropriate primary antibody for anti-SIRT3 (1 : 1000; Santa Cruz Biotechnology, St. Louis, MO, USA), anti-α-SMA, collagen I, collagen III (1 : 1000; Bioss, Beijing, China), anti-DRP1 (1 : 1000; Cell Signaling Technology, USA), anti-β-tubulin (1 : 3000; CMCTAG, Milwaukee, WI, USA), and anti-GAPDH (1 : 7000; Sigma-Aldrich, St. Louis, MO, USA) at 4°C. Next, membranes were incubated with horseradish peroxidase- (HRP-) labeled IgG at room temperature for 2 h. Enhanced chemiluminescence (ECL, Thermo Fisher Scientific Inc., Rockford, IL, USA) was dropped to visualize the protein blots.

2.14. Statistical Analysis. All data are shown as mean ± SEM and were analyzed by one-way ANOVA followed by the Bonferroni post hoc test (STATA 15.0). The values of P less than 0.05 were regarded as statistically significant.

3. Results

3.1. NaHS Inhibits Cell Proliferation but Enhances SIRT3 Transcription in Ang II-Stimulated Cardiac Fibroblasts. After

TABLE 1: Sequences of primers.

Gene	Sense primer	Antisense primer
Rat SIRT1	5′-CACCAGAAAGAACTTCACCACCAGA-3′	5′-ACCATCAAGCCGCCTACTAATCTG-3′
Rat SIRT2	5′-AGGGACAAGGAGCAGGGTTC-3′	5′-GAAGAGAGACAGCGGCAGGAC-3′
Rat SIRT3	5′-GAGGTTCTTGCTGCATGTGGTTG-3′	5′-AGTTTCCCGCTGCACAAGGTC-3′
Rat SIRT4	5′-TTGTGCCAGCAAGTCCTCCTC-3′	5′-GTCTCTTGGAAAGGGTGATGAAGC-3′
Rat SIRT5	5′-TCCAGCGTCCACACGAAACC-3′	5′-AACACCAGCTCCTGAGATGATGAC-3′
Rat SIRT6	5′-GCTGGAGCCCAAGGAGGAATC-3′	5′-AGTAACAAAGTGAGACCACGAGAG-3′
Rat SIRT7	5′-GAGCCAACCCTCACCCACATG-3′	5′-ACGCAGGAGGTACAGACTTCAATG-3′
Rat collagen I	5′-AGGGTCATCGTGGCTTCTCT-3′	5′-CAGGCTCTTGAGGGTAGTGT-3′
Rat collagen III	5′-AGCGGAGAATACTGGGTTGA-3′	5′-GATGTAATGTTCTGGGAGGC-3′
Mouse collagen I	5′-AAGAAGACATCCCTGAAGTCA-3′	5′-TTGTGGCAGATACAGATCAAG-3′
Mouse collagen III	5′-TTGGGATGCAGCCACCTTG-3′	5′-CGCAAAGGACAGATCCTGAG-3′
18S	5′-AGTCCCTGCCCTTTGTACACA-3′	5′-CGATCCGAGGGCCTCACTA-3′

NaHS (50 μM) administration for 4 h followed by Ang II (100 nM) stimulation for another 24 h, cell proliferation was evaluated by cell count analysis and hydroxyproline secretion. NaHS pretreatment significantly reduced cell numbers (Figure 1(a)) and reduced hydroxyproline content in the cell culture medium (Figure 1(b)) after Ang II stimulation. These data indicated that NaHS inhibited Ang II-induced cardiac fibroblast proliferation.

Next, we assessed the possible role of SIR2 family members in the attenuated effect of NaHS on cardiac fibroblast proliferation. The mRNA expressions of all seven members, SIRT1-SIRT7, were detected by real-time PCR. SIRT1 and SIRT3 were significantly decreased after Ang II stimulation, while SIRT2, SIRT4, SIRT5, SIRT6, and SIRT7 remained unchanged. Moreover, the decreased SIRT3 was corrected by NaHS preadministration for 4 h. However, there was no significant change in SIRT1 by NaHS, suggesting that SIRT1 was possibly not critical in the inhibitory effect of NaHS on Ang II-induced cardiac fibroblast proliferation. It is worth noting that there was no alteration on SIR2 mRNA of NaHS-treated cardiac fibroblasts without Ang II stimulation (Figure 1(c)). Moreover, NaHS also increased SIRT3 promoter activity in Ang II-stimulated cardiac fibroblasts (Figure 1(d)). Taken together, NaHS enhanced SIRT3 transcription in the inhibitory effect on Ang II-induced cardiac fibroblast proliferation.

3.2. NaHS Inhibits Ang II-Stimulated Cardiac Fibroblast Proliferation via SIRT3.
However, whether enhanced SIRT3 was crucial in the above effect remained to be elucidated. In our further study, SIRT3 was knocked down in cardiac fibroblasts by RNA interference technology. After specific SIRT3 siRNA transfection, SIRT3 was significantly reduced at both levels of mRNA and protein expressions (Figures 2(a) and 2(b)).

Then, cell numbers and hydroxyproline content of cardiac fibroblasts were assessed again after SIRT3 was silenced.

Our study showed that NaHS pretreatment significantly decreased cell numbers and reduced hydroxyproline content in Ang II-stimulated cardiac fibroblasts. However, the inhibitory effect was unavailable after SIRT3 was knocked down (Figures 2(c) and 2(d)). These results suggested that NaHS inhibited Ang II-stimulated cardiac fibroblast proliferation in a SIRT3-dependent manner.

3.3. NaHS Suppresses Collagen Expression in Ang II-Stimulated Cardiac Fibroblasts via SIRT3.
Next, the expression of collagen I and collagen III was also examined. We found that NaHS inhibited collagen I and collagen III expressions at both the mRNA and protein levels in Ang II-stimulated cardiac fibroblasts. However, the above protective effects by NaHS were absent after SIRT3 was silenced (Figure 3). It suggested that NaHS suppressed Ang II-stimulated cardiac fibroblast collagen expression in a SIRT3-dependent manner.

3.4. NaHS Inhibits α-SMA Expression in Ang II-Stimulated Cardiac Fibroblasts via SIRT3.
The expression of α-SMA is commonly regarded as a robust and sensitive marker of cardiac fibroblast differentiation [4]. The present studies found that the α-SMA expression was enhanced after Ang II stimulation, which was attenuated by NaHS pretreatment. However, the above inhibitory effect of NaHS on α-SMA expression was obviously blunted if SIRT3 was knocked down (Figure 4(a)). It suggested that NaHS inhibited α-SMA expression in Ang II-stimulated cardiac fibroblasts via SIRT3.

3.5. NaHS Attenuates Oxidative Stress in Ang II-Stimulated Cardiac Fibroblasts via SIRT3.
Previous studies have verified that excessive oxidative stress was a critical pathophysiological mechanism in several cardiovascular diseases including myocardial remodeling, atherosclerosis, myocardial ischemia-reperfusion injury, and diabetic cardiomyopathy
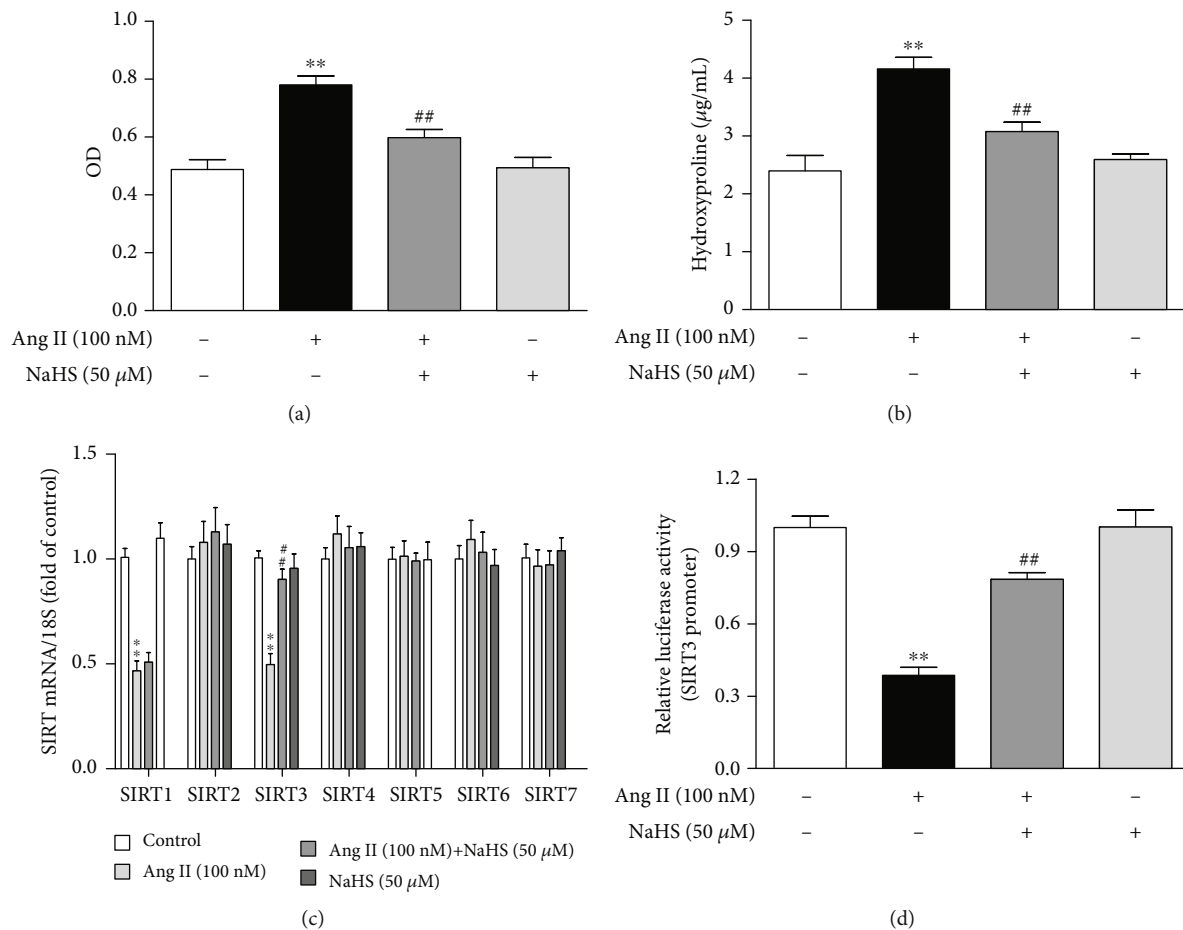
FIGURE 1: NaHS inhibits cell proliferation but enhances SIRT3 transcription in Ang II-stimulated cardiac fibroblasts. After pretreatment with NaHS (50 μM) for 4 h, neonatal rat cardiac fibroblasts were stimulated by Ang II (100 nM) for 24 h. (a) The number of cardiac fibroblasts was detected with CCK-8. (b) The content of hydroxyproline in the cell culture medium was measured. (c) Expression of SIR2 family (SIRT1-7) mRNA was measured by real-time PCR. (d) After the SIRT3 promoter luciferase plasmid was transfected into cardiac fibroblasts for 24 h, cells were pretreated with NaHS (50 μM) for 4 h followed by Ang II (100 nM) stimulation for another 24 h. Relative promoter activity of SIRT3 was detected with a dual-luciferase reporter assay system. $^{**}P < 0.01$ as compared with untreated cells; $^{##}P < 0.01$ as compared with Ang II alone-stimulated cells. $n = 6$.

[29, 30]. SIRT3, as a vital acetyl-lysine deacetylase, regulates mitochondrial function and reactive oxygen species (ROS) production [31]. Our present study found that NaHS alleviated DHE fluorescence intensity in Ang II-stimulated cardiac fibroblasts, suggesting that NaHS attenuated Ang II-stimulated ROS production. However, NaHS was no longer able to suppress DHE fluorescence intensity after SIRT3 was knocked down (Figure 4(b)). These data showed that NaHS attenuated oxidative stress in Ang II-stimulated cardiac fibroblasts via a SIRT3-dependent manner.

3.6. NaHS Improves Mitochondrial Respiration Function and Membrane Potential in Ang II-Stimulated Cardiac Fibroblasts via SIRT3. The above attenuated effects of NaHS on cardiac fibroblast proliferation suggested that mitochondrial function might also be improved by NaHS via SIRT3. To verify the hypothesis, the oxygen consumption rate (OCR) in Ang II-stimulated cardiac fibroblasts after NaHS administration with SIRT3 silencing was measured. Our study showed that NaHS significantly improved basal respi-

ration, ATP generation, respiratory reserve capacity, and maximal respiration in Ang II-stimulated cardiac fibroblasts, which was unavailable after SIRT3 silencing (Figures 4(c) and 4(d)). These data suggested that NaHS improved mitochondrial respiration function in Ang II-stimulated cardiac fibroblasts via SIRT3.

Next, the mitochondrial membrane potential of cardiac fibroblasts was measured by JC-1 staining. Cells with strong red fluorescence intensity indicated the normal mitochondrial membrane potential, while green fluorescence indicated a decreased one. Our results showed that NaHS increased red, but decreased green, fluorescence intensity in Ang II-stimulated cardiac fibroblasts, whereas the effect was significantly alleviated after SIRT3 was knocked down (Figure 4(e)). It suggested that NaHS improved mitochondrial membrane potential in Ang II-stimulated cardiac fibroblasts via a SIRT3-dependent manner.

3.7. NaHS Decreases Blood Pressure but Restores H_2S Levels and SIRT3 Expression in Mice with TAC. The above results
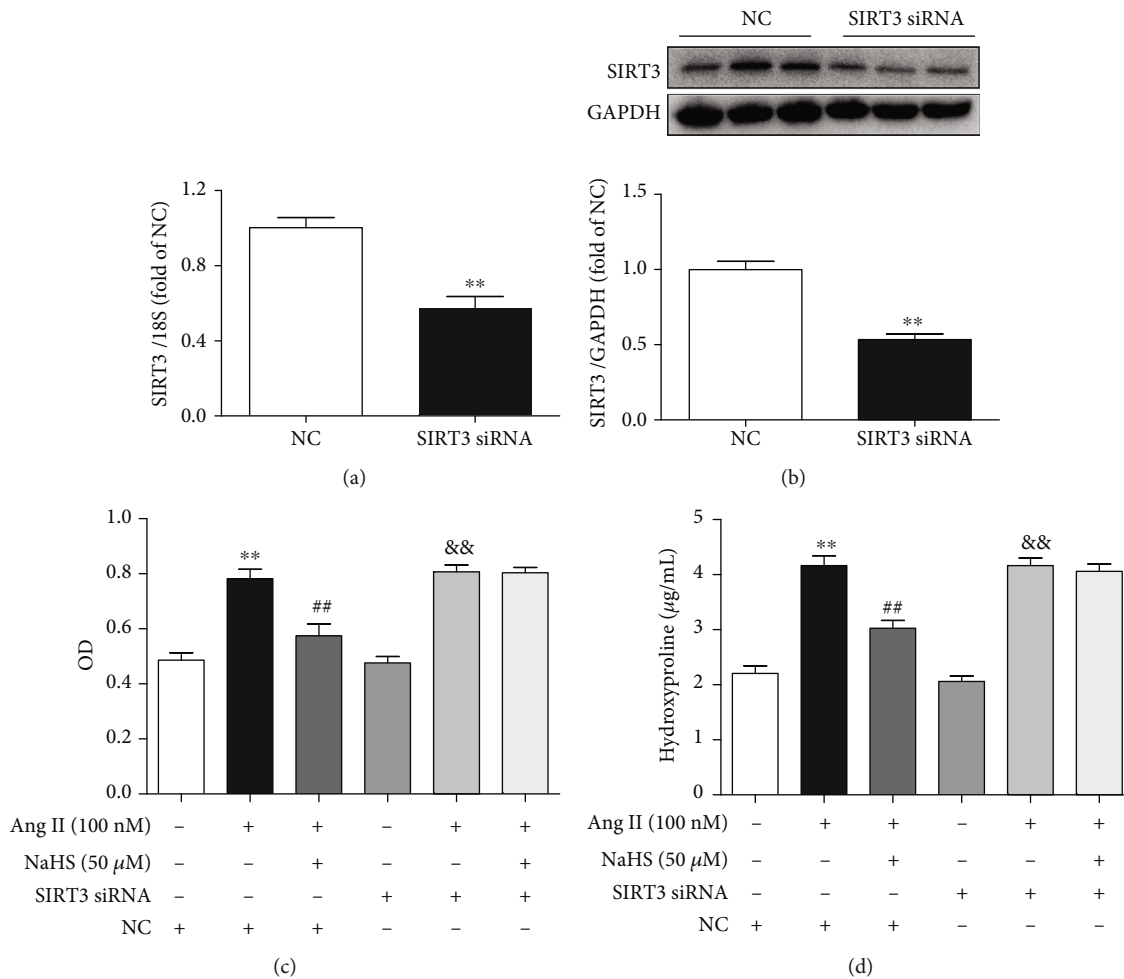
Figure 2: NaHS inhibits Ang II-stimulated cardiac fibroblast proliferation via SIRT3. (a, b) After SIRT3 siRNA or NC siRNA was transfected into neonatal rat myocardial fibroblasts for 48 h, expression of SIRT3 mRNA and protein was measured by real-time PCR and western blot, respectively. $^{**}P < 0.01$ as compared with cells with NC siRNA transfection. $n = 6$. (c) After SIRT3 siRNA or NC siRNA was transfected into cardiac fibroblasts for 24 h, the cells were pretreated with NaHS ($50\,\mu$M) for 4 h followed by Ang II (100 nM) stimulation for another 24 h. The number of cardiac fibroblasts was detected with CCK-8. (d) The content of hydroxyproline in the cell culture medium was measured. $^{**}P < 0.01$ as compared with untreated cells with NC siRNA transfection; $^{\#\#}P < 0.01$ as compared with Ang II alone-stimulated cells with NC siRNA transfection; $^{\&\&}P < 0.01$ as compared with untreated cells with SIRT3 siRNA transfection. $n = 6$.

showed that NaHS inhibited Ang II-induced cardiac fibroblast proliferation in a SIRT3-depended manner *in vitro*. Next, the role of SIRT3 in the protective effects of NaHS was investigated in mice. After TAC, SBP was significantly increased in WT and SIRT3 KO mice to the same extent in the next weeks. NaHS administration reduced SBP in both the WT and SIRT3 knockout mice (Figure 5(a)). H_2S concentration in the plasma and H_2S production in the myocardium were impaired after TAC, which was restored by the exogenous NaHS supplement in both WT mice and SIRT3 KO mice (Figures 5(b) and 5(c)). SIRT3 expression was decreased in the myocardium of WT mice after TAC, which was elevated by NaHS. And there was no SIRT3 expression in the myocardium of SIRT3 KO mice (Figure 5(d)). These data suggested that NaHS regulated blood pressure and H_2S levels regardless of the presence or absence of the SIRT3 gene.

3.8. NaHS Ameliorates Perivascular and Interstitial Collagen Deposition in the Myocardium of WT Mice but Not SIRT3 KO Mice with TAC.
Perivascular fibrosis and interstitial fibrosis are the main manifestations of myocardial fibrosis [32]. Collagen, shown in red by Sirius red staining, was significantly suppressed by NaHS in WT mice but not SIRT3 KO mice with TAC (Figure 6(a)). Statistical analysis showed that after TAC, both the ratio of PVCA to LA and the CVF in SIRT3 KO mice were higher than that in WT mice. NaHS decreased the ratio of PVCA to LA and reduced CVF in WT mice with TAC, which was unavailable in SIRT3 KO mice (Figures 6(b) and 6(c)). It indicated that NaHS ameliorated perivascular and interstitial collagen deposition in the myocardium of WT mice but not SIRT3 KO mice with TAC.

3.9. NaHS Reduces Collagen and α-SMA Expressions in the Myocardium of WT Mice but Not SIRT3 KO Mice with
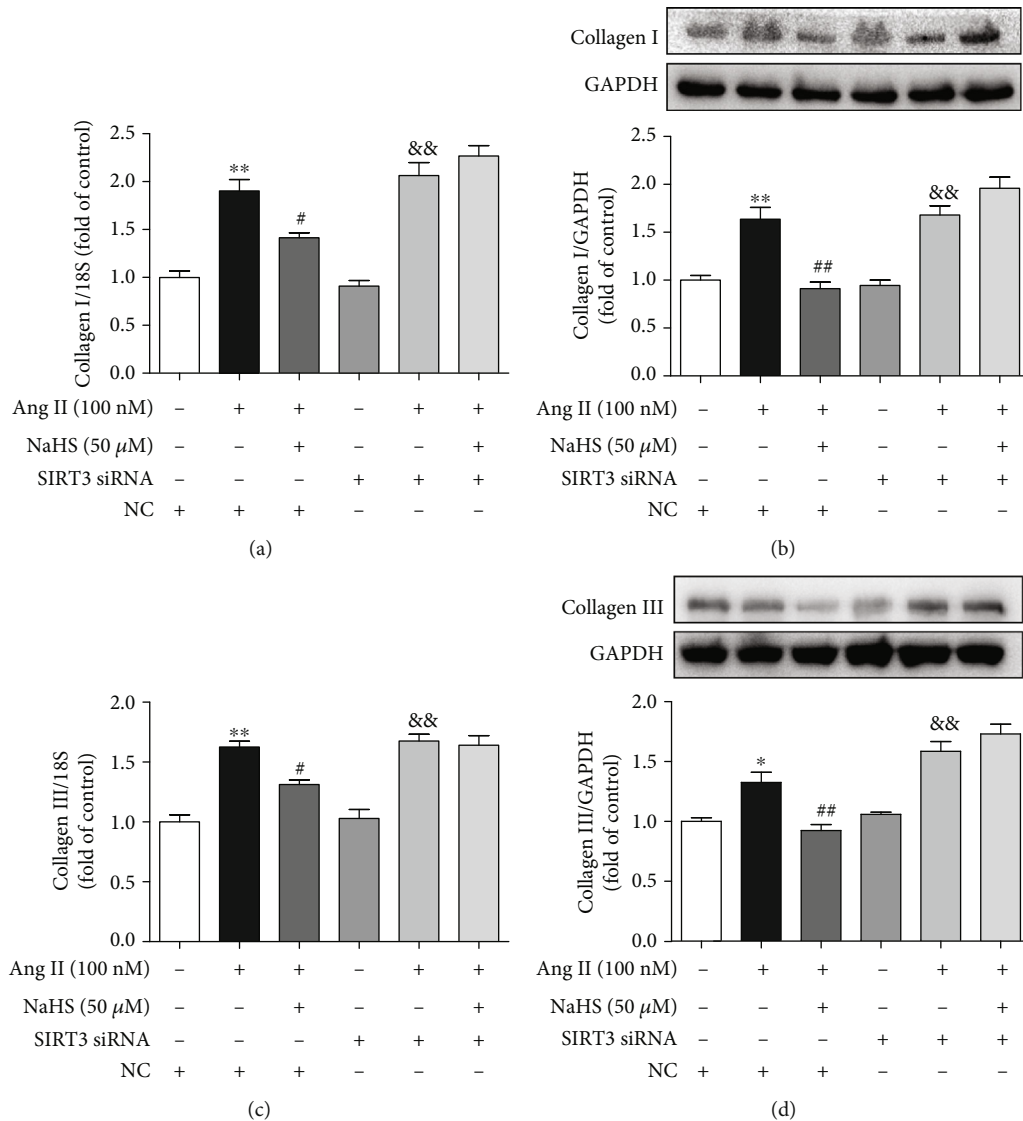
Figure 3: NaHS suppresses collagen expression in Ang II-stimulated cardiac fibroblasts via SIRT3. After SIRT3 siRNA or NC siRNA was transfected into neonatal rat cardiac fibroblasts for 24 h, the cells were pretreated with NaHS (50 μM) for 4 h followed by Ang II (100 nM) stimulation for another 24 h. (a, b) Expression of collagen I mRNA and protein was measured by real-time PCR and western blot, respectively. (c, d) Expression of collagen III mRNA and protein was measured by real-time PCR and western blot, respectively. $^*P < 0.05$ and $^{**}P < 0.01$ as compared with untreated cells with NC siRNA transfection; $^#P < 0.05$ and $^{##}P < 0.01$ as compared with Ang II alone-stimulated cells with NC siRNA transfection; $^{\&\&}P < 0.01$ as compared with untreated cells with SIRT3 siRNA transfection. $n = 6$.

TAC. The data *in vitro* suggested that NaHS reduced collagen expression in Ang II-stimulated cardiac fibroblasts via a SIRT3-dependent manner. Next, the possible protective effect *in vivo* was further investigated. We found that after TAC, there was more hydroxyproline content and collagen expression in SIRT3 KO mice than in WT mice. NaHS reduced hydroxyproline content and collagen expression in the myocardium of WT mice with TAC. However, there was no inhibitory effect of NaHS on the above indexes in SIRT3 KO mice with TAC (Figures 7(a)–7(c)). Similarly, there was more α-SMA expression in SIRT3 KO mice with TAC than in WT mice. NaHS suppressed α-SMA expression in the myocardium of WT mice but not SIRT3 KO mice with TAC (Figure 7(d)). Taken together, NaHS alleviated

myocardial fibrosis in mice with TAC via a SIRT3-dependent manner.

3.10. NaHS Restores DRP1 Expression in the Cardiac Fibroblasts with Ang II Stimulation and in the Myocardium of Mice with TAC via SIRT3. DRP1 is a protein associated with mitochondrial fission, which may induce structural damage and functional dysfunction of mitochondria [33]. Our present results showed that NaHS inhibited DRP1 expression in Ang II-stimulated cardiac fibroblasts. However, the inhibitory effect by NaHS was significantly weakened after SIRT3 was knocked down (Figures 8(a) and 8(b)). After TAC, there was more expression of DRP1 in the myocardium of SIRT3 KO mice than in WT mice. NaHS

α-SMA/DAPI

(a)

DHE/DAPI
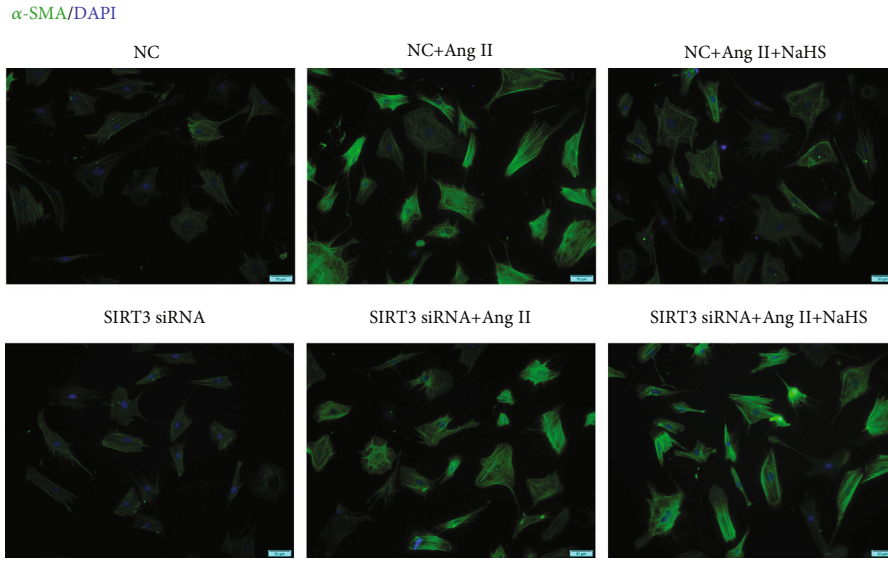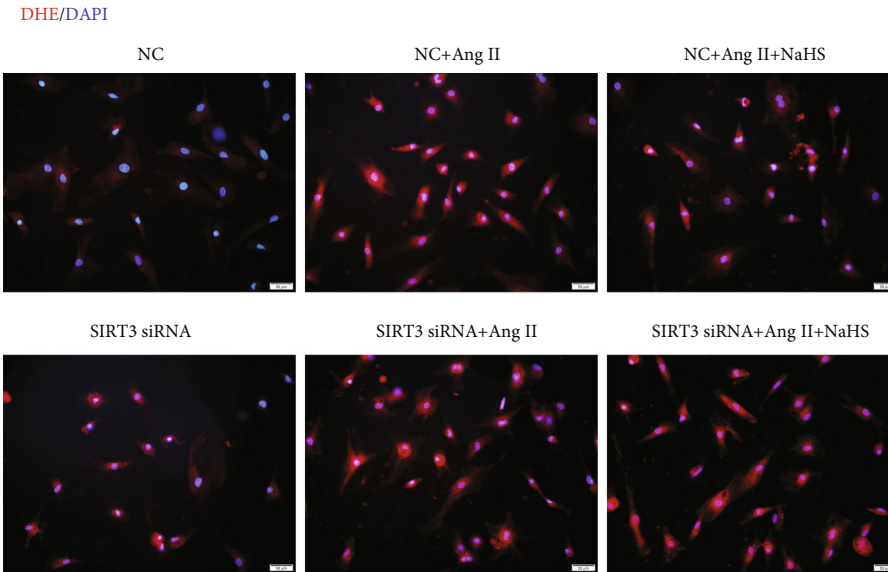
(b)
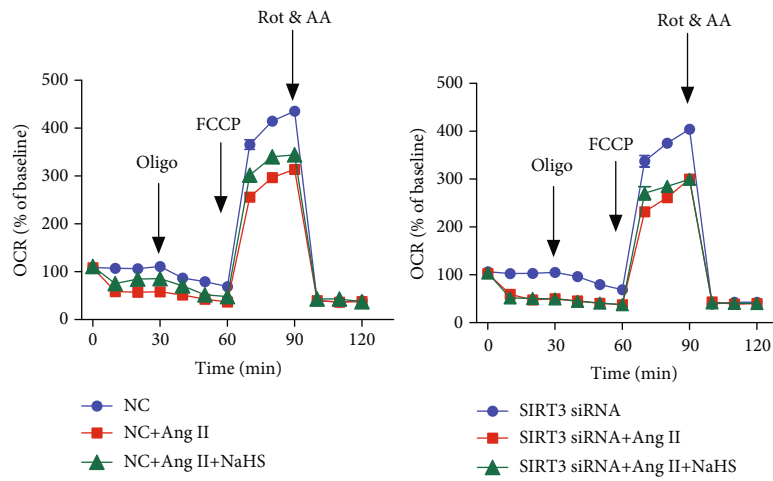
(c)

FIGURE 4: Continued.

(d)

(e)
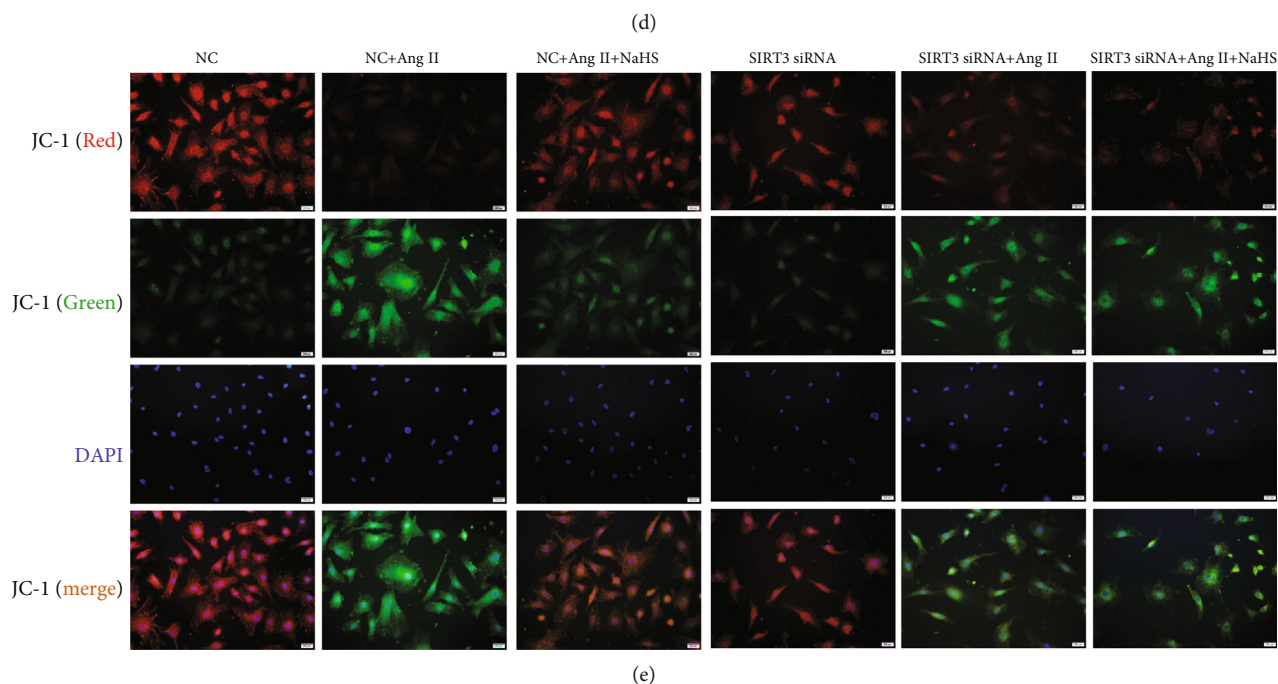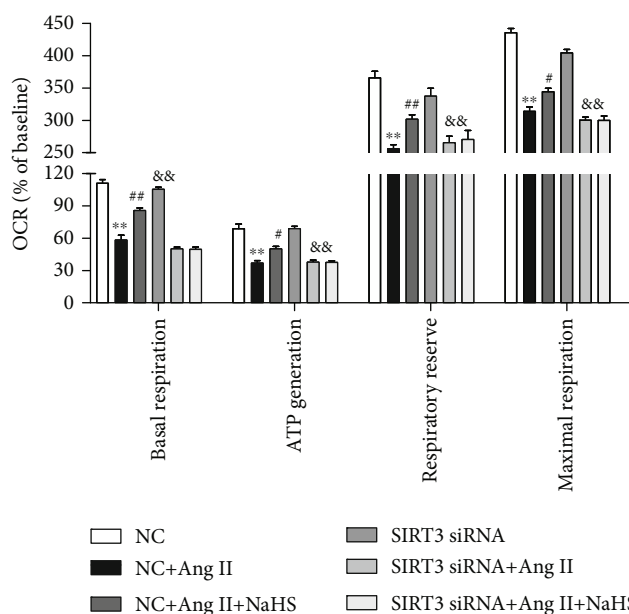
FIGURE 4: NaHS inhibits α-SMA expression and oxidative stress and improves mitochondrial respiration function and membrane potential in Ang II-stimulated cardiac fibroblasts via SIRT3. After SIRT3 siRNA or NC siRNA was transfected into neonatal rat cardiac fibroblasts for 24 h, the cells were pretreated with NaHS (50 μM) for 4 h followed by Ang II (100 nM) stimulation for another 24 h. (a) Expression of α-SMA in cardiac fibroblasts was measured by immunofluorescence with Alexa Fluor 488 (green)-conjugated IgG. The nuclei were stained using DAPI (blue). Bar = 50 μm. (b) ROS was detected with DHE staining. Bar = 50 μm. (c) The mitochondrial respiration function of cardiac fibroblasts was measured. (d) Quantitative analysis of basal respiration, ATP generation, respiratory reserve capacity, and maximal respiratory. $^{**}P < 0.01$ as compared with untreated cells with NC siRNA transfection; $^{#}P < 0.05$ and $^{##}P < 0.01$ as compared with Ang II alone-stimulated cells with NC siRNA transfection; $^{\&\&}P < 0.01$ as compared with untreated cells with SIRT3 siRNA transfection. $n = 6$. (e) Mitochondrial permeability potential was determined by JC-1 staining. Bar = 200 μm.

suppressed DRP1 expression in the myocardium of WT mice but not SIRT3 KO mice with TAC (Figure 8(c)). All these data verified that NaHS restored DRP1 expression in the cardiac fibroblasts with Ang II stimulation and in the myocardium of mice with TAC via a SIRT3-dependent manner.

4. Discussion

Myocardial fibrosis is the process of extracellular matrix remodeling to significantly increase myocardial stiffness and eventually results in heart failure and even sudden cardiac death [34]. The H$_2$S supplement might have protective
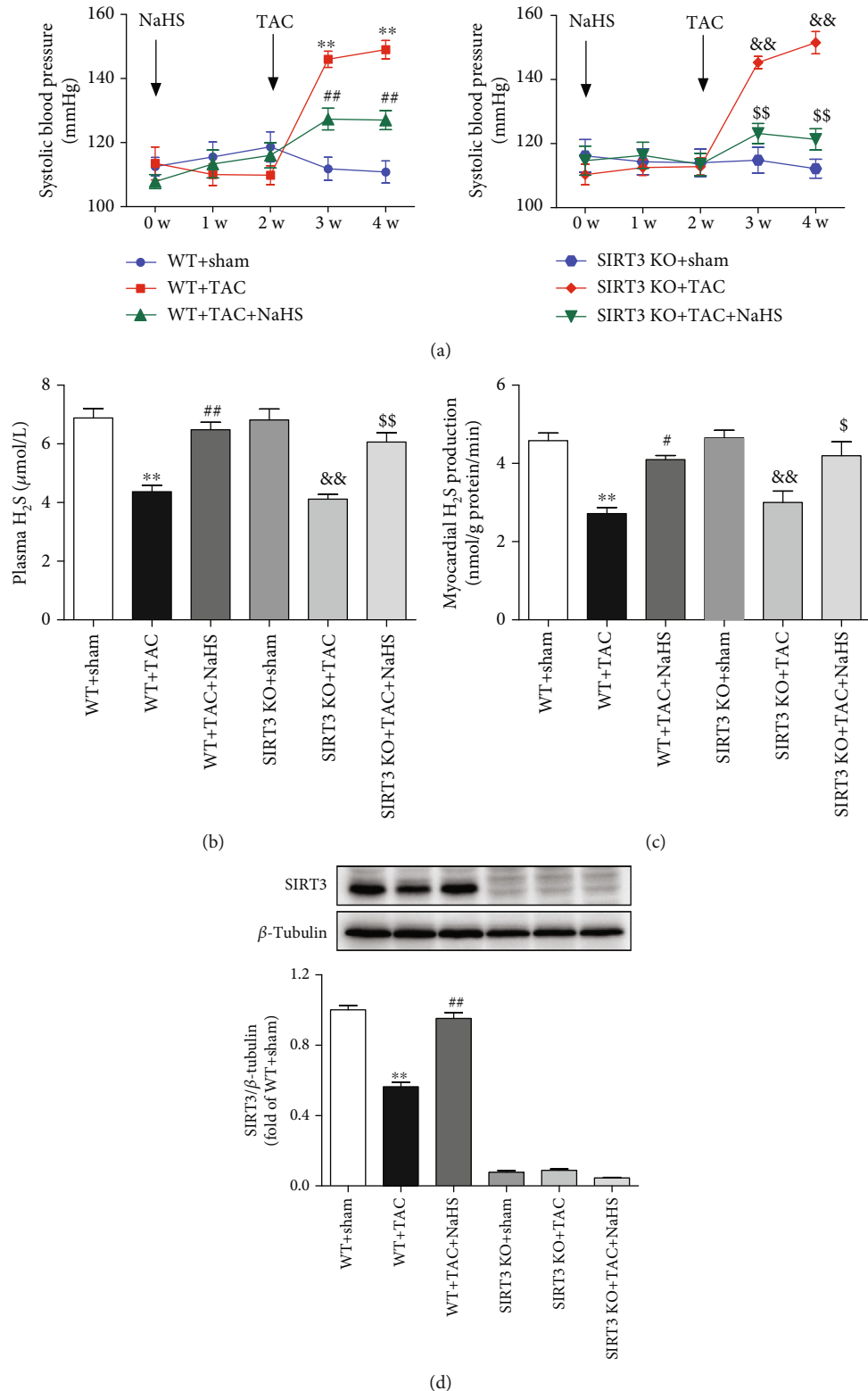
FIGURE 5: NaHS decreases blood pressure but restores H_2S levels and SIRT3 expression in mice with TAC. After intraperitoneal injection by NaHS ($50\,\mu mol \cdot kg^{-1} \cdot day^{-1}$) or normal saline (NS) for 2 weeks, male wild-type (WT) mice and SIRT3 knockout (SIRT3 KO) mice were subjected to transverse aortic constriction (TAC) surgery. NaHS or NS was administrated for another 2 weeks. (a) The level of SBP in WT mice and SIRT3 KO mice was monitored every week after NaHS administration. (b) H_2S concentration in the plasma was measured. (c) H_2S production in the myocardium was detected. (d) Expression of SIRT3 protein in the myocardium was measured by western blot. $^{**}P < 0.01$ as compared with WT+Sham; $^{\#}P < 0.05$ and $^{\#\#}P < 0.01$ as compared with WT+TAC; $^{\&\&}P < 0.01$ as compared with SIRT3 KO+Sham; $^{\$\$}P < 0.01$ as compared with SIRT3 KO+TAC. $n = 6$.

(a)

(b)

(c)
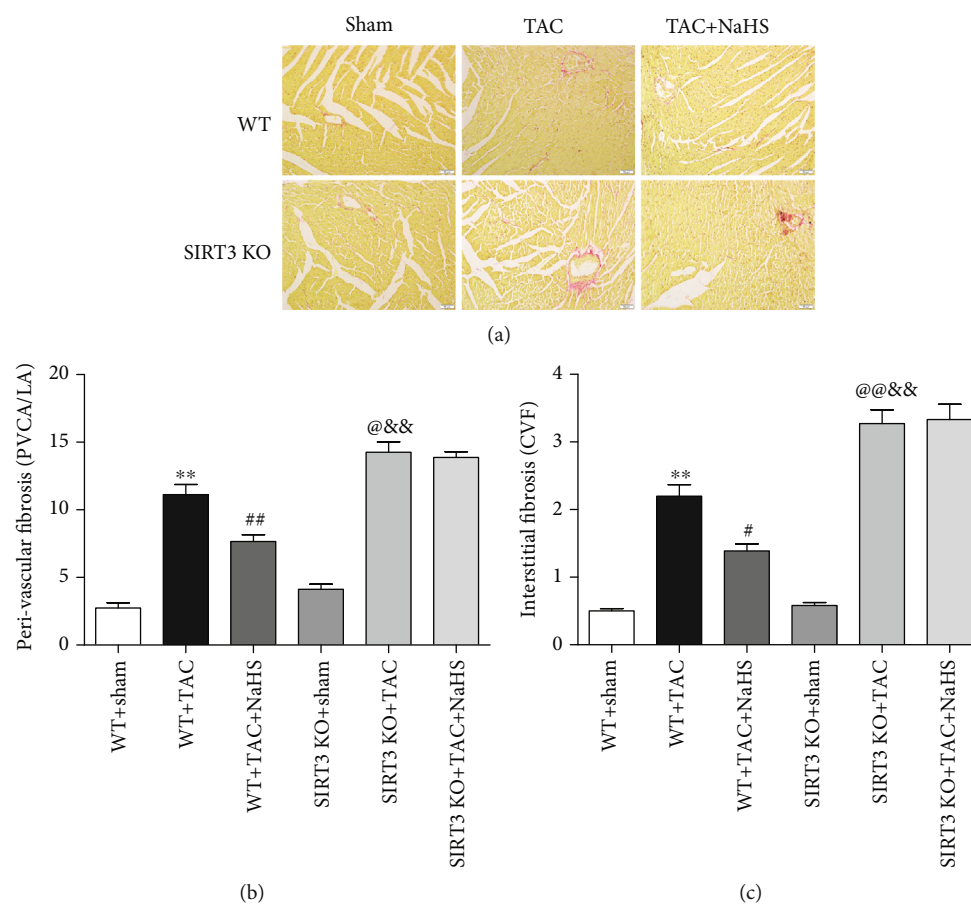
FIGURE 6: NaHS ameliorates collagen deposition in the myocardium of WT mice but not SIRT3 KO mice with TAC. After intraperitoneal injection by NaHS (50 μmol·kg^{-1}·day^{-1}) or NS for 2 weeks, male WT mice and SIRT3 KO mice were subjected to TAC surgery. NaHS or NS was administrated for another 2 weeks. (a) Collagen deposition in the myocardium was stained with saturated picric acid-Sirius red. Bar = 50 μm. (b) Perivascular fibrosis of the myocardium was assessed by the ratio of the perivascular collagen area (PVCA) to the luminal area (LA). (c) Interstitial fibrosis of the myocardium was assessed by the collagen volume fraction (CVF). **$P < 0.01$ as compared with WT+Sham; #$P < 0.05$ or @$P < 0.05$ and ##$P < 0.01$ or @@$P < 0.01$ as compared with WT+TAC; &&$P < 0.01$ as compared with SIRT3 KO +Sham. $n = 6$.

effects on myocardial ischemia-reperfusion injury, cardiac infarction, arrhythmia, cardiac hypertrophy, heart failure, and diabetic cardiomyopathy [35–37]. It is noted that H$_2$S suppressed cardiac fibroblast proliferation by inhibiting K$^+$ currents or channels and blocking the transformation of atrial fibroblasts into myoblasts [38]. NaHS administration ameliorated myocardial fibrosis via inhibiting cell aging in diabetic rats [39]. H$_2$S alleviated myocardial fibrosis and restored cardiac function in both the CSE KO and WT mice with myocardial infarction [40]. In our present experiment, we verified that NaHS inhibited cell numbers, hydroxyproline content, α-SMA expression, and collagen production but enhanced SIRT3 expression in the cardiac fibroblasts and the myocardium. It suggested the inhibitory effect of H$_2$S on both Ang II-induced cardiac fibroblast proliferation and TAC-induced myocardial fibrosis. Moreover, NaHS equally reduced blood pressure but enhanced the H$_2$S level in all mice, suggesting that the failure of NaHS to inhibit myocardial fibrosis in SIRT3 KO mice is due to SIRT3 deficiency but not blood pressure.

The key role of SIRT3 in mitochondrial function has been intensively investigated. However, the possible role of SIRT3 on the protective effects of H$_2$S against myocardial fibrosis was unknown. Our previous research studies have shown that H$_2$S increased SIRT3 expression in human umbilical vein endothelial cells and cardiomyocytes [16, 18, 41]. Other groups found that H$_2$S improved cardiac energy substrate metabolism via SIRT3 in db/db mice [42, 43]. H$_2$S activated SIRT3 through S-sulfhydration to attenuate cisplatin-induced acute kidney injury [44]. H$_2$S also attenuated hydrogen peroxide-induced NLR family pyrin domain-containing protein 3 (NLRP3) inflammasome activation via SIRT3 in macrophages [45]. Moreover, we verified that SIRT3 deficiency exacerbated diabetic cardiomyopathy and delayed diabetic skin wound healing [46, 47]. In our present experiment, mRNA expression of SIRT1 and SIRT3 was decreased, while other subtypes of the SIR2 family did not change significantly in cardiac fibroblasts with Ang II stimulation. Moreover, NaHS did increase SIRT3 transcription. Therefore, SIRT3 was focused on the possible pathway

(a)

(b)

(c)

(d)
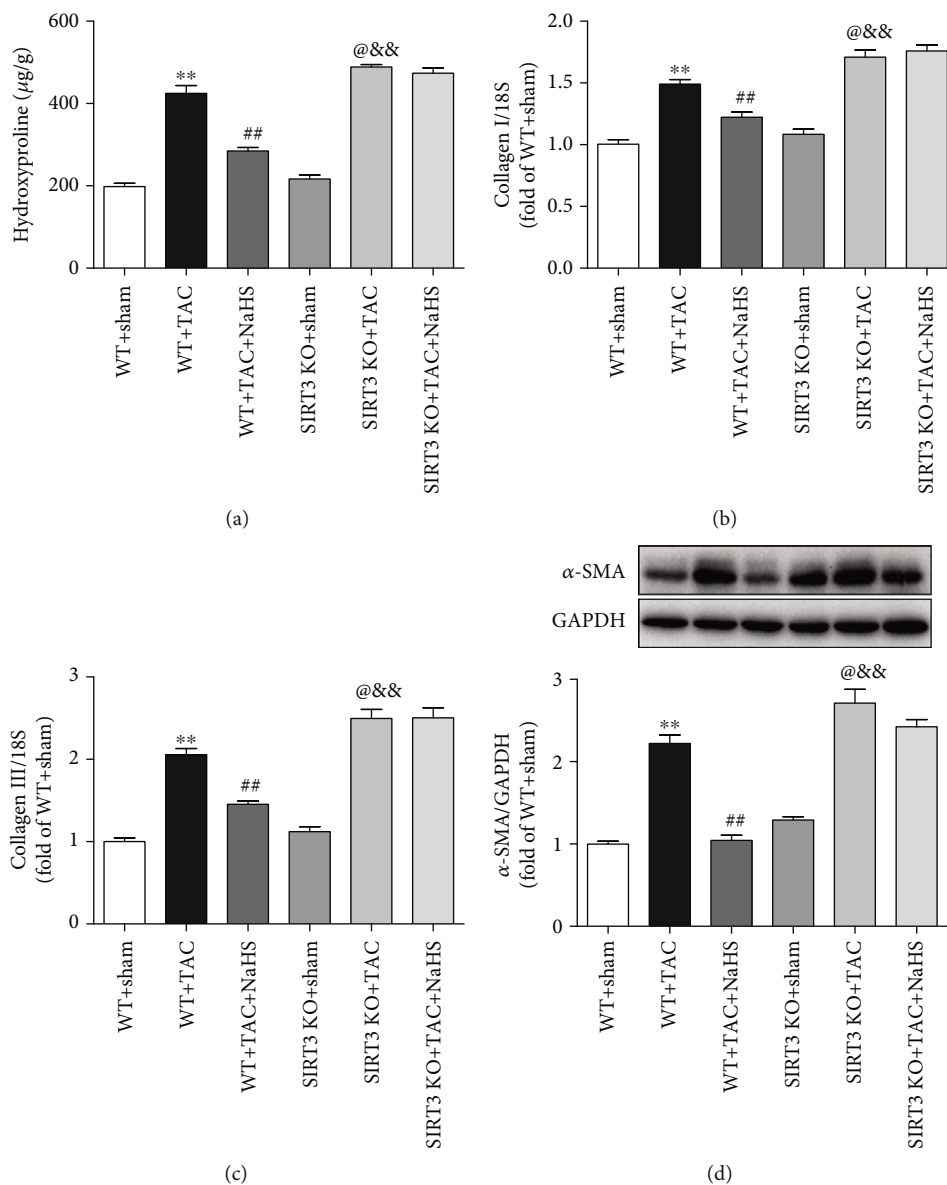
FIGURE 7: NaHS reduces collagen and α-SMA expressions in the myocardium of WT mice but not SIRT3 KO mice with TAC. After intraperitoneal injection by NaHS ($50\,\mu$mol·kg^{-1}·day^{-1}) or NS for 2 weeks, male WT mice and SIRT3 KO mice were subjected to TAC surgery. NaHS or NS was administrated for another 2 weeks. (a) The content of hydroxyproline in the myocardium was measured. (b, c) Expression of collagen I and collagen III mRNA in the myocardium was measured by real-time PCR. (d) Expression of α-SMA protein in the myocardium was measured by western blot. $^{**}P < 0.01$ as compared with WT+Sham; $^{##}P < 0.01$ or $^{@}P < 0.05$ as compared with WT+TAC; $^{\&\&}P < 0.01$ as compared with SIRT3 KO+Sham. $n = 8$.

of the protective effect on myocardial fibrosis next. We found that there was more serious fibrosis in SIRT3 KO mice after TAC, suggesting the protective role of SIRT3 in TAC-induced myocardial fibrosis. Cardiac fibroblasts with SIRT3 knockdown and mice with SIRT3 deficiency further verified the protective effect on myocardial fibrosis by H$_2$S via a SIRT3-depended manner. It is beneficial to clarify the mechanism of H$_2$S against myocardial fibrosis.

It is worth noting that the researchers know little about the detailed mechanism of how H$_2$S regulated SIRT3 transcription. Our previous study verified that H$_2$S increased activator protein 1 (AP-1) binding activity with the SIRT3

promoter to enhance SIRT3 transcription in hydrogen peroxide- (H$_2$O$_2$-) stimulated EA.hy926 endothelial cells [18]. Others demonstrated that the protective effect of H$_2$S in paraquat-induced liver injury was at least partly attributed to nuclear factor erythroid 2-related factor 2- (Nrf2-) dependent SIRT3 gene transcription [48]. H$_2$S can induce S-sulfhydration on specific cysteine residues of target proteins to alter protein function and signal transduction [13]. Some studies found that H$_2$S S-sulfhydrated c-Jun of AP-1 to enhance the transcriptional activity on SIRT3, which contributed to decrease ROS production in H$_2$O$_2$-stimulated macrophages [45]. However, the mechanism of how H$_2$S
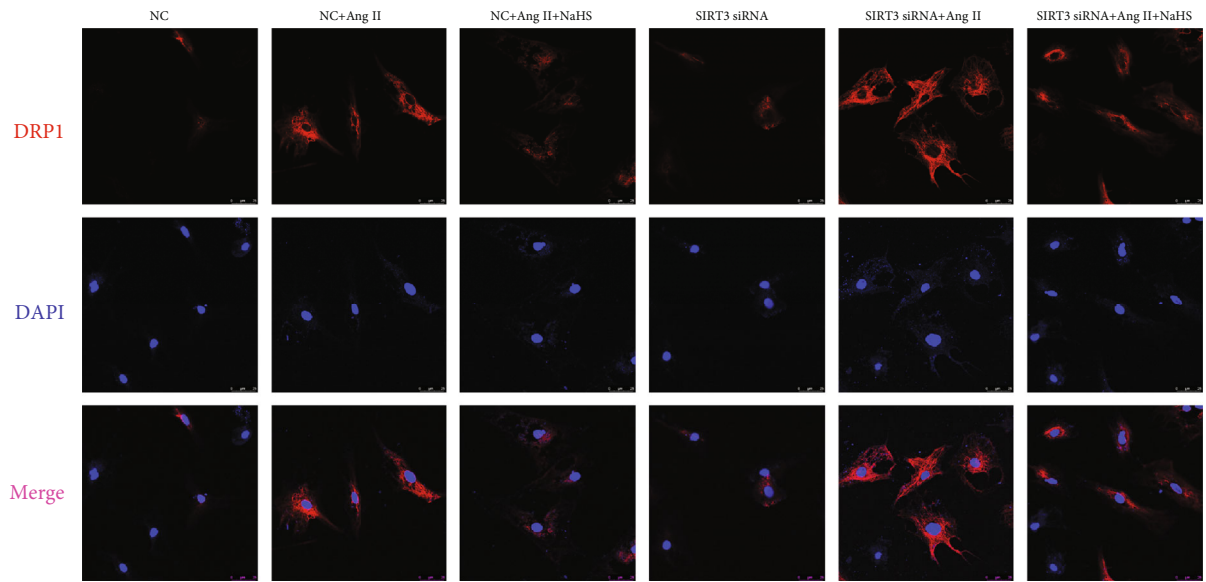
(a)
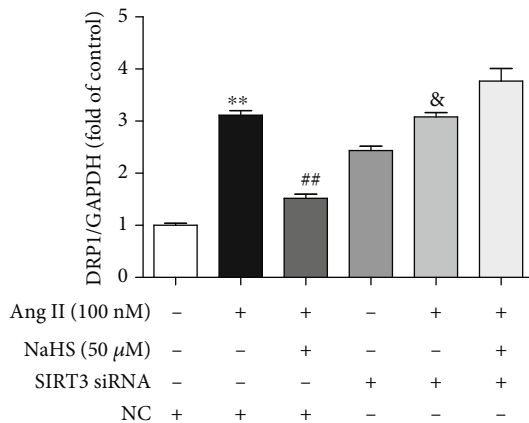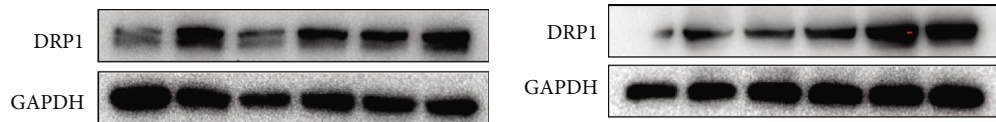
(b)
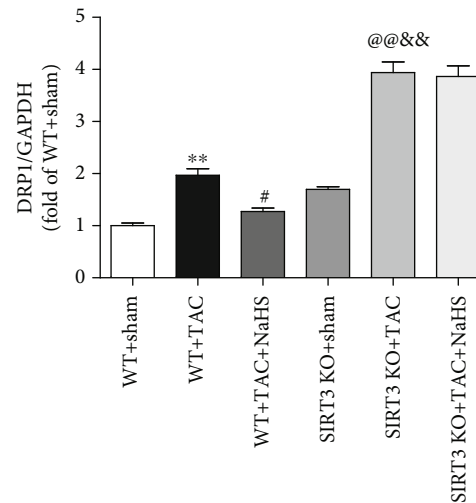
(c)

Figure 8: NaHS restores DRP1 expression in the cardiac fibroblasts with Ang II stimulation and in the myocardium of mice with TAC via SIRT3. (a) After SIRT3 siRNA or NC siRNA was transfected into neonatal rat cardiac fibroblasts for 24 h, the cells were pretreated with NaHS (50 μM) for 4 h followed by Ang II (100 nM) stimulation for another 24 h. DRP1 expression in cardiac fibroblasts was detected by immunofluorescence with Cy3 (red)-conjugated IgG. The nuclei were stained using DAPI (blue). Bar = 25 μm. (b) Expression of DRP1 protein was measured by western blot. $^{**}P < 0.01$ as compared with untreated cells with NC siRNA transfection; $^{##}P < 0.01$ as compared with Ang II alone-stimulated cells with NC siRNA transfection; $^{\&}P < 0.05$ as compared with untreated cells with SIRT3 siRNA transfection. $n = 6$. (c) After intraperitoneal injection by NaHS (50 μmol·kg^{-1}·day^{-1}) or NS for 2 weeks, male WT mice and SIRT3 KO mice were subjected to TAC surgery. NaHS or NS was administrated for another 2 weeks. Expression of DRP1 protein in the myocardium was measured by western blot. $^{**}P < 0.01$ as compared with WT+Sham; $^{#}P < 0.05$ or $^{@@}P < 0.01$ as compared with WT +TAC; $^{\&\&}P < 0.01$ as compared with SIRT3 KO+Sham. $n = 6$.

regulates SIRT3 transcriptional activity during myocardial fibrosis is not known at present and needs to be confirmed in further studies.

SIRT3 plays a vital role in mitochondrial biosynthesis and oxidative stress, which might be critical in the process of myocardial fibrosis [49]. Several studies also indicated
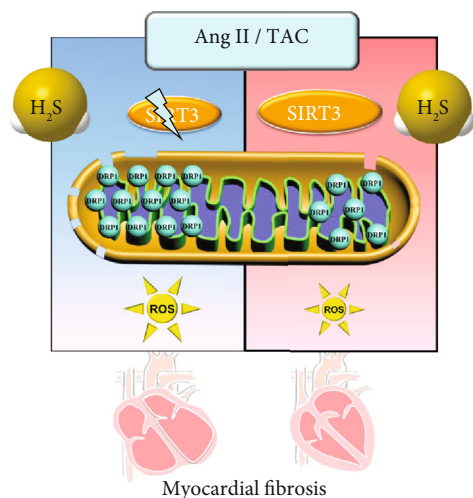
FIGURE 9: Illustration of the mechanism of protective effects on myocardial fibrosis by H_2S. H_2S enhanced SIRT3 transcription, decreased the DRP1 level, ameliorated mitochondrial membrane rupture, suppressed oxidative stress, and alleviated Ang II-induced cardiac fibroblast proliferation and TAC-induced myocardial fibrosis. However, these protective effects of H_2S were unavailable if SIRT3 was silenced in cells or deficient in mice. It suggested that H_2S attenuated myocardial fibrosis through oxidative stress inhibition via a SIRT3-dependent manner.

that H_2S was capable of attenuating oxidative stress and mitochondrial dysfunction [16, 50]. H_2S inhibited oxidative stress in the myocardium of chronic heart failure [51]. Studies have shown that impaired mitochondrial permeability transition pores reduced mitochondrial membrane potential depolarization and inhibited the activation of proapoptotic proteins [52]. It has been reported that H_2S effectively improved mitochondrial membrane potential in high glucose-stimulated human umbilical vein endothelial cells [53]. This may be one of the important mechanisms for protection against mitochondrial function by H_2S [54]. We found that NaHS significantly inhibited Ang II-induced ROS production, improved mitochondrial respiration function, and restored membrane potential in a SIRT3-dependent manner. However, the detailed mechanism of the SIRT3-mediated inhibitory effect on oxidative stress by H_2S was not known well now.

Mitochondria are highly dynamic organelles undergoing cycles of fusion and fission to modulate the morphology, distribution, and function. DRP1, a key protein to regulate mitochondrial fission, is related to clearing the damaged mitochondria and maintaining the process of cellular and organ dynamics [55]. However, an excessive increase of DRP1 will break the balance between mitochondrial fusion and fission to cause mitochondrial dysfunction. Therefore, mitochondrial fission manipulated by targeting DRP1 has been an appealing therapeutic strategy for cytoprotection [56]. We found that NaHS corrected the excessive enhancement of DRP1 in both the cardiac fibroblasts with Ang II stimulation and the myocardium with TAC via a SIRT3-mediated pathway. It clarified a novel mechanism for H_2S

and proposed an alternative approach for mitochondrial function protection.

In conclusion, NaHS, a H_2S donor, enhanced SIRT3 transcription and decreased the DRP1 level to possibly ameliorate mitochondrial membrane rupture, suppress oxidative stress, and alleviate Ang II-induced cardiac fibroblast proliferation and TAC-induced myocardial fibrosis. An illustration of the mechanism is outlined in Figure 9. However, these protective effects of H_2S were unavailable if SIRT3 was silenced in cells or deficient in mice. These results have shed new light on the molecular mechanism responsible for the cardioprotective effect of H_2S against myocardial fibrosis through SIRT3 activation, which might propose a novel strategy for myocardial fibrosis prevention and treatment.

Data Availability

The data used to support the finding of this study are available from the corresponding author upon request.

Conflicts of Interest

The authors declare that there is no conflict of interest regarding the publication of this paper.

Authors' Contributions

Lulu Liu and Weiwei Gong contributed equally to this study.

Acknowledgments

References

[1] N. G. Frangogiannis, "Cardiac fibrosis: cell biological mechanisms, molecular pathways and therapeutic opportunities," *Molecular Aspects of Medicine*, vol. 65, pp. 70–99, 2019.

[2] A. Gonzalez, E. B. Schelbert, J. Diez, and J. Butler, "Myocardial interstitial fibrosis in heart failure: biological and translational perspectives," *Journal of the American College of Cardiology*, vol. 71, no. 15, pp. 1696–1706, 2018.

[3] P. Wang, L. Luo, Q. Shen et al., "Rosuvastatin improves myocardial hypertrophy after hemodynamic pressure overload via regulating the crosstalk of Nrf2/ARE and TGF-β/ smads pathways in rat heart," *European Journal of Pharmacology*, vol. 820, pp. 173–182, 2018.

[4] Q. Song, L. Liu, J. Yu et al., "Dihydromyricetin attenuated Ang II induced cardiac fibroblasts proliferation related to inhibitory of oxidative stress," *European Journal of Pharmacology*, vol. 807, pp. 159–167, 2017.

[5] F. Xu, S. Sun, X. Wang, E. Ni, L. Zhao, and W. Zhu, "GRK2 mediates arginine vasopressin-induced interleukin-6 production via nuclear Factor-κB signaling neonatal rat cardiac fibroblast," *Molecular Pharmacology*, vol. 92, no. 3, pp. 278–284, 2017.

[6] M. Webber, S. P. Jackson, J. C. Moon, and G. Captur, "Myocardial fibrosis in heart failure: anti-fibrotic therapies and the role of cardiovascular magnetic resonance in drug trials," *Cardiology and Therapy*, vol. 9, no. 2, pp. 363–376, 2020.

[7] S. Smolgovsky, U. Ibeh, T. P. Tamayo, and P. Alcaide, "Adding insult to injury - inflammation at the heart of cardiac fibrosis," *Cellular Signalling*, vol. 77, p. 109828, 2021.

[8] Z. Li, D. J. Polhemus, and D. J. Lefer, "Evolution of hydrogen sulfide therapeutics to treat cardiovascular disease," *Circulation Research*, vol. 123, no. 5, pp. 590–600, 2018.

[9] H. Kimura, "Signalling by hydrogen sulfide and polysulfides via protein S-sulfuration," *British Journal of Pharmacology*, vol. 177, no. 4, pp. 720–733, 2020.

[10] X. Cao, L. Ding, Z. Z. Xie et al., "A review of hydrogen sulfide synthesis, metabolism, and measurement: is modulation of hydrogen sulfide a novel therapeutic for cancer?," *Antioxidants & Redox Signaling*, vol. 31, no. 1, pp. 1–38, 2019.

[11] C. R. Powell, K. M. Dillon, and J. B. Matson, "A review of hydrogen sulfide (H_2S) donors: chemistry and potential therapeutic applications," *Biochemical Pharmacology*, vol. 149, pp. 110–123, 2018.

[12] G. Yang, L. Wu, B. Jiang et al., "H_2S as a physiologic vasorelaxant: hypertension in mice with deletion of cystathionine gamma-lyase," *Science*, vol. 322, no. 5901, pp. 587–590, 2008.

[13] G. Meng, S. Zhao, L. Xie, Y. Han, and Y. Ji, "Protein S-sulfhydration by hydrogen sulfide in cardiovascular system," *British Journal of Pharmacology*, vol. 175, no. 8, pp. 1146–1156, 2018.

[14] Z. Liu, Y. Han, L. Li et al., "The hydrogen sulfide donor, GYY4137, exhibits anti-atherosclerotic activity in high fat fed apolipoprotein E(-/-) mice," *British Journal of Pharmacology*, vol. 169, no. 8, pp. 1795–1809, 2013.

[15] L. Xie, Y. Gu, M. Wen et al., "Hydrogen sulfide induces Keap1 S-sulfhydration and suppresses diabetes-accelerated atherosclerosis via Nrf2 activation," *Diabetes*, vol. 65, no. 10, pp. 3171–3184, 2016.

[16] G. Meng, J. Liu, S. Liu et al., "Hydrogen sulfide pretreatment improves mitochondrial function in myocardial hypertrophy via a SIRT3-dependent manner," *British Journal of Pharmacology*, vol. 175, no. 8, pp. 1126–1145, 2018.

[17] G. Meng, Y. Xiao, Y. Ma et al., "Hydrogen sulfide regulates Krüppel-Like factor 5 transcription activity via specificity protein 1 S-sulfhydration at Cys664 to prevent myocardial hypertrophy," *Journal of the American Heart Association*, vol. 5, no. 9, 2016.

[18] L. Xie, H. Feng, S. Li et al., "SIRT3 mediates the antioxidant effect of hydrogen sulfide in endothelial cells," *Antioxidants & Redox Signaling*, vol. 24, no. 6, pp. 329–343, 2016.

[19] J. Wang, W. Wang, S. Li et al., "Hydrogen sulfide as a potential target in preventing spermatogenic failure and testicular dysfunction," *Antioxidants & Redox Signaling*, vol. 28, no. 16, pp. 1447–1462, 2018.

[20] G. Meng, Y. Ma, L. Xie, A. Ferro, and Y. Ji, "Emerging role of hydrogen sulfide in hypertension and related cardiovascular diseases," *British Journal of Pharmacology*, vol. 172, no. 23, pp. 5501–5511, 2015.

[21] Y. Qiu, Y. Wu, M. Meng et al., "GYY4137 protects against myocardial ischemia/reperfusion injury via activation of the PHLPP-1/Akt/Nrf2 signaling pathway in diabetic mice," *The Journal of Surgical Research*, vol. 225, pp. 29–39, 2018.

[22] G. Meng, J. Zhu, Y. Xiao et al., "Hydrogen sulfide donor GYY4137 protects against myocardial fibrosis," *Oxidative Medicine and Cellular Longevity*, vol. 2015, Article ID 691070, 14 pages, 2015.

[23] Y. Wang, J. He, M. Liao et al., "An overview of sirtuins as potential therapeutic target: structure, function and modulators," *European Journal of Medicinal Chemistry*, vol. 161, pp. 48–77, 2019.

[24] T. Wang, Y. Wang, L. Liu et al., "Research progress on sirtuins family members and cell senescence," *European Journal of Medicinal Chemistry*, vol. 193, p. 112207, 2020.

[25] C. K. Singh, G. Chhabra, M. A. Ndiaye, L. M. Garcia-Peterson, N. J. Mack, and N. Ahmad, "The role of sirtuins in antioxidant and redox signaling," *Antioxidants & Redox Signaling*, vol. 28, no. 8, pp. 643–661, 2018.

[26] M. S. Elkhwanky and J. Hakkola, "Extranuclear sirtuins and metabolic stress," *Antioxidants & Redox Signaling*, vol. 28, no. 8, pp. 662–676, 2018.

[27] W. Sun, C. Liu, Q. Chen, N. Liu, Y. Yan, and B. Liu, "SIRT3: a new regulator of cardiovascular diseases," *Oxidative Medicine and Cellular Longevity*, vol. 2018, Article ID 7293861, 11 pages, 2018.

[28] T. Nagai, T. Anzai, H. Kaneko et al., "C-reactive protein overexpression exacerbates pressure overload-induced cardiac remodeling through enhanced inflammatory response," *Hypertension*, vol. 57, no. 2, pp. 208–215, 2011.

[29] J. N. Peoples, A. Saraf, N. Ghazal, T. T. Pham, and J. Q. Kwong, "Mitochondrial dysfunction and oxidative stress in heart disease," *Experimental & Molecular Medicine*, vol. 51, no. 12, pp. 1–13, 2019.

[30] Y. Zhang, P. Murugesan, K. Huang, and H. Cai, "NADPH oxidases and oxidase crosstalk in cardiovascular diseases: novel therapeutic targets," *Nature Reviews. Cardiology*, vol. 17, no. 3, pp. 170–194, 2020.

[31] J. Zhang, H. Xiang, J. Liu, Y. Chen, R. R. He, and B. Liu, "Mitochondrial sirtuin 3: new emerging biological function and therapeutic target," *Theranostics*, vol. 10, no. 18, pp. 8315–8342, 2020.

[32] R. B. van Heeswijk, J. A. M. Bastiaansen, J. F. Iglesias et al., "Quantification of myocardial interstitial fibrosis and extracellular volume for the detection of cardiac allograft vasculopathy," *The International Journal of Cardiovascular Imaging*, vol. 36, no. 3, pp. 533–542, 2020.

[33] S. T. Feng, Z. Z. Wang, Y. H. Yuan et al., "Dynamin-related protein 1: a protein critical for mitochondrial fission, mitophagy, and neuronal death in Parkinson's disease," *Pharmacological Research*, vol. 151, p. 104553, 2020.

[34] M. Gyongyosi, J. Winkler, I. Ramos et al., "Myocardial fibrosis: biomedical research from bench to bedside," *European Journal of Heart Failure*, vol. 19, no. 2, pp. 177–191, 2017.

[35] Y. D. Wen, H. Wang, and Y. Z. Zhu, "The drug developments of hydrogen sulfide on cardiovascular disease," *Oxidative Medicine and Cellular Longevity*, vol. 2018, Article ID 4010395, 21 pages, 2018.

[36] B. T. Hackfort and P. K. Mishra, "Emerging role of hydrogen sulfide-microRNA crosstalk in cardiovascular diseases,"

American Journal of Physiology. Heart and Circulatory Physiology, vol. 310, no. 7, pp. H802–H812, 2016.

[37] H. J. Sun, Z. Y. Wu, X. W. Nie, and J. S. Bian, "Role of endothelial dysfunction in cardiovascular diseases: the link between inflammation and hydrogen sulfide," *Frontiers in Pharmacology*, vol. 10, 2019.

[38] J. Sheng, W. Shim, H. Wei et al., "Hydrogen sulphide suppresses human atrial fibroblast proliferation and transformation to myofibroblasts," *Journal of Cellular and Molecular Medicine*, vol. 17, no. 10, pp. 1345–1354, 2013.

[39] Y. Li, M. Liu, X. Song et al., "Exogenous hydrogen sulfide smeliorates diabetic myocardial fibrosis by inhibiting cell aging through SIRT6/AMPK autophagy," *Frontiers in Pharmacology*, vol. 11, 2020.

[40] L. J. Ellmers, E. M. Templeton, A. P. Pilbrow et al., "Hydrogen sulfide treatment improves post-infarct remodeling and long-term cardiac function in CSE knockout and wild-type mice," *International Journal of Molecular Sciences*, vol. 21, no. 12, p. 4284, 2020.

[41] J. Zhang, J. Yu, Y. Chen et al., "Exogenous hydrogen sulfide supplement attenuates isoproterenol-induced myocardial hypertrophy in a sirtuin 3-dependent manner," *Oxidative Medicine and Cellular Longevity*, vol. 2018, Article ID 9396089, 17 pages, 2018.

[42] Y. Sun, Z. Tian, N. Liu et al., "Exogenous H_2S switches cardiac energy substrate metabolism by regulating SIRT3 expression in db/db mice," *Journal of Molecular Medicine (Berlin, Germany)*, vol. 96, no. 3-4, pp. 281–299, 2018.

[43] Y. Sun, Z. Teng, X. Sun et al., "Exogenous H_2S reduces the acetylation levels of mitochondrial respiratory enzymes via regulating the NAD+-SIRT3 pathway in cardiac tissues of db/db mice," *American Journal of Physiology. Endocrinology and Metabolism*, vol. 317, no. 2, pp. E284–E297, 2019.

[44] Y. Yuan, L. Zhu, L. Li et al., "S-sulfhydration of SIRT3 by hydrogen sulfide attenuates mitochondrial dysfunction in cisplatin-induced acute kidney injury," *Antioxidants & Redox Signaling*, vol. 31, no. 17, pp. 1302–1319, 2019.

[45] Z. Lin, N. Altaf, C. Li et al., "Hydrogen sulfide attenuates oxidative stress-induced NLRP3 inflammasome activation via S-sulfhydrating c-Jun at Cys269 in macrophages," *Biochimica et Biophysica Acta (BBA) - Molecular Basis of Disease*, vol. 1864, no. 9, pp. 2890–2900, 2018.

[46] S. Song, Y. Ding, G. L. Dai et al., "Sirtuin 3 deficiency exacerbates diabetic cardiomyopathy via necroptosis enhancement and NLRP3 activation," *Acta Pharmacologica Sinica*, vol. 42, no. 2, pp. 230–241, 2021.

[47] S. Yang, M. Xu, G. Meng, and Y. Lu, "SIRT3 deficiency delays diabetic skin wound healing via oxidative stress and necroptosis enhancement," *Journal of Cellular and Molecular Medicine*, vol. 24, no. 8, pp. 4415–4427, 2020.

[48] Z. Liu, X. Wang, L. Li, G. Wei, and M. Zhao, "Hydrogen sulfide protects against paraquat-induced acute liver injury in rats by regulating oxidative stress, mitochondrial function, and inflammation," *Oxidative Medicine and Cellular Longevity*, vol. 2020, Article ID 6325378, 16 pages, 2020.

[49] A. M. Rababa'h, A. N. Guillory, R. Mustafa, and T. Hijjawi, "Oxidative stress and cardiac remodeling: an updated edge," *Current Cardiology Reviews*, vol. 14, no. 1, pp. 53–59, 2018.

[50] I. Andreadou, R. Schulz, A. Papapetropoulos et al., "The role of mitochondrial reactive oxygen species, NO and H2S in ischaemia/reperfusion injury and cardioprotection," *Journal of Cellular and Molecular Medicine*, vol. 24, no. 12, pp. 6510–6522, 2020.

[51] E. Donnarumma, S. Bhushan, J. M. Bradley et al., "Nitrite therapy ameliorates myocardial dysfunction via H_2S and nuclear factor-erythroid 2-related factor 2 (Nrf2)-dependent signaling in chronic heart failure," *Journal of the American Heart Association*, vol. 5, no. 8, 2016.

[52] F. J. Bock and S. W. G. Tait, "Mitochondria as multifaceted regulators of cell death," *Nature Reviews. Molecular Cell Biology*, vol. 21, no. 2, pp. 85–100, 2020.

[53] J. Lin, X. Li, Y. Lin, Z. Huang, and W. Wu, "Exogenous sodium hydrosulfide protects against high glucoseinduced injury and inflammation in human umbilical vein endothelial cells by inhibiting necroptosis via the p38 MAPK signaling pathway," *Molecular Medicine Reports*, vol. 23, 2021.

[54] J. Jia, Z. Wang, M. Zhang et al., "SQR mediates therapeutic effects of H_2S by targeting mitochondrial electron transport to induce mitochondrial uncoupling," *Science Advances*, vol. 6, no. 35, p. eaaz5752, 2020.

[55] J. Y. Jin, X. X. Wei, X. L. Zhi, X. H. Wang, and D. Meng, "Drp1-dependent mitochondrial fission in cardiovascular disease," *Acta Pharmacologica Sinica*, vol. 42, no. 5, pp. 655–664, 2021.

[56] A. A. Rosdah, W. J. Smiles, J. S. Oakhill et al., "New perspectives on the role of Drp1 isoforms in regulating mitochondrial pathophysiology," *Pharmacology & Therapeutics*, vol. 213, p. 107594, 2020.

Research Article

Protection against Doxorubicin-Related Cardiotoxicity by Jaceosidin Involves the Sirt1 Signaling Pathway

Yuzhou Liu ⓘ, **Liying Zhou** ⓘ, **Binbin Du** ⓘ, **Yuan Liu** ⓘ, **Junhui Xing** ⓘ, **Sen Guo** ⓘ, **Ling Li** ⓘ, **and Hongrui Chen** ⓘ

Department of Cardiology, The First Affiliated Hospital of Zhengzhou University, Zhengzhou, Henan 450052, China

Correspondence should be addressed to Yuzhou Liu; 35507370@qq.com and Hongrui Chen; chruiga@163.com

The clinical use of doxorubicin (DOX) is largely limited by its cardiotoxicity. Previous studies have shown that jaceosidin has many biological activities. However, little is known about whether jaceosidin can attenuate DOX-related acute cardiotoxicity. Here, we investigated the therapeutic effects of jaceosidin on DOX-induced acute cardiotoxicity. Mice were intraperitoneally injected with a single dose of DOX to establish an acute cardiac injury model. To explore the protective effects, mice were orally administered jaceosidin daily for 7 days, with dosing beginning 2 days before DOX injection. The results demonstrated that jaceosidin dose-dependently reduced free radical generation, inflammation accumulation, and cell loss induced by DOX in cardiomyocytes. Further studies showed that jaceosidin treatment inhibited myocardial oxidative damage and the inflammatory response and attenuated myocardial apoptotic death, thus improving cardiac function in mice injected with DOX. The inhibitory effects of jaceosidin on DOX-related acute cardiotoxicity were mediated by activation of the sirtuin1 (Sirt1) signaling pathway. Jaceosidin lost its protective effect against DOX-related injury in Sirt1-deficient cardiomyocytes and mice. In conclusion, jaceosidin has protective potential in treating DOX-related cardiac injury through activation of the Sirt1 signaling pathway.

1. Introduction

Doxorubicin (DOX) has been widely used to treat solid and haematopoietic tumours; however, a major limiting factor for the clinical use of DOX is irreversible cardiac toxicity. DOX-induced cardiotoxicity is characterized by irreversible degenerative cardiomyopathy and congestive heart failure [1–3]. The pathogenesis of cardiotoxicity induced by DOX remains poorly understood, but accumulating evidence suggests the indispensable roles of free radical production and myocardial apoptosis [4]. DOX-induced cardiomyopathy occurs primarily through the generation of reactive oxygen species (ROS), which can induce myocardial lipid peroxidation and myofibre degeneration [5, 6]. Additionally, previous studies have linked ROS production to cardiomyocyte apoptosis [7]. It has been demonstrated that DOX-induced cardiotoxicity can be suppressed by the overexpression of superoxide dismutase (SOD) and catalase [8, 9]. These find-ings suggest that ROS production and myocardial apoptosis play important roles in DOX-induced cardiotoxicity. Therefore, we speculated that the suppression of ROS production and apoptotic cell death might largely rescue DOX-triggered cardiotoxicity.

Jaceosidin is a flavone isolated from medicinal plants of the genus *Artemisia* [10]. Jaceosidin has recently gained attention as a beneficial drug with low intrinsic toxicity. Moreover, jaceosidin has been demonstrated to possess antioxidative, anti-inflammatory, and immunosuppressive properties [11–13]. A recent study found that jaceosidin inhibits the inflammatory response and decreases complement levels in lipopolysaccharide- (LPS-) injected mice [14]. Fu et al. found that jaceosidin scavenged ROS and weakened mitochondrial lipid peroxidation in isolated rat livers [15]. In addition, jaceosidin ameliorated endoplasmic reticulum stress and insulin resistance by upregulating sarco-endoplasmic reticulum Ca2+-ATPase 2b [16]. However, the

effects of jaceosidin on DOX-related cardiac injury and the related signaling mechanisms remain unclear. Given the roles of inflammation and oxidative damage in DOX-related cardiac injury, the present study investigated whether jaceosidin attenuates DOX-related cardiac injury in vivo and in vitro.

2. Methods

2.1. Reagents. Jaceosidin (cat. no. 18085-97-7) and DOX (cat. no. 1515) were purchased from Sigma-Aldrich (St. Louis, MO, USA). Antibodies against nuclear factor E2-related factor 2 (Nrf2, cat. no. 12721S; 1 : 1000 dilution), haem oxygenase-1 (HO-1, cat. no. 43966; 1 : 1000 dilution), nuclear factor kappa-B (NF-κB, cat. no. 8242; 1 : 1000 dilution), phospho-IκB kinase β (P-IKKβ; cat. no. 2078; 1 : 1000 dilution), IKKβ (cat. no. 2687; 1 : 1000 dilution), Bax (cat. no. 5023; 1 : 1000 dilution), Bcl-2 (cat. no. ab32124; 1 : 1000 dilution), sirtuin1 (Sirt1, cat. no. 8469; 1 : 1000 dilution), and GAPDH (cat. no. 5174; 1 : 1000 dilution) were obtained from Cell Signaling Technology Inc. (Danvers, MA, USA).

2.2. Cell Culture and Treatment. Primary cultures of neonatal rat cardiac myocytes (NRCMs) were prepared as previously described [17]. The cells were cultured in Dulbecco's modified Eagle's medium supplemented with 10% heat-inactivated foetal bovine serum (FBS; Gibco; Thermo Fisher Scientific, Inc., Waltham, USA). Jaceosidin was dissolved in 0.1% dimethylsulfoxide (DMSO) for use in all in vitro experiments. To induce DOX-related injury, the cells were starved overnight in DMEM containing 0.5% FBS and then incubated with DOX (1 μmol/L) for 24 h. The cells were pretreated with different concentrations of jaceosidin (0, 2.5, 5, 10, 15 μmol/l) 6 hours before DOX administration. The dose of jaceosidin was determined according to a previous study [16]; the dose of DOX was also selected according to a previous study [2]. To knock down Sirt1 in cardiomyocytes, NRCMs were preincubated with siSirt1 (50 nmol/l) or siRNA (50 nmol/l) for 24 h and then subjected to DOX treatment for 24 h. siSirt1 and scrambled siRNA were obtained from Invitrogen. Cell viability was determined by a cell counting kit-(CCK-) 8 kit. Briefly, CCK-8 (10 μl) was added to the medium (100 μl) in each well of a 96-well plate and then incubated at 37°C for 2.5 hours. Optical density values were obtained at 450 nm using a BioTek Synergy HT Multi-Mode Microplate Reader.

2.3. Animals and Treatment. A total of 48 male C57BL/6 mice (age: 8-9 weeks; weight: 22-24 g) were purchased from the Experimental Animal Center of Zhengzhou University (Henan, China). The experimental protocols were approved by the Committee on Animal Care of The First Affiliated Hospital of Zhengzhou University (No. 8196437). All mice were allowed free access to food and water and were maintained on a 12 h light/dark cycle in a controlled temperature (20-25°C) and humidity (50 ± 5%) environment. After 1 week of adaptation, the mice were divided into four groups (n = 12 each): (1) vehicle+saline group, in which mice were orally administered 0.5% carboxymethylcellulose solution

(vehicle) daily for 7 days and received a saline injection on the second day of vehicle administration; (2) jaceosidin +saline group, in which mice were orally administered jaceosidin (4 mg/kg) daily for 7 days and received a saline injection on the second day of jaceosidin administration; (3) vehicle +DOX group, in which mice were orally administered 0.5% carboxymethylcellulose solution (vehicle) daily for 7 days and intraperitoneally injected with a single dose of DOX (15 mg/kg) on the second day of vehicle administration; and (4) jaceosidin+DOX group, in which mice were orally administered jaceosidin (4 mg/kg) daily for 7 days and intraperitoneally injected with a single dose of DOX (15 mg/kg) on the second day of jaceosidin administration. The dose of DOX was determined according to a previous study [2]. The jaceosidin suspension was prepared in 0.5% carboxymethylcellulose for the animal experiments. The dose of jaceosidin was selected according to a previous study [16]. Five days after DOX injection, the mice were sacrificed with a single overdose of pentobarbital sodium (200 mg/kg, ip), and blood samples and heart tissues were collected for further experiments.

To inhibit Sirt1 in vivo, mice were administered a specific inhibitor of Sirt1 (Ex527, 1 mg/kg) every other day for a total of 8 days beginning 3 days before DOX injection. The dose of Sirt1 was selected according to a previous study [18].

2.4. Haemodynamics Analysis. Cardiac function was assessed by a pressure-volume catheter at 5 days after DOX injection. Mice (n = 8 per group) were anaesthetized with ketamine (100 mg/kg) and xylazine (2.5 mg/kg) and then connected to a rodent ventilator after endotracheal intubation [19]. Cardiac catheterization was then performed using a 1.0-F catheter (SPR 839; Millar Instruments Inc.) inserted retrograde through the right carotid artery into the left ventricle. After stabilization for 10 min, the pressure signals and heart rate were recorded continuously with an ARIA pressure-volume conductance system coupled to a Powerlab/4SP A/D converter. The data were analysed using the LabChart software. All experiments were carried out in a blinded manner, and the data were analysed as previously described.

2.5. Western Immunoblot. Proteins from the heart samples were extracted with RIPA buffer. Nuclear proteins were extracted with NE-PER™ Nuclear and Cytoplasmic Extraction Reagents (Invitrogen). Proteins were separated by 10% SDS-PAGE and transferred onto polyvinylidene fluoride membranes. After blocking with 5% skim milk for 4 h at room temperature, the membranes were incubated with the primary antibodies at 4°C overnight. After incubation with the secondary antibody (1 : 10000, Thermo Fisher Scientific) for 2.5 hours at room temperature, the protein bands on the membranes were scanned using an enhanced chemiluminescence system and a BioSpectrum gel imaging system (CA, USA). Secondary antibodies and the enhanced chemiluminescence solution were purchased from Amersham. The band intensity was quantified by the ImageJ software, and GAPDH was used as the internal reference.

2.6. Real-Time Polymerase Chain Reaction. Total RNA was extracted using the RNeasy mini kit (Qiagen). cDNA was generated using Superscript III reverse transcriptase and random primers (Invitrogen). Real-time polymerase chain reaction (PCR) was performed using LightCycler 480 SYBR Green Master Mix (Roche Diagnostics). GAPDH was used as the internal reference.

2.7. Cell Injury Assay. Five days after DOX injection, blood samples were collected from the retro-orbital plexus of mice. The mouse cTnI ELISA kit (#CSB-E08421m) and mouse LDH ELISA kit (#CSB-E17733m) were purchased from CUSABIO. Plasma cardiac troponin I (cTnI) and lactate dehydrogenase (LDH) were detected using commercial kits according to the manufacturer's instructions. Optical density values were obtained at 450 nm using a BioTek Synergy HT Multi-Mode microplate reader. To evaluate cardiomyocytes in vitro, creatine kinase (CK) was detected using a CK assay kit (A032-1-1, Nanjing Jiancheng Bioengineering Institute).

2.8. Oxidative Status and Myocardial Cytokines. Five days after DOX injection, fresh heart samples were collected and homogenized to detect malondialdehyde (MDA) content, 4-hydroxynonenal (4-HNE), and total SOD activity using commercially available kits according to the manufacturer's instructions. Nrf2 binding activity was detected using the Nrf2 DNA binding ELISA kit (Active Motif). Cardiomyocytes were also collected to detect intracellular ROS, hydrogen peroxide, and superoxide production. The ROS assay kit was obtained from Abcam (#ab186027). This kit provides an ultrasensitive fluorometric one-step ROS assay that can be performed in a 96-well microtiter plate format. The signal was read by a fluorescence microplate reader at $Ex/Em = 520/605$ nm. The hydrogen peroxide assay kit was obtained from Biovision (Shanghai, China). This kit provides a highly sensitive, colorimetric assay for measuring H_2O_2 in biological samples. In this assay protocol, horseradish peroxidase (HRP) reacts with H_2O_2 to produce a product with red fluorescence ($Ex/Em = 535/587$ nm). The superoxide assay kit was obtained from Beyotime (Beijing, China). The protein carbonyl content in the supernatants of heart tissue homogenates was determined by using a protein carbonyl content assay Kit (K830-100, Biovision). The resulting signal was read by a fluorescence microplate reader at 375 nm. Oxidized glutathione (GSSG) and total glutathione concentrations were detected using a total glutathione/oxidized glutathione assay kit (A061-1-1; Nanjing Jiancheng Bioengineering Institute). Reduced glutathione (GSH) values were determined from the total and GSSG concentrations. The redox status was represented by the GSH/GSSG ratio.

The DNA-p65 NF-κB binding assay was performed with a Mercury TransFactor kit (BD Biosciences, Clontech). In addition, fresh heart samples were collected and homogenized to detect myocardial tumour necrosis factor- (TNF-) α and interleukin- (IL-) 6 expression. The TNF-α mouse ELISA kit (#BMS607-3) and IL-6 mouse ELISA kit (#BMS603HS) were purchased from Invitrogen.

2.9. HE Staining, TUNEL Analysis, and Caspase-3 Activity. For histological analysis, hematoxylin and eosin (H&E) staining was used. Fresh heart samples were sectioned to detect myocardial apoptosis with TdT-mediated dUTP nick end-labelling (TUNEL) using a CardioTACS kit (R&D Systems) according to the manufacturer's instructions. Cardiac caspase-3 activity was also measured with a CPP32/caspase-3 colorimetric protease assay.

2.10. Serum Transaminases and Creatinine Analyses. To evaluate the potential oral toxicity of jaceosidin, mice were orally administered jaceosidin (4 mg/kg) daily for 7 days. After that, the mice were sacrificed, and blood samples were collected to detect serum transaminases and creatinine. The kit for alanine transaminase (ALT), glutamate pyruvate transaminase (AST), and creatinine were provided by Nanjing Jiancheng Bioengineering Institute (Nanjing, China).

2.11. Statistical Analysis. The data are presented as the mean $\pm$ SEM. Statistical comparisons between two groups were performed using two-tailed Student's t-tests. Comparisons between multiple groups were performed using one-way ANOVA followed by a post hoc Bonferroni comparison analysis. Statistical significance was accepted at a value of $P < 0.05$.

3. Results

3.1. Jaceosidin Treatment Suppressed Intracellular ROS in DOX-Treated Cardiomyocytes. To investigate the effects of jaceosidin, NRCMs were pretreated with jaceosidin at different concentrations and subsequently treated with DOX for 24 hours. Jaceosidin significantly decreased the ROS production induced by DOX in a dose-dependent manner, with a maximal effect at a dose of 15 μmol/l (Figure 1(a)). We further investigated the inhibitory effect of jaceosidin on hydrogen peroxide and superoxide production in DOX-treated cells. We found that the elevations in hydrogen peroxide and superoxide in cardiac myocytes in response to DOX were significantly attenuated after jaceosidin treatment (Figures 1(b) and 1(c)). In addition, jaceosidin treatment markedly reduced myocardial MDA levels in DOX-treated cells (Figure 1(d)). DOX decreased the GSH/GSSG ratio and the total SOD activity; however, these alterations were largely inhibited by jaceosidin in a dose-dependent manner (Figures 1(e) and 1(f)). We also detected the protein carbonyl content, which is a representative product of protein oxidative damage. The results showed that jaceosidin dose-dependently decreased the protein carbonyl content in DOX-treated cells (Figure 1(g)).

3.2. Jaceosidin Treatment Suppressed Inflammation and Cell Loss in DOX-Treated Cardiomyocytes. We then examined NF-κB activity in DOX-treated cardiomyocytes. The DNA binding activity of NF-κB p65 was increased in DOX-treated cardiomyocytes. However, p65-DNA binding activity was suppressed by jaceosidin in a dose-dependent manner (Figure 2(a)). The gene expression levels of TNF-α and IL-6 were markedly elevated after DOX treatment. However, these increases in TNF-α and IL-6 were largely suppressed by
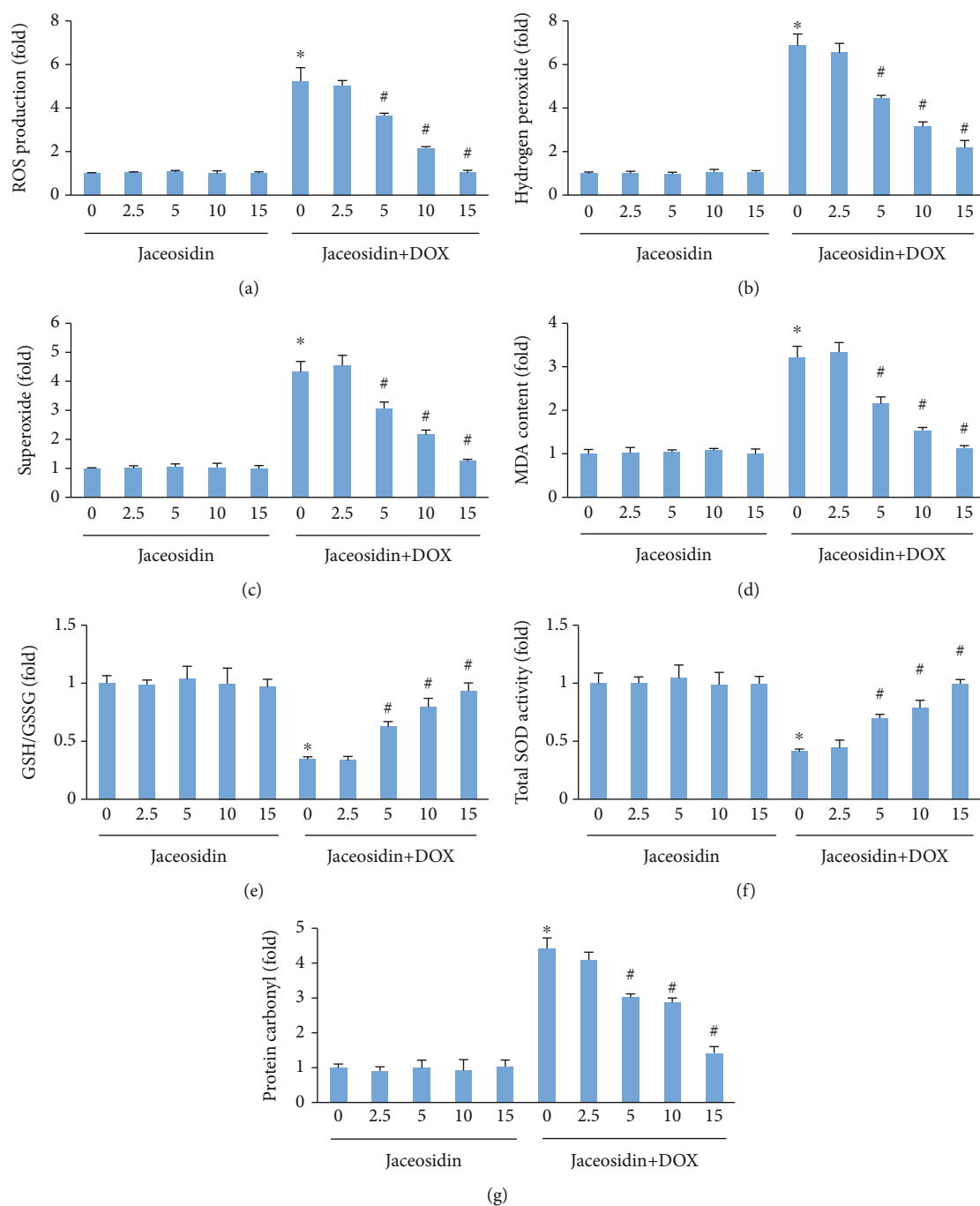
FIGURE 1: Jaceosidin inhibited reactive oxygen species (ROS) production in doxorubicin- (DOX-) treated cells. (a–c) The production of ROS, hydrogen peroxide, and superoxide in jaceosidin-treated cells ($n = 6$). (d) Malondialdehyde (MDA) content in jaceosidin-treated cells ($n = 6$). (e) The ratio of glutathione (GSH) to oxidized glutathione (GSSG) in jaceosidin-treated cells ($n = 6$). (f) Total superoxide dismutase (SOD) activity in DOX-treated cells. (g) Protein carbonyl content in the indicated groups ($n = 6$). For (a–g), cells were pretreated with various concentrations of jaceosidin (0, 2.5, 5, 10, 15 μmol/l) 6 hours before DOX (1 μmol/L) administration. The oxidative stress markers (a–g) were detected 24 hours after DOX administration. Data are shown as means ± SEM. Comparisons between multiple groups were performed using one-way ANOVA followed by a post hoc Bonferroni comparison analysis. *$P < 0.05$ compared with control. #$P < 0.05$ compared with DOX alone.
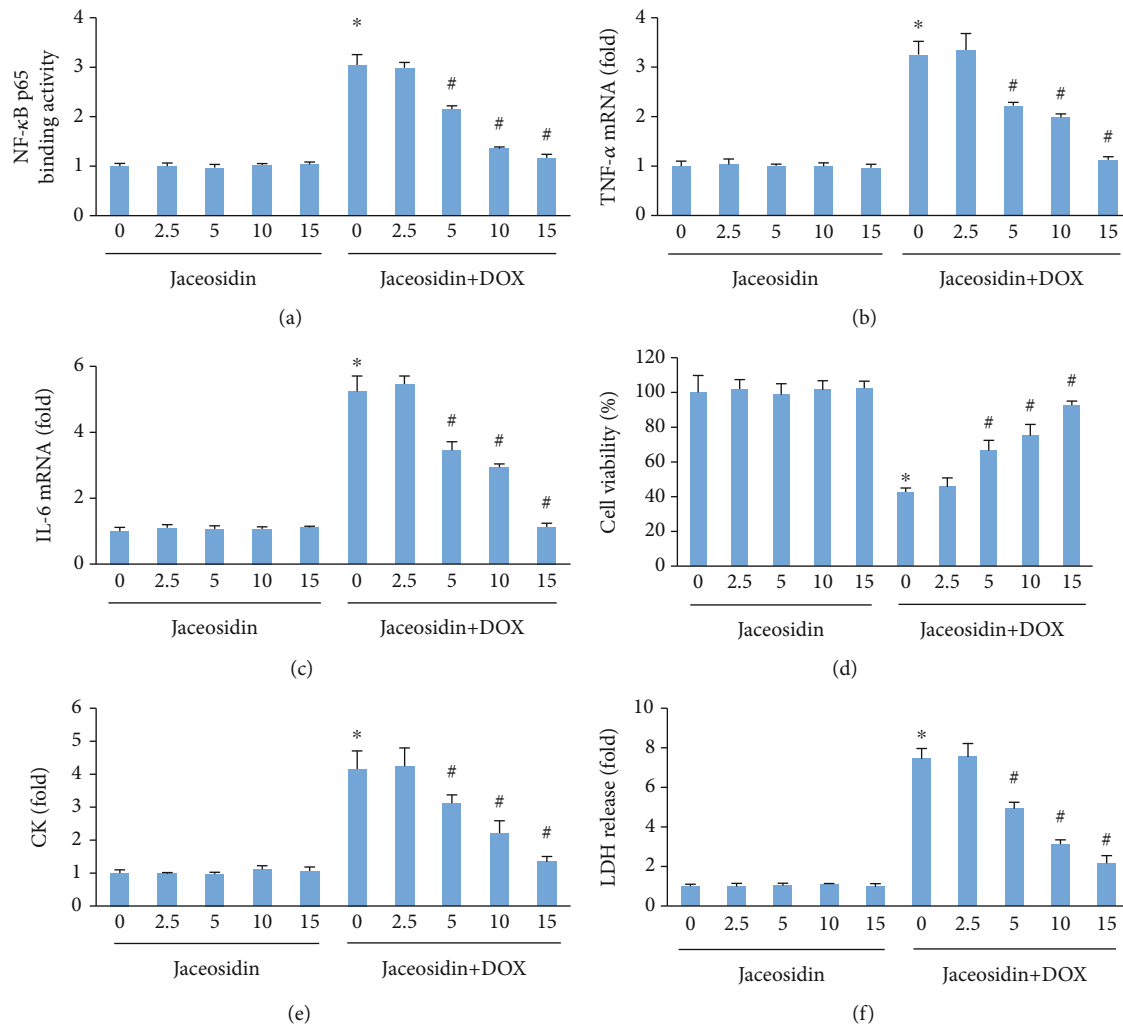
FIGURE 2: Jaceosidin inhibited the inflammatory response and cell loss in vitro. (a) Nuclear factor kappa-B (NF-κB) binding activity ($n = 6$). (b, c) The mRNA levels of inflammatory factors ($n = 6$). (d) Cell viability after doxorubicin (DOX) treatment ($n = 6$). (e, f) The release of lactate dehydrogenase (LDH) and creatine kinase (CK) in cells ($n = 6$). For (a–f), cells were pretreated with various concentrations of jaceosidin (0, 2.5, 5, 10, 15 μmol/l) 6 hours before DOX (1 μmol/L) administration. The inflammatory markers (a–f) were detected 24 hours after DOX administration. Data are shown as means ± SEM. Comparisons between multiple groups were performed using one-way ANOVA followed by a post hoc Bonferroni comparison analysis. $^{*}P < 0.05$ compared with control. $^{\#}P < 0.05$ compared with DOX alone.

jaceosidin (Figures 2(b) and 2(c)). DOX treatment impaired cardiomyocyte viability, and jaceosidin dose-dependently improved cell viability in response to DOX (Figure 2(d)). Jaceosidin treatment also dose-dependently decreased the release of CK and LDH in DOX-treated cardiomyocytes (Figures 2(e) and 2(f)).

3.3. Jaceosidin Treatment Attenuated DOX-Related Cardiac Injury in Mice.

To further determine the effects of jaceosidin, mice were administered a single injection of DOX to mimic DOX-induced acute cardiac injury. As shown in Figures 3(a) and 3(b), DOX significantly decreased the body weight and the ratio of heart weight to tibal length, and these effects were largely restored by jaceosidin treatment. Furthermore, treatment with jaceosidin reduced DOX-related cardiac injury, as indicated by the decrease in cTnI and LDH release (Figures 3(c) and 3(d)). Treatment with jaceosidin also improved cardiac function in DOX-treated mice, as indi-

cated by the improvements in EF, maximum first derivative of ventricular pressure with respect to time (+dP/dt) and stroke work, as well as the decrease in left ventricular end-diastolic pressure (LVEDP) (Figures 3(e)–3(h)). Histological examination showed that the number of cardiomyocyte vacuoles was increased in DOX-treated mice, and the change was significantly ameliorated in the DOX+jaceosidin group (Figure 3(i)).

3.4. Jaceosidin Treatment Inhibited Heart Oxidative Damage in DOX-Treated Mice.

Accumulating evidence suggests that oxidative damage plays an important role in the development of DOX-related cardiac injury [3, 20]. Our findings suggested that the reduction in the mRNA levels of SOD1, SOD2, and glutathione peroxidase 1 (Gpx1) was prevented by jaceosidin treatment (Figures 4(a)–4(c)). DOX also impaired total SOD activity, and this effect was prevented by jaceosidin treatment (Figure 4(d)). Jaceosidin reduced the increased levels of

(a)

(b)

(c)

(d)

(e)

(f)

Figure 3: Continued.

(g)

(h)

Vehicle Jaceosidin DOX DOX+jaceosidin

100 μm

(i)
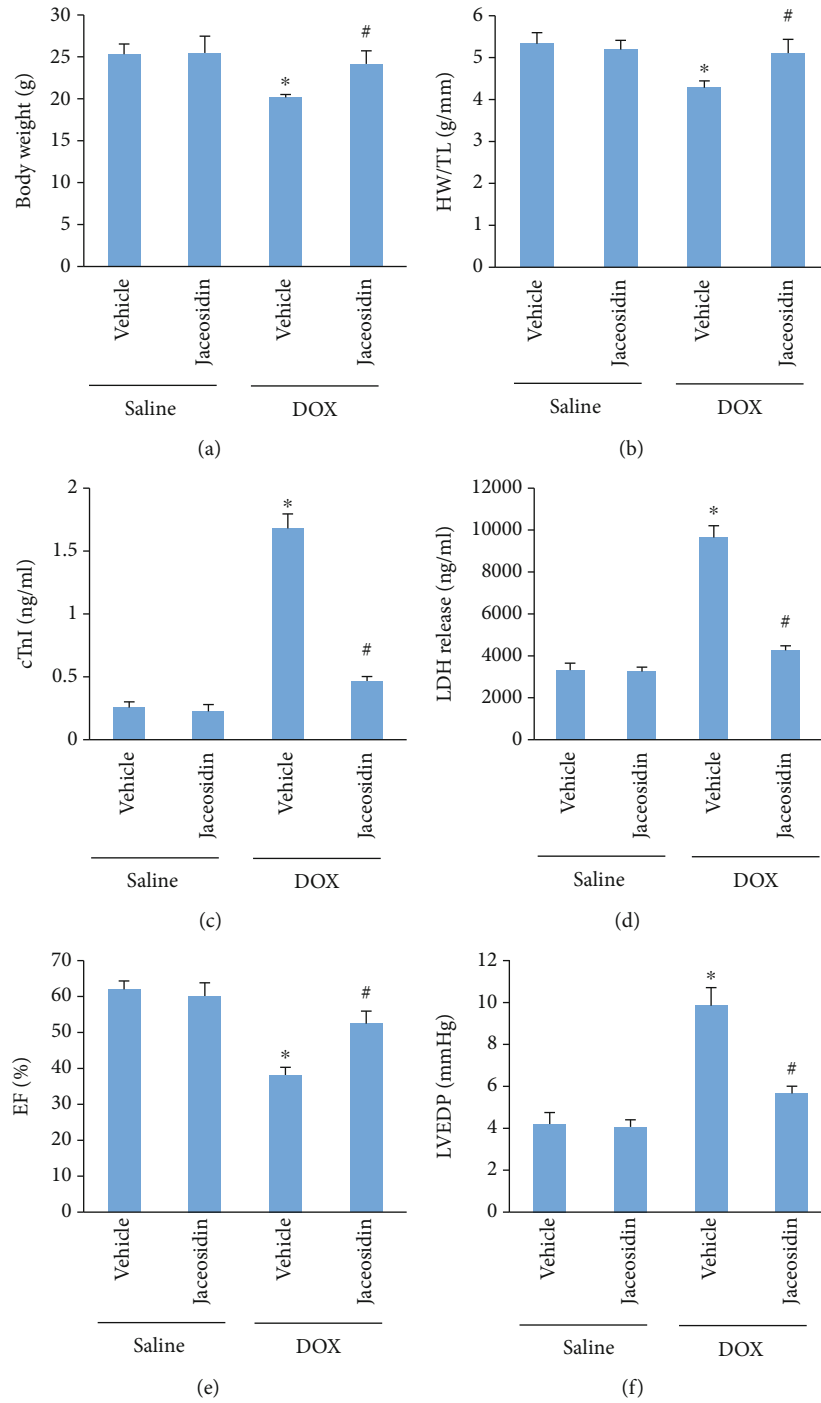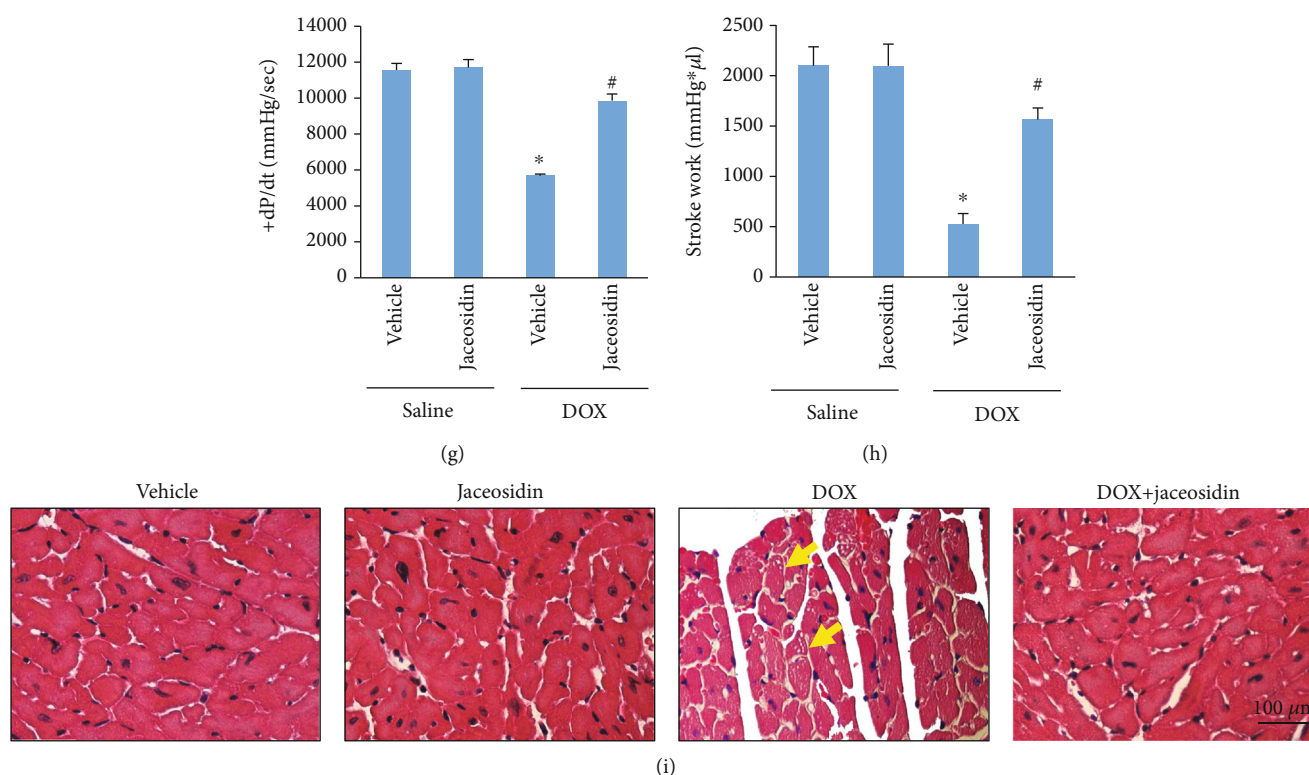
FIGURE 3: Jaceosidin (4 mg/kg) inhibited doxorubicin- (DOX-) related cardiac injury in vivo. (a) Body weight ($n = 12$). (b) The ratio of heart weight (HW) to tibia length (TL) ($n = 12$). (c, d) The plasma levels of cardiac troponin I (cTnI) and lactate dehydrogenase (LDH) ($n = 12$). (e) Ejection fraction (EF) in the mice ($n = 8$). (f, g) Left ventricular end-diastolic pressure (LVEDP) and the alteration in +dP/dt ($n = 8$). (h) The alteration in stroke work ($n = 8$). (i) Cardiomyocytes vacuolization were evaluated by HE staining. Mice were intraperitoneally injected with a single dose of DOX (15 mg/kg) to establish the acute cardiac injury model. Five days after DOX injection, blood samples and heart tissues were collected to assess cardiac injury, as reflected by (a–h). Data are shown as means ± SEM. Comparisons between multiple groups were performed using one-way ANOVA followed by a post hoc Bonferroni comparison analysis. $^{*}P < 0.05$ compared with saline. $^{\#}P < 0.05$ compared with DOX alone.

MDA and 4-HNE observed in the myocardium of vehicle-treated mice at 5 days post-DOX injection (Figures 4(e) and 4(f)). To further evaluate the oxidative stress caused by DOX, we assessed the GSH/GSSG ratio and the protein carbonyl content. DOX decreased the GSH/GSSG ratio but increased the protein carbonyl content, and these pathological alterations were prevented by jaceosidin treatment (Figures 4(g) and 4(h)). The decreased protein expression of Nrf2 and HO-1 induced by DOX was prevented by jaceosidin treatment (Figure 4(h)). Jaceosidin treatment also restored Nrf2 activity to normal levels in the hearts of DOX-treated mice (Figure 4(i)).

3.5. Jaceosidin Treatment Blunted the Inflammatory Response and Apoptotic Cell Death in DOX-Treated Mice.

To determine whether jaceosidin could suppress the inflammatory response in the hearts of DOX-treated mice, we first examined NF-κB p65 expression in the hearts. Jaceosidin was found to attenuate the increased expression of nuclear NF-κB p65 in response to DOX (Figure 5(a)). Jaceosidin treatment also suppressed IKKβ phosphorylation after DOX injection (Figure 5(b)). Jaceosidin treatment significantly decreased the mRNA levels of TNF-α, MCP-1, interferon-(IFN-) γ, and IL-17 in mice exposed to DOX (Figure 5(c)).

The protein levels of TNF-α and IL-6, as detected by ELISA, were markedly elevated after DOX treatment; however, these increases were suppressed in jaceosidin-treated mice (Figure 5(d)). The TUNEL staining data revealed significant myocardial apoptosis in the DOX group compared with the saline control, and jaceosidin treatment significantly attenuated DOX-induced myocardial apoptosis (Figure 5(e)). Jaceosidin decreased Bax protein expression but increased Bcl-2 protein expression in the heart tissue of DOX-treated mice (Figures 5(f) and 5(g)). Caspase-3 activity was markedly increased in DOX-treated mice. However, the activation of caspase-3 by DOX was abolished by jaceosidin (Figure 5(h)).

3.6. Jaceosidin Treatment Activated Sirt1 in the Hearts of DOX-Treated Mice.

We next detected the effect of jaceosidin on Sirt1 expression. As shown in Figure 6(a) and Figure S1, DOX decreased myocardial Sirt1 expression, and this effect was prevented by jaceosidin treatment. The in vitro analysis also revealed that jaceosidin increased Sirt1 expression in DOX-treated cardiomyocytes (Figure 6(b), Figure S1). The impaired Sirt1 activity in DOX-exposed cardiomyocytes was also improved after jaceosidin treatment (Figure 6(c)). To identify whether Sirt1 activation was responsible for the protective role of jaceosidin in DOX-related injury, we

(a)

(b)

(c)

(d)

(e)

(f)

Figure 4: Continued.

(g)

(h)

(i)

(j)
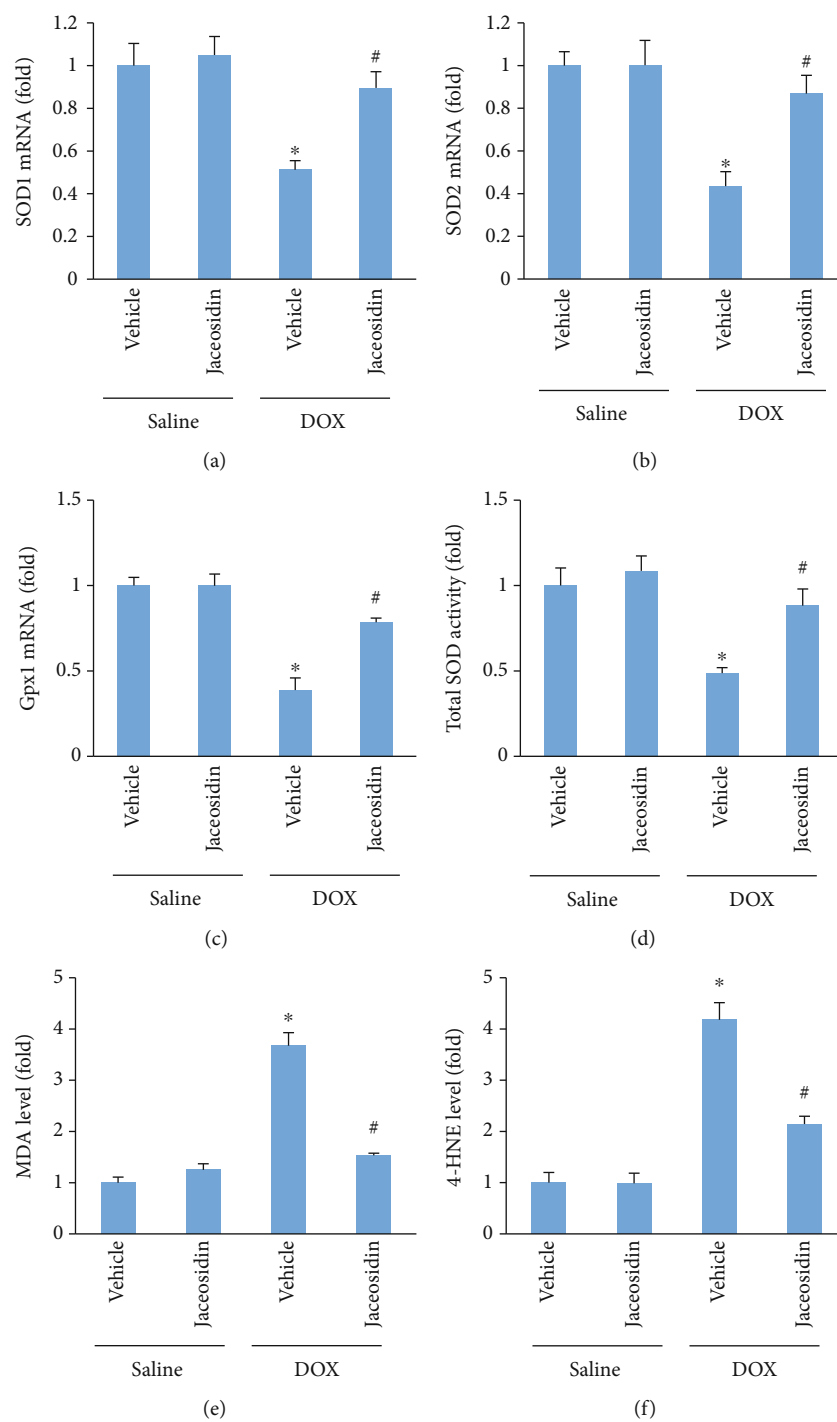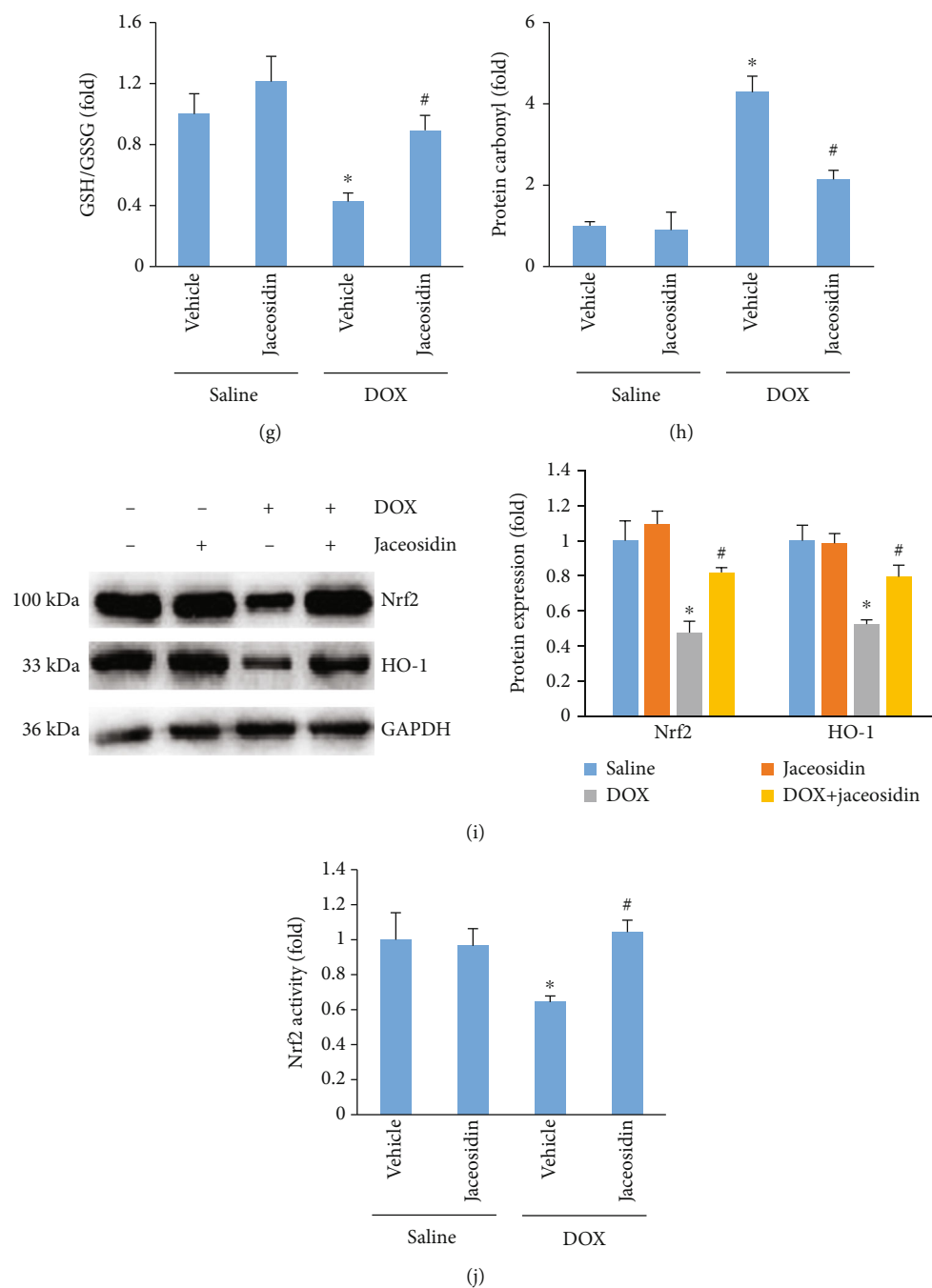
Figure 4: Jaceosidin (4 mg/kg) reduced oxidative stress in doxorubicin- (DOX-) treated mice. (a–c) The mRNA levels of superoxide dismutase 1 (SOD1), SOD2, and glutathione peroxidase 1 (Gpx1) in the hearts ($n = 6$). (b) Total SOD activity in the hearts ($n = 6$). (e, f) Malondialdehyde (MDA) and 4-hydroxynonenal (4-HNE) levels in the hearts ($n = 6$). (g) The ratio of glutathione (GSH) to oxidized glutathione (GSSG) in jaceosidin-treated mice ($n = 6$). (h) Protein carbonyl content in jaceosidin-treated mice ($n = 6$). (i) The protein expression of nuclear factor E2-related factor 2 (Nrf2) and haem oxygenase-1 (HO-1) in jaceosidin-treated mice ($n = 6$). (j) Nrf2 activity ($n = 6$). Mice were intraperitoneally injected with a single dose of DOX (15 mg/kg) to establish the acute cardiac injury model. Five days after DOX injection, heart tissues were collected to assess myocardial oxidative damage, as reflected by (a–j). Data are shown as means ± SEM. Comparisons between multiple groups were performed using one-way ANOVA followed by a post hoc Bonferroni comparison analysis. $^{*}P < 0.05$ compared with saline. $^{\#}P < 0.05$ compared with DOX alone.

depleted Sirt1 in cardiomyocytes. The results showed that jaceosidin was unable to protect against ROS production, increased MDA and TNF-α mRNA levels, and cell loss in Sirt1-deficient cells (Figures 6(d)–6(h)).

3.7. Jaceosidin Had No Protective Effect in Sirt1-Inhibited Mice. To confirm the role of Sirt1 in the effects of jaceosidin, mice were exposed to a Sirt1 inhibitor (Ex527). Extensive examinations indicated that unlike the ameliorated DOX-

(a)

(b)

(c)

(d)

FIGURE 5: Continued.

(e)

(f)

(g)

(h)
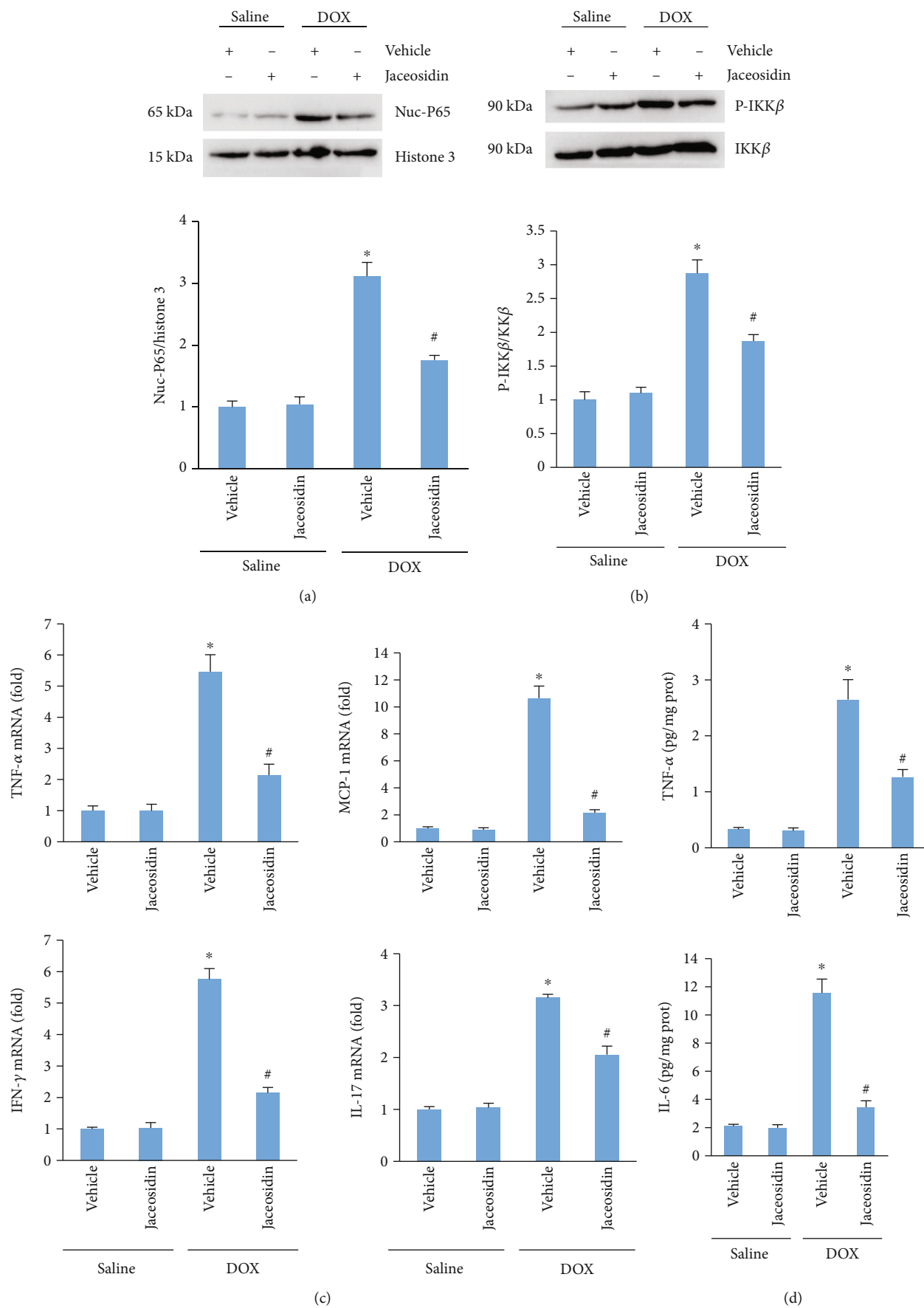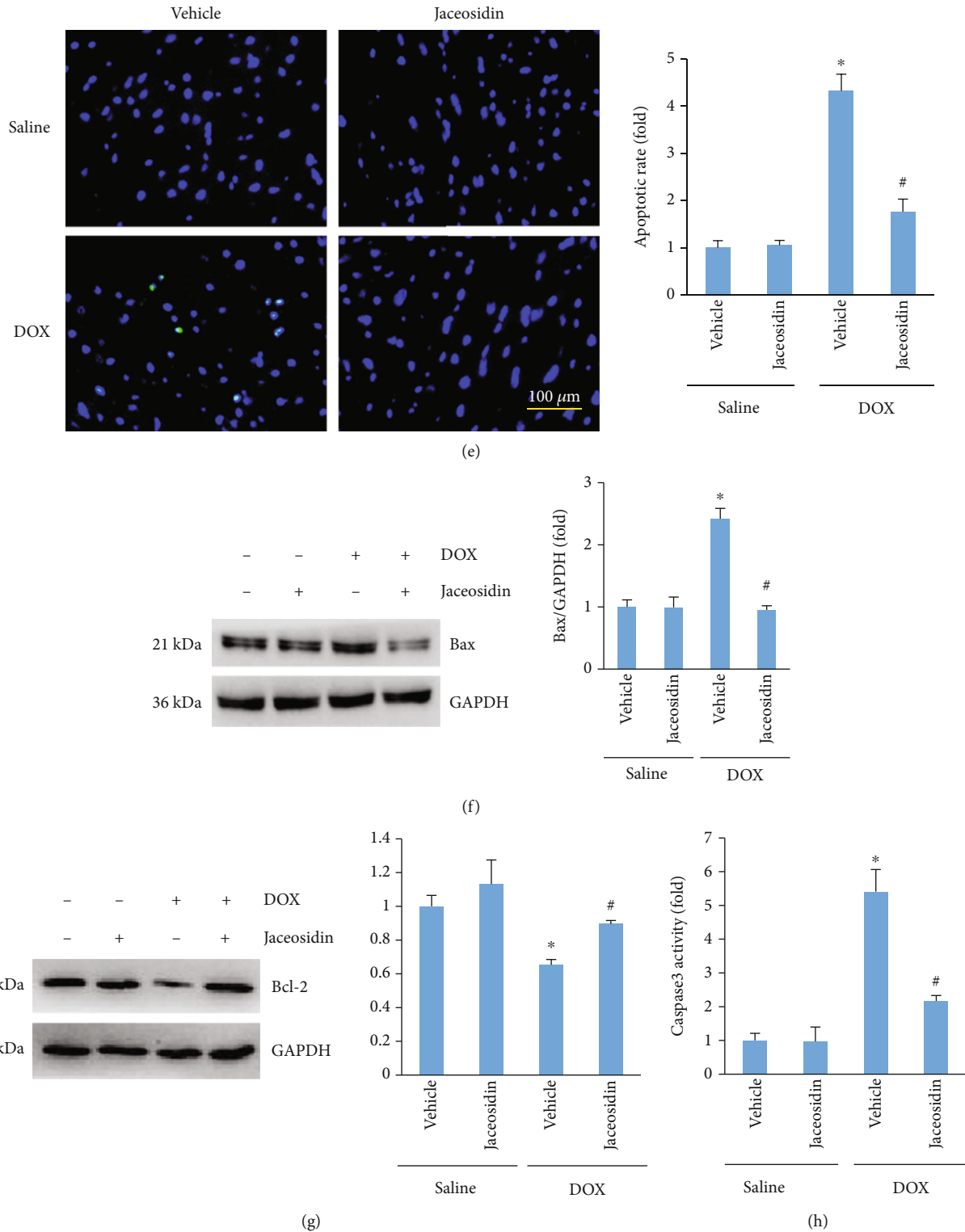
FIGURE 5: Jaceosidin (4 mg/kg) suppressed inflammation and cardiac apoptosis in doxorubicin- (DOX-) treated mice. (a, b) P65 and IκB kinase β (IKKβ) expression ($n = 6$). (c) mRNA levels of inflammatory factors in the hearts ($n = 6$). (d) Cytokine levels in the hearts ($n = 6$). (e) TUNEL staining in DOX-treated mice ($n = 6$). (f) Bax and Bcl-2 protein expression in DOX-treated mice ($n = 6$). (g) Caspase-3 activity in the hearts ($n = 6$). Mice were intraperitoneally injected with a single dose of DOX (15 mg/kg) to establish the acute cardiac injury model. Five days after DOX injection, heart tissues were collected to assess the myocardial inflammatory response and apoptosis, as reflected in (a–g). Data are shown as means ± SEM. Comparisons between multiple groups were performed using one-way ANOVA followed by a post hoc Bonferroni comparison analysis. $^*P < 0.05$ compared with saline. $^\#P < 0.05$ compared with DOX alone.

(a)

(b)

Figure 6: Continued.

(c)

(d)

(e)

(f)

FIGURE 6: Continued.

(g)

(h)
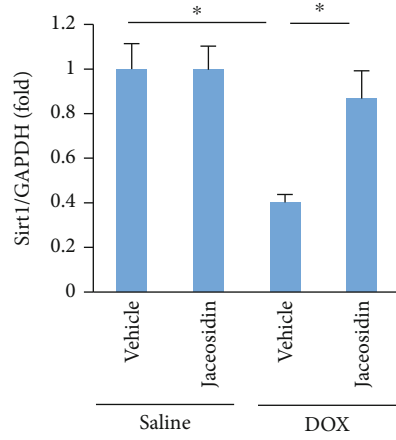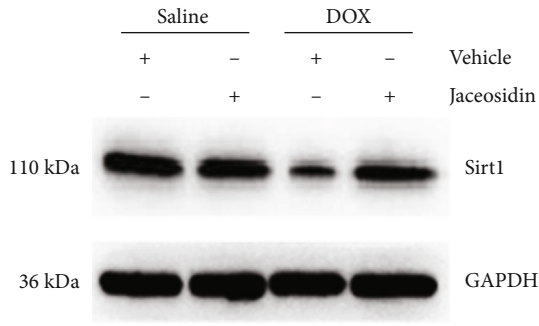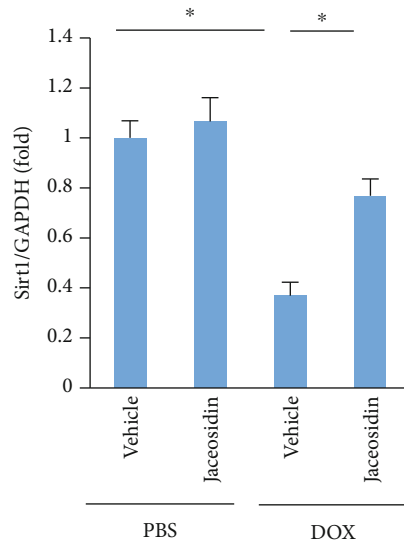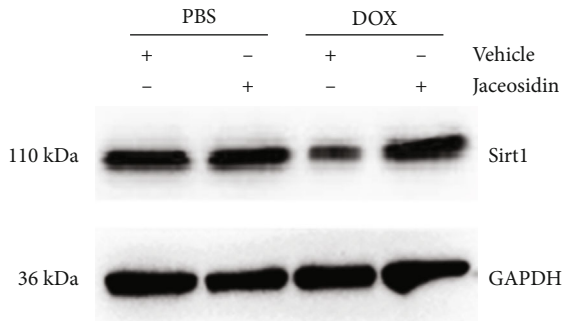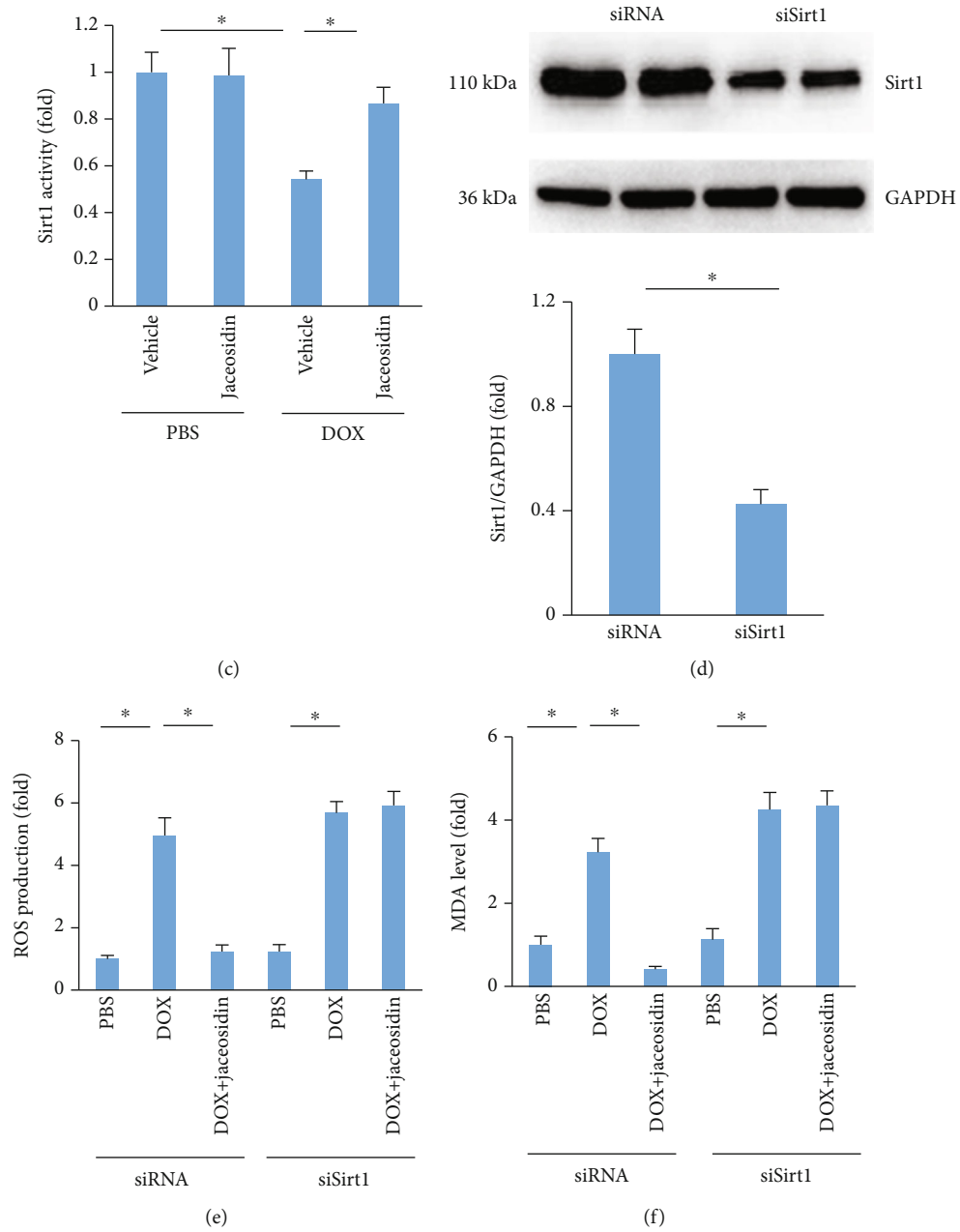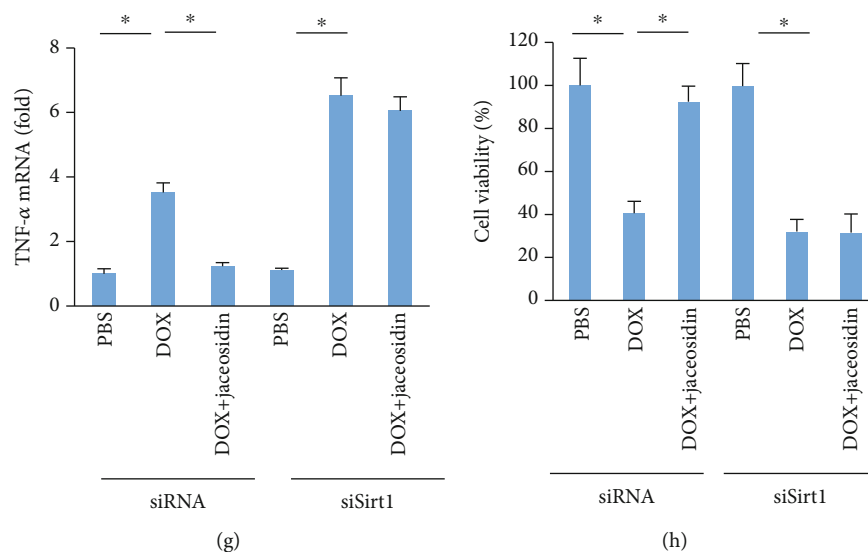
FIGURE 6: Jaceosidin (4 mg/kg) did not provide cardiac protection in sirtuin1- (Sirt1-) deficient cells. (a) Sirt1 protein expression in DOX-treated mice ($n = 6$). (b) Sirt1 protein expression in DOX-treated cells ($n = 6$). (c) Sirt1 activity in DOX-treated cells ($n = 6$). (d) Sirt1 protein expression in DOX-treated cells ($n = 6$). (e, f) ROS production and MDA content in DOX-treated cells ($n = 6$). (g) TNF-α mRNA level in DOX-treated cells ($n = 6$). (h) Cell viability after Sirt1 deficiency in DOX-treated cells ($n = 6$). For (b, c) and (e–h), cells were pretreated with jaceosidin (15 μmol/l) 6 hours before DOX (1 μmol/L) administration. To knock down Sirt1 in cardiomyocytes, NRCMs were preincubated with siSirt1 (50 nmol/l) or siRNA (50 nmol/l) for 24 hours. Data are shown as means ± SEM. For (d), comparisons were performed using two-tailed Student's t tests. For others, comparisons were performed using one-way ANOVA followed by a post hoc Bonferroni comparison analysis. $^{*}P < 0.05$ versus the matched control.

related cardiac injury in jaceosidin-treated mice, the extent of cardiac injury in the mice with DOX+jaceosidin+Ex527 was similar to that in mice with DOX+Ex527, as evidenced by alterations in the levels of EF, cTnI, +dP/dt, 4-HNE, inflammatory factors, and caspase-3 activity (Figures 7(a)–7(g)).

3.8. Oral Treatment of Jaceosidin Had No Liver or Renal Toxicity. To evaluate the potential oral toxicity of jaceosidin, mice were orally administered jaceosidin (4 mg/kg) daily for 7 days. After that, ALT, AST, and creatinine were detected. As shown in Figure S2A-C, jaceosidin administration cannot affect serum ALT, AST, and creatinine levels.

4. Discussion

Several ROS scavengers have been evaluated for their ability to limit DOX-induced cardiotoxicity, but with little success [21]. A low oxidant scavenging efficacy and/or the scavengers undergoing secondary reactions with other biomolecules might explain their lack of benefit [22]. Therefore, a strategy for preventing DOX-induced cardiotoxicity would help improve the quality of life of cancer patients. The present study demonstrated for the first time that jaceosidin can protect against DOX-related cardiac injury in mice and cardiomyocytes. We also found that jaceosidin supplementation can improve cardiac function and suppress DOX-induced oxidative stress, the inflammatory response, and myocardial apoptosis in mice through the activation of Sirt1. These data suggest that jaceosidin supplementation may be a promising avenue for improving cardiomyocyte survival in DOX-treated mice.

Several natural products have demonstrated the ability to protect against DOX-induced cardiotoxicity [20, 23]. However, these agents have adverse side effects, including weight loss and potentiation of doxorubicin-induced myelosuppression [24]. Jaceosidin has been shown to provide protection against several diseases [13, 14]. Jaceosidin attenuated osteoarthritic cartilage damage by blocking IκB degradation in mice [25], and it inhibited contact hypersensitivity in mice by downregulating IFN-γ signaling in T cells [26]. Jaceosidin has not been further investigated for its biological effect in the heart, particularly for the treatment of DOX-induced cardiotoxicity. As expected, we found that jaceosidin largely reduced DOX-related cardiac injury and improved cardiac function. To the best of our knowledge, this is the first report of the protective effect of jaceosidin in DOX-induced cardiotoxicity. Considering the translational potential of the present findings, it was important to confirm that jaceosidin treatment did not compromise the oncological efficacy of DOX. We did not evaluate the effects of jaceosidin on tumour growth and metastasis. However, several lines of evidence have demonstrated that jaceosidin can suppress the growth of several tumour types [27, 28], suggesting that jaceosidin would not compromise the oncological efficacy of DOX.

DOX has a high affinity for heart tissue and can abundantly accumulate in cardiomyocytes. DOX interferes with the normal electron transport chain to increase the production of free radicals and stimulate the oxidation of membrane lipids, leading to the accumulation of the highly reactive electrophile 4-HNE, which modifies various protein functions and impacts cardiac function [29]. A previous study indicated that amelioration of oxidative damage by FNDC5

(a)

(b)

(c)

(d)

(e)

(f)

Figure 7: Continued.

(g)
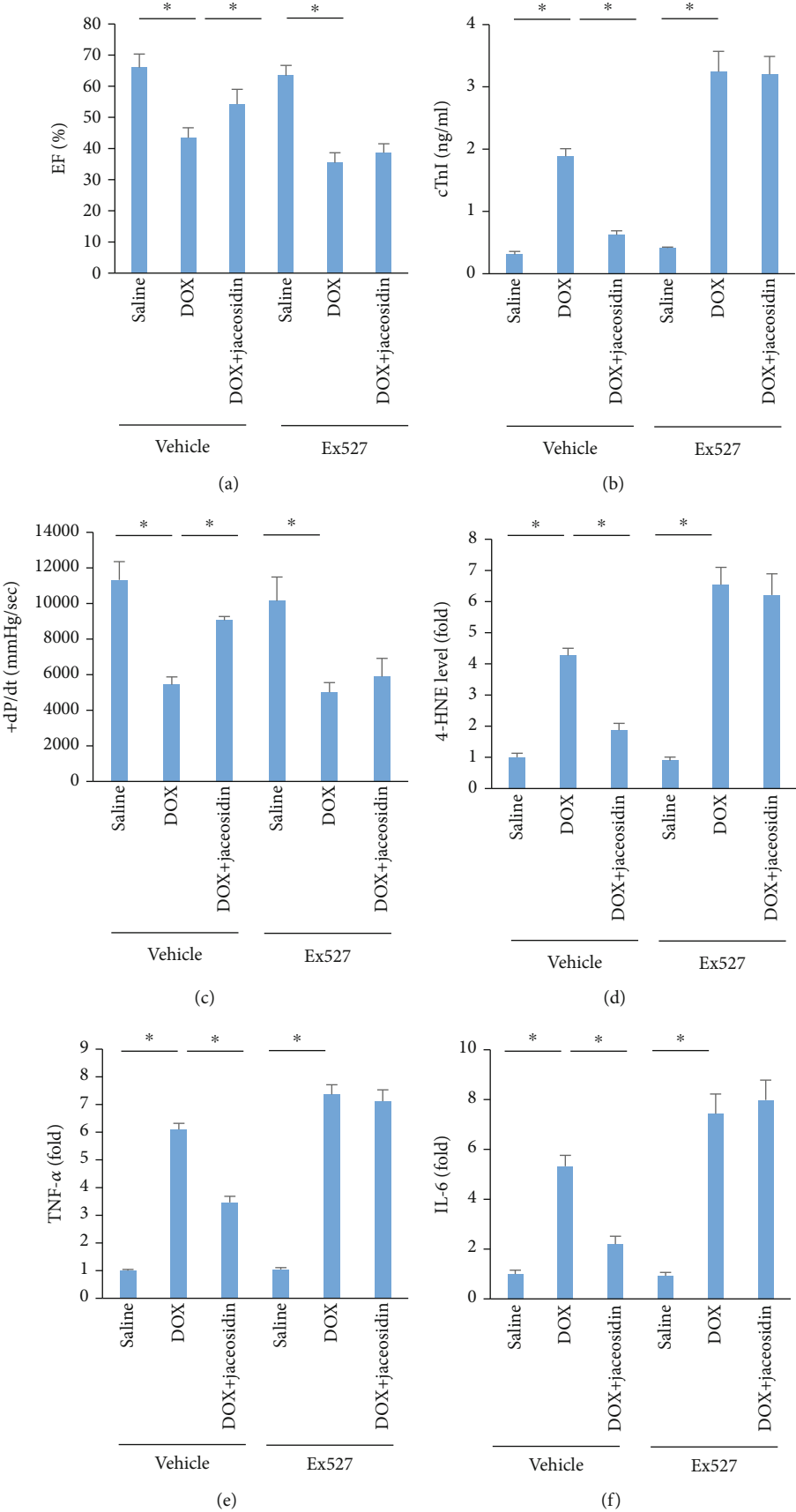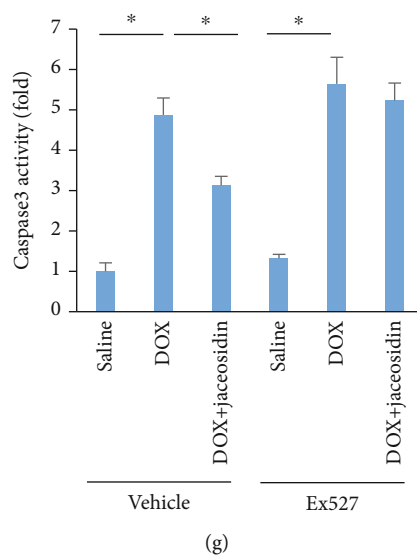
FIGURE 7: Jaceosidin (4 mg/kg) did not provide cardiac protection in mice with sirtuin 1 (Sirt1) inhibition. (a) Ejection fraction (EF) in DOX-treated mice ($n = 8 - 10$). (b) The level of cardiac troponin I (cTnI) in DOX-treated mice ($n = 6$). (C) +dP/dt in DOX-treated mice ($n = 6$). (d) The levels of 4-hydroxynonenal (4-HNE) in DOX-treated mice ($n = 6$). (e, f) The levels of tumour necrosis factor- (TNF-) α and interleukin- (IL-) 6 in DOX-treated mice ($n = 6$). (g) The activity of caspase-3 in mice ($n = 6$). To inhibit Sirt1 in vivo, mice were subjected to a specific inhibitor of Sirt1 (Ex527, 1 mg/kg) every other day for a total of 8 days beginning 3 days before DOX injection. Data are shown as means ± SEM. Comparisons were performed using one-way ANOVA followed by a post hoc Bonferroni comparison analysis. $^*P < 0.05$ versus the matched control.

overexpression helped alleviate DOX-related cardiac dysfunction [2]. In agreement with these previous reports, we found that DOX-induced ROS production, lipid peroxidation, and the impairment of SOD activity were blunted by jaceosidin treatment. Our findings are in agreement with a previous study showing that jaceosidin eliminated free radicals in LPS-induced RAW 264.7 macrophages [30]. However, there have been conflicting reports regarding the effects of jaceosidin. Kim et al. found that jaceosidin induced apoptosis in ras-transformed human breast epithelial cells through the generation of ROS. These discrepancies might be explained by the different roles of jaceosidin in different cells. A previous study reported that DOX-induced NF-κB activation occurred very early in the heart [31]. However, this activation could not be detected at 5 days after DOX injection [32]. Inconsistent with this study, we found that even at 5 days after DOX injection, NF-κB activation could still be detected in the heart tissue. Further assessment revealed that the mRNA levels of inflammatory factors and cytokine production were increased in the hearts of DOX-treated mice. These increases were largely blunted in jaceosidin-treated mice, which is in agreement with a study that found that jaceosidin attenuated lung histopathological changes, inhibited the expression of NF-κB, and decreased the levels of complement 3 (C3) [14]. These data imply that attenuation of oxidative damage and the inflammatory response are involved in jaceosidin-mediated inhibitory effects in DOX-related cardiac injury in mice.

Nrf2 has been recognized as one of the major cellular defence mechanisms against oxidative stress [33]. In response to ROS, Nrf2 is activated and mediates the induction of several cytoprotective enzymes [34]. It has been reported that elevated Nrf2 activity provides protection against DOX-induced cardiomyopathy [35]. Here, we tested the hypothesis that substantial Nrf2 activation, through jaceosidin induction, is involved in cardioprotection during DOX therapy. The results showed that jaceosidin restored Nrf2 protein expression in the hearts of DOX-treated mice. The mRNA levels of SOD1, SOD2, and Gpx, as well as SOD activity, were significantly decreased in the DOX group, and jaceosidin treatment was found to significantly, but not completely, prevent DOX-induced oxidative effects. These findings were consistent with a previous study showing that jaceosidin treatment increased the expression and activity of SOD in diabetic nephropathy [13]. These data suggest that jaceosidin may stimulate Nrf2-mediated downstream antioxidants to protect against DOX-induced damage.

Notably, DOX-induced oxidative stress activated apoptotic signaling and resulted in cardiomyocyte apoptosis in isolated cardiomyocytes, which was a key component in DOX-induced cardiotoxicity [36]. DOX caused the depletion of catalase and Gpx in the heart, thus creating an environment that promoted hydroxyl radical production, resulting in cytochrome c release followed by caspase-3 activation and myocardial apoptosis [7, 37]. We also found that jaceosidin largely attenuated DOX-induced myocardial apoptosis and cardiomyocyte loss. Jaceosidin treatment also decreased Bax expression and suppressed caspase-3 activity in DOX-exposed hearts. The attenuation of cell apoptosis also contributed to jaceosidin-mediated protection.

Sirt1, a histone deacetylase, is implicated in various cellular functions [38]. Sirt1 activation was shown to inhibit cardiomyocyte apoptosis in response to pathological stimuli [39]. Zhang et al. found that the Sirt1 protein level was

slightly increased in response to DOX [40]. Inconsistent with this study, we observed decreased Sirt1 expression in DOX-exposed hearts. This finding was in line with a previous study that found that DOX induced a significant decrease in Sirt1 activation and that activating Sirt1 prevented DOX-related cardiotoxicity in mice [41]. Here, we found, for the first time, that jaceosidin increased Sirt1 protein expression and activity in vivo and in vitro. Sirt1 knockdown abolished the protective effects provided by jaceosidin in DOX-induced cardiotoxicity. These data clearly indicated that jaceosidin-mediated protection against DOX-related cardiac injury was mediated by the activation of Sirt1.

In conclusion, the present study demonstrated that jaceosidin treatment inhibited myocardial oxidative and inflammatory damage and reduced apoptosis, thereby improving cardiac function after DOX treatment. Our results provide experimental evidence for the application of jaceosidin in the treatment of DOX-related cardiac injury.

Data Availability

The data that support the findings of this study are available from the corresponding author upon reasonable request.

Conflicts of Interest

The authors declare that they have no conflicts of interest.

Authors' Contributions

Yuzhou Liu, Liying Zhou, and Binbin Du contributed equally to this work.

Acknowledgments

Supplementary Materials

Figure S1: unedited and uncropped western blot images of Figures 6 (a) and 6 (b) and Figure 6 (d). Figure S2: the level of serum ALT, AST, and creatinine (a–c). Mice were orally administered jaceosidin (4 mg/kg) daily for 7 days ($n = 6$ for each group). Data are shown as means ± SEM. Comparisons were performed using two-tailed Student's t-tests. (Supplementary Materials)

References

[1] S. A. Brown, N. Sandhu, and J. Herrmann, "Systems biology approaches to adverse drug effects: the example of cardio-oncology," Nature Reviews. Clinical Oncology, vol. 12, no. 12, pp. 718–731, 2015.

[2] X. Zhang, C. Hu, C. Y. Kong et al., "FNDC5 alleviates oxidative stress and cardiomyocyte apoptosis in doxorubicin-induced cardiotoxicity via activating AKT," Cell Death and Differentiation, vol. 27, no. 2, pp. 540–555, 2020.

[3] Y. P. Yuan, Z. G. Ma, X. Zhang et al., "CTRP3 protected against doxorubicin-induced cardiac dysfunction, inflammation and cell death via activation of Sirt1," Journal of Molecular and Cellular Cardiology, vol. 114, pp. 38–47, 2018.

[4] V. J. Ferrans, J. R. Clark, J. Zhang, Z. X. Yu, and E. H. Herman, "Pathogenesis and prevention of doxorubicin cardiomyopathy," Tsitologiia, vol. 39, no. 10, pp. 928–937, 1997.

[5] W. Zhu, M. H. Soonpaa, H. Chen et al., "Acute doxorubicin cardiotoxicity is associated with p53-Induced inhibition of the mammalian target of rapamycin pathway," Circulation, vol. 119, no. 1, pp. 99–106, 2009.

[6] S. Zhou, A. Starkov, M. K. Froberg, R. L. Leino, and K. B. Wallace, "Cumulative and irreversible cardiac mitochondrial dysfunction induced by doxorubicin," Cancer Research, vol. 61, no. 2, pp. 771–777, 2001.

[7] A. C. Childs, S. L. Phaneuf, A. J. Dirks, T. Phillips, and C. Leeuwenburgh, "Doxorubicin treatment in vivo causes cytochrome C release and cardiomyocyte apoptosis, as well as increased mitochondrial efficiency, superoxide dismutase activity, and Bcl-2: Bax ratio," Cancer Research, vol. 62, no. 16, pp. 4592–4598, 2002.

[8] H. C. Yen, T. D. Oberley, S. Vichitbandha, Y. S. Ho, and D. K. St Clair, "The protective role of manganese superoxide dismutase against adriamycin-induced acute cardiac toxicity in transgenic mice," The Journal of Clinical Investigation, vol. 98, no. 5, pp. 1253–1260, 1996.

[9] Y. J. Kang, Y. Chen, and P. N. Epstein, "Suppression of doxorubicin cardiotoxicity by overexpression of catalase in the heart of transgenic mice (∗)," The Journal of Biological Chemistry, vol. 271, no. 21, pp. 12610–12616, 1996.

[10] D. M. Basso, M. S. Beattie, and J. C. Bresnahan, "Graded histological and locomotor outcomes after spinal cord contusion using the NYU weight-drop device versus transection," Experimental Neurology, vol. 139, no. 2, pp. 244–256, 1996.

[11] M. J. Kim, J. M. Han, Y. Y. Jin et al., "In vitro antioxidant and anti-inflammatory activities of Jaceosidin from Artemisia princeps Pampanini cv. Sajabal," Archives of Pharmacal Research, vol. 31, no. 4, pp. 429–437, 2008.

[12] V. Moscatelli, O. Hnatyszyn, C. Acevedo, J. Megias, M. J. Alcaraz, and G. Ferraro, "Flavonoids from Artemisia copa with anti-inflammatory activity," Planta Medica, vol. 72, no. 1, pp. 72–74, 2006.

[13] E. Park, K. Hong, B. M. Kwon, Y. Kim, and J. H. Kim, "Jaceosidin ameliorates insulin resistance and kidney dysfunction by enhancing insulin receptor signaling and the antioxidant defense system in type 2 diabetic mice," Journal of Medicinal Food, vol. 23, no. 10, pp. 1083–1092, 2020.

[14] X. L. Huang, X. C. Wei, L. Q. Guo et al., "The therapeutic effects of Jaceosidin on lipopolysaccharide-induced acute lung injury in mice," Journal of Pharmacological Sciences, vol. 140, no. 3, pp. 228–235, 2019.

[15] W. R. Fu, J. L. Chen, X. Y. Li, J. X. Dong, and Y. Liu, "Bidirectional regulatory mechanisms of Jaceosidin on mitochondria function: protective effects of the permeability transition and damage of membrane functions," The Journal of Membrane Biology, vol. 253, no. 1, pp. 25–35, 2020.

[16] Z. Ouyang, W. Li, Q. Meng et al., "A natural compound jaceosidin ameliorates endoplasmic reticulum stress and insulin resistance via upregulation of SERCA2b," Biomedicine & Pharmacotherapy, vol. 89, pp. 1286–1296, 2017.

[17] Z. G. Ma, Y. P. Yuan, X. Zhang et al., "C1q-tumour necrosis factor-related protein-3 exacerbates cardiac hypertrophy in mice," *Cardiovascular Research*, vol. 115, no. 6, pp. 1067–1077, 2019.

[18] T. Akimova, H. Xiao, Y. Liu et al., "Targeting sirtuin-1 alleviates experimental autoimmune colitis by induction of Foxp3+ T-regulatory cells," *Mucosal Immunology*, vol. 7, no. 5, pp. 1209–1220, 2014.

[19] Z. G. Ma, J. Dai, Y. P. Yuan et al., "T-bet deficiency attenuates cardiac remodelling in rats," *Basic Research in Cardiology*, vol. 113, no. 3, p. 19, 2018.

[20] D. Kumar, L. A. Kirshenbaum, T. Li, I. Danelisen, and P. K. Singal, "Apoptosis in adriamycin cardiomyopathy and its modulation by probucol," *Antioxidants & Redox Signaling*, vol. 3, no. 1, pp. 135–145, 2001.

[21] D. G. Deavall, E. A. Martin, J. M. Horner, and R. Roberts, "Drug-induced oxidative stress and toxicity," *Journal of toxicology*, vol. 2012, 2012.

[22] H. J. Forman, K. J. Davies, and F. Ursini, "How do nutritional antioxidants really work: nucleophilic tone and para-hormesis versus free radical scavenging in vivo," *Free Radical Biology & Medicine*, vol. 66, pp. 24–35, 2014.

[23] P. Nazeyrollas, A. Prevost, N. Baccard, L. Manot, P. Devillier, and H. Millart, "Effects of amifostine on perfused isolated rat heart and on acute doxorubicin-induced cardiotoxicity," *Cancer Chemotherapy and Pharmacology*, vol. 43, no. 3, pp. 227–232, 1999.

[24] X. Liu, Z. Chen, C. C. Chua et al., "Melatonin as an effective protector against doxorubicin-induced cardiotoxicity," *American Journal of Physiology. Heart and Circulatory Physiology*, vol. 283, no. 1, pp. H254–H263, 2002.

[25] H. Lee, D. Jang, J. Jeon et al., "Seomae mugwort and jaceosidin attenuate osteoarthritic cartilage damage by blocking IκB degradation in mice," *Journal of Cellular and Molecular Medicine*, vol. 24, no. 14, pp. 8126–8137, 2020.

[26] Y. Yin, Y. Sun, L. Gu et al., "Jaceosidin inhibits contact hypersensitivity in mice via down-regulating IFN-γ/STAT1/T-bet signaling in T cells," *European Journal of Pharmacology*, vol. 651, no. 1-3, pp. 205–211, 2011.

[27] S. M. Woo and T. K. Kwon, "Jaceosidin induces apoptosis through Bax activation and down-regulation of Mcl-1 and c-FLIP expression in human renal carcinoma Caki cells," *Chemico-Biological Interactions*, vol. 260, pp. 168–175, 2016.

[28] Z. Hajdu, J. Hohmann, P. Forgo, I. Mathe, J. Molnar, and I. Zupko, "Antiproliferative activity of Artemisia asiatica extract and its constituents on human tumor cell lines," *Planta Medica*, vol. 80, no. 18, pp. 1692–1697, 2014.

[29] E. A. Konorev, M. C. Kennedy, and B. Kalyanaraman, "Cell-permeable superoxide dismutase and glutathione peroxidase mimetics afford superior protection against doxorubicin-induced cardiotoxicity: the role of reactive oxygen and nitrogen intermediates," *Archives of Biochemistry and Biophysics*, vol. 368, no. 2, pp. 421–428, 1999.

[30] S. Li, S. Zhou, W. Yang, and D. Meng, "Gastro-protective effect of edible plant Artemisia argyi in ethanol-induced rats via normalizing inflammatory responses and oxidative stress," *Journal of Ethnopharmacology*, vol. 214, pp. 207–217, 2018.

[31] N. Nozaki, T. Shishido, Y. Takeishi, and I. Kubota, "Modulation of doxorubicin-induced cardiac dysfunction in toll-like receptor-2-knockout mice," *Circulation*, vol. 110, no. 18, pp. 2869–2874, 2004.

[32] Z. G. Ma, C. Y. Kong, H. M. Wu et al., "Toll-like receptor 5 deficiency diminishes doxorubicin-induced acute cardiotoxicity in mice," *Theranostics*, vol. 10, no. 24, pp. 11013–11025, 2020.

[33] J. D. Hayes and M. McMahon, "NRF2 and KEAP1 mutations: permanent activation of an adaptive response in cancer," *Trends in Biochemical Sciences*, vol. 34, no. 4, pp. 176–188, 2009.

[34] K. N. Ha, Y. Chen, J. Cai, and P. J. Sternberg, "Increased glutathione synthesis through an ARE-Nrf2-dependent pathway by zinc in the RPE: implication for protection against oxidative stress," *Investigative Ophthalmology & Visual Science*, vol. 47, no. 6, pp. 2709–2715, 2006.

[35] H. Benes, M. K. Vuong, M. Boerma, K. E. McElhanon, E. R. Siegel, and S. P. Singh, "Protection from oxidative and electrophilic stress in the Gsta4-null mouse heart," *Cardiovascular Toxicology*, vol. 13, no. 4, pp. 347–356, 2013.

[36] J. Nitobe, S. Yamaguchi, M. Okuyama et al., "Reactive oxygen species regulate FLICE inhibitory protein (FLIP) and susceptibility to Fas-mediated apoptosis in cardiac myocytes," *Cardiovascular Research*, vol. 57, no. 1, pp. 119–128, 2003.

[37] J. H. Doroshow, G. Y. Locker, and C. E. Myers, "Enzymatic defenses of the mouse heart against reactive oxygen metabolites: alterations produced by doxorubicin," *The Journal of Clinical Investigation*, vol. 65, no. 1, pp. 128–135, 1980.

[38] B. Osborne, N. L. Bentley, M. K. Montgomery, and N. Turner, "The role of mitochondrial sirtuins in health and disease," *Free Radical Biology & Medicine*, vol. 100, pp. 164–174, 2016.

[39] I. Lekli, G. Szabo, B. Juhasz et al., "Protective mechanisms of resveratrol against ischemia-reperfusion-induced damage in hearts obtained from Zucker obese rats: the role of GLUT-4 and endothelin," *American Journal of Physiology. Heart and Circulatory Physiology*, vol. 294, no. 2, pp. H859–H866, 2008.

[40] C. Zhang, Y. Feng, S. Qu et al., "Resveratrol attenuates doxorubicin-induced cardiomyocyte apoptosis in mice through SIRT1-mediated deacetylation of p 53," *Cardiovascular Research*, vol. 90, no. 3, pp. 538–545, 2011.

[41] E. D. Danz, J. Skramsted, N. Henry, J. A. Bennett, and R. S. Keller, "Resveratrol prevents doxorubicin cardiotoxicity through mitochondrial stabilization and the Sirt1 pathway," *Free Radical Biology & Medicine*, vol. 46, no. 12, pp. 1589–1597, 2009.

Review Article

The Involvement of the Oxidative Stress Status in Cancer Pathology: A Double View on the Role of the Antioxidants

Kamal Fatima Zahra,[1] **Radu Lefter,**[2] **Ahmad Ali** [ID],[3] **Ech-Chahad Abdellah,**[4] **Constantin Trus** [ID],[5] **Alin Ciobica** [ID],[6] **and Daniel Timofte**[7]

[1]*Faculty of Sciences and Techniques, Laboratory of Physical Chemistry of Processes and Materials/Agri-Food and Health, Hassan First University, B.P. 539, 26000 Settat, Morocco*

[2]*Center of Biomedical Research, Romanian Academy, 8th Carol I Avenue, 700506 Iasi, Romania*

[3]*Department of Life Sciences, University of Mumbai, Vidyanagari, Santacruz (East), Mumbai 400098, India*

[4]*Faculty of Sciences and Techniques, Laboratory of Physical Chemistry of Processes and Materials, Hassan First University, B.P. 539, 26000 Settat, Morocco*

[5]*Department of Morphological and Functional Sciences, Faculty of Medicine, Dunarea de Jos University, 800008 Galati, Romania*

[6]*Department of Biology, Faculty of Biology, Alexandru Ioan Cuza University, 11th Carol I Avenue, 700506 Iasi, Romania*

[7]*Faculty of Medicine, "Grigore T. Popa", University of Medicine and Pharmacy, Strada Universitatii 16, 700115 Iasi, Romania*

Correspondence should be addressed to Constantin Trus; dilconstantin@yahoo.com and Alin Ciobica; alin.ciobica@uaic.ro

Oxygen-free radicals, reactive oxygen species (ROS) or reactive nitrogen species (RNS), are known by their "double-sided" nature in biological systems. The beneficial effects of ROS involve physiological roles as weapons in the arsenal of the immune system (destroying bacteria within phagocytic cells) and role in programmed cell death (apoptosis). On the other hand, the redox imbalance in favor of the prooxidants results in an overproduction of the ROS/RNS leading to oxidative stress. This imbalance can, therefore, be related to oncogenic stimulation. High levels of ROS disrupt cellular processes by nonspecifically attacking proteins, lipids, and DNA. It appears that DNA damage is the key player in cancer initiation and the formation of 8-OH-G, a potential biomarker for carcinogenesis. The harmful effect of ROS is neutralized by an antioxidant protection treatment as they convert ROS into less reactive species. However, contradictory epidemiological results show that supplementation above physiological doses recommended for antioxidants and taken over a long period can lead to harmful effects and even increase the risk of cancer. Thus, we are describing here some of the latest updates on the involvement of oxidative stress in cancer pathology and a double view on the role of the antioxidants in this context and how this could be relevant in the management and pathology of cancer.

1. Introduction

In vivo synthesis of reactive oxygen and nitrogen species highlights either a physiological role necessary for normal cell function or oxidative stress characterized by excessive ROS production, thereby altering and damaging intracellular biomolecules, including nucleic acids, proteins, and lipids [1, 2]. Oxidative damage has been described as a serious mechanism in the initiation and progression of cancer.

Cancer is the most worrisome health problem that has received worldwide attention in the past decades. Currently, it is the second leading cause of death in developing countries after cardiovascular mortality [3]. More than 14 million new cancer cases occurred worldwide in 2012, according to the International Agency for Research on Cancer (IARC). The number of cancer deaths increased by 1.5 million, from 6.7 in 2002 to 8.2 million in 2012 [4]. By 2030, the global burden is expected to reach 21.7 million cancer cases and 13 million

cancer deaths [5]. This estimate of future burden growth is attributable to physical and environmental risk factors highlighted by globalization and socioeconomic metamorphoses such as pollution, UV radiation, adoption of new lifestyle, and unhealthy diet (poor diet, physical inactivity, smoking, etc.) [6].

There are many factors behind the process of carcinogenesis. Oxidation of DNA, proteins, and lipid peroxidation reactions generated by reactive intermediates, produced by oxidative stress, plays a major role in carcinogenesis. It has been suggested that 8-hydroxy-2-deoxyguanosine, malondialdehyde (MDA), 4-hydroxy-2-nonenal (4-HNE), and carbonylated proteins, by-products of oxidative damage, have mutagenic potential. Increased plasma and tissue concentrations of these oxidative stress second messengers have been reported in lung, gastric, colon, and breast cancers [7–10]. These findings call attention to the role of antioxidant deficiency or increased free radicals in producing such effects and provide a starting point for research into the therapeutic potential of antioxidants in cancer, which was later confirmed to be related to cellular and genetic damage induced by reactive forms of oxygen [11].

The growing knowledge of the mechanisms of oncogenesis related to oxidative stress has allowed the development of several treatments largely represented by the class of complementary alternative therapies, to target a specific mechanism without affecting quality of life, in contrast to less selective conventional chemotherapies [12]. In the last decades, antioxidant molecules have been recognized as one of the most effective forms of alternative and complementary therapy integrating a double therapeutic and preventive facet [13]. They are classified into different groups according to their properties: endogenous enzymatic antioxidants, endogenous nonenzymatic antioxidants, and exogenous antioxidants.

Thus, it was long considered antioxidants to be defensive weapons that can help prevent and suppress the development of cancerous processes, but lately a body of scientific evidence is emerging to challenge the efficacy or even the safety of these complementary alternative treatments calling for a reconsideration of a new paradoxical concept of double-edged antioxidants [14]. The topic on where the beneficial effects of the antioxidants become actually nocive in cancer therapy has been discussed in some relevant and recent reviews [15], or articles concerning (only) certain specific areas, such as bladder cancer development [16], or ROS-(reactive oxygen species-) based nanomaterials [17], but the exact role of antioxidants and the ambiguity of the oxidants-antioxidants interplay remain unclear. The current study is aimed at offering a comprehensive picture of oxidative stress implication in the various cancer developments and subsequently summarizing the most relevant findings of the anticancer role of all classes of antioxidants, presented here according to their conventional classification. The strategies to improve the efficacy of antioxidants in the clinical context have also been discussed. Data on the antioxidants and ROS controversial or contradictory roles in cancer, illustrative for the antioxidant paradox, the double-faceted impact in tumoral processes, are presented in the final part of this review.

2. Free Radicals, Oxidative Stress, and Cancer

2.1. Biology of Free Radicals. In the mid-1950s, Gerschman et al. were among the first to suggest that the deleterious effects of O_2 on the body could be attributed to the formation of oxygenated free radicals [18]. Inspired by their work, Denham Harman, the former chemist of the Shell Company, gave a hypothesis in 1956 famously known as "free radical theory of aging," postulating that aging and associated diseases are the consequence of a progressive alteration of cellular constituents under the effect of free radicals and ROS [19, 20]. In 1972, Harman extrapolated his theory to the "mitochondrial theory of aging," proposing that ATP synthesis in the mitochondria involved the electron transfer along a series of membrane multienzyme complexes until their ultimate recovery by molecular oxygen. During this transfer, reactive oxygen derivatives were produced that could generate mitochondrial and nuclear DNA mutations and damage the cellular constitutive proteins. These alterations in turn would cause other mutations promoting the synthesis of other ROS and thus the accumulation of free radicals in the affected cells. Today, the mitochondrial theory is privileged in the explanation of aging phenomena [21]. Harman's point of view was reinforced in 1969 when McCord and Fridovich isolated from human red blood cells the first enzymatic defense system against the superoxide anion produced by univalent reduction of the oxygen, the superoxide dismutase [22].

The discovery that the human body was capable of synthesizing free radicals has thereafter been the starting point for establishing the biological reality of free radicals and their possible pathophysiological roles. The most common radical species in biological systems are the oxygen-derived radicals also known as the reactive oxygen species (ROS). The ROS include oxygenated or primary free radicals such as superoxide anion ($O_2^{.-}$), hydroxyl radical ($OH^.$), or nitrogen monoxide ($NO^.$) and also nonradical highly toxic derivatives such as hydrogen peroxide (H_2O_2), peroxide anion (O_2^{2-}), and peroxynitrite ($ONOO^-$) [23]. The ROS, a natural consequence of aerobic metabolism, are synthesized during certain vital processes at a reasonable dose, their concentration being regulated by the balance between their rate of production and their rate of elimination by antioxidant systems [24–26]. When the balance between prooxidants and antioxidants is maintained, the ROS play a positive physiological role in the normal functioning of the cells, particularly in the phagocytosis process or the programmed cell death (apoptosis) [27–30]. However, when the homeostasis of oxygen becomes imbalanced in the prooxidant direction, it leads to a pathological state known as oxidative stress [31, 32]. Oxidative stress is a risk factor linked with mitochondrial dysfunction for numerous pathophysiological conditions in which cells are subjected to an endogenous or exogenous production of oxygenated free radicals that exceeds their antioxidant capacities and directly damage on contact macromolecules, including lipids, proteins, and DNA [33].

The lipid structures and in particular the cell membranes are the first targets of the ROS because of their richness in unsaturated fatty acids [34–36]. ROS reactions with

membrane lipids concretize in lipid peroxidation processes in cascade. Normally, the primary products of lipoperoxidation, the lipid hydroperoxides (LOOH), are detoxified through the enzymatic pathway of glutathione S-transferases (GST); however, when homeostasis is disturbed, the lipoperoxides escaping this detoxification led to toxic aldehydes; the best known of which is malondialdehyde (MDA) a highly reactive and mutagenic dialdehyde; the potential mutagen of MDA was detected in bacterial and mammalian cells [36–38]. MDA forms stable bonds with -NH$_2$ amine groups of biomolecules (proteins, phospholipids, or nucleic acids) to produce inter- and intramolecular bridges of amino-3-iminopropene and structural modifications, and thus, it diffuses easily and can reach the cellular nucleus. At this level, MDA can bind with the nucleotide bases, guanine and cytosine, creating bridges between the DNA strands that will lead to the cessation of the replication process or induce mutagenic effects [39]. In addition, the structures induced by MDA are recognized as nonautonomous by the immune system, resulting in an autoimmune response [40, 41].

Another major toxic by-product generated by lipid peroxidation is 4-hydroxy 2-nonenal (HNE) [42, 43]; the higher toxicity of 4-HNE can be explained by its rapid reactions with thiols and amino groups; 4-HNE formed in cells will modify proteins via Michael addition by reacting with compounds having a thiol group (GSH, Cys, and coenzyme A) [44, 45], but also, by the formation of adducts with three different side chains, by its reaction with the -SH groups of the cysteines, and by the formation of Schiff bases with the -NH$_2$ groups of the amino acids lysine and histidine [46, 47]. These adductions of HNE proteins modify and cause protein crosslinking and induce carbonyl stress, which contributes to the promotion of cytotoxic events such as cell growth arrest, mitochondrial dysfunction, apoptosis, and necrosis by modifying cellular proteins and nucleic acids, causing microinflammation that can damage neurons and to the progression of chronic schizophrenia, an Alzheimer's pathogenesis [48–51].

Carbonyl stress may also contribute to the progression of cancer; the concentrations of advanced glycation endproduct (AGE) marker of the carbonyl stress were found to be higher in the serum of breast cancer patients in the early stage of the disease, but also with advanced breast cancer (stage III and IV) [52]. HNE also forms adducts with DNA, reacting with the -NH$_2$ group of deoxyguanosine, resulting in DNA damage and mutagenic effects [53]. Not surprisingly, 4-HNE is considered a second toxic messenger of free radicals; it is found to be involved in a variety of pathologies, especially in humans, including atherosclerosis, Alzheimer's disease, Parkinson's disease, cirrhosis of the liver, and several cancers [54, 55]. Numerous pathologies are associated with lipid peroxidation, such as neurodegenerative diseases (Alzheimer, Parkinson), diabetes, cancers, inflammatory diseases, or aging [56–59].

Proteins also undergo direct and indirect damage following their interactions with the ROS, which are affecting their function by causing conformation modifications, fragmentations of the peptide chain, aggregation of cross-linked reaction products, changes in electrical charges, and increased susceptibility to proteolysis, resulting in loss of protein enzymatic activity and loss of function of receptor transporting proteins [37, 61].

The sulfur amino acids, such as methionine and cysteine, are particularly vulnerable to oxidation. Methionine is converted into methionine sulfoxide, then methionine sulfone that is heavily involved in neurodegenerative pathologies [61, 62]. The oxidation of the thiol group of cysteine (-SH) generates the sulfenic acid (-SOH) leading to the formation of S-S disulfide bridges or of sulfinic (-SO$_2$H) and sulfonic acid (-SO$_3$H) [60]. Tyrosine forms 3,4-dihydroxyphenylalanine; the nitration of this residue by peroxynitrite generates 3-nitrotyrosine detected in the plasma of diabetic subjects [64]. The basic amino acids lysine, arginine, and histidine constitute, in contact with free radicals, carbonyl derivatives such as 2-oxohistidine, α-aminoadipic semialdehyde, and glutamic semialdehyde. Carbonyl proteins are considered markers of the oxidative stress of proteins, and the increase in their rates is observed in a number of pathological conditions such as neurodegenerative diseases, muscular dystrophy [65], cataractogenesis, rheumatoid arthritis [66], and diabetes [67].

ROS from endogenous or environmental sources also pose a threat to the integrity of the genome by causing irreversible cellular changes in genomic components especially point mutations, deletions, gene rearrangements, and amplification [68]. The OH radical is the most important inducer of DNA oxidation reacting directly with all DNA components, such as purine and pyrimidine bases and the skeleton of deoxyribose sugar, and generating single-strand and double-strand breaks, abasic sites, and inter- and intrastrand covalent bonds as well as with the proteins and modified bases [69, 70]. Among the DNA bases, which are particularly sensitive to oxidation reactions, the most widely studied are the guanines as these have the lowest ionization potential and therefore constitute the main target of ROS [71, 72]. The ROS interaction with guanine will produce 8-oxo-7,8-dihydroguanine (8-oxodG) molecules by type I and type II photosensitization reactions [73, 74]. 8-oxodG has a high mutagenic potential leading to G : C to T : A transversions that have been observed in oncogenes and tumor suppressor genes (such as p53 gene), known to play an important role in carcinogenesis [39, 75, 76]. The accumulation of 8-oxodG was detected during liver carcinoma [77, 78]. 8-oxo-20-deoxyguanosine is also reported in the early stages of carcinogenesis [79].

2.2. Involvement of Oxidative Stress in Carcinogenesis. It is now well established that the uncontrolled production of reactive oxygen species and the products resulting from their reactions with biomolecules and cells contribute to the etiology of several pathologies, among which the most reported is cancer [25, 80, 81]. Carcinogenesis begins with genetic alterations, in which a very important role is played by high oxidative states [82]. The most frequent invasive cancers, according to GLOBOCAN 2018, an online database providing worldwide estimates of specific cancer incidence, are of prostate, breasts, lungs, gastric, and colorectal (Figure 1).
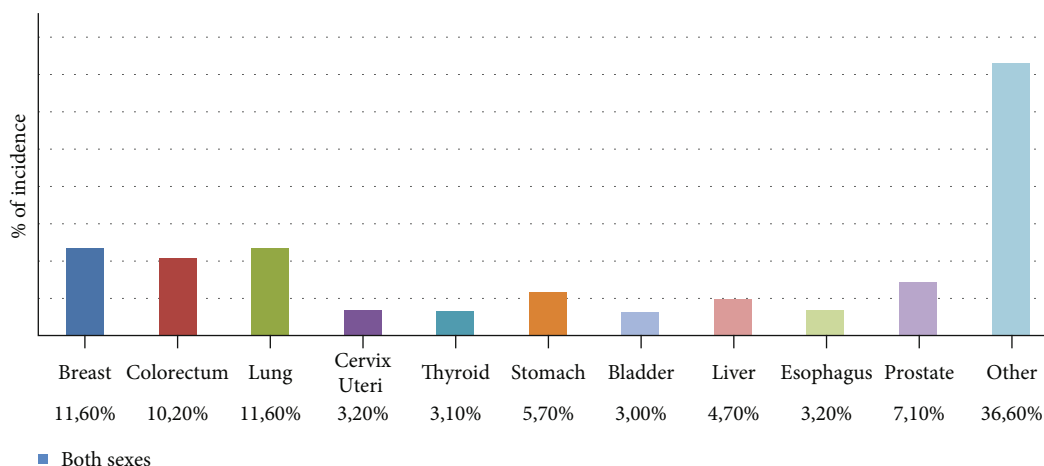
FIGURE 1: The distribution of cases for the 10 most common cancers in 2018 for both sexes (source: GLOBOCAN 2018 [83]).

2.2.1. Colorectal Cancer. Colorectal cancer is the third most common neoplastic disease in the world, and the fourth major cause of mortality [84]. The colon and rectum are permanently exposed to an uncontrolled rate of ROS from endogenous and exogenous sources that lead to the disruption of intestinal homeostasis and can contribute to an increased risk of cancer [85, 86]. Numerous studies have reported increased levels of phospholipase A_2 (PLA2) and myeloperoxidase (MPO) enzymes, associated with the production of high concentrations of free radicals, including RNS and ROS as well as increased levels of MDA and 4-HNE, major products of lipid peroxidation in patients with CRC [87–89]. 8-Oxo-7,8-dihydro-2′-deoxyguanosine, 8-hydroxydeoxyguanosine (8-OHdG), 2-hydroxyadenine, and 8-hydroxyadenine which resulted from DNA oxidation were 2-fold higher in colorectal cancers than in normal mucosa [90]. Similar results were detected in urine sample and peripheral blood leukocytes; a significant increase of 8-oxoGua and 8-oxodG excreted daily in urine additionally to 8-oxodG in leukocytes DNA was reported in colorectal cancer compared to healthy control [91].

2.2.2. Breast Cancer. A study conducted in western Algeria covering 62 breast cancer patients compared to 21 cancer-free controls, evaluating the levels of free oxygen radicals and antioxidants via FORD (free oxygen radicals defense) and FORT (free oxygen radicals test) tests, obtained significantly modified FORT/FORD ratio with increased FORT values and decreased FORD for the cancer patients [92]. The upregulation of oxidative stress markers and downregulation of the antioxidant defense system are considered one of the factors that correlate with the initiation and maintenance of breast cancer progression (Table 1) [92, 93]. DNA in breast cancer was reported to contain high concentrations of base modifications, products of DNA oxidation such as the 8-hydroxydeoxyguanosine, which seem to be involved in breast cancer [94–98]. High levels of urinary 8-OHdG have been detected in women with breast cancer, and the value of 8-OHdG becomes more significant in the later stage of cancer, suggesting that ROS may play an important role in the early carcinogenesis [99]. The ROS are also signaled in

the architectural distortion of the breast epithelium inducing fibroblast proliferation, hyperplasia of the epithelium, cellular atypia, and breast cancer [100].

2.2.3. Prostate Cancer. There is strong evidence that ROS from endogenous or exogenous sources are associated with the proliferation of prostate cancer cells [101–104]. The prostate epithelium of patients with this type of cancer is subjected to more intense oxidative stress as compared to men without the disease [102]. This increase in the generation of ROS is seemingly the result of the overexpression of the various isoforms of NAD(P)H oxidases (NOX), demonstrated in the cancer cells of the prostate [105, 106]. To identify the levels of ROS and the role of the extramitochondrial ROS generator, in the NOX system in prostate cancer cells, Kumar et al. used three cell lines (LNCaP, DU145, and PC3), normal prostate cell cultures (WPMY1, RWPE1, and primary normal epithelial cell cultures), and agents (the NOX inhibitor diphenyliodonium and the antioxidant N-acetyl-L-cysteine) that neutralize the effect of ROS and block their extramitochondrial generation. The results showed that NOX inhibition and ROS neutralization induced growth arrest and blocked proliferation of prostate cancer cell lines and that ROS generation was directly proportional to the aggressive phenotype [107]. A significant decrease in GPx–selenoenzyme and GSH in PC prostate cancer patients has been very well documented by Zachara et al. and Szewczyk-Golec et al., in tissue and serum compared to the control [108, 109]. These results showed that the lack of GPx defense system accompanied the increase of OS and thus the development of pathological prostate conditions. According to Miyamoto et al., the loss of GPx activity was associated with oxidative stress, through glycoxidative stress and two steps of nitroxidative stress, reversible by nitrosation of a selenium moiety, and irreversible by formation of a sulfur-seleno bridge between Cys91 and Sec 45 [110, 111].

2.2.4. Lung Cancer. Lung cancer is a leading cause of cancer-associated mortality worldwide, causing 1,000,000 deaths per year, due to a poor prognosis, high resistance to treatment, and poor survival rate [112, 113]. In lung cancer, oxidative

TABLE 1: The role of oxidative stress on cancer development.

Cancer type	Sample collection	Models	Biomarkers	Reference
CRC	Human colon tissue, males, mean age 67 yrs, range 60-83, normal tissue ($n = 2$) and cancerous tissue ($n = 5$)	In vivo	↑ROM ↑MPO	Keshavarzian et al. (1992) [87]
	Human colorectal mucosal tissues, normal tissue ($n = 20$) and tissue tumors ($n = 20$)	In vivo	↑MDA ↑MPO ↑PLA2	Otamiri et al. (1989) [88]
	Urine sample, cancer patients ($n = 222$) and healthy($n = 85$) Leukocyte DNA, healthy volunteers ($n = 134$), and malignant cancer patients ($n = 179$)	In vivo	↑8-oxoGua ↑8-oxodG ↑8-oxodG	Roszkowski et al. (2011) [91]
BC	Blood samples (plasma), women with breast cancer ($n = 62$) and healthy controls ($n = 21$)	In vivo	↑FORT ↓FORD	Tahari et al. (2013) [92]
	Blood samples, women BBC ($n = 50$), BC ($n = 50$), and healthy women ($n = 50$)	In vivo	↑8-OHdG	Eldin et al. (2019) [96]
	Urine sample, cancer patients ($n = 18$) or healthy control ($n = 10$)	In vivo	↑8-OHdG	Yamamoto et al. (1996) [99]
	Blood samples (serum), BC patients ($n = 35$) and healthy controls ($n = 35$)	In vivo	↑MDA ↑GSSG ↓GSH ↓TAC ↓GSH/GSSG	Hewala et al. (2019) [93]
PC	DU 145 LNCaP PC3	In vitro	↑H_2O_2 ↑O_2^- ↑Nox	Kumar et al. (2008) [107]
	Blood samples (erythrocytes and plasma), PC patients ($n = 30$; age 61 ± 8 years), BPH patients ($n = 30$; age 63 ± 8 years), and healthy men ($n = 25$; age 61 ± 14 years).	In vivo	↓GPx3	Szewczyk-Golec et al. (2015) [108]
	Human prostate tissue, PC ($n = 32$), BPH ($n = 40$) patients, and healthy subjects ($n = 39$)	In vivo	↓GSH-Px	Zachara et al. (2005) [109]
LC	A/J mice (female $n = 35$)	In vivo	↑8-OHdG	Xu et al. (1992) [119]

Abbreviations: 8-OHdG: 8-hydroxy-20–deoxyguanosine; 8-oxodG: 8-oxo-2′-désoxyguanosine; PLA2: phospholipase A2; MP: myeloperoxidase; CRC: colorectal cancer; BC: breast cancer; ROM: reactive oxygen metabolites; GSH: glutathione (total, reduced); GSSG: glutathione disulfide; LC: lung cancer; MDA: malondialdehyde; TAC: total antioxidant capacity; PC: prostate cancer.

stress is found to be a consequence of the disease as well as cooccurrence with smoking, which appears to be a major cause of lung cancer with 90% and 70-80% of cases of lung cancer men and women, respectively [114–118]. In a study conducted by Xu et al. 8-OHdG was elevated in mice treated with nitrosamine 4-(methylnitrosamino)-1-(3-pyridyl)-1-butanone (NNK) major components of tobacco that are associated with the etiology of lung cancer [119]. Smoking therefore contributes to the supply of oxidants not only by exogenous means but also by endogenous means through the induction of chronic inflammation of the respiratory tract with accumulation and activation of leukocytes. This activation leads to high concentrations of ROS/RNS and induces genetic mutations, incessant damage to DNA, inactivation of apoptosis, regulation of growth factors and cytokines, and activation of growth supporting genes, ultimately leading individuals to a high risk of lung cancer [114, 120–123]. The exogenous oxidants cause lung injury by a number of mechanisms, including depletion of glutathione and other antioxidants, initiation of redox cycling mechanisms, improvement of respiratory thrust in neutrophils and macrophages, inactivation of protease inhibitors such as a1-antitrypsin inhibitor, and direct damage to lipids, nucleic

acids, and proteins [124]. The reaction of NO with ROS altered the function of proteins by nitridation or induced structural alterations of DNA, including single- or double-strand DNA breaks, purine, pyrimidine, or changes in deoxyribose and reticulation of DNA; damage to DNA induced either stopping or induction of transcription, induction of DNA pathways signal transduction, replication errors, and genomic instability, contributing to the progression of pulmonary carcinogenesis [125].

2.2.5. Gastric Cancer. Gastric cancer is the fifth leading cause of cancer. It has a relatively rare occurrence in individuals less than 40 years of age [83]. However, the highly aggressive and heterogeneous nature of these cancers has made them the third leading cause of deaths in cancer patients, globally [126]. The stomach is continuously exposed to ingested pollutants and carcinogens. The ROS are also produced in large amounts due to bacterial metabolism and food digestion in a highly acidic environment. The cytoprotective mechanism of the gastric system and ingested antioxidants naturally prevent the above factors from affecting the stomach. However, several internal and external elements including lifestyle disorders, exposure to pollutants, and prevalence of *Helicobacter pylori*

infections can cause a disbalance in the cytoprotective mechanisms and lead to production of highly reactive and cytotoxic oxidative products like ketones, epoxides, and reactive aldehydes. These compounds trigger the formation of DNA adducts including malondialdehyde-deoxyguanosine, advanced lipid peroxidation end products, and AGEs and promote the prognosis of gastric cancer [127]. Although genetic factors predispose to development of gastric cancer, the above factors play a significant role in its development and prognosis [128].

Unlike other types of cancers, the correlation between dietary factors and reduced risk of development of gastric cancers is well established by the World Cancer Research Fund/American Institute for Cancer Research (WCRF/AICR). The antioxidant activity of flavonoids like quercetin and naringin present in apples and grape fruit, respectively, can inhibit carcinogen-activating enzymes in case of gastric cancers. The metabolism of toxins into carcinogens due to the expression of CYP1A1 (cytochrome P450 enzyme) is also inhibited which prevents DNA damage [129]. In general, it is known that the phytochemicals downregulate the β-catenin phosphorylation to enhance the apoptotic pathways in events of gastric cancer and simultaneously upregulate the AMPK pathway to support cellular homeostasis [130]. A recent study indicated a strong expression of the MUC4 gene in human gastric cancers. It was reported that the antioxidant alpha-lipoic acid inhibits the binding of STAT3 to the MUC4 promoter region to suppress the MUC4 expression and hence significantly reduces the proliferation of gastric cancers [131]. The anthocyanin (delphinidin)-rich extracts of calafate berries also significantly reduces the viability and migration of stomach cancer cells [132].

ROS appear to be involved in the progression of tumor progression [133], and a healthy organism must therefore be endowed with an adequate cellular defense to eliminate these molecules of extreme toxicity. These antioxygenic defense mechanisms are more precisely known as the antioxidants [134].

3. Antioxidants in Cancer Therapy

According to Tang and Halliwell, an antioxidant is defined as any substance that slows down, prevents or inhibits the generation of a toxic oxidant, neutralizes those already produced by donating their own electrons, and thereby prevents the harmful chain reactions caused by these oxidants [135]. Under this definition, antioxidants are classified according to their mode of action, their cellular location, and their origin into endogenous, enzymatic and nonenzymatic, and exogenous [136]. In recent years, the topic of antioxidants has become more famous in modern society in cosmetics and nutrition, but the use of antioxidants is at the center of the scientific debate when it comes to prevention or supplementation in oncology therapy, with benefits, but also harmful effects being reported [137].

3.1. Antioxidants, a Protection against Cancer. Many researchers have confirmed the involvement of the free radicals and ROS in the pathogenesis of many cancers [81, 138, 139], so it is logical to think that the alternative medicine of antioxidants acts in the prevention of this disease. Beyond their ability to trap ROS, antioxidants exhibit anticancer activities by increasing the immune response, stimulating cancer recessive genes, decreasing oncogene expression, or inhibiting tumor angiogenesis [140]. Below, we provide a summary of the strong evidence supporting the protective effect of the different classes of antioxidants.

3.2. Endogenous Enzymatic Antioxidants

3.2.1. Superoxide Dismutase (SOD). The superoxide dismutases, which make a class of metalloproteins, are one of the most effective antioxidant enzymes. In mammals, there are three isoforms, each of which has a metal ion as a cofactor: the cytosolic Cu/Zn-dependent SOD, the manganese mitochondrial SOD, MnSOD, and the extracellular Cu/Zn-SOD [141]; these differ in the chromosomal location of the gene, the nature of the active site metal, their quaternary structure, their cellular localization, and other characteristics [142], but they all catalyze the dismutation of the highly reactive superoxide anions to oxygen and the less reactive (but potentially toxic) hydrogen peroxide [143, 144]. SOD must therefore work in conjunction with other enzymes such as the iron-cofactor catalase and glutathione peroxidase, to eliminate the formed hydrogen peroxide [145].

There are numerous studies that have showed that the expression and enzymatic activities of all the three SOD isotypes are at a significant decrease across the majority types of cancers: CuZnSOD (SOD1) activity is decreased in breast carcinoma [146], gastric adenocarcinoma [147], and hepatocarcinogenesis [148] and MnSOD (SOD2) expression is downregulated in the ductal carcinoma tissues in patients with breast cancer [149] and skin cancers [150] and displays low levels which correlates with pancreatic cancerous tumor growth [151] and other primary ovarian and prostate tumors [152]. Extracellular SOD (SOD3) expression is downregulated in lung carcinomas [153] but also in prostate pancreatic, thyroid, or colorectal cancers according to Griess et al. [154]. Moreover, Bonetta [155] provides in a recent descriptive review evidence of multiple studies the relevance of MnSOD gene therapy [156] or of synthesized SOD mimetics in cancers [157, 158].

The diminished activity of SOD is associated with the destructive effects of O_2^- superoxide which by way of deprotonation of serine or threonine residues contribute to the accelerated rates of phosphorylation in many oncogenic signaling processes with subsequent antiapoptotic effect and tumoral progression [154].

The downregulation of MnSOD expression has been associated with changes in gene regulation mechanisms, such as altered DNA methylation patterns that involve abnormalities in transcription factor binding, such as the widely studied Sp1/Sp3 [159, 160], or decreased histone acetylation [161]. The aberrant DNA methylation, which can occur as either global hypomethylation in the early phase of neoplasia or regional hypermethylation of normally unmethylated CpG sites has been previously showed to be induced, among others, by reactive oxygen species and their derivatives DNA damage [162–164]. On the other hand, Robbins and Zhao

[159, 165] describe the antitumoral effect of MnSOD overexpression in a multistage skin carcinogenesis mouse model that was found in a previous study by [150], as involving suppression of activator protein-1 (AP-1) a transcription factor regulating oncogenic signaling. At the same time, the dimer AP-1 function depends on redox-sensitive Jun or Fos-type subunits and their phosphorylation states, which suggest the antioxidant capabilities of MnSOD in tumor suppression [159].

In light of these multiple results, the importance of SOD as a tumor suppressor seems well justified, in particular of MnSOD, whose active role in protecting mitochondria against increased oxidative stress may prevent defects in mitochondrial function that would lead to the development and progression of cancer [166].

However, there is yet a "puzzling dichotomy" on SOD role in cancer [167], as clinical and experimental studies bring enough evidence on unexpectedly high levels/activity of SOD in tumoral tissues [168–170]. In the most recent study on the antioxidant enzyme dichotomy, Gaya-Bover et al., assessed by western blot the levels of MnSOD, CuZn-SOD, CAT (Catalase), GPx, and other proteins both in tumor and nontumor adjacent tissue from colorectal cancer patients found that nontumor adjacent tissue of had higher levels of antioxidants enzymes that detoxify H_2O. However, tumor tissues showed higher levels of MnSOD and acetylated MnSOD that actually increased in stages II and III compared to stage I of malignancy and precancerous stage [171]. Palma et al. state that SOD2 undergoes a change of roles from a suppressor of tumor initiation to actually promoting tumor progression towards more malignant phenotypes, once the disease is established [167]. This observation is further contextualized by Kohan et al., when referring to the importance of aerobic glycolysis in tumor cell survival [168]. Thus, the MnSOD upregulation suppresses mitochondrial oxidative phosphorylation and leads to the activation of AMPK (AMP-activated protein kinase) that triggers the Warburg effect switch to glucose metabolization via glycolysis [168]. The glycolytic phenotype switch of the malignant cells is regarded as an adaptive advantage that decreases dependence on mitochondrial respiration and enables them to proliferate and invade into the peritumoral normal tissue [172].

3.2.2. Catalase (CAT).

Catalase, a heme oxidoreductase, strongly expressed in the liver, erythrocytes, and lungs [173] and located mainly in the peroxisomes [174] is composed of four polypeptide chains and contains iron atoms within the heme, which constitute the active sites of the protein [175]. The dismutation of the hydrogen peroxide by catalase happens with the heterolytic cleavage of the O-O bond of the hydrogen peroxide by the iron atoms of the heme group, thereby creating a water molecule and a highly oxidizing FeIV=O bond [143, 144]. The latter can oxidize a new molecule of hydrogen peroxide, generating dioxygen.

Catalase uses only H_2O_2 as a substrate and functions when it is present at high concentrations above physiological conditions; it does not eliminate all of the hydrogen peroxides and is quantitatively less effective than the glutathione peroxidase [176].

The overexpression of catalase in breast cancer cells MCF-7, a human-derived breast cancer cell line, not only impaired the proliferation and migration of the cancer cells but also improved sensitivity to anticancer treatments like doxorubicin, cisplatin, and paclitaxel when compared to parent cells and raised the resistance to the prooxidant combination ascorbate and menadione (Asc/Men) [177]. The elevated catalase activity confers strong protections against cancer by reversing the malignant phenotype via decreasing the cellular levels of ROS production (mainly H_2O_2) [177]. The high activity of CAT and when combined with chemotherapeutic drugs especially cCisplatin, 5-fluorouracil, and hydroxyurea correlate with decreased aggressiveness and suppress the proliferation of small lung cancer cell lines—A549 compared to untreated cells [178]. CAT treatment leads to disturbing the antioxidant defenses pathway and then a high production of intracellular H_2O_2 that could be responsible for the transcription factors NF-κB inactivation associated with promotion of tumorigenesis in A549 cells [178]. Bracalante et al. demonstrated that overexpression of catalase downregulates cell proliferation and reversed the amelanotic phenotype in clones A7 of the human A375 amelanotic melanoma cells compared with the parental cell lines [179]. A7 increased basal levels of hydrogen peroxide and as a result upregulated genes of the antioxidant system (AOS) induced and increased the ability of these cells to respond to oxidative stress, and then reduced the ROS levels, leading to less aggressive tumor cells [179].

The transfected RASMC vascular smooth muscle cells with AdCAT construct containing the human CAT (50-100-fold excess) reduced proliferation and DNA synthesis with increased spontaneous apoptosis through a COX-2-dependent mechanism compared with the corresponding parental cells [180]. The cell survival and the apoptosis resistance in RASMCs were maintained by H_2O_2; it is a downregulation by catalase-suppressed malignant phenotype [180, 181].

3.2.3. Glutathione Peroxidase (GPx).

Glutathione peroxidase, a selenium-dependent enzyme, present in extracellular fluids, cytosol, and mitochondria [182], was first identified by Mills in 1957 for its antioxidant activity [183]. Unlike catalase, glutathione peroxidase reduces a wide variety of organic hydroperoxides (ROOH) and neutralizes H_2O_2 using the reduced glutathione monomer (GSH) as a proton donor cofactor (H^+), which is subsequently converted into oxidized glutathione (GSSG); ultimately, the reactions lead to the formation of assimilable molecules, a cysteine or disulfide bridge, water molecules, and alcohol [144, 184].

Increased GPx levels were observed in many tumor cells, such as the oral squamous cell carcinoma (OSCC) [185], lung [186], colorectal [187], breast [188], and brain tumor [189] patients, compared with healthy controls. This can be explained by the fact that the tumor has high levels of oxidative stress; the body increases then the antioxidant system levels to compensate the increased levels of ROS as a natural defense against cancer [190]. Adenovirus-mediated human glutathione peroxidase gene (AdGPx) overexpression reduced the growth of pancreatic cancer cells in vitro and in vivo models. In vitro AdGPx enhanced the tumor-

suppressive effect of AdMnSOD; their combination slows the MIA PaCa-2 cells growth by 71% compared to parental cells. While after AdMnSOD and AdGPx injection into nude mice either alone or in combination showed a greatest effect by decreasing the tumorigenicity of pancreatic tumor cells [191]. The GPx increase is related to a H_2O_2 increase or other hydroperoxides caused by overexpression of MnSOD; the GPx activity neutralizes the increased hydrogen peroxide levels caused by overexpression of MnSOD to maintain intracellular homeostasis [191–194]. In addition, a high GPx expression drastically impeded tumor growth of weakly tumorigenic L929 fibrosarcoma cells injected subcutaneously into nude mice and increased the sensitivity of strongly tumorigenic B16BL6 melanoma cells to an angiodestructive therapy [195]. GPx4 inhibits tumor angiogenesis and malignancy through blocking eicosanoid synthesis, including COX-2, prevented TNF-mediated activation of cytokine-driven NF-κB and prostaglandin PGE2 production and abrogated PGE2-dependent COX-2 expression [195].

3.3. Endogenous Nonenzymatic Antioxidants

3.3.1. Bilirubin. The final product of the catalytic degradation reaction of heme and hemoglobin proteins by reticuloendothelial cells in the presence of two enzymes, heme oxygenase and biliverdin reductase [73], is considered a very important physiological antioxidant [196]. Bilirubin is remarkable for its powerful antioxidant potential against peroxyl radicals (ROO$\cdot$) and hydrogen peroxide [197, 198].

Due to its double action as a powerful antioxidant and as a prooxidant, bilirubin has been shown to have anticancer activity in both in vitro and in vivo, depending on the concentration and the cell type exposed to this pigment [199–202]. Emerging studies have suggested that serum bilirubin levels were negatively correlated with cancer risk and to cancer mortality [203–207]. In vitro, a 48 h treatment with a concentration of 10 μg/mL of bilirubin induced antiproliferative behavior in TMK-1 human gastric carcinoma cell line with a decrease close to 50% in cell population versus control and increased by more than twofold the intracellular radical levels after 6 h-24 h of incubation while no change was observed in control [202]. Bilirubin also caused a dose-dependent decrease (0–50 μM; for 48 h) in cell viability of colon adenocarcinoma cell lines [208]. The defense mechanisms by which bilirubin exhibits antitumor properties can be explained by the induction of prooxidant effects, apoptotic action, arresting cell cycle, and disrupting mitochondria dysfunction [202, 208].

In vivo, an intraperitoneal injection of 25 mg/kg of bilirubin in BALB/c nude mice bearing HRT-18 colon cancer xenografts increased plasma bilirubin levels around 35–40 mM and dramatically slower the tumor growth when compared to the control phosphate-buffered saline. The bilirubin exert anticancer activity by halting cell cycle progression at G1 phase through inducing p53 and the activation of MAPK/ERK-dependent p27 pathway which inhibits the activation of cyclin E/CDK2 and/or cyclin D/CDK4 complexes [209]. The same study describes an in vitro bilirubin dose-dependent model using multiple cell lines; at a lower dose (5 mM), bilirubin

inhibits cell proliferation of hepatocellular carcinoma HepG2 and NIH/3T3 immortalized mouse; the antiproliferative behavior of MDA-MB 231 human mammary gland ductal carcinoma cells, pancreatic PANC-1, malignant melanoma WM 266.4 including colonic HRT-18 studied in vivo can only be obtained in a concentration $\geq 25 \mu$M. The antioncogenic effect of bilirubinin was found to be partially dose dependent; at a high concentration, it acts as a proapoptotic factor in the tumor environment [209].

3.3.2. Coenzyme Q_{10} (CoQ_{10}). Coenzyme Q_{10}, known as ubiquinone, is a hydrophilic compound essential for the transport of electrons in the mitochondrial oxidative chain [210, 211, 298]. It is found in cell membranes, plasma, and lipoproteins where it acts as an antioxidant by trapping $RO_2\cdot$ radicals, thus inhibiting lipid peroxidation [198].

Because of its double role as a potent antioxidant molecule and as redox status at the mitochondria [213], the coenzyme Q has been proposed to have therapeutic potential for the treatment of several types of cancer [214–216]. Coenzyme Q_{10} deficiency has been reported in many cancer patients. A decreased mean value of blood vessels of coenzyme Q_{10} have been found in patients with breast and myeloma cancer compared to healthy controls [217]. In vitro, the response of PC3 human prostate cancer cells towards CoQ_{10} was markedly different compared to PNT2 human prostate nonmalignant cells. A 24 h incubation of cancer cells with different concentrations of coenzyme Q_{10} (50, 100, and 250 μM) significantly lowered cancer cells grow PC3 with no change on PNT2 noncancer cells compared to the control; the results showed also a greater free radical generation in PC3 [213]. Apparently, the abundance of ROS can explain the antitumor potential of CoQ_{10}; the cancer cell killing was found to be on Ros-induced cytotoxicity dependent through apoptosis, necroptosis, and autophagic cell death [218]. At high concentration, the CoQ_1, an analog of CoQ_{10}, showed remarkable antiproliferative effects in HepG2 human hepatocellular cancer cells. Although CoQ_1 was slightly more toxic to Hep G2, the anticarcinogenic effect of CoQ_1 can be attributed to its antimetabolite and cytotoxic activities, which disrupt normal biochemical reactions [219, 220].

Another analog of CoQ_{10} appears to be involved in the antitumor defense, the coenzyme Q_0 (2,3-dimethoxy-5-methyl-1,4-benzoquinone) decreased cell viability of A549 adenocarcinoma human alveolar basal epithelial cells and show a strong cytotoxicity towards both breast cancer cell lines MDA-MB-231 by arrest of G0/G1-phase cell cycle and S-phase cell cycle arrest in SKBr3 cells by inducing apoptogenic phenotype and promoting cell death [221, 222]. The anticancer efficacy and the cytotoxicity of the CoQ analogs can be also chain length dependent; the antiproliferative activity of CoQs was found to be negatively correlated with the length of CoQ's isoprenyl side chain [222].

In vivo supplementation with CoQ_{10} (0.4 mg/kgG1/day) has a therapeutic effect against hepatocellular neoplasia HCC induced by toxic agents such as trichloroacetic acid (TCA) in male Sprague-Dawley rats; these compounds exert a carcinogenic action by increasing oxidative stress, lipid peroxidation, and inflammation. The administration of CoQ_{10}

ameliorated the histopathological dysplastic changes, prevented the reduction of GSH and SOD activity, and significantly attenuated the expression of the nuclear factor-κB signaling pathway which enhances the transcription of TNF, iNOS, and COX-2 genes; CoQ_{10} reduced significantly both hepPar-1 and AFP immunomarkers of tumor in the liver cells of rats [223]. The CoQ_{10}-glucan synergies showed a high metastatic activity in Balb/c mice implanted with Ptas64 mammary carcinoma; the volume of tumors (mm^3) after CoQ_{10}-glucan supplementation was two times smaller than supplementation with glucan alone; the CoQ_{10} seems to reinforce the capacity of glucan to half the development of tumor through the stimulation of innate immune cells such as macrophages, dendritic cells, granulocytes, and natural killer cells and activation of mitogen-activated protein kinases (MAPKs) and nuclear transcription factor NF-κB p6512 [224, 225].

3.3.3. Melatonin.

Melatonin or N-acetyl-5-methoxytryptamine is a neurohormone mainly secreted by the pineal gland, but also in extrapineal organs including the retina, gastrointestinal tract, skin, bone, marrow, and lymphocytes, with an insignificant systemic contribution, and is synthesized from N-acetylation, followed by methylation of serotonin in the absence of light through the use of a methylation factor. It is synthesized by N-acetylation, followed by methylation of serotonin in the absence of light through 2 transferases: arylalkylamine-N-acetyltransferase (AANAT) and 5-hydroxy-indole-methyltransferase (5 HIOMT). Its first role was discovered in interaction with its organ of origin the pineal gland and was linked to its neuroendocrine function, in particular to the hypothalamo-pituitary-gonadal axis. A second obvious functional role of melatonin is involved in the synchronization of the sleep/wake cycle (chronobiotic role) [226]. Besides these functions, melatonin has been shown to act as a free radical scavenger and a potent endogenous antioxidant [227]. In *in vitro* cell-free systems, Tan et al. showed that melatonin (IC50 = 21 μM) quenches 50% of the adducts (DMPO-· OH) generated following exposure of H_2O_2 to ultraviolet light, five times more than GSH (IC50 = 123 μM) and thirteen times more than mannitol (IC50 = 283 μM) [228]. A structure-activity relationship was thus established, among the 3 indoleamine analogues of melatonin, 5-hydroxytryptamine (5-HT) lacking the methyl group in the 5-OH position of the indole ring and the acetyl group linked to the N position of the side chain; in N-acetyl-5-hydroxytryptamine (NA-5-HT) lacking the methyl group in the 5-OH position and 5-methoxytryptamine (5-MT) lacking an acetyl group in the N position of the side chain, only 5-MT reduced the formation of the adduct DMPO-· OH adduct with an efficiency lower than 60% of that of melatonin at high concentration [229]. These data show that the methyl group located at the 5-OH position of the indole ring of methionine gives it an important capacity for its hydroxyl radical trapping function, while the N-acetyl group produces a synergistic action. The melatonin (IC50 = 1.5 mM) has also been found to neutralize directly the nitric oxide generated by 1-hydroxy-2-oxo-3-(N-methyl-3-aminopropyl)-3-methyl-1-triazene (NOC-7) in a dose-dependent manner and more effectively than

N-acetylserotonin (IC50 = 20 mM), 5-hydroxytryptophan (IC50 = 15 mM), L-tryptophan (*IC*50 = 40 mM), and serotonin (IC50 = 8 mM), with a large biomolecular rate constant of 3.0×10^7 m^{-1} s^1. This potent ability to lower NO- concentrations can be explained either by direct scavenges or incapacitating its production while inhibiting its synthesis by lowering the activity of the prooxidative enzyme NO synthase [230]. This free radical scavenging ability extends to other radicals as well. Melatonin (ORAC peroxyl = 2.04) was found to be twice as effective as Trolox (ORAC peroxyl = 1.00) and vitamin C (ORAC peroxyl = 1.12) and three times more effective than reduced glutathione (ORAC peroxyl = 0.68) in detoxifying the peroxyl radicals ROO· generated by Azobis (2-methylpropionamidine)dihydrochloride (AAPH) [231]. Additionally ORAC-OH shows also that melatonin was 2-fold efficient than Trolox and 8-fold than dopamine, with GSH as a prooxidant [232]. Adding to its radical scavenging ability, melatonin also stimulated the levels of several antioxidative enzymes, including SOD, glutathione peroxidase, glutathione reductase, and catalase [233]. Melatonin administration (10 mg/kg) increased superoxide dismutase, GSH system like GPx, and catalase activities with a tissue-dependent degree and reduced MDA+4 HDA lipid peroxidation markers in the kidney, liver, and brain homogenates compared to the group of rats receiving twice weekly for 3 months 10 mg/kg of benzo(a)pyrene B(a)P alone [233]. A similar response was observed in xenografts (induced by the CT26 cell line) in BALB/c mice. Melatonin showed radioprotective action at 20 mg/kg in the lung and cardiac tissues after a single 5 Gy gamma ray exposure by stimulating GPx and SOD activities and depleting MDA level [234]. Melatonin not only upregulates antioxidant enzymes but also downregulates prooxidant enzymes such as myeloperoxidase, nitric oxide synthase, and eosinophil peroxidase [235, 236]. Also, AMK melatonin metabolites generated via the kynuric pathway acted as antioxidants and thus slowed down the prooxidative enzyme nitric oxide synthase (iNOS) [237, 238]. Another benefit of melatonin was recorded in the brain of rats treated with kainic acid, a neuronal excitotoxin. Melanonine played a protective role against DNA damage, by reducing the increase in oxidative marker 8-hydroxy-2-deoxyguanosine (8-OHdG) in both the frontal cortex and hippocampus. The proposed mechanism through which melatonin protects DNA from KA damage may be associated with nitric oxide (NOS) inhibition [239].

Melatonin has many therapeutic properties in the treatment of cancer through several mechanisms, including inhibiting cancer cell proliferation, decreasing oxidative stress, and increasing immune system activity. Liu et al. reported that 2 mM melatonin attenuates the proliferation of the MFC gastric cancer cell line in mice, by upregulating the mRNA expression of the transforming growth factor-β1 (TGF-β1) in tumor tissues. TGF-β1 has been shown to suppress tumor development in a time- and dose-dependent manner, by blocking the cell cycle (G1-phase arrest), via increasing cyclin-dependent kinase (cdks) inhibitor levels [240, 241]. This report was corroborated by Bizzarri et al. At physiological concentrations, the synergy of melatonin with low noncalcemic doses of 1,25-(OH) 2D3 significantly

inhibited the proliferation of rat RM4 breast cancer cells in the presence of estrogen by enhancing the TGF-β1 effect [242, 243]. In hepatocellular carcinoma, melatonin showed significant tumor growth inhibition both *in vitro* and *in vivo*. The melatonin potentiates sorafenib-induced apoptosis in 3 hepatoma cell lines HepG2, HuH7, and Hep3B via synergistic activation in a dose- and cell type-dependent manner, by enhancing ROS production, proapoptotic genes PARP hydroly and Bax, reducing the amount of mt-DNA in treated cells, and mitophagy-mediated by mitochondria and lysosome colocalization, rising the expression of mitophagy markers PINK1 and Parkin by downregulating heat shock protein 60 (Hsp60) [244]. Similar results were found *in vivo*; melatonine increased the therapeutic potential of mesenchymal stem cells (MSCs) in adult female rats after diethylnitrosamine- (DEN-) induced hepatocellular carcinoma (HCC). Melatonin thwart HCC carcinogenicity by inhibiting oxidative stress designated by the decrease in malondialdehyde levels and the increase in the activities of the enzymes superoxide dismutase, catalase, and glutathione peroxidase; inflammation by downregulating the expression of interleukin-1 beta, nuclear factor kappa B, vascular endothelial growth factor, and matrix metallopeptidase 9 genes; and upregulated expression of metalloproteinase inhibitor 1 gene, and induction of apoptosis indicated by increased activity of cleaved caspase-3 and Bax genes and downregulated expression of antiapoptotic genes Bcl2 and survivin [245]. Moreover, Yun et al. investigated the prooxidant and apoptotic efficacy of melatonin in a wild-type human colorectal cancer cell line (SNU-C5/WT) in a dose-time-dependent manner. The result showed that melatonin lessened SNU-C5/WT viability, through enhancing superoxide generation and reducing cellular prion protein (PrPC) expression, as well as PTEN-induced kinase 1 (PINK1) levels. This advanced mitochondria-mediated apoptosis and endoplasmic reticulum stress. This study highlights the promising strategy to target colorectal cancer [246]. Into the bargain, (20 μg/mL) melatonin and (50 mg/j) capecitabine synergized together and improved survival and tumor growth inhibition *in vivo* in pancreatic tissue of male Syrian hamsters injected with the carcinogen N-nitroso bis(2-oxopropyl) amine (BOP), compared to capecitabine alone; this combination showed an upgrade in the antioxidant enzymes GSH, SOD, CAT, and GSH-Px activities and a retrogression of lipid peroxidation products [247].

3.4. Exogenous Antioxidants

3.4.1. Trace Elements

(1) Selenium. A mineral micronutrient with strong antioxidant activity, essential for the defense of the body against damage caused by oxidative stress [248, 249], was acquired through diet; selenium is located mainly in the liver, kidneys, blood, brain, heart muscle, and testes. As a cofactor, selenium is incorporated in the form of selenocysteine into selenium-dependent enzymes, such as the GPx; hence, its role in free radical scavenging [250]. Selenium is also an antagonist of many metals (As, Cd, Pb, and Hg) and is therefore likely to modulate their toxicity which causes oxidative stress, disruption of pigment function, and alteration in protein activity [251, 252].

The selenoproteins act as a defensive barrier against reactive oxygen species and inflammatory responses [131]. Several studies have described the potential of selenium in the induction of apoptosis and selective cytotoxicity to cancer cell lines derived from the lung, colorectal, breast, esophageal, stomach, and prostate [132, 253, 254]. Recently, a study suggested that intracellular selenium and cisplatin may act synergistically and modulate the transient receptor potential vanilloid 1 (TRPV1) cation channel. These channels are responsible for the regulation of body temperature and sensing scalding sensory stimuli in events of distress. Hence, to some extent, relief from cancer-associated pain is possible through the above synergistic therapy. Besides, they also reported an increase in apoptotic proteins and a reduction in cell viability in the MCF-7 breast cancer cell line cultures on treatment with selenium as well as selenium+cisplatin. Also, an increase in ROS occurs on the use of chemotherapeutic agents including cisplatin. Selenium being an antioxidant overcomes the side effects of chemotherapy in general [255]. As a part of the recent development in cancer treatment, selenium-based nanobiocomposites of L-asparaginase have also been constructed which act as improved drug delivery systems with intact antioxidant function. Thus, it opens new dimensions to cancer therapy [256].

(2) Zinc. Zinc is the second most abundant elemental trace element in the body after iron, mainly found in bones, muscles, and liquids rich in proteins (plasma or cerebrospinal fluid) [257]. With indirect antioxidant property [258], this mineral participates in the structure or the regulation of more than 300 enzymes, in particular the antiradical enzymes involved in the protection against the toxic derivatives of oxygen, such as the superoxide dismutase [259]. Thus, the catalytic complexes that zinc and thiol groups form have been observed to stabilize and protect proteins against oxidation [260]. Zinc is also involved in maintaining the tissue functional levels of metallothionein, a molecule potentially capable of trapping free radicals [261].

Well-established evidence suggests decreased activity of ZIP1 (SLC39A1)-zinc uptake transporter in malignant cells. Although this indicates that zinc deficiency may be a triggering factor for cancer development, more studies are required to sustain the claim with absolute certainty [262]. However, zinc deficiency is strongly associated with esophageal squamous cell carcinoma, prostate cancer, and colon cancer [263]. It is also noted that zinc deficiency prominently causes oxidative DNA damage and simultaneously impairs the DNA repair ability in cells leading to increased frequency of mutations [264, 265]. The anticancer activity of zinc is associated with its significant role in promoting transcription factors for cellular propagation, antioxidant defense system, and DNA repair [263]. In prostate cancer, the modulation of cancerous cell growth is observed in the LNCaP cell-line with increased zinc supplementation. This is associated with the

activation of the ERK1/2 phosphorylation and reduction in VHR phosphatase and ZAP-70 kinase levels that together result in antiproliferative activities of zinc [266].

(3) Copper. Copper plays multiple roles in the metabolism of carbohydrates, lipids, and proteins, in the maintenance of bone mass and cartilages, and in the synthesis of hemoglobin and also contributes to immune defenses and the fight against the phenomenon of oxidation and aging [267–272]. In this regard, copper is a powerful antioxidant stimulating the activity of SOD, cytochrome C oxidase, and dopamine β-hydroxylase [73, 273].

Elemental copper is reported to be a strong modulator for the expression of several growth factors including vascular endothelial growth factor (VEGF), interleukins, and oxidative phosphorylation. Thus, it stimulates angiogenesis, cellular proliferation, migration, and oxidative stress. Hence, the anticancer therapies are largely based on anticopper (copper chelation) treatment approach, especially for metastatic cancers [274]. Copper complexes, on the other hand, show a spectrum of activities depending on the ligands attached to it and have been associated with both mitotic and apoptotic cancer cell deaths. The copper complexes prepared with N-benzyl 2-(diethyl amino) acetamide and 2-(diethyl amino) N-phenyl ethyl acetamide have shown anticancer activity in the U87 and HeLa cell lines [275]. The mixture of dithiocarbamates and copper salts react with cellular copper to form a proteasome that is responsible for inducing apoptosis [276] and also dismutates superoxides into harmless compounds [277]. Thus, they are emerging as promising metal-based cytotoxic agents for cancer therapy.

3.4.2. Vitamins

(1) Vitamin C. Vitamin C (ascorbic acid; $C_6H_8O_6$) is a heat and thermo labile antioxidant [278] that represents the most important line of defense against oxidative stress in extracellular fluids, acting as an antioxidant and cofactor in oxygen-catalyzed hydroxylation reactions [279]. It is a powerful scavenger of the ROS including the superoxide anion, singlet oxygen, H_2O_2, NO, and OH [280]. The antioxidant role of vitamin C is based on the inhibition of lipid peroxidation by reducing the oxidized vitamin E after its reaction with lipid radicals, generating the ascorbyl radical, which can be reduced by glutathione-dependent enzymes [281]. Vitamin C protects biomembranes and lipoproteins [282].

Dietary supplementation of vitamin C has been associated with improved patient outcome in advanced cancers of breast and pancreas [283]. Moreover, a synergistic action of ascorbic acid and anticancer agents like etoposide, cisplatin, and doxorubicin has also been reported. In 2015, a study reported selective death of cells with KRAS or BRAF mutations in human colorectal cancer cells. Interestingly, the dehydroascorbate (oxidized form of ascorbate) was found to compete with GLUT1 transporter (for glucose uptake) and reduced to ascorbic acid inside the cancer cells. The increased uptake of DHA and the subsequently increased concentration of vitamin C inside the cells can thus be correlated to death of cells undergoing above mutations [284]. Vitamin C-associated tumor inhibition and reduction in tumor aggressiveness have also been reported in gastric cancers [285].

(2) Vitamin E. The liposoluble vitamin E is the most important antioxidant of the hydrophobic interior sites of cell membranes [286]. Under this designation, the tocopherol and tocotrienol families are grouped, with alpha-tocopherol as the most abundant and most biologically active form [146, 287, 288]. This lipophilic antioxidant has the capacity of trapping and neutralizing free radicals such as lipoperoxides, forming nontoxic tocopheryl radicals and interrupting the lipid oxidation chain [73], and also increasing the activity of antioxidant enzymes such as SOD, GPx, catalase, glutathione transferase, and NAD(P)H reductase [289].

Vitamin E has been, most convincingly, identified as a potential adjuvant in the treatment of cancers. Dietary deficiency of vitamin E in generalized populations of Northern Europe and USA and their increased risk of colon and prostate cancer are clearly evident from epidemiological studies in literature [290, 291]. They also promote apoptosis and inhibit angiogenesis by modulating the immune system and structural proteins like sphingolipids and collagen [292, 293]. Moreover, vitamin E stimulates the p53 tumor suppressor gene and simultaneously downregulates mutant p53 proteins [294]. Vitamin E as well as its natural and synthetic isoforms exhibits strong antioxidation potential which further aids in therapies to overcome the side effects of anticancer drugs. Together, these factors prevent cancer development and proliferation [295].

An excellent experimental illustration of the antioxidant protective effect of vitamins and minerals was the famous French study started in 1994, Supplements in Vitamins and Minerals Antioxidants (SU.VI.MAX), a double-blind trial on 5034 men to test the impact of a daily intake of vitamin and mineral antioxidants in reducing the occurrence of prostate cancer. A supplement consisting of a combination of antioxidants at physiological doses of synthetic beta-carotene (6 mg), tocopherol (30 mg), vitamin C (120 mg), selenium (100 μg), and zinc (20 mg) or one placebo capsule was administered daily for 8 years. Overall, there was a moderate, nonsignificant reduction in the incidence of prostate cancer associated with supplementation; however, the effect was significantly different concerning the PSA (prostate-specific antigen). In men with normal initial PSA (<3 ng/mL), the supplement was associated with a significantly reduced rate of prostate cancer, which would support the consumption of antioxidant vitamins and minerals as a method of chemoprevention of prostate cancer [296].

Examining the relationship between MnSOD polymorphisms, a putative risk factor for prostate cancer, and status of exogenous dietary antioxidants—selenium, lycopene, a-tocopherol, and g-tocopherol—in modifying prostate carcinogenesisprocess in 567 cases and 764 controls, Li et al. [297] demonstrated that the combined status of the mentioned antioxidants is inversely associated with the risk of prostate cancer in patients with MnSOD polymorphism.

3.4.3. Polyphenols.

Polyphenols comprise more than 8000 hydrosoluble organic compounds, synthesized as secondary metabolites by plants [298, 299]. They are subdivided into several chemical groups and are characterized by the presence of at least two phenolic groups, one of which is directly associated with hydroxyl functions or engaged in another function: ether, ester, and heteroside [300]. Polyphenols are considered powerful antioxidants that prevent oxidative damage by not only trapping hydroxyl radicals, superoxides, and nitrites [301] but also by chelation of transition metals such as iron and copper essential catalysts of redox reactions [302], or by the inhibition of enzymes that produce free radicals [303, 304].

In the EPIC meta-analysis of data obtained from dietary questionnaires of 345,904 people, from seven European countries over a period of six years, Boeing et al. reported a significant inverse association between total fruit and vegetable consumption and risk of cancers of the upper aerodigestive tract of the oral cavity, pharynx, esophagus, and larynx at an 80 g/day intake [305].

Plant flavonoids are considered preventive therapies against cancer [306], and this important role of flavonoids was supported by the results of a recent study of Bondonno et al. analyzing the Danish nationwide dietary behavior over a 23-year period [307]. The researchers noted that a moderate intake of flavonoids was inversely associated with all-cause mortality including the cancer-related mortality, with the strongest associations between flavonoids and mortality being observed in high-risk populations of smokers and high alcohol consumers [307].

Quercetin is a unique flavonoid because of its biphasic oxidation properties. At cell concentrations in the 1-40 mM range, quercetin acts as an antioxidant and thus reduces the ability of ROS to damage cellular DNA [308], whereas at doses above 40 mM, quercetin acts as a prooxidant generating ROS which exert cytotoxic effects on the tumor [308]. Quercetin significantly inhibits NF-κB nuclear factor-kappa B activity activated by ROS [308–311]. The NF-κB is a master regulator of many genes involved in the carcinogenesisprocess through promotion of inflammation, cell growth, differentiation, and angiogenesis [312]. Its activation may regulate the production of prostaglandins via the gene cyclooxygenases-2 (COX-2), which promotes both angiogenesis and metastasis in certain tumor models, potentially through the regulation of vascular endothelial growth factor (VEGF) and MMPs [313–316]. NF-κB mediates a crosstalk between inflammation and the accumulation of proinflammatory cytokines cytokines such as TNF-alpha, and IL-6 in a tumor microenvironment with elevated NF-κB activity leads to the protumorigenic microenvironment [312]. The NF-κB is therefore a promising anticancer therapeutic pathway; the suppression of NF-κB leads to tumor regression [312]. Min and Ebeler revealed that treatments with 1 mM quercetin prevent H_2O_2-induced DNA oxidative damage in Caco-2 human epithelial colorectal adenocarcinoma cells by improving the DNA repair process [317]. Moreover, the same researchers observed that treatment with quercetin (1-100 μM) induces the expression of the mRNA of human 8-oxoguanine DNA glycosylase (hOGG1), an enzyme involved in the DNA repair [317]. In addition, quercetin has been shown to inhibit cell proliferation in the human breast carcinoma cell line MCF-7 by inhibiting cell cycle progression at G2 and M phases, in addition to induction of the apoptosis pathway [318]. This mechanism involved was the inhibition of cyclin B1-Cdc2 kinase enzymatic complex activity [318], critically involved otherwise in the unfolding of early mitotic events [319].

4. Nanoantioxidant Strategies

In spite of the anticancer effectiveness of antioxidants, they remain a growing challenge for clinicians due to their instability, limited bioavailability, poor solubility, and low selectivity, which limit their therapeutic uses in cancer. To overcome these pharmacokinetic limitations, a promising nanotechnology offers the possibility of delivering bioactive compounds directly into tumor tissues, and therefore providing their maximal anticancer therapeutic activities. A variety of novel nanoantioxidant-based delivery systems to target cancer have been reported [320].

4.1. Lipid-Based Nanoparticles.

Solid lipid nanoparticles (SLNs) are the novel generation of submicron-sized colloidal nanocarriers ranging from 50 to 1000 nm where the liquid-lipid has been replaced by a solid-lipid such as mono-, di-, or triglycerides, phospholipids, lipid acids, glyceride mixtures or waxes, and cholesterol and surfactants. SLNs offer relevant characteristics such as site-specific targeting, long-term physical stability, large surface area, and low toxicity and therefore have immense antiproliferative potential in cancer therapy by delivering antioxidant drugs incorporating them into the SLN formulation in order to improve the drug pharmacokinetics and/or reduce their toxicities [321]. The SLNs-antioxidant contributions have been reported in curcumin, a natural antioxidant compound with anticancer potential [322]. Wang et al. showed that curcumin- (cur-) loaded SLNs exhibited higher antiproliferative activity in a dose-dependent manner and induced strong cytotoxicity and apoptosis by enhancing ROS production in SKBR3 cells, resulting in a decrease in the Bax/Bcl-2 ratio, as well cyclin-dependent kinase 4 (CDK4) and cyclin D1 expression compared to free curcumin. These findings indicate that cur–SLNs might be an efficient chemodrug against breast cancer [323]. Similar to this, the incorporation of sesame into SLNs showed its ability to induce the normalization of skin cancers after [324].

4.2. Micelles.

Micelles are defined as the self-assembly of colloidal nanometries (diameter less than 50 nm) and consist of a hydrophobic core and a hydrophilic shell and are therefore used to transport hydrophilic and lipophilic molecules. Their surfactant structures can be aggregated by cationic, anionic, zwitterionic, or nonionic groups depending on the nature of the head groups, their origin, and the length of the alkyl chains. These polymers have been considered promising nanocarriers in cancer clinical trials for their capacity, critical size, drug incorporation efficiency, stability, and release rate [325]. Quercetin-loaded polymeric micelles showed significant antiproliferative and apoptotic potential in vivo and

in vitro in CT26, PC3, and H22 tumor-bearing mice, enhanced cytotoxicity in the MCF-7 human breast cancer cell line, and improved drug accumulation in the A549 cancer cell line and murine xenograft model [326]. Furthermore, Hasegawa et al. demonstrated that administration of catechol in micelles thwart cancer by inhibiting ROS-mediated angiogenesis and thus the formation of capillary networks in the tumor tissue environment in the chicken ex ovo chorioallantoic membrane assay [327].

4.3. Cyclodextrin. Cyclodextrins are cyclic oligosaccharides formed from α-(1,4)glycosidic units by the enzymatic degradation of starch by cyclodextrin glucanotransferase, resulting in a toroidal structure and are water soluble in nature with a hydrophobic core 0.5 to 1.0 nm in diameter and a hydrophilic outer surface. The cyclodextrin complex confers high aqueous solubility, dissolution rate, and bioavailability to poorly water-soluble drugs. Their unique characteristics predispose them to applications in the design of an efficient cancer drug delivery system [320]. The encapsulation of vitamin E into the inclusion complex β-cyclodextrin (β-CD) showed fast dissolving nanofibers accompanied with efficient antioxidant properties and light and shelf stability compared to its uncomplexed form. Moreover, even after 3 years of storage, the vitamin E/HP-B-CD nanofibers preserved its antioxidant hallmark. Along the same lines [328], Dhakar et al. reported an improvement of water solubility and antioxidant property with no cytotoxicity of kynurenic acid (4-hydroxyquinoline-2- carboxylic acid, KYNA) loaded in cyclodextrin nanosponges compared to free kynurenic acid [329].

5. Antioxidants and Controversies

The antioxidants and ROS display yet controversial or contradictory roles in tumorigenesis, as ROS which more often are involved in tumor development and progression, are also toxic to cancer cells, and can potentially induce apoptosis at high levels [330], and conversely antioxidants may cause an increase in the risk of cancer [331].

Against the general opinion favoring the anticancer role of antioxidants, a 2014 study in mouse models of BRAF and KRAS oncogenes-induced lung cancer found that nutrient supplementation with the antioxidants N-acetylcysteine and vitamin E significantly accelerated tumor cell proliferation and growth by reducing ROS, damaging DNA and preventing tumor suppressor p53 activation [332], which leads to the cessation of its roles in the response to DNA damage such as DNA damage repair, cell cycle arrest, senescence, and apoptosis, all of which are in place to prevent mutations from being passed on down the lineage, its inactivation therefore promotes the development of many types of tumors [332–334].

The above study suggested that the antioxidants in lung cancer cells may downregulate the endogenous ROS defense through feedback mechanism on supplementation with N-acetylcysteine and vitamin E. As a result, a significant decrease can be noted in oxidative DNA damage, which in turn, suppresses the activation of the p53 gene. These outcomes were based on the findings that the antioxidant selectively supported proliferation of lung cancer cells with wild-type p53 and was not observed in cells with mutant or inactivated p53. In general, it is suggested that the continuous use of antioxidants like glutathione, superoxide dismutase, catalase, and thioredoxin may prevent the ROS levels from inducing anticancer mechanisms (mainly apoptosis) by keeping them in check [14]. Also, since tumor cells themselves produce antioxidants to overcome oxidative damage, the additional supplements may allow tumor cells to store surplus antioxidants and promote its survival and further proliferation [335]. A recent observational study of 2014 patients demonstrated an association between antioxidant supplements (including vitamins, carotenoids, and coenzyme Q_{10}) and increased risk for breast cancer recurrence and death [336].

In a large-scale research on the potential effects of daily antioxidant supplementation (120 mg of vitamin C, 30 mg of vitamin E, 6 mg of beta-carotene, 100 μg of selenium, and 20 mg of zinc) against the risk of skin cancers, with a median follow-up period of 7.5 years, Hercberg et al. reported more beneficial effects in men, whose prior antioxidant status was lower (for beta-carotene and vitamin C), but not in women, who had an increased rate of melanoma compared to the placebo group [337].

A meta-analysis of four randomized clinical trials involving 109,394 subjects investigating the effect of beta-carotene supplementation on the incidence of lung cancer among smokers and/or male asbestos workers surprisingly showed that high-dose beta-carotene supplementation (30 mg daily) related to tobacco was significantly associated with an increased lung cancer risk; a high concentration of beta-carotene in interaction with cigarette smoke promotes lung carcinogenesis by acting as a prooxidant exacerbating oxidative damage [338]. The reactive nitrogen species (RNS) found in the gaseous phase of cigarette smoke triggers the prooxidant behavior of β-carotene, generating wider range of oxidation products, including 4-nitro-β-carotene which induced more lipid peroxidation and DNA damage [339–342]. Besides the effect of high concentration, at a high partial pressure of oxygen, may also affect the antioxidants function of β-carotene in favor of prooxidant behavior due to autooxidation [343].

6. Conclusions

Under physiological conditions, both endogenous and exogenous antioxidants are undoubtedly important and interdependent to circumscribe the prooxidative damage of the ROS. Multiple factors ranging from genetics to imbalanced lifestyle can disrupt oxidative homeostasis leading to oxidative stress, high generation of reactive oxygen species (ROS), and free radicals that consequently assault the structure of DNA molecules, proteins, and increased lipid peroxidation. During these damaging processes, a variety of molecules are produced, including 8-OH deoxyguanosine, malondialdehyde, and 4-hydroxy 2-nonenal, participate to promote the risk of mutagenesis, and are significantly correlated with carcinogenesis.

As such, a strong enzymatic and nonenzymatic antioxidant defense system to efficiently scavenge the ROS and

prevent oxidative damage is essential in the prophylaxis against the development of cancerous processes. Numerous reports ranging from *in vitro* and animal experimental to clinical and large observational studies have shown the antitumoral efficacy of the antioxidants and the potential for reducing the side effects of the chemotherapy and radiotherapy regimens. The use of conventional antioxidants-free therapies has been limited in biomedical trials due to their poor permeation across cell membranes and cell internalization, easier degradation, and limited bioavailability. To overcome these barriers, a recent nanoantioxidant system may provide potential solutions to enhance antioxidant efficiency and to offer target delivery.

However, inclusion of antioxidants in cancer therapy is controversial due to their unpredictable interaction with chemodrugs. Furthermore, recent research has revealed the overconsumption of antioxidants (and in particular synthetic antioxidants) can promote the survival and growth of cancer cells; a phenomenon known as the antioxidant paradox. A high antioxidant supplementation that exceeds safe levels can cause "antioxidant stress" and can fuel the metastasis-promoting physiological imbalance. In light of all these data, great caution is advised in the use of large doses of supplements. The natural state of health is a question of balance. A balanced diet of antioxidants can thus hold the key to cancer prevention.

Data Availability

All data used is available on request.

Conflicts of Interest

The authors declare that there are no conflicts of interest.

Authors' Contributions

Kamal Fatima Zahra and Radu Lefter equally contributed to this manuscript.

References

[1] A. Paramanya and A. Ali, "Role of oxidative stress in biological systems," *Middle East Journal of Science*, vol. 5, no. 2, pp. 155–162, 2019.

[2] A. Ali, A. Paramanya, D. K. Prairna, and S. Zehra, "Antioxidants in glycation related diseases," in *Oxidative Stress and Antioxidant Defense: Biomedical Value in Health and Diseases*, M. S. Uddin and A. Upaganlawar, Eds., pp. 465–488, NOVA Science Publishers, Hauppauge, USA, 2019.

[3] Gbd 2015 Mortality and Causes of Death Collaborators, "Global, regional, And national life expectancy, all-cause mortality, and cause-specific mortality for 249 causes of death, 1980-2015: a systematic analysis for the Global Burden of Disease Study 2015," *Lancet*, vol. 388, no. 10053, pp. 1459–1544, 2016.

[4] D. M. Parkin, F. Bray, J. Ferlay, and P. Pisani, "Global cancer statistics, 2002," *CA: a cancer journal for clinicians*, vol. 55, no. 2, pp. 74–108, 2005.

[5] F. Bray, A. Jemal, N. Grey, J. Ferlay, and D. Forman, "Global cancer transitions according to the Human Development Index (2008-2030): a population-based study," *Lancet Oncol.*, vol. 13, no. 8, pp. 790–801, 2012.

[6] M. Maule and F. Merletti, "Cancer transition and priorities for cancer control," *The Lancet. Oncology*, vol. 13, no. 8, pp. 745-746, 2012.

[7] J. Shen, P. Deininger, J. D. Hunt, and H. Zhao, "8-Hydroxy-2′-deoxyguanosine (8-OH-dG) as a potential survival biomarker in patients with nonsmall-cell lung cancer," *Cancer: Interdisciplinary International Journal of the American Cancer Society*, vol. 109, no. 3, pp. 574–580, 2007.

[8] S. S. Khanzode, S. D. Khanzode, and G. N. Dakhale, "Serum and plasma concentration of oxidant and antioxidants in patients of Helicobacter pylori gastritis and its correlation with gastric cancer," *Cancer letters*, vol. 195, no. 1, pp. 27–31, 2003.

[9] N. Knoll, C. Ruhe, S. Veeriah et al., "Genotoxicity of 4-hydroxy-2-nonenal in human colon tumor cells is associated with cellular levels of glutathione and the modulation of glutathione S-transferase A4 expression by butyrate," *Toxicological Sciences*, vol. 86, no. 1, pp. 27–35, 2005.

[10] P. Rossner Jr., M. B. Terry, M. D. Gammon et al., "Plasma protein carbonyl levels and breast cancer risk," *Journal of cellular and molecular medicine*, vol. 11, no. 5, pp. 1138–1148, 2007.

[11] C. Valadez-Vega, L. Delgado-Olivares, J. A. Morales González et al., "The role of natural antioxidants in cancer disease," in *Oxidative Stress and Chronic Degenerative Diseases - a Role for Antioxidants*, J. A. En Morales-González, Ed., pp. 391–418, Technical Editor, Croatia, 2013.

[12] L. Dany, P. Cannone, E. Dudoit, and R. Favre, "Patients et médecins face à la chimiothérapie," *Journal international sur les représentations sociales*, vol. 2, no. 1, pp. 57–67, 2005.

[13] Q. Kong, J. A. Beel, and K. O. Lillehei, "A threshold concept for cancer therapy," *MedicalHypotheses*, vol. 55, no. 1, pp. 29–35, 2000.

[14] M. Asadi-Samani, N. Farkhad, M. Mahmoudian-Sani, and H. Shirzad, "Antioxidants as a Double-Edged Sword in the Treatment of Cancer," in *Antioxidants*, E. Shalaby, Ed., IntechOpen, 2019.

[15] A. Deledda, G. Annunziata, G. C. Tenore, V. Palmas, A. Manzin, and F. Velluzzi, "Diet-derived antioxidants and their role in inflammation, obesity and gut microbiota modulation," *Antioxidants*, vol. 10, no. 5, p. 708, 2021.

[16] P. Wigner, R. Grębowski, M. Bijak, J. Saluk-Bijak, and J. Szemraj, "The interplay between oxidative stress, inflammation and angiogenesis in bladder cancer development," *International Journal of Molecular Sciences*, vol. 22, no. 9, p. 4483, 2021.

[17] Y. Li, J. Yang, and X. Sun, "Reactive oxygen species-based nanomaterials for cancer therapy," *Frontiers in Chemistry*, vol. 9, 2021.

[18] R. Gerschman, D. L. Gilbert, S. W. Nye, P. Dwyer, and W. O. Fenn, "Oxygen poisoning and X-irradiation—a mechanism in common," *Science*, vol. 119, no. 3097, pp. 623–626, 1954.

[19] D. Harman, "Aging: a theory based on free radical and radiation chemistry," *J Gerontol*, vol. 11, no. 3, pp. 298–300, 1956.

[20] D. Harman, "Free radical theory of aging," *Mutation Research/Dnaging*, vol. 275, no. 3-6, pp. 257–266, 1992.

[21] D. Harman, "The biologic clock: the mitochondria?," *Journal of the American Geriatrics Society*, vol. 20, no. 4, pp. 145–147, 1972.

[22] J. M. McCord and I. Fridovich, "Superoxide Dismutase: an enzymic function for erythrocuprein (hemocuprein)," *J. Biol. Chem.*, vol. 244, no. 22, pp. 6049–6055, 1969.

[23] J. M. C. Gutteridge and B. Halliwell, "1 Iron toxicity and oxygen Radicals," *Baillière's Clinical Haematology*, vol. 2, no. 2, pp. 195–256, 1989.

[24] S. di Meo, T. T. Reed, P. Venditti, and V. M. Victor, "Role of ROS And RNS sources in physiological and pathological conditions," *Oxidative Medicine and Cellular Longevity*, vol. 2016, Article ID 1245049, 44 pages, 2016.

[25] P. Jia, C. Dai, P. Cao, D. Sun, R. Ouyang, and Y. Miao, "The role of reactive oxygen species in tumor treatment," *Rsc Advances*, vol. 10, no. 13, pp. 7740–7750, 2020.

[26] S. G. Rhee, "Cell signaling: H_2O_2, a necessary evil for cell signaling," *Science*, vol. 312, no. 5782, pp. 1882-1883, 2006.

[27] K. Brieger, S. Schiavone, J. Miller, and K. H. Krause, "Reactive oxygen species: from health to disease," *Swiss Medical Weekly*, vol. 142, article W13659, 2012.

[28] N. Faust, F. Varas, L. M. Kelly, S. Heck, and T. Graf, "Insertion of enhanced green fluorescent protein into the lysozyme gene creates mice with green fluorescent granulocytes and macrophages," *Blood, the Journal of the American Society of Hematology*, vol. 96, no. 2, pp. 719–726, 2000.

[29] C. Migdal and M. Serres, "Espèces réactives de l'oxygène et stress oxydant," *Médecine/Sciences*, vol. 27, no. 4, pp. 405–412, 2011.

[30] B. Salehi, M. Martorell, J. L. Arbiser et al., "Antioxidants: positive or negative actors?," *Biomolecules*, vol. 8, no. 4, p. 124, 2018.

[31] L. Castro and B. A. Freeman, "Reactive oxygen species in human health and disease," *Nutrition*, vol. 17, no. 2, pp. 161–165, 2001.

[32] S. D. Swain, T. T. Rohn, and M. T. Quinn, "Neutrophil priming in host defense: role of oxidants as priming agents," *Antioxid Redox Signal*, vol. 4, no. 1, pp. 69–83, 2002.

[33] J. S. Bhatti, G. K. Bhatti, and P. H. Reddy, "Mitochondrial dysfunction and oxidative stress in metabolic disorders – A step towards mitochondria based therapeutic strategies," *Molecular basis of disease*, vol. 1863, no. 5, pp. 1066–1077, 2017.

[34] A. J. Hulbert, "On the importance of fatty acid composition of membranes for aging," *J Theor Biol*, vol. 234, no. 2, pp. 277–288, 2005.

[35] R. Pamplona, M. Portero-Otín, C. Ruiz, R. Gredilla, A. Herrero, and G. Barja, "Double bond content of phospholipids and lipid peroxidation negatively correlate with maximum longevity in the heart of mammals," *Mech Ageing Dev*, vol. 112, no. 3, pp. 169–183, 2000.

[36] M. Singh, D. Shrivastava, and R. Kale, "Antioxidant potential of Asparagus adscendens," *Antioxidant Enzyme*, vol. 323, 2012.

[37] K. B. Beckman and B. N. Ames, "Oxidative Decay of DNA," *J. Biol. Chem*, vol. 272, no. 32, pp. 19633–19636, 1997.

[38] H. H. Draper and M. Hadley, "A review of recent studies on the metabolism of exogenous and endogenous malondialdehyde," *Xenobiotica*, vol. 20, no. 9, pp. 901–907, 1990.

[39] A. R. Collins, J. Cadet, L. Mőller, H. E. Poulsen, and J. Viña, "Are we sure we know how to measure 8-oxo-7,8-dihydro-guanine in DNA from human cells?," *Archives of Biochemistry and Biophysics*, vol. 423, no. 1, pp. 57–65, 2004.

[40] S. K. Das, S. Maji, S. L. Wechman et al., "Mda-9/Syntenin (Sdcbp): novel gene and therapeutic target for cancer metastasis," *Pharmacological Research*, vol. 155, p. 104695, 2020.

[41] G. Wang, P. Cai, G. A. S. Ansari, and M. F. Khan, "Oxidative and nitrosative stress in trichloroethene-mediated autoimmune response," *Toxicology*, vol. 229, no. 3, pp. 186–193, 2007.

[42] H. Esterbauer, R. J. Schaur, and H. Zollner, "Chemistry and biochemistry of 4-hydroxynonenal, malonaldehyde and related aldehydes," *Free Radical Biology and Medicine*, vol. 11, no. 1, pp. 81–128, 1991.

[43] C. M. Spickett, "The lipid peroxidation product 4-hydroxy-2-nonenal: advances in chemistry and analysis," *Redox Biology*, vol. 1, no. 1, pp. 145–152, 2013.

[44] H. Esterbauer, H. Zöllner, and N. Scholz, "Reaction of glutathione with conjugated carbonyls," *Zeitschrift Für Naturforschung C*, vol. 30, no. 7-8, pp. 466–473, 1975.

[45] R. J. Schaur, "Basic aspects of the biochemical reactivity of 4-hydroxynonenal," *Molecular Aspects of Medicine*, vol. 24, no. 4-5, pp. 149–159, 2003.

[46] G. Brambilla, L. Sciabà, P. Faggin et al., "Cytotoxicity, DNA fragmentation and sister-chromatid exchange in Chinese hamster ovary cells exposed to the lipid peroxidation product 4-hydroxynonenal and homologous aldehydes," *Mutation Research/Genetic Toxicology*, vol. 171, no. 2-3, pp. 169–176, 1986.

[47] M. Perluigi, R. Coccia, and D. A. Butterfield, "4-Hydroxy-2-nonenal, a reactive product of lipid peroxidation, and neurodegenerative diseases: a toxic combination illuminated by redox proteomics studies," *Antioxidants & Redox Signaling*, vol. 17, no. 11, pp. 1590–1609, 2012.

[48] C. H. Chen, A. U. Joshi, and D. Mochly-Rosen, "The role of mitochondrial aldehyde dehydrogenase 2 (Aldh2) in neuropathology and neurodegeneration," *Acta Neurologica Taiwanica*, vol. 25, no. 4, pp. 111–123, 2016.

[49] S. Dalleau, M. Baradat, F. Guéraud, and L. Huc, "Cell death and diseases related to oxidative stress:4-hydroxynonenal (HNE) in the balance," *Cell Death & Differentiation*, vol. 20, no. 12, pp. 1615–1630, 2013.

[50] V. Ergin, R. E. Hariry, and C. Karasu, "Carbonyl stress in aging process: role of vitamins and phytochemicals as redox regulators," *Aging and Disease*, vol. 4, no. 5, pp. 276–294, 2013.

[51] T. Ohnuma, S. Nishimon, M. Takeda, T. Sannohe, N. Katsuta, and H. Arai, "Carbonyl stress and microinflammation-related molecules as potential biomarkers in schizophrenia," *Frontiers in Psychiatry*, vol. 9, p. 82, 2018.

[52] P. Tesarová, M. Kalousová, B. Trnková et al., "Carbonyl and oxidative stress in patients with breast cancer–is there a relation to the stage of the disease?," *Neoplasma*, vol. 54, no. 3, pp. 219–224, 2007.

[53] F. L. Chung, R. G. Nath, J. Ocando, A. Nishikawa, and L. Zhang, "Deoxyguanosine adducts of T-4-hydroxy-2-nonenal are endogenous DNA lesions in rodents and humans: detection and potential sources," *Cancer Research*, vol. 60, no. 6, pp. 1507–1511, 2000.

[54] M. Umberto Dianzani, "4-Hydroxynonenal from pathology to physiology," *Molecular Aspects of Medicine*, vol. 24, no. 4-5, pp. 263–272, 2003.

[55] N. Zarkovic, "4-Hydroxynonenal as a bioactive marker of pathophysiological processes," *Molecular Aspects of Medicine*, vol. 24, no. 4-5, pp. 281–291, 2003.

[56] R. A. Adarsh Pal Vig, "Lipid peroxidation: a possible marker for diabetes," *Journal of diabetes and metabolism*, vol. 11, pp. 1–6, 2012.

[57] G. Barrera, "Oxidative stress and lipid peroxidation products in cancer progression and therapy," *ISRN Oncology*, vol. 2012, Article ID 137289, 21 pages, 2012.

[58] D. A. Butterfield, M. L. Bader Lange, and R. Sultana, "Involvements of the lipid peroxidation product, HNE, in the pathogenesis and progression of Alzheimer's disease," *Biochimica et Biophysica Acta (BBA)-Molecular and Cell Biology of Lipids*, vol. 1801, no. 8, pp. 924–929, 2010.

[59] V. Ruipérez, F. Darios, and B. Davletov, "Alpha-synuclein, lipids and Parkinson's disease," *Progress in Lipid Research*, vol. 49, no. 4, pp. 420–428, 2010.

[60] S. B. Farr and T. Kogoma, "Oxidative stress responses in Escherichia coli and Salmonella typhimurium," *Microbiological Reviews*, vol. 55, no. 4, pp. 561–585, 1991.

[61] E. R. Stadtman, H. Van Remmen, A. Richardson, N. B. Wehr, and R. L. Levine, "Methionine oxidation and aging," *Biochimica et Biophysica Acta (BBA)-Proteins and Proteomics*, vol. 1703, no. 2, pp. 135–140, 2005.

[62] R. Shringarpure and K. J. Davies, "Protein turnover by the proteasome in aging and disease1, 2," *Free Radical Biology and Medicine*, vol. 32, no. 11, pp. 1084–1089, 2002.

[63] E. R. Stadtman, "Oxidation of free amino acids and amino acid residues in proteins by radiolysis and by metal-catalyzed reactions," *Annual review of biochemistry*, vol. 62, no. 1, pp. 797–821, 1993.

[64] A. Ceriello, F. Mercuri, L. Quagliaro et al., "Detection of nitrotyrosine in the diabetic plasma: evidence of oxidative stress," *Diabetologia*, vol. 44, no. 7, pp. 834–838, 2001.

[65] M. E. Murphy and J. P. Kehrer, "Oxidation state of tissue thiol groups and content of protein carbonyl groups in chickens with inherited muscular dystrophy," *Biochemical Journal*, vol. 260, no. 2, pp. 359–364, 1989.

[66] M. L. Chapman, B. R. Rubin, and R. W. Gracy, "Increased carbonyl content of proteins in synovial fluid from patients with rheumatoid arthritis," *J. Rheumatol.*, vol. 16, no. 1, pp. 15–18, 1989.

[67] R. H. Jones and J. S. Hothersall, "The effect of diabetes and dietary ascorbate supplementation on the oxidative modification of rat lens β_L crystallin," *Biochemical medicine and metabolic biology*, vol. 50, no. 2, pp. 197–209, 1993.

[68] A. L. Jackson and L. A. Loeb, "The contribution of endogenous sources of DNA damage to the multiple mutations in cancer," *Mutation Research/Fundamental and Molecular Mechanisms of Mutagenesis*, vol. 477, no. 1-2, pp. 7–21, 2001.

[69] B. Halliwell and G. Jm, *Free Radicals in Biology and Medicine*, Oxford University Press, Midsomer Norton, Third edition, 1999.

[70] J. Imlay and S. Linn, "DNA damage and oxygen radical toxicity," *Science*, vol. 240, no. 4857, pp. 1302–1309, 1988.

[71] C. J. Burrows and J. G. Muller, "Oxidative nucleobase modifications leading to strand scission," *Chemical Reviews*, vol. 98, no. 3, pp. 1109–1152, 1998.

[72] L. P. Candeias and S. Steenken, "Reaction of HO- with guanine derivatives in aqueous solution: formation of two different redox-active OH-adduct radicals and their unimolecular transformation reactions. Properties of G (-H)," *Chemistry– A European Journal*, vol. 6, no. 3, pp. 475–484, 2000.

[73] J. Haleng, J. Pincemail, J. O. Defraigne, C. Charlier, and J. P. Chapelle, "Le stress oxydant," *Revue médicale de Liège*, vol. 62, no. 10, pp. 628–638, 2007.

[74] G. T. Wondrak, M. K. Jacobson, and E. L. Jacobson, "Endogenous UVA-photosensitizers: mediators of skin photodamage and novel targets for skin photoprotection," *Photochemical & photobiological sciences*, vol. 5, no. 2, pp. 215–237, 2006.

[75] B. N. Ames, "Dietary carcinogens and anticarcinogens: oxygen radicals and degenerative diseases," *Science*, vol. 221, no. 4617, pp. 1256–1264, 1983.

[76] H. Sp and H. Cc, "Molecular epidemiology of human cancer: contribution of mutation spectra studies of tumor suppressor genes," *Cancer Research*, vol. 58, pp. 4023–4037, 1998.

[77] M. Ichiba, Y. Maeta, T. Mukoyama et al., "Expression of 8-hydroxy-2'-deoxyguanosine in chronic liver disease and hepatocellular carcinoma," *Liver International*, vol. 23, no. 5, pp. 338–345, 2003.

[78] K. B. Schwarz, M. Kew, A. Klein et al., "Increased hepatic oxidative DNA damage in patients with hepatocellular carcinoma," *Digestive Diseases and Sciences*, vol. 46, no. 10, pp. 2173–2178, 2001.

[79] J. H. Lee, I. Hwang, Y. N. Kang, I. J. Choi, and D. K. Kim, "Genetic characteristics of mitochondrial DNA was associated with colorectal carcinogenesis and its prognosis," *PLoS One*, vol. 10, no. 3, article e0118612, 2015.

[80] A. Görlach, E. Y. Dimova, A. Petry et al., "Reactive oxygen species, nutrition, hypoxia and diseases: problems solved?," *Redox Biology*, vol. 6, pp. 372–385, 2015.

[81] S. Reuter, S. C. Gupta, M. M. Chaturvedi, and B. B. Aggarwal, "Oxidative stress, inflammation, and cancer: How are they linked?," *Free Radical Biology and Medicine*, vol. 49, no. 11, pp. 1603–1616, 2010.

[82] J. E. Klaunig, L. M. Kamendulis, and B. A. Hocevar, "Oxidative stress and oxidative damage in carcinogenesis," *Toxicologic Pathology*, vol. 38, no. 1, pp. 96–109, 2010.

[83] F. Bray, J. Ferlay, I. Soerjomataram, R. L. Siegel, L. A. Torre, and A. Jemal, "Global Cancer Statistics 2018: GLOBOCAN estimates of incidence and mortality worldwide for 36 cancers in 185 countries," *Ca: A Cancer Journal for Clinicians*, vol. 68, no. 6, pp. 394–424, 2018.

[84] F. A. Haggar and R. P. Boushey, "Colorectal cancer epidemiology: incidence, mortality, survival, and risk factors," *Clinics in Colon and Rectal Surgery*, vol. 22, no. 4, pp. 191–197, 2009.

[85] S. Blau, A. Rubinstein, P. Bass, C. Singaram, and R. Kohen, "Differences in the reducing power along the rat GI tract: lower antioxidant capacity of the colon," *Molecular and Cellular Biochemistry*, vol. 194, no. 1, pp. 185–191, 1999.

[86] J. Guz, M. Foksinski, A. Siomek et al., "The relationship between 8-oxo-7,8-dihydro-2'-deoxyguanosine level and extent of cytosine methylation in leukocytes DNA of healthy subjects and in patients with colon adenomas and carcinomas," *Mutation Research/Fundamental and Molecular Mechanisms of Mutagenesis*, vol. 640, no. 1-2, pp. 170–173, 2008.

[87] A. Keshavarzian, D. Zapeda, T. List, and S. Mobarhan, "High levels of reactive oxygen metabolites in colon cancer tissue: analysis by chemiluminescence probe," *Nutrition and Cancer*, vol. 17, no. 3, pp. 243–249, 1992.

[88] T. Otamiri and R. Sjodahl, "Increased lipid peroxidation in malignant tissues of patients with colorectal cancer," *Cancer*, vol. 64, pp. 422–425, 1989.

[89] E. Skrzydlewska, S. Sulkowski, M. Koda, B. Zalewski, L. Kanczuga-Koda, and M. Sulkowska, "Lipid peroxidation and antioxidant status in colorectal cancer," *World journal of gastroenterology: WJG*, vol. 11, no. 3, p. 403, 2005.

[90] H. Wiseman and B. Halliwell, "Damage to DNA by reactive oxygen and nitrogen species: role in inflammatory disease and progression to cancer," *Biochemical Journal*, vol. 313, Part 1, p. 17, 1996.

[91] K. Roszkowski, W. Jozwicki, P. Blaszczyk, A. Mucha-Mal-ecka, and A. Siomek, "Oxidative damage DNA: 8-oxoGua and 8-oxodG as molecular markers of cancer," *Medical Science Monitor*, vol. 17, no. 6, pp. CR329–CR333, 2011.

[92] Z. Tahari, A. Medjdoub, T. Sahraoui et al., "Analyse de l'état du stress oxydatif dans le cancer du sein à l'Ouest algérien via les tests FORD et FORT et corrélation avec le grade histopronostique SBR," *Journal Africain du Cancer / African Journal of Cancer*, vol. 5, no. 1, pp. 16–21, 2013.

[93] T. I. Hewala and M. R. A. Elsoud, "The clinical significance of serum oxidative stress biomarkers in breast cancer females," *Medical Research Journal*, vol. 4, no. 1, pp. 1–7, 2019.

[94] S. Bjelland and E. Seeberg, "Mutagenicity, toxicity and repair of DNA base damage induced by oxidation," *Mutation Research/Fundamental and Molecular Mechanisms of Mutagenesis*, vol. 531, no. 1-2, pp. 37–80, 2003.

[95] R. S. Devaux and J. I. Herschkowitz, "Beyond DNA: the role of epigenetics in the premalignant progression of breast cancer," *Journal of Mammary Gland Biology and Neoplasia*, vol. 23, no. 4, pp. 223–235, 2018.

[96] E. E. M. Nour Eldin, M. Z. el-Readi, M. M. Nour Eldein et al., "8-Hydroxy-2'-deoxyguanosine as a Discriminatory Biomarker for Early Detection of Breast Cancer," *Clinical Breast Cancer*, vol. 19, no. 2, pp. E385–E393, 2019.

[97] D. H. Kang, "Oxidative stress, DNA damage, and breast cancer," *Aacn Advanced Critical Care*, vol. 13, no. 4, pp. 540–549, 2002.

[98] C. Y. Ock, E. H. Kim, D. J. Choi, H. J. Lee, K. B. Hahm, and M. H. Chung, "8-Hydroxydeoxyguanosine: Not mere biomarker for oxidative stress, but remedy for oxidative stress-implicated gastrointestinal diseases," *World Journal of Gastroenterology*, vol. 18, no. 4, pp. 302–308, 2012.

[99] T. Yamamoto, K. I. Hosokawa, T. Tamura, H. Kanno, M. Urabe, and H. Honjo, "Urinary 8-hydroxy-2 '-deoxyguanosine (8-OHdG) levels in women with or without gynecologic cancer," *Journal of Obstetrics and Gynaecology Research*, vol. 22, no. 4, pp. 359–363, 1996.

[100] T. G. C. Murrell, "Epidemiological and biochemical support for a theory on the cause and prevention of breast cancer," *Medical hypotheses*, vol. 36, no. 4, pp. 389–396, 1991.

[101] R. S. Arnold, J. He, A. Remo et al., "Nox1 Expression Determines Cellular Reactive Oxygen and Modulates c-fos-Induced Growth Factor, Interleukin-8, and Cav-1," *The American journal of pathology*, vol. 171, no. 6, pp. 2021–2032, 2007.

[102] L. Khandrika, B. Kumar, S. Koul, P. Maroni, and H. K. Koul, "Oxidative stress in prostate cancer," *Cancer Letters*, vol. 282, no. 2, pp. 125–136, 2009.

[103] B. Oh, G. Figtree, D. Costa et al., "Oxidative stress in prostate cancer patients: a systematic review of case control studies," *Prostate International*, vol. 4, no. 3, pp. 71–87, 2016.

[104] S. C. Sikka, "Role of oxidative stress response elements and antioxidants in prostate cancer pathobiology and chemoprevention–a mechanistic approach," *Current Medicinal Chemistry*, vol. 10, no. 24, pp. 2679–2692, 2003.

[105] S. S. Brar, Z. Corbin, T. P. Kennedy et al., "Nox5 NAD(P)H oxidase regulates growth and apoptosis in Du 145 prostate cancer cells," *American Journal of Physiology-Cell Physiology*, vol. 285, no. 2, pp. C353–C369, 2003.

[106] T. Kamata, "Roles of Nox1 and other Nox isoforms in cancer development," *Cancer science*, vol. 100, no. 8, pp. 1382–1388, 2009.

[107] B. Kumar, S. Koul, L. Khandrika, R. B. Meacham, and H. K. Koul, "Oxidative stress is inherent in prostate cancer cells and is required for aggressive phenotype," *Cancer Research*, vol. 68, no. 6, pp. 1777–1785, 2008.

[108] K. Szewczyk-Golec, J. Tyloch, and J. Czuczejko, "Antioxidant defense system in prostate adenocarcinoma and benign prostate hyperplasia of elderly patients," *Neoplasma*, vol. 62, no. 1, pp. 119–123, 2015.

[109] B. Zachara, K. Szewczyk-Golec, J. Tyloch et al., "Blood and tissue selenium concentrations and glutathione peroxidase activities in patients with prostate cancer and benign prostate hyperplasia," *Neoplasma*, vol. 52, no. 3, pp. 248–254, 2005.

[110] Y. Miyamoto, Y. H. Koh, Y. S. Park et al., "Oxidative stress caused by inactivation of glutathione peroxidase and adaptive responses," *Biological Chemistry*, vol. 384, no. 4, pp. 567–574, 2003.

[111] N. TANIGUCHI, M. TAKAHASHI, H. SAKIYAMA et al., "A common pathway for intracellular reactive oxygen species production by glycoxidative and nitroxidative stress in vascular endothelial cells and smooth muscle cells," *Annals of the New York Academy of Sciences*, vol. 1043, no. 1, pp. 521–528, 2005.

[112] A. Jemal, L. X. Clegg, E. Ward et al., "Annual report to the nation on the status of cancer, 1975–2001, with a special feature regarding survival," *Cancer: Interdisciplinary International Journal of the American Cancer Society*, vol. 101, no. 1, no. 1, pp. 3–27, 2004.

[113] M. J. Rathos, "Potentiation of in vitro and in vivo antitumor efficacy of doxorubicin by cyclin-dependent kinase inhibitor P276-00 in human non-small cell lung cancer cells," *Bmc Cancer*, vol. 13, no. 1, pp. 1–10, 2013.

[114] N. Azad, Y. Rojanasakul, and V. Vallyathan, "Inflammation and lung cancer: roles of reactive oxygen/nitrogen species," *Journal of Toxicology and Environmental Health, Part B*, vol. 11, no. 1, pp. 1–15, 2008.

[115] E. Barreiro, V. I. Peinado, J. B. Galdiz et al., "Cigarette smoke–induced oxidative stress: a role in chronic obstructive pulmonary disease skeletal muscle dysfunction," *American Journal of Respiratory and Critical Care Medicine*, vol. 182, no. 4, pp. 477–488, 2010.

[116] W. Macnee, "Pulmonary and systemic oxidant/antioxidant imbalance in chronic obstructive pulmonary disease," *Proceedings of the American Thoracic Society*, vol. 2, no. 1, pp. 50–60, 2005.

[117] M. Parkin, T. Je, P. Boffetta, J. Samet, P. Shields, and N. Caporaso, "Tumours of The Lung," in *World Health Organization Classification of Tumors. Pathology and Genetics of Tumors of The Lung, Pleura, Thymus and Heart*, pp. 9–124, IARC Press, Lyon, 2004.

[118] K. Zabłocka-Słowińska, S. Płaczkowska, K. Skórska et al., "Oxidative stress in lung cancer patients is associated with

altered serum markers of lipid metabolism," *Plos One*, vol. 14, no. 4, article E0215246, p. e0215246, 2019.

[119] Y. Xu, C. T. Ho, S. G. Amin, C. Han, and F. L. Chung, "Inhibition of tobacco-specific nitrosamine-induced lung tumorigenesis in A/J mice by green tea and its major polyphenol as antioxidants," *Cancer Research*, vol. 52, no. 14, pp. 3875–3879, 1992.

[120] B. N. Ames, L. S. Gold, and W. C. Willett, "The causes and prevention of cancer," *Proceedings of the National Academy of Sciences*, vol. 92, no. 12, pp. 5258–5265, 1995.

[121] J. A. Cook, D. Gius, D. A. Wink, M. C. Krishna, A. Russo, and J. B. Mitchell, "Oxidative stress, redox, and the tumor microenvironment," *Seminars in Radiation Oncology*, vol. 14, no. 3, pp. 259–266, 2004.

[122] E. Filaire, C. Dupuis, G. Galvaing et al., "Lung cancer: What are the links with oxidative stress, physical activity and nutrition," *Lung Cancer*, vol. 82, no. 3, pp. 383–389, 2013.

[123] W. S. Joshua Loke, M. Y. Lim, C. R. Lewis, and P. S. Thomas, "Oxidative stress in lung cancer," *Cancer*, vol. 1, pp. 23–32, 2014.

[124] R. P. Bowler, P. J. Barnes, and J. D. Crapo, "The role of oxidative stress in chronic obstructive pulmonary disease," *COPD: Journal of Chronic Obstructive Pulmonary Disease*, vol. 1, no. 2, pp. 255–277, 2004.

[125] D. G. Yanbaeva, M. A. Dentener, E. C. Creutzberg, G. Wesseling, and E. F. Wouters, "Systemic effects of smoking," *Chest*, vol. 131, no. 5, pp. 1557–1566, 2007.

[126] J.-P. Gao, W. Xu, W. T. Liu, M. Yan, and Z.-G. Zhu, "Tumor heterogeneity of gastric cancer: from the perspective of tumor-initiating cell," *World Journal of Gastroenterology*, vol. 24, no. 24, pp. 2567–2581, 2018.

[127] J. Kanner, J. Selhub, A. Shpaizer, B. Rabkin, I. Shacham, and O. Tirosh, "Redox homeostasis in stomach medium by foods: The Postprandial Oxidative Stress Index (POSI) for balancing nutrition and human health," *Redox biology.*, vol. 12, pp. 929–936, 2017.

[128] J. Machlowska, J. Baj, M. Sitarz, R. Maciejewski, and R. Sitarz, "Gastric cancer: epidemiology, risk factors, classification, genomic characteristics and treatment strategies," *International Journal of Molecular Sciences*, vol. 21, no. 11, p. 4012, 2020.

[129] "Diet, nutrition, physical activity and stomach cancer," *continuous update project: analysing research on cancer prevention and survival*, 2018, https://www.Wcrf.Org/Sites/Default/Files/Stomach-Cancer-Report.Pdf.

[130] R. K. Al-Ishaq, A. J. Overy, and D. Büsselberg, "Phytochemicals and gastrointestinal cancer: cellular mechanisms and effects to change cancer progression," *Biomolecules*, vol. 10, no. 1, p. 105, 2020.

[131] H. W. Tan, H. Y. Mo, A. T. Y. Lau, and Y. M. Xu, "Selenium species: current status and potentials in cancer prevention and therapy," *International Journal of Molecular Sciences*, vol. 20, no. 1, p. 75, 2019.

[132] M. Kieliszek, B. Lipinski, and S. Blazejak, "Application of sodium selenite in the prevention and treatment of cancers," *Cells*, vol. 6, no. 4, p. 39, 2017.

[133] V. Aggarwal, H. S. Tuli, A. Varol et al., "Role of reactive oxygen species in cancer progression: molecular mechanisms and recent advancements," *Biomolecules*, vol. 9, no. 11, p. 735, 2019.

[134] J. Cadet, J. L. Ravanat, M. Tavernaporro, H. Menoni, and D. Angelov, "Oxidatively generated complex DNA damage:

[135] S. Y. Tang and B. Halliwell, "Medicinal plants and antioxidants: what do we learn from cell culture and Caenorhabditis elegans studies?," *Biochemical and Biophysical Research Communications*, vol. 394, pp. 1–5, 2010.

[136] D. Durand, M. Damon, and M. Gobert, "Oxidative stress in farm animals: General aspects," *Cahiers De Nutrition ET De Diététique*, vol. 48, no. 5, pp. 218–224, 2013.

[137] N. S. Chandel and D. A. Tuveson, "The promise and perils of antioxidants for cancer patients," *New England Journal of Medicine*, vol. 371, no. 2, pp. 177-178, 2014.

[138] M. Valko, D. Leibfritz, J. Moncol, M. T. D. Cronin, M. Mazur, and J. Telser, "Free radicals and antioxidants in normal physiological functions and human disease," *The International Journal of Biochemistry & Cell Biology*, vol. 39, no. 1, pp. 44–84, 2007.

[139] P. Storz, "Reactive oxygen species in tumor progression," *Frontiers in Bioscience*, vol. 10, no. 1-3, pp. 1881–1896, 2005.

[140] G. Shklar, "Mechanisms of cancer inhibition by anti-oxidant nutrients," *Oral oncology*, vol. 34, no. 1, pp. 24–29, 1998.

[141] K. Rahman, "Studies on free radicals, antioxidants, and cofactors," *Clin. Interv.Aging*, vol. 2, no. 2, pp. 219–236, 2007.

[142] I. N. Zelko, T. J. Mariani, and R. J. Folz, "Superoxide dismutase multigene family: a comparison of the CuZn-SOD (SOD1), Mn-SOD (SOD2), and EC-SOD (SOD3) gene structures, evolution, and expression," *Free Radical Biology and Medicine*, vol. 33, no. 3, pp. 337–349, 2002.

[143] J. É. M. MatÉs, C. Pérez-Gómez, and I. N. de Castro, "Antioxidant enzymes and human diseases," *Clinical biochemistry*, vol. 32, no. 8, pp. 595–603, 1999.

[144] J. M. Matés, "Effects of antioxidant enzymes in the molecular control of reactive oxygen species toxicology," *Toxicology*, vol. 153, no. 1-3, pp. 83–104, 2000.

[145] H. E. Ganther, "Selenium metabolism, selenoproteins and mechanisms of cancer prevention: complexities with thioredoxin reductase," *Carcinogenesis*, vol. 20, no. 9, pp. 1657–1666, 1999.

[146] J. Kasapović, S. Pejić, A. Todorović, V. Stojiljković, and S. B. Pajović, "Antioxidant status and lipid peroxidation in the blood of breast cancer patients of different ages," *Cell Biochemistry and Function: Cellular Biochemistry and Its Modulation by Active Agents or Disease*, vol. 26, no. 6, pp. 723–730, 2008.

[147] M. Monari, A. Trinchero, C. Calabrese et al., "Superoxide dismutase in gastric adenocarcinoma: is it a clinical biomarker in the development of cancer?," *Biomarkers*, vol. 11, no. 6, pp. 574–584, 2006.

[148] S. Elchuri, T. Oberley, W. Qi et al., "CuZnSOD deficiency leads to persistent and widespread oxidative damage and hepatocarcinogenesis later in life," *Oncogene*, vol. 24, no. 3, pp. 367–380, 2005.

[149] T. Sm, W. S. Hou Mf, B. Hu et al., "Expression of manganese superoxide dismutase in patients with breast cancer," *The Kaohsiung Journal of Medical Sciences*, vol. 27, no. 5, pp. 167–172, 2011.

[150] Y. Zhao, L. Chaiswing, T. D. Oberley et al., "A mechanism-based antioxidant approach for the reduction of skin carcinogenesis," *Cancer Research*, vol. 65, no. 4, pp. 1401–1405, 2005.

[151] J. J. Cullen, C. Weydert, M. M. Hinkhouse et al., "The role of manganese superoxide dismutase in the growth of pancreatic

adenocarcinoma," *Cancer Research*, vol. 63, no. 6, pp. 1297–1303, 2003.

[152] J. G. Wilkes, M. S. Alexander, and J. J. Cullen, "Superoxide dismutases in pancreatic cancer," *Antioxidants*, vol. 6, no. 3, p. 66, 2017.

[153] M. L. Teoh-Fitzgerald, M. P. Fitzgerald, T. J. Jensen, B. W. Futscher, and F. E. Domann, "Genetic and epigenetic inactivation of extracellular superoxide dismutase promotes an invasive phenotype in human lung cancer by disrupting ECM homeostasis," *Molecular Cancer Research*, vol. 10, no. 1, pp. 40–51, 2012.

[154] B. Griess, E. Tom, F. Domann, and M. Teoh-Fitzgerald, "Extracellular superoxide dismutase and its role in cancer," *Free Radical Biology and Medicine*, vol. 112, pp. 464–479, 2017.

[155] R. Bonetta, "Potential therapeutic applications of MnSODs and SOD-mimetics," *Chemistry–A European Journal*, vol. 24, no. 20, pp. 5032–5041, 2018.

[156] M. W. Epperly, H. Wang, J. A. Jones, T. Dixon, C. A. Montesinos, and J. S. Greenberger, "Antioxidant-chemoprevention diet ameliorates late effects of total-body irradiation and supplements radioprotection by MnSOD-plasmid liposome administration," *Radiation Research*, vol. 175, no. 6, pp. 759–765, 2011.

[157] J. Alexandre, C. Nicco, C. Chéreau et al., "Improvement of the therapeutic index of anticancer drugs by the superoxide dismutase mimic mangafodipir," *Journal of The National Cancer Institute*, vol. 98, no. 4, pp. 236–244, 2006.

[158] B. Gauter-Fleckenstein, K. Fleckenstein, K. Owzar, C. Jiang, I. Batinic-Haberle, and Z. Vujaskovic, "Comparison of two Mn porphyrin-based mimics of superoxide dismutase in pulmonary radioprotection," *Free Radical Biology and Medicine*, vol. 44, no. 6, pp. 982–989, 2008.

[159] D. Robbins and Y. Zhao, "The role of manganese superoxide dismutase in skin cancer," *Enzyme Research*, vol. 2011, Article ID 409295, 7 pages, 2011.

[160] I. N. Zelko, M. R. Mueller, and R. J. Folz, "Cpg methylation attenuates Sp1 and Sp3 binding to the human extracellular superoxide dismutase promoter and regulates its cell-specific expression," *Free Radical Biology and Medicine*, vol. 48, no. 7, pp. 895–904, 2010.

[161] M. Hitchler, K. Wikainapakul, L. Yu, K. Powers, W. Attatippaholkun, and F. Domann, "Epigenetic regulation of manganese superoxide dismutase expression in human breast cancer cells," *Epigenetics*, vol. 1, no. 4, pp. 163–171, 2006.

[162] R. Franco, O. Schoneveld, A. G. Georgakilas, and M. I. Panayiotidis, "Oxidative stress, DNA methylation and carcinogenesis," *Cancer Letters*, vol. 266, no. 1, pp. 6–11, 2008.

[163] X. Gào, Y. Zhang, B. Burwinkel et al., "The associations of DNA methylation alterations in oxidative stress-related genes with cancer incidence and mortality outcomes: a population-based cohort study," *Clinical Epigenetics*, vol. 11, no. 1, p. 14, 2019.

[164] N. Nishida and M. Kudo, "Oxidative stress and epigenetic instability in human hepatocarcinogenesis," *Digestive Diseases*, vol. 31, no. 5-6, pp. 447–453, 2013.

[165] D. Robbins and Y. Zhao, "Manganese superoxide dismutase in cancer prevention," *Antioxidants & Redox Signaling*, vol. 20, no. 10, pp. 1628–1645, 2014.

[166] R. Kohan, A. Collin, S. Guizzardi, N. Tolosa de Talamoni, and G. Picotto, "Reactive oxygen species in cancer: a paradox between pro- and anti-tumour activities," *Cancer Chemotherapy and Pharmacology*, vol. 86, no. 1, pp. 1–13, 2020.

[167] F. R. Palma, C. He, J. M. Danes et al., "Mitochondrial superoxide dismutase: what the established, the intriguing, and the novel reveal about a key cellular redox switch," *Antioxidants & Redox Signaling.*, vol. 32, no. 10, pp. 701–714, 2020.

[168] S. K. Dhar, J. Tangpong, L. Chaiswing, T. D. Oberley, and D. K. St Clair, "Manganese superoxide dismutase is a P53-regulated gene that switches cancers between early and advanced stages," *Cancer Research*, vol. 71, no. 21, pp. 6684–6695, 2011.

[169] A. Kim, "Modulation of MnSOD in cancer: epidemiological and experimental evidences," *Toxicological Research*, vol. 26, no. 2, pp. 83–93, 2010.

[170] M. Malafa, J. Margenthaler, B. Webb, L. Neitzel, and M. Christophersen, "MnSOD expression is increased in metastatic gastric cancer," *Journal of Surgical Research*, vol. 88, no. 2, pp. 130–134, 2000.

[171] A. Gaya-Bover, R. Hernández-López, M. Alorda-Clara et al., "Antioxidant enzymes change in different non-metastatic stages in tumoral and peritumoral tissues of colorectal cancer," *The International Journal of Biochemistry & Cell Biology*, vol. 120, p. 105698, 2020.

[172] R. A. Gatenby and E. T. Gawlinski, "The glycolytic phenotype in carcinogenesis and tumor invasion: insights through mathematical models," *Cancer Research*, vol. 63, no. 14, pp. 3847–3854, 2003.

[173] D. V. Ratnam, D. D. Ankola, V. Bhardwaj, D. K. Sahana, and N. M. V. R. Kumar, "Journal of Controlled Release," *Journal of Controlled Release*, vol. 113, no. 3, pp. 189–207, 2006.

[174] J. Goudable and A. Favier, "Oxidative free radicals and antioxidants," *Nutrition clinique et métabolisme*, vol. 11, no. 2, pp. 115–120, 1997.

[175] D. Quinton, A. Galtayries, F. Prima, and S. Griveau, "Functionalization of titanium surfaces with a simple electrochemical strategy," *Surface and Coatings Technology*, vol. 206, no. 8-9, pp. 2302–2307, 2012.

[176] G. Cohen and P. Hochstein, "Glutathione peroxidase: the primary agent for the elimination of hydrogen peroxide in erythrocytes," *Biochemistry*, vol. 2, no. 6, pp. 1420–1428, 1963.

[177] C. Glorieux, N. Dejeans, B. Sid, R. Beck, P. B. Calderon, and J. Verrax, "Catalase overexpression in mammary cancer cells leads to a less aggressive phenotype and an altered response to chemotherapy," *Biochemical Pharmacology*, vol. 82, no. 10, pp. 1384–1390, 2011.

[178] V. A. de Oliveira, L. L. da Motta, M. A. de Bastiani et al., "In vitro evaluation of antitumoral efficacy of catalase in combination with traditional chemotherapeutic drugs against human lung adenocarcinoma cells," *Tumor Biology*, vol. 37, no. 8, pp. 10775–10784, 2016.

[179] C. Bracalente, I. L. Ibañez, A. Berenstein et al., "Reprogramming human A375 amelanotic melanoma cells by catalase overexpression: upregulation of antioxidant genes correlates with regression of melanoma malignancy and with malignant progression when downregulated," *Oncotarget*, vol. 7, no. 27, pp. 41154–41171, 2016.

[180] M. R. Brown, F. J. Miller Jr., W. G. Li et al., "Overexpression of human catalase inhibits proliferation and promotes apoptosis in vascular smooth muscle cells," *Circulation Research*, vol. 85, no. 6, pp. 524–533, 1999.

[181] T. Jc, M. Jain, H. Cm et al., "Induction of apoptosis by pyrrolidinedithiocarbamate and N-acetylcysteine in vascular smooth muscle cells," *Journal of Biological Chemistry*, vol. 271, no. 7, pp. 3667–3670, 1996.

[182] S. H. Akbas, A. Yegin, and T. Ozben, "Effect of pentylenetetrazol-induced epileptic seizure on the antioxidant enzyme activities, glutathione and lipid peroxidation levels in rat erythrocytes and liver tissues," *Clinical biochemistry*, vol. 38, no. 11, pp. 1009–1014, 2005.

[183] G. C. Mills, "Hemoglobin catabolism: I. Glutathione peroxidase, an erythrocyte enzyme which protects hemoglobin from oxidative breakdown," *Journal of Biological Chemistry*, vol. 229, no. 1, pp. 189–197, 1957.

[184] M. Valko, C. J. Rhodes, J. Moncol, M. Izakovic, and M. Mazur, "Free radicals, metals and antioxidants in oxidative stress-induced cancer," *Chemico-Biological Interactions*, vol. 160, no. 1, pp. 1–40, 2006.

[185] K. C. Deshpande, M. M. Kulkarni, and D. V. Rajput, "Evaluation of glutathione peroxidase in the blood and tumor tissue of oral squamous cell carcinoma patients," *Journal Of Oral And Maxillofacial Pathology*, vol. 22, no. 3, p. 447, 2018.

[186] J. A. Cook, H. I. Pass, S. N. Iype et al., "Cellular glutathione and thiol measurements from surgically resected human lung tumor and normal lung tissue," *Cancer Research*, vol. 51, no. 16, pp. 4287–4294, 1991.

[187] F. Y. F. Lee, A. Vessey, E. Rofstad, D. W. Siemann, and R. M. Sutherland, "Heterogeneity of glutathione content in human ovarian cancer," *Cancer Research*, vol. 49, no. 19, pp. 5244–5248, 1989.

[188] R. R. Perry, J. Mazetta, M. Levin, and S. C. Barranco, "Glutathione levels and variability in breast tumors and normal tissue," *Cancer*, vol. 72, no. 3, pp. 783–787, 1993.

[189] H. Kudo, T. Mio, T. Kokunai, N. Tamaki, K. Sumino, and S. Matsumoto, "Quantitative analysis of glutathione in human brain tumors," *Journal of Neurosurgery*, vol. 72, no. 4, pp. 610–615, 1990.

[190] M. Strycharz-Dudziak, M. Kiełczykowska, B. Drop et al., "Total antioxidant status (TAS), superoxide dismutase (SOD), and glutathione peroxidase (GPx) in oropharyngeal cancer associated with EBV infection," *Oxidative Medicine and Cellular Longevity*, vol. 2019, Article ID 5832410, 15 pages, 2019.

[191] J. Liu, M. M. Hinkhouse, W. Sun et al., "Redox regulation of pancreatic cancer cell growth: role of glutathione peroxidase in the suppression of the malignant phenotype," *Human Gene Therapy*, vol. 15, no. 3, pp. 239–250, 2004.

[192] M. J. Boden, A. E. Brandon, J. D. Tid-Ang et al., "Overexpression of manganese superoxide dismutase ameliorates high-fat diet-induced insulin resistance in rat skeletal muscle," *American Journal of Physiology-Endocrinology and Metabolism*, vol. 303, no. 6, pp. E798–E805, 2012.

[193] T. B. Mysore, T. A. Shinkel, J. Collins et al., "Overexpression of glutathione peroxidase with two isoforms of superoxide dismutase protects mouse islets from oxidative injury and improves islet graft function," *Diabetes*, vol. 54, no. 7, pp. 2109–2116, 2005.

[194] W. Zhong, L. W. Oberley, T. D. Oberley, and D. K. S. Clair, "Suppression of the malignant phenotype of human glioma cells by overexpression of manganese superoxide dismutase," *Oncogene*, vol. 14, no. 4, pp. 481–490, 1997.

[195] I. Heirman, D. Ginneberge, R. Brigelius-Flohe et al., "Blocking tumor cell eicosanoid synthesis by Gpx4 impedes tumor growth and malignancy," *Free Radical Biology and Medicine*, vol. 40, no. 2, pp. 285–294, 2006.

[196] T. Jansen and A. Daiber, "Direct antioxidant properties of bilirubin and biliverdin. is there a role for biliverdin reductase? Frontiers in," *pharmacology*, vol. 3, p. 30, 2012.

[197] A. J. Gross and A. J. Downard, "Regeneration of pyrolyzed photoresist film by heat treatment," *Analytical chemistry*, vol. 83, no. 6, pp. 2397–2402, 2011.

[198] S. K. Powers and M. J. Jackson, "Exercise-induced oxidative stress: cellular mechanisms and impact on muscle force production," *Physiological Reviews*, vol. 88, no. 4, pp. 1243–1276, 2008.

[199] G. O. Noriega, M. L. Tomaro, and A. M. C. del Batlle, "Bilirubin is highly effective in preventing in vivo δ-aminolevulinic acid- induced oxidative cell damage," *Biochimica Et Biophysica Acta (Bba)-Molecular Basis of Disease*, vol. 1638, no. 2, pp. 173–178, 2003.

[200] S. Lee, Y. Lee, H. Kim, D. Y. Lee, and S. Jon, "Bilirubin nanoparticle-assisted delivery of a small molecule-drug conjugate for targeted cancer therapy," *Biomacromolecules*, vol. 19, no. 6, pp. 2270–2277, 2018.

[201] Y. Lee, S. Lee, D. Y. Lee, B. Yu, W. Miao, and S. Jon, "Multistimuli-responsive bilirubin nanoparticles for anticancer therapy," *Angewandte Chemie International Edition*, vol. 55, no. 36, pp. 10676–10680, 2016.

[202] P. Rao, R. Suzuki, S. Mizobuchi, T. Yamaguchi, and S. Sasaguri, "Bilirubin exhibits a novel anti-cancer effect on human adenocarcinoma," *Biochemical and Biophysical Research Communications*, vol. 342, no. 4, pp. 1279–1283, 2006.

[203] C. P. Wen, F. Zhang, D. Liang et al., "The Ability of bilirubin in identifying smokers with higher risk of lung cancer: a large cohort study in conjunction with global metabolomic profiling," *Clinical Cancer Research*, vol. 21, no. 1, pp. 193–200, 2015.

[204] L. J. Horsfall, G. Rait, K. Walters et al., "Serum bilirubin and risk of respiratory disease and death," *Jama*, vol. 305, no. 7, pp. 691–697, 2011.

[205] M. F. McCarty, ""Iatrogenic Gilbert syndrome"- A strategy for reducing vascular and cancer risk by increasing plasma unconjugated bilirubin," *Medical Hypotheses*, vol. 69, no. 5, pp. 974–994, 2007.

[206] S. Ching, D. Ingram, R. Hahnel, J. Beilby, and E. Rossi, "Serum levels of micronutrients, antioxidants and total antioxidant status predict risk of breast cancer in a case control study," *The Journal of Nutrition*, vol. 132, no. 2, pp. 303–306, 2002.

[207] S. D. Zucker, P. S. Horn, and K. E. Sherman, "Serum bilirubin levels in the U.S. population: gender effect and inverse correlation with colorectal cancer," *Hepatology*, vol. 40, no. 4, pp. 827–835, 2004.

[208] P. Keshavan, S. Schwemberger, D. Smith, G. Babcock, and S. Zucker, "Unconjugated bilirubin induces apoptosis in colon cancer cells by triggering mitochondrial depolarization," *International Journal of Cancer*, vol. 112, no. 3, pp. 433–445, 2004.

[209] R. Ollinger, P. Kogler, J. Troppmair et al., "Bilirubin inhibits tumor cell growth via activation of ERK," *Cell Cycle*, vol. 6, no. 24, pp. 3078–3085, 2007.

[210] J.-J. Dugoua, "Vitamins, minerals, trace elements, and dietary supplements," in *Clinical Pharmacology during Pregnancy*, pp. 367–382, Elsevier, 2013.

[211] S. Tsalamandris, E. Oikonomou, A. Papamikroulis, and D. Tousoulis, "Anti-oxidant treatment," in *Coronary Artery Disease*, pp. 273–300, Elsevier, 2018.

[212] R. E. Beyer, "The relative essentiality of the antioxidative function of Coenzyme Q–the interactive role of DT-diaphorase," *Molecular aspects of medicine*, vol. 15, pp. s117–s129, 1994.

[213] J. L. Quiles, A. J. Farquharson, M. C. Ramírez-Tortosa et al., "Coenzyme Q differentially modulates phospholipid hydroperoxide glutathione peroxidase gene expression and free radicals production in malignant and non-malignant prostate cells," *Biofactors*, vol. 18, no. 1-4, pp. 265–270, 2003.

[214] E. G. Bliznakov, "Coenzyme Q in experimental infections and neoplasia," *Biomedical and Clinical Aspects of Coenzyme Q10*, vol. 1, pp. 73–84, 1984.

[215] K. Folkers, "The potential of coenzyme Q 10 (Nsc-140865) in cancer treatment," *Cancer Chemotherapy Reports. Part 2*, vol. 4, no. 4, pp. 19–22, 1974.

[216] S. Hodges, N. Hertz, K. Lockwood, and R. Lister, "CoQ10: Could it have a role in cancer management?," *Biofactors*, vol. 9, no. 2-4, pp. 365–370, 1999.

[217] K. Folkers, A. Osterborg, M. Nylander, M. Morita, and H. Mellstedt, "Activities of Vitamin Q_{10} in Animal Models and a Serious Deficiency in Patients with Cancer," *Biochemical and Biophysical Research Communications*, vol. 234, no. 2, pp. 296–299, 1997.

[218] B. Perillo, M. di Donato, A. Pezone et al., "Ros in cancer therapy: the bright side of the moon," *Experimental & Molecular Medicine*, vol. 52, no. 2, pp. 192–203, 2020.

[219] K. Folkers and T. H. Porter, "Antimetabolites of coenzyme Q and their potential clinical use as antitumor agents: a new biochemical approach to cancer chemotherapy," *Journal of Chemical Education*, vol. 61, no. 10, p. 892, 1984.

[220] G. Galati and P. J. O'brien, "Cytoprotective and anticancer properties of coenzyme Q versus capsaicin," *Biofactors*, vol. 18, no. 1-4, pp. 195–205, 2003.

[221] C.-H. Chung, S.-C. Yeh, C.-J. Chen, and K.-T. Lee, "Coenzyme Q0 from Antrodia cinnamomea in submerged cultures induces reactive oxygen species-mediated apoptosis in A549 human lung cancer cells," *Evidence-Based Complementary and Alternative Medicine*, vol. 2014, Article ID 246748, 10 pages, 2014.

[222] T. J. Somers-Edgar and R. J. Rosengren, "Coenzyme Q0 induces apoptosis and modulates the cell cycle in estrogen receptor negative breast cancer cells," *Anti-Cancer Drugs*, vol. 20, no. 1, pp. 33–40, 2009.

[223] A. A. Fouad, A. S. Al-Mulhim, and I. Jresat, "Therapeutic effect of coenzyme Q10 against experimentally-induced hepatocellular carcinoma in rats," *Environmental Toxicology and Pharmacology*, vol. 35, no. 1, pp. 100–108, 2013.

[224] G. C. F. Chan, W. K. Chan, and D. M. Y. Sze, "The effects of β-glucan on human immune and cancer cells," *Journal of Hematology & Oncology*, vol. 2, no. 1, pp. 1–11, 2009.

[225] V. Vetvicka and J. Vetvickova, "Combination Therapy with glucan and coenzyme Q10 in murine experimental autoimmune disease and cancer," *Anticancer Research*, vol. 38, no. 6, pp. 3291–3297, 2018.

[226] C. Q. Chen, J. Fichna, M. Bashashati, Y. Y. Li, and M. Storr, "Distribution, function and physiological role of melatonin in the lower gut," *World journal of gastroenterology: WJG*, vol. 17, no. 34, pp. 3888–3898, 2011.

[227] D. Zhao, Y. Yu, Y. Shen et al., "Melatonin synthesis and function: evolutionary history in animals and plants," *Frontiers in endocrinology*, vol. 10, p. 249, 2019.

[228] D. X. Tan, "Melatonin: a potent, endogenous hydroxyl radical scavenger," *Endocrine Journal*, vol. 1, pp. 57–60, 1993.

[229] D. X. Tan, R. J. Reiter, L. C. Manchester et al., "Chemical and physical properties and potential mechanisms: melatonin as a broad spectrum antioxidant and free radical scavenger," *Current topics in medicinal chemistry*, vol. 2, no. 2, pp. 181–197, 2002.

[230] Y. Noda, A. Mori, R. Liburdy, and L. Packer, "Melatonin and its precursors scavenge nitric oxide," *Journal of pineal research*, vol. 27, no. 3, pp. 159–163, 1999.

[231] C. Pieri, M. Marra, F. Moroni, R. Recchioni, and F. Marcheselli, "Melatonin: a peroxyl radical scavenger more effective than vitamin E," *Life sciences*, vol. 55, no. 15, pp. -PL271–PL276, 1994.

[232] E. Sofic, Z. Rimpapa, Z. Kundurovic et al., "Antioxidant capacity of the neurohormone melatonin," *Journal of neural transmission*, vol. 112, no. 3, pp. 349–358, 2005.

[233] E. Murawska-Ciałowicz, Z. Jethon, J. Magdalan et al., "Effects of melatonin on lipid peroxidation and antioxidative enzyme activities in the liver, kidneys and brain of rats administered with benzo(a)pyrene," *Experimental and toxicologic pathology*, vol. 63, no. 1-2, pp. 97–103, 2011.

[234] S. H. M. H. Abadi, A. Shirazi, A. M. Alizadeh et al., "The effect of melatonin on superoxide dismutase and glutathione peroxidase activity, and malondialdehyde levels in the targeted and the non-targeted lung and heart tissues after irradiation in xenograft mice colon cancer," *Current molecular pharmacology*, vol. 11, no. 4, pp. 326–335, 2018.

[235] D. Pozo, R. J. Reiter, J. R. Calvo, and J. M. Guerrero, "Physiological concentrations of melatonin inhibit nitric oxide synthase in rat cerebellum," *Life Sciences*, vol. 55, no. 24, pp. PL455–PL460, 1994.

[236] R. J. Reiter, D. X. Tan, and A. Galano, "Melatonin: exceeding expectations," *Physiology*, vol. 29, no. 5, pp. 325–333, 2014.

[237] T. K. Kim, Z. Lin, W. Li, R. J. Reiter, and A. T. Slominski, "N 1-Acetyl-5-methoxykynuramine (AMK) is produced in the human epidermis and shows antiproliferative effects," *Endocrinology*, vol. 156, no. 5, pp. 1630–1636, 2015.

[238] R. J. Reiter, L. Fuentes-Broto, S. D. Paredes, D. X. Tan, and J. J. Garcia, "Melatonin and the pathophysiology of cellular membranes," *Marmara Pharmaceutical Journal.*, vol. 14, pp. 1–9, 2010.

[239] L. Tang, R. J. Reiter, Z. R. Li, G. G. Ortiz, B. P. Yu, and J. J. Garcia, "Melatonin reduces the increase in 8-hydroxy-deoxyguanosine levels in the brain and liver of kainic acid-treated rats," *Molecular and cellular biochemistry*, vol. 178, no. 1/2, pp. 299–303, 1998.

[240] H. Liu, Y. Zhu, H. Zhu et al., "Role of transforming growth factor β1 in the inhibition of gastric cancer cell proliferation by melatonin in vitro and in vivo," *Oncology reports*, vol. 42, no. 2, pp. 753–762, 2019.

[241] H. Kamesaki, K. Nishizawa, G. Y. Michaud, J. Cossman, and T. Kiyono, "TGF-beta 1 induces the cyclin-dependent kinase inhibitor p27Kip1 mRNA and protein in murine B cells," *The Journal of Immunology*, vol. 160, no. 2, pp. 770–777, 1998.

[242] M. Bizzarri, A. Cucina, M. G. Valente et al., "Melatonin and vitamin D_3 increase TGF-β_1 release and induce growth inhibition in breast cancer cell cultures," *Journal of Surgical Research*, vol. 110, no. 2, pp. 332–337, 2003.

[243] E. Batlle and J. Massagué, "Transforming growth factor-β signaling in immunity and cancer," *Immunity*, vol. 50, no. 4, pp. 924–940, 2019.

[244] N. Prieto-Domínguez, R. Ordóñez, A. Fernández et al., "Melatonin-induced increase in sensitivity of human hepatocellular carcinoma cells to sorafenib is associated with reactive oxygen species production and mitophagy," *Journal of Pineal Research*, vol. 61, no. 3, pp. 396–407, 2016.

[245] M. A. el-Magd, Y. Mohamed, E. S. el-Shetry et al., "Melatonin maximizes the therapeutic potential of non-preconditioned MSCs in a DEN-induced rat model of HCC," *Biomedicine & Pharmacotherapy*, vol. 114, p. 108732, 2019.

[246] C. W. Yun, S. Kim, J. H. Lee, and S. H. Lee, "Melatonin promotes apoptosis of colorectal cancer CellsviaSuperoxide-mediated ER stress by inhibiting cellular prion protein expression," *Anticancer research*, vol. 38, no. 7, pp. 3951–3960, 2018.

[247] J. Ruiz-Rabelo, R. Vázquez, A. Arjona et al., "Improvement of capecitabine antitumoral activity by melatonin in pancreatic cancer," *Pancreas*, vol. 40, no. 3, pp. 410–414, 2011.

[248] D. Fernández-Lázaro, C. I. Fernandez-Lazaro, J. Mielgo-Ayuso, L. J. Navascués, A. Córdova Martínez, and J. Seco-Calvo, "The role of selenium mineral trace element in exercise: antioxidant defense system, muscle performance, hormone response, and athletic performance. A Systematic Review," *Nutrients*, vol. 12, no. 6, p. 1790, 2020.

[249] U. Tinggi, "Selenium: it's role as antioxidant in human health," *Environmental Health and Preventive Medicine*, vol. 13, no. 2, pp. 102–108, 2008.

[250] J. T. Rotruck, A. L. Pope, H. E. Ganther, A. B. Swanson, D. G. Hafeman, and W. G. Hoekstra, "Selenium: biochemical role as a component of glutathione peroxidase," *Science*, vol. 179, no. 4073, pp. 588–590, 1973.

[251] L. Rastgoo, A. Alemzadeh, A. M. Tale, S. E. Tazangi, and T. Eslamzadeh, "Effects of copper, nickel and zinc on biochemical parameters and metal accumulation in Gouan,'Aeluropus littoralis'," *Plant Knowledge Journal*, vol. 3, no. 1, p. 42, 2014.

[252] G. N. Schrauzer, "Selenium and selenium-antagonistic elements in nutritional cancer prevention," *Critical Reviews in Biotechnology*, vol. 29, no. 1, pp. 10–17, 2009.

[253] H. Ren, J. Mu, J. Ma et al., "Selenium inhibits homocysteine-induced endothelial dysfunction and apoptosis via activation of Akt," *Cellular Physiology and Biochemistry*, vol. 38, no. 3, pp. 871–882, 2016.

[254] M. Suzuki, M. Endo, F. Shinohara, S. Echigo, and H. Rikiishi, "Differential apoptotic response of human cancer cells to organoselenium compounds," *Cancer Chemotherapy and Pharmacology*, vol. 66, no. 3, pp. 475–484, 2010.

[255] E. Sakallı Çetin, M. Nazıroğlu, B. Çiğ, I. S. Övey, and P. Aslan Koşar, "Selenium potentiates the anticancer effect of cisplatin against oxidative stress and calcium ion signaling-induced intracellular toxicity in MCF-7 breast cancer cells: involvement of the TRPV1 channel," *Journal of Receptors and Signal Transduction*, vol. 37, no. 1, pp. 84–93, 2017.

[256] G. Baskar, K. Lalitha, and G. B. George, "Synthesis, characterization and anticancer activity of selenium nanobiocomposite of L-asparaginase," *Bulletin of Materials Science*, vol. 42, no. 1, 2019.

[257] H. Tapiero and K. D. Tew, "Trace elements in human physiology and pathology: zinc and metallothioneins," *Biomedicine & Pharmacotherapy*, vol. 57, no. 9, pp. 399–411, 2003.

[258] M. Stefanidou, C. Maravelias, A. Dona, and C. Spiliopoulou, "Zinc: a multi-purpose trace element," *Archives of Toxicology*, vol. 80, no. 1, pp. 1–9, 2006.

[259] L. Rink and P. Gabriel, "Zinc and the immune system," *Proceedings of the Nutrition Society*, vol. 4, pp. 541–552, 2000.

[260] P. I. Oteiza, K. L. Olin, C. G. Fraga, and C. L. Keen, "Zinc deficiency causes oxidative damage to proteins, lipids and DNA in rat testes," *The Journal of nutrition*, vol. 125, no. 4, pp. 823–829, 1995.

[261] R. W. Olafson, "Intestinal metallothionein: effect of parenteral and enteral zinc exposure on tissue levels of mice on controlled zinc diets," *The Journal of Nutrition*, vol. 113, no. 2, pp. 268–275, 1983.

[262] L. C. Costello and R. B. Franklin, "Cytotoxic/tumor suppressor role of zinc for the treatment of cancer: an enigma and an opportunity," *Expert Review of Anticancer Therapy*, vol. 12, no. 1, pp. 121–128, 2012.

[263] D. K. Dhawan and V. D. Chadha, "Zinc: a promising agent in dietary chemoprevention of cancer," *The Indian Journal of Medical Research*, vol. 132, no. 6, pp. 676–682, 2010.

[264] Y. Song, S. W. Leonard, M. G. Traber, and E. Ho, "Zinc deficiency affects DNA damage, oxidative stress, antioxidant defenses, and DNA repair in rats," *The Journal of Nutrition*, vol. 139, no. 9, pp. 1626–1631, 2009.

[265] A. Witkiewicz-Kucharczyk and W. BAL, "Damage of zinc fingers in DNA repair proteins, a novel molecular mechanism in carcinogenesis," *Toxicology Letters*, vol. 162, no. 1, pp. 29–42, 2006.

[266] R. B. Franklin and L. C. Costello, "Zinc as an anti-tumor agent in prostate cancer and in other cancers," *Archives of Biochemistry and Biophysics*, vol. 463, no. 2, pp. 211–217, 2007.

[267] J. L. Burkhead and S. Lutsenko, "The role of copper as a modifier of lipid metabolism," in *In Lipid Metabolism*, Intechopen, 2013.

[268] H. Chen, Z. K. Attieh, B. A. Syed et al., "Identification of zyklopen, a new member of the vertebrate multicopper ferroxidase family, and characterization in rodents and human cells," *The Journal of Nutrition*, vol. 140, no. 10, pp. 1728–1735, 2010.

[269] J. R. Faryniarz and J. E. Ramirez, *U.S. Patent No. 7,927,614*, Patent and Trademark Office, Washington, Dc: U.S, 2011.

[270] M. Fields, R. J. Ferretti, J. M. Judge, J. C. Smith, and S. Reiser, "Effects of different dietary carbohydrates on hepatic enzymes of copper-deficient rats," *Proceedings of the Society for Experimental Biology and Medicine*, vol. 178, no. 3, pp. 362–366, 1985.

[271] D. Huster, T. D. Purnat, J. L. Burkhead et al., "High Copper Selectively Alters Lipid Metabolism and Cell Cycle Machinery in the Mouse Model of Wilson Disease∗ ," *Journal of Biological Chemistry*, vol. 282, no. 11, pp. 8343–8355, 2007.

[272] K. Plawecki and K. Chapman-Novakofski, "Bone health nutrition issues in aging," *Nutrients*, vol. 2, no. 11, pp. 1086–1105, 2010.

[273] A. Martin, "The "Apports Nutritionnels Conseillés (Anc)" for the french population," *Reproduction Nutrition Development*, vol. 41, no. 2, pp. 119–128, 2001.

[274] S. Baldari, G. Di Rocco, and G. Toietta, "Current biomedical use of copper chelation therapy," *International Journal of Molecular Sciences*, vol. 21, no. 3, p. 1069, 2020.

[275] A. P. Singh, N. K. Kaushik, A. K. Verma, and R. Gupta, "Synthesis, structure and anticancer activity of copper (II) complexes of N-benzyl-2- (diethylamino) acetamide and 2-(diethylamino)-N-phenylethylacetamide," *Indian Journal of Chemistry Section –A*, vol. 50, p. 474, 2010.

[276] C. Santini, M. Pellei, V. Gandin, M. Porchia, F. Tisato, and C. Marzano, "Advances in copper complexes as anticancer agents," *Chemical Reviews*, vol. 114, no. 1, pp. 815–862, 2014.

[277] H. Khalid, M. Hanif, M. Hashmi, T. Mahmood, K. Ayub, and M. Monim-ul-Mehboob, "copper complexes of bioactive ligands with superoxide dismutase activity," *Mini Reviews In Medicinal Chemistry*, vol. 13, no. 13, pp. 1944–1956, 2013.

[278] J. L. S. Barrita and M. D. S. S. Sánchez, "Antioxidant Role of Ascorbic Acid and His Protective Effects on Chronic Diseases. Oxidative Stress Chronic Degener. Dis," *Role Antioxidants*, vol. 449, pp. 450–484, 2013.

[279] P. Patak, H. S. Willenberg, and S. R. Bornstein, "Vitamin C is an important cofactor for both adrenal cortex and adrenal medulla," *Endocrine research*, vol. 30, no. 4, pp. 871–875, 2004.

[280] L. J. Machlin and A. Bendich, "Free radical tissue damage: protective role of antioxidant nutrients," *The Faseb Journal*, vol. 1, no. 6, pp. 441–445, 1987.

[281] J. E. Packer, T. F. Slater, and R. L. And Willson, "Direct observation of a free radical interaction between vitamin E and vitamin C," *Nururr*, vol. 278, pp. 737-738, 1979.

[282] R. Bouldjadj, *Study of the antidiabetic and antioxidant effect of the lyophilized aqueous extract of Artemisia herba alba Asso in healthy rats and streptozotocin-diabetic rats Thesis of Magister*, Mentouri Constantine University, 2009.

[283] E. Pawlowska, J. Szczepanska, and J. Blasiak, "Pro- and Antioxidant Effects of Vitamin C in Cancer in correspondence to Its Dietary and Pharmacological Concentrations," *Oxidative Medicine and Cellular Longevity*, vol. 2019, Article ID 7286737, 18 pages, 2019.

[284] J. Yun, E. Mullarky, C. Lu et al., "Vitamin C selectively kills KRAS and BRAF mutant colorectal cancer cells by targeting GAPDH," *Science*, vol. 350, no. 6266, pp. 1391–1396, 2015.

[285] B. V. Hoang, J. Lee, I. J. Choi, Y. W. Kim, K. W. Ryu, and J. Kim, "Effect of dietary vitamin C on gastric cancer risk in the Korean population," *World Journal of Gastroenterology*, vol. 22, no. 27, pp. 6257–6267, 2016.

[286] E. Birben, U. M. Sahiner, C. Sackesen, S. Erzurum, and O. Kalayci, "Oxidative stress and antioxidant defense," *World Allergy Organization Journal*, vol. 5, no. 1, pp. 9–19, 2012.

[287] B. B. Frei and B. N. Ames, "Relative importance of vitamin E in antiperoxidative defences in human blood and low-density lipoprotein (LDL)," *Vitamin E in health and diseases*, M. Dekker, Ed., pp. 131–141, Academic Press, New York, 1998.

[288] K. Hensley, E. J. Benaksas, R. Bolli et al., "New perspectives on vitamin E: Γ-tocopherol and carboxyethylhydroxychroman metabolites in biology and medicine," *Free Radical Biology and Medicine*, vol. 36, no. 1, pp. 1–15, 2004.

[289] R. Brigelius-Flohé, F. J. Kelly, J. T. Salonen, J. Neuzil, J. M. Zingg, and A. Azzi, "The European perspective on vitamin E: current knowledge and future research," *The American Journal of Clinical Nutrition*, vol. 76, no. 4, pp. 703–716, 2002.

[290] S. Vertuani, A. Angusti, and S. Manfredini, "The antioxidants and pro-antioxidants network: an overview," *Current pharmaceutical design*, vol. 10, no. 14, pp. 1677–1694, 2004.

[291] Q. Jiang, S. Christen, M. K. Shigenaga, and B. N. Ames, "Γ-Tocopherol, The major form of vitamin E in the US diet, deserves more attention," *The American Journal of Clinical Nutrition*, vol. 74, no. 6, pp. 714–722, 2001.

[292] C. Tappeiner, A. Meyenberg, D. Goldblum et al., "Antifibrotic effects of tocotrienols on human tenon's fibroblasts," *Graefe's Archive for Clinical and Experimental Ophthalmology*, vol. 248, no. 1, pp. 65–71, 2010.

[293] S. Lemaire-Ewing, C. Desrumaux, D. Néel, and L. Lagrost, "Vitamin E transport, membrane incorporation and cell metabolism: is alpha-tocopherol in lipid rafts an oar in the lifeboat?," *Molecular Nutrition & Food Research*, vol. 54, no. 5, pp. 631–640, 2010.

[294] J. Schwartz, G. Shklar, and D. Trickler, "P53 in the anticancer mechanism of vitamin E," *European Journal of Cancer Part B: Oral Oncology*, vol. 29, no. 4, pp. 313–318, 1993.

[295] S. Takahashi, K. Takeshita, A. Seeni et al., "Suppression of prostate cancer in a transgenic rat model via gamma-tocopherol activation of caspase signaling," *Prostate*, vol. 69, no. 6, pp. 644–651, 2009.

[296] F. Meyer, P. Galan, P. Douville et al., "Antioxidant vitamin and mineral supplementation and prostate cancer prevention in the SU.VI.MAX trial," *International Journal of Cancer*, vol. 116, no. 2, pp. 182–186, 2005.

[297] H. Li, P. W. Kantoff, E. Giovannucci et al., "Manganese superoxide dismutase polymorphism,prediagnostic antioxidant status,and risk of clinical significant prostate cancer," *Cancer Research*, vol. 65, no. 6, pp. 2498–2504, 2005.

[298] W. E. Hardman, "Diet components can suppress inflammation and Reduce cancer risk," *Nutrition Research and Practice*, vol. 8, no. 3, pp. 233–240, 2014.

[299] S. Khatri, A. Paramanya, and A. Ali, "Phenolic acids and their health promoting activity," in *In Plant and Human Health, Volume 2 - Phytochemistry and Molecular Aspects*, M. Ozturk and K. R. Hakeem, Eds., pp. 661–680, Springer, Nature Switzerland, 2019.

[300] J. Bruneton, *Pharmacognosy, Phytochemistry - Medicinal Plants 3rd Ed Techniques And Documentation*, Lavoisier, Paris, 1999.

[301] Y. Li and R. C. G. Martin, "Herbal medicine and hepatocellular carcinoma: applications and challenges," *Evidence-Based Complementary and Alternative Medicine*, vol. 2011, Article ID neq044, 14 pages, 2011.

[302] H. M. Yang, Y. M. Ham, W. J. Yoon et al., "Quercitrin protects against ultraviolet B-induced cell death in vitro and in an in vivo zebrafish model," *Journal of Photochemistry and Photobiology B: Biology*, vol. 114, pp. 126–131, 2012.

[303] O. Benavente-García, J. Castillo, F. R. Marin, A. Ortuño, and J. A. Del Río, "Uses and properties ofCitrusFlavonoids," *Journal of Agricultural and Food Chemistry*, vol. 45, no. 12, pp. 4505–4515, 1997.

[304] S. A. B. E. Van Acker, D. Van Den Berg, M. N. J. L. Tromp et al., "Structural aspects of antioxidant activity of flavonoids," *Free Radical Biology and Medicine*, vol. 20, no. 3, pp. 331–342, 1996.

[305] H. Boeing, T. Dietrich, K. Hoffmann et al., "Intake of fruits and vegetables and risk of cancer of the upper aerodigestive tract: the prospective epic-study," *Cancer Causes Control*, vol. 17, no. 7, pp. 957–969, 2006.

[306] P. G. Pietta, "Flavonoids as antioxidants," *Journal of natural products*, vol. 63, no. 7, pp. 1035–1042, 2000.

[307] B. N. E. T. Coll, "Flavonoid intake is associated with lower mortality in the Danish Diet Cancer and Health Cohort," *Nature communications*, vol. 10, no. 1, pp. 1–10, 2019.

[308] A. J. Vargas and R. Burd, "Hormesis and synergy: pathways and mechanisms of quercetin in cancer prevention and management," *Nutrition Reviews*, vol. 68, no. 7, pp. 418–428, 2010.

[309] N. Chekalina, Y. Burmak, Y. Petrov et al., "Quercetin reduces the transcriptional activity of NF-kb in stable coronary artery disease," *Indian Heart Journal*, vol. 70, no. 5, pp. 593–597, 2018.

[310] M. Mouria, A. S. Gukovskaya, Y. Jung et al., "Food-derived polyphenols inhibit pancreatic cancer growth through mitochondrial cytochrome C release and apoptosis," *International Journal of Cancer*, vol. 98, no. 5, pp. 761–769, 2002.

[311] R. Schreck, P. Rieber, and P. A. Baeuerle, "Reactive oxygen intermediates as apparently widely used messengers in the activation of the Nf-kappa B transcription factor and HIV-1," *The Embo Journal*, vol. 10, no. 8, pp. 2247–2258, 1991.

[312] Y. Xia, S. Shen, and I. M. Verma, "NF-κb, an active player in human cancers," *Cancer Immunology Research*, vol. 2, no. 9, pp. 823–830, 2014.

[313] F. Colotta, P. Allavena, A. Sica, C. Garlanda, and A. Mantovani, "Cancer-related inflammation, the seventh hallmark of cancer: links to genetic instability," *Carcinogenesis*, vol. 30, no. 7, pp. 1073–1081, 2009.

[314] S. Huang, C. A. Pettaway, H. Uehara, C. D. Bucana, and I. J. Fidler, "Blockade of NF-κb activity in human prostate cancer cells is associated with suppression of angiogenesis, invasion, and metastasis," *Oncogene*, vol. 20, no. 31, pp. 4188–4197, 2001.

[315] A. John and G. Tuszynski, "The role of matrix metalloproteinases in tumor angiogenesis and tumor metastasis," *Pathology Oncology Research*, vol. 7, no. 1, pp. 14–23, 2001.

[316] F. A. Kuehl and R. W. Egan, "Prostaglandins, arachidonic acid, and inflammation," *Science*, vol. 210, no. 4473, pp. 978–984, 1980.

[317] K. Min and S. E. Ebeler, "Quercetin inhibits hydrogen peroxide-induced DNA damage and enhances DNA repair in Caco-2 cells," *Food and Chemical Toxicology*, vol. 47, no. 11, pp. 2716–2722, 2009.

[318] J.-A. Choi, J.-Y. Kim, J.-Y. Lee et al., "Induction of cell cycle arrest and apoptosis in human breast cancer cells by quercetin," *International Journal of Oncology*, vol. 19, no. 4, pp. 837–844, 2001.

[319] D. O. Morgan, "Principles of CDK regulation," *Nature.*, vol. 374, no. 6518, pp. 131–134, 1995.

[320] D. Kashyap, H. S. Tuli, M. B. Yerer et al., "Natural product-based nanoformulations for cancer therapy: opportunities and challenges," in *In Seminars in cancer biology*, Academic Press, 2019.

[321] B. García-Pinel, C. Porras-Alcalá, A. Ortega-Rodríguez et al., "Lipid-based nanoparticles: application and recent advances in cancer treatment," *Nanomaterials*, vol. 9, no. 4, p. 638, 2019.

[322] R. S. Ramsewak, D. L. DeWitt, and M. G. Nair, "Cytotoxicity, antioxidant and anti-inflammatory activities of Curcumins I-III from _Curcuma longa_," *Phytomedicine*, vol. 7, no. 4, pp. 303–308, 2000.

[323] W. Wang, T. Chen, H. Xu et al., "Curcumin-loaded solid lipid nanoparticles enhanced anticancer efficiency in breast cancer," *Molecules*, vol. 23, no. 7, p. 1578, 2018.

[324] T. Geetha, M. Kapila, O. Prakash, P. K. Deol, V. Kakkar, and I. P. Kaur, "Sesamol-loaded solid lipid nanoparticles for treatment of skin cancer," *Journal of drug targeting*, vol. 23, no. 2, pp. 159–169, 2015.

[325] Y. Wang, B. Tao, Y. Wan et al., "Drug delivery based pharmacological enhancement and current insights of quercetin with therapeutic potential against oral diseases," *Biomedicine & Pharmacotherapy*, vol. 128, p. 110372, 2020.

[326] M. Vinayak and A. K. Maurya, "Quercetin loaded nanoparticles in targeting cancer: recent development," *Anti-Cancer Agents in Medicinal Chemistry (Formerly Current Medicinal Chemistry-Anti-Cancer Agents)*, vol. 19, no. 13, pp. 1560–1576, 2019.

[327] U. Hasegawa, M. Moriyama, H. Uyama, and A. J. Van Der Vlies, "Catechol-bearing block copolymer micelles: Structural characterization and antioxidant activity," *Polymer*, vol. 66, pp. 1–7, 2015.

[328] A. Celebioglu and T. Uyar, "Antioxidant vitamin E/cyclodextrin inclusion complex electrospun nanofibers: enhanced water solubility, prolonged shelf life, and photostability of vitamin E," *Journal of agricultural and food chemistry*, vol. 65, no. 26, pp. 5404–5412, 2017.

[329] N. K. Dhakar, F. Caldera, F. Bessone et al., "Evaluation of solubility enhancement, antioxidant activity, and cytotoxicity studies of kynurenic acid loaded cyclodextrin nanosponge," *Carbohydrate polymers*, vol. 224, p. 115168, 2019.

[330] A. Glasauer and N. S. Chandel, "Targeting antioxidants for cancer therapy," *Biochemical pharmacology*, vol. 92, no. 1, pp. 90–101, 2014.

[331] K. le Gal, M. X. Ibrahim, C. Wiel et al., "Antioxidants can increase melanoma metastasis in mice.," *Science Translational Medicine*, vol. 7, no. 308, pp. 308re8–308re8, 2015.

[332] V. I. Sayin, M. X. Ibrahim, E. Larsson, J. A. Nilsson, P. Lindahl, and M. O. Bergo, "Antioxidants accelerate lung cancer progression in mice," *Science translational medicine*, vol. 6, no. 221, pp. 221ra15–221ra15, 2014.

[333] M. Lacroix, L. K. Linares, and L. Le Cam, "Rôle du suppresseur de tumeurs p53 dans le contrôle du métabolisme," *Médecine/Sciences*, vol. 29, no. 12, pp. 1125–1130, 2013.

[334] T. Shi and T. B. Dansen, "Reactive oxygen species induced p53 activation: DNA damage, redox signaling, or both?," *Antioxidants & Redox Signaling*, vol. 33, no. 12, pp. 839–859, 2020.

[335] M. W. Moyer, *Antioxidants may make cancer worse*, 2015, https://www.Scientificamerican.Com/Article/Antioxidants-May-Make-Cancer-Worse/.

[336] C. B. Ambrosone, *Antioxidant supplements linked to increased risk for breast cancer recurrence, death*, 2020, https://www.Healio.Com/News/Hematology-Oncology/20200116/Antioxidant-Supplements-Linked-To-Increased-Risk-For-Breast-Cancer-Recurrence-Death.

[337] S. Hercberg, K. Ezzedine, C. Guinot et al., "Antioxidant supplementation increases the risk of skin cancers in women but not in men," *The Journal of nutrition*, vol. 137, no. 9, pp. 2098–2105, 2007.

[338] T. Tanvetyanon and G. Bepler, "Beta-carotene in multivitamins and the possible risk of lung cancer among smokers versus former smokers: a meta-analysis and evaluation of national brands," *Cancer*, vol. 113, no. 1, pp. 150–157, 2008.

[339] A. Arora, C. A. Willhite, and D. C. Liebler, "Interactions of beta-carotene and cigarette smoke in human bronchial epithelial cells," *Carcinogenesis*, vol. 22, no. 8, pp. 1173–1178, 2001.

[340] D. L. Baker, E. S. Krol, N. Jacobsen, and D. C. Liebler, "Reactions of β-carotene with cigarette smoke oxidants. identification of carotenoid oxidation products and evaluation of the prooxidant/antioxidant effect," *Chemical Research in Toxicology*, vol. 12, no. 6, pp. 535–543, 1999.

[341] L. Gallicchio, K. Boyd, G. Matanoski et al., "Carotenoids and the risk of developing lung cancer: a systematic review," *The American Journal of Cinical Nutrition*, vol. 88, no. 2, pp. 372–383, 2008.

[342] A. Rahman, S. S. I. Bokhari, and M. A. Waqar, "Beta-carotene degradation by cigarette smoke in hexane solution in vitro," *Nutrition Research*, vol. 21, no. 6, pp. 821–829, 2001.

[343] A. J. Young and G. M. Lowe, "Antioxidant and prooxidant properties of carotenoids," *Archives of Biochemistry and Biophysics*, vol. 385, no. 1, pp. 20–27, 2001.

Research Article

Enhanced Sensitivity of Nonsmall Cell Lung Cancer with Acquired Resistance to Epidermal Growth Factor Receptor-Tyrosine Kinase Inhibitors to Phenformin: The Roles of a Metabolic Shift to Oxidative Phosphorylation and Redox Balance

Suntae Kim,[1] Ji Hye Im,[1,2] Wan Kyu Kim [ID],[3] Young Jae Choi,[4,5] Ji-Yoon Lee,[4] Sang Kyum Kim,[4] Sun Jo Kim,[1] Sung Won Kwon,[1] and Keon Wook Kang [ID] [1]

[1]College of Pharmacy and Research Institute of Pharmaceutical Sciences, Seoul National University, Seoul 08826, Republic of Korea
[2]Department of Cancer Control, National Cancer Center Graduate School of Cancer Science and Policy, National Cancer Center, Goyang 10408, Republic of Korea
[3]Department of Life Sciences, Ewha Womans University, Seoul 03760, Republic of Korea
[4]College of Pharmacy, Chungnam National University, Daejeon 34134, Republic of Korea
[5]Bioanalysis and Pharmacokinetics Research Group, Korea Institute of Toxicology, Daejeon 34114, Republic of Korea

Correspondence should be addressed to Keon Wook Kang; kwkang@snu.ac.kr

Received 28 May 2021; Accepted 29 June 2021; Published 29 July 2021

Academic Editor: Jolanta Czuczejko

Background. Although the efficacy of epidermal growth factor receptor-tyrosine kinase inhibitor (EGFR- TKI) therapy has been proven in non-small cell lung cancer (NSCLC) patients, acquired resistance to EGFR-TKIs presents a serious clinical problem. Hence, the identification of new therapeutic strategy is needed to treat EGFR-TKI-resistant NSCLC. *Methods.* Acquired EGFR-TKI-resistant lung cancer cell lines (HCC827, H1993, and H292 cells with acquired resistance to gefitinib or erlotinib) were used for cell-based studies. IncuCyte live cell analysis system and XFp analyzer were used for the determination of cell proliferation and energy metabolism, respectively. *In vivo* anticancer effect of phenformin was assessed in xenografts implanting HCC827 and gefitinib-resistant HCC827 (HCC827 GR) cells. *Results.* HCC827 GR and erlotinib-resistant H1993 (H1993 ER) cells exhibited different metabolic properties compared with their respective parental cells, HCC827, and H1993. In EGFR-TKI-resistant NSCLC cells, glycolysis markers including the glucose consumption rate, intracellular lactate level, and extracellular acidification rate were decreased; however, mitochondrial oxidative phosphorylation (OXPHOS) markers including mitochondria-driven ATP production, mitochondrial membrane potential, and maximal OXPHOS capacity were increased. Cell proliferation and tumor growth were strongly inhibited by biguanide phenformin via targeting of mitochondrial OXPHOS complex 1 in EGFR-TKI-resistant NSCLC cells. Inhibition of OXPHOS resulted in a reduced $NAD^+/NADH$ ratio and intracellular aspartate levels. Recovery of glycolysis by hexokinase 2 overexpression in erlotinib-resistant H292 (H292 ER) cells significantly reduced the anticancer effects of phenformin. *Conclusion.* Long-term treatment with EGFR-TKIs causes reactivation of mitochondrial metabolism, resulting in vulnerability to OXPHOS inhibitor such as phenformin. We propose a new therapeutic option for NSCLC with acquired EGFR-TKI resistance that focuses on cancer metabolism.

1. Background

Epidermal growth factor receptor-tyrosine kinase inhibitors (EGFR-TKIs) such as gefitinib and erlotinib have generally been used in non-small cell lung cancer (NSCLC) patients as first-line targeted therapy since 2003, and their prognosis has significantly improved with the targeted therapy. Unfortunately, long-term treatment with EGFR-TKIs frequently

causes resistance to targeted therapy, which led to the development of second- and third-generation EGFR-TKIs that avoid point mutations in the EGFR tyrosine kinase domain [1]. The T790M point mutation in EGFR exon 20 was reported as a major cause of EGFR-TKI resistance [1, 2]. Consequently, diverse resistance research was conducted on the H1975 NSCLC cell line carrying the T790M mutation, and a third-generation EGFR-TKI, osimertinib (Tagrisso®), which targets T790M, has been approved by the United States Food and Drug Administration as first-line therapy for metastatic lung cancer patients with an EGFR exon 19 deletion or L858R mutation [3]. However, acquired resistance to EGFR-TKIs may not be solely due to point mutations in some patients [2]. Although several molecular mechanisms for acquired resistance to EGFR-TKIs have been suggested, clinically available new therapeutic strategies are still needed [1].

Because a principal hallmark of cancer cells is rapid growth, a sufficient supply of nutrients is a critical requirement for cancer cells. Therefore, understanding cell type-specific metabolic processes that consume or use nutrients in cancer is important and could offer potential target(s) for cancer chemotherapy. After the discovery of the Warburg effect (metabolic dependency on glycolysis even under aerobic conditions), metabolic reprogramming in tumors has been extensively studied, and several clinically effective targets for controlling cancer cell-specific metabolism have been identified [4, 5]. In the present study, a new therapeutic strategy for treating EGFR-TKI-resistant NSCLC that focuses on cancer metabolism is proposed and the pharmacological efficacy of phenformin, a biguanide agent was elucidated.

2. Materials and Methods

2.1. Reagents and Antibodies. Antibodies recognizing Hexokinase I (C35C4), Hexokinase II (C64G5), phospho-pyruvate kinase isozymes M2 (PKM2) (Tyr105), PKM2 (D78A4), α-tubulin, phospho-EGFR (Tyr1068) (1H12), phospho-AKT (Ser473), and phospho-p44/42 mitogen-activated protein kinase (MAPK) (Thr202/Tyr204) (20G11) were purchased from Cell signaling Technology (Danvers, MA, USA). Anti-Pyruvate Dehydrogenase E1-alpha subunit (S293) and total OXPHOS human antibody cocktail were obtained from Abcam (Cambridge, United Kingdom). Antiglyceraldehyde-3-phosphate dehydrogenase (GAPDH) was supplied from Millipore (Burlington, MA, USA) and anti-Flag was purchased from Sigma Aldrich (St. Louis, MO, USA). Epidermal growth factor (EGF), sodium 2-oxobutyrate (AKB), and L-aspartic acid were supplied from Sigma Aldrich. Gefitinib and osimertinib were obtained from MedChemExpress (Monmouth Junction, NJ, USA). Erlotinib, phenformin, and rotenone were purchased from Cayman (Ann Arbor, MI, USA).

2.2. Cell Culture and Establishment of Stably Hexokinase II Overexpressing H292 ER Cells. Human lung cancer cells H1993, H1993 ER, H292, and H292 ER cells were kind gifts of Dr. Sang Kook Lee (Seoul National University, Seoul, Republic of Korea). HCC827, HCC827 GR, H1975, H1993,

H1993 ER, H292, and H292 ER cells were cultured in RPMI 1640 medium (Hyclone, Logan, UT, USA) with 10% fetal bovine serum (Biowest, MO, USA) and 1% penicillin/streptomycin (100 U/mL, Hyclone). All cells were maintained in an incubator humidified 5% CO_2 at 37°C.

To establish hexokinase II stably overexpressing cells, pCAG-Flag-HK2-IRES-Blas plasmid was transfected to H292 ER cells using Lipofectamine 2000 as specified by the manufacturer's instruction (Invitrogen, Carlsbad, CA, USA). Colonies were selected by incubation with blasticidin (15 μg/mL, Invitrogen). pCAG-Flag-IRES-Blas vector was used for mock transfection. pCAG-Flag-IRES-Blas and pCAG-Flag-HK2-IRES-Blas plasmids were kindly donated from Dr. Hong-Duk Youn (Department of Molecular Medicine & Biopharmaceutical Sciences, Graduate School of Convergence Science, Seoul National University, Seoul, Republic of Korea).

2.3. Cell Proliferation. Cells were seeded in a 96-well plate (2×10^3 cells/well) and cultured for 72 h. To determine cell proliferation, real-time scanned phase-contrast images were acquired and integrated confluence was analyzed by Incu-Cyte® ZOOM™ Live Cell Analysis system (Essen BioScience, Ann Arbor, MI, USA).

2.4. Genomic DNA Sequencing. Genomic DNA from lung cancer cell lines was extracted with lysis buffer (10% sodium dodecyl sulfate (SDS), 100 mM NaCl, 100 mM ethylenediaminetetraacetic acid (EDTA), 50 mM Tris (pH 8.0)) and proteinase K (15 mg/mL). Exon 18-21 region of EGFR gene was amplified by polymerase-chain-reaction (PCR). Thermal cycler settings include an initial denaturation at 95°C for 3 min followed by 40 cycles of denaturation at 95°C for 20 sec, annealing at 59.1°C for 10 sec, and extension at 72°C for 30 sec. Primers for exon 18 (sense: CAAATGAGCTG GCAAGTGCCGTGTC, antisense: GAGTTTCCCAAACA CTCAGTGAAAC), exon 19 (sense: GCAATATCAGCCTT AGGTGCGGCTC, antisense: CATAGAAAGTGAACAT TTAGGATGTG), exon 20 (sense: CCATGAGTACGTAT TTTGAAACTC, antisense: CATATCCCCATGGCAAACT CTTGC), and exon 21 (sense: CTAACGTTCGCCAGCC ATAAGTCC, antisense: GCTGCGAGCTCACCCAGAATG TCTGG) were used, and capillary electrophoresis sequencing was performed in Macrogen (Seoul, South Korea).

2.5. Immunoblot Analysis. After washing with cold sterile PBS, cells were lysed with lysis buffer containing 20 mM Tris-Cl (pH 7.5), 1% Triton X-100, 137 mM sodium chloride, 1 mM sodium orthovanadate, 10% glycerol, 2 mM EDTA, 25 mM β-glycerolphosphate, 1 mM phenylmethylsulfonyl-fluoride, 2 mM sodium inorganic pyrophosphate, and 1 μg/mL leupeptin. Total cell lysates were separated using SDS polyacrylamide gel and electrophoretically transferred to nitrocellulose membranes. After serial incubation of the membranes with primary antibodies and horseradish peroxidase- (HRP-) conjugated anti-IgG antibodies, the membranes were exposed to enhanced chemiluminescence (ECL) reagent (Millipore, Burlington, MA, USA), and images were obtained using LAS3000 mini (Fujifilm, Tokyo, Japan).

2.6. 2-Deoxyglucose- (2-DG-) Uptake Assay. Cells seeded in a 96-well plate (2×10^4 cells/well) were incubated with 1 mM 2-DG for 10 min. 2-deoxyglucose-6-phosphate (2-DGP) was determined using Glucose uptake-Glo assay kit (Promega, Madison, WI, USA) following the manufacturer's instruction.

2.7. Determination of NAD$^+$/NADH Ratio. Cells were plated in a 96-well plate and treated with the indicated concentration of phenformin for 24 h. Using NAD$^+$/NADH Glo Assay (Promega), the NAD$^+$/NADH ratio was calculated [6].

2.8. Determination of Glucose Consumption in Culture Medium. Cell culture media were collected 24 h after incubation, and a 1000-fold diluted solution was achieved by adding ice-cold 50% methanol. The solution was introduced to 1 equivalent volume of chloroform for phase separation. Samples were vortexed for 10 s and subsequently centrifuged at 16,000 rcf for 5 min. The upper hydrophilic phase was transferred to a microcentrifuge tube, and the extraction was repeated once with the remaining lower phase. The collected hydrophilic phase was dried under gentle stream of nitrogen. Dried samples were reconstituted with 100 μL methoxyamine hydrochloride (20 mg/mL, Sigma Aldrich) in pyridine and incubated at 37°C for 90 min. Following cool-down, samples were introduced to 100 μL N,O-bis(trimethylsilyl)trifluoroacetamide solution with 1% trimethylchlorosilane (Sigma Aldrich) and derivatized at 60°C for 40 min. Glucose contents were analyzed by the Shimadzu GCMS-QP2010 (Tokyo, Japan) system equipped with DB-5MS (30 m, 0.25 mm, 0.25 μm; Agilent Technologies, DE, USA). Inlet temperature was set at 270°C, and the samples were injected in split mode (1 : 2). Column oven temperature was maintained as the following gradient: 0 min, 80°C; 2 min, 80°C; 7 min, 100°C; 10 min, 100°C; 35 min, 200°C; 36 min, 200°C; 48.5 min, 300°C; and 50.5 min, 300°C. Mass scan ranged from 40 to 600 m/z with 3.06 scan/s of scan rate. Absolute quantitative values were calculated with peak area based on calibration curve by external glucose standard solutions and normalized by total protein contents.

2.9. Determination of Intracellular Lactate and Aspartate Levels. The sample injection volume was 5 μL, and peak separation was performed on a Hypersil GOLD C_8 (2.1×150 mm, 5 μm, Thermo Scientific, Waltham, MA) maintained at 30°C. The analysis was performed to gradient condition using Agilent 1290 infinity II system with autosampler, column oven, and binary pump (HPLC water containing 0.01% (v/v) formic acid, A; 100% methanol, B), and flow rate was 0.2 mL/min. LC-MS/MS data were acquired with an Applied Biosystems SCIEX 4000 QTRAP hybrid triple quadrupole-linear ion trap mass spectrometer equipped with a Turbo V ionization source. The detection was conducted using multiple reaction monitoring (MRM) of the transitions of m/z 89 > 43 for lactate, m/z 132 > 88 for aspartate, and m/z 157 > 112 for $^{13}C_5$, D_5, ^{15}N-glutamate (ISTD) in the negative ion mode. Acquisition and analysis data were performed with Analyst® software (ver.1.6.2; Applied Biosystems, Foster City, CA, USA).

2.10. Determination of Mitochondria ATP Production Rate, Oxygen Consumption Rate (OCR), and Extracellular Acidification Rate (ECAR). OCR and ECAR were determined using XFp analyzer (Seahorse Bioscience, North Billerica, MA, USA). XFp cell mito-stress test kit, XFp glycolysis stress test kit, and XFp Real-Time ATP rate assay kit (Seahorse Bioscience) were used to detect OCR, ECAR, and ATP ratio, respectively. All the reagents and assay conditions were followed by manufacturer's instructions.

2.11. RNA Preparation and RNA Sequencing. Total RNA was extracted from HCC827 and HCC827 GR cells using TRIzol reagent (Invitrogen). Purity and concentration of RNA samples were evaluated by NanoDrop Lite (Thermo Scientific, MA, USA), and transcriptome RNA-sequencing of the samples was performed by Macrogen.

2.12. Transmission Electron Microscopy. Cells were fixed with Karnovsky's fixative and fixed with 2% osmium tetroxide. 0.5% uranyl acetate was used for staining, and propylene oxide and ethanol were used for dehydration. By using Spurr's resin, cells were embedded and polymerized at 70°C. After embedding, blocks were trimmed with ultramicrotome (EM UC7, Leica, Wetzler, Germany) and detected with Transmission Electron Microscope (JEM1010, JEOL, Tokyo, Japan).

2.13. Flow Cytometry Analysis to Determine Mitochondria Membrane Potential. Tetramethylrhodamine methyl ester perchlorate (TMRM) (Sigma-Aldrich, MO, USA) was prepared as 100 μM stock solution in dimethyl sulphoxide. Cancer cells were incubated with 100 nM TMRM for 30 min at 37°C. After trypsin treatment, the detached stained cells were analyzed by Novocyte flow cytometer (Agilent, CA, USA).

2.14. Xenograft Assay. Five-week-old male Balb/c-nu mice were supplied from Raon Bio Inc. (Seoul, South Korea). Animal studies were performed according to the institute regulation and approval from Seoul National University Institutional Animal Care and Use Committee (Approval #: SNU-170717-6-1). Mice were kept in SNU semipathogen-free animal facility, with five mice in each cage. After anesthesia with Zoletil®/Rompun® mixture, 3.5×10^6 HCC827 or 3×10^6 HCC827 GR cells were inoculated on right flanks of mice. One week after inoculation, the mice were randomly divided into two groups (vehicle control group and phenformin treatment group (300 mg/kg/day, P.O.)). Animal number in xenograft study is 6-10 per group. Mice were monitored every other day, tumor length and width were detected by calipers, and tumor volume was calculated using the formula (length $\times$ width^2) $\times$ 0.5. Animals were sacrificed by carbon dioxide inhalation in euthanasia chamber.

2.15. Statistics. Student's t-test was performed to compare the difference between two groups. One-way ANOVA and Tukey's post hoc was used to analyze differences in multiple comparison. Statistical analysis was calculated using SigmaPlot (version 12.5). The statistical significance was accepted at $*P < 0.05$, $**P < 0.01$, and $***P < 0.001$; $^\#P < 0.05$, $^{\#\#}P < 0.01$, and $^{\#\#\#}P < 0.001$.

3. Results

3.1. Long-Term Treatment with EGFR-TKIs Induces Acquired Resistance with Downregulation of EGFR Signaling in Lung Cancer Cells.

Gefitinib-resistant NSCLC HCC827 (HCC827 GR) cells were established via long-term exposure of the cells to stepwise escalation of gefitinib. HCC827 GR cells exhibited resistance to gefitinib at a level similar to that in H1975 cells (T790M mutation). Other lung cancer cell lines, H1993 (NSCLC) and H292 (mucoepidermoid lung cancer) cells, also exhibited resistance to erlotinib after long-term treatment (H1993 ER and H292 ER, respectively) (Figure 1(a)). Osimertinib, a third-generation EGFR-TKI, strongly inhibited H1975 cell proliferation but marginally affected cell proliferation in the lung cancer cell lines with acquired EGFR-TKI resistance (HCC827 GR, H1993 ER, and H292 ER) (Figure 1(b)). Because various mutations in the EGFR tyrosine kinase domain associated with gefitinib resistance have been reported [7], DNA sequencing of EGFR exons 18 to 21 was performed for HCC827, HCC827 GR, H1975, H1993, H1993 ER, H292, and H292 ER cells. An exon 19 deletion mutation and inherited gefitinib resistance, T790M, were found in HCC827 and H1975 cells, respectively (Figure 1(c)). However, mutations were not detected in all the lung cancer cells with acquired EGFR-TKI resistance tested (Figure 1(c)). Furthermore, EGF-induced phosphorylation of EGFR (Tyr1068) and its downstream kinases, phosphorylation of AKT (Ser473) or p44/p42 MAPK (Thr202/Tyr204), was not observed or was weaker in the three acquired-resistance cells compared with their parental cell lines. In addition, the EGFR tyrosine kinase-inhibiting effects of gefitinib, erlotinib, and osimertinib were weaker (Figure 1(d)). Conversely, EGFR phosphorylation and its downstream signals were successfully suppressed by osimertinib but not by gefitinib or erlotinib in H1975 cells (T790M) (Figure 1(d)). The results showed that the acquisition of EGFR-TKI resistance by long-term treatment with gefitinib or erlotinib led to relatively minimal effects on EGFR activity, and these cells subsequently exhibited decreased sensitivity to EGFR-TKIs, even osimertinib.

3.2. Glycolysis Activity Is Decreased in Lung Cancer Cells with Acquired EGFR-TKI Resistance.

EGFR signaling promotes aerobic glycolysis in triple-negative breast cancer (TNBC) [8], and the inhibition of EGFR reverses the Warburg effect and reactivates oxidative phosphorylation (OXPHOS) in NSCLC cells [9]. Because EGFR signaling is suppressed in the three acquired-resistance lung cancer cell lines (HCC827 GR, H1993 ER, and H292 ER), we examined glucose metabolism in these cancer cells. The 2-DG uptake assay showed that glucose uptake in all three resistant cancer cell lines was decreased (Figure 2(a)), and the glucose consumption assay showed that the amount of glucose remaining in the culture medium was higher in HCC827 GR cells compared with HCC827 parental cells (Figure 2(b)). Using the XFp analyzer with a glycolysis stress kit, changes in the extracellular acidification rate (ECAR) representing glycolysis were estimated. After being exposed to the same amount of glucose (10 mM), HCC827 GR and H1993 ER cells

showed less changes compared with their parental cells (Figure 2(c)). Furthermore, expression levels of enzymes involved in glycolysis (HK1, HK2, and GAPDH) were lower in the two resistant cell lines (HCC827 GR and H1993 ER) (Figure 2(d)), whereas the dimer (inactive) form of Tyr105-phosphorylated PKM2 was slightly reduced in HCC827 GR and H1993 ER cells (Figure 2(d)). Notably, H292 ER cells lacked both HK1 and HK2, first-step enzymes in glycolysis, and the Tyr105-phosphorylated PKM2 level was upregulated (Figure 2(d)), indicating that glycolysis dysfunction in the H292 ER cells was mainly due to HK1/2 defects. The mRNA expression associated with the glycolysis gene set was further analyzed using RNA sequencing for both HCC827 and HCC827 GR cells. However, mRNA expression patterns associated with glycolysis in the two cell types did not exhibit any specific trends (Figure S1A). Although metabolic differences were not clearly identified at the mRNA or protein level in glycolytic enzymes, the metabolic data indicate that glycolysis capacity was decreased in the lung cancer cells with acquired EGFR-TKI resistance.

3.3. Reactivation of Mitochondrial OXPHOS Function in Lung Cancer Cells with Acquired EGFR-TKI Resistance.

Because glycolysis is the main energy process using glucose in rapidly growing cancers, glycolysis is considered a hallmark of cancer (Warburg effect) [10]. However, the role of mitochondrial OXPHOS in cancer progression has also been studied [4, 5, 11, 12]. Because EGFR inhibition induces the reactivation of mitochondrial OXPHOS in NSCLC cells [9], and the lung cancer cells with acquired EGFR-TKI resistance exhibited decreased EGFR kinase signaling activities (Figure 1(d)), OXPHOS activities in the three lung cancer cell lines with acquired EGFR-TKI resistance were compared with those in their parental cell lines. Using the XFp analyzer with a cell mito stress test kit, oxygen consumption rate (OCR) changes were monitored after treatment with OXPHOS modulators (1.5 μM oligomycin, 0.5 μM trifluoromethoxy carbonylcyanide phenylhydrazone (FCCP), and a mixture of 0.5 μM rotenone and 0.5 μM antimycin A). ATP-linked mitochondrial respiration increased in HCC827 GR and H1993 ER cells compared with their parental cells (Figure 3(a)). In H292 ER cells, maximal respiration in mitochondria increased but ATP-associated respiration did not change significantly compared with the parental cells (Figure 3(a)). Then, the ATP production ratio was compared between glycolysis and OXPHOS using the XFp analyzer with an ATP real-time rate assay kit. ATP production in the HCC827 cells was highly dependent on glycolysis (88.75%), but not on OXPHOS (11.25%). However, HCC827 GR cells had more ATP production that depended on mitochondrial OXPHOS (27.14%) than did HCC827 cells (Figure 3(b)). Mitochondrial membrane potential is induced by a proton pump in OXPHOS and regarded as an essential component during mitochondrial ATP production. Mitochondrial membrane potential in HCC827 and HCC827 GR cells was analyzed via staining with tetramethylrhodamine methyl ester (TMRM, red dots). As shown in Figure 3(c), total integrated red fluorescence intensity versus cell confluence
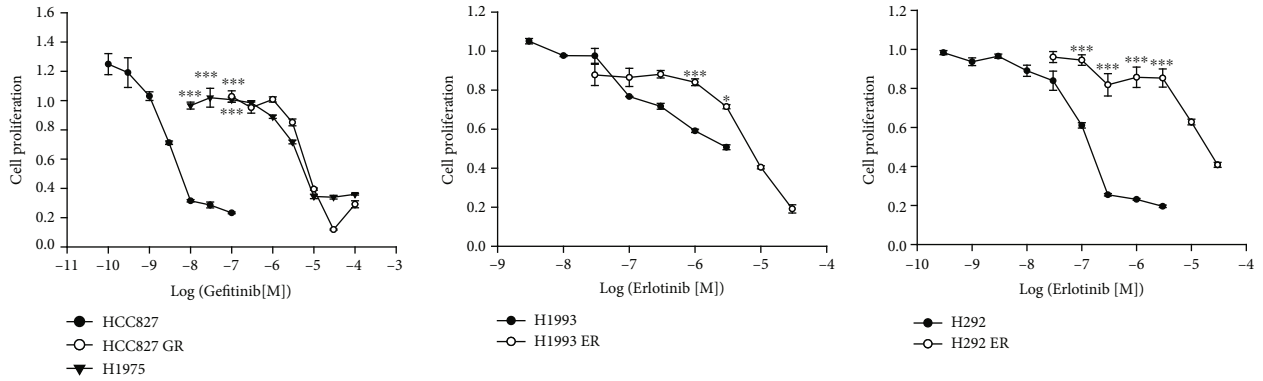
(a)
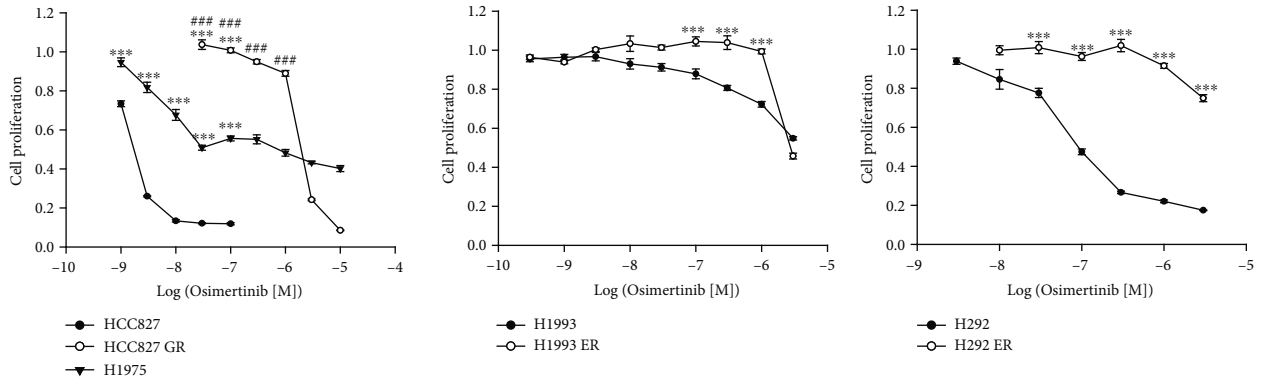
(b)

	EGFR mutation (exon18~21)
HCC827	Del (E746-A750)
HCC827 GR	X
H1975	T790M, L858R
H1993	X
H1993 ER	X
H292	X
H292 ER	X

(c)

FIGURE 1: Continued.

(d)
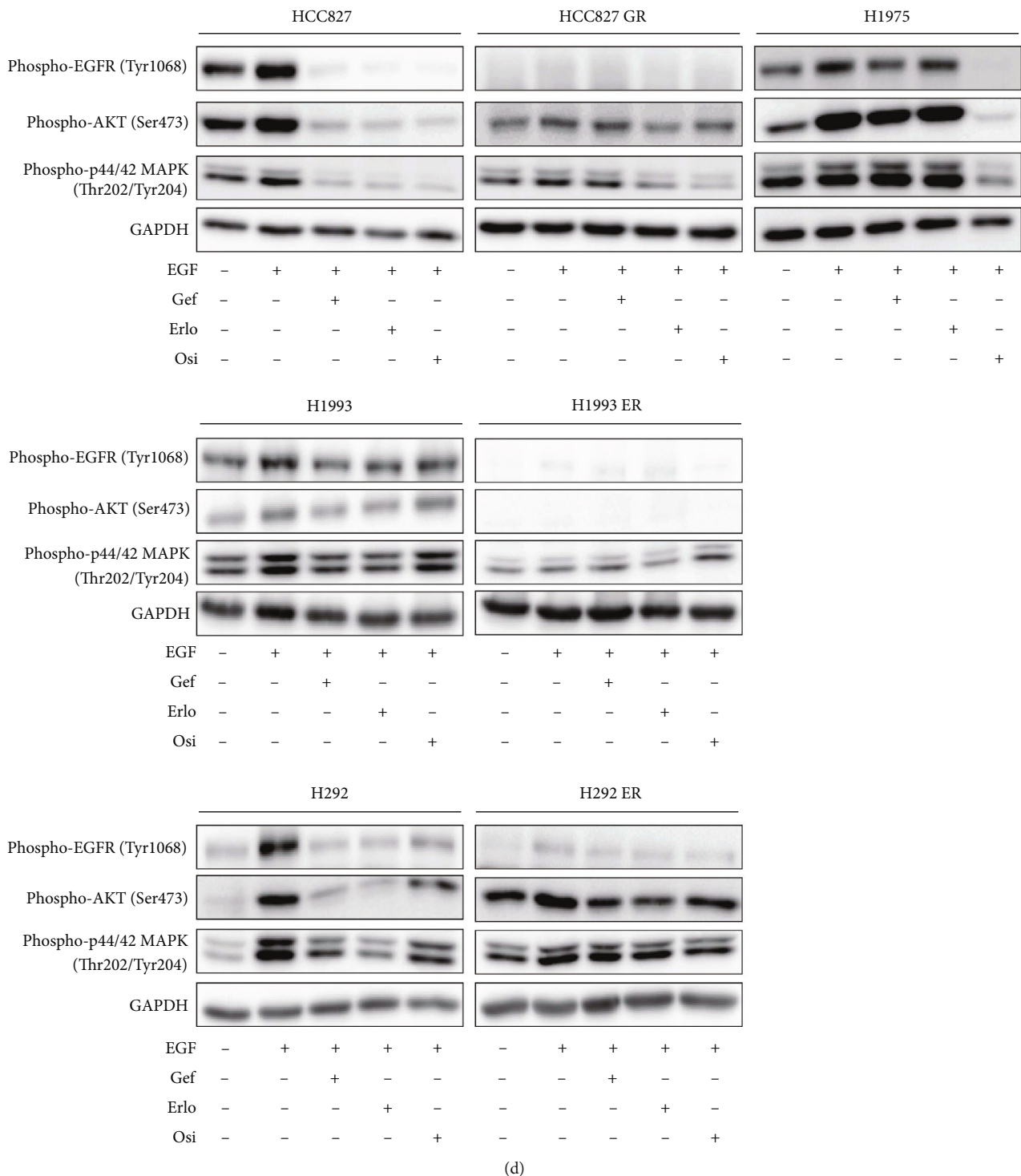
Figure 1: Acquisition of EGFR-TKI resistance by long-term treatment of gefitinib or erlotinib in NSCLCs. (a and b) Effects of EGFR TKIs on cell proliferation of EGFR TKI-resistant lung cancer cells. HCC827, HCC827 GR, H1993, H1993 ER, H292, H292 ER, and H1975 cells were incubated with various concentrations of gefitinib or erlotinib (a) and osimertinib (b), and cell proliferation was monitored for 72 h by IncuCyte ZOOM analyses. Data represent means $\pm$ S.E.M. ($n = 3 - 6$, $*P < 0.05$, $**P < 0.01$, $***P < 0.001$ vs. parental cell line; $^{\#\#\#}P < 0.001$ vs. H1975). (c) Genomic DNA sequencing of EGFR exon 18 to 21. (d) EGFR and its downstream signaling activities in HCC827, HCC827 GR, H1993, H1993 ER, H292, and H292 ER cells. All cells were pretreated with vehicle or 100 nM gefitinib, erlotinib, or osimertinib for 1 h and then exposed to 100 ng/mL EGF for 5 min. Total cell lysates were subjected to immunoblottings for phospho-EGFR (Tyr1068), phosphor-AKT (Ser473), or phosphor-p44/p42 MAPK (Thr202/Tyr204).

(a)

(b)

(c)
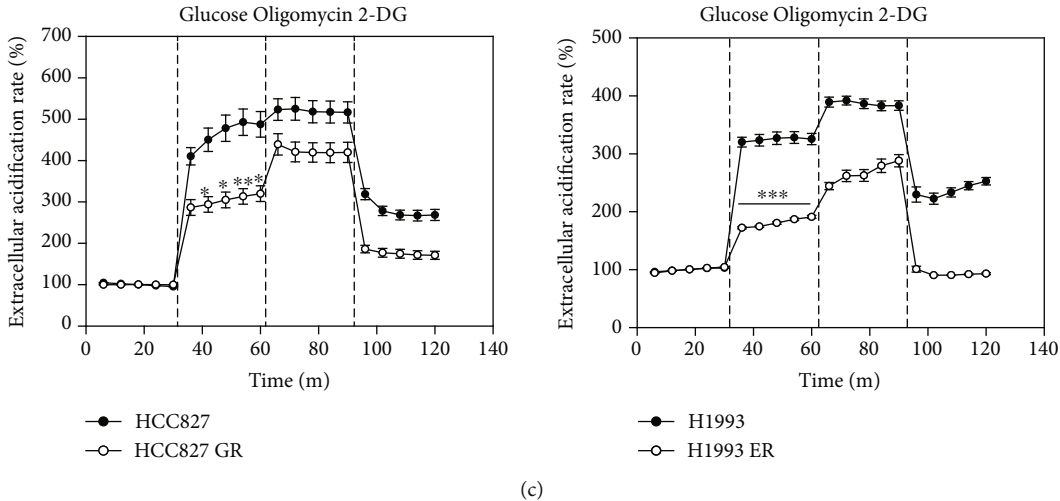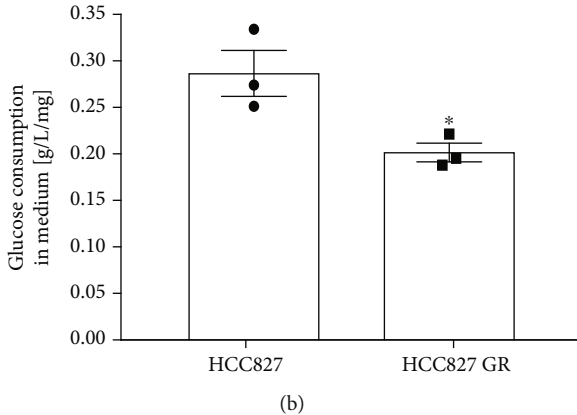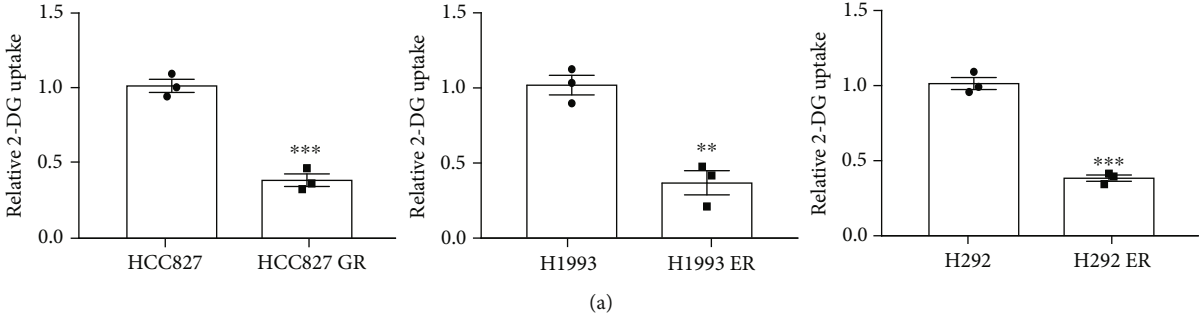
Figure 2: Continued.

(d)
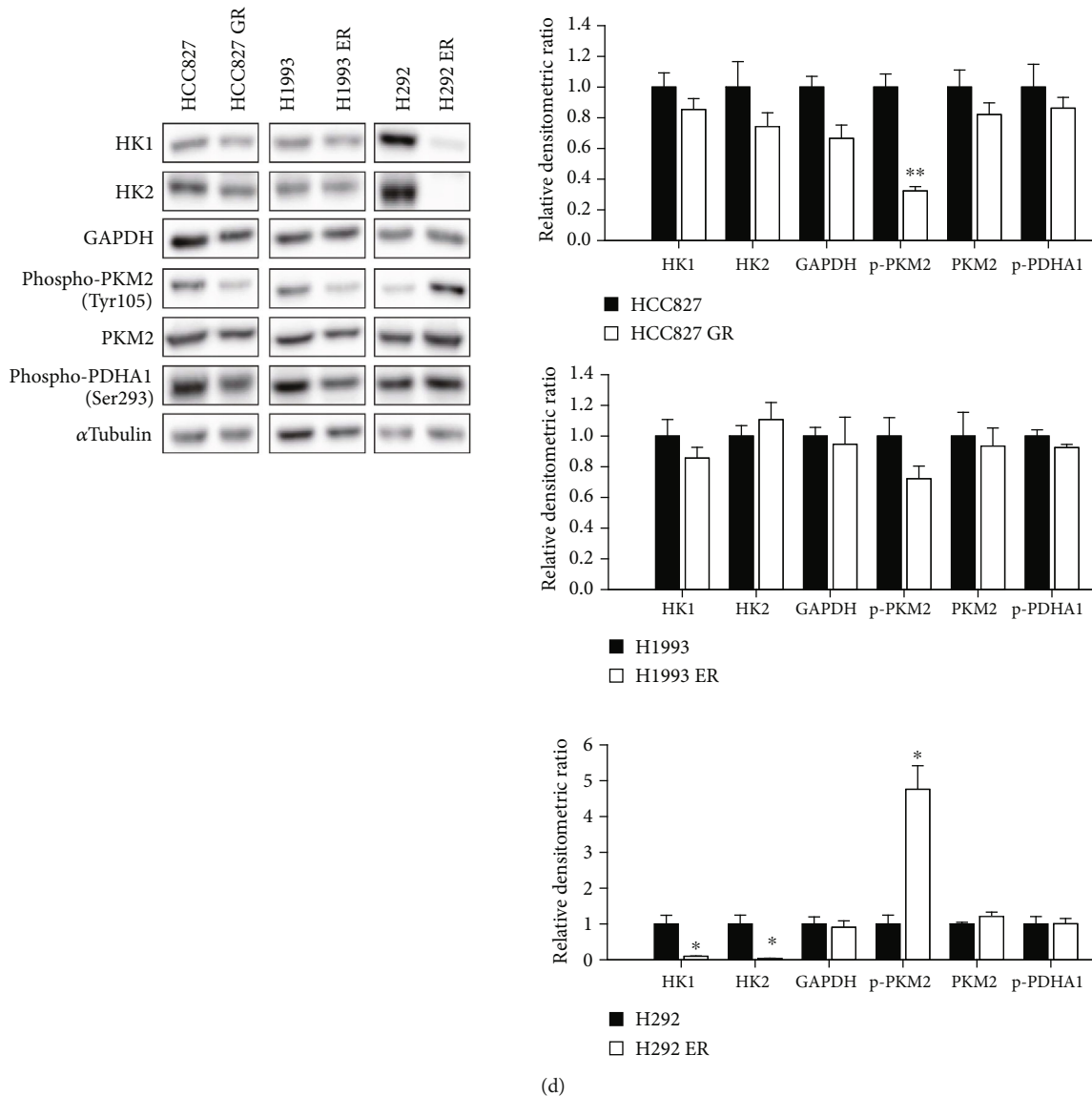
FIGURE 2: Decreased glycolysis activity in acquired EGFR-TKI-resistant lung cancer. (a) Relative glucose consumption by 2-DG uptake assay. Data represent means ± S.E.M. ($n = 3$, $**P < 0.01$, $*** P < 0.001$ vs. 2-DG uptake in parental cell line). (b) Glucose contents in culture media. Glucose level was determined by GC-MS in culture media from HCC827 and HCC827 GR cells incubated for 24 h. Glucose concentration was normalized by total protein amounts. Data represent means ± S.E.M. ($n = 3$, $*P < 0.05$ vs. HCC827). (c) ECAR changes. ECAR values were obtained from glycolysis stress test using XFp analyzer. Glucose (10 mM), oligomycin (1 μM), and 2-DG (50 mM) were added at indicated time points. Data represent means ± S.E.M. ($n = 3$, $*P < 0.05$, $**P < 0.01$, $*** P < 0.001$ vs. parental cell line). (d) Basal protein expression levels of glycolysis enzymes. Protein expression of hexokinase (HK)1, HK2, GAPDH, phosphor-PKM2 (Tyr105), PKM2, and phospho-PDHA1 (Ser293) was assessed by immunoblottings.

was significantly higher in HCC827 GR cells. Conversely, the basal intracellular level of lactate, the end product of glycolysis, was significantly decreased in HCC827 GR cells compared with HCC827 cells (Figure 3(d)). Inhibition of OXPHOS can cause a compensatory increase in glycolysis resulting in the conversion of pyruvate to lactate. The lactate level increased in phenformin- (OXPHOS inhibitor-) treated HCC827 GR cells; however, a difference in HCC827 cells was not detected (Figure 3(d)). These results indicate that mitochondrial OXPHOS was reactivated in the NSCLC cell lines with acquired EGFR-TKI resistance (HCC827 GR and H1993 ER). Next, we assessed morphological changes in

the mitochondria as well as the protein and mRNA expression of OXPHOS subunits. Transmission electron microscopy images showed no differences in the size and number of mitochondria in both HCC827 and HCC827 GR cells (Figure 3(e)). The expression of OXPHOS subunit proteins (complex 2, 3, 5) was slightly increased in HCC827 GR cells compared with HCC827 cells; however, the OXPHOS subunits expression in H1993 ER and H292 ER cells was not significantly different from that in their parental cells (Figure 3(f)). The distribution of expression levels of different mRNAs associated with OXPHOS subunits was viewed as a MA plot. Significant fold-changes between HCC827 and

(a)

(b)

(c)

(d)

(e)
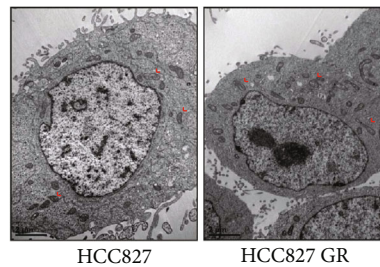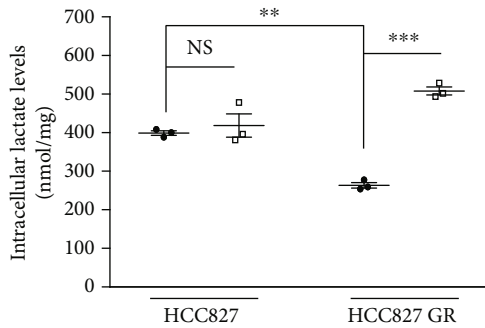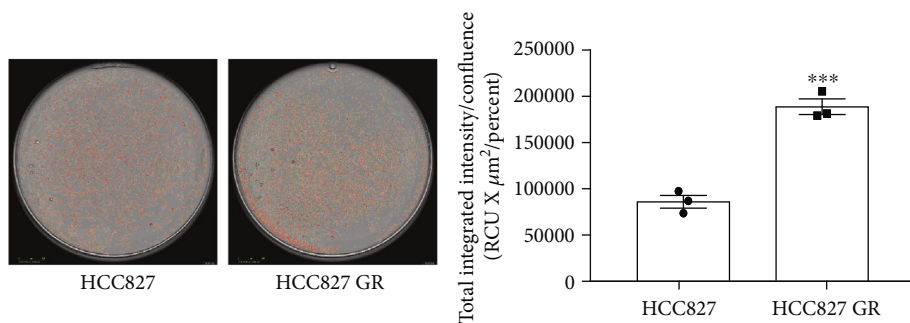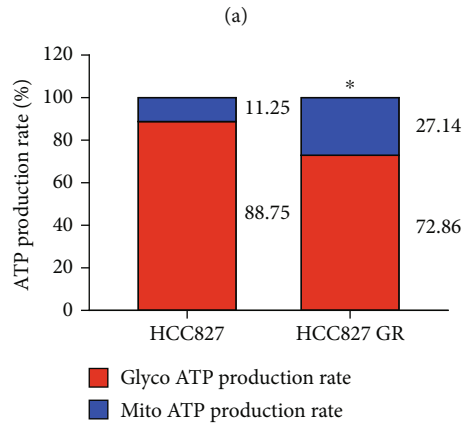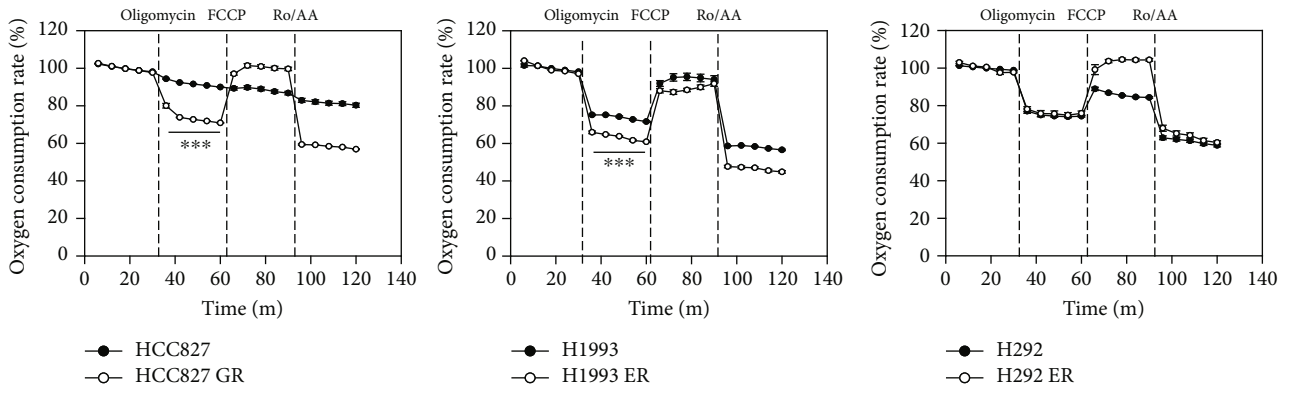
Figure 3: Continued.
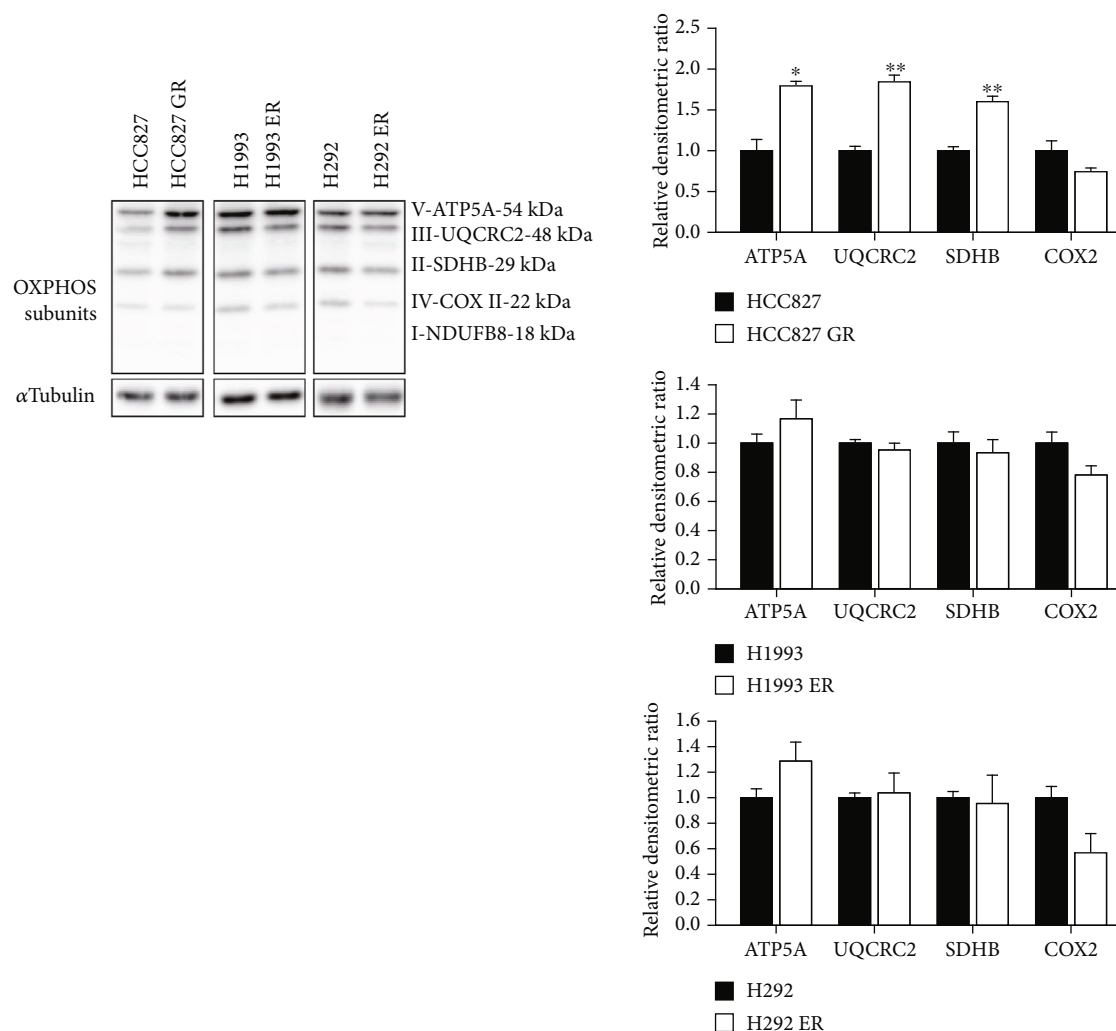
(f)

FIGURE 3: Reactivation of mitochondria function in acquired EGFR-TKI-resistant lung cancer. (a) OCR values were measured by XFp analyzer with cell mito stress kit. Oligomycin ($1.5\,\mu M$), FCCP ($0.5\,\mu M$), and mixture of rotenone (Ro, $0.5\,\mu M$) and antimycin A (AA, $0.5\,\mu M$) were treated at indicated time points. Data represent means $\pm$ S.E.M. ($n = 3$, $***\,P < 0.001$ vs. parental cell line). (b) Relative contribution of glycolysis and OXPHOS to ATP production. Using XFp real-time ATP rate assay kit, ATP production rate from glycolysis and OXPHOS was simultaneously determined in HCC827 and HCC827 GR cells. Data represent means ($n = 3$, $*P < 0.05$ vs. mito ATP production rate in HCC827). (c) Mitochondrial membrane potential. HCC827 and HCC827 GR cells were incubated with 100 nM TMRM for 30 min, and fluorescence signals were detected by IncuCyte ZOOM. Total integrated intensity of TMRM (red fluorescence) was normalized with cell confluence (outlined with yellow line). Data represent means $\pm$ S.E.M. ($n = 3$, $***\,P < 0.001$ vs. HCC827). (d) Intracellular lactate levels. HCC827 and HCC827 GR cells were treated with $100\,\mu M$ phenformin for 24 h, and lactate levels in cell lysates were determined by LC-MS/MS. Intracellular lactate level was normalized with total protein amounts. Data represent means $\pm$ S.E.M. ($n = 3$, $**P < 0.01$, $***\,P < 0.001$ significant difference between the two indicated groups). (e) Number and size of mitochondria (red arrows) in HCC827 and HCC827 GR cells were analyzed by TEM. (f) Protein level of OXPHOS subunits (ATP5A, UQCRC2, SDHB, COX II, and NDUFB8) was detected by immunoblotting.

HCC827 GR cells were not found (Figure S1B). The data indicated that increased OXPHOS capacity in EGFR-TKI-resistant NSCLC is associated with enhanced mitochondrial function but not with changes in related gene expression.

3.4. Inhibition of Proliferation in Lung Cancer Cells with Acquired EGFR-TKI Resistance Is Caused by Phenformin. Biguanides, the most prescribed anti-diabetic agents, have been recognized for their anticancer effects, and many clinical trials are currently in progress [13–16]. The repositioning

of biguanides as anticancer agents is attracting much attention due to the cost benefit and minimal safety issues. In a recent study, the combination of osimertinib with phenformin delayed osimertinib resistance in a preclinical NSCLC model [17]. We hypothesized that phenformin, an OXPHOS complex 1 inhibitor, would selectively inhibit the proliferation of lung cancer cells with acquired EGFR-TKI resistance that mainly employ mitochondrial OXPHOS. A prototype biguanide, phenformin, more effectively inhibited the proliferation of HCC827 GR and H1993 ER cells than their

(a)

(b)

(c)

(d)

HCC827

Vehicle ($n = 6$)

Phenformin ($n = 6$)

HCC827 GR

Vehicle ($n = 10$)

Phenformin ($n = 7$)

(e)

FIGURE 4: Continued.

(f)
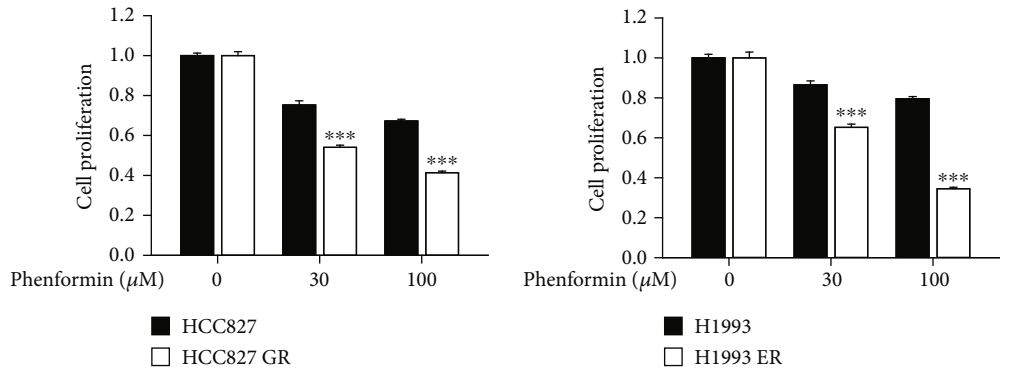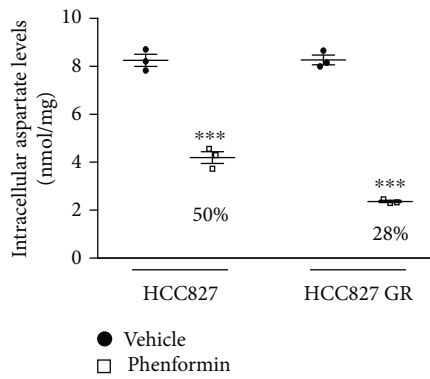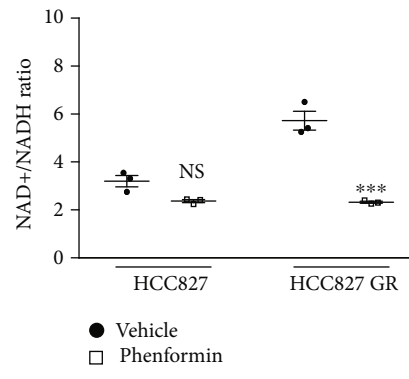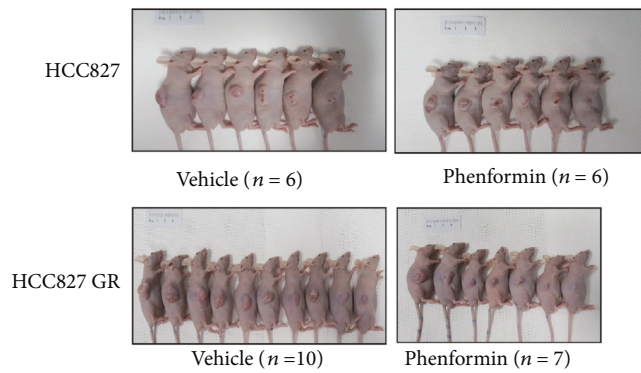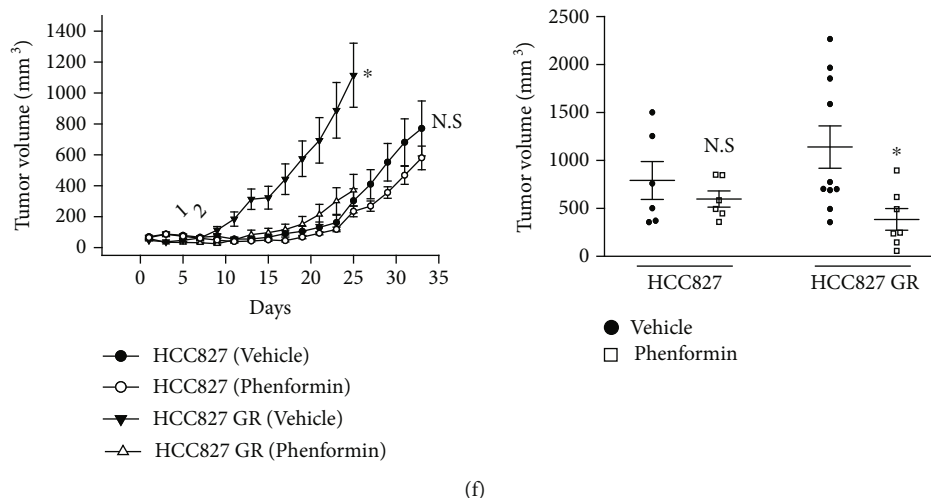
FIGURE 4: Selective anticancer effect of phenformin in acquired EGFR-TKI-resistant lung cancer. (a) HCC827, HCC827 GR, H1993, and H1993 ER cells were exposed to phenformin (30 and 100 μM) for 72 h, and cell proliferation was monitored by IncuCyte ZOOM. Data represent means ± S.E.M. ($n = 6$, $***P < 0.001$ vs. parental cell line). (b) Intracellular aspartate level. HCC827 and HCC827 GR cells were treated with 100 μM phenformin for 24 h, and aspartate levels in cell lysates were determined by LC-MS/MS. Data represent means ± S.E.M. ($n = 3$, $***P < 0.001$ vs. vehicle-treated group). (c) Potentiation of redox stress by phenformin in acquired EGFR-TKI-resistant cancer cells. Intracellular $NAD^+/NADH$ ratio was analyzed in HCC827 and HCC827 GR cells 24 h after exposure with vehicle or 100 μM phenformin. Data represent means ± S.E.M. ($n = 3$, $***P < 0.001$ vs. vehicle-treated group). (d) Reversal of antiproliferative effect of phenformin by electron acceptor or aspartate. Cell proliferation was monitored for 72 h in HCC827 and HCC827 GR cells treated with phenformin (30 and 100 μM) in the presence or absence of 1 mM AKB or 10 mM aspartate. Data represent means ± S.E.M. ($n = 6$, $**P < 0.01$, $***P < 0.001$ vs. vehicle-treated group). (e and f) In vivo anticancer effect of phenformin on tumor growth of EGFR-TKI-resistant lung cancer. HCC827 and HCC827 GR cells were inoculated into right flank of Balb/c nude mice, and the mice were orally administered with 300 mg/kg phenformin or tap water (vehicle) once a day. (e) Representative images. (f) Tumor volumes were measured every other day. Data represent means ± S.E.M. ($n = 6 - 10$, $*P < 0.05$ vs. vehicle-treated group).

parental cell lines (Figure 4(a)). However, the growth-inhibiting effect of phenformin was not enhanced in H292 ER cells compared with H292 cells (Figure S2C), which is consistent with the data showing no difference in ATP-associated OCR change (Figure 3(a)). Next, the potential mechanism by which phenformin inhibits the proliferation of EGFR-TKI-resistant NSCLC cells was assessed. Because OXPHOS is required for aspartate biosynthesis in proliferating cells [6, 18], intracellular aspartate level was measured after exposing HCC827 and HCC827 GR cells to phenformin. The intracellular aspartate level decreased to a greater extent in HCC827 GR cells than in HCC827 cells after exposure to phenformin (Figure 4(b)). Inhibition of aspartate biosynthesis occurs due to an imbalance in the $NAD^+/NADH$ ratio. When the cellular $NAD^+/NADH$ ratio was measured, phenformin-mediated $NAD^+/NADH$ imbalance was only observed in HCC827 GR cells (Figure 4(c)). α-Ketobutyrate (AKB) is a representative electron acceptor that participates in regenerating NAD^+ [6]. The addition of both AKB and aspartate partially alleviated the growth-inhibiting effects of phenformin in HCC827 GR cells (Figure 4(d)). To assess if mitochondrial OXPHOS complex I is a target of phenformin, the effects of rotenone, a potent OXPHOS complex 1 inhibitor, were investigated. TMRM-based mitochondria membrane potential in HCC827 GR cells was more potently reduced by rotenone treatment than HCC827 cells (Figure S2A). As expected, rotenone exerted strong growth-inhibiting effects in HCC827

GR cells, and its antiproliferative effect was reversed with AKB treatment (Figure S2B). To evaluate the anticancer effects of phenformin in vivo, Balb/c nude mice were implanted with HCC827 or HCC827 GR cells. In xenografts inoculated with HCC827 GR cells, oral administration of phenformin (300 mg/kg/day) significantly reduced tumor growth derived from HCC827 GR cells. Conversely, phenformin administration did not significantly affect tumor growth in xenografts inoculated with HCC827 cells (Figures 4(e) and 4(f)).

3.5. Reversal of Anticancer Effects of Phenformin Is Caused by Glycolysis Reactivation in Lung Cancer Cells with Acquired EGFR-TKI Resistance.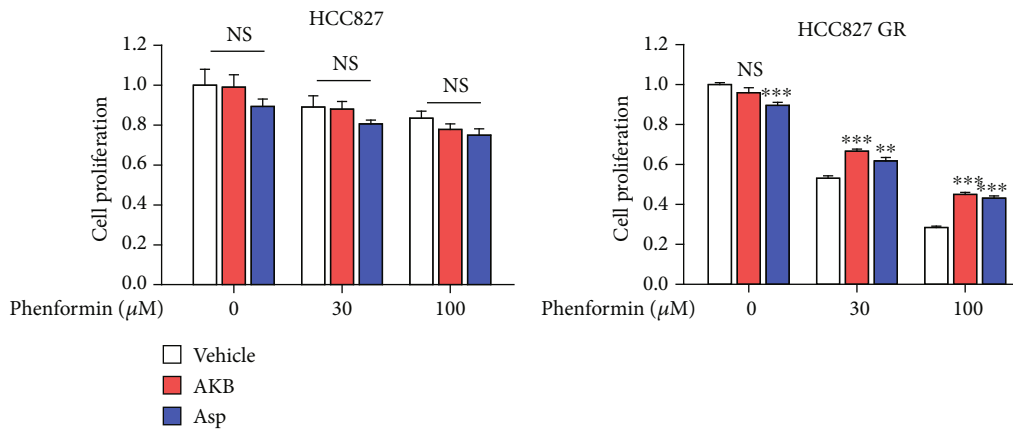 Because the reactivation of OXPHOS in most of the lung cancer cell lines with acquired EGFR-TKI resistance was observed, we hypothesized that phenformin sensitivity could be diminished by the restoration of glycolysis (Warburg effect) in the resistant cell types. Hexokinase (HK) is a first-step glycolytic enzyme that converts glucose into glucose 6-phosphate. Among the five HK isoforms, HK2 is highly expressed and functions as the predominant form in cancer cells [19]. Because HK2 and HK1 expressions were absent in H292 ER cells (Figure 2(d)), we hypothesized that HK enzyme deficiency is a key event for the metabolic shift to OXPHOS in H292 ER cells. HK2-overexpressing H292 ER cells (H292 ER-HK2) were established by transfection with a Flag-tagged human HK2 overexpression vector (Figure 5(a)). XFp analysis with a

(a)

(b)

(c)

(d)

Figure 5: Continued.

(e)
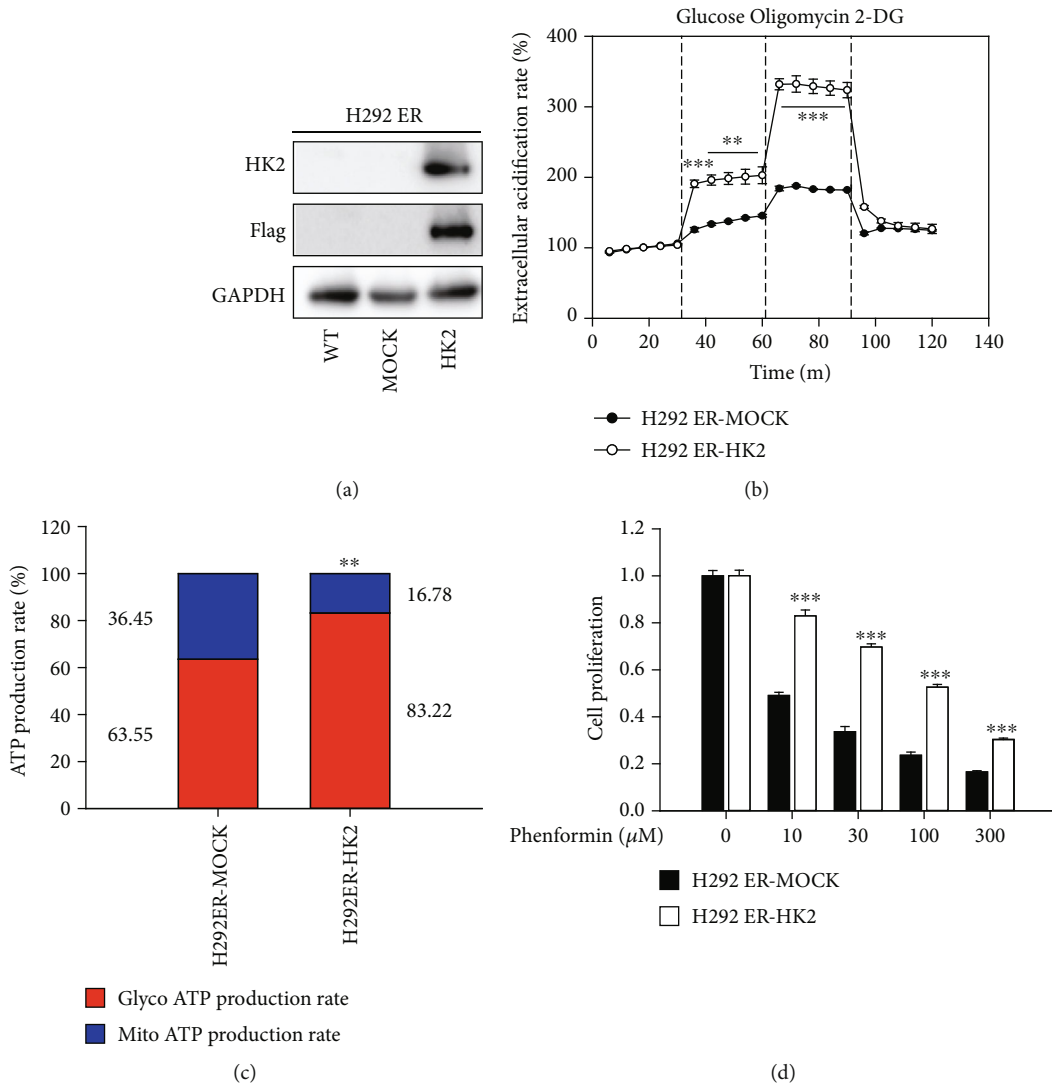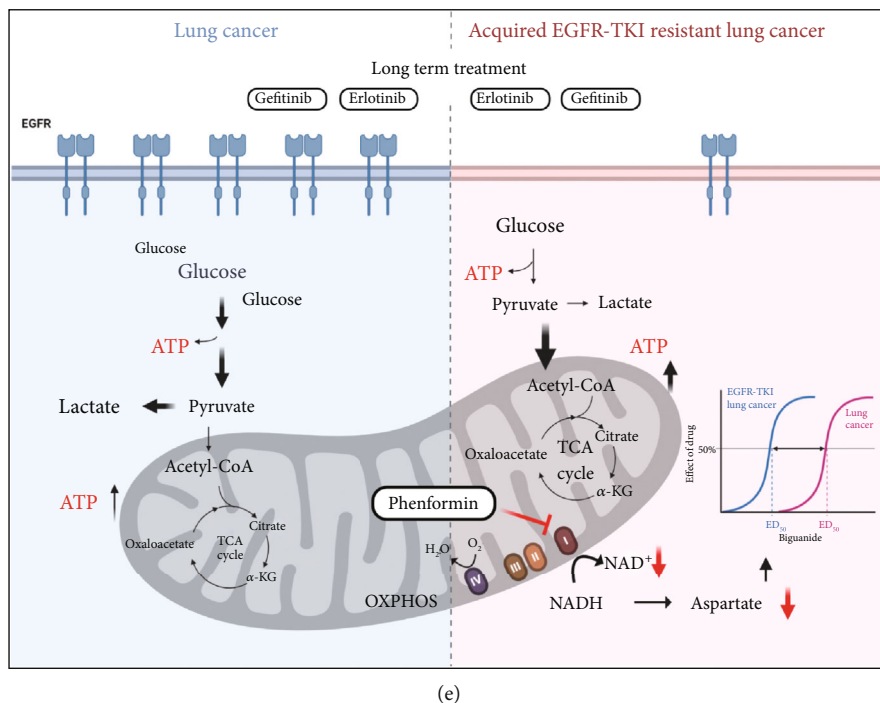
Figure 5: Reversal of antiproliferation effect of phenformin by glycolysis reactivation. (a) Establishment of hexokinase2 overexpressing H292 ER cells (H292 ER-HK2). H292 ER cells were transfected with pCAG-Flag-HK2-IRES-Blas or pCAG-Flag-IRES-Blas and protein expression was confirmed by immunoblotting. (b) ECAR values in H292 ER-MOCK and H292 ER-HK2 cells. Glycolysis stress test was performed by XFp analyzer, and ECAR was measured and normalized with basal ECAR level. Data represent means ± S.E.M. ($n = 3$, ∗∗$P < 0.01$, ∗∗∗$P < 0.001$ vs. H292 ER-MOCK). (c) Relative contribution of glycolysis and OXPHOS to ATP production in H292 ER-MOCK and H292 ER-HK2 cells. Using XFp real-time ATP rate assay kit, ATP production rate from glycolysis and OXPHOS was measured in H292 ER-MOCK and H292 ER-HK2 cells. Data represent means ($n = 3$, ∗∗$P < 0.01$ vs. mito ATP production rate in H292 ER-MOCK). (d) Alleviated antiproliferative effect of phenformin by HK2 overexpression. H292 ER-MOCK and H292 ER-HK2 cells were treated with vehicle or phenformin and cell proliferation rate was monitored for 72 h by IncuCyte ZOOM. Data represent means ± S.E.M. ($n = 6$, ∗∗∗$P < 0.001$ vs. H292 ER-MOCK). (e) Schematic illustration for metabolic shift to OXPHOS and the enhanced biguanide responsiveness in acquired EGFR-TKI resistant lung cancer.

glycolysis stress test kit showed that ECAR changes representing glycolysis and its capacity were greater in H292 ER-HK2 cells compared with mock-transfected cells (Figure 5(b)). The ATP production ratio from glycolysis also increased from 63.55% to 83.22% (Figure 5(c)). Furthermore, the inhibitory effects of phenformin on the proliferation of H292 ER cells were significantly decreased by HK2 overexpression, indicating that enhanced glycolysis reduces the anticancer effects of phenformin in lung cancer cells with acquired EGFR-TKI resistance (Figure 5(d)).

4. Discussion

EGFR overexpression has been detected in approximately half of NSCLC patients and is associated with poor prognosis, whereas EGFR-TKIs such as gefitinib and erlotinib significantly increase the survival rate of patients without serious side effects (6). Unfortunately, most patients acquire resistance to EGFR-TKIs within 6–12 months [20, 21]. Several heterogeneous mechanisms, such as *de novo* mutation, amplification, and downstream pathway activation of EGFR or the activation of bypass pathways (e.g., pathways involving c-Met, Axl, insulin-like growth factor receptor, and other members of the EGFR family), explain the acquired EGFR-

TKI resistance in NSCLC [22–25]. Osimertinib (Tagrisso®, a third-generation EGFR-TKI) has been approved for the treatment of patients with metastatic and EGFR T790M mutation-positive NSCLC [26]. However, several cases of patients resistant to osimertinib have been reported in clinics [26]. Although phenotype characteristics of EGFR-TKI-resistant lung cancer cells can be classified as EGFR-dependent and EGFR-independent growth [26], deciding an appropriate treatment strategy is difficult due to the acquired resistance being driven by heterogeneous mechanisms. Herein, we propose a plausible therapeutic strategy targeting the cancer metabolism of EGFR-TKI-resistant lung cancer cells that focuses on the metabolic shift to mitochondrial OXPHOS.

In the tested lung cancer cell lines, the metabolic use of glucose differed between EGFR-TKI-sensitive and EGFR-TKI-resistant lung cancer cells. Both glucose uptake and glycolytic capacity were significantly reduced in lung cancer cell lines with acquired EGFR-TKI resistance compared with their parental cell lines. Conversely, the overall function of mitochondria was enhanced in the resistant cell lines, as evidenced by increases in mitochondrial ATP production and mitochondrial membrane potential. Reportedly, EGFR stimulation accelerates glycolysis in TNBC cell lines [8].

Furthermore, suppression of EGFR signaling in NSCLC cells reverses the Warburg effect and reactivates OXPHOS [9]. Because EGFR-TKI-resistant lung cancer cell lines (HCC827 GR, H1993 ER, and H292 ER) acquired resistance via stepwise exposure to EGFR-TKIs over a long-term period [21, 27] and exhibited downregulated signaling activity of EGFR (Figure 1(d)), compensatory activation of mitochondrial OXPHOS in the resistant NSCLC cell lines appears reasonable.

Cancer metabolism is an emerging research area in cancer biology. Based on the reprogrammed pathways of nutrient utilization and metabolism in cancer cells, several metabolic characteristics have been identified as hallmarks of cancer and recognized as promising therapeutic targets for cancer chemotherapy [10, 28–32]. The metabolic processes of mitochondria have attracted attention as part of the development of treatment strategies targeting cancer metabolism [5]. In particular, biguanides inhibiting mitochondrial complex I could be of interest because metformin has been used for an extended period as an effective type 2 diabetes agent, and its safety is proven [14]. However, clear evidence showing the successful anticancer efficacy of biguanides has not been reported in numerous clinical trials, which may be due to the nonselection of either a proper biomarker that determines the reactivity of biguanide or an appropriate biguanide-responding carcinoma [33–35]. In the present study, phenformin strongly inhibited cell proliferation and tumor growth in NSCLC with acquired EGFR-TKI resistance (Figure 4).

We demonstrated that the anticancer effects of phenformin depend on the metabolic status of cancer cells, ATP production via glycolysis, or mitochondrial OXPHOS (Figure 5(c)). Although diverse cellular proteins including AMP-activated protein kinase, liver kinase B1 [36], OXPHOS complex 1 [37], and mitochondrial glycerolphosphate dehydrogenase [38] have been suggested as pharmacological targets of biguanides, we considered the NAD$^+$/NADH imbalance caused by OXPHOS complex 1 inhibition a plausible mechanism by which phenformin acts on EGFR-TKI-resistant NSCLC. Because NAD$^+$ is required to activate cytosolic malate dehydrogenase to generate oxaloacetate and then for the synthesis of aspartate through aspartate aminotransferase, a key function of mitochondrial OXPHOS and the redox balance in cancer cells is the biosynthesis of aspartic acid for the rapid growth of cancer [6, 18]. As shown in Figure 4, the intracellular aspartate level was decreased by phenformin in EGFR-TKI-resistant NSCLC. Because the metabolic shift to mitochondrial OXPHOS is triggered by long-term exposure to EGFR-TKIs, biguanide targeting OXPHOS may result in sustained redox stress as well as a subsequent aspartic acid deficiency and can be proposed as a new therapeutic option for NSCLC with acquired EGFR-TKI resistance. Consistent with our data, the combination of phenformin with osimertinib delayed the occurrence of resistance in a preclinical model of NSCLC in a recent study [17].

The present study has several limitations. First, all lung cancer cell lines did not exhibit a metabolic shift from glycolysis to mitochondrial OXPHOS under long-term exposure to EGFR-TKIs. In fact, phenformin sensitivity in H292 ER cells was of a similar intensity to that of its parental H292 cells (Figure S2C). Second, a proper biomarker indicating if a metabolic shift had occurred was not suggested. The expression levels of glycolytic enzymes, such as HK1, HK2, and GAPDH, were downregulated in HCC827 GR and H1993 ER cells. Conversely, Tyr105-phosphorylated PKM2, an inhibitory form of PKM2, and S293-phosphorylated PDHA1, which converts pyruvate into acetyl-CoA, were also downregulated in HCC827 GR and H1993 ER cells. Based on our results showing that the expression levels of glycolytic enzymes, such as HK1 and HK2, were low and those of the inactive form of PKM2 (Tyr105-phosphorylated PKM2) and S293-phosphorylated PDHA1 were high, H292 ER cells should be more dependent on OXPHOS and more vulnerable to phenformin. However, significant differences were not observed in terms of inhibitory effects of phenformin on the proliferation of H292 and H292 ER cells (Figure S2C). Because the metabolic processes of cancer cells are diverse, elucidating an indicator that defines the metabolic characteristics of cancer is challenging. Although specific genes that uniquely control the metabolic status of cancer cells have been successfully elucidated in a few studies [33, 35, 39], we could not find a common metabolic point for which mitochondrial function is upregulated in three different EGFR-TKI-resistant lung cancer cell lines. However, we presume that biguanide sensitivity in NSCLC with acquired EGFR-TKI resistance relies on mitochondrial OXPHOS activity. Because mitochondrial function is precisely controlled by numerous enzymes involved in several biochemical cycles, predicting the responsiveness to biguanide by only assessing specific gene expression is difficult.

5. Conclusions

Long-term treatment with EGFR-TKIs induces chemoresistance with a metabolic shift from glycolysis to OXPHOS in lung cancer cells. Suppressing OXPHOS by phenformin causes redox imbalance, leading to inhibition of aspartate biosynthesis and ultimately cancer cell growth. Our research provides pharmacological evidence for a therapeutic strategy using biguanides for EGFR-TKI-resistant NSCLC (Figure 5(e)).

Abbreviations

2-DG:	2-Deoxyglucose
AA:	Antimycin A
AKB:	Sodium 2-oxobutyrate
Asp:	Aspartate
ECAR:	Extracellular acidification rate
EGF:	Epidermal growth factor
EGFR:	Epidermal growth factor receptor
Erlo:	Erlotinib
FCCP:	Trifluoromethoxy carbonylcyanide phenylhydrazone
GAPDH:	Glyceraldehyde-3-phosphate dehydrogenase
Gef:	Gefitinib

H1993 ER:　　　Erlotinib-resistant H1993 cells
H292 ER:　　　Erlotinib-resistant H292 cells
HCC827 GR:　Gefitinib-resistant HCC827 cells
HK1:　　　　　Hexokinase 1
HK2:　　　　　Hexokinase 2
NSCLC:　　　　Nonsmall cell lung cancer
OCR:　　　　　Oxygen consumption rate
Osi:　　　　　　Osimertinib
OXPHOS:　　　Oxidative phosphorylation
PDHA1:　　　　Pyruvate dehydrogenase E1-alpha subunit
Phen:　　　　　Phenformin
PKM2:　　　　　Pyruvate kinase isozymes M2
Ro:　　　　　　Rotenone
TKI:　　　　　　Tyrosine kinase inhibitor
TMRM:　　　　Tetramethylrhodamine methyl ester.

Data Availability

Data is contained within the article or supplementary material.

Ethical Approval

Animal studies were approved by Seoul National University Institutional Animal Care and Use Committee (Approval #: SNU-170717-6-1).

Conflicts of Interest

The authors declare that they have no competing interests.

Authors' Contributions

KWK and SK designed experiments and wrote the manuscript. WKK helped analyzing RNA sequencing results. SKK and SWK helped determination of cell metabolites. SK, JHI, YJC, JYL, and SJK performed experiments.

Acknowledgments

Supplementary Materials

Supplemental Figure 1: (a) MA plot showing differential RNA expression levels in HCC827 GR versus HCC827 cells. Genes related to glycolysis were highlighted in red. (b) MA plot showing differential RNA expression in HCC827 and HCC827 GR cells. Genes related to OXPHOS subunits were highlighted in blue. Supplemental Figure 2: (a) Effect of rotenone, a representative complex 1 inhibitor, on cell proliferation of HCC827 and HCC827 GR cells. Both the cell types were exposed to $0.1 \mu M$ rotenone and/or 1 mM AKB for 72 h, and cell proliferation was assessed by IncuCyte ZOOM. Data represent means ± S.E.M. ($n = 6$, $***P < 0.001$ vs. vehicle-treated group; $^{\#}P < 0.05$, $^{\#\#\#}P < 0.001$ vs. rotenone-treated group). (b) Effect of rotenone on mitochondria membrane potential. HCC827 and HCC827 GR cells were treated with rotenone for 1 h, and TMRM fluorescence was detected by flow cytometry. Data represent means ± S.E.M. ($n = 3$, $***P < 0.001$ vs. vehicle-treated HCC827 cells). (c) H292 and H292 ER cells were treated with vehicle or phenformin (30 and 100 μM) for 72 h, and cell proliferation was analyzed with IncuCyte ZOOM. Data represent means ± S.E.M. ($n = 6$). *(Supplementary Materials)*

References

[1] G. Recondo, F. Facchinetti, K. A. Olaussen, B. Besse, and L. Friboulet, "Making the first move in _EGFR_ -driven or _ALK_ -driven NSCLC: first- generation or next-generation TKI?," *Nature Reviews Clinical Oncology*, vol. 15, no. 11, pp. 694–708, 2018.

[2] H. A. Yu, M. E. Arcila, N. Rekhtman et al., "Analysis of tumor specimens at the time of acquired resistance to EGFR-TKI therapy in 155 patients with EGFR-mutant lung cancers," *Clinical Cancer Research*, vol. 19, no. 8, pp. 2240–2247, 2013.

[3] "FDA resources for Information. Food and Drug Administration Web site," 2018, https://www.accessdata.fda.gov/drugsatfda_docs/label/2018/208065s008lbl.pdf.

[4] R. J. DeBerardinis and N. S. Chandel, "Fundamentals of cancer metabolism," *Science Advances*, vol. 2, no. 5, article e1600200, 2016.

[5] T. M. Ashton, W. G. McKenna, L. A. Kunz-Schughart, and G. S. Higgins, "Oxidative phosphorylation as an emerging target in cancer therapy," *Clinical Cancer Research*, vol. 24, no. 11, pp. 2482–2490, 2018.

[6] L. B. Sullivan, D. Y. Gui, A. M. Hosios, L. N. Bush, E. Freinkman, and M. G. Vander Heiden, "Supporting aspartate biosynthesis is an essential function of respiration in proliferating cells," *Cell*, vol. 162, no. 3, pp. 552–563, 2015.

[7] S. V. Sharma, D. W. Bell, J. Settleman, and D. A. Haber, "Epidermal growth factor receptor mutations in lung cancer," *Nature Reviews Cancer*, vol. 7, no. 3, pp. 169–181, 2007.

[8] S. O. Lim, C. W. Li, W. Y. Xia et al., "EGFR signaling enhances aerobic glycolysis in triple-negative breast cancer cells to promote tumor growth and immune escape," *Cancer Research*, vol. 76, no. 5, pp. 1284–1296, 2016.

[9] V. De Rosa, F. Iommelli, M. Monti et al., "Reversal of Warburg effect and reactivation of oxidative phosphorylation by differential inhibition of EGFR signaling pathways in non-small cell lung cancer," *Clinical Cancer Research*, vol. 21, no. 22, pp. 5110–5120, 2015.

[10] D. Hanahan and R. A. Weinberg, "Hallmarks of cancer: the next generation," *Cell*, vol. 144, no. 5, pp. 646–674, 2011.

[11] C. T. Hensley, B. Faubert, Q. Yuan et al., "Metabolic heterogeneity in human lung tumors," *Cell*, vol. 164, no. 4, pp. 681–694, 2016.

[12] C. Lehuede, F. Dupuy, R. Rabinovitch, R. G. Jones, and P. M. Siegel, "Metabolic plasticity as a determinant of tumor growth and metastasis," *Cancer Research*, vol. 76, no. 18, pp. 5201–5208, 2016.

[13] K. M. Schuler, B. S. Rambally, M. J. DiFurio et al., "Antiproliferative and metabolic effects of metformin in a preoperative window clinical trial for endometrial cancer," *Cancer Medicine*, vol. 4, no. 2, pp. 161–173, 2015.

[14] A. Vancura, P. L. Bu, M. Bhagwat, J. Zeng, and I. Vancurova, "Metformin as an anticancer agent," *Trends in Pharmacological Sciences*, vol. 39, no. 10, pp. 867–878, 2018.

[15] S. Niraula, R. J. O. Dowling, M. Ennis et al., "Metformin in early breast cancer: a prospective window of opportunity neoadjuvant study," *Breast Cancer Research and Treatment*, vol. 135, no. 3, pp. 821–830, 2012.

[16] A. M. Joshua, V. E. Zannella, M. R. Downes et al., "A pilot 'window of opportunity' neoadjuvant study of metformin in localised prostate cancer," *Prostate Cancer and Prostatic Diseases*, vol. 17, no. 3, pp. 252–258, 2014.

[17] M. J. Martin, C. Eberlein, M. Taylor, S. Ashton, D. Robinson, and D. Cross, "Inhibition of oxidative phosphorylation suppresses the development of osimertinib resistance in a preclinical model of EGFR-driven lung adenocarcinoma," *Oncotarget*, vol. 7, no. 52, pp. 86313–86325, 2016.

[18] K. Birsoy, T. Wang, W. W. Chen, E. Freinkman, M. Abu-Remaileh, and D. M. Sabatini, "An essential role of the mitochondrial electron transport chain in cell proliferation is to enable aspartate synthesis," *Cell*, vol. 162, no. 3, pp. 540–551, 2015.

[19] D. DeWaal, V. Nogueira, A. R. Terry et al., "Hexokinase-2 depletion inhibits glycolysis and induces oxidative phosphorylation in hepatocellular carcinoma and sensitizes to metformin," *Nature Communications*, vol. 9, no. 1, p. 446, 2018.

[20] F. Morgillo, C. M. Della Corte, M. Fasano, and F. Ciardiello, "Mechanisms of resistance to EGFR-targeted drugs: lung cancer," *Esmo Open*, vol. 1, no. 3, article e000060, 2016.

[21] D. Kim, D. H. Bach, Y. H. Fan et al., "AXL degradation in combination with EGFR-TKI can delay and overcome acquired resistance in human non-small cell lung cancer cells," *Cell Death & Disease*, vol. 10, no. 5, p. 361, 2019.

[22] J. A. Engelman, K. Zejnullahu, T. Mitsudomi et al., "MET amplification leads to gefitinib resistance in lung cancer by activating ERBB3 signaling," *Science*, vol. 316, no. 5827, pp. 1039–1043, 2007.

[23] Z. F. Zhang, J. C. Lee, L. P. Lin et al., "Activation of the AXL kinase causes resistance to EGFR-targeted therapy in lung cancer," *Nature Genetics*, vol. 44, no. 8, pp. 852–860, 2012.

[24] F. Morgillo, J. K. Woo, E. S. Kim, W. K. Hong, and H. Y. Lee, "Heterodimerization of insulin-like growth factor receptor/epidermal growth factor receptor and induction of survivin expression counteract the antitumor action of erlotinib," *Cancer Research*, vol. 66, no. 20, pp. 10100–10111, 2006.

[25] K. Takezawa, V. Pirazzoli, M. E. Arcila et al., "HER2Amplification: a potential mechanism of acquired resistance to EGFR inhibition in EGFR-mutant lung cancers that lack the Second-SiteEGFRT790MMutation," *Cancer Discovery*, vol. 2, no. 10, pp. 922–933, 2012.

[26] A. Leonetti, S. Sharma, R. Minari, P. Perego, E. Giovannetti, and M. Tiseo, "Resistance mechanisms to osimertinib in _EGFR_ -mutated non-small cell lung cancer," *British Journal of Cancer*, vol. 121, no. 9, pp. 725–737, 2019.

[27] D. H. Bach, D. Kim, S. Y. Bae et al., "Targeting Nicotinamide *N*-Methyltransferase and miR-449a in EGFR-TKI- Resistant Non-Small-Cell Lung Cancer Cells," *Molecular Therapy-Nucleic Acids*, vol. 11, pp. 455–467, 2018.

[28] B. J. Altman, Z. E. Stine, and C. V. Dang, "From Krebs to clinic: glutamine metabolism to cancer therapy," *Nature Reviews Cancer*, vol. 16, no. 10, pp. 619–634, 2016.

[29] R. Bajpai and M. Shanmugam, "Targeting cancer metabolism through synthetic lethality-based combinatorial treatment strategies," *Current Opinion in Oncology*, vol. 30, no. 5, pp. 338–344, 2018.

[30] R. J. Klement, "The emerging role of ketogenic diets in cancer treatment," *Current Opinion in Clinical Nutrition and Metabolic Care*, vol. 22, no. 2, pp. 129–134, 2019.

[31] A. Luengo, D. Y. Gui, and M. G. Vander Heiden, "Targeting metabolism for cancer therapy," *Cell Chemical Biology*, vol. 24, no. 9, pp. 1161–1180, 2017.

[32] C. M. Cheng, F. Geng, X. Cheng, and D. L. Guo, "Lipid metabolism reprogramming and its potential targets in cancer," *Cancer Communications*, vol. 38, no. 1, p. 27, 2018.

[33] K. Birsoy, R. Possemato, F. K. Lorbeer et al., "Metabolic determinants of cancer cell sensitivity to glucose limitation and biguanides," *Nature*, vol. 508, no. 7494, pp. 108–112, 2014.

[34] D. Y. Gui, L. B. Sullivan, A. Luengo et al., "Environment dictates dependence on mitochondrial complex I for NAD+ and aspartate production and determines cancer cell sensitivity to metformin," *Cell Metabolism*, vol. 24, no. 5, pp. 716–727, 2016.

[35] D. B. Shackelford, E. Abt, L. Gerken et al., "LKB1 inactivation dictates therapeutic response of non-small cell lung cancer to the metabolism drug phenformin," *Cancer Cell*, vol. 23, no. 2, pp. 143–158, 2013.

[36] R. J. Shaw, K. A. Lamia, D. Vasquez et al., "The kinase LKB1 mediates glucose homeostasis in liver and therapeutic effects of metformin," *Science*, vol. 310, no. 5754, pp. 1642–1646, 2005.

[37] H. R. Bridges, A. J. Y. Jones, M. N. Pollak, and J. Hirst, "Effects of metformin and other biguanides on oxidative phosphorylation in mitochondria," *Biochemical Journal*, vol. 462, no. 3, pp. 475–487, 2014.

[38] S. Thakur, B. Daley, K. Gaskins et al., "Metformin targets mitochondrial glycerophosphate dehydrogenase to control rate of oxidative phosphorylation and growth of thyroid cancer in vitro and in vivo," *Clinical Cancer Research*, vol. 24, no. 16, pp. 4030–4043, 2018.

[39] J. Chiche, J. Reverso-Meinietti, A. Mouchotte et al., "GAPDH expression predicts the response to R-CHOP, the tumor metabolic status, and the response of DLBCL patients to metabolic inhibitors," *Cell Metabolism*, vol. 29, no. 6, pp. 1243–1257.e10, 2019.

Review Article

Oxidative Stress Markers among Obstructive Sleep Apnea Patients

Agata Stanek (iD),[1] **Klaudia Brożyna-Tkaczyk** (iD),[2] **and Wojciech Myśliński** (iD)[2]

[1]*Department and Clinic of Internal Medicine, Angiology and Physical Medicine, Faculty of Medical Sciences in Zabrze,*
Medical University of Silesia, Batorego 15 St., 41-902 Bytom, Poland
[2]*Chair and Department of Internal Medicine, Medical University of Lublin, Staszica 16 St., 20-081 Lublin, Poland*

Correspondence should be addressed to Agata Stanek; astanek@tlen.pl
and Klaudia Brożyna-Tkaczyk; klaudiabrozyna19@gmail.com

Agata Stanek and Klaudia Brożyna-Tkaczyk contributed equally to this work.

Obstructive sleep apnea (OSA) is a chronic respiratory disorder, which can be present in up to 50% of the population, depending on the country. OSA is characterized by recurrent episodes of partial or complete obstruction of the upper airways with consistent movement of the respiratory musculature during sleep. Apneas and hypopneas can lead to a decrease in oxygen saturation, an increase in carbon dioxide in the blood, and subsequent arousals and sleep fragmentation caused by repetitive activation of the central nervous system. As a consequence, intermittent hypoxemia and consequent reoxygenation result in the production of reactive oxygen species, leading to systematic oxidative stress, which is postulated to be a key mechanism of endothelial dysfunction and increased risk for cardiovascular disorders in patients with OSA. In this review, various biomarkers of oxidative stress, including high-sensitivity C-reactive protein, pregnancy-associated plasma protein-A, superoxide dismutase, cell-free DNA, 8-hydroxy-2-deoxyguanosine, advanced oxidation protein products, lipid peroxidation products, receptor for advanced glycation end-products, and thioredoxin are discussed. Biomarkers of oxidative stress have the potential to be used to assess disease severity and treatment response. Continuous positive airway pressure (CPAP) is one of the most common noninvasive treatments for OSA; it keeps the upper airways open during sleep. This reduces episodes of intermittent hypoxia, reoxygenation, and arousal at night. CPAP has been shown to have anti-inflammatory properties and decrease oxidative stress. The administration of certain compounds, like vitamins A, C, and E as well as N-acetylcysteine and allopurinol, can decrease oxidative stress markers. However, their role in the treatment of OSA remains unclear.

1. Introduction

Obstructive sleep apnea (OSA), a chronic respiratory disorder, is present in up to 50% of the population, depending on the country, and affects nearly 1 billion adults aged 30–69 years [1]. OSA is characterized by recurrent episodes of partial or complete obstruction of the upper airways, with consistent movement of the respiratory musculature during sleep [2]. Apneas and hypopneas can lead to a decrease in oxygen saturation, an increase of carbon dioxide in the blood, and subsequent arousals and sleep fragmentation caused by repetitive activation of the central nervous system [3]. Frequent awakening during sleep is followed by somnolence during the day, lack of concentration, and chronic fatigue.

The main risk factor for OSA is obesity; other risk factors include postmenopausal status in women, craniofacial dysmorphisms, alcohol use, overuse of hypnotics, and advanced age [4]. The risk of developing cardiovascular disorders such as ischemic heart disease, heart failure, arrhythmia, stroke, and transient ischemic attack is relatively high in patients with OSA [5, 6]. In addition, OSA can predispose patients to hypertension, irrespective of other factors. OSA may cause cognitive dysfunction as well and accelerate aging [7].

The first-choice method for diagnosing OSA is overnight polysomnography, which can assess the severity of OSA in terms of apneas and hypopneas per hour (AHI). OSA severity is divided into mild, moderate, and severe, depending on AHI per hour; mild patients have 5 to 14 episodes per hour,

moderate cases have 15 to 29 per hour, and severe cases have over 30 per hour [8]. Additional parameters, such as oxygen desaturation index (ODI), measured as the mean number of oxygen hemoglobin saturation drops of 3% or more per hour of subjective sleep duration, mean blood hemoglobin oxygen saturation (SpO_2), and duration of oxygen blood saturation below 90% ($TSpO_2 < 90\%$) may also be measured during polysomnography [9, 10]. The gold standard of treatment for OSA is a continuous positive airway pressure (CPAP), which can be delivered using a wide variety of devices. CPAP keeps the upper airways open during sleep and, as a consequence, reduces apneas and hypopneas [11].

2. Oxidative Stress in OSA

Recurrent episodes of disturbed airflow due to obstruction during sleep in patients with OSA can lead to apneas/hypopneas and sequent fluctuations in blood oxygenation, with intermittent hypoxemia and hypercapnia. As a consequence, intermittent hypoxemia and the consequent reoxygenation result in the production of reactive oxygen species (ROS), leading to systemic oxidative stress [12]. ROS can react with nucleic acids, proteins, and lipids leading to DNA alterations, cellular damage, and inflammation [6, 13]. Moreover, intermittent hypoxemia stimulates the production of proinflammatory factors and promotes metabolic dysregulation and platelet aggregation [14].

The systemic oxidative stress present in OSA may represent a key mechanism of endothelial dysfunction and a primary reason for the increased risk of cardiovascular found in this patient population [15, 16]. More specifically, ROS induce endothelial dysfunction in the early stages of OSA by increasing the expression of leukocyte-specific (L-selectin and integrins) and endothelial-specific adhesion molecules (E-selectin, P-selectin, ICAM-1, and VECAM-1). Additionally, endothelial dysfunction may also cause microvascular damage [17].

Sampol et al. first showed that patients who underwent thoracic aortic dissection had a high prevalence of previously undiagnosed and frequently severe OSA [18]. It was postulated that aortic dissection may relate to ROS production induced by intermittent hypoxia and hypoxia-inducible factor-1 (HIF-1). Moreover, the progression of aortic dissection is also affected by this pathway, which promotes the expression of vascular endothelial growth factor (VEGF), as well as matrix metalloproteinases 2 and 9 in the aortic wall [19].

Obesity, which occurs in more than 50% of OSA patients, is itself a chronic inflammatory state related to systematic oxidative stress and increased cardiovascular morbidity [6, 20]. Simiakakis et al. [21] showed that systemic oxidative stress in patients with OSA is not associated with disease severity but rather with the presence of obesity, smoking, and female sex.

2.1. Biomarkers of Oxidative Stress in OSA Patients.
In the following section, biomarkers of oxidative stress in patients with OSA will be discussed in more detail. For this purpose, Medline and Embase databases were queried, and only papers published in the last 20 years were analyzed. We used key words such as "obstructive sleep apnea," "oxidative stress," "CPAP," and "antioxidants." The present systematic review was reported based on the guidelines of the Preferred

Reporting Items for Systematic Reviews and Meta-Analysis (PRISMA) Statement (Figure 1).

In our review, we only studied English articles, using systemic reviews, meta-analyses, prospective studies, and case reports. Biomarkers of oxidative stress in patients with OSA are presented in Table 1.

2.1.1. High-Sensitivity C-Reactive Protein.
A high-sensitivity C-reactive protein (hsCRP) is an acute-phase protein, in which high levels represent a marker of inflammation [22], though hsCRP may also be an oxidative stress marker [23]. There is a positive correlation between the levels of hsCRP and the parameters used to assess OSA severity, such as AHI, ODI, and $SpO_2 < 90\%$ [24]. Obesity, assessed by body mass index (BMI), is a common comorbidity among OSA patients and is associated with increased oxidative stress, independently from presence of OSA [25]. While some view OSA as independent from obesity and elevated CRP levels [26], Volná et al. [24] reported a significant difference in the serum levels of hsCRP in patients without OSA compared to severe OSA after correction for BMI.

2.1.2. Pregnancy-Associated Plasma Protein-A.
Pregnancy-associated plasma protein-A (PAPP-A) belongs to the metalloproteinase family. PAPP-A is synthesized by the placenta during pregnancy; therefore, it is widely used as a marker for prenatal genetic screening [27]. Moreover, PAPP-A is produced by the colon, kidneys, endometrium, bones, and testicles, among other organs [28]. PAPP-A was found to be a marker of instability in atherosclerosis in coronary syndromes. Moreover, high levels of PAPP-A have been reported to be present in patients with asthma, chronic obstructive pulmonary disease, and lung cancer [29, 30]. Thus, a high level of PAPP-A may signal the presence of inflammation and oxidative stress and could be used as a biomarker of risk for patients with atherosclerosis [31–33]. Results from previous reports assessing the levels of PAPP-A in OSA patients remain ambiguous. Cengiz et al. [34] showed that PAPP-A levels were significantly higher in OSA patients compared with a control group. In this study, a negative correlation between AHI and the levels of PAPP-A was reported. Surprisingly, patients with moderate OSA were found to have higher levels of PAPP-A compared with those who had mild or severe OSA [34]. In contrast, Volná et al. reported no significant correlation between AHI and the severity of OSA [24]. The ambiguity of these results may be due to a relatively small study sample.

2.1.3. Superoxide Dismutase Activity.
Superoxide dismutase (SOD) is an essential antioxidant enzyme that eliminates ROS in a similar fashion to catalase and peroxidase. Lower activity levels of SOD were present in OSA patients compared with healthy subjects [35]. A significant reduction in SOD activity was reported in those who had mild to moderate OSA [13].

2.1.4. Cell-Free DNA.
High cell free-DNA (cfDNA) levels are considered a serum marker of many inflammatory diseases, such as stroke, ischemic heart failure, acute coronary syndrome, and OSA [21, 36, 37]. Free radicals in OSA
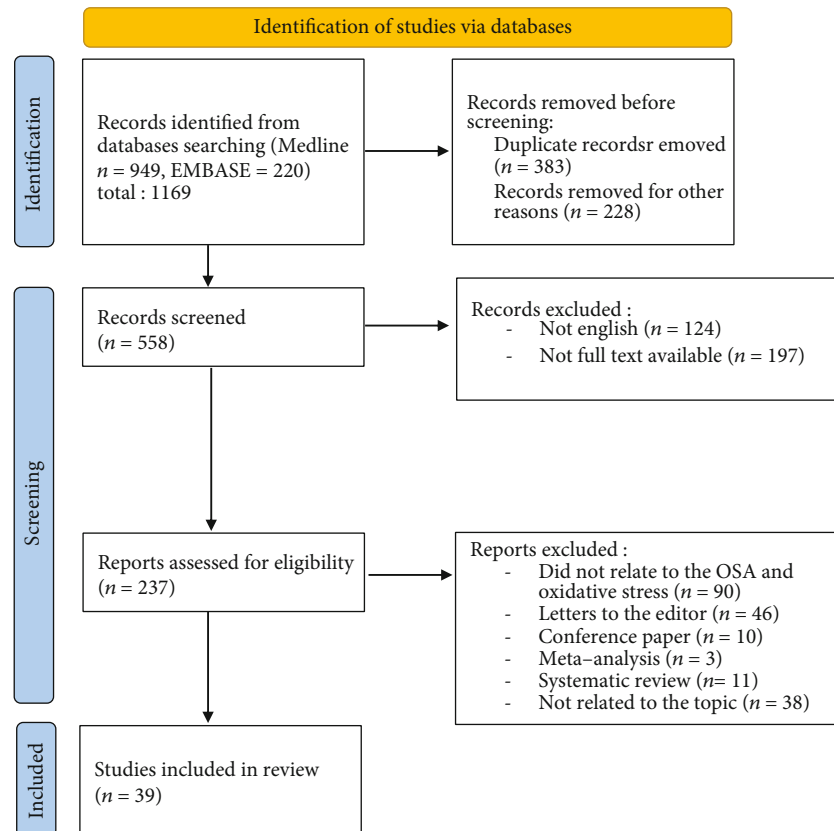
FIGURE 1: PRISMA flow diagram showing the study selection and identification.

patients destroy nucleic acids and lead to a higher level of free nucleosomes and cfDNA [38]. The levels of cfDNA were found to be significantly higher in OSA patients compared with healthy subjects [39]. Moreover, a linear correlation between cfDNA concentration and severity of disease was observed [40].

2.1.5. 8-Hydroxy-2-deoxyguanosine. 8-Hydroxy-2-deoxyguanosine (8-OHdG) is a product of DNA oxidation and has been used as a biomarker of oxidative stress. Significantly higher urinary 8-OHdG excretion has been observed in patients with severe OSA. In the same study, a positive correlation between 8-OHdG and AHI, ODI, and $TSpO_2 < 90\%$ was observed [41]. In contrast, Jordan et al. [42] showed that the concentration of 8-OhDG correlates with a duration of lower saturation. However, urinary excretion remained within the normal range in OSA patients. Presumably, in this group, hypoxemia and consequent reoxygenation did not induce strong DNA damage.

2.1.6. Advanced Oxidation Protein Products. Advanced oxidation protein products (AOPP) are a group of oxidized proteins that are produced by oxidation overload [43]. AOPP is a marker of both oxidative stress and inflammation [44]. They represent a more stable biomarker than products of lipid oxidation [45]. A study by Tóthová et al. [46] showed that AOPP concentrations in saliva samples are higher in the morning compared with the evening in patients with OSA. Thus, hypoxia, which occurs

during sleep in OSA patients, induces oxidative stress. Yağmur et al. [47] discovered a positive correlation between AOPP blood concentrations and AHI, TSpO2 < 90%, and ODI. Moreover, higher levels of AOPP are observed in patients with severe and moderate OSA compared with those who had mild OSA or were healthy subjects. Mancuso et al. [48] published contradicting results, where there was no correlation between polysomnography parameters and AOPP concentrations.

2.1.7. Lipid Peroxidation Products. End-products of lipid peroxidation include oxononenal (ONE), malondialdehyde (MDA), and hydroxynonenal (HNE). Lipid oxygenation is typically assessed by measuring the plasma concentrations of thiobarbituric acid-reactive substances (TBARS), which contain MDA and lipid peroxides. Hopps et al. [49] detected significantly higher levels of lipid peroxidation in patients with severe OSA compared with those who had mild and moderate disease severity. In all OSA patients ($n = 48$), positive correlations between AHI and TBARS and between ODI and TBARS were detected. Moreover, neck circumference, which is an anthropometric parameter used as a screening tool for obesity, was positively correlated with TBARS [49]. 8-Isoprostane is a product of the oxidation of arachidonic acid and is considered to be a reliable marker of oxidative stress because of its chemical stability [50]. Urinary excretion of 8-isoprostane was higher in OSA patients compared with healthy individuals [51].

TABLE 1: Characteristics of oxidative stress markers in obstructive sleep apnea (OSA) patients.

Author	Study population	Marker	Outcome
Volná J. et al. 2011 [24]	51 men divided into groups according to AHI values	hsCRP sRAGE PAPP-A	(i) Positive correlation between AHI, ODI, TSpO$_2$ < 90%, and hsCRP levels ($p < 0.001$) (ii) Significant difference between hsCRP levels in severe OSA (AHI ≥ 30) compared to healthy individuals (AHI ≤ 5) ($p = 0.039$) (iii) Negative correlation between sRAGE and AHI ($p = 0.044$) and between sRAGE and ODI ($p = 0.027$) (iv) No correlation between OSA parameters and PAPP-A levels
Cengiz A. et al. 2018 [34]	44 OSA 44 control group	PAPP-A	(i) PAPP-A levels significantly higher in OSA, particularly in patients with moderate severity, compared to the control group ($p < 0.001$) (ii) Negative correlation between AHI and PAPP-A (iii) Positive correlation between minimum and mean oxygen levels at night and PAPP-A
Wysocka E. et al. 2008 [35]	41 OSA 39 control group	SOD	(i) Decreased activity of SOD in OSA compared to controls, particularly in those with moderate to severe severity ($p = 0.006$)
Bauça J. et al. 2017 [39]	62 OSA 52 control group	cfDNA	(i) Increased concentration of dsDNA in OSA compared to controls ($p = 0.007$)
Ye L. et al. 2010 [40]	127 OSA (43 mild, 39 moderate, and 45 severe) 52 control group	cfDNA	(i) Positive correlation between level of cfDNA and AHI and ODI (ii) Linear correlation between cfDNA concentration and severity of OSA
Yamauchi M. et al. 2005 [41]	75 OSA (17 nonsevere [AHI < 30], 58 severe [AHI ≥ 30]	8-OHdG	(i) Urinary excretion of 8-OHdG higher in severe OSA ($p = 0.03$) (ii) Positive correlation between 8-OHdG urinary excretion and AHI, ODI, and TSpO$_2$ < 90%
Jordan W. et al. 2006 [42]	25 OSA (20 moderate to severe, 5 UARS or mild OSA)	8-OHdG	(i) 8-OHdG concentration slightly higher in patients with moderate to severe OSA (NS)
Tóthová L. et al. 2019 [46]	24 OSA (AHI > 30)	AOPP	(i) Salivary AOPP concentrations higher in the morning compared to evening ($p < 0.05$)
Yağmur A. et al. 2020 [47]	125 OSA (32 mild, 34 moderate, 59 severe) 40 control group	AOPP	(i) Higher levels of AOPP in severe and moderate OSA subjects compared to mild OSA subjects and healthy controls ($p < 0.05$) (ii) Positive correlation between AOPP blood concentration and AHI, TSpO$_2$ < 90%, and ODI ($p < 0.001$)
Mancuso M. et al. 2012 [48]	41 OSA (7 mild, 15 moderate, and 19 severe) 32 control group	AOPP	(i) No correlation between AOPP levels and AHI
Hopps E. et al. 2014 [49]	48 OSA (21 low [AHI < 30], 27 high [AHI > 30])	TBARS	(i) Positive correlation between AHI, ODI, and TBARS concentration ($p < 0.0001$)
Cherneva R. et al. 2017 [51]	86 OSA (ESS < 11) 45 control group	8-Isoprostane	(i) Higher urinary excretion in OSA patients compared to controls ($p = 0.028$)
Cai W. et al. 2015 [55]	139 OSA (46 with AHI < 42, 46 with 42 ≤ AHI < 66, 47 with AHI ≥ 66)	sRAGE esRAGE	(i) Negative correlation between sRAGE and esRAGE expression and AHI ($p < 0.05$)
Guo Q. et al. 2013 [57]	54 OSA (14 mild, 11 moderate, and 29 severe)	Trx	(i) Positive correlation between AHI and Trx concentration ($p < 0.05$)

2.1.8. Receptor for Advanced Glycation End-Products. Advanced glycation end-products (AGE) are the results of the nonenzymatic glycation of proteins. This reaction can occur during intermittent hypoxia and hyperglycemia [52, 53]. Receptor for advanced glycation end-products (RAGE) is a multiligand cell-surface receptor that interacts with AGE. Interaction between the receptor and its ligand activates nuclear factor-kappa B (NF-κB) and stimulates oxidative stress and inflammatory marker production. RAGE is expressed in podocytes, mesangial cells, and renal tubules, among other tissues [54]. Soluble RAGE (sRAGE) and endogenous secretory RAGE (esRAGE) were recently identified as two isoforms of this receptor. In OSA patients, sRAGE and esRAGE expression negatively correlated with AHI,

ODI, and BMI [24, 55]. In addition, esRAGE expression relates to systolic and diastolic blood pressure; the lower the blood pressure, the higher the expression of esRAGE [55]. However, such a correlation was not found for sRAGE. Thus, it was suggested that these isoforms may have differing roles in OSA progression.

2.1.9. Thioredoxin. Thioredoxin (Trx), along with NADPH and thioredoxin reductase (TrxR), is part of the Trx system, which is present in all living organisms. The main role of this system is to regulate a variety of cellular redox reactions and signaling pathways, such as antioxidant defense and gene transcription [56]. Guo et al. [57] found a positive correlation between the concentrations of Trx and the severity of OSA.

Increased Trx levels were proportional to reduced O_2 saturation and increased AHI values.

3. The Impact of CPAP on Oxidative Stress in OSA

CPAP is one of the most common noninvasive methods of treating OSA; by keeping the upper airways open during sleep, CPAP reduces episodes of intermittent hypoxia, reoxygenation, and arousal during the night. CPAP is also reported to decrease oxidative stress [58, 59]. The efficacy of CPAP depends on the duration of therapy. Alzoghaibi and BaHammam [60] showed that even one night of overnight CPAP treatment impacts lipid peroxidation and decreases TBARS concentrations. However, such a short therapy does not affect antioxidant production, and SOD activity remains unchanged after CPAP therapy. In contrast, decreased concentrations of 8-isoprostane from exhaled breathe were reported after only 2 days of CPAP therapy [61]. Likewise, three months of CPAP treatment led to a significant reduction in 8-isoprostane serum concentrations [58]. Borges et al. [62] reported that 8-week CPAP therapy had no significant impact on oxidative stress biomarkers, including SOD and AOPP. However, sleep efficiency and hours of sleep significantly improved. In several studies, AOPP concentrations remained unchanged after 3 months of CPAP therapy; however, the number of patients who underwent reevaluation after therapy was small ($n = 7$) [48]. Eight-week CPAP therapy also significantly decreased the levels of 8-OHdG [63]. With regard to Trx, studies have shown that one-month therapy significantly decreases the concentrations of this biomarker in patients with severe OSA [64].

4. The Role of Antioxidants in OSA

4.1. Vitamins and Microelements. Vitamins C, E, and A are essential microelements that act as antioxidants to protect lipids, proteins, nucleic acids, and other important biomolecules against oxidative stress damage [65, 66]. Their antioxidant properties are related to their ability to donate electrons. Selenium (Se), a metalloid, is present as selenoproteins, which are important in many reactions, such as the formation of thyroid hormones and antioxidant defense [67].

The role of antioxidants in OSA has been reported in many studies, though opinions may differ. Several studies reported decreased levels of vitamins A and E in OSA patients compared with healthy individuals [68, 69]. In contrast, Saruhan et al. [70] found that concentrations of vitamin A are increased in OSA patients and are positively correlated with AHI. The levels of vitamin E were also higher in OSA patients compared with healthy individuals, but the difference was not statistically significant, possibly due to the different sample sizes of the groups used in the study (47 vs. 114). Vitamins A and E, fat-soluble compounds, are stored in adipose tissue and the liver; oxidative stress and inflammation induce an increased release of vitamins from adipose tissue. Moreover, oxidative stress in OSA patients upregulates the expression of α-tocopherol transfer protein (αTTP),

which is responsible for vitamin E transfer between the liver and other tissues [71]. However, the concentrations of vitamin C, a water-soluble compound, were significantly decreased in OSA patients compared with healthy subjects [70]. Opinions regarding the correlation between selenium levels and OSA also differ. Chen et al. [72] demonstrated that selenium concentrations are decreased in newly diagnosed OSA patients with mild to moderate severity. In contrast, Saruhan et al. [70] found significantly higher selenium levels in OSA patients compared with healthy subjects. In both studies, patients with comorbidities, which could impact the results, were excluded. The disparity between these studies could also result from varying sample sizes.

In the literature, several studies have investigated the use of antioxidants as therapy for OSA. Grebe et al. [73] performed measurements of flow-mediated dilation (FMD) on brachial artery by ultrasonography. FMD is a parameter that assesses endothelial function. FMD values were decreased in OSA patients; however, after intravenous administration of vitamin C, FMD increased in these patients, but not in the control group. In addition, animal models, including rats, have been used to assess the influence of vitamins C and E on oxidative stress. Intermittent hypoxia generated by obstruction of the trachea led to higher concentrations of MDA and AOPP, both indicators of oxidative stress. The administration of antioxidants significantly decreased AOPP levels, with no impact on MDA concentrations [59].

4.2. Medications and Perspective for Future OSA Therapy. Several medications frequently used to treat diseases other than OSA have antioxidant properties. NAC is well-known as a mucolytic drug and is used in acetaminophen intoxication. Moreover, NAC is essential to glutathione synthesis and has an antioxidant effect. A 30-day oral administration of N-acetylcysteine (NAC) has been previously tested in OSA patients. This study reported that in NAC-treated patients, lipid peroxidation products were significantly decreased and levels of glutathione were increased after treatment [13]. Allopurinol, which is commonly used in urate-lowering therapy, has additional properties, such as scavenging free radicals and inhibition of lipid peroxidation [74]. An animal model study, performed on rats, reported a significant decrease in lipid peroxidation products in allopurinol-treated rats [75].

5. Conclusion

Taken together, oxidative stress in patients with OSA arises as a consequence of intermittent hypoxia during the night. Biomarkers of oxidative stress may be used to assess disease severity as well as the individual response to treatment. Several of these markers, including high-sensitivity CRP, 8-hydroxy-2-deoxyguanosine, thioredoxin, advanced oxidation protein products, and lipid peroxidation, have positive correlations with AHI, ODI, and $SpO_2 < 90\%$.

CPAP therapy is essential to treat OSA due to its antioxidative properties. Many studies have reported a significant decrease in the concentrations of many oxidative markers, such as 8-isoprostane, 8-hydroxy-2-deoxyguanosine, and

thioredoxin. The impact on the reduction of oxidative stress is greater the longer the therapy. However, SOD activity did not differ after the treatment. Likely, it is necessary to conduct further studies with a longer period of CPAP treatment and a wider study group.

In addition, surveys on the administration of antioxidants such as vitamins and antioxidant medications demonstrated decreased levels of markers of oxidative stress. However, several were performed on animal models, and further experimentation is warranted. Nonetheless, antioxidants may one day be utilized as complementary therapy for OSA, with potential benefits for patients who are intolerant to CPAP.

Conflicts of Interest

The authors declare no conflict of interests.

Authors' Contributions

Agata Stanek and Klaudia Brożyna-Tkaczyk contributed equally to this work.

References

[1] A. V. Benjafield, N. T. Ayas, P. R. Eastwood et al., "Estimation of the global prevalence and burden of obstructive sleep apnoea: a literature-based analysis," *The Lancet. Respiratory Medicine*, vol. 7, no. 8, pp. 687–698, 2019.

[2] V. K. Kapur, D. H. Auckley, S. Chowdhuri et al., "Clinical practice guideline for diagnostic testing for adult obstructive sleep apnea: an American Academy of Sleep Medicine clinical practice guideline," *Journal of Clinical Sleep Medicine*, vol. 13, no. 3, pp. 479–504, 2017.

[3] J. M. Parish and V. K. Somers, "Obstructive sleep apnea and cardiovascular disease," *Mayo Clinic Proceedings*, vol. 79, no. 8, pp. 1036–1046, 2004.

[4] P. E. Peppard, T. Young, J. H. Barnet, M. Palta, E. W. Hagen, and K. M. Hla, "Increased prevalence of sleep-disordered breathing in adults," *American Journal of Epidemiology*, vol. 177, no. 9, pp. 1006–1014, 2013.

[5] T. D. Bradley and J. S. Floras, "Obstructive sleep apnoea and its cardiovascular consequences," *The Lancet*, vol. 373, no. 9657, pp. 82–93, 2009.

[6] H. J. Eisele, P. Markart, and R. Schulz, "Obstructive sleep apnea, oxidative stress, and cardiovascular disease: evidence from human studies," *Oxidative medicine and cellular longevity*, vol. 2015, Article ID 608438, 9 pages, 2015.

[7] Y. Li and Y. Wang, "Obstructive sleep apnea-hypopnea syndrome as a novel potential risk for aging," *Aging and disease*, vol. 12, no. 2, pp. 586–596, 2021.

[8] M. Semelka, J. Wilson, and R. Floyd, "Diagnosis and treatment of obstructive sleep apnea in adults," *American Family Physician*, vol. 94, no. 5, pp. 355–360, 2016.

[9] P. Mayer, A. Herrero Babiloni, G. Beetz et al., "The evaluation of autonomic arousals in scoring sleep respiratory disturbances with polysomnography and portable monitor devices: a proof of concept study," *Nature and Science of Sleep*, vol. -Volume 12, no. 12, pp. 443–451, 2020.

[10] S. Kainulainen, J. Töyräs, A. Oksenberg et al., "Severity of desaturations reflects OSA-related daytime sleepiness better than AHI," *Journal of Clinical Sleep Medicine*, vol. 15, no. 8, pp. 1135–1142, 2019.

[11] A. Antonescu-Turcu and S. Parthasarathy, "CPAP and bi-level PAP therapy: new and established roles," *Respiratory Care*, vol. 55, no. 9, pp. 1216–1229, 2010.

[12] L. Lavie, "Oxidative stress in obstructive sleep apnea and intermittent hypoxia - revisited - the bad ugly and good: implications to the heart and brain," *Sleep Medicine Reviews*, vol. 20, pp. 27–45, 2015.

[13] A. B. Lira and C. F. de Sousa Rodrigues, "Evaluation of oxidative stress markers in obstructive sleep apnea syndrome and additional antioxidant therapy: a review article," *Sleep and Breathing*, vol. 20, no. 4, pp. 1155–1160, 2016.

[14] M. Yamauchi and H. Kimura, "Oxidative stress in obstructive sleep apnea: putative pathways to the cardiovascular complications," *Antioxidants and Redox Signaling*, vol. 10, no. 4, pp. 755–768, 2008.

[15] L. Lavie and P. Lavie, "Molecular mechanisms of cardiovascular disease in OSAHS: the oxidative stress link," *European Respiratory Journal*, vol. 33, no. 6, pp. 1467–1484, 2009.

[16] F. Wang, Y. Liu, H. Xu et al., "Association between upper-airway surgery and ameliorative risk markers of endothelial function in obstructive sleep apnea," *Scientific Reports*, vol. 9, no. 1, p. 20157, 2019.

[17] A. Maniaci, G. Iannella, S. Cocuzza et al., "Oxidative stress and inflammation biomarker expression in obstructive sleep apnea patients," *Journal of Clinical Medicine*, vol. 10, no. 2, p. 277, 2021.

[18] G. Sampol, O. Romero, A. Salas et al., "Obstructive sleep apnea and thoracic aorta dissection," *American Journal of Respiratory and Critical Care Medicine*, vol. 168, no. 12, pp. 1528–1531, 2003.

[19] W. Liu, W. Zhang, T. Wang et al., "Obstructive sleep apnea syndrome promotes the progression of aortic dissection via a ROS- HIF-1α-MMPs associated pathway," *International Journal of Biological Sciences*, vol. 15, no. 13, pp. 2774–2782, 2019.

[20] R. Mehra and S. Redline, "Sleep apnea: a proinflammatory disorder that coaggregates with obesity," *The Journal of Allergy and Clinical Immunology*, vol. 121, no. 5, pp. 1096–1102, 2008.

[21] M. Simiakakis, F. Kapsimalis, E. Chaligiannis, S. Loukides, N. Sitaras, and M. Alchanatis, "Lack of effect of sleep apnea on oxidative stress in obstructive sleep apnea syndrome (OSAS) patients," *PLoS One*, vol. 7, no. 6, p. e39172, 2012.

[22] J. Y. Yeun and G. A. Kaysen, "C-reactive protein, oxidative stress, homocysteine, and troponin as inflammatory and metabolic predictors of atherosclerosis in ESRD," *Current Opinion in Nephrology and Hypertension*, vol. 9, no. 6, pp. 621–630, 2000.

[23] S. Cottone, G. Mule, e. nardi et al., "Relation of C-reactive protein to oxidative stress and to endothelial activation in essential hypertension," *American Journal of Hypertension*, vol. 19, no. 3, pp. 313–318, 2006.

[24] J. Volna, D. Kemlink, M. Kalousova et al., "Biochemical oxidative stress-related markers in patients with obstructive sleep apnea," *Medical Science Monitor*, vol. 17, no. 9, pp. CR491–CR497, 2011.

[25] A. M. J. de Lima, C. M. R. Franco, C. M. M. B. de Castro, A. A. Bezerra, L. Ataíde Jr, and A. Halpern, "Obstructive sleep apnea contribution to oxidative stress in obesity," *Arquivos Brasileiros de Endocrinologia & Metabologia*, vol. 52, no. 4, pp. 668–676, 2008.

[26] S. Firat Guven, M. H. Turkkani, B. Ciftci, T. Ulukavak Ciftci, and Y. Erdogan, "The relationship between high-sensitivity C-reactive protein levels and the severity of obstructive sleep apnea," *Sleep and Breathing*, vol. 16, no. 1, pp. 217–221, 2012.

[27] S. Berk, O. T. Dogan, E. I. Aydemir, A. Bingol, S. L. Ozsahin, and I. Akkurt, "Diagnostic usefulness of pregnancy-associated plasma protein-A in suspected pulmonary embolism," *Multidisciplinary Respiratory Medicine*, vol. 8, no. 1, 2013.

[28] I. Bulut, E. Gulcan, A. Coskun et al., "Relationship between pregnancy-associated plasma protein-A and lung cancer," *American Journal of the Medical Sciences*, vol. 337, no. 4, pp. 241–244, 2009.

[29] F. Talay, M. Tosun, Z. A. Yaşar et al., "Evaluation of pregnancy associated plasma protein-A levels in patients with chronic obstructive pulmonary disease and associations with disease severity," *Inflammation*, vol. 39, no. 3, pp. 1130–1133, 2016.

[30] A. Coskun, O. Balbay, S. Duran et al., "Pregnancy-associated plasma protein-A and asthma," *Advances in Therapy*, vol. 24, no. 2, pp. 362–367, 2007.

[31] L. Fialová, M. Kalousová, J. Soukupová et al., "Relationship of pregnancy-associated plasma protein-A to renal function and dialysis modalities," *Kidney and Blood Pressure Research*, vol. 27, no. 2, pp. 88–95, 2004.

[32] C. Heeschen, S. Dimmeler, C. W. Hamm et al., "Pregnancy-associated plasma protein-A levels in patients with acute coronary syndromes: comparison with markers of systemic inflammation, platelet activation, and myocardial necrosis," *Journal of the American College of Cardiology*, vol. 45, no. 2, pp. 229–237, 2005.

[33] A. Stanek, A. Cholewka, T. Wielkoszyński, E. Romuk, K. Sieroń, and A. Sieroń, "Increased levels of oxidative stress markers, soluble CD40 ligand, and carotid intima-media thickness reflect acceleration of atherosclerosis in male patients with ankylosing spondylitis in active phase and without the classical cardiovascular risk factors," *Oxidative Medicine and Cellular Longevity*, vol. 2017, Article ID 9712536, 8 pages, 2017.

[34] A. Cengiz, S. Konuk, and T. Tuğ, "The relation between pregnancy-associated plasma protein A and obstructive sleep apnea syndrome," *Canadian Respiratory Journal*, vol. 2018, Article ID 3297810, 6 pages, 2018.

[35] E. Wysocka, S. Cofta, M. Cymerys, J. Gozdzik, L. Torlinski, and H. Batura-Gabryel, "The impact of the sleep apnea syndrome on oxidant-antioxidant balance in the blood of overweight and obese patients," *Journal of Physiology and Pharmacology*, vol. 59, Supplement 6, pp. 761–769, 2008.

[36] A. Shimony, D. Zahger, H. Gilutz et al., "Cell free DNA detected by a novel method in acute ST-elevation myocardial infarction patients," *Acute Cardiac Care*, vol. 12, no. 3, pp. 109–111, 2010.

[37] N. W. Tsai, T. K. Lin, S. D. Chen et al., "The value of serial plasma nuclear and mitochondrial DNA levels in patients with acute ischemic stroke," *Clinica Chimica Acta*, vol. 412, no. 5–6, pp. 476–479, 2011.

[38] A. V. Ermakov, M. S. Konkova, S. V. Kostyuk, V. L. Izevskaya, A. Baranova, and N. N. Veiko, "Oxidized extracellular DNA as a stress signal in human cells," *Oxidative Medicine and Cellular Longevity*, vol. 2013, Article ID 649747, 12 pages, 2013.

[39] J. M. Bauça, A. Yañez, L. Fueyo et al., "Cell death biomarkers and obstructive sleep apnea: implications in the acute coronary syndrome," *Sleep*, vol. 40, no. 5, 2017.

[40] L. Ye, G.-H. Ma, L. Chen et al., "Quantification of circulating cell-free DNA in the serum of patients with obstructive sleep apnea-hypopnea syndrome," *Lung*, vol. 188, no. 6, pp. 469–474, 2010.

[41] M. Yamauchi, H. Nakano, J. Maekawa et al., "Oxidative stress in obstructive sleep apnea," *Chest*, vol. 127, no. 5, pp. 1674–1679, 2005.

[42] W. Jordan, S. Cohrs, D. Degner et al., "Evaluation of oxidative stress measurements in obstructive sleep apnea syndrome," *Journal of Neural Transmission*, vol. 113, no. 2, pp. 239–254, 2006.

[43] V. Witko-Sarsat, M. Friedlander, C. Capeillère-Blandin et al., "Advanced oxidation protein products as a novel marker of oxidative stress in uremia," *Kidney International*, vol. 49, no. 5, pp. 1304–1313, 1996.

[44] M. Skvarilová, A. Bulava, D. Stejskal, S. Adamovská, and J. Bartek, "Increased level of advanced oxidation products (AOPP) as a marker of oxidative stress in patients with acute coronary syndrome," *Biomedical Papers*, vol. 149, no. 1, pp. 83–87, 2005.

[45] Z. A. Massy and T. Nguyen-Khoa, "Oxidative stress and chronic renal failure: markers and management," *Journal Nephrology*, vol. 15, no. 4, pp. 336–341, 2002.

[46] Ľ. Tóthová, P. Celec, I. Mucska, and J. Hodosy, "Short-term effects of continuous positive airway pressure on oxidative stress in severe sleep apnea," *Sleep and Breathing*, vol. 23, no. 3, pp. 857–863, 2019.

[47] A. R. Yağmur, M. A. Çetin, S. E. Karakurt, T. Turhan, and H. H. Dere, "The levels of advanced oxidation protein products in patients with obstructive sleep apnea syndrome," *Irish Journal of Medical Science*, vol. 189, no. 4, pp. 1403–1409, 2020.

[48] M. Mancuso, E. Bonanni, A. LoGerfo et al., "Oxidative stress biomarkers in patients with untreated obstructive sleep apnea syndrome," *Sleep Medicine*, vol. 13, no. 6, pp. 632–636, 2012.

[49] E. Hopps, B. Canino, V. Calandrino, M. Montana, R. Lo Presti, and G. Caimi, "Lipid peroxidation and protein oxidation are related to the severity of OSAS," *European Review for Medical and Pharmacological Sciences*, vol. 18, no. 24, pp. 3773–3778, 2014.

[50] J. L. Cracowski, T. Durand, and G. Bessard, "Isoprostanes as a biomarker of lipid peroxidation in humans: physiology, pharmacology and clinical implications," *Trends in Pharmacological Sciences*, vol. 23, no. 8, pp. 360–366, 2002.

[51] R. V. Cherneva, Z. V. Cherneva, O. B. Georgiev, D. S. Petrova, and J. I. Petrova, "8-isoprostanes and resistin as markers of vascular damage in non- hypersomnolent obstructive sleep apnoea patients," *Clinical Physiology and Functional Imaging*, vol. 37, no. 6, pp. 695–702, 2017.

[52] Y. Xu, F. Toure, W. Qu et al., "Advanced glycation end product (AGE)-receptor for AGE (RAGE) signaling and up-regulation of Egr-1 in hypoxic macrophages," *Journal of Biological Chemistry*, vol. 285, no. 30, pp. 23233–23240, 2010.

[53] D. G. Dyer, J. A. Blackledge, S. R. Thorpe, and J. W. Baynes, "Formation of pentosidine during nonenzymatic browning of proteins by glucose. Identification of glucose and other carbohydrates as possible precursors of pentosidine in vivo," *Journal of Biological Chemistry*, vol. 266, no. 18, pp. 11654–11660, 1991.

[54] E. J. Lee, E. Y. Park, H. Mun et al., "Soluble receptor for advanced glycation end products inhibits disease progression

in autosomal dominant polycystic kidney disease by down-regulating cell proliferation," *The FASEB Journal*, vol. 29, no. 8, pp. 3506–3514, 2015.

[55] W. Cai, J. F. Sun, Y. Liu et al., "Relationship between serum levels of endogenous secretory RAGE and blood pressure in male nondiabetic patients with obstructive sleep apnea," *Journal of Human Hypertension*, vol. 29, no. 12, pp. 713–718, 2015.

[56] J. Zhang, X. Li, X. Han, R. Liu, and J. Fang, "Targeting the thioredoxin system for cancer therapy," *Trends in Pharmacological Sciences*, vol. 38, no. 9, pp. 794–808, 2017.

[57] Q. Guo, Y. Wang, Q. Y. Li, M. Li, and H. Y. Wan, "Levels of thioredoxin are related to the severity of obstructive sleep apnea: based on oxidative stress concept," *Sleep and Breathing*, vol. 17, no. 1, pp. 311–316, 2013.

[58] H. Karamanlı, D. Özol, K. S. Ugur et al., "Influence of CPAP treatment on airway and systemic inflammation in OSAS patients," *Sleep and Breathing*, vol. 18, no. 2, pp. 251–256, 2014.

[59] P. Celec, I. Jurkovičová, R. Buchta et al., "Antioxidant vitamins prevent oxidative and carbonyl stress in an animal model of obstructive sleep apnea," *Sleep and Breathing*, vol. 17, no. 2, pp. 867–871, 2013.

[60] M. A. Alzoghaibi and A. S. BaHammam, "The effect of one night of continuous positive airway pressure therapy on oxidative stress and antioxidant defense in hypertensive patients with severe obstructive sleep apnea," *Sleep and Breathing*, vol. 16, no. 2, pp. 499–504, 2012.

[61] G. E. Carpagnano, S. A. Kharitonov, O. Resta, M. P. Foschino-Barbaro, E. Gramiccioni, and P. J. Barnes, "8-Isoprostane, a marker of oxidative stress, is increased in exhaled breath condensate of patients with obstructive sleep apnea after night and is reduced by continuous positive airway pressure therapy," *Chest*, vol. 124, no. 4, pp. 1386–1392, 2003.

[62] Y. G. Borges, L. H. C. Cipriano, R. Aires et al., "Oxidative stress and inflammatory profiles in obstructive sleep apnea: are short-term CPAP or aerobic exercise therapies effective?," *Sleep and Breathing*, vol. 24, no. 2, pp. 541–549, 2020.

[63] B. Jurado-Gamez, M. C. Fernandez-Marin, J. L. Gomez-Chaparro et al., "Relationship of oxidative stress and endothelial dysfunction in sleep apnoea," *European Respiratory Journal*, vol. 37, no. 4, pp. 873–879, 2011.

[64] K. I. Takahashi, K. Chin, H. Nakamura et al., "Plasma thioredoxin, a novel oxidative stress marker, in patients with obstructive sleep apnea before and after nasal continuous positive airway pressure," *Antioxidants and Redox Signaling*, vol. 10, no. 4, pp. 715–726, 2008.

[65] A. Carr and B. Frei, "Does vitamin C act as a pro-oxidant under physiological conditions?," *The FASEB Journal*, vol. 13, no. 9, pp. 1007–1024, 1999.

[66] F. Shahidi and A. C. De Camargo, "Tocopherols and tocotrienols in common and emerging dietary sources: occurrence, applications, and health benefits," *International Journal of Molecular Sciences*, vol. 17, no. 10, p. 1745, 2016.

[67] Y. Mehdi, J. L. Hornick, L. Istasse, and I. Dufrasne, "Selenium in the environment, metabolism and involvement in body functions," *Molecules*, vol. 18, no. 3, pp. 3292–3311, 2013.

[68] A. Barceló, F. Barbé, M. de la Peña et al., "Antioxidant status in patients with sleep apnoea and impact of continuous positive airway pressure treatment," *European Respiratory Journal*, vol. 27, no. 4, pp. 756–760, 2006.

[69] L. V. Sales, V. M. S. de Bruin, V. D'Almeida et al., "Cognition and biomarkers of oxidative stress in obstructive sleep apnea," *Clinics*, vol. 68, no. 4, pp. 449–455, 2013.

[70] E. Saruhan, E. Sertoglu, Y. Unal, S. Bek, and G. Kutlu, "The role of antioxidant vitamins and selenium in patients with obstructive sleep apnea," *Sleep and Breathing*, vol. 25, no. 2, pp. 923–930, 2021.

[71] L. Ulatowski, C. Dreussi, N. Noy, J. Barnholtz-Sloan, E. Klein, and D. Manor, "Expression of the α-tocopherol transfer protein gene is regulated by oxidative stress and common single-nucleotide polymorphisms," *Free Radical Biology and Medicine*, vol. 53, no. 12, pp. 2318–2326, 2012.

[72] P. C. Chen, C. H. Guo, C. J. Tseng, K. C. Wang, and P. J. Liu, "Blood trace minerals concentrations and oxidative stress in patients with obstructive sleep apnea," *The Journal of Nutrition, Health and Aging*, vol. 17, no. 8, pp. 639–644, 2013.

[73] M. Grebe, H. J. Eisele, N. Weissmann et al., "Antioxidant vitamin C improves endothelial function in obstructive sleep apnea," *American Journal of Respiratory and Critical Care Medicine*, vol. 173, no. 8, pp. 897–901, 2006.

[74] W. Doehner, N. Schoene, M. Rauchhaus et al., "Effects of xanthine oxidase inhibition with allopurinol on endothelial function and peripheral blood flow in hyperuricemic patients with chronic heart failure: results from 2 placebo-controlled studies," *Circulation*, vol. 105, no. 22, pp. 2619–2624, 2002.

[75] A. L. Williams, L. Chen, and S. M. Scharf, "Effects of allopurinol on cardiac function and oxidant stress in chronic intermittent hypoxia," *Sleep and Breathing*, vol. 14, no. 1, pp. 51–57, 2010.

Research Article

Oxidative Stress in Association with Metabolic Health and Obesity in Young Adults

Grzegorz K. Jakubiak [iD],[1,2] **Kamila Osadnik** [iD],[1] **Mateusz Lejawa** [iD],[1] **Sławomir Kasperczyk** [iD],[3] **Tadeusz Osadnik** [iD],[1,4] **and Natalia Pawlas** [iD][1]

[1]*Department of Pharmacology, Faculty of Medical Sciences in Zabrze, Medical University of Silesia, Jordana 38, 41-808 Zabrze, Poland*
[2]*Department and Clinic of Internal Medicine, Angiology and Physical Medicine, Faculty of Medical Sciences in Zabrze, Medical University of Silesia, Batorego 15, 41-902 Bytom, Poland*
[3]*Department of Biochemistry, Faculty of Medical Sciences in Zabrze, Medical University of Silesia, Jordana 19, 41-808 Zabrze, Poland*
[4]*2nd Department of Cardiology and Angiology, Silesian Center for Heart Diseases, Marii Skłodowskiej-Curie 9, 41-800 Zabrze, Poland*

Correspondence should be addressed to Grzegorz K. Jakubiak; grzegorz.k.jakubiak@gmail.com

Introduction. Obesity is one of the most important public health problems in the world. Among obese people, there are those who, apart from excessive body weight, do not exhibit other metabolic dysfunctions, have a lower risk of developing cardiovascular diseases (CVDs), and show lower mortality. According to the theory, they are referred as metabolically healthy obese (MHO), in contrast to metabolically unhealthy obese (MUO). Metabolic disturbances occurring with obesity have been well established to be associated with oxidative stress. *Aim.* The purpose of this study was to analyse the association between selected anthropometric and biochemical parameters with oxidative stress in MHO, MUO, and normal weight young adults. *Material and Methods.* Individuals with age between 18 and 36 years with no history of chronic diseases and use of medicaments, with or without obesity, participated in the study. Complete blood counts, biochemical measurements, and parameters of oxidative stress such as total antioxidant capacity (TAC), total oxidative status (TOS), oxidative stress index (OSI), serum concentration of malondialdehyde (MDA), ceruloplasmin, thiol groups and lipid hydroperoxides (LPH), concentration of lipofuscin (LPS) in erythrocytes, and the activity of superoxide dismutase (SOD) were measured. *Results.* 422 patients who met the inclusion criteria were enrolled in the study. Among the study participants, 208 people (49.29%) were offspring of patients with angiographically confirmed coronary artery disease. Among the participants, 16 patients have been included in the group of metabolically healthy obese (MHO) people and 61 patients in the group of metabolically unhealthy obese (MUO) people and 345 patients had normal body weight. Significant differences between metabolically unhealthy obese and normal weight patients, as well as between women and men, have been found. *Conclusions.* We showed significant differences in the selected parameters of oxidative stress between metabolically unhealthy obese (MUO) individuals and young volunteers with normal body weight as well as without significant medical history.

1. Introduction

Obesity is a significant risk factor for metabolic disorders leading to multiple diseases such as diabetes mellitus, cancer, and cardiovascular diseases [1]. It has been observed that there is a subgroup of patients, called metabolically healthy obese (MHO), with no metabolic abnormalities despite excessive body weight. Patients with metabolic disorders in the course of obesity belong to metabolically unhealthy obese (MUO) individuals [2]. According to the current definition, body mass index (BMI) above $30 \, \text{kg/m}^2$ allows the diagnosis of obesity. Obesity causes worsening of quality of life and

poses economic burden for countries worldwide [3]. The prevalence rate of obesity increased by 27.5% between 1980 and 2013 [4].

Cardiovascular diseases (CVDs), such as coronary heart disease and stroke, belong to the most important causes of mortality worldwide [5, 6]. The incidence of CVDs among young people has increased past two decades, and it may be associated with increasing incidence of obesity [7]. Atherosclerosis is the main mechanism leading to CVDs [8]. Oxidative stress is suspected to play an important role in the pathogenesis of atherosclerosis [9].

Oxidative stress results from imbalance between prooxidative and antioxidant factors in favour of prooxidative factors [10]. Representatives of reactive oxygen species (ROS), highly reactive radical or nonradical molecules generated in the course of oxygen metabolism, are superoxide anion, hydroxyl radical, and hydrogen peroxide [11]. Superoxide dismutase (SOD), glutathione peroxidase, and catalase are main antioxidant enzymes in humans [12]. Ascorbic acid, glutathione, beta-carotene, tocopherols, and tocotrienols belong to nonenzymatic antioxidants [13]. Reactive oxygen species can damage macromolecules such as proteins, lipids, and deoxyribonucleic acid (DNA) [14]. Lipid peroxidation assessment by measurement of malondialdehyde blood concentration is a useful marker of oxidative stress [15]. Oxidative stress was shown to be a distinctive feature of obesity [16].

Although there is a distinction between MHO and MUO, research results show that MHO individuals have a greater risk of developing cardiovascular diseases and cardiovascular events than normal weight individuals but less than MUO individuals. Research on the differences in metabolic status between MUO and MHO individuals may contribute to a better understanding of the metabolic heterogeneity phenomenon in obese people and the pathogenesis of cardiovascular disease in the course of obesity. It was recently documented that such abnormalities as increased serum myeloperoxidase (MPO) activity, nitric oxide (NO) formation, and nitrosative damage to proteins are associated with the progression of metabolic disturbances of obesity as well as elevated ONOO—blood concentration may be a valuable predictor of development of hypertension and metabolic syndrome in obese individuals [17].

The purpose of this study was to analyse the association between selected anthropometric and biochemical parameters with oxidative stress in young healthy adults with and without obesity and metabolic disturbances.

2. Materials and Methods

Blood samples were taken from healthy volunteers, both descendants of people with premature angiographically confirmed CHD and healthy volunteers from the MAGNETIC study (Metabolic and Genetic Profiling of Young Adults with and without a Family History of Premature Coronary Heart Disease). The detailed recruitment procedure of the MAGNETIC study, which was a case-control study, was published [18]. Individuals were recruited from offspring of patients hospitalized in the Silesian Centre for Heart Diseases due to premature CHD and from untreated people aged 18–36 years

without a family history of CHD. From the whole group of recruited volunteers, we selected obese individuals and those with normal weight. The group was divided into two subgroups: metabolically healthy obese (MHO) persons and metabolically unhealthy obese (MUO) persons. The control group constituted of normal weight persons without the metabolic syndrome. Criteria of metabolic health according to Buscemi et al. have been used [19]. Subjects who met at least two of the following conditions are considered metabolically unhealthy: (1) systolic blood pressure (SBP) ≥ 130 mmHg or diastolic blood pressure (DBP) ≥ 85 mmHg or use of antihypertensive medication; (2) triglycerides ≥ 150 mg/dL or use of lipid-lowering medication; (3) high density lipoprotein (HDL) cholesterol < 40 mg/dL (1.0 mmol/L) (men) or < 50 mg/dL (1.2 mmol/L) (women); (4) total cholesterol > 200 mg/dL (5.2 mmol/L) or use of cholesterol-lowering medication; (5) glucose > 100 mg/dL (5.55 mmol/L) or diabetes mellitus type 2. People who met one or no criterion are considered metabolically healthy.

Inclusion criteria for the study group were as follows: (1) age between 18 and 36 years, (2) obesity, (3) no use of medicaments, and (4) agreement for participation in trial. Inclusion criteria for the control group were as follows: (1) age between 18 and 36 years, (2) normal weight, (3) no metabolic syndrome, (4) no use of medicaments, and (5) agreement for participation in the trial. Exclusion criteria for both groups were as follows: (1) age below 18 years or above 36 years, (2) use of medicaments, and (3) acute or chronic disease.

Blood pressure was measured with a certified automatic apparatus. Blood samples were obtained from every individual between 7 am and 9 am, approx. 8–10 h after the last meal. The serum sample was obtained for oxidative stress analyses and frozen immediately at -80 C. Complete blood counts (CBC) were analysed by a Sysmex XE2100 (Sysmex Corporation, Kobe, Japan). Biochemical measurements were analysed by a Cobas 6000 (Roche Diagnostics, Indianapolis, IN, USA) using Roche reagents. The following parameters were assessed: uric acid, total cholesterol, low density lipoprotein (LDL) cholesterol, high density lipoprotein (HDL) cholesterol, triglycerides, and glucose. The measurements were done in a clinical laboratory. In all patients, the body mass, height, BMI, waist-hip ratio (WHR), visceral adipose index (VAI), SBP, and DBP were measured. VAI was calculated from waist circumference (WC), BMI, triglycerides (TG) blood concentration, and high density lipoprotein (HDL) concentration based on the methodology described by Amato et al. [20] according to the following rules:

$$\text{Males}: \text{VAI} = \left(\frac{\text{WC}}{39.68 + 1.88 \times \text{BMI}}\right) \times \left(\frac{\text{TG}}{1.03}\right) \times \left(\frac{1.31}{\text{HDL}}\right),$$

$$\text{Females}: \text{VAI} = \left(\frac{\text{WC}}{36.58 + 1.89 \times \text{BMI}}\right) \times \left(\frac{\text{TG}}{0.81}\right) \times \left(\frac{1.52}{\text{HDL}}\right).$$

(1)

The thiol (SH) group serum concentration was measured according to the methodology described by Koster et al. 5,5′ -Dithiobis (2-nitrobenzoic acid) (DTNB) is reduced by

compounds containing SH groups, yielding the yellow anion derivative, 5-thio-2-nitrobenzoate, absorbing at a wavelength of 412 nm [21]. An automated PerkinElmer analyser was applied. Results have been shown as the thiol group concentration per gram of protein.

Total antioxidant capacity (TAC) was determined by the colorimetric method developed by Erel. Ions 2,2′-azinobis-3-ethylbenzothiazoline-6-sulfonate change colour, and they are measured as the modification in absorbance at 660 nm [22]. This procedure was conducted in an automated PerkinElmer analyser calibrated with Trolox.

The methodology described by Erel has been used to measure serum total oxidative status (TOS). Oxidizing agents in an acidic medium cause the oxidation of ferrous ions to ferric ions. Xylenol orange changes colour in the presence of ferric ions, and it is measured as the change in absorbance at 560 nm [23]. This assay was conducted in an automated analyser (PerkinElmer) calibrated with hydrogen peroxide.

Oxidative stress index (OSI) has been calculated as percentage ratio of TOS to TAC.

Malondialdehyde (MDA) serum concentration was measured fluorometrically according to Ohkawa et al. with modifications. Samples were mixed with 8.1% sodium dodecyl sulfate, 20% acetic acid, and 0.8% 2-thiobarbituric acid. Samples were vortexed and then incubated for one hour at 95 Celsius degrees. In the next step, butanol-pyridine 15 : 1 (v/v) was added. The mixture was shaken for ten minutes and then centrifuged. The butanol-pyridine layer was measured fluorometrically at 552 nm and 515 nm excitation (PerkinElmer, Waltham, Massachusetts). Tetraethoxypropane was used as the standard. 2-Thiobarbituric acid-reactive substance concentration values are expressed as MDA equivalents [24].

Ceruloplasmin (CER) serum concentration has been determined by the methodology described by Richterich. It is based on the ability of ceruloplasmin to catalyse the oxidation of p-phenylenediamine to the coloured product which can be detected spectrophotometrically [25].

Measurements of lipid hydroperoxides (LPH) concentration were conducted basing on the methodology developed by Sődergren et al. It is associated with colour change of xylenol orange in the presence of ferric ions, followed by the addition of methanol and butylated hydroxytoluene (BHT). The change of absorbance was measured at 560 nm in the Victor X3 automated analyser (PerkinElmer), which was calibrated with hydrogen peroxide [26].

Concentration of lipofuscin (LPS) in erythrocytes has been measured according to Jain as fluorescence of the extraction of erythrocytes in a mixture of isopropanol and chloroform [27]. Results were shown in relative units (RUs).

The activity of superoxide dismutase (SOD) has been measured according to the method published by Oyanagui. In this method, the activity of SOD is negatively proportional to the concentration of coloured product generated in the reaction of nitric ions with naphthalene diamine and sulfanilic acid. Nitric ions are products in the reaction of superoxide ions (generating by xanthine oxidase) with hydroxylamine. Absorbance was measured using an automated PerkinElmer analyser at a wavelength of 550 nm. The enzymatic activity of SOD was expressed in nitric units (NUs). The activity of

SOD isoenzymes such as MnSOD and CuZnSOD has been determined using KCN as the inhibitor of the CuZnSOD activity [28].

The experimental protocol has been approved by the Bioethics Committee at the Institute of Occupational Medicine and Environmental Health in Sosnowiec (no. 03/2013) and further extended by the Bioethics Committee at the Medical University of Silesia (no. KNW/0022/KB1/118/18/19).

Statistical analysis has been performed by Statistica 10 (Statsoft, Tibco). The normality of distribution was checked with the Shapiro-Wilk as well as Lilliefors test. Spearman's rank correlation has been performed for the analysis of correlations between determined parameters in the group of all participants and for both men and women separately. Mann–Whitney U test has been used to analyse the associations of measured parameters with sex. Kruskal-Wallis ANOVA and post hoc test were used to find differences between MHO, MUO, and metabolically healthy normal weight (MHNW) participants. Statistical tests were performed correcting for multiple comparisons (Dunn's test). Frequencies of categorical values were compared using the χ^2 test. Box plots and respective tests were prepared in the R software.

3. Results

422 patients who met inclusion criteria have been enrolled in the study. In this group, 44.8% (189) were men and 55.2% (233) were women. The average age was 27.67 ± 4.48 years in the whole group, 27.69 ± 4.41 years among men and 27.64 ± 4.54 years among women. 16 patients were classified as metabolically healthy obese people (7 women and 9 men). 61 patients met the definition of metabolically unhealthy obese (19 women and 42 men). 345 patients were classified as metabolically healthy with normal weight (MHNW) (207 women and 138 men). Among the study participants, 208 people (49.29%) were offspring of people with angiographically confirmed CHD (98 men and 110 women). 76 participants were current smokers (37 men and 39 women), 47 persons were past smokers (27 men and 20 women), and 298 participants had never smoked (125 men and 173 women). Differences between MHNW, MHO, and MUO individuals in terms of epidemiologic, anthropometric, and biochemical data are presented in Table 1.

There were significant differences between men and women in biochemical parameters and unhealthy behaviour such as alcohol consumption between men and women as well as the parameters of oxidative stress (Table 2). Oxidative stress parameters assessed in the study may be divided into three groups: antioxidant barrier (SH groups, SOD, MnSOD, CuZnSOD, and CER), parameters associated with total antioxidant/oxidant status (TAC, TOS, and OSI), and oxidative damage (MDA, LPH, and LPS). In the whole group of participants, TOS, OSI, and SOD activities (total SOD, MnSOD, and CuZnSOD) and LPS and ceruloplasmin concentrations were significantly higher among women than men. The thiol group concentration per gram of protein was significantly lower among women than men. In both males and females, TAC positively correlated with uric acid concentration.

Table 1: Differences between MHNW, MHO, and MUO in terms of epidemiologic, anthropometric, and biochemical data.

Variable	MHNW		MHO		MUO		MHNW vs. MHO*	MHNW vs. MUO*	MHO vs. MUO*
	N	Mean (SD) (n (%))	N	Mean (SD) (n (%))	N	Mean (SD) (n (%))			
Age (years)	344	27.05 (4.44)	16	30.53 (2.91)	61	30.22 (3.73)	0.0052	<0.001	ns
Females (%)	344	206 (59.9%)	16	7 (43.8%)	61	19 (31.2%)	ns#	ns#	ns#
Alcohol (yes)	345	260 (75.4%)	16	13 (81.2%)	61	42 (68.8%)	ns#	ns#	ns#
Smoking (i) Current		56 (16.33%)		4 (25%)		16 (26.23%)			
vs. (ii) Past	343	257 (74.93%)	16	8 (50%)	61	32 (52.46%)	ns#	ns#	ns#
(iii) Never		30 (8.75%)		4 (25%)		13 (21.31%)			
Family history of premature coronary heart disease (CHD) (yes)	345	154 (44.6%)	16	10 (62.5%)	61	44 (72.1%)	ns#	ns#	ns#
Family history of type 2 diabetes (T2D) (yes)	345	177 (51.3%)	16	7 (43.7%)	61	38 (62.3%)	ns#	ns#	ns#
Total cholesterol (TC) (mmol/L)	344	4.68 (0.87)	16	4.57 (0.69)	61	5.67 (1.07)	ns	<0.001	0.0015
High density lipoprotein cholesterol (HDL-C) (mmol/L)	344	1.75 (0.41)	16	1.44 (0.35)	61	1.12 (0.25)	0.0065	<0.001	0.033
Low density lipoprotein cholesterol (LDL-C) (mmol/L)	344	2.66 (0.78)	16	2.79 (0.65)	61	3.76 (0.94)	ns	<0.001	0.0030
Triglycerides (TG) (mmol/L)	344	0.83 (0.36)	16	1.1 (0.36)	61	2.56 (2.27)	0.014	<0.001	0.019
Glucose (mmol/L)	344	4.87 (0.37)	16	5.03 (0.3)	61	5.43 (0.59)	ns	<0.001	ns
Uric acid (UA) (μmol/L)	344	277.65 (63.71)	16	332.13 (73.84)	61	381.15 (61.74)	0.014	<0.001	ns
Body mass index (BMI) (kg/m^2)	344	21.74 (1.79)	16	32.27 (1.83)	61	33.77 (2.69)	ns	<0.001	ns
Waist-hip ratio (WHR)	338	1.1 (5.45)	16	0.89 (0.05)	60	0.94 (0.08)	<0.001	<0.001	ns
VAI	338	1.06 (5.47)	16	1.27 (0.56)	60	3.88 (4.75)	<0.001	<0.001	0.040
Systolic blood pressure (SBP) (mmHg)	334	122.42 (12.0)	15	133.47 (22.93)	60	138.05 (14.86)	ns	<0.001	ns
Diastolic blood pressure (DBP) (mmHg)	335	76.63 (9.46)	15	78.67 (11.36)	58	85.81 (10.01)	ns	<0.001	0.023

Mean (SD): mean value (standard deviation) calculated for quantitative features; n (%): the number of people (the percentage of this number in relation to the subgroup) given in the case of qualitative features; N: size of the subgroup; MHNW: metabolically healthy normal weight individuals; MHO: metabolically healthy obese individuals; MUO: metabolically unhealthy obese individuals; ns: not significant. * p values according to Kruskal-Wallis test; # p values according to χ^2 test.

TABLE 2: Differences between men and women in terms of biochemical and oxidative stress parameters as well as epidemiologic and anthropometric data.

Variable	Men Mean (SD) (n (%))/ median (Q1; Q3)	N	Women Mean (SD) (n (%))/ median (Q1; Q3)	N	p value U Mann–Whitney/χ^{2*}
Age (years)	27.69 (4.41)	189	27.6374 (4.54)	233	ns
Alcohol (yes)	159 (84%)	189	155 (67%)	232	0.001*
Smoking (i) Current vs. (ii) Past (iii) Never	37 (20%) 27 (14%) 125 (66%)	189	39 (17%) 20 (9%) 172 (74%)	231	ns*
Family history of premature coronary heart disease (CHD) (yes)	98 (52%)	189	109 (47%)	232	ns*
Family history of type 2 diabetes (T2D) (yes)	91 (48%)	189	130 (56%)	232	ns*
Total cholesterol (TC) (mmol/L)	4.83 (1.06)	189	4.82 (0.86)	233	ns*
Low density lipoprotein cholesterol (LDL-C) (mmol/L)	2.98 (0.96)	189	2.70 (0.81)	233	0.0072
High density lipoprotein cholesterol (HDL-C) (mmol/L)	1.44 (0.35)	189	1.82 (0.44)	232	<0.001
Triglycerides (TG) (mmol/L)	1.32 (1.52)	189	0.91 (0.50)	232	0.00049
Glucose (mmol/L)	5.06 (0.46)	188	4.87 (0.43)	232	<0.001
Uric acid (UA) (μmol/L)	342.63 (64.03)	189	255.67 (55.81)	233	<0.001
Body mass index (BMI) (kg/m^2)	25.52 (5.20)	189	22.54 (4.27)	233	<0.001
Systolic blood pressure (SBP) (mmHg)	130.89 (14.64)	189	120.35 (11.79)	233	<0.001
Diastolic blood pressure (DBP) (mmHg)	79.76 (10.58)	189	76.55 (9.45)	233	0.0022
Thiol group concentration (PSH) (μmol/g protein)	4.39 (4.00; 4.70)	189	4.00 (3.60; 4.20)	233	<0.001
Ceruloplasmin (CER) (mg/dL)	36.10 (31.80; 41.40)	189	45.10 (38.70; 55.10)	233	<0.001
Total antioxidant capacity (TAC) (mmol/L)	1.02 (0.950; 1.130)	189	1.04 (0.940; 1.130)	233	0.905
Total oxidative status (TOS) (μmol/L)	4.70 (3.600; 6.100)	189	5.300 (4.40; 6.950)	232	0.0024
Oxidative stress index (OSI) (%)	0.45 (0.36; 0.61)	189	0.51 (0.41; 0.67)	232	0.0034
Lipid hydroperoxides (LPH) (μmol/L)	2.39 (1.90; 3.10)	188	2.50 (2.00; 3.10)	232	0.36
Superoxide dismutase (SOD) (NU/mL)	19.63 (18.44; 21.651)	189	21.10 (19.70; 22.70)	233	<0.001
MnSOD (NU/mL)	10.80 (9.77; 11.90)	189	11.40 (10.10; 12.50)	233	0.0015
CuZnSOD (NU/mL)	9.066 (8.10; 10.30)	189	9.80 (8.60; 11.00)	233	0.00026
Lipofuscin (LPS) (RU/L)	190.30 (114.01; 302.30)	189	275.20 (196.40; 350.20)	233	<0.001
Malondialdehyde (MDA) (μmol/L)	1.66 (1.29; 2.06)	186	1.690 (1.310; 2.110)	233	0.52

Mean (SD): mean value (standard deviation) calculated for quantitative features; n (%): the number of people (the percentage of this number in relation to the subgroup) given in the case of qualitative features; N: size of the subgroup; MHNW: metabolically healthy normal weight individuals; MHO: metabolically healthy obese individuals; MUO: metabolically unhealthy obese individuals; ns: not significant; Q1: first quartile; Q3: third quartile. *χ^2 test.

Among men, significant differences associated with metabolic status in LPH and LPS blood concentration and SOD blood activity (total and CuZnSOD, but not MnSOD) were observed. LPH concentration in MUO was higher than in MHNW. LPS concentration was the highest in MHNW and the lowest in MHO. SOD total blood activity and CuZnSOD activity were highest in MHNW (Figure 1, Supplementary table 1). There were no differences between MHO and MUO regarding oxidative stress parameters.

Among women, significant differences associated with metabolic status in SH group concentration per gram of protein (PSH), TAC, and total SOD activity (but not MnSOD and CuZnSOD) were observed. TAC was the highest in MUO and the lowest in MHNW. Total SOD activity was higher in MHNW than in MUO (Figure 2, Supplementary table 2).

In men, we observed significant negative correlation between age and TAC, SOD, and CuZnSOD. The LPS negatively correlated with age, total cholesterol, LDL, triglycerides, BMI, WHR, and VAI while positively with HDL. SOD activity negatively correlated with triglycerides, BMI, WHR, and VAI, while opposite correlation was found between the latter parameters and LPH. TAC was negatively correlated with age and HDL cholesterol, while positively with triglycerides, uric acid, and VAI (Table 3).
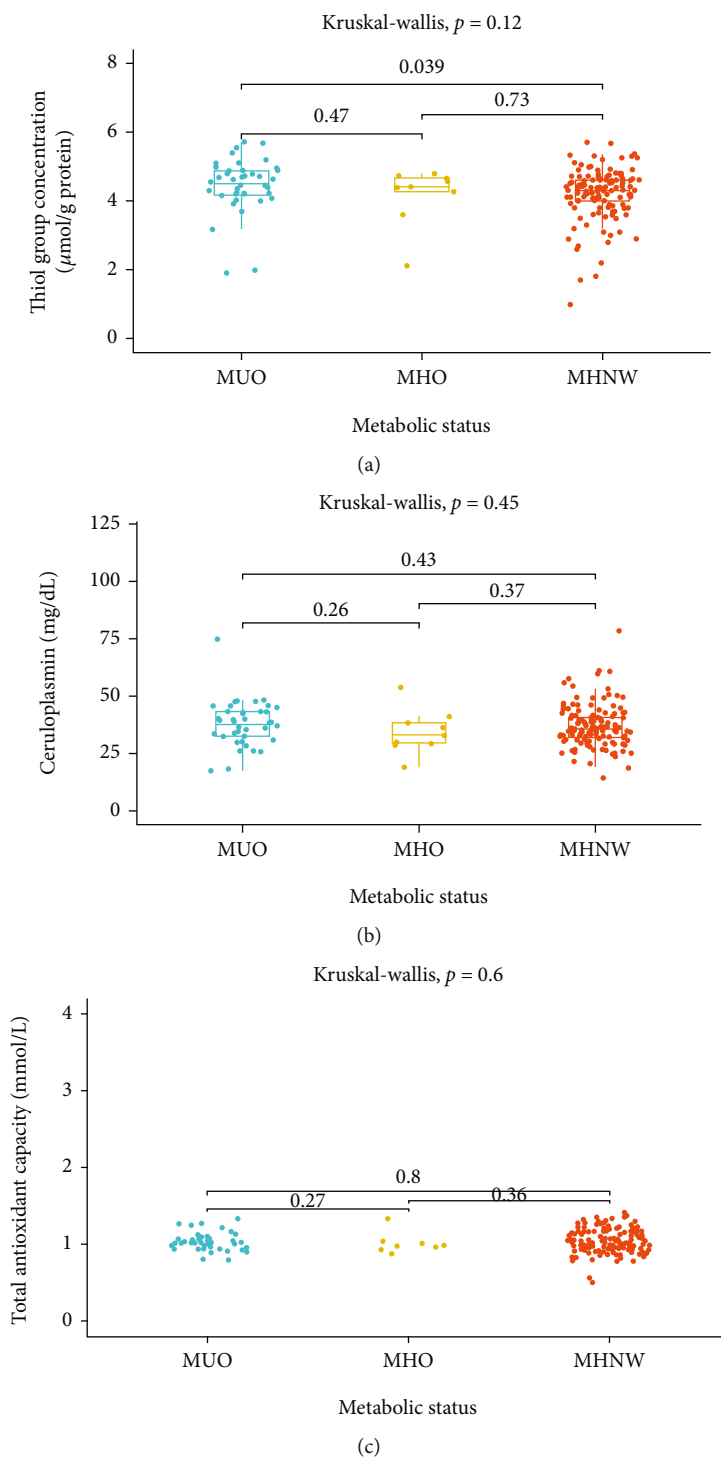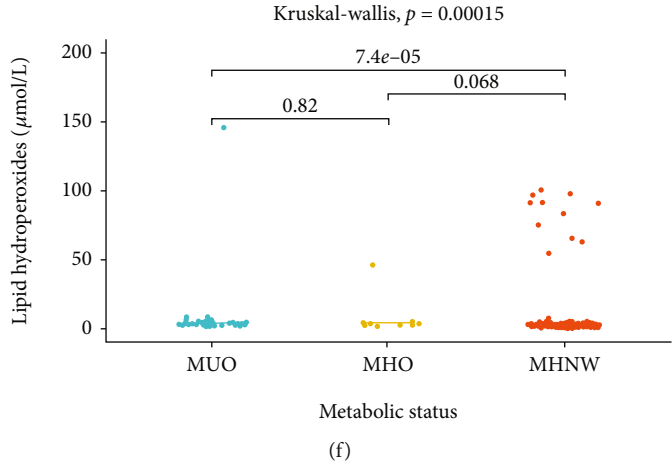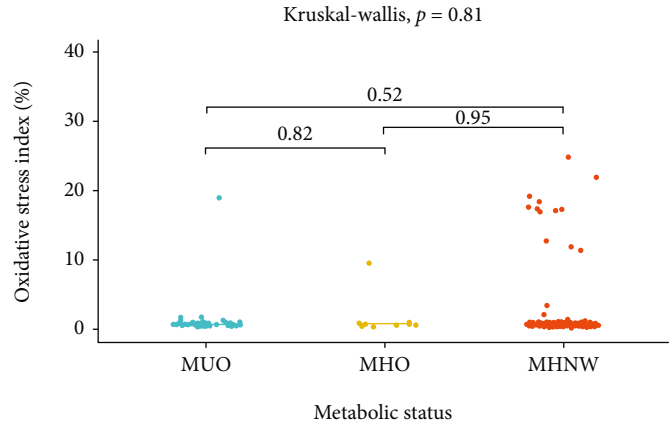
(a)

(b)

(c)

FIGURE 1: Continued.

(d)

(e)

(f)

Figure 1: Continued.

(g)

(h)

(i)

(j)

FIGURE 1: Continued.

Kruskal-wallis, $p = 0.77$

(k)
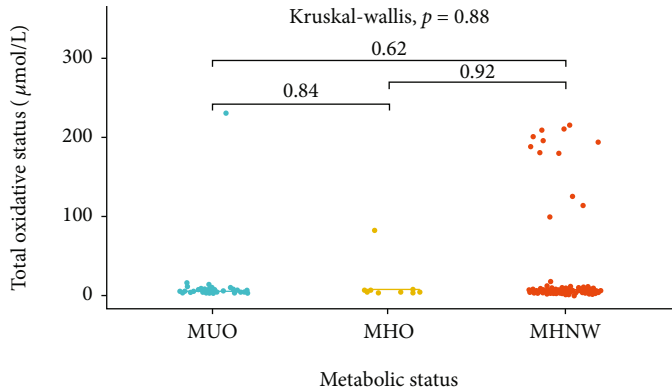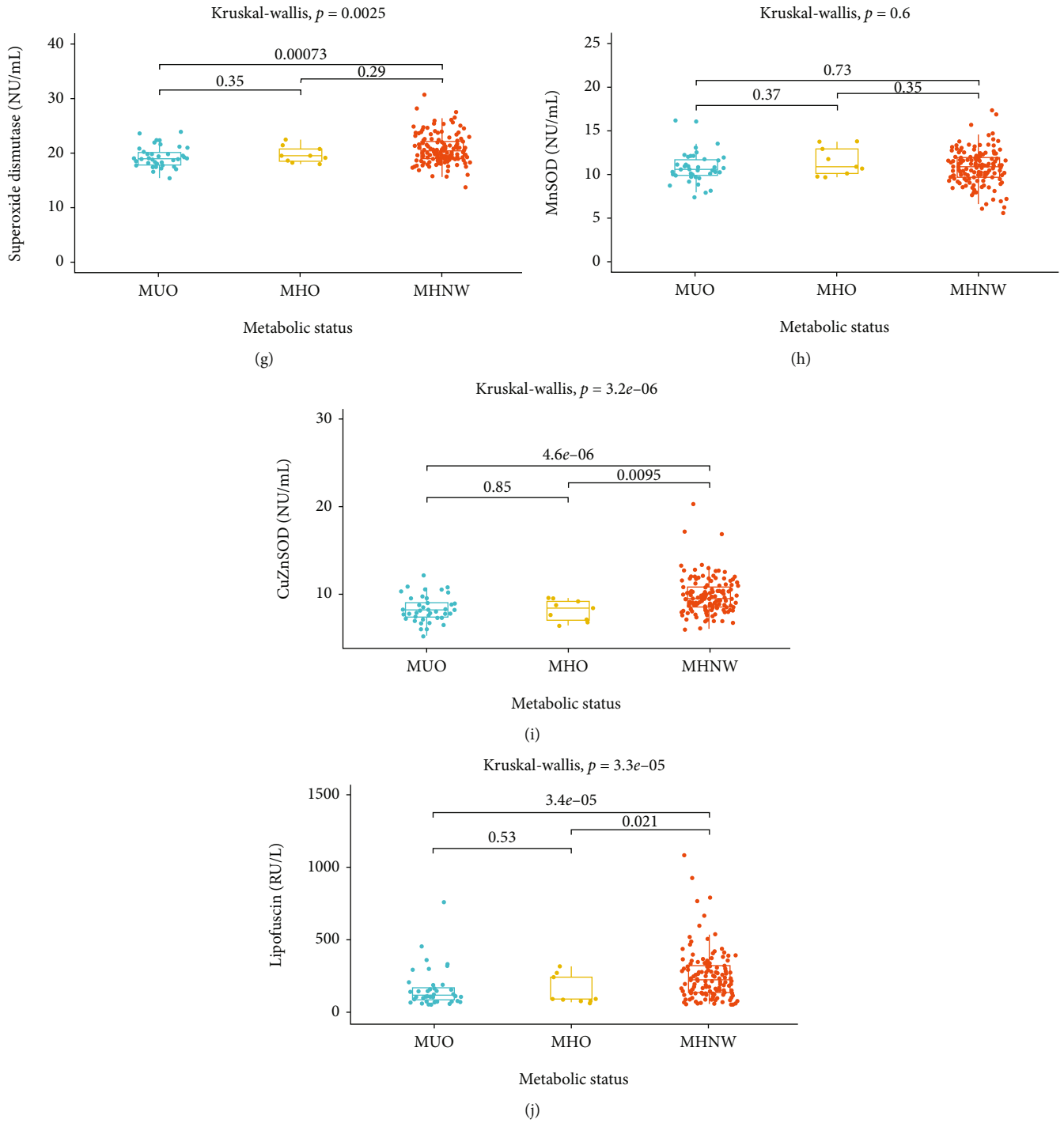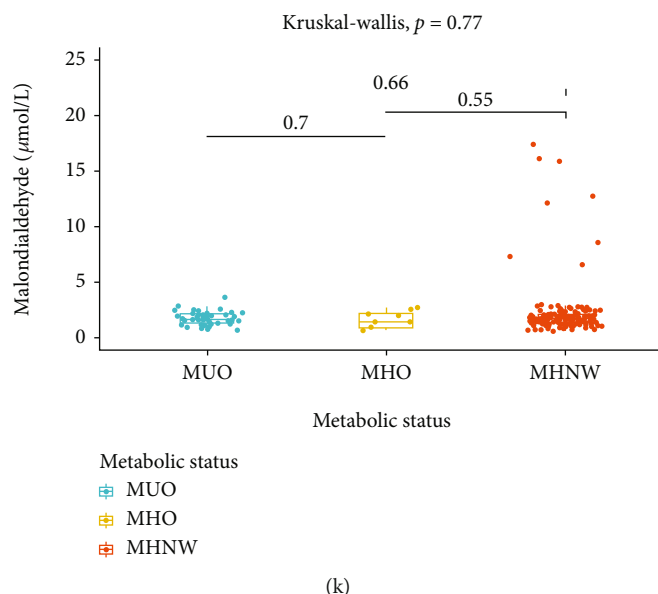
FIGURE 1: Oxidative stress parameters—differences between men with different metabolic status. MHNW: metabolically healthy normal weight individuals; MHO: metabolically healthy obese individuals; MUO: metabolically unhealthy obese individuals. Data are presented in boxes as median, first, and third quartile values. (a) Thiol group concentration; (b) ceruloplasmin; (c) total antioxidant capacity; (d) total oxidative status; (e) oxidative stress index; (f) lipid hydroperoxides; (g) superoxide dismutase; (h) Mn-dependent superoxide dismutase; (i) Cu- and Zn-dependent superoxide dismutase; (j) lipofuscin; (k) malondialdehyde.

In women, we observed significant negative correlation between age and SOD and CuZnSOD, while positive with TAC and LPS. The LPH positively correlated with triglycerides, SBP, and VAI. TAC was positively correlated with cholesterol, triglycerides, and uric acid (Table 4).

4. Discussion

Our results show that gender differences have a significant impact on parameters related to oxidative stress. In some parameters, we observed a significant trend related to the number of metabolic disturbances from healthy persons with normal weight to metabolically unhealthy obese. Comparing to other studies, our subjects were younger and they were not treated for any disease.

The strength of our study is undoubtedly the participation of young people, without a significant medical history and medication administration. The limitation of our work is the design and the lack of follow-up which could allow us to investigate the relationship between selected parameters of oxidative stress, in the predisposition to develop coronary artery disease. The prospective studies are needed. The study presented by us is a case-control study; therefore, it allows only to determine the presence of specific correlations, not a cause-and-effect relationship. Another limitation of the study is the lack of evaluation of oxidative stress in red blood cells and the lack of oxidative nucleic acid as well as protein damage. Another limitation is the lack of one accepted definition of MHO and MUO; thus, the necessity to choose one of the suggested. We used the criteria according to Buscemi, which take into account parameters such as blood pressure, blood glucose concen-

tration, and plasma lipid profile (TG, TC, and HDL-C). The criteria for the diagnosis of MUO developed by other authors take into account also other parameters. For example, the Karelis criteria and the Wildman criteria include the value of the homeostasis model assessment of insulin resistance (HOMA-IR) index [29], which was not calculated in our study.

4.1. Gender Differences in Terms of Oxidative Stress. According to the results of the study conducted on the healthy population by Brunelli et al., the state of oxidative stress is higher in women than in men. In this study, such parameters as diacron reactive oxygen metabolite (dROM) and biological antioxidant potential (BAP) have been assessed [30]. Higher lipid peroxidation among women has been reported in the study conducted by Block et al. [31] In the other study, higher oxidative stress in men than in women measured by blood concentration of the thiobarbituric acid-reacting substances (TBARS) and urinary concentration of 8-iso-PGF2α has been documented [32]. Nielsen et al. have shown that MDA concentration is slightly but significantly higher in men than in women [33]. The data available in the literature therefore show discrepancies in the relationship between sex and oxidative stress, which our study also confirms; however, we have also shown higher intensity of oxidative stress in women than in men regarding following parameters: PSH, CER, TOS, SOD, MnSOD, CuZnSOD, and LPS.

Due to the described differences between men and women in terms of the parameters of oxidative stress in our cohort, we decided to analyse the relationship between body weight and metabolic health status and the parameters of oxidative stress separately for women and men.

(a)

(b)

(c)
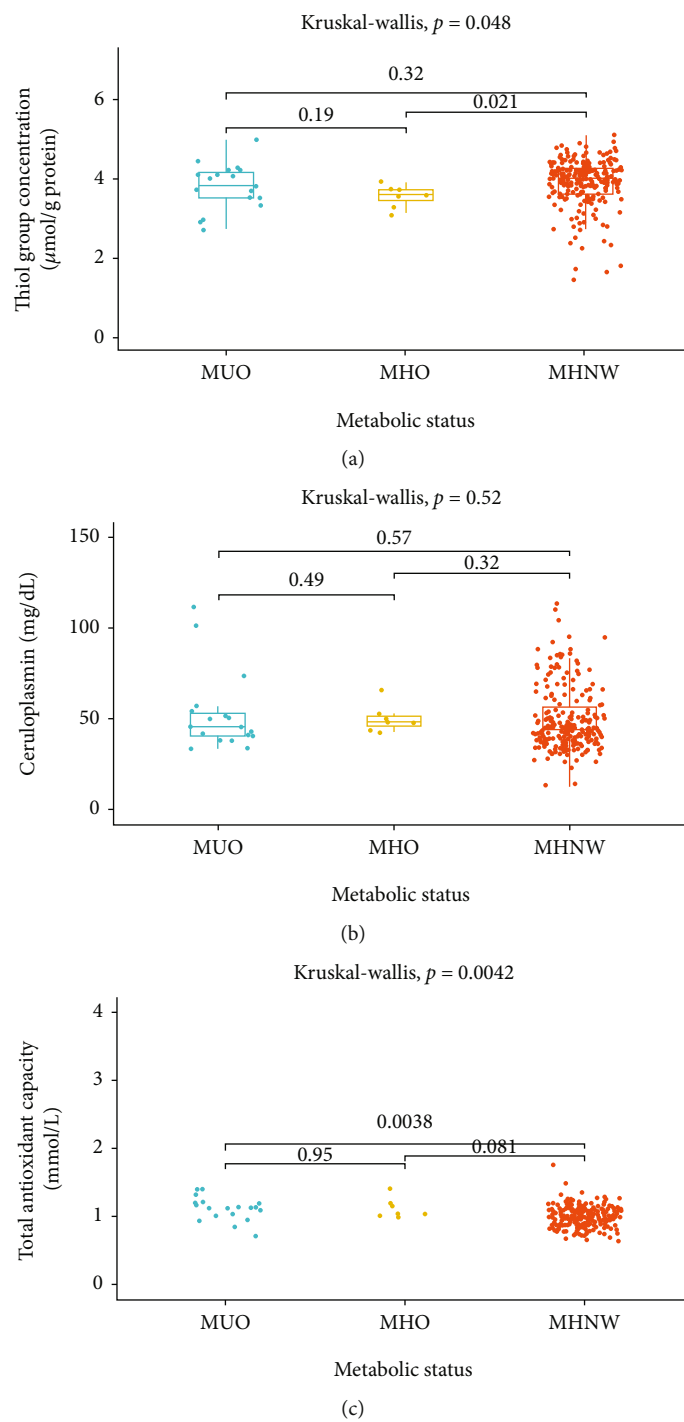
FIGURE 2: Continued.

(d)

(e)

(f)

Figure 2: Continued.

(g)

(h)

(i)

(j)

(k)
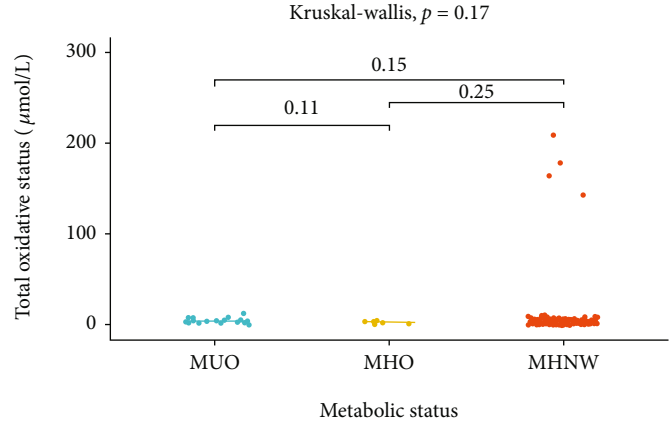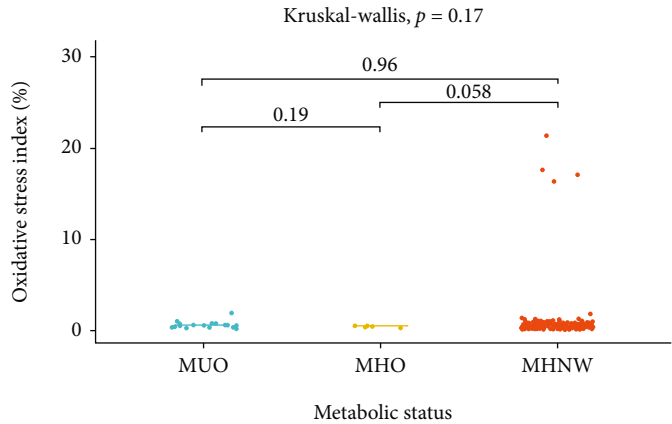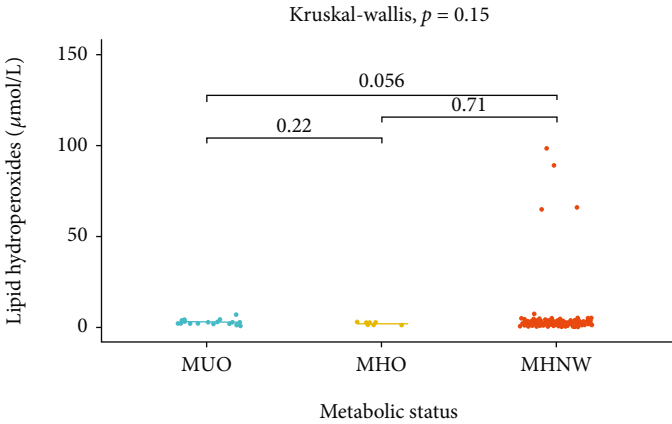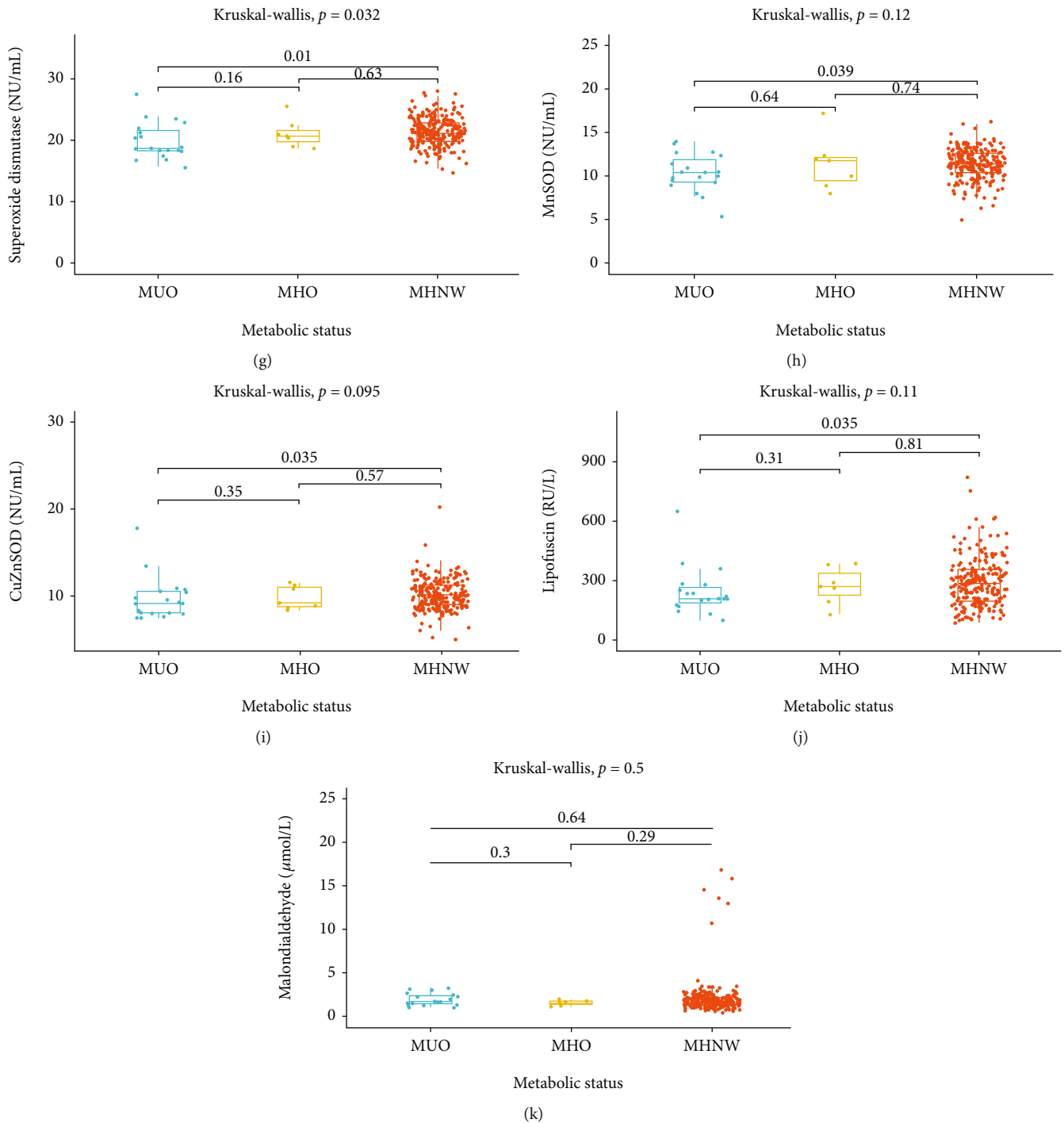
FIGURE 2: Oxidative stress parameters—differences between women with different metabolic status. MHNW: metabolically healthy normal weight individuals; MHO: metabolically healthy obese individuals; MUO: metabolically unhealthy obese individuals. Data are presented in boxes as median, first, and third quartile values. (a) thiol group concentration; (b) ceruloplasmin; (c) total antioxidant capacity; (d) total oxidative status; (e) oxidative stress index; (f) lipid hydroperoxides; (g) superoxide dismutase; (h) Mn-dependent superoxide dismutase; (i) Cu- and Zn-dependent superoxide dismutase; (j) lipofuscin; (k) malondialdehyde.

4.2. Oxidative Stress in Association with Body Weight and Metabolic Health

4.2.1. Oxidative Stress Parameters Related to Antioxidant Barrier.
Gol et al. studied the differences in the concentration of native thiol groups (-SH) and the total concentration of

thiol groups (-SH and -S-S-) between people who lead a sedentary lifestyle, people who are overweight or obese, and people who exercise regularly. There was no significant difference between these groups in the native thiol groups. In terms of the total number of thiol groups, the highest value was found among people who exercise regularly and the

TABLE 3: Spearman correlations R between oxidative stress parameters in men and anthropometric and biochemical measurements.

Variables	Thiol group concentration (PSH)	Ceruloplasmin (CER)	Total antioxidant capacity (TAC)	Total oxidative status (TOS)	Oxidative stress index (OSI)	Lipid hydroperoxides (LPH)	Superoxide dismutase (SOD)	MnSOD	CuZnSOD	Lipofuscin (LPS)	Malondialdehyde (MDA)
Age	-0.026	-0.034	-0.198**	-0.112	-0.054	-0.022	-0.156*	-0.013	-0.260***	-0.217**	0.023
Total cholesterol (TC)	0.0039	-0.00054	-0.028	0.0064	0.022	0.108	-0.136	-0.0090	-0.209**	-0.256***	-0.012
Low density lipoprotein cholesterol (LDL-C)	0.0135	0.046	0.0030	-0.022	-0.012	0.0782	-0.12	-0.0202	-0.17	-0.246***	-0.0034
High density lipoprotein cholesterol (LDL-C)	-0.187*	-0.128	-0.186*	-0.111	-0.0625	-0.271***	0.116	0.0276	0.171*	0.182*	-0.0061
Triglycerides	0.191**	0.014	0.173*	0.12	0.070	0.224**	-0.184*	-0.0832	-0.216**	-0.256***	-0.029
Glucose	0.089	-0.075	0.018	-0.048	-0.024	0.011	-0.037	0.044	-0.101	-0.116	0.030
Uric acid (UA)	0.144*	0.148*	0.362****	-0.027	-0.12	0.102	-0.0065	0.053	-0.093	-0.198**	-0.014
Body mass index (BMI)	0.063	-0.041	-0.017	0.040	0.044	0.272***	-0.237**	-0.05	-0.299***	-0.313***	0.045
Systolic blood pressure (SBP)	0.087	0.024	-0.108	0.0784	0.11	0.218**	-0.0296	0.143	-0.187*	-0.0434	-0.0273
Diastolic blood pressure (DBP)	0.088	0.096	-0.142	0.0656	0.0742	0.176*	0.0282	0.204**	-0.201**	-0.122	-0.036
Waist-hip ratio (WHR)	0.049	0.054	0.105	-0.056	-0.086	0.101	-0.241***	-0.039	-0.329***	-0.160*	0.089
Visceral adipose index (VAI)	0.188*	0.068	0.207**	0.112	0.052	0.239**	-0.202**	-0.083	-0.253***	-0.237**	0.0034

$*p < 0.05$; $**p < 0.01$; $***p < 0.001$.

TABLE 4: Spearman correlations R between oxidative stress parameters and anthropometric and biochemical measurements in women.

Variables	Thiol group concentration (PSH)	Ceruloplasmin (CER)	Total antioxidant capacity (TAC)	Total oxidative status (TOS)	Oxidative stress index (OSI)	Lipid hydroperoxides (LPH)	Superoxide dismutase (SOD)	MnSOD	CuZnSOD	Lipofuscin (LPS)	Malondialdehyde (MDA)
Age	-0.102	0.138*	0.131*	0.0095	-0.037	0.0217	-0.155*	-0.038	-0.177**	0.131*	0.091
Total cholesterol (TC)	-0.070	0.234***	0.134*	0.143*	0.075	0.109	-0.071	-0.092	-0.013	0.010	0.157*
Low density lipoprotein cholesterol (LDL-C)	-0.032	0.105	0.114	0.027	-0.022	0.021	-0.159*	-0.189**	-0.048	-0.036	0.121
High density lipoprotein cholesterol (HDL-C)	-0.050	0.103	-0.051	0.077	0.104	0.038	0.069	0.086	0.030	0.111	0.043
Triglycerides	-0.160*	0.386***	0.151*	0.246***	0.131*	0.261***	-0.104	-0.128	-0.035	0.028	0.212**
Glucose	-0.040	-0.113	0.067	0.021	-0.0011	0.038	-0.0091	0.019	-0.0504	0.099	0.0205
Uric acid (UA)	-0.058	-0.053	0.447***	-0.029	-0.214**	-0.018	0.040	0.016	0.022	0.041	0.0050
Body mass index (BMI)	-0.146*	0.142*	0.084	0.029	-0.021	0.090	-0.072	-0.076	-0.061	-0.030	0.047
Systolic blood pressure (SBP)	-0.062	0.232***	-0.010	0.134*	0.12	0.17**	0.026	0.101	-0.077	-0.025	-0.012
Diastolic blood pressure (DBP)	-0.061	0.205**	-0.057	0.101	0.11	0.12	0.0077	0.054	-0.079	0.069	0.054
Waist-hip ratio (WHR)	0.0089	-0.013	0.120	-0.027	-0.076	-0.018	-0.024	-0.0099	-0.053	-0.045	0.014
Visceral adipose index (VAI)	-0.110	0.287***	0.126	0.154*	0.057	0.181**	-0.1099	-0.133*	-0.041	-0.019	0.147*

*$p < 0.05$; **$p < 0.01$; ***$p < 0.001$.

lowest among people who lead a sedentary lifestyle [34]. In our study, we assessed the concentration of thiol groups per gram of protein. In women, the value of this parameter was decreased both in MHO and in MUO, which implies the higher intensity of oxidative stress, and was negatively correlated with triglycerides and BMI and there was no association with uric acid, while in men, the parameter positively correlated with triglycerides and uric acid, while negatively with HDL cholesterol concentration. Decreased concentration of reduced thiol groups may be a result of increased oxidative stress in those individuals and indicated different prooxidant and antioxidant mechanisms in men and in women.

Alissa et al. published the results of a study aimed at assessing the relationship between selected parameters of iron metabolism and dietary iron supply and risk factors for coronary heart disease among men from Saudi Arabia. 270 men participated in the study: 130 of whom underwent coronary angiography (<50% stenosis was found) constituted the study group and 140 persons without grounds for suspecting coronary artery disease constituted the control group. There was a significantly higher incidence of such cardiovascular risk factors as diabetes mellitus, hypertension, and metabolic syndrome in the research group. People in the study group were also significantly older than those in the control group (55.6 ± 1.1 vs. 41.2 ± 1.5 years). It was found that in the research group, the concentration of ceruloplasmin in the blood was significantly higher [35]. In our study, no significant differences in the concentration of ceruloplasmin were found between the groups with or without metabolic disturbances; however, we observed that it was significantly higher in women. Perhaps the increase in ceruloplasmin concentration occurs only at a later stage of metabolic disorder progression than in the population we studied.

SOD is one of the most important antioxidant enzymes in the human organism [36]. Baynes and Thorpe suggested that in response to oxidative stress, cells increase the production of this enzyme to prevent mitochondria from oxidative damage [37, 38]. The function of this enzyme is to catalyse the dismutation reaction of the highly reactive superoxide radical anion. SOD occurs in the form of three isoenzymes: cytosolic CuZnSOD, mitochondrial MnSOD, and extracellular SOD (EC-SOD). It has been shown that oxidative stress causes increase in the expression of antioxidant enzymes such as SOD [39]. The data available in the literature on the dependence of SOD activity on body weight and metabolic health status are not unequivocal. Isogawa et al. published data that gave partially similar conclusions to ours. According to the results of their study, SOD activity negatively correlates with BMI. They have shown also that lower SOD activity correlates with increased carotid intima-media thickness which is a well-known indicator of increased cardiovascular risk, but on the other hand, existence of carotid plaque positively correlates with SOD activity [40]. Among the population we studied, the relationship is even stronger in obese individuals with a metabolically unhealthy phenotype and is slightly greater in women than in men. Yubero-Serrano et al. showed that the activity of SOD in patients with two components of metabolic syndrome is signifi-

cantly lower than in patients with three or more concomitant components of the metabolic syndrome. They have concluded that SOD activity could be the most relevant biomarker of oxidative stress in patients suffering from metabolic syndrome [41]. It is noteworthy that in both above-mentioned studies, mean age of participants was similar and higher than in our study. Isogawa et al. performed their study on the group of patients in which only some of the participants had components of the metabolic syndrome, but Yubero-Serrano et al. enrolled only people with metabolic syndrome. Farah et al. have shown no significant difference in SOD activity between MHO and MUO patients [42]. According to our results, the total blood SOD activity was significantly lower in MUO than in MHNW, both in women (difference 6.37%; $p = 0.0025$) and in men (difference 11.79%; $p = 0.0321$). According to our research, the determination of total blood SOD activity could be a marker of obesity-related metabolic disorders, both in women and in men.

4.2.2. Oxidative Stress Parameters Related to Total Antioxidant/Oxidant Status.

The term TAC of plasma or tissue fluid refers to the total capacity to neutralize the prooxidative potential of reactive oxygen species. It is important that the determination of the TAC takes into account the synergistic or antagonistic effect of the various antioxidants present in the plasma or tissue fluid, as opposed to the measurement of the concentration of individual antioxidants [43]. A high fraction of TAC is attributed to uric acid as the endogenous antioxidant molecule [44]. That is why we observed a strong correlation in the whole group.

OSI is the percentage ratio of TOS to TAC. In a study by Nowicki et al., in which people after cardiovascular events (study group) and those without a history of cardiovascular events (control group) participated, no significant difference was found in OSI between the research and the control group, as well as no significant correlation was found between OSI and BMI [45]. Our study also showed no significant difference in terms of OSI between the MUO, MHO, and MHNW groups. Romuk et al. conducted a study to investigate the differences in the parameters of oxidative stress between patients with ischemic and nonischemic cardiomyopathy. It has been found that in patients with ischemic cardiomyopathy, the TAC value is significantly higher and the OSI value is significantly lower. There were no significant differences in TOS. In the study, people with normal body weight or overweight participated [46]. In obese and overweight adolescents, TAC and TOS measured in the plasma and saliva were documented to be higher than in the control group [47]. Higher BMI was shown to be an independent risk factor for the lower total antioxidant status (TAS) which may be correlated with increased carotid intima-media thickness in patients with arterial hypertension [48]. In our study, TAC was significantly higher in obese women with metabolic diseases, and we found an increasing correlation of TAC with increasing metabolic disorders, measured as total cholesterol and triglyceride level. This may suggest that obesity and related metabolic disturbances may contribute to the development of coronary artery disease

in a young population. In our results, the TAC among MHO women was 2.91% higher than that among MHNW women, and the TAC value among MUO women was 10.68% higher than that among MHNW women ($p = 0.0042$). Our results suggest that TAC could be a marker of metabolic disorders developing in the course of obesity in women, but more research is needed in this direction.

4.2.3. Oxidative Stress Parameters Related to Oxidative Damage.
Simão et al. conducted a study that compared the parameters of oxidative stress in patients who had suffered an ischemic stroke, depending on the coexistence or absence of features of the metabolic syndrome. In the group of patients with metabolic syndrome, a significantly higher concentration of lipid hydroperoxides and a significantly higher value of the oxidative stress index were found. In the entire population studied by us, as well as among men analysed separately, the concentration of lipid hydroperoxides was significantly higher in metabolically obese patients (MUO) but, as already mentioned, without significant differences in OSI [49]. As shown in this study, MUO subjects had increased hydroperoxide lipid levels compared to MHNW and MHO individuals. It has been previously demonstrated that hydroperoxides derivatives are the main primary products of lipid oxidation, particularly in several human inflammatory diseases including diabetes, hypertension, dyslipidaemia, and metabolic syndrome [50, 51].

Lipofuscin is a conglomerate of highly oxidized proteins and lipids considered to be a marker of cell aging. Oxidative stress plays a role in the formation of lipofuscin [52]. There is not a large amount of data elucidating the clinical relevance of LPS measurement in metabolic syndrome. Cazzola et al. have documented that overweight and obesity are associated with increased LPS content in erythrocytes. Taking into account the overall results of this study, it is probably associated with increased lipid peroxidation and the making of aldehydes promoting the formation of cross-links between proteins and phospholipids. Only metabolically healthy females have been enrolled into the study [53]. Our results are therefore not fully comparable as we showed a downward trend for LPS content with increasing metabolic abnormalities. Further studies are needed to better understand the role of LPS as a possible marker of oxidative stress in the course of metabolic disorders.

Research shows that metabolically healthy obesity (MHO) is not a permanent condition. Echouffo-Tcheugui et al. showed that in a four-year follow-up, 43% of MHO women and 46% of MHO men develop disorders that allow them to qualify as metabolically obese patients (MUO) [54]. Moreover, even obese people who are metabolically healthy have an increased health risk. According to the results of the meta-analysis carried out by Zheng et al., MHO individuals have a significantly higher risk of cardiovascular events than metabolically healthy normal weight people (MHNW) (RR 1.5; 95% CI 1.27–1,77) [55]. Bell et al. demonstrated an increased risk of developing type 2 diabetes in this population [56], and Arnlöv et al. showed an increased risk of developing CVD [57]. The state of MHO should therefore not be regarded as completely normal but rather as a transition period between the state of health and the development of overt metabolic syndrome, as well as a condition associated with an increased risk of morbidity.

4.3. Can Supplementation of Antioxidants Be a Useful Direction in Therapy?
The results presented in this study show that obese people with metabolic disorders show more disturbances in the parameters of oxidative stress than people with normal body weight without metabolic disorders. The literature suggests the usefulness of many nutraceuticals with antioxidant properties in obese patients, but much of the information on this topic is based mainly on the results of basic research [58]. Recently, the role of isoflavones in the prevention and therapy of type 2 diabetes has been described in detail [59], as well as the properties of phytoestrogens in the context of their use in the prevention of obesity and the resulting disorders [60]. However, it should be noted that this subject is of great interest, and in recent years, the results of clinical trials and meta-analyses evaluating the importance of antioxidant supplementation in the context of the treatment of obesity and related metabolic disorders have been published. Suliburska et al. presented the results of a randomized, double-blind study, which showed that a 3-month supplementation of green tea extract has a positive effect on body weight, lipid profile, blood glucose concentration, and TAS in obese people, as well as on zinc and magnesium metabolism [61]. A systematic review and meta-analysis of clinical trials showed that spirulina supplementation is associated with weight loss in obese subjects [62]. Saffron has documented beneficial effects on waist circumference and fasting blood glucose [63]. The supplementation of certain nutraceuticals with antioxidant properties has a beneficial effect on the metabolic status of obese people and may be considered in the treatment of obese people. However, it should be remembered that such an approach should be of an auxiliary nature and cannot replace a lifestyle change, including a rational diet and exercise, leading to weight loss.

5. Summary

Our findings suggest that metabolically unhealthy obese patients have more pronounced oxidative stress parameters comparing to those with normal weight without metabolic disturbances. The significant differences between men and women may imply different mechanisms leading to oxidative stress and its complications. Our results are partially confirmed by the studies that have been conducted so far, which, however, mainly concerned patients with already developed disease entities, which are complications of obesity.

An important achievement of our research is the demonstration that the total SOD activity is statistically significantly lower in MUO compared to MHNW in both women and men, while the TAC value increases significantly in MUO women. Our study involved young people, untreated for chronic diseases; therefore, these parameters of oxidative stress could be considered for use in clinical practice as early markers of the development of metabolic disorders with weight gain. More research is needed. These results show that

obesity is always a pathological condition, despite the lack of specific disease entities already developed.

Abbreviations

BMI:	Body mass index
CBC:	Complete blood count
CER:	Ceruloplasmin
CHD:	Coronary heart disease
CI:	Confidence interval
CuZnSOD:	Copper- and zinc-containing superoxide dismutase
CVD:	Cardiovascular disease
DBP:	Diastolic blood pressure
EC-SOD:	Extracellular superoxide dismutase
HDL:	High density lipoprotein
HDL-C:	High density lipoprotein cholesterol
HOMA-IR:	Homeostasis model assessment of insulin resistance
HR:	Hazard ratio
LDL:	Low density lipoprotein
LDL-C:	Low density lipoprotein cholesterol
LPH:	Lipid hydroperoxides
LPS:	Lipofuscin
MDA:	Malondialdehyde
MHNW:	Metabolically healthy normal weight
MHO:	Metabolically healthy obese/obesity
MnSOD:	Manganese-containing superoxide dismutase
MPO:	Myeloperoxidase
MUO:	Metabolically unhealthy obese/obesity
NU:	Nitric unit
OSI:	Oxidative stress index
oxLDL:	Oxidized low density lipoproteins
PSH:	Thiol group concentration per gram protein
ROS:	Reactive oxygen species
RR:	Relative risk
RU:	Relative unit
SBP:	Systolic blood pressure
SOD:	Superoxide dismutase
TAC:	Total antioxidant capacity
TAS:	Total antioxidant status
TBARS:	Thiobarbituric acid-reacting substances
TC:	Total cholesterol
TG:	Triglycerides
TOS:	Total oxidative status
UA:	Uric acid
VAI:	Visceral adipose index
WC:	Waist circumference
WHR:	Waist-hip ratio.

Data Availability

The data presented in this study are available on request from the corresponding author.

Conflicts of Interest

The authors declare no conflict of interest.

Supplementary Materials

Supplementary Table 1: oxidative stress parameters—differences in men with different metabolic status. Supplementary Table 2: oxidative stress parameters—differences in women with different metabolic status. (Supplementary Materials)

References

[1] Y. C. Chooi, C. Ding, and F. Magkos, "The epidemiology of obesity," *Metabolism*, vol. 92, pp. 6–10, 2019.

[2] N. Stefan, H. U. Häring, F. B. Hu, and M. B. Schulze, "Metabolically healthy obesity: epidemiology, mechanisms, and clinical implications," *Lancet Diabetes and Endocrinology*, vol. 1, no. 2, pp. 152–162, 2013.

[3] C. M. Apovian, "Obesity: definition, comorbidities, causes, and burden," *American Journal of Managed Care*, vol. 22, 7 Suppl, pp. S176–S185, 2016.

[4] M. Ng, T. Fleming, M. Robinson et al., "Global, regional, and national prevalence of overweight and obesity in children and adults during 1980-2013: a systematic analysis for the Global Burden of Disease Study 2013," *Lancet*, vol. 384, no. 9945, pp. 766–781, 2014.

[5] P. L. Schnall, M. Dobson, and P. Landsbergis, "Globalization, work, and cardiovascular disease," *International Journal of Health Services*, vol. 46, no. 4, pp. 656–692, 2016.

[6] H. Thomas, J. Diamond, A. Vieco et al., "Global atlas of cardiovascular disease 2000-2016: the path to prevention and control," *Global Heart*, vol. 13, no. 3, pp. 143–163, 2020.

[7] C. Andersson and R. S. Vasan, "Epidemiology of cardiovascular disease in young individuals," *Nature Reviews Cardiology*, vol. 15, no. 4, pp. 230–240, 2018.

[8] J. Frostegard, "Immunity, atherosclerosis and cardiovascular disease," *BMC Medicine*, vol. 11, no. 1, article 117, 2013.

[9] N. R. Madamanchi, A. Vendrov, and M. S. Runge, "Oxidative stress and vascular disease," *Arteriosclerosis, Thrombosis and Vascular Biology*, vol. 25, no. 1, pp. 29–38, 2005.

[10] K. Cervantes Gracia, D. Llanas-Cornejo, and H. Husi, "CVD and oxidative stress," *Journal of Clinical Medicine*, vol. 6, no. 2, p. 22, 2017.

[11] M. P. Murphy, "How mitochondria produce reactive oxygen species," *Biochemical Journal*, vol. 417, no. 1, pp. 1–13, 2009.

[12] M. Wołonciej, E. Milewska, and W. Roszkowska-Jakimiec, "Trace elements as an activator of antioxidant enzymes," *Postępy Higieny i Medycyny Doświadczalnej*, vol. 70, pp. 1483–1498, 2016.

[13] A. M. Kabel, "Free radicals and antioxidants: role of enzymes and nutrition," *Journal of Nutrition and Health*, vol. 2, no. 3, pp. 35–38, 2014.

[14] S. Biswal, H. Rizwan, S. Pal, S. Sabnam, P. Parida, and A. Pal, "Oxidative stress, antioxidant capacity, biomolecule damage, and inflammation symptoms of sickle cell disease in children," *Hematology*, vol. 24, no. 1, pp. 1–9, 2019.

[15] F. Ito, Y. Sono, and T. Ito, "Measurement and clinical significance of lipid peroxidation as a biomarker of oxidative stress:

oxidative stress in diabetes, atherosclerosis, and chronic inflammation," *Antioxidants*, vol. 8, no. 3, p. 72, 2019.

[16] F. Pietrocola and J. M. Bravo-San Pedro, "Targeting autophagy to counteract obesity-associated oxidative stress," *Antioxidants*, vol. 10, no. 1, p. 102, 2021.

[17] B. Choromańska, P. Myśliwiec, M. Łuba et al., "The impact of hypertension and metabolic syndrome on nitrosative stress and glutathione metabolism in patients with morbid obesity," *Oxidative Medicine and Cellular Longevity*, vol. 2020, Article ID 1057570, 10 pages, 2020.

[18] T. Osadnik, K. Osadnik, N. Pawlas et al., "Metabolic and genetic profiling of young adults with and without a family history of premature coronary heart disease (MAGNETIC). Study design and methodology," *Archives of Medical Science*, vol. 15, no. 3, pp. 590–597, 2019.

[19] S. Buscemi, P. Chiarello, C. Buscemi et al., "Characterization of metabolically healthy obese people and metabolically unhealthy normal-weight people in a general population cohort of the ABCD study," *Journal of Diabetes Research*, vol. 2017, Article ID 9294038, 9 pages, 2017.

[20] M. C. Amato, C. Giordano, M. Galia et al., "Visceral adiposity index: a reliable indicator of visceral fat function associated with cardiometabolic risk," *Diabetes Care*, vol. 33, no. 4, pp. 920–922, 2010.

[21] J. F. Koster, P. Biemond, and A. J. Swaak, "Intracellular and extracellular sulphydryl levels in rheumatoid arthritis," *Annals of the Rheumatic Diseases*, vol. 45, no. 1, pp. 44–46, 1986.

[22] O. Erel, "A novel automated direct measurement method for total antioxidant capacity using a new generation, more stable ABTS radical cation," *Clinical Biochemistry*, vol. 37, no. 4, pp. 277–285, 2004.

[23] O. Erel, "A new automated colorimetric method for measuring total oxidant status," *Clinical Biochemistry*, vol. 38, no. 12, pp. 1103–1111, 2005.

[24] H. Ohkawa, N. Ohishi, and K. Yagi, "Assay for lipid peroxides in animal tissues by thiobarbituric acid reaction," *Analytical Biochemistry*, vol. 95, no. 2, pp. 351–358, 1979.

[25] R. Richterich, *Chemia Kliniczna: Teoria i Praktyka*, PZWL, Warszawa, 1971.

[26] E. Sődergren, J. Nourooz-Zadeh, L. Berglund, and B. Vessby, "Re-evaluation of the ferrous oxidation in xylenol orange assay for the measurement of plasma lipid hydroperoxides," *Journal of Biochemical and Biophysical Methods*, vol. 37, no. 3, pp. 137–146, 1998.

[27] S. K. Jain, "In vivo externalization of phosphatidylserine and phosphatidylethanolamine in the membrane bilayer and hypercoagulability by the lipid peroxidation of erythrocytes in rats," *Journal of Clinical Investigation*, vol. 76, no. 1, pp. 281–286, 1985.

[28] Y. Oyanagui, "Reevaluation of assay methods and establishment of kit for superoxide dismutase activity," *Analytical Biochemistry*, vol. 142, no. 2, pp. 290–296, 1984.

[29] A. Tsatsoulis and S. A. Paschou, "Metabolically healthy obesity: criteria, epidemiology, controversies, and consequences," *Current Obesity Reports*, vol. 9, no. 2, pp. 109–120, 2020.

[30] E. Brunelli, F. Domanico, D. La Russa, and D. Pellegrino, "Sex differences in oxidative stress biomarkers," *Current Drug Targets*, vol. 15, no. 8, pp. 811–815, 2014.

[31] G. Block, M. Dietrich, E. P. Norkus et al., "Factors associated with oxidative stress in human populations," *American Journal of Epidemiology*, vol. 156, no. 3, pp. 274–285, 2002.

[32] T. Ide, H. Tsutsui, N. Ohashi et al., "Greater oxidative stress in healthy young men compared with premenopausal women," *Thrombosis and Vascular Biology*, vol. 22, no. 3, pp. 438–442, 2002.

[33] F. Nielsen, B. B. Mikkelsen, J. B. Nielsen, H. R. Andersen, and P. Grandjean, "Plasma malondialdehyde as biomarker for oxidative stress: reference interval and effects of life-style factors," *Clinical Chemistry*, vol. 43, no. 7, pp. 1209–1214, 1997.

[34] M. Gol, B. Özkaya, C. Yildirim, and R. Bal, "Regular exercise, overweight/obesity and sedentary lifestyle cause adaptive changes in thiol-disulfide homeostasis," *Annals of the Brazilian Academy of Sciences*, vol. 91, no. 2, article e20180547, 2019.

[35] E. M. Alissa, W. H. Ahmed, N. Al-ama, and G. A. A. Ferns, "Relationship between indices of iron status and coronary risk factors including diabetes and the metabolic syndrome in Saudi subjects without overt coronary disease," *Journal of Trace Elements in Medicine and Biology*, vol. 21, no. 4, pp. 242–254, 2007.

[36] H. Sies, "Oxidative stress: oxidants and antioxidants," *Experimental Physiology*, vol. 82, no. 2, pp. 291–295, 1997.

[37] J. W. Baynes, "Role of oxidative stress in development of complications in diabetes," *Diabetes*, vol. 40, no. 4, pp. 405–412, 1991.

[38] J. W. Baynes and S. R. Thorpe, "Role of oxidative stress in diabetic complications: a new perspective on an old paradigm," *Diabetes*, vol. 48, no. 1, pp. 1–9, 1999.

[39] J. É. M. MatÉs, C. Pérez-Gómez, and I. N. de Castro, "Antioxidant enzymes and human diseases," *Clinical Biochemistry*, vol. 32, no. 8, pp. 595–603, 1999.

[40] A. Isogawa, M. Yamakado, M. Yano, and T. Shiba, "Serum superoxide dismutase activity correlates with the components of metabolic syndrome or carotid artery intima-media thickness," *Diabetes Research and Clinical Practice*, vol. 86, no. 3, pp. 213–218, 2009.

[41] E. M. Yubero-Serrano, J. Delgado-Lista, P. Peña-Orihuela et al., "Oxidative stress is associated with the number of components of metabolic syndrome: LIPGENE study," *Experimental and Molecular Medicine*, vol. 45, no. 6, p. e28, 2013.

[42] R. Farah, P. Gilbey, M. Grozovski, H. Asli, R. Khamisy-Farah, and N. Assy, "Antioxidant enzyme activity and cognition in obese individuals with or without metabolic risk factors," *Experimental and Clinical Endocrinology and Diabetes*, vol. 124, no. 9, pp. 568–571, 2016.

[43] C. G. Fraga, P. I. Oteiza, and M. Galleano, "In vitro measurements and interpretation of total antioxidant capacity," *Biochimica et Biophysica Acta*, vol. 1840, no. 2, pp. 931–934, 2014.

[44] A. Gawron-Skarbek, A. Guligowska, A. Prymont-Przymińska, D. Nowak, and T. Kostka, "Plasma and salivary non-urate total antioxidant capacity does not depend on dietary vitamin C, E, or β-carotene intake in older subjects," *Molecules*, vol. 23, no. 4, p. 983, 2018.

[45] G. J. Nowicki, B. Ślusarska, A. Prystupa, M. Polak, M. Czubaj-Kowal, and E. Rudnicka-Drożak, "Oxidative/antioxidative status in patients after myocardial infarction and in those without cardiovascular event depending on anthropometric factors defining body weight," *International Journal of Environmental Research and Public Health*, vol. 16, no. 21, p. 4077, 2019.

[46] E. Romuk, C. Wojciechowska, W. Jacheć et al., "Comparison of oxidative stress parameters in heart failure patients depending on ischaemic or nonischaemic aetiology," *Oxidative*

Medicine and Cellular Longevity, vol. 2019, Article ID 7156038, 13 pages, 2019.

[47] A. Zalewska, A. Kossakowska, K. Taranta-Janusz et al., "Dysfunction of salivary glands, disturbances in salivary antioxidants and increased oxidative damage in saliva of overweight and obese adolescents," *Journal of Clinical Medicine*, vol. 9, no. 2, p. 548, 2020.

[48] P. Gać, M. Poręba, L. Januszewska et al., "The total antioxidant status, serum selenium concentrations and the ultrasound assessment carotid intima media thickness in patients with arterial hypertension," *Antioxidants*, vol. 10, no. 1, p. 63, 2021.

[49] A. N. C. Simão, M. F. Lehmann, D. F. Alfieri et al., "Metabolic syndrome increases oxidative stress but does not influence disability and short-time outcome in acute ischemic stroke patients," *Metabolic Brain Disease*, vol. 30, no. 6, pp. 1409–1416, 2015.

[50] N. Houstis, E. D. Rosen, and E. S. Lander, "Reactive oxygen species have a causal role in multiple forms of insulin resistance," *Nature*, vol. 440, no. 7086, pp. 944–948, 2006.

[51] A. Fortuno, G. San Jose, M. U. Moreno, O. Beloqui, J. Diez, and G. Zalba, "Phagocytic NADPH oxidase overactivity underlies oxidative stress in metabolic syndrome," *Diabetes*, vol. 55, no. 1, pp. 209–215, 2006.

[52] T. Jung, N. Bader, and T. Grune, "Lipofuscin: formation, distribution, and metabolic consequences," *Annals of the New York Academy of Sciences*, vol. 1119, no. 1, pp. 97–111, 2007.

[53] R. Cazzola, M. Rondanelli, S. Russo-Volpe, E. Ferrari, and B. Cestaro, "Decreased membrane fluidity and altered susceptibility to peroxidation and lipid composition in overweight and obese female erythrocytes," *Journal of Lipid Research*, vol. 45, no. 10, pp. 1846–1851, 2004.

[54] J. B. Echouffo-Tcheugui, M. I. Short, V. Xanthakis et al., "Natural history of obesity subphenotypes: dynamic changes over two decades and prognosis in the Framingham Heart Study," *Journal of Clinical Endocrinology and Metabolism*, vol. 104, no. 3, pp. 738–752, 2019.

[55] R. Zheng, D. Zhou, and Y. Zhu, "The long-term prognosis of cardiovascular disease and all-cause mortality for metabolically healthy obesity: a systematic review and meta-analysis," *Journal of Epidemiology and Community Health*, vol. 70, no. 10, pp. 1024–1031, 2016.

[56] J. A. Bell, M. Kivimaki, and M. Hamer, "Metabolically healthy obesity and risk of incident type 2 diabetes: a meta- analysis of prospective cohort studies," *Obesity Reviews*, vol. 15, no. 6, pp. 504–515, 2014.

[57] J. Arnlöv, E. Ingelsson, J. Sundström, and L. Lind, "Impact of body mass index and the metabolic syndrome on the risk of cardiovascular disease and death in middle-aged men," *Circulation*, vol. 121, no. 2, pp. 230–236, 2010.

[58] H. A. Hassan and N. E. El-Gharib, "Obesity and clinical riskiness relationship: therapeutic management by dietary antioxidant supplementation – a review," *Applied Biochemistry and Biotechnology*, vol. 176, no. 3, pp. 647–669, 2015.

[59] A. Kuryłowicz, "The role of isoflavones in type 2 diabetes prevention and treatment – a narrative review," *International Journal of Molecular Sciences*, vol. 22, no. 1, p. 218, 2021.

[60] A. Kuryłowicz, M. Cąkała-Jakimowicz, and M. Puzianowska-Kuźnicka, "Targeting abdominal obesity and its complications with dietary phytoestrogens," *Nutrients*, vol. 12, no. 2, p. 582, 2020.

[61] J. Suliburska, P. Bogdanski, M. Szulinska, M. Stepien, D. Pupek-Musialik, and A. Jablecka, "Effects of green tea supplementation on elements, total antioxidants, lipids, and glucose values in the serum of obese patients," *Biological Trace Element Research*, vol. 149, no. 3, pp. 315–322, 2012.

[62] S. Moradi, R. Ziaei, S. Foshati, H. Mohammadi, S. M. Nachvak, and M. H. Rouhani, "Effects of Spirulina supplementation on obesity: A systematic review and meta- analysis of randomized clinical trials," *Complementary Therapies in Medicine*, vol. 47, article 102211, 2019.

[63] J. Rahmani, E. Bazmi, C. Clark, and S. S. Hashemi Nazari, "The effect of saffron supplementation on waist circumference, HA1C, and glucose metabolism: a systematic review and meta-analysis of randomized clinical trials," *Complementary Therapies in Medicine*, vol. 49, article 102298, 2020.